PROCEEDINGS
NINTH WORKSHOP
GEOTHERMAL RESERVOIR ENGINEERING

December 13-15, 1983



Henry J. Ramey, Jr., Paul Kruger, Frank G. Miller,
Roland N. Horne, William E. Brigham,
and Jon S. Gudmundsson
Stanford Geothermal Program
Workshop Report SGP-TR-74*

*Sponsored by the Geothermal and Hydropower Technologies Division of the U.S. Department of Energy, Stanford-DOE Contract No. DE-AT03-80SF11459

Library of Congress Catalogue Card No. 85-081236

TABLE OF CONTENTS

Page

Preface . . . . . -vii-

Introduction

DOE's Current Geothermal Reservoir Programs and Comments on International Cooperation in Hydrothermal Research - R.S.H. Toms 1

Field Development

Geothermal Field Development in the European Community Objectives, Achievements and Problem Areas - P. Ungemach 5

Present Status and Future Prospects of Geothermal Development in Italy - R. Cataldi, G. Neri, and G. Manetti 17

Geothermal Field Developments in Iceland G. Palmason, V. Stefansson, S. Thorhallsson, and T. Thorsteinsson 37

Multiple Reservoirs in the Mofete Field, Naples, Italy R. Carella, and M. Guglielminetti 53

Overview of Geothermal Development at Olkaria in Kenya - A. Svanbjornsson, J. Matthiasson, H. Frimannsson, S. Arnorsson, S. Bjornsson, V. Stefansson, and K. Saemundsson 65

Resource Evaluation and Development Plans for a 120 MW Geothermal Power Plant on Milos Island, Greece - M.J. Economides, C.A. Ehlig-Economides, G. Speliotis, and F. Vrouzi 73

Geothermal Field Development in Mexico - H. Alonso E. 81

Some Comments on the La Primavera Geothermal Field Mexico B. Dominguez A., and M.J. Lippmann 87

A Status Report on the Exploitation Conditions of the Ahuachapan Geothermal Field - J. Rivera-R, A. Vides-R., G. Cuellar, F. Samaniego-V, and G. Neri-I 97

Recent Developments in Reservoir Engineering in New Zealand M.A. Grant, P.F. Bixley, M.J. O'Sullivan, and J.D. Leaver 107

Geothermal Field Developments in Japan - S. Hirakawa 115

Reservoir Engineering Aspects of the Philippines Geothermal Developments in Leyte and Southern Negros - R. Kingston, and A. Watson 121

Geothermal Energy Development in China - K. Xin, and Q. Yang 127

Hydrothermal Systems

Exploration, Drilling, and Development Operations in the Bottle Rock Area of the Geysers Steam Field with New Geologic Insights and Models Defining Reservoir Parameters - J.J. Hebein 135

Geologic Model of the Baca Geothermal Reservoir, Valles Caldera, New Mexico - D.L. Nielson, and J.B. Hulen 145

Desert Peak: A Geothermal Field in Churchill County, Nevada K.P. Goyal, W.R. Benoit, J.P. Maas, and J.R. Rosser 151

The Generating Capacity of the Heber Geothermal Field, California M.J. Lippmann, and G.S. Bodvarsson 157

Page

Well Testing

A Summary of Geothermal Exploration and Data from Stratigraphic Test Well No. 1 Makushin Volcano, Unalaska Island - D.A. Campbell, and M.J. Economides 167

Well Test Analysis in Naturally Fissured, Geothermal Reservoirs with Fracture Skin - A.F. Moench 175

Slug Test Data Analysis in Reservoirs with Double Porosity Behavior K. Mateen, and H.J. Ramey, Jr. 181

Interpretation of Interference Data from the Klamath Falls, Oregon Geothermal Resource - S.M. Benson 187

Evaluating Geothermal Reserves with Application of Well Interference and Pressure Buildup Tests - T.L. Chiu, C.Y. Chiang, and T.S. Wu 193

Analysing Spinner Measurements from Well Tests Using Computerized Interpretation Techniques - R.N. Horne, A. Guillot, and A. Rosa 199

The Development and Use of a High Temperature Downhole Flowmeter for Geothermal Well Logging - R.D. Solbau, C.B. Goranson, and S.M. Benson 205

Nonisothermal Injectivity Index Can Infer Well Productivity and Reservoir Transmissivity - O. Sigurdsson, G.S. Bodvarsson, and V. Stefansson 211

Effect of Scaling on Downhole Pressure Transient Data - S. Petty 217

Reservoir Chemistry

Effects of Natural Recharge on Gas Composition in the Larderello-Castelnuovo Area - F. D'Amore, R. Celati, C. Calore, and R. Bertrami 221

Gas Chemistry in Geothermal Systems - S. Arnorsson, and E. Gunnlaugsson 231

Permeability Reduction due to Precipitation of Quartz under Nonisothermal Conditions - L.A. Keith, P.T. Delaney, and D.E. Moore 239

Hypotheses on Possible Equilibria between N_2 and Other Gases at Larderello and Cerro Prieto - F. D'Amore, R. Celati, and C. Calore 247

Heterogeneity of the Liquid Phase, and Vapor Separation in Los Azufres (Mexico) Geothermal Reservoir - D. Nieva, L. Quijano, A. Garfias, R.M. Barragan, and F. Laredo 253

Simulation of Radon Transport in Geothermal Reservoirs - L. Semprini, and P. Kruger 261

Mineralogy and Distribution of Hydrothermal Mineral Zones in Los Azufres (Mexico) Geothermal Field - M. Cathelineau, R. Oliver, G. Izquierdo, A. Garfias, D. Nieva, and O. Izaguirre 269

Production

One Year Experience with Portable Back-Pressure Turbines in Los Azufres G. Hiriart L. 275

One Component Two Phase Flow in Horizontal and Vertical Ducts: Some Basic Considerations - P.F. Maeder, D.A. Dickinson, and D.E. Nikitopoulos 279

Page

A Method to Recover Useful Geothermal-Reservoir Parameters from Production Characteristic Curves (1) Steam Reservoirs - E. Iglesias, V. Arellano, A. Garfias, C. Miranda, J. Hernandez, and J. Gonzales 285

A Method to Recover Useful Geothermal-Reservoir Parameters from Production Characteristic Curves (2) Hot Water Reservoirs - E. Iglesias, V. Arellano, and R. Molinar 291

Injection

Tracer Recovery and Mixing from Two Geothermal Injection-Backflow Studies R.M. Capuano, M.C. Adams, and P.M. Wright 299

Physical Model of a Fractured Reservoir - L.C. Hull, and K.N. Koslow 305

Response of East Mesa and Raft River Reservoirs to Injection-Backflow Testing - B.F. Russell, L.C. Hull, and W.F. Downs 311

Disposal of Flashed Brine Dosed with $CaCO_3$ Scale Inhibitor: What Happens when the Inhibitor is Exhausted - D.E. Michels 317

Matrix Diffusion and Its Effect on the Modeling of Tracer Returns from the Fractured Geothermal Reservoir at Wairakei, New Zealand . . . . . 323 C.L. Jensen, and R.N. Horne

Doublet Tracer Testing in Klamath Falls, Oregon - J.S. Gudmundsson, S.E. Johnson, R.N. Horne, P.B. Jackson, and G.G. Culver 331

Laboratory Physical Model for Pattern Injection in Geothermal Systems M. Parlaktuna, and E. Okandan 339

Simulation

Analysis of Production Data from the Krafla Geothermal Field, Iceland K. Pruess, G.S. Bodvarsson, and V. Stefansson 345

Modeling Studies of Geothermal Systems with a Free Water Surface G.S. Bodvarsson, and K. Pruess 351

Reservoir Simulation on the Cerro Prieto Geothermal Field: A Continuing Study M. Castaneda, R. Marquez, V. Arellano, and C.A. Esquer 357

Numerical Simulations of the Hydrothermal System at Lassen Volcanic National Park - M.L. Sorey, and S.E. Ingebritsen 365

A Fundamental Approach to the Simulation of Flow and Dispersion in Fractured Media - J.D. Miller 373

Petrothermal

Rock Failure in Compression - S. Nemat-Nasser, and H. Horii 381

Pressure Transient Analysis for Large Scale Hydraulic Injections in the Carnmenellis Granite, England - R.J. Pine 387

Variation of Fracturing Pressures with Depth near the Valles Caldera Z. Dash, and H. Murphy 397

Behaviors of Crack-Like Reservoirs by Means of Fracturing at Nigorikawa and Kakkonda Geothermal Fields - H. Abe, H. Takahashi, K. Nakatsuka, H. Niitsuma, and M. Takanohashi 403

The Cost Effectiveness of Fracture Stimulation in Increasing the Flow from Geothermal Wells - G.L. Brown 409

Page

Crustal Rock Fracture Mechanics for Design and Control of Artificial Subsurface Cracks in Geothermal Energy Extraction Engineering (Γ -Project) H. Abe, and H. Takahashi 415

Reservoir Physics

Mapping the Acid Stimulation in the Beowawe Geothermal Field using Surface Electrical Potentials - C.M. Hart, D. Engi, and H.E. Morris 421

Thermal Expansion Behavior of Cerro Prieto Sandstones and Other Sedimentary Rocks under Stress - E. Contreras, and F. Bermejo 427

Design and Development of a Test Facility to Study Two-Phase Steam/Water Flow in Porous Media - A.K. Verma, K. Pruess, G.S. Bodvarsson, C.F. Tsang, and P.A. Witherspoon 443

Radial Flow of Pressured Hot Water through Narrow Cracks - R. James 449

List of Participants 455

PREFACE

The Ninth Workshop on Geothermal Reservoir Engineering was held at Stanford University on December 13-15, 1983. The attendance at the Workshop was similar to last year's with 123 registered participants of which 22 represented 8 foreign countries.

A record number of technical papers (about 60) were submitted for presentation at the Workshop. The Program Committee, therefore, decided to have several parallel sessions to accommodate most of the papers. This format proved unpopular and will not be repeated. Many of the participants felt that the Workshop lost some of its unique qualities by having parallel sessions.

The Workshop has always been held near the middle of December during examination week at Stanford. This timing was reviewed in an open discussion at the Workshop. The Program Committee subsequently decided to move the Workshop to January. The Tenth Workshop will be held on January 22-24, 1985.

The theme of the Workshop this year was "field developments worldwide." The Program Committee addressed this theme by encouraging participants to submit field development papers, and by inviting several international authorities to give presentations at the Workshop. Field developments in at least twelve countries were reported: China, El Salvador, France, Greece, Iceland, Italy, Japan, Kenya, Mexico, New Zealand, the Philippines, and the United States. There were 58 technical presentations at the Workshop, of which 4 were not made available for publication. Several authors submitted papers not presented at the Workshop. However, these are included in the 60 papers of these Proceedings.

The introductory address was given by Ron Toms of the U.S. Department of Energy, and the banquet speaker was Al Cooper of Chevron Resources Company.

An important contribution was made to the Workshop by the chairmen of the technical sessions. Other than Stanford Geothermal Program faculty members, they included: Don White (Field Developments), Bill D'Olier (Hydrothermal Systems), Herman Dykstra (Well Testing), Karsten Pruess (Well Testing), John Counsil (Reservoir Chemistry), Malcolm Mossman (Reservoir Chemistry), Greg Raasch (Production), Manny Nathenson (Injection), Susan Petty (Injection), Subir Sanyal (Simulation), Marty Molloy (Petrothermal), and Allen Moench (Reservoir Physics).

The Workshop was organized by the Stanford Geothermal Program faculty, staff and students. We would like to thank Jean Cook, Joanne Hartford, Terri Ramey, Amy Osugi, and Marilyn King for their valued help with the Workshop arrangements and the Proceedings. We also owe thanks to the program students who arranged and operated the audio-visual equipment.

The Ninth Workshop was supported by the Geothermal and Hydropower Technologies Division of the U.S. Department of Energy through contract DE-AT03-80SF11459. We deeply appreciate this continued support.

H. J. Ramey, Jr., R. N. Horne, P. Kruger,
W. E. Brigham, F. G. Miller,
J. S. Gudmundsson

Proceedings Ninth Workshop Geothermal Reservoir Engineering
Stanford University, Stanford, California, December 1983
SGP-TR-74

DOE's CURRENT GEOTHERMAL RESERVOIR PROGRAMS AND COMMENTS ON INTERNATIONAL COOPERATION IN HYDROTHERMAL RESEARCH

Ronald S. H. Toms

United States Department of Energy
Washington, D. C., 20585

ABSTRACT

DOE's geothermal program continues to emphasize a range of reservoir-related programs in reservoir definition, brine injection, stimulation, hot dry rock, geopressured resources and, now, magma resources. These programs are described briefly. Programs in international cooperation between the U.S. and 23 other countries on hydrothermal research have produced important gains in knowledge over the past ten years. Although the activity has diminished, a resurgence is anticipated.

CURRENT RESERVOIR-RELATED PROGRAMS

DOE's interest in geopressured resources is to determine the economics and to provide a technology base that industry will exploit. The three existing deep wells that were drilled in the Gulf Coast geopressured reservoirs will be continuously flow-tested this year to determine the drawdown and changes in fluid composition and gas content. EPRI is planning a total energy extraction experiment that will give further impetus to industry involvement.

In hot dry rock we plan this year to complete the Phase II thermal loop at Fenton Hill, New Mexico, to the originally planned size, and to begin extended operation of the loop to assess reservoir longevity, operating performance and environmental effects. We also plan to model the reservoir that we will have created.

Our experimental work in well stimulation was completed last year, and this year we will study the lessons learned and perform additional analyses of new techniques before embarking on more experimental work. However, through our hard rock penetration research studies we have identified the use of a tailored-pulse loading, by a slow-burning propellant as a promising technique, and work on this will proceed.

Brine injection technology has become an important program in hydrothermal research. We will continue to develop tracer, geophysical and modeling techniques to monitor and predict migration of spent brines injected into reservoirs. We will also continue the development of chemical conditioning methods to prevent unwanted chemical reactions in the well and in the adjacent injected zone. We plan to develop well completion technology to enhance the acceptance of injected brines by the well and thus extend its useful life.

Our efforts on reservoir definition will continue on many fronts. We will continue the development and validation of reservoir models capable of predicting productivity and depletion rates. We will evaluate surface and subsurface geophysical techniques capable of mapping natural fracture systems within reservoirs. Specific study areas will include Cerro Prieto and Los Azufres, Klamath Falls, the Newberry Caldera and others to be determined.

Under our State assistance programs we will continue programs in resource assessment, resource development, technical assistance and technology transfer. There will be an emphasis on high temperature resources, especially the Cascades and other prospects associated with shallow magma bodies.

In conjunction with reservoir productivity we are continuing the work in two-phase flow in the well-bore. This includes studies into the fundamental phenomena in facilities using freon and air-in-water to simulate well-bore conditions.

As part of our effort in hard rock penetration research we are developing techniques for precise borehole mapping. We have already adapted an inertial navigation system to map a relatively cold well-bore, and temperature hardening is the next step.

The proposal last year to provide a hole-of-opportunity in the Salton Sea for scientific research, under the Continental Scientific Drilling Program, has resulted in funding that will be used for a competitive solicitation for deepening or drilling a well to 18,000 feet in the Salton Sea KGRA. It is anticipated that this effort will provide valuable geothermal research into the understanding of the formation of the Salton Sea geothermal anomaly, the nature of any underlying reservoirs, and new estimates of geothermal potential, as well as a variety of important answers in the earth

sciences.

Finally, we are this year taking an engineering look at the potential for magma energy extraction. The scientific feasibility for this was established by the "magma tap" experiments at Kilauea Iki in Hawaii. We will review the candidate shallow magma bodies in the continental U.S. to evaluate their characteristics and location. We will estimate the cost of drilling and extracting energy from selected prospects, and consider their potential economics with regard to potential users and transmission lines. If the estimates are sufficiently promising we will then plan a definitive experiment for the future.

INTERNATIONAL COOPERATION

In view of the international theme of this meeting and the presence of so many distinguished geothermal experts from around the world, I will now give a short review of DOE's cooperation in international research. A meeting such as this one is an ideal forum for experts to exchange information. The world's geothermal community has a good record of informally sharing its research results, but as you know there are other, more formal ties between nations through which even closer interactions among researchers are fostered. Specifically it is DOE's cooperative agreements in geothermal energy and the outlook for the future that I will now discuss.

Since the days of its predecessor agencies, the Atomic Energy Commission and the Energy Research and Development Administration, DOE has actively pursued international cooperation in geothermal research. Ten years ago, in 1973, we joined with Iceland in a program of information exchange on direct heat applications and advanced energy conversion systems. Also in that year the United States was a party, along with fourteen other countries, in a geothermal pilot study sponsored by NATO's Committee on the Challenges of Modern Society (CCMS). This study examined a broad spectrum of geothermal topics including reservoir assessment, direct heat applications, small power plants, and hot dry rock.

The NATO-CCMS pilot study was a benchmark for future international cooperation in geothermal research. During the past decade nearly every international agreement concerning geothermal energy came about, either directly or indirectly, as a result of this pioneering effort. Not only was international cooperation stimulated, but the study spawned a renewed awareness in many countries of geothermal energy's potential. While perhaps not contributing directly to power on line, the NATO-CCMS work highlighted the many benefits of joint research among nations while also promoting geothermal energy as a real alternative in a petroleum-based world economy.

DOE perceives at least four principal values or benefits from its international cooperative agreements. First of all, such agreements enhance our domestic research programs by bringing a larger pool of talent and data to bear on technical problems. For instance, the knowledge we have gained about production from a liquid-dominated field through our bilateral agreement with Mexico will serve as a model for production in the Imperial Valley.

Secondly, we realize substantial cost savings through task sharing. The outstanding example of this benefit is our IEA Cooperative Agreement with Germany and Japan in hot dry rock technology. Under that agreement Germany and Japan each contribute up to 25 percent of the budget to operate the Fenton Hill Project in New Mexico. In return, both countries receive all project findings and may assign scientific and technical personnel to work with LANL Fenton Hill for extended periods.

The remaining benefits of our cooperative agreements are less tangible but no less important. We believe that cooperative R&D in alternative energy sources will encourage and accelerate a transition from dependency on imported oil and gas, thereby increasing this nation's and other nations' energy security. Lastly, but an important benefit, we regard our cooperative projects as a most positive step to improved relations between the U.S. and other nations.

Since the NATO-CCMS study, DOE has participated in ten other international cooperative arrangements. Of these, six were direct, bilateral agreements; the remainder were agreements involving three or more countries conducted under the auspices of an umbrella organization such as the IEA. The eleven agreements involved a total of 23 other countries. Italy has participated with us in four of those agreements, while Mexico, Japan, and Germany each have been party to three.

Whereas the legacy of international cooperation over the past decade has been rich, we have apparently reached a low point in that cooperation. Of the eleven agreements mentioned before, only two are actually active at present: (i) the IEA Agreement on Hot Dry Rock Technology and (ii) the bilateral arrangement between DOE and ENEL (Italy). Even the DOE-ENEL agreement, probably the one having the most interest to reservoir engineers, has been largely inactive of late while new tasks are being negotiated.

A number of reasons can be cited for the slackened interest in cooperation on geothermal research. The recent worldwide oil surplus coupled with a pervasive recession caused many nations to reevaluate their energy research programs. With fewer incentives and less funds for research, many countries chose to deemphasize their international programs; greater emphasis was

placed on purely domestic R&D activities. During this period DOE strived to fulfill its international commitments. The Department was reluctant, for budgetary reasons, to assume new obligations.

Although, today, budget constraints are still very much present, DOE understands the usefulness and importance of cooperative research and development. Some of geothermal's remaining problems can best be solved through the combined efforts of experts from many countries. Accordingly, we are negotiating a new U.S.-Mexico Agreement covering both the Cerro Prieto and Los Azufres fields.

We particularly endorse arrangements which maximize information exchange among countries working on similar technical problems. In this regard DOE has begun negotiations with the United Kingdom's Department of Energy on a comprehensive program of information exchange in hot dry rock technology.

The benefits of international cooperation and technology exchange among nations are again being evaluated. We predict that the next decade will witness a revitalization of many past ties in cooperative research and the forging of new ones. Certainly experience has taught that no single country can solve all technical problems confronting us, and that by working together we will reach solutions a great deal faster.

Proceedings Ninth Workshop Geothermal Reservoir Engineering
Stanford University, Stanford, California, December 1983
SGP-TR-74

GEOTHERMAL FIELD DEVELOPMENT IN THE EUROPEAN COMMUNITY OBJECTIVES, ACHIEVEMENTS AND PROBLEM AREAS

Pierre Ungemach

Commission of the European Communities
Rue de la Loi 200, 1049 Brussels, Belgium

ABSTRACT

Achievements and problem areas are reviewed with respect to various engineering implications of geothermal field development in the European Community (EC). Current and future development goals address three resource settings.

(a) low enthalpy sources (30-150°C), an outlook common to all Member states as a result of hot water aquifers flowing in large sedimentary units with normal heat flow, widespread throughout the EC;
(b) high enthalpy sources (<150°C) in areas of high heat flow which, as a consequence of the geodynamics of the Eurasian plate, are limited to Central and South-West Italy and to Eastern Greece;
(c) hot dry rocks (HDR), whose potential for Europe, and also the difficulties in implementing the heat mining concept, are enormous. A large scale experiment conducted at medium depth in Cornwall (UK) proves encouraging though. It has provided the right sort of scientific inputs to the understanding of the mechanics of anisotropic brittle basement rocks.

Development of low grade heat deposits is strongly resource but moreover utilisation dependant under present technological and economic heating standards. This practically restricts commercial exploitation to district heating of large urgan areas whenever exists a dependable aquifer. The most significant development takes place in the Paris Basin with 50 geothermal well pairs (doublet) due to operate by late 1984. This concentration might at a stage cause producing and injector wells to interfere. Other development prospects are shaping in Aquitaine (SW France), Denmark, United Kingdom, Italy and Germany. Many of these aquifers consist of clastic sediments, and therefore arise the problem of reinjecting safely a solid free brine to secure well lifetime and prevent formation invasion by fine particles.

Ten high enthalpy fields have been identified to date of which five, all of the liquid dominated type, have been discovered in the past decade. Yet none of them has moved to commercial production for a variety of technical, economical and environmental reasons.

In particular volcano-tectonic geothermal systems are not fully understood as to their permeability-fracture pattern and their agressive fluid thermochemistry.

Topical R&D actions in the fields of geochemistry, geophysics, reinjection, well stimulation, induced seismicity and reservoir simulation are described whenever they relate to reservoir engineering concerns.

Hot dry rocks. There is a background of seven years of R&D on the topic, since the early modelling and laboratory studies and field experiments at shallow depths which led to the large scale, intermediate depth, test site in Cornwall.

The major questions arisen by the current Cornish project are (a) how to control the growth of a HDR reservoir under strongly anisotropic in-situ stresses and subsequent shear fracturing, and (b) how to reliably assess the volume of fluid filled, artificial and reactivated, joint sets, and the heat exchange are?

1. EC GEOTHERMAL ENVIRONMENTS

Exploration and development of geothermal sources is largely dictated by the geodynamics of the Eurasian lithospheric plate which defines the main European geothermal provinces shown in Fig. 1.

Therefore present and prospective development objectives address three resource settings, namely:

(a) low enthalpy sources. Exploitation of warm water aquifers (30-150°C) is an outlook common to all EC Member states because of the presence of widespread - intracratonic and foredeep - sedimentary basins displaying near to normal heat flow (50 to 100 mW/m^2) and of hydrothermal convection - hot springs - systems of more local occurence in tectonised areas close to border faults of tertiary grabens and to orogenic belts. Highly compartmented tertiary grabens, subjected to distensive transverse faulting, may constitute an objective intermediate between low and high enthalpy uses.

(b) high enthalpy sources. Dry and wet steam resources are limited to those areas, the closing Mediterranean, where the collision of the Eurasian and African plates give rise to typical attributes such as subduction trenches, active volcanic island arcs, marginal basins, anatectic magmatism, extensional horst and graben structures e.g. to Central and South-Western Italy and to Eastern Greece.

(c) hot dry rocks (HDR). So far present projections on the amount of energy ultimately recoverable from natural hot wet sources is limited: 5 million tons of oil equivalent (TOE) per year corresponding to maximum installed capacities of 1,500 MWE (electricity generation) and 7,000 MWT (direct uses) respectively. Not surprising therefore is the considerable interest raised in the EC by the HDR concept of heat mining. Feasible engineering of man made geothermal reservoirs, irrespective of the site specific constraints inherent to natural sources, could multiply by an order of magnitude the EC geothermal reserve.

2. LOW ENTHALPY FIELDS

There are ten or so proven regional aquifers with dependable reservoir performance, among which the Jurassic limestones in the Paris suburban area and Cretaceous sandstones in Aquitaine (South West France) are the most extensively developed for district heating purposes. In the Paris area exploitation of saline waters by means of production-reinjection doublets is the rule whereas in Aquitaine singlet production wells are used instead (fresh water).

Particularly in the first case where about 50 such doublets will be operating in late 1984 there are serious risks of interferring wells with subsequent cooling breakthroughs. In Aquitaine excessive pressure depletions are feared in the near future. Hence the implementation of adequate reservoir management policies becomes urgent and regional simulation of heat and mass transfer is underway to attempt optimizing heat extraction and reservoir lifetime.

In Aquitaine injector wells will be required at a stage to sustain reservoir pressure above the critical matrix 'crushing' threshold. In the Paris basin two alternative strategies are being considered either (a) horizontal wells that allow for larger heat capacities and longer system lifetime, or/and (b) exploitation of underlying Triassic sandstones. The latter depends on procedures for securing reinjection of large quantities of cooled brines over often limited net pay intervals. Two test sites in the Paris Basin experienced severe problems notably sand face bridging due to odd well completions (partial or no gravel packing) and formation invasion by fine particles (see Fig. 2).

Emphasis is placed on developing suitable engineering technologies, through core tests and pilot filtering hardware, for feasibly mastering reinjection in clastic sediments, a geological environment common to many hot water deposits throughout the EC.

3. HIGH ENTHALPY FIELDS

The three dry steam fields of Larderello, Travale and Monte Amiata in Central Tuscany and Northern Latium are a long established geothermal assett with an installed capacity amounting to 440 MWE.

At Larderello the recent reinjection of steam condensates should prove beneficial a practice, as shown in Fig. 3. Elsewhere most problems are posed by liquid dominated sources such as in Torre Alfina (high CO_2 content), Cesano where the thermochemistry of a near saturated brine is very similar to that encountered in the Imperial Valley of California and Latera, a volcano- sedimentary field with a puzzling, fracture dominated, porosity pattern, which penalizes commercial production (and reinjection).

Last but not least, the Mofete and San Vito fields near Naples illustrate the foregoing difficulties to which ought to be added the environmental risk of investigating and developing a field in an active volcanic, seismic and densely populated area. It is a fact of evidence that the development of liquid sources has not progressed at the expected pace.

As a result Community supported research has focused with varying success on the following topic areas:

(a) reinjection and well stimulation. On the Latera field where reinjection of the separated brine is a practical and environmental necessity a series of dry holes were selected as candidates for well stimulation to attempt turning them into commercial injectors. Field procedures combined massive and progressively increasing cold water injection and acid treatment with a view to add the effects of thermal stress cracking, hydraulic fracturing and self propping of induced and/or reactivated fractures. These experiments completed on more or less empirical bases - no back-up by dynamic hydro-mechanical and leaching tests on core - achieved a significant increase of well injectivities, 100 T/h below fracturing pressures (see test and stimulation schedule in Table 1).

(b) well testing. Test hardware using pressurised separators and suitable fluid sampling facilities, are progressively substituted for the standard Russell-James method of testing two-phase flow wells. However, more sophisticated procedures are required to thoroughly appraise well and reservoir performance and fluid behaviour under a variety of thermodynamic conditions.

(c) reservoir simulation. Two - one industry, the other research oriented - computer codes of the 3D two phase flow type were applied to the simulation of the Mofete (liquid) and Travale (steam) fields, the latter benefitting from 10 years long production-pressure histories (Fig. 4). Indeed these complex models are worth using for better comprehending reservoir structure and physics rather than as accurate prediction tools. In fact available pressure temperature sequences are more characteristic of well and very near wellbore flow than of long term reservoir response and boundary influences. Along this line progress is noticed in the implementation of more realistic wellbore two phase flow simulators accounting for CO_2 partial pressure, non condensable H_2S, CH4, and brine evolution.

(d) induced seismicity. The impact of geothermal exploitation on the seismicity of areas with active tectonics and volcanism is monitored by a series of stations in the main fields. At Latera a more refined network using three component seismometers has been installed with a view to detect eventual acoustic emissions generated by well stimulation and water injection operations. After long well shut-ins there is evidence of a fairly intense background seismicity. During injection swarms of events are generated (Fig. 5) with foci locations ordered along two, apparently coherent, tectonic trends. Until now geothermal exploitation has not, in seismic terms, proven harmful to the environment and seismic monitoring when adequately designed has shown to be a valuable reservoir investigations tool.

(e) geophysics and geochemistry. Integrated geophysical investigations were undertaken on the well documented Travale field chosen as a test site for evaluating the potential of various, conventional and exotic, geophysical techniques in prospecting high enthalpy sources. Some results are not indifferent to reservoir engineers in particular (i) transient electromagnetic recording which applies an IP criterion at great depth. Positive anomalies of amplitude residuals proved strongly correlated with known steam producing zones, which is interpreted as the existence, locally, of polarising mineral bodies formed as consequence of hydrothermal convection e.g. of fracturing (see Fig. 6), (ii) reflection seismics using P and S sources. Contrasts appeared between tight compact and porous fractured rocks especially on S sections structurally more sensitive to shear and fracturation, and (iii) microearthquake recording by a dense array of three component seismometers. There is an organised trend of seismic velocity and attenuation signatures consistent with the model of a fissured reservoir filled at various saturations by either steam or water (Fig. 7). Apart from the usual water rock interactions studied from the fundamental point of view in the laboratory, isotope geochemistry and particularly $^3He/^4He$ ratios provided fascinating clues in perfecting the conceptual model of the Larderello system (heat sources and deep convecting fluid flow paths (shown in Fig. 8 sketch).

Active geochemistry, using a set of five complexed rare earth tracers, combining ideal (non adsorbing) and non ideal (adsorbing) properties has achieved a convincing performance in characterizing a shallow HDR system (Fig. 9). As a matter of fact geochemistry and geophysics, whatever speculative their outcome, often appeared as a valuable tool in conceptual modelling of hydrothermal reservoirs. Yet this opinion is not fully accepted by all specialists.

4. HOT DRY ROCKS

HDR research has associated a variety of early laboratory experiments and model calculations, with field fracturing and circulation tests at shallow depths prior to commissioning the large scale intermediate depth, stimulation project at the Rosemanowes Quarry site in British Cornwall.

Laboratory research dealt with the mechanics and hydraulics of rock fracturing, thermal stress cracking, mathematical and physical modelling of crack propagation and linking on somewhat idealised elastic bodies. Enhancement of fracture conductivity by means of fatigue micropressurisation and chemical leaching by Soda compounds were also studied in some detail.

Preliminary field experiments made it possible (a) to test equipments and procedures - in-situ stress measurements, fracturing and linking processes, fracture detection and microseismic control, and (b) to select the most promising stimulation concept now implemented in Cornwall.

The idea behind this concept is to stimulate large volumes of a jointed rock mass by taking advantage precisely of this basic feature of crystalline and metamorphic basement rocks, by reactivating natural joints. The candidate process combines explosive pretreatment and massive hydraulic fracturing. Unfocused explosives, fired below the plastic limit, are assumed to develop a near wellbore system of radially oriented self-propped fractures resulting in a strong negative skin. The fractures ease the access to the natural joints which is completed by repeated massive pressurisation and venting cycles. This sequence tested successfully at shallow depth is presently being validated at a greater depth (2200 m) under a state of stress representative of target HDR depths.

It is possible to draw of few tentative conclusions from early loop circulation tests:
(a) over 300,000 m^3 of water have been injected in the HDR reservoir and hardly 100,000 m^3 recovered so far;
(b) the system can be circulated at 30 l/s ca. (below 10 MPa WHP) but at the expense of severe losses resulting from, mainly downward, fracture growth away from the recovery well;
(c) because of a peculiar situation where the well axis and the major natural joint strike are misaligned with the maximum in-situ horizontal stress, shearing instead of tension (jacking) appears as the dominant factor in fracture propagation. Alternatively shear triggered an intense microseismic activity which allowed for a consistent reservoir evaluation from foci clustering. Shear fracturing should prevail on most HDR sites because of anisotropic in-situ stresses and the anisotropy in rock strength,a distinctive attribute of basement rocks;
(d) although pressure records tend to indicate natural joint reactivation, reservoir growth has proceeded normal to the minimum horizontal stress and not along a known joint direction. Connections consist of reactivated joints contained by in-situ stresses;
(e) there is evidence, from seismo-acoustic emission and event mapping , hydraulic, thermal and tracer testing of a large stimulated volume (1 km^3 ca.) displaying rock/fluid contact areas of at least 1 km^2. However, neither can seismicity nor tracers define either fluid filled fractures or heat exchange areas. Aseismic (deaf) zones are manifest (Fig. 10) within the pressurised volume and a number of events are triggered far beyond the hydraulically stimulated area in the early fracturing stages. Hence seismo-acoustic mapping can only produce an enveloppe not the stimulated volume proper. Tracers can define adsorbed areas which do not fit necessarily the effective heat exchange area. Tracers on the other hand can best discriminate the main flow conduits of a multipath well connection.
(f) The HDR loop operates as a large volumetric diffusive system between two, weakly connected, performant wells rather than as a connection through a highly conductive fracture.

In summary nothing worked as anticipated. Fractures grew downwards, and not upwards, the major fractures did no propagate along the planes of weakness of the natural joints and there were no indications of channelling and well shortcircuiting whatsoever; The project is very stimulating indeed and has provided already invaluable scientific information.

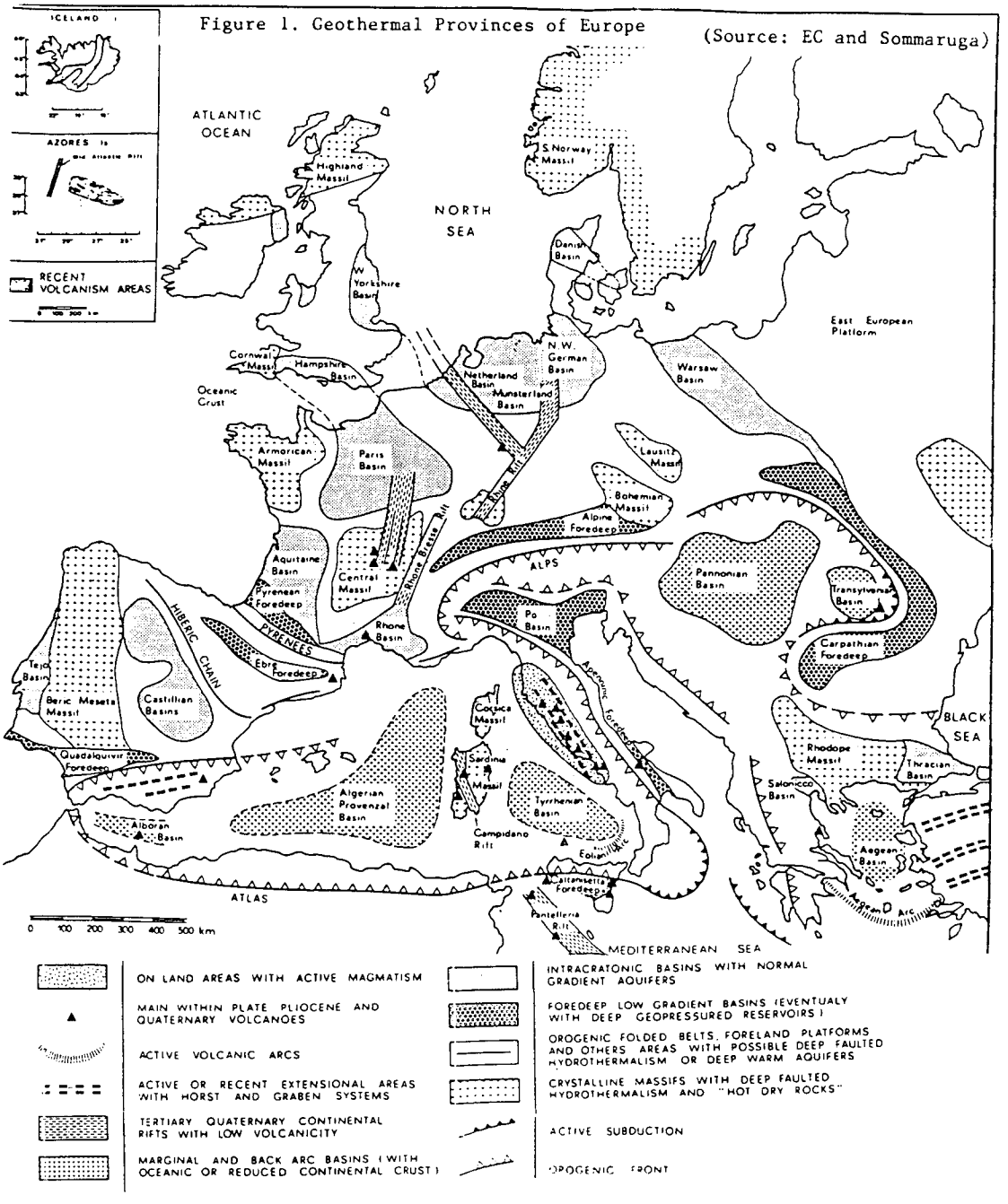
Stage 2 of the Cornish programme will consist of drilling a third well in order to intersect the main reservoir structure.

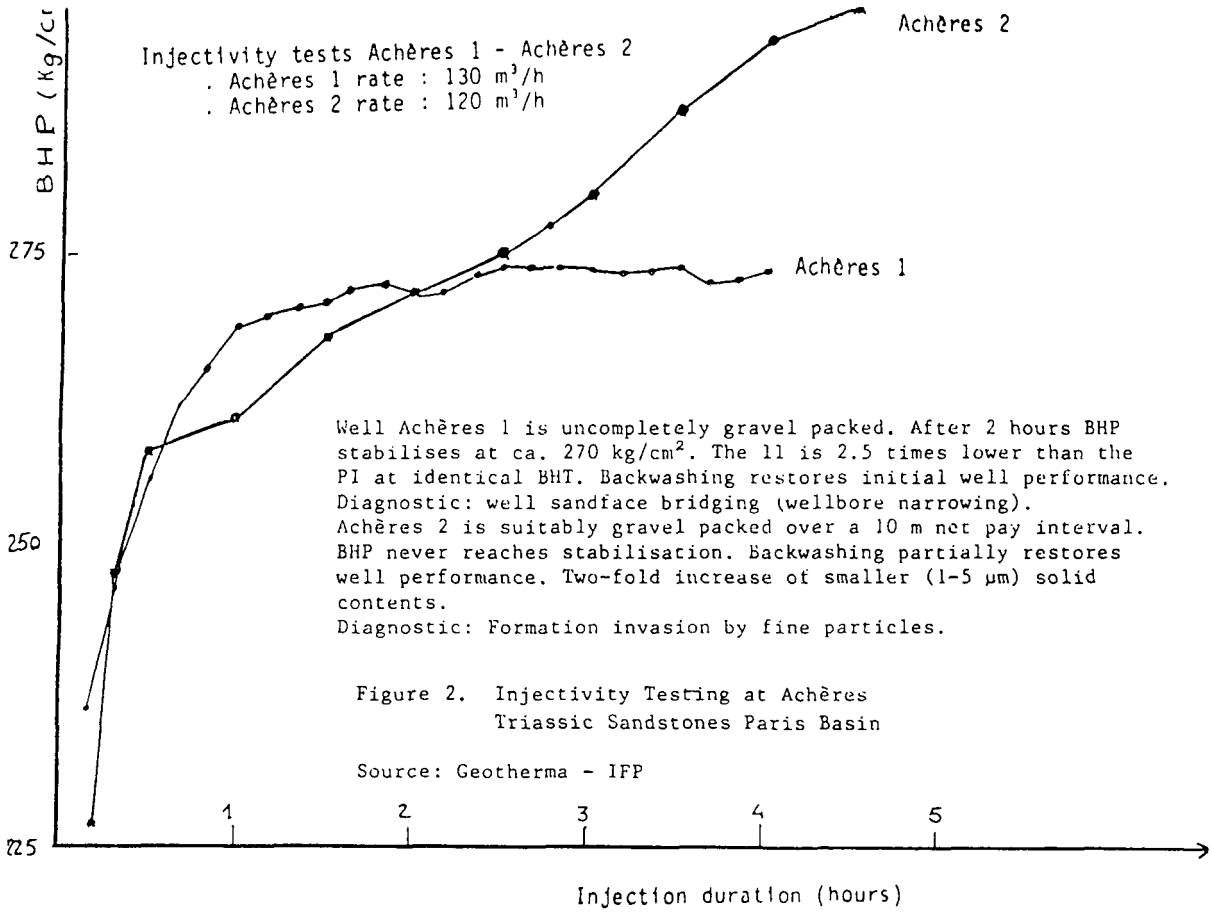
An alternative process for stimulating jointed rocks, known as the oriented hydraulic fracturing concept, has been tested in the laboratory and in the field at shallow depth. Validation at greater depth could be given a chance on a second large scale experiment in Central France.

ACKNOWLEDGEMENTS

Most if not all the material of this extended summary is borrowed to the current 2nd R&D programme of the Commission of the European Communities whose authorisation for publication is appreciated. The author wishes to extend his thanks to R. Oxburgh (Univ. of Cambridge), G. Chierici (AGIP), G. Capetti (ENEL-UNG), A. Duprat (CGG), M. Gobelet (ENSMP) and A.S. Batchelor (CSM) for stimulating discussions on various reservoir engineering matters and related topics, discussed in this paper.

Figure 1. Geothermal Provinces of Europe (Source: EC and Sommaruga)





Well Achères 1 is uncompletely gravel packed. After 2 hours BHP stabilises at ca. 270 kg/cm². The II is 2.5 times lower than the PI at identical BHT. Backwashing restores initial well performance.
Diagnostic: well sandface bridging (wellbore narrowing).
Achères 2 is suitably gravel packed over a 10 m net pay interval. BHP never reaches stabilisation. Backwashing partially restores well performance. Two-fold increase of smaller (1-5 µm) solid contents.
Diagnostic: Formation invasion by fine particles.

Figure 2. Injectivity Testing at Achères
Triassic Sandstones Paris Basin

Source: Geotherma - IFP

Source: Geotherma - IFP

Figure 2. Injectivity Testing at Achères
Triassic Sandstones Paris Basin

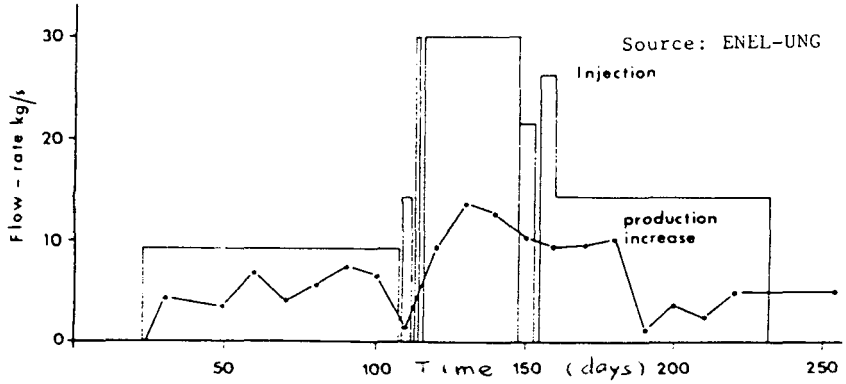
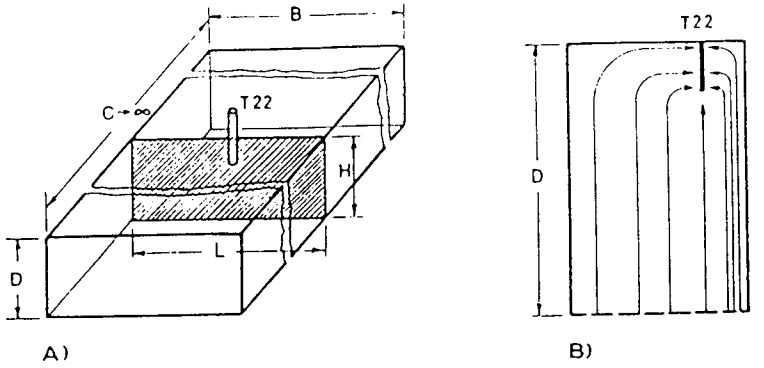


Figure 3 Injection experiment in Larderello.
Condensates are reinjected in a well at a distance varying from 0.2 to 3 km to steam producing wells



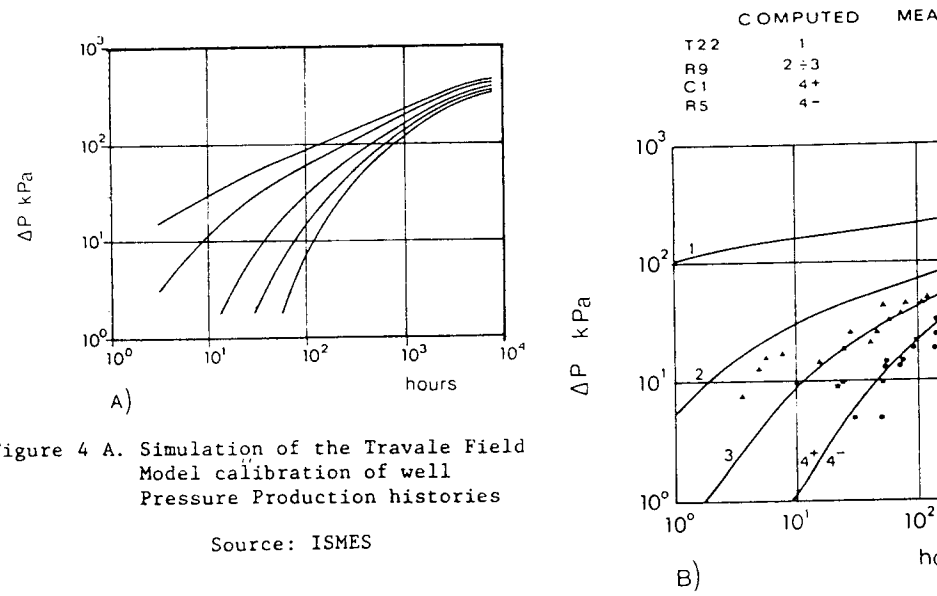
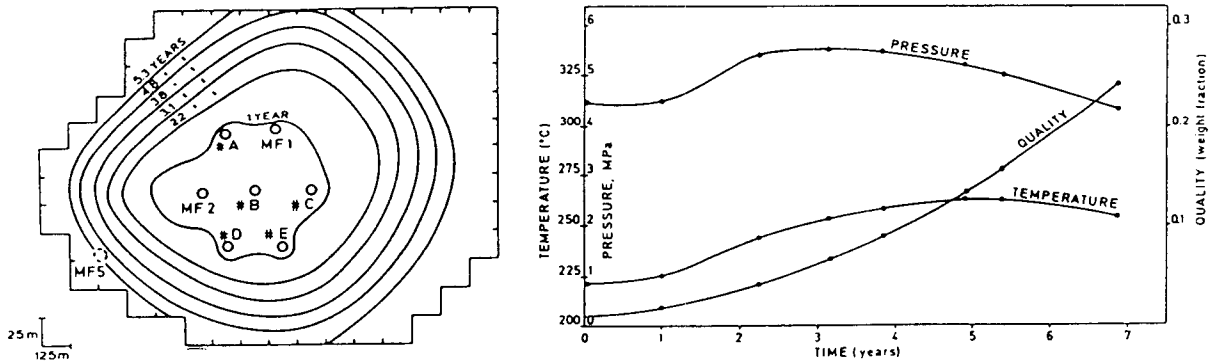


Figure 4 A. Simulation of the Travale Field
Model calibration of well
Pressure Production histories

Source: ISMES

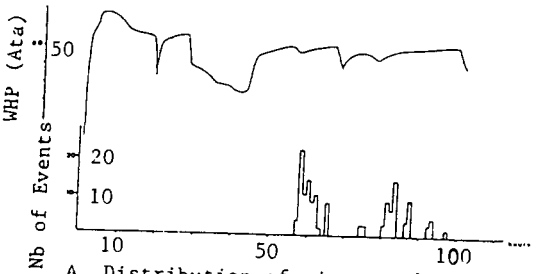


a. Top metamorphic formation.
Model layer n° 12. Evolution of
the flashing front with time.

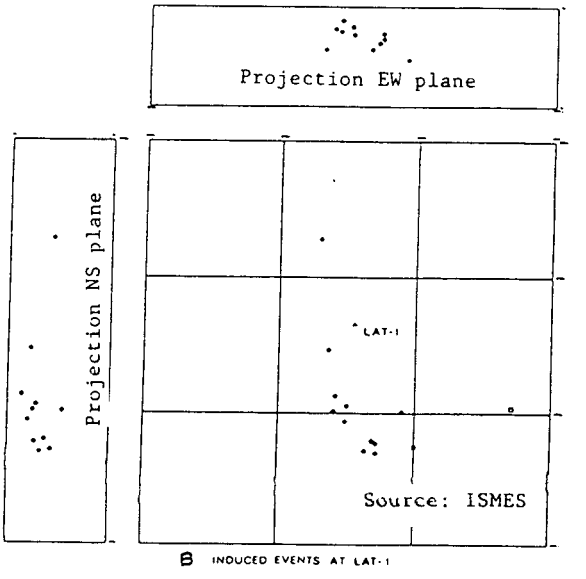
b. Change of well head conditions for an average well

Source: AGIP

Figure 4 B. Simulation of the Mofete Field.
Case: 7 producers, no injector



A. Distribution of microearthquakes during injection at well L.1



B INDUCED EVENTS AT LAT-1

Figure 5. Induced Seismicity at Latera
Total earthquakes recorded: 148

Only strongest events are shown in Fig. B

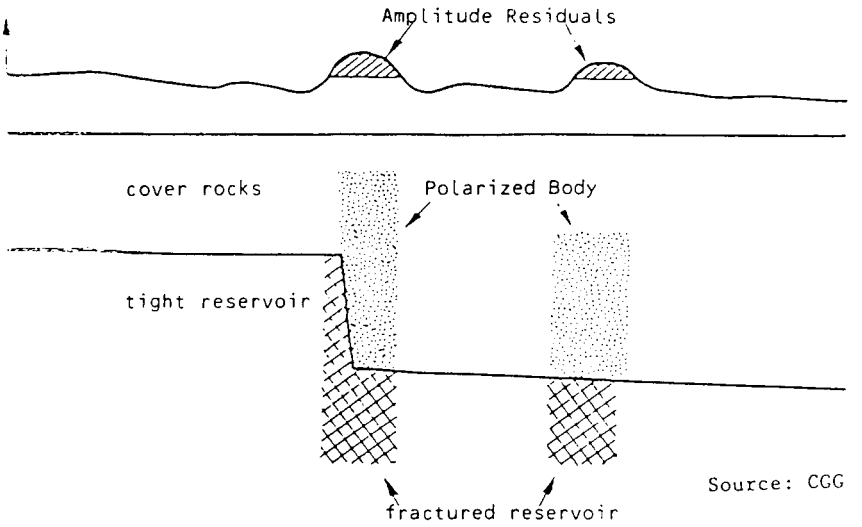


Figure 6 Trasient EM Recording at Travale Interpretative Model, Polarised Bodies are attributed to hydrothermal mineralisation (pyritisation ...).

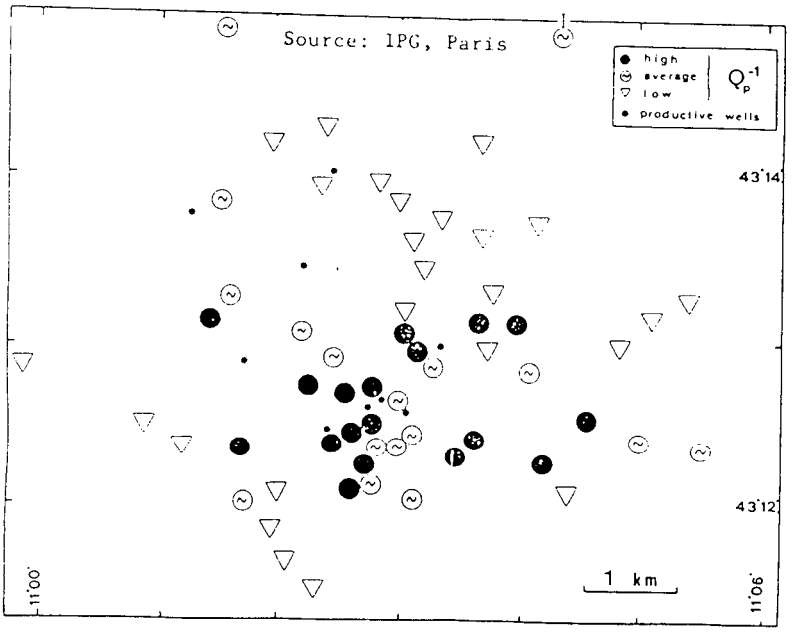


Figure 7 Experimental Seismology at Travale. Mapping of relative attenuation Q_P^{-1} of P waves calculated from distant shots. Q_P^{-1} is derived from slopes of spectral ratios respective to the average spectrum (over the whole network) for each individual wave.

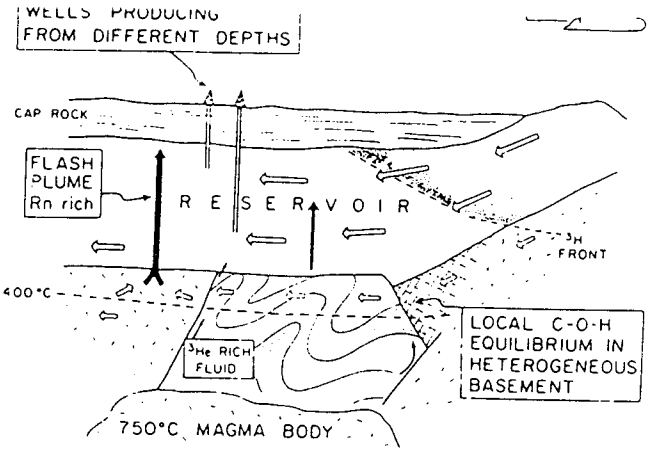


Figure 8 An Updated Conceptual Model of the Larderello Field based on rare gas isotope geochemistry

Source: Univ. of Cambridge

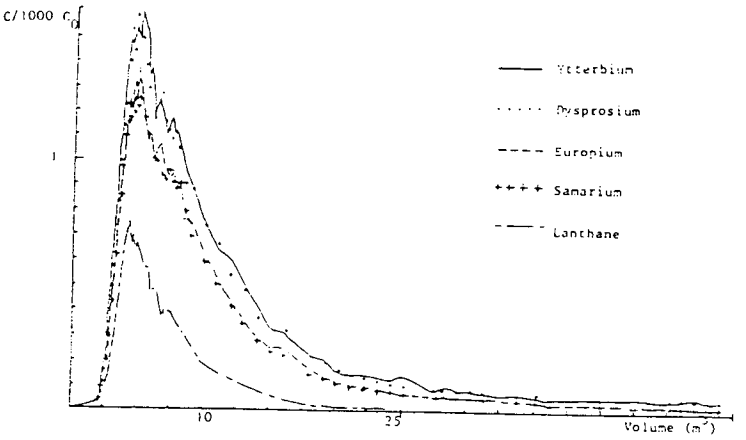
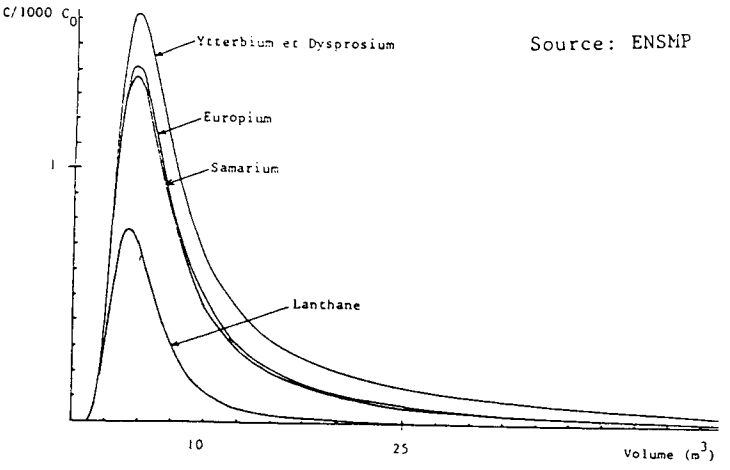
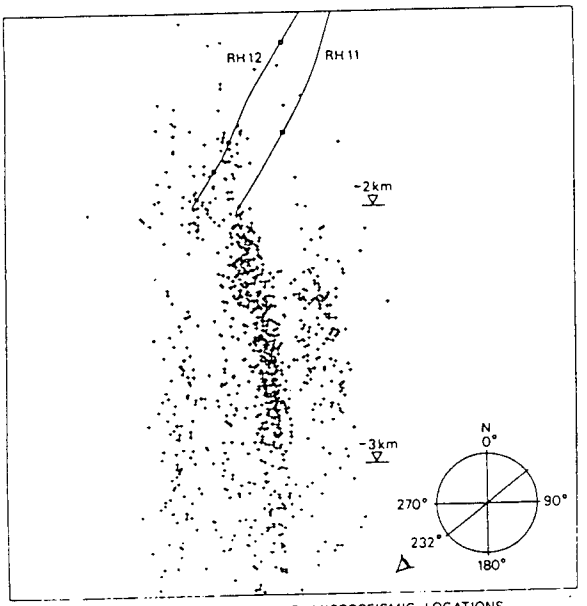


Figure 9a. Experimental tracer restitution curve

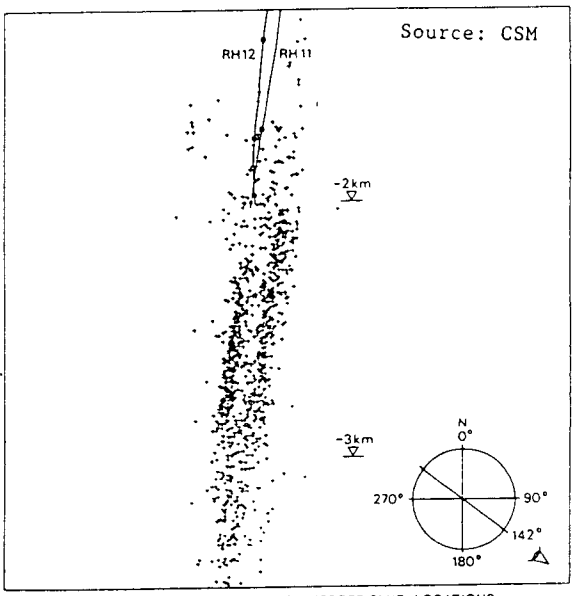


Source: ENSMP

Figure 9b. Model calculated restitution curve



A VERTICAL SECTION SHOWING MICROSEISMIC LOCATIONS VIEWED FROM THE SOUTH WEST



B VERTICAL SECTION SHOWING MICROSEISMIC LOCATIONS VIEWED FROM THE SOUTH EAST

Figure 10 Locations of seismo-acoustic events monitored during fracturing and circulation

Proceedings Ninth Workshop Geothermal Reservoir Engineering
Stanford University, Stanford, California, December 1983
SGP-TR-74

PRESENT STATUS AND FUTURE PROSPECTS OF GEOTHERMAL DEVELOPMENT IN ITALY

by
R. CATALDI and A. CALAMAI

WITH AN APPENDIX ON RESERVOIR ENGINEERING
by
G. NERI and G. MANETTI

ENEL/National Geothermal Unit - Pisa, Italy

ABSTRACT

This paper consists of two parts and an appendix.

In the first part a review is made of the geothermal activity in Italy from 1975 to 1982, including electrical and non-electrical applications. Remarks then follow on the trends that occurred and the operational criteria that were applied in the same period, which can be considered a transitional period of geothermal development in Italy.

Information on recent trends and development objectives up to 1990 are given in the second part of the paper, together with a summary on program activities in the various geothermal areas of Italy.

The appendix specifically reviews the main reservoir engineering activities carried out in the past years and the problems likely to be faced in the coming years in developing Italian fields.

In particular, production and injection well-testing in high and low enthalpy liquid-dominated reservoirs are illustrated, as well as:

- reinjection tests carried out in the Larderello field with the aim of enhancing heat extraction from the upper steam-dominated part of the reservoir;
- flow-rate transient tests in the Larderello and Travale fields.

1. INTRODUCTION

In Italy the utilization of geothermal resources for industrial purposes dates back to about 150 years ago. Exploitation of by-products associated with hot fluids and direct use of heat for chemical processing until 1913, combined electrical and chemical production between 1913 and 1965, and electric generation alone from 1965 to 1980 are the three main steps of geothermal development in Italy.

Where the direct use of geoheat is concerned, apart from balneotherapy, examples of agricultural applications and space heating are surely not lacking; but until the energy crisis exploded in the past decade little attention was paid to this problem.

Throughout the period of geothermal development in Italy, and particularly after 1960, hundreds of specific notes and general papers were published by Italian authors illustrating the various aspects of the research and the utilization of this energy source. Two progress reports, in particular, presented by CATALDI et al. (1970) and CERON et al. (1975) at the U.N. Geothermal Symposium in Pisa and the U.N. Geothermal Conference of San Francisco, respectively, outline the geothermal situation in Italy at the beginning and the middle of the 1970s. Both of these reports, however, confine themselves to illustrating the state of research and exploration for the purposes of geothermoelectric production, without making any mention of direct uses of geothermal heat.

The first part of this paper will start from the situation illustrated by the above-mentioned progress report of CERON et al. in order to give an organic, although general, account of the geothermal development in Italy after 1975, including electric production and direct applications of geoheat.

The second part of the paper illustrates the objectives and summarizes the program of activities scheduled up to 1990.

Appended to this paper is a note by G. MANETTI and G. NERI, dealing specifically with the

main activities carried out in reservoir engineering during the past years, together with and overview of the problems likely to be faced in the future in this branch of geothermal activity.

In this way, the Authours of both the paper and the appendix hope to make a general as well as a specific contribution to the Ninth Stanford Workshop on Geothermal Reservoir Engineering.

PART I

2. SITUATION IN 1982 AS COMPARED TO THAT IN 1975

To facilitate comparison of the results obtained in the period in question, it seems appropriate to consider separately two groups of activities: those carried out or in progress having the main goal of producing electricity, and those conducted or still ongoing with the chief aim of directly using the terrestrial heat.

With respect to drilling, however, this distinction is not easy to make, and Table 1 summarizes all geothermal wells drilled in Italy up to the end of 1982.*

* Excluded from Table 1 are only the wells drilled in the 1940s in the Phlaegrean Fields, and a few other wells drilled in the 1950s in the island of Ischia, Sciacca and Viterbo.

With reference to the central section of Table 1, attention must be drawn to three points:

- wells have been considered productive only where they have encountered fluids with physicochemical characteristics permitting their utilization (at present or in the near future) for the production of electric power and/or for other uses. It is clear that this represents a limitation, since many wells that are now non-commercial, and are thus considered dry, due to insufficient temperatures or for other reasons (rapid scaling, for example), might, in a few years, fall within the category of productive wells;
- the flow-rate of the various productive wells is expressed in terms of the total output of fluid, which, from case to case, may be superheated steam, saturated steam,water/steam mixture or water only. In all cases, however, the gas flow-rate has been deducted;
- the delivery pressure to which the flow-rate figures refer generally ranges between 5 and 15 atm.

2.1 - First group: electrical uses

In Italy the production of electric energy from geothermal fluids is currently limited to the zones of Larderello, Travale, Radicondoli and Mt. Amiata. However, considering their perspectives, the new areas of Latera, Torre Alfina, Cesano and Phlaegrean Fields have been included in this first group as well. Indeed, the studies in the these areas indicate in some

Table 1 - WELLS DRILLED - MARCH 1975 AND DECEMBER 1982

ZONE	SITUATION AT JANUARY 1975			FROM JANUARY 1975 TO DECEMBER 1982				SITUATION AT DECEMBER 1982		
	WELLS DRILLED (no.)	AVERAGE DEPTH (m)	WELLS /km^2 (no.)	WELLS DRILLED (no.)	AVERAGE DEPTH (m)	PRODUCTIVE WELLS (no.)	FLOW-RATE t/h*	WELLS DRILLED (no.)	AVERAGE DEPTH (m)	WELLS /km^2 (no.)
LARDERELLO	539	656	3.08	34	1642	11	350	573	714	2.86
TRAVALE-RADICONDOLI	34	644	4.86	20	1703	9	810	54	1036	1.46
Mt. AMIATA	60	780	1.50	8	2882	4	270	68	1027	1.46
LATERA	-	-	-	8	2129	3	1200	8	2129	0.61
CAMPI FLEGREI	-	-	-	9	2226	4	520	9	2226	1.80
CESANO	-	-	-	11	2274	4	750	11	2274	0.59
TORRE ALFINA	5	742	1.67	4	1766	3	500	9	1197	1.38
OTHER ZONES	12	951	-	5	2210	2	300	17	1321	-
TOTAL	650	673	2.83	99	1951	40	4700	749	842	2.24

* STEAM AND/OR WATER (SEE TEXT)

cases (Latera and Phlaegrean Fields) that electric generation is already feasible, and in other cases (Torre Alfina and Cesano) that this generation might become feasible in the future.

The situation in the old and new zones (see Fig. 1 for the locations and Table 2 for the plants) can be summarized as follows.

- Larderello. Of a total of 573 wells existing in this zone (see Table 1), only 34 were drilled in the period in question. Since 1975 drilling has been carried out mainly in the peripheral areas with the aim of exploring the margins of the field and delimiting the size of the main reservoir, which is chiefly made up of carbonate rocks.

  During these years, moreover, the average depth was considerably increased (more than 1600 m), since exploration was directed at locating permeable horizons within the metamorphic basement down to approx. 4 km.

  The fluid produced in this zone is generally superheated steam.

  Aside from the exploration activities, the reinjection activity in this zone is worth mentioning. It was started a few years ago with the aim of gradually attaining (by 1985) a total subsurface disposal of approx. 600 t/h of condensing water. The results so far obtained with reinjection into the carbonate reservoir are encouraging both from the stand point of the increase in flow rate and the containment of the decline in pressure in the older producing wells.

  In addition, a modernization program has been initiated on the old generating units; the program also provides for a more rational location of some smaller plants. The recovery of efficient power achieved with this program from 1975 to the present is estimated at approx. 25-30 MW.

- Travale-Radicondoli. In this zone a small geothermal field was discovered in the 1950s which for a brief period supplied a 3 MW

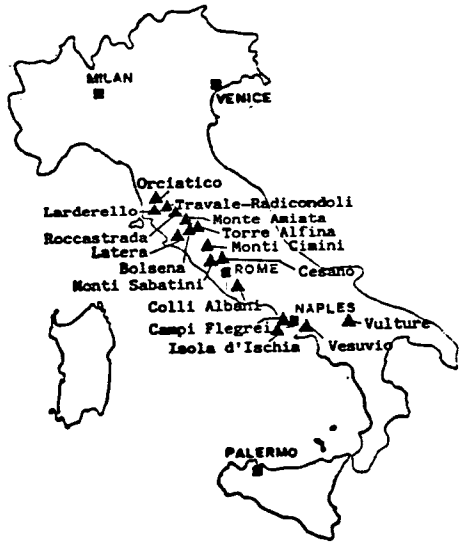


Fig. 1 - Location of high enthalpy zones

Table 2 - INSTALLED CAPACITY OF ITALIAN GEOTHERMOELECTRIC POWER PLANTS

REGION	POWER PLANT	JANUARY 1975			DECEMBER 1982		
		NO. OF UNITS	UNIT RATING (MW)	TOTAL INST.CAP. (MW)	NO. OF UNITS	UNIT RATING (MW)	TOTAL INST.CAP. (MW)
LARDERELLO	LARDERELLO 2	4	14.5	69	4	14.5	58
		1	11		-	-	
	LARDERELLO 3	3	26		3	26	
		1	24	120	1	24	111
		2	9		1	9	
	GABBRO	1	15	15	1	15	15
	CASTELNUOVO	2	11		2	11	
		1	26	50	1	26	50
		1	2		1	2	
	SERRAZZANO	2	12.5		2	12.5	
		2	3.5	47	2	3.5	47
		1	15		1	15	
	SASSO 2	1	12.5		1	12.5	
		1*	3.2	22.7	1*	3.2	22.7
		2	3.5		2*	3.5	
	LAGO 2	1	12.5		1	12.5	
		1	6.5	33.5	1	6.5	33.5
		1	14.5		1	14.5	
	MONTEROTONDO	1	12.5	12.5	1	12.5	12.5
	VALLESPICO	1*	0.9	0.9	1*	0.9	0.9
	MOLINETTO	1*	3.5	3.5	1	8	8
	LAGONI ROSSI 1	1*	3.5	3.5	1*	3.5	3.5
	LAGONI ROSSI 2	1*	3	3	-	-	-
	LAGONI ROSSI 3	-	-	-	1	8	8
	S. MARTINO	-	-	-	1	9	9
Subtotal		33	-	380.6	32	-	379.1
TRAVALE RADICONDOLI	TRAVALE 2	1*	15	15	1	15	
		-	-	-	1	3	18
	RADICONDOLI	-	-	-	2	15	30
Subtotal		1		15	4	-	48
Mt. AMIATA	BAGNORE 1	1*	3.5	3.5	1*	3.5	3.5
	BAGNORE 2	1*	3.5	3.5	1*	3.5	3.5
	PIANCASTAGNAIO	1*	15	15	1*	15	15
Subtotal		3	-	22	3	-	22
TOTAL		37	-	417.6	39	-	449.1

* Discharging-to-atmosphere units

discharging-to-atmosphere power plant. But the shallow depth of the reservoir and the proximity of large outcrops of permeable rocks communicating with it rapidly led to the thermal degradation of the fluid produced and to the impossibility of continuing the electric power generation.

Subsequently, a new geothermal field having been located in the early 1970s a few km NE of the old production area, exploration and exploitation activities were concentrated in the new zone. As at Larderello, the main reservoir is made up of carbonate formations, but productive horizons are also present in the schistose-quartzitic formations below. Approximately 75% of the fluid produced in the new fields is constituted by superheated or saturated steam, while 25% is made up of water/steam mixture.

The installed capacity, which was 15 MW in 1975, reached 48 MW in 1982. Moreover, fluid is available for supplying some additional 30 MW.

- Mt. Amiata. The generating units installed in this region (at Bagnore and Piancastagnaio, for a total of 22 MW) are fed with generally saturated steam produced by a shallow reservoir (500-1000 m) made up of carbonate formations.

  In 1979, however, exploration of the schistose-quartzitic basement underlying the aforementioned reservoir was begun in order to individuate deep permeable horizons down to 3-4 km. This deep exploration, which explains the sizeable increase in the average depth of the wells (see Table 1), is giving very encouraging results at Piancastagnaio where the presence of permeable layers has been ascertained between 2500 and 3500 m.

  It is still too early to say whether these layers belong to a second reservoir which is completely separate from the first; what it is clear for the moment is the fact that the fluid produced is (at least initially) a water/steam mixture having pressures and temperature (300-350°C) greatly higher than those of the fluid yielded by the carbonate reservoir.

  The fluid produced by the deep horizons will therefore feed a new 15 MW geothermoelectric group which is already under construction.

- Latera. ENEL and AGIP, working in joint venture, discovered a new geothermal field of the water-dominated type in this zone in 1980.

  The top of the reservoir (600-1500 m deep) is made up of Mesozoic carbonate rocks whose structural attitude is controlled by a recumbent fold. The temperature of the fluid is of the order of 200-230°C, with TDS of 8-10 g/l. Although there are problems of carbonate scaling during both production and reinjection, the feasibility study (now approaching conclusion) indicates that the fluid can be utilized for generating electric power. It is thus planned to install a provisional 3.5 MW generating plant in the near future, to be followed by a first 15 MW power plant.

- Phlaegrean Fields (Mofete). Setting aside the activities carried out in the 1940s, it can be said that the systematic exploration of this zone was first begun by the AGIP-ENEL joint venture towards the end of the 1970s.

  The wells drilled thus far (of which nearly half are productive - see Table 1) indicate that in this volcanic area the production of fluids does not stem from a reservoir that can be unambiguously defined in lithological and geometrical terms. A certain fortuitousness of production is in fact found in correspondence with a few fracture systems which in some places are sealed and in others open. It would thus seem that there are various productive horizons, but actually, at least up to approx. 3 km down, it is a matter of discountinuities oriented almost vertically. The production of greatest interest has been found between 1300 and 1600 m, with wellbottom temperatures of around 250-300°C.

  The fluid produced is a water/steam mixture with a salinity of the order of 35-40 g/l or more, mainly controlled by sodium chloride.

  While the feasibility study is still in progress, the orientation is towards installing a 4-5 MW discharging-to atmosphere power unit in the near future, which would also serve for testing the field.

- Cesano. Here we have a field of the "hot brine" type, with a total salinity varying between a minimum of 70-80 and a maximum of 300-350 g/l. The highest salinity values (which is of the sulfate-alkalic type in all cases) are found in the central part of the field in correspondence to fractures connected with the explosion chimneys. Temperature in the reservoir ranges between 120-130°C on the periphery of the field and 220-230°C in its central part.

Given the marked scaling properties of the fluids (ALLEGRINI et al., 1982), various possibilities of utilization of the fluid are being experimented for separate sectors of the field.

As far as generating electricity is concerned, based on experimentation of various flash processes (and also tests made by using a helical screw expander), it has been concluded that the production of electricity alone in this field is not economically profitable. Therefore, the orientation is towards achieving an integrated utilization of the resource: electrical production, subordinate to the extraction of chemicals and/or the direct use of the geothermal heat (see also Cesano Project in section 2.2.1).

- Torre Alfina. In this zone about 1000 t/h of fluid can be drawn from a shallow carbonate reservoir (500-1000 m) in which the temperature is 140-160°C.

  It is a water-dominated field in which the fluid produced, although not having a very high salinity (TDS = 7000 ppm), but being saturated with CO_2, determines severe carbonate scaling phenomena.

  Mainly on account of this, but also because of other problems linked to disposal of the waste waters, it was decided to postpone for the time being the utilization of this kind of resource. Nevertheless, the Alfina zone will be brought back under consideration to explore the schistose-quartzitic basement and see whether it is possible (as in the Mt. Amiata zone) to achieve the production of fluid from deep layers with better chemical and physical characteristics than those mentioned above.

- Other regions. In addition to the zones described above, surface exploration activities have been carried out from 1975 to the present in a certain number of other zones considered of potential interest for finding high temperature fluids. These zones are: Orciatico-Montecatini and Roccastrada in Tuscany; Volsini Mountains, Cimini Mountains, Sabatini Mountains and Albani Hills in Latium; Vesuvius in Campania; Vulture in Basilicata.

  In one of these zones (Sabatini Mountains), deep exploration has already begun; but the first well drilled here, even though it encountered a temperature at the bottom (2500m) of over 280°C, turned out to be dry. This because of the lack of permeability, due to a marked self-sealing process of the fractures in the carbonate formations, which were expected to constitute the reservoir of the geothermal fluids.

  Naturally, the deep exploration in this zone will be continued and will soon be started in some of the other new zones mentioned above.

  A summary of the fluid found in recent years in the various zones examined in this section, not yet utilized but nonetheless already available for feeding new geothermoelectric groups, is given in Table 3 below.

Tab. 3 - Fluid available at Dec.'82 for the supply of new geothermoelectric units

REGION	FLUID AVAILABLE (t/h)	EXPECTED CAPACITY (MW)
- Larderello	200	20
- Travale-Radicondoli	300	30
- Mt. Amiata	180	18
- Latera	1200	10
- Cesano	750	5
- Phlaegrean Fields (Mofete)	520	9
TOTAL	3150	92

The total capacity corresponding to this fluid (∿92 MW), which will be installed gradually in the next few years, will constitute part of the increase is geothermoelectric capacity that is planned to install by 1990 in accordance with the objectives of the Italian National Energy Plan, as will be more fully reported in section 4.

2.2 - Second group: non-electrical and combined uses

2.2.1 - Projects already realized or in the course of realization (locations in Fig. 2)

- Abano. This town, located near Padua, is one of the best-known European spas with a very fluorishing balneotherapeutic activity. The hot water (65-90°C) produced by some 120 wells (250-400 m deep) is utilized, through heat exchangers, firstly for space heating and hot sanitary water production and later for supplying spas. Some 75 hotels, each having its own well(s) and heating circuit, in addition to many homes, are heated in this way (BARBIER, 1977).

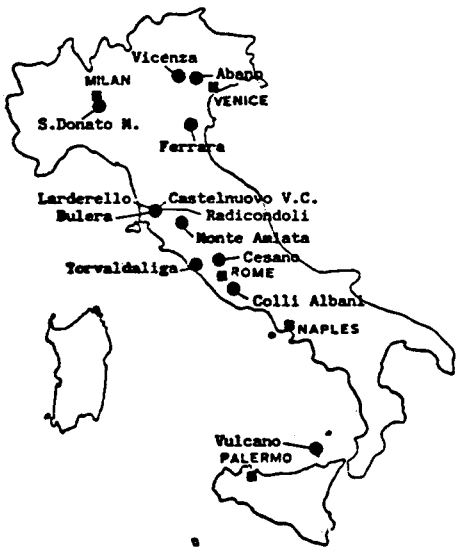


Fig. 2 - Location of low enthalpy zones

- Galzignano. This village is located in the same geological district as that of Abano. Near it some 20,000 m^2 of greenhouses have been in operation for about 25 years, producing mainly decorative plants and flowers. Low-salinity water at 65°C is yielded by a 300 m deep artesian well which supplies the greenhouses heating circuit 28 km long (BARBIER, 1977).

- Vicenza. A well drilled 15 km north of Vicenza for oil exploration yielded some 100 m^3/h of very low salinity water at 65-70°C. This is a very favorable circumstance in that, after its use as heat source, the water can be used for civil and/or agricultural purposes.

  Two district areas of the town, suitable for geothermal heating, were selected after the feasibility study (ELECTROCONSULT, 1982): the first one includes a group of private houses (about 656,000 m^3) having an expected energy consumption of nearly 20,000 Gcal per year and a required peak power of 8.6 Gcal/h. This group needs a distribution network 3500 m long.

  The second area, including military barracks and the prison being constructed nearby, requires no new distribution network, because both barracks and prison have their own heating systems. The volume to be heated in this second area is 561,600 m^3, with an estimated yearly consumption of 20,300 Gcal and a required peak power of 9.9 Gcal/h.

  The previously mentioned existing well will not be used, because it is too far from Vicenza; therefore, two new wells (one north and one southeast of the town) will be drilled near the utilization areas. Heat pumps will be used to increase the energy recovery.

  The water temperature in the distribution circuit will be 75°C at the inlet and 60°C at the outlet. Moreover, a network of pipes, parallel to heat-transport ones, will deliver hot water for sanitary uses.This water will be directly supplied by the production wells due to the fact that water in the whole sedimentary basin near Vicenza has a very low saline content.

- San Donato. This project is aimed at heating the SNAM's buildings (a company of the ENI group), located in the outskirts of Milan, for a total volume of 467,000 m^3.

  One producing well (100 m^3/h of water at 65°C) and one reinjection well, both 2000 m deep, will be used in this project. The maximum thermal power available from the geothermal fluid is expected to be 4.4 Gcal/h, supplying an annual geoheat content of 15,000 Gcal (CERON-SOMMARUGA, 1979). Due to the low fluid temperature, a heat pump will be employed to enhance heat extraction from geothermal water.

- Ferrara. Two wells located about 4 km outside this town spontaneously produce some 250 m^3/h of water at nearly 100°C; but the flow-rate can be increased by means of submerged pumps.

  A market survey of the potential users concluded that some 7,500 apartments can be heated by using the water of these wells. The district heating system envisages an overall yearly consumption of 110,000 Gcal, out of which about two thirds will be of geothermal origin whereas the remaining part should be provided by a backup liquid fuel heater. The heat distribution network will have a total length of approx. 20 km with operation temperatures of 90°C at the inlet and 53°C at the outlet (INVERNIZZI-SARTI, 1982).

- Larderello. Low-temperature fluids (70-130°C) have been used in this area since 1827 for several purposes: extraction of valuable chemicals (mainly boron compounds) and drying of saline solutions until 1950, greenhouses and space heating until now-a-day.

  At present, non-electrical applications concern district heating(office and residential

buildings) and greenhouses only by using low-pressure/low-temperature steam produced by shallow, old wells. An indirect-cycle system is now adopted in both cases; steam is made to flow through shell-and-tube exchangers and heats fresh waters running in conventional circuits. A total volume of nearly 350,000 m^3 of district heating and some 15,000 m^3 of greenhouses (growing mainly vegetables) are heated in this way at Larderello and surrounding villages (ALLEGRINI, 1976).

- Castelnuovo V.C. Waste low-pressure/low-temperature steam available in this area from shallow, almost exhausted wells will be used for heating 154 buildings (approx. 200,000 m^3) in this village located near Larderello.

  The steam will be condensed in a mixture condenser and the hot water produced, at a temperature of about 95°C, will be conveyed to a plate heat exchanger, where it will heat the secondary water of a distribution circuit. The users will draw heat from the distribution through other plate heat exchangers, each serving a small group of consumers.

  The heat distribution system will be rated for a peak power of 7 Gcal/h, out of which 5 Gcal/h will be obtained by the geothermal heat recovery plant. The backup and the reserve will be supplied by liquid fuel heaters.

  The annual consumption of geoheat in this system (including sanitary water) is expected to be some 7800 Gcal.

- Bulera. This is a particular type of integrated project which is being implemented by ENEL for demonstration purposes. It is aimed at producing electric power and heat by using the geothermal fluid of the well Bulera 1, near Larderello. The fluid is made up of steam at 120°C with a very high uncondensable gas content (over 50%). Steam will be condensed and the resulting water at 85-90°C will be used in a binary cycle to evaporate a low-boiling fluid (freon) whose vapour will drive a 50 kW_e turbogenerator. After this heat exchange, the outflowing water (at about 70°C) will be used to heat several greenhouses, where ornamental plants and vegetables will be grown. Lastly, before being reinjected, the geothermal water will heat water for catfish breeding and water-hyacinth growing.

  The project will involve the exploitation of geothermal heat for a total of 1.35 Gcal/h, out of which 0.6 will be required by the binary cycle plant. Moreover, the unconsensable gas, made up almost entirely of CO_2, will be recovered and used in the greenhouses to improve the plant growing.

- Amiata. This is a typical example of multi-purpose utilization projects, recently implemented in an area characterized by underemployment and other socioeconomic problems.

  In this area two back-pressure power plants were installed by ENEL, one at Bagnore and the other at Piancastagnaio (see section 2.1), discharging steam into the atmosphere at nearly 100°C.

  To exploit the heat of this (previously wasted) steam at Piancastagnaio, an agricultural development project was set up for a nearby area (approx. 42 hectares) some years ago and has recently (1983) come into operation. More than half of the project area is used for growing ornamental plants and flowers in glass-covered greenhouses heated by a secondary circuit. Moreover, a drying plant is connected with these greenhouses, which also serves other nearby greenhouses where vegetables are grown.

  Modifications of the power station were necessary to allow the recovery of waste heat. The geoheat utilization scheme, described in detail by FRANCIA et al. (1982), basically consists of:
  - a heat recovery circuit (including a mixture condenser and a 50 m high gas escape chimney) and a reinjection circuit;
  - a heat transport circuit supplied by clean water and including surface heat exchangers at both ends of the circuit, as well as a pumping system;
  - a distribution circuit, including the pipe network and the circulating pumps.

  The estimated yearly heat consumption is 150,000 Gcal for the greenhouses and 200,000 Gcal for the drying plants.

- Cesano. As mentionned in section 2.1, the central part of this hot brine field features temperatures of the order of 230°C and salinity of 300-350 g/l, whereas the peripheral part of the reservoir has temperatures of 120-170°C and salinity of 80 to 150 g/l (BALDI et al.,1982; ALLEGRINI et al., 1982).

  Due to these peculiar characteristics, a feasibility study is under way concerning the integrated utilization of the resource: electric energy production, chemicals recovery (mainly glaserite and subordinately bromide

and iodine), and geoheat for district heating.

As regards the latter utilization in particular, a project is being set up for the central heating of the military buildings and facilities pertaining to the Cesano Infantry School, totalling a volume of about 350,000 m^3 space heating (ENEL, 1982). The estimated yearly energy consumption is 8600 Gcal, with a peak power of 6.7 Gcal/hr (out of which 5.6 are for space heating and 1.1 for sanitary water heating).

The distribution network (5.7 km long, made of a preinsulated double pipe buried under the ground level) will enable circulation of pressurized water having a maximum pressure of 17 bar, inlet temperature of 120°C and outlet temperature of 60°C.

Table 4 summarized dimensions and heat data of the projects summarized above, while Fig. 2 shows their location.

Tab. 4 - Geoheat of Italian district heating and greenhouse projects under development in Dec. 1982

PROJECT	DISTRICT HEATING VOLUME (m^3)	GREENHOUSE AREA (m^2)	ANNUAL GEOHEAT (Gcal)	ANNUAL OIL SAVING (PET)
Abano and Galzignano	100,000	20,000	150,000	20,000
Vicenza	1,118,000	-	23,000	4,200
San Donato	467,000	-	15,000	2,100
Ferrara	2,100,000	-	75,000	9,000
Larderello	350,000	15,000	90,000	14,000
Castelnuovo V.C.	20,000	-	7,800	1,100
Bulera	-	5,500	2,200	300
Amiata	-	220,000	350,000	54,000
Cesano	350,000	-	8,600	1,300
TOTAL	4,505,000	260,500	721,600	106,000

2.2.2 - Projects under preliminary study

In addition to the projects above, many prefeasibility studies are being carried out in other areas, aimed at exploiting geothermal fluids for direct or combined uses. Among them, it is worth mentioning the following.

- Radicondoli. This project envisages heating 24,000 m^2 of greenhouses for flower and vegetable growing. The forecasted heat consumption is some 23,000 Gcal per year, with a peak of 7.5 Gcal/h. The geothermal fluid will be used in an indirect cycle, heating (through a heat exchanger) the water of a secondary circuit.

- Torvaldaliga. In this area, near Civitavecchia, a large low-temperature (50-60°C) reservoir exists at relatively shallow depth (500-600 m). Wells drilled in this area are of the artesian type and water has a low salinity.

  A project is under study to use hot water for pre-heating fuel oil supplying a large thermoelectric power plant operated by ENEL in that locality.

- Colli Albani. A preliminary market survey carried out in this region has individuated a number of high consumption areas where geothermal energy might profitably be used for non-electrical applications. Based on this survey and on the geological situation of this region, a series of possibilities are being considered to provide mainly industries and, to a lesser extent, district heating systems and agricultural activities with geothermal heat. Should the market conditions prove to be attractive, geothermal heat for direct uses could be available within a few years for an energetic content corresponding to 5000 PET/y.

- Vulcano. On this island of the Aeolian archipelago a project is being implemented aimed at producing electricity and fresh water by means of high-temperature fluids likely to exist within 1500-2000 m depth. The objective is to install a 5 MW_e power plant and to use geoheat to obtain approx. 1.1 million cubic meters of fresh water per year from the sea water or from steam condensate or residual geothermal water. Production of both electricity and fresh water should suffice for meeting energy and hydric demand of the three main Aeolian isalnds, i.e. Vulcano, Lipari and Salina.

2.3 - Remarks on the development between 1975 and 1982

As can be inferred from the summary presented in the preceding sections, and by comparing

the information given in this paper with that contained in the progress report of CERON et al. (1975), the geothermal situation in Italy in the period considered here has changed remarkably with respect to the preceding years.

Indeed, up to beginning of the 1970s, the production of electric energy being the sole industrial objective to pursue, the interest in the development of Italian geothermal resources was concentrated chiefly in the areas of Larderello, Travale and Mt. Amiata, and secondarly in a few other zones of the pre-Apennine belt in Tuscany, Latium and Campania where it was thought that the geological conditions could be favorable for finding steam or, at least, fluids at temperatures over 180°C. In the subsequent period, however, and particularly towards the end of the 1970s, boosted by the energy and economic crises following the events of 1973, exploration was gradually expanded to numerous other zones with the objective not only of producing electric power, but of utilizing geothermal resources for direct and combined applications to the greatest extend possible. For this reason fluids with temperatures of 100°C or even less have been considered of possible industrial interest.

A prominent aspect of the period in question is that of "deep exploration". By this is meant the fact that, whereas up to the first years of the past decade the extraction of geothermal fluids was limited in the areas of Larderello, Travale and Mt. Amiata to the reservoir made up of Mesozoic carbonate formations and to the upper part of the positive structures of the metamorphic basement, after 1975 a program was launched (called, as a matter of fact, "deep exploration") directed at verifying two hypotheses: the first concerning the existence within the metamorphic complex (at depths between 2500 and 5000 m) of permeable horizons capable of forming a deeper reservoir; the second regarding the possibility of extracting, from deep layers, fluids of higher temperature and pressure than those contained in the part of the reservoir exploited so far.

As mentioned in section 2.1, this programme has already begun to produce very encouraging results both in the Larderello area and, in particular, at Piancastagnaio.

In the new areas, on the other hand, the objectives of "deep exploration" seemed premature in the period from 1975 to present-day, since it was firstly necessary to verify the existence of a first reservoir. However, with the increased competitivity of geothermal energy, the average depth limit in drilling has now been fixed at 3000 m, as opposed to the earlier limit of 1500-2000 m.

Another important program in the period considered is reinjection, which was launched in the mid 70s as a means of: i) discharging the waste condensate from the Larderello powerplant back into the underground; ii) attempting a partial recharge of the field (which has a strong deficit in the mass balance between water inflow and fluid out-flow); and iii) slowing down pressure drawdown in the more intensely exploited area.

Reinjection tests were initially carried out in the more marginal areas of the field, and were later extended gradually to the central areas affected by a more intense and prolonged exploitation. The results are very satisfactory in all instances.

Further aspects of geothermal activity in the 1975-1982 period include: improving of certain exploration methodologies, study and experimentation of utilization of hot brine resources, study and application of reservoir engineering techniques, various injection and production tests on certain wells in the water dominated fields, application of various stimulation and fracturing tecniques, design and construction of new instrumentation for high temperature and pressures, modernization and rationalization of the steam pipelines, modernization of some old generating units, resiting of some small power-plant, extension of the remote control system in the power-plant, design of new types of generating units.

This is clearly a very wide spectrum of activity that reflects a profound shift on the Italian geothermal scene. The results of these activities were already gratifying, but hopefully will become even more fruitful in the future, thus contributing to attain the geothermal objectives of the National Energy Plan for 1990. These objectives and the future activities are outlined in the second part of this paper.

PART II

3. TYPE OF RESOURCES AND GEOTHERMAL POTENTIAL OF ITALY

High (> 150°C), intermediate (100-150°C) and low temperature (< 100°C) resources are known to exist in Italy. If reference is made to 3 km depth, the thermal situation of Italy can be schematically illustrates as in Fig. 3.

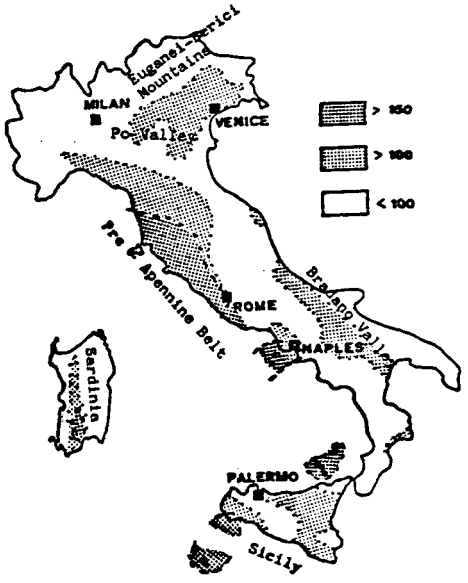


Fig. 3 - Sketch map of the temperature (°C) at a depth of 3000 m b.g.l. (from Fanelli et al. - 1979 modified)

Where the type of geothermal systems are concerned the following can be said: hydrothermal convection systems predominate in the pre-Apennine belt (western Tuscany, Latium and Campania) and occur also in a few other geologic provinces of the peninsula (Euganei-Berici Mts., Bradano Valley and Vulture) and of the islands (Ischia, Aeolian archipelago, eastern and southwestern Sicily, and southern Sardinia); magmatic systems are likely to exist below 2.5-3 km in some active or recent volcanic areas (Vesuvius, Phlaegrean Fields, Pantelleria); geopressurized systems are known to exist below 3 km in the central sector of the Po Valley and near the shore of Northern Adriatic Sea, but their existence at great depth cannot be ruled out in other sedimentary basins of Italy; conduction-dominated systems (due to insufficient permeability rather than lack of water) have been documented in an area of the Northern Sabatini region and are likely to exist also in some geologic structures of the Alps, in some zones of Tuscany (Apuan Alps, and other areas) and in central Sardinia; normal gradient systems feature the remaining part of Italy, i.e. most of the Alpine chain, western and central Po Valley, the whole Apennine range, the southeastern belt of the peninsula, southern and northeastern Sicily and eastern Sardinia.

Assessment of geothermal potential for part of the Italian territory or for the whole country has been made on several occasions during the past decade (BARELLI et al., 1975a and 1975b; CATALDI et al. 1978); CATALDI-SQUARCI, 1978); but the methodologies and the results of these studies are being reviewed at present, also on the basis of the criticism made by CATALDI-CELATI (1983). However, the most recent data available are those published by CATALDI et al. (1978) for central and southern Tuscany and by CATALDI-SQUARCI (1978) for the whole country. Both studies are based on the terminology and methodology proposed by MUFFLER-CATALDI (1978). These data refer to a depth of 3 km and can be summarized here as follows:*

- accessible resource base (ARB) ..... 3×10 GW_y (thermal)
- resources (RSS) 5×10^4 GW_y (thermal)
- reserves (RSV) 12×10^3 " "

With reference to the last figure it is estimated that nearly 30% ($\sim$3500 GWy_t) are characterized by temperatures sufficiently high to be used for electric generation, some 50% ($\sim$6000 GWy_t) could be suitable for non-electrical applications and some 20% ($\sim$2500 GWy_t) have temperatures insufficient (at least for the moment) for any kind of use.

Where geothermoelectric generation is concerned, it is estimated that some 110 GWy (electric) could be obtained from the reserves. Duly taken into account the part of reserves already exploited thus far at Larderello, Travale and Mt. Amiata ($\sim$10 GWy_e), the remaining 100 GWy_e would correspond to 2000 MW_e for 50 years. However, when formulating industrial scale programs, the geothermoelectric potential of Italy, to be on the safe side, should be kept at 1000 MW_e for 50 years (PACCHIAROTTI-PARIS, 1979).

More than 90% of the high-temperature reserves, related to hydrothermal convection systems, are expected to come from the pre-Apennine belt of Italy (western Tuscany, Latium and Campania), with the remaining 10% attributable mainly to the islands. The intermediate and low-temperature reserves, on the contrary, are to be found not only in the abovesaid areas but also in many other regions of Italy.

---

* The temperature limits considered in this assessment are:

- mean annual temperature (reference temperature) ..... 15°C
- minimum reservoir temp. for non-electrical uses .....60°C
- minimum reservoir temp. for electrical generation ..... 130°C

4. RECENT TRENDS, DEVELOPMENT OBJECTIVES AND EFFORT UNTIL 1990

In one of the preceding sections it was said that the five year period 1975-1980 can be considered a transitional period as far as geothermal development in Italy is concerned. The re-examination of previous experience carried out during these five years in light of the profound changes that had occured on the world market of energy sources has led to the identification of the following main areas of activities for the future geothermal development in Italy:

- intensification of study, research and experimental activities in all sectors of exploration and utilization technologies;
- expanding prospecting and drilling zones to include not only areas with strong and moderate thermal anomalies, but in some cases also areas with normal temperature gradients, with the aim of taking in the whole spectrum of the possible uses of geothermal resources: electrical, non electrical and combined;
- deepening drilling in the old fields up to a maximum of 5000 m, and increasing the average depth of wells in new fields up to a mean value of approximately 3000 m, with the objective of exploring deep levels and recovering fluids at higher pressures and temperatures;
- modernization of power stations and/or replacement of old generating units with the aim of improving by 20-25% the mean efficiency of the present geothermoelectric plants;
- reducing the time elapsing between the discovery and utilization of the fluids, either by more widespread use of small, mobile, discharging-to-atmosphere plants in the initial production stage in new fields or for decentralized wells, or by ordering the condensation units in advance;
- designing new types of turbines with greater flexibility (in terms of pressure, temperature, gas content, etc.) than the ones used in the past, and thus adaptable to various production characteristics;
- normalization of the sizes of the individual units according to three basic values (4-5 MW for those discharging to atmosphere, 20 MW and 55-60 MW for the condensation ones) in order to standardize the constructional and operational components of the plants.

On the basis of these working lines, the geothermal objectives of Italy by the end of the current decade in the framework of the National Energy Plan established by the Italian government can be summarized as follows.

As far as electric production is concerned, bearing in mind that the 450 MW presently installed permitted generating 2.7 billion kWh on 1982 (a figure corresponding to approx. 1.5% of the total electric energy produced and 0.4% of the overall energy consumption in Italy in the past year) , it is envisaged to attain an increase of about 250 MW for the year 1990, therefore, the net geothermoelectric capacity installed is expected to reach some 700 MW with a production of 4.2 billion kWh in 1990. The last figure correspond to 1.7% of the total electricity likely to be produced in Italy by the end of this decade.

Where the direct applications are concerned, in addition to the projects mentioned in one of the preceding sections, a number of other initiatives are planned for the coming years, with the goal of achieving in 1990 the utilization of low-to-moderate enthalpy fluids for an energetic content corresponing to 300,000 PET/year.

The aggregate energy contribution of electrical and non-electrical uses of geothermal resources is thus expected to increase from the present 0.4% to 0.6% of the overall Italian energy consumption in the year 1990.

To reach this objective, a total capital investement of 1000* billion Italian liras has been allocated for the decade 1981-90, accounting for exploitation of known and new geothermal areas, as well as for the modernization of old power stations and the construction of new plants. This is therefore a great effort, that involves, among other things, drilling wells for a total of about 400,000 m.

However, as regards the type of fluid necessary to attain the abovesaid objectives, the situation differs greatly with respect to direct and indirect applications. Indeed, for indirect utilization (i.e. for electric energy generation), there is no problem of end-product consumption, and the only limitation derives from the relative scarcity of high-enthalpy resources; on the contrary, for direct heat uses one can count on a huge amount of low-enthalpy resources in Italy, but so far a strong demand has been lacking. Hence, from the latter point of view, the problem of creating a demand for low-to-moderate temperature

* Figure refered to constant money value 1980. At the rate change of that year this figure corresponds to 1.2 billion US $.

heat and the location of its utilization poles will have to be faced.

To solve this problem two lines of action are being pursued: the first, provided for by a specific law, is to stimulate the demand by supplying incentives (grants, soft loans, free-of-charge consulting and other subsidiary means) for the direct applications of geothermal energy wherever it is technically possible and economically convenient to use geoheat in place of fuel oil and/or electric energy; the second is a market survey aimed at individuating any a significant users (industries, farms, district heating systems, etc.) of low-to-moderate enthalpy fluids with the objective of "addressing" as much as possible the exploration of geothermal resources towards the most important consumption areas.

If these actions bear fruit as hoped, the direct uses of geothermal heat at low or moderate temperature could, by 1990, reach values even considerably higher than those corresponding to the 300,000 PET foreseen by the National Energy Plan.

Furthermore, in order to give a continuing and more significant boost to direct uses of geothermal heat, in the spirit of the actions aimed at stimulating demand, ENEL is soon to organize a "Demonstration Center" in Larderello which will be provided with test facilities, plant schemes, models and informational material that will be put at the disposal of any users interested in knowing and/or developing non-electrical applications of terrestrial heat.

5. PROSPECT AREAS AND IMPLEMENTATION OF PROGRAMS

In order to achieve the objectives described in sect.4. highest priority has been given to the development of hydrothermal systems, whereas all the other systems mentioned in section 3 will be the subject of studies or, at the most, experimental activities until the end of the present decade.

Particular attention will be paid to the high enthalpy systems that are now being exploited, or have recently been discovered. With regard to the reservoir already being exploited at Larderello, effort will continue on reinjection of waste condensate and the modernization and optimization of the utilization plants, in order to increase the generating capacity by about 50 MW.

Exploitation of the shallow reservoir will continue in Travale-Radicondoli, Latera, Cesano and Phlaegrean Fields (Mofete) with the objective of installing an aggregate capacity of 100-110 MW by the end of 1990. Moreover, in the other prospect areas discovered in Tuscany, Latium, Campania and Basilicata, all the prefeasibility studies are expected to be completed by 1990 and deep exploration begun in some.

Where the deep reservoir is concerned, exploitation will continue at Larderello and Piancastagnaio and exploration will begin at Travale-Radicondoli and Bagnore, with the objective of increasing generating capacity by an estimated 100 MW.

With regard to the implementation of the activities mentioned above, ENEL will be the sole operator at Larderello, Travale-Radicondoli, Mt. Amiata, Alfina and Cesano, whereas ENEL and AGIP will operate as a joint-venture in the remaining areas. In particular situations, such as the Vulcano Project (Aeolian islands, Sicily), the joint venture is extented to other operators. ENEL will thus be responsible of about 80% of the activities directed at the production of high temperature fluids.

With regard to the implementation of projects for the direct use of terrestrial heat, ENEL and AGIP have so far operated as a joint venture in most cases; however, in future other public or private organizations might be involved in low-enthalpy projects.

As far as base and applied research is concerned, in addition to ENEL and AGIP, other organizations (Universities, Laboratories, Enterprises, etc.) are involved in developing the geothermal activities. Particularly worth of mention, for its contribution to the background development of geothermal energy, is the National Research Council of Italy, whose effort is achieved either through the International Institute for Geothermal Research or in the frame of the "Energetics" Finalized Project.

Finally, mention should be made of the fact that some R. and D. activities, as well as a certain number of demonstration projects, are partly financed by the European Economic Community, as part of the programmes launched by the EEC in 1975 to promote the development of new and renewable sources of energy.

BIBLIOGRAPHY

ALLEGRINI G., 1976: "Non electric uses of endogenous fluids at Larderello". Symposium International Energia Geotermica, Guatemala City.

ALLEGRINI G., CORSI R., CULIVICCHI G., DI FALCO R., FIORDELISI A., GRASSI A., NARDINI G., NENCETTI G.F., TOMEI B., 1982: "Fluid management of the Cesano reservoir: experimental activity". 1st. Turkish-Italian Seminar on Geothermal Energy, Ankara.

BALDI P., BUONASORTE G., CAMELI G.M., CIGNI U., FUNICIELLO R., PAROTTO M., SCANDIFFIO G., TONEATTI R., 1982: "Exploration methodology, deep drilling and geothermal model of the Cesano field (Latium, Italy)". 1st. Turkish-Italian Seminar on Geothermal Energy, Ankara.

BARBIER E., 1977: "L'energia geotermica in agricoltura, nel riscaldamento di ambienti ed in processi industriali". National Meeting "Geothermal Energy and Regions". Chianciano (Italy).

BARELLI A., CALAMAI A., CATALDI R., 1975a: "Stima del potenziale geotermico della fascia Pre-Apenninica centro-meridionale". ENEL CRG, T3/1492, pp.33.

BARELLI A., CALAMAI A., CATALDI R., 1975b: "Estimation of the geothermal potential of the Pre-Apennine belt of central-southern Italy". 2nd United Symposium on the Development and Use of Geothermal Resources, S. Francisco, Abstract I-3.

CATALDI R., CERON P., DI MARIO P., LEARDINI T., 1970: "Progress report on geothermal development in Italy". Geothermics, Special Issue 2, Vol. 2, p.77.

CATALDI R., LAZZAROTTO A., MUFFLER L.J.P., SQUARCI P., STEFANI G.C., 1978: "Assessment of geothermal potential of central and southern Tuscany". Geothermics, Vol. 7.

CATALDI R., SQUARCI P., 1978: "Valutazione del potenziale geotermico in Italia con particolare riguardo alla Toscana centrale e meridionale". Congresso AEI, Vol. 1, p. 1-32.

CATALDI R., CELATI R., 1983: "Review of Italian experience in geothermal resources assessment". Journal of Volcanology and Geothermal Research, Vol. 1, pp. 168-184, Stuttgard.

CERON P., DI MARIO P., LEARDINI T., 1975: "Progress report on geothermal development in Italy from 1969 to 1974 and future prospects". 2nd United Nations Symposium, S. Francisco.

CERON P., SOMMARUGA C., 1979: "Aspetti economici connessi con l'impiego dell'energia geotermica". Congresso di Bari.

ELECTROCONSULT, 1982: "Teleriscaldamento geotermico Città di Vicenza, Studio di Fattibilità". Unpublished Report.

ENEL, 1982: "Revisione e sintesi dello studio di Fattibilità del sistema di teleriscaldamento alimentato da energia geotermica per la Scuola di Fanteria di Cesano". Unpublished Report.

FRANCIA C., CALCARA F., MARIANI G., 1982: "Multipurpose Utilization of Geothermal energy: INDENI-ENEL Geothermal project on the Amiata". BHRA Int. Conf. on Geothermal Energy. Florence, Vol. 2, p. 43.

INVERNIZZI G., SARTI G., 1982: "Note sul progetto di teleriscaldamento geotermico di alcuni quartieri di Ferrara". 9th National Meeting of Plant Engineering. Milano.

MUFFLER L.J.P., CATALDI R., 1982: "Methods for regional assessment of geothermal resources". Geothermics, Vol. 7.

PACCHIAROTTI E., PARIS L., 1979: "L'Energia geotermica per la produzione di energia elettrica: Stato attuale e prospettive". Convegno "Fonti Energetiche Nazionali per l'Elettricità". Siena.

APPENDIX

OVERVIEW OF RESERVOIR ENGINEERING IN THE ITALIAN GEOTHERMAL FIELDS

FOREWORD

The reservoir engineering studies conducted during the last few years by ENEL as part of the testing, development and management of its geothermal fields can be ascribed to the following four main sectors: reinjection, well and field tests, stimulation and instrumentation.

A description is given below of the programs of the above sectors, the results obtained, future programs and the objective set by ENEL.

1. REINJECTION

I.A - Criteria

ENEL has reinjected spent geothermal fluids since the mid-70s, with the objective of increasing energy production from particular reservoirs and avoiding with the minimum economic outlay, eventual adverse effects on the environment caused by discharging these fluids into the sea or rivers. The first reinjection project involved various known reservoirs in the Larderello and Mt. Amiata* zones, which are vapour-dominated high enthalpy and lower enthalpy (corresponding to satured steam) systems respectively.

Recently reinjection has also been extended to the liquid dominated reservoir of the recently discovered Latera field.

The criteria followed in planning reinjection are tied to the objective of these projects, and can be summarized as follows.

Objective: Recovery of energy from the rocks in vapour-dominated systems

- Reinjection into the top of the "dry" volume of the reservoir, in wells with a low hydraulic resistance and intersecting vertical fractures. Injection pressure in the reservoir is lower than the saturated vapour pressure corresponding to rock temperature (∿250°C).
- Reinjection into deep layers of the dry reservoir (2000-2500 m below the top of the reservoir) where temperature is around 300°C.

Objective: Discharge waste into the underground

- Reinjection into the aquifers next to the vapour-dominated reservoir, preferably where there is a small hydraulic gradient in the direction of the reservoir. Restrictive legislation prohibits any discharge into the underground beyond the geothermal reservoir.
- Reinjection into the liquid-dominated reservoir at safe distances from the productive wells.

The safe distance is evaluated theoretically on the basis of various conceptual schemes of the flow regime between the reinjection well and productive well.
Preliminary tests tracers are contemplated in order to verify the compatibility between the theoretical results and the effective flow regime in the reservoir.

I.B - Experiments and projects

Heat recovery from a geothermal reservoir is undoubtely the most attractive objective of every reinjection project. It seems particularly propitious for vapour-dominated reservoir such as that at Larderello, where large volumes of rock (many km^3) at temperatures of about 250°C are saturated in superheated steam at pressures of a few bars.

Extraction of a small fraction of the thermal energy of the dry rock would theoretically allow to stabilize the decline in production for many years or, if necessary, to increase steam production and reservoir pressure for a more limited period of time. This objective cannot be set for areas of the Larderello field in which the steam reservoir interfere naturally with relatively cold aquifers; nor is it viable in the Mt. Amiata reservoir where the steam is, in the best of circumstances, dry saturated steam and the recent meteoric waters flowing through the volcanic chimneys, that out crop on the surface, contribute to the natural recharge of the reservoir.

The first reinjection tests were accompanied by preliminary theoretical studies to evaluate, at least approximately, the effects of reinjection on vapour- and liquid-dominated and two-phase fluid reservoirs.

The first reinjection test into the dry volume of the Larderello system began in 1979, using an old shallow well that was no longer producing at a significant level. The criteria used in choosing this well were as described above. The test was performed in two phases: at first 30-40 m^3/h of water were injected for a few months and, after a short interval, ∿140 m^3/h of fluid were again injected; the test continued in this way for 30 months. The same qualitative results were obtained in both phases: almost total vaporization of the injected water, no decrease in the temperature of the fluid produced by the wells known to interfere with the reinjection well.

Further tests were carried out in the various wells of the reservoir, not always producing as satisfactory results as these described

---

* In this section we refer to the shallow reservoir of Mt. Amiata region. A second productive level of the reservoir also exists in this region at a depth of about 3000 m; it is under exploration at present.

earlier.

The main conclusion to be drawn from these reinjection tests at Larderello is that energy could be recovered from the dry rocks of the system. The success of such an operation depends mainly on permeability distribution around the reinjection well, so that, in practical terms, it is essentially a question of selecting the reinjection wells.

The program of activity for the Larderello system for the next few years includes reinjection of vast quantities of water in order to try to maintain the present production rates and increase wellhead pressure to 10 bar.

The quantity of reinjected water should gradually be increased over 400 m^3/h, which is far higher than the amount available as discharge from the power-plants.

The problems raised by this program are: selection of reinjection wells, reinjection flow-rates for each of the latter, methods and techniques for monitoring the effects of these tests on the thermodynamic state of the reservoir, monitoring of induced seismicity and recovery of the quantities of water required in the tests.

II. WELL AND FIELD TESTS

During the last few years well tests, which are a routine operation after completing a well, have been conducted in the wells of the new geothermal fields still under exploration; i.e., at Latera and the deep reservoir at Mt. Amiata.

The field tests have involved part of the Larderello reservoir and all of the Travale field.

II.A - Well tests

A few deep wells (2600-3500 m) drilled into the deep reservoir at Mt. Amiata have revealed the existence of a reservoir containing pressurized water in the 300-340°C temperature range. Four wells have been put into production - PC 26, PC 27, PC 29 and PC 30 - and the reservoir is estimated to cover such a wide area that 50 production wells are programmed for the next ten years.

The low permeability of the rocks limits the productive capacity of the single wells. The flow-rates of the productive wells vary from 25 to 40 t/h of steam and uncondensable gas (0.04-0.09 by weight) at a wellhead pressure of 11 bar, together with a few t/h of water in the liquid phase.

During production liquid flashing begins first in the well, and then spreads to the surrounding formation, thus producing a temporal increase in fluid enthalpy at well-head, which stabilizes after 20-30 hours of production.

This corresponds to the "stabilization"* of the vaporization front around the wellbore. The position of this front, and the specific enthalpy of the fluid produced, depend on wellhead pressure.

Let us take as an example some results of a well test in Piancastagnaio 27 well (PC 27).

Pressure and temperature logs obtained along the bore-hole in static and dynamic conditions, show a marked decrease in pressure at wellbottom in flow conditions caused by the low permeability of the rocks. This phenomenon affects the back-pressure curve, which is almost flat in the well utilization pressure range.

The pressure build-up occuring after shut-in shows the trend typical of fractures media. The instability regime occuring 17 hours after shut-in is caused by in-hole fluid condensation. After the condensation phase pressure starts to rise again, returning to its static value before the well was opened.

The behaviour of the wells at Latera is quite different, because of the different nature of the reservoir. Although it is a liquid-dominated reservoir, it is characterized by a gas cap lying between the cover rocks and the liquid surface, at depths between 500 and 1600 m. The reservoir fluid contains sodium chloride, alkaline sulphates and boric acid, at temperature between 210°C and 232°C.

Three productive wells, L2, L3D and L4, produce a two-phase mixture of water, gas and steam, with a specific enthalpy of 215-240 Kcal/kg; the flow-rates of the first two wells have been estimated at 500-600 t/h.

Based on the results of the preliminary tests, the CO_2 content in the reservoir fluid has been evaluated at 0.025-0.06 of the water. The carbonate rocks of the reservoir, along with the CO_2 in the fluid, produce large-scale calcium carbonate precipitations during production, and consequent scaling in the casing. Scaling inhibitors have proved very successful in some tests, even in small doses, and it does seem

* The vaporization front continually moves away from the wellbore, but at an ever decreasing rate.

possible to combat this phenomenon.

In this exploitation program for the Latera reservoir, well L3D and L2 will be used as production and reinjection well, respectively. The distance between the well (∿1800 m) and formation permeability should theoretically guarantee that the warm front of the production well will not be broken until after 30 years of exploitation.

II.B - Field tests

The development programme for the Larderello reservoir envisages an increase in steam pressure by means of reinjection, concentrating production during daytime in order to preserve the reservoir.

With these programs in mind and considering past policy, some tests have been conducted in the Larderello field to evaluate reservoir volume where the steam phase is continuous and the hydraulic resistance between the reservoir and the steam manifolds in the utilization plants.

The field tests involved a 10% reduction in the flow-rate of the production wells, which was achieved by temporarily shutting off a turboalternator unit. The consequent increase in production pressure, measured at the manifolds of the production plants, was analysed using a conceptual scheme of the reservoir with concentrated parameters.

This model assumes that the reservoir is intensely fractured, and that a variation in pressure is propagated much faster than usually occurs in a porous medium, from one end of the reservoir to the other.

The empty volume is thus evaluated at $\sim 10^9$ m^3, which is compatible with the values attainable using other methods.

The tests in the Travale field entailed total shut-in of the wells producing superheated steam for 10 days; after re-opening the wells flow-rate was reduced to 60% of the pre-test value.

The objective of the test was to evaluate pressure recovery in the reservoir to verify the results obtained with a mathematical model of the field, and to obtain the necessary information for optimizing management of the Travale reservoir, which is affected by meteoric waters that infiltrate the nearby outcrops of reservoir rocks and which may impair fluid quality.

Although these tests are still under way, the results so far corroborate qualitatively the reservoir scheme based on past experience and studies, and are also quantitatively comparable with the results of the mathematical model.

The pressure build-up in the wells that were specifically shut-in for the tests reveals the typical trend of flow in fractures and some short term storage effects in well R8.

Field development at Travale will in future be directed at exploiting the deepest layers of the reservoir where the liquid and steam phases coexist. At the same time production will be limited in the uppermost layers of the reservoir so as to facilitate recovery of steam pressure and reduce the flow of meteoric waters.

Instrumentation

One of the main activities in reservoir engineering is the development of measuring tecniques for use in the bore and on the surface during well and field tests.

Among the characteristics required of this instrumentation, in geothermal wells in particular, is the ability to operate in high temperatures, to record data in real time and to provide accurate and immediate readings.

Because of the well-known drawbacks in adopting mechanical instrumentation, we have chosen electrical ones. Development has automatically been hampered by the temperature limitations in electronic components (125-130°C) and in plastic materials (FEP, PTFE, PFA: 260-280°C).

Our temperature and pressure probes have non built-in electronic sensors, are run on direct current, and transmit the data analogically from the probe to the surface using multiconductor cables.

-: The modular design of the instruments includes:
   - a 7 conductor cable
   - truck with hoist
   - data acquisition system comprising computer and peripherals, magnetic tape unit, printer and plotter for direct log recording.
-: These instruments are the results of several years experience in the development of equipment for well-logging applications.

The equipment from the CISE geothermal line are at present adopted regularly by ENEL at Larderello during intense geothermal exploitation and have proved to be reliable, sturdy and versatile.

The main characteristics of the various instru-

ments already in use or in the experimental phase are:

1) Probe for temperature and pressure measurements (TP probe)
The probe, is 52 mm in diameter, 0.5 m in length and 4.5 kg in weight.
- maximum temperature 300°C
- maximum pressure 50 MPa (500 bars) (in dependence on the transducer mounted in the probe)
- maximum depth 4000 m
- temperature accuracy ± 0.2°C
- temperature resolution 0.01°C
- time constant 6 s
- pressure accuracy ± 0.3% of the transducer capacity
- pressure resolution 0.004% of the transducer capacity.

2) Caliper
The caliper, is 120 mm in diameter, 3 m in length and 160 kg in weight.
It performs the simultaneous measurements of two orthogonal diameters of a borehole cross-section and of the velocity drift of the fluid emitted (during production tests) or injected (during injection tests).
- maximum temperature 250°C
- maximum pressure 35 MPa (350 bars)
- maximum depth 4000 m
- diameter measurements from 120 to 650 mm
- diameter measurements accuracy ± 5 mm
- fluid velocity accuracy ± 10%

3) Bottom sampler
The tool, collects fluid samples in the well at the wanted depth. It consists of a bottle and two valves, and is sent down the well with the two valves closed: when it reaches the wanted depth, an electric motor opens the two valves in order to let the fluid enter into the bottle and the air come out of it. When the bottle is filled, the same electric motor closes the two valves and the tool is lifted with the sample. The tool can be used at:
- maximum temperature 250°C
- maximum pressure 25 MPa (250 bars).

4) Fluid level gauge
Slow variation of fluid level in deep wells measurements, no electric signal; useful in presence of evaporating fluid. Housed in a valise (weight 40 kg; max. detectable variation 10 m; accuracy ± 1 cm; max. depth 800 m).

5) Heat conductivity gauge
Thermal conductivity measurements for hard rocks; direct reading; computerized data analysis (specific linear power-T vs time-thermal conductivity); Von Hertzen-Maxwell needles (O.D.: 0.8 to 15 mm; lenght: few centimeters to 1 m; range: 0.003 to 0.3 W cm^{-1} $°C^{-1}$; accuracy: better than 3%).

6) Electric clinometer
The clinometer is provided with a magnetic compass and carries out the measurement of borehole drift angles and their direction with reference to the geographic coordinates. Owing to the compass, it cannot be used in cased holes and is affected by the possible formation magnetism. A second version with a gyro-compass is begin planned. The instrument is 4.4 m long and can be extended to 6.9 m, its weight is 65 Kg. It is provided with three different interchangeable measurement equipments. Its characteristics are:
- maximum temperature 300°C
- maximum pressure 50 MPa (500 bars)
- maximum depth 4000 m
- borehole diameters from 120 to 400 mm
- drift angle measurements:
  0÷15° with accuracy better than ± 1°
  0÷30° " " of ± 1°
  0÷60° " " of ± 2°
- direction error ± 3°40'.

7) Recovery electromagnets
These tools are used to pick up small steel objects fallen into the boreholes. In order to identify the objects, the electromagnets are provided with a specially designed load cell that can measure the object weight directly at the well bottom with consequent better accuracy.
Four tools have been constructed having the following characteristics:
- diameter 116 mm - maximum liftable weight 600 N
- diameter 175 mm - maximum liftable weight 900 N
- diameter 250 mm - maximum liftable 1400 N
- diameter 400 mm - maximum liftable 2000 N.

A study is now being made of a tool for measuring scaling in casings in geothermal bores.

The use of probes with no built-in electronic parts means that the temperature limit of the cable must be increased to a least 400°C. Consequently experiments are now being conducted on developing a multi-conductor cable capable of operating in temperature conditions of at least 400°C; this cable is now being constructed.

As the same time we have also developed thick film ceramic transducers to obtain a more

intense starting signal.

Another innovative concept, aimed at overcoming the limitations of electric insulators, is the development of an optical temperature probe, together with optical cable and surface electronics. This instrument can be adopted in temperature conditions up to 500°C and to depths of 3500 m.

Stimulation

Another important activity of the last few years and which is expected to be of considera ble interest in future is the development of pratical methods for stimulating wells that are no longer commercial but could at least be used as reinjection wells.

The poor local permeability encountered by these wells is normally responsible for their decreased productivity and/or injectivity.

For some time now ENEL has been conducting hydraulic stimulation tests, sometimes using chloric acid, as the formations are usually carbonates.

The results of these experiments have been analyzed by a theoretical model (numerical simulation), as well as by well test analyses, in order to achieve a greater under-standing of the phenomenology involved in stimulation operations.

Two types of stimulation have been tested:
- removal of skin effects with a high matrix permeability
- creation and/or propagation of fracture systems connected with the wells.

In the first case, removal of skin effect generally succeeds in vastly improving injection properties.

The test results obtained so far in the second type of operation are encouraging, but cannot be considered totally adeguate for practical purposes.

In this cases stimulation by pressurized injec tion until hydraulic fracturing is achieved results in:
- the creation or propagation of a fractured zone
- a gradual shift in skin from positive to negative values
- a reduction in the initial over-pressure limit
- an improvement in injectivity for increasingly longer injection times
- a hydraulic behaviour typical of fractured media.

These results are interpreted as follows:
- the fractures remain partly open as injection pressure ends
- thermal stress, by reducing effective stress in the fracture zone, explains the permeability increase on the fracture surface;
- because of the low heat conductivity of the rocks, this increase in permeability is maintained with time.

However, as the effects are confined to a small part of the medium and increase in its average permeability not expected, more satisfactory results can only be achieved when the artificial fractured surface reaches a high permeability zone.

Tests will be held in future in wells sited in particular conditions.

BIBLIOGRAPHY

R.C. SCHROEDER, M.J. D. SULLIVAN, K. PRUESS, R. CELATI, C. RUFFILLI: "Reinjection studies of vapour-dominated systems". Proc. 2nd DOE-ENEL Workshop Oct. 1980.

A. BARELLI, R. CORSI, S. D'OFFIZI, F. LOVARI, G. MANETTI, U. ROSSI: "Results of drilling exploration in the Latera geothermal area: Uti lization project of a water-dominated reser voir". Presented at the 3rd EC Internation Seminar "European Geothermal Update". Munich, Nov. 1983.

G. CAPPETTI, A. GIOVANNONI, C. RUFFILLI, C. CALORE, R. CELATI: "Reinjection in the Larderel lo geothermal fields". Proc. Int. Conf. on Geothermal Energy Florence, May 1982.

G. CARRADORI and G.NERI: "The simulation of well tests and production data of the Travale geothermal field by a mathematical model". Note Presented at the U.N. Seminar on utilization of geothermal energy for electric power production and space heating Florence, May, 1984.

G. CARRADORI, P. CERON, G. NERI, A. PEANO: "Assessment of the role of numerical simulation in modelling Travale geothermal field". Presented at the 3rd EC International Seminar "European Geothermal Update". Munich, Nov. 1983.

A. BARELLI: "Rapporto sulle attività e sperimen tazioni eseguite ai pozzi di Latera". ENEL/ UNG Internal Report 1983.

"Simulazione dello stress termico dovuto ad iniezione in pozzi fratturati". ISMES. Inter nal report 1983.

M. ADORNI, A. PARMEGGIANI, L. CEPPATELLI, P. ROSSELLI: "New developments in geothermal instrumentation: the overcoming of the thermal barriers". Proc. Int. Conf. On Geothermal Energy, Vol. 1 Florence May, 1982.

Proceedings Ninth Workshop Geothermal Reservoir Engineering
Stanford University, Stanford, California, December 1983
SGP-TR-74

GEOTHERMAL FIELD DEVELOPMENTS IN ICELAND

G. Pálmason, V. Stefánsson, S. Thórhallsson, and T. Thorsteinsson

Orkustofnun
Grensásvegur 9, 108 Reykjavík, Iceland

INTRODUCTION

Commercial exploitation of geothermal resources in Iceland dates back to the 1920's. The first district heating system, in the capital Reykjavík, began operation on a small scale in 1930 with the heating of a few buildings including a school house and a public swimming hall. The water, 15 kg/s, 93°C, was taken from shallow wells in what is now known as the Laugarnes field, which was at that time outside the town. In the 1940's the Reykjavík heating system was expanded considerably utilizing water issuing from wells less than 600 m deep in the Reykir geothermal field about 17 km away from the town. Rapid development followed, especially after the impetus given by the increase in oil prices during the 1970's. The main emphasis was on space heating, but other uses began to emerge at the same time. In 1976 the diatomite plant at Mývatn began operation using steam from the Námafjall field for drying. In 1969 a small non-condensing turbine was set up in the same place for generation of electricity. And about 1974 work started on the Krafla power plant which was to consist of two 30 MW units, of which only one has been operating yet. At the Svartsengi field which is used mainly for district heating, three small electric generating units of 8 MW total capacity have been installed. For more details on the utilization of geothermal energy the reader is referred to Gudmundsson (1982, 1983).

Today geothermal energy plays a relatively large role in the energy economy of Iceland. About 80% of the space heating requirements are met with geothermal energy at an average cost to the consumer which is about 18% of the cost of oil heating. The remaining needs are met with hydroelectricity (13%) and oil (7%). Space heating accounts for about 40% of the total energy consumption in Iceland. In terms of energy content geothermal provides about 40% of the total energy sold to users. In terms of oil equivalents the fraction is 27%. Fig. 1 shows how geothermal energy has steadily grown in importance relative to other primary energy sources in the past decades. At the present time the annual saving in imported oil due to the use of geothermal energy amounts to US$ 560 per capita.

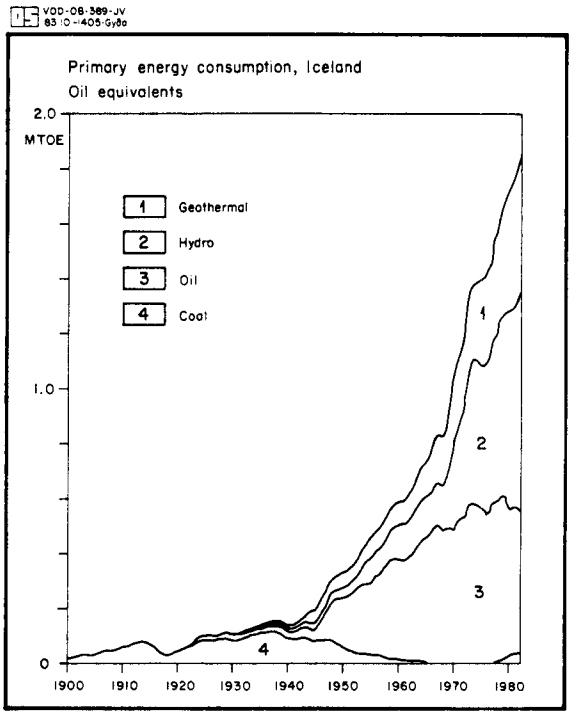


Fig. 1. The role of geothermal energy in the energy economy of Iceland, expressed in million tons of oil equivalents per year.

The exploration and research carried out in conjunction with the exploitation of the various geothermal fields has vastly deepened our understanding of the hydrothermal systems in Iceland. They have proved to be more diverse with respect to physical state, chemical composition, hydrological properties, and geological control than previously thought. The purpose of the present paper is to review the present state of knowledge regarding the Icelandic geothermal systems, with emphasis on the production and reservoir engineering aspects.

ASSESSMENT OF THE GEOTHERMAL RESOURCES

The geothermal fields in Iceland have long been classified into high-temperature and low--temperature fields on the basis of the concept of base temperature (Bodvarsson, 1961). This division remains a useful one. The high--temperature fields are all within the active neovolcanic zones while the low-temperature activity occurs in flank areas where the crustal rocks are older and the temperature within the crust lower than in the neovolcanic zone.

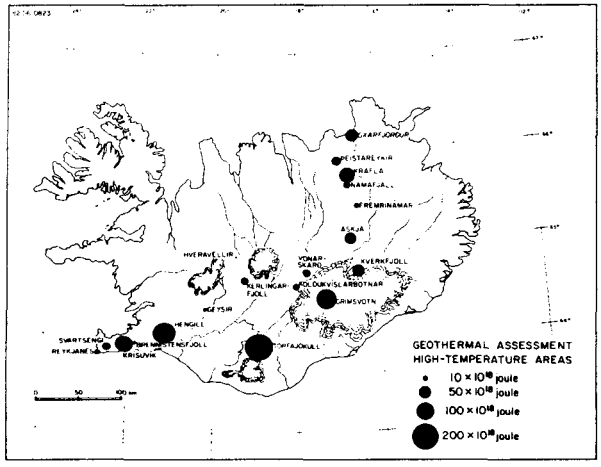


Fig. 2. A total stored-heat geothermal assessment of the high-temperature fields.

A revised assessment of the geothermal potential of the high-temperature fields has recently been made by the Geothermal Division of Orkustofnun (Pálmason, 1981). It is based on stored heat calculations and an assumed geothermal recovery factor of 20%. The area of the fields is estimated on the basis of surface manifestations and geophysical surface surveys where they are available. The reservoir thickness from which production can be obtained is assumed to be 3 km. The stored heat in the various high-temperature fields is shown in Fig. 2. The total available heat from these fields, taking into account recovery- and accessibility factors, is estimated to be 10^{20} Joule, or, when converted to electricity, 175,000 MWyrs. On the basis of geological considerations it seems possible that an additional potential of 2-3 times the above values may lie hidden without direct surface expression within the neovolcanic zone.

The assessment makes no predictions of the rate at which the energy can be withdrawn. Experience alone can add this dimension to the assessment. A considerable body of production data is gradually accumulating, both from high-temperature and low-temperature fields. Some of this is reviewed in the following.

THE REYKJAVÍK FIELDS

The Reykjavík Municipal District Heating Service utilizes geothermal water from low-temperature fields located within or relatively near to the city. These fields are (Fig. 3) Reykir, which supplies about 3/4 of the water used, Ellidaár and Laugarnes, which are located within the city. In addition, the Seltjarnarnes field which supplies the adjacent community of Seltjarnarnes with hot water is located within that community.

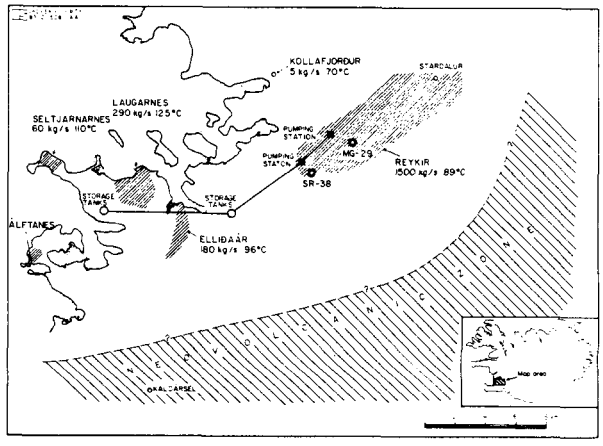


Fig. 3. A location map of the Reykjavík low-temperature fields. Also shown are maximum pumping rates from each field.

In the Laugarnes field, where exploitation was initiated in 1930, deep drilling (>1000 m) began in 1958, and soon after the first wells were connected to the district heating system in Reykjavík. The early production experience from this system has been reported by Thorsteinsson and Elíasson (1970). The main reservoir to a depth of 1250 m has a temperature of about 135°C, but the deepest well at that time, about 2200 m, encountered a deeper producing horizon with a temperature of about 145°C near its bottom. The water from this field is low in total dissolved solids, about 350 ppm, of which 35 ppm is chloride. Two deeper drillholes, to 2857 and 3085 m, were sunk in the production area in 1979 in order to explore possible deeper aquifers. Production was obtained all the way to the bottom, where the temperature was 155°C. In the deepest well the salinity of the water proved higher than in other wells in the Laugarnes field, with about 200 ppm of chloride (Gunnlaugsson, pers. comm.).

The permeability-thickness product in the Laugarnes field was estimated by Thorsteinsson and Elíasson (1970) on the basis of interference tests of 10-20 hours' duration to be about 110 darcy-m. Assuming a thickness of 1000 m for the producing reservoir, this gives a permeability of 110 millidarcys. A per-

meability of a few darcys was obtained by Bodvarsson (1978) on the basis of water level recovery data from one well. These values are rather high and may be affected by specific aquifer structures near the wells. On the basis of annual total production variations and accompanying water level changes, Pálmason (1967) estimated with a crude steady-state model a permeability of 35 millidarcys for the formations surrounding the production area. Bodvarsson (1978), using the same data and a more sophisticated model obtained a value of 10 millidarcys for the global permeability of the Laugarnes field. These estimates show wide discrepancies which need to be explained.

An opportunity for a pressure buildup test of the Laugarnes field as a whole presented itself in 1982, when pumping was temporarily discontinued from all the wells in the area for 4 months. The water level was monitored in several wells. The short-time buildup showed a proportionality to the square root of time (Fig. 4), indicating fracture permeability

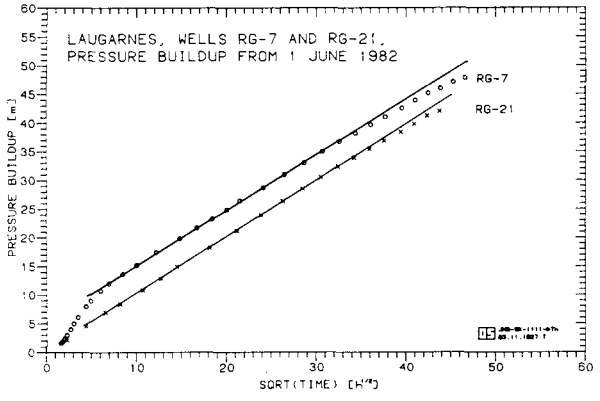


Fig. 4. Pressure buildup in the Laugarnes field, showing a linear change with the square root of time over a certain time interval.

(Gringarten et al., 1972a and b). The longer-time pressure buildup (Fig. 5) indicates a global permeability-thickness product of about 15 darcy-m. With a production zone thickness of about 1000 m this gives 15 millidarcys as a global permeability for the Laugarnes field.

The Reykir field was the principal source of thermal water for the Reykjavík District Heating Service from 1944 until 1959, when the redevelopment of the Laugarnes field began. In 1955 the production of 350 kg/s at an average temperature of 86°C was by free flow from 69 shallow wells. It was realized that the production could be increased by deeper drilling and by pumping from the wells. A redevelopment program was started in 1970, and by early 1975 29 new wells of 800-2040 m depth (average 1616 m) had been drilled. Well completions are of the open hole type. Prior to late 1973 production casing diameters were 9 5/8" up to 200 m depth, and hole size was 8 1/2". Later wells have 13 3/8" casings (200 m) and 12 1/4" hole size to 1400-1600 m. Typical pumping rates from the older wells are 30-40 kg/s but 90-100 kg/s from the later wells. The higher production rates are attributable to larger pumps and to improved productivity characteristics of the larger diameter wells.

The production history from 1971 to 1975 has been reported by Thorsteinsson (1976). In 1974 the annual discharge by pumping had reached 18.2 gigaliters, while the free flow from the older wells had ceased completely due to pressure drawdown in the reservoir. The average temperature of the pumped water was 83.5°C.

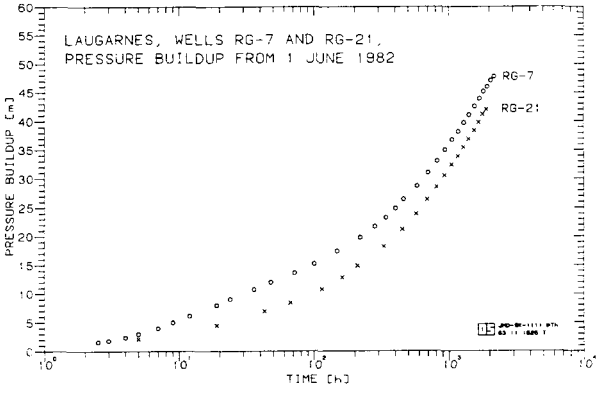


Fig. 5. Pressure buildup in the Laugarnes field, used for estimating the global permeability of the field.

On the basis of interference tests Thorsteinsson (1976) estimated the transmissivity in the Reykir production area to be in the range (0.48 - 2.7) x 10^{-2} m^2/s. With a 1000 m thickness of the producing reservoir this corresponds to a permeability range of 150 - 860 millidarcys. Since 1975 10 additional wells have been drilled in the Reykir field, expanding the production area considerably to the east, in the direction towards the neovolcanic zone. The production history for 1976-1982 and water levels from two observation wells is shown in Fig. 6. The pressure variations due to the seasonal variations in pumping rate are propagated over considerable distances as evidenced by the 204 m deep Stardalur observation well about 7 km to the northeast (Fig. 3), where 65% of the pressure amplitude in the production area is observed. The global permeability estimated from the long-term pressure decline is about 70 millidarcys, significantly lower than that obtained from the interference tests. This probably reflects similar conditions as in the Laugarnes field, although the permeabilities in general are higher in the Reykir field.

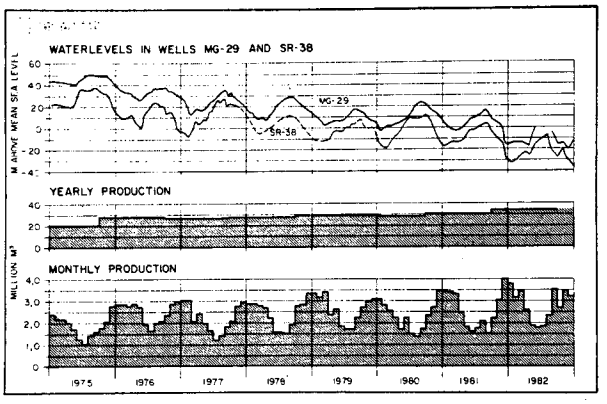


Fig. 6. The production history and pressure decline of the Reykir low-temperature field.

The water from the Reykir field is relatively low in dissolved solids, about 200 ppm, of which 10-15 ppm is chloride.

The Ellidaár field is relatively small, and was discovered in 1967 when the first well was drilled there. Although the field is only 2-3 km away from the Laugarnes field, its water is distinctly different, more dilute and of a lower temperature. It resembles more the Reykir water with regard to temperature, chemical and isotopic composition. The peak pumping rate from this area has been around 180 kg/s. Thorsteinsson (1976) has estimated the transmissivity within the production area to be 3.5×10^{-3} m^2/s on the basis of short-term interference tests. This indicates a permeability similar to that found for the Laugarnes field from similar tests.

Some cooling, up to 10°C, has been observed in wells in the Ellidaár field. It is believed to be caused by infiltration of colder water from the surroundings or by downflow of colder groundwater in non-producing wells. This phenomenon is presently under study.

The Seltjarnarnes field which is located 3-4 km west of the Laugarnes field has five wells, 860-2000 m deep, of which three are producing. The peak pumping rate is 60 kg/s and the reservoir temperature is 80-125°C. Interference tests indicate a permeability about one half that of the Laugarnes field. The water is distinctly more mineralized than the Laugarnes water, with about 1600 ppm total dissolved solids of which 670 ppm is chloride. Because of the high salinity and corrosive nature of this water heat exchangers have to be used.

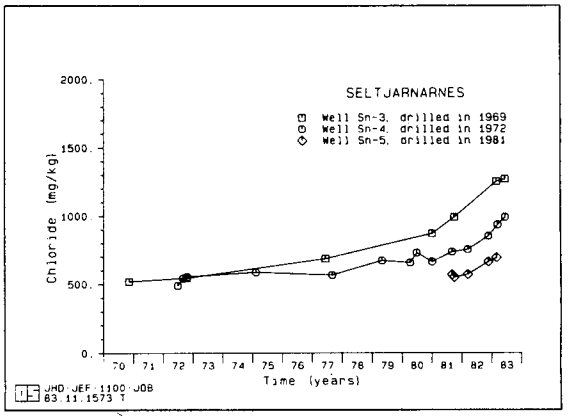


Fig. 7. Changes in chloride content of water from wells in the Seltjarnarnes low-temperature field.

In recent years the salinity of the water pumped from the Seltjarnarnes field has increased considerably (Fig. 7), while the temperature has remained constant. A possible explanation of this is that mixing with a few percent of sea-water is taking place.

Besides the four main low-temperature fields described above there are indications from exploration work that other fields may exist in the Reykjavík area. One of them is the Álfta-

TABLE 1. TRANSMISSIVITIES AND PERMEABILITIES IN THE REYKJAVÍK LOW-TEMPERATURE GEOTHERMAL FIELDS

Field	Short time interference tests (1 - 4 days)		Long time values	
	Transmissivity m^2/s	Permeability millidarcy	Transmissivity m^2/s	Permeability millidarcy
Laugarnes	6.0×10^{-3}	110	7.4×10^{-4}	14
Ellidaár	3.5×10^{-3}	100		
Reykir	4.8×10^{-3}-2.7×10^{-2}	150 - 860	2.2×10^{-3}	70
Seltjarnarnes	2.5×10^{-3}	50		

nes field shown in Fig. 3. Little is known, however, about the production characteristics outside the fields presently being exploited.

Table 1 summarizes the transmissivities and permeabilities that have been deduced for the Reykjavík fields.

THE SVARTSENGI HIGH-TEMPERATURE FIELD

The existence of the Svartsengi field was proved in 1971 by the first well drilled in that area to a depth of 240 m. The field is located within the axial zone of the Mid-Atlantic Ridge on the Reykjanes peninsula. The field is exploited by the Sudurnes Regional Heating service which was established in 1975 to provide district heating to several communities on the Reykjanes peninsula (Thórhallsson, 1979). Electricity is also generated by 3 small turbine units of 8 MW total capacity.

Eleven holes have been drilled in an area of about 1.5 km^2 to depths of 240-1998 m. The hydrothermal system in its natural state is liquid-dominated with a reservoir temperature of 240°C. The geothermal fluid is a brine with a salinity of 2/3 that of seawater(12500 ppm Cl).

Production data, including fluid discharge rate, pressure drawdown, downhole pressure, dissolved solids and gas, and downhole temperature, have been collected regularly since the beginning of the operations. Annual fluid production has been increased steadily reaching about 8.7 million tons in 1981 and 1982 (Fig. 8). The used fluid has been disposed of by surface drainage in the surrounding lava field, causing substantial silica deposition in the disposal pond. Reinjection experiments have been started (Gudmundsson 1983a) and will be continued.

Short-time interference tests have been made between wells spaced about 200 m apart. They have given rather high values of permeability, about 1 darcy. The drawdown history of the field (Figs. 8 and 9) suggests that the high permeability zone may be bounded by rather impermeable walls in one or more directions, and model studies have been made with this assumption (Kjaran et al., 1979). By analogy with the Laugarnes field described earlier one might also suspect that the short-time interference tests are primarily affected by fractures in the vicinity of the wells and that the longer-time drawdown behavior is controlled by lower global permeability values in the rocks surrounding the production area.

The geological strata in the Svartsengi wells consist of alternating suites of basalt lavas and hyaloclastites (Franzson, 1983). Below about 800 m depth 20-40% of the succession are basaltic intrusives. A comparison between aquifer occurrences and geological structures reveals that aquifers in the upper 600 m are largely due to primary permeability along stratification boundaries, whereas below that depth, i.e. within the reservoir proper, the aquifers are associated with intrusives and near vertical fractures, but there the primary pores have largely been filled with secondary minerals.

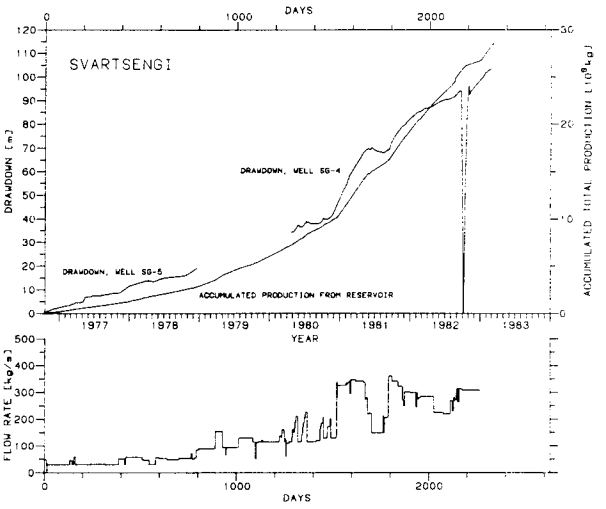


Fig. 8. Production history and pressure decline of the Svartsengi high-temperature field.

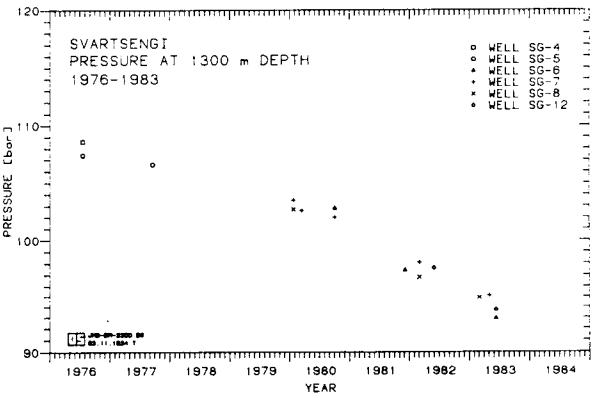


Fig. 9. Downhole pressure measurements in the Svartsengi wells.

The geothermal fluid composition has been monitored in all the wells. There are irregular variations with time but no long-term trends are visible. The gas content is more variable. In most wells it is about 0.2% by weight of the steam but in the shallow wells it reaches about 2%. Calcite scaling takes place inside the production casing where flashing occurs (Arnórsson, 1978), and the deposits are cleaned regularly by drilling.

The production characteristics of the Svartsengi wells are typical of high-permeability liquid-dominated reservoirs. The maximum

wellhead pressure is about 20 bar, and the maximum flow depends primarily on the well diameter. The older wells 4,5 and 6 had a 9 5/8" production casing and a typical mass flow of 60 kg/s (at 10-15 bar , WHP), while the later wells have a 13 3/8" casing and a typical mass flow of 120 kg/s. Delivery curves for wells 4 and 10, showing the benefits of the larger casing program, are shown in Fig. 10.

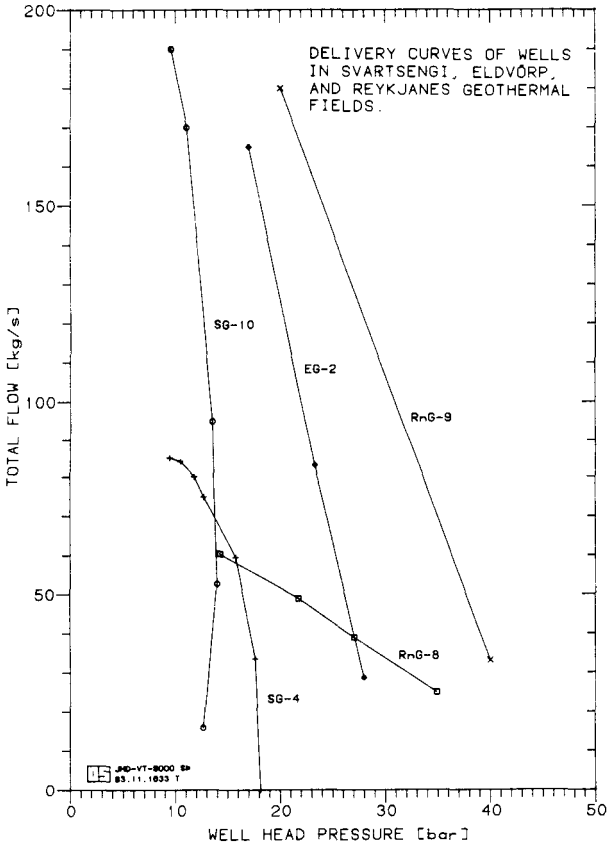


Fig. 10. Delivery curves of wells in the Svartsengi (SG-4, SG-10), Eldvörp (EG-2) and Reykjanes (RnG-8, RnG-9) fields.

The Eldvörp area, about 6 km southwest of the Svartsengi production area, is probably a part of the Svartsengi field, as indicated by electrical resistivity measurements (Georgsson, 1981). The first well was drilled in 1983 to a depth of 1265 m. It is of the same design as the newer Svartsengi wells with 13 3/8" production casing. First tests indicate that the well will be a good producer, similar to the Svartsengi wells.

THE REYKJANES HIGH-TEMPERATURE FIELD

The Reykjanes field is located on the south--western tip of the Reykjanes peninsula, about 8 km southwest of the Eldvörp area. Early exploration of the field has been described by Björnsson et al. (1972). Additional work on the well discharge characteristics was reported by Gudmundsson et al. (1981). The field is at present exploited by a sea-chemicals production company, which operates a small-scale plant for the production of salt, as well as for generating electricity for its own use. A fish-meal plant is under construction in the area. It will purchase geothermal steam from the sea-chemicals company for process heating.

Several wells were drilled in the Reykjanes field in 1968 and 1969, to a maximum depth of 1754 m. In 1983 an additional well (No. 9) was drilled to a depth of 1445 m. It was of the same design (13 3/8" production casing) as the recent Svartsengi wells. The delivery curves of wells 8 and 9 are shown in Fig. 10, demonstrating clearly the increased output for the larger diameter well.

The Reykjanes field is liquid-dominated as the other nearby fields on the Reykjanes peninsula. The geothermal fluid is a brine, considered to originate as mostly seawater, although other possibilities have been suggested (e.g. Gudmundsson et al., 1981). The total dissolved solids content is similar to that of seawater. Individual components differ from seawater, in particular magnesium, sulfate, potassium and calcium, which are determined by ionic exchange equilibria between rock and water. The silica content is determined by the temperature, which in the Reykjanes reservoir is 270-290°C.

The main reservoir is capped by a zone of heavy calcite deposition between 500 and 700 m depth. The strata consist of alternating sequences of lavas, hyaloclastites and tuffaceous sediments. Intrusives are rare. Aquifers appear to correlate mostly with horizontal stratification boundaries as well as with (near vertical) fracture planes.

THE KRAFLA HIGH-TEMPERATURE FIELD

The development of the Krafla field in the northern part of the neovolcanic zone was started in 1974, with a view to generating 60 MW of electricity. A detailed description of the field development up to 1979 is given by Stefánsson (1981). Further details are given by Ármannsson et al (1981), Stefánsson and Steingrímsson (1980), G.S. Bodvarsson et al (1981, 1982, 1983a, 1983b, 1983c), Pruess et al (1983), Kristmannsdóttir (1981).

At the end of 1983 23 wells have been drilled in the Krafla field. They are located in three drilling areas, which are here termed Leirbotnar, Southern Slopes and Hvíthóll. Their location is shown in Fig. 11.

In the beginning of the development (1975) in Leirbotnar it seemed that the reservoir was boiling, giving a saturation pressure and temperature with depth. In 1976 it was found that the reservoir was divided into an upper zone (down to 1000 m depth) of single phase 210°C water and a lower zone (beneath 1100 m depth) which is boiling and with a temperature in the

range 300-350°C. Late in 1975 magmatic activity started about 2 km from the drilling area resulting in substantial influence on the geothermal reservoir. The effect of the magmatic gases on the reservoir fluid resulted in severe deposits in wells (Ármannsson et al.,

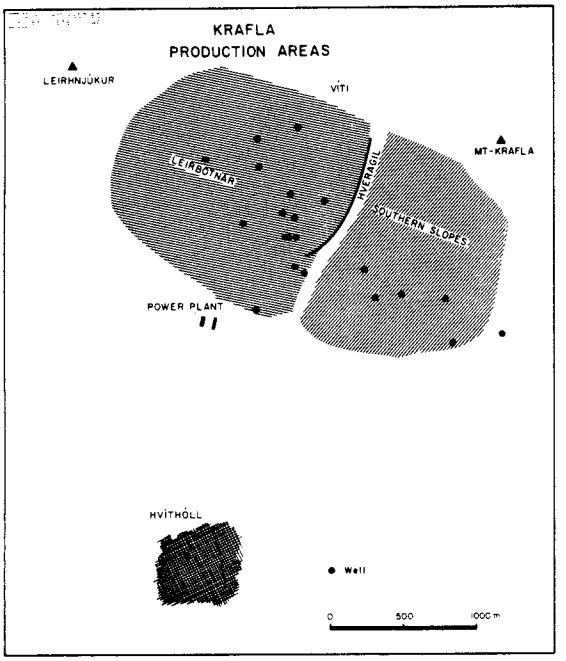


Fig. 11. A location map of the Krafla production areas, showing also the distribution of wells. Leirhnjúkur, on the eruptive fissure swarm, is in the upper left hand corner.

1981). Further drilling was carried out east of Leirbotnar, in the second production area, the Southern Slopes of Mt. Krafla. The chemical properties turned out to be favorable, but this second production area was found to be too small for the 60 MW power plant.

A third production area at Hvíthóll was tested in 1982 and 1983. In this case, the chemical characteristics turned out to be favorable also, but the reservoir system is apparently too small. The presently available steam from the three areas suffices for 35 MW, of which 25 MW is connected.

The experience in Krafla has shown that this is one of the most complex geothermal systems described in the literature. Not only are the conditions complex but the production characteristics vary considerably within the geothermal system. Fig. 12 shows the temperature distribution within the three production areas so far tested in the Krafla field. The usual classification of reservoirs into vapor-dominated, liquid-dominated and two-phase boiling reservoirs does not seem to apply for the geothermal system as a whole, as in the Krafla field we might have all three cases present in one geothermal system.

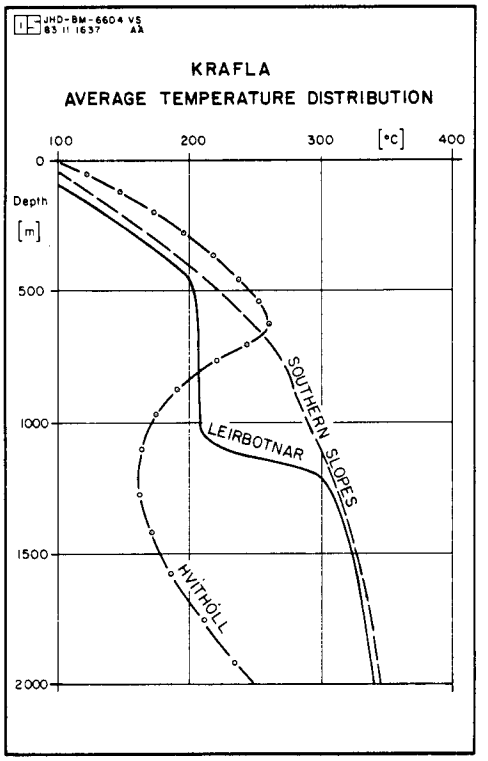


Fig. 12. Average temperature distribution in the three production areas in the Krafla field.

Most of the wells in the Krafla field produce from a boiling reservoir with a temperature of 300-350°C. The delivery curves of these wells contrast sharply with similar curves for single-phase reservoirs, e.g. Svartsengi. The flow is almost constant regardless of the wellhead pressure (Fig. 13). The enthalpy on the other hand is high, usually in the range 2000-2700 kJ/kg. A peculiar behavior is found for well KJ-11 (Fig. 13), which is open to two types of reservoirs, an upper liquid-dominated zone and a lower boiling zone. For certain conditions of pressure at the wellhead the upper zone controls the flow giving a delivery curve which changes considerably with wellhead pressure. For other pressure conditions the lower feed zone is activated giving a flow that is almost constant with varying wellhead pressure.

The wells tapping the two-phase reservoir in Krafla do not reach stable conditions of flow and enthalpy until after weeks or months of production. An example is given by well KJ-14 in Krafla (Fig. 14). The reason for this behavior is that in two-phase reservoirs a very large local drawdown is created around the well, which propagates very slowly in the reservoir due to the high compressibility of the system. When stable conditions are reached in

in the reservoir the flow rate and the enthalpy remain relatively constant.

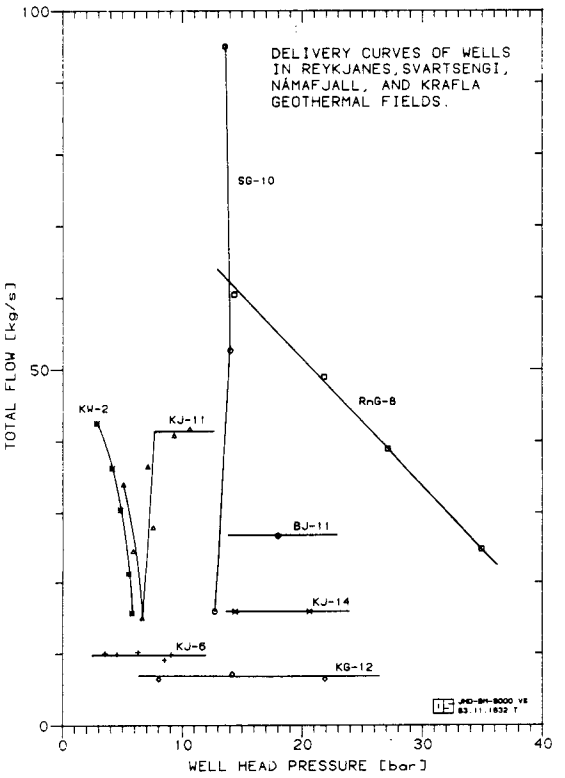


Fig. 13. Delivery curves of wells in the Krafla (KW-2), KJ-6, KJ-11, KG-12, KJ-14) and Námafjall (BJ-11) fields. For comparison two wells from the Svartsengi and Reykjanes fields are shown.

Reinjection into the Krafla reservoir has not been carried out yet. Fig. 15 shows the effect of an unintentional interference test, when during cleaning operations cold water was injected into a well for about 3 days. Two days after the start of the injection the flow characteristics of the nearby well KJ-13 changed as shown in Fig. 15. The flowing enthalpy decreased and the water phase in the discharge increased, while the steam phase remained more or less constant.

Numerical studies of the effect of reinjection into the Krafla reservoir (Pruess et al., 1983) have given similar results to those observed in well KJ-13. Reinjection into two-phase reservoirs will not increase the steam flow from existing wells, but will increase the longevity of the reservoir considerably as is also the case for single-phase reservoirs.

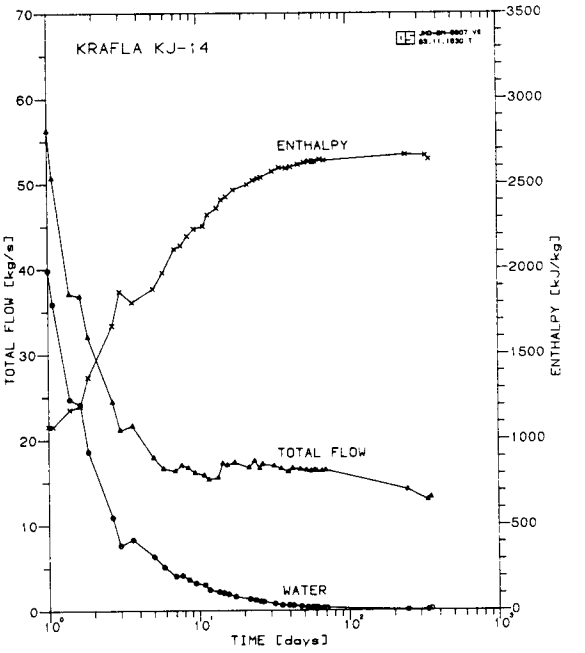


Fig. 14. Production history of well KJ-14 in Krafla.

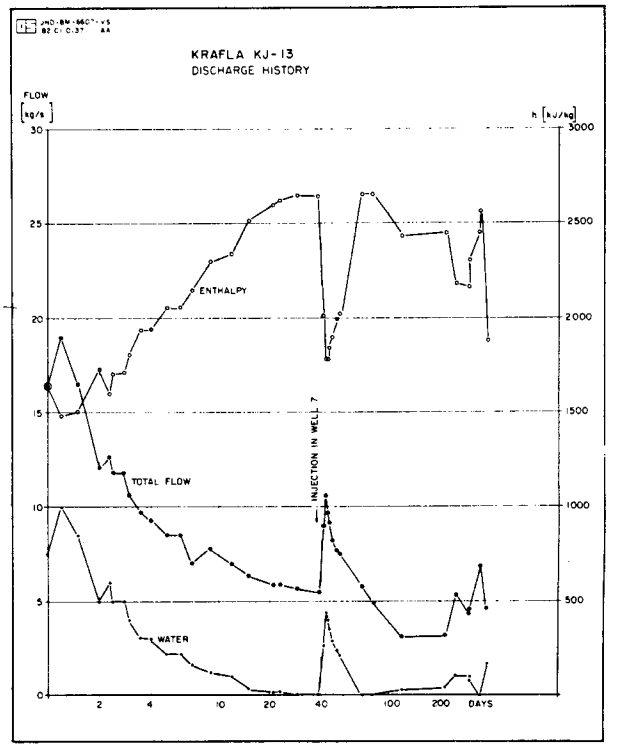


Fig. 15. Production history of well KJ-13 in Krafla, showing the effect of a cold water injection into a nearby well.

The magmatic activity which started in 1975 in the vicinity of Leirhnjúkur (Fig. 11) northwest of the drilling area has influenced the geothermal reservoir in various ways, and has provided an opportunity to study some interrelationships between the two kinds of phenomena. On the basis of attenuation of seismic S-waves a magma chamber has been inferred at a depth of approximately 3-7 km beneath the Krafla caldera (Einarsson, 1978). Large changes in the ground surface elevation have taken place over a period of 5-6 years. They have reflected the pressure variations associated with the movement of magma beneath the Krafla fissure swarm where the volcanic activity was concentrated (Björnsson et al., 1979).

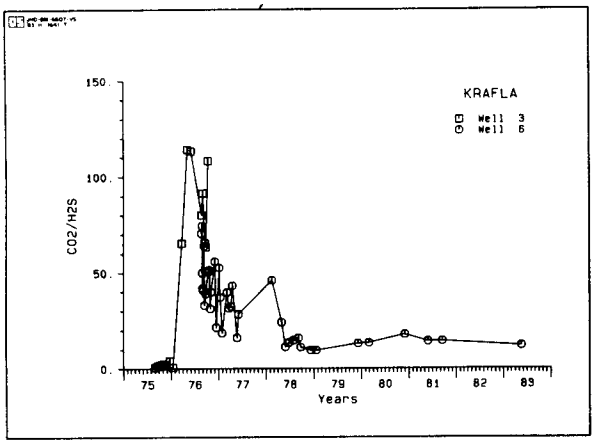


Fig. 16. The variation of gas content in wells in Leirbotnar, due to the nearby magmatic activity.

The chemical composition of the reservoir fluid in Krafla has been strongly influenced by the magmatic activity. Fig. 16 shows the CO_2/H_2S ratio in the discharge from wells KG-3 and KJ-6 in Leirbotnar during the period 1975-1983. An increase by a factor of 100 was observed in the beginning of the magmatic activity, but the effect seems to be fading out at present. The concentration of CO_2 is now (1983) only about five times higher than before the magmatic episode.

An interesting phenomenon from a reservoir engineering point of view was a pressure pulse which was observed in well KG-5 at the beginning of a volcanic eruption about 5 km away (Fig. 17). The well is mainly open to the single-phase upper part of the reservoir, and the pulse seems to be an example of the response of a confined reservoir to an instanteneous point like pressure change. The average transmissivity deduced from the pulse for the single-phase upper zone of the reservoir, $kh/\mu=1.7\times10^{-8}$ $m^3/Pa.s$ (Sigurdsson and Tiab, 1983), is in good agreement with

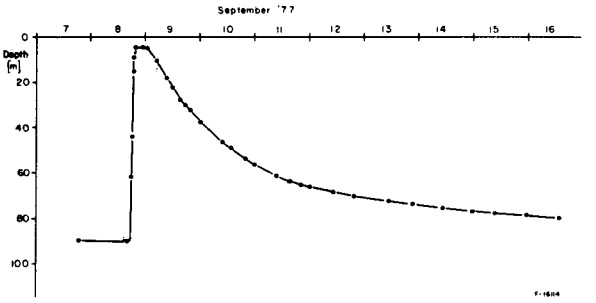


Fig. 17. A pressure pulse in well KG-5 in Leirbotnar caused by volcanic activity about 5 km away. The vertical scale shows depth to the water level.

what is obtained from injection tests of individual wells (Sigurdsson, 1978).

THE NÁMAFJALL HIGH-TEMPERATURE FIELD

The Námafjall field supplies steam for process heating in a diatomite plant and for the generation of electricity in a 3 MW noncondensing station. Its exploitation began in 1967,

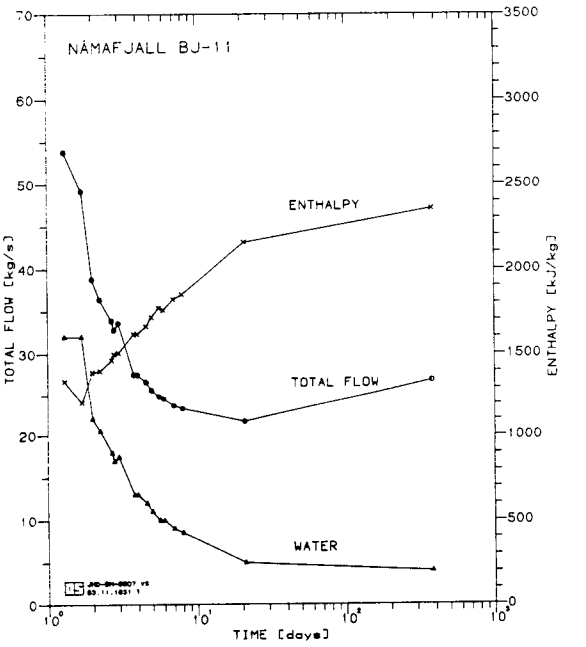


Fig. 18. Production history of well BJ-11 at Námafjall.

and to date 12 wells have been drilled. Changes in the chemistry of the discharged fluid in 1970-1976 have been reported by Arnórsson (1977).

The field which is located about 8 km south of the Krafla field was affected to some degree by the volcanic activity which began in 1975.

Some of the older wells were damaged by movement on faults. Two new wells were drilled in 1979 and 1980 to depths of 1923 and 1999 m. They show in many ways similar characteristics as some of the Krafla wells. The reservoir is boiling and a steady state production is not reached until after several weeks. Fig. 18 shows the production history of well BJ-11. An interesting feature is the increase in flow rate with time. This is believed to be caused by thermal contraction associated with a cooling of the reservoir rock under boiling conditions.

THE AKUREYRI LOW-TEMPERATURE FIELDS

Several hydrothermal systems in the valley of Eyjafjörður in northern Iceland are here termed the Akureyri fields (Fig. 19), because they are utilized for district heating in the town of Akureyri (13,000 inh.). The first successful drilling was carried out in Laugaland in 1976, and at the present time a total of 19 wells, 800 to 2800 m deep, have been

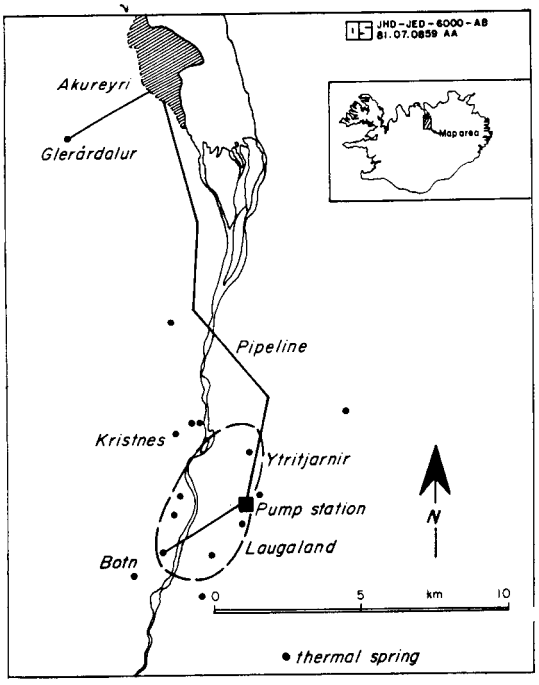


Fig. 19. A location map of the Akureyri low-temperature fields. The dashed curve encloses a low resistivity area.

drilled in the Akureyri fields. The development in these fields to 1981 has been described by Björnsson (1981).

The reservoir temperature is mostly in the range 80-100°C, and the water is low in dissolved solids, 200-300 ppm, of which 10-15 ppm is chloride. The aquifers are found in the depth range 300-2500 m.

The reservoir rocks are gently dipping (5-7°) plateau basalts of Tertiary age (8-10 Myrs). They are cut by numerous dikes, trending approximately north-south. The aquifers seem to be associated with some of the dikes and with interlayers between lavas, the best aquifers occurring at intersections between these two kinds of permeable structures. Because of the nature of the aquifers, non-productive wells are relatively common in these fields, the success ratio being rather low, about 50% of all drilled wells.

Because of the low overall permeability of the reservoirs the pressure drawdown is relatively high. Fig. 20 shows the drawdown for the Laugaland system as measured in several wells.

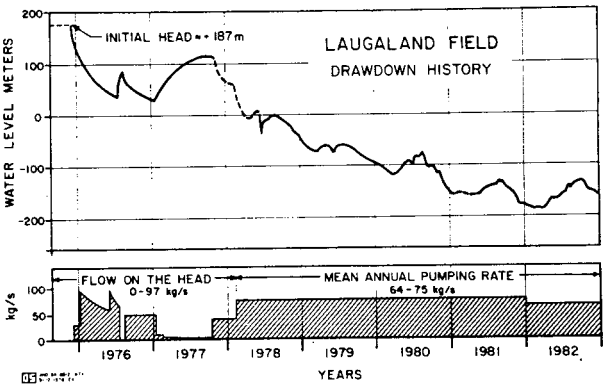


Fig. 20. Production history and pressure decline of the Laugaland low-temperature field.

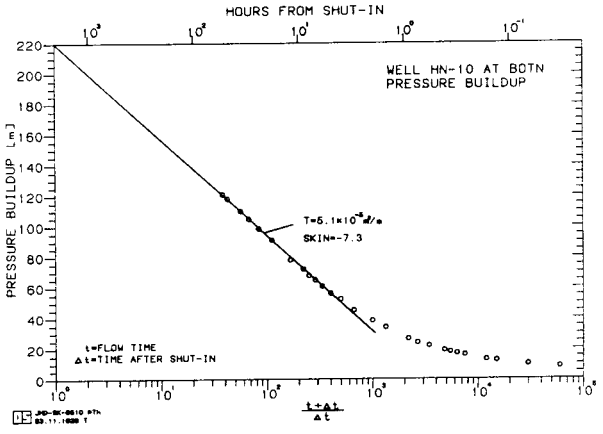


Fig. 21. A Horner diagram of pressure buildup at the Botn low-temperature field.

Original pressure corresponded to +187 m water level relative to the top of well LN-10, while six years later the level was down to about -180 m, a total decline of about 370 m. The total accumulated flow from the field at the end of 1981 was about 12 gigaliters. Seasonal variations in production rate are reflected in the drawdown diagrams.

An example of a Horner diagram from a pressure buildup test at the Botn field adjacent to the Laugaland field is shown in Fig. 21. The calculated permeability-thickness product is 1.8 darcy-m, corresponding to about 2 millidarcys, which is significantly lower than in most other exploited fields in Iceland.

Fig. 22 shows the drawdown in the Ytritjarnir field just north of the Laugaland field, due to a production of 46 kg/s. The approximate proportionality to the square root of time indicates that the flow is mainly along fractures, in good agreement with what is expected on the basis of the geological structure in the area.

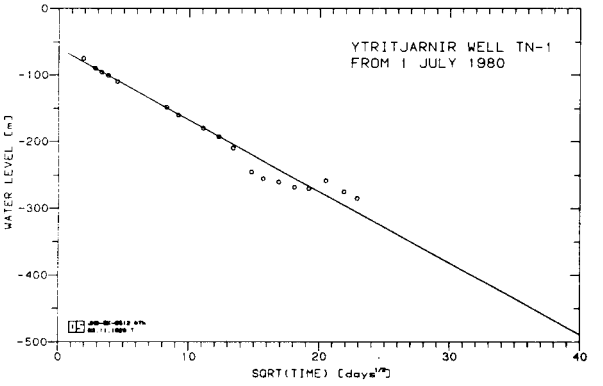


Fig. 22. Pressure drawdown in the Ytritjarnir field, showing an approximately linear variation with the square root of time. The deviations from the line are due to changes in flow rate.

THE NESJAVELLIR HIGH-TEMPERATURE FIELD

The Nesjavellir field is located in the northern part of the Hengill geothermal area (Bodvarsson 1951, Árnason et al., 1969). It is being explored with a view to a possible use for district heating in Reykjavík and for generation of electricity. Drilling started in the sixties and was resumed in 1982 after about 10 years' halt in development.

Well NG-6 which was drilled in 1982 has indicated the possibility of a 300°C steam zone at 800-1000 m depth. Fig. 23 shows the interpreted pressure profile in the reservoir at the location of this well. The reservoir seems to be overpressured to approximately 800 m depth, but the main feeder at 1085 m has an undisturbed pressure of 86 bar. The pressure profile in the reservoir thus indicates a steam zone of 86 bar pressure and 300°C temperature in the depth range 800-1000 m.

So far, vapor-dominated reservoirs have generally been found to have steam zones of about 240°C temperature and 32 bar pressure. The results from well NG-6 at Nesjavellir seem to indicate that steam zones outside the magical numbers of 240°C, 32 bar are possible in Nature. Further drilling, which is planned in the Nesjavellir field, will probably throw further light on this question.

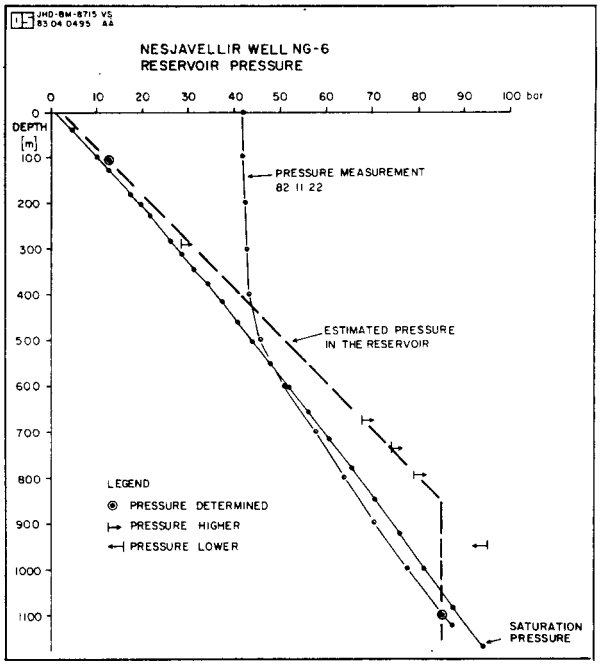


Fig. 23. A pressure profile in well NG-6 at Nesjavellir, indicating a 300°C steam zone at 800-1000 m depth.

DISCUSSION

The exploitation of geothermal fields in Iceland for a large variety of uses, especially in the past 2-3 decades, has provided a wealth of new data on the reservoir properties of the hydrothermal systems, and has shown that they are more diverse than previously thought.

Reservoir engineering studies were initiated in the Laugarnes low-temperature field in the middle 1960's, after several wells had been drilled in that area to depths of 1000-2000 m. When a sufficient number of wells became available in high-temperature fields, especially in the Svartsengi and Krafla fields, reservoir studies were also started in these fields. The main results of this work are reviewed in this paper. Several fields which have been exploited on a smaller scale, have not been mentioned, although they are of interest from the reservoir engineering point of view. These include the Selfoss low-temperature field (Tómasson and Halldórsson, 1981) in southern Iceland, and the Urridavatn low-temperature field in the Tertiary plateau basalts of eastern Iceland, both of which are used for district heating.

TABLE 2. PRODUCTION DATA FOR WELLS IN HIGH-TEMPERATURE FIELDS

Field	Well*) No	Year meas.	P_o (bar)	Tot.flow (kg/s)	Enthalpy (kJ/kg)	Steam (6 bar) (kg/s)	Power**) (MW_e)
Reykjanes	8	71	10	80	1100	16.5	7.5
	8	83	10	66.6	1102	13.8	6.3
	9	83	21	180	1300	54.4	24.7
Eldvörp	2	83	18	165	1270	47.5	21.6
Svartsengi	(2)	72	7.0	50	850	4.3	2.0
	3	72	7.5	72	990	11.1	5.0
	(4)	74	11.0	85	1040	15.1	6.9
	5	79	15	72	1040	12.8	5.8
	6	79	6.8	84	1040	14.9	6.8
	7	80	18.4	57	1040	10.1	4.6
	8	80	16.0	160	1040	28.4	12.9
	9	80	16.0	160	1040	28.4	12.9
	10	80	14.0	160	1000	25.3	11.5
	11	80	16.0	160	1040	28.4	12.9
Nesjavellir	5	77	7.0	33	1130	7.3	3.3
(N-Hengill)	6	83	9.1	26.7	2005	17.1	7.8
Hveragerði	6	79	6.7	58	1000	9.2	4.2
(S-Hengill)	7	79	3.4	32	870	3.1	1.4
	8	61	8.0	97	1140	21.9	10.0
Krafla	(1)	74	-	17.2	1675	8.3	3.8
	(3)	75	8.5	68	1100	14.0	6.4
	6	76	8.2	16.2	1486	6.3	2.9
	6	83	2.5	6.7	1248	1.9	0.9
	7	76	10.7	13.4	1780	7.1	3.2
	7	83	9.0	8.1	1214	2.1	1.0
	9	77	18.0	42.2	1230	11.3	5.1
	9	83	10.0	22.5	988	3.4	1.5
	(10)	76	23	52	1360	17.2	7.8
	11	77	10	44.2	1300	13.4	6.1
	11	83	10.4	4.6	1816	2.5	1.1
	12	79	7.9	6.5	>2676	6.4	2.9
	12	83	12.4	3.6	>2676	3.5	1.6
	13	83	8.5	9.2	2393	7.6	3.5
	14	83	11.9	12.7	2642	12.0	5.5
	15	83	7.6	3.5	2676	3.4	1.5
	16	83	3.8	8.0	1515	3.2	1.5
	17	83	14.2	10.7	1340	3.4	1.5
	19	83	12.2	8.9	2626	8.3	3.8
	20	83	12.9	10.0	1941	6.1	2.8
	21	83	20.3	27.4	1652	12.9	5.9
	22	83	5.3	30.9	1103	6.4	2.9
Námafjall	(4)	77	10.2	-	-	7.0	3.2
	(6)	77	9.0	-	-	3.8	1.7
	(7)	77	11.4	52.3	1288	15.5	7.0
	(8)	77	29.0	44.4	1093	9.0	4.1
	(10)	77	28.0	89.2	1270	25.7	11.7
	11	83	16.2	25.3	2320	20.0	9.1
	12	83	18.2	16.9	2260	12.9	5.9

*)Wells in parenthesis are damaged.
**)Calculated electric power based on 1 MW_e = 2.2 kg/s steam at 6 bar.

The temperatures encountered in the geothermal reservoirs range from less than 100°C in the low-temperature fields to over 300°C in some of the high-temperature fields. The geothermal fluids are usually low in dissolved solids and gases. An exception is the fields on the outer part of the Reykjanes peninsula, where seawater circulates in the neovolcanic zone which connects with the submarine axial zone of the Mid-Atlantic Ridge.

An interesting recent result of the work in the low-temperature fields, especially Laugarnes and Akureyri, is that the pressure buildup (drawdown) behavior supports strongly the assumption that the flow is mainly associated with fracture permeability. This result is not unexpected on geological grounds as surface outflow from hydrothermal systems is often observed to be along dikes, faults or boundaries between lava flows. There are some indications that similar conditions may exist in the high-temperature fields as well.

Permeabilities have been estimated for the various reservoirs exploited to date. These show wide variations between fields, and also within fields depending on the method used. Great care is needed in interpreting data from fractured reservoirs. Short-time interference tests usually give much higher permeabilities than longer-time tests, which probably reflects the nature of the flow along mostly linear fractures.

Overall global permeabilities for the various fields have been estimated using a thickness of 1000 m for the production reservoir, as most of the production wells are 1000-2000 m deep. The highest permeability, some 100 millidarcys, is found in the Reykir low-temperature field and in the Svartsengi high-temperature field. The lowest values, some 2 millidarcys, are found in the Akureyri fields. In Krafla, permeabilities of some 1-10 millidarcys are indicated. Intermediate values are found e.g. in the Laugarnes field, about 15 millidarcys.

The physical state of the high-temperature hydrothermal systems varies from one field to another, and also within one and the same field. The fields on the Reykjanes peninsula (Svartsengi, Eldvörp, Reykjanes) are liquid-dominated in their natural state, but the experience from Krafla, Námafjall and Nesjavellir shows that two-phase boiling systems may be just as common. The difference in well production characteristics from the two kinds of reservoirs is clearly demonstrated in Figs. 10 and 13. In the single-phase systems the well total flow is usually large and primarily controlled by the diameter of the well, while in the two-phase systems the total flow is smaller and is governed by conditions within the reservoir outside the well, and largely unaffected by the wellhead pressure. Some production data from individual wells in the various high-temperature fields have been compiled and are given in Table 2.

Another difference between the single- and the two-phase reservoirs concerns the changes in flow with time. In single-phase reservoirs the decrease in flow with time is primarily governed by the overall drawdown in the reservoir, and the flowing enthalpy remains constant. In two-phase reservoirs both mass flow and enthalpy change initially with time (Figs. 14, 15 and 18), while the long-term decline depends more on local conditions around each well.

ACKNOWLEDGEMENTS

We thank the State Electric Power Works and the District Heating systems of Reykjavík, Sudurnes, Akureyri and Seltjarnarnes for permission to use data from their fields. Many colleagues at Orkustofnun, in particular H. Jakobsson, have contributed to the preparation of this paper. Their contributions are greatfully acknowledged.

REFERENCES

Ármannsson, H., G. Gíslason and T. Hauksson, 1982. Magmatic gases in well fluids and the mapping of the flow pattern in a geothermal system. Geochim. Cosmochim. Acta, 46, 167-177.

Árnason, B., P. Theodórsson, S. Björnsson and K. Saemundsson, 1969. Hengill, a high-temperature thermal area in Iceland. Bull. Volcanol., 33, 245-260.

Arnórsson, S., 1977. Changes in the chemistry of water and steam discharged from wells in the Námafjall geothermal field, Iceland, during the period 1970-76. Jökull (Reykjavík), 27, 47-59.

Arnórsson, S., 1978. Precipitation of calcite from flashed geothermal waters in Iceland. Contr. Mineral. Petrol., 66, 21-28.

Björnsson, A., 1981. Exploration and exploitation of low-temperature geothermal fields for district heating in Akureyri, North-Iceland. Geoth. Resources Council Trans., 5, 495-498.

Björnsson, A., G. Johnsen, S. Sigurdsson, G. Thorbergsson and E. Tryggvason, 1979. Rifting of the plate boundary in North Iceland 1975-1978. J. Geophys. Research, 84, 3029-3038.

Björnsson, S., S. Arnórsson and J. Tómasson, 1972. Economic evaluation of the Reykjanes thermal brine area, Iceland. Am. Ass. Petrol. Geologists Bull., 56, 2380-2391.

Bodvarsson, G., 1951. Report on the Hengill thermal area. J. Engineer's Assoc. Iceland,

36, 1-48 (in Icelandic with a summary in English).

Bodvarsson, G., 1961. Physical characteristics of natural heat resources in Iceland. Jökull, (Reykjavík), 11, 29-38.

Bodvarsson, G., 1978. A field example of free surface testing. Proc. Fourth Workshop Geothermal Reservoir Engineering, Stanford, SGP-TR-30, 153-159.

Bodvarsson, G.S., S. Benson, O. Sigurdsson, G.K. Halldórsson and V. Stefansson, 1981. Analysis of well data from the Krafla geothermal field in Iceland. Proceedings Seventh Workshop Geothermal Reservoir Engineering, Stanford. SGP-TR-55, 71-76.

Bodvarsson, G.S., K. Pruess, V. Stefansson and E.T. Elíasson, 1982. Modeling studies of the natural state of the Krafla geothermal field, Iceland. Proceedings Eight Workshop Geothermal Reservoir Engineering. Stanford, SGP-TR-60, 211-217.

Bodvarsson, G.S., S.M. Benson, O. Sigurdsson, V. Stefansson, and E.T. Elíasson. The Krafla geothermal field, Iceland. 1. Analysis of well test data. Water Resources Research (in press).

Bodvarsson, G.S., K. Pruess, V. Stefansson, and E.T. Elíasson. The Krafla geothermal field, Iceland. 2. The natural state of the system. Water Resources Research (in press).

Bodvarsson, G.S., K. Pruess, V. Stefansson, and E.T. Elíasson. The Krafla geothermal field, Iceland. 3. The generating capacity of the field. Water Resources Research (in press).

Einarsson, P., 1978. S-wave shadows in the Krafla caldera in NE-Iceland, evidence for a magma chamber in the crust. Bull. Volcanol., 41, 1-9.

Franzson, H., 1983. The Svartsengi high-temperature field, Iceland. Subsurface geology and alteration. Geoth. Resources Council Trans., 7, 141-145.

Georgsson, L.S., 1981. A resistivity survey on the plate boundaries in the western Reykjanes peninsula, Iceland. Geoth. Resources Council Trans., 5, 75-78.

Gringarten, A.C., H.J. Ramey Jr., and R. Raghaven, 1972a. Pressure analysis for fractured wells. SPE Paper 4051, presented at the SPE 47th Annual Fall Meeting, San Antonio, Texas.

Gringarten, A.C., and P.A. Witherspoon, 1972b. A method of analysing pump test data from fractured aquifer. Proc. Symp. Percolation Fissured Rock, Int. Soc. Rock. Mech., Stuttgart, T3, 1-9.

Gudmundsson, J.S., 1983a. Injection testing in 1982 at the Svartsengi high-temperature field in Iceland. Geoth. Resources Council Trans., 7, 423-428.

Gudmundsson, J.S., 1982. Low-temperature geothermal energy use in Iceland. Geothermics, 11, 59-68.

Gudmundsson, J.S., 1983. Geothermal electric power in Iceland: Development in perspective. Energy, 8, 491-513.

Gudmundsson, J.S., T. Hauksson and J. Tómasson, 1981. The Reykjanes geothermal field in Iceland: Subsurface exploration and well discharge characteristics. Proceedings Seventh Workshop Geothermal Reservoir Engineering, Stanford, Dec. 1981. SGP-TR-55, 61-69.

Kjaran, S.P., G.K. Halldórsson, S. Thorhallsson and J. Elíasson, 1979. Reservoir engineering aspects of Svartsengi geothermal area. Geoth. Resources Council Trans., 3, 337-339.

Kristmannsdóttir, H., 1981. Wollastonite from hydrothermally altered basaltic rocks in Iceland. Min. Mag., 44, 95-99.

Pálmason, G., 1967. On heat flow in Iceland in relation to the Mid-Atlantic Ridge. In: Iceland and Mid-Ocean Ridges (ed. S. Björnsson), Soc. Sci. Islandica, Publ. 38, 111-127.

Pálmason, G., 1981. An assessment of the geothermal resources in Iceland. Proc. Energy Conf. Reykjavík, June 1981, 121-137.

Pruess, K., G.S. Bodvarsson, V. Stefansson, and E.T. Elíasson. The Krafla geothermal field, Iceland. 4. History match and prediction of individual well performance. Water Resources Research (in press).

Sigurdsson, O., 1978. Flow properties of the upper reservoir system in Krafla. Orkustofnun Report OSJHD7851 , 36 pp. (in Icelandic).

Sigurdsson, O. and D. Tiab, 1983. Analysis of pressure pulses resulting from magmatic activity in the vicinity of geothermal wells. Paper SPE 11751 presented at the 1983 California Regional Meeting, Ventura, Calif., March 23-25, 1983.

Stefansson, V., 1981. The Krafla geothermal field, Northeast Iceland. In: Geothermal Systems: Principles and Case Histories (ed. L. Rybach and L.J.P. Muffler), John Wiley & Sons, 273-294.

Stefansson, V. and B. Steingrímsson, 1980. Production characteristics of wells tapping two phase reservoirs at Krafla and Námafjall.

Proceedings Sixth Workshop Geothermal Reservoir Engineering, Stanford, SGP-TR-50, 49-59.

Thórhallsson, S., 1979. Combined generation of heat and electricity from a geothermal brine at Svartsengi in S.W. Iceland. Geoth. Resources Council Trans., 3, 733-736.

Thorsteinsson, T., 1976. Redevelopment of the Reykir hydrothermal system in southwestern Iceland. Proceedings Second United Nations Symposium on the Development and Use of Geothermal Resources. Lawrence Berkeley Lab., Univ. of Calif., 2173-2180.

Thorsteinsson, T. and J. Elíasson, 1970. Geohydrology of the Laugarnes hydrothermal system in Reykjavík, Iceland. Geothermics, Spec. Iss. 2, v. 2, 1191-1204.

Tómasson, J. and G.K. Halldórsson, 1981. The cooling of the Selfoss geothermal area, S-Iceland. Geoth. Resources Council Trans., 5, 209-212.

Proceedings Ninth Workshop Geothermal Reservoir Engineering
Stanford University, Stanford, California, December 1983
SGP-TR-74

MULTIPLE RESERVOIRS IN THE MOFETE FIELD, NAPLES, ITALY

R. Carella, M. Guglielminetti

Agip S.p.A.
Milan, Italy

ABSTRACT

Mofete field, located near Naples, in southern Italy, lies within the large Campi Flegrei caldera.
Drilling for geothermal fluids was carried out unsuccessfully in 1939-1954. AGIP, in joint venture with the national utility ENEL, after intensive exploration efforts, resumed drilling at the end of 1978; several new deep wells indicate the presence of a water dominated field in Mofete with three reservoirs (only the shallowest of which was reached by previous wells). The deepest aquifer, tapped by well Mofete 5 at the depth of about 2700 m, contains hypersaline fluids(about 516 000 ppm TDS at atmospheric conditions corresponding to about 150 000 ppm in the reservoir) with a bottom hole temperature of about 360°C. The intermediate level, reached by well Mofete 2 at 1900 m depth, is characterized by low salinity fluids (about 38 000 ppm TDS at the surface corresponding to 18 000 ppm calculated in the reservoir) with a reservoir temperature of 340°C. The uppermost reservoir, tapped by wells Mofete 1, 3D, 7D, 8D and 9D ranges between 550 and 1500 m depth and has water with salinity ranging from 40 000 to 76 000 ppm TDS at the surface corresponding to 28 000 to 52 000 ppm in the reservoir with a bottom temperature of 230-308°C. The uppermost aquifer is in fractured volcanic rocks while the other two are in a metamorphosed volcano-sedimentary complex.
Long term production and injection tests will be carried out shortly to ascertain the main characteristics of the field.

INTRODUCTION

Location

The Mofete field is located within the Campi Flegrei caldera, near Naples, in southern Italy (see Fig. 1). The caldera extends west of Naples for about 15 km. The Mofete field lies at the western limit of the caldera, along an isthmus between the Gulf of Pozzuoli and the Tyrrhenian sea.

The area, occupied by low hills and with a mean elevation of 50-100 meters, is highly inhabited.

Summary history of exploration and development

Exploration for steam in the Mofete area began in 1939 where the local utility,through its geothermal subsidiary SAFEN, started exploration work interrupted by the war in 1943 and resumed in the years 1949-1954.
Several shallow and some deep wells were drilled, which indicated the presence of a hot salt water dominated system at shallow depth and temperatures as high as 325°C at a depth of 1800 m. The then existing techniques were not mature and the company abandoned its efforts. In 1978 AGIP, the Italian state owned oil & gas company, acting as operator, in joint venture with the national utility ENEL, was granted a lease and resumed the activities in the area. An extensive exploration programme was carried out which included geology, geochemistry, gravity and magnetic surveys, as well as some seismic lines.
The gravity data indicated a regional subcircular negative anomaly centered in the Gulf of Pozzuoli, surrounded by a ring of positive anomalies. Magnetically large positive anomalies are located offshore, as well as on land in the Astroni area of the positive gravity ring.
Most of the remaining positive gravity anomalies are characterized by negative magnetic anomalies (Fig. 2). The electric surveys show at shallow levels strong resistivity minima in correspondence to several areas, the origin of which is probably due to presence of hot saline waters (Fig. 3). The overall geologic interpretation of the geophysical picture (as shown in the interpretative schematic section in Fig. 4) is that of a ring of lava intrusions which locally have been altered by hot saline fluids rising through radial faults. The presence of such fluids is indicated by the low resistivity values which are coupled with a marked reduction of the magnetic susceptivity of the altered rocks.
The seismic results have been very poor and dif-

ficult to interpret.
The geochemical surveys indicate that the thermal waters of the Campi Flegrei caldera are a mix of local meteoric waters and deep hot waters of marine origin with indications of local leakage of steam.
The first AGIP deep well, Mofete 1, was drilled in 1978 to the depth of 1606 m and indicated the presence of a water dominated reservoir at 500-900 m in fractured volcanics with large quantities of saline water (43 000 ppm TDS, corresponding to 30 000 ppm TDS at reservoir conditions) with a temperature of 247°C. Uncommercial quantities of fluids (65 000 ppm TDS at surface, corresponding to 39 500 ppm in the reservoir) were produced from below 1223 m. Well Mofete 2, drilled in 1979 (500 m NW of well n° 1) to TD 1989 m has encountered in fractured volcano-sedimentary rocks (around 1300 and 1990 m) saline fluids (38 000 ppm TDS, corresponding to 18 200 ppm at reservoir conditions) with a temperature of 337°C.
AGIP subsequently completed the deep well n° 5, at TD 2700 m, and the directionally drilled n° 3D, 7D, 8D and 9D at depths between 907 and 1909 m; deviated drilling was carried out in order to make the best use of the limited available land in this highly inhabited region. Well n° 5 produced for a short period from 2700 m very hypersaline fluids (over 500 000 ppm TDS at atmospheric conditions corresponding to about 150 000 ppm in the reservoir) at a bottom hole temperature of 347°C. Well 3D, 7D, 8D and 9D tapped the Mofete 1 reservoir between 500 and 1500 m vertical depth (with a bottom temperature of 230-308°C and an average salinity of 40 000-76 000 ppm TDS at atmospheric conditions, corresponding to 28 000-52 000 ppm in the reservoir).

GEOLOGY

The Campi Flegrei caldera, on the western flank of which is located the Mofete field, has a diameter of 15 km. The core of this large geologic feature lies in the sea (Gulf of Pozzuoli) and only its northern half is preserved on land, albeit substantially modified by collapses, sea ingressions followed by emergence and local volcanic episodes.
The latest volcanic event is the formation of the Monte Nuovo volcano in 1538, but the continuing strong ground deformation episodes and connected microseismic events indicate a permanent underground activity due to magmatic and phreato-magmatic phenomena. Fumaroles and hydrothermal activity are recorded on the sea bottom in the Gulf of Pozzuoli, as well as on land at the Solfatara, at Agnano and in the Mofete area. Outcrops in Mofete area consist of volcanics ("yellow tuffs"). In this area faults with WSW-ENE, N-S and NNW-SSE directions have been located either through direct examination or by interpretation of an elongated area of altered outcrops. Circular structures of volcanic origin abound in and around Mofete.
The subsurface, as indicated by the wells drilled, consists in volcanic and volcano-sedimentary rocks. The lithologic succession and relevant thickness, from top to bottom, is as follows (see Fig. 5):
1) Yellow, green and gray tuffs: 180-590 m.
2) Tuffs of marine origin with some interbedded lava beds: 500-800 m.
3) Trachitic-latitic lavas (10-550 m).
4) Tuffs with interbedded quartzitic-feldspathic siltites: 500-600 m.
5) Trachitic-latitic lavas with interbedded tuffs and siltites (deep section in well Mofete 5): 800 m.

There are no clear marker beds and therefore correlation between wells is extremely difficult. From the hydrothermal paragenesis point of view, the following zones and relevant alteration minerals can be detected (depth ranges of top of zone in brakets).
- argillitic zone (outcropping): montmorillonite, zeolite, calcite;
- phyllic zone (250-400 m): chlorite, calcite;
- phyllic-propylitic zone (500-800 m): chlorite, illite, calcite, adularia, epidote, pyrite;
- propylitic-potassic zone (850-1300 m): quartz, calcite, illite, adularia, calcite, epidote;
- low rank thermometamorphic zone (1700-2200 m): actinolite, diopside, tourmaline, garnet, pyrrhotite.

The hydrothermal minerals in the lowermost section (presence of garnet) are indicative of temperature above 320°C, whilst the propylitic epidote-bearing zone should indicate a temperature of 240-260°C. The depth of the various alteration zones varies with location: well n° 2 is the more strongly altered and at shallower depth than the other wells, while n° 5 shows the less alteration.

FIELD DESCRIPTION

Reservoirs

A shallow zone from surface to a depth of a few hundred meters is highly permeable. Below it, tuffs, alterated to argillaceous and argillaceous phyllic rocks, provide an adeguate caprock also through self sealing processes, due to hydrothermal circulation. The deeper section is still basically impervious except when fractured zones provide sufficient permeability to act as reservoir. As indicated, rocks are generally compact and permeability is mainly due to

faulting and fracturing. Therefore the location of the reservoirsis erratic and unpredictable. Core examination has indicated the existence of fractures with inclination from 45° to subvertical; such fractures are frequently cemented by hydrothermal minerals such as illite, chlorite, epidote and quartz. Open fractures are indicated by loss of circulation zones, sometimes very conspicuous; potential productive zones are shown by temperature logs.

In well n° 1 total loss of circulation was encountered at 300-450 m, and partial losses at 850 and 1450 m. Temperature logs show from 600 to 1000 m and between 1200 and 1400 m isothermal zones which could be fluid bearing. Finally at 1550 m a sharp temperature reversal could be due to water influx. Tests have confirmed water bearing reservoirs at 600-1000 m and at 1223-1606 m.

Well n° 2 incurred severe losses of circulation in the 1300-1400 m interval and at 1950 m. Temperature logs show a zero increase at 1300-1350 m and between 1900 and 1989 m. Tests of the interval 1272-1989 m indicate one or more producing levels, possibly in corrispondence with the lost circulation zones at the top and bottom of the interval.

Well n° 3D, which encountered a conspicuous loss of circulation zone at 250-400 m, has an isothermal profile between 400 and 700 m (with a temperature decrease at 600 m) and between 1300 and 1450 m. Tests below 1297 m had negative results, while the perforated interval at 440-665 m is a poor producer, possibly due to formation damage and to the presence of two separate productive levels at different temperature (higher in the upper level) thereby creating an interference and thus showing an intermittent production pattern.

In well n° 5 formation were tight, even in the lowermost section, in which during a short production test a flow of highly saline brine could not be sustained.

Wells 7D, 8D and 9D show evidence,on the basis of fluid chemistry and testing, of a substantial common reservoir at 500-1500 m (vertical depth), which is the same shallow reservoir of wells 1 and 3D. In well n° 7D substantial losses of circulation were met at a deviated depth of 1250-1411 m (1100-1300 m vertical depth); the top of such zone is permeable from the temperature log interpretation.

Well n° 8D has a good permeability at 600-700 m deviated depth (515-650 m vertical depth).

In well n° 9D there is a highly permeable interval at 750-790 m deviated, corresponding to 720-760 m vertical depth. A deep level (1042-1648 m) produced limited amounts of brine.

Temperature distribution

Several temperature logs were run in the various wells. Although different instruments were used, the main tool has been the Amerada-Kuster recorder. The logs selected for an estimate of the equilibrium temperature of reservoir are in general the ones which were run as long as possible after the end of circulation or testing. For the purpose of locating the permeable zones, the temperature logs run shortly after completion of drilling were considered.

An example of temperature profiles interpretation in the Mofete field is hereafter given for well n° 1 (Fig. 6). The temperature profile immediately after drilling (prof. 1) shows two zones of likely convection, at the depths of 550-950 and 1200-1400 m; at both depths some minor losses of circulation occurred.

By the time this profile was run, the shallower horizon was already cased off, since higher temperatures were encountered at greater depth. The well was completed at the deepeer horizon, with a 5" slotted liner.

The equilibrium temperature profile (prof. 2) two months after the end of drilling, again shows the same convective horizons, but confirming the shallow and minimizing the deepeer one. After displacement with nitrogen, the well proved fluid inflow from the deepeer horizon at a limited flow-rate. The well was therefore perforated at the shallower horizon (550-896 m)obtaining a good production; even though the reservoir temperature was lower than that of the previously tested zone, its well head temperature was higher because of higher well head pressure due to higher permeability.

Table 1 - Mofete field - Maximum measured temperatures at equilibrium (°C)

	Well 1	Well 2	Well 3D	Well 5	Well 7D	Well 8D	Well 9D
Shallow reservoir	247	-	230-275	-	301	234	210-308 (°)
Intermediate reservoir	-	337	-	-	-	-	-
Deep reservoir	-	-	-	347	-	-	-

The temperatures measured in the wells (Table 1) are in good agreement with the temperatures derived from mineral alteration studies and with Na^+/K^+ geothermal data (except for well n° 5). The highest gradient is shown by well n° 2 with almost 340°C at 1989 m (TD), whilst the highest

(°) - Temperature recorded during drilling (not stabilized).

temperature was measured in well n° 5 at 2700 m (347°C). Isotherm maps (Fig. 7) clearly indicate a closed round anomaly with a radius of 0.5 km near surface, centered on wells 2 and 3D. The shallow isotherms show a culmination in correspondence to well n° 3D with 150°C at a depth of only 200 m. Well n° 3, deviated to the west, has shown evidences of a temperature plume with a decrease in temperature at about 600 m.

Fluid characteristics and theoretical model of the field

Chemical composition of the brine was measured at atmospheric pressure and is given in Table 2 hereunder; however data were also calculated at reservoir conditions for some selected wells (see Table 3). As can be seen from the chemical data, the composition and ratios of elements in well n° 1, shallow pay, are similar to those of the fluids tapped in well 3D, 7D, 8D and 9D. An increase of salinity with depth is recorded in the wells n° 1 and n° 9D brines. Such increase can be due to the higher formation temperatures, which rise with depth from 230 to 308°C. As concern comparison of the brines of the shallow pay with those of the intermediate pay of well n° 2, some ratios, like Na/Cl, point to a common origin. However the much lower salinity of n° 2 well brines at the same depth and at a short distance from the deeper part of the shallow aquifer can be explained by considering the two reservoirs separated.
The brines of the deep section in well n° 5 are conspicuously different from the rest; water-rock interaction could have played a role.
A possible model of how the Mofete field originated, taking into account fluid chemistry and other elements, can be envisaged as follows: in a first deep reservoir (evidenced in well Mofete 5) the original sea water brine was concentrated to the present values because of evaporation due to the effect of the high temperature and limited recharge; consequently there was a loss of steam which migrated to the upper reservoirs. During its ascent the steam entered into the Mofete 2 reservoir and by condensing, because of lower temperature, caused a consistent dilution of the Mofete 2 brine which again one must suppose poorly connected with the seawater recharge zone. A very minor quantity of steam remained to alter only marginally the upper reservoir (wells 1, 3D, 7D, 8D and 9D) better connected with the sea, and to escape at surface.

Pressure distribution

Pressure was measured by different tools with the main instrument used being the Kuster-Amerada recorder. A reconstruction of the static pressure versus depth (see Fig. 8) with measurements recorded in each well in correspondence to the different reservoir levels, shows a common line corresponding to the hydrostatic pressure line, except for the points related to well n° 5 wich are shifted towards higher pressures. We therefore conclude that the reservoir of all wells (except n° 5) are interconnected and in communication approximately at sea level.

WELL LOGGING AND TESTING

Well logging

Since Mofete field is in volcanic formation, reliability of conventional electric logs is problematic; in effect a calibration for quantitative estimate of petrophysical parameters is not available at the moment. A complete set of logs was run in the first wells in order to examine the possibility of an integrate interpretation of the data. The interpretation led to a reduced log programme including DLL, GR, SP, BGT, DDDHC, HTT; the GR log has proved particularly useful to recognize the lithology and the other logs to detect the fractured layers.

Well testing

Up to now, only short tests have been carried out on Mofete wells, with a maximum amount of liquid discharged at surface of about 5000 m^3 per test (due to the pit dimensions). In the course and at the end of drilling, tests were at first carried out through drill strings (DST); these tests, later abandoned, provided results which permitted to select possible pay zones, even though only on a qualitative basis. A test that has been commonly used, during and at the end of the drilling, has been the injectivity test; this test is conducted whenever potential interesting intervals are indicated by temperature trends, circulation losses and mineral alterations. The procedure for injectivity test is as follows: (1) Injecting for short periods (15 min each) at different flow rates in order to be able to select a proper flow rate for a prolonged injection; (2) injecting at the selected flow rate, observing pressure build-up for 12 hours; (3) stopping injection and observing fall-off for 12 hours. Opposite the intervals selected for production, slotted liners are installed to prevent well sloughing. The wells are discharged, with the drilling rig still on site, through a test line which includes a silencer and allows to obtain the production parameters (flow rate, enthalpy, pressures, temperatures) with the Russel James method. Other parameters, like the transmissivity and skin

factor, are obtained by pressure build-up and drawdown. These tests are generally short lasting, because of the limited volume of storing pits and provide only preliminary data. In some cases, when a potential production zone has been cased-off because a deeper pay was the target but its test was unsuccessful, casing was perforated by shaped charges. Notwithstanding the method is not the optimal for geothermal production, it was successful in the case of Mofete 1 well; shooting density was of 13 charges per m, from 550 to 896 m depth, resulting in a commercial production.

Once the drilling rig has been moved, beside the measurements with the Russel James method, in some wells (Mofete 1, 2) a pressure separator was used to allow production measurements and sampling of the two separated phases with more accuracy (Fig. 9). At the end of the production test, when the well was shut-up, a pressure build-up was carried out with a bottom-hole gauge, while initial draw-down could be conducted only when nitrogen displacement to induce the well was not necessary.

In Table 4 the data and the results of tests conducted in the field are indicated.

As can be seen from the above mentioned table, the upper reservoir has an enthalpy of 1100 kJ/kg while the intermediate one has 1600 kJ/kg. The transmissivity of the upper reservoir(20E-9 m^3/Pa s) is higher than the one of the intermediate reservoir (4E-9 m^3/Pa s).

The reservoir fluid in Mofete field, under static conditions, is single phase (liquid), with a dissolved CO_2 content varying from 1% to 5% by weight with the exception of well n° 2 reservoir in which the CO_2 was calculated to be flashed at static reservoir conditions.

The thermal and hydrogeologic conditions cause a two-phase state in the reservoir under dynamic conditions, because of pressure losses leading to evaporation. As a consequence the two phase fluid increases its enthalpy in its way towards the wellbore (since the rocks at a higher temperature transfer heat to the cooler boiling fluid) and upflows at nearly constant enthalpy (a slight decrease is due to work against gravity and to heat losses) whithin the wellbore (fig. 10). Because of CO_2 content, the fluid state is actually two-phase, two component, with the liberated CO_2 being present at slightly higher pressures than H_2O vapour.

FUTURE PROGRAMS

The next step foreseen consists of the evaluation of the size and behaviour of the reservoir and of the complementary corrosion and scaling studies. For the development of this state of experimentation it is necessary to put a well into long term production; the separated liquid will be disposed off by reinjecting it into another well.

To conduct the long term production-reinjection tests, two wells drilled from the same platform have been selected, to avoid installing long pipelines between platforms in the highly urbanized area of Mofete.

Wells n° 1 and n° 7D were selected as production and reinjection wells respectively, both in upper reservoir; 3 other wells will serve as observers for pressure interference. They are n° 2, in the intermediate reservoir, and n° 8D and N° 9D in the upper reservoir. During these tests the productive and reinjective performances of the wells will be observed for a period of 2 months; the hydrothermal conditions of the wells will be determinated to evaluate possible production regimes and to create the basis for a techno-economical evaluation of the field exploration. Moreover, the feasibility of reinjecting the separated liquid will be verified at selected temperatures, chosen on the basis of actual computation of the deposition kinetics of various elements, to avoid the scaling at the surface and in the reservoir.

The test plant was designed according to the scheme indicated in Fig. 11 with the purpose of allowing continuity of operations, flexibility of operating condition, bleeding of the fluids for chemical testing and accurate measurements of the flow rates. The second separation stage is foreseen to feed the chemical testing section at different temperatures independently from the temperature in the reinjection line. Injection of chemical inhibitors is foreseen, and several point of injection and sampling are envisaged to control the fluids, with various dosage units available. Corrosion tests are planned with the aim of finding out the most suitable materials for the future plants; they will be carried out not only on liquids but also on steam with the use of specimens and spools.

Immediately after the long term test and on the basis of results obtained, work-overs are planned to be carried out on some wells of the field. For instance, the well n° 9D, that in the course of drilling has encountered an upper interval with a good transmissivity, is actually completed in a deeper interval with poor productive characteristics; therefore the upper interval shall be opened to the production, perforating the casing with shaped charges. The wells 7D and 8D will be again put into production and the fluid will be reinjected for the time necessary (10-12 day) to evaluate their stabilized characteristics.

Moreover a research program of stimulation in-

terventios is being completed and a pilot stimulation job could be carried out by mid 1984 in well n° 3D (perforated interval 430-665 m). The testing program will provide the main information for the installation of a small plant for the experimental generation of electric energy. It is thought that a back pressure turbogenerator of 3 MW can be installed at the end of 1984. If such activity is successfull frilling of new wells both for production and reinjection purposes will be carried out both from the existing pads and from new ones mainly through deviated wells.
Concurrently a first commercial power plan of 15-20 MW could be installed in the next few years.

ACKNOWLEDGEMENTS

The authors wish to thank the management of Agip S.p.A. for permission to publish this paper. They extend their appreciation to the Staff of Geothermal Exploration and Production Departments and to Mr. P.E. Liguori of DAL who cooperated in this work.

REFERENCES

1. P. Armienti et al.: "Magma evolution within a shallow chamber: the Phlegraean Fields" Journal of volcanology and geothermal research, Dec. 1982.
2. P. Bruni et al.: "Risultati gedlogici preliminari dell'esplorazione geotermica nell'area dei Campi Flegrei", Rend. Soc. Geol. It. 1981.
3. G.L. Chierici et al.: "Mofete field, Italy numerical model study", European Geothermal Update, Munich Dec. 1983.
4. D. Cioppi et al.: "Evaluation of the Mofete High Enthalpy Reservoir"CEC , Second Int. Seminar Geothermal Research,Strasburg; March 1980.
5. P. La Torre et al.: "Geothermal well location in southern Italy": the contribution of geophysical methods" Boll. Soc. Geof. Teor. e Appl. Sept. 1980.
6. R. Nannini et al.: "Geothermal exploration" Boll. Geof. Sept. 1982.
7. M. Rosi et al.: "Phlegraean Fields", Journal of volcanology Dec. 1982.

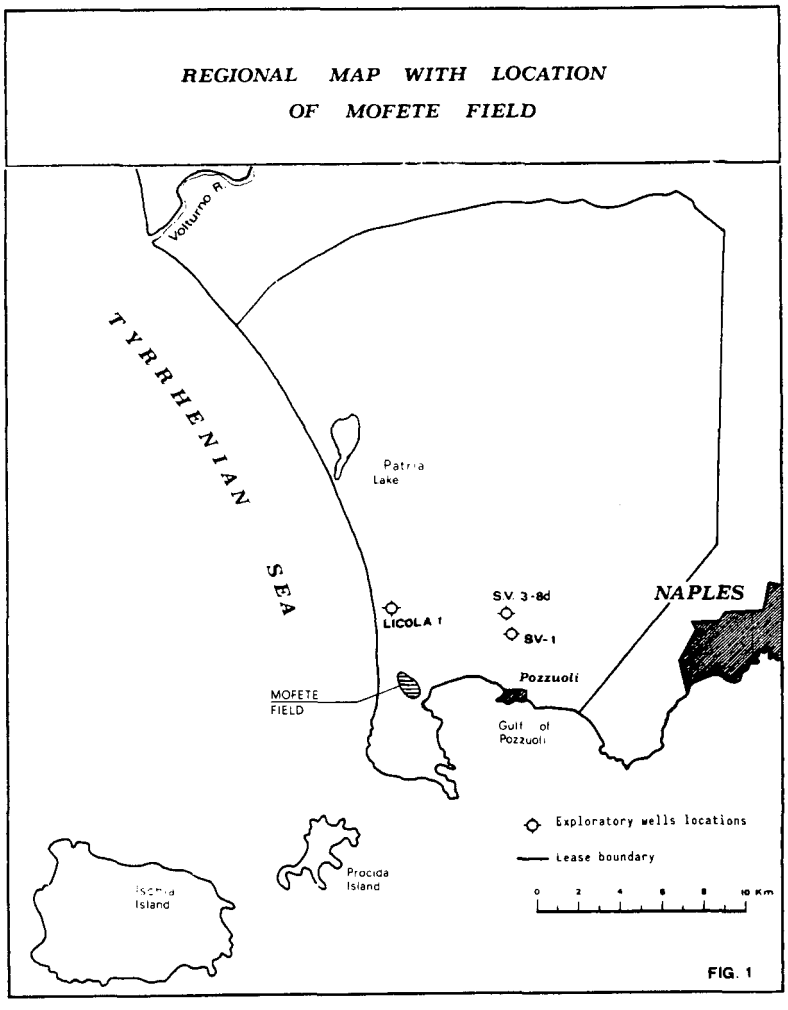


FIG. 1

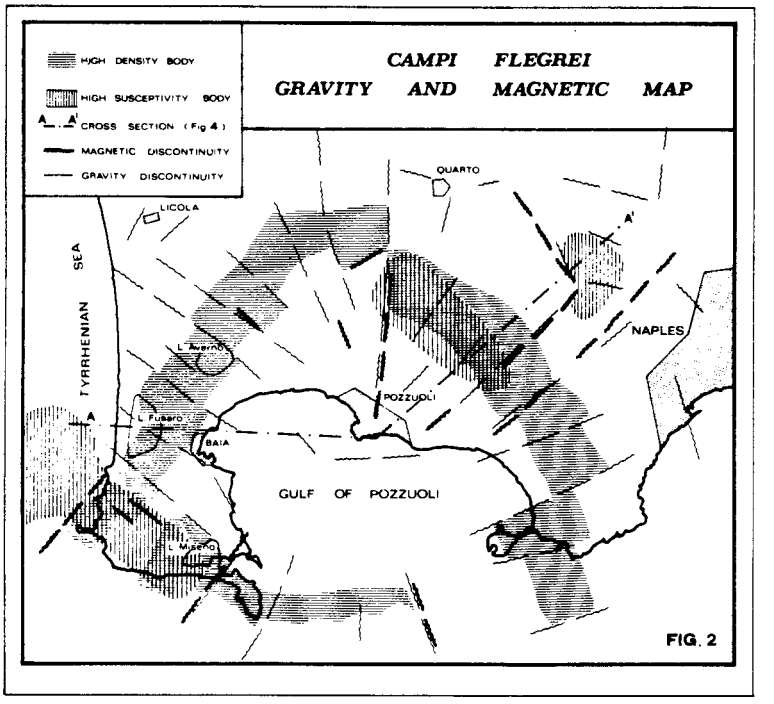

HIGH DENSITY BODY
HIGH SUSCEPTIVITY BODY
A A' CROSS SECTION (Fig 4)
MAGNETIC DISCONTINUITY
GRAVITY DISCONTINUITY
CAMPI FLEGREI
GRAVITY AND MAGNETIC MAP
QUARTO
LICOLA
SEA
TYRRHENIAN
A
A'
NAPLES
L. Averno
POZZUOLI
L. Fusaro
BAIA
GULF OF POZZUOLI
L. Miseno

FIG. 2

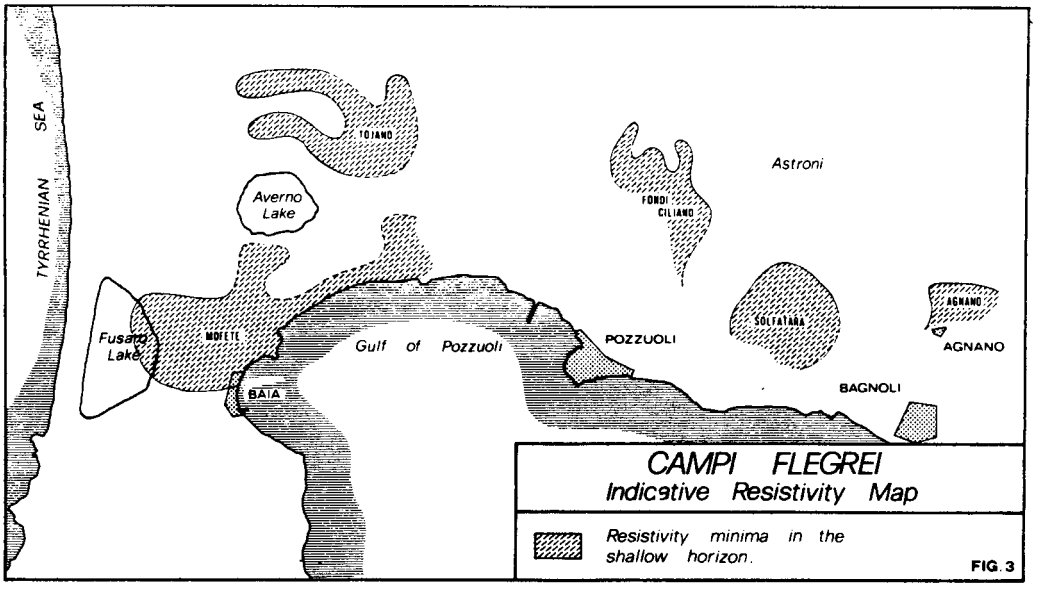

TYRRHENIAN SEA
TOIANO
Averno Lake
Astroni
FORDI CILIANO
Fusaro Lake
MOFETE
Gulf of Pozzuoli
POZZUOLI
SOLFATARA
AGNANO
AGNANO
BAGNOLI
BAIA
CAMPI FLEGREI
Indicative Resistivity Map
Resistivity minima in the shallow horizon.

FIG. 3

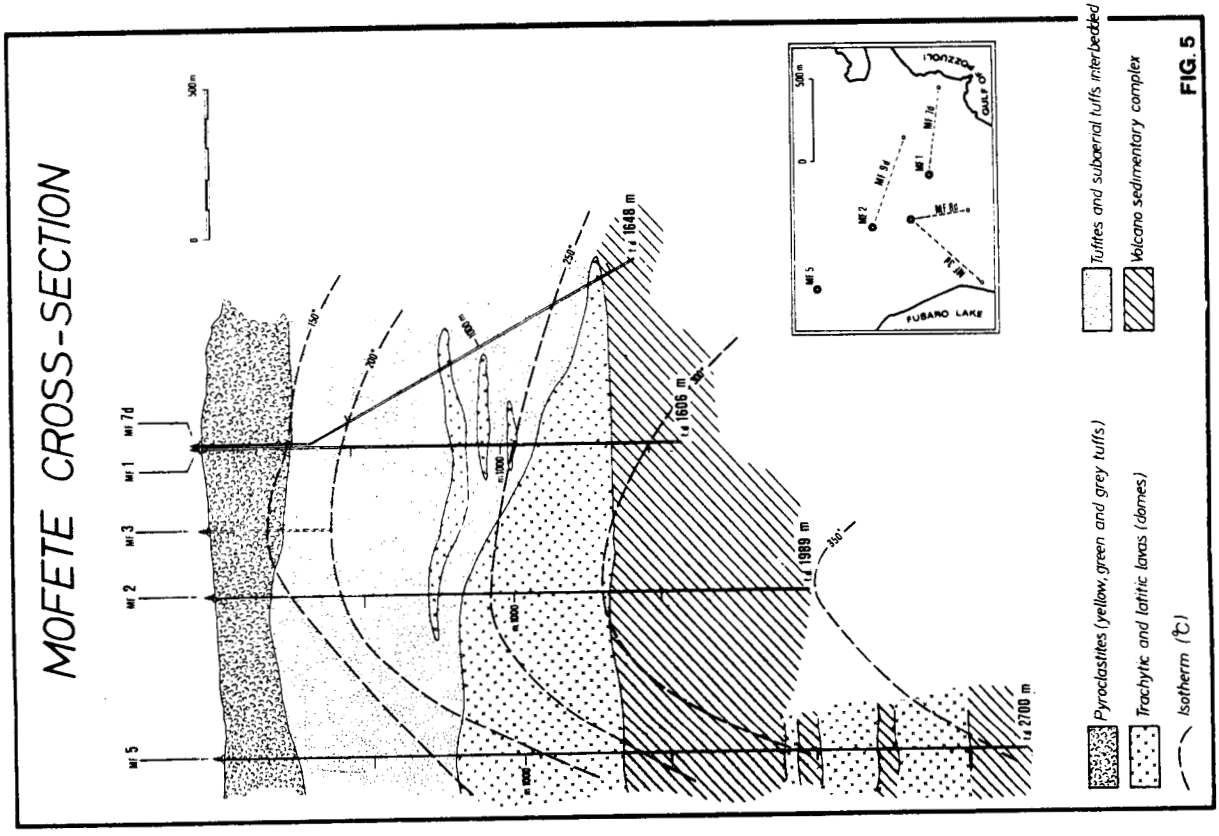

MOFETE CROSS-SECTION
MF 7d
MF 1
MF 3
MF 2
MF 5
1648 m
1606 m
1989 m
2100 m
250°
300°
350°
1000
1500
2000
500m
0
POZZUOLI
GULF OF
MF 7d
MF 1
MF 3
MF 2
MF 5
FUSARO LAKE
Tufites and subaerial tuffs interbedded
Volcano sedimentary complex
Pyroclastites (yellow, green and grey tuffs)
Trachytic and latitic lavas (domes)
Isotherm (°C)

FIG. 5

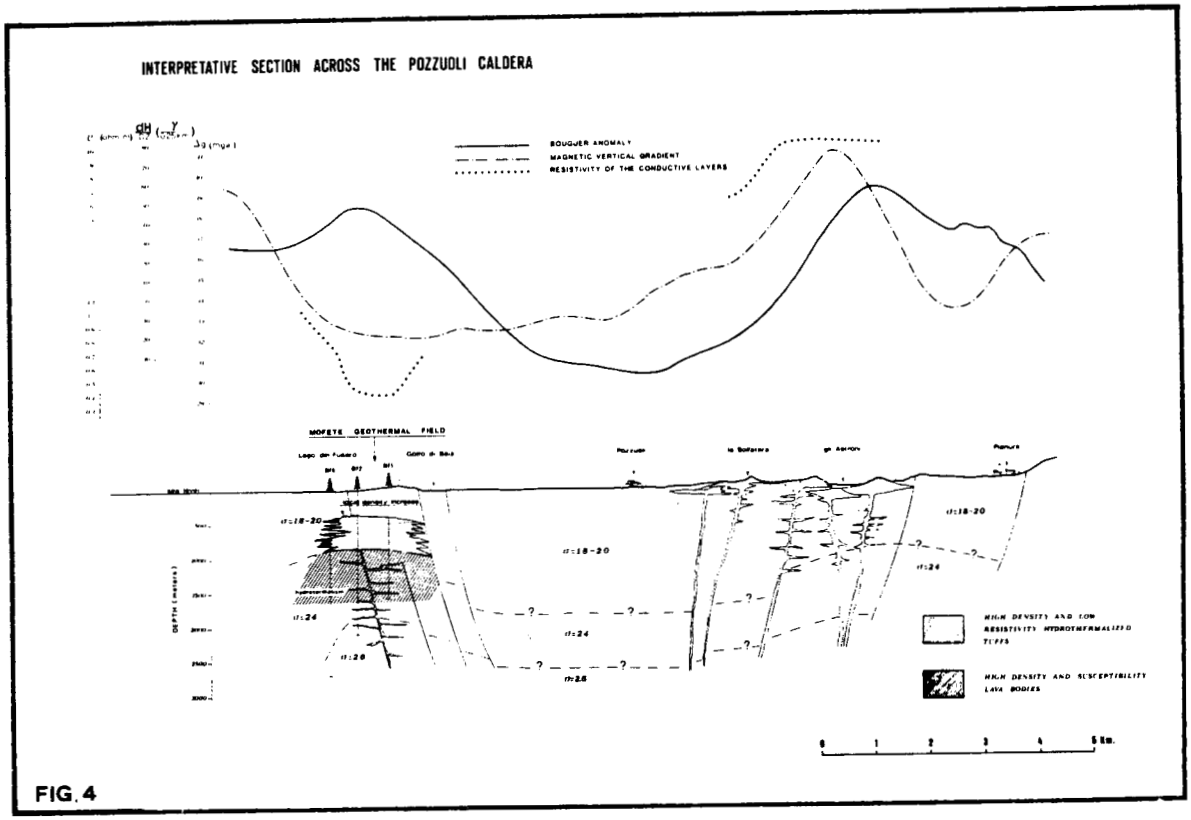

INTERPRETATIVE SECTION ACROSS THE POZZUOLI CALDERA
BOUGUER ANOMALY
MAGNETIC VERTICAL GRADIENT
RESISTIVITY OF THE CONDUCTIVE LAYERS
MOFETE GEOTHERMAL FIELD
Lago del Fusaro
Cigno di Baia
Baia
Miseno
Monte
Solfatara
Averno
Pozzuoli
MF 6
MF 7
MF 1
rt:18-20
rt:24
rt:28
HIGH DENSITY AND LOW RESISTIVITY HYDROTHERMALIZED TUFFS
HIGH DENSITY AND SUSCEPTIBILITY LAVA BODIES
0 1 2 3 4 5 Km.

FIG. 4

WELL MOFETE 1
STATIC TEMPERATURE PROFILES

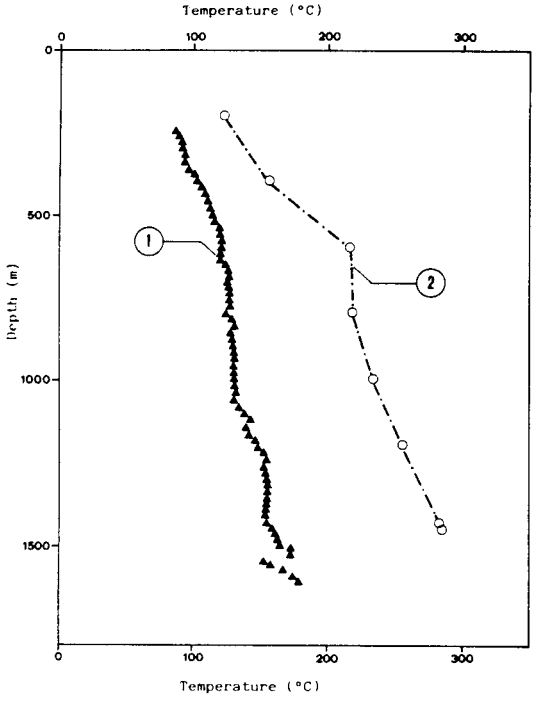
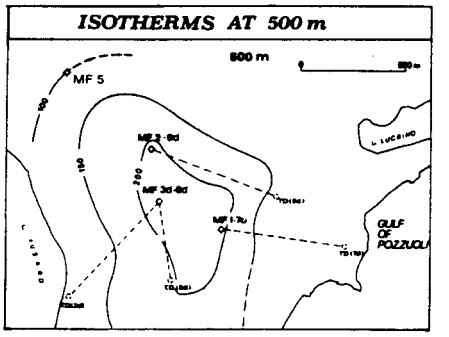


FIG. 6

MOFETE FIELD ISOTHERMS (°C)



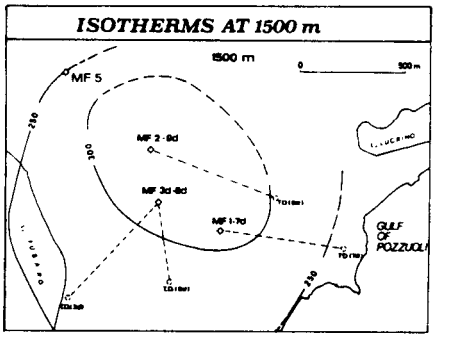


FIG. 7

MOFETE FIELD PRESSURE-DEPTH RELATIONSHIP

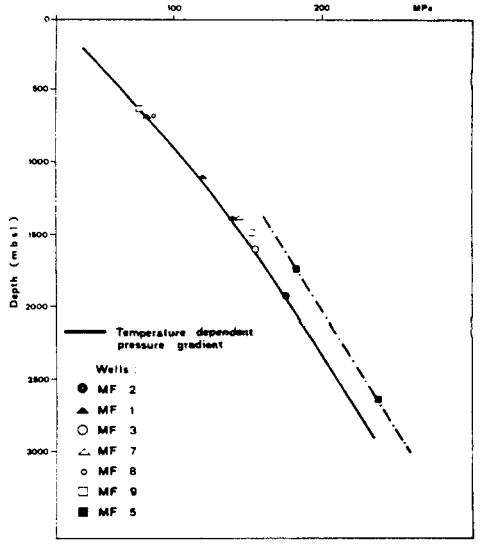


FIG. 8

MOFETE PIT-TEST UNIT
WITH PRESSURE SEPARATOR

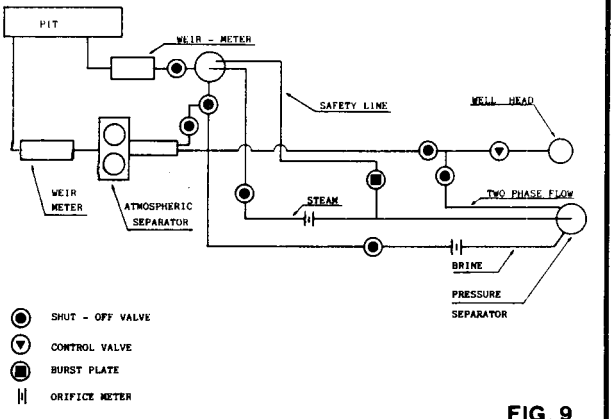
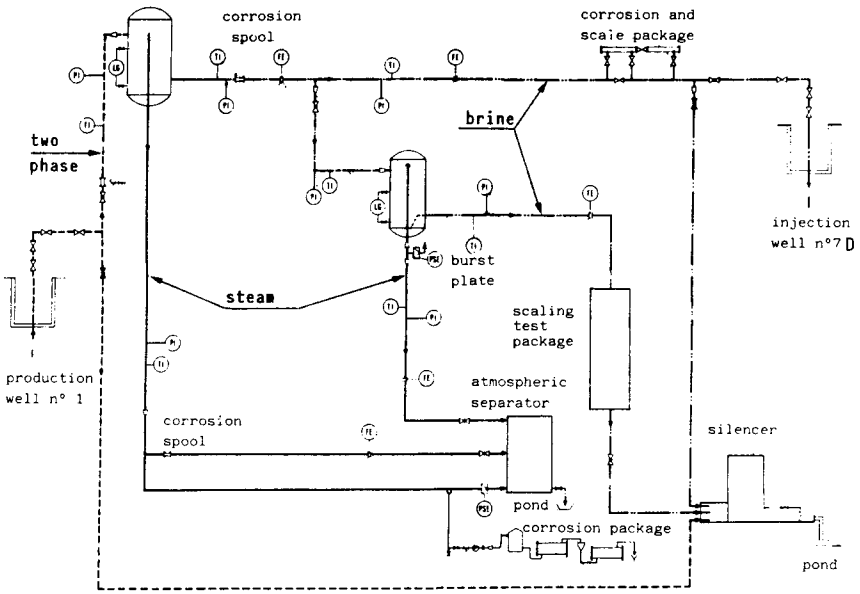
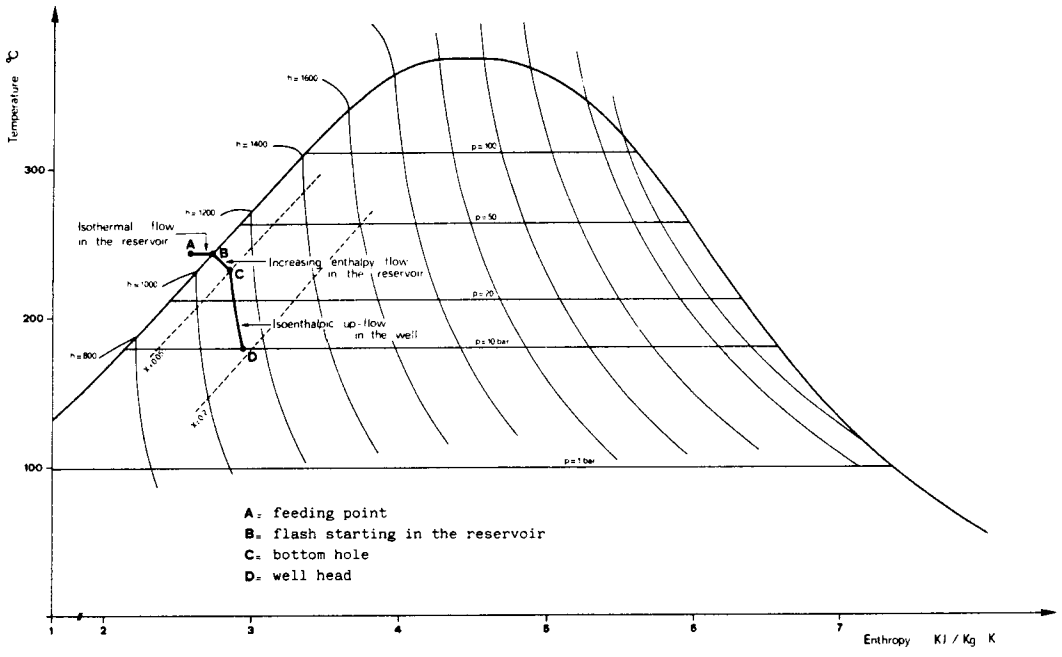


FIG. 9



Mofete Field
Long term test unit

FIG. 11



A = feeding point
B = flash starting in the reservoir
C = bottom hole
D = well head

Mofete Field:
Thermodynamic pattern from reservoir to well head

FIG. 10

TABLE 2

MOFETE FIELD

CHEMISTRY OF WATER SEPARATED AT ATMOSPHERIC PRESSURE (ppm)

	Shallow Reservoir						Intermediate Reservoir	Deep Reservoir
	Well N° 1 (550-896 m)	Well N° 1 (1273-1606 m)	Well N° 3D (430-665 m)	Well N° 7D (1110-1648 m)	Well N° 8D (662-907 m)	Well N° 9D (1339-1749m)	Well N° 2 (1275-1989m)	Well N° 5 (2310-2699 m)
Na	14320	20860	13790	14760	14590	21300	10600	85160
K	1760	3880	1122	2610	1626	4410	2467	43380
Ca	792	2124	714	790	752	3520	1005	53950
B	178	183	106	144	90	288	295	231
Sr	49	68	43	26	41	64	30	1310
As	13	17	16	26	15	32	22	-
Li	36	46	34	56	37	56	28	480
Mn	10	28	4	10	8	55	52	5510
Fe	1	3	3	21	1	2	1	9450
SiO_2	568	690	425	639	454	578	938	210
Cl	25304	37800	23393	26650	25171	43897	21169	313850
HCO_3	116	77	110	195	98	73	85	TRACES
SO_4	72	7	156	70	82	14	12	TRACES
TDS	42860	65509	39428	45997	42965	75695	37880	515902
Na/Li	398	453	406	264	394	380	379	177
Cl/B	142	207	221	185	280	152	72	1359
Na/Cl	0.57	0.55	0.59	0.55	0.58	0.49	0.50	0.27
pH	7.5	6.5	7.5	7.2	7.7	6.9	6	4.5

TABLE 3

MOFETE FIELD

WATER CHEMISTRY FOR SELECTED SAMPLES CALCULATED AT RESERVOIR CONDITIONS (ppm)

	Shallow Reservoir		Intermediate Reservoir
	Well N° 1 (550-896 m)	Well N° 1 (1273-1606 m)	Well N° 2 (1275-1989 m)
Na	10025	12589	5090
K	1230	2342	1180
Ca	555	1281	480
B	125	110	140
Sr	34	41	14
As	9	11	11
Li	25	28	13
Mn	7	17	25
Fe	1	2	1
SiO_2	398	417	450
Cl	17710	22810	10200
HCO_3	81	46	41
SO_4	50	4	6
TDS	30000	39500	18200
Na/Li	398	453	391
Cl/B	142	207	73
Na/Cl	0.57	0.55	0.50

TABLE 4

RESULTS OF TESTING OF MOFETE WELLS

WELL (total depth-m)	INJECTION					PRODUCTION					
						LIP METHOD			PRESSURE	SEPARATOR	METHOD
	TESTED INTERVALS (m)	INTERVAL TEMPERATURE (°C)	W H P (MPa)	FLOW RATE (m^3/h)	TRANSMISSIVITY (m^3/Pa s)	RELEVANT DATA	ENTHALPY (kJ/kg)	TRANSMISSIVITY (m^3/Pa s)	RELEVANT DATA	ENTHALPY (kJ/kg)	TRANSMISSIVITY (m^3/Pa s)
MOF 1 (1606 vert.)	550-896 csg 7"-9" 5/8	247	-	-	-	WHT=220°C WHP=2.35 MPa Q_s = 25 t/h Q_t = 70 t/h	1100	-	WHT=220°C WHP=1.27 MPa Q_s = 31 t/h Q_t = 210 t/h	1100	-
	1223-1469 liner 5"	295	-	-	-	WHT=165°C WHP=0.49 MPa Q_s = 9.5 t/h Q_t = 24 t/h	1100	-	WHT=140°C WHP=0.4 MPa Q_s = 7 t/h Q_t = 23 t/h	1100	0.5×10^{-9}
MOF 2 (1989 vert.)	1272-1989 liner 7"	337	3.86 4.90 5.90	36 55 95	6×10^{-9}	WHT=200°C WHP=0.52 MPa Q_s = 35 t/h Q_t = 61 t/h	1600	-	WHT=200°C WHP=0.92 MPa Q_s =27 t/h Q_t =66 t/h	1600	4.7×10^{-9}
MOF 3d (1909 dev. 1749 vert.)	430-665 csg 9" 5/8	230	-	-	-	LOW PRODUCTION		-	-	-	-
	1302-1900 liner 7"	275	3.5 3.5 3.8 4.9	27 87 126 162	0.7×10^{-9} 0.6×10^{-9} 0.6×10^{-9} 1.1×10^{-9}	NO PRODUCTION		-	-	-	-
MOF 5 (2700 vert.)	1627-1960 liner 7"	286	3.5	60	0.5×10^{-9}	LOW PRODUCTION		-	-	-	-
	2310-2699 liner 5"	362	7.03	19	0.7×10^{-9}	VERY FAST SALT DEPOSITION INTERRUPTS PRODUCTION		-	-	-	-
MOF 7d (1648 dev. 1476 vert.)	1042-1646 liner 7"	301	0.1 0.6 0.8	38 133 181	10×10^{-9}	WHT=165°C WHP=0.68 MPa Q_s =20 t/h Q_t =60 t/h	1150	5×10^{-9}	-	-	-
MOF 8d (907 dev. 800 vert.)	660-907 liner 7"	234	0.1 0.45 0.17	36 61 95	20×10^{-9}	WHT=155°C WHP=0.89 MPa Q_s = 18 t/h Q_t = 200 t/h	950	17×10^{-9}	-	-	-
MOF 9d (1745 dev. 1582 vert.)	694-1004 O.H. 12" 1/4	210	0.8 1.4	54 115	22×10^{-9}	NOT YET TESTED		-	-	-	-
	1342-1745 liner 7"	308	0.1 4.3 4.5	9.5 39 83	2×10^{-9}	LOW PRODUCTION		-	-	-	-

Proceedings Ninth Workshop Geothermal Reservoir Engineering
Stanford University, Stanford, California, December 1983
SGP-TR-74

OVERVIEW OF GEOTHERMAL DEVELOPMENT AT OLKARIA IN KENYA

Andrés Svanbjörnsson, Jónas Matthíasson, Hreinn Frímannsson, Stefán Arnórsson, Sveinbjörn Björnsson, Valgarður Stefánsson and Kristján Sæmundsson

VIRKIR Consulting Group Ltd., Reykjavík, Iceland

ABSTRACT

The Olkaria geothermal field has been under continuous development since 1970. A feasibility study, completed in 1976, after six wells had been drilled and tested, indicated that development of the Olkaria field was feasible. The feasibility study was followed by production drilling and the construction of three 15 MW generating units. The first unit was brought on stream in July 1981, the second in December, 1982, and the third unit is scheduled to be completed in early 1985. The current output of 19 productive wells is equivalent to 46 MW_e.

Distribution of fumaroles and resistivity surveys indicate an areal extent of some 80 km^2 for the Olkaria geothermal field. Gas chemistry of fumaroles indicates comparable underground temperatures over the whole field, 200-250°C. The capacity of the resource has been estimated to be 500-1000 MW electric for a production period of 25 years.

Most of the drilling has been confined to a small part of the geothermal field. Here maximum recorded downhole temperature is 339°C and temperatures follow the boiling point curve with depth. A thin steam zone at 240°C is observed in the top of the reservoir at approximately 600-700 m depth. The reservoir fluid is dilute, of the sodium chloride type, contains chloride in the range of 200-700 ppm. The reservoir rocks consist of a sequence of near horizontal lavas and tuffs of trachytic composition, but basaltic andesites have also been identified. The drilled rocks at Olkaria are of relatively low permeability, the average yield of wells being equivalent to about 2.5 MW_e.
Exploratory drilling is presently in progress in the Olkaria field, the aim being to locate new production areas within the field. Three holes have been completed and the forth and last hole under the present plan is being drilled.

INTRODUCTION

The VIRKIR Consulting Group Ltd. has been engaged in consultation for geothermal development at Olkaria since 1976, first in collaboration with SWECO in Stockholm and later with Merz and McLellan in Newcastle. VIRKIR's participation has involved assessment of the reservoir characteristics, siting of wells and design of wellhead equipment and the steam supply system. This article focuses on the reservoir aspects but it describes also how the flow characteristics of wells affected decision on the design of the steam supply system and turbine inlet pressure.

The reservoir data have been mostly collected by experts of the Kenya Power Company Ltd. Interpretation has been jointly by these experts and VIRKIR experts. Various aspects of the geothermal development at Olkaria and detailed evaluation of the scientific data has been described in numerous reports, mostly of the Kenya Power Company Ltd. Some key references include Bhogal (1980), Bodvarsson and Pruess (1981), Brown (1981), Glover (1972), Kenya Power Company (1977, 1979, 1980, 1981, 1982, 1983a), McCann (1974), Muna (1982), Mwangi (1982), Naylor (1972), Ndombi (1980), Nganga (1982), Noble and Ojiambo (1975), Odongo (1983), Ojiambo et al. (1982), UN-EAPL (1972, 1976), and Waruingi (1983).

The Olkaria Geothermal Project has been financed by the Kenyan Government, the World Bank, the Commonwealth Development Corporation, and the European Investment Bank.

OVERALL FIELD CHARACTERISTICS

The Olkaria geothermal field is located in the Gregory Rift Valley, 5-10 km south of Lake Naivasha and some 100 km northwest of Nairobi (Fig. 1). The Olkaria geothermal system is considered to be related to a mature central volcano near the western marginal faults of the Rift Valley. The geothermal field occupies the greater part of a caldera or ring structure which is at least 80 km^2 in size (Naylor, 1972; KPC, 1979). There has been some disagreement on the existence of the ring structure (KPC, 1981) which is mostly inferred from circular arrangement of comendite domes (Fig. 2). A fissure zone, active both tectonically and volcanologically, trends N-S through the western part of the inferred ring structure. WSW-striking faults have been observed in the area. Recent evidence from drillings indicates

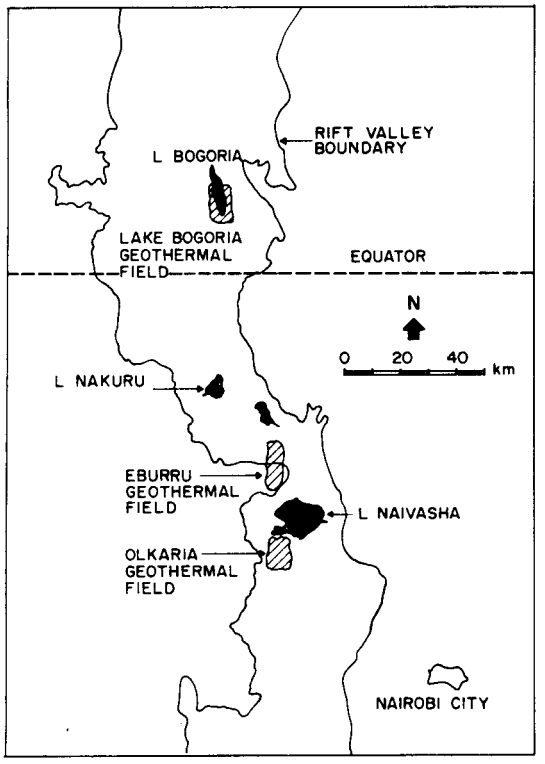


Fig. 1 Location of the Olkaria geothermal field in the Rift Valley.

that these faults may be major upflow zones.

The youngest volcanic eruption in the Olkaria area occurred some 300 ± 100 years ago producing the Ololbutot flow and several smaller flows on a crater line which coincides with the N-S fissure zone. It is not possible to predict when another volcanic eruption is due but very probably it will occur in the same fissure zone as previous eruptions.

The areal extent of the Olkaria geothermal field has been inferred on the basis of 1) the occurrence of fumaroles and hot ground, 2) anomalous shallow ground temperatures, and 3) anomalies of low bedrock resistivity (Noble and Ojiambo, 1975). A conservative estimate based on 1) and 2) lies in the range 50 km^2. Resistivity surveys strongly suggest a larger field, totalling about 80 km^2 (Fig. 2). Natural heat loss of the Olkaria system has been estimated by Glover (1972) to be 400 MW thermal corresponding to a steam flow of 140 kg/sec, or the steam required for 50 MW electric power production. Gas geothermometry results indicate that subsurface temperatures of 250°C and higher are to be expected over the entire field (KPC, 1983b). The area in the southern part of the field by the fissure swarm and near the first exploration hole represents a major upflow according to the most recent geothermometry interpretation (KPC, 1983b) as steam condensation in the upflow is here at minimum.

A critical review of available resistivity data carried out in 1980 favoured Schlumberger soundings as the most appropriate for evaluation of the deep resistivity structure (KPC, 1980). Re-interpretation of the deepest soundings revealed regional low resistivity in the south of the field below 2000 m and updoming to some 1400 m in the northwest. This updoming resistivity low is most likely due to hydrothermal alteration. It has been postulated that the northwest region is a primary upflow of the hottest reservoir fluid (KPC, 1980).

The catchment area to the north of the Olkaria field is over 3000 km^2. Mean annual precipitation within the catchment area varies between 650 and 1500 mm. Potential evaporation is estimated as 1700-2100 mm/year (McCann, 1974). The rain pattern is, however, such that an excess of water joins the ground water after losses by evaporation. Lake Naivasha is a fresh water lake. There is no surface outflow so underground seepage must occur and to the south. The subsurface drainage has been estimated as 8 m^3/sec and more than 4.7 m^3/sec have been estimated to recharge on average the Olkaria geothermal reservoir (McCann, 1974, Noble and Ojiambo, 1975). Calculations indicate that recharge into the Olkaria reservoir is not a limiting factor to exploitation, even considering a reasonably large geothermal power plant (UN-EAPL, 1976).

OUTLINE OF HISTORY OF DEVELOPMENT

Exploration of the Olkaria geothermal field was initiated in the year 1956 and has been continuous since 1970. The early exploration involved the drilling of two holes. High temperatures were encountered but attempts to bring the holes into production were not successful. In 1970 a geothermal exploration project was initiated in Kenya and was jointly financed by the United Nations Development Programme and the Kenyan Government. During 1971 and 1972 exploration was carried out in the Olkaria geothermal field. It consisted of geological mapping and geophysical and geochemical surveys as well as further investigations on the two exploration holes drilled in 1956-58. The surface exploration work was followed by a Technical Review Meeting to assess the exploration results. The Meeting recommended the drilling of four exploratory holes in the Olkaria field. Drilling started in 1973. The second hole was successful and further drilling was concentrated around that hole. By 1976 six holes had been drilled at Olkaria. The drilling was succeeded by a feasibility study the results of which indicated that development of the geothermal resource at Olkaria was attractive and Kenyan authorities decided to construct a 30 MW power plant of two 15 MW units with possible extension by the addition of a third 15 MW unit. The first unit was brought on stream in July, 1981, the second in December, 1982 and the third unit is scheduled to be commissioned in early 1985.

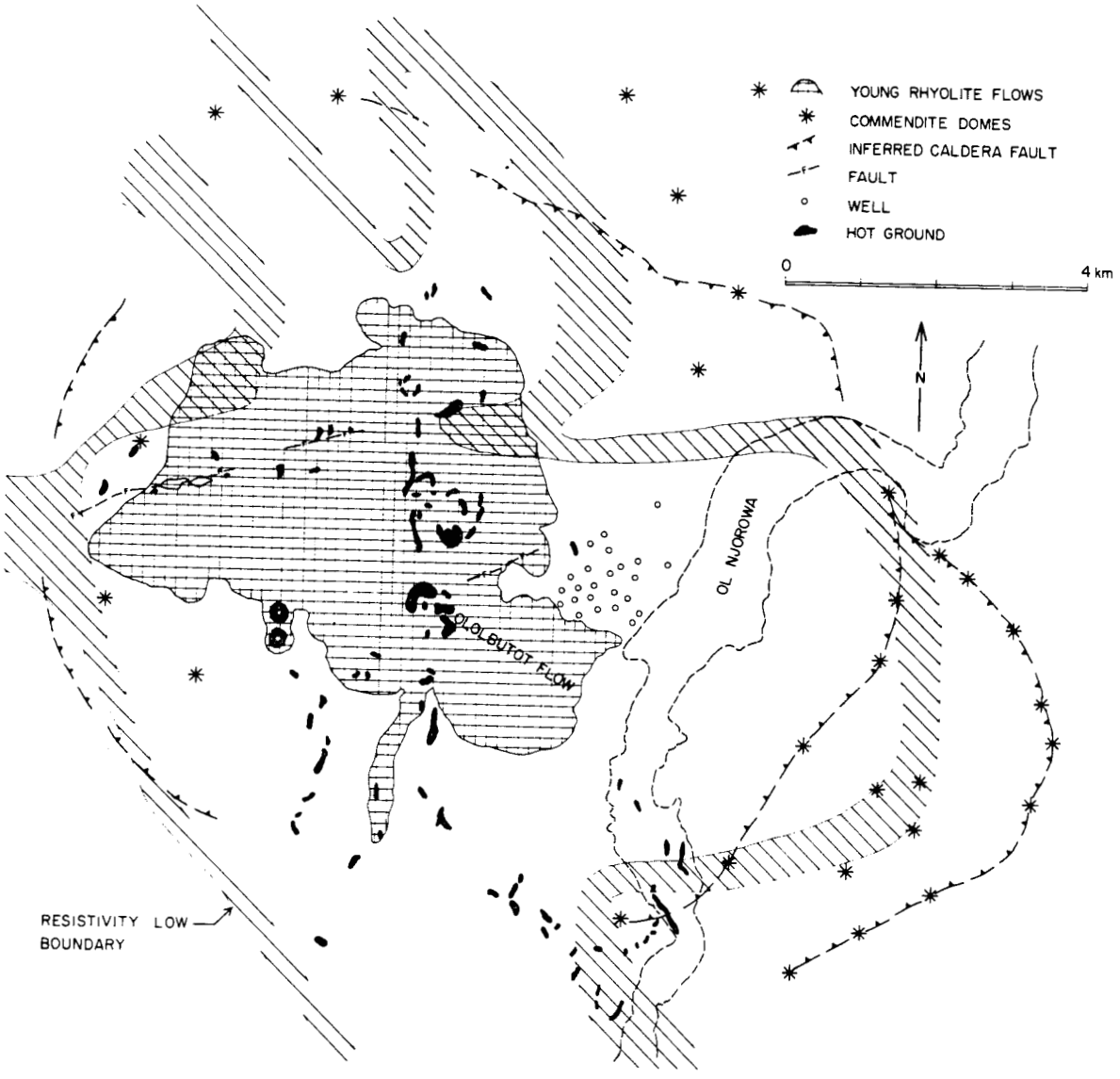


Fig. 2 Combined map showing geological feature and boundary of bedrock resistivity anomaly.

In 1980 the Kenya Power Company Ltd. organized a second Scientific Review Meeting, the aim of which was to give recommendations on exploration of the Olkaria geothermal field beyond the present production area. The Meeting recommended the drilling of exploration holes at four new sites to be followed by appraisal drilling where the exploration drillings were successful. Three of the exploration holes have now been completed and the fourth hole is being drilled.

THE BOREFIELD CHARACTERISTICS

After the successful drilling of the second exploratory hole (OW-2) in 1974 later appraisal and production drilling has been concentrated in that part of the Olkaria field. It was visualized that early demonstration of feasible use of the geothermal resource was desirable rather than more exploratory drilling in other parts of the Olkaria field that might have discovered better production areas. The present borefield is about 2 km^2 and now (November, 1983) 24 wells have been completed and the 25th well is being drilled. Of the 24 wells, 19 are productive yielding steam equivalent to 46 MW_e. The wells range in depth from 901 to 2485 m, most of them being in the range 1200-1400 m.

Physical State - Temperature and Pressure

In the production field perched salty aquifers are underlain by a shallow, low pressure steam zone at 1600-1700 m elevation (the borefield is

at 1920-1950 masl). Between 1275 and 1625 masl liquid near boiling temperature controls the pressure. The observed temperature profile in this depth interval (Fig. 3) can be explained by the rise of steam through rock composed of layers of alternating poor and good permeability. In Fig. 3 one may recognise sections of linear gradients in aquicludes, boiling curve segments in layers of better permeability and intervals of constant temperature, where the fluid is convecting in layers of highest permeability.

At 1130-1275 m elevation the wells penetrate a steam zone near 240°C and 35 bars abs. pressure. The pressure gradient in this zone is controlled by the vapour phase although both phases, steam and water, are coexisting. Below 1130-1210 masl the wells reach a liquid dominated boiling water reservoir with a pressure potential corresponding to a rest water level of boiling water at 1550-1620 masl.

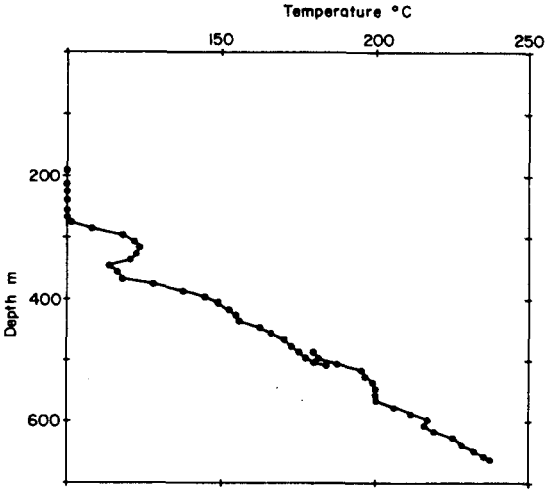


Fig. 3 Temperature in well OW-2 above the steam zone.

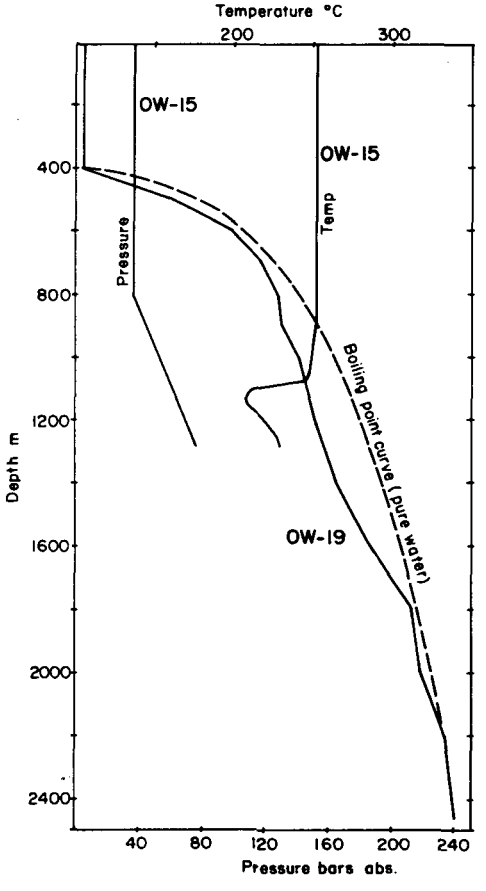


Fig. 4 Temperature and pressure profiles in selected wells. The logs for well OW-15 show the features characterising the steam zone and a temperature reversal below that zone considered to be due to cooling by injected water 21 days before the temperature run was taken.

Temperatures in the water reservoir appear to follow the boiling point curve at least to the drilled depth of 2485 m. This is not easily confirmed as most temperature logs are severely disturbed by cooling effects of injected water and cooling due to boiling in the formation during flow tests (Fig. 4). The highest recorded temperatures are 304°C at 1651 m depth in well OW-4 and 296°C and 339°C at 1600 m and 2460 m in wells OW-6 and OW-19 respectively. All are slightly below the boiling point for pure water at these depths but dissolved gases may have lowered the boiling temperature.

Pressure logs have been analysed to infer the pressure potential of the dominating aquifers in the water reservoir. These aquifers are found at various depths in wells. In order to obtain a common reference level for the pressure potential the level of the 35 bar abs. isobaric surface has been estimated assuming a vertical pressure gradient of hydrostatic water of boiling temperature. The isobaric surface is found to slope up towards north by 0.14 m/m indicating a lateral flow component from the north through the borefield.

Stratigraphy and Hydrothermal Alteration

The rocks penetrated by drillholes in the production area are exclusively volcanic except for the topmost 100-150 m. No significant sedimentary intercalations have been discovered. The stratigraphic sequence consists mostly of near horizontal lavas of fine grain and some tuffs. They are generally of trachytic composition but rhyolites have been identified. Less differentiated rocks, probably basaltic andesite are conspiceous at 500-700 m depth. They overlie the steam zone and probably act as caprock for the geothermal reservoir. Channelways for the geothermal fluid are probably lava contacts, scoria zones and coarse pyroclastic interbeds, but also contraction joints in the lavas.

The hydrothermal alteration of the reservoir rocks has been studied by Browne (1981). The mineral assemblage is that typically found in rocks altered by hydrothermal fluids above 200°C (see Browne, 1978). Prominent alteration minerals include chlorite, calcite, quartz, pyrite, fluorite, epidote, albite and adularia. Calcite occurs in greatest abundance above 600-800 m depth. As its formation is associated with boiling it is inferred that significant steam formation starts at this level. Epidote distribution, but this mineral forms at temperatures above about 250°C, indicates that the southernmost wells in the borefield are located on the periphery of the steam zone.

The abundance of adularia and albite in the altered rock has been used as a semiquantitative indicator of permeability (Browne, 1981). At Olkaria they are most abundant in the westernmost part of the borefield but here wells tend to be poor producers. It is expected that the amount of albite and adularia in altered rock is determined by the total quantity of water passing, together with water salinity and boiling, and may not represent present-day permeability. Alteration leads to reduction in permeability. In order to explain the positive correlation between albite and adularia abundance and permeability, observed in some geothermal fields (Browne, 1981) a mechanism which rejuvenates the permeability must be postulated such as tectonic movements. The apparent negative correlation between alteration and permeability at Olkaria would by this argument indicate insignificant tectonic movements in the present borefield.

Fluid Chemistry

Waters discharged from wells at Olkaria are of the sodium chloride type (Table 1). Compared with waters in geothermal systems located in acid volcanics in many other parts of the world the chloride concentrations are relatively low at Olkaria or in the range 200-500 ppm when correction has been made for steam loss. The concentrations of compatible major components, including gases, are governed by equilibria with alteration minerals in the rock.

An increase in the chloride concentrations is observed with increasing depth of the producing aquifers. Also chloride concentrations increase from south to north across the borefield. The positive relation observed between chloride levels and Na-K geothermometry temperatures have been taken to indicate that the northernmost wells are closest to a major upflow (KPC, 1982). The chloride-depth gradient is believed to have development by downward percolation of condensate from the steam zone into the boiling water reservoir as a result of heat loss through the caprock.

Permeability

Permeable zones have been identified by circulation losses during drilling, or inflow, as well as from analysis of pressure and temperature logs obtained during injection tests and recovery of temperature and pressure after completion of the wells.

Table 1. Composition of water and steam from selected wells at Olkaria at atmospheric pressure (0.8 bars abs.). From Muna (1982).

	OW-6	OW-10	OW-12
Water phase (ppm)			
pH/°C	9.25/20	8.58/20	9.10/20
SiO_2	762.0	734.0	880
B	5.6	8.0	6.4
Na	495.0	734.0	476.0
K	70.2	147.4	72.2
Ca	0.82	0.92	0.62
Mg	0.009	0.032	0.018
CO_2[a]	48.8	34.4	71.1
SO_4	38.6	30.1	44.1
H_2S[a]	2.9	0.62	1.46
Cl	482.2	1140.2	629.9
F	49.5	57.0	67.5
Steam phase (immoles/kg steam)			
CO_2	62.24	41.71	38.00
H_2S[a]	10.91	5.12	5.09
H_2	5.67	4.02	5.14
CH_4	0.78	0.42	1.69
N_2[b]	0.98	1.38	0.98
Discharge enth.J/g	2316	2378	2209

[a]Total carbonate and total sulphide.
[b]Residual gas.

Most of the wells have encountered permeable horizons within the steam zone at 600-800 m depth. This corresponds with the bottom of the basaltic-andesite series and the top of the underlying rhyolites. Many other wells have encountered aquifers at 1000-1150 m depth in trachyte lavas within the boiling water reservoir. Some wells have also penetrated permeable zones at 900-1000 m depth. Only three wells penetrate significantly below 1400 m. Of these only one well, OW-19, has struck a significant aquifer below this depth, or at 1500 m.

Transmissivity (permeability-thickness product) has been estimated by several methods. They include pressure build-up during injection of water of constant flow rate and pressure fall off after injection is stopped. Also by recording drawdown of pressure in producing aquifers under stable discharge conditions and by studying the gradual recovery of that pressure to undisturbed values after the well has been closed. There is often considerable discrepancy between the results of the different test methods but interpretation in a two phase reservoir is complicated. Values obtained for the transmissivity in individual wells lie generally in the range 1-5 Darcy-meters but the highest values recorded are 13 Dm for well OW-12.

These results show, compared with many other exploited geothermal fields, that permeability is relatively low at Olkaria, at least within the present borefield.

Well Performance

Most of the wells are fed by a number of aquifers at different levels. Clearly many wells have a significant contribution from the steam zone. Wells dominated by feeders in the steam zone show rapid build up of shut-in pressure to about 35 bars. On the other hand wells dominated by aquifers in the water reservoir have a tendency to build up higher wellhead pressures. The flow from these latter group of wells shows little decline with rising wellhead pressures up to 20 bars whereas wells dominated by feeders in the steam zone cannot maintain their output at such a high wellhead pressure.

The enthalpy of the well discharges is variable, although high on average, or about 2200 J/g. A few wells discharge practically dry steam. During the early periods of discharge the enthalpy may correspond with that of steam saturated water at the respective aquifer temperature but its value gradually rises within a few weeks to about 2000 J/g or more.

The steam flow from the wells is low on the whole as would be expected from the low reservoir permeability. For exploitable wells it lies in the range 10-60 tonnes/hour at 6 bars abs. wellhead pressure, the weighted average being about 25 tonnes/hour. During the 2 year production period of the Olkaria geothermal power station some wells have shown decline in output by as much as 20% whereas other wells have remained stable. The cause has not yet been satisfactorily explained.

The best wells are located on a rather narrow belt on either side of a ravine running N-S and immediately east of the power station. It may be that this ravine is the surface expression of a fracture zone.

Conceptual Field Model

The main features of a model for the present borefield are as follows: Boiling water reservoir is overlain by a steam zone of 50-150 m thickness capped by a sequence of basaltic-andesite lavas. There is a strong component of lateral flow through the borefield from north to south as indicated by the pressure gradient and fluid chemistry, possibly from a major upflow along the WSW trending fault just north of the borefield. During the lateral movement of the fluid, boiling and phase separation occurs, leading to the formation of the steam zone. The lateral movement from the major upflow may be concentrated on a N-S trending fracture zone represented by a topographical ravine immediately east of the power station. Heat loss through the cap rock causes some steam condensation and descending condensate produces rather strong salinity gradient in the uppermost part of the hot water reservoir as well as a gradient in the direction of the flow.

Generating Capacity of the Reservoir

The longevity of the reservoir around the present borefield has been predicted by numerical simulation (Bodvarsson and Pruess, 1981). The approach taken was to assume that the pressure declines uniformly throughout the borefield as a consequence of fluid extraction. The borefield was thus modelled as one block within which there are no spatial variations in pressure. The recharge into the reservoir was accurately modelled. Furthermore the fluid mass in the steam zone was neglected and the reservoir fluid was extracted from the uppermost 550 m of the water reservoir.

The results of the numerical simulation study showed that the most critical factors controlling the generating capacity are horizontal and vertical permeabilities. Fig. 5 shows examples of predicted pressure decline for different assumed vertical permeability values. From the simulation studies and available data on transmissivity it was concluded that the geothermal reservoir around the present borefield can supply steam for the 45 MW power plant over at least 30 years (KPC, 1982).

THE STEAM SUPPLY SYSTEM

A wellhead separator and wellhead silencer is installed at each well. The steam is piped from the separator to the power station passing through a moisture separator prior to admission to the turbines. Steam pressure is controlled accurately by automatic exhaust valves located near the power house and blowing excess steam to atmosphere. The water from the silencers is discharged into special infiltration ponds.

The steam supply system was designed to accomodate the observed well characteristics as well as the predicted response of the reservoir to the production load. The water fraction in the well descharges was low and it was anticipated that it would decrease still with time. It was, therefore, not attractive to exploit this water phase by a second flash at low pressure. The admission pressure to the turbines was selected at 5 bars abs. by making a compromise between hardware economy and the cost of steam winning with due regard to possible future decline in wellhead pressure and steam flow due to reservoir drawdown.

FUTURE DEVELOPMENT

In December, 1980, the Kenya Power Company Ltd. organized a Scientific Review Meeting the aim of which was to assess all available data on the Olkaria geothermal field and forward recommendations for exploration and development beyond the present 45 MW power station. The Meeting recommended the drilling of deep (2500 m) exploratory holes at four new sites to be followed by appraisal drilling where there was success. Successful exploratory hole was defined as one that discharged sufficient steam to generate at least 4 MW electric. At this time (November, 1983) exploratory holes have been drilled at three of these sites and drilling is in progress at the last site. It is visualized that appraisal drilling will be

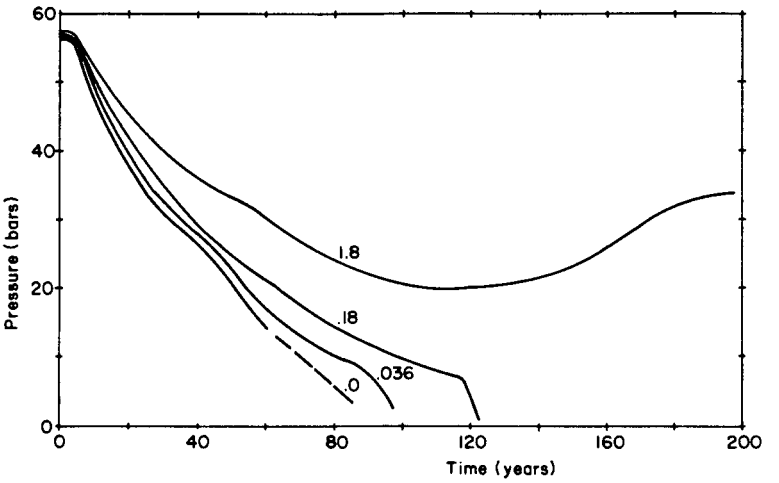


Fig. 5 An example of predicted pressure decline in the borefield. The following assumptions were made: Production area 2 km^2. Reservoir area 12 km^2. Horizontal transmissivity 4.0 Darcy-meters. Figures on graph show vertical permeability in mD. Corey relative permeability curves were used. From Bodvarsson and Pruess (1981).

commenced after thorough evaluation of the exploratory well data and it is anticipated that units of 30 MW will be suitable for economy reasons and market requirements.

Kenya does not possess fossil fuel reserves and most of the economically attractive hydropower schemes have already been developed. In view of this and the successful development at Olkaria, geothermal resources will, we believe, play an increasingly important role in Kenya's power generation.

ACKNOWLEDGEMENTS

The authors wish to thank the Kenya Power Company Ltd. for permitting publication of this article. Although we have taken the task to write the present summary on geothermal development at Olkaria, the results on which it is based are not only ours but the outcome of intergrated work of the VIRKIR Group, Merz and McLellan and experts from the East African Power and Lighting Company who work for the Kenya Power Company Ltd. The following individuals are specially thanked for long and fruitful collaboration on the Olkaria geothermal project: P. Getecha, J. Ouma, S. Bwire-Ojiambo, M. E. O. Odongo, M. N. Mwangi, Z. W. Muna and C. B. Haukwa of the East African Power and Lighting Company and T. E. Norris, D. Woodruff and J. S. Shaw of Merz and McLellan. We also wish to thank many experts of GENZL for their joint work on the Olkaria geothermal project.

REFERENCES

Bhogal,P.S. (1980), "Electrical Resistivity Investigations at the Olkaria Geothermal Field, Kenya", Geothermal Resources Council, Transactions, 4, 9-12.

Bödvarsson, G. and Pruess K. (1981), "Olkaria Geothermal Field - Numerical Studies of the Generating Capacity of the Reservoir," A report prepared for the Kenya Power Company Ltd.

Browne, P.R.L. (1981), "Petrographic Study of Cuttings from Ten Wells Drilled at the Olkaria Geothermal Field, Kenya," Geothermal Institute, University of Auckland, NZ. Report for KPC, Nov., 1981.

Browne, P.R.L. (1978), "Hydrothermal Alteration in Active Geothermal Fields", Ann. Rev. Earth Planet. Sci. 6, 229-250.

Glover, R.I. (1972), "Chemical Characteristics of Water and Steam Discharges in the Rift Valley," UN Geothermal Resources Exploration Project Report.

The Kenya Power Company Ltd. (1977), "Report on Geothermal Development at Olkaria," prepared by Merz and McLellan and Virkir Ltd., Oct., 1977.

The Kenya Power Company Ltd. (1979), "Progress Report on Steam Production," prepared by Merz and McLellan and Virkir Ltd., Apr., 1979.

The Kenya Power Company Ltd. (1980), "Scientific Review of Olkaria Geothermal Reservoir," A report prepared for the Scientific Review Meeting by GENZL, Nov., 1980.

The Kenya Power Company Ltd. (1981), "Recommendations for Further Geothermal Exploration at Olkaria," A report prepared by Merz and McLellan and Virkir Ltd., May, 1981.

The Kenya Power Company Ltd. (1982), "Status Report on Steam Production," A report prepared by Merz and McLellan and Virkir Ltd., May, 1982.

The Kenya Power Company Ltd. (1983a), "Status Report on Steam Production," A report prepared by Merz and McLellan and Virkir Ltd., Jan., 1983.

Mwangi, M.N. (1982), "Two-Dimensional Interpretation of Schlumberger Soundings and Head-On Data with Examples from Eyjafjordur Iceland, and Olkaria, Kenya," United Nations University Geothermal Training Programme, Iceland, Report 1982-9, 72 pp.

Naylor, W.I. (1972), "The Geology of the Eburru and Olkaria Geothermal Prospects," UN Geothermal Resources Exploration Project Report.

Ndombi, J.M. (1981), "The Structure of the Shallow Crust Beneath Olkaria Geothermal Field, Kenya," Deduced from Gravity Studies, J. Volc. Geothermal Research, 9, 237-251.

Nganga, J.N. (1982), "Comparison of Drilling in High Temperature Fields in Olkaria, Kenya, and Krafla, Iceland," United Nations University Geothermal Training Programme, Iceland, Report 1982-10, 59 pp.

The Kenya Power Company Ltd. (1983b), "Status Report on Steam Production," A report prepared by Merz and McLellan and Virkir Ltd., Nov., 1983.

McCann, D.L. (1974), "Hydrogeologic Investigations of the Rift Valley Catchments," UN Geothermal Resources Exploration Project Report.

Muna, Z.W. (1982), "Chemistry of Well Discharges in the Olkaria Geothermal Field, Kenya," United Nations University Geothermal Training Programme, Iceland, Report 1982-8, 38 pp.

Noble, J.W. and Ojiambo, S.B. (1975), "Geothermal Exploration in Kenya," In Proceedings of the Second United Nations Symposium on the Development and Use of Geothermal Resources, San Francisco 20-29 May, 1975, 1, 189-204.

Odongo, M.E.O. (1983), "Geological Report of OW-1 Well," Kenya Power Company Ltd. Geothermal Project Report GL/OW/1/013.

Ojiambo, S.B., Odongo, M.E.O., Maina, S.K. and Haukwa, C.B. (1982), "First Year Operation Experience of the Olkaria Geothermal Power Station," Kenya Power Company Ltd. Geothermal Project Report.

United Nations - East African Power and Lighting Company (1972), "Report of Technical Review Meeting, December, 1972," UN Geothermal Resources Exploration Project Report.

United Nations - East African Power and Lighting Company (1976), "Feasibility Report for the Olkaria Geothermal Project," prepared by Sweco and Virkir Ltd., Dec., 1976.

Warningi, S.N. (1983), "Two Years Production Period at the Olkaria Geothermal Field, Kenya," Kenya Power Company Ltd. Geothermal Project Report.

Proceedings Ninth Workshop Geothermal Reservoir Engineering
Stanford University, Stanford, California, December 1983
SGP-TR-74

RESOURCE EVALUATION AND DEVELOPMENT PLANS FOR A 120 MW GEOTHERMAL POWER PLANT ON MILOS ISLAND, GREECE

M.J. Economides[1], C.A. Ehlig-Economides[1],
G. Speliotis[2], F. Vrouzi[2]

[1]University of Alaska, Fairbanks
[2]Public Power Corporation (Greece),

ABSTRACT

Five deep wells have been drilled on the Island of Milos, Greece, identifying a high-temperature, high-enthalpy geothermal reservoir. The thermodynamic properties of the fluid, and the estimated porosity and presumed thickness of the formation suggest a fluid and heat storage capacity that could support a 60 MWe power plant for 85 years or a 120 MWe for half that time.

The existing five wells can deliver 180 t/h of steam at 10 bar abs pressure, capable of generating a maximum electric power output of slightly less than 20 MWe.

This paper describes the geology, the drilling and the well testing results pertaining to the five wells, and discusses the reservoir potential for a 60 MWe geothermal power plant.

INTRODUCTION

Milos Island, a member of the Cyclades Group in the Aegean Sea, is part of the active Aegean Volcanic Arc of which the islands of Santorini and Nisyros are also members. The Island of Milos and Nisyros have been been the sites of major drilling activity. Figure 1 based on the work by McKenzie[1] shows the location of Milos Island within the volcanic arc in the Aegean Sea.

Two exploratory wells, MA-1 and MZ-1, drilled in 1975-76 proved productive. The former was drilled in the Adamas area, while the latter was drilled in the Zephyria area. Three other wells drilled during 1980-82 (M-1, M-2 and M-3) all proved productive. Figure 2 positions the wells on the map of the island.

GEOLOGY

The Island of Milos may be represented by the generalized model shown on Figure 3 offered by Vrouzi[2]. The schematic represents a W-E cross-section of the island at the latitude of the Zephyria plane. The model shows an infiltration zone in the west (associated with several lava domes), a partial deep discharge towards the east, the development of a series of convective circuits within the reservoir (metamorphic complex), some upward leakages through the main fault systems, a cover made up of widespread hydrothermal alterations of a polygenic formation, and some local intrusions connected with the few domes outcropping in the south-eastern sector of the island. The latter intrusions, however, represent a local hydrogeological disturbance to the deep system.

Because of the reasonably flat surface terrain and the proximity to population centers, the Eastern part of the Island, and especially the Zephyria-Agrilies and the Adamas regions were sited for the contemplated geothermal development.

DRILLING AND SUBSURFACE LITHOLOGY

Table 1 presents a summary of the well diameters and depths for the three newer wells (M-1, M-2, and M-3).
The sequence of terrains crossed by each well is summarized below.

M-1: A shallow interval of alluvia (0-20 m) is made of stratified flood deposits. From 20-60 m there is the chaotic formation made of melange comprised of schists, micaschists, quartz, limestones and extremely altered materials. Beneath this terrain there is a thick metamorphic layer (60 m to T.D.) consisting of schist primarily of the green schist facies. Epidote is a prominent mineral in this complex.

M-2: The alluvia terrain is again a shallow terrain (0-15 m) composed of stratified flood desposits. A thin layer (15-25 m) of grey tuff and other new volcanics is present. From 25-145 m, there is the chaotic formation consisting of a melange of various lithotypes. Metamorphic fragments (quartz, mica-schists, chloro-schists) are

TABLE 1

DRILLING STATISTICS FOR WELLS M-1, M-2, and M-3

Depth	M-1 1180 m	M-2 1381	M-3 1017 m
Well Diameter			
24"	0-99.5 m	0-169 m	0-186 m
17 1/2"	99.5-399 m	169-600 m	186-637
12 1/4"	399-903 m	600-1381 m	637-1017 m
8 1/2"	903-1180 m		

followed by volcanic fragments, some sedimentary blocks and hydrothermal material. Below 149 m (to T.D.) a thick metamorphic formation similar to the one under M-1 is found.

M-3: No alluvia deposits were found in the case of M-3. Instead, a chaotic melange consisting of metamorphic and volcanic fragments is evident (0-20 m).

A volcanic formation (20-125 m) is characterized by intense hydrothermal alteration rendering much of the original structure of the rock unrecognizable.

This layer is underlain by a sedimentary formation (125-173 m) formed by the Neogenic marine ingression. The formation contains carbonaceous quartz arenites, sandstones, arenaceous carbonate rocks, limestones and dolomites and some shales.

Finally, the thick metamorphic layer observed in M-1 and M-2 is found below 173 m (to T.D.).

The terrain sequences found in the three wells is summarized in schematic form in Figure 4. A geologic history of the structures may then be reconstructed.

A pull-apart fault probably caused the block of rock beneath well M-3 to subside, followed by the marine ingression which led to the deposition of the Neogenic formation (125-173 m). Generally, the sediments are well sorted. Sometime later in the geologic history, the magma from a molten rock body under the metamorphic rock complex intruded upward pushing the whole block upward, depositing it above the neogenic formation by uplifting the overlying melange deposits. Another possibility is that magma formed a volcanic cone around the vent above the neogenic sediments. Then melange and alluvial formations were deposited later above the cone.

The location of the M-3 on the top of the hill forming the uplifted horst that borders the Zephyria plain suggests the presence of two faults (see cross-section) around M-3. This hypothesis is further strengthened by the presence of neogenic sediments in M-3 and their absence in M-1 and M-2.

Considering the mineralogy and lithology of the rocks pierced by the wells, it can be suggested that the metamorphic trend is from M-2 to M-3 to M-1.

Presence of calcite mineral above 900 m and its absence at lower depths can be directly related to the pattern of underground water movement.

FLOW AND TRANSIENT PRESSURE WELL-TESTING

The three new wells have been flowtested and Table 2 contains the pertinent flowrate and enthalpy data.

A large number of injection tests have been done on all three wells. Cold seawater was injected and the ensuing buildup of pressure was allowed to fall off. Nine such tests were done for well M-1. The injection time for each was approximately 30 minutes. Nine similar tests were done for M-2 and three more were done for M-3.

The tests were performed at various well intervals for the evaluation of the reservoir transmissivity. Log-log graphs of these tests were utilized as diagnostic tools. Figure 5 is a log-log graph of three injection fall-off tests from M-1, while Fig. 6 is a similar graph of three injection fall-off tests from M-3.

In general, most of the data demonstrate the presence of fractures, as identified by the half-slope behavior on the log-log graph evident at early time. The data trend then flattens out, a frequent indicator of double porosity systems. A "rule of thumb" known as the "double Δp rule" identifies the

TABLE 2

WELL FLOW DATA

	M-1	M-2	M-3
Total Production Rate at 12 kg/cm^2 (175 psi) wellhead pressure	119 t/h	47 t/h	126 t/h
Enthalpy	1450 kJ/kg	2200 kJ/kg	1600 kJ/kg
Quality at 10 kg/cm^2 (150 psi)	0.35	0.71	0.42
Steam Flow Rate	41.7 t/h	33.4 t/h	52.9 t/h
Condensing Power Plant Maximum Electricity Capacity (20,000 PPH/MWe)	4.6 MWe	3.7 MWe	5.8 MWe
Production Interval	900-T.D.	940-T.D.	900-T.D.
Total Dissolved Solids	120,000 PPM	140,000 PPM	130,000 PPM
Bottom-Hole Temperature	323°C	282°C	300°C+
Bottom-Hole Pressure	~ 120 kg/cm^2	~ 120 kg/cm^2	~ 120 kg/cm^2

commencement of the straight line behavior in a semi-logarithmic graph of the data. According to the rule, data following two times the Δp from the deviation from the half slope will fall on a semi-log straight line. Unfortunately, most of the tests were not run for a sufficiently long time for any sustained or even certain appearance of the semi-log straight line as is evident from Figs. 5 and 6. Further, the short duration of the tests limits the value of the data for interpretation of the double porosity behavior. (These tests, run by the contractor, were not designed by the authors of this report.)

The calculated storage capacity of well M-1 is 43 m^3 (8 1/2" by 1180 m). A half hour injection at 100 m^3/h (as it was done for most tests) would barely unload the original wellbore contents into the formation.

Semi-log graphs of the data are presented in Fig. 7. Injection tests #4 and #9 were selected for analysis since they were done over roughly the same completion interval. The extrapolation of the time function $(t+\Delta t)/\Delta t$ to unity (infinite fall-off time, Δt) would result in the initial reservoir pressure). Hence, since the tests were done for the same depth, the extrapolation of these straight lines must converge at approximately the same value of pressure. The slopes for the two straight lines were thus obtained and were calculated as 9 kgr/cm^2/cycle (for test #4) and 3.6 kgr/cm^2/cycle (for test #9).

The pertinent equation for calculating the permeability is:

$$k = \frac{526\, q\mu}{mh} \qquad (1)$$

where k in md, q in m^3/hr, μ in cp and h in m.

The permeability values obtained from these two tests were 11.5 md and 14 md, respectively.

The wellbore drainage factor or skin effect may be calculated using the equation:

$$S = 1.151\left(\frac{p_{1hr}-p_i}{m} - \log \frac{k}{\phi\mu c_t r_w^2} + 3.11\right) \qquad (2)$$

where k in md, μ in cp, c_t in (kgr/cm^2)$^{-1}$ and r_w in m.

Equations 1 and 2 were developed for the above units from the well equations, widely used in petroleum reservoir engineering.

Using Eq. 2, the skin effect for both tests was calculated as S = -7. The negative value for the skin further supports the notion that the well has penetrated a natural fracture.

Injection test #2, done at a shallower interval was also analyzed providing a permeability value of 3.7 md and a skin factor of -6.

The injection tests performed during the drilling operation provided a number of useful results about the formation and the wells. The diagnostic log-log plots gave evidence of the presence of natural fractures, a widespread feature of

geothermal reservoirs elsewhere. The flattening out of the data trends gave indication of two porosity systems also evident in other geothermal formations. Analysis of three of these tests provided estimates for the formation permeability and the open hole wellbore condition. The negative value of the skin effect provided additional evidence of the penetration of natural fractures by the wells.

Short-time injection tests, utilizing alien to the formation fluids (seawater) at much lower temperature would create other phenomena (such as thermal fracturing) that would mask or alter certain formation characteristics. At the present time, drawdown/buildup and interference well tests are contemplated in order to evaluate formation characteristics as well as the principal axes of permeability. The latter are extremely important in any future re-injection schemes which must be planned in conjunction with the development of the power plant.

RESERVE ESTIMATION

Assuming a maximum of 25 km^2 areal extent with a 1000 m thick reservoir (much of it will be accessible through vertical fractures touching the well, not through drilling) a bulk volume of 2.5×10^{10} m^3 may be calculated. Using a porosity value of 5%, the pore volume may then be calculated as 1.25×10^9 m^3. The liquid specific volume at reservoir conditions (p=120 kg/cm^2) is 1.53×10^{-3} m^3/kg. Hence, the mass present is $1.25 \times 10^9 / 1.53 \times 10^{-3}$ or 8.18×10^{11} kg. Since 20,000 lb/hr or 9100 kg/hr have been traditionally used per 1 MWe, the total flow need for a 60 MWe, assuming 50% quality is 1.09×10^5 kg/hr. Hence, the expected longevity of the resrvoir is calculated as 85 years.

DEVELOPMENT PLANS

At the time of writing this paper, the Public Power Corporation is in the first phase of the development of the geothermal reservoirs of Milos, and is in the process of contracting the design and installation of a small 1.5-2 MWe condensing power plant by mid 1985. This pilot facility will provide a means for testing prototype separators, pipelines, turbines, condensers and re-injection schemes for problems associated with scaling and corrosion. In addition, extended fluid production and re-injection will provide more definitive data on the reservoir and on the sustained deliverability and injectivity characteristics of the wells.

The second phase will include the drilling of five new geothermal wells, testing and measurements, the study of a plausible geothermal model and the determination of the total power capacity (expected to be about 60 MWe) resulting in the design, procurement and installation of a 60 MWe power plant by late 1989. The installation of the first network of submarine cables for the transmission of the generated power will also take place during this phase.

The third phase will include the drilling of approximately 20 new geothermal wells, appropriate testing and measurements aiming towards the procurement and installation of a second 60 MWe power plant by late 1992. This phase will include the installation of a second network of submarine cables for the transmission of the additional 60 MWe.

Since the power output is expected to greatly outpace the demand for Milos or that of the islands in its immediate proximity, the installation of the submarine cables for power transmission to the Greek mainland is considered of utmost importance and is contemplated at the present time by the PPC.

REFERENCES

1. McKenzie, D.P.,: "Active Tectonics of the Mediterranean Region: R. Astron. Soc., Geophys. J., v. 30, no. 2. p. 105-185, 1972.

2. Vrouzi, F.: Research and Development of Geothermal Resources in Greece: Present Status and Future Prospects, Public Power Corporation Report, Athens, 1983.

ACKNOWLEDGEMENTS

The authors wish to thank Messrs. Shaukat A. Khan and Timothy Collett for their input in the geological analysis contained herein.

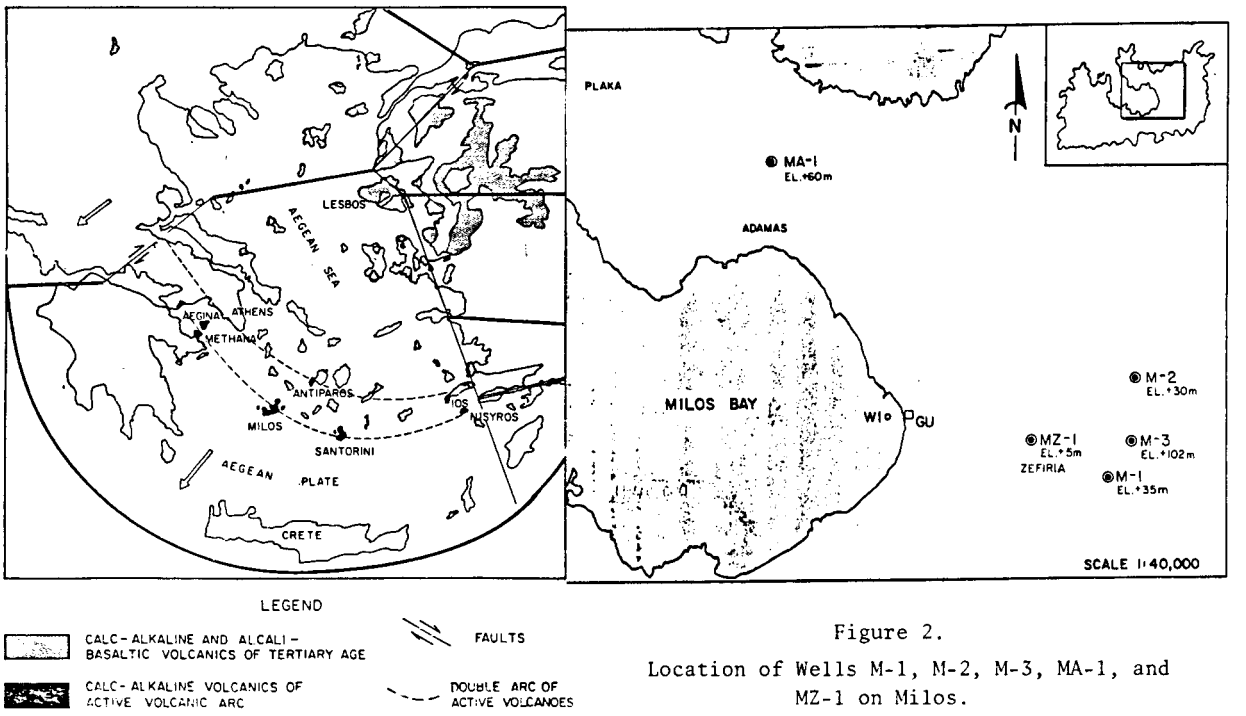


Figure 1.
Distribution of Volcanic Rocks of Tertiary and Quaternary Age in the Aegean Region.

Figure 2.
Location of Wells M-1, M-2, M-3, MA-1, and MZ-1 on Milos.

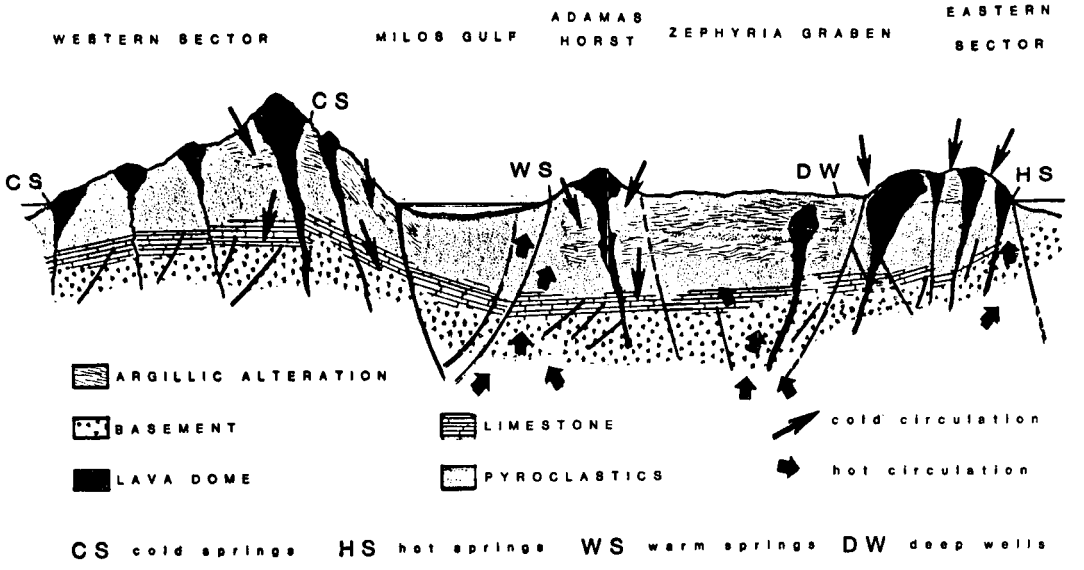


Figure 3.

Sketch of geothermal model of the Island of Milos (From Ref. 2).

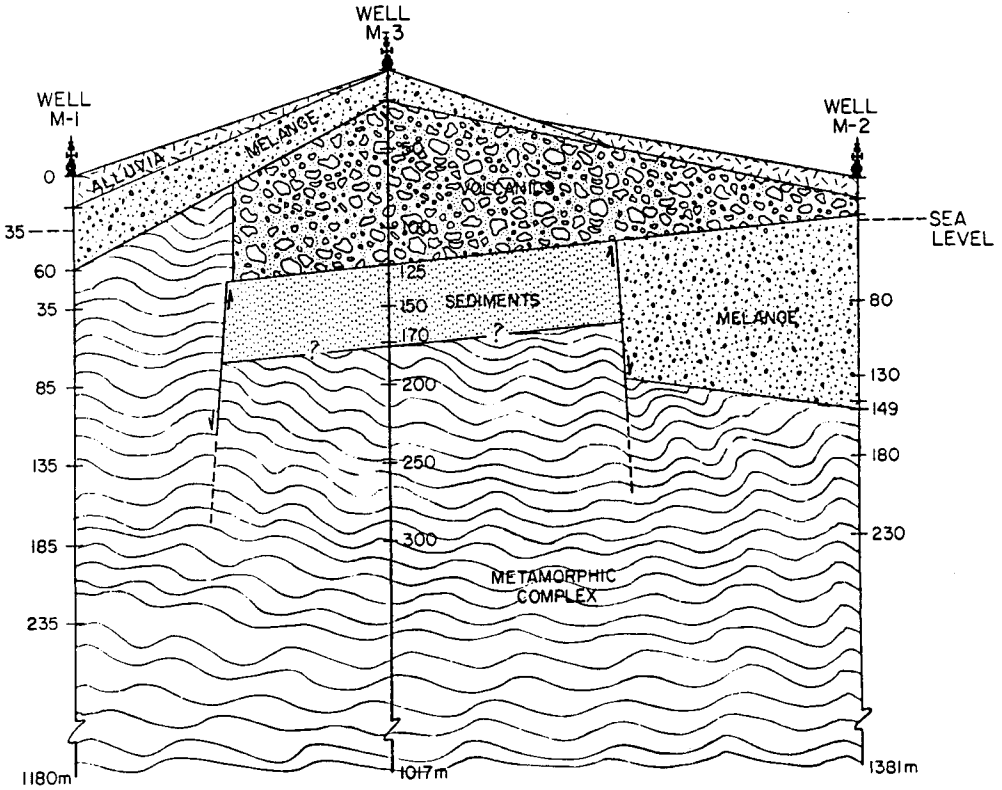


Figure 4

Terrain Sequences penetrated by wells M-1, M-2 and M-3, N-S Cross section.

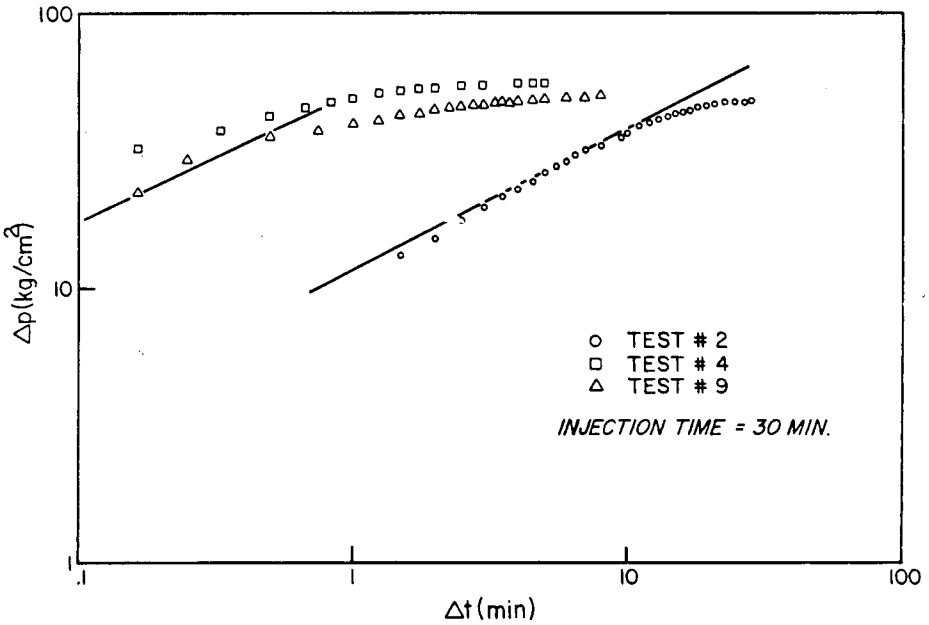


Figure 5
Injection Fall-off Pressure Transients Tests for M-1

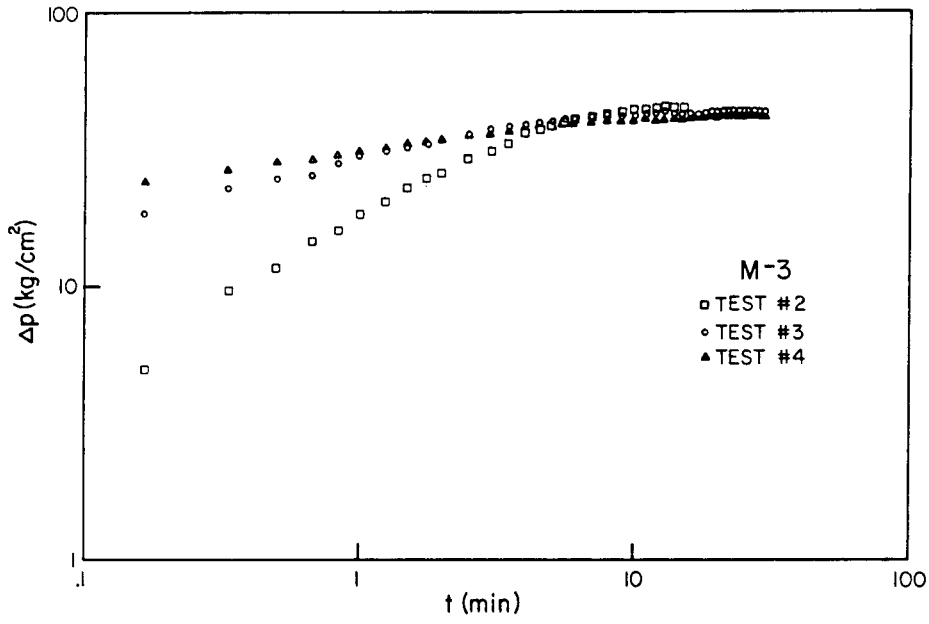


Figure 6
Injection Fall-off Pressure Transients Tests for M-3

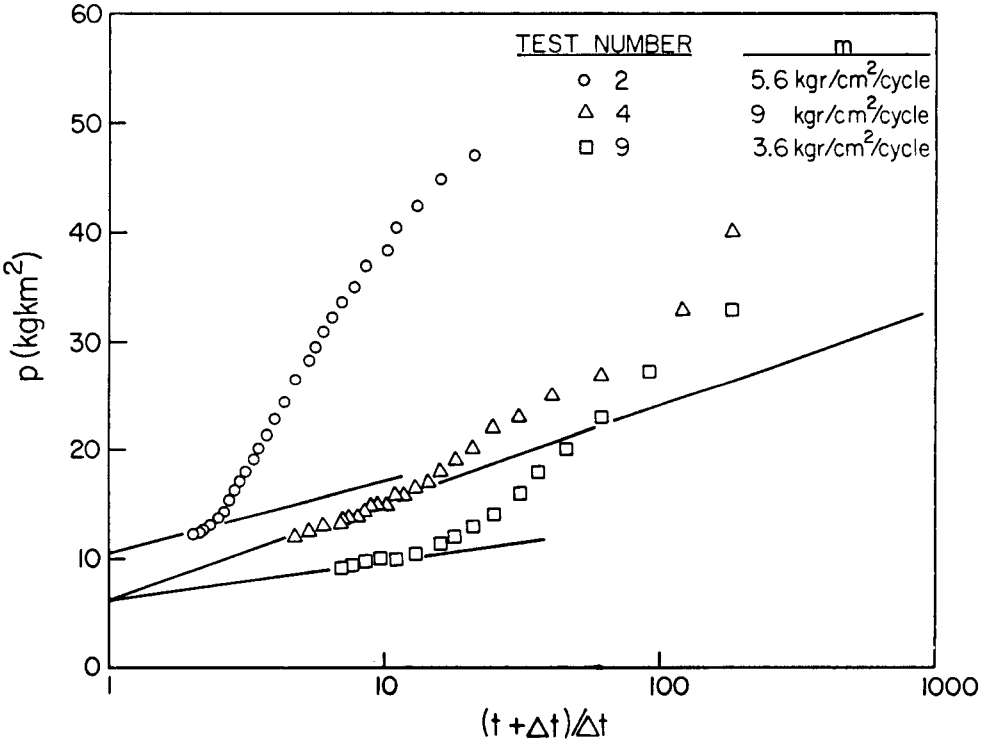


Figure 7
Semi-logarithmic Analysis of Pressure Transients Data for Well M-1.

Proceedings Ninth Workshop Geothermal Reservoir Engineering
Stanford University, Stanford, California, December 1983
SGP-TR-74

GEOTHERMAL FIELD DEVELOPMENT IN MEXICO

ING. HECTOR ALONSO ESPINOSA

COMISION FEDERAL DE ELECTRICIDAD
GERENCIA DE PROYECTOS GEOTERMOELECTRICOS
MORELIA, MICHOACAN, MEXICO.

ABSTRACT.

Mexico is a Country characterized by -- its diversified means of Power Genera - tion. Actual installed capacity is al- most 19 000 MW, of which 205 MW corres- ponds to Geothermal Plants, that is, -- 180 MW in Cerro Prieto and 25 MW of Por table Plants in Los Azufres.

To date, 346 areas with exploita - tion possibilities, are known. They -- are mainly distributed along the Volca- nic Belt where the most prominent are, - Los Azufres, La Primavera, Los Humeros, Ixtlan De Los Hervores and Los Negritos, among others. Proved reserves are 920 MW, and the accessible resource base are 4 600 MW identified and 6 000 MW undis- covered.

The long range construction studies- intends to achieve a total installed -- capacity of 100 000 MW, by the end of - this century, including 2 000 MW Geother- mal, through conventional and Portable- Plants. It is not a definite program,- but a development strategy. The carry- ing out of a definite program, will de- pend upon the confirmation of Hypothesis made in previous studies, and the econo mic decisions related to the financial- sources availability, and technologies- to be used in the future as well.

GENERAL ASPECTS OF ACTUAL POWER GENERATION.

The Comision Federal de Electrici- dad (CFE), is a Federal Government Agen cy created to generate and distribute - power in Mexico. Its main objectives - are basically:

- Planning the National Electric - System.
- Generation, Transmission and Dis tribution of Electric Power.
- Construction of all Power Plants. Installations and Works that re- quire Planning, Execution, ---- Operation and Maintenance of the National Electric System.
- Promote scientific research as - well as National Technology in - Electrical Aplications.
- Promote National Manufacturers - of Electrical Equipment and those related.

C.F.E. is organized basically in - five (5) operational interconnection -- systems, which are located geographically - as shown on Fig. 1, with an actual power generating capacity of 18 390 MW integra ted through different types of Power -- Plants as per Table 1, according to its capacity.

One Nuclear Plant (Two 654 MW Units) is under construction as well as multiple other installations for wind and solar- studies.

During the last year, the total -- Electric Energy Consumption was -- 73 200 X 10^6 KWH (73.2 TWH), that is - approximately 1 000 KWH/ person. The- source of this energy in 1982 and its - consumption since 1976, is shown on -- Tables 2 and 3.

If taken an average of 9% as a re- presentative of the values for the pre vious table, and in the case that only- half corresponds to a Power Generation, by means of Conventional Thermoelectrics, should be necessary to burn up almost - 1.8 X 10^6 barrels of oil per day, by the year 2010.. Growth in this manner can - not be afforded, since Hydro Generation could not go as much as three times its actual installed capacity, coal is very limited and Nuclear so expensive.

Therefore, it seems more convenient for Mexico to elaborate a short and long range planning, for the construction of Power- Plants, based on the availability of altern -- sources of energy, of which Mexico is plentiful.



fig. 1 ELECTRIC SYSTEMS & INTERCONNECTION MAIN LINES C.F.E.

SYSTEM	TYPE OF POWER PLANT							TOTAL
	HIDRO	STEAM	COMBINED CYCLE	TURBO GAS	DIESEL	GEOTHERM	COAL	
INTERCONECTADO DEL SUR (SIS)	6172	4091	791	572	9	25	—	11660
INTERCONECTADO DEL NORTE (SIN)	378	3505	432	753	—	—	300	5368
TIJUANA - MEXICALI	—	287	—	209	—	180	—	676
PENINSULAR (YUCATAN)	—	367	—	120	30	—	—	517
LA PAZ — SISTEMAS AISLADOS	—	75	—	32	62	—	—	169
TOTAL	6550	8325	1223	1686	101	205	300	18390

TABLE 1. POWER GENERATION (MW) As Of 1982

OIL AND COAL	49.2	TWH
GEOTHERMIC	1.3	TWH
HYDRO	22.7	TWH
TOTAL	73.2	TWH

TABLE 2.- ELECTRIC ENERGY CONSUMPTION BY TYPE OF SOURCE IN 1982.

YEAR	TWH	GROWTH (%)
1976	44.6	—
1977	48.9	9.6
1978	53.0	8.4
1979	58.1	9.7
1980	61.9	6.5
1981	67.9	9.7
1982	73.2	7.8

TABLE 3.- ELECTRIC ENERGY CONSUMPTION SINCE 1976

GEOTHERMAL RESERVES.

To date in Mexico are known 346 -- areas with possibilites for Power Generation, most of them distributed along the Volcanic Belt as indicated on Fig. 2.

RESERVE	MW
PROVED	920
IDENTIFIED	4600
UNDISCOVERED	6000
TOTAL	11520

TABLE 4.- MEXICO GEOTHERMAL RESERVES



FIG. 2.- GEOTHERMAL LOCALIZATION OF GEOTHERMAL AREAS.

The application of multiple exploratory and production techniques as well as mathematical modeling to predict and evaluate Geothermal Potencial of such - areas, has permitted to classify the -- reserves as per Table 4.

The distribution of these reserves are:

- Proved reserves; determined through exploratory and production wells; and as a result of using mathematical model to evaluate potential- and assure no less than 20 years operation.

CERRO PRIETO	700 MW
LOS AZUFRES	165 MW
LOS HUMEROS	55 MW
TOTAL PROVED	920 MW

Within the accessible resource --- base, as defined by the U.S.G.S.:

- Identified reserves; characterized by drilling or by geochemical, - geophysical and geological evidence.

LOS AZUFRES MICH.	492 MW
LOS HUMEROS, PUE.	668 MW
LA PRIMAVERA, JAL.	148 MW
SAN MARCOS, JAL.	260 MW
CERRO PRIETO, B.C.	108 MW
SAN AGUSTIN, MICH.	260 MW
ARARO, MICH.	260 MW
SAN BARTOLOME, GTO.	460 MW
IXTLAN DE LOS HERVORES, MICH.	72 MW
TAXHIDO, HGO.	247 MW
LOS NEGRITOS, MICH.	143 MW
PUROAGUITA, GTO.	164 MW
HERVORES DE LA VEGA, JAL.	143 MW
LA CIENEGA, SIN.	143 MW
CULIACAN, SIN.	143 MW
OTHERS	857 MW
TOTAL IDENTIFIED	4,600 MW

-Undiscovered reserves; unspecified-concentratios of Geothermal Energy surmised to exist on the basis of broad geologic, and geochemical - knowledge and theory.

From all the rest of the 346 areas, was estimated 6 000 MW as possible.

POWER PLANTS CONSTRUCTION PROGRAM.

As of the moment, the program indicated on Table 5 is included in the --- construction and investment program of- the Electric Sector (POISE). Graphic - Representation is made in Fig. 3.

FIELD	CAPACITY		OPERATION	
CERRO PRIETO II	UNIT 1	110 MW	MAY.	1984
	UNIT 2	110 MW	OCT.	1984
CERRO PRIETO III	UNIT 1	110 MW	OCT.	1984
	UNIT 2	110 MW	JUL.	1985
CERRO PRIETO IV	UNIT 1	110 MW	MAY.	1992
LOS AZUFRES I	UNIT 1	55 MW	MAR.	1988
	UNIT 2	55 MW	JUN.	1988
LOS AZUFRES II	UNIT 1	55 MW	MAR.	1991
	UNIT 2	55 MW	JUN.	1991

TABLE 5.- POISE GEOTHERMAL POWER PLANTS. CONSTRUCTION PROGRAM

One year experience, operating 5 - MW portable units in Los Azufres, has - demonstrated the convenience of using - them especially as complement of Power- Plant with condenser.

One of the main attractives of --- using these plants is its relative small size and short time for hook up and running it after well completion, which -- saves money and gives very useful reservoir information before deciding the -- installation of a formal Power Plant.

An intermediate alternate is the - utilization of 10 MW small plants with- condenser. These are not as portable - as the 5 MW plants but more efficient.

The possibility of using small --- plants looks attractive for Mexico, --- since National Manufacturers are able - to produce them not totally but in great part.

In table 6, is shown the alternative to modify the Geothermal Power --- Plants construction of POISE, but subject to financial and economical relation -- ships of the country.

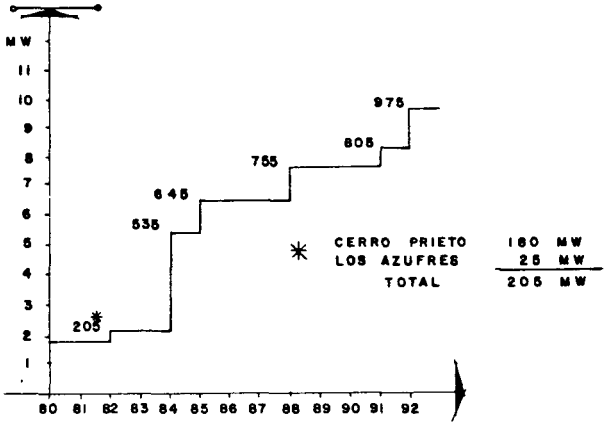
The installation cost per KW for - the different types of plants is as --- follows:

COST IN USCY/KW

	POWER PLANT	WELLS
100 MW	500	200 (1)
55 MW	700	400 (2)
5 MW	350	500 (2)

(1) TAKEN FROM CERRO PRIETO II

(2) TAKEN FROM LOS AZUFRES



3.- GRAPHIC REPRESENTATION OF CONSTRUCTION POROGRAM.

YEAR	POWER (MW)		ACUMMULATED POWER (MW)		TOTAL
	SMALL PLANTS	FORMAL PLANTS	SMALL PLANTS	FORMAL PLANTS	POWER TO INSTALL
ACTUAL	25	180	25	180	205
1983	—	—	25	180	205
1984	20	330	45	510	555
1985	20	110	65	620	685
1986	20	—	85	620	705
1987	20	—	105	620	725
1988	20	110	125	730	855
1989	25	—	150	730	880
1990	30	—	180	730	910
1991	35	110	215	840	1055
1992	40	110	255	955	1205
1993	45	—	300	950	1250
1994	50	55	350	1005	1355
1995	55	—	405	1005	1410
1996	60	110	465	1115	1580
1997	60	—	525	1115	1640
1998	60	110	585	1225	1810
1999	60	—	645	1225	1870
2000	60	110	705	1335	2040

TABLE 6.-ALTERNATIVE TO CONSTRUCTION PROGRAM OF POISE

In order to attain an energy generation as mentioned before, it will be necessary to drill at a pace of 30 to 35 wells per year as an average.

Drilling and related activities such as exploration, reservoir engineering and surface installations design, will require an adequate training program of human resources.

The forecasts obtained for the year 2000 have been based on the following presumptions:

EXPLORATION.

Sustainment of the exploration activities utilizing five groups each consisting of 1 Geologist, 1 Geophysicit, 1 Geochemist and 1 Reservoir Engineer, besides the auxiliary nonspecialized personnel.

According to our present organizational diagram, interpretation and evaluation of the compiled data, would take place at the Central Offices where 5 Geologists, 3 Geophysicist, 5 Specialists in Petrography and 5 in Hydrology would be required.

DRILLING.

If one equipment is considered to drill 3 1/2 wells per year, 10 drilling equipments will be necessary in order to achieve the established annual goal of 35 wells. This means for CFE to have 10 Drilling Engineers, 30 Supervisors, 10 Specialists in Electric Well Logs plus some 50 Technicians able to handle the logging equipments. On each field where drilling is taking place it will be required in addition, 1 Geologist, 1 Geochemist, 1 Environmental Protection Engineer, 2 Reservoir Engineers and 2 Well Termination Specialists. To this we must add the respective Field and Laboratory Technicians.

PRODUCTION.

During the exploitation of a field, permanent activities of well repair, maintenance, hydrology, evaluation of the reservoir evolution and field operations are required. For this purpose we are considering for each field being exploited, 2 Drilling Engineers, 8 Technicians on Well Repair, 3 on Geochemistry, 2 on Reservoirs, 12 on Production/Generation and 4 on Specialized Maintenance (Instrumentation).

PRELIMINARY PLANS:

With the purpose of interpreting the geothermal data and studying the most adequate technical options for exploitation, it is necessary to carry out the appropriate factibility studies and preliminary plan where the thermodynamic cycle, separation and well head pressures, and policies for best resource exploitation be established. This involves the participation of Engineers Specialists on Geothermal Preliminary Plans in addition to the Mechanical, Civil, Chemical and Electrical Engineers.

SCIENTIFIC SUPPORT:

As in geothermics exceptional cases are the common rule, it will be necessary to count on a group of high level specialists dedicated to the study and solving of the specific problems arising on each field. This group must include at least one Specialized Engineer on each of the following areas: Reservoirs, Thermodynamics, Corrosion, Geohydrology, Geochemistry, Geophysics, Drilling, Environmental Protection, Chemistry and Mechanics.

We are considering that the plant design and construction activities could be performed by the highly qualified personnel the Central Organization should have for the execution of a construction program.

All human resources mentioned until now are intended to continue receiving the support of companies dedicated to the research of subjects related to Geothermics and of those Institutions, National or International, involved as producing, coordinating or research and development entities.

Moreover, our experience seems to indicate that for Mexico it would be very enticing to manufacture, and to a certain degree design with its own technology, geothermal turbogenerators of small capacity to be used as important complement to the future geothermal development.

We will conclude saying the panorama we have presented over the geothermal development in Mexico is ambitious but realistic. To be able to carry out the proposed plan it will be necessary to carefully establish a program for the formation of qualified personnel which includes formal room instruction as well as practical field training.

PERSONNEL	EXPLORATION	DRILLING	PRODUCTION	TOTAL
GEOLOGIST	10	1		11
GEOPHYSICIST	8			8
GEOCHEMIST	5	1	3	9
PETROLEUM ENGINEER		10	2	12
RESERVOIR SPECIALIST	1	2	3	6
PETROLEUM SPECIALIST	5			5
ENVIRONMENTAL SPECIALIST		1		1
GEOHYDROLOGY SPECIALIST	5		2	7
WELL TERMINATION SPECIALIST.		2		2
WELL REPAIRING SPECIALIST			8	8
PRODUCTION SPECIALIST			12	12
MAINTENANCE SPECIALIST			12	12
INSTRUMENTATION ESPECIALIST			2	2
WELL LOGS SPECIALIST		10		10
TOTAL	34	27	44	105

REFERENCES.

(1) "SITUACION ACTUAL Y PROGRAMA FUTURO DE LOS APROVECHAMIENTOS GEOTERMICOS DE LA REPUBLICA MEXICANA". — ING. HECTOR ALONSO ESPINOSA, COMISION FEDERAL DE ELECTRICIDAD, COORDINADORA EJECUTIVA DE CERRO PRIETO.

(2) "DESARROLLO DEL MERCADO ELECTRICO (1977-1991)". — COMISION FEDERAL DE ELECTRICIDAD SUBDIRECCION DE CONSTRUCCION.

(3) "ELECTRIC POWER DEVELOPMENT PLANS IN MEXICO". — ING. RAFAEL MOLINAR CESEÑA, COMISION FEDERAL DE ELECTRICIDAD, COORDINADORA EJECUTIVA DE CERRO PRIETO.

(4) "ASSESMENT OF GEOTHERMAL RESOURCES OF THE UNITED STATES 1978". — L. JP. MUFFLER AND MARIANNE GUFFANTI.

(5) "ESTADO DE LA GEOTERMIA EN MEXICO RESERVAS Y ESTRATEGIAS DE DESARROLLO". — COMISION FEDERAL DE ELECTRICIDAD GERENCIA DE PROYECTOS GEOTERMOELECTRICOS.

Proceedings Ninth Workshop Geothermal Reservoir Engineering
Stanford University, Stanford, California, December 1983
SGP-TR-74

SOME COMMENTS ON THE LA PRIMAVERA GEOTHERMAL FIELD, MEXICO

Bernardo Domínguez A.,
Gerencia de Proyectos Geotermoeléctricos,
Comisión Federal de Electricidad,
Morelia, Michoacán, México,

Marcelo J. Lippmann,
Earth Sciences Division
Lawrence Berkeley Laboratory,
University of California
Berkeley, California 94720

ABSTRACT

The La Primavera geothermal field is located about 20 km west of the city of Guadalajara, Jalisco, in the western part of the Mexican Neovolcanic Axis. Initial results of five deep exploration wells (down to 2000 m depth) were very promising; measured downhole temperatures exceed 300°C. During production, however, downhole temperatures dropped, and the chemistry of the fluids changed. The analysis of geologic, mineralogic, geochemical, and well completion data indicate that colder fluids flow down the wellbore from shallower aquifers cooling the upper zones of the geothermal reservoir. This problem is attributed to inadequate well completions.

Doubts have arisen about continuing the exploration of the field because of the somewhat disappointing drilling results. However, a more thorough analysis of all available data indicates that a good geothermal prospect might exist below 3000 m, and that it could be successfully developed with appropriately located and completed wells.

INTRODUCTION

The La Primavera geothermal field lies in the late Pleistocene ryholitic complex of the same name, located about 20 km west of Guadalajara, Jalisco, Mexico (Fig. 1). Associated with faults related to caldera collapse and later magma injection, the Sierra La Primavera contains abundant fumaroles near its center and large-volume hot springs around its western boundary (Mahood et al., 1983). The temperature of these springs is about 65°C, their discharge is significant, i.e.: Río Caliente (73 L/s), Arroyo Verde (43 L/s), and Agua Brava (156 L/S). Because of these important surface manifestations the Comisión Federal de Electricidad (CFE) began in 1978 a program of geothermal exploration and evaluation. By late 1980 the first exploratory well was completed; presently five deep wells have been drilled within the caldera (Fig. 2).

The initial results of the exploratory drilling were encouraging. However, the prospects for a commercial system became less bright mainly because of a reduction in downhole temperatures as the wells were allowed to flow. We summarize in this paper the data obtained from the La Primavera wells and we offer an explanation as to the behavior of the wells during production. Finally, the location and completion of new wells, and the deepening of some of the existing ones is proposed.

AVAILABLE DATA

The bulk of the information on the exploration and development of the La Primavera field is contained in internal CFE reports, written in Spanish (Benegas, 1983; Casarrubias, 1983; Gutierrez, 1983; Munguia, 1983; Pérez, 1983; Ramírez, 1983; Romero, 1983; Torre, 1983; Villa, 1983). One of the purposes of this paper is to make available part of this information.

Mahood (1980, 1981a, and b) extensively studied the geology and petrology of the Sierra La Primavera. She characterizes the system as a late Pleistocene rhyolitic center consisting of lava flows and domes, ash flow tuffs, air fall pumices, and caldera lake sediments. Recently, Mahood et al. (1983) published the results of a reconnaissance geochemical study of the geothermal area itself. Their model of the geothermal system suggests that the heat source could be a melt zone or magma chamber approximately 15 km in diameter and 2-5 km below the surface. Most of the shallow heat would be available where permeable zones associated with deep faults have permitted convection of hydrothermal fluids.

According to Mahood et al. (1983) the geothermal reservoir is largely in volcanic rocks that predate the Primavera caldera, consisting of silicic ash-flow tuffs and lava flows, and andesitic to basaltic lavas. Therefore, the reservoir rocks will present a wide range of permeabilities and porosities. Their model shows (Fig. 3) that near the center of the Sierra La Primavera hot water (>300°C) rises to shallow depths, where it boils to form a shallow vapor-dominated zone. Steam of this zone heats meteoric water in a shallow, high permeability aquifer (in the Tala Tuff) from which steam separates at about 170°C. Part of the steam escapes to the surface through fault-related fractures cutting the less permeable zones of the Tala Tuff which act as a cap rock to the geothermal system. The remaining geothermal fluid then flows laterally as a two-phase fluid, cooling by conduction, emerging as hot (about 65°C) springs at the western margin of the Sierra.

The mass recharge to the geothermal system indicated by the downward arrows shown in Figure 3, could be significant. According to Ramfrez (1983) the potential infiltration in the area would be approximately 5.9 x 10^6 m^3/year. However, not all of it would reach the geothermal reservoir, part will feed the important near-surface aquifer. The leakage of meteoric waters to the geothermal reservoir is rather slow. On the basis of tritium analyses, Mahood et al. (1983) indicate a minimum age for the geothermal waters of 50 years.

WELLS

To date five exploratory wells have been drilled at the La Primavera geothermal field (Fig. 2): Primavera 1 (PR-1), Río Caliente 1 (RC-1), Primavera 2 (PR-2), Primavera 4 (PR-4), and Primavera 5 (PR-5). They are located in, or near, areas of geothermal manifestations. Each well was drilled to intersect the structures (faults, fractures) which permit the ascent of geothermal fluids from depth. Well data on the lithology, cutting mineralogy, lost circulation, completion, and temperature will be described below.

Primavera 1 (Fig. 4). This is the first deep well drilled in La Primavera. It is located in the fumarole area of "Las Barrancas" in the southern part of the caldera; its total depth is 1226 m. The lithologic column in PR-1, as in all La Primavera wells, is composed mainly by pyroclastic and volcanic rocks.

Important fractures were encountered, resulting in high, and sometimes total, circulation losses. These zones occurred mainly in the Tala Tuff between 36 and 380 m depth, and below 700 depth. The mineralogy of the cuttings indicate moderate temperatures, especially in the upper 1000 m; pyrite and epidote appear near the bottom of the hole.

During the drilling of the upper 600 m the temperature of the mud at the outlet never exceeded 52°C, and the difference between inlet and outlet temperatures was small. However, for some zones between 690 and 1100 m depth (corresponding to lost circulation zones) the outlet mud temperature exceeded 60°C. For that interval, the average maximum outlet temperature was 40°C and the inlet-outlet difference sometimes was greater than 10°C. Toward bottomhole the outlet mud temperature reached and exceeded 60°C, and the temperature difference was only about 5°C. With a static mud column in the borehole for 25 hours, the temperature near the bottom of the well was slightly above 200°C.

The completion of the well is shown on Figure 4. A long slotted liner was installed between 659 and 1159 m, allowing the communication between different feed zones of contrasting temperatures. This was reflected by the behavior of the well during production, as will be discussed below.

Río Caliente 1 (Fig. 5). RC-1 was drilled near the western edge of the caldera, in an area of high-discharge hot springs. It was intended to intersect the high-angle faults bounding the caldera.

The 1900-m deep well was drilled through rocks with few fractures; no circulation losses were observed. The mineralogy of the cuttings, the temperature of the drilling mud and the downhole temperature profiles indicate that RC-1 is a low temperature well. The borehole was left open below 297 m depth.

The model of Mahood et al. (1983) (Fig. 3) shows that this well was drilled in a discharge area, away from the hot water source near the central part of the caldera.

Primavera 2 (Fig. 6). This well is located in the central part of the caldera, in the "La Azufrera" area where vigorous sulfur-depositing steam vents exit. Drilled to 2000-m, PR-2 is the deepest La Primavera well.

Important loss-of-circulation zones were encountered in the upper 500 m, mainly in the Tala Tuff, and below 1500 m, in the microlitic andesites. Generally, the cutting mineralogy indicates moderate temperatures. However, epidote was observed at about 500 m, suggesting higher temperature alteration associated with a fault intersected at that depth. Epidote was also found near bottomhole; pyrite occurred between about 800 and 1300 m, and below 1600 m depth.

The outlet mud temperature during drilling sometimes exceeded 70°C; the inlet-outlet temperature differential, 10°C. The highest mud temperatures were observed between about 1600 and 1800 m depth, related to the partial lost circulation zones. The downhole temperatures measured after 24 hours with a static mud column in the borehole indicate boiling at about 700 m depth, and a maximum temperature of about 265°C at bottomhole.

Casing was installed and cemented to 998 m depth, and a partially slotted liner was suspended below it. The open part of the liner, below 1567 m depth, is adjacent to the zone of highest measured temperatures. However, the long open hole interval, behind the liner, allows the down-flow of colder waters within the borehole influencing the production characteristics of the well. A maximum temperature of 307°C at 2000 m, with a static water column in the wellbore, was recorded.

Primavera 4 (Fig. 7). PR-4 was drilled to a total depth of 668 m in the Cerritos Colorados graben, an area of active fumaroles. During drilling serious circulation problems were encountered, requiring the use of air and foam for some zones. All data indicate low temperatures for the drilled interval. The fractures in the microcrystalline rhyolite and Tala Tuff not only create drilling problems but also allow deep infiltration of shallow, cold ground waters, "drowning" any possible geothermal anomaly. Casing was cemented to 305 m depth. Below that the borehole is open except for a cement plug between 637 and 668 m.

Primavera 5 (Fig. 8). This well is located 580 m east of PR-1; its total depth is 1215 m. Major lost circulation problems were encountered which, sometimes, even prevented the retrieval of cuttings.

The mineralogy of the cuttings, the temperature of the mud during drilling, and the temperature profiles in the mud colum after 61 hours of static conditions--showing a maximum temperature of about 230°C--indicated better thermal conditions than in the other four wells.

PR-5 was completed with cemented casing and liner down to 879 m in an attempt to isolate the lower units from colder aquifers above. However, the slotted liner installed between 879 and 1213 m was left open to some of the moderate temperature zones in the lithic tuffs where some major circulation losses occurred. This allows the intrusion of colder fluids into the deeper part of the borehole and reservoir.

HYDROTHERMAL ALTERATION

The distributions of lithologies and hydrothermal alteration as determined from well cuttings, are shown schematically in Figure 9. The nonuniform percentage of alteration minerals reflects the interaction of the rocks with waters of different temperatures. Where higher temperatures are found, such as where hotter fluids ascend through faults and fractures, a larger percentage of alteration is observed. Conversely, where colder waters circulate and descend along faults and fractures, the alteration is less prevalent.

Figure 9 clearly indicates the highest temperatures toward the south-central part of the caldera, near wells PR-1 and PR-2, and the lowest temperatures towards its periphery (e.g. well RC-1). This thermal structure is consistent with Mahood et al's. (1983) model (Fig. 3).

BEHAVIOR OF WELL PR-1

To illustrate the characteristics of the La Primavera field, the behavoir of well PR-1 is discussed. The temperature logs taken after drilling completion are shown in Figure 10. After 25 hours with a static column of water in the borehole the highest measured temperature, about 210°C, was at total depth. During the well warmup period (Fig. 11) significant temperature increases were observed. Bottomhole temperatures above 280°C were measured.

The changes in the temperature profiles with production are shown in Figure 12. The first two logs (T-59 and T-60) taken with the well producing through a 10-in.-diam. line show rather low temperatures, possibly because some of the large volumes of cold water injected into the formation during drilling (about 3200 m^3 between 700 and 1226 m depth) are flowing back into the borehole. Profiles T-61 and T-62 (well flowing through two 2-in.-diam. lines) indicate a general increase of temperature with time. Log T-63 (well producing through a 1-1/2-in.-diam. orifice) shows the highest temperatures (maximum about 255°C) because of the low flow rate.

The later profiles T-66, 67 and 70 (well flowing through a 3-1/2 inch orifice or a 4-1/2 inch nozzle) indicate a significant drop in temperatures; the maximum measured is about 235°C. A break in the profile is shown between 800 and 900 m depth, indicating the influx of colder water. During drilling a zone of partial lost circulation was encountered at about 880 m (Fig. 4). The evolution of the downhole temperature profiles with time and production, indicates that more than one zone is feeding the well. The communication between aquifers of different temperatures behind the long slotted casing, is affecting adversely the production characteristics of this well. Similar behavior was observed in other La Primavera wells.

When a well intersects multiple feed zones, its performance during production might be unstable in response to the entrance of fluids of different enthalpies at various times (Grant et al., 1979). In PR-1 some instabilities are evident from variations in the chemistry of the produced fluids (Fig. 13). The fluid samples were taken during and after the time the downhole temperatures discussed above were measured. Until about February 1981 the produced fluids show an increasing proportion of geothermal waters, and a decreasing amount of low temperature injected water. After that time, there is general slow decrease in chloride, silica and boron, and an increase in bicarbonate and sulfate. These changes reflect an increasing proportion of colder waters in the fluids produced by PR-1. The oscillations in the content of some of these components could be due to the instabilities in the well resulting from its multiple feed zones.

SUMMARY AND CONCLUSIONS

The five wells completed to date at La Primavera indicate that the highest temperatures in the field are found in the south-central part of the caldera where faults and fractures carry geothermal fluids to shallower depths. In that area, a temperature of 307°C was measured in well PR-2 at 2000 m depth. Temperatures slightly above 200°C were recorded at 1200 m in wells PR-1 and PR-5.

With the exception of RC-1, important lost circulation zones, associated with fractures and contacts, were encountered. Because of the way the wells were completed with long open intervals, communication between different feed zones occurs, resulting in downflow of colder water in the borehole and progressive cooling of the produced fluids.

The mineralogy of the cuttings correlates well with the temperature of the formations at depth. Zones permeated by colder waters leaking from shallow aquifers show low percentage of alteration minerals; in areas where upflow of geothermal fluids occurs, the percentage is high.

On the basis of the data obtained from the five wells, it is felt that temperatures above 300°C could be found at about 2000 m depth in the area of wells PR-1 and PR-5. These wells could be deepened or new wells could drilled in that part of the caldera. Another region to be explored with drilling is south of these two wells, where the distribution of alteration minerals and the geologic structure suggest the existence of high subsurface temperatures. The exploration wells should be at least 3000 m deep, preferably 3500 m.

Based on the experience gained from the existing wells we emphasize that the completion of any new well should be carefully designed using all available data, in order to isolate the geothermal aquifers from colder, shallower water-bearing zones. Only with these deeper and properly designed wells will one be able to evaluate the geothermal potential of the La Primavera field.

ACKNOWLEDGEMENTS

We gratefully acknowledge the assistance of our colleagues of the Gerencia de Estudios Geotérmicos of the Comisión Federal de Electricidad for sharing their information. We wish to thank N.E. Goldstein and H.A. Wollenberg of the Lawrence Berkeley Laboratory for discussing and reviewing the manuscript. Part of this work was supported by the Assistant Secretary for Conservation and Renewable Energy, Office of Renewable Technology, Division of Geothermal and Hydropower Technologies of the U.S. Department of Energy under Contract No. DE-AC03-76SF00098.

REFERENCES

Benegas S., S. 1983. La Primavera - Geología regional. Com. Fed. Electr., internal report.

Casarrubias U., Z., 1983. La Primavera - Geología de detalle y del subsuelo. Com. Fed. Electr., internal report.

Grant, M. A., P. F. Bixley, and M. C. Syms, 1979. Instability in well performance. Geothermal Resources Council Trans. v.3, p. 275-278.

Gutierrez N., L. C., 1983. La Primavera - Mineralogía hidrotermal. Com. Fed. Electr., internal report.

Mahood, G. A., 1980. Geological evolution of a Pleistocene rhyolitic center - Sierra La Primavera, Jalisco, Mexico. J. Volcanol. Geotherm. Res., v. 8, p. 199-230.

Mahood, G. A., 1981a. Chemical evolution of a Pleistocene rhyolitic center - Sierra La Primavera, Jalisco, Mexico. Contrib. Mineral Petrol., v. 77, p. 129-149.

Mahood, G. A., 1981b. A summary of the geology and petrology of the Sierra La Primavera, Jalisco, Mexico. J. Geophys Res., v. 86, p. 10137-10152.

Mahood, G. A., A. H. Truesdell, and L. A. Templos M., 1983. A reconnaissance geochemical study of La Primavera geothermal area, Jalisco, Mexico. J. Volcanol. Geotherm. Res., v. 16, p. 247-261.

Munguía B., F., 1983. La Primavera - Geoquímica de los fluidos de los pozos. Com. Fed. Electr., internal report.

Pérez Y. y Z., J., 1983. La Primavera - Perforación de pozos. Com. Fed. Electr., internal report.

Ramírez S., G. R., 1983. La Primavera - Hidrogeología de la zona geotérmica. Com. Fed. Electr., internal report.

Romero G., J. C., 1983. La Primavera - Exploración geofísica. Com. Fed. Electr., internal report.

Torre R., M. A., 1983. La Primavera - Producción y evaluación de pozos. Com. Fed. Electr., internal report.

Villa M., S. J., 1983. La Primavera - Exploración geoquímica. Com. Fed. Electr., internal report.

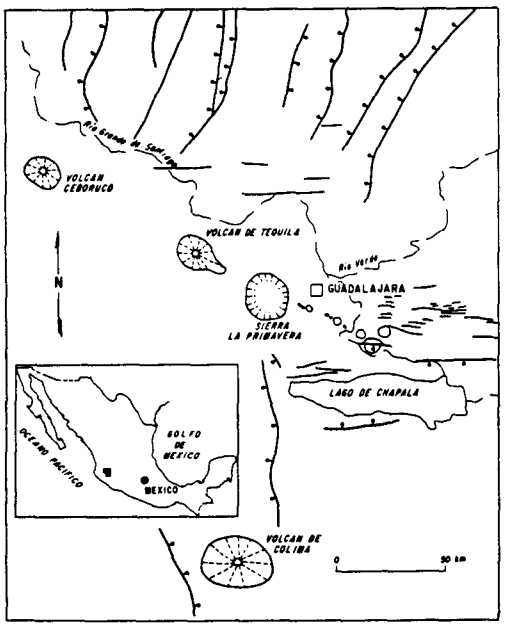


Figure 1. Location of the Sierra La Primavera, west of Guadalajara, Jalisco, Mexico (from Mahood, 1980).

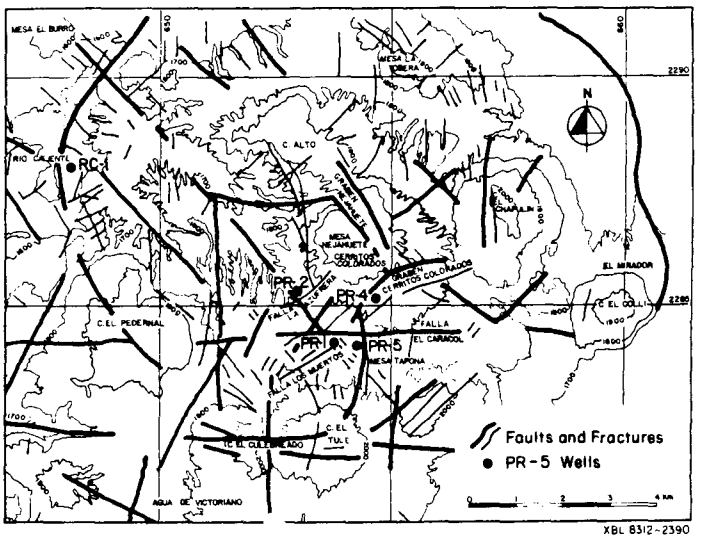


Figure 2. Structural map of the La Primavera field showing the location of the exploration wells.

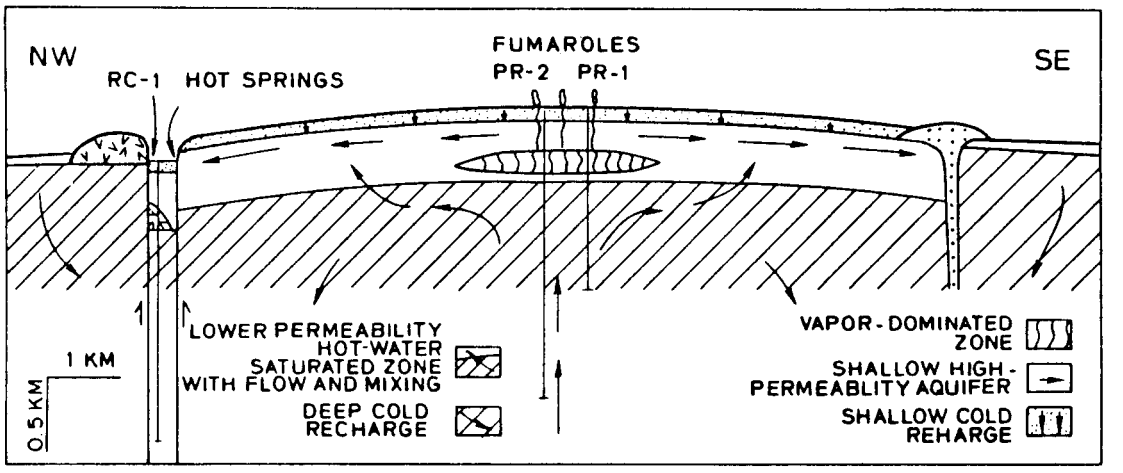


Figure 3. Schematic model for the La Primavera geothermal system developed by Mahood et al. (1983). Diagonal ruling, pre-Primavera volcanic rocks; V-pattern, precaldera lavas; unpatterned, (mainly) Tala Tuff; light stipple, lacustrine sediments; rectilinear dots, ring domes.

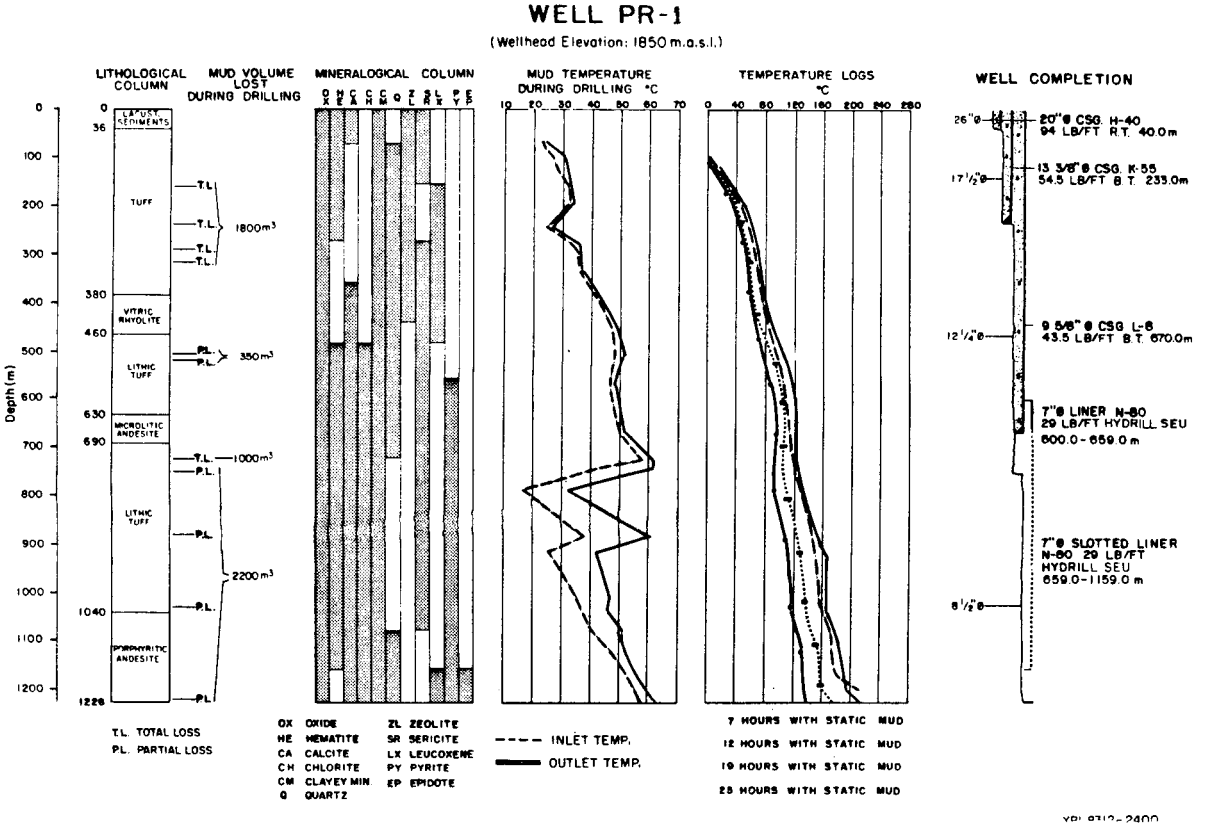


Figure 4. Well PR-1. Drilling and completion data.

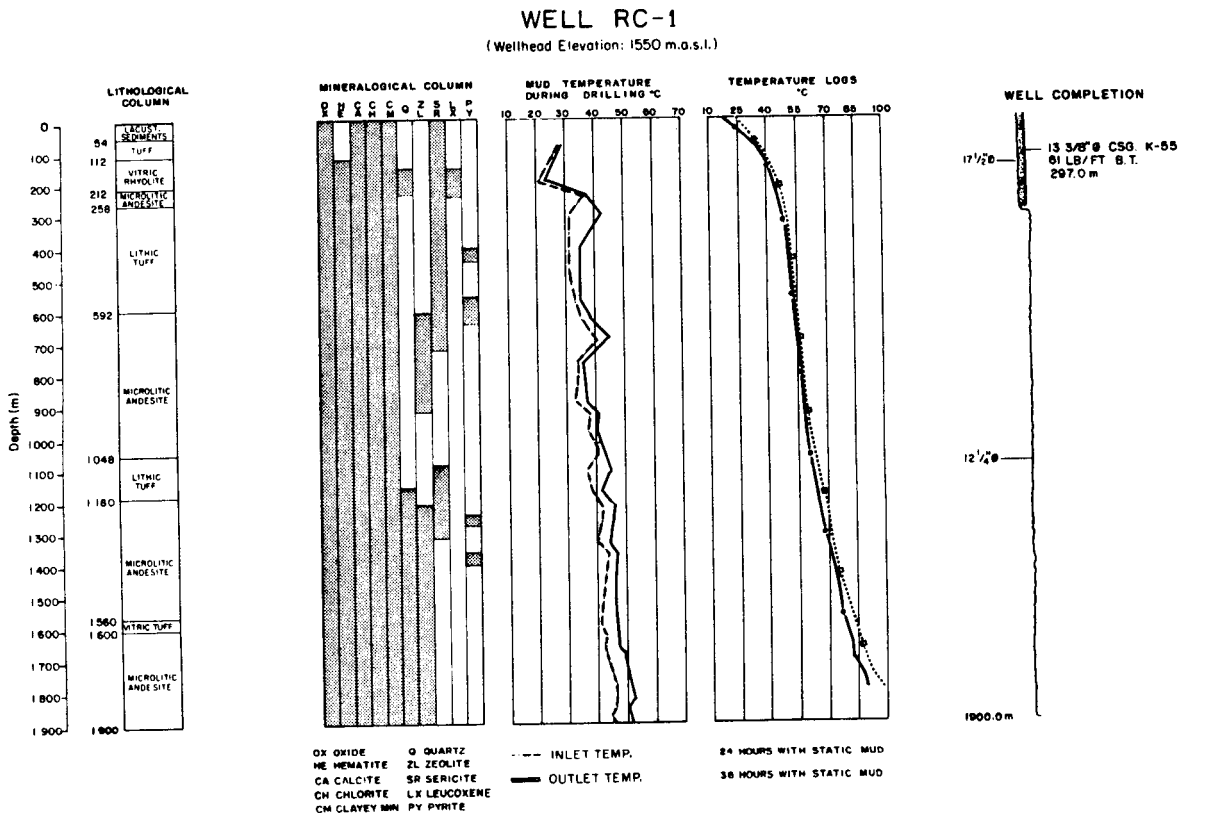


Figure 5. Well RC-1. Drilling and completion data.

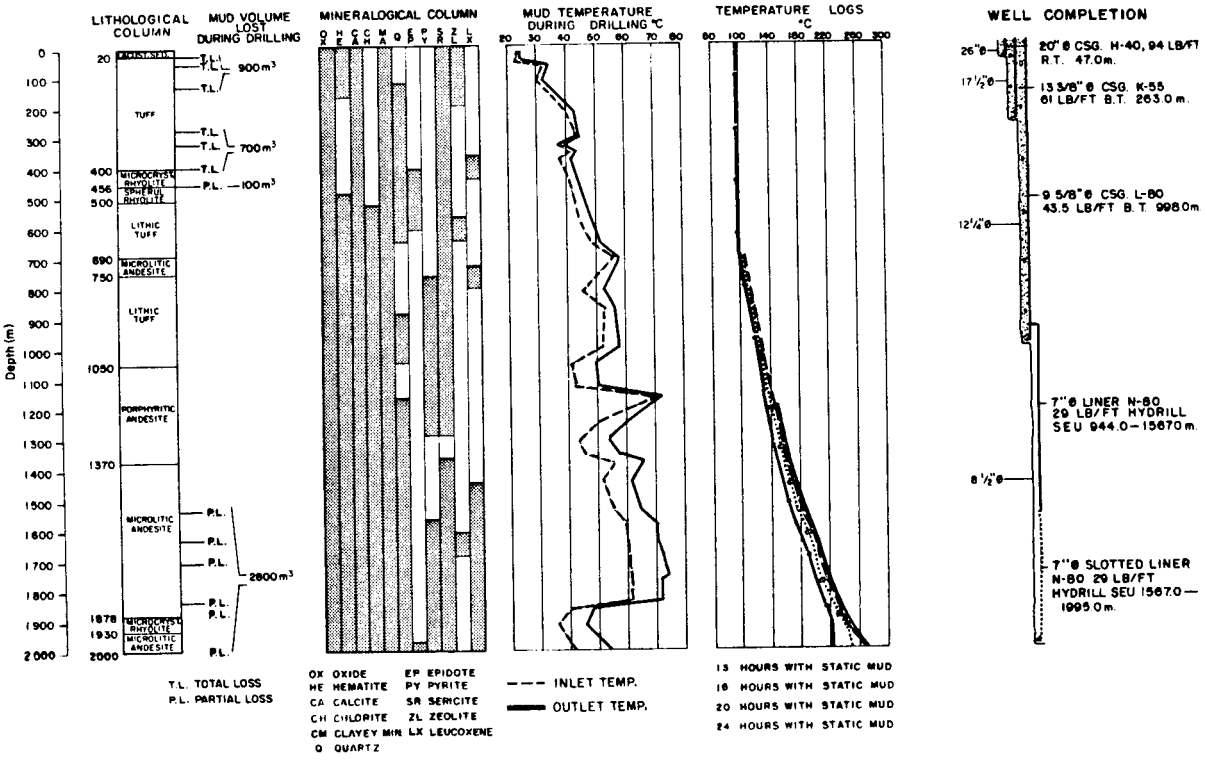


Figure 6. Well PR-2. Drilling and completion data.

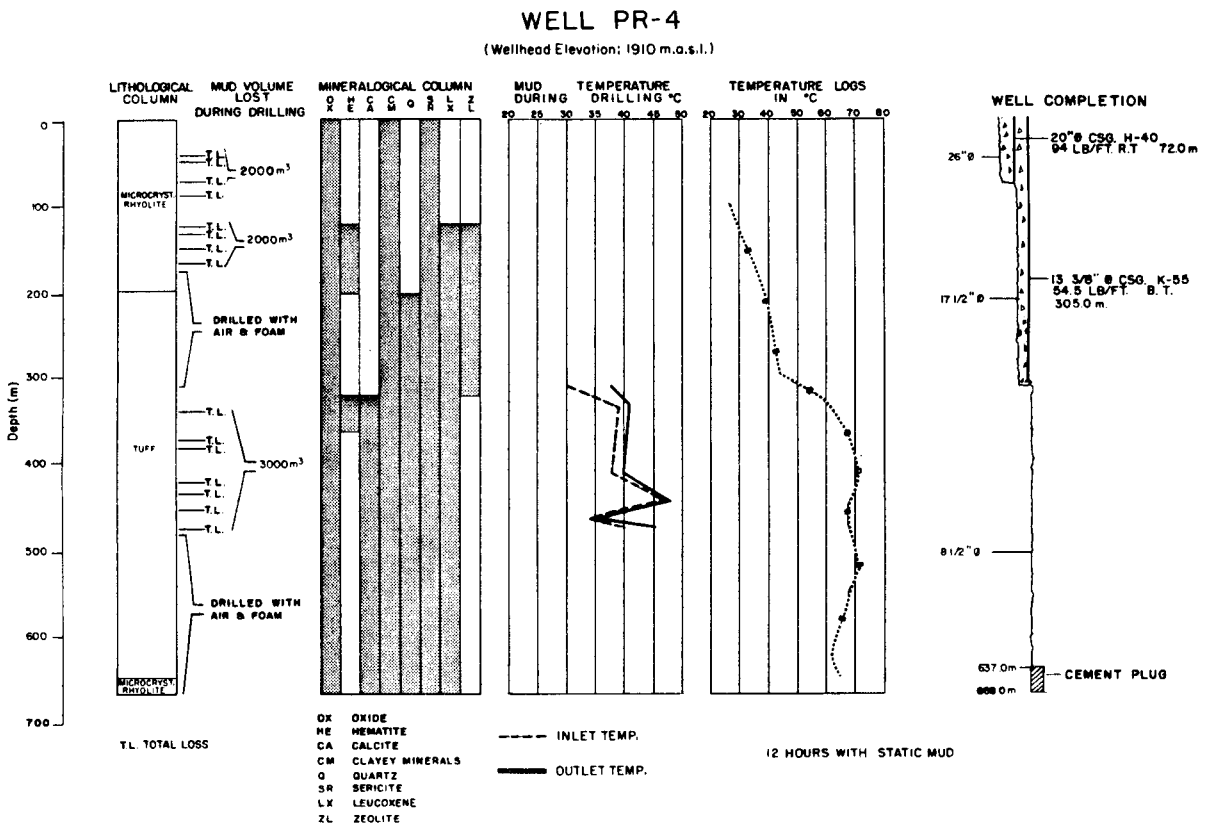


Figure 7. Well PR-4. Drilling and completion data.

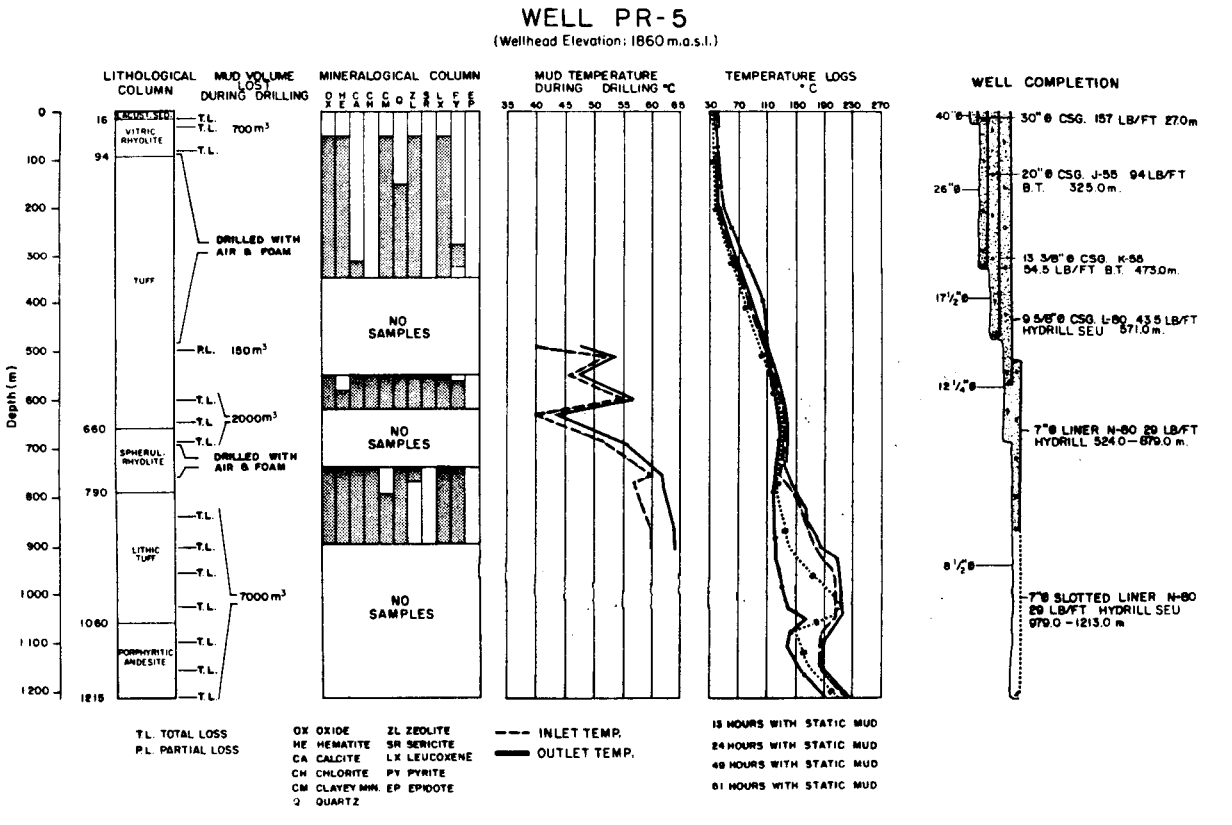


Figure 8. Well PR-5. Drilling and completion data.

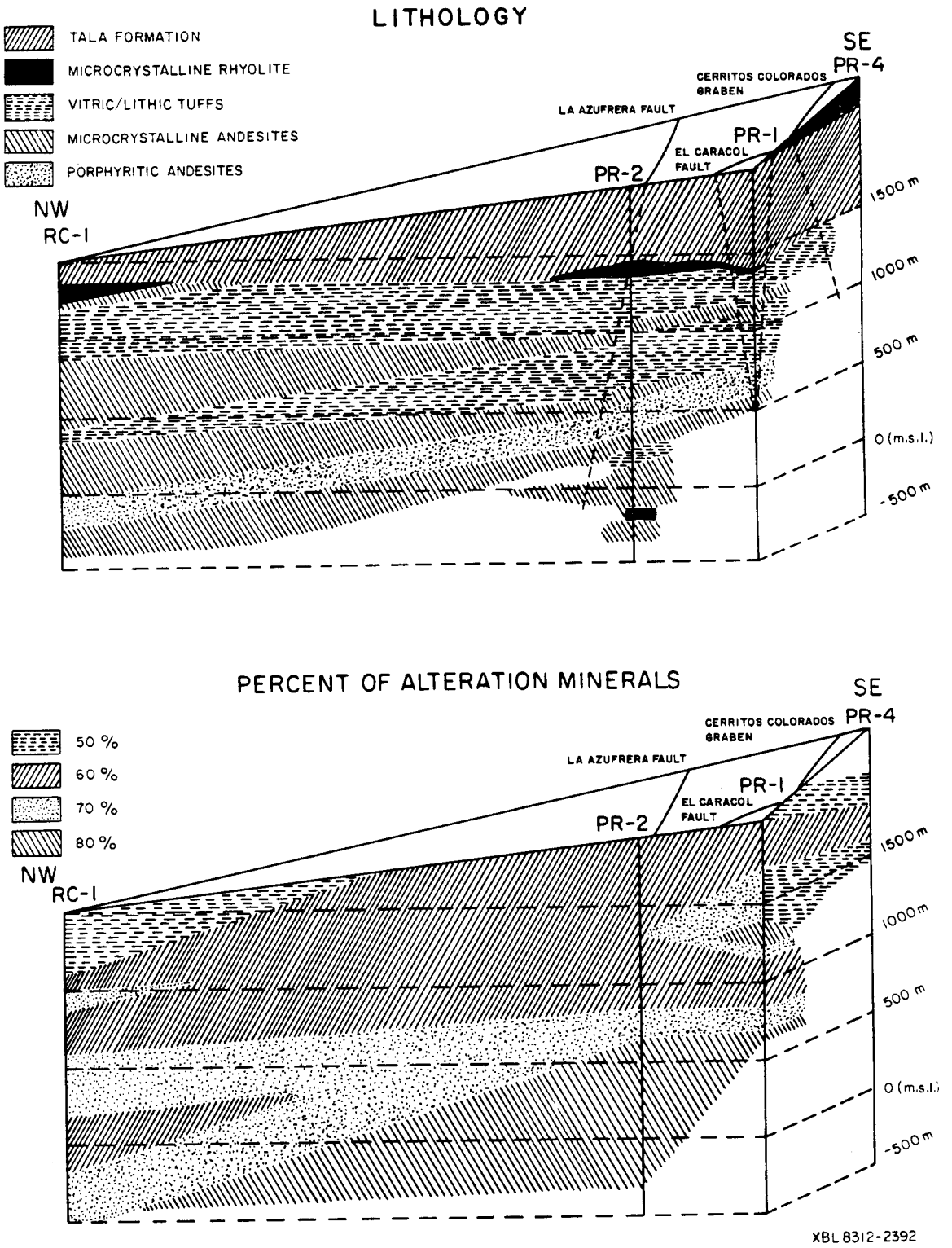


Figure 9. Distribution of lithologies and alteration minerals in the La Primavera geothermal field.

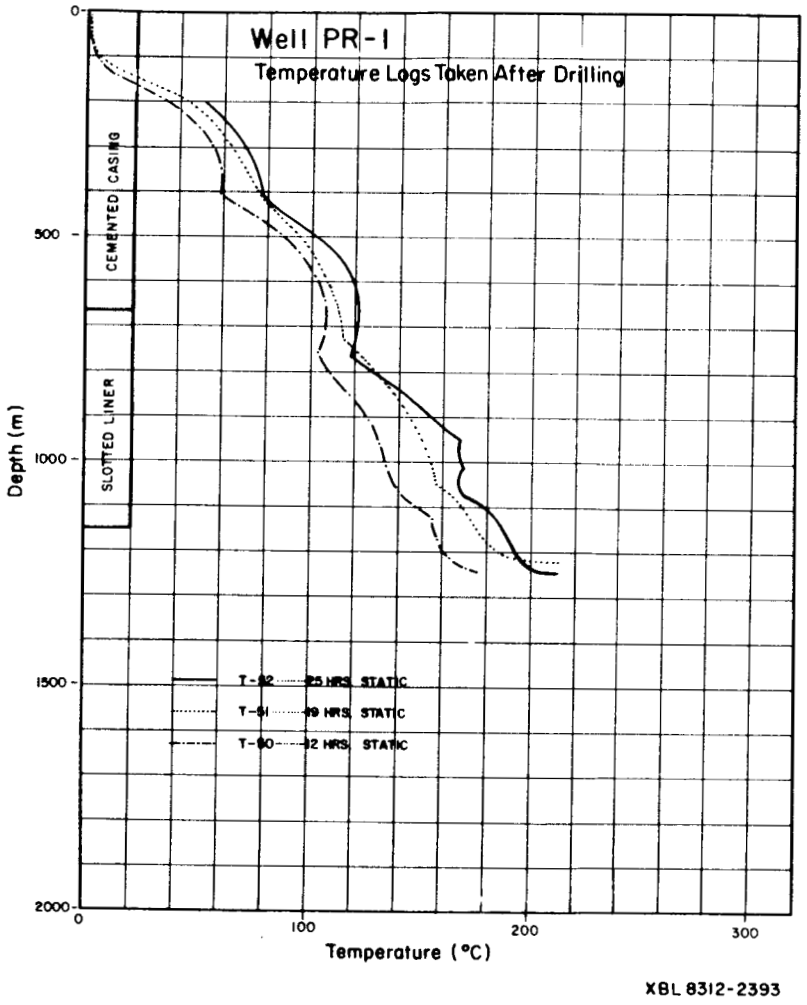


Figure 10. Well PR-1. Temperature logs taken after completion of drilling.

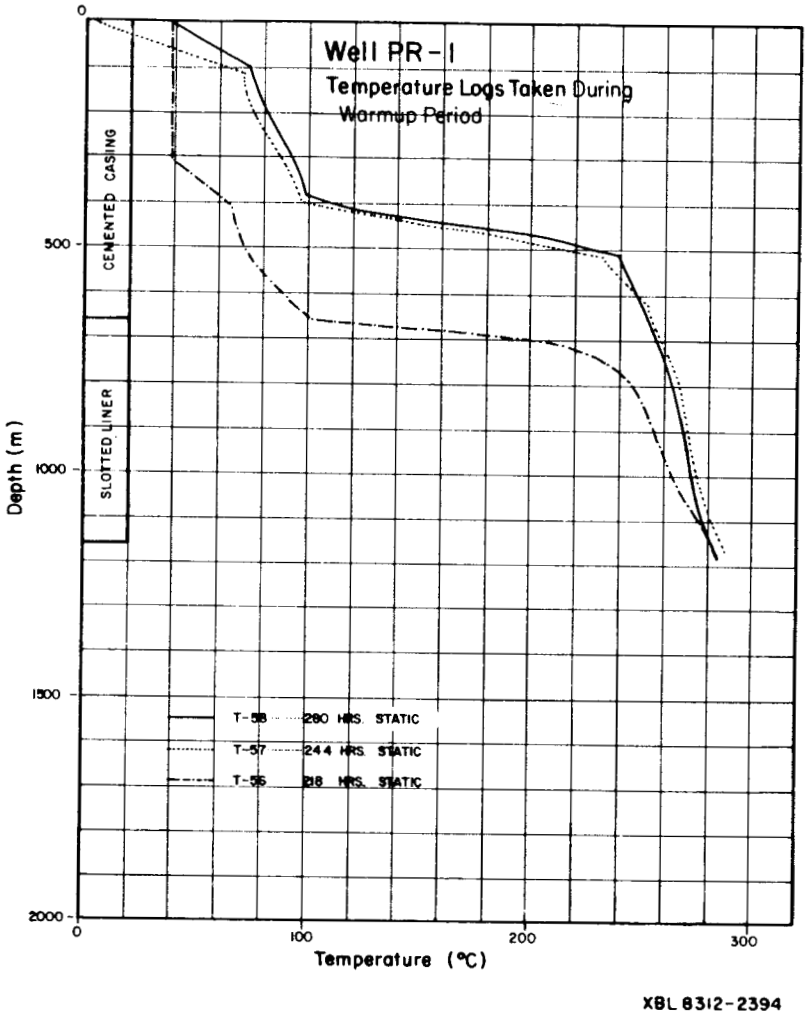


Figure 11. Well PR-1. Temperature logs taken during warmup period.

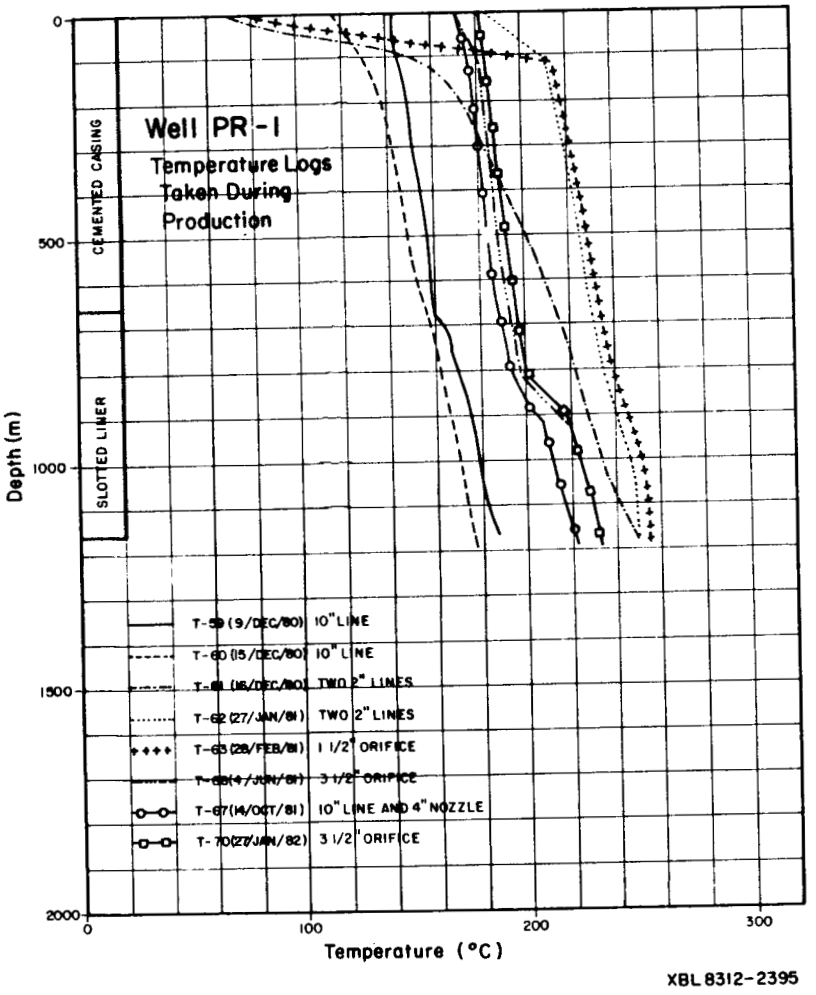


Figure 12. Well PR-1. Temperature logs taken during production.

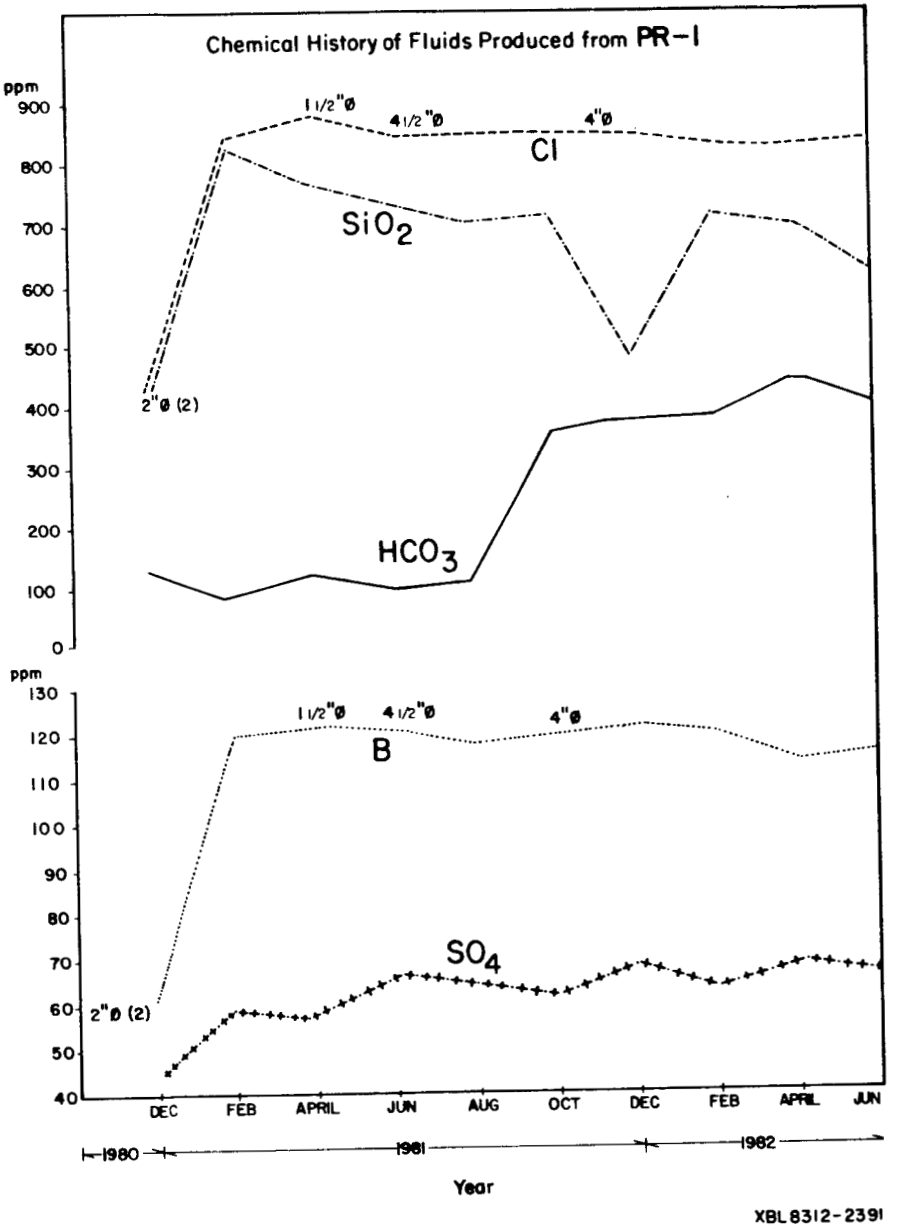


Figure 13. Well PR-1. Chemical history of produced fluids.

Proceedings Ninth Workshop Geothermal Reservoir Engineering
Stanford University, Stanford, California, December 1983
SGP-TR-74

A STATUS REPORT ON THE EXPLOITATION CONDITIONS OF THE AHUACHAPAN GEOTHERMAL FIELD

Rivera-R., Jesus,* Vides-R., Alberto,** Cuellar, Gustavo,*** Samaniego-V., Fernando,* and Neri-I., Gustavo**

ABSTRACT

The present exploitation conditions of the Ahuachapan field are discussed. The high well density in a small area has resulted in a significant reservoir pressure decrease due to the inherent reservoir over-exploitation. The average pressure in the exploitation zone has decreased from the 1975 value of 34 kg/cm^2 to the May 1983 value of 23 kg/cm^2. The production decline characteristics of the Ahuachapan wells were examined, concluding that all wells but Ah-22 show exponential decline. The cumulative production-reinjection for the field up to April 1983 is 159.090 x 10^6 tons, and 37.592 x 10^6 tons, respectively. The effect of reinjection upon field behavior is evident when observing the pressure decline characteristics of the field. It is seen that for injection fraction related to total mass extracted above 30 percent, the average decline pressure in the production area becomes approximately stabilized. If this condition is not met the reservoir pressure decreases sharply. From this finding it is concluded that a careful and properly planned reinjection program is a must for the field.

The observed temperature reduction in some of the wells seems to be the result of two operating mechanisms. First, we have the pressure decline that produces water vaporization and the consequent temperature descend. Analysis of information available shows no clear indication of deleterious temperature effects on the producing wells due to injection. The only exception observed to date is well Ah-5 that because its close distance and its relative structural position and direct hydraulic connection to injector Ah-29, presented conditions for fast displacement of the thermal front, resulting in unsufficient contact area and residence time for reheating of the injected water.

INTRODUCTION

The geothermal investigation at Ahuachapán started at about the end of 1965 with financial support from the United Nations. Since that date, numerous studies on the geology, geophysics, geochemistry and reservoir performance of Ahuachapán geothermal field have been carried out, specially after the successful completion of well Ah-1 in 1968. At present 30 wells have been drilled, 12 of them feeding the power plant, 5 more reserved for injection purposes and 13 remain under observation conditions aimed at properly defining its potential.

The reservoir behavior was considered normal up to November 1980 when the third 30 mw unit went into operation, with the inherent increase in mass output, resulting in a sharp decrease in reservoir pressure. A temperature reduction being only partially attributed to the pressure decline has been observed in some of the wells, producing water vaporization. Another possible cause of the temperature lowering effect would be the relatively cool water injected at different times into the reservoir.

This abnormal reservoir behavior prompted the Comisión Hidroelectrica del Río Lempa to undertake a thorough revision of the exploitation conditions of Ahuachapán field. This study reports on the first stage of this work, based mainly on a preliminary analysis of all of the extensive amount of information on the field that has accumulated and therefore reference will be made to results that have been prepared by other investigators.

GEOLOGICAL BACKGROUND

The Ahuachapan Geothermal Field is located in the northwestern part of El Salvador, Central America. As it is shown in Fig. 1, it is located some 20 km from the border with Guatemala and 40 km from the Pacific Ocean. The average

* Universidad Nacional Autonoma de Mexico (UNAM), Mexico, D.F.

** Comision Ejecutiva Hidroelectrica del Rio Lempa (CEL), San Salvador, El Salvador

*** Organizacion Latinoamerica de Energia (OLADE), Quito, Ecuador

elevation of the field is about 800 m above sea level and it is sitted on the northeastern slopes of a range of composite volcanoes of Quaternary age.

The thermal anomaly responsible for the occurrence of the Ahuachapan Field is due to its location at the edge of the central graben of El Salvador[1]. The geothermal field is situated in the vicinity of the intersection of the central graben and the main axis of a sinking transversal geological structure. This structural location favors deep hot fluid assent through a marginal set of faults and further lateral fluid migration along a NO-SE oriented transversal fault system (Fig. 1). The most permeable horizon along the intersection of these system of faults is constituted by an alternated andesitic mass with the presence of breccia and fine pyroclastics. As is illustrated in Fig. 2, this andesitic mass is known as the Ahuachapan Andesite and constitutes the main hot fluid producing horizon for the geothermal field.

PRODUCING CONDITIONS.

It is shown in Fig. 3 that the current drilled area for the field is of about 6.4 sq km while exploitation is concentrated in a smaller area of 0.6 sq km, with 16 wells completed and only 12 of them feeding the power plant.

It is evident that the actual production area is overexploitated, resulting in a pronounced pressure decrease in the center of the field. The magnitude of this decrement can be observed in Fig. 4 through the isobaric pressure distributions measured in December 1975 and May 1983. It can be observed that the pressure decrement has been uniform throughout the field but a focus is located in its center. It can be seen that in the outer area pressure has gone down in this period from 40 to 30 kg/cm^2, while the exploitation zone was encompass by the isobaric line of 34 kg/cm^2 in 1975 and in May 1983 by the 24-23 kg/cm^2 line.

Figs. 5 and 6 show the variation of mass production, reinjection and average reservoir pressure versus time. Fig. 7 presents the data of the two previous figures in an alternate manner; this is an updated version of a similar figure included in reference 3, where reinjection is shown as a percent of total mass produced. It can be seen that for an injection fraction above 30 percent approximately, the average pressure decline in the production area becomes nearly stabilized. This stabilization is evident in the period between November 1978 September 1980 (see Fig. 6). During this time mass reinjected accounted for 30 percent of total mass extracted and it was preceeded by two injection periods, the first from September 1976 to August 1977 with a 39 percent reinjection and the second from September 1977 to October 1978 with a 44 percent reinjection. The effect of reinjection during these three periods resulted in a almost stabilized reservoir pressure of 28 kg/cm^2.

From November 1980 to the first quarter of 1982, the geothermal system presented non-equilibrium conditions as a result of a 23 percent increment in mass extraction with respect to production during the previous stabilized production-injection period. This in addition to a 43 percent reduction in reinjection resulted in a change of the pressure decline gradient from -0.37 (kg/cm^2/year) during the stabilized period to -2.91 (kg/cm^2/year). As recognized earlier, this sharp pressure decline coincides with the start of operation of unit 3 in November 1980. The overexploitation effect is clearly apparent in the results of average pressure versus cumulative production of Fig. 8. This graph shows the additional pressure drop caused by the increment of mass extraction needed for the operation of unit 3.

Fig. 9 presents the variation of mass extracted per unit pressure drop versus producing time. These results indicate the energy utilized in the production of the geothermal fluids. Fig. 10 shows extra indication of the efficiency of exploitation in terms of mass production weighted with respect to the number of producing wells versus producing time, clearly indicating that the decreasing tendency has been stopped, reaching an approximate constant value as of the first quarter of 1983.

Decline curve theory has been successfully applied to Ahuachapán wells. In this study several production histories for different wells were analyzed reaching the previous conclusion of earlier investigators that all Ahuachapán wells but Ah-22 show exponential decline. This particular well shows a hyperbolic decline as shown in Fig. 11. A key well because of its position in the field and of its behavior is well Ah-1 (see Fig.3) Fig. 12 illustrates the production history of this well, where two well defined production trends are identified; the first goes from 1976 to the end of 1980, denoted by the straight line 1 and the second begins from this latter time when unit 3 started operations and continues through the end of 1982 and it is represented by straight line 2. The extrapolation of straight line 1 represents the production decline expected for well Ah-1 if the production conditions of the field would have not been drastically incremented at the end of 1980; on the other side, the extrapolation of straight line 2 represents the production decline expected for the well if production would continue at the 1982 level.

An alternate very useful way to analyze the production decline characteristics of a well is through the Fetkovich's type curve method, Figs.13 and 14 illustrate the use of this technique for the production data of wells Ah-22 and Ah-1, previously presented in Figs.

11 and 12. The resulting matches confirm the findings previously discussed for these wells.

REINJECTION OF WASTE WATER

By the end of the 1960's[9] it became apparent that in order to properly develop the Ahuachapan Geothermal Field, a suitable waste water disposal system had to be established. At that time, there were several options available; disposal into rivers, conduction of the brine to the Pacific Ocean through a mountain range by means of a canal, or reinjection of the spent water either outside or in the geothermal field. After evaluating each one of these options[1], it was decided to carry out large-scale reinjection experiments at the field. In 1970-71 almost 2×10^6 m^3 of water at 150°C were injected at rates of 91 of 164 lt/sec, without any evident technical difficulty. Results of these tests are fully described elsewhere[10]. Based upon these results, it was decided to reinject within the high-temperature system in such a way as to establish a secondary heat-sweep of the reservoir rock and also as a hydraulic support for natural water recharge to the system.

Unit 1 of Ahuachapan began electricity production in June 1975 and residual water injection started in August 1975 by using well Ah-2 as an injector (see Figs. 3 and 5). As waste water output from the reservoir was continuously increasing, more wells had to be used for injection purposes. In January 1976 well Ah-8 was converted to reinjection, followed by Ah-29 in April and Ah-17 in October of the same year. Amount of waste water increased further after start up of Unit 2 in July 1976. By the end of 1975 there was an estimated total extraction of 28.716×10^6 tons from which only 2.151×10^6 ton of water had been reinjected by means of Ah-2; meanwhile, as April 1983 a gross total 159.090×10^6 tons of water had been extracted and 37.592×10^6 tons of waste brine had been conducted back to the reservoir through those four wells mentioned before.

Through the life of the project, not all injection wells had been active at all times. As shown in Fig. 1, due to the location of injector wells, it is convenient to separate injection history into two distinctive areas; the northeastern area which comprises well Ah-29 and Ah-2, and the western area that contemplates injectors Ah-17 and Ah-8. It is important to notice that due to their structural situation as well as to their particular completion and total depth, wells Ah-2 and Ah-8 can be considered somewhat marginal to the main geothermal system, meanwhile Ah-17 and Ah-29 are closely related to the productive horizon. Therefore, reservoir response to cool waste water injection could be expected to be different for all of them. Average reservoir temperature is in the order of 230°C, meanwhile waste brine is reinjection at about 150°C.

At western area, reinjection of separated water from wells Ah-6 and Ah-21 at Ah-17 started in October 1976 and ended in May 1978. Total estimated mass injected in this well was in the order of 113.526×10^6 ton. Its main injection period went from February 1977 up to May 1978 with injection rates ranging from 0.23 to 0.38×10^6 ton/month, with an estimated average of approximately 0.28×10^6 ton/month over this period[3]. As shown in Fig. 1, production wells Ah-6 and Ah-24 are within a 250 m radius of this injection well. This fact in addition to the highly fractured nature of Ahuachapan's reservoir rock, has raised some controversy as to the magnitude of possible detrimental thermal effect that injected cool waste water has had on the production characteristics of those wells. At present, no conclusive results have been reached. Further study in this direction is needed and is being carried out. After suspension of injection in Ah-17, this well was successfully converted to producer, having shown a satisfactory temperature recovery.

Well Ah-8 is also located in the western area of reinjection. Its structural position seems to be marginal as far as to the main system of faults is concern. Injection in this well started as early as January 1976 and went on in an almost uninterrupted manner until May 1982. Injection in this period showed a peak of about 0.165×10^6 ton/month in 1976 and then diminished fluctuating around an average of 0.11×10^6 ton/month up to the middle of 1981. It is unlikely that any important thermal contamination of the reservoir have occurred due to injection at this well; however, as mentioned, further studies have to be conducted in order to arrive to a final conclusion.

Injection well Ah-29 is located in the northwestern area of reinjection. Its structural position and open interval places this well within the productive horizon of the Ahuachapan Field. Besides this, tracer studies[10] performed during an injection long-term test in near by well Ah-5, showed good transmisivity in the block cointaining both wells, as well as some kind of hydraulic communication with wells located at the center of the field, such as Ah-1 and to a lesser degree, wells Ah-6 and Ah-7. As a consequence, reinjection in well Ah-29 has resulted in early break through in well Ah-5 with an observable decrease in enthalpy of produced fluids from this well. This effect can easily be seen from Fig. 15. Injection in Ah-29 started in April 1976 and continued until November 1982.

Well Ah-2 is also located in the northweastern area of reinjection. Its situation seems to be marginal to the main producing area, although there is direct communication with the productive horizon, mainly through fractures. Its position seem to be the best suited of all injector wells placed until now. It started injection in April 1975 and except for short periods, it was on operation until August 1982.

In summary, reinjection of waste water into the producing horizon at Ahuachapan has proven to be helpful in reducing pressure declination rates, in those periods when mass extraction has been balanced with a given percentage of mass reinjected. As it can be seen from Figs. 6 and 7, when percent mass injected is less than some critical value, reservoir pressure declines rather sharply. Fig. 7 is an updated version of Fig. 9 of Ref. 3.

One of main objections mentioned in the literature to reinjection of waste water into the producing formation has been the danger of thermal contamination of the hot reservoir, adversely affecting produced enthalpy. The injection arrangement set up for Ahuachapan is not the most adequate. However, and with the exception of the special case of wells Ah-29-Ah-5, discussed previously, it has not been possible until now to clearly separate temperature effects in produced fluids due to pressure drops and those resulting from possible mixtures with colder injected water. Fig. 6 shows the behavior of well Ah-1, the oldest producing well of the field, in which no thermal effect coming from cooling with injected fluids is apparent.

CONCLUSIONS

Further studies need to be carried out in Ahuachapan in order to establish a better definition of several important parameters for a more appropriate management of the field. Among these parameters the following are considered to be of prime importance:

1. Connectivity in the reservoir, in order to define the most probable direction of movement of injected fluids.
2. Better control of injection depth at injection wells.
3. Expanding the exploitation area of the reservoir, drilling new wells to the South and Southwest of the presently exploited area.
4. Establish a better geological definition of the reservoir and of the heat source and fluid recharge.
5. Perform model studies in order to establish a more adequate reinjection system for the reservoir.
6. Review and reinterpretation of field date under the new conception of the reservoir.

REFERENCES

1. ELC: "Ahuachapan Status Report." (1982)
2. Sección de Ingeniería, Superintendencia de Recursos Geotérmicos, personal communication .
3. Witherspoon, P.: "Analysis of Reservoir at Ahuachapán Geotermal Field", May, 1979.
4. "Indicios de Sobre-Explotación en el Campo Geotermico de Ahuachapán", Sección de Ingenieria, Superintendencia de Recursos Geotérmicos, CEL Report, June 1982.
5. "Resultados del Cierre de Pozos en el Campo Geotérmico de Ahuachapán, Junio-Septiembre 1982", Subsección de Investigaciones Geotérmicas, Superintendencia de Recursos Geotérmicos, CEL Report, October 1982.
6. "Comportamiento del Campo Geotérmico de Ahuachapán Durante 1981", Superintendencia de Recursos Geotérmicos, CEL Report, May 1982.
7. Fetkovich, M.: "Decline Curve Analysis Using Type Curves", J. Pet. Tech. (June, 1980), 1065-1077.
8. Rivera, R.J.: "Application of Type Curve Procedures for the Analysis of Production Data from Geothermal Wells", Geothermal Resources Council, Trans., Vol. 2 (July, 1978) 575-578.
9. Einarsson, S.S., "Review of the Water Disposal Problem in Ahuachapan and its Implications: UN Development Programme Survey of Geothermal Resources, El Salvador, Project Report (August, 1970)
10. Einarsson, S.S., Vides-R,A., and Cuellar, G., "Disposal of Geothermal Waste Water by Reinjection", Proceedings, U.N. Symposium, San Francisco (1975) 1349-1363.

ACKNOWLEDGMENTS

The authors wish to express their gratitude to the personnel of the geothermal laboratory; without his help this study could not be made. Also the colaboration of the Facultad de Ingeniería of the Universidad Nacional de México is greatly appreciated. Finally the support of the Organización Latinoamericana de Energía (OLADE) and Comisión Hidroeléctrica del Río Lempa (CEL) is also recognized. Permission from CEL and OLADE to publish data included in this paper is also acknowledged.

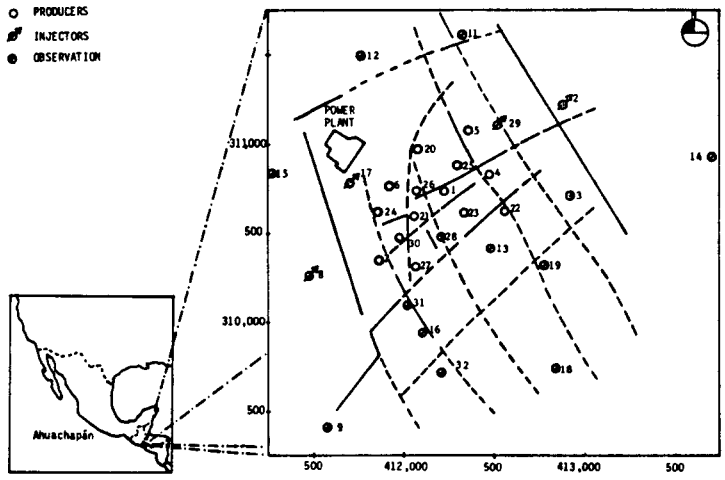


FIG.1 LOCATION OF AHUACHAPAN GEOTHERMAL FIELD AND WELL DISTRIBUTION

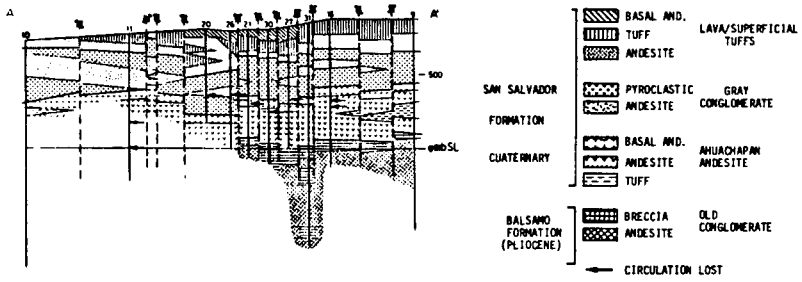


FIG. 2 STRATIGRAPHY OF THE AHUACHAPAN GEOTERMAL FIELD

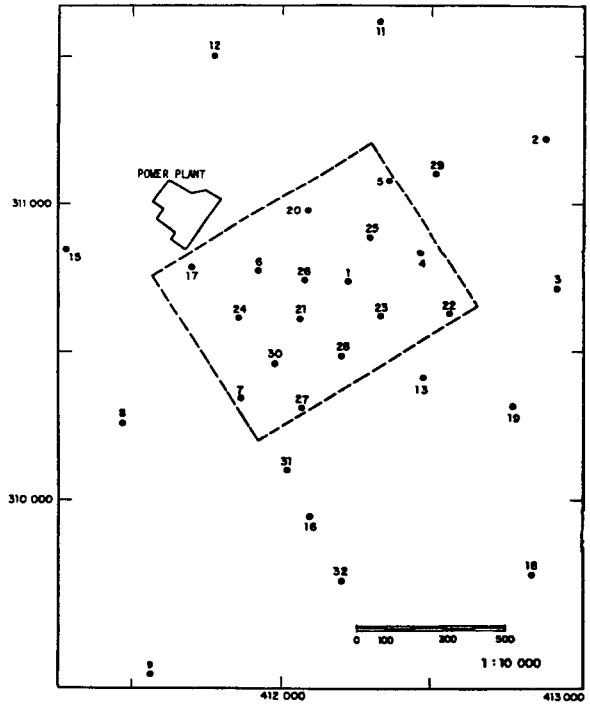


FIG 3 LOCATION OF WELLS IN THE AHUACHAPAN FIELD.

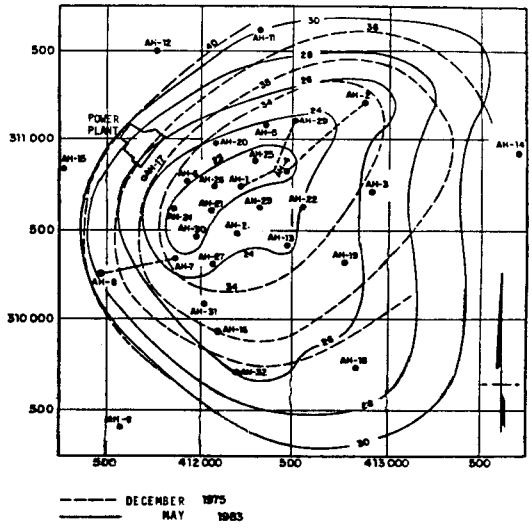


FIG 4 ISOBARIC LINES FOR PRESSURE CONDITIONS PREVAILING IN DECEMBER 1975 AND MAY 1983.

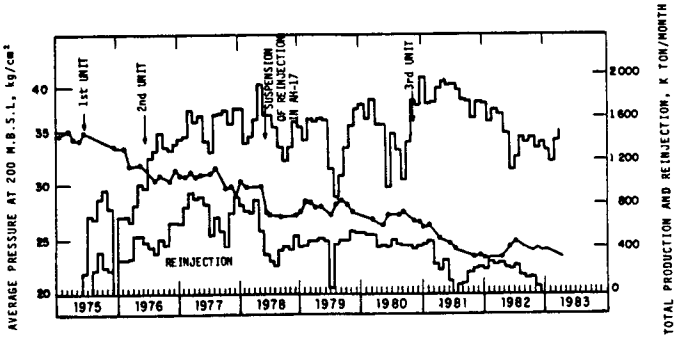


FIG 5 VARIATION OF PRODUCTION, REINJECTION AND AVERAGE RESERVOIR PRESSURE VS TIME.

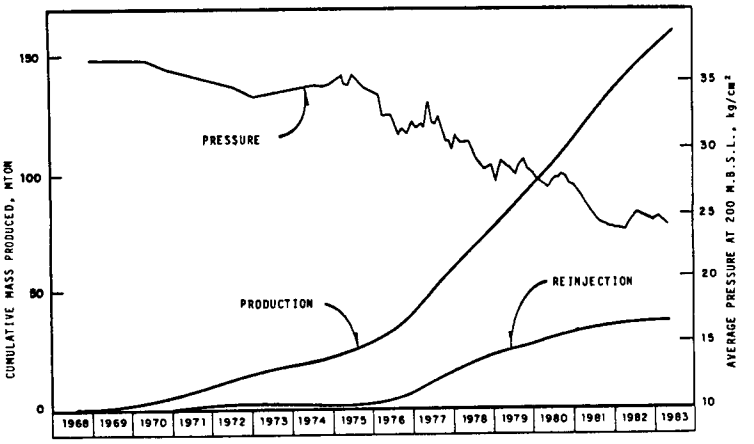


FIG 6 AVERAGE PRESSURE BEHAVIOR AS A FUNCTION OF CUMULATIVE PRODUCTION AND REINJECTION.

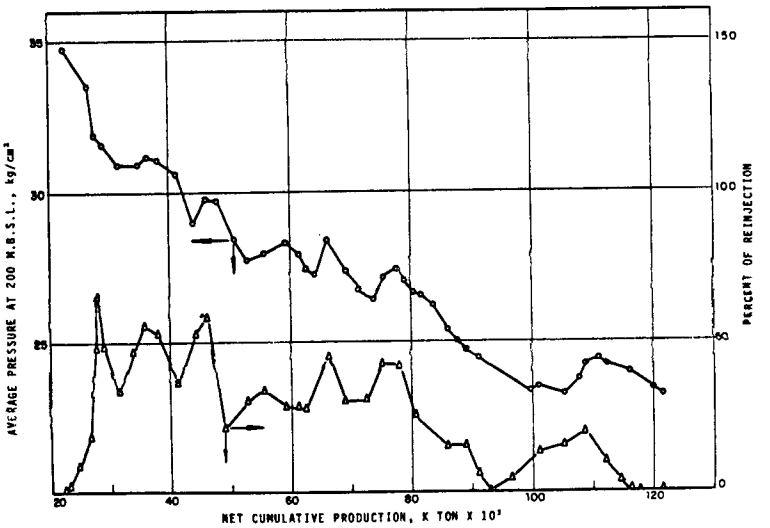


FIG 7 EFFECT OF WATER REINJECTION ON THE VARIATION OF AVERAGE PRESSURE.

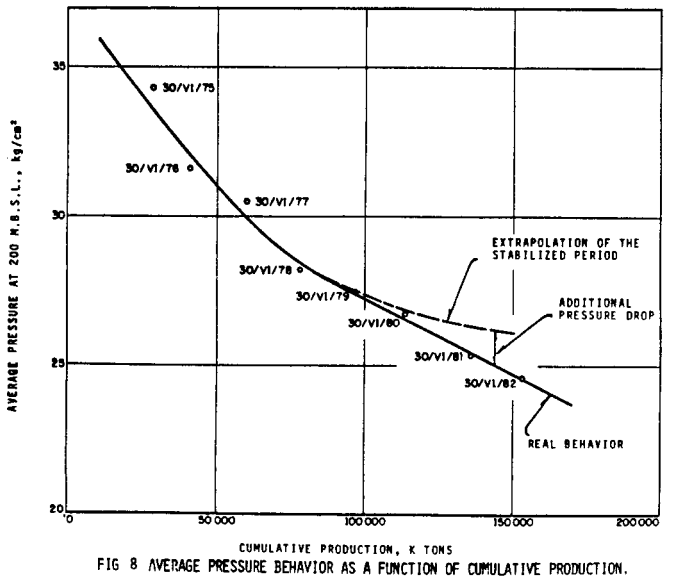


FIG 8 AVERAGE PRESSURE BEHAVIOR AS A FUNCTION OF CUMULATIVE PRODUCTION.

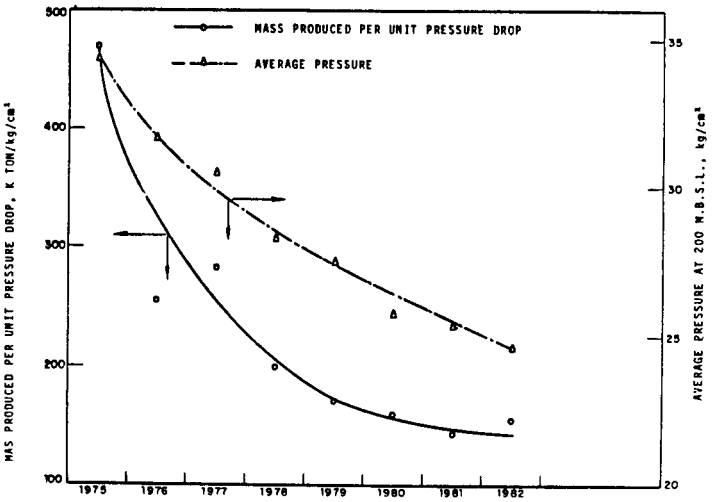


FIG 9 EFFECT OF AVERAGE PRESSURE DECLINE ON MASS PRODUCED PER UNIT PRESSURE DROP.

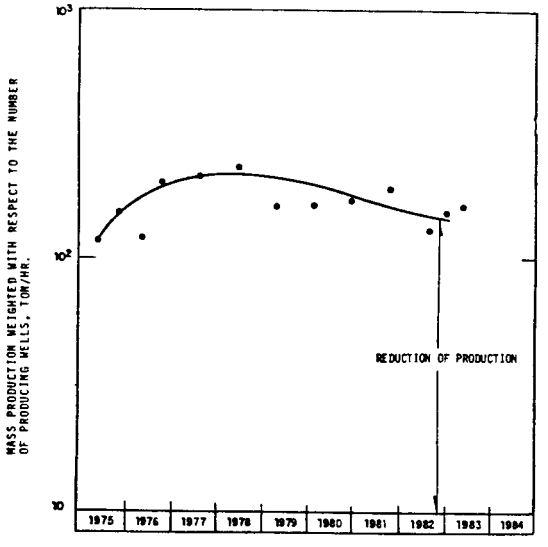


FIG 10 VARIATION OF MASS PRODUCTION WEIGHTED WITH RESPECT TO THE NUMBER OF PRODUCING WELLS VS TIME.

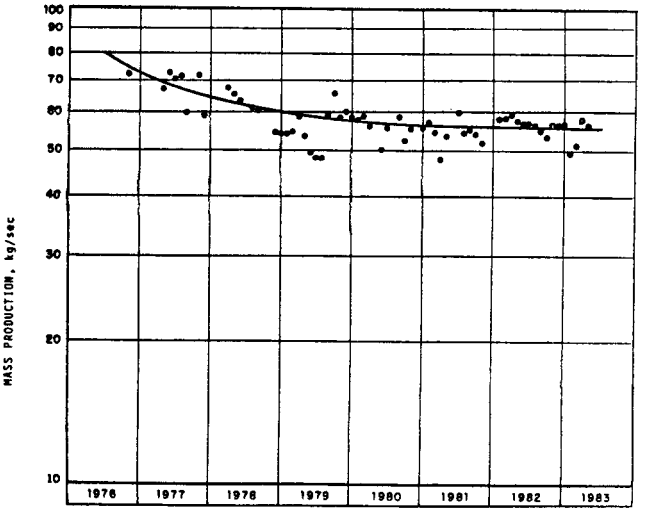


FIG 11 HYPERBOLIC PRODUCTION DECLINE FOR WELL AH-22

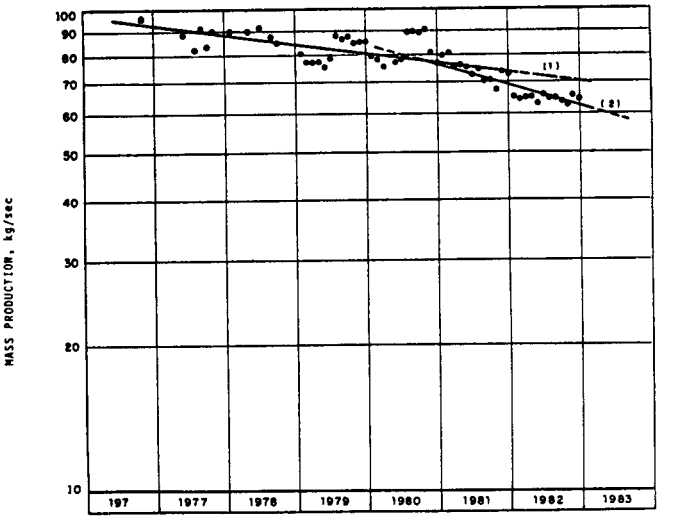


FIG 12 EXPONENTIAL DECLINE FOR WELL AH-1

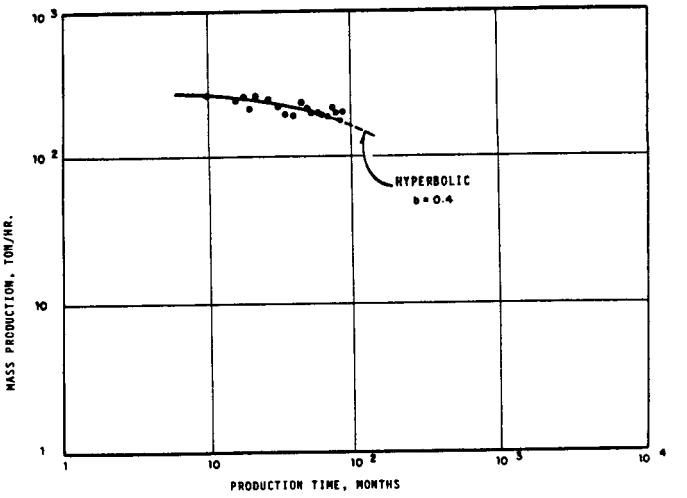


FIG 13 MATCH OF PRODUCTION DECLINE DATA OF WELL AH-22 TO THE FETKOVICH'S TYPE CURVE.

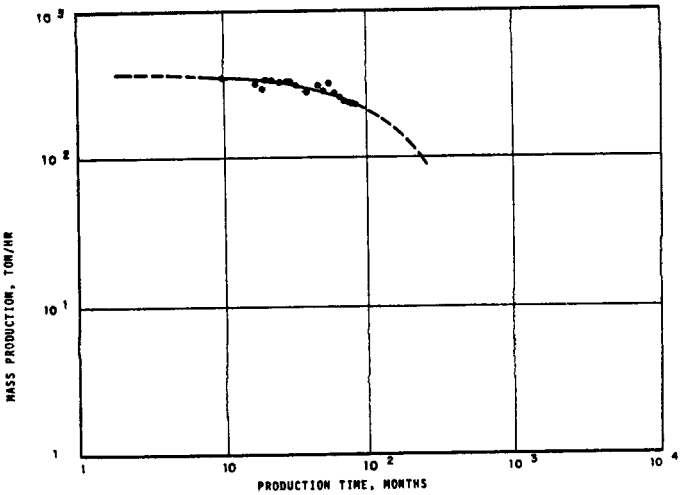


FIG 14 MATCH OF PRODUCTION DECLINE DATA OF WELL AH-1 TO THE FETKOVICH'S TYPE CURVE.

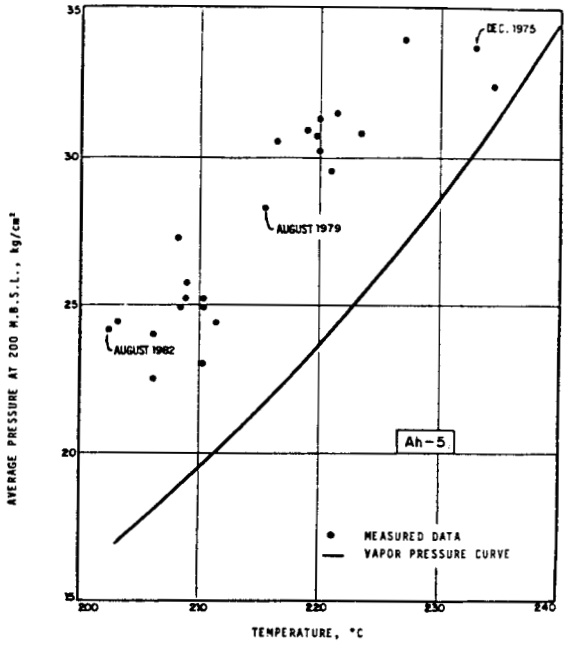


FIG 15 AVERAGE RESERVOIR PRESSURE VERSUS TEMPERATURE FOR WELL AH-5 FOR THE PERIOD DECEMBER 1975 - AUGUST 1982

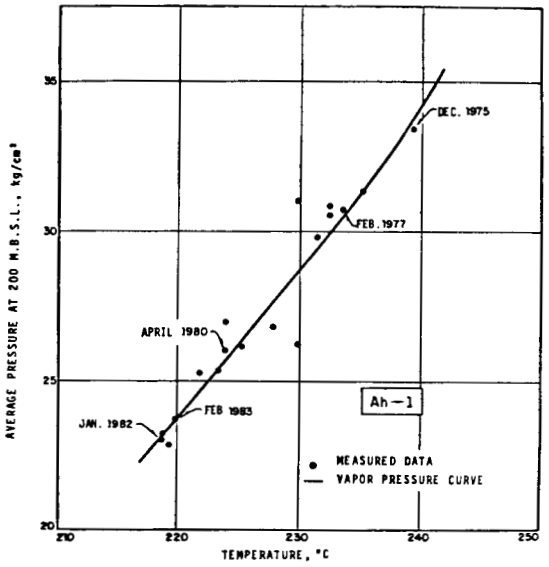


FIG 16 AVERAGE RESERVOIR PRESSURE VS TEMPERATURE FOR WELL AH-1 FOR THE PERIOD DECEMBER 1975 - FEBRUARY 1983.

Proceedings Ninth Workshop Geothermal Reservoir Engineering
Stanford University, Stanford, California, December 1983
SGP-TR-74

RECENT DEVELOPMENTS IN RESERVOIR ENGINEERING IN NEW ZEALAND

M.A. Grant*, P.F. Bixley**, M.J. O'Sullivan† and J.D. Leaver**

* Applied Mathematics Division, DSIR, Wellington
** Ministry of Works and Development, Wairakei
† Auckland University, Auckland

ABSTRACT

Over 1982-83 there have been substantial increases in the reservoir engineering contribution to the New Zealand geothermal programme. This has taken four forms:

- more extensive and detailed analysis of pre- and post-production performance, primarily at Broadlands;
- the extensive use of high-resolution pressure gauges to carry out interference tests at Rotorua, Ngawha and Broadlands;
- the installation of an extensive monitoring system at Rotorua;
- the commencement of detailed simulation of Broadlands.

Past modelling of Broadlands used a lumped-parameter model. More detailed data analysis has produced clearly-defined histories of the two productive areas of the field, and more detailed estimates of the amounts of recharge deriving from deep and shallow sources. Some interference tests at Broadlands show results which fit closely to the line source solution or the line source solution with barrier. An extensive monitoring system is being installed to record changes in the Ohaaki rhyolite, a shallow very permeable aquifer extending far beyond field boundaries.

Interference tests at Ngawha, using Paroscientific gauges mounted at wellhead or within the casing have shown responses over a distance of several kilometres, and transmissivities of several hundred darcy-metres. Similar tests at Rotorua over shorter distances have shown major structure or anisotropy within a very permeable aquifer, and anomalously large storativity.

Monitoring of reservoir pressures by water level or transducer at Rotorua has shown these to respond to barometric pressure, earth tides, fluctuations in domestic withdrawal and level of Lake Rotorua. Instrumentation of springs and geysers has just been completed.

Detailed numerical modelling of Broadlands has been started, initially with a model of the natural state. Results are expected to be used in detailed design of the reinjection system. Analysis of detailed chemical and enthalpy transients at BR21 demonstrate that the well produces from a fractured medium.

INTRODUCTION

Figure 1 shows the location of the fields referred to in the text. The geothermal program consists of maintenance work at Wairakei and Kawerau, development at Broadlands for the 102MW station to come on line in 1988, exploration work at Ngawha and Mokai, and at Rotorua the monitoring program.

ROTORUA

Rotorua field supports a major tourist attraction, the Whakarewarewa Thermal Reserve ("Whaka"), which contains some geysers and numerous springs and other surface manifestations. The field underlies part of Rotorua city and here it supports the discharge of over 400 domestic and industrial wells.

The development of the geothermal resource for such heat supply began significantly in the 1950's and has accelerated rapidly. Simultaneously, there has been an apparent decline in the surface activity of Rotorua, both in the Thermal Reserve and elsewhere. The present balance of discharge is a flow of about 100 kg/s from Whaka, and about 400 kg/s from the wells, most of which is reinjected into producing or shallower levels.

The inference that declining surface activity is caused by the increasing exploitation has led to the establishment of a monitoring programme for Rotorua. The object of this program is

to more accurately define the structure of the field and the relation between exploitation and changes in surface activity, and hopefully to contribute to an ultimate management plan.

Past records at Rotorua are scarce and generally of poor quality. There are available good histories of neither surface activity nor wells. The lack of past data severely limits present attempts to model reservoir processes. The present monitoring program consists of series of monitor wells, of groundwater wells, of instruments on springs and of well discharge measurements. Figure 2 shows a map of the city and the resistivity boundary. The major surface discharge is now at Whaka and apparently also directly into Lake Rotorua. The monitor wells are drilled to depths typical of production wells, but differ from typical wells in that they have only a very short open interval, at a loss zone, to eliminate internal flows. The monitor wells are equipped with a float recorder, if they have a water level, or else a pressure gauge. The groundwater wells are shallow wells recording the local groundwater table. Two have float recorders and the remainder are measured two or three times weekly.

A number of springs, pools or geysers in Whakarewarewa are instrumented. Variables recorded are some of: water level, temperature, time in eruption and conductivity. Puarenga stream, which drains Whaka, also has gauging stations above and below at which flow rate and temperature are recorded. Chemical samples are taken from wells and springs at intervals.

Discharge and injection tests have been carried out on a number of wells, and five interference tests utilising pairs or groups of wells.

The monitoring system is not yet quite complete, and records are available so far from only part of the system. The interference tests with several observation wells have produced puzzling responses, with quite inconsistent results at the different observation wells. In general permeability is high and storativity often larger than for a liquid aquifer. The most interesting result so far is the interference test in which water level in the observation well fell in response to cold water injection in the source well. The source well penetrated boiling temperatures. Monitor well records have been analysed for correlation with barometric pressure, lake level, earth tides and demand fluctuations. All effects are

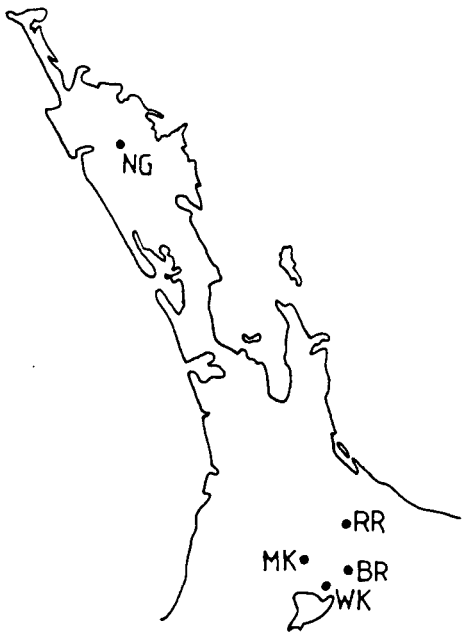


Figure 1. Northern part of North Island. Fields are labelled by their prefix: BR = Broadlands, MK = Mokai, RR = Rotorua, WK = Wairakei (all in the Central Volcanic Region) and NG = Ngawha in Northland.

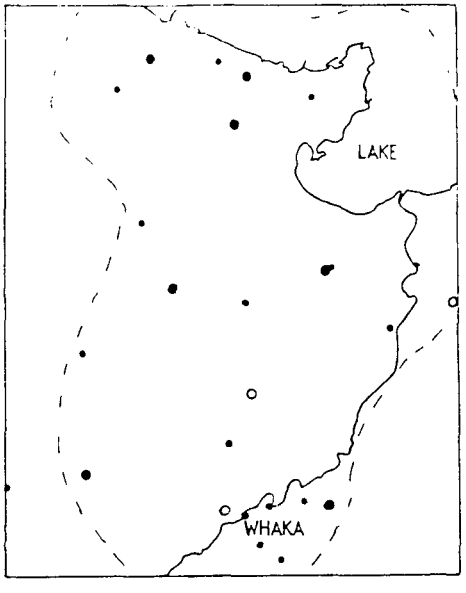


Figure 2. Rotorua field. Dashed line is approximate field boundary. Large circles are monitor wells (open circles undrilled) and small circles groundwater wells. After Grant and Bradford, 1983b.

present but not consistently. Some events are seen right across the field, confirming high permeability.

Since the monitoring program was first proposed in 1979, several more springs have failed, temporarily or permanently. Public concern over the last was such that the monitoring program's results have been partially anticipated: a task force has been established to provide technical assistance to well users to reduce flow rates. It is believed that the inefficiency of present use is so great that substantial reductions can be achieved at little cost to users, and the immediate aim of the task force is such reductions as can easily and cheaply be achieved. The longer management of the field is still unclear, and this remains the ultimate objective of the monitoring program.

WAIRAKEI

Recently work has been completed on a simple model of the Wairakei reservoir (see Blakeley and O'Sullivan, 1982). The model is rather idealised as radial symmetry is assumed and the discretisation is quite coarse. The block layout is shown in Figure 3.

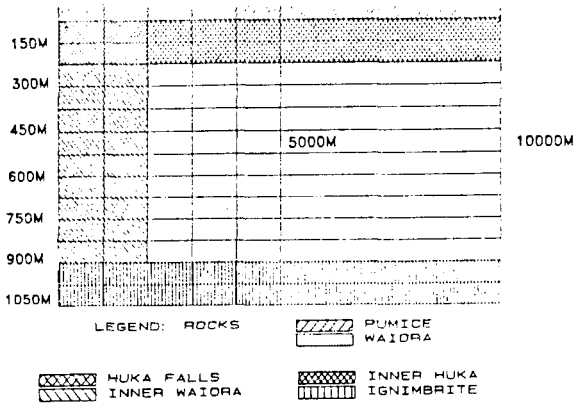


Figure 3. Wairakei field axisymmetric model.

The basic aim of the modelling study was to construct a simple model which was able to perform three tasks:

(i) reproduce a natural state similar to that observed at Wairakei before exploitation;
(ii) match the production history;
(iii) produce a plausible long-term future.

Also the model was designed to be independent of external assumptions as far as possible. Therefore a large total volume was considered so that the inevitable boundary conditions do not significantly affect the performance of the model over the simulation time of 70 years (1953-2023).

The results from the model were good. An excellent match to the pressure response was obtained (any two parameter model can achieve this) and a reasonable match to production enthalpy was obtained. A small number of parameters was used. As Figure 3 shows, different properties were used for each of the major material types (idealised here as uniform constant thickness layers), and in tuning the model to match the production history it was found to be necessary to have different permeabilities inside and outside the production zone. Further discussion of the model and the results are given by Blakeley and O'Sullivan (1982). Perhaps the most interesting results are the temperature and saturation distributions at various stages of exploitation shown in Figure 4.

They illustrate the stages of development of the Wairakei reservoir. First the two-phase zone expands as the pressure in the production zone drops rapidly. This stage continues until a quasi-equilibrium state is attained where the lateral inflow to the production zone matches the production rate. After this time the pressure drop slows and the production zone is gradually cooled by the cooler recharge water.

In fact, Wairakei is not radially symmetric or perfectly uniform, and the intrusion of cooler recharge water along faults to some parts of the production zone is already noticeable. The future predicted by the model should be regarded, therefore, as the "best possible" case.

NGAWHA

During 1983 a set of Paroscientific quartz pressure gauges and data logging equipment was purchased by Ministry of Works and Development for use on interference testing. These gauges have a resolution of 1-10 millibar depending on the individual gauge full scale range and the capabilities of the data logger.

At Ngawha we are fortunate that many of the well will stand shut with a liquid column to the wellhead and a stable pressure of 4-12 bars. So by simply attaching a high resolution gauge to the wellhead, interference observations can be made.

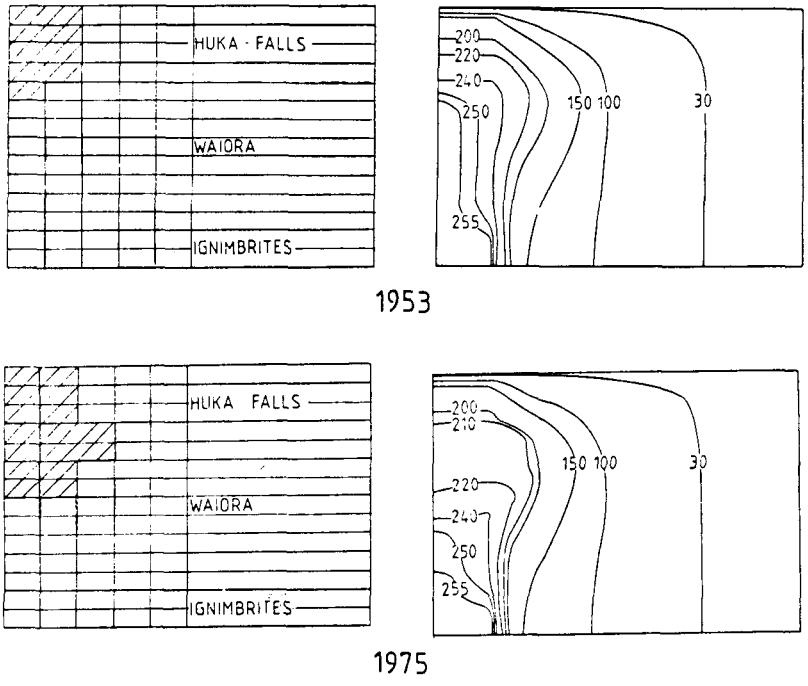


Figure 4. Wairakei model results at two times. Shaded area on left block is two-phase zone.

A section of the Ngawha field is shown on Figure 5, showing observation and production wells. In all wells except NG13 feed points are at 700-1000 m; in NG13 they are between 960-1600 m.

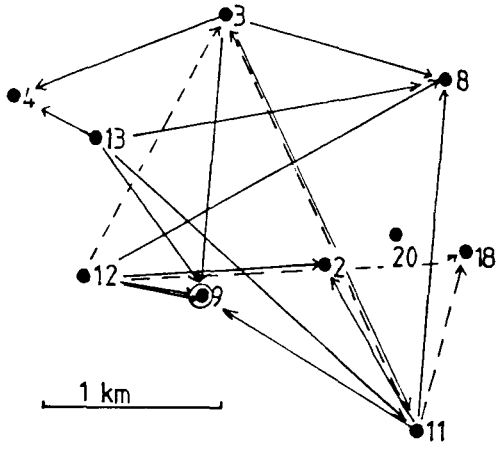


Figure 5. Ngawha field layout and interference tests. Solid lines indicate response, dashed lines no response. NG9 has a dual completion.

Ngawha reservoir is overlain by a caprock of breccia of very low permeability. The reservoir rock is fractured greywacke. Within this greywacke is a zone of very high permeability, containing liquid water at 220-230°C and 1-2%CO_2. Beneath the permeable layer temperatures rise rapidly.

Analysis of the interference test results has been difficult. There are significant instrumental problems, producing a drift in the recorded results that is difficult to correct for. Another instrumental problem is that cable coatings are palatable to cattle. There are also difficulties in the interpretation of the real data. This has been shown most strikingly in the response of NG9, 2 and 8, to NG12. Each observation well produces a result that fits well to the line source solution, but the three wells have nearly identical responses despite different distances. Work continues on a structural model.

MOKAI

Mokai field, located 25 km northwest of Taupo, is the most recent exploration target, and the most promising field yet drilled in New Zealand. The resistivity boundary contains 18 km^2 (Bibby et al., 1981). The six wells drilled so far have found that part is cool (150-220°C); part is very hot, at boiling point to above 320°C, and permeable.

The initial assessment of the reservoir has used detailed interpretation of the reservoir pressure distribution (Bixley and Grant, 1981) and the natural flow

to determine that overall reservoir values are $k_h h \geq 100$ d-m, and $k_v A \cong 20$ md-km^2, where k_v and k_h are vertical and horizontal permeabilities and h and A are aquifer thickness and area. In an exploited reservoir at boiling point vertical fluxes are important. Simulations of vertical fluid distribution under exploitation (Figure 6), implemented using the Auckland University geothermal reservoir simulator (Zyvoloski and O'Sullivan, 1980), show that for $k_v > 10$ md no deep production wells will be required. By such simple modelling studies it is hoped to optimise development strategy.

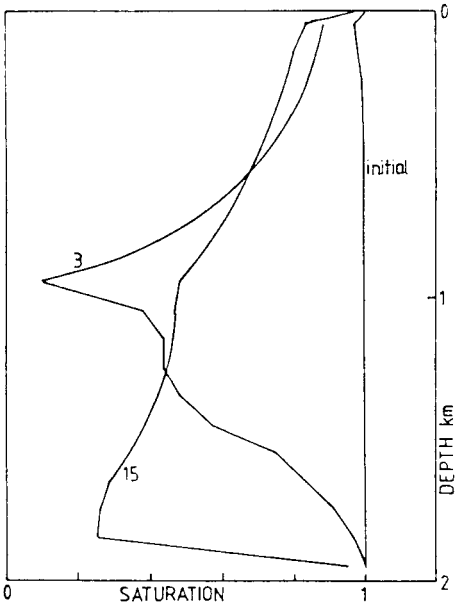


Figure 6. Mokai vertical scenarios. Sensitivity to vertical permeability. Figure shows saturation profile initially, and after 12 years withdrawal at 1000 kg/s, for k_v = 3 and 15 md. From Grant and Bradford, 1983b.

BROADLANDS

The greatest variety and depth of reservoir work has been done at Broadlands. This includes interference testing, detailed interpretation of pressure-temperature data and simulation.

Interference testing

Several of the investigation and production wells drilled at Broadlands will stand open with a stable water level, unless stimulated into production. Since 1979 most of these wells have been used to monitor interference effects from single well production or injection tests. Most of the wells are drilled to about 1200 m and have feed points at 800-1000 m. Nine interference tests were done, including one well pair where the observation and production wells were reversed, and later an injection test was performed. Results from most of these tests have been previously analysed using semi-log analysis methods and are reported by Grant, Donaldson and Bixley (1983).

In May 1983 Professor H.J. Ramey Jnr visited New Zealand and gave a series of lectures on well test analysis. As part of these lectures the Broadlands interference tests were re-evaluated using log-log matching to the line source solution. Examples of curve matching are shown in Figure 7.

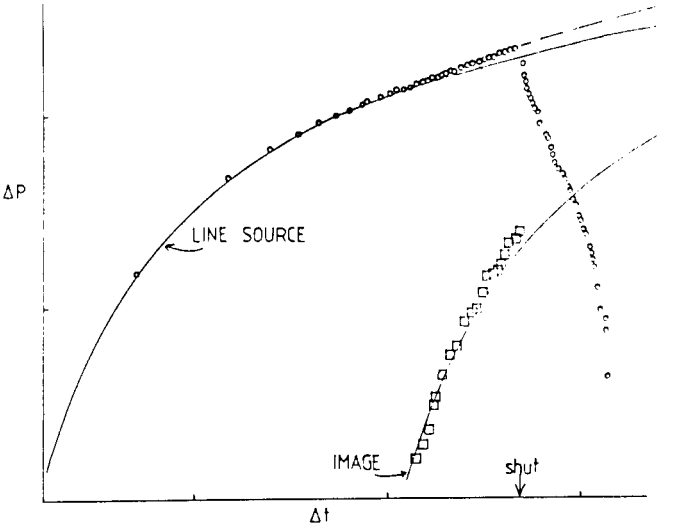


Figure 7. BR13 response to BR23 production, log-log plot. Boundary effect after 11 hrs production.

In general the observed data corrected for changes in atmosphere pressure - the water levels were 0-90 m below surface and were recorded with a resolution of 1-3 cm, i.e. 1-3 millibar - give very good matches with the line source solution, and display a range of characteristic responses. Figure 7 shows a boundary effect commencing during the production period.

Results are summarised in Table 1, together with those presented by Grant, Donaldson and Bixley, using semi-log analysis. Image distances obtained from the line source analysis are somewhat erratic, but permeability-thickness values are quite consistent showing an area with kh of 70-100 d-m in the known, hot, productive section of the reservoir and a more extensive area to the south with a lower permeability-

Observation well	Prodn well	r m	SEMILOG ANALYSIS kh (d-m)	SEMILOG ANALYSIS ϕch (x 10^{-7} m/Pa)	LINE SOURCE ANALYSIS kh (d-m)	LINE SOURCE ANALYSIS ϕch (x 10^{-7} m/Pa)	LINE SOURCE ANALYSIS image (m)	LINE SOURCE ANALYSIS duration (hr)
13	23	280	90	7.8	93	0.7	2400	140
23	13*	"	120	3.1	72	1.3	3600	500
23	13(I)	"	95	2.8	68	2.1	900	50
23	19	360	80	5.6	93	3.1	1100	190
34	31	570	-	-	20	6.4	-	300
34	23	790	-	-	27	3.6	-	200
34	19	740	-	-	29	4.0	3400	500

TABLE 1. BROADLANDS INTERFERENCE TEST RESULTS

* For this test choosing the correct straight line is very difficult and the line source match is not as good as for other tests.

thickness of 20-30 d-m and cooler formation - say 200°C compared with 260-270°C in the productive reservoir.

Further testing

During December 1983 an extensive interference testing program will commence at Broadlands to determine reservoir parameters at the production level (600-1000 m) and in cooler aquifers overlying the production field. In this program up to 20 wells, of a range of depths from deep production wells (1200 m), through monitor wells (150-500 m) to groundwater holes (10 m), will be monitored continuously for response to production or injection at various levels of the system.

Reservoir interpretation

Past modelling of Broadlands relied upon a single average pressure history against which a lumped-parameter model was calibrated (Grant, 1977). There is in fact considerable detail in the pressure distribution, both in area and depth, over time. More detailed reservoir histories have been constructed. Figure 8 shows pressure drawdown in 1980-81. Two well-defined areas, W (West or Ohaaki) and E (Eastern) appear. Also shown is an anomalous zone in which pressures are consistently high, conjectured as the upflow region of the field.

Using pressure histories for Eastern and Western fields, and of shallow and deep zones of Ohaaki, more detailed mass and energy balances have been made. Of the 30 Mt discharged from Ohaaki 1968-71, it is estimated that 15 Mt was replaced from the East and 10 Mt by downflow from the rhyolites above the reservoir. Most of the 10 Mt loss from the rhyolite was in turn made up by return of water disposed at surface.



Figure 8. Isobars of drawdown, 1980-81. Pressure drop is marked in bars. Solid circles are productive wells and open circles non-productive. From Grant and Iles, 1981.

Simulation

The Broadlands geothermal reservoir presents a difficult modelling task because it contains significant quantities of carbon dioxide in the reservoir fluid. However, there are plenty of data available enabling approximate pressures, temperatures and chemical compositions to be deduced over a large part of the field. Also, a large discharge of the reservoir, with a resulting large pressure drop, was made during the period 1968-71. The behavior of the reservoir during this period and its

subsequent recovery from 1971-74 and beyond was extensively monitored, thus providing an excellent data base for model calibration.

Work is proceeding on various modelling studies of the Broadlands geothermal field with the aim of setting up a model to assist with the planning of the development of the field.

Some related generic studies of the behavior of gas-rich geothermal reservoirs have been carried out in collaboration with scientists at Lawrence Berkeley Laboratory (O'Sullivan et al., 1983).

The most simple model of the Broadlands reservoir is a single block with a pressure-dependent recharge. Grant (1977) used such a model to produce a good fit to the production history at Broadlands from 1967-71 and the recovery from 1971-74.

Grant's results have been reproduced using reservoir simulators with the capability of modelling gas-rich reservoirs (Zyvoloski and O'Sullivan, 1983). The main problem with simple lumped parameter models of Broadlands is their long-term behavior depends on external recharge assumptions. In order to model the actual change of recharge properties with time, some spatial variation is required.

To further study the permeability structure of Broadlands several modelling studies are being carried out. The first of these involves a simple 1-D vertical model designed to assist with understanding the vertical permeability structure of Broadlands and to help explain the pressure, temperature and CO_2 distribution in the reservoir. The model produces a good match to the observed pressure and temperature distributions in the upflow zone in the Ohaaki section of the reservoir.

The model has also been used to simulate the reservoir behavior during the 1968-74 period. The vertical discretisation of this simple model results in a better match to production enthalpy and CO_2 content histories. However, lateral recharge is still represented only by pressure-dependent sources and therefore this model cannot be used for long-term predictions, a criticism which applies even more directly to the lumped-parameter model (Grant, 1983). Detailed results are given by Blakeley et al., 1983.

Some progress has been made on a 3-D model of the natural state of the

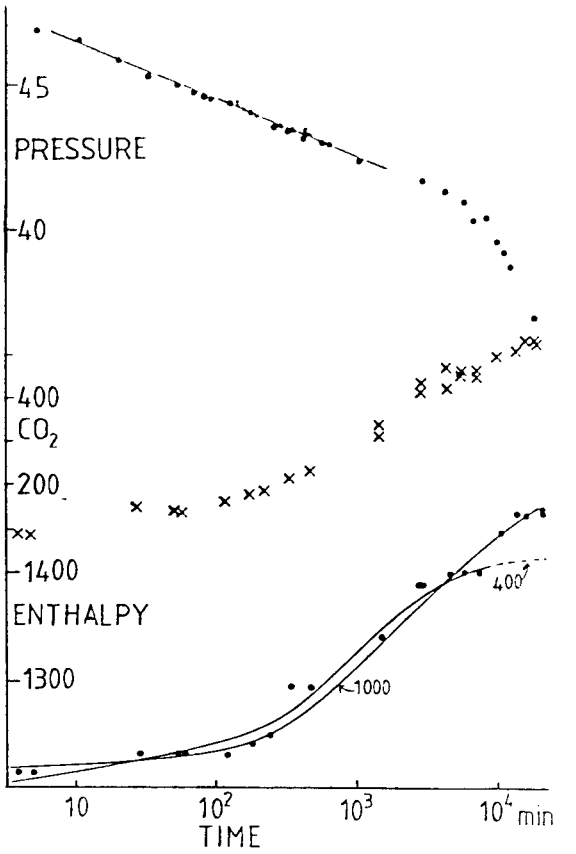


Figure 9. Changes during two weeks discharge of BR21. Pressure at principal feedpoint in bar; CO_2 content in mmol/100mol of total discharge and enthalpy in kJ/kg. From Grant and Glover (1984).

Broadlands reservoir. Also, work is proceeding on modelling the highly permeable Ohaaki rhyolite.

Other scientific work

In March-April 1982 BR21 was discharged for four weeks to obtain detailed measurements of the transient changes in enthalpy and gas and water chemistry of a two-phase well. The pressure transient results were presented at the previous workshop (Grant et al., 1982). Figure 9 shows some changes over two weeks flow at near-constant rate.

The enthalpy and chemical changes do not conform to flow in a homogeneous porous medium. Both took long to stabilise, and indeed probably did not attain stability within the test. This can be explained by modelling the reservoir as fractured, in which case the stabilisation time is increased to the block relaxation time. Correlations between chemical composition and enthalpy indicate a high residual saturation (≥80%),

assuming fracture relative permeabilities. For more details see Grant and Glover (1984).

CONCLUSION

The reservoir engineering program in New Zealand, like those elsewhere, has expanded in scope and responsibility. The combination of increased experience, better instrumentation and simulation capability means that operators now expect predictions of future behavior rather than qualitative answers.

REFERENCES

Bibby, H.M., Dawson, G.B., Rayner, H.H., Stagpoole, V.M. & Graham, D.J. (1981), "Geophysical investigations of the Mokai geothermal field", Report 184, Geophysics Div., DSIR.

Bixley, P.F. & Grant, M.A. (1981), "Evaluation of pressure-temperature profiles in wells with multiple feed points", Proc. N.Z. Geothermal Workshop, 121-124.

Blakeley, M.R. & O'Sullivan,M.J. (1982), "Modelling of production and recharge at Wairakei", Proc. N.Z. Geothermal Workshop, 23-31.

Blakeley, M.R., O'Sullivan, M.J. & Bodvarsson, G.S. (1983), "A simple model of the Ohaaki geothermal reservoir", Proc. N.Z. Geothermal Workshop, 11-15.

Grant, M.A. (1977), "Broadlands - a gas-dominated geothermal field", Geothermics, 6, 9-29.

Grant, M.A. (1983), "Geothermal reservoir modelling", Geothermics, 12(4).

Grant, M.A. & Bradford, E. (1983a), "Mokai reservoir assessment 3: Simple modelling and suggested exploration", Report 113, App. Math. Div., DSIR.

Grant, M.A. & Bradford, E. (1983b), "Measurements of the Rotorua reservoir", Proc. N.Z. Geothermal Workshop.

Grant, M.A., Donaldson, I.G. & Bixley, P.F. (1983), "Geothermal Reservoir Engineering", Academic Press, New York.

Grant, M.A. & Iles, D.W. (1981), "A simple model of the connection between the eastern and western sections of Broadlands geothermal field", unpub. report.

Grant, M.A. & Glover, R.B. (1984), "Two-phase heat and mass transfer experiment at well BR21 Broadlands", Geothermics, 13(3).

O'Sullivan, M.J., Bodvarsson, G.S., Pruess, K. & Blakeley, M.R. (1983), "Fluid and heat flow in gas-rich geothermal reservoirs", SPE paper 12102, presented at 58th Annual Tech. Conf. and Ex., San Francisco, Oct.5-8, 1983.

Zyvoloski, G.A. & O'Sullivan, M.J. (1980), "Simulation of a gas-dominated two-phase geothermal reservoir", Soc. Pet. Eng. J., 20(1), 52-58.

Proceedings Ninth Workshop Geothermal Reservoir Engineering
Stanford University, Stanford, California, December 1983
SGP-TR-74

GEOTHERMAL FIELD DEVELOPMENTS IN JAPAN

Seiichi Hirakawa

The University of Tokyo, Faculty of Engineering
Bunkyo-ku, Tokyo 113, JAPAN

ABSTRACT

The present situation of the geothermal field developments in Japan is such that eight geothermal power stations are being operated, while there are still many geothermal areas to be explored. Up to this day, the target of geothermal exploration has mainly been the areas by surface geological survey and the existing geothermal reservoirs are located not deeper than 1,500m depth. Recent geothermal energy development shows a trend from the study on vapor dominated or liquid dominated hydrothermal resources in shallow zones to that on hydrothermal resources in deeper zones. Exploration wells of 3,000m depth class have been drilled in Japan.

INTRODUCTION

There are altogether eight geothermal power plants in operation in Japan. They are, in order of commencement of operation, the Matsukawa Power Plant of the Japan Metals and Chemicals Co., Ltd. (Matsuo-mura, Iwate Prefecture), the Otake Power Plant of the Kyushu Electric Power Co., Ltd. (Kokonoe-machi, Oita Prefecture), the Onuma Power Plant of the Mitsubishi Metal Corporation (Hachimantai, Akita Prefecture), the Onikobe Power Plant of the Electric Power Development Co., Ltd. (Naruko-machi, Miyagi Prefecture), the Hatchobaru Power Plant of the Kyushu Electric Power Co., Ltd. (Kokonoe-machi, Oita Prefecture), the Kakkonda Power Plant (Shizukuishi-machi, Iwate Prefecture) of the Japan Metals and Chemicals Co., Ltd., and the Tohoku Electric Power Co., Ltd., the Suginoi Power Plant (Beppu-shi, Oita Prefecture) that was constructed as a non-utility power plant by the Suginoi Hotel Co., Ltd., and the Mori Power Plant (Mori-machi, Hokkaido) that was put in operation on November 26, 1982 by the Donan Geothermal Energy Co., Ltd., and the Hokkaido Electric Power Co., Ltd. These geothermal fields, except Matsukawa of the vapor dominated type, are mostly the water dominated type. Then, under expansion are the Hatchobaru and Kakkonda Power plants, where development works are presently in progress. The eight geothermal power plants mentioned above have generated a combined power of 1,203 x 10^6 kWh/yr, and the mean working rate and load factor of all these power plants combined lie on a high level of 95.4% and 87.3%, respectively, reflecting the very high reliability levels of these geothermal power plants.

The work of surveying and developing geothermal energy resources in Japan is being advanced under consignment by the New Energy Development Organization (NEDO), the central organ in the country for geothermal energy development, with aid extended by the Ministry of International Trade and Industry (MITI). Although there are still many geothermal areas to be explored, it will take a long time to realize their steam production. These exploration and development of geothermal resources are mostly based on the organized basic investigation, which has started from the fiscal year 1973 by the Geological Survey of Japan. According to the reports by the G.S. group, the distribution of thermal areas in Japan is geologically divided into five categories as follows: (1) Neogene Tertiary green tuff areas, (2) Neogene Tertiary sedimentary basins, (3) Neogene Tertiary plutonic rock areas, (4) Pliocene-Quaternary sedimentary basins, and (5) Quaternary volcanic areas. Among these, the Pliocene-Quaternary sedimentary basins are areas of normal terrestrial heat flow. The Tertiary plutonic rock areas have locally abnormal heat flow, but heat flow from the Tertiary sedimentary basins and green tuff areas is generally higher than that of normal heat flow areas. There are one hundred and eleven sites of steam fumaroles, boiling springs and hot springs with water temperature higher than 90°C in the abovementioned areas and most of these are distributed in the Quaternary volcanic areas.

To promote geothermal development, the G.S. of Japan picked up thirty high potentiality geothermal areas characterized by remarkable geothermal anomaly. Most of these areas have often been designated as national parks or

quasi-national parks, and the geothermal development within these areas needs beforehand permission of the Environment Agency. The Japan Geothermal Energy Development Center has investigated geothermal potentiality and feasibility of its development through surface survey and well drilling (about 1,000m depth) under instructions from the Power Generation Section and Geothermal Resources Development Investigation Committee, which belong to MITI.

Before 1977, the target of geothermal exploration has mainly been the areas by surface geological survey and the existing geothermal reservoirs are located not deeper than 1,500m depth. In 1977, the G.S. of Japan selected the fifteen promising geothermal areas based on the items of (1) indication of large scale geothermal reservoir, (2) detection of 3,000m - 4,000m depth reservoir, (3) relationship on volcano distribution and (4) geothermal activities in Neogene Tertiary sedimentary basins and Quaternary volcanic areas. The exploration wells of 3,000m depth class were drilled from 1978 by MITI to make clear of the deep geothermal reservoirs in Hohi area where Otake and Hachobaru power stations are located.

MATSUKAWA

The Matsukawa power plant is located about 50 km north west of Morioka City, about one and half hours drive. It occupies the southern corner of the Towada Hachimantai National Park and is in a basin of the upper stream of the Matsukawa river with an altitude of 900m above sea level. Mt. Iwate, an active volcano, can be seen in a north west direction from here. Matsukawa has been known as a sulphuric hotspring area from old times.

In January 1964, drilling of the first production well at Matsukawa turned out to be very successful. The amount of steam from a well which was 945m deep reached more than 60 t/h which represents a possible output of 5,000 kw. The first in Japan and the world's fourth geothermal power plant of 22 MW capacity was constructed here in October 1966.

Geologically, this area is covered by Quaternary volcanic rocks, with existence of a caldera around Mt. Marumori and a steep cliff consisting of altered rocks along the Matsukawa river presents wild topographical features made by the violent volcanic activity of early times. In spite of the fact that there were but a few geothermal manifestations without a boiling point like substance at the surface, simple steam and hot water emitted from the wells when drilled by the Field Office to a depth of about 300m. The first geothermal energy investigation was started in 1956. The Geological Survey of Japan, belonging to the Agency of Industrial Science and Technology, joined the investigation. Thus, a cooperative study between the Geological Survey and JMC (Japan Metals and Chemicals Co.,Ltd.) was commenced in 1958. From then forward for ten years much effort for development was exerted until the project finally reached its goal with the completion of the geothermal power plant.

Based on the data obtained from the drillings, the geological succession in this area can be described as follows: from upper to lower; Quaternary Matsukawa andesite; the Tertiary Pliocene Tamagawa welded tuff formation; Miocene Yamatsuda; Koshidomaezawa; and the Sakamotozawa and Kunimitoge formations, respectively. Seven production wells are divided into three types by their steam characteristics. The first type is the well characterized by the emission of wet steam for some periods before becoming a superheated steam; for a period of five months in the case of the No.2 well and for one year in the case of the No.1 well. The second type is the well which has a continuous emission of wet steam up to the present. The No.3 well corresponds to this category. The last type is the well which has had a continuous emission of superheated steam so far, but producing dry steam when the emission first started. Well No.5, 6 and 7 which are located at the upper stream of Akagawa river are of this type. It goes without saying that this last type is most useful for generating power.

Geophysical prospecting carried out at two levels; one is at the surface, the other is in the bore holes. The VES (vertical electric sounding) method has been applied for gathering information about geologic structure and rock alteration. In order to survey the geologic structure and fractured zones concerned with producing geothermal steam, a large scale seismic survey has been conducted in this area. From the method of seismic reflection with four fold, much information about the underground structure in the base rocks covered by the Quaternary volcanic complex has been obtained. It goes without saying that core samples obtained by drilling give important information about the geologic structure and the occurrence of geothermal fluid. Besides core survey, it is possible to get data on subsurface structure from the survey by the geophysical logging of a hole. To facilitate this type of survey, temperature and electric loggings have been made in all exploration and production wells in this area.

Eight production wells 945 - 1,500m deep have been drilled so far in the Matsukawa area, among which seven wells (except the No.4 well) supply steam for the power station. A typical arrangement of insertion of casing pipes in

this area has been as follows: from upper to lower, 30m of surface C.P. of 18", 250m of conductor C.P. of 13 3/8" and 500m of production C.P. of 9 5/8" which are surrounded by cementing material. From 500m deep to the bottom of hole, slotted 7" pipe is inserted into the remaining 8 5/8" of the hole after drilling is completed.

The slits in the slotted pipes are arranged in a zig zag formation with 14 lines per 220 mm in length. Each line has an area of 80mm x 5.5mm and total lines occupy 5 - 7% of he surface area of a slotted pipe.

Except where steam begins to flow out naturally, a blow out of steam is caused artificially by using a sand pump or a bailer. In Matsukawa, the No.7 exploration well was drilled by a method of directional drilling. Directional drilling was undertaken by using a turbo-drill of 6 5/8" diameter at a depth of 292m, with a horizontal distance from the well head to the bottom of the hole being 175.85m at a depth of 600m. By using this directional method, it is possible to reduce the area of the drilling site and thereby the total length of the steam gathering pipe lines.

ONUMA

The Onuma geothermal field began steam production in 1973. As for geology of this field, Quaternary volcanic rocks (70 to 150m thick) and Tertiary formation (more than 2,000m thick) have been confirmed in the course of geologic survey. The Quaternary andesitic rocks cover most of the area. The Tertiary formation consists mainly of dacite and andesite and their pyroclastics and sediments of Miocene to Pliocene age. Many volcanoes are known to be distributed on the uplifted block formed by a series of faults and folds. Prevailing geologic structure in the area is N-S and NW-SE trending tectonic lines which are characterized by the faults, block movement and graben structure. Geothermal manifestations such as geysers, fumaroles, mud pots and hot spring are found along the subsided structure of the graben trending in N-S which is confirmed by the regional gravity survey. A number of zones of surface alteration due to geothermal activities have been recognized covering a total area of more than 5 km^2. The elongation of the surface alteration in E-W and N-S directions reflects the subsurface geologic structure. The E-W trending alteration zone represents the tectonic line of Tamagawa to Goshogake and the N-S trend of alteration zone appears to be along the graben structure.

Gravity survey and electrical one were carried out in this area. Using La Coste G type gravimeter, gravity survey was conducted in order to determine significant subsurface geologic structure prevailing in the area. In Ohnuma, Bouguer anomaly values varying from -65 to -38mgal were found. Therefore, this area lies in a typical negative Bouguer anomaly area. A large and elongated low gravity zone having graben structure has been confirmed which trends N-S from Shibari to Goshogake. Ohnuma geothermal plant is considered to be located at the center of this graben structure. Schlumberger array employing direct current resistivity method was used throughout the survey covering a total length of 72 line km. Low resistivity zone with values less than 10Ωm in AB/2 = 800m extends continuously from north to south. A specific low resistivity zone was distinguished to appear from Sumikawa passing through Ohnuma, then to Komonomori in the graben structure.

Based on the chemical composition of hot spring waters from the area, they are classified into three groups; SO_4 type is the most abundant among three groups. Weak alkaline to neutral NaCl type occurs only at Shibari and Zenikawa on the northern part of the area. Tamagawa hot spring is famous as HCl type with low pH value. Analysis of the discharged water from the production wells of the Ohnuma power plant shows 2,500 to 3,000 ppm solids content, mainly of sodium chloride and silica.

Five production wells have been drilled by rotary drilling machine with final diameter of 8 5/8 inches and slotted pipes of 7 inches in diameter in the deeper parts. At about 1,300 to 1,700m depth thick piles of dacite, andesite and their pyroclastics are closely interbedded with each other and strongly fractured forming hot water reservoir. Being closely spaced between production wells, mutual interference on their production output is noted. However, the annual decrement of the steam production is very small. As geothermal steam is accompanied with hot water, the steam separator at the wellhead effectively separates steam from hot water. The separated steam is transmitted to the power station through the main steam pipe. Condensed steam is recycled as cooling water. A part of hot water is being utilized to fresh water by means of heat exchanger and the remainning is re-injected into the ground through re-injection wells.

OTAKE

The Otake area, covering Kokonoe Town, Kusu District, Oita Prefecture, is located at 6km northwest of Mt. Kuji in the central part of the Northern Kyushu. As for topography, it lies between Mt. Kuroiwa at its south-east, Mt. Waita at its north-west and Mt.Misokobushi at its west. They are dormant volcanoes, and constitute a valley of Kusu River, running from south to north. And its elevation is in

the range from 900m to 1,100m above sea level. Natural steam fumarole zone is distributed in the direction of south-north, and also fumarloes and hot springs are located in this neighborhood. Main ones of them are arranged from the south in the order of Komatsu-, Otake- and Kawara-Fumaroles and Sujiyu- and Hizenyu-Hot Springs.

The Otake area was selected for the geothermal development as follows; (1) It is in natural steam fumarole zone among mountain ranges of Kuju, and in the vicinity of this area such surface manifestations of geothermal activity as Fumaroles and hot springs are brisk. (2) Near Kawara-Fumarole, a well was drilled in 1927 and steam obatined at the depth of 84m. It has been spouting steam-water mixture for 30 years approximately, though the steam production from the well was decreased gradually and stopped lately. (3) It gives comparatively less influence to the hot springs or private houses in the neighborhood, though situated rather inconveniently. Besides, the residents are generally cooperative.

Results from the preliminary survey revealed that comparatively new hornblende andesite and volcanic complex of Mt. Kuroiwa covers the Mt. Waita and Mt. Ichimoku. At Komatsu-Fumarole there exists clay-soil originated by considerable hydrothermal alteration, and underground water is stored to be comparatively scarce. At both Otake- and Kawara-Fumaroles there are more pyroclastic rocks than clayey ones.

The activity of steam fumaroles at Komatsu-

Fumarole was powerful over wide areas. Otake-

Fumarole was more or less weaker than the former. Kawara-Fumarole was the weakest of all three, and also its range in activity was narrow. The scale and activity of three Fumaroles grew smaller toward the north. As to the traffic convenience, Kawara-Fumarole is best, since it is close to the road, while Otake-Fumarole is located at about 200m east to the road, from which a mountain path leads to it. Komatsu-Fumarole is located in the distance of 800m south from the terminal, and is most inconvenient of all, though it is reached by a mountain path.

Based on the results of preliminary surveys, steam wells were drilled in Otake area to obtain super-heated natural steam. Sites of wells were selected near Otake-Fumarole, which is convenient for transportation of drilling equipment and preparatory works, and also in the neighborhood of Kawara-Fumarole and between two Fumaroles. During the term between February 1953 and December 1956, 4 steam wells were drilled at the depth of 300m to 900m. The whole well produced powerful discharges of steam-water mixture instead of super-heated steam. At that time, it was considered from the surrounding geological conditions that the steam reservoir existed in the tertiary sediment, of which the depth were estimated in the range of 500m to 600m. Nevertheless, the drilling operation for Otake well No.3 drilled to the depth of 900m did not proved the existence of the tertiary sediment. Of course, it was found after the well-completion that the discharge from the well was also the mixture of steam and hot water. In such a manner, it was impossible to get the superheated steam from the well for primary object in the geothermal power generation.

In December 1961, steam of 16 t/h was obtained by separating the steam-water mixture from geothermal well mentioned above. Accordingly, geothermal exploration and researches were enterprised for the object to generate electric power using separated steam. In order to develop the geothermal power generation, it is essentially need to collect the information in detail on the range of geothermal areas, conditions of subsurface structure to be stored the mixture of steam and hot water as well as the production capacity, well performance and the life of wells.

At first, it was decided to apply some geophysical exploration (magnetic, gravity, resistivity and temperature) to the wide area including Otake and Hatchobaru areas, and secondly to investigate further subsurface condition by boring. In conclusion, such geophysical explorations revealed the possible existence of geothermal hot water, channels suppling heat and connecting to thermal source, and the promising geothermal area of ellipse with major axis of 3 km extending from south to north and minor axis of 1.5 km extending from east to west including Otake and Hatchobaru areas, which is indicated by low resistivity zone. To confirm the results of geophysical exploration, to clarify geological structure and to investigate the existence of geothermal steam and hot water, two test borings of 1,000 meter class were carried out in the southern area of Otake geothermal field.

A possibility of geothermal field development was obtained by the test results of Otake Well No.5 in Dec. 1961. Accordingly, a plan was made on the drilling of 5 productive wells, Nos.6 through 10, during the term from December 1963 to March 1966. Otake power station has a capacity of 12.5 MW, and has been operating since 1967. At that time, Otake Wells No.6 through No.10 produced the steam, but Otake Well No.6 ceased production in the end of 1967, Well No.7 in 1975, Well No.8 in 1977, Well No.10 in 1980 due to a loss in enthalpy, respectively. Since that time, steam production had declined. In 1979 and

1981, production was raised by the directional drilling of new production wells No.14, No.15 and No.16. At present, the output of Otake power plant keeps about 8 MW with four production wells (these three wells and Well No.9) and four reinjection wells (Nos. 10 through 13).

HATCHOBARU

Hatchobaru No.1 Unit (55 MW) was completed in 1977 as the world's first double-flash type geothermal power plant and has been operating satisfactorily. Kyushu Electric Power Co. has been conducting the development of geothermal steam and the construction and operation of power plants under an integrated system from geothermal exploration to power plants, and completed Otake No.1 Unit (12.5 MW) in 1967 and Hatchobaru No.1 Unit (55 MW) in 1977. When Hatchobaru started operation, the output was 23 MW due to insufficient steam production and reinjection capacity caused by a delay in drilling. However, the output increased steadily with successful drilling, reaching the rated output of 55MW in 1980. It has since then been operating satisfactorily at an average annual capacity factor of about 90%, though the amount of steam sometimes runs low.

When the geology of Kyushu is examined macroscopically, there are two major rifts running from east to west and from north to south, effusing a large number of volcanoes. A section of the east-west rift, i.e., Oita-Kumamoto line, is occupied by the Kuju volcanic group which is the heat source of the Hatchobaru geothermal field. The depth of the geothermal reservoir at Hatchobaru was previously 800 -1,500m (lower Hohi stratum or Usa stratum). However, as a result of drilling of a 2,000m class production well (H-17) in 1980 and a 3,000m exploratory well (HT-5-1) in 1982 as part of the survey for the development of No.2 Unit, the geotectonic condition has been ascertained to a considerable extent. As regards the order of strata from the surface, Kuju volcanic rocks (Quaternary), Hohi volcanic rocks (Quaternary), Usa strata (Tertiary) and the basement rocks (Mesozoic era) are found. The basement rocks appear at a depth of about 2,000m with granite intruding into metamorphic rocks (crystalline schists) and forming alternating strata. The hydrothermal alterated minerals (epidote and calcite) found in small cracks in the basement rocks suggest the possible existence of a deep reservoir zone.

A total of 18 production wells have been drilled so far in the Hatchobaru area, 12 of which with successful blowing. The number of currently blowing wells is 10, generating 55 MW. The geothermal reservoir zone in the Hatchobaru area is assumed to be fractures which developed along a fault. Therefore, the probability of successful blowing is high if the production well is drilled through fault planes. Two faults, Komatsu-ike sub-fault and Hatchobaru fault, have been confirmed in the Hatchobaru area. In particular, the former is a major discharge fault and successful blowing resulted in most of those wells drilled through this fault at 1,000 - 2,000m. The characteristics of production wells vary from well to well. However, the ratio of steam to hot water in the blowing fluid is about 1:2 (mouth pressure of about 8 kg/cm^2g) with the non-condensable gas content averaging 0.5% (weight %). Since the output of production wells has been decreasing at a rate of about 10% per year, it is necessary to drill an additional well every year.

A total of 17 reinjection wells have been drilled so far in the Hatchobaru area, 14 of which are in current use. In addition, three of unsuccessful steam production wells have been used as reinjection wells. There is no complete failure for reinjection wells. Even in the case of a completely dry hole, it is possible to develop lost circulation of water artificially by patiently repeating appropriate pressurization and boiling out. There are two major problems involved in reinjection wells: a rapid fall in reinjection capacity and the interference of reinjection with the steam production zone. As for the reinjection capacity, since it decreases by about 20% every year, it is necessary to provide from two to three additional wells annually. This seems to be primarily due to the silica content in the hot water. The interference with the steam production zone poses an extremely serious problem in the Hatchobaru area. Since this area offers few locations suitable for reinjection, e.g., recharge fault, many reinjection wells were drilled near the steam production stratum at the early stage of development. As a result, gradual cooling of production wells occurred and, in particular, two production wells situated relatively near reinjection wells stopped blowing (H-4 and H-6). In order to prevent the cooling of production wells due to reinjection, it is desirable to completely stop reinjection in the neighboring area. However, this is not possible under the present conditions. Accordingly, of the total hot water of 750 t/h, about 250 t/h is diverted to the Otake area for reinjection to ease the effect.

SUGINOI

Suginoi geothermal power plant of the Suginoi Hotel, having the capacity of 3 MW, the smallest in Japan, started operation in Aug. 1981. The attention of Japanese people interested in geothermal field development is directed to this plant operation because of its unique features characterized by the multipurpose utilization including electricity generation, heating and cooling energy, recreation and therapy in baths and spas and so on. Seven wells were drilled from 180m to 400m depth. At present, these wells produce steam of 50 t/h and hot water of 25 t/h

from bottom hole where temperature is 90°C - 230°C.

ONIKOBE

The Onikobe power plant is located in Onikobe Katayama district, Naruko-machi, Miyagi Prefecture and is operated by the Electric Power Development Company, Ltd. Licensed plant capacity is 12.5 MW, total steam production in twelve wells is about 50 t/h and hot water reinjection rate in two wells is about 150 t/h. Most of production well concentrate to the shallow zone (depth 200 - 400 meters) with lower steam productivity. One directional well drilled in 1980 produced steam of 17 t/h and PH 5 hot water of 50 t/h from a 1,000m zone.

MORI

The Mori power plant in Nigorikawa geothermal field located in Southern Hokkaido is a 50 MW station operated by Donan Geothermal Energy Co. Ltd., and the Hokkaido Electric Power Co. Ltd. It has been producing since Nov. in 1982. In this field, it is necessary to pay much attention to the high CO_2 gas content in the steam, and high HCO_3 ion content in the hot water. The plugging of scale deposit in pipe intercepts the output of Mori power plant.

KAKKONDA

The Kakkonda power station in the Takinoue geothermal field located in Iwate prefecture, northeastern part of Honshu, Japan is a 50 MW station operated by JMC and Tohoku Electric Power Company. It has been producing since May in 1978.

Based on the results of the detailed surveys made during the period from 1967 to 1972, drilling of six exploration wells of 700 - 1,000m deep was commenced in September, 1972 and completed in February, 1974. By the data obtained from drilling and geological and geophysical loggings made in the wells, possibility of geothermal development in this area was furthermore supported. Thus, based on the results of the synthetic analyses of the surface and subsurface exploration, drilling of the production and reinjection wells started in August, 1974, for the purpose of geothermal development in this area. During the period from August 1974 to August 1977, 11 production wells of 1,000 - 1,600m deep and 15 reinjection wells of 500 -700m deep were drilled. On the other hand, construction of wellhead equipment and steam gathering pipelines was commenced in May, 1975 and completed in November, 1977. At that moment, all the construction works of steam supply system came to an end.

Installations related to steam supply system include geothermal wells, separators, steam gathering pipelines, steam header and silencer. Among these, geothermal wells are divided into two types, one for production and another for reinjection. Because Takinoue is located in the National Park, where land use for construction of roads, drilling sites, steam gathering pipelines and power plant is normally prohibited by environmental concerns, a grouping method was adopted in Takinoue for the drilling of the geothermal wells, which meant that two or three wells were grouped in small base areas. Due to the reasons mentioned above, five drilling base areas, named A, B, C, D and E, were prepared in Takinoue. Accordingly, most wells in a base area were drilled by directional drilling with such an arrangement as multi-legs of an octopus. Moreover, to drill production wells, air drilling method was adopted in this area. In this method, air is used as circulating fluid for mud water and it has such merits that drilling rate is increased, long life of drilling bits can be kept, permeable cracks are protected from plugging by cuttings and fractures with geothermal fluid can be checked. Nine among 11 production wells were drilled by air drilling, showing that this method can be used in such a hot water area as Takinoue.

Compared to Matsukawa which is one of the vapour-dominated areas, Takinoue is a typical hot water area as mentioned already. Therefore, much hot water gushes out from the production wells with steam. The separator is used for separating steam from hot water at the ground surface. Separated hot water is sent to the reinjection wells, while steam is transported by pipelines and is gathered in a steam header. In Takinoue, the steam header is set up in B base area which is located near the power plant. The dry steam is sent to the steam header and the separated hot water is disposed into the reinjection wells in B and A base areas.

Acknowledgements

For giving the field information and/or printed matter used in this review work, the author deeply appreciates the contribution of Japan Geothermal Energy Association, Kyushu Electric Power Co. Inc., Japan Metals and Chemicals Co. Ltd., Mitsubishi Metal Corporation, and Electric Power Development Co. Ltd.

Proceedings Ninth Workshop Geothermal Reservoir Engineering
Stanford University, Stanford, California, December 1983
SGP-TR-74

RESERVOIR ENGINEERING ASPECTS OF THE PHILIPPINES GEOTHERMAL DEVELOPMENTS IN LEYTE AND SOUTHERN NEGROS

R. Kingston
A. Watson

KRTA Limited
Auckland, New Zealand

ABSTRACT

The current state of development of the Tongonan and Puhagan geothermal fields in the Philippines is presented and the nature of the reservoirs is described. In the latter part of the paper, reservoir engineering techniques which have been found to be particularly valuable are discussed and some aspects which give rise to problems are identified.

INTRODUCTION

The Tongonan and Puhagan geothermal fields are water dominated fields on the islands of Leyte and Negros respectively - (Fig. 1). The Tongonan field currently supports the Tongonan I, 112 MW(e) power station which was commissioned earlier this year and the Puhagan field supports the Palinpinon I, 112 MW (e) station which is still in commissioning. In contrast to the Tiwi and Mak-Ban fields on the island of Luzon, which were developed by non-Philippine companies and the steam sold to Philippine National Power Corporation (NPC) power stations, Tongonan and Puhagan have been developed by the Energy Development Corporation of the Philippine National Oil Company (EDC-PNOC). Exploration began with the help of a New Zealand - Philippines Economic Co-operation programme in which KRTA were New Zealand Government representatives. The field development phases were carried out by EDC-PNOC, with the aid of a joint venture company formed by EDC-PNOC and KRTA: the scope of work covered geoscience, drilling management and reservoir engineering as well as the design, construction and commissioning of all field surface works.

So far as the power stations are concerned, both are owned and operated by NPC. Tongonan I design, construction management and commissioning was carried out by KRTA over the period 1979 to 1983. Palinpinon I was started later and, of largely prefabricated construction, was designed, constructed and commissioned by 1983 under a turnkey contract by a Japanese manufacturer.

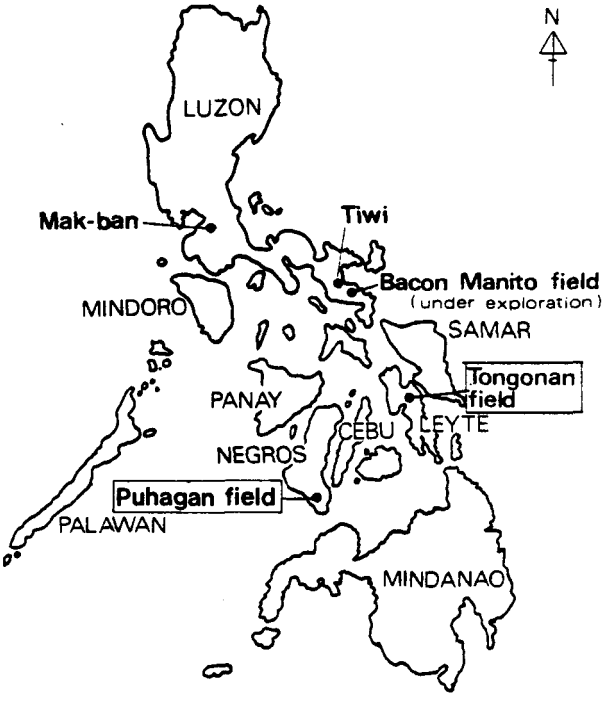


Fig. 1. Field locations in the Philippines.

CURRENT STATE OF DEVELOPMENT OF THE FIELDS

The two developments are rather similar in terms of operating parameters and general type. Each field provides single flash dry saturated steam to its 112 MW(e) power station at 0.6 MPa abs from production wells supplying a two-phase mixture to cyclone separators. The separators operate at about 0.7 MPa abs and the waste water is fed to reinjection wells without any further cooling. In plan view, however, the developments have distinct differences - Figs 2(a) and (b). The Tongonan two-phase pipelines are long and follow the main river valleys to separator stations situated about 400m from the power station. In the Mahiao sector of the field there are 6 vertical production wells spaced at 200-300m in almost a straight line; in the

Sambaloran sector there are 6 vertical production wells in a random cluster with rather wider spacings. The Puhagan development on the other hand, is one in which deviated wells have been drilled from four multi-well pads situated within 500m of the power station. The longest two-phase line is about 300m and a single separator station is situated about 200m from the power station. Both field developments have been constrained by topography, being located in very steep and easily eroded terrain. In both, the reinjection wells have been sited so as to be downhill from the separator stations.

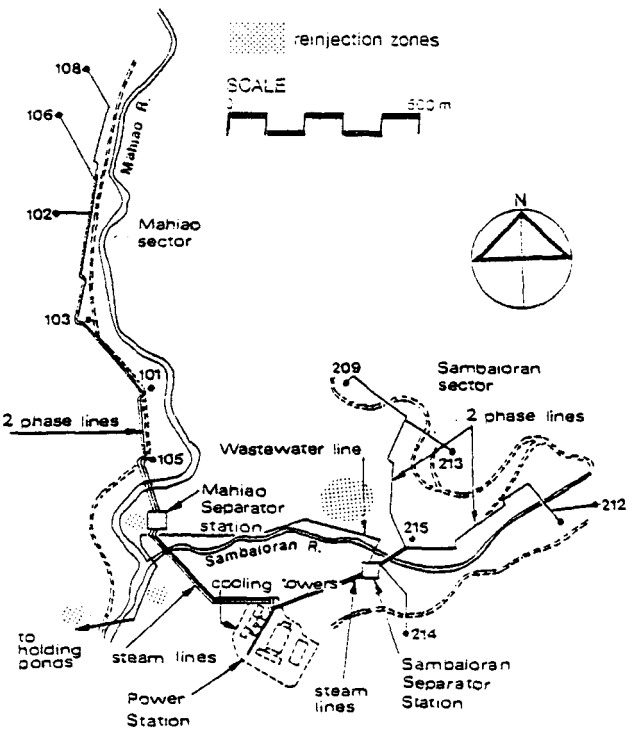


Fig. 2(a). The Tongonan field.

As indicated briefly in the introduction, major production from the Tongonan field started in April 1983 and from Puhagan more recently. Leyte has no major electrical grid; the load for Tongonan I is made up mainly by a nearby copper smelter which has several items of equipment that present large electrical loads and can be switched on and off almost instantaneously. The fluctuating load which results is not ideal for a geothermal power plant, however, the steam gathering system was designed with such conditions in mind and so far has performed well.

Southern Negros has a more developed electrical grid system and Palinpinon I should not have to operate with major load variations. In both fields the main power station was preceded by the installation of small non-condensing units, 3 MW(e) at Tongonan and four 1.5 MW(e) units at

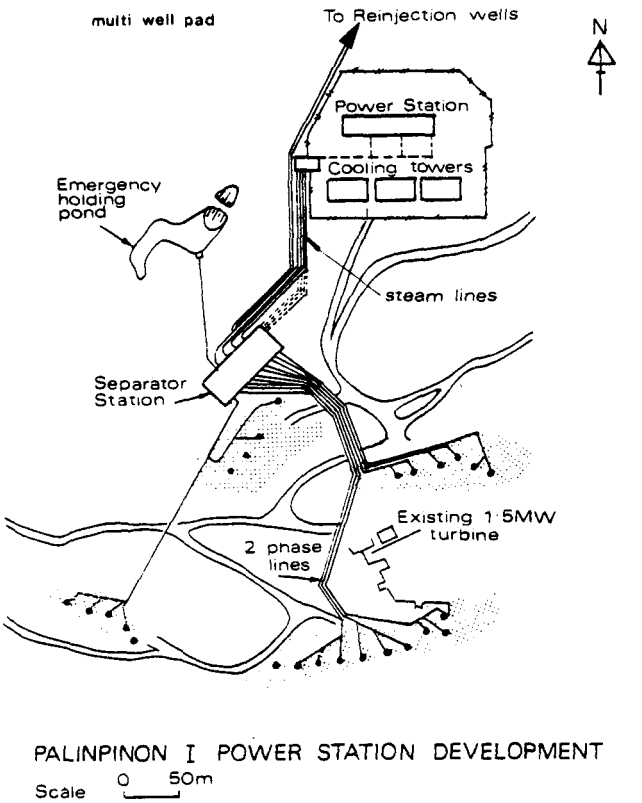


Fig. 2(b). The Puhagan field.

Puhagan. These have provided useful electricity generation as well as field operations experience.

A major feature of both fields is that full reinjection is designed for. Silica concentrations in the waste water are such that supersaturation and deposition can only be avoided by using waste water temperatures of 165-180°C, which is the temperature level after the first flash stage. Fortunately an economic assessment showed that a second stage flash was not clearly cost beneficial and the single flash cycle was adopted. From the surface engineering point of view, reinjection at either field presented no major problems. The cold standing water level in the wells is sufficiently low that injection pumps are not required, particularly at Puhagan where it was so low (in excess of 600m in some wells) as to cause difficulties in promoting discharge. In addition the layout of pipelines and separator stations was done with reinjection areas in mind, to take advantage of local topography. The choice of areas in which to reinject was not easy and to some extent is rather subjective. Reinjection tests lasting several months have been carried out at Tongonan in order to provide experience on which to base the selection of waste water temperatures etc.

THE NATURE OF THE RESERVOIRS

Tongonan

Many more wells have been drilled in Tongonan than are needed for Tongonan I as a deliberate policy for additional power plant and these give a good spread of data points to help understand the field. As mentioned previously the wells are mainly vertical and of depth less than 3000m. Usually at least two production zones occur in a well; there does not seem to be major disequilibrium between the zones, as judged by the tendency for internal flows in wells. Internal flows do occur however, for example, a two-phase upflow in well 209. This leads us to the most significant geological feature - the principle production zone is a contact zone between the upper surface of a quartz diorite plutonic intrusion and the overlying volcanics. The upper surface contours of the pluton are shown in Fig. 3 from which it can be seen that the Sambaloran wells are grouped around a local high point whilst the Mahiao valley wells follow a steeply dipping edge. How much production can be gained by drilling into the pluton is still a point of conjecture; certainly well 209 penetrates 600m into the pluton and seems to produce from well below the pluton surface. It has the highest output of any Philippines well at about 25 MW(e) equivalent, but it is blocked to instruments at depth and the nature of the deep production cannot be examined. The contact zone contains propylitised andesites and andesite/microdiorite breccias and is of varying thickness across the field, up to a maximum of about 500m. It is heavily fractured.

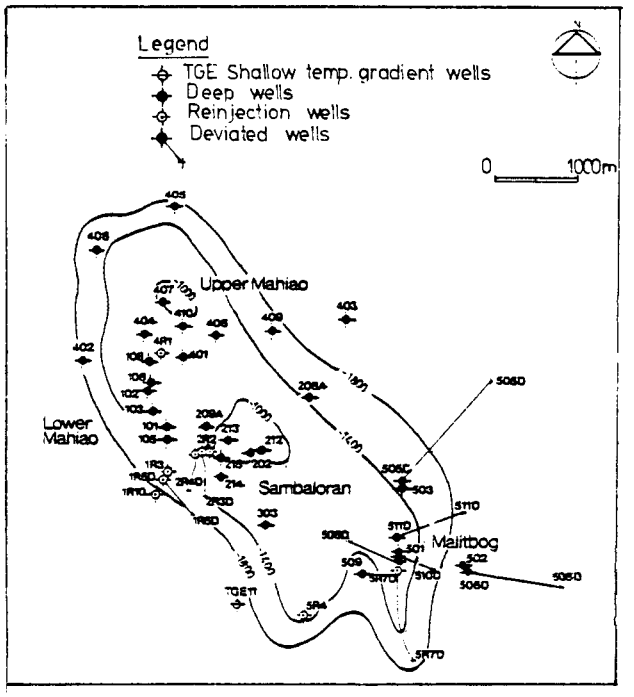


Fig. 3. Pluton surface contours at Tongonan.

The overlying layers are mainly volcanic andesites, breccias and tuffs, and although certain well defined sequences such as thin beds of sandstones and siltstones and some dykes are evident, they have no major effect on reservoir performance. Gross transmissivity of the wells is between 1 and 8 darcy-m as measured by pressure buildup and pressure falloff tests. It is KRTA/EDC practice to measure injectivity by injecting water on well completion, and values between 20 and 60 ℓ/s MPa are typical. Temperature contours on a plane at 900m below MSL show a similar general shape to the pluton surface contours, suggesting that the contact zone which 'cloaks' the pluton itself contains the highest temperature fluid. Maximum temperatures are about 320°C, and production from the contact zone is single-phase saturated liquid. Production from within the pluton in the case of well 209 is two-phase and there are two-phase zones at shallow levels in the reservoir. These appear to be naturally occurring, and their presence leads to discharge enthalpies which are quite strong functions of wellhead pressure. The extent to which discharge tests could be carried out was limited by environmental restrictions on allowable discharge to the rivers in the 'dry' seasons and by pipeline construction in the case of Tongonan I wells, but as shown by Lovelock, Cope and Baltasar (1982) correlation of discharge enthalpy with chloride concentration in discharge has proved to be very instructive as regards natural fluid movements in the field. Under full bore discharge the output enthalpy is higher than that of liquid from the contact zone because of steam production from the upper zones. With the discharge restricted so that wellhead pressure is high, steam production is suppressed and the discharge enthalpy is that of liquid at depth. Fig. 4 shows the chloride concentration in the total discharge plotted as a function of discharge enthalpy for one particular well. The linear plot is an indication that the discharge consists of a mixture of two fluids with different chloride concentrations and enthalpies. The points with numbers attached refer to restricted output - the restriction and hence the wellhead pressure is greatest for

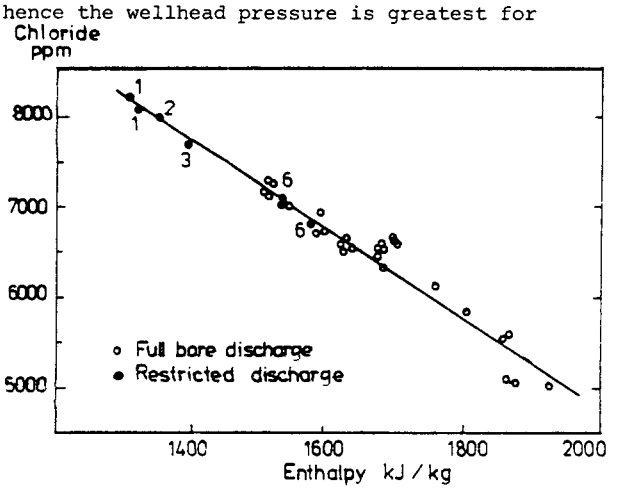


Fig. 4. Chloride-enthalpy plot for a Tongonan well.

points marked 1 and number 6 is almost an unrestricted full bore discharge. The high enthalpy full bore discharge points in Fig. 4 represent different mixes of steam and water produced probably because of drawdown whilst the low enthalpy points suggest that the 'primary' reservoir fluid for this well has an enthalpy of about 1300 kJ/kg and hence a temperature of about 290°C. This is supported by the Na-K-Ca geothermometer and SiO_2 geothermometer results.

Applying the same technique over the rest of the field gives an indication of the chloride concentration of the local geothermal fluid. Assuming that the chloride concentrations vary due to mixing with meteoric water, then the shape of the contours of this variable over the field gives some indication of the natural flow of geothermal fluid. The suggestion is that the fluid is at maximum concentration and possibly rises in the Upper Mahiao Valley region and that a major percolation of this primary fluid into the Bao Valley region has taken place, which fits with the interpretation of the early exploration drilling results. Lovelock, Cope and Baltasar go into more detail about the interpretation of natural flows. It is of interest to note that the Malitbog area wells display temperature inversions, which are consistent with the natural flow interpretation.

Puhagan

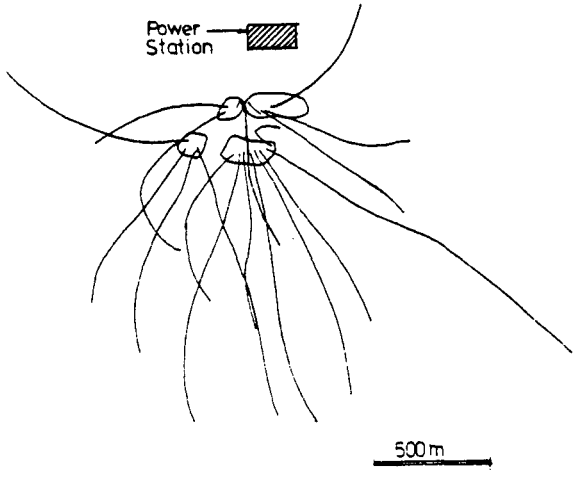


Fig. 5. Well tracks at Puhagan.

A plan view of the well tracks is shown in Fig. 5 and it will be immediately clear that the spread of data points for establishing temperature contours etc. is not so good as at Tongonan. An additional complicating factor in establishing undisturbed reservoir temperatures from the wells is the frequent occurrence of downflows. This feature is consistent with the idea of the permeability being fracture dominated with the reservoir composed of low permeability material. Detailed descriptions of the stratigraphy have been given by Leach and Bogie (1982) and Maunder, Brodie and Tolentino (1982). A further indication of the localised nature of the permeability is that the variation of chemical constituents in a well output in response to variations in wellhead pressure is rather random, in contrast to Tongonan wells, which suggests that different fluids can occur in isolation throughout the reservoir. Fig. 6 represents a cross section of the reservoir showing the main geological components. The near-horizontal sill is fairly influential in channelling ground water into the reservoir, giving rise to calciting problems in some wells. As in Tongonan, it has been established that production occurs from within the pluton; well SG1 is cased into the pluton and has a power output of about 5 MW(e) and maximum temperatures of 277°C, however its ability to provide for long term production still needs to be established.

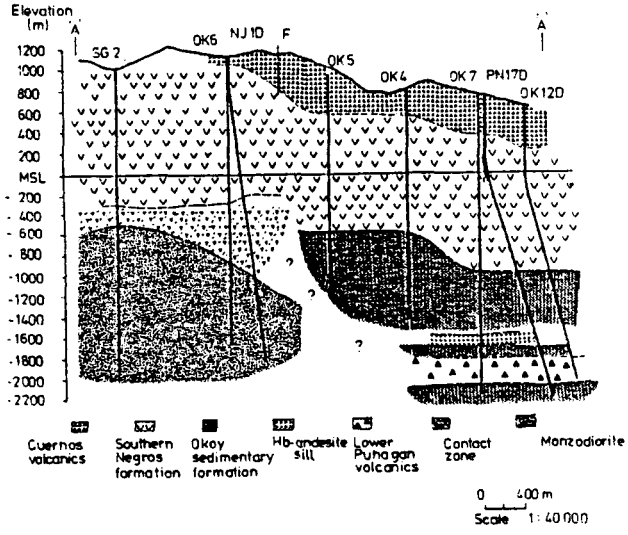


Fig. 6. Cross section of Puhagan.

RESERVOIR ENGINEERING TECHNIQUES

Well Discharge Stimulation

The wells in the Puhagan field were drilled from a high elevation and it is mainly these which caused us to examine the problem of how to discharge reluctant wells. Water levels 600m below the wellhead were encountered. A column of liquid standing in the well exerts a hydrostatic pressure at the production zone which is just sufficient to balance the reservoir pressure. The problem of how to get the well to discharge continuously may be considered to be that of reducing the density of the column to such an extent that the length needed to balance off the reservoir pressure will not fit in the available length of wellbore. This becomes more difficult as the empty part of the wellbore occupies a greater proportion of the well, however if it can be achieved then the well will flow. If the reservoir fluid entering the well is hot enough it will flash and provide the expansion needed to

keep the well discharging. An obvious method to try is pumping, to remove some of the cold water, cause the formation to flow and hence fill the wellbore with flashing water. Airlifting has been used on occasions in the Philippines, but is inappropriate for Puhagan wells because of the very large compressor which would be needed. At the other extreme of sophistication, liquid nitrogen injection via a continuous tubing unit is prohibitively expensive in this instance. The two methods which are used are air compression and steam heating.

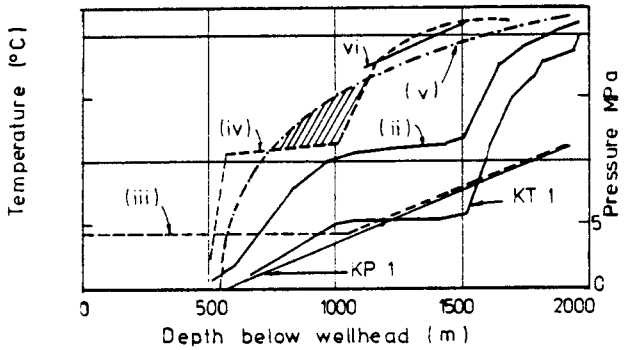


Fig. 7. Temperature and pressure profiles in a well with compression.

Fig. 7 shows the interpretation of events in a well which was compressed. The example chosen is one in which air compression was tried but appeared at the outset to be marginal and in fact did not work. Curve (i) shows early temperature and pressure, and curve (ii) a 25 day shut temperature profile. The well was then compressed to a wellhead pressure of about 4.5 MPa, curve (iii), and the well allowed to stand for the fluid to reach thermal equilibrium with its new surroundings.

Curve (iv) shows the temperature distribution which would have existed in the water after the air release, superimposed on the temperature distribution which would be expected of a column of boiling water with its surface at 550m, curve (v). The hatched area shows the length of the well which clearly would have contained liquid water. The water above this, from 750m upwards, would have expanded into the cool upper portion of the well. It appears as if liquid below 1150m would have found itself above local saturation temperature, however it must be remembered that the liquid filled length exerts a greater hydrostatic pressure than the equivalent length of boiling liquid so the local saturation temperature is raised from curve (v) to curve (vi) in this region. The degree of superheat in the lower section of the well is now only marginal. In addition, the fluid entering the well from the reservoir is likely to come from the region between 1100m and 1500m deep, so no superheat at all may occur below 1100m. In the event, the well did not discharge by compression.

The steam heating technique is simply to inject into the well to be discharged either steam from a boiler or the two-phase discharge from a neighbouring well. Quite long temporary (welded steel) pipelines have been used to transport well outputs and have been found to be reliable and economic. The boiler used was a once-through packaged type which could be transported with fuel and water treatment plant, to where it was required. Brodie, Dobbie and Watson (1981) provide a simple analysis to show that heat loss to the upper levels of the casing of the well significantly reduces the degree of expansion of fluid achieved by the testing process. Steam heating of this section of the well counteracts this problem.

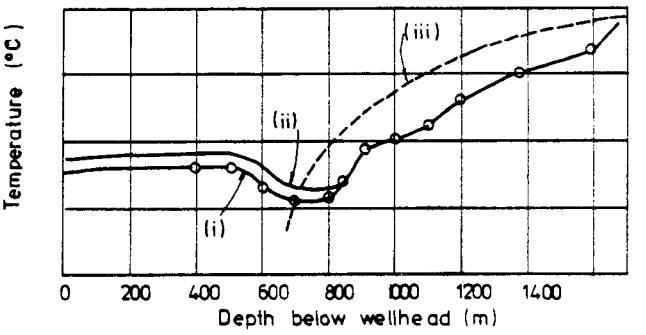


Fig. 8. Temperature profiles in a well with steam heating.

Fig. 8 shows the temperature distributions in the well to which Fig. 7 refers, after 1 day of heating (curve (i)) and 7 days of heating (curve (ii)), at which time the wellhead pressure was 1.5 MPa. abs. Curve (iii) shows the temperature distribution in the well required to make all of the column boil; it would only boil at the top, but this would (and did) unload the well and lead to discharge. The current position is that we have an empirical correlation to guide us in judging whether steam heating or merely air compression is necessary for any particular well.

Reinjection Studies

In order of priority, concerns about reinjection performance relate to reinjection capacity of the chosen part of the reservoir, life expectancy of wells because of the risk of silica deposition, the possibility of rapid returns of reinjection fluid reducing the output of production wells, and the risk of induced seismicity. Various trials have been carried out over the last few years, for example in Tongonan wells 401 and 404 supplied a 3 MW(e) turbine for several years and the waste water was reinjected to well 4R1. Reinjection at low temperatures (less than 140^{0}C) was examined using Tongonan wells 103 and 101 as producers and 105 as the reinjection well. This was a difficult trial to interpret as it was interrupted by pipeline construction which took

higher priority, but it led conclusively to the idea that reinjection at less than 160°C was not possible at Tongonan, and that the waste water should not be allowed to dissolve oxygen from the atmosphere. The interpretation of more recent tests at Tongonan is currently under way. In these, the waste has been kept free of oxygen and has been reinjected at about 165°C. If there has been any reduction in 'injectivity' of the well it is very small and has caused us to examine our interpretation of injectivity tests. These are normally carried out after well completion and the results used for field design, for which they are adequate. For the more precise evaluation of reinjection damage more detailed analysis methods are needed, such as those used by Mangold, Tsang, Lippman and Witherspoon (1981) and Benson and Bodvarrson (1982), in which the effects of radial temperature variations are modelled using a simulator.

The risk of induced seismicity appears at first sight to be higher at Puhagan than at Tongonan since the terrain is generally steeper and more fracture dominated, and the wellheads are high above the standing water level in wells. Estimates of tectonic stress have been made from well measurements and appear to be higher at Tongonan than Puhagan, however, which could redress the balance. Seismic monitoring is being carried out in both fields.

Other Reservoir Engineering Aspects

KRTA/PNOC-EDC carry out a full range of reservoir engineering measurements and geochemical sampling of well fluids. We consider that these two topics taken together give the best possibility of understanding field behaviour during production. KRTA use the Shaft 79 numerical simulator and having carried out studies of the behaviour of individual Philippines wells and a full reservoir study for Hatchobaru in Japan, are convinced of the value of numerical simulation. There remains, however, a gap in predictive ability at the power station planning stage in the development of a field. At this time too little production has taken place to tune a simulator for performance predictions, and the assessment of field production capacity rests on the ideas of field hydrology gained during exploration. Our view is that it is unreasonable to expect reservoir engineering to bridge this gap and that a recourse to economic risk analysis is necessary.

ACKNOWLEDGEMENTS

The authors are indebted to The Energy Development Corporation of the Philippine National Oil Company for permission to publish this paper.

REFERENCES

Benson S.M. and Bodvarsson G.S. (1982)
Non-isothermal effects during injection and falloff tests, SPE 11137.

Leach T.M. and Bogie I. (1982)
Overprinting of hydrothermal regimes in the Palinpinon geothermal field, Southern Negros, Philippines.
Pacific Geothermal Conference, Auckland, New Zealand.

Lovelock B.G., Cope D.M. and Baltasar A.J. (1982)
A hydrogeochemical model of the Tongonan geothermal field. ibid.

Maunder B.R., Brodie A.J. and Tolentino B.S.(1982)
The Palinpinon geothermal resource, Negros, Republic of the Philippines - an exploration case history. ibid.

Mangold D.C., Tsang C.F., Lippman M.J. and Witherspoon P.A. (1981).
A study of thermal discontinuity in well test analysis, JPT, 33, 6, June '81.

Brodie A.J., Dobbie T.P. and Watson A. (1981)
Well discharge stimulation techniques in hot water dominated geothermal fields.
Proc. 2nd ASCOPE Conf., Manila, Oct. 1981.

Proceedings Ninth Workshop Geothermal Reservoir Engineering
Stanford University, Stanford, California, December 1983
SGP-TR-74

GEOTHERMAL ENERGY DEVELOPMENT IN CHINA

Xin Kuide Yang Qilong

Bureau of Hydrogeology and Engineering Geology,
Ministry of Geology and Mineral Resources,
Beijing, China

INTRODUCTION

China's geothermal resources are mainly of low - medium temperature. More than 30 geothermal areas have been or are being explorated. According to the geology, economy and technology of geothermal energy development main efforts are concentrated in some places with better conditions and can be exploited effectively in the near future, such as low temperature geothermal fields in Beijing and Tianjin, Yangbajain and Dengchong high temperature geothermal fields respectively in Tibet and Yunnan province.

In Beijing and Tianjin the geothermal water is used for space heating, bathing, medical treatment, greenhouse, raising tropical fish, industry and so on. In Beijing now more than 200 thousand sq. m. of indoor floor is being heated with geothermal water and about 50 thousand persons per day use it to take bath. In future, the low temperature geothermal water utilization in these big cities would flourish.

In 1970 the first experimental geothermal power plant using the flashing method was built in Dengwu, Guangdong province. In 1977 one MW experimental wet steam power plant was built in Yangbajain, Tibet, and a 6 MW power plant in 1981 (Photo 1). And another 3 MW generator is expected to complete in 1985.

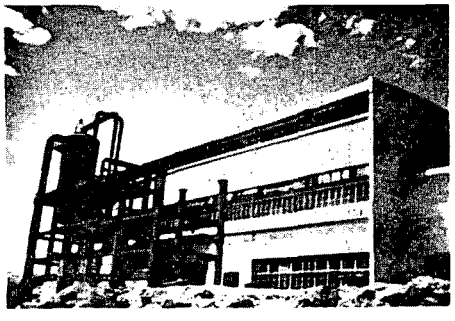


Photo 1: The 6 MW Experimental Power Plant at Yangbajain

This paper is intended to summarize some important results of exploration, particularly in the geothermal reservoir engineering.

GEOLOGICAL CHARACTERISTICS OF GEOTHERMAL RESOURCES (Fig. 1)

The distribution of geothermal fields in China is closely related to the geotectonic feature, the magma and earthquake activities. The high temperature geothermal fields (> 150°C) are mainly situated in southern Tibet, western Yunnan and Taiwan. The west-southern China is effected by Indian Plate. The Himalayan tectonic zone is located in the collision zone between Eurasian and Indian Plates and Taiwan - between Eurasian and Pacific Plates - is at the same time subjected to the northwestward compression of the Philippine Plate (Luo Huanyan, 1979). In all these areas the plate movement, magma and earthquake activities are quite strong and have no doubt provided the conditions for intense hydrothermal activity.

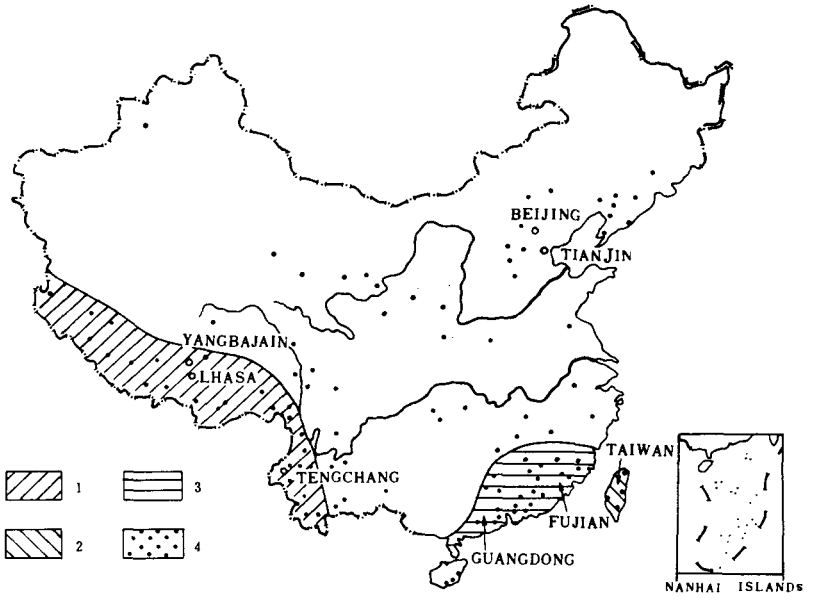
The medium- and low- temperature geothermal fields (< 150°C) are mainly distributed in the coastal region in East China, including Fujian, Guangdong and Hunan provinces, in which the Yanshanin movement since the Mesozoic gave a great influences, The geothermal fluid is contained in the granite with strong silicified alteration.

The low temperature geothermal fields (< 100°C) are distributed almost all over the country, notably the Songliao Plain, North China Plain, Liaodong Peninsula and other areas. The geothermal water is related to faults, magma activities and basement uplift.

BEIJING AND TAINJIN LOW TEMPERATURE GEOTHERMAL FIELDS

1. Regional geology and geothermal feature

Beijing and Tainjin geothermal fields are situated in North China Plain and face the Bohai Gulf on the east. There are a series of deep faults with NE - SW directions between grabens and horsts (Fig. 2). The geothermal fields coincide with the local uplifts within the grabens, but the place with the maximum geothermal gradient in cap



(1) Southern Xizang (Tibet) - Western Yunnan High Temperature Geothermal Zone (2) Taiwan High Temperature Geothermal Zone
(3) Southeast Coast Medium Temperature Geothermal Zone
(4) Main Geothermal Fields

Fig. 1: The distribution of geothermal resources in China

rock is not at the top of the local uplift, but at the steep fault zone between the uplift and centre of graben.

The geotectonic and geothermal activities in the east is stronger than in the west - the main feature of geotectonic and geothermal condition in North ChinaPlain. For instance, the temperature of basement aquifer in Tainjin is 58 - 96 °C and in Beijing - 40 - 79 °C.

According to the seismic record and observation data of artificial earthquake, the crust thickness of North China Plain is approximately 30 - 45 km, with the trend generally being thin in the east and relatively thick in the west. The neighbourhood of Tainjin, having a Conrad and a Moho respectively of about 17 and 32 - 33 km, is a region which is relatively thinner in the North China Plain (Qin Jiafa and Gu Datong 1981).

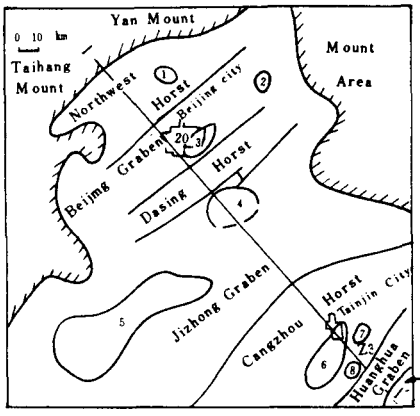
From Isotope data the geothermal fields are recharged by precipitation in the mountain areas, circulated through the basement aquifers and faults. Measured in a bore located in the NW side of Beijing Graben (near the mountain) at depth of 1 km, the temperature only reached 19 °C. It shows the precipitation recharge sweeps the heat from this part of sediment and makes it cooler. The deep water circulation can also be determined by the analyses of the chemical content of geothermal fluids. In Beijing area the mineralization of geothermal water from basement aquifers is low (0.4 - 0.7 g/l), the type of it - HCO_3 - Na. But in Tainjin area the mineralization is high (1.58 - 4.4 g/l), the type - $Cl \cdot HCO_3$ - Na. It appeared that groundwater runoff and recharge in Tainjin is even smaller compared with Beijing.

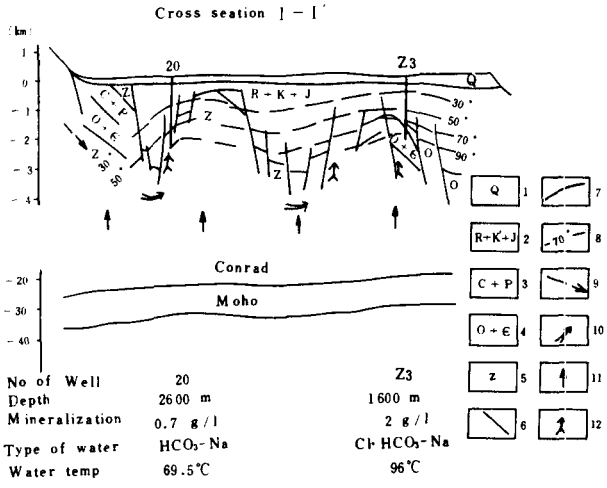
2. Reservoir characteristics

The dolomite or limestone basement of Paleozoic and Proterezoic era in North China Plain is characterised by many fissures, fractures and karst. For example, in wells 5 and 7 in Beijing city, the karst caves have been found at depth of 938.6 - 939.3 m and 730 - 735 m respectively. And the fissure with width of 1 cm at depth of 721.9 m in well 32 have been seen by the downhole TV (Photo 2). And in Tianjin while drilling wells 2 and 4 in the limestones, the bits were dropped several times.

Fig. 3 shows the distribution of two aquifers (Tieling and Wumishan groups, Z_{jt} and Z_{jw}), their top depth, the water temperature at wellhead and specific capacities for each well. The basement structure is a monoclinal stratum with dip angle about 10° towards south. It is clear that the dolomite of Tieling group (about 300 m in thickness) distributes only in the south part of the geothermal field with top depth of 587 m in well 3 in the east to 1200 m in well R1 in the west, and the water temperature rises with increase of top depth from 39.2 °C in well 3 to 53 °C in well R1. The dolomite of the Wumishan group distributes in all area. The thickness of it may reach several km and is the main reservoir in Beijing. The shollowest top of it (517 m in well 21) is in the central part of the field and it increases rapidly towards the NW direction (in well 20 2456 m). The water temperature rises also with increase of the top depth of the dolomite reaching 69 °C in well 20 at wellhead and 79.6 °C at the bottom of well 38 (2600 m). The well production varies from 30 to 96 m^3/hr and specific capacities - from 0.2 to 3.4 kg/s.m.

Between these two dolomite aquifers and above Tieling dolomite there are the shales of Hongshaizhuang (about 300 m in thickness) and Xiamaling (about 90 m) groups (Z_{jx} and Z_{jh}) respectively. And the basement is overlaid with formations of Mesozoic and Cenozoic era. Since the shales have low resistivity (< 150 om.m.) and high radiativity (3000 - 15000 n/m), the





(1) Quaternary system (2) Tertiary and Mesozoic system (3) Permian and Carboniferous system (4) Ordovician and Cambriam system (5) Proterozoic system (6) Fault (7) Geological line (8) Isotherm line (°C) (9) Cold recharge water (10) Deep circular hot water (11) Terrestrial heat flow (12) Upflow along faults

Fig. 2: Schematic of hydrogeology features of North China Plain

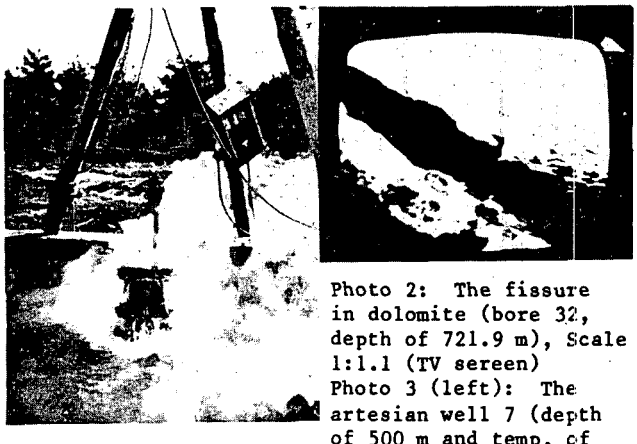


Photo 2: The fissure in dolomite (bore 32, depth of 721.9 m), Scale 1:1.1 (TV sereen)
Photo 3 (left): The artesian well 7 (depth of 500 m and temp. of 62°) in Xiaotangshan, Beijing

border of them can be determined clearly by logging.

To determine the parameters of aquifers 3 sets of interference pumping tests have been done in Beijing. The data from an interference well test are shown in Table 1 The water table was recorded in well T2 while well T1 was flowing at a rate of 95.5 m^3/hr. A log-log graph of the drawdown pressures in well T2 versus time was analyzed by type curve matching with the line source solution, as shown in Fig. 4. From the pressure match, the permeability (k) is estimated at 3.06 Darcy (the thickness is 100 m). The time match gives a porosity of 1.6 %, which results in an estimate of 4.5×10^{-5}(kg/cm^2)$^{-1}$ for the compressibility.

Table 1
Pressure interference data between wells T1 and T2 (1983)

T (day)	S(m)/P(psig)	T(day)	S(m)/P(psig)
0	0 / 0	0.42	0.24/0.341
0.04	0 / 0	0.50	0.28/0.398
0.08	0.02/0.028	0.58	0.37/0.526
0.125	0.03/0.043	0.67	0.40/0.569
0.17	0.06/0.085	0.75	0.41/0.583
0.21	0.09/0.128	0.92	0.43/0.612
0.25	0.11/0.156	1.08	0.49/0.697
0.29	0.14/0.199	1.25	0.51/0.725
0.33	0.17/0.242	1.42	0.55/0.782
0.38	0.20/0.284	1.67	0.60/0.853

Distance between wells = 230 m
Water viscosity = 0.6 cp

Other methods are also used to determine the porosity of aquifers. For instance, 1.78 - 3.6 % has been calculated by sound-wave logging in 6 wells at depth of 705 - 1575 m. In addition, the porosity of 7 dolomite cores collected from a well were measured in lab to be 0.4 - 6 % (av. 2.77%). And Prof. Bodvarsson estimated the porosity to be 3 %, assuming the resistivity of dolomite aquifer and local water 400 and 12 om.m. respectively.

The fact that the results of the interference test agree with other data suggests that the dolomite or limestone aquifers in Beijing, or even in North China Plain, has high permeability (k about 3 Darcy) and low porosity (about 2.5 %), indicating a fractured and/or solution opening situation. Finally it should be noted that besides basement aquifer there are some aquifers in Tertiary and Jurassic sedimentary or volcanic rocks, but their temperature is low. Particularly in Tianjin, the sediment aquifer now is the main geothermal production aquifer.

3. The long-term observed water level and geothermal resource assessment

The drawdown on wells during the exploitation depends on the well production. The

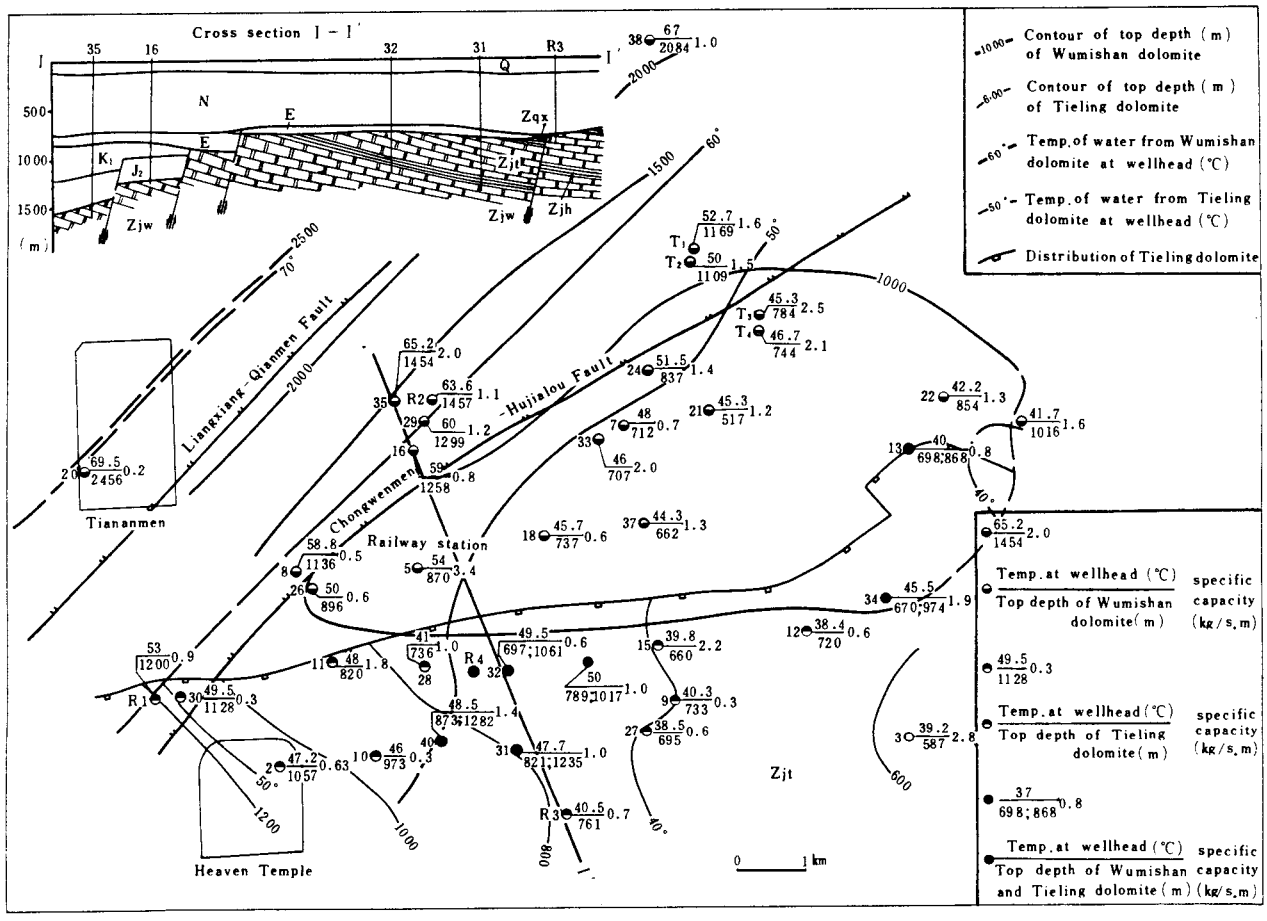


Fig. 3: Distribution of aguifers, their top depth and water temperature by Daofu, Yang Qilong and Bai Tieshan

drawdown curves of 4 typical wells in the city of Beijing, their production increased from 4.9×10^5 m³ in 1971 to 3.3×10^6 m³ in 1981, are shown in Fig 5. And in the city of Tianjin, 259 wells have been drilled since 1970. The water level has dropped to 40 - 60 m below surface (Fig. 6). The basement limestone water is still artesian, because the production rate is limited.

3.1. Estimation of maximum well production

The exploitation period from 1971 to 1981 was divided into four stages (Fig. 5). Based on the functional relationship between specific production rate in whole area and drawdown of water level (from original static water level) the *maximum* production was estimated. The specific yield (q) and depth of water table[5] for each stage were 3.2×10^5, 6.9×10^5, 1.3×10^6, 1.9×10^6 m³ and 11.3, 15.1, 18.9, 22.9 m respectively. After distinguishing the relationship between q and s in various way, the power functional equation $Lg\ q = -1.05 + 2.44Lgs$ has been got (Fig. 6). If the drowdown rate is 1.5 m/yr, the water table would be increased from 22.9 m at the end of 1981 to 35 m in 1990 (dynamic table may reach 60 - 80 m), the production being 7.7×10^6 m³/yr.

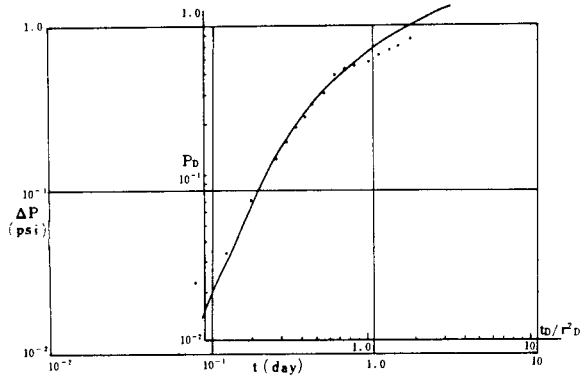


Fig. 4: Type-curve matching of the pressure interference data between wells T_1 and T_2

Prof. Bodvarsson wrote in his consult report:" Based on the data from observation well 3, the equilibrium dynamic drawdown at constant total pumping rate of 6500 m³/d is about 10 m, that is 18 m below ground surface. Without difficulty, the drawdown could be increased by a factor 6 to 10. It is prudent to limit the estimate to a factor of 5 such that without fluid reinjection the yearly average total pumping rate could be increased to 3×10 m³/d" (1.1×10^7 m³/yr.).

3.2. Estimation of total energy reserves

Assuming that the thickness of aquifer is 300 m, temperature at wellhead and for waste water - 55 and 35 °C respectively, volumetric specific heat of rock/water - 0.5 cal/cm·°C, recovery factor - 0.2, the energy reserves of 3×10^{13} kcal was estimated for 50 km², where the exploitation depth is less than 1.5 km. And the heat energy for an other 50 km² (depth of 1500 - 2500 m) is 9×10^{13} kcal (500 m in thickness of aquifer and 70°C of temperature at wellhead are adopted). So the total heat energy inthe geothermal area of 100 km² in the city of Beijing could reach 1.2×10^{14} kcal(equals to the energy released by burning 1.7×10^{7} tons of coal). Assuming active reservoir life to be 25 yr., heat energy of 4.8×10^{12} kcal/yr can be extracted. If 2/3 of the hot water is used for space heating, the floor area would reach 2.6×10^{7} sq.m. (Assuming the heating period is 3 months and heat standard - 40 kcal/sq.m·hr).

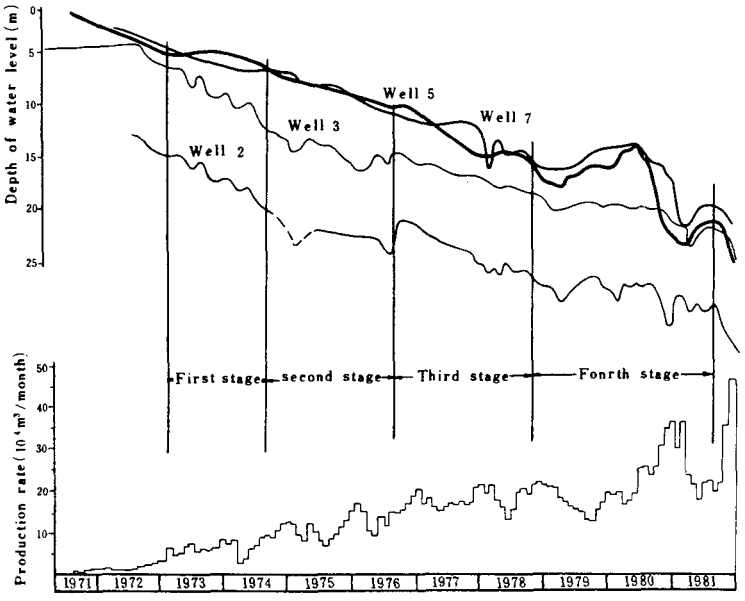


Fig. 5: Drawdown curves of water level in 4 typical wells (1971-1981) by Liu Shufang

In the city of Tianjin the geothermal field (about 100 km²) has the total energy of 1.4 10^{14}kcal, if the thickness and temperature of basement aquifer assumed to be 400 m and 70 °C, and other parameters are the same as mentioned above.

It is clear that a sufficient degree of heat sweeping from aquifer can be obtained only by successful reinjection. In Beijing city well R4 (depth of 1274 m) has been used for reinjection of waste water (at the end of heating system) for two years. The production well 32 (depth of 1151 m) at a distance of 200 m from well R4, had a rate of 36 m³/hr with temperature of 49 °C at wellhead, providing a heating floor area of 11,000 sq.m. After the waste water with temp. of 38 °C was reinjected into well R4 the water table rised only by 2.8 m. After stopping reinjection of 1.2×10^{4} m into R4 for 8 months, the water temperature in the dolomite recovered to 49.5 °C (the original temp. was 52 °C). Since the heating period in North China lasts only 4 months, the water temperature can recover in an other 8 months. Up to now, no temp. drop in surrounding wells has been observed yet.

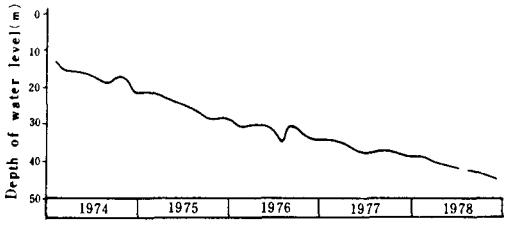


Fig. 6: Variations of underground water level of one geothermal well in Tianjin

HIGH TEMPERATURE GEOTHERMAL FIELD IN YANGBAJAIN, TIBET (Fig. 8)

1. Regional and field geology feature

Just an hour's drive northwest of Lhasa, the capital of Tibet, is the Yangbajain Geothermal Field, located in the elongate basin about 5 km wide and 100 km long at the foot of Mt. Nyaigentanglha. Here there are many geothermal fields and new tectonic movement and earthquake are very active. Folds and faults can be seen in Quaternary layers. The main rocks in Yangbajain and the surrounding area are gneiss, slate, tuff and granite.

In the southern part of the field there are many hot or boiling springs (Photo 4), boiling mud pools, silica sinters, hot water lake and so on. The northern part of the field is an alteration area (about 4 km²). Here, due to intense thermo-chemical action, the colorful rock has been reduced to white, powdery kaolin. In some places, just a few centimeters beneath the

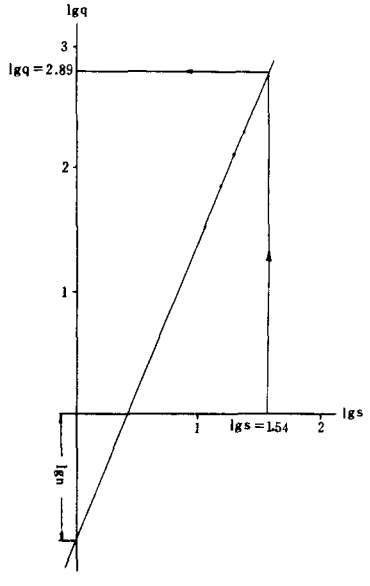


Fig. 7: The line shows the equation of lgq=f (lgs)

ground, the temperature exceeds the local boiling point of 86°C (4300 m above sea level). And sulphur is also being mined. Based on data from wells, the vertical zonation of sulphur and sulphide has been found. At depth of 20 m the Quaternary layers content pyrite (FeS_2). And semi-transparent sulphur crystals (S) appeared at crack from surface to 10 m. In more oxidation condition, sulphate occurred and the layers became kaolinized and alunitized.

2. Temperature and pressure of geothermal fluid (Fig. 9 and 10)

The maximum temperature of geothermal fluid changes from 172°C in the northern part of the field to 160°C in the southern part. On the other two sides, the temperature reduces to 112 - 142°C. Well 19 shows a trend toward a maximum temp. of 152°C at depth of 140 m, followed by a geothermal gradient of 3.1°C/100 m that was recorded from 810 m down to 1000 m. The geothermal gradient of well 7 is 4°C/100 m. So far only these two wells, 19 (1000 m) and 7 (603 m), are deep enough to determine the geothermal gradient at depth, showing temp. trends that would intersect at 178.4 °C at depth of 2600 m (the method provided by Michel J. Economides, etc. 1982). It should be noted that this source temperature is lower than that of 207 - 222°C estimated by geothermometers, so the real source depth might be deeper.

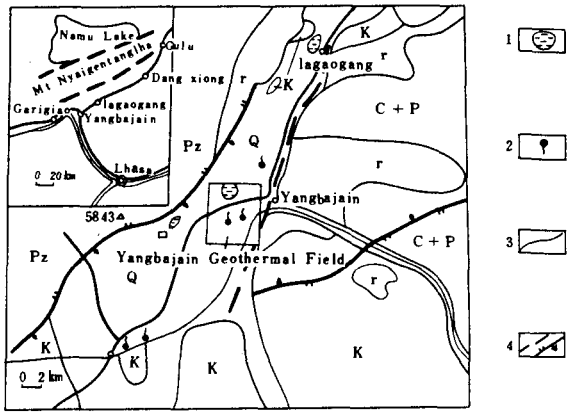
The begining point of increased geothermal gradient changes from 810 m(122.9°C) in well 19 to 460 m (92°C) in well 7. After expanding the gradient to surface the temp. of 97.7°C and 74.4°C (much higher than local average atmospheric temp. of 11°C) have been got.

Depending on the drilling stabilized mud density, Mr. Wang Zongying calculated the downhole water pressure. The altitude of the zero pressure in wells decreases from NW to SE, having the same tendency as the temperature and relief changes (Fig. 9).

3. The geothermal system model

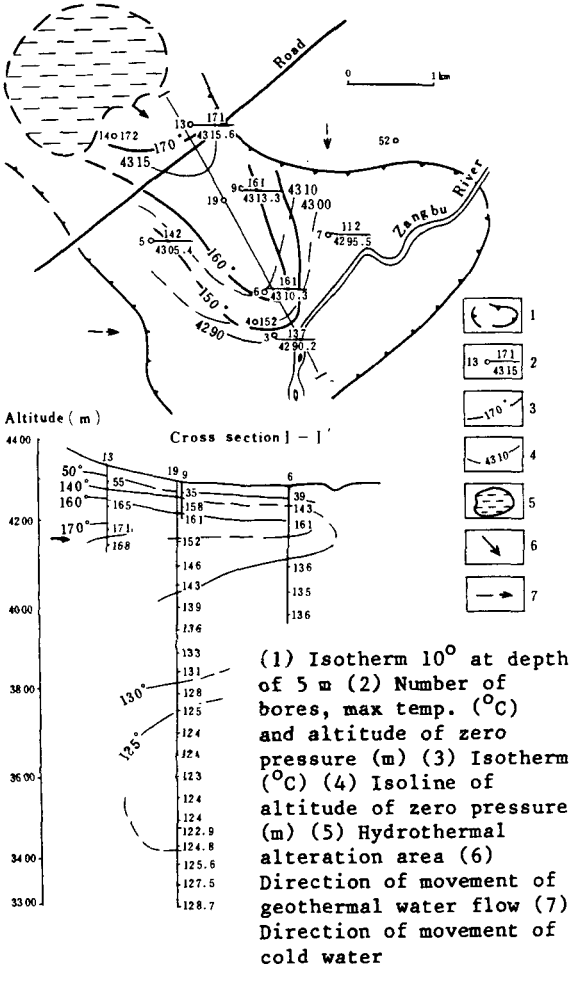
The silicified sandstone distribution and chemical content of geothermal fluid are also important to prove the lateral water flow in Yangbajain Geothermal Field.

Fig. 11 shows the relation of temp. of fluid with silicified sandstone. The highest temp. are recorded all in the silicified sandstones, which have high resistivity. The silicified sandstone appears in a form of "tongue", that is, the top of it varies from a depth 150 m in north to a depth of 70 m in south, and in thickness from 250 to 100 m. As there are a lot of fractures in it, the permeability is high. For instance, well 9 has the best parameters: depth 89.3 m, 169 tons of water and 21 tons of steam per hour at a wellhead



(Q) Quaternary sand and till; (K) Cretaceous tuff, C + P - Carboniferus and Permian slate; (Pz) Pareozoic gneiss, (r) Granite; (1) Hydorthermal alteration area; (2) Hot and boiling springs; (3) Geological line; (4) Fault

Fig. 8: Geology may Yangbajain and surrounding area



(1) Isotherm 10° at depth of 5 m (2) Number of bores, max temp. (°C) and altitude of zero pressure (m) (3) Isotherm (°C) (4) Isoline of altitude of zero pressure (m) (5) Hydrothermal alteration area (6) Direction of movement of geothermal water flow (7) Direction of movement of cold water

Fig. 9: Temperature and pressure distribution in Yangbajain

temp. of 148 °C and pressure of 4.7 atm. The estimated electricity potential is 1978 kw (Photo 5).

Fig. 12 shows the mineralization and ion content of fluid in wells are proportional. They decrease from NW To SE and from the "tongue" to surrounding area. The fluid collected from well 13 contains mineralization (2.2 g/l), Cl (651 mg/l) and HBO_2 (298 mg/l), the highest among all existing wells. This kind of water mixes cold water with low mineralization and high HCO_3 from outside the field and Cl - HCO_3 mixed water is formed.

Accordingly, it is presumed that the present activity of the field is the post-intrusive action magma. Cold recharge water(1) passes a nearby heating volume beneath the sulphur deposit or even farther and mixes with juvenile water from cooling magma, rising in temp.,decreasing in density, and forming a deep thermal fluid(2), which rises along the fault. Due to pressure reduction and changes in the oxide-reductive conditions, sulphur steam(3),mercury,etc. are separated and produce hydrothermal alteration and sulphur deposit. Then as it is pushed by cold water at the foot of Mt. Nyaingentanglha(4), the deep thermal fluid turns to the horizontal movement to be mixed-thermal fluid(5), Fig. 13.

4. Reservoir parameters and resource assessment (Fig. 14)

Thirteen geothermal wells have been drilled here up to 1980. They have the parameters: depth 68 - 1000 m, total flowrate 82 - 191 tons/hr at a wellhead temperature of 120 - 148 °C and pressure of 2.3 - 4.7 atm. The total estimated electricity potential is 15.3 MW.

The energy reserves are estimated to be 4.5×10^{13}kcal for the Quaternary aquifer, as the geothermal area is 10 km^2(the maximum temp. in wells is higher than 150 °C). This area consists of 6 km^2 in the north of the road(the thickness of 300 m and temp. of 170 °C) and 4 km^2 in the south (150 m and 160 °C). The waste water temp. is 90 °C, the specific volume of rock/water - 0.6 cal/cm^3·°C the heat recovery - 0.2. If the pipe and power plant efficiency is 0.1, the electricity potential - 65.4 MW. If the exploitation period covers 25 years, the electric potential of 26 MW is estimated.

The fact,that the Yangbajain Geothermal Field has the lateral water flow,can not be negleted in its resource assessment. The following equations were used to determine reservoir permeability(k) in well 13.

$$K = \frac{QLgR/r}{2.73MS} \qquad S = 2.32\times10^{5}\,\frac{QV_w\mu^{0.15}}{t^3\times10^9\,d^{0.85}}$$

Put Q = 141 m^3/hr, R = 400 m, r = 0.2, M = 58 m, μ = 0.09 cp, t = 3 mm(width of fissure determined from core) and V_w = 1.125



Photo 4: Morning in Yangbajain

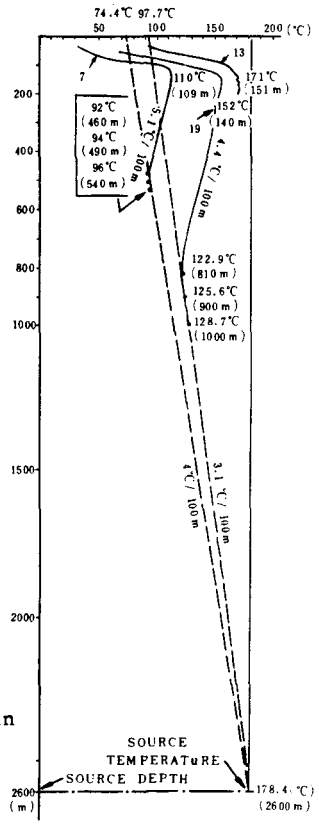


Fig. 10 (right): The shallow reservoir and source temp. at Yangbajain Geothermal Field

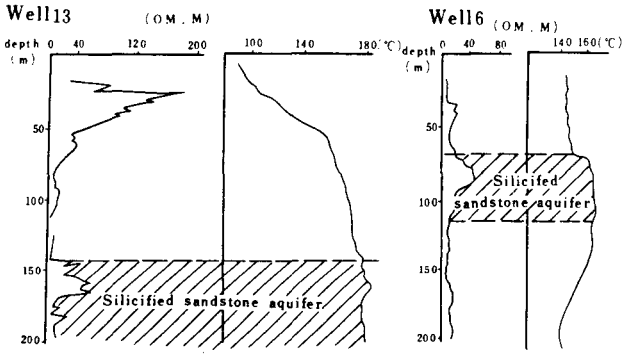


Fig. 11: Relation of temp. and resistivity with silicified sandstone

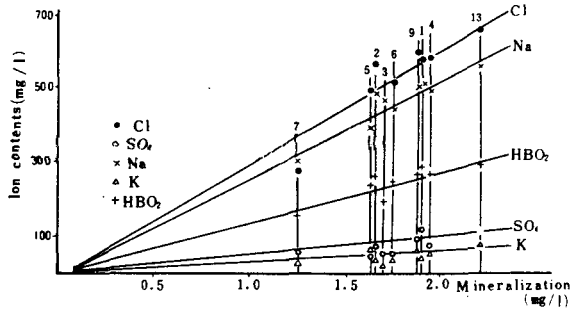


Fig. 12: Relation between mineralization and ion contents of geothermal fluids sampled from bores in Yangbajain

cm³/g into the equations, we got S = 5.1 m and K = 14.3 m/day for well 13. Adopting the width of the cross section I - I' of 2 km, the thickness of aquifer 300 m, water level gradient of 1.5 % (calculated from isoline of altitude of zero pressure) - the cross section water flow of 5363 m³/hr has been obtained. In Yangbajain a water flowrate of 100 m³/hr can produce 1 MW, so 54 MW might be produced by using above mentioned flowrate. Finally, the total electricity potential of the Quaternary aquifer in Yangbajain is estimated to be 80 MW.

SUMMARY

Geothermal energy is one of the important new energy resources in China. In Beijing, Tainjin, Tibet, Yunnan, Fujian, Guangdong and many other places it is under exploration and utilization. The preliminary resource assessment in this paper shows the promising prospects of production of geothermal energy in Beijing, Tainjin and Yangbajain.

In North China the dolomite or limestone of Paleozoic and Proterezoic era has higher temp. and good permeability. Important thing is to find and explorate more new geothermal fields in local uplift within grabens. In Yangbajain the silicified sandstone or conglomerate controls the Quaternary aquifer. The most improtant task is to find the high temperature geothermal fluid in the basement.

ACKNOWLEDGEMENTS

Thanks are given to the Beijing Hydrogeology Company, the Geothermal Geology Team in Tibet, and Mr. Zhang Hongren, Mrs. Shen Minzi, Mr. Bai Tieshan and Mrs. Gong Meizhen for their invaluable help in making this manuscript possible.

REFERENCES

Bodvarsson, G.S. (1982) Technical Evaluation of Geothermal Resources and their Development in Beijing Area of the People's Republic of China, Report on a Misson as a Consult in Reservoir Engineering.

Gin Jiafa and Gu Datong, (1981) Prospecting and Utilization of the geothermal Resource of Tainjin, Paper on the Sino/US Geothermal Resources Conference.

Michel J. Economides, Christine A. Ehlig Economides, Jay F, Kunze, Ben Lofgren (1982) A Fieldwide Reservoir Engineering Analysis of the Pilgrim Springs, Alaska, Geothermal Reservoir, Proceedings, Eighth Workshop on Geothermal Reservoir Engineering, pp. 25-30

Xin Kuide and Zhang Xigen, (1982) Geothermal Resources in China, GEOTHERMICS, V. 11, No. 4, pp. 281-187.

Yang Qilong. (1982) Geotemperature Measurement in Geothermal Exploration, Proceedings Pacific Geothermal Conference 1982 and 4th New Zealand Geothermal Workshop, Part 2, pp. 485-489.

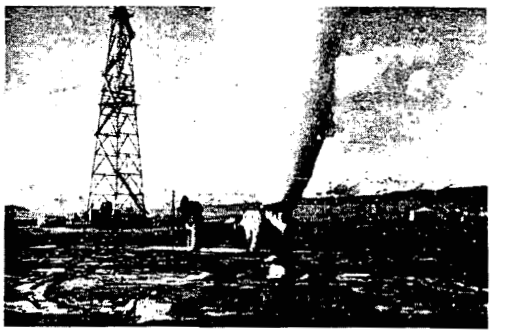
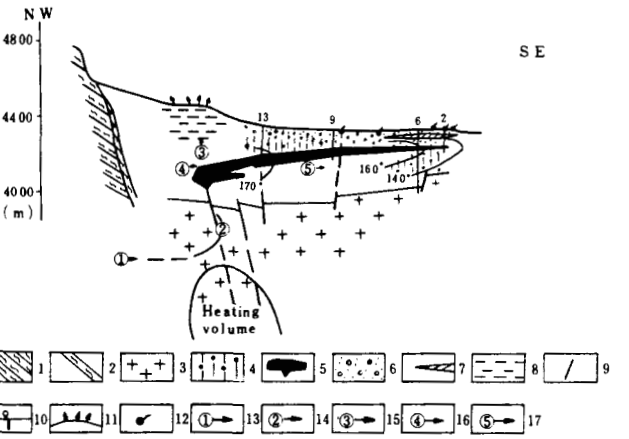


Photo 5: The well 9 spouts



(1) Gneiss of Paleozoic era (2) Breccia
(3) Granite (4) Till of Quaternary
(5) Silicified grit controlled aquifer
(6) Grit (7) Clay (8) Alteration area
(9) Fault (10) Wells (11) Steam ground
(12)Hot or boiling springs (13) Cold recharge water (14) Deep thermal water flow (15) Sulfur steam (16) Cold water at the foot of Mt. Nyaingentanglha (17) Mixed geothermal water flow

Fig. 13: Geothermal system model of Yangbajain Geothermal Field

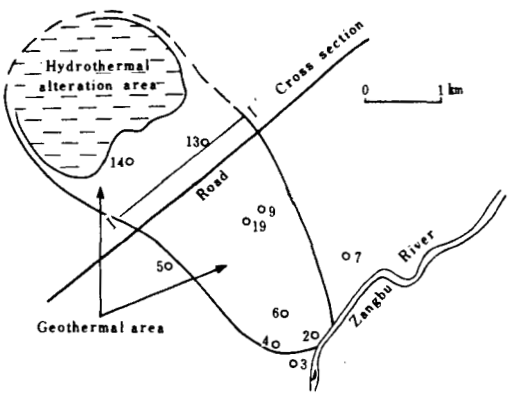


Fig 14: Map shows the geothermal area and cross section for reservoir assessment

Proceedings Ninth Workshop Geothermal Reservoir Engineering
Stanford University, Stanford, California, December 1983
SGP-TR-74

EXPLORATION, DRILLING, AND DEVELOPMENT OPERATIONS IN THE BOTTLE ROCK AREA OF THE GEYSERS STEAM FIELD, WITH NEW GEOLOGIC INSIGHTS AND MODELS DEFINING RESERVOIR PARAMETERS.

Jeffrey J. Hebein

MCR Geothermal Corporation
10880 Wilshire Boulevard
Los Angeles, California 90024

ABSTRACT

MCR Geothermal Corporation pioneered successful exploratory drilling the Bottle Rock area of the Geysers Steam Field in 1976. The wellfield is characterized by a deep reservoir with varied flowrates, temperatures, pressures, and steam chemistries being quite acceptable. More detailed reservoir engineering tests will follow as production commences.

Subsurface geology is comprised of a deep main graywacke rock(s) with overlying cap, condensation, and highly altered reservoir zones. Liquid reserves for steam production probably exist in the condensation zone fractures and alteration pores(?), and by physical adsorption in micropores along fracture surfaces, since interstitial porosities and the presence of a basal boiling brine have been ruled out.

The steam reservoir evolved from ancestral liquid-dominated hydrothermal systems and possesses an extremely viable fracture system comprised of tectonic rubble breccias. Essentially, the steam reservoir(s) are huge tectonic breccias superimposed on (mimicing) and now overlapping huge ancestral hydrothermal breccias. While earlier reservoir models utilized a boiling-brine and/or Raleigh-plume dispersion mode of existance and operation, geological data now suggests that the reservoir may be a system of verticle steam-filled fractures with a separate condensation zone held somewhat immobile along the top and flank boundaries of the fracture networks.

Local extensional tectonics have and continue to play a very important role in the formation and continuance of both the ancestral liquid and active vapor systems in the steam field. Accordingly so, drilling programs should be designed with tectonics in mind so as to maximize well deliverabilities.

The Francisco lease will supply steam to power a 55 MW powerplant presently under construction by the California Department of Water Resources.

INTRODUCTION

Figure 1 is a location map illustrating MCR's developments. Entex Petroleum, Inc., Houston, Texas is a partner in the current Francisco production venture.
MCR's stepout into the Bottle Rock area confirmed a boundary addition to the extremely large and prolific Geysers field. Public information on the characteristics of the field has been sparse. This presentation, however, should stimulate discussion of technical information regarding the Bottle Rock area and assist total steam field comprehension.

WELLFIELD CHARACTERISTICS - FRANCISCO LEASE

Area:	380 acres, 3 pad locations
Wells:	12 drilled to date, 1 used as injector, 2 not to be used.
Depths (drilled):	8606 to 10,586 feet.
Flowrates:	47,000 to 179,000 Lbs/Hr @ 125 psig; average 110,000 Lbs/Hr
Times:	generally 12 wks to drill, production casing at 6500'-6700'
Steam entries:	5 (minimum) to 21 (maximum) 6575'/6310' (TVD) to 10,560'/10,240' (TVD); range 2-3000 Lbs/Hr. to 90,000 Lbs/Hr.

Some wells are drier and show superheat at the wellhead, some discharge a wetter steam Initially, Francisco 1-5 was drilled to 8970 feet in 1976 and produced 108,000 Lbs/Hr steam @ 109 psig with 6" bore. MCR's minimum economic limit is 75,000 lbs/hr, although lower output wells would be connected to the gathering system.

Reservoir temperatures average 247°C/477°F and pressures range from 500-550 psig. These temperatures and pressures appear to exceed values given for other parts of the steam field (Cochran, 1979; Ramey, 1968; Lipman, et al., 1977). Temperatures and pressures tend to climb slightly as depth is increased within the reservoir. These variances from other reservoir values may

indicate differing conditions in separate field cells or that the Francisco lease has very "virgin" conditions in the reservoir. Shut in wellhead pressures hold at 400-455 psig.

Steam chemistry is within field ranges and is highly acceptable. Table 1 is an analysis of condensate and non-condensables from a typical well.

TABLE 1

Arsenic	(ug/l)	< 10
Mercury (Total)	"	22
Iron	(mg/l)	0.63
Calcium	"	< 0.080
Boron	"	7.8
Chloride	"	5.0
Fluoride	"	< 0.10
Sulfate	"	2.6
Bicarbonate Alkalinity	"	170
Carbonate Alkalinity	"	0
Nitrate	"	0.49
Specific Conductance	(umhos)	430
ph		6.2
T.D.S.	(mg/l)	12
Suspended solids	"	< 2
Noncondensables	(ppm/wt)	4,300
Water vapor	"	996,000
Carbon dioxide	"	3,700
Sulfur (as H_2S)	"	219
Ammonia	"	64.6
Methane	"	104
Nitrogen	"	143
Hydrogen	"	75
Radon 222 (pico cur/l noncond.)		480

Rate:	121,000 LBS/Hr.
T°:	352°F

Transient well testing and tracer tests will follow in hope that general values for reservoir transmissivity and draw-down can be obtained. Inhomogenities in geologic structure (fracture framework) may also be implied through these tests.

WELL AND SUBSURFACE GEOLOGY

Figure 2 represents a generalized geologic section of lease wells. McLaughlin (1981) and Thomas (1981) both define a "lithocap" above the steam reservoir. This cap is comprised of a massive Franciscan melange up to 6000-6700 feet in thickness under the Bottle Rock area.

The main graywacke's upper portions show Franciscan metamorphic alteration (calcite) and the mid to lower portions exhibit massive quaternary hydrothermal alteration. Alteration appears similar to accounts for other wells throughout the steam field (Lambert, 1976; Lockner et al., 1982); Sternfeld, 1981) with the exception that Bottle Rock wells encounter these conditions at much greater depth. MCR's wells encroach upon an apparent contact metamorphic zone (migmatites) at depth. In two wells, drilling encountered fine grained felsic volcanic dike rocks of dacitic to rhyolitic composition.

Coring of the main graywacke beneath the Francisco lease was above the reservoir section as was coring from other parts of the field (Lockner et al., 1982). The cores show excellent fresh enechelon, concentric fractures which probably relate to fresh fracturing associated with recent tectonic extension. This upper portion of the main graywacke is massively calcite veined, very dense, virtually non-porous (thin sectioned), and appreciably brittle. Petrographically, these rocks are albite-sericite-epidote-chlorite-quartz altered. This rock would make an excellent initially fractured reservoir rock in the ancestral liquid systems of the Geysers field. Interstratified argillites are dense, carbonaceous black, moderately calcite veined, and well sheared with glassy slickensides associated with actinolite/chlorite-like recrystallization. It is highly conceivable that these argillites (and other melange types) could hold steam bearing fractures if such fractures communicate with fractures in massive graywacke bodies.

A condensation zone (maximum three to five hundred feet thick)definitely exists above the steam reservoir (Fig. 2) and is probably found in some form in all other parts of the steam field. This zone is characterized by liquid saturated fractures and perhaps some pore saturation with specific rock alteration. The hydrothermal alteration process is probably phyllic (sericitic) alternation, where steam condensate alters and leaches rocks within the zone. Here, detrital and hydrothermal feldspars are altered to clay group (illite) minerals and zeolites, quartz is augmented, and realgar is viewed in traces. Steam and water entries are commonly encountered while drilling in this zone. The water usually dissipates after a day or two of drilling but in one instance a water entry was so large that the zone(s) required plugging off before air drilling could resume.

Ramey (1968) reported the presence of a water body (condensation zone) between the shallow upper and lower reservoirs in the Sulphur Bank area of the steam field. Several researchers (White et al., 1971; Truesdell and White, 1973; D'Amore and Truesdell, 1979) have speculated on the occurrence of this zone with MCR's drilling confirming its presence. Weres et al. (1977) reported the alteration of reservoir rocks with the formation of minute, sand-like particles (smectite?) in the pores of the graywacke encountered in wells in the Castle Rock Springs area of the Geysers

field. This probably represents a condensation zone and is quite similar to MCR's findings.

Table 2 is an analysis of fluids (flashed to some unknown extent) from the condensation zone penetrated by a well. The well is the same one whose steam analysis is presented in Table 1.

TABLE 2

Potassium	(mg/l)	110
Calcium	"	96
Sodium	"	270
Iron	"	2.3
Arsenic	(ug/l)	320
Mercury	"	3.2
Chloride	(mg/l)	250
Sulfate	"	400
Sulfide (H_2S)	"	< 0.10
Silica	"	2.0
Bicarbonate Alkalinity	"	230
Total Carbon dioxide	"	170
Boron	"	14
Ammonia	"	< 0.20

The actual reservoir rocks are highly hydrothermally altered, non-porous in thin section and are probably composed of numerous diffusion microfractures and flow fractures. Petrographically, these rocks are albite-illite-smectite-chlorite-epidote-zeolite-quartz altered. Smectite pore fill has destroyed former residual interstitial porosity. The fracture model by Norton and Knapp (1977) is utilized for fracture porosity definition. Porosity estimates are speculative, if not near unobtainable because the reservoir has fracture porosity. Diffusion and residual porosity can be determined but flow porosity is destroyed during coring. Overall fracture porosity is probably less than 5%, both in the main reservoir and the condensation zone. Thermogenics (Caupuano, 1979) estimates overall reservoir fracture porosity at 1-3%, while Union Oil Co. (Lipman, et al., 1977) estimates a 3-7% interstitial porosity (irrelevant?) from cores probably retrieved above the reservoir section itself (Lockner et al., 1982). Residual porosity fluids are probably very limited and immobile, excluding the effects of any secondary surface adsorption in micropores.

Ancestral hydrothermal veining comprised of quartz-epidote-feldspar is abundant in brecciated zones with this mineralization also found in disseminated veins and interstitial pores somewhat removed from the massive breccias. Sporatic, continuous occurrences of these massive hydrothermal brecciations and mineralizations strongly suggest the penetration of ancestral liquid dominated conduits as wells are laterally directionally drilled. The quartz-epidote alterations still remain the best indicator of upcoming steam entries although minor steam occurrences can occur in relatively clean rock, even in the calcite-rich rock near the top of the reservoir graywacke. Analysis of cuttings from other wells in the field (Sternfeld, 1981) show similar traits to Bottle Rock well cuttings. Frye (1976) discusses the importance of silica content in enhancing reservoir rocks with respect to steam occurrence in Aminoil's production area.

Ocasionally, semi-massive, very argillite-rich units within the main graywacke are penetrated. A dramatic loss of quaternary hydrothermal alteration and steam potential is usually witnessed. The argillites can become very clay-like or schistose and flakey, causing major sloughing problems. If sloughing is too severe, wellbores may collapse inward and raise considerable havoc while air drilling. Encountering such bodies at greater depths had actually prohibited the continuance of air drilling in one instance.

RESERVES

Where are the liquid reserves in the Geysers reservoir(s)? The condensation zone probably has substantial liquid reserves in place in both diffusion and flow fracture porosity. Fractures in the condensation zone should communicate with reservoir fractures intersected by the wellbores. Capillarity condensation (Hsieh and Ramey, 1983) may be responsible for holding fluids in the fractures of the condensation zone whereby the hydrostatic head of fluids in these fracture systems is less than underlying reservoir pressure, thus enabling such fluids to stay relatively in place. Since clay minerals (illite) found as traces to 15% of total rock volume in the condensation zone are hygroscopic, small reserves may be found in these altered pore spaces. Weres et al. (1977) inferred that these pore voids are responsible for overall reservoir fluid storage, but the author suggests that this potential storage medium only pertains to the condensation zone.

Since the physical surface adsorption of liquids into heated rocks has been demonstrated in the laboratory (Hsieh and Ramey, 1983), it can be assumed that this phenomena does exist along reservoir fractures. Liquids in micropores along fracture pathlines may contribute to reserves for steam formation, those liquids probably being a major reserve source. Of course, steam already in place in fractures is also part of the total reserves.

The suggestions that the reservoir rocks are a "cracked sponge" (Weres et al., 1977) or that substantial matrix porosity/permeability (mobile liquid saturation) exists

(Pruess and Narasimhan, 1981), should be dismissed. The reservoir rocks are virtually interstitially filled with solids. Determination of potential steam reserves may be very difficult if not unrealistic in a fractured, gas-drive reservoir where reserve porosity parameters are only implied and geologic inhomogenities are apparent throughout the reservoir.

The presence of a basal boiling brine overlain by an isothermal vapor zone such as is commonly found in near-surface fumarolic/hot spring-type geothermal regimes has been suggested as a major source of steam in large vapor systems such as the Geysers (White et al., 1971, Truesdell and White, 1973; D'Amore and Truesdell, 1979). Since no basal boiling water table has ever been found at the Geysers and other geologic features offer modes for potential storage of liquid reserves, this concept is deemed superficial and should not be utilized until direct supportive evidence is offered by field operators.

DEVELOPMENT OF LIQUID AND VAPOR SYSTEMS

The vapor system within the Geysers field was once a very prolific liquid system, therefore one must look upon the reservoir in terms of its past functions so as to more fully comprehend its present functions. Several successive liquid hydrothermal stages or phases (Lambert, 1976) did exist in at least several parts of the steam field.

Continual extensional tectonics over the last two to three million years in the Geysers region (McLaughlin, 1981) is probably responsible for all past and present igneous hydrothermal activity in this region. Thomas (1981) reports that felsic igneous intrusives occur under many of the anomaly crests within the steam field. It is highly plausible that intrusive masses (stock-like) underlie many key areas of the steam field and were directly responsible for the driving of ancestral convective liquid systems in separate or twinned locations in the Geysers field. Liquid system development probably evolved just as the active Wairakei and Broadlands systems (Grindley and Browne, 1975) now function with Rayleigh plume dispersion (Henley, 1973; Elder, 1981) as an acceptable mode of fluid circulation. MCR's drilling experiences provide evidence that the current vapor system is a direct result of a deep massive ancestral liquid system. One major contributing factor to system development was that the initial reservoir graywackes were already dense and brittle (low tensile strength) which offered an excellent host rock for fracture systems to develop within. Tectonic extension and intense heat flow will continue as the liquid system now becomes quite mature, seals itself and becomes a candidate for vapor-domination. A good qualitative scenario for the evolution of a vapor system is given by Pruess and Truesdell (1980). As the system boils down and more vaporous conditions start to prevail on the top, the lower body liquid portions may themselves reseal, refracture, brecciate by steam explosions and hydraulic fracturing, and again reseal such as happened in intermediate depth systems such as those at Wairakei and Broadlands (Grindley and Browne, 1975). A previously boiling environment represented by deposition of minerals such as adularia, etc. (Ellis and Mahon, 1977) is encountered by drilling in MCR's wells and other parts of the field (Sternfeld, 1981; Lockner et al., 1982). Continual boil down must have occurred in the reservoir(s) since former hydrostatic pressures would have then been too high to allow for the boiling of a mildly saline single-phase liquid at appreciable depths. However, the author strongly disagrees (discussion forthcoming) with Sternfeld's rendition of successive boil-down levels involving imbricate thrust zones.

FRACTURE MODELS

Fracture properties are the key factors determining how the Geysers reservoir(s) respond. McLaughlin (1981, Figs. 8,9) presented models using near verticle fracturing stemming from extensional tectonics, which should be quite accurate. Thermogenics, Inc. (Caupuano, 1979), Shell Oil Co. (Hite and Fehlberg, 1976), and Union Oil Co. (Lipman et al., 1977) prefer a near verticle orientation for reservoir fractures or perhaps fractures just above the reservoir. MCR's drill core and drilling experiences strongly suggest that reservoir fractures are near-verticle. The author believes the idea of high volume near-verticle steam filled fractures in the Geysers reservoir(s) (Ramey and Gringarten, 1975) is quite realistic. H.J. Ramey stated (Kennedy, 1974), that numerous well tests in the Geysers field showed evidence of tremendous verticle fractures intersecting the wellbores. The pressure-time data suggests "cavernous" bodies exist in parts of the steam field. MCR's deep drilling experiences adequately confirms those speculations.

Drilling occasionally encounters drill breaks of say six inches to a foot of sudden drop. These breaks are usually associated with steam entries but sometimes yield little or no steam. Wellbores have penetrated what appears to be massive cavernous fractures, (rubble breccias) with very large steam entries coming forth from breaks of 5 or 6 feet in a minute or two. Massive ancestral hydrothermal brecciation is an

excellent indicator. As tectonic extention continues, fractures will grow wider instead of veinfilling as in the ancestral liquid system, whereas steam is a relatively poor solvent and mineralizer with respect to the mineralizing effectiveness of hot water. As large fractures grow, steam-bearing conduits could penetrate into relatively unaltered rock, as is seen in several instances while drilling.

RESERVOIR MODELS

Early models (White et al., 1971; Truesdell and White, 1973) of steam reservoirs (the Geysers) depicted a basal boiling brine feeding steam filled fractures and an overlying condensation zone. D'Amore and Truesdell (1979) and Thomas (1981) utilized a Rayleigh condensation model based almost entirely on geochemical parameters. Thomas' data strongly suggests the presence of several higher level core-type reservoir anomalies within the steam field. Many anomalies probably have top-bounded closure, being asymetrically similar to a dome and/or plunging anticlinal form. While the D'Amore and Truesdell model is an excellent geochemical critique, it uses superficial geologic thought. The author strongly disagrees with the ideas of dissolution of a detrital and hydrothermal quartz-rich reservoir rock (perhaps a bit of dissolution in the condensation zone) and movement of steam and/or condensate through subhorizontal lateral fractures networks (Thomas, 1981). Figure 3 depicts a conception of reservoir (cell) anomalies according to MCR's data and other privileged data.

Rayleigh plume models may not necessarily be realistic or accurate in modeling a steam/gas drive reservoir. If the idea of a basal boiling brine is dismissed, the steam reservoir(s) may be no more than an essentially isobaric/isothermal saturated steam convection cell overlain by a condensation zone formed by the contact of very hot steam with a cooler cap rock. The accumulated condensate probably flows outward somewhat to form huge saturated bodies on the outmost flanks of the reservoir. This may account for the dirtier steam chemistry found in outer flank wells, due to the increased size and increased non-condensable gas volume of the condensation zone. As the hydrostatic head of the condensation zone becomes greater than the reservoir pressure, a small amount of condensate may dribble down into reservoir fractures and become vaporized, that is in an unexploited system. Water entries encountered by Aminoil (Frye 1976) while laterally drilling may emanate from large condensate bodies on the outermost flanks of a particular anomaly.

Whereas flank wells possess lower deliverabilities are wetter, and probably penetrate a larger condensation zone, potential liquid reserves for those wells may be higher with decline rates possibly being less severe.

The areas that crest the various field anomalies are known (public and privileged data) to harbor well deliverabilities in the 300,000+ Lbs/Hr class from very shallow wells (4,000 - 5,000 feet) with production coming beneath a thin lithocap from say 2 or 3 very large steam entries. Such wells decline in flowrate at much faster rates than do outer flank wells. It is proposed that these cores are huge tectonic breccia chimneys and that the Geysers reservoir(s) is basically a huge steam and condensate filled tectonic breccia(s) superimposed upon (mimicing) and now overlapping a huge ancestral hydrothermal breccia(s). The field anomaly cores may have been the highly altered or mineralized cores of a former liquid "mushroom" plume such as presently exists at Wairakei. These cores can fracture to more prolific degrees because of either locally enhanced tectonics (minimum principal stress) and/or a greater reduction in tensile strength due to enhanced mineralization. The core of the Squaw Creek anomaly is probably such an area with very high productivity, while MCR's leases represent the middle portions of the flank. In comparison, data from Shell Oil Co. (Cochran, 1979) and public drilling records strongly infers that Shell's leases occupy the core and steep flanks of such a field anomaly.

The Geysers field is probably composed of numerous reservoirs (cells) that are separated by relatively impermeable rock. There may be some minor cross flow between individual cells. Pressure mapping and tracer tests can identify such trends. MCR will initially consider the Francisco Lease area to be part of the Squaw Creek (Unit 17 and/or 11) cell(s) until pressure monitoring indicates otherwise.

How deep does the reservoir fracture system penetrate? With no significant evidence of a bottom, it can be confidently assumed that the reservoir will cease at some depth(s) determined by a localized dramatic change in the physical nature (tensile strength) of the rocks or a reduction in extensional tectonics (minimum principle stress). Encountering a contact metamorphic zone and/or felsic intrusive basement at depth may indicate a lithologic change substantial enough to no longer allow propogation of permeable fractures.

GENERAL GEYSERS FIELD TECTONICS

McLaughlin (1981, Figures 7 and 8) demonstrates the probable results of extentional forces in the Geysers Field area agreeing well with the shear strain ellipsoid of Crowell and Ramirez (1979) and the

visible lineaments and topographic drainage throughout the field. Accordingly so, drilling programs should be designed with tectonics in mind.

The idea of sub-horizontal partings existing in the steam reservoir(s) (McLaughlin, 1981, Figure 8) may only apply to the very shallow tops of anomalies such as the Big Geysers anomaly where verticle lithostatic pressures are low. However, the contributory effects in deeper reservoirs (below 2000 - 3000 feet) is probably nil. As the tight top of the main graywacke is penetrated, permeability in the reservoir section quickly opens up, the only conclusion to be offered is that fractures pinch in going upward into the lithocap as is suggested by McLaughlin (1981, Figure 11). Primary horizontal extension in the form of large fractures and tectonic caverns are certain while secondary permeability in the form of hairline fractures is less certain but must exist. The secondary permeability may develop along synthetic and antithetic shear planes. Block faulting seen in cross section (Thomas, 1981), occurring along the strikes of recent shear planes, may also indicate enhanced secondary permeability pathlines. Gulati et al. (1978) suggest through tritium injection surveys, that injected fluids disperse radially in a Geysers reservoir from an injection point. This phenomena implied that there is lateral permeability along more than one pathline. Varying quantitative recovery values imply that permeabilities and pathline lengths/attitudes vary in different directions. Semprini and Kruger (1980) present evidence that suggests physical processes (structured features) control radon tracer flow through a Geysers Field reservoir. Geologically speaking, the Geysers reservoir(s) must therefore not be homogeneously fractured.

Several earlier ideas by various authors concerning permeability pathlines within the steam reservoir(s) are most likely obsolete. The idea of reservoir fracture permeability pathlines following old imbricate/subduction related thrust faults is poorly conceived. These faults are of mesozoic and tertiary age and are undoubtedly gouge gangue-sealed by former (tertiary and quaternary) mineralization, judging by what is seen in graywacke core rocks that have been altered by former events of hydrothermal metamorphism. Speculations of dipping soft, unfractured graywacke layers (slabs) sandwiched in between alternating hard fractured layers are also unsound. Quaternary age shear and extensional tectonics that vertically penetrate all graywacke grades should be thought of as the prominent factor in reservoir formation. Drilling experiences show that steam entries can occur in all three graywacke grades of former regional metamorphism.

DRILLING METHODOLOGY

What are the real benefits of directional drilling in the Geysers field? Most wells are probably drilled directionally for two reasons, one to minimize well pad locations in rought terrain and the other to penetrate more fracture systems through lateral penetration.

MCR's approach is to drill across inferred primary extensional permeability trends (verticle fractures) utilizing deep lateral penetration. Whereas near-verticle extensional fractures should form perpendicular to the extensional component (minimum principle stress), drilling should be oriented parallel to that stress. Drilling wells to the northwest or southeast has been highly successful with the northwest direction preferred because deviation control is much better. Drilling elsewhere usually results in very poor wells. Drilling should never proceed vertically, with the steam field offering good examples of deep verticle wells completed dry, and then turned into prolific producers when they were plugged back and sidetracked laterally.

Some may argue that wells can be fanned out in any direction, becoming adequate producers, thus contradicting the approach suggested here. This may be factual in rare isolated areas where tectonics forces deviate from the normal or in the core areas of the field's anomalies where fracturing is more pervasive and permeable. However, the extensional component philosophy is still considered to be the most appropriate within the steam field.

When is the time to set production casing and proceed to air drill into the reservoir? First, the top of the main graywacke must be identified. Then, evidence of the condensation zone along with drilling mud temperatures and bottoms up mud temperatures must be utilized in deciding where to set production casing. The use of elaborate temperature logging is not actually required.

CONCLUDING REMARKS

Aside from MCR's current area of interest two other wells (Figure 1) were drilled in other parts of the Geysers area. Both wells were subsequently plugged and abandoned and the leases released after varying and interesting results. Newfield 1-33 was drilled from the eastern side of the Collayomi Fault Zone, through the fault and massive ophiolite, then into reservoir rocks consisting of a silicified melange type. This well penetrated to 8985 feet and produced about 30,000 Lbs/Hr of steam, thus revealing that some vestige of the steam reservoir exists all the way over to the

fault zone. Tellyer 1-24 was drilled to 12,194 feet in deep massive graywackes and encountered numerous water, steam, and gas entries but was unable to sustain any degree of production.

Condensed steam will be reinjected at rates up to 750 gallons per minute through one well placed deep into the reservoir. Depletion wells will be drilled from existing pads as steam declines warrant. Approximately 1,100,000 Lbs/Hr of steam will be initially available to the powerplant in order to combat initial declines.

ACKNOWLEDGEMENT

The views and conclusions expressed in this article are those of the author and may not necessarily be those those of MCR Geothermal Corporation, its affiliated companies, or partners.

REFERENCES

Capuano, L.E., 1979, How Geysers steam wells are drilled and equipped: World Oil, February 1, 1979, P.69-72

Cochran, L.E., 1979, Formation evaluation in the geothermal environment, the Geysers Steam Field, California: Society of Petroleum Engineers, SPE 8452, 12 pp.

Crowell, J.C. and Ramirez, V.R., 1979, Late Cenezoic faults in southeastern California: in Tectonics of the Juncture between the San Andreas Fault System and the Salton Trough, Southestern California - A Guidebook; University of California-Santa Barbara Department of Geological Sciences, P.27 -39

D'Amore, F. and Truesdell, A.H., 1979, Models for steam chemistry at Larderello and the Geysers: Proceedings of Fifth Geothermal Reservoir Engineering Workshop, Stanford University, Stanford, California, P.283-297

Elder, J., 1981, Geothermal Systems, Academic Press, San Francisco, 508 pp.

Ellis, A.J. and Mahon, W.A. J., 1977, Chemistry and Geothermal Systems, Academic Press, New York, 392 pp.

Frye, G.A., 1976, Investigation of a fluid boundary: Summaries of Second Workshop Geothermal Reservoir Engineering, Stanford Univeristy, Stanford, California, P.30-33

Grindley, G.W., and Browne, P.R.L., 1975, Structural and hydrological factors controlling the permeabilities of some hot-water geothermal fields: Second United Nations Symposium on the Development and Use of Geothermal Resources, San Francisco, California, vol. 1, P.377-386

Gulati, M.S., Lipman, S.C., and Strobel, C.J., 1978, Tritium Tracer survey at the Geysers: Geothermal Resources Council Transactions, vol. 2, P.237-239

Henley, R.W., 1973, Some fluid dynamics and ore genesis: Institution of Mining and Metalurgy, February, 1973, P.B1-B7

Hsieh, C.H., and Ramey, H.J., 1983, Vapor-pressure lowering in Geothermal systems: Society of Petroleum Engineers Journal, February, 1983, P.157-167

Kennedy, G., 1974, Geothermal fields and self-sealing cap rock: in Proceedings - The Utilization of Volcano Engergy, Hilo, Hawaii (1974), P.299-306

Lambert, S.J., 1976, Stable Isotope Studies of Some Active Hydrothermal Systems: Ph.D Thesis, California Institute of Technology, (1976), 362pp

Lipman, S.C., Strobel, C.J., and Gulati, M.S., 1977, Reservoir performance of the Geysers Field: in Larderello Workshop on Geothermal Resource Assessment (1977), Larderello, Italy, 13pp, 9 figs.

Lockner, P.A., Summers, R., Moore, D., and Byerlee, J.D., 1982, Laboratory measurements of reservoir rock from the Geysers Geothermal Field, California: International Journal Rock Mechanics, Mineral Science, and Geomechanics, vol. 19, P.65-80

McLaughlin, R.J., 1981, Tectonic setting of pre-Tertiary rocks in its relation to geothermal resources in the Geysers-Clear Lake area; in Research in the Geysers-Clear Lake Geothermal Area, Northern California: United States Geological Survey Professional Paper 1141, P.3-24

Norton, D. and Knapp, R., 1977, Transport phenomena in hydrothermal systems: the nature of porosity: American Journal of Science, vol. 277, P.913-936

Pruess, K. and Narasimhan, T.N., 1981, On Fluid Reserves and the Production of Superheated Steam From Fractured, Vapor-Dominated Geothermal Reservoirs: Lawrence Berkeley Laboratory, LBL-12921, 35pp

Pruess, K. and Truesdell, A.H., 1980, A numerical simulation of the natural evolution of vapor dominated hydrothermal systems: in Proceedings of Sixth Workshop Geothermal Reservoir Engineers, Stanford University, Stanford, California, P.194-203

Ramey, H.J., 1968, A reservoir engineering study of the Geysers Geothermal Field: Submitted as Evidence, Reich and Reich, Petitioners vs Commissioner of Internal

Revenue, 1969 Tax Court of the United States, 52, T.C. #74, 1970

Ramey, H.J., and Gringarten, A.C., 1975, Effect of high-volume vertical fractures on geothermal steam well behavior: in Second United Nations Symposium on the Development and Use of Geothermal Resources, San Francisco, California, vol. 3, P.1759-1762

Semprini, L. and Kuger, P., 1980, Radon Transect Analysis in Geothermal Reservoirs: Society of Petroleum Engineers, SPE 8890, 8pp

Sternfeld, J.N., 1981, The Hydrothermal Petrology and Stable Isotope Geochemistry of Two Wells in the Geysers Geothermal Field, Sonoma County, California: M.S. Thesis, University of California, Riverside, UCR/16PP-81/7, 202pp

Thomas, R.P., 1981, Subsurface Geology: in Reservoir Assessment of the Geysers Geothermal Field, California Division of Oil and Gas, TR27, P9-20

Truesdell, A.H. and White, D.E., 1973, Production of Superheated steam from vapor dominated geothermal reservoirs: Geothermics, vol. 2, #3-4, P.154-175

Weres, O., Tsao, K., and Wood, B., 1977, Resource, Technology, and Environment at the Geysers: Lawrence Berkeley Laboratory, LBL-5231, P.IV1-57

White, D.E., Muffler, L.J.P., Truesdell, A.H., 1971, Vapor-dominated hydrothermal systems compared with hot-water systems: Economic Geology, vol. 66, P.75-97

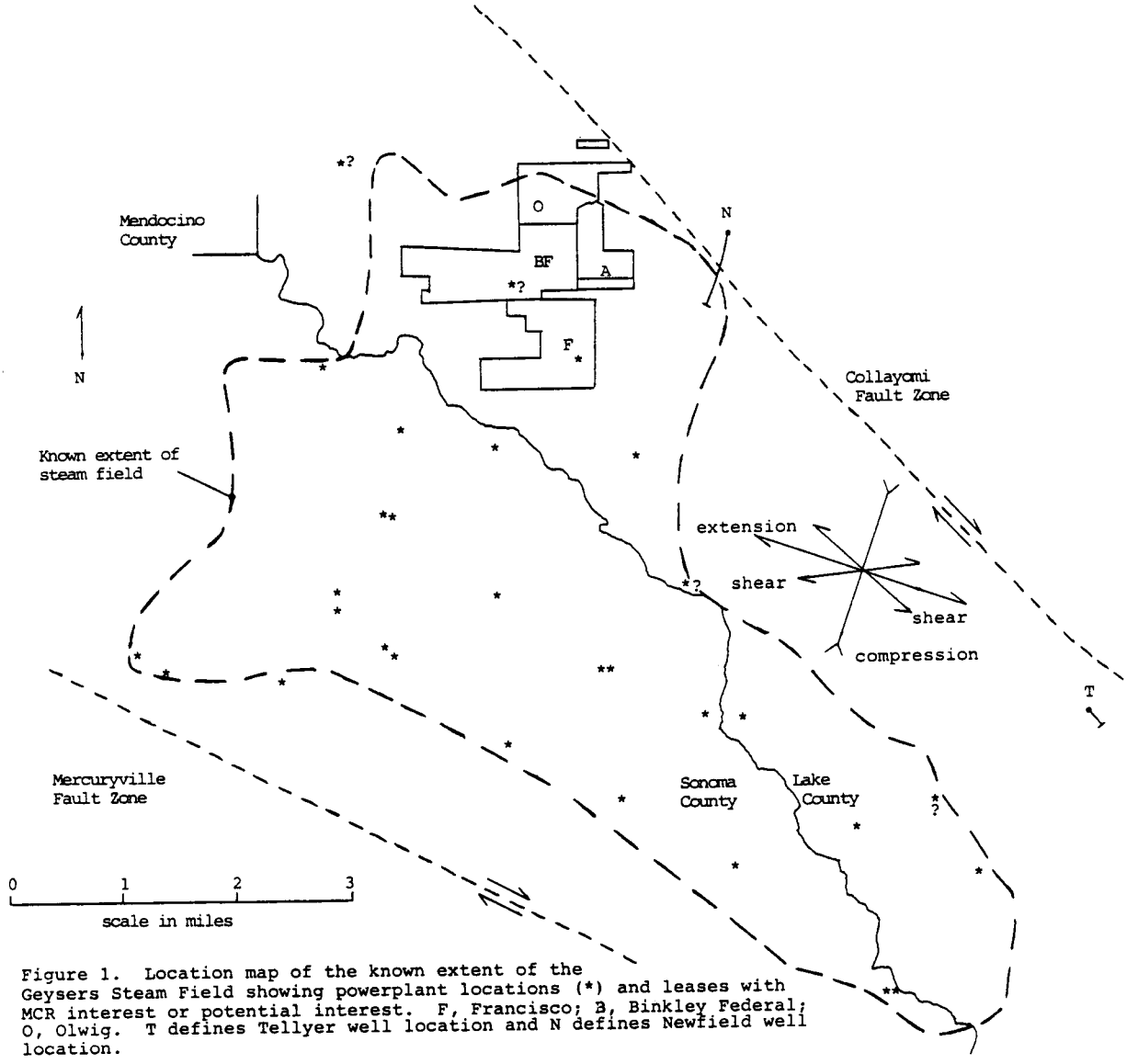


Figure 1. Location map of the known extent of the Geysers Steam Field showing powerplant locations (*) and leases with MCR interest or potential interest. F, Francisco; B, Binkley Federal; O, Olwig. T defines Tellyer well location and N defines Newfield well location.

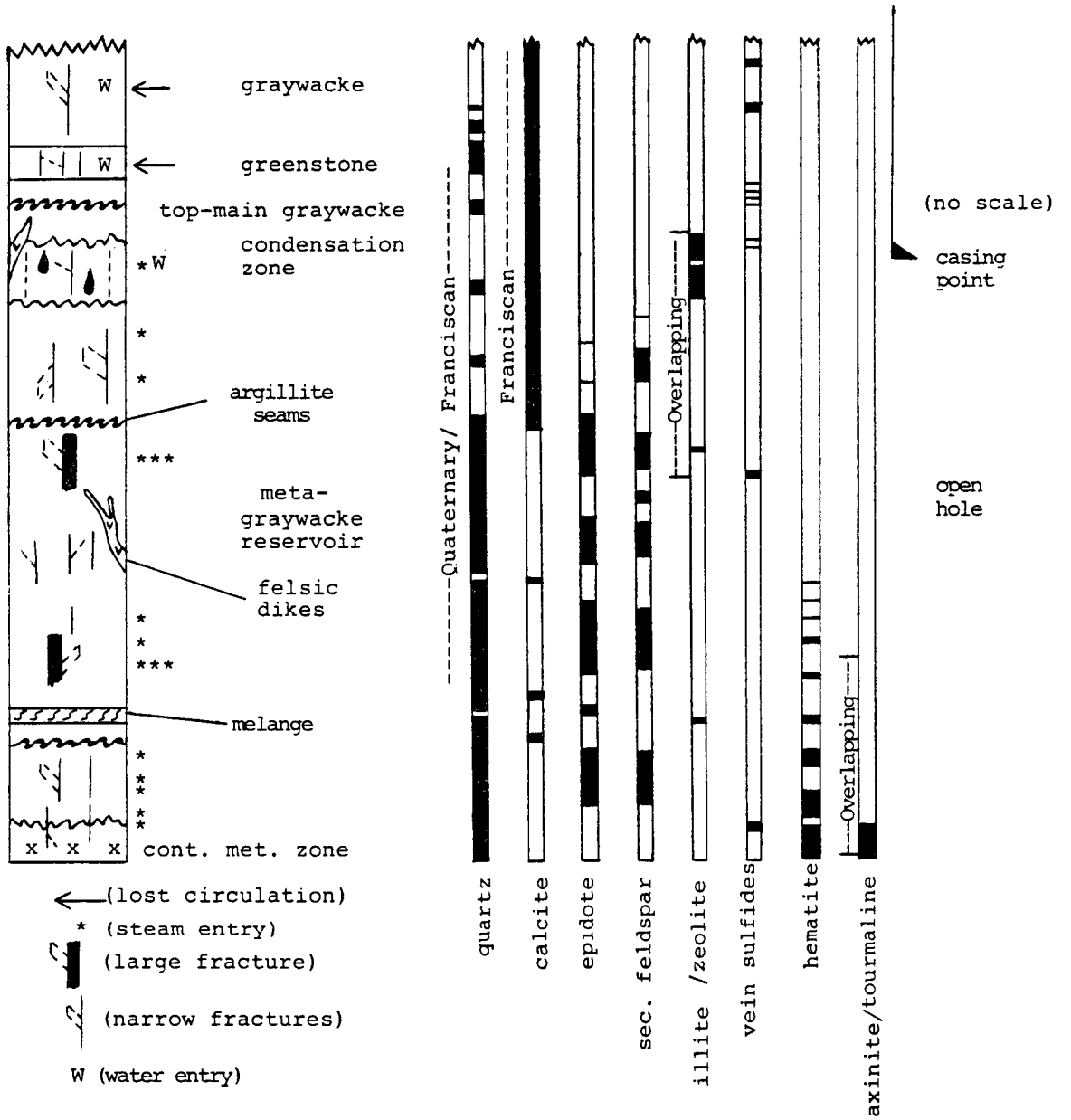


Figure 2. Generalized lithologic section and mineralogical zoning of a typical Francisco lease well, showing permeable traits.

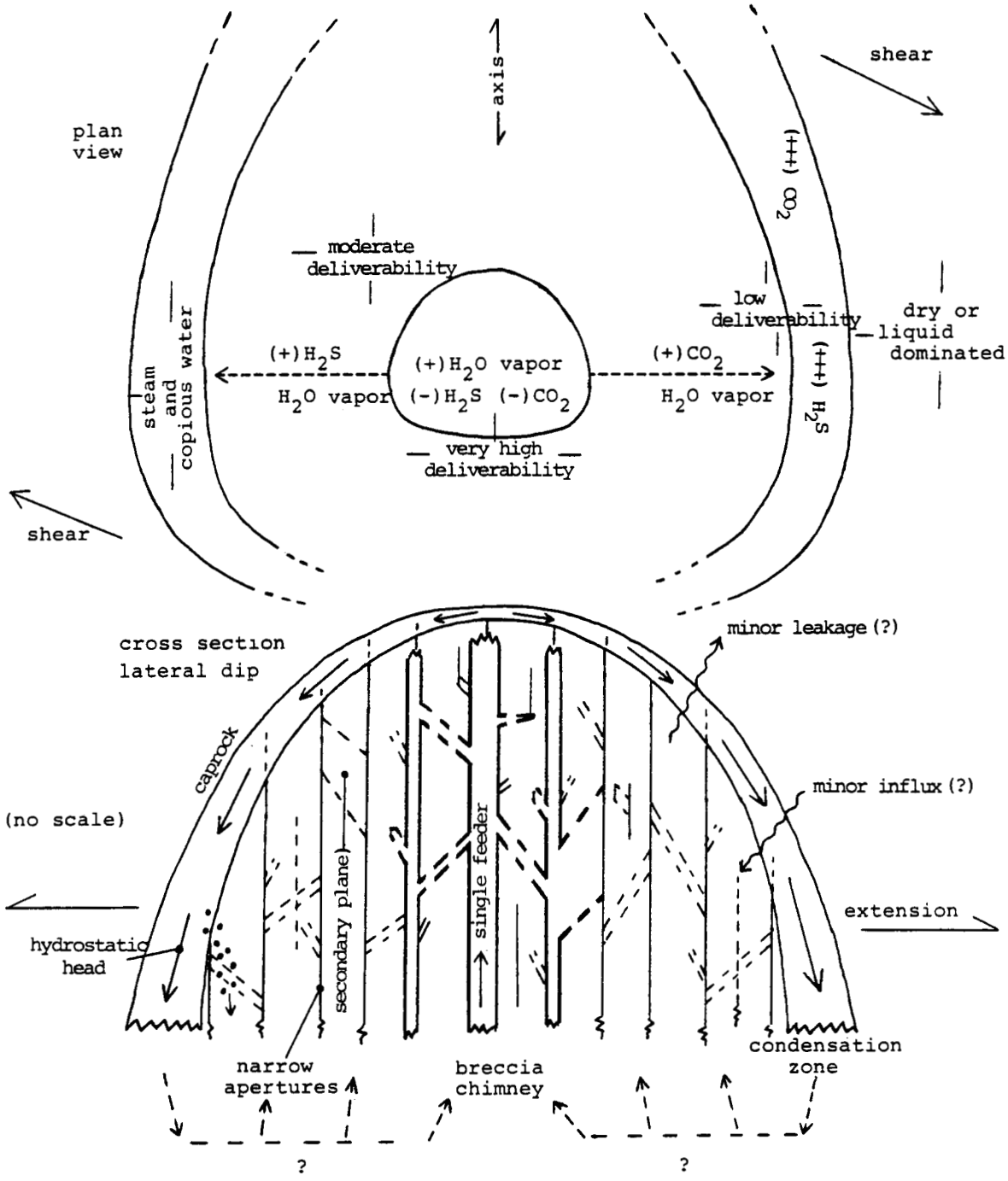


Figure 3. Illustration defining a conceptual view across the lateral dip of Geysers reservoir(s). A huge breccia chimney is developed in the core with variances in steam (probably condensate also) chemistry throughout the system. The presence of a basal boiling brine is questionable. Changes in permeability may relate to differing structural stresses/strains across any field anomaly. This is two-dimensional. As the fringe of the cell is approached, the effects of a massive condensation zone and the eventual end of the reservoir are shown.

Proceedings Ninth Workshop Geothermal Reservoir Engineering
Stanford University, Stanford, California, December 1983
SGP-TR-74

GEOLOGIC MODEL OF THE BACA GEOTHERMAL RESERVOIR, VALLES CALDERA, NEW MEXICO

Dennis L. Nielson and Jeffrey B. Hulen

Earth Science Laboratory, University of Utah Research Institute
420 Chipeta Way, Suite 120
Salt Lake City, UT 84108

ABSTRACT

Logging of drill cuttings from Union Oil Company's Baca geothermal project has resulted in a detailed geologic picture of the Baca geothermal reservoir. The reservoir is located in a complex geologic environment with both fracture and stratigraphic permeability, which have been modified (largely reduced) by hydrothermal alteration. The geothermal system is principally hosted by ash-flow tuffs and volcaniclastic rocks associated with the development of the Valles and Toledo calderas and preceding explosive rhyolitic eruptions. The cooling history of these rocks has produced non-welded tuffs, with considerable intergranular permeability and extensive hydrothermal alteration, through densely welded ash-flow tuffs with little intrinsic permeability. Lithologic units beneath the ash-flow tuff sequence are commonly altered and metamorphosed but contain few hot-water entries, although some, such as the Madera Limestone, are regional groundwater aquifers outside the caldera.

Previous workers have reported that the Baca field has a permeability-thickness product of about 6,000 md-ft, which is low compared with other producing geothermal areas. A model for the development of the Redondo Creek resurgent dome, within which the Baca field is located, explains these low permeabilities by emphasizing the nature of strain and resulting fracture permeability in the host lithologies. The model also helps emphasize the importance of inherited structures in the formation of the dome and suggests that these faults may be the principal conduits for geothermal fluids from depth in the system. Another implication of modeling dome development is that the magmatic heat source for the geothermal system lies beneath present drilling depths.

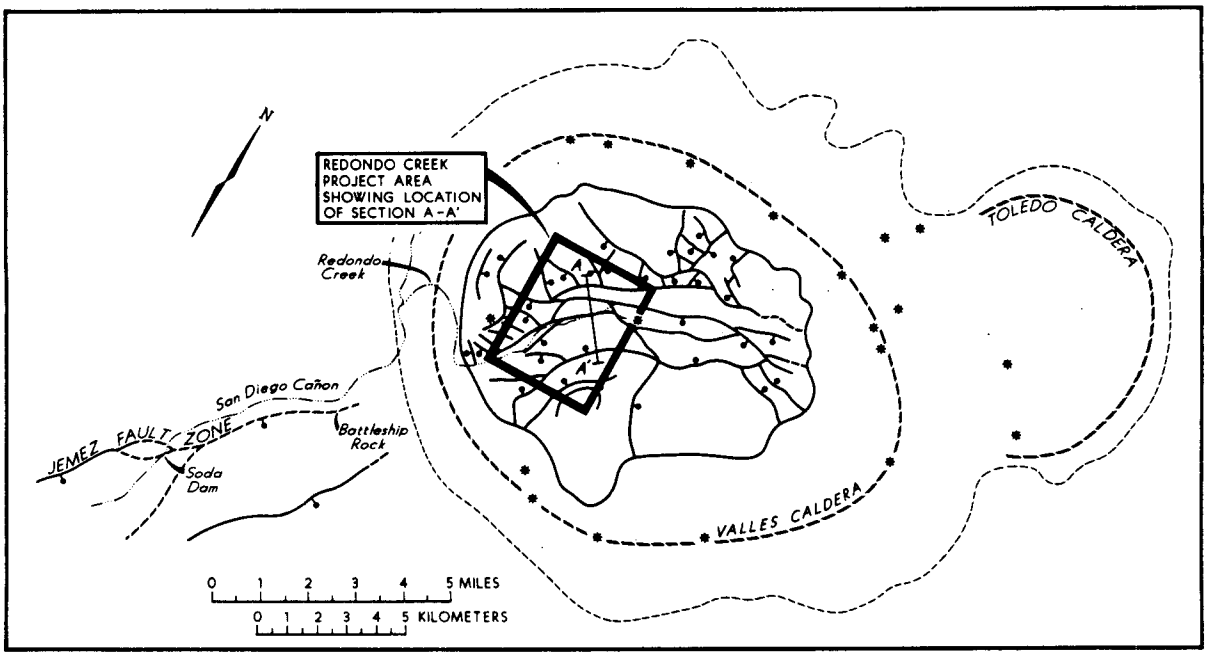


Figure 1. Index map showing location of the Valles-Toledo caldera complex.

The stratigraphic and structural hydrothermal fluid paths at Baca can be characterized as follows: 1) those sealed by alteration, 2) those which do not produce fluids but do accept fluids, and 3) those which produce geothermal fluids.

INTRODUCTION

The caldera environment represents a complex interaction of volcanic, structural, and often, hydrothermal processes. As a result calderas are often targets for geothermal exploration and development. From the standpoint of the reservoir engineer, such geothermal systems would be hosted by rocks that display a complex interplay of stratigraphic permeability, structural permeability (both faults, fractures and joints), and changing permeability which results from the process of hydrothermal alteration and new fracture generation. The purpose of this paper is to present a geologic model of the Baca geothermal reservoir which is situated within a small portion of the Valles caldera in New Mexico (Fig. 1.). The geologic history of the Valles caldera is presented in Smith and Bailey (1968). The data we present is largely based on our studies of subsurface samples from Union Oil Company's Baca project area. Additional results of our work have been published previously (Hulen and Nielson, 1982, 1983; Nielson and Hulen, in press).

STRATIGRAPHY

The Precambrian to Quaternary stratigraphic sequence penetrated by deep Union wells in the Redondo Creek area of the Valles caldera has been characterized in the reports cited immediately above and to which the reader is guided for more detailed description of individual lithologies. This paper will restrict discussion of these rocks mostly to features related to structural or stratigraphic permeability.

The Baca geothermal reservoir is hosted principally by a sequence of Pleistocene felsic ash-flow tuffs and associated volcaniclastic sediments locally exceeding 1800 m in thickness within the Valles caldera. The two members of the Bandelier Tuff, the Otowi and overlying Tshirege, form the middle portion of this sequence (Fig. 2). The Tshirege is overlain by the "Upper Tuffs" (Nielson and Hulen, in press), dominantly non-welded to poorly welded felsic ash-flow tuffs; the Otowi rests unconformably on complexly interstratified, variably welded felsic ash-flow tuffs and sediments of limited local extent grouped by Nielson and Hulen (in press) as the "Lower Tuffs".

Permeability (and former permeability) in the felsic tuff sequence at Redondo Creek is both structural and stratigraphic. Stratigraphic permeability is controlled by thin, intra-tuff sandstones, discrete, non-welded tuff horizons and perhaps air-fall pumice beds (Hulen and Nielson, 1982). Structural permeability is developed along high-angle normal faults disrupting the felsic tuff sequence as well as underlying units. We believe these faults to be the principal paths along which thermal fluids ascend. Once within the felsic tuff sequence, however, the fluids appear to be diverted in part into intra-tuff stratigraphic aquifers (Fig. 2), creating an intricate circulation system requiring much more caution in targeting from the surface than a fault-controlled system alone.

The Otowi and Tshirege Members of the Bandelier Tuff (Fig. 2), initially deposited as thick, hot (600-700°C) ash flows, have undergone profound compaction, welding, devitrification (a process by which silica minerals and feldspar nucleate from the glass initially present) and widespread granophyric crystallization. As a result, both members, generally exceeding 300 m in thickness in the Redondo Creek wells, are typically dense and impermable except where faulted or fractured or where they include thin permeable strata. The Otowi and Tshirege, in fact, may serve as local caprocks above geothermal fluids circulating in the Lower Tuffs and underlying rocks.

Several productive thermal fluid entries have been encountered in the Paliza Canyon Formation, a sequence of Pliocene intermediate-composition flows, tuffs, subvolcanic intrusives (?) and volaniclastic rocks beneath the "Lower Tuffs". The Paliza Canyon has not been sufficiently investigated to state with certainty that the entries are stratigraphically or structurally controlled. Furthermore, one of the most productive Paliza Canyon entries occurs at the bottom of well B-24, where the nature of permeability control cannot be ascertained.

Stratigraphic geothermal targets in sub-Paliza Canyon rocks included friable arkose of the Tertiary Santa Fe Sandstone/Abiquiu Tuff (Fig. 2), red-bed arkose of the Permian Abo Formation, solution voids/karstic terrain in limestone of the Pennsylvanian Madera Formation and gruss developed on deep Precambrian granitic rocks. No thermal fluid entries were penetrated beneath the Paliza Canyon Formation. Lost-circulation zones, however, were very common (Molloy and Laughlin, 1982). This implies locally adequate permeability in these rocks, but either no connection with major thermal fluid conduits or perhaps pervasive underpressuring of the reservoir at depth.

STRUCTURE

Nielson and Hulen (in press) have modeled the development of the Redondo dome following the philosophy developed by Johnson (1970) for the emplacement of the Henry Mountains

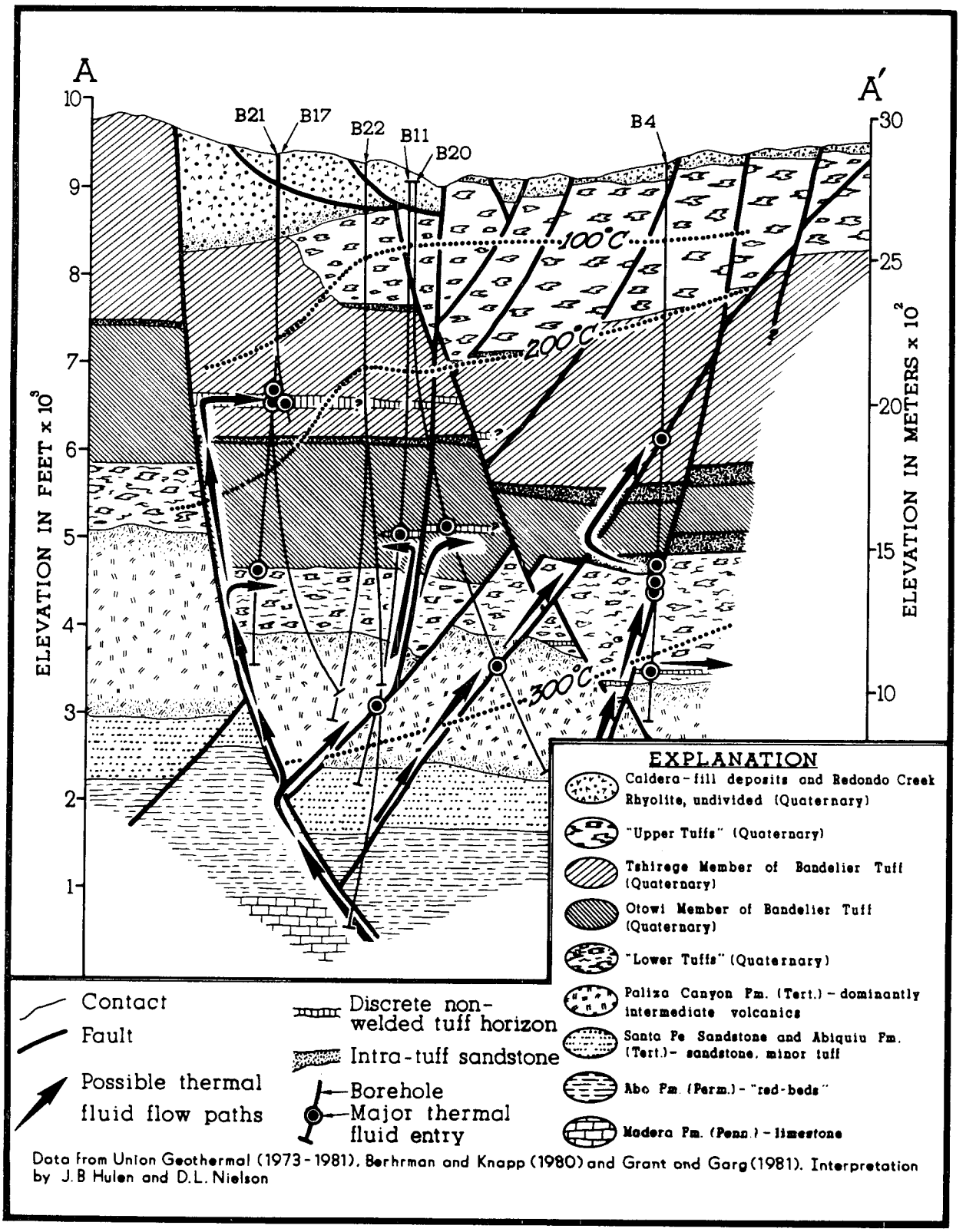


Figure 2. Geologic cross-section through the Redondo Creek project area, showing possible thermal fluid migration channels.

laccolith in Utah. We did not intend to model rigorously the formation of the Redondo Dome, but rather to use theoretical concepts of dome formation to help explain the permeabilities found in the Baca project area.

Most workers agree that resurgent domes are formed after caldera collapse by upward pressure of still molten magma. This upward pressure results in the formation of a structural dome, generally in the center of the caldera. As a result of the doming process, the affected strata are subjected to differential stresses. In the upper portions of the dome, the rocks are under tension. This results in the development of faulting along the crest of the dome that forms most of the fracturing that is often identified as an apical graben of the dome. Approximately half way down through the dome, a surface called the neutral plane separates the upper tensional environment from a lower region characterized by compression. In contrast to the normal faults above the neutral plane, the region below the neutral plane will be characterized by the development of conjugate shears.

On the basis of consideration of the dome development process, Nielson and Hulen (in press) concluded that the idealized model of dome development was modified by the reactivation of older structures associated with the Jemez fault (Fig. 1). These structures were steep, throughgoing fault zones prior to the formation of the Redondo dome, and they have continued to maintain that character during and after the formation of the dome. These faults may extend to depths where they intersect crystallized magma which is the cause of the structural doming. It is our opinion that these reactivated faults are the principal conduits of upwelling hydrothermal fluids, and that successful wells in the field intersect these fractures, or fractures or stratigraphic horizons which communicate with these principal fluid conduits.

In conjunction with injection studies at Baca, Riney and Garg (1982) have commented on the ability of some permeable zones to serve as fluid producers while other zones in the same well serve as fluid acceptors. It is clearly possible that the zones which serve as fluid acceptors were fractures formed solely as a result of dome formation while those that act as fluid producers are part of, or connect with, the reactivated structures which we feel are transporting the geothermal fluids from depth.

The conceptualization of the stress fields and related faulting and fracturing is also important in the planning and implementation of stimulation experiments. The fracturing of the region around the well bore will not necessarily result in sustained increased production unless that artificial fracturing is able to intersect the principal fracture zones which carry the geothermal fluids. In addition, in the stress field above the neutral plane, it is probable that stimulation will open fractures which are associated with extension along the top of the domed structure rather than the reactivated structures which we feel may be the more important geothermal conduits.

One conclusion from our structural work at the Baca project area has been that resurgent domes are inherently impermeable due to their mode of structural development. Observations of other resurgent dome features tend to support this conclusion. In most hydrothermally active caldera systems (such as Yellowstone), hot spring and fumarolic activity are spatially associated with the margins of resurgent domes, where these dome structures are thought to intersect the ring fracture system of the caldera. Very little hot spring or fumarolic activity is present on the dome itself. This conclusion seems also to be borne out in older calderas which have been dissected by erosion, such as the Creede caldera. In these instances, hydrothermal mineralization is marginal to the resurgent dome or even outside the caldera structure.

Another interesting result is that the structural model can be used to predict the depth to the magma body which produced the resurgent doming (Johnson, 1970). If the Redondo dome is approximated by a circular feature with a diameter of 10,900 m, the depth to the top of the intrusive is approximately 4,700 m. The deepest hole in the field is Baca-12 which is 3,242 m deep and bottoms in Precambrian granite. Neither Baca-12 nor any of the other holes in the field intersect significant amounts of intrusive rock which can be related to the resurgent doming process.

HYDROTHERMAL ALTERATION AND ITS INFLUENCE ON PERMEABILITY

Beneath a zone of high-level clay alteration, the thick felsic tuff sequence which includes the Bandelier Tuff within the project area is largely unaltered. However, restricted fracture zones, faults, and some stratigraphic horizons are pervasively altered. In particular, non-welded ash-flow tuffs and volcaniclastic sediments are commonly highly altered, indicating the passage of hydrothermal solutions. Many of these zones are not fluid producers at the present time, the most obvious reason being that the alteration has reduced permeability and choked off the hydrothermal channels. Alteration assemblages within the Bandelier tuff are dominated by illite, suggesting the fixation of potassium and the release of sodium during the alteration process.

Studies by Hulen and Nielson (1983) in the

high-level clay alteration zone in the upper portion of well Baca-20 have demonstrated the presence of smectite and allevardite-ordered illite-smectite (I/S) mixed-layer clay in the formerly permeable "Upper Tuffs". Present temperatures of about 30°C in this upper zone contrast with temperatures of formation of allevardite-ordered I/S of between 100° and 175°C. Thus, this pervasive clay-rich alteration was probably developed at an earlier stage in the evolution of the hydrothermal system, when temperatures were higher than they are at the present time. It was also the suggestion of Hulen and Nielson (1983) that this upper level alteration may be the "cap rock" postulated by Hartz (1976) and Grant and Garg (1981). It also represents a zone, which is over 300 meters thick in Baca-20, that should demonstrate relatively low electrical resistivity. This overlies the reservoir zone itself which should be of higher electrical resistivity due to the narrow production zones within largely unaltered thick sequences of Bandelier Tuff. The electrical resistivity structure has important implications for the use of resistivity methods for both resource exploration and development of the field.

Productive thermal fluid entries, both stratigraphically and structurally controlled, are invariably associated with moderate to intense hydrothermal alteration. The alteration assemblages, as yet incompletely characterized, are apparently dependent in part on host rock composition. Fluid entries in the felsic Bandelier Tuff and "Lower Tuffs", for example, are associated with the assemblage illite-calcite-pyrite with calcite subordinate. Altered rock from an unusual entry of this type at a depth of 811 m in well B-17 contains, as indicated by semi-quantitative XRD, 56% pyrite, 32% illite and 9% calcite with only a few percent (presumably) original rock-forming quartz and feldspar. A clay separate prepared from this sample contains, in addition, traces of smectite and chlorite. Entries in the intermediate-composition Paliza Canyon Formation contain abundant chlorite (and chlorite-rich mixed-layer chlorite-smectite) in addition to calcite, illite, pyrite and minor epidote, plagioclase and potassium feldspar, but some or all of these phases could predate the present geothermal system. Alteration zones mineralogically and texturally similar to those described above, but not associated with active fluid entries, are relatively common in the Baca wells. It seems very likely that these zones represent former fluid flow channels now completely sealed by alteration.

Other zones which resulted in extreme lost circulation problems during drilling operations demonstrate little or no alteration suggesting lack of communication with the hydrothermal system.

In summary, the fluid conduits at Baca can be categorized in the following manner.

1. Former fluid channels sealed by alteration. These include both stratigraphic and structurally controlled fluid entries.

2. Open conduits which do not produce geothermal fluids. Again, these are both stratigraphic and structural intervals and are characterized as lost circulation zones. These constitute the stratigraphic and structural intervals which do not communicate with the reactivated fault zones which are thought to be the principal fluid conduits in the system.

3. Geothermal production zones. All commercial production zones apparently are structurally controlled while subcommercial zones are controlled by both structures and stratigraphic intervals.

Fluid entries have been documented only within the Bandelier Tuff and Paliza Canyon Formations, although this may be a function of drilling depths within the system.

ACKNOWLEDGEMENTS

This work was funded by the U.S. Department of Energy under contract number DE-AC07-80ID12079. The lithologic samples studied were provided through the courtesy of Union Geothermal Division of the Union Oil Company of California. Samples for XRD were prepared and run by Frank Bakke and Louise McPherson. Illustrations were drawn by Pat Daubner. The manuscript was organized and typed by Joan Pingree.

REFERENCES

Behrman, P. G., and Knapp, R. B. (1980), "Structure of the Redondo Creek area, Baca project, New Mexico--implications concerning the nature of permeability and production and recommendations for future drilling", Union Oil Co. Internal Rept., Univ. of Utah Research Inst., Earth Sci. Lab., Open-File Rept. NM/Baca/101.

Grant, M. A., and Garg, S. K. (1981), "Baca geothermal demonstration project--interpretation of downhole data from the Baca geothermal field: Systems, science and software", Topical Rept. No. DOE/ET/27163-12.

Hartz, J. D. (1976), "Geothermal reservoir evaluation of the Redondo Creek area, Sandoval County, New Mexico", Union Oil Co., Geoth. Div., Internal Rept.

Hulen, J. B., and Nielson, D. L. (1982), "Stratigraphic permeability in the Baca geothermal system, Redondo Creek area, Valles Caldera, New Mexico", Geothermal Resources Council Transactions, v. 6, p. 27-30.

Hulen, J. B., and Nielson, D. L. (1983), "Stratigraphy of the Bandelier tuff and characterization of high-level clay alteration in borehole B-20, Redondo Creek area, Valles Caldera, New Mexico", Geothermal Resources Council Transactions, v. 7, p. 163-168.

Johnson, A. M. (1970), "Physical processes in geology", San Francisco, Freeman, Cooper and Co., 577 p.

Molloy, M. W., and Laughlin, A. W. (1982), "Drilling problems (in the Redondo Creek project area)", in Goldstein, N. E., Holman, W. R., and Molloy, M. W., eds., Final report of the Department of Energy reservoir definition review team for the Baca Geothermal Demonstration Project, Lawrence Berkeley Laboratory Rept. LBL-14132, p. 22-25.

Nielson, D. L., and Hulen, J. B. (in press), "Internal geology and evolution of the Redondo Dome, Valles Caldera, New Mexico", Journal of Geophysical Research.

Riney, T. D. and Garg, S. K. (1982), "Evaluation of injection test data from a Baca well", Eighth Workshop on Geothermal Reservoir Engineering, Stanford University.

Smith, R. L., and Bailey, R. A. (1968), "Resurgent cauldrons", in Coats, R.R., Hay, R. L., and Anderson, C. A. (eds)., Studies in Volcanology, Geological Society of America Memoir 116 , p. 613-662.

Union Oil Company of California, Union Geothermal Division (1970-1981), ""Mud" logs (generalized lithology, drilling rate and temperature) for wells Baca 4-6 and 9-24".

Proceedings Ninth Workshop Geothermal Reservoir Engineering
Stanford University, Stanford, California, December 1983
SGP-TR-74

DESERT PEAK: A GEOTHERMAL FIELD IN CHURCHILL COUNTY, NEVADA

K. P. Goyal, W. R. Benoit, J. P. Maas, and J. R. Rosser

Phillips Petroleum Company
655 East 4500 South
Salt Lake City, Utah 84107

ABSTRACT

The 400°F liquid dominated Desert Peak geothermal reservoir produces from fractures associated with intersecting north-northeast and east-northeast trending normal faults. Fractures occur in intrusive basement rocks, pre-Tertiary metasedimentary and metavolcanic rocks, and Tertiary volcanic rocks. Static temperature surveys from six deep wells indicate that the reservoir has both recharge and discharge in the vicinity of wells B21-1 and 86-21.

Interference data, from a 30-day flow test of 86-21 show high reservoir connectivity. The calculated transmissivity is an order of magnitude higher in a north-south direction than in an east-west direction. A reservoir thickness on the order of thousands of feet and disturbed reserves in excess of 7 billion barrels are estimated.

A conceptual model of the Desert Peak system contains meteoric water derived from the Carson and Fernley Sinks. Heated at depth, water rises up along normal faults into highly fractured rocks between the depths of 3000 and 9000 feet, forming a geothermal reservoir. The thermal water naturally rises or leaks out of the reservoir up normal faults to within a few hundred feet of the surface until it has reached hydrostatic equilibrium or is blocked by discontinuous impermeable lacustrine sedimentary rocks. In the latter case it spreads out laterally creating a huge near surface thermal anomaly.

INTRODUCTION

The Desert Peak geothermal field is located approximately 50 miles east-northeast of Reno, Nevada in northwestern Churchill County (Fig. 1). It underlies the northern part of the Hot Springs Mountains which form part of the northwestern margin of the Carson Sink. To date six deep wells and numerous shallow and intermediate depth temperature-gradient holes have been drilled at Desert Peak. Only one of these wells has not intersected the geothermal reservoir. These wells have discovered a liquid dominated reservoir with an average temperature of 400°F. The wells produce from depths between 3000 and 9000 feet. The produced fluid is a sodium chloride water with a total dissolved solids content of 6700 mg/l. The dissolved gas content is between .02 and .04% by weight. The Desert Peak geothermal field is blind in that there is very little geological evidence exposed on the surface to indicate its presence (Benoit et al., 1982). At the present time, the proposed field development by Phillips Petroleum Company calls for a 9 MW demonstration power plant to be built and operating by 1985.

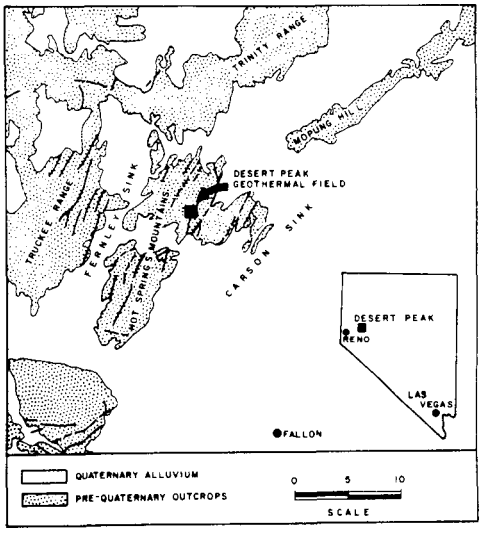


Figure 1. The Location Map.

GEOLOGY AND GEOPHYSICS

The Hot Springs Mountains are a low relief, highly fragmented horst block. In the northern half of the range, the general stratigraphy consists of intrusive rocks ranging from hornblendite to granite in composition below depths of 7000 feet. These have intruded and contact metamorphosed a Mesozoic (?) sequence of marine metasedimentary and metavolcanic rocks

which lie between depths of 3000 and 7000 feet. Argillite, quartzite and phyllite are the dominant lithologies with lesser limestone and metavolcanic rocks also being present. Tertiary volcanic rocks overlie the pre-Tertiary section. This volcanic section can be broken into a lower rhyolitic unit composed primarily of ash flow tuffs and an upper basaltic unit known as the Chloropagus Formation. The combined thickness of this volcanic unit is between 2500 and 3000 feet. Overlying these volcanic rocks is a sequence of lacustrine sedimentary rocks known as the Truckee Formation which is up to 600 feet thick in the vicinity of the wells. Lastly, Quaternary alluvium and a thin veneer of windblown sand cover most of the area in the immediate vicinity of the wells.

Structurally, the northern Hot Springs Mountains have been broken into numerous rhombohedral blocks by intersecting north-northeast and east-northeast trending normal faults. Recent mapping and drilling indicates that drape folds overlie many of these normal faults in the vicinity of the deep wells. These drape folds can be exposed where well-bedded Tertiary sedimentary rocks have been preserved above an elevation of about 4500 feet. In the immediate vicinity of the wells the sedimentary rocks are either eroded or are poorly exposed so the drape folds are much more difficult to recognize. The locations of the deep wells and the faults inferred on the basis of a drape folding interpretation are shown in Fig. 2. The locations of these faults are different than those presented earlier (Benoit et al., 1982; Hiner, 1979).

Self-potential and ground magnetic surveys have been used at Desert Peak to help in locating possible hydrothermally active buried faults. The trends of both geologically and geophysically interpreted faults, as shown in Fig. 2, are similar. The elevation contours of the 400°F temperature, also shown in this figure, depict a dome with its peak around well B21-1. This indicates that the hot liquid rises up along normal faults in the vicinity of this well. Earlier reports (Benoit et al., 1982) have demonstrated that near the surface this thermal water

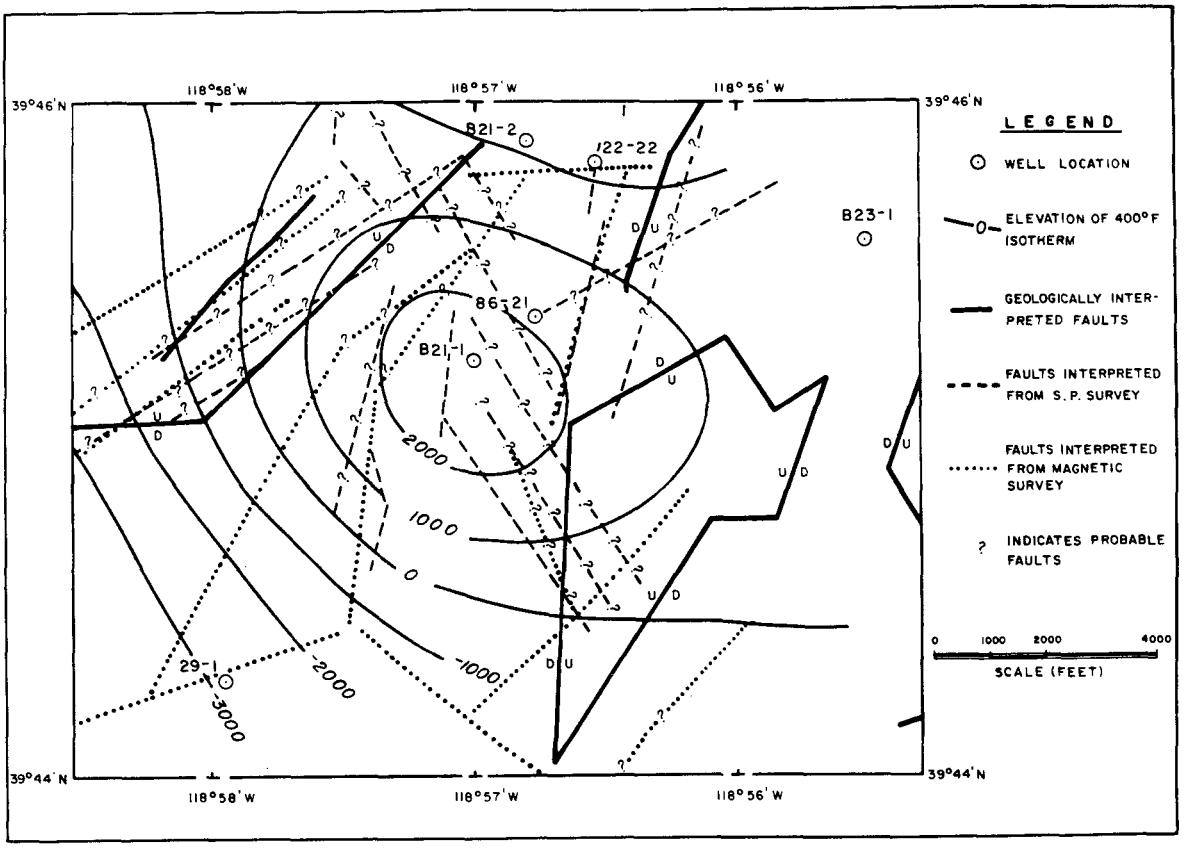


Figure 2. Inferred faults, well locations and evaluation contours of 400°F temperature in Desert Peak.

moves laterally down gradient through available permeability.

A plot of static formation temperatures versus elevation in all the Desert Peak wells is shown in Fig. 3. In a broad sense, these temperature profiles are of three types. First, wells B21-1 and 86-21 are the hottest wells at the shallowest depths with continuously decreasing temperature gradients. These wells are believed to be closer to a hot discharge zone of the system than the other wells in the field. A comparison of the deep isothermal temperatures in the wells suggests that wells B21-1 and 86-21 are also closer to the recharge source of the system than well B21-2. The isothermal temperature in B21-1 and 86-21 is 406°F compared to that of 392°F in B21-2.

The second type of profiles are those measured in wells B23-1 and 22-22.

The temperatures at shallow depths in these wells are lower than those obtained in B21-1 and 86-21, but are similar at greater depths. The profiles of the third type are the reversible temperature profiles measured in wells B21-2 and 29-1. The main difference between these two wells is that the well B21-2 intersected the geothermal reservoir while the well 29-1 is located outside the reservoir. The high temperature gradients at shallow depths in these two wells appear to have been caused by lateral flow of hot water. The reversal in 29-1 is caused by hot water originating in the vicinity of wells B21-1 and 86-21 flowing outward over colder local waters. The cause of the reversal in B21-2 needs further study.

The production zones defined from well logs and drilling reports are also shown in Fig. 3. It is believed that the well B23-1 intersects two different hot water aquifers, however only one is shown in this figure. Based on successive temperature surveys, Urban and Diment (1982) delineated a shallow aquifer between 330 and 1645 foot elevation (2950 and 4265 foot depth), as shown in Fig. 3. Well B23-1 apparently produces from below the 7000 foot depth, indicating a deeper reservoir extending below this depth. The geothermal reservoir, as presently known, in the Desert Peak area lies below an elevation of 1900 feet.

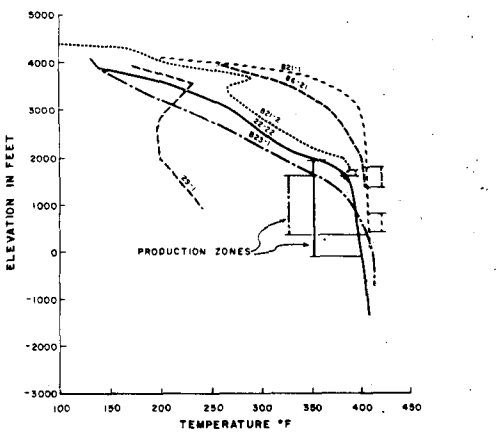


Figure 3. Static temperatures in Desert Peak Wells.

INTERFERENCE TESTING

Well 86-21 was flow tested for 30 days in the fall of 1982. It produced about 550,000 lbm/hr at an average wellhead pressure and temperature of 85 psig and 325°F respectively. A total of 1.3 million barrels of fluids was produced during this test. Wells B21-1 and B21-2, located respectively 1315 feet southwest and 3190 feet north from 86-21, were monitored for the interference data (Fig. 2).

The observation wells were equipped with downhole pressure chambers connected to high accuracy Heise gauges by capillary tubing. The monitoring system was pressurized with nitrogen to minimize response time. An hourly reading of the interference data was taken during the test. It was noticed that the wells B21-1 and B21-2 responded within 8 and 12 hours, respectively, to the flowing of 86-21. This indicates that the wells in this reservoir are well connected.

A log-log plot of drawdown versus time is shown in Fig. 4 for both wells. A maximum pressure drop of about 34 psi was noted in well B21-1 and that of about 12.5 psi in well B21-2. The line source solution match of the field data and the nondimensional coordinates of the matched point are also shown in this figure.

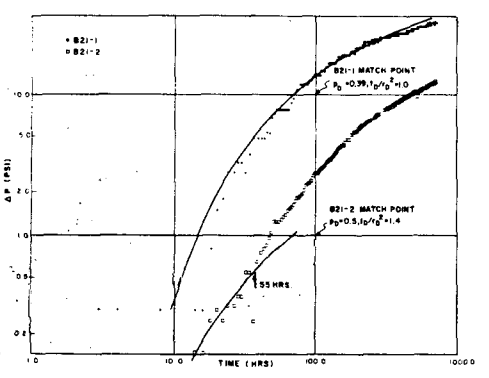


Figure 4. Drawdown-type curve match for Wells B21-1 and B21-2.

The Horner buildup plots of both wells are presented in Fig. 5. The data of the well B21-1, shown in Figs. 4 and 5, do not point toward the existence of a permeability barrier. However, the plots of the well B21-2 do display the existence of a discontinuity after 55 hours during drawdown and 142 hours during buildup.

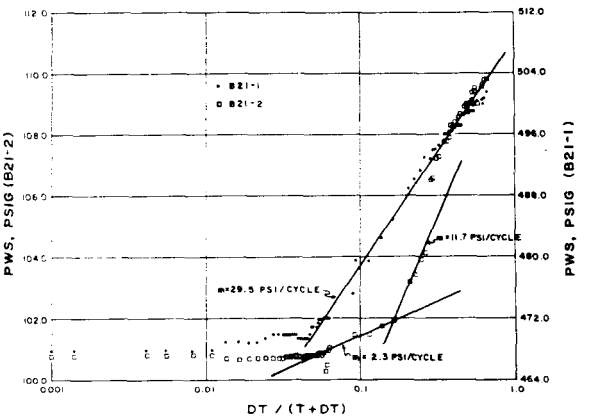


Figure 5. Horner buildup plots for wells B21-1 and B21-2.

For an average production rate of 550,000 lbm/hr and a reservoir temperature of 405°F, the following reservoir parameters may be obtained from Figs. 4 and 5 (Earlougher, 1977).

Observation Well B21-1

Drawdown: $kh = 33{,}000$ md-ft
$\phi C_t h = 37 \times 10^{-4}$ ft/psi

Buildup: $kh = 33{,}000$ md-ft
$\phi C_t h = 27 \times 10^{-4}$ ft/psi

Observation Well B21-2

Drawdown: $kh = 423{,}200$ md-ft
$\phi C_t h = 57 \times 10^{-4}$ ft/psi
distance to the discontinuity 5600 feet

Buildup: $kh = 423{,}800$ md-ft
$\phi C_t h = 70 \times 10^{-4}$ ft/psi
distance to the discontinuity 8150 feet

These results imply that the thickness of the reservoir is in thousands of feet rather than hundreds of feet. Based on the interference data, the reserves disturbed during the 30-day flow exceed 7 billion barrels. Northeast-southwest trending faults located north of well 22-22 may be interpreted as possible permeability barriers.

CONCEPTUAL MODEL

A conceptual model of the Desert Peak geothermal field is shown in Fig. 6. The depth of the upper mantle in the Basin and Range province varies from 15 to 20 miles (Stauber, 1983). Previously discussed stratigraphy and the thicknesses of various formations encountered in this field are also shown in this figure.

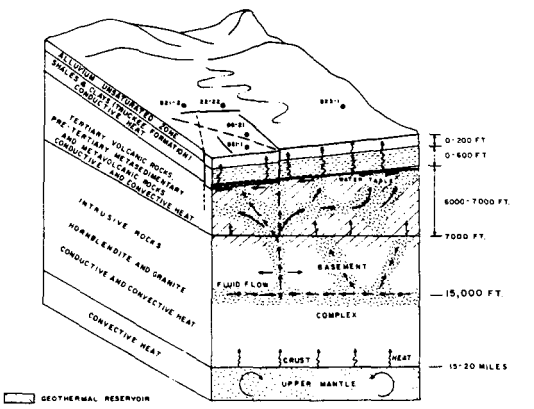


Figure 6. Conceptual Model of Desert Peak Geothermal Field.

The fractures in hard basement rocks which result from normal faulting are expected to increase vertical permeability much more than the horizontal permeability. The heat transfer mechanism in the basement complex is expected to be controlled by convection in open fractures and by conduction in low permeability rocks. Well B23-1 is believed to produce from the granite below 7000 feet.

Wells B21-1 and B21-2 produce from the pre-Tertiary section. Well 86-21 produces from rhyolite near the bottom of the Tertiary volcanic section where both vertical and horizontal water flow has been observed. In the Tertiary volcanic section, heat transfer is primarily by convection. It is presumed that heat transfer in the pre-Tertiary metasedimentary and metavolcanic rocks is by both convection and conduction depending upon the presence or absence of fluid movement. The known geothermal reservoir is shown schematically by hatched lines in Fig. 6.

Fine grained lacustrine sedimentary rocks of the Truckee Formation overlie Tertiary volcanic rocks and act as local caps for near surface horizontal movement of thermal water. However, in many areas the water table is several hundred feet deep. This means that often the relatively thin Truckee Formation does not have a chance to act as a cap rock

because it is completely above the water table. At this time, it is not known whether or not an effective cap exists for the Desert Peak reservoir.

The uppermost layer in Fig. 6 consists of alluvium to a maximum depth of 200 feet. This layer is almost always above the water table.

The reservoir is highly fractured with faults concentrated in northeasterly and northwesterly directions, as shown in Fig. 2. Faults shown in Fig. 6 are schematic, but do represent the reservoir concept as known to date.

In summary, the vertical as well as horizontal permeability in the basement and in the geothermal reservoir is mostly due to fractures. The major source of fluids in the Desert Peak area is thought to be seepage from the Carson and Fernley Sinks, which are located respectively to the east and west of the Hot Springs Mountains (Fig. 1). It is postulated that this water percolates gradually into the sediments and basement rock over an area considerably larger than the Desert Peak anomaly. Heated at depth by an as yet undefined source, the liquid rises into the high permeability fractured fault zones, convecting energy toward the surface. The ascending hot water charges the highly fractured main geothermal reservoir which is believed to exist between 3000 feet and 9000 feet depth. The thermal water either continues to rise or leaks out of the reservoir to within a few hundred feet of the surface until it has reached hydrostatic equilibrium or it is blocked by impermeable lacustrine sedimentary rocks. In the latter case, it flows laterally down gradient along available flow path permeability between depths of 200 to 1000 feet. This lateral hot water flow has created a huge, intense near-surface thermal anomaly which obscures the location of the smaller actual produceable reservoir (Fig. 3). It is believed that the three shallowest producing wells (B21-1, B21-2 and 86-21) produce from normal faults concealed by overlying drape folds.

CONCLUSIONS

Geological and well testing data indicate that the fractured geothermal reservoir lies in various rock types. The fractures, at least in the immediate vicinity of wells B21-1, B21-2 and 86-21, display a strong north-south trend. The interference data indicates that the wells intersect a highly permeable reservoir. The north-south transmissivity is an order of magnitude higher than that in east-west direction. This agrees well with the fault orientation in the field. The transmissivity and storativity calculations indicate that the thickness of the Desert Peak reservoir is on the order of thousands of feet. This agrees well with the interpretation that the fracture zones are associated with steeply dipping normal faults. A conceptual model, involving deep circulation of meteoric water through normal faults, explains various features associated with the Desert Peak geothermal reservoir.

REFERENCES

1. Benoit, W. R., J. E. Hiner and R. T. Forest (1982) "Discovery and Geology of the Desert Peak Geothermal Field: A Case History", Nevada Bureau of Mines and Geology, University of Nevada, Reno, Bulletin 97, p. 82.

2. Earlougher, Jr., R. C. (1977) "Advances in Well Test Analysis", Monograph volume 5, Henry L. Doherty Series, Society of Petroleum Engineers of AIME, New York, p. 264.

3. Hiner, J. E. (1979) "Geology of the Desert Peak Geothermal Anomaly, Churchill County, Nevada": Masters Thesis, Univeristy of Nevada, Reno, p. 84.

4. Stauber, D. A. (1983) "Crustal Structure of North Central Nevada from Seismic Refraction, Gravity and Surface Wave Data", in Abstracts of the Symposium on the Role of Heat in the Development of Energy and Mineral Resources in the Northern Basin and Range Province. Geothermal Resources Council, p. 26.

5. Urban, T. C. and W. H. Diment (1982) "An Interpretation of Precision Temperature Logs in a Deep Geothermal Well near Desert Peak, Churchill County, Nevada", Transactions, Geothermal Resources Council, v.6, pp 317-320.

Proceedings Ninth Workshop Geothermal Reservoir Engineering
Stanford University, Stanford, California, December 1983
SGP-TR-74

THE GENERATING CAPACITY OF THE HEBER GEOTHERMAL FIELD, CALIFORNIA

M. J. Lippmann and G. S. Bodvarsson

Earth Sciences Division
Lawrence Berkeley Laboratory
University of California
Berkeley, CA 94720

ABSTRACT

Using numerical simulation techniques and the radial model developed for the study of the natural state of the Heber field (Lippmann and Bodvarsson, 1983b), the response of this geothermal system to exploitation is analyzed. In this study the generation rate in the field is allowed to build up over a period of 10 years; after that, 30 years of constant power production is assumed. Full (100%) injection of the spent brines is considered, the fluids being injected 2250 m ("near injection") or 4250 m ("far injection") from the center of the system. The study shows that a maximum of 6000 kg/s (equivalent to approximately 300 MW_e) of fluids may be produced for the near injection case, but only 3000 kg/s (equivalent to approximately 150 MW_e) for the far injection case. The results indicate that the possible extraction rates (generating capacity) generally are limited by the pressure drop in the reservoir. The average temperature of the produced fluids will decline 10-18°C over the 40-year period.

INTRODUCTION

Construction of the first power plant at the Heber geothermal field (Fig. 1) began in June 1983. It will be a 45 MW_e (net) binary plant and is scheduled to come on-line in 1985. The construction of a second facility, a 47 MW_e (net) dual-flash power plant, will begin in early 1984; its completion is also targeted for 1985. Further development at Heber might follow. Chevron Geothermal Co., the operator of the field, estimates that the Heber anomaly can support a power generation of 500 MW_e for at least 30 years (Salveson and Cooper, 1981; California Division of Oil and Gas, 1983).

The objective of this paper is to evaluate the generating capacity of the Heber system under different production-injection scenarios. The response of the field to exploitation is calculated using a numerical simulator that computes heat and mass transport in geothermal systems. The initial temperature and pressure distributions and the boundary conditions assumed in these calculations correspond to those determined by the natural state model of Heber developed previously (Lippmann and Bodvarsson, 1983b).

PREVIOUS WORK

The only published modeling study on the exploitation of the Heber reservoir is that by Tansev and Wasserman (1978). They use a three-dimensional, single-phase (liquid) non-isothermal simulator. Their model of the geothermal reservoir covers a 30.3 km^2 area and consists of two main zones: Zone 1, from 2000 to 4000 ft (600 to 1200 m) depth, and Zone 2, from 4000 to 6000 ft (1200 to 1800 m) depth. Zone 1 is subdivided into 15 horizontal sand and shale layers, and Zone 2, into 13 layers. The model is further divided into 8 areal pies, each consisting of 15 rows.

Tansev and Wasserman (1978) assume that: (1) the sand and shale layers are continuous, homogeneous and isotropic, (2) the initial temperatures vary only as a function of the radial coordinate, and do not vary vertically in a given zone, (3) the regional ground water movement is negligible, (4) no heat (or mass) recharge occur from the underburden (below 1800 m), and (5) (in most cases studied) no cross flow exists between the pies into which the model is divided. No data is given on the thermal and hydraulic properties assigned to the different layers.

Fluids are assumed to be produced from both zones (between 600 and 1800 m depth) to sustain a constant 200 MW_e total generating capacity. Hot fluids are extracted near the axis of the system and the spent brine is reinjected near its periphery (the exact locations are not given). The initial total fluid production rate is 4.56 m^3/s, but as the temperature of the produced fluids decreases the production rate increases. Some of the conclusions reached by Tansev and Wasserman (1978) are: (1) both zones show a 16.7°C temperature decline over a thirty year production period, (2) the Heber system between 600 and 1800 m (Zones 1 and 2) alone can support 250 MW_e power production, and (3) in general, the generating capacity of Heber will be restricted mainly by the pressure drop rather than by the temperature decline (a temperature of 160°C for the power plant is assumed as a economic cutoff point).

AVAILABLE DATA

Only information on the reservoir development plan will be reviewed since the published data on the subsurface characteristics of the Heber system have been summarized elsewhere (Lippmann and Bodvarsson, 1983b).

According to Tansev and Wasserman (1978), Chevron plans to develop a nearly circular 30.3 km^2 area with each plant increment representing a pie-shaped segment. Salveson and Cooper (1981) indicate that the "wells will be directionally drilled for production from surface islands into the high temperature part of the thermal anomaly. Bottom hole locations will be evenly distributed in a circular pattern having a radius of about 600 m.

The power plants will be located near the producing islands to minimize heat loss during transit of the hot brine. Cooled brine will be piped from the power plants to injection islands on the periphery of the field. There, 2.4-4.0 km from the center of the anomaly, the spent brine will be reinjected through directionally drilled wells to the present position of the 129°C isotherm."

For the production depths assumed by Tansev and Wasserman (1978) -- 600 to 1800 m -- 2.28 m^3/s of fluid will initially be required to generate 100 MW_e. For a fluid density of 900 kg/m^3, this would correspond to about 2050 kg/s. Lacey and Nelson (1982; Fig. 2) state that 995 kg/s of geothermal fluids are needed for the 45 MW_e (net) binary plant. For the 47 MW_e (net) dual flash plant De Haven (1982) mentions a rate of about 1020 kg/s. In other words, about 1000 kg/s of fluid will be required to generate 50 MW of electrical power.

One hundred percent of the fluids produced from the reservoir will be reinjected; some makeup waters from surface sources will be required. For the 45 MW_e (net) plant the temperature of the injected fluids will be 72.2°C (Lacy and Nelson, 1982; Fig. 2). No other reference indicating the temperature of the injected brines was found in the literature.

METHODOLOGY

LBL's three-dimensional simulator PT (Bodvarsson, 1982) is used to compute the heat and mass flow through the system in response to different assumed development plans. The change of reservoir pressures and the average temperature of the produced fluids are the main parameters used to establish the feasibility of the fluid production-injection schemes considered in this study.

DESCRIPTION OF THE MODEL

The model used in the simulations is almost identical to the one applied for studying the natural state of the Heber system (Lippmann and Bodvarsson, 1983b). The radially symmetric model presents five zones of different material properties (Fig. 2).

Boundary conditions. The outer boundary of the model, 10 km from the axis, is assumed to be open to heat and mass flow and have constant temperatures and pressures. The temperatures at the outer boundary are assumed to increase linearly with depth with a gradient of 50°C/km. The pressures used at the outer boundary are hydrostatic for the assumed temperature distribution.

The top boundary is considered open only to heat flow; it is kept at a constant temperature of 22°C, which corresponds to the mean annual temperature in the area. Most of the bottom boundary, at 4950 m depth, is assumed to be closed to fluid flow and to have a constant temperature of 269.5°C, computed from the assumed geothermal gradient and surface temperature. However, in a circular area around the axis of the system, 1000-m in radius, the lower boundary is left open to fluid flow. This area has a constant temperature and pressure of 244.5°C and 456.7 bars, respectively. Under natural state conditions these parameters result in a mass recharge through the axial lower area of the system. This is equal to that of the 14.6 kg/s convective heat source inferred to exist at the bottom of the upflow zone at the Heber field (Lippmann and Bodvarsson, 1983b). During the simulation of the exploitation of the system, this rate of recharge will increase with time as the reservoir pressure in the upflow zone decreases. Thus, the modeling of the upflow zone using a constant pressure boundary is an optimistic assumption. The different treatment of the inner lower boundary (constant pressure as opposed to constant flow rate) is the only disparity between the models used to simulate the behavior of the system before and during exploitation.

Initial conditions. The initial temperature and pressure conditions used in simulating the exploitation of the field correspond to those of the natural state model discussed by Lippmann and Bodvarsson (1983b). Figure 3 shows the initial distribution of temperatures (because of symmetry only half of the cross section is given).

Rock properties. The reservoir system is divided into 5 zones with different rock properties, primarily different permeability values (Table 1). Zones 1 and 2 are 550 m thick and represent the caprock. Zone 3, which corresponds to a cylinder of 1000 m radius, is the hot water upflow zone. Zones 4 and 5 correspond to the outer regions of the field.

The most important reservoir parameters controlling the distribution of temperature and pressure in the system under natural (steady-state) conditions are the permeability and thermal conductivity. These are determined for the different zones by modeling Heber in its pre-exploitation state (Lippmann and Bodvarsson, 1983b). To our knowledge no values have been published on the porosity of the Heber reservoir. In our work we use porosities which are in the range of those found in other geothermal fields of the Salton Trough (Riney et al., 1980; Lippmann and Bodvarsson, 1983a).

Fluid properties. The geothermal fluid is assumed to be pure water; its density, viscosity and compressibility are allowed to vary with temperature and pressure. The specific heat of the fluid is kept constant (4,200 kJ/kg); its thermal expansivity is neglected.

Produced zones. Fluids are produced from the 1000-m radius upflow zone (Zone 3). In two of the four cases studied (Cases 1 and 2) production is uniformly distributed between depths of 650 m and 2950 m. This production scheme is similar to the one discussed by Salveson and Cooper (1981).

In Cases 3 and 4, the production is assumed to be restricted to deeper formations (the 1950-2950 m depth interval) facing the higher permeability Zone 5 (Fig. 2).

Production rates. The main objective of this study is to find out what extraction rates (i.e., generating capacity) are possible at Heber for different injection scenarios. It is assumed that during a

10-year period the installed generating capacity at Heber increases linearly with time, from zero MW_e at t = 0 to a maximum value at 10 years. From then on, the electrical power generation remains constant at the maximum level.

The simulations are carried out until boiling is observed in some part of the system (this always occurs in the shallow reservoir region near the axis), or to 100 years, whichever occurs first. When boiling occurs, the reservoir pressure at the upper part of the produced zone (at 750 m depth in Cases 1 and 2) generally drops about 40 bars, a drawdown considered to be excessive for a pumped system like that planned at Heber. Based on the published data noted above, it is assumed that 1000 kg/s of geothermal fluids are required to generate 50 MW_e.

Injected zones. One hundred percent of the fluids extracted from the reservoir are reinjected. At each depth interval the same mass of fluid is injected as is produced. Several radial distances from the axis of the system are considered for reinjection (Fig. 4). Two extreme situations are discussed here.

Near Injection: Uniform injection into a circular region extending between 2000 and 2500 m from the axis of the system (Cases 1 and 3);

Far Injection: Uniform injection into a circular region extending between 4000 and 4500 m from the axis (Cases 2 and 4).

These two extremes bound the radial distances indicated by Salveson and Cooper (1981) for the location of the injected zones; i.e., 2.4-4.0 km.

Temperature of the injected brine. Following Lacy and Nelson (1982; Fig. 2) it is assumed that the injected fluid has a temperature of 72.2°C.

RESULTS

Four reservoir development plans (cases) are discussed (see Table 2). In the first two cases fluid is produced from between 650 and 2950 m depths; the plan is similar to that described by Salveson and Cooper (1981). Cases 3 and 4 study the effect of producing (and injecting) all fluid from a deeper 1000-m thick interval located adjacent to (or in) the higher permeability Zone 5.

The computed changes in reservoir pressures and average temperature of the produced fluids for the four cases are given in Figures 5 to 15. For Case 1, the temperature, pressure and mass flow distribution in the system are shown in Figures 16 to 18. The production characteristics after 40 years of development for all cases studies are summarized in Table 3.

Reservoir Pressures

The shape of the pressure versus time graphs for the production nodes reflects the assumed field development plan. Between 0 and 10 years the total production rate increases linearly with time, from zero to a maximum rate at 10 years. This causes large pressure declines at early times. Later on, pressures tend to stabilize due to constant extraction rates and injection effects.

In Cases 1 and 2 the drawdown in the upper part of the produced interval (Fig. 5 and 8) is much larger than that in the lower part (Fig. 6 and 9). This is mainly due to the limited fluid recharge to the shallower zones of the production region. In the upper part of the production zone, the lateral recharge is limited because of the relatively low horizontal permeability (10 md) of Zone 4. In comparison, for the lower part of the production zone, the horizontal permeability of the neighboring Zone 5 is 115 md. The effect of the permeability distribution on the pressure drop in the reservoir is evident in Figure 17 which shows pressure contours for Case 1 after 40 years of exploitation. The effect of permeability contrast is also evident in the magnitude of the recharge to the different regions of the production zone, as illustrated in Figure 18; the length of the arrows is proportional to the mass flow rate.

In order to circumvent the effect of the lower permeability Zone 4, in Cases 3 and 4 the production and injection was restricted to the 1950-2950 m depth interval (Table 2). In these cases, even though the fluid extraction rate per unit volume of production zone has more than doubled with respect to Cases 1 and 2, the drawdown has been reduced considerably. No boiling occurs in the system even when the production rate is as high as 10,000 kg/s (Fig. 12 and 14).

The reservoir pressure support of the reinjection operations is clearly evident when one compares, e.g., the 4000 kg/s examples, for Cases 1 and 2 (Fig. 5 and 8, and 6 and 9). The closer to the production zone injection takes place, the greater is the pressure support. However, if fluids are injected too close to the production region, detrimental decreases in the temperature of the produced fluids occur (see below).

The pressures in the injection nodes located in Zone 4 are illustrated in Figure 11 (for Cases 1 and 2). There is a rapid rise in pressure as the injection (and production) rate increases during the first 10 years. From then on, as the rate is kept constant, the pressure stabilizes (Case 1) or even slowly decreases (Case 2). On the other hand, the pressure in the injection nodes located in the higher permeability zone (Zone 5) only changes slightly with time. For example, in Case 4 (far injecton) the total pressure rise after 40 years of injection at a rate of 10,000 kg/s is 3.5 bars.

Average Production Temperature

The temperatures reported here are the average temperatures of the produced fluids at the reservoir level; to obtain the temperature of the fluids at the inlet to the power plant one must consider the heat losses in the wellbore and also those in the surface hot water transmission pipes.

With production uniformly distributed over the 1000-m radius cylinder the initial average temperature of the produced fluids (weighted by mass) is 178.7°C for Cases 1 and 2, and 177.8°C for Cases

3 and 4. Because of the characteristic mushroom shape of the isotherms in the reservoir (Fig. 3), these average initial temperatures would be a few degrees higher if production is increased towards the axis of the system, and correspondingly reduced in the outer regions of the production cylinder. The changes in average fluid production temperatures with time for the different cases are given in Figures 7, 10, 13 and 15. The temperature of the produced fluids decreases significantly faster in Cases 1 and 3 (near injection) than in Cases 2 and 4 (far injection), because of the smaller distance between injection and production areas.

In Cases 3 and 4 the higher mobility of the injected fluids results in high overall temperature drops due to the larger permeability of Zone 5 and higher production/injection rates per unit volume. For equal total rates the temperature reductions are far greater than in Cases 1 and 2 (see Fig. 13 and 15). The higher mobility of the injected fluids in Zone 5 relative to that for Zone 4 is reflected, for Case 1 by the shape of the isotherms after 40 years of exploitation (Fig. 16), especially that of the 120°C isotherm.

The temperature of the produced fluids is not significantly affected if the temperature of the injected fluids is increased slightly (e.g., 100°C instead of 72.2°C). For example, in Case 1 (6000 kg/s), the average temperature after 40 years only increases from 163.6 to 163.9°C. However, because 100°C fluids have significantly lower viscosity than 72.2°C fluids, injection of higher temperature fluids is preferential for pressure support. In the example discussed above, the 100°C injection increases the "longevity" of the system from about 58 to about 70 years (Table 4).

"Longevity" of the System

The "longevity" of the system, considered here to correspond to the time boiling occurs somewhere in the system (excessive pressure drops), is given in Table 4 for the different cases studied. Based upon this criterion, and a minimum acceptable 40-year period, the results show that for Cases 1 and 2 the system cannot be produced at rates greater than 6000 and 3000 kg/s, respectively.

In Cases 3 and 4 the fluid extraction rate could reach, and possibly exceed, 10,000 kg/s (equivalent to about 500 MW_e). But, in these two cases the temperature reduction of the produced fluids, and not the drop in reservoir pressure, controls the maximum allowable fluid production rate. If one uses an economic temperature limit of 160°C for the power plant as indicated by Tansev and Wasserman (1978), and neglects any heat losses during transport in wellbore and surface pipes (i.e., temperature of the fluids at the reservoir equal to that at the power plant inlet), the maximum allowable production rate for a 40-year period is less than 6000 kg/s for Case 3 and slightly below 3000 kg/s for Case 4.

CONCLUSIONS

If one assumes a 40-year lifetime for the project, with 10 years to build up to the total electrical generating capacity and 30 years of maximum constant electrical power output, the results obtained show that (Table 3):

(1) For injection between 2000 and 2500 m from the axis of the system (near injection) a maximum production rate of 6000 kg/s (about 300 MW_e) is possible. However, it should be stressed that in Case 1, after 40 years of exploitation, the total pressure drop in the upper part of the produced region is 35.9 bars, and the average temperature of the produced fluids (at reservoir level) will have declined about 15°C, to about 164°C. For Case 3, the maximum possible mass extraction rate is below 6000 kg/s; for that rate after 40 years the production temperature would drop about 34°C, to about 144°C.

(2) For injection between 4000 and 4500 m (far injection) the maximum feasible production rate is 3000 kg/s (about 150 MW_e). In Case 2, after 40 years, the maximum drawdown in the reservoir (at r = 100 m, z = -750 m) is approximately 30 bars and the average temperature of production fluids 170°C. In Case 4, the pressure drop in the reservoir, at r = 100 m, z = -2700 m, is 12.0 bars and the temperature of the produced fluids will have dropped about 18°C, to about 159°C.

ACKNOWLEDGEMENTS

We thank our colleagues C. Doughty and J. Wang for reviewing the manuscript, as well as P. Fuller and C. Doughty for generating the computer plots used in the paper. This work was supported by the Assistant Secretary for Conservation and Renewable Energy, Office of Renewable Technology, Division of Geothermal and Hydropower Technologies of the U.S. Department of Energy under Contract No. DE-AC03-76SF00098.

DISCLAIMER

"This paper was prepared as an account of work sponsored by an agency of the United States Government. Neither the United States Government nor any agency thereof, nor any of their employees, makes any warranty, express or implied, or assumes any legal liability or responsibility for the accuracy, completeness, or usefulness of any information, apparatus, product, or process disclosed, or represents that its use would not infringe privately owned rights. Reference herein to any specific commercial product, process, or service by trade name, trademark, manufacturer, or otherwise, does not necessarily constitute or imply its endorsement, recommendation, or favoring by the United States Government or any agency thereof. The views and opinions of authors expressed herein do no necessarily state or reflect those of the United States Government of any agency thereof."

REFERENCES

Bodvarsson, G.S., 1982. Mathematical modeling of the behavior of geothermal systems under exploitation (Ph.D. thesis). Lawrence Berkeley Laboratory, report LBL-13937, 353 p.

California Division of Oil and Gas, 1983. Chevron, Dravo, may be partners in Heber dual flash project. Geothermal Hot Line, v. 13, No. 1, p. 7-8.

De Haven, N.J., 1982. Heber geothermal project. Geothermal Resources Council Trans., v. 6, p. 339-341.

Elders, W.A., J.R. Hoagland, E.R. Olson, S.D. McDowell, and P. Collier, 1978. A comprehensive study of samples from geothermal reservoirs. Riverside, Calif., Univ. of Calif. report UCR/IGPP-78/26, 264p.

Lacy, R.G. and T.T. Nelson, 1982. Heber binary project--Binary cycle geothermal demonstration power plant. Proc. Sixth Annual Geothermal Conference and Workshop, Electric Power Research Institute report EPRI AP-2760, p. 5-1 to 5-7.

Lippmann, M.J. and G.S. Bodvarsson, 1983a. Numerical studies of the heat and mass transport in the Cerro Prieto geothermal field, Mexico. Water Resour. Res., v. 19, p. 753-767.

Lippmann, M.J. and G.S. Bodvarsson, 1983b. A modeling study of the natural state of the Heber geothermal system, California. Geothermal Resources Council, Trans., v. 7, p. 441-447.

Riney, T.D., J.W. Pritchett, and L.F. Price, 1980. Integrated model of the shallow and deep hydrothermal systems in the East Mesa area, Imperial Valley, California. La Jolla, Calif., S-Cubed report SSS-R-80-4362, 116 p.

Salveson, J.O., and A.M. Cooper, 1981. Exploration and development of the Heber geothermal field, Imperial Valley, California. Proc. 1981 New Zealand Geothermal Workshop, p. 3-6.

Tansev, E.O., and M.L. Wasserman, 1978. Modeling the Heber geothermal reservoir. Geothermal Resources Council Trans., v. 2, p. 645-648.

Table 1. Rock properties used in the model.

Zone	Porosity	Horizontal Permeability (md)	Vertical Permeability (md)	Conductivity Rock-water Mixture (W/m°C)	Density (kg/m^3)
1	.30	5	0.5	1.088	2650
2	.30	5	0.05	1.088	2650
3	.23	125	12.5	2.000	2650
4	.25	10	0.1	2.000	2650
5	.23	115	11.5	2.000	2650

Note. Rock compressibility and thermal expansion are neglected.

Table 2. Reservoir development plans studied for the Heber field.

Case	Production/Injection depth intervals (m)	Average radial distance to injecton zones (m)
1	650 - 2950	2250
2	650 - 2950	4250
3	1950 - 2950	2250
4	1950 - 2950	4250

Note. In all cases fluid is produced from a 1000-m radius axial cylinder.

Table 3. Production characteristics after 40 years.

Fluid Production Rate (kg/s)	Reservoir* Pressure (bars)	ΔP^* (bars)	Average Temperature of Produced Fluids (°C)	$\Delta\overline{T}$ (°C)
		Case 1		
4000	55.5	-23.1	168.0	-10.7
5000	49.3	-29.4	165.8	-12.9
6000	42.8	-35.9	163.6	-15.1
		Case 2		
2000	59.1	-19.6	172.7	-6.0
3000	49.1	-29.6	170.1	-8.6
		Case 3		
6000	234.6	-19.7	144.1	-33.6
10,000	217.4	-37.0	126.8	-51.0
		Case 4		
3000	242.4	-12.0	159.2	-18.5
10,000	212.7	-41.7	146.0	-31.8

Note. *: For Cases 1 and 2 reservoir pressures correspond to the production node at r = 100 m and z = -750 m; for Cases 3 and 4, to the node at r = 100 m and z = -2700 m.

Table 4. "Longevity" of the System.[1]

Fluid Production Rate (kg/s)	Generating Capacity (MW_e)	Boiling in the system occurs after:
	Case 1	
4000	~200	>100 yrs
5000	~250	>100 yrs
6000	~300	~58 yrs (~70 yrs)[2]
7000	~350	~25 yrs
	Case 2	
2000	~100	>100 yrs
3000	~150	>100 yrs
4000	~200	~12.2 yrs
	Case 3	
6000	~300	>100 yrs[3]
10,000	~500	>100 yrs[3]
	Case 4	
3000	~150	>100 yrs[3]
10,000	~500	>100 yrs[3]

Notes. (1): See text for definition. (2): Injection of 100°C water.
(3): Based on pressure considerations only.

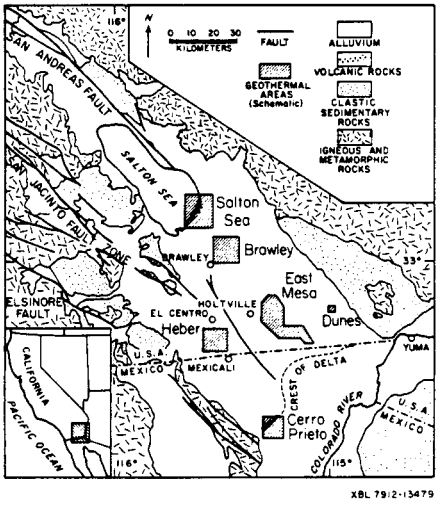


Figure 1. Location of geothermal areas in the Salton Trough (from Elders et al., 1978).

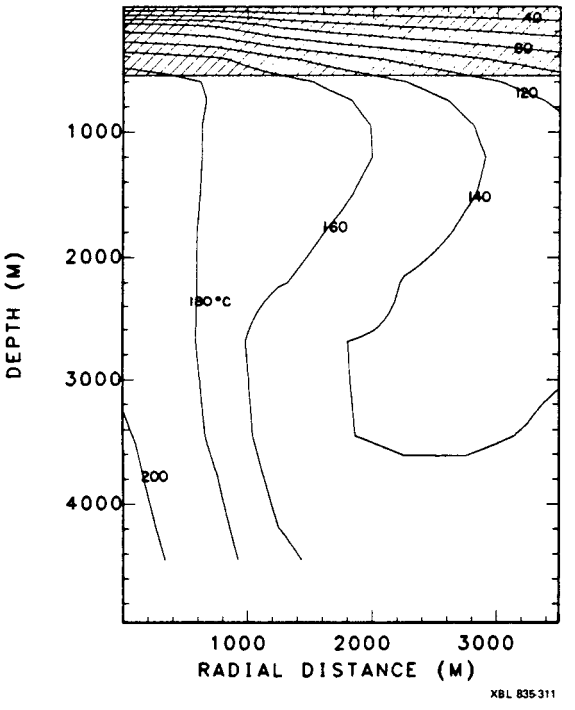


Figure 3. Initial distribution of temperatures in the system. Hatched layer represents the caprock (from Lippmann and Bodvarsson, 1983b).

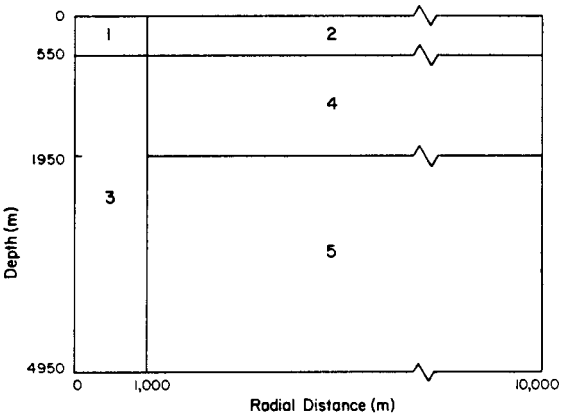


Figure 2. Different zones used in the model.

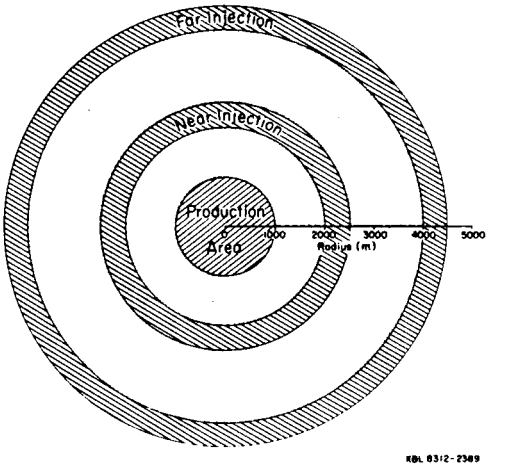


Figure 4. Plan view of the production/injection model used for Heber.

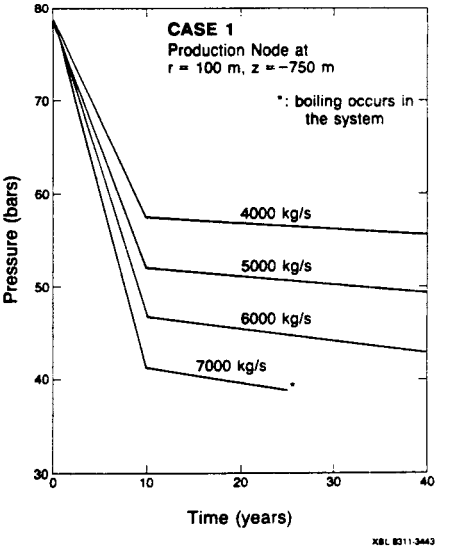


Figure 5. Case 1. Pressure in production node at r = 100 m, z = -750 m.

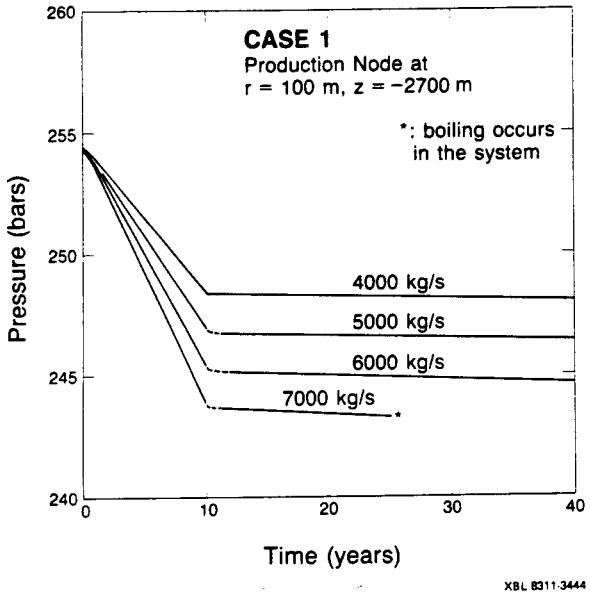


Figure 6. Case 1. Pressure in production node at r = 100 m, z = -2700 m.

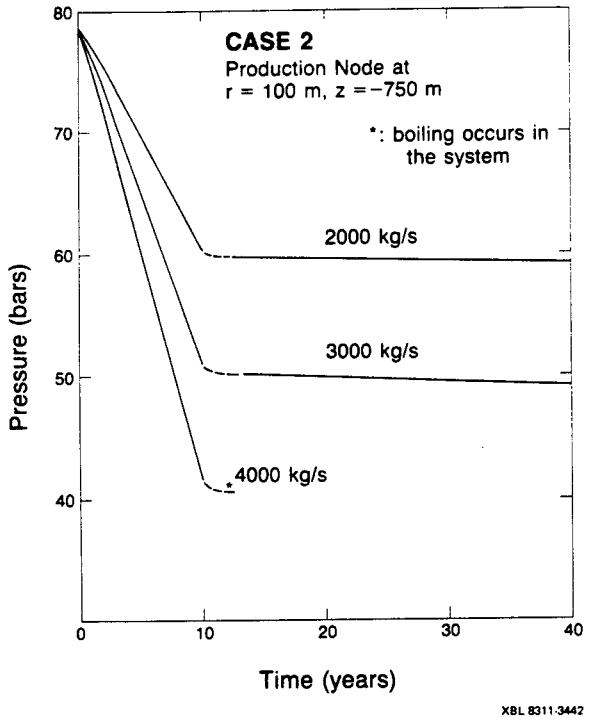


Figure 8. Case 2. Pressure in production node at r = 100 m, z = -750 m.

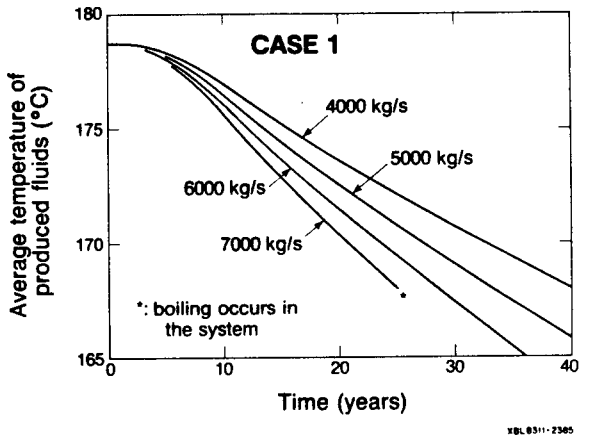


Figure 7. Case 1. Average temperature of produced fluids.

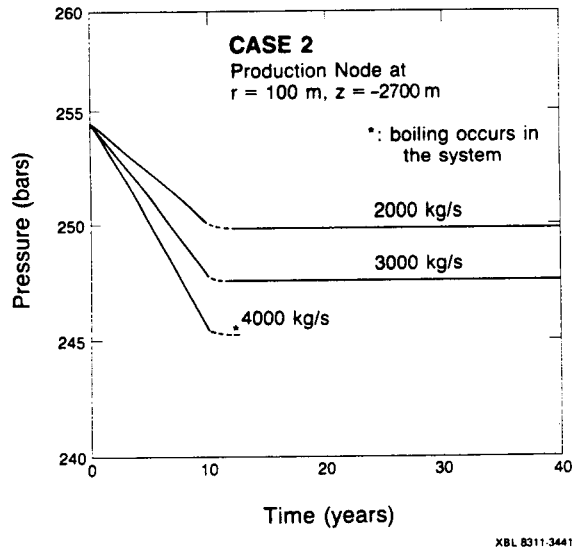


Figure 9. Case 2. Pressure in production node at r = 100 m, z = -2700 m.

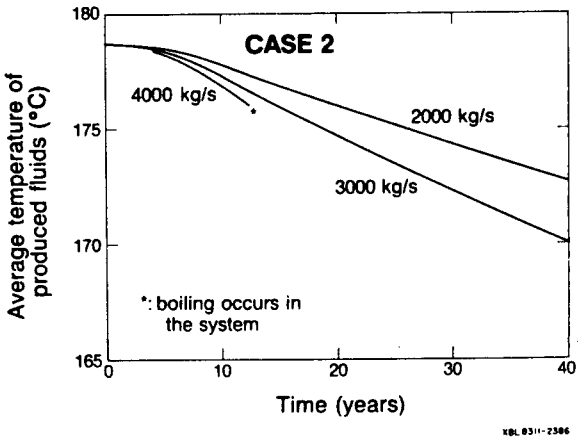


Figure 10. Case 2. Average temperature of produced fluids.

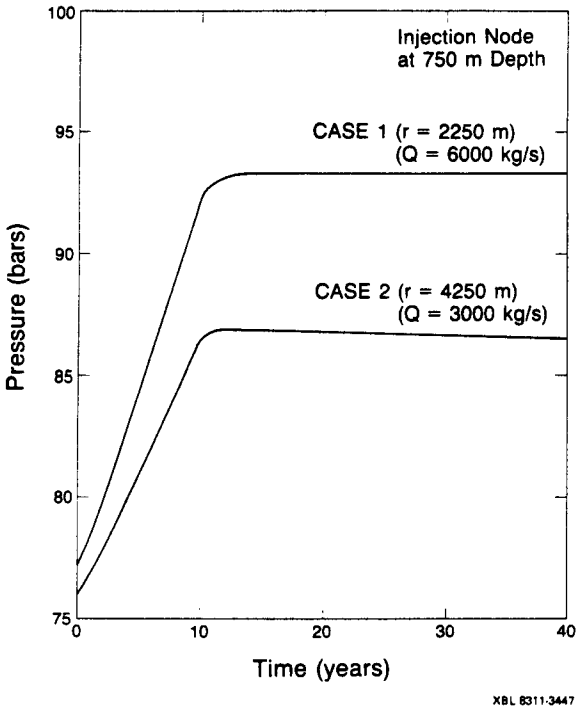


Figure 11. Cases 1 and 2. Pressure in injection node at 750 m depth.

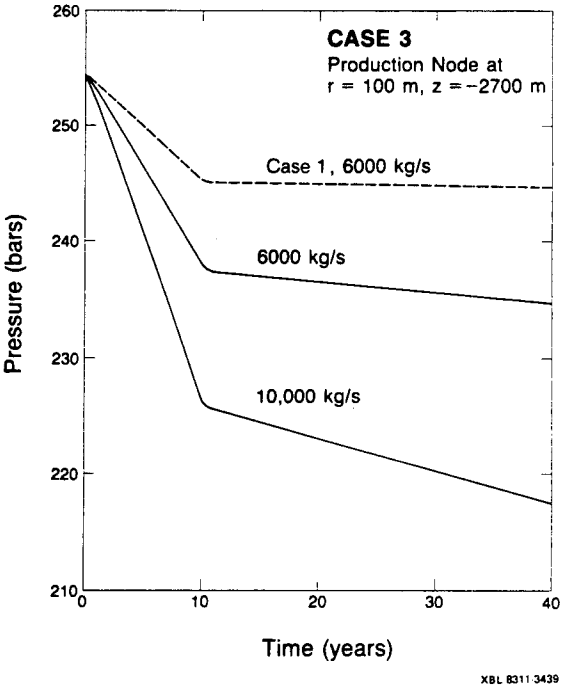


Figure 12. Case 3. Pressure in production node at r = 100 m, z = -2700 m.

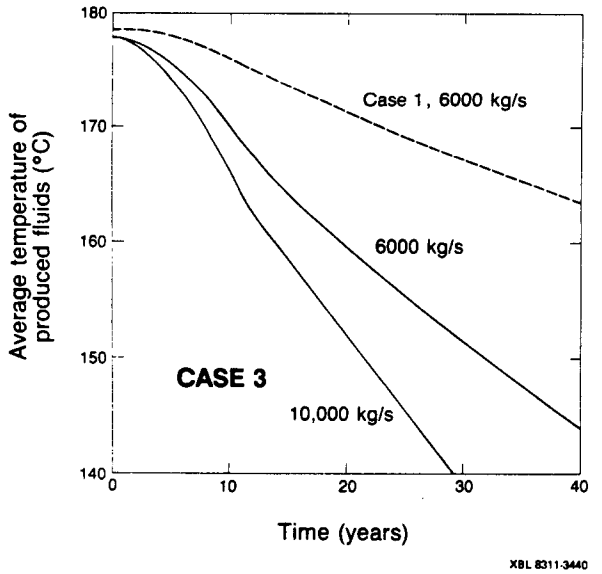


Figure 13. Case 3. Average temperature of produced fluids.

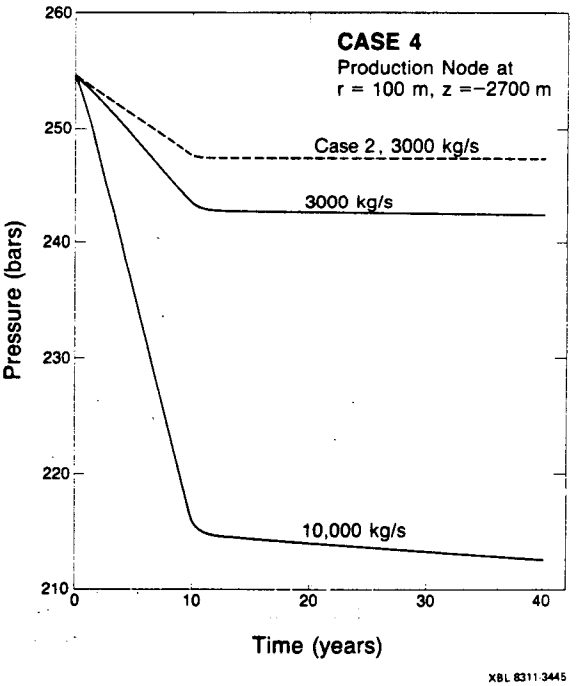


Figure 14. Case 4. Pressure in production node at r = 100 m, z = -2700 m.

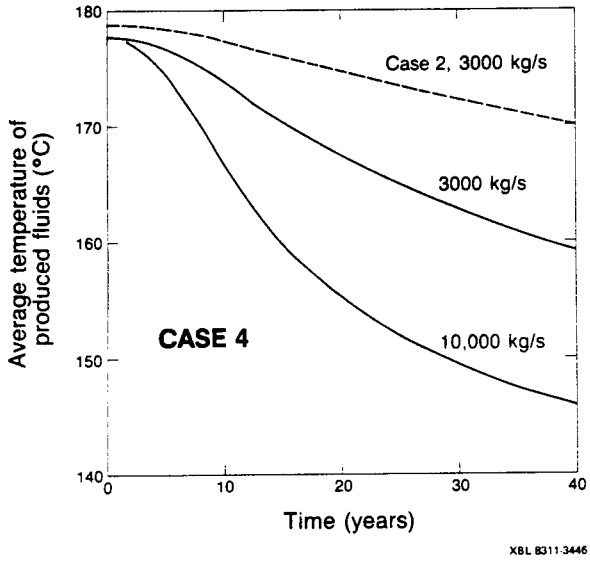


Figure 15. Case 4. Average temperature of produced fluids.

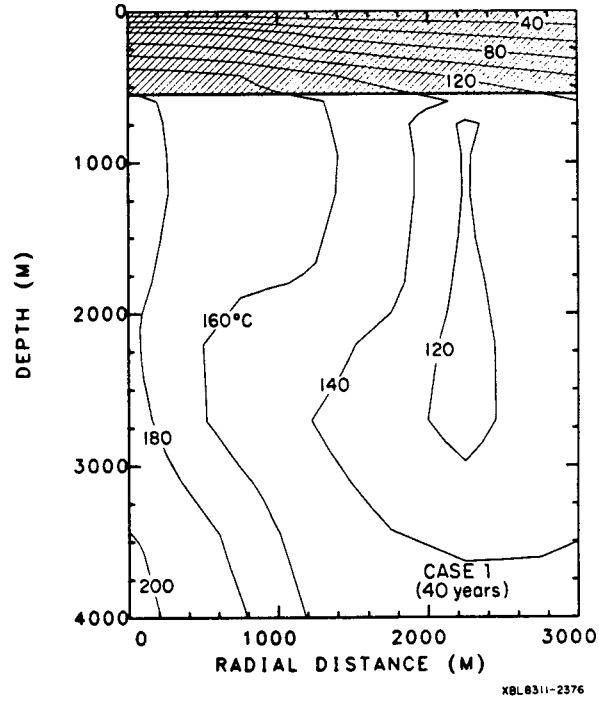


Figure 16. Case 1. Computed temperature distribution in the system after 40 years of exploitation. Hatched region represents the caprock.

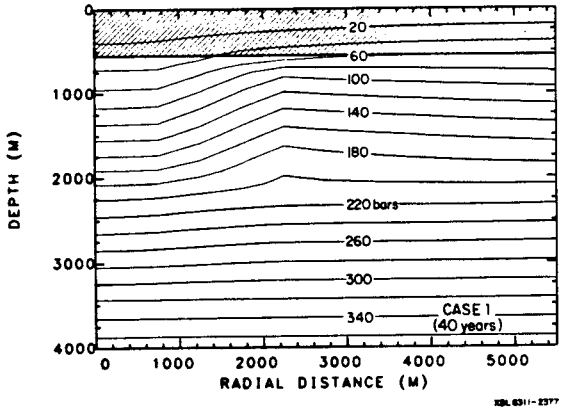


Figure 17. Case 1. Computed pressure distribution in the system after 40 years of exploitation. Hatched region represents the caprock.

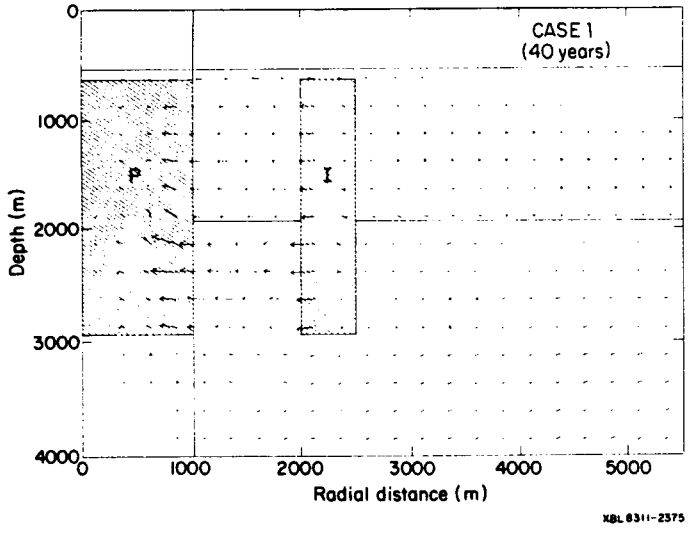


Figure 18. Case 1. Computed mass-flow pattern in the system after 40 years of exploitation. Length of arrows is scaled with respect to the largest mass flow rate. Lines delimit the different zones in the model. The hatched region represents the production (P) and injection (I) regions.

Proceedings Ninth Workshop Geothermal Reservoir Engineering
Stanford University, Stanford, California, December 1983
SGP-TR-74

A SUMMARY OF GEOTHERMAL EXPLORATION AND DATA FROM STRATIGRAPHIC TEST WELL NO. 1 MAKUSHIN VOLCANO, UNALASKA ISLAND

Don A. Campbell[1] and Michael J. Economides[2]

[1]Republic Geothermal, Inc., Santa Fe Springs, CA
[2]University of Alaska, Fairbanks, AK

ABSTRACT

Geothermal resource investigations have been conducted for the past four years on Unalaska Island in the Aleutian Chain. The focus of the work has been Makushin Volcano, about 12 miles from the cities of Unalaska and Dutch Harbor.

In the summer of 1982, three widely spaced deep temperature gradient holes were drilled which encountered high temperatures. During the summer of 1983, a three inch diameter "slim hole" well, ST-1, was drilled to 1,949 feet. A shallow, low pressure, steam zone and a relatively productive hot water zone at total depth were encountered. The lower zone produced 47,000 lb/hr, limited by reaching critical mass velocity at the orifice. The static bottomhole pressure and temperature were 478 psig and 379°F, respectively.

Analysis of transient pressure and flow data yielded a productivity index of 3,470 lb/hr/psi and a permeability-thickness of 50,900 md-ft for the three-foot (at the wellbore) lower zone fracture. A preliminary reservoir/wellbore flow evaluation for a possible power plant indicates two commercial-size wells could fuel a 10 megawatt facility.

INTRODUCTION

Unalaska Island, located approximately 900 miles southwest of Anchorage, Alaska, is one of the Fox Islands in the central portion of the Aleutian Islands arc (Figure 1). Makushin Volcano, the 6,680-foot high active volcano situated on the northern end of Unalaska Island, has numerous fumarole fields on its eastern flanks, suggesting the presence of geothermal resources beneath the volcano.

The cities of Unalaska and Dutch Harbor, which together comprise the primary northern Pacific port for the crabbing and bottom fishing industries, are located approximately 12 miles east of Makushin Volcano on Unalaska Bay. The area's electrical demand of approximately 11 megawatts is presently satisfied by diesel generators. Because fossil fuel costs (and thus electric power costs) are high on Unalaska Island, both the local community and the state of Alaska have been interested in evaluating the potential for economically exploiting geothermal energy. To this end, in late 1981 the Alaska Power Authority (APA), advised by the University of Alaska and the Alaska Geological Survey, contracted with Republic Geothermal, Inc. (Republic) to explore the vicinity of Makushin Volcano for geothermal resources. The multiyear exploration project was to include geological, geochemical, and geophysical field work and culminate in the drilling and testing of a resource exploration well. Should a commercial resource be identified, additional work beyond the scope of the project could lead to the construction of a small geothermal electrical generating facility to provide economical, reliable electrical energy for the island.

This report first briefly reviews the results of the 1982 exploration program, principally data from three thermal gradient holes and the geothermal resource model that was developed. The focus of the discussion which follows thereafter is the data from the drilling and testing of the first stratigraphic test well, ST-1, completed during the summer of 1983.

DRILLING OPERATIONS AND LOGISTICS

Drilling operations and logistics were unique in many respects because they were significantly influenced by a combination of rugged topography, limited access, available equipment, and adverse weather. The topography of northern Unalaska Island is a mixture of glaciated (U-shaped) valleys, cirques, and aretes; volcanic (lava and pyroclastic) plateaus and cliffs; and deep, steep-sided stream and river valleys. Areas of reasonably gentle relief capable of adequately accommodating a deep wellsite (without the need for extensive earthmoving) were limited over much of the geothermal area.

The rugged topography also limited overland access to the area. Although this problem should not prevent the construction of a road if a power plant is eventually built, budget limitations required that both the exploration program and the deep well drilling be supported entirely by helicopter.

Weather probably provided the biggest operational constraint, because it limited the project to a relatively short summer field season (approximately May 1 to September 15). Snow was up to eight feet deep at the base camp plateau (1,200 feet) in mid-May, and remained on the ground at that elevation well into late-June. Snow and freezing rain were common early and late in the season, and rain was prevalent throughout the operations. The two biggest weather constraints, however, were wind and fog. Winds of 40 to 50 mph were common, and gusts of hurricane force were not infrequent. These conditions often hampered helicopter transport of materials by sling. Fog also frequently grounded the helicopter.

TEMPERATURE GRADIENT HOLES

Following geological, geophysical, and geochemical surveys of the Makushin geothermal area, three ±1,500-foot temperature gradient holes were sited and drilled in the summer of 1982[1]. Temperature gradient hole D-1 was drilled on a plateau approximately one mile northwest of the base camp (Figure 1). The hole was spudded in glacial boulder till that mantled a sequence of Makushin Volcanics extending to 1,220 feet. The volcanics are a series of essentially unaltered andesite flows with interbeds of cinders, lahars, and gravel. Below the volcanics, from 1,220 feet to total depth (T.D.) at 1,429 feet, the hole

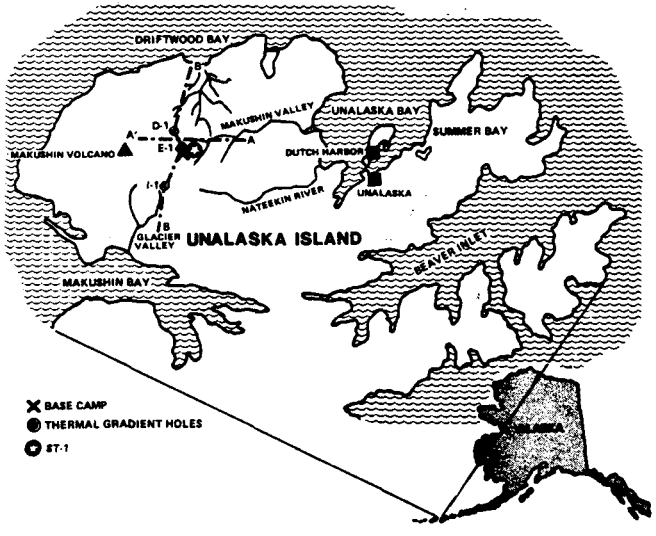


FIGURE 1. UNALASKA GEOTHERMAL EXPLORATION
PROJECT LOCATION MAP

penetrated a highly altered and fractured, fine-grained diorite. The diorite was intensely fractured and veined in the upper portion, with most fractures having near-vertical inclinations. Alteration minerals included sulfur, pyrite, kaolinite, calcite, epidote, quartz, anhydrite, and chlorite. Most of these minerals are products of the reaction between the rock and high temperature (>300°F) hydrothermal fluids.

Temperature measurements made in D-1 (Figure 2) indicated essentially isothermal convective conditions (ground water circulation) to approximately 700 feet. Below this depth the temperature increased at a high rate (22°F/100 ft) in a conductive (linear) manner to T.D. The elevated temperature recorded at T.D. (212°F), the high gradient, and the high temperature alteration of the surrounding rock all suggest the presence of a relatively shallow (±4,000 feet) hydrothermal system.

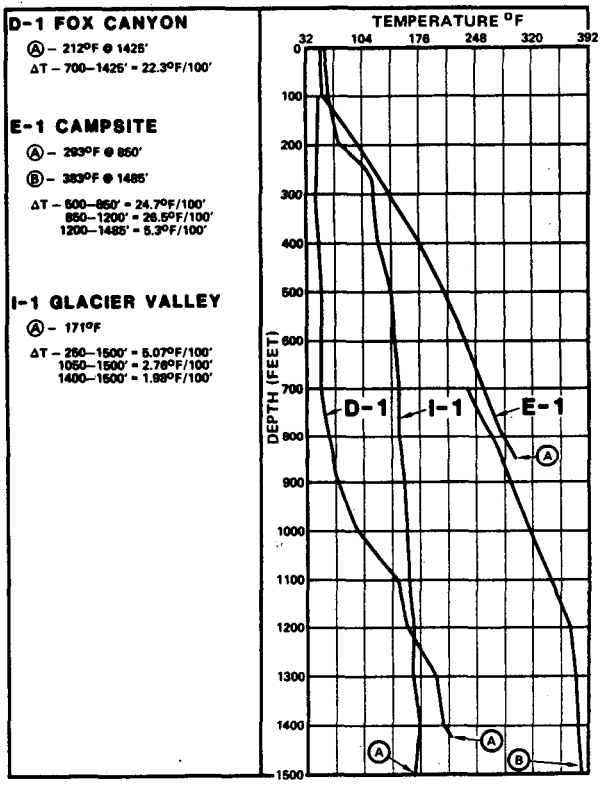


FIGURE 2. TEMPERATURE GRADIENT HOLES

The E-1 hole, located near the base camp, penetrated a sandy tuff from surface to approximately 40 feet (Figure 1). It then encountered weathered diorite which quickly graded into relatively fresh, hard, massive diorite. The diorite extended from 40 feet to T.D. at 1,501 feet, in marked contrast to the D-1 hole in which andesites and other volcanic rocks comprise the first 1,220 feet of hole. Veins and fractures were present throughout the hole, but were commonly found in 10 to 15-foot thick zones separated by massive unfractured diorite. The major fractures were dominantly vertical, with the smaller fractures and veins dipping about 45° to the core axis. The alteration and vein-filling minerals were essentially the same as those in the D-1 hole, with quartz, epidote, and anhydrite representing the higher temperature hydrothermal alteration minerals.

The temperature profile in E-1 was essentially conductive from surface to T.D. Gradients in the first 1,200 feet were quite consistent and high, and averaged 26°F/100 ft (Figure 2). At 1,200 feet, the profile began to roll over and the gradients declined abruptly to about 5°F/100 ft over the last 285 feet. This was taken to indicate that the hole had nearly penetrated the self-sealed zone and that it was approaching a convective hydrothermal system.

Temperature gradient hole I-1 was located in Glacier Valley, approximately three miles south-southwest of the camp and the E-1 site (Figure 1). Stratigraphically, I-1 was very similar to E-1, and confirmed the hitherto unknown wide distribution of the diorite intrusive body. The hole was spudded on the remnant of a terrace underlain by glacial till and pyroclastic materials about 40-feet thick. From 40 feet to T.D. at 1,500 feet, the rock drilled consisted of massive, cryptocrystalline to medium-grained diorite.

The diorite is generally altered, as in E-1, with alteration minerals including chlorite, quartz, carbonate, clay, and epidote. The upper third of the hole contained pervasive fractures commonly lined with pyrite, quartz, and epidote that were deposited during an older, high-temperature hydrothermal episode. Fractures filled with a variety of secondary minerals were, as in the other holes, distributed throughout the bottom two-thirds of the hole.

The temperature data recorded in I-1 (Figure 2) was quite different from that found in the first two holes. The profile indicated two separate thermal regimes. The first was a shallow (surface to 225± feet) system that produced large flows (>150 gpm) of 64°F to 77°F artesian water while drilling. The second system extended from about 250 feet to T.D. and appears to be a relatively conductive system, with gradients of 2°F/100 ft to 5°F/100 ft and a maximum temperature of 176°F at 1,400 feet. The data in Figure 2 also shows that there is a small temperature reversal (4°F) over the last 100 feet of the hole.

The overall temperature regime and profile of this hole indicates that it is on the southern edge of the present geothermal system, at least for this depth range, although the intense fracturing and mineralization indicates the previous presence of a high temperature geothermal system.

The geochemistry of the cuttings from the gradient holes (e.g., enrichments of Hg, F, Li, As, S) suggests the existence of a liquid-dominated reservoir not far below 1,500 feet. The local existence of fumarolic activity and of chloride-poor thermal waters implies that a steam cap overlies the hot-water reservoir. A vapor zone does not appear to be ubiquitous, but may be limited to areas beneath the active fumaroles where open fractures permit boiling. Lower elevation hot springs in Glacier and Driftwood Bay Valleys are chloride-rich.

The static temperature measured in E-1 suggests that the subsurface geothermal reservoir temperature exceeds 380°F. The geochemical signatures of the core recovered from E-1 imply a fluid temperature greater than 390°F. Calculations utilizing four different geochemical thermometers and samples from the fumaroles and hot springs indicate resource temperatures as high as 570°F.

GEOTHERMAL RESOURCE MODEL

The geothermal resource model described below was developed following synthesis of the results of studies conducted on the Makushin volcano geothermal area through 1982.(2) Figure 1 depicts the surface locations of the geologic cross sections contained in Figure 3. These north-south and east-west cross sections best illustrate the proposed model of the Makushin geothermal system. Figure 3 also includes temperature isotherms that have been overlain on the geology.

The heat source of the Makushin geothermal system appears to be a buried igneous intrusion associated with the volcano. Fourteen historical eruptions of Makushin suggest that molten or partially molten rock is currently likely to exist. The temperature and post-glacial volcanic distributions suggest that the heat source for the system is not directly beneath the summit, but rather is offset asymmetrically to the east.

The geothermal reservoir is probably situated primarily within the Makushin dioritic stock at commercially exploitable depths. The occurrence of most of the surface geothermal manifestations within diorite outcrops, the high, conductive temperature profiles recorded in the diorite, and the elevated observed temperatures are all evidence for a diorite reservoir. Some volcanic rocks act as a seal for the reservoir, as seen in D-1, while chemical precipitates appear to have "self-sealed" the diorite, as seen in E-1.

The location of the geothermal reservoir appears to be structurally controlled by a major northeasterly striking fracture zone. This zone is a long, wide, older tectonic feature whose inherent weakness probably played a major role in the intrusion of the original diorite stock. This zone has been refractured at least twice since the initial dioritic intrusion, as shown by several sequences of vein-filling minerals in the three gradient holes. More recent movement along this northeastern-trending zone maintains the permeability with fractures in the present-day geothermal reservoir, as well as the ruptures in the impermeable cap along which the majority of the surface geothermal manifestations occur. The gravity data and

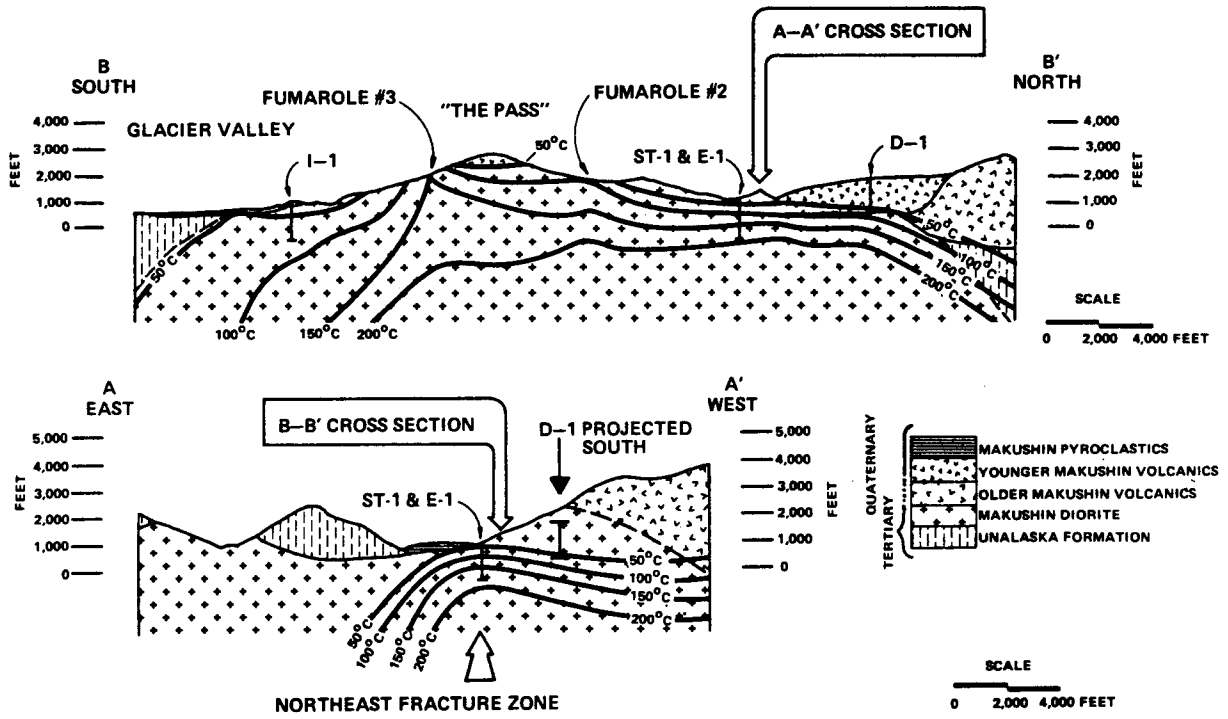


FIGURE 3. GEOLOGIC CROSS SECTIONS DEPICTING THE MODEL OF THE MAKUSHIN VOLCANO GEOTHERMAL AREA

mercury soil anomalies confirm the position and extent of the northeasterly trending fracture zone.

In summary, the Makushin geothermal system appears to be a liquid-dominated resource with temperatures in excess of 390°F. It is situated in fractured diorite within a northeasterly trending zone about two miles wide. The commercially exploitably reservoir is probably below 2,000 feet and may cover more than seven square miles. Reservoir waters rising upward (convecting) boil below an elevation of 1,200 feet in localized open fractures to form a steam cap that is limited in size and extent. Leakage of steam from this cap feeds fumaroles and mixes with ground waters to form chloride-poor hot springs. Reservoir waters appear to be mixing with ground waters before exiting in Glacier and Driftwood Bay valleys as chloride-rich hot springs.

This model of the hydrothermal system, in conjunction with logistical considerations, was used as a basis for selecting the test well location drilled in the summer of 1983.

DRILLING OF ST-1

The decision to support the deep drilling operations by helicopter placed certain limitations on the drilling equipment which could be used. "Helicopter" rotary rigs, which have been modified so that all loads are smaller than 4,000 pounds (the maximum lift capacity of a medium helicopter), have been created for use in similar situations, but few now exist. The two which were located were both rated to 16,000 feet and would require the support of at least two medium helicopters. This pushed the estimated cost of drilling a full-size deep well to approximately $6,000,000. Because the Longyear 38 continuous wireline coring rig used to drill the three 1,500-foot temperature gradient holes had performed well, it was decided instead to drill a small-diameter stratigraphic test well using a Longyear 44, a slightly larger wireline diamond core drilling rig. This lowered the cost to about one-third of that estimated for the rotary rig, although the lesser depth capability of the rig (4,000 feet) and smaller diameter of the bottomhole (2-3 inches) somewhat limited the amount of reservoir productivity data obtainable.

Stratigraphic Test Well No. 1 (ST-1) was spudded on July 2, 1983 near the E-1 temperature gradient hole (Figure 1). The well was intended to provide a "slim hole" (three inch diameter) test of the stratigraphy and the geothermal resource to about 4,000 feet. A number of drilling problems were encountered. These were primarily associated with boulders in the shallow volcanic tuff/lahar, lost circulation zones, low strength (small diameter) core pipe, and limited cementing capabilities. Mechanically, the well was completed with H.Q. core pipe (3.06 inches I.D.) cemented to 650 feet, and 2.98 inch diameter open hole below to a total depth of 1,949 feet.

Diorite with varying degrees of alteration and fracturing was cored continuously from below the shallow volcanics (170± feet) to T.D. The first significant open fractures were encountered at 672 feet. Limited testing at this depth indicated a steam zone with a shut-in pressure of +109 psig and bottomhole temperature in excess of 310°F. Flow rates with only 13 psig wellhead pressure were less than 5,000 lb/hr. The zone was mostly shut-off with lost circulation material and cement, and coring continued.

Due to continuing severe lost circulation problems, the wellbore was cemented from 1,056 feet to 550 feet and then redrilled. It is unclear whether these lost circulation problems were due to the breakdown of the zone at 672 feet or to multiple fracture zones below this point. Below 1,056 feet coring continued with 90 percent returns to 1,916 feet, where total lost circulation was experienced again. The well was cored "blind" (no circulation) to 1,926 feet and then a test was attempted, but sustained flow could not be obtained.

After coring blind an additional 20 feet (to 1,946 feet), the drillstring dropped free for three feet, indicating a major void. In a preliminary test, the well flowed steam and water for three hours with a gradually increasing wellhead pressure. After shut in wellhead pressure reached 102 psig, with the well reportedly standing full of water. Preparations for a formal test were begun.

TEST FACILITIES AND INSTRUMENTATION

Logistical considerations severely limited the type of test facilities and instrumentation which could cost-effectively be employed to test ST-1. A relatively simple two-phase orifice meter and James tube were installed at the end of a flow line to measure the flow rate. Upstream/downstream orifice pressures were recorded continuously with a differential pressure flow meter. James tube lip pressure was monitored continuously and manually recorded at frequent intervals using a carefully pre-calibrated test quality gauge. Pressure and temperature were also recorded frequently at the wellhead and elsewhere using conventional gauges.

In the absence of a separator or weir, it was necessary to estimate the fluid enthalpy to calculate a flow rate from the James[3] tube pressure. This was done using the two-phase orifice pressure drop data and/or by estimation from the measured pre-flash flowing wellbore temperature adjusted for uphole heat losses.

Downhole pressure and temperature were measured using conventional Amerada instruments modified for high temperature service. Two elements of each type were available and each was calibrated before and after testing. Temperature elements with a 200-500°F range, sensitivity of one part in 2,000, and accuracy of ±2°F were employed. Pressure elements with a 0-4,000 psig range, one part in 2,000 (±2 psig) sensitivity, and ±8 psig accuracy were used.

The inaccuracy, insensitivity, and erratic response of the pressure elements in the low pressure, 0-500 psig, range later proved to be a major problem. However, it should be noted that initial planning was for reservoir pressures of about 1,600 psig (±4,000-foot T.D.). Even when testing was initiated, about 900 psig was anticipated (1,950-foot T.D., ±100 psig shut-in wellhead pressure). When the critical value of the 0-500 psig range was recognized after the first survey, the end of the "summer" operating season was near. Delay of the testing to locate, modify (for geothermal), and calibrate new instruments was not feasible.

FLOW TEST MEASUREMENTS

The flow test plan was a simple one consisting of: (1) initial static pressure/temperature (P/T) surveys; (2) flow until stable at the highest practical rate with bottomhole P/T measurements; (3) flow at a reduced rate until stable with P/T measurements in the hole during the rate change; (4) shut in and build-up with two pressure instruments in the hole; and (5) final static P/T surveys. Instruments could not be in the hole during the initial drawdown because of the danger of "floating" in the small hole, which could not be evaluated until the rate was known. Extreme turbulence in the two-phase flow region also prevented any meaningful data from being measured above the flash point.

Figure 4 shows static pressure traverses measured in ST-1 before (Run 1) and after (Run 7) the flow period. Figure 5 shows corresponding static temperature data. At the

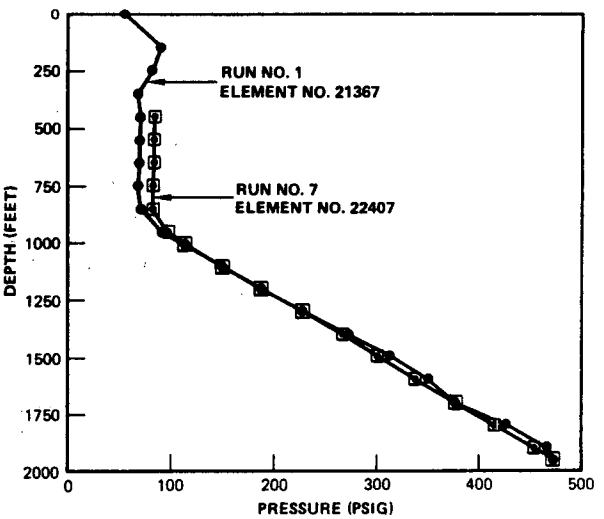


FIGURE 4. MAKUSHIN ST-1 UNALASKA ISLAND STATIC PRESSURE PROFILES

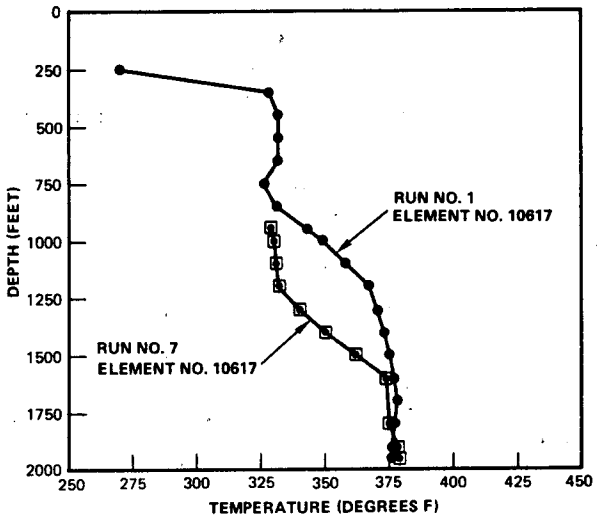


FIGURE 5. MAKUSHIN ST-1 UNALASKA ISLAND STATIC TEMPERATURE PROFILES

selected bottomhole datum of 1,900 feet, a substantially subhydrostatic initial pressure of 478 psig was measured. After the flow, element No. 21367 returned to 473 psig, which is essentially the same as the initial pressure within the rated accuracy of the instrument. However, element No. 22407 was lower by about 20 psig. This element (No. 22407) suffered severe buffeting in the two-phase zone on its initial run into the well while flowing (Run 3) and is suspect in all its subsequent measurements (even though it recalibrated "OK" after the test). Both temperature runs are in reasonable agreement with a bottomhole temperature of 379°F at 1,900 feet.

The most striking feature of the static surveys is the presence of a gas zone above 900 feet, both before and after the flow. Steam apparently refluxes up to about 300 feet, with a noncondensable gas (> 95% CO_2) "cap" above that. A maximum stable shut-in wellhead pressure of 136 psig has since been measured (two months later). This can only be attributable to noncondensable gas evolution from the shallow dry steam zone, inasmuch as the noncondensables measured in the flowing fluid were extremely low (<300 ppm). Apparent differences in the gas zone pressure between runs may either be attributable to the erratic response of the elements in this low pressure range, to variable shut-in times, or to slight pressure leak-off at the lubricator packing upon initiation of each run.

Two additional features of the static temperature surveys deserve comment. The cooling anomaly in Run 1 at about 700 feet probably reflects the continuous loss of drilling fluids to the lost circulation zone at 672 feet. The apparent cooling in the wellbore above 1,600 feet after the flow (Run 7) is extremely puzzling. Flashing was always above 1,000 feet as shown by the existence of liquid gradients in the wellbore during flow from T.D. to at least this depth.

The test rate/wellhead pressure history is shown on Figure 6 along with the downhole pressures measured at the 1,900-foot datum throughout the test. Wellhead pressure declined from 108 psig to a stable 36 psig within 15 minutes of opening the well. The rate stabilized at 47,000 lb/hr in the same 15-minute period. Calculations showed that at this rate, the well was limited by reaching critical mass velocity at the orifice. Only minor perturbations associated with running the Amerada instruments in and out were experienced thereafter. The flowing pressure measured at 1,900 feet several hours after opening the well was stable. The absolute value of the indicated drawdown of 25 to 30 psig is suspect (element No. 22407), however, because (as previously noted) the element was possibly damaged during the run-in through the two-phase zone and later returned to a "static" value which was about 20 psig low. The same element 19 hours later again indicated stability, but 5 psig higher.

Upon lowering the rate to 34,700 lb/hr, the wellhead pressure rose to 52 psig within five minutes and was stable until shut in. The downhole pressure showed no change for over an hour after the rate change and then went down about one psig rather than up (No. 22407). While the absolute pressure magnitudes are suspect, both pressure elements also exhibited this phenomena of declining pressure upon shut-in. Both elements exhibit similar character during the buildup, first declining one to two hours after shut-in, then flattening and then rising slowly for many hours, with a curious more rapid rise in the last three hours. The static survey a day later showed that no further pressure increase had occurred.

PRESSURE/FLOW "ANALYSIS"

Any analysis of the transient pressure data described above would be speculative at best at this stage because: (1) the pressure drawdown achievable from this reservoir with a three-inch wellbore is apparently slight; (2) the response of element No. 22407 is suspect for the reasons previously mentioned; (3) the apparently valid response of element No. 21367 is within the range of its rated accuracy (i.e., ±8 psig); and (4) some limited communication between the shallow steam zone and the main liquid reservoir (1,946-49 feet) exists, at least at the wellbore, and may be influencing the apparent responses (e.g., crossflow or high compressibility steam cap).

Nonetheless, the data from element No. 21367 should be analyzable in principle, and may actually represent a valid reservoir response. At a minimum, it is possible to calculate a productivity index (PI) and, from it, a permeability-thickness (kh) based on a porous media, radial flow model as follows:

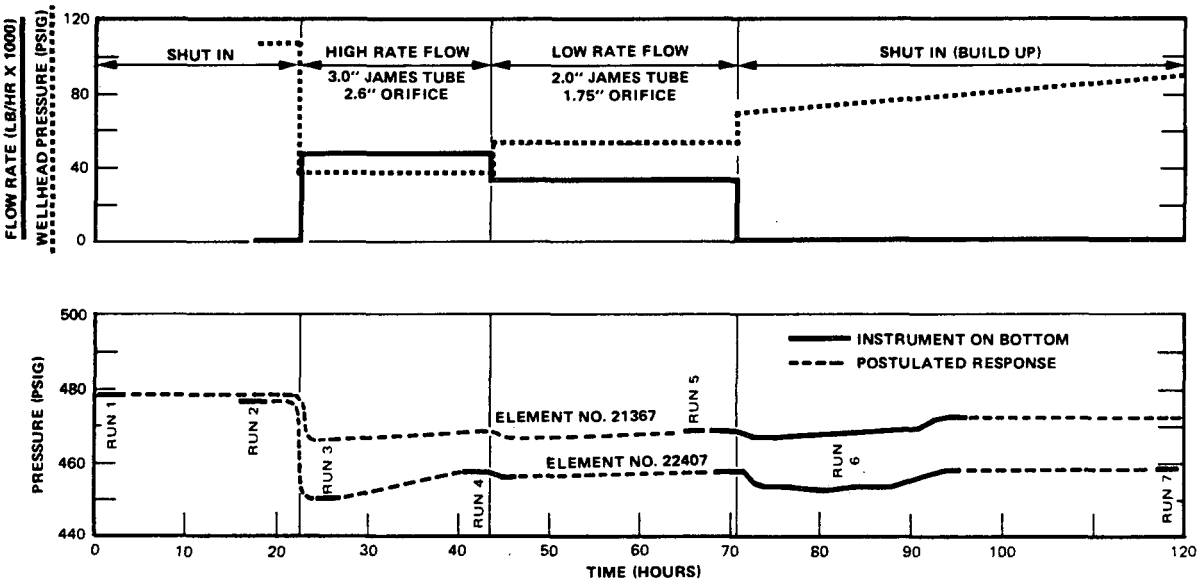


FIGURE 6. MAKUSHIN ST-1 UNALASKA ISLAND FLOW TEST HISTORY AND PRESSURE AT 1900 FEET (8/31/83 THROUGH 9/5/83)

$$PI = \frac{q}{P_i - P_f} = \frac{kh}{(10.21)\, B\mu\, \ln (re/rw)}$$

Where:

q = 34,700 lb/hr
(flow rate)

$P_i - P_f$ = 478-468 psig = 10 psig
(initial pressure-flowing pressure)

B = 1.14
(formation volume factor)

μ = 0.14 cp
(viscosity)

ln re/rw = 9 (40-acre radial drainage assumed)
(ratio of effective drainage radius to wellbore radius)

$$PI = 3,470 = \frac{kh}{14.67}$$

kh = 50,900 md-ft

A linear flow model may be more appropriately applied to the Makushin fractured reservoir, but possible interpretations are highly sensitive to assumed fracture dimensions which are unknown. Attempts at matching/analysis of the buildup data employing conventional type curves, etc., were unsuccessful.

It must be concluded that either the reservoir response is exceedingly complex, or that the instrumentation sensitivity/accuracy is inadequate for this application. It is intended that testing over a longer period during the summer of 1984 will be performed employing a quartz crystal pressure transducer and capillary tube in order to at least resolve the instrumentation ambiguities.

POWER POTENTIAL

The estimation of individual well power potential for commercial operations requires the fundamental assumption that an extensive reservoir can be represented by the fluid properties, initial pressure, temperature, and productivity index derived from the slim hole data. Given this as a bases, then a wellbore flow model yielding wellhead pressure vs rate must first be validated against the measured slim hole conditions. Once a match is achieved, then wellhead pressure vs rate curves for various commercial-size wellbore configurations may be generated and related to appropriate power cycles with some degree of confidence.

The flow simulator used for this study was developed by Intercomp[3] and has been used extensively by the industry for geothermal and geopressured wellbore flow calculations for several years. It is a commercially available, vertical, multiphase flow simulator which incorporates treatment for variable well diameter with depth, heat losses, and non-condensable gases. The "nominal" commercial well conditions arrived at were as follows:

Initial Pressure	= 478 psig @ 1,900 feet
Bottomhole Temp.	= 379°F @ 1,900 feet
Salinity	= 6,000 ppm TDS
CO_2 Content	= 300 ppm
Productivity Index	= 3,470 lb/hr/psi
13-3/8 inch casing to	1,750 feet
12-1/4 inch open hole to	1,900 feet

Using these conditions, a cross-plot of a double flash steam cycle and the simulator generated curve for wellhead pressure vs flow rate was constructed. An optimum output of 870,000 lb/hr at 60 psia wellhead pressure was found to generate six gross megawatts of power

(Figure 7). Thus, two commercial-size wells could supply the 10 megawatts desired to service the current needs of Dutch Harbor and Unalaska.

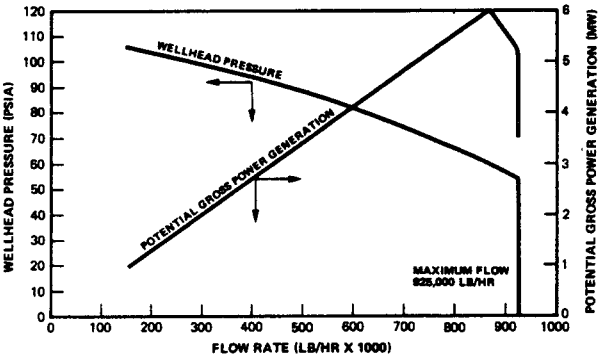


FIGURE 7. COMMERCIAL SIZE WELL – FLOW RATE vs. WELLHEAD PRESSURE AND POTENTIAL POWER GENERATION

CONCLUSIONS

The Unalaska geothermal exploration program has been very successful thus far. Geological, geophysical, and geochemical surveys of the Makushin area resulted in the siting of three temperature gradient holes in 1982. Two of these holes provided strong evidence of a geothermal resource while the third defined a southern limit. The resource model subsequently developed was then tested with the drilling of a deep slim hole production well in the summer of 1983.

Results from the slim hole confirmed the basic model of a shallow steam zone overlying a liquid-dominated reservoir in fractured diorite. Temperature (379°F) was about 10°F lower than predicted, but the well barely penetrated the top of the reservoir at 1,949 feet. Planned deepening next summer (1984) may yield substantially higher temperatures if some of the geochemical indicators are valid.

Flow testing of the well proved that the reservoir is potentially highly productive, with only three feet of fractured interval (at the wellbore) producing 47,000 lb/hr through three inch pipe and little reservoir pressure drawdown. Unfortunately, problems with insensitive and/or inaccurate pressure instrumentation in the unexpectedly low pressure range encountered does not allow rigorous analysis. A "ball park" productivity index of 3,470 lb/hr/psi and permeability-thickness of 50,900 md-ft can be calculated. Additional testing next summer with improved instrumentation is expected to resolve present ambiguities.

Assuming the conditions encountered in the slim hole are representative of an extensive reservoir, the power potential of a commercial-size well is estimated to be in the range of six megawatts. Given the relatively small requirement for power on Unalaska (currently about 11 megawatts) and the estimated seven square mile resource extent, there is strong indication even at this early stage that a more than adequate geothermal power facility can be developed.

REFERENCES

1. Isselhardt, C. F., et al (1983), "Temperature Gradient Hole Results from Makushin Geothermal Area, Unalaska Island, Alaska," Geothermal Resources Council Transactions, Vol. 7, October 1983, pgs. 95-98.

2. Isselhardt, C. F., et al (1983) "Geothermal Resource Model for the Makushin Geothermal Area, Unalaska Island, Alaska," Geothermal Resources Council Transactions, Vol. 7, October 1983, pgs. 99-102.

3. James, Russell (1980), "A Choke-Meter for Geothermal Wells Which Measures Both Enthalpy and Flow," Geothermal Energy, May 1980, pgs. 27-30.

4. "Vertical Steam-Water Flow in Wells With Heat Transfer," Scientific Software - Intercomp, February 1982.

ACKNOWLEDGEMENTS

The authors wish to thank the Alaska Power Authority for their support and numerous members of Republic's staff for their input to this report.

Proceedings Ninth Workshop Geothermal Reservoir Engineering
Stanford University, Stanford, California, December 1983
SGP-TR-74

WELL TEST ANALYSIS IN NATURALLY FISSURED, GEOTHERMAL RESERVOIRS WITH FRACTURE SKIN

A.F. Moench

U.S. Geological Survey, Menlo Park, CA

ABSTRACT

Mineral deposition or alteration is commonly found at fracture-block interfaces in fissured, geothermal reservoirs. In response to pressure reduction in the fissures such mineralization, if less permeable than the matrix rock, will retard the flow of fluid from the blocks to the fissures and is termed fracture skin in this paper. The problem of fluid flow to a production well in a double-porosity reservoir with fracture skin was analyzed theoretically. One of the findings of the analysis was that fully transient block-to-fissure flow can be approximated by pseudo-steady state flow if fracture skin permeability is sufficiently low. Type curves generated by numerical inversion of Laplace transform solutions are used to illustrate this effect. They are also used to corroborate the results of a finite-difference model of steam transport to a well in a naturally fissured, geothermal reservoir with fracture skin.

INTRODUCTION

Geothermal reservoirs are commonly composed of fractured rocks that have been subjected in varying degrees to hydrothermal alteration. Quartz, calcite, and other minerals are often found lining or filling fractures in surface outcrops and well-core samples. Interconnected, highly permeable fissures serve as primary conduits for mineral-charged water circulating naturally in geothermal reservoirs. Such fluids, when not in chemical equilibrium with the wall rock, alter or deposit minerals at fissure-block interfaces. The particular products of hydrothermal alteration or deposition depend upon physical and chemical parameters that vary from place to place. Types of products that occur in geothermal systems are described by Ellis and Mahon (1977). Such alteration products are termed "fracture skin" in this paper and are assumed to impede the free exchange of fluid between blocks and fissures.

Naturally fissured reservoirs are often treated mathematically as double-porosity systems whereby primary porosity blocks of low permeability and high storage capacity are separated by secondary porosity fissures of high permeability and low storage capacity. Two approaches have been taken to problems of well-test analysis in double-porosity reservoirs: one approach assumes that flow from blocks to fissures occurs under pseudo-steady state conditions and the other assumes fully transient conditions. In the pseudo-steady state approximation, one neglects divergence of flow within the primary porosity blocks. Therefore, this approach lacks the firm theoretical foundation of the transient-flow assumption. However, well-test data exist that support both approaches (Bourdet and Gringarten, 1980; Streltsova, 1983).

Moench (1983) has reviewed the theory of flow in double-porosity reservoirs. By introducing fracture skin to the theoretical analysis, he showed that the pseudo-steady state approximation is a special case of the theory that is based upon transient block-to-fissure flow. For large fracture skin it was shown graphically that the divergence of the flow in the blocks is small and thus the pseudo-steady state approximation is reasonable. In this paper dimensionless pressure responses obtained by numerical inversion of Laplace transform solutions are used to illustrate the effects of fracture skin. Results are compared to the response predicted by a finite-difference model described by Moench and Denlinger (1980) that was modified to incorporate fracture skin.

MATHEMATICAL MODELS

De Swaan (1976) proposed the use of either slab-shaped or sphere-shaped blocks to represent the geometry of the matrix rocks in a double-porosity reservoir and presented the equations that describe the transient flow of fluids in the fissures and blocks. In this study both these geometries are used.

Figure 1 shows a schematic diagram of a thin but finite-thickness skin of low-permeability material on the surface of a hypothetical block in a naturally fractured reservoir. It is assumed that the permeability of the skin is less than that of the block and possesses no storage capacity. Flux of fluid from the block to the fissure is assumed to be perpendicular to the interface and to obey Darcy's law. By continuity at the block-fissure interface

$$k_s \frac{(p')_{y=b'} - p}{b_s} = -k'\left(\frac{\partial p'}{\partial y}\right)_{y=b'} \quad (1)$$

where y is a generalized coordinate with its origin at the center of the block. Symbols are defined in the nomenclature and in Figure 1.

In accordance with commonly used definitions, dimensionless pressure is defined as

$$p_D = \frac{2\pi kH}{q\mu}(p_i - p) \quad (2)$$

dimensionless time is defined as

$$t_D = \frac{kt}{\mu\phi c_t r_w^2} \quad (3)$$

and dimensionless distance is defined as

$$r_D = r/r_w \quad (4)$$

Because of the low permeability of the matrix rock, the problem of flow to a production well is usually solved by assuming fluid enters the wellbore only through fissures and not through matrix rock. The mathematical development requires that gravitational effects are negligible and that pressure in the reservoir is initially uniform throughout. Further details and complete boundary value problems are given by Moench (1983). Assuming radial flow to a fully penetrating well discharging at a constant rate from an infinitely extensive double-porosity reservoir confined above and below by impermeable formations, the Laplace transform, line-source solution for dimensionless pressure drawdown in the fissure system is

$$\bar{p}_D = \frac{1}{s} K_o(r_D\sqrt{s + \bar{q}_D}) \quad (5)$$

where, for slab-shaped blocks,

$$\bar{q}_D = \frac{\gamma^2 m \tanh(m)}{1+S_F m \tanh(m)} \quad (6)$$

and, for sphere-shaped blocks,

$$\bar{q}_D = \frac{3\gamma^2[m\coth(m)-1]}{1+S_F[m\coth(m)-1]} \quad (7)$$

where $S_F = \frac{k'b_s}{k_s b'}$ (8)

The parameter m is defined as

$$m = \frac{\sqrt{\sigma s}}{\gamma} \quad (9)$$

where

$$\sigma = \frac{\phi' c_t'}{\phi c_t} \quad (10)$$

$$\gamma^2 = \left(\frac{r_w}{b'}\right)^2 \frac{k'}{k} \quad (11)$$

If the dimensionless fracture skin, S_F, is zero these solutions reduce to previously published solutions (see, for example, Deruyck and others, 1982; Gringarten, 1982).

The pressure response predicted by models that assume sphere-shaped blocks is very similar to that obtained by assuming slab-shaped blocks. Examination of (6) and (7) reveals that for $S_F=0$ and at early time, $\bar{q}_D=\gamma\sqrt{\sigma s}$ for slab-shaped blocks, and $\bar{q}_D= 3\gamma\sqrt{\sigma s}$ for sphere-shaped blocks. Hence at early time, the response due to sphere-shaped blocks will be the same as that due to slab-shaped blocks if the permeability of the sphere-shaped blocks is reduced by a factor of nine (see Figure 2). At late time the responses will be the same by virtue of the fact that $\bar{q}_D=\sigma s$ in (6) and (7).

For the special case in which dimensionless fracture skin is large and m is small (6) becomes

$$\bar{q}_D = \frac{\gamma^2 m^2}{1+S_F m^2} \quad (12)$$

and (7) becomes

$$\bar{q}_D = \frac{3\gamma^2 m^2}{3+S_F m^2} \quad (13)$$

The expressions (12) and (13) when combined with (5) can be shown to be identical to the commonly used pseudo-steady state, block-to-fissure flow models for double-porosity systems. It is necessary, however, to substitute fracture-skin permeability for block permeability in the pseudo-steady state flow model (Moench, 1983). The dimensionless parameter, λ, defined by Warren and Root (1963) to relate block and fissure system permeability, becomes

$$\lambda = \frac{k_s r_w^2}{k\, b' b_s} = \frac{\gamma^2}{S_F} \qquad (14)$$

for slap-shaped blocks, and

$$\lambda = \frac{3k_s r_w^2}{k\, b' b_s} = \frac{3\gamma^2}{S_F} \qquad (15)$$

for sphere-shaped blocks. Substitution of these expressions into (12) and (13) yields

$$\bar{q}_D = \frac{s}{1/\sigma + s/\lambda} \qquad (16)$$

Although expressed in different notation, (16) and (5) combine to form the same solution as given by Kazemi and others (1969) which is an extension for interference tests of the Warren and Root model.

For the purpose of analyzing production-well data it is often necessary to include effects of wellbore storage and skin. In this paper, for the purpose of simplicity, wellbore skin is neglected. The Laplace transform solution that included effects of wellbore storage but neglects wellbore skin is

$$\bar{p}_D = \frac{K_o(r_D x)}{s\left[sC_D K_o(x) + xK_1(x)\right]} \qquad (17)$$

where $x = \sqrt{s+\bar{q}_D}$

The wellbore storage parameter is defined in the usual manner as

$$C_D = \frac{C}{2\pi r_w^2 \phi c_t H} \qquad (18)$$

TYPE CURVES

The Laplace transform solutions given by (5) and (17) are easily inverted with the Stehfest (1970) algorithm. Figure 2 shows a comparison of line-source type curves for slab-shaped blocks and sphere-shaped blocks, using (5)-(7), in the absence of fracture skin. Only for large values of $(r_D\gamma)^2$ do the type curves for the two geometries deviate from one another significantly. Also shown in Figure 2 and in the figures that follow are two dashed curves that are the Theis curve (σ=0) and the Theis curve shifted to the right by a factor of $1+\sigma$. These can be obtained from (5) by letting $\bar{q}_D = \sigma s$.

Figure 3a shows line-source type curves for different values of S_F for slab-shaped blocks. The same curves plotted on semi-logarithmic paper are shown in Figure 3b. In the absence of fracture skin Figure 3b shows the expected semi-logarithmic half slope during the intermediate-time transition period. As S_F increases the response approaches that expected for pseudo-steady state, block-to-fissure flow.

Figure 4 shows a comparison of the type curves in Figure 3a with the corresponding curves for the pseudo-steady state approximation. The latter were obtained using (5) and (16) where $r_D^2\lambda = (r_D\gamma)^2/S_F$, as required by (14) for slab-shaped blocks. As S_F increases the two type curves approach one another. A similar correspondence can be shown for sphere-shaped blocks.

Similar type curves were used by Moench (1983) to analyse groundwater pumping-well and observation-well data from the fractured, hydrothermally altered, volcanic rock terrane of the Nevada Test Site. The data compare favorably with the theory for double-porosity reservoirs with fracture skin.

COMPARISON WITH FINITE-DIFFERENCE MODEL

The finite-difference model for steam transport in a naturally fissured, vapor-dominated, reservoir described by Moench and Denlinger (1980) was modified to incorporate fracture skin at the surface of the slab-shaped blocks. It was assumed that pore water and adsorbed water were absent so that the steam behaved as a noncondensable gas. In the absence of vaporization or adsorption the finite-difference model becomes isothermal. The well discharge rate was made sufficiently small so that the pressure changes that occur in the fissures and blocks do not introduce nonlinear effects. Since the finite-difference model was designed for slab-shaped blocks and includes wellbore storage the comparison with the analytical model is made using (6) and (17).

For steam transport, assuming rock compressibility is negligible compared with steam compressibility, the dimensionless parameters, are the following:

$$p_D = \frac{2\pi k_f b M_w}{q_f \mu Z R T}\left(p_i^2 - p^2\right)$$

$$t_D = \frac{k_f t}{\mu \phi_f \beta r_w^2}$$

$$\gamma^2 = \left(\frac{r_w}{b'}\right)^2 \frac{k'b'}{k_f b}$$

$$\sigma = \frac{\phi' b'}{\phi_f b}$$

$$C_D = \frac{\pi r_w^2 L}{2\pi r_w^2 \phi_f \frac{b}{b'} \beta H}$$

$$= \frac{L}{4\phi_f bn}$$

where $n = \frac{H}{2b'}$

Figures 5 and 6 show the results obtained with the finite-difference model using the reservoir parameters listed in Table 1. Results obtained by numerical inversion of the Laplace transform solution, also shown in Figures 5 and 6, appear to corroborate the results obtained with the finite-difference model.

CONCLUSIONS

The graphical results presented in Figures 2-4 show that fracture skin can have a profound influence on the pressure response in a naturally fractured reservoir. They also show that the prevailing theories of flow that assume either transient or pseudo-steady state, block-to-fissure flow can be unified by incorporating fracture skin in the mathematical development.

Because of fracture skin, data plotted on semi-logarithmic paper may appear to have an intermediate-time slope of between zero and one-half that of the late-time slope. Hence caution is urged in the use of the standard semi-logarithmic, straight-line method for evaluating the permeability-thickness product. This is especially true if the test is too short for the late-time portion of the pressure response to manifest itself.

NOMENCLATURE

$2b$	average aperture of fissure
$2b'$	average fracture spacing
b_s	average thickness of fracture skin
C	wellbore storage coefficient
C_D	dimensionless wellbore storage
c_t	fissure system compressibility
c_t'	block system compressibility
H	reservoir thickness
k	$[=k_f b/b']$ fissure system permeability
k_f	$[=(2b)^2/12]$ average fissure permeability
k'	block system permeability
k_s	average fracture skin permeability
K_o	modified Bessel function of the first, second and order zero
K_1	modified Bessel function of the first, second and order unity
L	length of wellbore
m	defined by (9)
M_w	molecular weight of water
n	number of producing fissures
p	pressure in fissure
p'	pressure in block
p_D	dimensionless pressure in fissure
$\bar{p}_D$	Laplace transform of p_D
p_i	initial pressure
q	total well discharge rate
q_f	discharge rate to well from an average fissure
q_D	source term for flow from blocks to fissures
$\bar{q}_D$	Laplace transform of q_D
r	radial distance
r_w	effective radius of pumped well
R	gas constant
s	Laplace transform variable
S_F	dimensionless fracture skin defined by (8)
t	time
T	temperature
y	generalized block coordinate
Z	steam compressibility factor (deviation from ideal gas)
λ	parameter defined by Warren and Root (1963) and by (14) and (15)
μ	viscosity of the fluid
ϕ	$[\phi_f b/b']$ fissure system porosity
ϕ_f	average fissure porosity
ϕ'	block system porosity
σ	defined by (10)
γ	defined by (11)
β	steam compressibility

REFERENCES

Bourdet, D., and A.C. Gringarten, Determination of fissure volume and block size in fractured reservoirs by type-curve analysis, Unpublished preprint, SPE-9293, presented at 55th Annual Fall Technical Conference and Exhibition of the Society of Petroleum Engineers of AIME, Dallas, TX, Sept. 21-24, 1980.

Deruyck, B.G., D.P. Bourdet, G. DaPrat, and H.J. Ramey, Jr., Interpretation of interference tests in reservoirs with double porosity behavior - theory and field examples, Unpublished preprint, SPE-11025, presented at 57th Annual Fall Technical Conference and Exhibition of Society of Petroleum Engineers of AIME, New Orleans, LA, Sept. 26-29, 1982.

Ellis, A.J., and W.A.J. Mahon, Chemistry and Geothermal Systems, Academic Press, Inc., New York, 392 pp., 1977.

Gringarten, A.C., Flow-test evaluation of fractured reservoirs, in Recent Trends in Hydrogeology, Geol. Soc. Amer., Special Paper 189, 237-263, 1982.

Kazemi, H., M.S. Seth, and G.W. Thomas, The interpretation of interference tests in naturally fractured reservoirs with uniform fracture distribution, Trans., AIME, 246: Soc. Petr. Eng. J.. 463-472, Dec. 1969.

Moench, A.F., Double-porosity models for a fissured groundwater reservoir with fracture skin, Water Resour. Res., in review, 1983.

Moench, A.F., and R. Denlinger, Fissure-block model for transient pressure analysis in geothermal steam reservoirs, Proc. sixth workshop on Geothermal Reservoir Engineering, Stanford University, Stanford, CA, p. 178-187, 1980.

Streltsova, T.D., Well pressure behavior of a naturally fractured reservoir, Soc. Petr. Eng. J., 769-780, 1983.

Stehfest, H., Numerical inversion of Laplace transforms, Commun. ACM, 13(1), 47-49, 1970.

deSwaan-O.,A., Analytic solutions for determining naturally fractured reservoir properties by well testing, Trans., AIME, 261; Soc. Petr. Engr. J. 117-122, 1976.

Warren, J.E., and P.J. Root, The behavior of naturally fractured reservoirs, Trans., AIME, 228; Soc. Petr. Engr. J., 3(3), 245-255, Sept. 1963.

Table 1. Parameters Used in Simulations*

2b	0.02 cm
b'	1640 cm
b_s	0.1 cm
L	10^5 cm
H	0.492×10^5 cm
r_w	16 cm
n	15
ϕ_f	0.5
ϕ'	0.0005
k_f	3.3×10^{-5} cm^2
k'	10^{-12} cm^2 (0.1 millidarcys)
k_s	10^{-17} and 10^{-16} cm^2 (1 and 10 nanodarcys)
kH	9.84×10^{-6} cm^3 (9.84 darcy-meters)
q_f	2.77 g/s
T	234°C
p_i	30 bars

*parameters not listed are known properties of water at prevailing temperature and pressure.

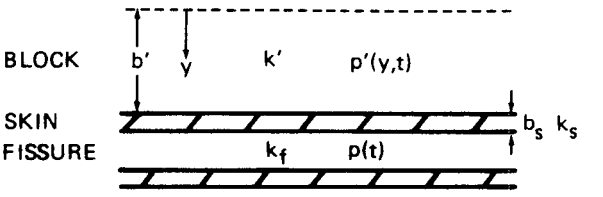


Figure 1. Schematic diagram of block and fissure with fracture skin.

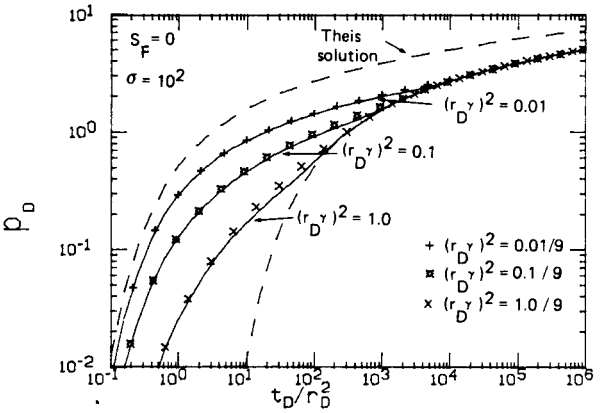


Figure 2. Line-source, type curve comparisons for slab-shaped blocks (solid lines) and sphere-shaped blocks (symbols) without fracture skin.

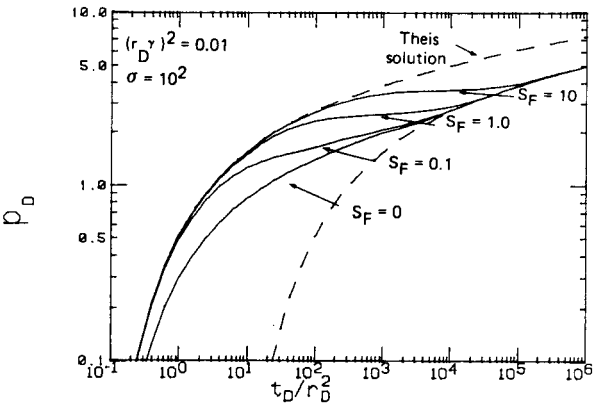


Figure 3a. Line-source type curves for transient flow from slab-shaped blocks with fracture skin

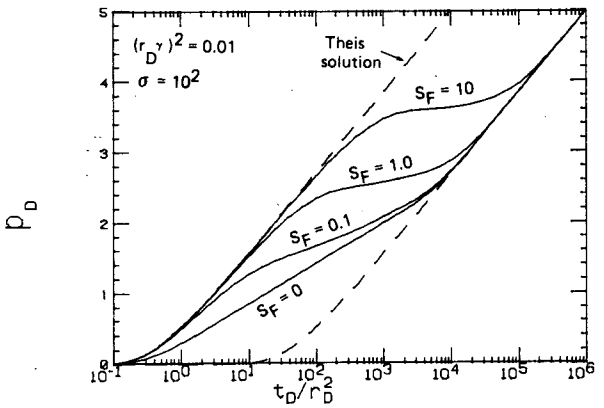


Figure 3b. Semi-logarimthmic plot of Figure 3a.

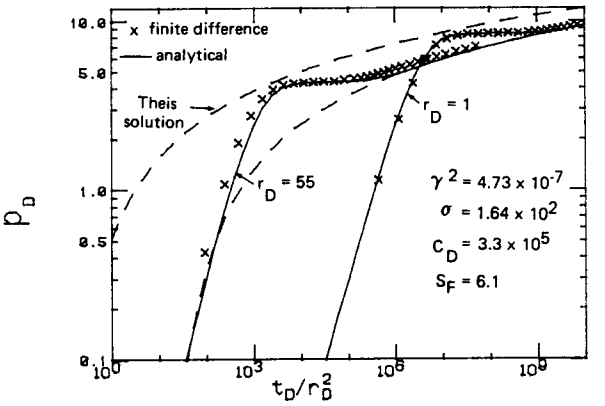


Figure 5. Comparison of the finite-difference model for simulated pressure drawdown in a dry-steam, double-porosity reservoir with the analytical model for the indicated parameters.

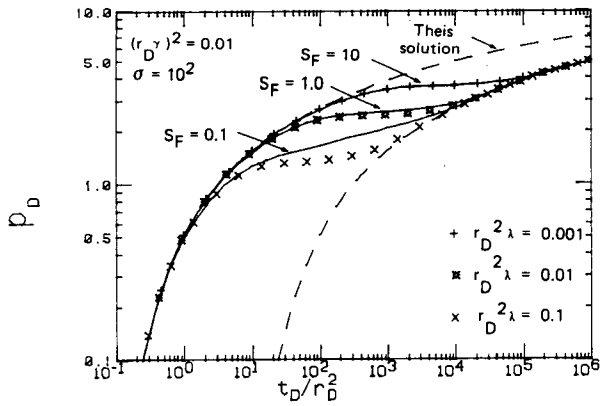


Figure 4. Comparison of type curves for transient flow from slab-shaped blocks with fracture skin (solid lines) with corresponding type curves for the pseudo-steady state flow model (symbols).

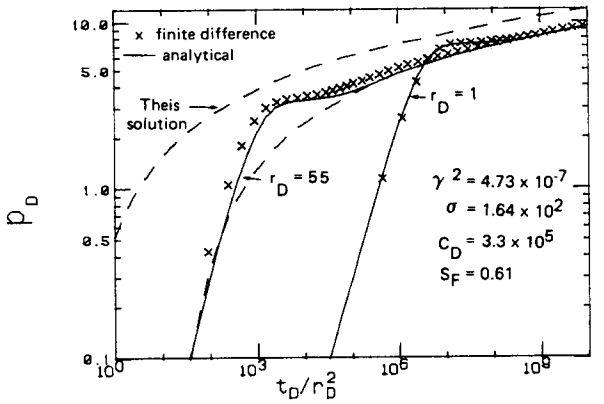


Figure 6. Comparison of the finite-difference model for simulated pressure drawdown in a dry-steam, double-porosity reservoir with the analytical model for the indicated parameters.

Proceedings Ninth Workshop Geothermal Reservoir Engineering
Stanford University, Stanford, California, December 1983
SGP-TR-74

SLUG TEST DATA ANALYSIS IN RESERVOIRS WITH DOUBLE POROSITY BEHAVIOUR

Khalid Mateen and Henry J. Ramey Jr.

Stanford University

ABSTRACT

Pressure analysis for a slug test which corresponds to the flow period of a Drill Stem test is extended to wells in reservoirs with double-porosity behaviour.

Solutions are obtained for either pseudo-steady state or transient interporosity flow. The distinctive specific features of both solutions are identified. Results presented are applicable to both naturally-fractured and layered reservoirs with the more permeable layer connecting to the wellbore.

Type curves based on the pseudo-steady or transient interporosity flow are presented. These type curves are similar to the existing homogenous single layer type curve with addition of interporosity flow lines indicating double-porosity behaviour.

INTRODUCTION

The slug test problem is posed by a formation with a pressure which is, at most, great enough to lift a column of reservoir fluid just to the surface of the earth. The initial production rate is high and gradually declines as the accumulating fluid in the drill string increases the back pressure.

The slug test was introduced in ground water hydrology by Ferris and Knowles in 1954. An analogous heat conduction test was reported by Jaeger (1956). In 1967, Cooper et al. presented a solution for a well of a finite diameter and showed the line source approximation of Ferris and Knowles to be valid for large times.

Neglecting inertial and friction effects the liquid column is assumed to be in static equilibrium with the wellbore. Slug test formulations based on liquid column height and that based on bottom hole pressure were separately proposed. Liquid column height is measured in ground water hydrology, whereas bottom hole pressure is measured in petroleum industry.

In 1972, Ramey and Agarwal presented a detailed derivation for the DST problem with skin effect. These authors obtained a solution to the problem in the form of an inversion integral by Laplace transformation. Ramey, Agarwal and Martin (1975) correlated the solution for DST problem using a wellbore storage coefficient and dimensionless time based on effective wellbore radius, a technique used by Earlougher and Kersh (1974) in conventional well testing. More detail on pertinent literature has been presented by Mateen(1983).

Extensive work has been done in recent years to explain the transient pressure behaviour

of naturally-fractured or fissured reservoirs. Such reservoirs have homogenously distributed regions of primary and secondary porosity. One medium(fissure) presents a high conductivity and drains the reservoir fluid to the well, the other(matrix) has a much lower conductivity and feeds only to the fissure medium. They are termed two-porosity reservoirs. Naturally-fractured reservoirs and layered reservoirs with only the more permeable layer conducting to a wellbore exhibit the same double porosity behaviour.
Warren and Root(1963) mathematically modelled
such reservoirs. They assumed pseudo-steady interporosity flow and showed interporosity flow parameter λ, and a storativity ratio ω, were sufficient to characterize the flow model. In this study diffusivity equations for matrix and fissures were formulated and combined assuming either pseudo steady state or transient interporosity flow.

The characteristic double-porosity diffusion equation was then coupled in Laplace space with wellbore pressure through inner boundary conditions of a steady- state pressure drop occuring at the sand face (skin effect), and a wellbore storage effect. Type curves based on either pseudo-steady state or transient interporosity flow were developed.

PROBLEM SOLUTION

The details of the problem solution are presented by Mateen (1983). Only the reults will be discussed here. However it is necessary to define useful dimensionless groups, they are defined as:

$$P_{wfD} = \frac{P_i - P_{wf}}{P_i - P_o} \quad \text{.....(1)}$$

$$t_D = \frac{k_f t}{[\ (\phi Vc_t)_f + (\phi Vc_t)_m\ ]\ \mu r_w^2} \quad (2)$$

$$r_D = \frac{r}{r_w} \quad \text{.....(3)}$$

$$C_D = \frac{C}{2\pi h[\ (\phi Vc_t)_f + (\phi Vc_t)_m] r_w^2} \quad \text{..(4)}$$

$$\omega = \frac{(\phi Vc_t)_f}{[\ (\phi Vc_t)_f + (\phi Vc_t)_m]} \quad \text{...(5)}$$

$$\frac{t_D}{C_D} = \frac{2\pi k_f h\ \Delta t}{\mu\ C} \quad \text{....(6)}$$

$$\lambda = \frac{\alpha\ k_f\ r_w^2}{k_m} \quad \text{...(7)}$$

where "α" is interporosity shape factor, defined by Warren and Root (1956) as

$$\alpha = \frac{4\ n\ (n+2)}{l} \quad \text{.....(8)}$$

where "n" is the number of normal subsets of fissures and "l" is a characteristic dimension of the matrix.

The behaviour at early and late times is that of a homogenous reservoir and corresponds to two different curves on the type curves introduced by Ramey et al.(1975). At intermediate times for the pseudo-steady interporosity flow model the pressure response depends on λe^{-2S}. At

intermediate times for transient interporosity flow the pressure response depends upon a dimensionless parameter β.

For slab-shaped matrix blocks, β is given by:

$$\beta = \frac{3\ C_D\ e^{2S}}{\lambda\ e^{-2S}} \qquad .....(9)$$

For spherically-shaped matrix blocks, β is equal to:

$$\beta = \frac{3\ C_D\ e^{2S}}{5\ \lambda\ e^{-2S}} \qquad ....(10)$$

Type Curve Analysis For Pseudo Steady State Interporosity Flow

The interporosity flow effect for a double-porosity reservoir with λe^{-2S} as the governing parameter is shown in Fig. 1

The corresponding pressure response in a Slug test for a well in double-porosity reservoir is therefore obtained by superposing the curves of early and late homogenous behaviour, with the curves of intermediate interporosity flow behaviour, and is presented in Fig. 2. A typical result for a wellbore pressure in a two porosity reservoir is given in Fig. 3. At early times, production comes from the fissure system with $C_D=C_{Df}$. As the matrix starts feeding into the fissures, pressure leaves the C_De^{2S} curve and follows λe^{-2S} curve, until production comes from the entire system. At this stage pressure follows a new C_De^{2S} with $C_D=C_{Df+m}$, below the first curve

Assuming (ϕhc_t) and the wellbore storage coefficient (C) are known, a semilog or a log-log type curve analysis of pressure response can yield all the system parameters. Transmissivity can be obtained from the time match, skin factor(S) from C_De^{2S} match, λ from λe^{-2S} match, and storativity ratio ω, from the ratio of C_De^{2S} value of last curve to C_De^{2S} value of the first curve. Determination of ω is not always possible, specially when pressure follows the transition curve from very early times.

Type Curve Analysis For Transient Model Interporosty Flow Model

As for the pseudo-steady state interporosity model, the mechanism of fluid flow in double-porosity reservoirs with transient interporosity flow involves three successive flow regimes. At early times, there is a homogenous system behaviour with only fissures contributing to the flow. At intermediate times, a transition occurs and the matrix contributes progressively. Response is described by one of the β curves in Fig. 4. At late times, the behaviour is again homogenous with both matrix and fissures contributing. A typical two-porosity case with the transient flow assumption is portrayed in Fig. 5. Type curves for the transient interporosity flow model are obtained by superposing curves of transition curves from Fig. 4 on the homogenous system type curves of Ramey et al.(1975)

A semi-log or a log-log type curve analysis can be used to evaluate reservoir parameters in the same way as for the pseudo-steady state model. However, during the transition period, pressure follows a curve corresponding to some β value. Determination of the interporosity flow parameter β, therefore, requires additional knowledge about the geometry of the matrix blocks.

Knowledge that either the reservoir is fissured or layered can be obtained through logging, or other geological evidences.

Pseudo Steady State Model as compared to Transient Interporosity Flow Model

Both the pseudo-steady state and transient models yields the same flow pattern: fissure-homogenous at early times, transition at intermediate times, and total-homogenous at late times.

The principal difference between the two models is the shape and duration of the transition curve. The difference is more pronounced on the left side of the type curve, that is for large values of λe^{-2S} Transition curves for the pseudo-steady state model in this range of time are steeper than for the transient inter-porosity flow model. This fact causes the transition duration to be shorter than for transient inter porosity flow model. Also the transition from the early and late time curves is less smooth than that for the transient model. For small values of λe^{-2S}, the pressure response of these two models becomes almost identical.

Results indicate that under certain ranges of values of ω and λ the double porosity effects are not distinguishable from those of a homogenous reservoir. Pressure in both pseudo steady state and transient interporosity flow models responds in a similar way to a given change in parameters ω and λ.

Nomenclature

c_t : total compressibility, atm
C : wellbore storage constant, cc/atm
C_D : dimensionless wellbore storage constant
h : formation thickness, cm
k_f : permeability of fissure, darcys
p_i : Initial pressure, psi
p_o : Cushion pressure, psi
p_{wf} : pressure in the fissure medium within the wellbore, atm
p_{wfD} : dimensionless pressure drop in the fissure medium within the wellbore
r : radial distance from the well, cm
r_w : radius of the wellbore, cm
S : dimensionless skin factor
t : time, sec
t_D : dimensionless time
V : ratio of volume of one porous system to bulk volume
α : interporosity shape factor, cm^2
β : interporosity flow group
λ : interporosity flow parameter
μ : viscosity, cp
ω : storativity ratio
ϕ : porosity of the medium, fraction

References

Cooper, H. H., Jr., Bredehoeft, J. D., and Papadopulous, I. S. : "Response of a Finite-diameter Well to Instantaneous Charge of Water", Water Resources Research (1967), Vol. 3, No. , 263-269.

Earlougher, R. C., Jr., and Kersch, K. M. : " Analysis of Short-Time Transient Test Data by Type Curve Matching", J. Pet. Tech. (July 1974), 793.

Ferris, J. G., and Knowles, D. B. : "The Slug Test for Estimating Transmissibility", U.S. Geol. Survey Ground Water Note 26, 1-7, 1954.

Ramey, H. J., Jr., and Agarwal, R. G. : "Annulus Unloading Rates as Influenced by Wellbore Storage and Skin Effect",Soc. Pet. Engrs. Jour., October, 1972, p-453

Ramey, H. J., Jr., Agarwal, R. G., and

Martin, I. : "Analysis of 'Slug Test' or DST Flow Period Data", Can. Pet. Jour., July, 1975.

Warren , J. E., and Root, P. J.: "The Behaviour of Naturally Fractured Reservoirs" Soc. Pet. Eng. J., (Sept., 1963), 245-255.

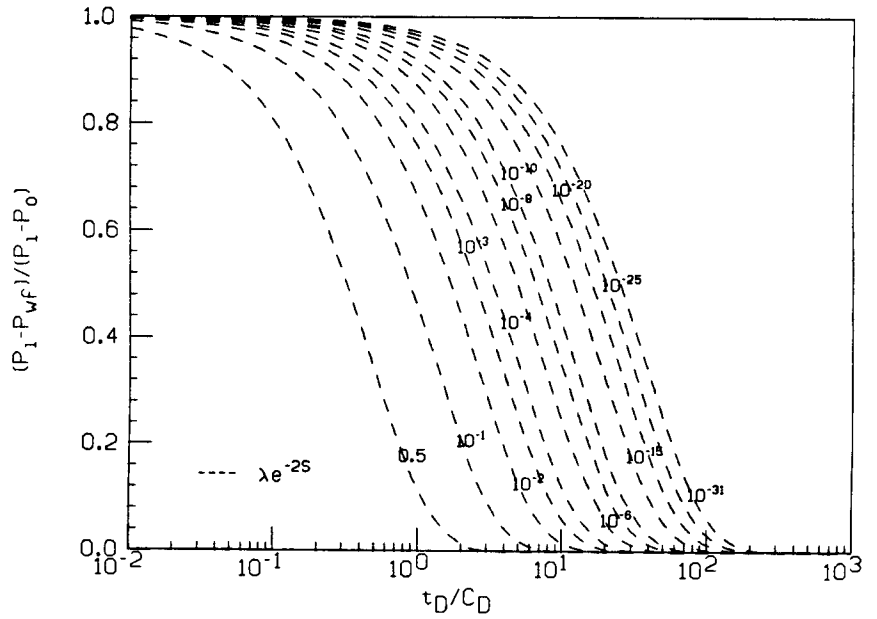


Figure 1: Transition pressure in double porosity reservoir (PSS) (Semi-log)

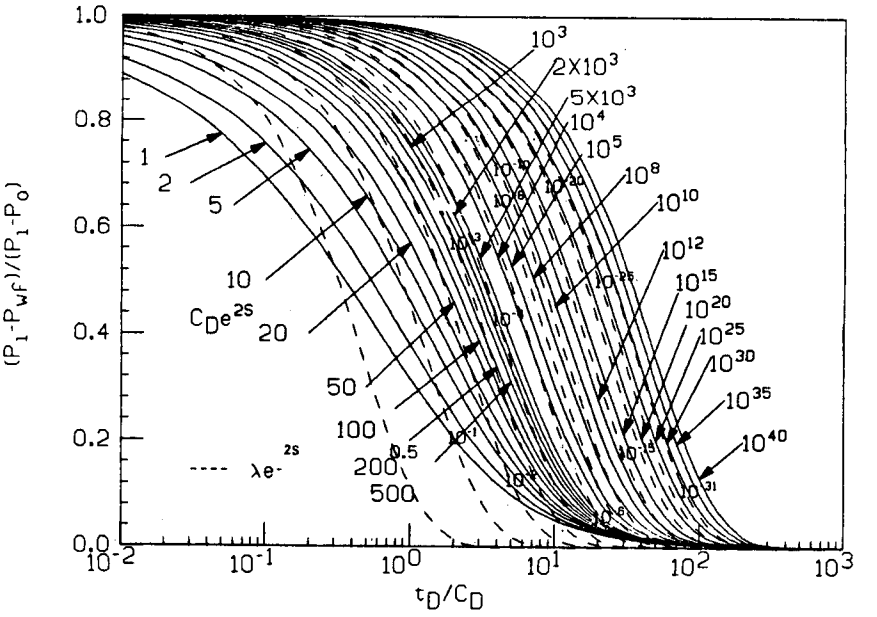


Figure 2: Semi-log double porosity type curve (PSS)

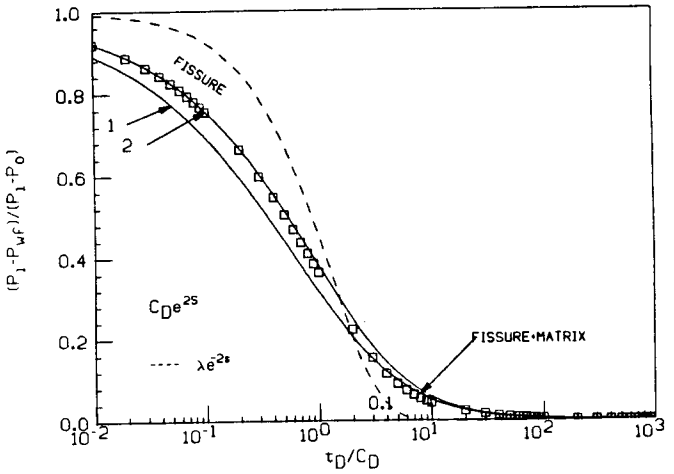


Figure 3: Example of semi-log double porosity behavior (PSS)
($\omega = 0.5$, $\lambda * e^{-2S} = 0.1$)

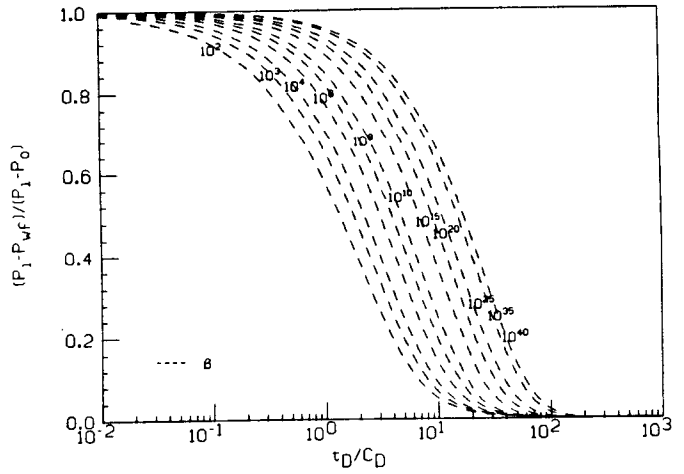


Figure 4: Transition pressure in double porosity reservoir
Transient Model

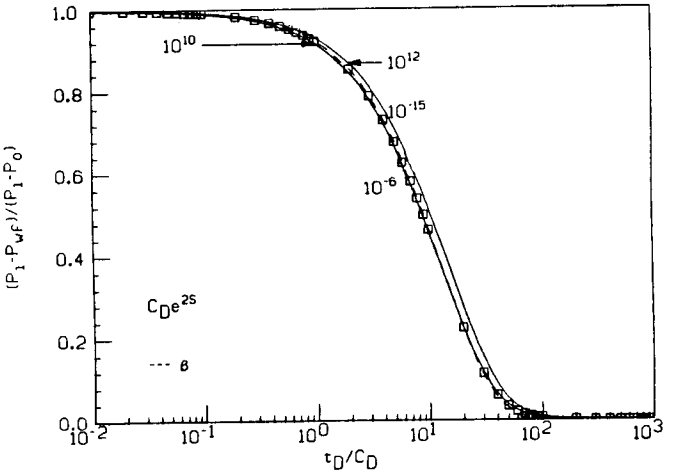


Figure 5: Example of semilog double porosity behavior (Transient)
($\omega = 0.01$, $\beta = 3.0\,D + 21$)

Proceedings Ninth Workshop Geothermal Reservoir Engineering
Stanford University, Stanford, California, December 1983
SGP-TR-74

INTERPRETATION OF INTERFERENCE DATA FROM THE KLAMATH FALLS, OREGON GEOTHERMAL RESOURCE

S. M. Benson

Earth Sciences Division
Lawrence Berkeley Laboratory
University of California
Berkeley, California

ABSTRACT

Data from a seven week pressure interference test in the Klamath Falls, Oregon geothermal resource have been analyzed. The data indicate that productive wells are fed by a highly permeable fracture network and that the less permeable matrix blocks contribute significantly to the reservoir storage capacity. Detailed analysis of data from two wells is presented. Data from both of the wells yield a reservoir permeability-thickness (kh) of approximately $1.3X10^{6}$ md-ft and a storativity ($\phi c_t h$) of $6.8X10^{-3}$ ft/psi. The parameters (λ and ω), which are determined by the distribution of permeability and storativity between the matrix and fractures, vary by more than an order of magnitude. A sensitivity study shows that for these wells, the pressure transients are not very sensitive to the distribution of permeability and storativity between the fractures and matrix blocks. No hydrologic boundaries were detected during the test. This indicates that the fault which supplies hot water to the shallow hydrothermal system does not behave according to the classical model of either a barrier or constant potential boundary.

INTRODUCTION

The City of Klamath Falls, Oregon (see location map in Figure 1) is underlain by a low to moderate temperature (<110°C) geothermal resource. Although located in close proximity to the Cascade Range, the geothermal system is more typical of the fault-charged reservoirs of the Basin and Range Province to the east (Sammel, 1980). Presumably, hot water upwells along a major range front fault and flows laterally in the highly permeable near surface rocks. The subsurface geology is extremely complex; rock units are fractured, faulted and thermally altered (Peterson and McIntyre, 1970; O'Brien and Benson, 1981). Correlation of marker beds between wells is often impossible. To date, over 400 shallow wells (<400 m) have been drilled and are currently in use for space heating, domestic hot water or small scale industrial processing (OIT, 1978).

In 1979 the City of Klamath Falls drilled the first of two wells to be used to supply hot water to a district heating system. On completion of the second well, the district heating supply and distribution network were installed. Short term testing of both wells indicated that they were sufficiently productive to provide the 750 gpm peak load requirement of the heating system and that the impact on existing users would be small (Benson et al., 1980; Benson, 1982a; and Benson 1982b). Concern over the impact of pumping hot water from the resource to supply the district heating system resulted in the passage of an ordinance that prohibited pumping of geothermal fluid without returning it to the well from which it was pumped. Additionally, concern over the lack of a sufficient data base on the geothermal system resulted in a comprehensive resource study that was funded by the U. S. Department of Energy. The study, coordinated by the U. S. Geological Survey, included geochemical analysis of the reservoir fluids, tracer studies, background data monitoring and the seven week interference test that will be discussed here.

TEST DESCRIPTION

The interference test consisted of monitoring water level changes in more than 40 wells while hot water was pumped from one well for 3 weeks and concurrenty reinjected into another well for an additional 4 weeks. Twelve of the observation wells were instrumented with high resolution downhole instruments that incorporate quartz crystal pressure transducers and thermistor temperature sensors (Solbau et al., 1981). Data from these twelve wells were transmitted to one of two central locations where they were processed and recorded. This allowed synchronous data recording, which resulted in the collection of very accurate early time pressure transient data. The locations of these wells are shown in Figure 2. Also shown are the locations of the production well (CW-1) and the injection well (County Museum Well). Detailed analysis of the data from the Head and Page wells (shown in Figure 2) will be discussed here.

During the first three weeks of the test well CW-1 was pumped at a rate of 43.5 kg/s. The produced water was disposed of in an irrigation canal. During the last four weeks of the test, pumping continued but the water was reinjected into the County Museum well. The back pressure at the Museum well resulted in a slightly lower and somewhat variable pumping rate (42 to 40 kg/s). The pumping rate during the test is shown in Figure 3. The injection rate during the last four weeks of the test was identical to the pumping rate.

Well Descriptions

The pumped well, CW-1, is approximately 274.3 m deep and is cased from the surface to a depth of 109.7 m. Initial testing of the well indicated that the rock units from 109.7 m to 274.3 m were of low permeability and produced very little fluid. Subsequently, the well was slotted from approximately 59.4 m to 73.1 m. A short test proved this interval to be very permeable. Essentially all of the water enters the bore between 59.4 m to 73.1 m.

The injection well, the County Museum well, was originally drilled to a depth of 376.4 m. Sinker bar runs indicate that the wellbore now has approximately 16.7 m of fill. The well is cased from the surface to a depth of 137.3 m. The remainder of the well is open hole. A spinner survey was run and showed that two intervals were accepting fluid, one between 143 - 159 m and a second between 310 - 329 m. Each interval appears to accept approximately 50% of the injected fluid. The completion data from the observation wells and the active wells are summarized in Table 1.

Interference Data

The interference data from the Head and Page wells are shown in Figures 4 and 5. Both of the wells exhibited the same basic behavior. Pressures (water levels) decreased while only the pumping well was active. The drawdown at the Head well (1.74 psi) was larger than at the Page well (1.1 psi) because it is closer to the pumped well. When injection began the water levels in both wells rose rapidly. Since the Page well is closer to the injection well than it is to the pumped well, the water level rose above its pre-test level.

Essentially all of the wells monitored during the test had this type of response. In general the largest drawdowns attributed to pumping (2ϕ psi) occurred in the wells closest to the pumped well. The rapid pressure transient responses in all of the observation wells, to both injection and production, indicates that there are no hydrologic discontinuities (barriers, faults) within the region examined by the monitor wells. Qualitatively, all of the wells behaved in a uniform manner. This is suprising in light of the complexity and heterogeneity of both the lithology and thermal regime in the Klamath Falls geothermal anomaly.

DATA ANALYSIS

The fractured and heterogeneous nature of the system and the interpretation of previous short term tests suggested that a double porosity model would best describe the pressure transient behavior in the observation wells (Benson et al., 1980; Deruyck et al., 1982). The log-log plots of the drawdown data from the Head and Page wells (shown in Figures 6 and 7) are typical of double porosity reservoirs with transient interporosity flow. The data were matched to the double porosity type curves published by Deruyck et al., 1982. The best matches are shown in each instance. The calculated permeability-thickness products, total storativity and the double porosity parameters (λ and ω) are given in Table 2. The parameters λ and ω are those defined by Warren and Root, (1963):

$$\omega = \frac{(\phi c_t)_f}{(\phi c_t)_f + (\phi c_t)_m}$$

and

$$\lambda = \alpha r_w^2 \frac{k_m}{k_f}$$

The kh and the $\phi c_t h$ values are in good agreement with one another. The parameters λ and ω differ by more than the order of magnitude.

It is of interest to note that several other type curve matches are possible with this data. The log-log plot of the Page well data, shown in Figure 7, is a good example. In addition to the double porosity type curve match, shown by the solid line, two other type curve matches are shown. Fitting the early time data, up to approximately ten hours, with the conventional line source solution (Theis), gives an excellent match. The kh calculated from this curve is approximately three times the value obtained from the double porosity type curve match. Also, the departure of the data from this match after approximately ten hours would indicate the presence of a no-flow boundary. This illustrates the dangers of running a short term test in a heterogeneous system, and explains why interpretation of the previous short term tests overestimated the reservoir permeability (Benson et al., 1980). A second type curve match is also possible using the middle and late time data. The data from approximately 5 hours onward can be nicely matched with the line source solution (Theis). This match is also shown in Figure 7. Analysis based on this interpretation yields approximately the same kh and bulk $\phi c_t h$ as the double porosity type curve match. As the drawdowns measured prior to 5 hours are relatively small (<0.10 psi) one might feel confident in such a match by assuming the very early time data were inaccurate or unimportant. Using this approach, the correct values for the bulk system properties are obtained. This however is not always the case and ones confidence in the analysis increases if all of the data are considered. The double porosity interpretation yields an excellent match throughout the entire test period, thus lending credence to this interpretation.

Pressure transient data during the injection phase of this test were analyzed by assuming that the pressure transients due to the initial pumping period had reached steady state and therefore could be ignored in the subsequent calculations. In light of the background noise (other well users and seasonal

water level changes), this assumption does not appear to create any additional ambiguity in the analysis. During the injection phase, flow rates were slightly variable (42 - 40 kg/s). This variation was also neglected in the analysis because water level changes due to other sources (barometric pressure fluctuations and other well uses) were of the same order of magnitude as those resulting from the flowrate variations and do not effect the overall data interpretation.

Log-log plots of the pressure buildup data and type curve matches at the Head and Page wells are shown in Figures 8 and 9. The matches between the observed data and the double porosity type curves are excellent. Data from the Head well can also be fit to a Theis curve if the first several hours of the tests are neglected. The results of both analyses are similar and are given in Table 2. Data from the Page well are best fit to a double porosity type curve with pseudo-steady state interporosity flow. All of the other test data are more accurately described with a transient interporosity flow model. This is probably the result of its being closer to the active well, which tends to exagerate the effects of the double porosity system. Once again, the values of kh and the $\phi c_t h$ are in good agreement but λ and ω vary substantially.

As can be seen from Table 2, the parameters kh and $\phi c_t h$ all in good agreement. On the other hand, λ and ω both vary by more than an order of magnitude. To assess the significance of the variation of these parameters, a sensitivity study was conducted to determine their uniqueness. The data were re-analyzed using the method described by Lai et al., (1983). They have developed a semi-analytic solution for analyzing pressure transients in double porosity reservoirs with block-like geometry and transient interporosity flow. A semi-log plot of the data match obtained from the analysis of the drawdown at the Page well is shown in Figure 10. The same values for kh and $\phi c_t h$ were obtained. However, values of $\lambda = 1.05X10^{-6}$ and $\omega = 4X10^{-3}$ were calculated. These values differ by more than an order of magnitude from the values obtained with the log-log type curve match. Also shown in Figure 10 are the drawdowns calculated using several other values of λ and ω (varying by more than 2 orders of magnitude). It can be seen that for all practical purposes these curves are almost indistinguishable. The implication is that for observation wells far from the active well, in a high permeability reservoir, the data analysis may not uniquely determine the parameters λ and ω.

SUMMARY

Analysis of the data from a 7 week interference test show that all of the shallow geothermal wells in the Klamath Falls geothermal resource penetrate a single continuous aquifer. Local heterogeneities (rock type and temperature) do not appear to significantly affect the hydrologic behavior of the system. The responses of individual wells to pumping and/or reinjection are consistent with this observation. Detailed analyses of the data from two of the observation wells show that the aquifer behaves as a double porosity medium. The fractures and high permeability strata provide pathways along which the fluid moves easily. The less permeable matrix blocks store the bulk of the hot geothermal water. No hydrologic boundaries to the geothermal system were apparent in the interference data. However, the effects of the other users and the seasonal rise in water level may have masked the effects of a boundary in the very late time data. It can be estimated that there are no hydrologic boundaries within a 1 mile radius of the pumped well. This sheds a new light on the hydrologic properties of the fault that is known to transect the area and is the postulated source of the near surface hot water. The fault does not behave according to the classical models for either a barrier or constant potential boundary. Instead, it is essentially invisible to hydrologic testing. Several hypothesis can explain this observation. First, the hot water may upwell over a broad region rather than along a single fault zone that would be detected hydrologically. Second, the fault permeability may be on the same order of magnitude as the permeability of the near surface aquifers and hence, indistinguishable. Third, a single fault may provide the conduit for upwelling from great depth but as the fault approaches the surface, the width of the fractured zone increases which creates a diffuse upwelling region in the near surface. Without more information it is not possible to determine which one of these possibilities (or others) is the correct one.

COMMENTS

Analysis of this interference data points out some of the limitations of and provides guidelines for interference testing and data analysis in highly heterogeneous systems. These are summarized as follows.

1) Short term tests can lead to overestimation of reservoir permeability.

2) Analysis of moderate to late time data with the line source solution may yield the correct bulk values of kh and $\phi c_t h$.

3) Data from a test of proper duration and obtained with sufficiently sensitive instrumentation can be analyzed using a double porosity model to evaluate kh and $\phi c_t h$ with a high level of confidence.

4) It may not be possible to uniquely determine values for the double porosity parameters (λ and ω) in highly permeable reservoirs and/or observation wells far from the flowing well

All of these observations are consistent with theoretical results. However, the limitations of analysis methods are not always apparent by examination of mathematical solutions.

Analysis of this data demonstrates that even with a very high quality data set, there are limitations to the amount of information that can be obtained. Additional interpretation requires input from other disciplines such as well logging/or and detailed lithologic evaluation.

ACKNOWLEDGEMENTS

The invaluable assistance of Ray Solbau, who helped collect this data, is gratefully acknowledged. Thanks are also due to C. H. Lai who performed the parameter sensitivity analysis. Thanks are also due to many others who helped conduct this test, especially Dr. E. A. Sammel of the U.S.G.S. who coordinated and facilitated the entire research program. This work was supported by the Assistant Secretary for Conservation and Renewable Energy, Office of Renewable Technology, Division of Geothermal and Hydropower Technologies of the U. S. Department of Energy under Contract No. DE-AC03-76SF00098.

References

Benson, S. M., Goranson, C. B., and Schroeder, R. C., 1980, Evaluation of City Well 1, Klamath Falls, Oregon, Lawrence Berkeley Report LBL-10848.

Benson, S. M., 1982a. Klamath Falls (WP-1 and WP-2) System Check, September 29 through 30, 1981, unpublished report to the City of Klamath Falls, OR.

Benson, S. M., 1982b. Klamath Falls WP-1, Supply and Distribution Network, Museum Well) System check, February 8 through 12, 1982, unpublished report to the city of Klamath Falls, OR.

Deruyck, B. G., Bourdet, D. P., Da Prat, G., and Ramey, H. J., 1982, Interpretation of Interference Tests in Reservoirs with Double Porosity Behavior-Theory and Field Examples, Presented at the 57th Annual Fall Technical Conference and Exhibition of the Society of Petroleum Engineers; New Orleans, LA., SPE-11025.

Lai, C. H., and Bodvarsson, G. S., 1983, A New Model for Well Test Data Analysis for Naturally Fractured Reservoirs, Presented at the 1983 California Regional Meeting of the Society of Petroleum Engineers; Ventura, California, SPE-11688.

O'Brien, M. T., and Benson, S. M., 1981, Reservoir Evaluation of Klamath Falls, Oregon, In the 1980 Annual Report of the Earth Sciences Division, Lawrence Berkeley Laboratory; Berkeley, California; LBL-12100, p. 140-147.

Oregon Institute of Technology, 1978, Geothermal Hydrology and Geochemistry of Klamath Falls, Oregon, Urban Area, Final Report for USGS Contract #14-08-0001-6-791.

Peterson, N. V., and McIntyre, J. R., 1970, The Reconnaissance Geology and Mineral Resources of Eastern Klamath County and Western Lake County, Oregon, Oregon Dept. Geol. Min. Ind. Bul. 66.

Sammel, E. A., 1980, Hydrogeologic Appraisal of the Klamath Falls Geothermal Area, Oregon, U.S.G.S. Prof. Paper 1044-G.

Solbau, R. D., Goranson, C. B., and Benson, S. M., 1981. Recently Developed Well Test Instrumentation for Low-to-Moderate Temperature Hydrothermal Reservoirs, Lawrence Berkeley Laboratory Report, LBL-13260.

Warren, J. E., and Root, P. J., 1963, The Behavior of Naturally Fractured Reservoirs, Society of Petroleum Engineers Journal, v. 3, p. 245-255.

Table 1. Well Completion Data

Well	Depth (m)	Elevation* (m)	Cased Depth (m)	Distance to* CW-1 (m)	Distance to Museum Well (m)
CW-1	274.3	1272	109.7**	-	838
County Museum	376.4	1252	137.3	838	-
Head	76.2	1278	18.3	320	640
Page	141.7	1256	45.4	671	259

* Distances and elevations are approximate.

** Slotted from 59.4 - 73.1 m.

Table 2. Well Test Data Analysis Results

Observation Well	Active Well	kh(md-ft)	φch(ft/psi)	λ	ω
Head	CW-1	$1.29X10^{6}$	$9.6X10^{-3}$	$6.8X10^{-9}$	0.01
Page	CW-1	$1.38X10^{6}$	$4.3X10^{-3}$	$1.8X10^{-7}$	0.3
Head	Museum	$1.23X10^{6}$	$5.7X10^{-3}$	$5.1X10^{-7}$	0.3
Page	Museum	$1.41X10^{6}$	$7.7X10^{-3}$	$2.4X10^{-7}$	0.06

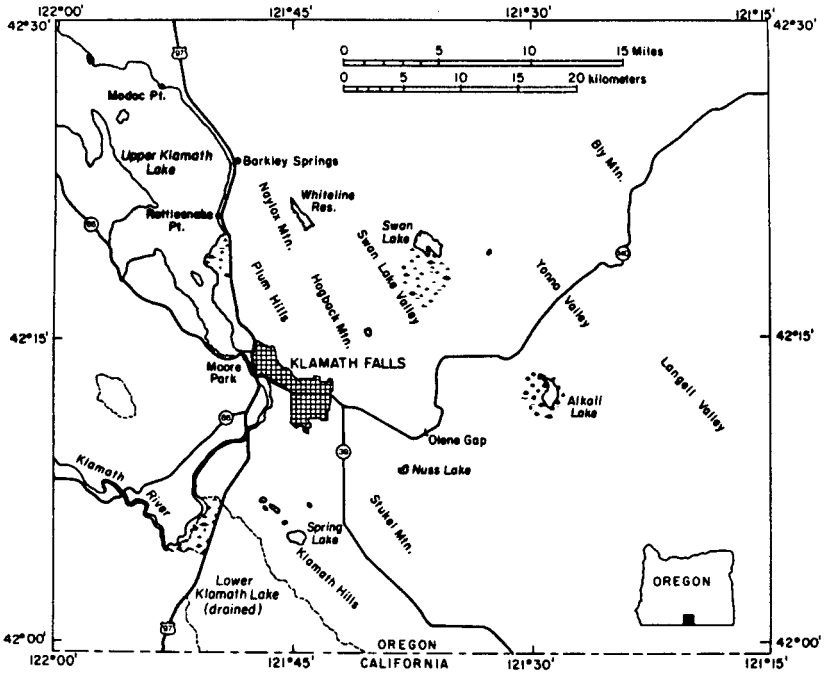


Figure 1. Location map of Klamath Falls, OR.

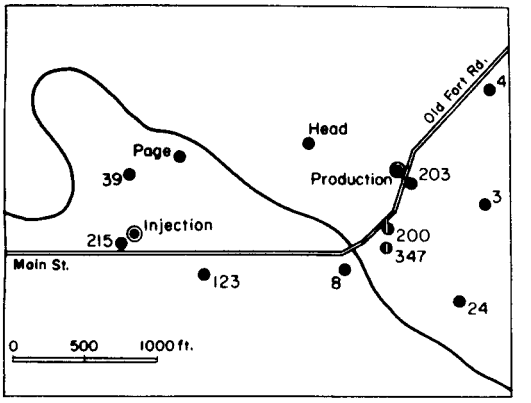


Figure 2. Well location map.

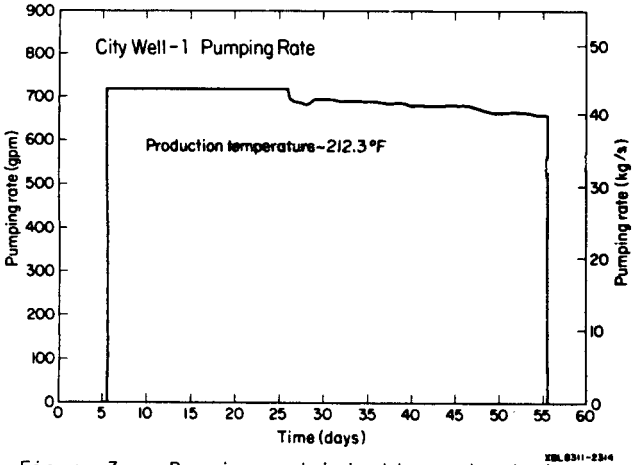


Figure 3. Pumping and injection rate during the interference test.

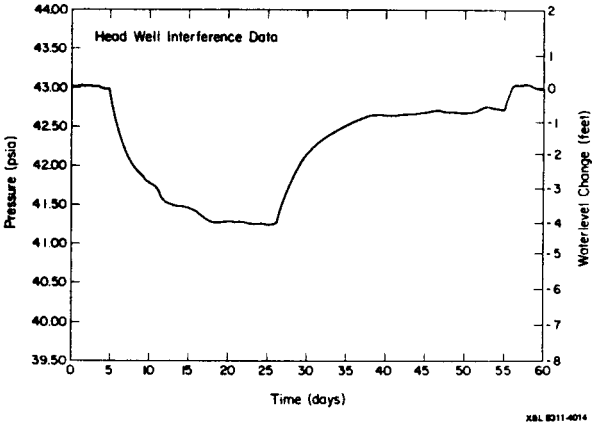


Figure 4. Head well interference data.

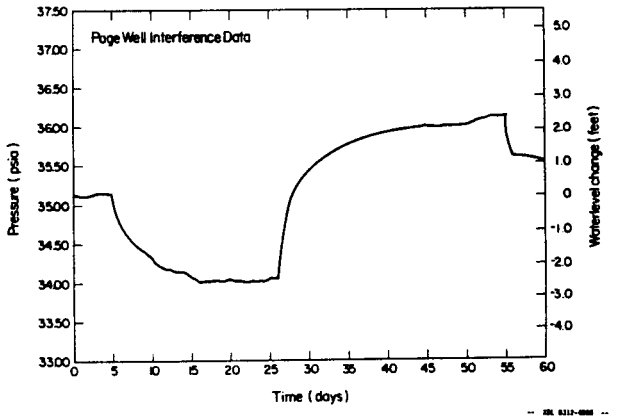


Figure 5. Page well interference data.

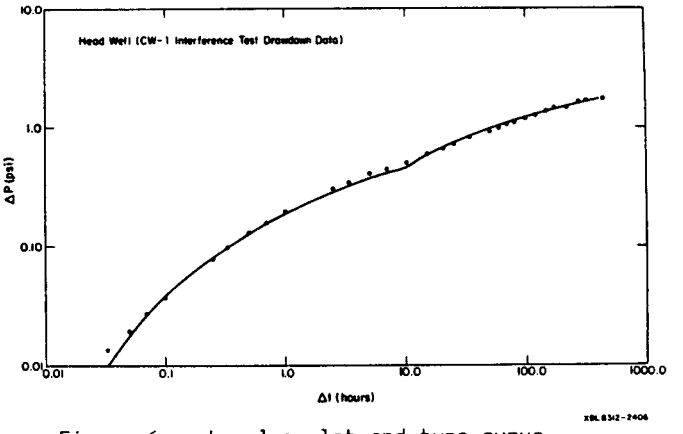


Figure 6. Log-log plot and type curve match the Head well drawdown data.

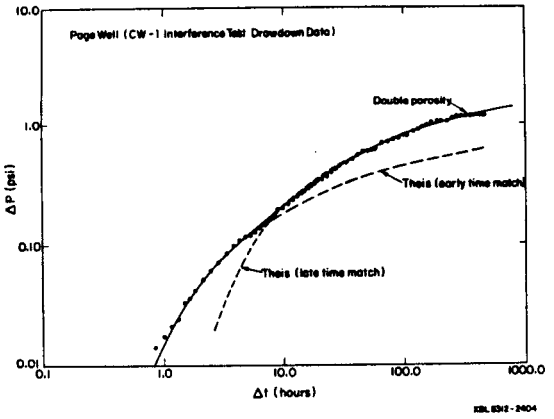


Figure 7. Log-log plot and type curve match of the Page well drawdown data.

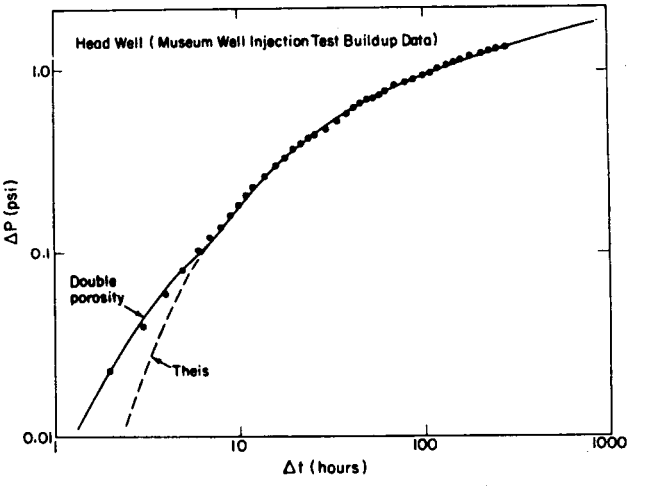


Figure 8. Log-log plot and type curve match of the Head well buildup data.

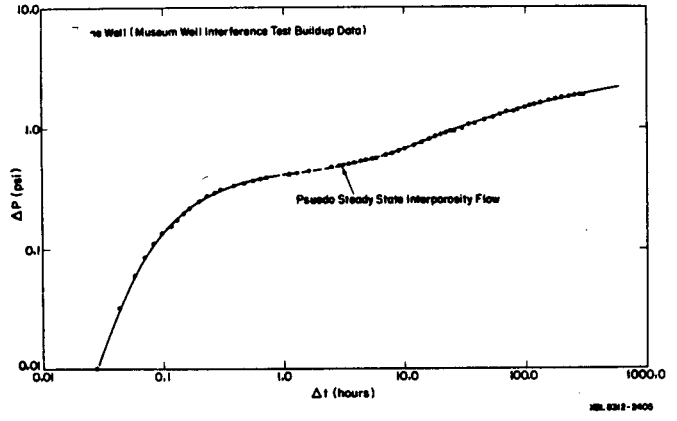


Figure 9. Log-log plot and type curve match of the Page well buildup data.

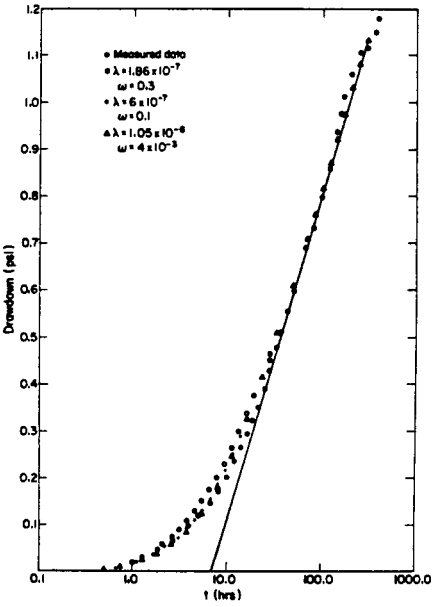


Figure 10. Semi-log plot and analysis of the Page well buildup data.

Proceedings Ninth Workshop Geothermal Reservoir Engineering
Stanford University, Stanford, California, December 1983
SGP-TR-74

Evaluating Geothermal Reserves with Application of Well Interference and Pressure Buildup Tests

T. L. Chiu, C. Y. Chiang, and T. S. Wu

Taiwan Petroleum Exploration Division
Chinese Petroleum Corporation
Miaoli, Taiwan 360

ABSTRACT

In order to evaluate geothermal reserves, it is necessary to estimate the porosity-thickness product of the reservoir. This paper deals with the method for estimating the porosity-thickness product of geothermal reservoirs by means of combining well interference and pressure buildup tests. A field study from the Chingshui geothermal area in Taiwan is given to illustrate the application of the method.

INTRODUCTION AND THEORIES

It is necessary to estimate the porosity-thickness (ϕh) product of the reservoir for evaluating geothermal reserves. This paper proposes a method to evaluate the ϕh value for that purpose. The authors derived equations, which demonstrate the relation between the pressure drop and the ϕh value of the observation well, from combining the theories of pressure buildup and interference tests. By using the equations and plotting the field surveying data on semilog paper, the ϕh value can be obtained.

Suppose well No.1 is a production well and well No.2 an observation well. By an interference test for the infinite reservoirs, the pressure drop in the close-in observation well due to continued production in well No.1 is given by

$$P_e - P_{abs} = \frac{q_1 B_w \mu}{6.15\ kh} \log \left(\frac{14.22\ kt}{\mu c \phi r^2} \right) \quad \text{---------- (1)}$$

In Eq.(1), the kh value can be estimated by the pressure buildup test on well No.2. The pressure buildup test is better done prior to the interference test which, however, should not be conducted until the pressure in well No.2 becomes quite stable. By the pressure buildup test, the pressure of well No.2 which has been shut-in for a time δ will be

$$P_\delta = P_e - \frac{q_2 B_w \mu}{6.15\ kh} \log \left(\frac{\delta}{T+\delta} \right) \text{----(2)}$$

Now if we write

$$m = \frac{q_2 B_w \mu}{6.15\ kh} \quad \text{---------- (3)}$$

then

$$P_\delta = P_e - m \log \left(\frac{\delta}{T+\delta} \right) \text{ -------- (4)}$$

Eq.(4) indicates that the buildup pressure P_δ plotted versus $\frac{\delta}{T+\delta}$

on semilog paper will be a straight line of slope m, expressed in psi per cycle, and from the value of m obtained graphically, the kh value may be found as

$$kh = \frac{q_2 B_w \mu}{6.15\, m} \qquad \text{---------- (5)}$$

Substituting Eq.(5) in Eq.(1)

$$P_e - P_{abs} = \frac{q_1 m}{q_2} \log \left(\frac{2.312\, q_2 B_w t}{C\phi h m r^2}\right)$$

or

$$P_e - P_{abs} = \frac{q_1 m}{q_2} \log \left(\frac{2.312\, q_2 B_w}{C\phi h m r^2}\right) + \frac{q_1 m}{q_2} \log t$$

$$\text{-------- (6)}$$

If we write

$$b = (P_e - P_{abs})_{t=1}$$

then

$$b = \frac{q_1 m}{q_2} \log \left(\frac{2.312\, q_2 B_w}{C\phi h m r^2}\right) \text{ ------ (7)}$$

and

$$P_e - P_{abs} = b + \frac{q_1 m}{q_2} \log t \text{ ----- (8)}$$

Eq.(8) indicates that the pressure drop $(P_e - P_{abs})$ plotted versus t on semilog paper will be a straight line (Fig.1), and from the value of b obtained graphically, the ϕh value may be found as

$$\phi h = \frac{2.312\, q_2 B_w}{C m r^2 \log^{-1}\left(\frac{b q_2}{m q_1}\right)} \qquad \text{------- (9)}$$

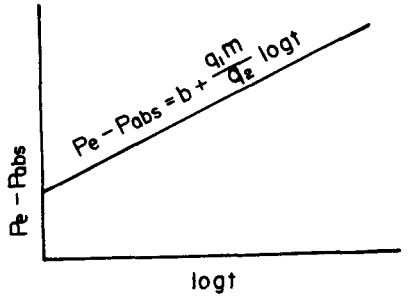


Figure 1. $(P_e - P_{abs})$ plotted versus t on semilog paper

Then the producible fluid content in reservoir per square kilometer can be calculated by

$$W = \frac{\phi h \rho \times 10^6}{3.281\, B_w} \qquad \text{------ (10)}$$

FIELD TEST RESULTS

The reservoir of the Chingshui geothermal field, a liquid-dominated system, was estimated by combining pressure buildup and interference tests. The stable flowing rate of well 4T was

q_2 = 132.6 ton/hr = 138.1 kl/hr=20848 bbl/day

Table 1 presents the pressure buildup data. Figure 3 is the Horner pressure-time semilog plot. From the straight line on the graph m = 37 psi/cycle.

Table 1. Pressure Buildup Data
(t = 60.56 hr)

Δt(hr)	$\frac{t+\Delta t}{\Delta t}$	P(psig)	ΔP	Δt(hr)	$\frac{t+\Delta t}{\Delta t}$	P (psig)	ΔP
0	-	350	0				
0.083	730.6	444	94	3.00	21.2	928	578
0.167	363.6	580	230	3.50	18.3	932	
0.250	243.2	703	353	4.00	16.1	935	585
0.333	182.9	778	428	5.00	13.1	940	590
0.417	146.2	802	452	6.00	11.1	940	590
0.500	122.1	833	483	7.00	9.65	940	590
0.583	104.9	848	498	8.00	8.57	944	
0.667	91.8	850	500	9.00	7.73	947	
0.750	81.7	855	505	10.00	7.06	949	599
0.833	73.7	862	512	11.00	6.51	949	
1.000	61.6	874	524	12.00	6.05	949	
1.167	52.9	887	537	13.00	5.66	949	
1.333	46.4	896	546	14.00	5.33	949	
1.500	41.4	901	551	15.00	5.04	952	
1.667	37.3	906	556	16.00	4.79	952	
1.833	34.0	911	561	17.00	4.56	954	
2.000	31.3	913	563	18.00	4.36	954	
2.333	27.0	920	570	19.00	4.19	954	
2.667	23.7	923	573	20.00	4.03	954	
				21.00	3.88	957	
				22.00	3.75	957	

When the pressure in well 4T is quite stable, after the well was shut-in, the interference test was started. During the interference test period, well 16T was producing, and pressure responses were observed in well 4T.

In Table 2, the flow rates of the production well were taken from the out-put of the well as given in Figure 3.

The pressure drop (P_e-P_{abs}) plotted versus t on seimilog paper is a straight line (Fig.4). From the straight line on the graph,

$$b = (P_e - P_{abs})_{t=1} = 2$$

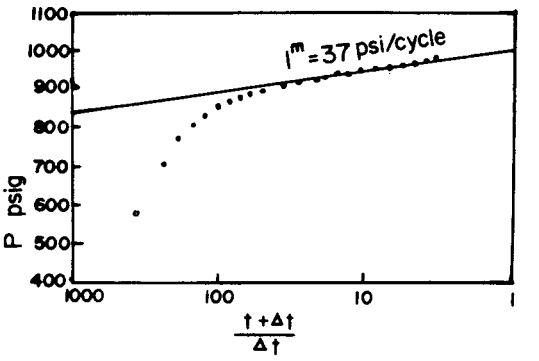


Figure 2. Pressure buildup curve

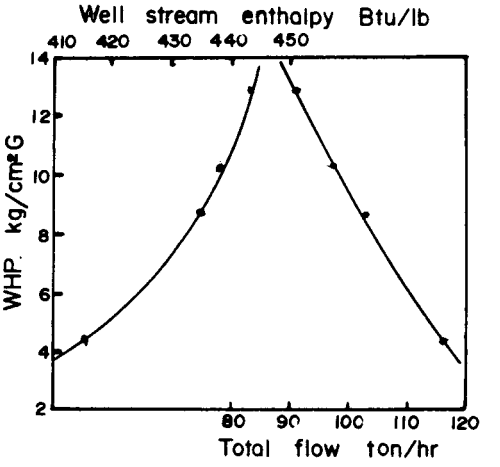


Figure 3. Out-put curve of well 16T

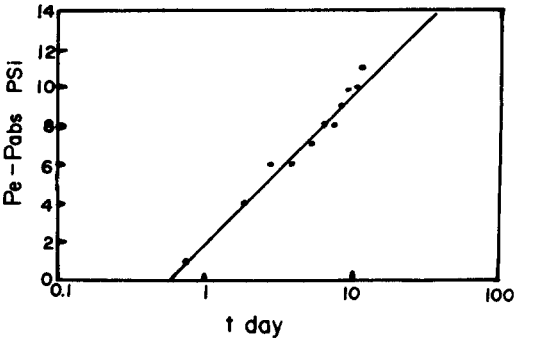


Figure 4. (P_e-P_{abs}) plotted versus t on semilot paper

Table 2. Interference data

Observation well: Well 4T
Flowing well : Well 16T

Flowing time		Pressure in observation well	P_e-P_{abs}	Pressure in production well	Flow rate of production well	Cumulative liquid production	Average flow rate	
hr	day	psig	psi	kg/cm$_2$ G.	ton/hr	ton	ton/hr	bbl/day
0	0	172		18.2	0	0		
18.5	0.77	171	1	4.9	114.5	1059		
42.5	1.77	168	4	4.1	117.5	3843		
66.5	2.77	166	6	3.9	118.0	6669		
90.5	3.77	166	6	3.9	118.0	9501		
114.5	4.77	165	7	3.9	118.0	12333		
138.5	5.77	164	8	3.9	118.0	15165		
162.5	6.77	164	8	3.8	118.5	18003		
186.5	8.77	163	9	3.8	118.5	20843		
210.5	9.77	162	10	3.7	118.6	23692		
234.5	10.77	162	10	3.7	118.6	26537		
258.5	11.77	161	11	3.7	118.6	29384	113.7*	17872

*113.7 ton/hr = 118.4 kl/hr = 17,872 bbl/day

Besides, other data were given:

$T = 405^{o}F$

$\rho = 0.857$ g/cm^3

$P = 1625$ psia

$B_w = 1.0+1.2\times10^{-4}(T-60)+1.0\times10^{-6}(T-20)^2 -3.33\times 10^{-6} P$

$= 1.0+1.2\times10^{-4}(405-60) +1.0\times10^{-6}(405-60)^2-3.33\times10^{-6}\times1625$

$= 1.155$

$C \fallingdotseq 1 \times 10^{-5}$ psi^{-1}

$r = 1{,}000$ ft

and from Table 2

$q_1 = 17{,}872$ STB/day

Substituting above information in Eq.(9)

$$\phi h = \frac{2.312\, q_2 B_w}{cmr^2 \log^{-1}(\frac{bq_2}{mq_1})}$$

$$= \frac{2.312\times20848\times1.155}{37\times10^{-5}\times(1000)^2 \log^{-1}(\frac{2\times20848}{37\times17872})}$$

$= 130$ ft $= 40$ m

and then,

$$W = \frac{\phi h \rho \times 10^6}{3.281\, B_w} = \frac{130\times0.857\times10^6}{3.281\times1.155}$$

$= 29.4 \times 10^6$ ton/km^2

CONCLUSION

1. Geothermal reserves can be evaluated by means of combining pressure buildup and interference tests. The evaluating method proposed by this paper demands that the pressure buildup and interference tests be performed respectively and successively. Generally, interference test requires more time than pressure buildup test. For saving time, it is advisable to conduct pressure buildup test prior to interference test.
2. The evaluation method given in this paper is suitable for a liquid-dominated geothermal system, since the pressure of such a system very easily becomes stable.

NOMENCLATURE

B_w = fluid formation volume factor, bbl/STB
C = fluid compressibility, psi^{-1}
h = net pay thickness, ft
k = permeability, darcy
m = slope of Honor pressure build up line, psi/cycle
P_e = static pressure of the reservoir, psia
P_δ = pressure measured in well No.2 when the well has been shut-in for a time δ during pressure buildup test, psia
q_1 = the rate of production of well No.1 during interference test. STB/day
q_2 = the rate of production of well No.2 prior to shut-in of the well during the pressure buildup test, STB/day
r = the distance between well No.1 and well No.2, ft
T = producing time of well No.2 prior to shut-in of the well, day
t = producing time of well No.1, day
W = producible fluid content in reservoir, ton/km^2
δ = shut-in time of well No.2 after flowing for a time during the pressure buildup test, day
μ = fluid viscosity, CP
ρ = density of fluid in reservoir, g/cm^2
ϕ = porosity

ACKNOWLEDGMENTS

The authors wish to acknowledge their indebtedness to K. L. Lo, S. C. Chiang S. C. Hsiao, C. Y. Huang, and S. L. Chang of the Taiwan Petroleum Exploration Division of the Chinese Petroleum Corporation for their helpful suggestions during the development of this paper, and to the management of the Chinese Petroleum Corporation for permission to publish this paper.

REFERENCE

(1) Craft, B. C., and Hawkins, M. F., (1969): "Petroleum Reservoir Engineering".

(2) Matthews, C. S., and Russell, D. G., (1967): "Pressure Buildup and Flow Test in Wells".

(3) Ramey, Henry J. Jr., and Chang, Carl R. Y., (1979): "A Preliminary Reservoir Engineering Study of the Chinshui Geothermal Field, Taiwan".

Proceedings Ninth Workshop Geothermal Reservoir Engineering
Stanford University, Stanford, California, December 1983
SGP-TR-74

Analysing Spinner Measurements from Well Tests Using Computerized Interpretation Techniques

Roland N. Horne, Alain Guillot and Adalberta Rosa*

Stanford University

ABSTRACT

The development of reliable spinner tools may help avoid much of the ambiguity which often accompanies well tests in geothermal wells, due to interlayer flows through the well bore. However, the use of both pressure and flow rate changes requires new methods of well test interpretation. The Stanford Geothermal Program has been developing microcomputer-based techniques for the simultaneous analysis of pressure and flow rate measurements. There are two key steps in the procedure. Firstly, the non-linear regression is achieved by calculating the gradients of the response (with respect to the unknown reservoir parameters) in Laplace space, and inverting numerically. Secondly, the variable flow rate is represented in terms of a superposition of many step changes - this was found to work better than a spline fit to the data. One problem was encountered when attempting to analyze data in which the spinner "stalled", causing a jump to zero flow rate.

The method shows great promise in that the degrees of freedom on the interpretation are greatly reduced, the well bore storage effect disappears, and inter-feed flows do not affect the results.

INTRODUCTION

Well test analysis is often hampered by complicating factors such as wellbore storage (afterflow) and multi-phase flow. As a result, great care is required in associating any portion of data with the "correct semilog straight line". The difficulties are often greater in the case of geothermal wells since the wellbore storage effect is usually substantial, and the additional problem of multiple feed points in the same well makes the analysis ambiguous. One solution to these various problems is the use of a spinner to measure downhole flow rate during a test. Provided the feed point is properly located, and the downhole pressure and flow rate measured at an appropriate place, it then no longer matters whether that feed zone produces (or accepts) all or only some of the test fluid; nor does it matter if the feed zone produces (or accepts) fluid to (or from) other feed zones in the same well rather than to (or from) the surface--the spinner will always monitor the actual reservoir flow rate. At present stages of technological development, spinners can operate in geothermal wellbore environments (although with safety mainly in injection tests), and combined tools with simultaneous pressure, flow rate and temperature measurements have been used (Benson, Goranson, Solbur and Biocca, 1981). At the present time however, conventional well test analysis techniques cannot easily use these new measurements, except when they serve only to show that the flow rate is constant. New interpretation techniques are required.

Stanford University's Department of Petroleum Engineering has been developing computerized pressure transient techniques, using non-linear regression to fit field data to a reservoir model. The first problem to overcome was the difficulty in describing the reservoir model in a closed analytic form, since many conventional type curves have been developed using numerical techniques. Rosa and Horne (1983) showed a way of formulating the reservoir model in Laplace space (in which most solutions exist in closed form), and then numerically inverting the transforms of the solution and its derivatives with respect to the unknown reservoir parameters. The numerical inversion was performed using an algorithm by Stehfest (1970). Experimentation with non-linear regression methods indicated that variable projection (Kaufman, 1975) or Gauss-Marquardt with penalty functions (Bard, 1974) would be the preferred methods to use.

Following the successful development of a set of methods capable of fitting a wide range of common type curves using a computer, the next step was to extend the work to encompass reservoir models that cannot be represented graphically in a type curve. Included in these is the case where flow rate is not constant. This work by Guillot (1983), examined the advantages of representing the variable flow rate in terms of a superposition of step functions, or in a spline approximation.

This paper will summarize the results of both works, discussing first the advantages in performing the interpretation using the computer, and second the specific case of variable flow rate tests.

Computerized 'Type Curve' Matching

Well test interpretation in the conventional manner usually requires the separate analysis of one, two, three or more different portions of the pressure-time response. Commonly the early time response is used to estimate wellbore storage and skin effects, and also to correctly locate the start of the "correct semilog straight line" which is the second (intermediate time) response. The semilog straight line occurs when the fluid flows radially

*Present Address: Petrobras, Brazil

through the reservoir and no external boundary effects have been reached. Recognition of the correct straight line is one of the more frequent sources of error in well test interpretation since several different semilog straight lines may be apparent in some real data. The slope of the straight line is used to estimate permeability-thickness product (kh). The third region that may be analyzed is the late time response, which indicates the presence of and distance to reservoir boundaries.

Interpretation of a well test may be difficult or impossible if one or more of the separate responses is absent. For example, a well with a large storage volume, close to a fault or boundary, may show a response which changes from storage-dominated to boundary-dominated without ever showing a semilog straight line. Worse still a spurious straight line may be apparent in the data, resulting in an erroneous interpretation. For this, and other reasons, it is also possible to obtain different estimates for the reservoir parameters from different parts of the response.

Many of these problems may be overcome with computerized curve matching. Using non-linear regression algorithms, a computer can fit curves as easily as straight lines and is therefore not dependent on the sometimes subjective choice of "the semilog straight line". The algorithm also does not obtain its estimates from a sub-region of the data, thus it cannot obtain different parameter estimates from different sub-regions. The procedure fits the entire pressure response at one time, regardless of its straightness or otherwise, and obtains a set of parameter estimates consistent with the whole data set. These estimates may still be in error if the model used was inappropriate, but on the whole the number of degrees of freedom (i.e. possibilities for error) are reduced relative to conventional graphical methods.

The analysis method proceeds as follows:

Define:

$\left[\Delta p_{wf}\right]_{t=t_i}$ = theoretical value of pressure drop at the wellbore at time $t=t_i$, as defined by the reservoir model

Δp_{wf_i} = recorded value of that pressure drop

The least squares procedure calls for minimization of the sum of squares of the residuals, defined by:

$$SSR(\vec{\theta}) = \sum_{i=1}^{n} \left\{ \left[\Delta p_{wf}\right]_{t=t_i} - \Delta p_{wf_i} \right\}^2 \qquad (1)$$

$\vec{\theta} = (\theta_1, \theta_2, \ldots, \theta_{np})^t$ is a vector of the np unknown reservoir parameters.

SSR is called the objective function and we seek the vector $\vec{\theta}^*$ at which it attains its minimum. This process of minimization is an optimization and if we constrain the parameters we will refer to the process as nonlinear programming.

The system of equations of condition is given by:

$$F_1 \equiv \left[\Delta p_{wf}\right]_{t=t_1} - \Delta p_{wf_1} = 0 \qquad (2)$$

$$\vdots$$

$$F_n \equiv \left[\Delta p_{wf}\right]_{t=t_n} - \Delta p_{wf_n} = 0$$

The equations in this system are nonlinear with respect to the unknown reservoir and well parameters. The basis of the Gauss method is linearization of the equations by expanding each function F_i in a Taylor series up to the first derivative term. We note that the derivatives cannot always be easily obtained in real space because the functions F_i are known only in the Laplace domain. However, we employ one of the theorems of the Laplace transform theory:

$$\frac{\partial F}{\partial \theta_p}(\vec{\theta},t) = L^{-1}\left\{\frac{\partial f}{\partial \theta_p}(\vec{\theta},z)\right\} \qquad (3)$$

where:

p = parameter number

θ_p = reservoir parameter

$\vec{\theta}$ = vector having the reservoir parameters as components

f = function F in the Laplace domain, i.e., $\overline{\Delta p}_{wf}(\vec{\theta},z)$.

After linearizing the system of equations (2) the normal equations are constructed by the usual procedure. Then, the normal equations are solved, the corrections added to the solution vector to form a new estimate of the unknowns. We repeat the process until convergence within a prescribed accuracy.

The Gauss method is known to be very sensitive to the initial guess and may converge slowly or even diverge if it is too far from the true solution. It may be improved greatly using the Marquardt (1963) modification and further improved by the addition of penalty functions (Rosa and Horne, 1983).

The inversion of the equation from Laplace space to real space was done numerically using the Stehfest (1970) algorithm. The accuracy variable N in that algorithm was chosen to be 8. With this value results from the evaluation of the pressure at the wellbore agree closely with those presented by Agarwal (Al-Hussainy and Ramey, 1970), within four or five significant figures.

Table 1 presents data obtained from a pressure drawdown test on a new oil well, which is strongly influenced by wellbore storage.

TABLE 1

DATA FOR EXAMPLE TEST

After Earlougher and Kersch (1974)

q_{sc} = 179 STB/d C_t = 8.2 x 10^{-6} psi^{-1}

B_o = 1.2 bbl/STB ϕ = 0.18

h = 35 ft μ = 1.0 cp

r_w = 0.276 ft

Drawdown Pressure Data

Δt(hr)	Δp_{wf}(psi)
0.2	19.7
0.3	28.1
0.5	43.1
0.7	58.3
1.0	75.1
2.0	114.5
3.0	135.5
5.0	152.2
7.0	163.2
10.0	166.7
20.0	171.2
30.0	173.9
50.0	175.2
70.0	177.1

Figure 1 shows the log-log plot. Matching with the Gringarten et al (1979) type curves we estimated:

k = 104 md = 0.104 darcy
s = 12.3
C = 0.08659 bbl/psi = 202,386. cm^3/atm

Earlougher and Kersch (1974) obtained the following results using type curve matching:

k = 132 md = 0.132 darcy
s = 18
C = 0.0942 bbl/psi = 220,172. cm^3/atm

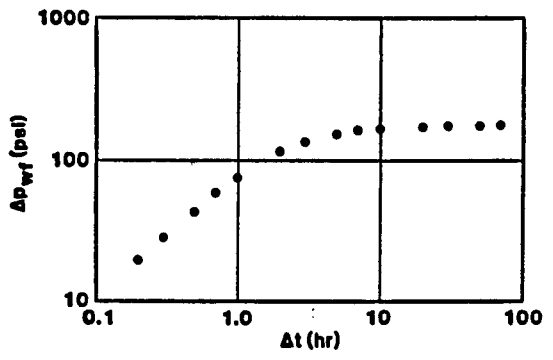


Fig 1. Log-log plot of example data (after Earlougher and Kersch, 1974).

We performed the semi-log analysis, as presented in Figure 2, and calculated:

k = 102.6 md = 0.103 darcy
s = 12.1

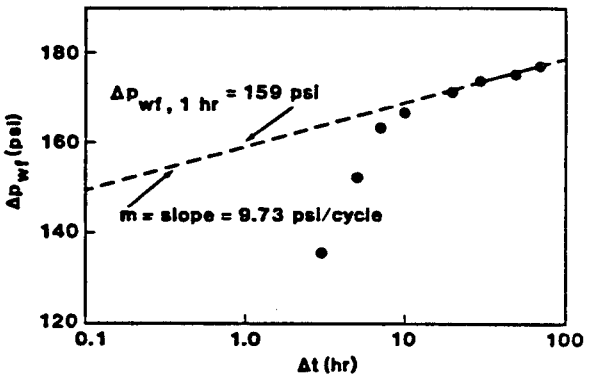


Fig 2. Semi-log plot of example data.

According to the approximate start of semi-log straight line indicated by the matching with the Gringarten et al (1979) type curves, only two or at most three points fall on that line. This makes the conventional analysis rather difficult and subjective. In order to investigate this point, we employed the Gauss method using all the data points but also without some of them. The results are summarized in Table 2.

The matching using all the data points gave a sum of squares of residuals of 0.0478 atm^2 and the largest individual residual, not shown, was 2.3 psi. The estimated permeability from the conventional semi-log analysis is 13.6% above the result from the Gauss method and the skin factor is 23.6% above.

The conventional semi-log analysis is difficult with so few points on the straight line, so it is interesting to observe what happens if the last two data points are not present. In this case the conventional analysis would be impossible but the automated matching still produces reasonable figures for permeability and skin, within 18%, and practically the same wellbore storage coefficient.

Excluding the first three points it would be impossible to estimate the wellbore storage by conventional analysis using the unit slope line. However, the Gauss method yields almost the same results as those obtained when using all the data points.

These examples point out the efficacy of the automated procedure. It is clear that it is feasible to estimate the three reservoir parameters using data that fall only in the transition region between the unit slope line (dominated by storage effects) and the semi-log straight line (no storage effects anymore). The only way of performing this analysis is automatically, using a regression technique as proposed, because there is no simple analytical expression for the pressure drop in the transition region and the visual matching becomes completely subjective.

TABLE 2 - RESULTS OF THE GAUSS METHOD

Data from Table 1

Example	Number of Data Points	Initial Guess (Darcy System of Units)			Solution (Darcy System of Units)			Iterations	SSR $(atm)^2$
		k	s	C	k	s	C		
1	14	0.100	18.	220,000.	0.0903	9.87	201,840.	6	0.0478
2	12 (excluding the last two points)	0.104	12.3	202,386.	0.0806	8.07	200,360.	4	0.03857
3	11 (excluding the first three points)	0.100	18.	220,000.	0.0899	9.79	201,490.	6	0.04524
4	10 (excluding the first two & last three points)	0.104	12.3	202,386.	0.0810	8.14	200,560.	4	0.03811

Quite apart from this, the automatic approach also permits confidence intervals to be placed on all the parameter estimates, as shown in Rosa and Horne (1983). This quantification of the "fuzziness" of the estimates is not possible in the conventional analysis.

Variable Flow Rate

Given that the model pressure drop $\left[\Delta p_{wf}\right]_{t=t_i}$ and its derivatives can be obtained by numerical inversion of their Laplace transforms, it is no longer necessary to require that the flow rate be constant during the test - provided it has been measured. For the simple case without storage and skin, the model function can be written down in terms of the exponential integral function E_1, without recourse to the Laplace transform:

$$\left[\Delta p_{wf}\right]_{t=t_i} = \frac{\mu}{4\pi kh}\sum_{j=0}^{n-1}\frac{q(\tau_{j+1})+q(\tau_j)}{2}\left[E_1\frac{\varphi\mu c r_w^2}{4k(t_i-\tau_j)} - E_1\frac{\varphi\mu c r_w^2}{4k(t_i-\tau_{j+1})}\right] \quad (4)$$

Here $q(\tau_j)$ are the set of n flow rates measured throughout the test - each treated as constant from time τ_j to time τ_{j+1}. Guillot (1983) also examined the case where the variable flow rate is fitted using a spline, however the step function approach was found to give better results in much less computer time. Figure 3 shows an example of a flow rate variation and its approximation in terms of (a) step functions and (b) a cubic spline. The resulting pressure histories are shown in Figure 4. The non-linear regression program can fit both pressure curves with good accuracy; however only the step function approach arrives at estimates of the reservoir parameters which coincide with the values used to generate the data. The spline approximation approach gives answers which deviate as much as 10% from the actual values.

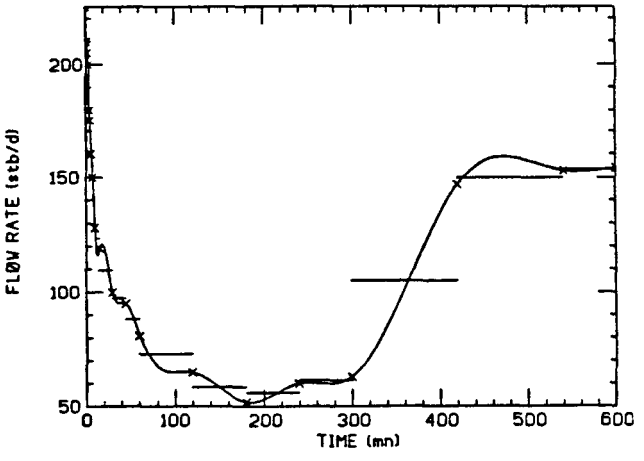


Fig 3. Flow rate vs. time: x = data; broken curve - step functions; solid curve - spline approximation.

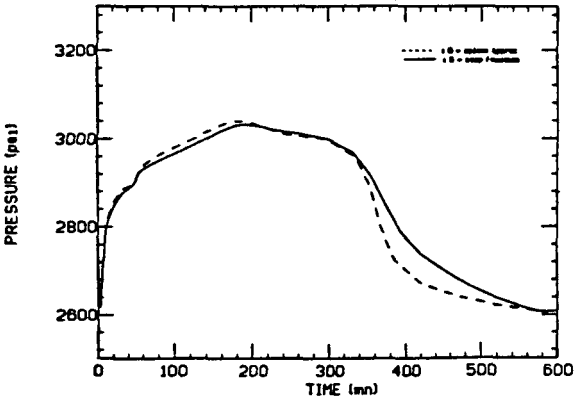


Fig 4. Pressure vs. time resulting from the flow rate approximations of Fig 2.

This difficulty in smoothing the data manifests itself in an important way in real data. There is commonly a "step" in flow rate measurements when the spinner stalls as the flow becomes small. This step is not a true representation of the actual calculated pressure response in the same manner as the "wiggles" produced by the spline. Examples considered by Guillot (1983) showed two difficulties in fitting such real data - firstly, the algorithm has difficulty converging on the observed data (since the model forces the non-existent step), and secondly the fit eventually obtained does not give reasonable values of the reservoir parameters. Using only that part of the data which precedes the stalling of the spinner results in a much better fit. This again emphasizes the efficacy of the computerized technique, since the reservoir estimates are obtained purely from what would normally be the afterflow period - before the downhole flow rate reaches zero in a buildup test. The additional hours of data collected in pursuit of the correct straight line is not required, and in fact make the fit more difficult to obtain.

Summary

(1) The use of the Laplace transform of a reservoir model pressure transient (and its derivatives with respect to unknown reservoir parameters) makes possible computerized fitting of many common type curves. The transforms need to be inverted numerically in most cases.

(2) The computerized method does not analyze a sub-region of the data (such as the semilog straight line), but fits all the data at once. It is therefore possible to correctly fit many data sets that do not demonstrate easily recognizable graphical features.

(3) By fitting the whole data set at one time the reservoir parameter estimates obtained are at least consistent. The reduction in degrees of freedom is also likely to make the estimates more correct.

(4) The flow rate need not be constant, provided it has been measured. Analysis of variable flow rate tests gives better answers than constant rate tests since wellbore storage effects do not effect the results, and the number of degrees of freedom are substantially reduced.

(5) The computerized well test analysis procedure is capable of fitting data from much shorter tests than are necessary for conventional analysis. This represents a significant saving in time for wire-line crews, and a shortening of exposure of the tools to the downhole environment.

(6) The methods are sensitive to errors in the measurements, but fortuitously less sensitive to flow rate errors than to pressure errors. An exception is the flow rates indicated when the spinner "stalls", and this data requires careful handling.

ACKNOWLEDGEMENT

This research was supported by a grant from Schlumberger.

REFERENCES

1. Agarwal, R.G., Al-Hussainy, R. and Ramey, H.J., Jr.: "An Investigation of Wellbore Storage and Skin Effect in Unsteady Liquid Flow: I. Analytical Treatment", *Soc. Pet. Eng. J.* (September, 1970), 279; *Trans.*, AIME, 249.
2. Bard, Y.: *Nonlinear Parameter Estimation*, Academic Press, Inc. Ltd., New York, 1974.
3. Benson, S.M., Goranson, C., Solbur, R., and Biocca, A.B.: "The LBL Combined PTQ Tool", Annual Report 1980, Earth Science Division, Lawrence Berkeley Laboratory, Report No. LBL-12100, July 1981, p. 121-124.
4. Earlougher, R.C., Jr. and Kersch, K.M.: "Analysis of Short-Time Transient Test Data by Type-Curve Matching", *J. Pet. Tech.* (July, 1974) 793; *Trans.*, AIME, 257.
5. Gringarten, A.C., Bourdet, D.P., Landel, P.A. and Kniazeff, V.J.: "A Comparison Between Different Skin and Wellbore Storage Type-Curves for Early-Time Transient Analysis", paper SPE 8205, presented at the SPE-AIME 54th Annual Technical Conference and Exhibition, Las Vegas, Nevada, September, 23-26, 1979.
6. Guillot, A.Y.: "Automatic Type Curve Matching With Non-Constant Flow Rate", M.S. Report, Stanford University Department of Petroleum Engineering, June, 1983.
7. Kaufman, L. "A Variable Projection Method for Solving Separable Nonlinear Least Squares Problems", B.I.T. 15, 49-57 (1975).
8. Marquardt, D.W.: "An Algorithm for Least-Squares Estimation of Nonlinear Parameters", *J. Soc. Indust. Appl. Math.* (June, 1963), 11, No. 2.
9. Rosa, A.J., and Horne, R.N.: "Automated Type Curve Matching in Well Test Analysis Using Laplace Space Determination of Parameter Gradients", paper SPE 12131 presented at the 1983 Annual Fall Meeting of the Society of Petroleum Engineers, San Francisco, California, October, 1983.
10. Stehfest, H.: "Numerical Inversion of Laplace Transforms", *Communications of the ACM* (January, 1970), *13*, No. 1, Algorithm 368.

Proceedings Ninth Workshop Geothermal Reservoir Engineering
Stanford University, Stanford, California, December 1983
SGP-TR-74

THE DEVELOPMENT AND USE OF A HIGH TEMPERATURE DOWNHOLE FLOWMETER FOR GEOTHERMAL WELL LOGGING

R.D. Solbau, C.B. Goranson*, and S.M. Benson

Earth Sciences Division
Lawrence Berkeley Laboratory, University of California
Berkeley, California 94720
*BGI, 2000 Center St., Berkeley, CA. 94704

ABSTRACT

This paper discusses the development and use of a high temperature (300°C) downhole flowmeter for geothermal well logging. The availability of the instrument gives the reservoir engineer a powerful tool for formation evaluation and studying wellbore dynamics. The instrument components, their function, and temperature limitations are discussed in detail. Several field examples of spinner log interpretation are also presented.

INTRODUCTION

The Earth Sciences Division at the Lawrence Berkeley Laboratory has developed a reliable high temperature (300°C) downhole flowmeter. The utility of downhole flowmeters for locating production and injection zones in petroleum reservoirs has resulted in their use for many years. The high temperatures, corrosive brines and very high fluid velocities encountered in geothermal wells prohibited the use of conventional downhole flowmeters. In the mid 1970's both the U.S. government and private industry put a significant effort into developing high temperature instruments (including downhole flowmeters) suitable for use in geothermal wells (Veneruso et al, 1979; Lawton et al, 1982). This ongoing effort has resulted in the development and testing of high temperature components and instruments. However, the difficulty in making reliable high temperature instruments persists. Using a very simple design concept and a minimum of downhole electronic components, a successful design for a reliable high temperature (300°C) downhole flowmeter (spinner) has been realized. The availability of a high temperature spinner has demonstrated its use for several purposes:

1) Locating production and injection zones;

2) Indicating changes in production and injection zones resulting from acidizing or fracturing;

3) Locating the flashpoint or bubble point in a wellbore;

4) Reflecting scale buildup, casing damage, plugged perforations or thief zones.

To make downhole measurements, the flowmeter is attached to a high temperature single conductor armored logging cable. It is lowered into the well with a conventional logging hoist. As the flowmeter is lowered into the well, the vertical fluid velocity causes an impeller to rotate. The rotational speed is sensed and recorded at the surface. Changes in the vertical fluid velocity can be used to indicate the items previously mentioned.

BACKGROUND

A general utility geothermal downhole flowmeter should have a temperature rating of at least 300°C and an operating pressure of 10,000 psi. In 1977, when research in this area began, the only high temperature downhole flowmeter available was a subsurface recording unit with a temperature rating of 260°C (Kuster). A stylus would scribe a number of marks on a metal chart located inside the body of the flowmeter. Each mark on the chart represented a certain number of turns of the impeller. A survey would require making stops of equal length in time at various well depths, never knowing if the instrument was still functioning or if zones of interest had been located and properly identified. Other downhole flowmeters had been used extensively in oil wells but were not well suited for the high temperatures in geothermal wells. Most of these

used pivot bearings and had rather sophisticated downhole electronics. The downhole electronic packages typically had a maximum temperature rating of 177°C. Due to the high wellbore velocities, thermal and mechanical shock, scaling and the corrosive nature of geothermal fluids, conventional pivot bearings and unprotected ball bearings were unreliable.

FLOWMETER

The basic concept of the spinner is that the fluid flowing up or down a wellbore and passing through the flow passage of the instrument will rotate the impeller inside the flowmeter at a rate that is proportional to the fluid velocity. The impeller in turn rotates a magnet assembly. The rotating magnet opens and closes a reed switch, thus generating a frequency signal which is recorded electronically at the surface. The frequency signal is proportional to the number of revolutions per minute at which the impeller is rotating. The spinner rotates at approximately 150 revolutions per minute for each foot per second of fluid velocity (for liquid water). The volumetric flowrate is calculated by multiplying the measured fluid velocity by the cross-sectional area of the bore. A photograph of the flowmeter is shown in Figure 1. The total length of the instrument is 2 feet and its maximum outside diameter is 2 inches without the centralizer. The flowmeter makes a pressure tight connection to a high temperature cablehead with the aid of metal to metal seals and high temperature elastomer o-ring seals.

Components

Table 1 lists the major components used in the instrument. The advantages of these components in hostile downhole conditions are discussed below. Downhole geothermal environments are particularly harsh on instruments due to:

1) High temperatures;
2) Corrosive liquids and gases;
3) Scale formation;
4) Sand production;
5) Very high fluid velocities in the flash zones.

To design and fabricate a high temperature flowmeter that will function reliably under these conditions, several design criteria must be met. First, the downhole electronics should be simple and function reliably at high temperatures. Second, the bearings must be shock resistant, have a high operating temperature and be protected from the geothermal brine. Finally, all components exposed to the brine must be corrosion and abrasion resistant in the operating environment.

The first objective was accomplished by using a reed switch* to sense the rotation of the impeller. This simple device eliminates the need for any active downhole electronics such as voltage regulators, voltage to frequency converters or signal amplifiers which may be temperature sensitive. The reed switch assembly operates in the following manner. The reed switch, enclosed in a stainless steel tube, is placed in close proximity to a magnet which is fastened to the top of the shaft (Figure 2). As the impeller rotates it opens and closes the reed switch. This creates a frequency signal which can be monitored and recorded at the surface. Two types of bearings are frequently used in downhole flowmeters, pivot bearings and ball bearings. Pivot bearings are more commonly used in conventional flowmeters but for the reasons discussed previously they may not be best suited for geothermal applications. Ball bearings, if kept clean and well lubricated will function extremely

*A reed switch is a passive electronic device. It has electrically insulated contacts that can be made to close by passing a magnetic field in close proximity of the device, and will open when the magnetic field is removed.

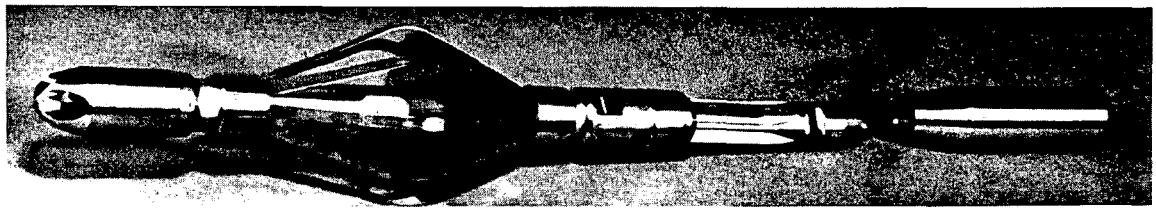


Figure 1. Photograph of the downhole flowmeter.

reliably at high temperatures and high rotational speeds. In addition, their successful use in the early subsurface recording units made them a logical choice. Two bearings are used (shown in Figure 2), one close to the impeller and the other near the top of the shaft. The two precision bearings let the 1/8 inch diameter impeller shaft rotate freely. They are protected from the corrosive wellbore fluid by an oil bath reservoir. The oil is prevented from leaving the enclosure at the lower bearing by capillary action due to the close fit of the impeller shaft and the shaft exit port located below the bottom bearing. After the flowmeter is lowered into a well, the higher specific gravity and the pressure of the brine prevents the turbine oil from leaving the enclosure.

To protect the instrument from the corrosive and abrasive downhole environments in geothermal wells the body was fabricated of type 304 stainless steel. A titanium impeller was chosen and fabricated because of the very high strength to weight ratio and high resistance to corrosion in geothermal brines. The aluminum and plastic impellers used in many downhole flowmeters are usually destroyed within a short time by the brines and high temperatures.

The fluid in production wells enters the flowmeter through the holes in the bullnose, rotating the impeller, and escapes through the externally fluted area of the bearing and shaft housing (see Figure 2). During use in injection wells, a collapsible funnel is usually attached at the fluted area of the bearing and shaft housing, which diverts the well fluid through the impeller housing, rotating the impeller and exiting at the bullnose.

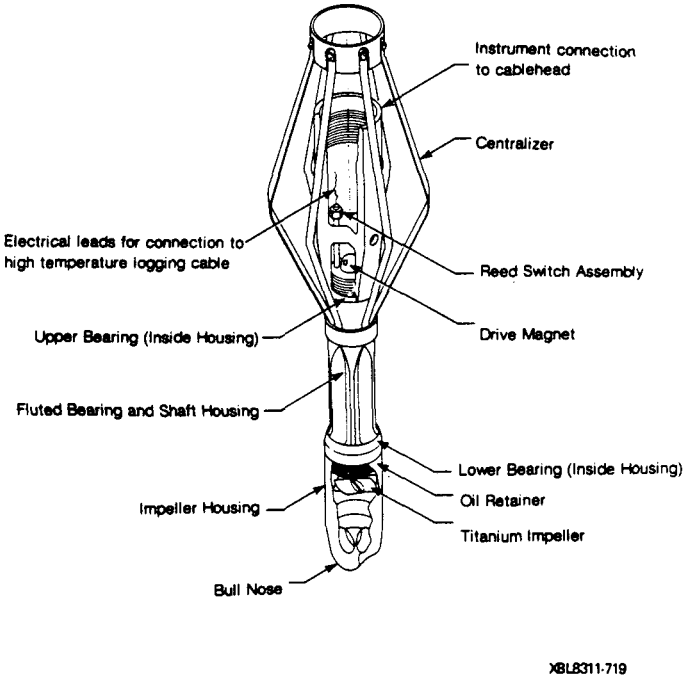


Figure 2. Schematic of the downhole flowmeter.

EXAMPLES

Downhole flowmeters have many applications in geothermal well testing, formation evaluation, and wellbore dynamics. In the following section three examples are given which demonstrate their utility and illustrate some of the difficulties with the interpretation of spinner logs. In theory, interpretation of spinner logs is very straight forward, but in practice it is often complicated by bore diameter variation and erratic

Table 1. Spinner components and temperature ratings.

Component	Type	Temperature Rating
Bearings	Shielded Precision Ball Bearings (many manufacturers)	480°C
Reed Switch	Hermetically Sealed (many manufacturers)	300°C*
Lubricating Oil	High Temperature Turbine Oil (Union 32 or equivalent)	300°C
Magnet	Alnico 5 or Alnico 8	400°C

*No temperature rating given. This value was determined experimentally and the true value may be significantly higher. The only reed switch tested is manufactured by the Calectro Company.

fluid flow near fractures or perforations. Methodical evaluation of the spinner log can resolve some of these complications and result in quantitative evaluation of production and injection zones. The first two examples are spinner surveys obtained from wells in the Imperial Valley, Calif. The first one demonstrates a conventional interpretation of a spinner survey from a well completed in a sandstone and shale reservoir. The second demonstrates flash point location in a very hot well which produces highly saline brine. The last example demonstrates the interpretation of a spinner log in a well with an openhole completion.

Flowmeter logs are obtained by lowering the instrument into the well. The log can be obtained while the instrument is lowered down the bore at a constant rate or with stops made at regular intervals. Logging at a constant speed has the advantage that the line speed can be sufficient to overcome the starting velocity (0.25 ft/s) of the spinner. On the other hand, it has been found that the precision of the survey is far greater if stops are made. During logging runs it is also important to ensure that the instrument is adequately centralized in the bore throughout the survey. This can be a problem in large diameter wells or wells with significant bore diameter changes. In that case the centralizer is chosen to fit the region of major interest.

Imperial Valley, California: Well 1

Wells completed in sandstone formations may have an even permeability distribution over the bore length or it may be concentrated in discrete intervals. Wells in the Imperial Valley may have open intervals up to several thousand feet. Detailed reservoir engineering studies and well workovers require knowledge of the permeability distribution in the formation(s) penetrated. Correlation of geophysical borehole logs can be used for this purpose but rarely with sufficient confidence. Spinner surveys provide a direct method of determining the distribution of well productivity over the borehole length. Comparison of the productivity distribution to cuttings and borehole log analyses can be used to infer both the formation permeability and near-bore permeability damage.

A typical spinner survey from such a well is shown in Figures 3 and 4. The well completion is shown in Figure 5. In Figure 3, the casing profile is shown. At the very top of the well the fluid velocity is relatively high (reflected by the rotation rate of over 300 RPM). At 225 feet, the fluid velocity drops to zero. This reflects the transition from the flashed to the unflashed brine in the wellbore (the flash depth). From 225 feet to 1750 feet the fluid velocity is below the starting velocity of the spinner. Therefore no fluid velocity is registered. From 1750 feet to the bottom of the casing (4700 feet), the fluid velocity remains nearly constant (with the exception of the higher velocities at the casing shoe).

Data from the spinner survey in the slotted liner is shown in Figure 4. Analysis of the data indicates that two intervals produce at least 73% of the fluid. The upper zone located between 4700 feet and 4720 feet produces approximately 18% of the total flow. Between 4720 feet and 4980 feet only 7% of the total flow is produced. The second major productive interval lies between 4980 feet and 5100 feet. At least 55% of the flow is produced from this interval. Because of the low fluid velocity below 5100 feet, it is not possible to determine if any fluid is being produced. Approximately 20% of the total fluid may be produced from below this depth.

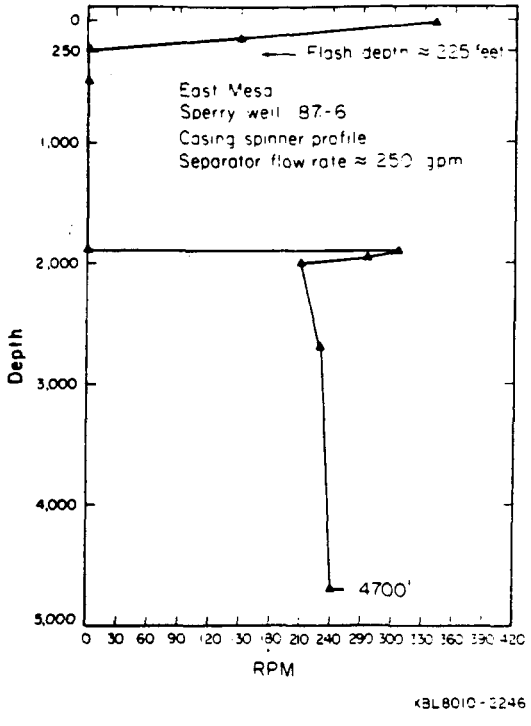


Figure 3. Casing spinner survey from well 87-6, Imperial Valley, Calif.

This is a good example of a conventional spinner log interpretation, and several key points are illustrated. First, the spinner easily detects the flash depth in the well. Second, the low flowrate (250 gpm) at which the survey was conducted created a relatively large uncertainty in the quantity of flow that was coming from below 5100 feet (20% uncertainty). Therefore, it would seem desirable to conduct the survey at a higher flowrate. However, there is a disadvantage to this, in that the flow regime in the vicinity of the perforations may become erratic at higher production rates. This results in a further ambiguity in the interpretation of the survey.

Imperial Valley, California: Well 2

The depth of the flash point in a well is typically inferred from abrupt changes in the slopes of flowing temperature and pressure profiles. In wells producing from gas rich reservoirs with highly saline brine, the slope of the pressure and temperature profiles change gradually, creating uncertainty in the true depth of the flashpoint. The spinner profile obtained from the upper portion of such a well is shown in Figure 6. Near the top of the well the fluid velocity is very high, reflecting a high steam content in the fluid. With increasing depth the fluid velocity gradually decreases (due to lower steam quality). Below 3000 feet the fluid velocity stabilizes, indicating that only a liquid phase is present. The spinner survey precisely locates the flash depth.

Wendel, California

The velocity of the fluid as it travels up the well is inversely proportional to the square of the bore radius. Therefore, even small changes in the radius can result in large changes in the fluid velocity. In openhole completions the bore diameter is often highly variable resulting in erratic fluid velocities. These changes are often so large that interpretation of the spinner data is very difficult. However, if a caliper survey is available, careful correlation of the two logs can result in quantitative evaluation of the spinner survey. This is demonstrated by the following example which was obtained from a geothermal well completed in a naturally fractured granitic rock. The spinner and caliper surveys from this well are shown in Figure 7. From the caliper survey (right side of Figure 7) it can be seen that the bore diameter is highly

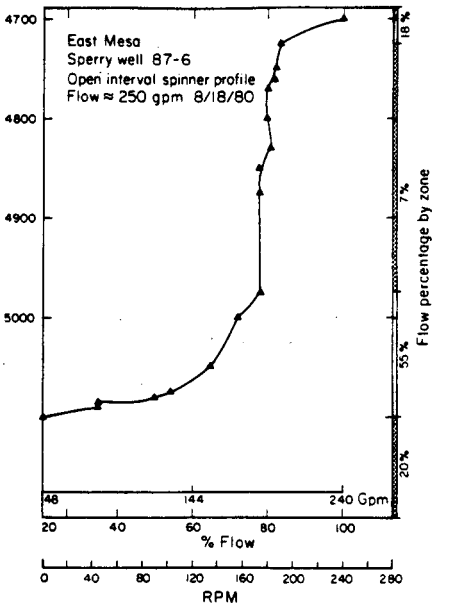


Figure 4. Open interval spinner survey from well 87-6, Imperial Valley, Calif.

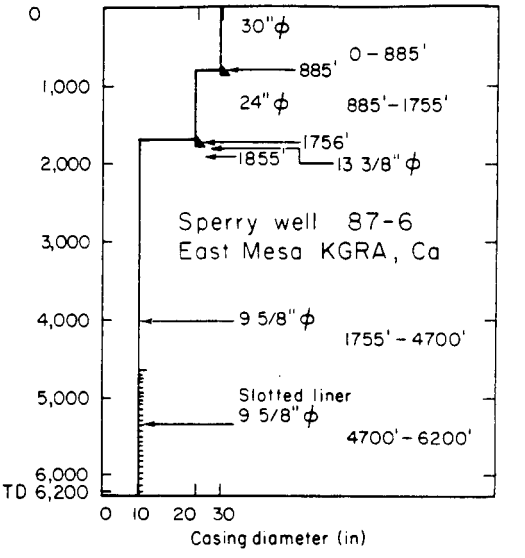


Figure 5. Casing schedule, well 87-6, Imperial Valley, Calif.

erratic. This is reflected in the variations in the fluid velocity shown in the spinner survey (left side of Figure 7). By comparing the flow velocity to the caliper survey at the depths at which the bore diameter is that of the originally drilled hole (13 inches to 5300 feet) the distribution of production intervals can be determined. The survey showed that 7% of the flow was entering the bore between 5120 feet to 5180 feet, 13% between 5190 feet and 5260 feet, and the remaining 80% between 5280 feet and

5320 feet. Below 5320 feet the impeller stopped rotating, indicating that the fluid velocity had dropped below the running velocity. Because the survey was conducted at a relatively high flowrate (680 gpm) it can be determined that less than 6% of the flow (40 gpm) was entering the well below 5320 feet.

This example demonstrates the extreme sensitivity of the flowmeter results to changes in the bore diameter. Whereas for conventional applications this may be a drawback, it can be very useful for detecting scale buildup or casing collapse in a wellbore. Because the spinner can be run while the well is under production, the spinner can be used as a production mode borehole caliper. This has the advantage in that scale buildup or casing problems can be diagnosed without shutting in the well.

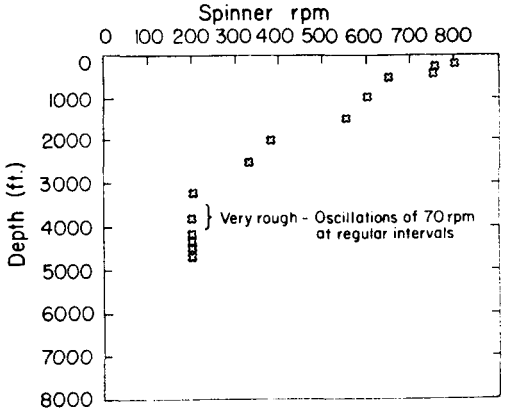


Figure 6. Spinner survey through the flash zone.

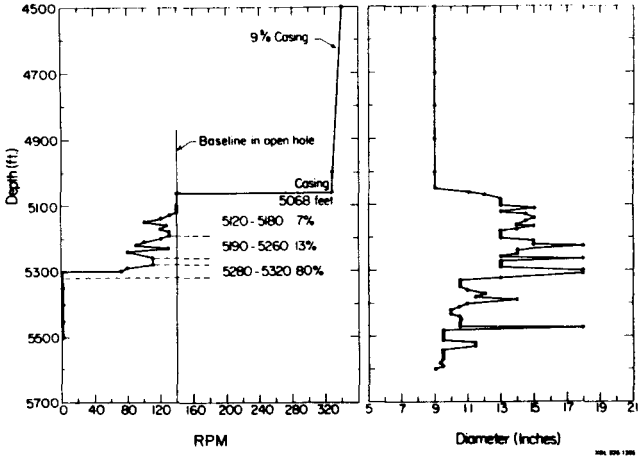


Figure 7. Spinner and caliper surveys from a well with an open hole completion.

CONCLUSION

By using existing technology a high temperature (300°C) downhole flowmeter can be constructed. In addition to the conventional uses, downhole flowmeters can be used for 1) locating the flash point in a well, and 2) as a very sensitive production mode borehole caliper. Careful analysis is required to avoid erroneous interpretation of the data and to extract the maximum amount of information from the survey. If a caliper survey is available, a spinner survey can be used successfully in an openhole completion.

There are several practical guidelines to follow in order to obtain the best quality spinner data.

1) Ensure that the instrument is adequately centralized during the survey.

2) A combination of logging at a constant line speed with regular stops throughout the regions of interest will provide the most accurate record.

3) Conduct the survey at the maximum flowrate possible without developing a highly erratic flow regime around the perforations. This flowrate must be determined empirically.

4) Expect to spend a fair amount of time on the analysis of the data.

ACKNOWLEDGEMENTS

This work was supported by the Assistant Secretary for Conservation and Renewable Energy, Office of Renewable Technology, Division of Geothermal and Hydropower Technologies of the U.S. Department of Energy under Contract No. DE-AC03-76SF00098.

REFERENCES

Kuster Flowmeter MK II: Instructions, Operations and Maintenance Manual, Kuster Company, Long Beach, CA.

Lawton, R., Kolar, J., and Todd, B. (1982), Fluid Velocity Sensor Development Report, Hot Dry Rock Geothermal Energy Development Project, Los Alamos National Laboratory, Los Alamos, New Mexico 87545.

Veneruso, A.F., Simpson, R.S., Charles, A. (1980), High Temperature and Instrumentation Seminar Proceedings, Sandia National Laboratory, Albuquerque, New Mexico 87185.

Proceedings Ninth Workshop Geothermal Reservoir Engineering
Stanford University, Stanford, California, December 1983
SGP-TR-74

NONISOTHERMAL INJECTIVITY INDEX CAN INFER WELL PRODUCTIVITY AND RESERVOIR TRANSMISSIVITY

Omar Sigurdsson, Gudmundur S. Bodvarsson[+] and Valgardur Stefansson

Orkustofnun, Grensasvegur 9, 108 Reykjavik, Iceland.

ABSTRACT

In geothermal wells injection tests are commonly used to obtain well and reservoir data. These tests are typically conducted in a series of step rates followed or preceded by a complete shutin. Usually the temperature of the injected fluid is different from that of the reservoir fluid. Because of the strong temperature dependence of fluid viscosity and to a lesser extent, fluid density, nonisothermally related pressure responses must be considered. The nonisothermal injectivity index obtained from these tests depends on the mobility ratio of the cold region to the hot reservoir and the extent of the cold spot. This paper proposes a method of estimation of the apparent viscosity which accounts for these effects and relates the nonisothermal injectivity index to the isothermal injectivity index.

INTRODUCTION

In geothermal wells injection tests are commonly used to obtain well and reservoir data. The temperature of the injected fluid is invariably different from the temperature of the in situ reservoir fluid. Since fluid mobility, k/μ, plays the major role in pressure transient behavior, the strong temperature dependence of fluid viscosity and to a lesser extent, fluid density, has a large impact on the test. The dynamic viscosity of water changes by an order of magnitude between 20 °C and 300 °C, the major changes ocurring between 20 °C and 100 °C. However, the decrease in fluid density from 20 °C to 300 °C is approximately 30%. To interpret such tests the nonisothermally related pressure transient must be considered.

Several authors have discussed the interpretation of pressure transients during cold water injection into hot reservoirs. In particular, Bodvarsson and Tsang (1980) and Mangold et. al. (1981) considered the behavior of nonisothermal pressure transients in geothermal reservoirs and illustrated the effect of the temperature dependent fluid properties, viscosity and density. Tsang and Tsang (1978) developed a semi-analytic solution for pressure transients during cold water injection tests. O'Sullivan and Pruess (1980) and Garg (1980) discussed the analysis of injection and falloff tests in two-phase geothermal reservoirs. These studies demonstrated that the pressure transients during injection tests can be used to determine the transmissivity of the reservoir. In recent studies by Benson and Bodvarsson (1982) and Benson (1982) methods for calculating the skin factor and reservoir properties from nonisothermal injection tests were developed and the conditions in which the pressure transients behaved like a composite reservoir or moving front dominated problem for both single- and step-rate tests discussed. In the present study their work is extended by relating the nonisothermal injectivity to the reservoir transmissivity.

FORMULATION OF THE PROBLEM

Injection of cold water is frequently used as a testing procedure for geothermal wells, as for example in completion tests at the end of drilling. Injection tests are typically conducted in a series of step rates followed or preceded by a complete shutin. Since the duration of each step is seldom very long, usually few hours, stabilized time is usually not reached. The observed pressure is therefore transient and the injectivity so obtained only an approximation.

Now consider the system illustrated in Figure 1. It is that of a single well at the axis of a radial system of two concentric regions which can have different properties. Defining nondimensional time, radius and pressure as:

$$t_{DR} = \frac{k_1 t}{\phi_1 \mu_1 c_1 R^2} \qquad ....(1)$$

$$r_D = \frac{r}{R} \qquad ....(2)$$

+ Lawrence Berkeley Laboratory, Berkeley, California

References and illustrations at end of paper.

$$P_{D1} = \frac{2\pi k_1 h \rho_1}{q \mu_1} (P_i - P_1) \; ; \; 0<r_D<1 \quad (3)$$

$$P_{D2} = \frac{2\pi k_2 h \rho_2}{q \mu_2} (P_i - P_2) \; ; \; 1 < r_D \quad (4)$$

Then the flow equations in the two regions are:

$$\frac{\partial^2 P_{D1}}{\partial r_D^2} + \frac{1}{r_D} \frac{\partial P_{D1}}{\partial r_D} = \frac{\partial P_{D1}}{\partial t_{DR}} \quad ....(5)$$

and

$$\frac{\partial^2 P_{D2}}{\partial r_D^2} + \frac{1}{r_D} \frac{\partial P_{D2}}{\partial r_D} = \frac{1}{\gamma} \frac{\partial P_{D2}}{\partial t_{DR}} \quad ....(6)$$

where

$$\gamma = \frac{\{k/\phi\mu c\}_2}{\{k/\phi\mu c\}_1} \quad ....(7)$$

Initial conditions are P_1 and P_2 are P_i everywhere so:

$$P_{D1}(r_D,0) = P_{D2}(r_D,0) = 0 \quad ....(8)$$

There are three boundary conditions to consider; the inner boundary, the discontinuity and the outer boundary. At the inner boundary the condition is:

$$\lim_{r_D \to 0} r_D \frac{\partial P_{D1}}{\partial r_D} = -1 \quad ....(9)$$

At the discontinuity, the flux and pressure must be continuous so:

$$P_{D1} = P_{D2} \quad ....(10)$$

$$\frac{\partial P_{D1}}{\partial r_D} = \delta \frac{\partial P_{D2}}{\partial r_D} \quad ....(11)$$

where

$$\delta = \frac{\{k\rho/\mu\}_2}{\{k\rho/\mu\}_1} \quad ....(12)$$

Here, only the infinite outer boundary case is considered. Then the outer boundary condition is:

$$\lim_{r_D \to \infty} P_{D2}(r_D,t_{DR}) = 0 \quad ....(13)$$

RESULTS

Following the procedure of Horne et. al. (1980) the long time solution for P_{D1} can be written as:

$$P_{D1} = \frac{1}{2} \{ - Ei(-\frac{r_D^2}{4t_{DR}}) + Ei(-\frac{1}{4t_{DR}}) - \frac{1}{\delta} Ei(-\frac{1}{4\gamma t_{DR}}) \} \quad ....(14)$$

For a large time this may be approximated as:

$$P_{D1} = \frac{1}{2} \{ \ln(r_D^2) + \frac{1}{\delta} \ln(\frac{1.781}{4\gamma t_{DR}}) \} \quad (15)$$

In real space Eq. 15 becomes:

$$P_1 = P_i + \frac{q\mu_1}{4\pi k_1 h \rho_1} \{ \ln(\frac{R}{r})^2 + (\frac{k_1 \rho_1 \mu_2}{k_2 \rho_2 \mu_1}) \ln(\frac{2.246 k_2 t}{\phi_2 \mu_2 c_2 R^2}) \} (16)$$

For an isothermal homogeneous geothermal system the pressure at the well during injection can be written as:

$$P_{wf} = P_i + Bq + Cq^2 \quad ....(17)$$

where C is a constant governed by the pore structure of the porous medium, the radius and the condition of the well. The quadratic flow rate term accounts for the non-Darcy's flow effects. Assuming these effects to be negligible for the purpose of this study, the injectivity index can be expressed as:

$$II = \frac{q}{P_{wf} - P_i} = \frac{1}{B} \quad ....(18)$$

Because of the relatively short duration of each injection step in the test, the pressure at the well is considered to be transient. Then B can be approximated as:

$$B = \frac{\mu}{4\pi k h \rho} \ln(\frac{2.246kt}{\phi\mu c_t r_w^2}) \quad ....(19)$$

For homogeneous rock properties and single phase condition, Eqs. 16 and 17 along with Eq. 19 yield:

$$\frac{\mu_a}{\rho_a} \ln(\frac{2.246kt}{\phi\mu_a c_t r_w^2}) = \frac{\mu_1}{\rho_1} \{ \ln(\frac{R}{r_w})^2 + (\frac{\rho_1 \mu_2}{\rho_2 \mu_1}) \ln(\frac{2.246kt}{\phi\mu_2 c_t R^2}) \} \ ...(20)$$

Eq. 20 is a root solving problem to find the apparent viscosity which will represent the nonisothermal effect in a conventional manner. Figures 2 - 4 show how this apparent viscosity is related to the position of the thermal front

and the duration of the injection steps for the properties listed in table I. Thus the nonisothermal injectivity index is for engineering purposes approximately related to the isothermal injectivity index as:

$$II_{ISOTH} \simeq \left(\frac{\mu_a \rho_2}{\rho_a \mu_2} \right) II_{NONISOTH} \qquad (21)$$

DISCUSSION

Figure 5 has been constructed using the data in table I and the apparent viscosity relative to the cooled radius. It shows the transmissivity of the hot reservoir as a function of the injectivity depending on the size of the cooled radius. Figure 5 could equally well have been constructed from a rearrangement of Eq. 16. Figure 5 shows that when the nonisothermal injectivity and the size of the cooled zone are known (see Benson, 1982), the transmissivity of the reservoir can be determined. If the transmissivity and the nonisothermal injectivity are known, the size of the cold spot can be estimated. It is also possible to project the well productivity as its temperature recovers from the injection and the cold zone diminishes. Here it is assumed that the reservoir transmissivity does not change between injection and production. However, as Grant (1982) has pointed out, the injection transmissivity is in many instances observed to be several times greater than that for production. This might be due to an increase in permeability with injection either because of hydraulic fracturing or thermal contraction of rock and opening of fissures.

It has been pointed out (Benson and Bodvarsson 1982, Benson 1982) that the presence of a cooled zone around the well acts as an apparent positive skin. Hence, the presence of a positive skin will shift the curves on Figure 5 up and to the left while the presence of a negative skin will shift them down and to the right. Of particullar interest is the effect of fractures, since transmissivity or injectivity is usually dominated by natural fractures in geothermal systems. The presence of fractures will contribute to a negative skin, but the extent of a cooled zone is much greater at the fracture feed points than in the rock matrix. How these effects counteract each other is not fully known, but numerical studies indicate that the heat transfer from rock matrix to fissures significantly changes the radius of the zone occupied by the cold injection fluid (Bodvarsson and Tsang 1982).

EXAMPLES

A simulated nonisothermal step rate injection test was run on the numerical simulator, PT (Pressure - Temperature) (Bodvarsson 1981). The test consisted of three six-hour steps with injection rates of 0.10, 0.15 and 0.20 kg/s/m of 20 °C fluid into a 300 °C reservoir followed by a complete shutin. The reservoir properties used for the simulation are given in table I. The reservoir is a liquid saturated homogeneous porous medium. No cold spot exists around the well prior to injection. The observed injectivity at the end of each step is shown in Figure 6, which is similar to Figure 5. Since the transmissivity of the hot reservoir is constant during the test, one can see that the decrease in injectivity is a result of an increasing cold spot around the well. The size of the cold spot as determined by the transmissivity and the injectivity for each step is in good agreement with the location of the thermal front according to the simulator which is shown in Figure 6. Assuming that the isothermal injectivity is identical to the well productivity, the production index can be estimated by extrapolation, using Figure 6, as the well warms up.

The transmissivity and the injectivity index for a few of the wells in the Krafla geothermal field are plotted in Figure 7. The Krafla geothermal reservoir is fracture dominated so an average skin factor of s = -5 is assumed for the field. Following the methodology developed by Benson and Bodvarsson 1982, and Benson 1982, the size of the cold spot around the wells due to drilling and injection testing is estimated to be 2 to 3 m on the average. However, since the reservoir is fracture dominated, the distance to the thermal front can be considerably greater in the fractures or around the feed points in the wells. On the other hand the distance to the thermal front in the nearly impermeable rock matrix, between the feed points in the wells, can be of the order of a few cm and is controled by the thermal conduction of the rock matrix. The size of the cold spot as obtained from Figure 7 when the data is plotted according to the methodology of this paper is therefore some weighted average of these two distances. It seams therefore that the existence of a cold spot around the feed points in a well in a hot fractured reservoir has very litle effect on the relationship between transmissivity and injectivity. Other factors such as the skin effect are problably dominating the effect of the cold invasion zone in fracture dominated reservoirs.

CONCLUSIONS

Through theoretical considerations an apparent viscosity has been established which relates the nonisothermal injectivity index, obtained from nonisothermal step rate tests, to the isothermal injectivity index. Thus it is possible to use the nonisothermal injectivity index to estimate the reservoir transmissivity and infer the well productivity.

NOMENCLATURE

c_t = total system compressibility, Pa^{-1}
C_r = specific heat capacity, J/kg°C
h = thickness, m
II = injectivity index, kg/sPa
k = permeability, m^2
P = pressure, Pa
q = mass flow rate, kg/s
r = radius, m
R = radius of cold spot, m
t = time, s
T = temperature, °C
μ = dynamic viscosity, Pa s
ρ = density, kg/m^3
ϕ = porosity
λ = thermal conductivity, W/m°C

Subscripts

a = apparent
c = cold
D = dimensionless
i = initial
inj = injection
r = rock
w = well
wf = well flowing
1 = inner (cold) region
2 = outer (hot) region

ACKNOWLEDGMENTS

We thank Rafmagnsveitur Rikisins, Krofluvirkjun for permission to use data from the Krafla geothermal field.

REFERENCES

1. Benson, S. M. and Bodvarsson, G. S.: "Non-isothermal Effects During Injection and Falloff Tests," paper SPE 11137, presented at the SPE 57th Annual Fall Technical Conference and Exhibition, New Orleans, Louisiana, 1982.

2. Benson, S.: "Interpretation of Noniso-thermal Step-Rate Injection Tests," Proceedings 8th Workshop on Geothermal Reservoir Engineering, Stanford University, Stanford, California (Dec. 1982).

3. Bodvarsson, G. S. and Tsang, C. F.: "Thermal Effects in the Analysis of Fractured Reservoirs," 3rd Invitational Well Testing Symposium, Lawrence Berkeley Laboratory Report, LBL-12076, Berkeley, California (March 1980).

4. Bodvarsson, G. S.: "Mathematical Modelling of the Behavior of Geothermal Systems Under Exploitation," Ph. D. dissertation, University of California, Berkeley, 1981.

5. Bodvarsson, G. S. and Tsang, C. F.: "Injection and Thermal Breakthrough in Fractured Geothermal Reservoirs," J. Geophys. Res., v. 87, No 82 (Feb. 1982) 1031-1048.

6. Garg, S. K.: "Pressure Transient Analysis for Two-Phase (Water/Steam) Geothermal Reservoirs," Soc. Pet. Eng. J. (June 1980) 206-214.

7. Grant, M. A.: "The Measurement of Permeability by Injection Tests," Proceedings 8th Workshop on Geothermal Reservoir Engineering, Stanford University, Stanford, California (Dec. 1982).

8. Horne, R. N., Satman, A. and Grant, M. A.: "Pressure Transient Analysis of Geothermal Wells with Phase Boundaries," paper SPE 9274 presented at the SPE 55th Annual Fall Technical Conference and Exhibition, Dallas, Texas (1980).

9. Mangold, D. C., Tsang, C. F., Lippmann, M. J. and Witherspoon, P. A.: "A Study of Thermal Discontinuity in Well Test Analysis," J. Pet. Tech. (June 1981) 1095-1105.

10. O'Sullivan, M. J. and Pruess, K.: "Analysis of Injection Testing of Geothermal Reservoirs," Geothermal Resources Concil Transactions, vol. 4 (1980).

11. Tsang, Y. W. and Tsang, C. F.: "An Analytic Study of Geothermal Reservoir Pressure Response to Cold Water Reinjection," Proceedings 4th Workshop on Geothermal Reservoir Engineering, Stanford University, Stanford, California (Dec. 1978).

Table I. Reservoir Properties

Permeability, k_r	$1.0 \cdot 10^{-14}$ m^2
Thickness, h	1.0 m
Porosity, ϕ	0.20
Specific heat capacity, C_r	1000.0 J/kg°C
Density, ρ_r	2200.0 kg/m^3
Thermal conductivity, λ	2.0 W/m°C
Total system compressibility, c_t	$1.0 \cdot 10^{-9}$ Pa^{-1}
Wellbore radius, r_w	0.10 m

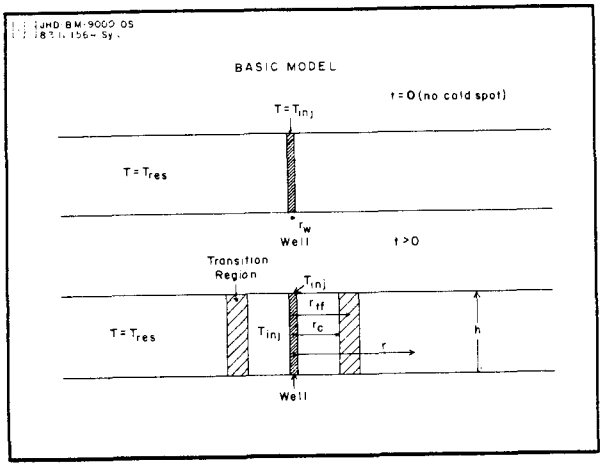


Figure 1. Schematic picture of the reservoir system before and after nonisothermal injection

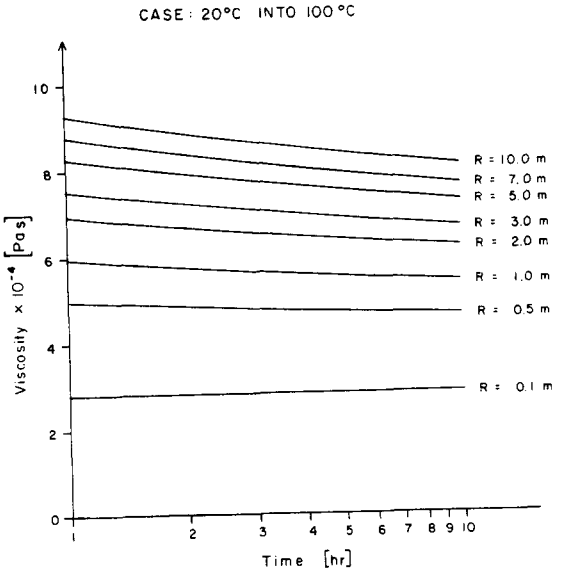


Figure 2. Apparent viscosity as a function of the duration of the injection steps and the size of the cold spot for injection of 20 °C water into 100 °C reservoir.

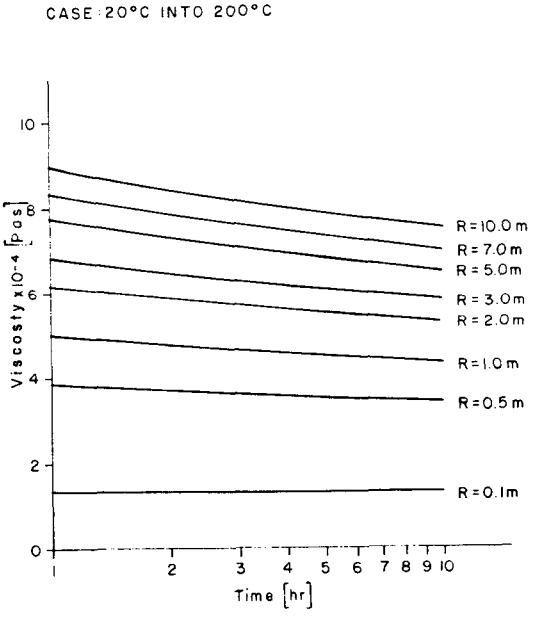


Figure 3. Apparent viscosity as a function of the duration of the injection steps and the size of the cold spot for injection of 20 °C water into 200 °C reservoir.

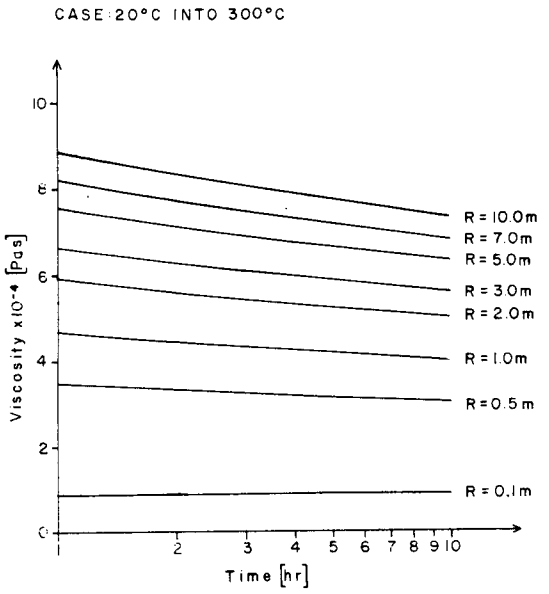


Figure 4. Apparent viscosity as a function of the duration of the injection steps and the size of the cold spot for injection of 20 °C water into 300 °C reservoir.

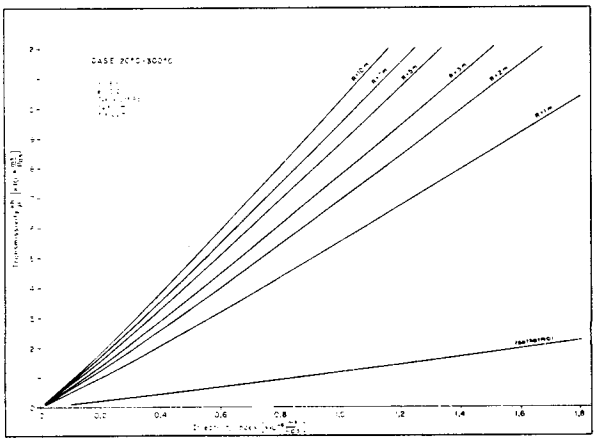


Figure 5. Transmissivity as a function of the injectivity and the size of the cold spot.

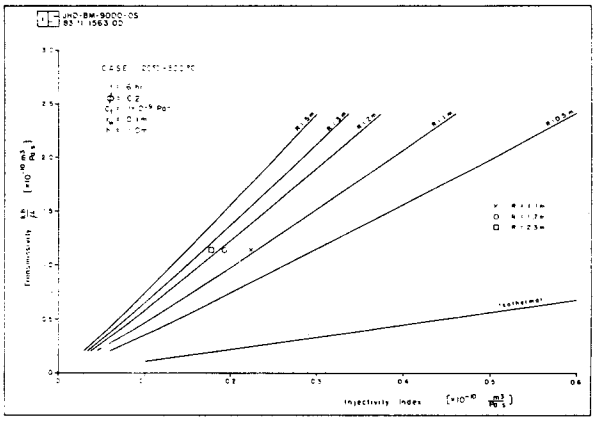


Figure 6. The relationship between transmissivity and injectivity for the simulated example.

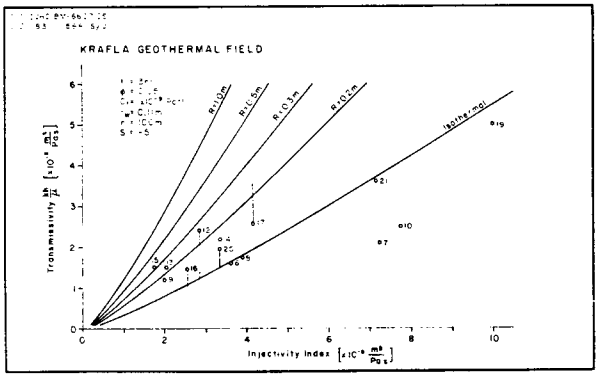


Figure 7. The relationship between transmissivity and injectivity for a few of the wells in the Krafla geothermal field.

Proceedings Ninth Workshop Geothermal Reservoir Engineering
Stanford University, Stanford, California, December 1983
SGP-TR-74

EFFECT OF SCALING ON DOWNHOLE PRESSURE TRANSIENT DATA

Susan Petty

Well Production Testing, Inc.
P.O. Box 69
Carlsbad, CA 92008

ABSTRACT

Test data from several wells where scale either formed in the wellbore or in the reservoir have been observed. Some generalizations can be made about the behavior of downhole and wellhead pressure during drawdown and build-up. In addition, estimates of the size of the obstruction can be made in the field. Reservoir parameters can be calculated from pressure build-ups, after the problem of downhole scaling has been identified.

INTRODUCTION

During many long-term test situations in geothermal wells, scale deposits accumulate in the wellbore or in the reservoir. This obstruction to the flow clearly influences test results, as well as causing problems in future production operations. Scale control and clean-up methods are available, but to evaluate the economics of production, we need some idea of the rate of scale build-up, the location of the scale and some estimates of reservoir parameters despite the scale. Since the flow regime in the wellbore is generally two-phase and, in the presence of a rapid change in the size and shape of the flow path, also non-equilibrium, modeling the deposition of scale isn't an easy task. We can, however, use the data collected during long-term tests to evaluate well productivity and make some predictions about rate of scale formation if we collect both downhole and wellhead pressure data. Also, in order to avoid losing or damaging tools used for downhole measurements during production testing, we can make some estimates of the size of the hole remaining in the obstruction.

TEST OBSERVATIONS

Scaling downhole has been observed during several test situations. The most useful data was obtained where both downhole and wellhead pressure were measured. For ease of discussion, scaling is designated as being either in the wellbore or outside the wellbore and, therefore, in the reservoir. Scale in the reservoir may be very close to the wellbore and/or in the liner perforations. Test observations discussed here include three cases:

CASE 1: WELLBORE SCALE - CONSTANT RATE TEST

Scale forms in the wellbore during a constant rate test.

CASE 2: WELLBORE SCALE - FALLING RATE AND PRESSURE

Scale forms in the wellbore during a test where rate and pressure are allowed to drop.

CASE 3: RESERVOIR SCALE - CONSTANT RATE

Scale forms in the reservoir near the wellbore during a constant rate test.

Scale deposition should be most rapid in the zone where flashing occurs, regardless of the type of scale being formed. Initially, the length of the wellbore over which vapor bubbles are nucleating may be short, or if dissolved gases are present, quite long. As pressure draws down in the reservoir, the flash zone will move down the borehole. Thus, wellhead pressure will be the result of the

saturation pressure at the reservoir temperature, pressure drops due to frictional losses in the two-phase flow region, head loss due to heat transfer in the borehole, head loss due to the length of the two-phase zone and expansion and vaporization of the fluid as head is reduced. As drawdown in the reservoir slows with time, the flash zone will remain close to the same point in the borehole. When drawdown is rapid, scale will be deposited in a thin layer over a long section of casing. As drawdown slows, scale will begin to build-up into an obstruction which causes a rapid change in borehole diameter. Since the position of the obstruction is keeping up with the flash point, it is reasonable to assume that the fluid eventually is two-phase above the obstruction and a single-phase liquid below it. Observations of scale build-up in surface piping show that scale takes the approximate shape of the flow lines.

CASE 1: WELLBORE SCALE - CONSTANT RATE TEST

When flow rate is controlled and kept constant at the surface, the downhole pressure can be expected to continue to drop as the reservoir pressure drops, despite the increase in size of the obstruction. The wellhead pressure will drop rapidly, however, as the test choke or valve is opened to maintain the flowrate. At some point, the obstruction chokes the flow and the mass flux across the constriction is limited; further reductions in wellhead pressure will not result in increased flow rate and the test will become a falling rate test unless a decision is made to shut-in the well and observe recovery. At this point, the pressure in the reservoir will begin to level out or rise as the choke limits flow rate.

If scale accumulation is very slow and choking does not occur, the wellhead pressure should drop as the scale increases pressure loss due to increased friction in the borehole and decreased size of the borehole. However, these quantities make up less than 10% of the total pressure loss in the borehole and the difference in rate of change of the wellhead pressure compared to downhole pressure may be difficult to detect before a fairly large amount of scale has accumulated. This is particularly true if the reservoir is fractured or if boundaries occur in the reservoir, since these changes may obscure the scale problem until it becomes severe.

CASE 2: WELLBORE SCALE - VARIABLE RATE/PRESSURE TEST

When flow rate is allowed to fall as reservoir pressure drops, the effect of scale build-up in the wellbore will be seen as an increased rate of drop in the wellhead pressure and flow rate. The downhole pressure levels off and finally increases, due to the decreased flow rate. Again, choking will occur when the obstruction is large enough, but before choking occurs, the flow rate will already have begun decreasing more rapidly due to the frictional losses. The wellhead pressure will drop reflecting the increased heat loss in the wellbore due to the lower velocities, but this drop will be minor compared to the rapid drop in wellhead pressure which occurs when the obstruction becomes large enough to choke the flow downhole. (See Figure 1.) Figure 2 shows the very rapid drop in flow rate and wellhead pressure associated with scaling in the borehole. This data was collected at the end of a three-month flow test where scale deposition was very slow and probably spread over a long section of the borehole during early parts of the test, due to a large amount of dissolved CO_2.

CASE 3: SCALE IN THE RESERVOIR - CONSTANT RATE TEST

If flow rate is held constant while scale accumulates either in the reservoir or at the perforations of a liner, downhole pressure will give the appearance of a reservoir with either a no-flow or low-permeability boundary. (See Figure 3.) As reservoir scale continues over a long time period, it will become impossible to maintain a constant rate due to very large pressure losses and reduced permeability, especially near the wellbore. Reservoir scale is much more likely when a single-phase reservoir becomes two-phase, due to pressure drops caused by production. The largest flow volume through the smallest area occurs near the wellbore with the result that scale will build-up

most rapidly in this zone. For this reason, pressure build-up in a well where scale has occured in the reservoir should show a large skin effect where skin effect during drawdown would be much smaller. (See Figure 4.) Pressure build-up data also should not show any boundary effects.

CONCLUSIONS

Observations of test results show that build-up of scale in the wellbore is difficult to detect during early time. Increased frictional pressure losses due to the thin layer of scale deposited in the two-phase region make up a small percentage of the total pressure losses contributing to the wellhead pressure and may result in a decrease in wellhead pressure of less than 2 psi in 5000 feet of wellbore.

The build-up of scale in the reservoir will give erroneous results if reservoir properties are calculated from drawdown curves. Build-up curves will show extremely large skin effects. Since pressure drop across the obstruction may lower the flash point in the wellbore, downhole pressure measurements may be slightly affected by scaling during a constant rate test. Drawdown and build-up curves should be compared to see if this effect is present.

When scale begins to build in one section of the borehole, however, it is very likely the flashing will occur in the narrowest part of this obstruction, due to the rapid pressure drop (Simoneau, 1975). The speed of sound in a two-phase liquid is given by the equation:

$$\frac{1}{c^2} = -\rho^2 \left(\frac{d\bar{v}_\ell}{dP} (1-x) + \frac{d\bar{v}_g}{dP} x + \frac{dx}{dP} \bar{v}_{g-\ell} \right)$$

where c is the speed of sound, ρ is the density of the mixture, x the quality, $\bar{v}_\ell$ is the specific gravity of the liquid and $\bar{v}_g$ is the specific gravity of the gas. Combining this with the Clausius - Clapeyon equation and looking at the limit for zero quality we have:

$$\lim_{x \to o} \frac{1}{c^2} = -\rho^2 \left(\frac{d\bar{v}_\ell}{dP} - \frac{\bar{v}^2_{g-\ell} C_\ell T}{L^2} \right)$$

where C_ℓ is the specific heat of the liquid, T is the temperature, and L^2 is the heat of vaporization (Rohatgi, 1975). This gives a velocity for the speed of sound right at the point where nucleation of vapor begins in water at atmospheric pressure of 6 ft/sec, which is a great deal less than 4794 ft/sec, the velocity of sound in liquid water. At a mass flux of 300,000 lb/hr, choking would occur in an opening 14 inches in diameter. For water at saturation pressure for 400° F, this discontinuity is less and an opening of 2 inches will choke the flow. Since changes in upstream pressure in a choked flow will not cause changes in the flow rate, we can determine the point when choking occurs by opening a throttle valve or test choke if we are throttling the well. We can then determine the speed of sound for the inception of boiling for the reservoir temperature and calculate the size of the opening needed to cause choking using the equation:

$$A = \frac{Q}{\rho c}$$

where A is the cross-sectional area at the obstruction, Q is the mass flux, ρ is the density of the liquid and c is the speed of sound at the flash point.

REFERENCES

1. Rohatgi, U.S. and Reshotko, E.: "Non-Equilibrium One-Dimensional Two-Phase Flow in Variable Area Channels," in Non-Equilibrium Two-Phase Flows, American Society of Mechanical Engineers, November, 1975.

2. Simoneau, R. J.: "Pressure Distribution in a Converging-Diverging Nozzle During Two-Phase Choked Flow of Subcooled Nitrogen," in Non-Equilibrium Two-Phase Flows, American Society of Mechanical Engineers, November, 1975.

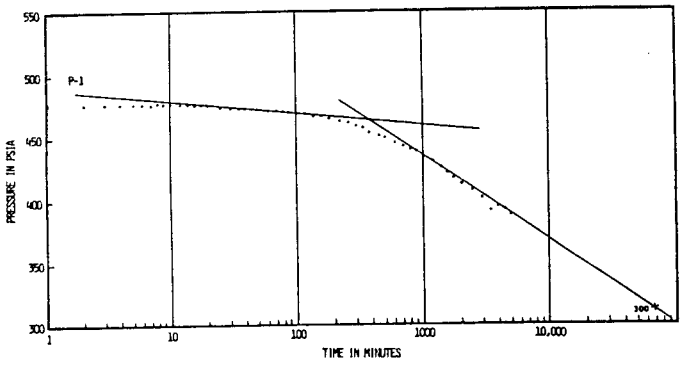


Figure 1. Constant Rate Test - Pressure Drawdown (7/12 - 7/19/82).

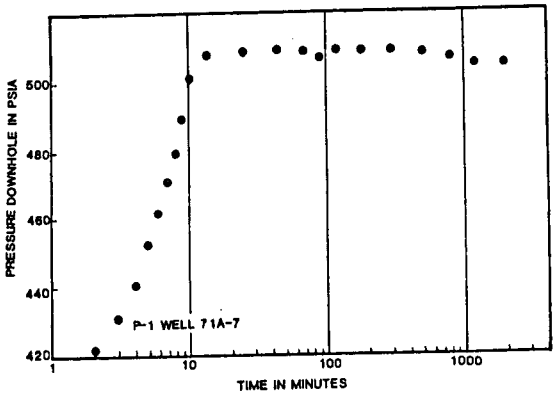


Figure 2. Constant Rate Test - Pressure Build-up (7/19 - 7/23/82).

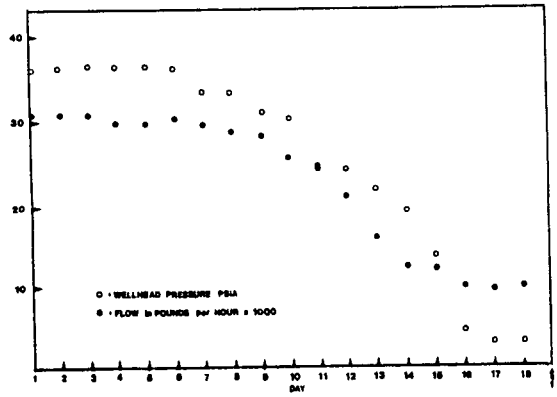


Figure 4. Falling Rate Test - Wellhead Pressure & Flowrate.

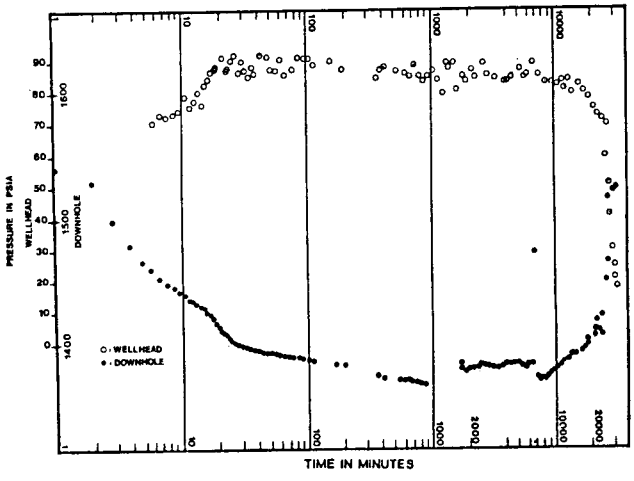


Figure 3. Falling Rate Test - Wellhead & Downhole Pressure.

Proceedings Ninth Workshop Geothermal Reservoir Engineering
Stanford University, Stanford, California, December 1983
SGP-TR-74

EFFECTS OF NATURAL RECHARGE ON GAS COMPOSITION IN THE LARDERELLO - CASTELNUOVO AREA

Franco D'Amore*, Romano Celati*, Claudio Calore*, Rino Bertrami**

*CNR-Istituto Internazionale per le Ricerche Geotermiche
PISA, Italy

**ENEL-Unità Nazionale Geotermica
PISA, Italy

ABSTRACT

A study of the temporal behaviour of gas composition in the Larderello-Castelnuovo area shows that this behaviour varies, depending on whether the wells are affected or not by natural recharge. Where no natural recharge exists, gas composition seems to be governed by chemical equilibria. The recharge water, and the steam it produces, mix with the fluid already existing in the reservoir. At Larderello (far from absorption areas) the gas composition resulting from this mixing does not undergo further changes by chemical reactions. This is due either to a lack of reactivity where there is no liquid phase or to an ineffective fluid-rock interaction. At Castelnuovo (close to absorption areas) the H_2S and CH_4 contents in the gas have gradually decreased with the increase in recharge effects. The decrease in H_2S can be attributed to dissolution in liquid water and oxidation. Various hypotheses have been forwarded for the methane. The correlation existing between CH_4 and N_2 concentrations, even when the methane decreases in the areas affected by recharge, suggests that CH_4 may be governed by more than just the Fisher-Tropsch reaction.

INTRODUCTION

In an earlier paper (Calore et al.,1982) the spatial and temporal variations in gas/steam ratio and the isotopic composition of the steam were studied in the Larderello-Castelnuovo area. This study showed that fluid composition in these zones of the field is mainly controlled by a mixing between the fluid originally present in the reservoir and recent meteoric waters. The areas affected by natural recharge were also gradually expanding. This paper deals with the variation in uncondensable gas composition in the area affected by natural recharge. A comparison is also made with fluid composition in areas unaffected by this phenomenon.

FLUID COMPOSITION IN THE LARDERELLO-CASTELNUOVO AREA

H_2 and H_2S concentrations in the uncondensable gas are plotted in Figs.1 and 2 versus gas/steam ratio. The evolution with time of gas/steam ratio is different in the wells unaffected by recharge (D'Amore & Truesdell, 1979; D'Amore et al.,1981; D'Amore et al.,1982) compared to wells affected by this phenomenon (Calore et al.,1982). In the latter case the typical trend exhibits strong decreases in gas/steam ratio within a relatively short time, accompanied by a shift in $\delta^{18}O$ towards more negative values and, in many cases, by the appearance or increase of the tritium content in the steam. This behaviour has been attributed to a mixing between the steam originally present in the reservoir and the steam formed by the vaporization of the recharge water containing tritium, with very negative $\delta^{18}O$ and almost no gas.

In the zones unaffected by recharge of recent meteoric waters, the H_2 and H_2S contents in the steam (Figs.1 and 2) vary inversely with the gas/steam ratio (D'Amore et al.,1982). The bands shown in these Figures include the Larderello wells with estimated reservoir temperatures in the 240°-260°C range. The trend is the same for different wells and for each single well in different periods, whether the gas/steam ratio increases or decreases.

In the wells affected by recharge, the percentage of H_2 in the uncondensable gas remains more or less constant with the decrease in gas/steam ratio, both at Larderello and Castelnuovo. This means that the H_2/H_2O ratio varies proportionally with the gas/H_2O ratio, as if the original steam was simply diluted by a gas-free vapour. The H_2S content in the uncondensable gas exhibits a different trend at Larderello from that at Castelnuovo. In the former area it remains

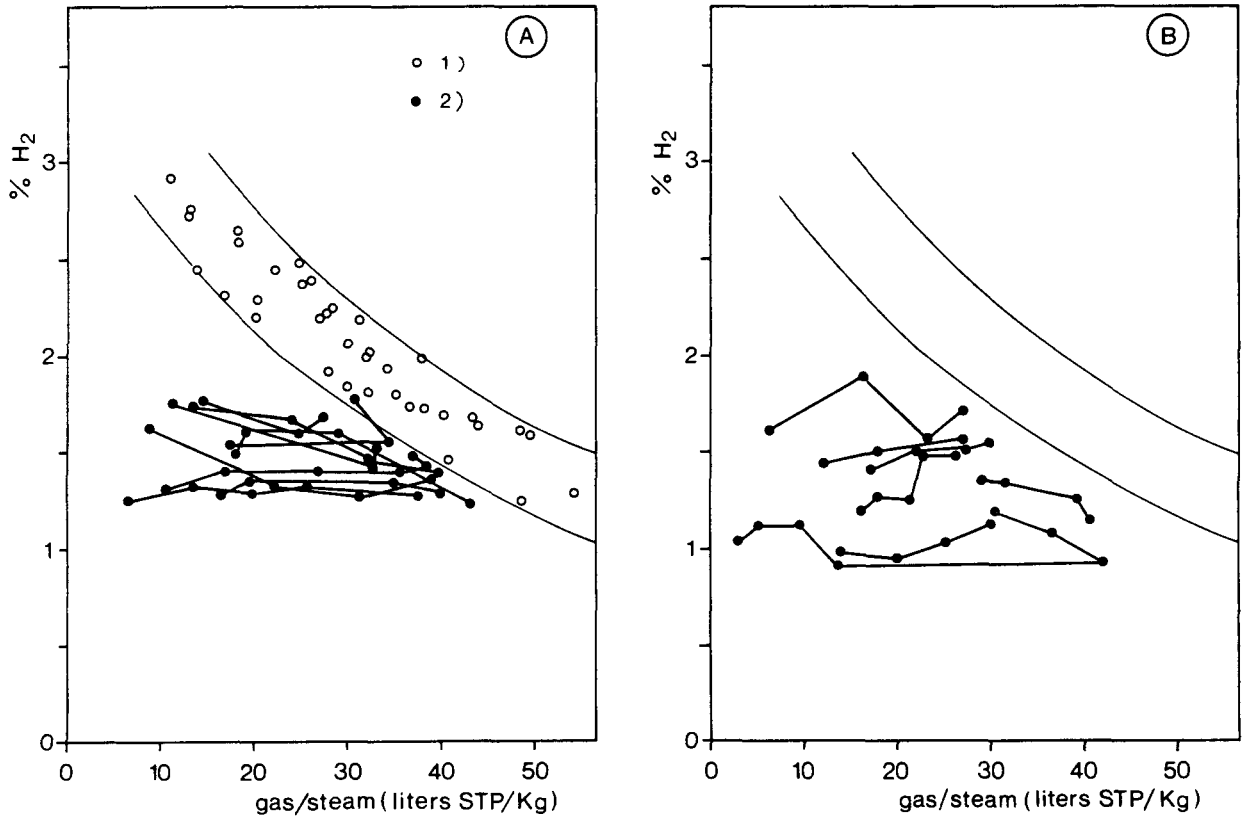


Figure 1. H_2 (molar percent in the uncondensable gas) versus gas/steam ratio. A) Larderello area; B) Castelnuovo area. 1)wells unaffected by recharge; 2)wells affected by recharge. The band in Fig. 1A is shown in Fig.1B for comparison.

practically constant, whereas in the latter it shows a strong decrease with the decrease in gas/steam ratio. Figure 3 shows the zone of the field for which there is no evidence of recharge effects and the zones, affected by recharge, where the H_2S content remains constant (Larderello) or decreases (Castelnuovo).

The percentage of CH_4 in the uncondensable gas shows no correlation with the gas/steam ratio in the areas unaffected by recharge (Table 1); on the other hand, its areal distribution in that area is well defined, and similar temporal trends are shown by groups of neighbouring wells. Figure 4 illustrates the CH_4 trend in the Larderello area before recharge had any effect on the zone. The Castelnuovo area is excluded from this map as there were not enough data available to define any temporal behaviour before the effects of recharge. Two zones can be distinguished in Fig.4 in which the CH_4 molar percentage remained constant with time, at values of 0.2-0.5 and 1-2 respectively. In the intermediate zone the $\%CH_4$ increased considerably (as much as 100%) before recharge effects became evident.

In the Castelnuovo area the methane content in the gas showed a well-defined areal distribution during the period 1940-1950. It increased regularly from about 0.1 on the southernmost margin to 1-1.5 on the northern margin.

Recharge produced a general strong decrease in the CH_4/gas ratio at Castelnuovo (Table 2).At Larderello the most conspicuous decreases caused by recharge occurred in the wells that initially had the highest percentages of CH_4, whereas in the wells with the lowest initial values the latter remain constant or decrease very little. It is difficult to distinguish any trend in the case of the lowest values, however, as the analytical errors are of the same order of magnitude as the variations.

A general correlation was noted throughout the whole Larderello field between CH_4 and N_2.This correlation is shown by D'Amore et al.(1983). Figure 5 shows that this correlation holds even when $\%CH_4$ decreases in the wells affected by recharge.

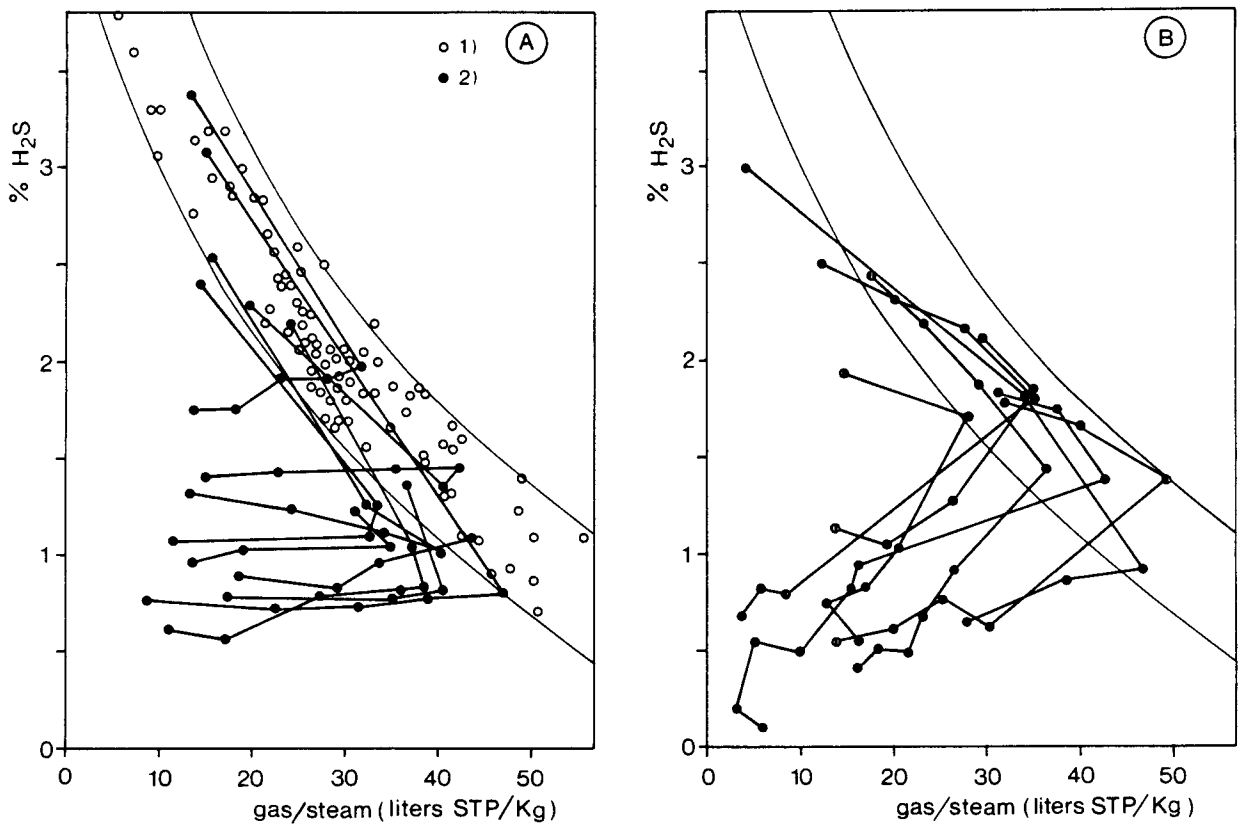


Figure 2. H_2S (molar percent in the uncondensable gas) versus gas/steam ratio. See Fig.1 for symbols.

DISCUSSION

Fluid composition in zones unaffected by recharge

According to the conceptual model of D'Amore & Truesdell (1979), different parts of the reservoir with different fluid compositions and liquid saturations can be distinguished in a vapour-dominated system. Temporal variations in the gas/steam ratio have been explained by the fact that expansion of the drainage volume is accompanied by a temporal variation in the contribution to production of various zones of the reservoir. D'Amore et al.(1982) have shown that H_2 and H_2S contents in the fluid are governed by the following two equilibria in adequate redox conditions (oxygen and sulphur fugacity):

$$H_2O = H_2 + \tfrac{1}{2}O_2 \qquad (1)$$

$$H_2S = H_2 + \tfrac{1}{2}S_2 \qquad (2)$$

Equations (11) and (17) in D'Amore et al.(1982) have been modified, for oxygen fugacity, according to D'Amore & Gianelli (1984):

$$\log f_{O_2} = -3.808 - 13708.3/T - 2.075 \times 10^6/T^2 \qquad (3a)$$

and, for sulphur fugacity, according to the following empirical correlation (valid for the Larderello field):

$$\log f_{S_2} = 5.706 - 9767/T \qquad (3b)$$

These equations can be rewritten as:

$$\log\left(\frac{n_{H_2}}{n_{H_2O}}\right)_{WH} = \log\left(\frac{n_{H_2}}{n_{gas}}\right)_{WH} + \log\left(\frac{n_{gas}}{n_{H_2O}}\right)_{WH}$$

$$= 4.556 - 5922/T + 1.038 \times 10^6/T^2 + \log\left(y + \frac{1-y}{B_{H_2}}\right) \qquad (4)$$

$$\log\left(\frac{n_{H_2S}}{n_{H_2O}}\right)_{WH} = \log\left(\frac{n_{H_2S}}{n_{gas}}\right)_{WH} + \log\left(\frac{n_{gas}}{n_{H_2O}}\right)_{WH}$$

$$= 7.539 - 6410.75/T - 0.79 \log T + 1.038 \times 10^6/T^2 + \log\left(y + \frac{1-y}{B_{H_2S}}\right) \qquad (5)$$

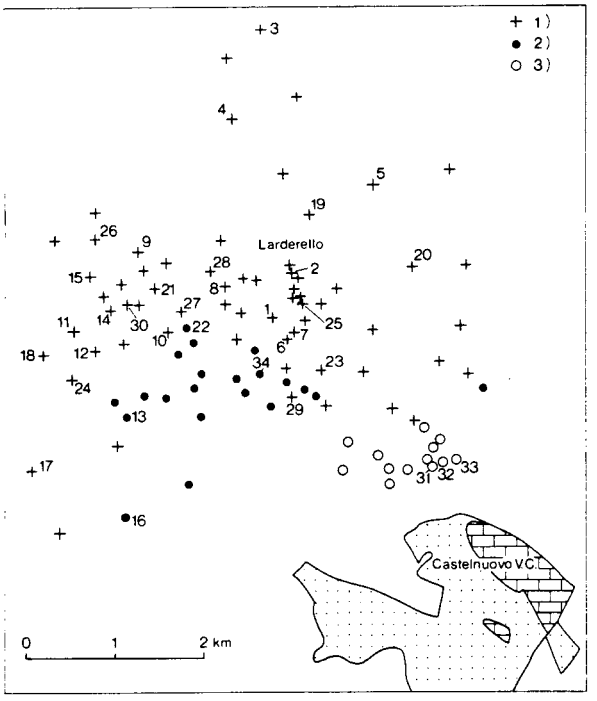


Figure 3. Location of wells with different evolution of $\%H_2S$ in the uncondensable gas. 1) Wells unaffected by recharge; 2) wells affected by recharge, with constant $\%H_2S$; 3) wells affected by recharge, with decreasing $\%H_2S$.

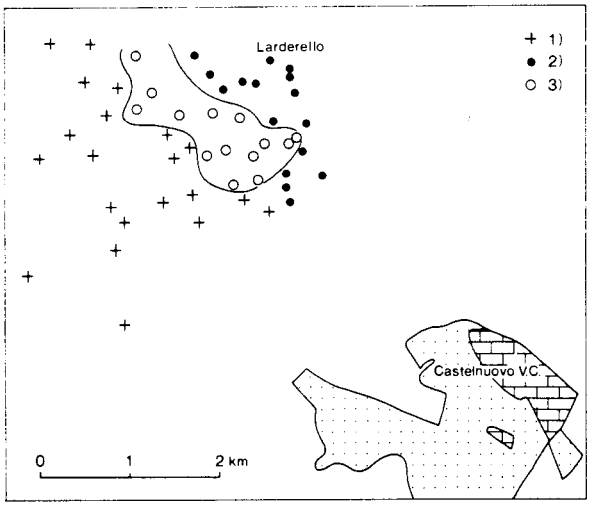


Figure 4. Areal distribution and temporal evolution of CH_4 (molar percent in the uncondensable gas) for the Larderello wells before recharge effects became evident. 1) $\%CH_4$ constant in the range 0.2-0.5; 2) $\%CH_4$ constant in the range 1-2; 3) $\%CH_4$ increasing with time towards values of 1-2.

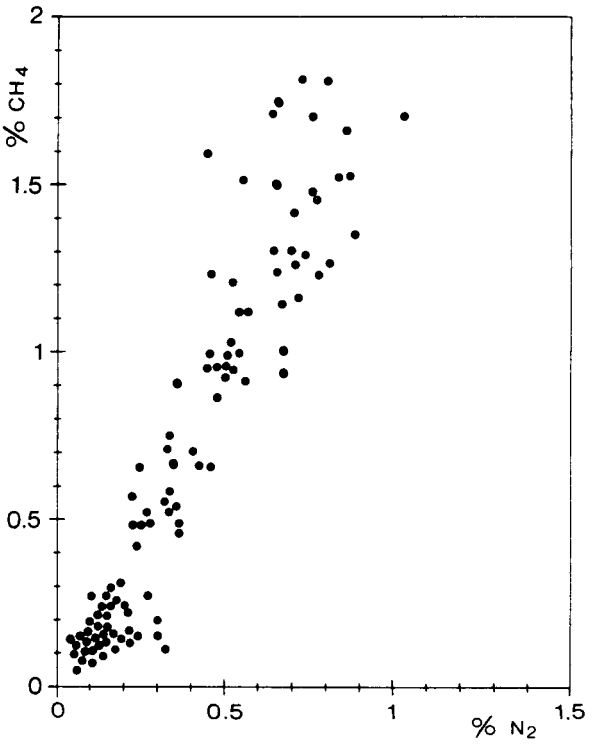


Figure 5. Correlation between $\%CH_4$ and $\%N_2$ in the uncondensable gas from nine wells affected by natural recharge.

where n is the number of moles, T is temperature in °K, B_i is the distribution coefficient of the species i between steam and liquid water, and y is the molar fraction of steam in the steam-water mixture in the reservoir. These equations are valid in the following conditions (D'Amore & Celati, 1983):

- the fluid produced comes from one two-phase source in chemical and phase equilibrium;
- the two-phase fluid present in the reservoir is transferred to the well with no chemical reactions and no gain or loss of mass, although it may undergo phase changes (liquid boiling).

From the above equations it follows that the H_2 and H_2S concentrations in the gas vary inversely with the gas/steam ratio (for constant T and y), and increase as a function of T and y. The field data shown in Figs. 1 and 2 are clustered within relatively narrow bands for two reasons:

a) the selected wells have rather uniform reservoir temperatures;
b) all other conditions being equal (temperature, fluid composition in the steam phase, etc.), the gas/steam ratio increases with y.

Table 1 gives fluid composition for some wells at Larderello during a period in which their gas/steam ratio remained more or less constant. Also shown are estimated reservoir temperatures based on production data and in-hole logs. In order to verify whether eqs.(4) and (5), at these temperatures, are consistent with fluid analyses, we calculated y for each well from eqs.(4) and (5) (y_H and y_S). The y values obtained are plausible, and there is usually a satisfactory agreement between the y values from these two equations.

As regards CH_4, assuming that the Fisher-Tropsch reaction

$$CO_2 + 4H_2 = CH_4 + 2H_2O \qquad (6)$$

is in equilibrium in a two-phase system, and that the hypotheses made for eqs.(4) and (5) are valid, then:

$$\log\left(\frac{n_{CH_4}}{n_{gas}}\right)_{WH} = \log\left(\frac{n_{CO_2}}{n_{gas}}\right)_{WH} + 4\log\left(\frac{n_{H_2}}{n_{H_2O}}\right)_{WH} + 0.26 + 5227/T - 4\log\left(y + \frac{1-y}{B_{H_2}}\right) - \log\left(y + \frac{1-y}{B_{CO_2}}\right) + \log\left(y + \frac{1-y}{B_{CH_4}}\right) \qquad (7)$$

Equation (7) does not satisfactorily explain the variations in CH_4/gas ratio observed in the area. According to the y values calculated from eq.(7) (y_{FT} in Table 1) the low CH_4/gas ratios should be tied to high y values. The y values obtained from eq.(7) in this case are, however, systematically higher than those obtained from eqs.(4) and (5). Note that eqs.(4), (5) and (7) are valid only for one two-phase source of fluid. Following the model of D'Amore & Truesdell (1979), however, the fluid may come from various zones of the reservoir with possibly different fluid compositions and physical characteristics. The y value obtained when assuming a single source is still meaningful in the case of various sources, if the latter have the same temperature and steam phase composition. In this case the calculated term $y + \frac{(1-y)}{B}$ represents the weighted average of these terms of the various sources.

The correlation between CH_4 and N_2 at Larderello cannot be explained by considering reaction (6) as the only possible equilibrium controlling methane concentration. If at least some of the methane derives from the products of decomposition of organic nitrogenous compounds (C, N_2, H_2), on the other hand, then CH_4 and N_2 could be linked together in the same chemical reaction. D'Amore et al.(1983) have considered the reaction:

$$C + \frac{1}{2}N_2 + 7/2\ H_2 = CH_4 + NH_3 \qquad (8)$$

In the same hypotheses on chemical equilibria and the boiling process formulated for reactions (1),(2) and (6), we obtain:

$$\log\left(\frac{n_{NH_3}}{n_{H_2O}}\right)_{WH} + \log\left(\frac{n_{CH_4}}{n_{H_2O}}\right)_{WH} - \frac{7}{2}\log\left(\frac{n_{H_2}}{n_{H_2O}}\right)_{WH} - \frac{1}{2}\log\left(\frac{n_{N_2}}{n_{H_2O}}\right)_{WH} = 0.14 + 2737.5/T + \log\left(y + \frac{1-y}{B_{NH_3}}\right) + \log\left(y + \frac{1-y}{B_{CH_4}}\right) - \frac{7}{2}\log\left(y + \frac{1-y}{B_{H_2}}\right) - \frac{1}{2}\log\left(y + \frac{1-y}{B_{N_2}}\right) \qquad (9)$$

The y values calculated from eq.(9) for the field data (y_{CN} in Table 1) are generally in good agreement with those calculated from the H_2 and H_2S concentrations (eqs.(4) and (5)).

The temporal increases in CH_4/gas ratio observed at Larderello occurred in a zone lying between the central zone of Larderello, with a relatively high CH_4/gas ratio, and the south-western zone, with a low CH_4/gas ratio. Since several sources at varying depths contribute to fluid production, we may assume that the contribution from the deepest sources gradually increased with time in the zone with an increasing CH_4/gas ratio. Fluid composition thus gradually came closer to that in the adjacent central zone, where the contribution from depth was already quite large (D'Amore & Truesdell, 1979).

Fluid composition in the zones affected by recharge

At Larderello the constant values of H_2 and H_2S (Figs.1A, 2A) are indicative of a mixing in the steam phase with no further changes due to chemical reactions.

The recharge water during its flow towards the centre of the field is assumed to be totally vaporized after a rather short distance. The steam produced in this way has probably a low gas content. During its flow within the field this 'recharge steam' mixes with the steam and gas rising from the deeper boiling zones, and the resulting fluid is, in part, extracted

through the productive wells along this flow-path. The gradients observed in the gas/steam ratio and in isotopic composition (Calore et al.,1982) can be ascribed to this process. This gradual mixing process does not change the H_2 and H_2S concentrations in the gas,since these concentrations are almost uniform in the deep steam all along the flow-path, as indicated by the H_2 and H_2S concentrations observed before recharge effects became important in the area. This is not the case for methane, whose concentration was not uniform in the area. The lowest values occur in the southern zone, i.e. in the first part of the flow-path of the recharge fluid. Thus the mixing produced a decrease in CH_4 concentration in the gas of the wells furthest from the recharge areas, which had a high CH_4 content before mixing.

When an excess of water is present as steam in the fluid resulting from the mixing, the equilibria considered in the system unaffected by recharge generally no longer hold for the mixture. A new equilibrium is apparently not attained for H_2. This may be the result of the lack of a liquid phase, or of the limited rock volumes capable of interacting with the fluid: if the fluid flows prevalently through a small number of large fractures, then the contact surface will be small and the buffer capacity of the rock next to the walls of the fracture may be used up or covered. Note that in the latter case equilibrium (1) may be attained with no detectable change in $\%H_2$, but with an increase of f_{O_2} . The mixing produces a decrease in H_2/H_2O ratio with respect to the original fluid, and f_{O_2} may increase to a new equilibrium value by dissociation of a minimum amount of H_2O, being $f_{O_2} \ll f_{H_2}$. This hypothesis could be verified by independent determination of f_{O_2} (e.g. by CO/CO_2 ratio measurements). With regard to reaction (2), the dilution phenomenon does not affect the H_2/H_2S ratio in the gas, so that f_{S_2} should remain constant.

Reaction (6) in the steam phase, on the other hand, could produce important variations in gas composition, as the fluid contains appreciable quantities of all the species involved in this reaction. A decrease in H_2/H_2O ratio might lead to the decrease in CH_4/CO_2 ratio observed in several wells. However, reaction (6) does not explain the simultaneous decrease in N_2/gas ratio.

At Castelnuovo, which is the zone nearest the recharge area, fluid composition is probably affected by the presence of a large amount of liquid water in the reservoir.

H_2S is probably the gas component most affected by the presence of liquid, as it has a high solubility and can be quickly oxidized to HSO_4^- . Very young infiltration waters can be expected to retain a certain oxidizing capacity. Note that H_2S could equilibrate with HSO_4^- in the presence of $CaCO_3$ and $CaSO_4$ (with $0.7\%H_2S$ in the gas and a gas/steam ratio of 5 litres STP/kg as typical values of the area), with $\log f_{O_2} = -38.5$ at 200°C.This is still a very low value (the value expected in a water-rock equilibrium at the same temperature is $\log f_{O_2} = -42$).

There is no indication of any trend to restore the previous H_2/H_2O ratio in the fluid when the gas/steam ratio decreases, as the majority of the Castelnuovo data indicate an approximately constant concentration of H_2 in the gas. This does not exclude that eq.(1) re-equilibrates with a higher oxygen fugacity. Calculations made at the same f_{O_2} considered for H_2S oxidation reproduce the observed H_2/H_2O ratio with plausible low values of y.

More processes can be considered possibly responsible for the strong decrease in $\%CH_4$ in the gas.

1) Partial re-equilibration after mixing. At Castelnuovo the mixing of 'original steam' and recharge fluid occurs in the presence of a liquid phase which may facilitate chemical reactions. If reaction (6) takes place, the decreased H_2/H_2O ratio entails a strong decrease in $\%CH_4$ in the gas. However, once again reaction (6) cannot explain the simultaneous decrease in CH_4 and N_2. Equation (9), for fixed temperature and y can be re-written as:

$$\log\left(\frac{n_{CH_4}}{n_{gas}}\right)_{WH} = 7\log\left(\frac{n_{H_2}}{n_{gas}}\right)_{WH} - \log\left(\frac{n_{CH_4}}{n_{N_2}}\right)_{WH}$$

$$+ 4\log\left(\frac{n_{gas}}{n_{H_2O}}\right)_{WH} - 2\log\left(\frac{n_{NH_3}}{n_{gas}}\right)_{WH} + \text{const.}$$

In the study area n_{H_2}/n_{gas} and n_{CH_4}/n_{N_2} are more or less constant, so that n_{CH_4}/n_{gas} should decrease with an increase in n_{NH_3}/n_{gas} and a decrease in n_{gas}/n_{H_2O}. A strong increase in n_{NH_3}/n_{gas} and a decrease in gas/steam ratio have actually been observed at Castelnuovo.

A complete re-equilibration appears unlikely in the upper parts of the reservoir, considering the fast circulation of recharge water, the imperfect mixing and the short time available for chemical reactions.

2) Variations in flow pattern. The fluid variations observed at Castelnuovo during exploitation suggest lateral fluid flow from the outer towards the central area. Increased contribution from the south-west zone to production in the central area of Castelnuovo must lead to a decrease in CH_4 in the gas,with minor changes to H_2 and H_2S. In fact, the south-west zone is characterized by very low concentrations of CH_4 and N_2, and H_2 and H_2S concentrations similar to the central zone. This process could also explain the simultaneous variation in CH_4 and N_2.

REFERENCES

Calore, C., Celati,R., D'Amore, F., Noto, P. (1982),"Geochemical Evidence of Natural Recharge in Larderello and Castelnuovo Areas", Proc.8th Workshop Geothermal Reservoir Engineering, Stanford, Dec.14-16,1982,323-328.

D'Amore, F., Calore, C., Celati, R. (1981), "Temporal Evolution of the Composition of the Fluid from Serrazzano Zone (Larderello)", Proc. 7th Workshop Geothermal Reservoir Engineering, Stanford, Dec.15-17, 1981, 91-96.

D'Amore, F., Celati, R. (1983),"Methodology for Calculating Steam Quality in Geothermal Reservoirs", Geothermics, vol.12, no.2/3, 129-140.

D'Amore, F., Celati, R., Calore, C. (1982) "Fluid Geochemistry Applications in Reservoir Engineering (Vapor-Dominated Systems)", Proc. 8th Workshop Geothermal Reservoir Engineering Stanford, Dec.14-16,1982,295-308.

D'Amore, F., Celati, R., Calore, C. (1983) "Hypotheses on Possible Equilibria between NH_3 and Other Gases Present in Geothermal Fluids", this Workshop.

D'Amore, F., Gianelli, G. (1984), "Mineral Assemblages and Oxygen and Sulphur Fugacities in Natural Water-Rock Interaction Processes", Geochim. et Cosmochim. Acta, in press.

D'Amore, F., Truesdell, A.H. (1979)," Models for Steam Chemistry at Larderello and The Geysers", Proc. 5th Workshop Geothermal Reservoir Engineering, Stanford, Dec.12-14, 1979, 283-297.

Table 1. Averages of gas/steam ratios and major gas analyses from steam samples from Larderello wells before any recharge effects. Compositions are in mole percent of total dry gas. NH_3 is in ppm in the steam condensate. y_H, y_S, y_{FT} and y_{CN} are the molar fractions of steam in the steam-water mixture in the reservoir, computed from eqs.(4),(5),(7) and (9) respectively.

Well	Years	T_{res} °C	Gas/steam litres STP/kg	$\%H_2$	$\%H_2S$	$\%CH_4$	$\%N_2$	$\%CO_2$	NH_3 ppm	y_H	y_S	y_{FT}	y_{CN}
1	70-76	250	29.8 ± 1.7	1.96 ± 0.14	1.91 ± 0.11	1.42 ± 0.10	0.74 ± 0.09	94.12 ± 0.50	130 ± 8	0.44	0.53	0.49	0.44
2	70-76	250	31.0 ± 0.8	2.06 ± 0.11	2.02 ± 0.15	1.32 ± 0.13	0.69 ± 0.06	93.95 ± 0.44	119 ± 19	0.48	0.58	0.54	0.51
3	71-77	260	51.0 ± 1.6	1.53 ± 0.06	1.38 ± 0.11	0.69 ± 0.02	0.60 ± 0.08	95.79 ± 0.19	177 ± 13	0.50	0.53	0.71	0.62
4	71-76	260	38.1 ± 0.8	1.76 ± 0.07	1.48 ± 0.07	1.93 ± 0.07	1.28 ± 0.07	93.56 ± 0.21	172 ± 16	0.43	0.42	0.47	0.40
5	70-76	240	51.8 ± 1.6	1.42 ± 0.12	1.37 ± 0.08	0.88 ± 0.04	0.69 ± 0.07	95.66 ± 0.21	197 ± 30	0.65	0.81	0.78	0.60
6	71-76	260	39.7 ± 1.5	1.77 ± 0.09	1.97 ± 0.10	1.52 ± 0.07	0.83 ± 0.05	93.92 ± 0.21	123 ± 22	0.45	0.60	0.52	0.50
7	71-76	260	40.5 ± 0.6	1.72 ± 0.10	1.98 ± 0.16	1.52 ± 0.04	0.90 ± 0.10	93.76 ± 0.39	121 ± 6	0.45	0.62	0.52	0.51
8	70-76	270	21.6 ± 0.6	2.49 ± 0.10	2.58 ± 0.14	1.38 ± 0.09	0.69 ± 0.04	92.85 ± 0.15	105 ± 11	0.29	0.33	0.37	0.38
9	71-76	250	25.4 ± 1.2	2.40 ± 0.08	2.34 ± 0.13	1.25 ± 0.07	0.71 ± 0.04	93.28 ± 0.17	157 ± 9	0.46	0.55	0.53	0.46
10	70-75	250	44.2 ± 1.2	1.61 ± 0.06	1.00 ± 0.05	0.43 ± 0.05	0.23 ± 0.02	96.71 ± 0.15	151 ± 15	0.54	0.40	0.81	0.65
11	70-76	240	49.8 ± 1.1	1.34 ± 0.10	0.87 ± 0.06	0.36 ± 0.02	0.14 ± 0.01	97.29 ± 0.09	138 ± 15	0.59	0.48	0.89	0.65
12	71-76	240	52.4 ± 1.5	1.31 ± 0.06	0.86 ± 0.06	0.33 ± 0.02	0.16 ± 0.02	97.33 ± 0.09	131 ± 21	0.61	0.51	0.93	0.71
13	71-76	240	32.2 ± 1.1	1.40 ± 0.06	1.08 ± 0.05	0.32 ± 0.02	0.15 ± 0.03	97.06 ± 0.07	307 ± 18	0.40	0.39	0.62	0.30
14	71-76	250	73.5 ± 2.0	1.07 ± 0.07	0.51 ± 0.05	0.26 ± 0.03	0.13 ± 0.01	98.03 ± 0.05	178 ± 16	0.59	0.34	1.0	0.70
15	73-77	250	84.1 ± 3.3	0.98 ± 0.04	0.46 ± 0.03	0.30 ± 0.06	0.17 ± 0.02	98.09 ± 0.08	177 ± 7	0.62	0.35	1.0	0.72
16	71-75	230	33.9 ± 1.2	1.49 ± 0.10	1.03 ± 0.10	0.19 ± 0.01	0.08 ± 0.01	97.22 ± 0.13	485 ± 29	0.52	0.44	0.89	0.35
17	71-76	260	19.6 ± 0.6	2.21 ± 0.06	2.02 ± 0.10	0.42 ± 0.03	0.13 ± 0.01	95.21 ± 0.15	293 ± 18	0.28	0.29	0.44	0.24
18	71-76	240	44.3 ± 1.2	1.38 ± 0.06	0.92 ± 0.05	0.30 ± 0.01	0.14 ± 0.03	97.27 ± 0.10	166 ± 11	0.54	0.45	0.85	0.56
19	70-76	250	32.1 ± 1.8	1.99 ± 0.17	1.99 ± 0.14	1.37 ± 0.08	0.80 ± 0.04	93.76 ± 0.33	168 ± 31	0.48	0.59	0.54	0.45
20	70-76	240	89.3 ± 5.8	1.02 ± 0.18	1.00 ± 0.09	1.20 ± 0.07	0.93 ± 0.03	95.84 ± 0.28	165 ± 12	0.80	1.0	0.88	0.75
21	70-76	240	25.2 ± 0.9	2.31 ± 0.09	2.03 ± 0.08	1.02 ± 0.07	0.53 ± 0.04	94.08 ± 0.20	129 ± 10	0.52	0.57	0.59	0.52
22	70-76	250	19.4 ± 0.6	2.78 ± 0.19	2.09 ± 0.11	0.87 ± 0.04	0.39 ± 0.05	93.88 ± 0.20	121 ± 9	0.41	0.36	0.51	0.47
23	71-76	240	46.8 ± 2.6	1.69 ± 0.11	1.29 ± 0.05	0.97 ± 0.05	0.54 ± 0.05	95.43 ± 0.29	155 ± 6	0.70	0.69	0.81	0.71
24	71-76	240	27.8 ± 1.0	1.96 ± 0.05	1.78 ± 0.05	0.83 ± 0.04	0.38 ± 0.02	94.97 ± 0.22	117 ± 21	0.48	0.56	0.58	0.50
25	71-76	250	37.2 ± 2.5	1.71 ± 0.06	1.55 ± 0.06	0.97 ± 0.10	0.53 ± 0.06	95.24 ± 0.21	182 ± 15	0.48	0.54	0.59	0.45
26	70-76	250	46.0 ± 4.0	1.44 ± 0.10	0.98 ± 0.15	0.64 ± 0.05	0.36 ± 0.05	96.55 ± 0.20	172 ± 7	0.50	0.41	0.69	0.51
27	70-76	260	22.1 ± 0.5	2.56 ± 0.17	2.28 ± 0.09	1.11 ± 0.08	0.51 ± 0.04	93.54 ± 0.21	108 ± 14	0.36	0.38	0.46	0.45
28	71-76	250	30.3 ± 0.9	2.08 ± 0.19	1.69 ± 0.11	1.17 ± 0.03	0.62 ± 0.05	94.38 ± 0.34	152 ± 25	0.47	0.47	0.55	0.46
29	70-75	240	28.0 ± 0.5	2.51 ± 0.15	2.26 ± 0.11	1.68 ± 0.08	0.75 ± 0.16	92.78 ± 0.26	115 ± 12	0.62	0.72	0.63	0.63
30	71-76	270	26.3 ± 1.4	2.23 ± 0.15	1.84 ± 0.11	0.90 ± 0.03	0.47 ± 0.03	94.51 ± 0.23	153 ± 13	0.32	0.29	0.44	0.35

Table 2. Variations in fluid composition with time for some wells affected by recharge

Well	Year	Gas/steam litres STP/kg	%H_2	%H_2S	%CH_4	%N_2	%CO_2	NH_3 ppm
31	1948	35.4	1.60	2.80	1.16	0.68	93.76	180
	1965	9.4	1.70	0.82	0.19	0.13	97.16	144
	1982	2.5	1.34	0.49	0.07	0.10	98.00	119
32	1948	44.9	0.91	1.45	0.85	0.54	96.25	310
	1965	15.8	0.98	0.95	0.25	0.15	97.70	270
	1973	4.0	1.18	0.54	0.12	0.13	98.00	137
33	1948	49.6	0.74	1.40	0.76	0.50	96.60	370
	1966	26.0	1.12	0.77	0.30	0.13	97.69	283
	1979	18.0	1.01	0.56	0.25	0.16	98.01	186
34	1966	31.0	1.93	1.93	1.60	0.43	94.11	119
	1976	21.4	2.48	1.90	1.13	0.51	93.98	177
	1981	13.7	2.20	1.75	0.85	0.47	94.73	140
16	1973	34.5	1.32	1.12	0.20	0.10	97.27	468
	1978	18.9	1.67	1.10	0.07	0.03	97.12	408
	1981	13.5	1.55	0.97	0.06	0.05	97.35	350

Proceedings Ninth Workshop Geothermal Reservoir Engineering
Stanford University, Stanford, California, December 1983
SGP-TR-74

GAS CHEMISTRY IN GEOTHERMAL SYSTEMS

Stefán Arnórsson, Science Institute, University of Iceland, Reykjavík, Iceland
Einar Gunnlaugsson, Reykjavík Municipal District Heating Service, Reykjavík, Iceland

ABSTRACT

Five new gas geothermometers are introduced. They are useful for predicting subsurface temperatures in water dominated geothermal systems. The geothermometers use data on CO_2, H_2S and H_2 concentrations in fumarole steam as well as CO_2/H_2 and H_2S/H_2 ratios. It is demonstrated that the gas composition of fumarole steam may be used with or without drillhole data to evaluate steam condensation in the upflow zones of geothermal systems. Uncertainty exists, however, in distinguishing between the effects of steam condensation and phase separation at elevated pressures. The gas content in steam from discharging wells and the solute content of the water phase can be used to evaluate which boiling processes lead to "excess steam" in the discharge and at which temperature this "excess steam" is added to the fluid moving through the aquifer and into the well. Examples, using field data, are given to demonstrate all the mentioned applications of geothermal chemistry.

INTRODUCTION

Various aspects of the use of gas chemistry for the exploration for geothermal resources and their development are summarized in this contribution. They are relevant for water dominated reservoirs. The aspects include prediction of subsurface temperatures from the gas content of fumarole steam, estimation of steam condensation in upflow zones and evaluation of boiling mechanisms in aquifers around producing wells. Emphasis is laid on the principles of the different applications but they are elucidated with examples of field data.

THE GAS CONTENT OF WATER IN GEOTHERMAL RESERVOIRS

Geochemical studies during the last few years have demonstrated that gas concentrations and gas ratios in drillhole discharges correlate with the undisturbed temperature of the producing aquifers (Giggenbach, 1980; D'Amore and Panichi, 1980; Nehring and D'Amore, 1981; Arnórsson et al., 1983). It has further been demonstrated that the fugacities of CO_2, H_2S and H_2 are buffered by hydrothermal mineral assemblages (Arnórsson and Gunnlaugsson, 1983). Arnórsson et al. (1983) proposed temperature functions for CO_2 and H_2S which are valid up to 250°C. Giggenbach (1980) and Arnórsson (1983) have expressed temperature functions in terms of gas pressures for CO_2 and CO_2, H_2S and H_2 respectively in geothermal waters. Table 1 gives temperature functions for CO_2, H_2S and H_2 concentrations in geothermal waters which are valid up to 350°C as indicated.

Alteration processes in geothermal systems involve dissolution of the primary rock constituents and precipitation of new ones via transfer of matter through the aqueous phase. Which new minerals are precipitated depends on the temperature of the water, kinetic factors and the composition of the rock, or better the composition of the geothermal system. It is a well known problem in metamorphic geology that different minerals or mineral assemblages have similar solubilities. This implies that different minerals will often produce similar aqueous solute concentrations for compatible components at equilibrium. Compatible components are those incorporated in mineral phases. This is well demonstrated by the results of Bird and Norton (1981) on the Salton Sea geothermal system. A mineral zonation is observed with depth in that system and each zone is characterised by a particular mineral assemblage. Chemical thermodynamic calculations show that any of these assemblages give about the same fluid composition (the observed composition) at equilibrium for the compatible components. Yet, in strict terms, it is very important to realise that the temperature functions given in Table 1 are valid only for certain mineral assemblages, assemblages which form when volcanic rocks of basic to acidic composition are altered because they have been derived from data from geothermal systems located in such rocks. These temperature functions may not be valid for geothermal systems located in other rock types, particularly if their composition differs much from the mentioned rock types. Alteration may lead to the formation of different mineral assemblages that would buffer gas fugacities at a significantly different level at any temperature.

For H_2S and H_2 two functions are presented in Table 1, each valid over a fixed range of water

Table 1. Temperature functions for gas concentrations (as log moles) in geothermal reservoir waters.

Gas		Temperature function (°K)	Remarks
CO_2	-1.09	-3894.55/T +2.532·logT	All waters
H_2S	-11.80	-0.06035·T -17691.09/T +27.163·logT	All waters above 300°C and waters in the
H_2	-3.04	-10763.54/T +7.003·logT	range 200-300°C if Cl>500ppm
H_2S	-1.24	-4691.84/T +2.830·logT	All waters below 200°C and waters in the
H_2	+11.98	+0.08489·T +8254.09/T -27.587·logT	range 200-300°C if Cl<500ppm

salinity and temperature. Water salinity may to some extent reflect rock type. Different rock types have different concentrations of the incompatible component chloride and it is the availability of this component which governs water salinity.

It has not been established which minerals control CO_2, H_2S and H_2 fugacities as described by the functions in Table 1 below some 200-250°C. At higher temperatures the assemblage epidote-prehnite-calcite-quartz seems to control CO_2 levels. For water containing less than 500 ppm chloride and below 300°C pyrite, pyrrhotite, epidote and prehnite appear to buffer H_2S and H_2 fugacities but pyrite, epidote, prehnite and magnetite or chlorite seem to be involved in the case of waters containing over 500 ppm chloride.

GEOTHERMOMETRY

The drillhole data on which the functions in Table 1 are based have been used to calibrate several gas geothermometers. The application of these gas geothermometers involves the sampling and analysis of fumarole steam and derivation of subsurface temperatures with the aid of the functions in Table 2. These functions refer to gas concentrations in steam at atmospheric pressure and assume adiabatic boiling of the parent water and equilibrium degassing (Arnórsson and Gunnlaugsson, 1983). Conde sation of steam in the upflow and phase separation at pressures above atmospheric cause high temperature estimates for the CO_2, H_2S and H_2 geothermometers as they are based on concentration in steam. On the other hand the geothermometers which use gas ratios (CO_2/H_2 and H_2S/H_2) are not significantly affected by these processes as the dissolved gases are practically quantitatively transferred to the steam phase already at the early stages of boiling. The geothermometers which use gas concentrations are advantageous over the gas ratio geothermometers when steam condensation or phase separation produces less deviation from the adiabatic boiling model adopted than gas reactions in the upflow. Arnórsson and Gunnlaugsson (1983) have demonstrated, by comparing measured temperatures in wells and data from fumaroles, that the predicted geothermometry temperatures compare generally well with the temperatures actually encountered in drillholes at depths as great as 1000 m or more. Their work shows that H_2S and to a lesser extent H_2 tend to be removed from the steam in the upflow presumably as a result of reactions with alteration minerals in the wall rock or oxidation. Therefore CO_2/H_2 ratios may be regarded to yield conservative estimates of subsurface temperatures as this ratio increases with decreasing temperatures as may be seen the respective temperature functions in Table 2. CO_2 temperatures can be expected to be on the high side as this gas does not seem to be lost from the steam in the upflow. H_2S and H_2 temperatures are often intermediate between the CO_2/H_2 and the CO_2 temperatures as the effect of condensation is counterbalanced to a greater or lesser extent by the removal of these gases from the steam in the upflow. H_2S/H_2 temperatures yield high values when H_2S has been removed preferrentially to H_2 in the upflow.

Data from fumaroles in Hveragerdi are used here as an example to illustrate gas geothermometry results (Fig.1). Many wells have been sunk in this area which forms the southernmost part of the Hengill geothermal field in southwest Iceland. Xi-Xiang (1980) has recently summarized the temperature distribution in the Hveragerdi reservoir from measurements in wells. In general temperature increases northwards from about 150°C in the village of Hveragerdi to 230°C in the far north in well 1 (Fig. 1). A temperature maximum is observed in most wells which has been interpreted by lateral flow from the central part of the Hengill geothermal field (Árnason et al., 1968).

For convenience for discussing and comparing measured temperatures in wells and gas geothermometry temperatures the Hveragerdi field is divided into two areas, one around wells 2, 4 and 5 and the other at the head of the valley running north from Hveragerdi where wells, 1, 3, 6, 7 and 8 are located. Here fumaroles are concentrated on high ground on the northern valley slopes, and in smaller V-valleys dissecting these slopes.

Table 2. Temperature functions for gas geothermometers. Gas concentrations are in mmoles per kg of steam.

Geothermometer	Temperature function	Mean dev.°C	Standard dev.°C	Remarks
CO_2	-44.1 +269.25Q -76.880Q^2 +9.520Q^3	20[a]	21[a]	All waters
H_2S	+246.7 +44.810	14	9	All waters above 300°C
H_2	+277.2 +20.990	8	6	and waters in the range
CO_2/H_2	+341.7 -28.570	14	8	200-300°C if chloride
H_2S/H_2	+304.1 -39.460	11	8	>500 ppm.
H_2S	+173.2 +65.040	15	13	All waters below 200°C
H_2	+212.2 +38.590	19	14	and waters in the range
CO_2/H_2	+311.7 -66.720	28	23	200-300°C if chloride <500 ppm.

Q designates the logarithim of the respective gas concentration or the gas ratio.
[a]Data points with aquifer temperatures below 150°C were omitted.

CO_2/H_2 temperatures for fumaroles around wells 2, 4 and 5 are in the range 117-172°C but CO_2 temperatures range from 237° to 255°C. These temperatures are to be compared with the range 181-198°C measured in the nearby wells. According to earlier statement the highest CO_2/H_2 temperatures should be regarded as a conservative value for subsurface temperatures and CO_2 temperatures are possibly too high. For the upper area maximum CO_2/H_2 temperature is 233°C but the highest recorded downhole temperature is 230°C in well 1. CO_2 temperatures range from 257° to 278°C.

Inspection of Fig. 1 reveals that H_2 temperatures tend to lie inbetween the CO_2 and CO_2/H_2 temperatures. CO_2 concentrations do not change as rapidly with temperature as do H_2 concentrations according to the gas geothermometry functions. Therefore the discrepancy between the CO_2, H_2 and CO_2/H_2 geothermometry results can be explained by steam condensation/phase separation et elevated pressure or removal of H_2 from the steam in the upflow or a combination of these processes.

H_2S temperatures compare well with H_2 temperatures in the lower area. However, in the upper area they tend to be lower and also lower than the CO_2/H_2 temperatures. In the upper area the fumaroles are mostly located on high ground and well above the water table. According to Arnórsson and Gunnlaugsson (1983) H_2S is particularly prone to be removed from the steam under conditions of low water table.

EVALUATION OF CONDENSATION

The discrepancy between the CO_2/H_2 geothermometry results on one hand and the CO_2 or H_2 results on the other hand may be used to evaluate steam condensation in upflow zones of geothermal systems. The evaluation involves calculation of CO_2 or H_2 concentrations from the CO_2/H_2 temperature and the respective functions in Table 2. The ratio of the calculated CO_2 (or H_2) concentration divided by the analysed concentration equals the fraction of steam, Y, which has not condensed and (1-Y), is therefore the condensed fraction. Since H_2 tends to be removed in the upflow, CO_2/H_2 temperatures tend to be low giving high values for (1-Y). For the Hveragerdi fumaroles (Fig. 1) this method indicates that 59-95% of the steam has condensed in the upflow and 77% on average.

Another method to estimate condensation involves comparison between the gas content in fumaroles and in steam discharged from wells at atmospheric pressure. Using CO_2 data from wells 2 and 4 (aquifer temperatures 182° and 181°C) condensation is indicated which amounts on average to 73% in the lower area, the range being 65-79%. The same approach for the upper area using well 7, with aquifer temperature of 225°C, give a range of 68-84%, the average being 77%.

Although numerous boiling hot springs occur in the Hveragerdi area, it may be that the discrepancy between the gas concentrations in fumarole steam and in steam from wells after the discharge has flashed to atmospheric pressure is not due to condensation but to separation of the steam from the water in the upflow at pressures above atmospheric. Study of fumarole chemistry in several geothermal fields in Iceland by Arnórsson and Gunnlaugsson (1983) shows that there is some relation between the discrepancy between CO_2 (and H_2) temperatures on one hand and CO_2/H_2 temperatures on the other and the age of the rocks. The difference tends to be largest in the oldest rocks. It is generally accepted that the permeability of the volcanic rocks in Iceland decreases with time due to compaction and hydrothermal alteration. It is to be

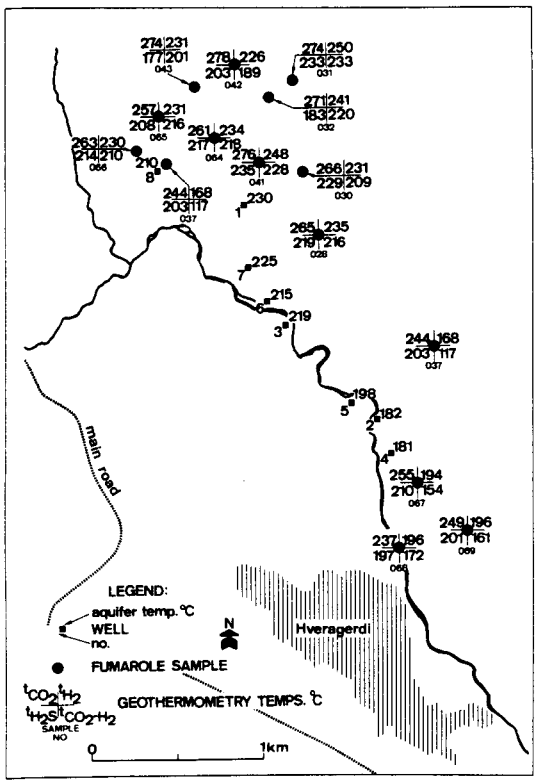


Fig. 1. Gas geothermometry results for the Hveragerdi area, southwest Iceland.

expected that low permeability in upflow zones where boiling occurs will favour phase separation. It is concluded that fumarole chemistry can be affected by both steam condensation and phase separation but further study is required to evaluate the relative magnitude of these processes in different fields. The results may contribute to early evaluation of permeability in geothermal systems but also to estimation of natural heat loss.

EVALUATION OF BOILING PROCESSES

It is often observed that the enthalpy of wet-steam well discharges varies with wellhead pressure but also with time, generally towards increasing steam to water ratios. As far as the present authors know discharge enthalpy changes are confined to wells fed by a two phase mixture of water and steam. Changes in the fluid chemistry (or lack of changes) which accompany discharge enthalpy changes can be useful in evaluating the processes which are involved. Results pertinent to this aspect of applied geochemistry have been described by Arnórsson (1981), Glover et al. (1981) and Grant and Glover (1983).

Steam is excess of that formed by adiabatic boiling of water of a particular aquifer temperature is here termed "excess steam".

It is visualized that "excess steam" in wet-steam well discharges may be the outcome of either of two processes, or a combination of them. One of these processes involves phase separation in the aquifer and preferrential movement of the steam into the well. The other process involves evaporation of pore water as a result of heat transfer from the rock to the fluid. Pressure drop caused in the aquifer around a producing well will cool the fluid by boiling and initiate heat transfer from the rock.

In the present contribution it is demonstrated how fluid chemistry may be used to evaluate the relative magnitude of these two processes for individual wells. The evaluation makes use of both gas composition and solutes in the aqueous phase. Data from Nesjavellir, Iceland and Olkaria, Kenya, are used to elucidate this application of chemistry.

If relative permeability is the cause of high discharge enthalpy, i.e. "excess steam", it is to be expected that the concentrations of gases in the steam phase at a particular pressure remain constant despite changes in the discharge enthalpy. If, on the other hand, evaporation of pore water was responsible, it is to be expected that gas concentrations in the total discharge would remain constant and the gas content of the steam phase would thus decrease in proportion to the amount added of pore water derived steam. It is logical to assume that the pore water would become degassed during the early stages of boiling and further evaporation would yield practically gas free steam.

The data on CO_2 from well 6 at Nesjavellir, Iceland (Fig. 2) indicates that the relative permeability effect is for all practical purposes the sole cause of the increased discharge enthalpy from 1290 to 2140 J/g that occurred during one week after the well was discharged for the first time (see Stefánsson et al., 1983).

The temperature, or more accurately the enthalpy, of the "excess steam" added may affect evaporation of the water fraction in well discharges. If the steam is added at a pressure close to the sampling pressure, i.e. close to the well, the addition will not affect the aqueous solute concentrations. If, on the other hand, the steam is added at a significantly different pressure so that its enthalpy differs markedly from that of steam at the sampling pressure, its presence and relative amount will affect the evaporation of the discharged water.

Fig. 3 shows variation in silica and sodium concentrations in the water discharged from well 6 at Nesjavellir with discharge enthalpy during the first week of flow. The horizontal lines represents expected relative concentrations if the "excess steam" was added at a pressure equal to the sampling pressure but the curves represent calculated relative solute concentration variations if the steam was added

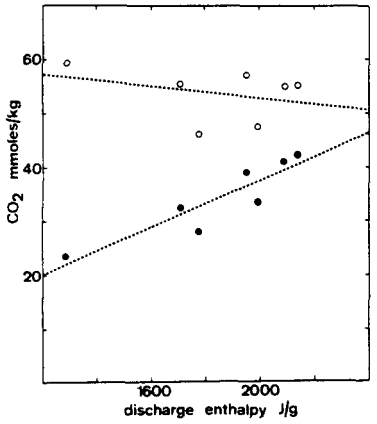


Fig. 2. CO_2 concentrations in well 6 at Nesjavellir during the first week of discharge in December, 1982. Filled symbols designate concentrations in the total discharge and open symbols concentrations in the steam at atmospheric pressure.

at 290°C, i.e. the undisturbed temperature of the dominant feeder. The results for sodium favour that the "excess steam" was added at 290°C but silica concentrations do not. It is possible that the silica concentrations do not give a reliable picture of the situation. They are sensitive to temperature variations in the formation. Initial silica concentrations are low but later they correspond well with the aquifer temperature of 290°C assuming equilibrium with quartz.

Data on the composition of water and steam from wet-steam wells may not be sufficiently complete to permit correlation of possible chemical changes with changes in discharge enthalpy. A single analysis of the steam fraction and measurement of the discharge enthalpy may be tentatively used to evaluate the relative magnitude of the two boiling processes in the aquifer with the aid of the equations in Table 1. If evaporation of pore water only was responsible for the "excess steam" in a well discharge, the gas content of the total discharge should be equal to that described by the respective functions in Table 1 at a specified aquifer temperature. If the relative permeability effect was the cause of "excess steam", the gas content in the steam phase of the discharge multiplied by calculated steam fraction equal to that obtained by adiabatic boiling should conform with the functions in Table 1.

Fig. 4 shows data on the gas content in steam from selected wells at Olkaria in Kenya. The spread of data points indicates that wells with the lowest Na-K geothermometry temperatures owe their "excess steam" dominantly to phase separation but for wells with Na-K temperatures significantly over 240°C pore water evaporation appears to dominate. A steam zone of 240°C caps a boiling water reservoir at Olkaria (Svanbjörnsson et al., 1983). The wells which have Na-K temperatures significantly higher than 240°C are dominated by feeders in the boiling water reservoir but wells with Na-K temperatures of 240°C of somewhat less appear to be dominantly fed from the steam zone. It can be noted from Fig. 4 that the gas content of all the wells are very similar and correspond rather closely with gas geothermometry temperatures of 240°C. It is a plausible explanation, although considered unlikely in view of flow characteristics of wells (see Svanbjörnsson et al., 1983), that the steam in the well discharges is dominantly derived from the steam zone and Na-K temperatures reflect some water inflow from variable depths within the boiling water reservoir.

QUALITY OF STEAM

The gas content of steam at a particular separation pressure may be predicted in the case of CO_2, H_2S and H_2 with the use of the equations in Table 1. Usually these gases constitute far the larger part of the total gas in geothermal fluids although CH_4 and N_2 may

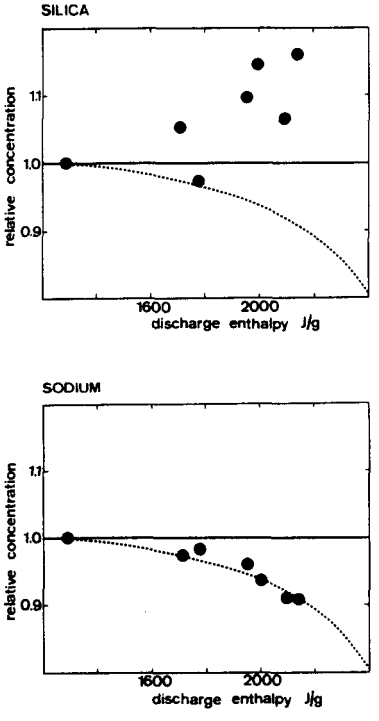


Fig. 3. Relative changes with discharge enthalpy in the silica and sodium concentrations in water (at atmospheric pressure) from well 6 at Nesjavellir. Straight lines correspond with concentrations, if the "excess steam" was added at a pressure equal to the sampling pressure but curves if steam at 290°C (the aquifer temperature for the well) was added.

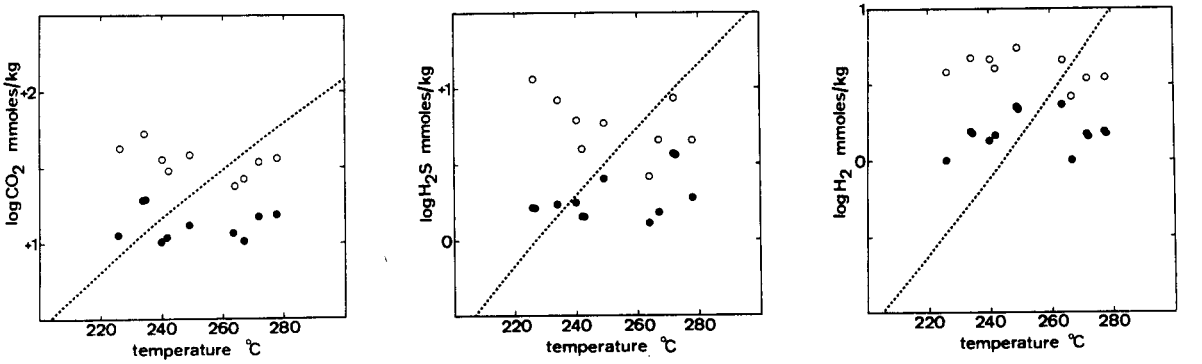


Fig. 4. CO_2, H_2S and H_2 concentrations in fluid discharged from wells at Olkaria. Open symbols represent actual concentrations in the total discharge and correspond therefore with the "excess steam" being derived from evaporation of degassed pore water. Filled symbols show calculated concentrations in the reservoir water on the assumption that the "excess steam" in the discharges was caused by phase separation in the aquifer and preferrential movement of the steam into the wells. The curves designate gas concentrations in equilibrated geothermal reservoir waters according to Table 1. The data are from Muna (1982).

sometimes contribute significantly. The steam fraction, X, formed by adiabatic boiling of water equals $(h-h_p)/L_p$ where h and h_p represent the enthalpies of steam saturated water at a specified aquifer temperature and the enthalpy of water at steam pressure respectively. L_p is the latent heat of vaporization at that pressure. By dividing X into a calculated gas concentration derived from the equations in Table 1 the gas concentrations in the steam are obtained. This is the maximum anticipated concentration in the steam phase. If increased well discharge enthalpy was caused by phase separation in the aquifer, the gas content in the steam would not change and therefore stay at the theoretical maximum level. Pore water evaporation, as a cause of increased discharge enthalpy, would on the other hand lower gas concentrations from this maximum. As an example it can be mentioned that gas $(CO_2+H_2S+H_2)$ in steam at 6 bars abs. calculates to be 0.35 and 1.1% by volume at maximum for aquifer temperatures of 250° and 300°C respectively. For a discharge enthalpy of 2200 J/g and pore water evaporation the corresponding figures are 0.10% and 0.48% respectively. It is considered to be useful to predict the quality of geothermal steam with respect to gas content already at the geochemical survey phase in geothermal exploration. This can be done by making use of estimated subsurface temperatures using geothermometry.

REFERENCES

Árnason, B., Theódórsson, P., Björnsson, Sv. and Saemundsson, K. (1968), "Hengill, a High Temperature Thermal Area in Iceland," Bull. Volcanologique, 33, 245-260.

Arnórsson, S. (1981), In "Status Report on Steam Production," Report prepared by VIRKIR and Merz and McLellan for the Kenya Power Company Ltd., July, 1981, 31p.

Arnórsson, S. (1983), "Gas Pressures in Geothermal Systems," Chemical Geology, submitted.

Arnórsson, S. and Gunnlaugsson, E. (1983), "New Gas Geothermometers for Geothermal Exploration - Calibration and Application," In preparation.

Arnórsson, S., Gunnlaugsson, E. and Svavarsson, H. (1983), "The Chemistry of Geothermal Waters in Iceland. I. Mineral Equilibria and Independent Variables Controlling Water Compositions," Geochim. Cosmochim. Acta, 47, 547-566.

Bird, D.K. and Norton, D.L. (1981) "Theoretical Predictions of Phase Relations Among Aqueous Solutions and Minerals; Salton Sea Geothermal System," Geochim. Cosmochim. Acta, 45, 1479-1494.

D'Amore, F. and Panichi, C (1980), "Evaluation of Deep Temperatures of Hydrothermal Systems by a New Gas Geothermometer. Geochim. Cosmochim. Acta, 44, 549-556.

Giggenbach, W.F. (1980), "Geothermal Gas Equilibria," Geochim. Cosmochim. Acta, 44, 2021-2032.

Glover, R.B., Lovelock, B. and Ruaya, J.R. (1981), "A Novel Way of Using Gas and Enthalpy," Proc, N.Z. Geothermal Workshop, Auckland University, Nov. 9-11, 163-170.

Grant, M.A. and Glover, R.B. (1980), "Two Phase Heat and Mass Transfer Experiment at Well BR21, Broadlands," Geothermics, submitted.

Muna, Z.W. (1982), "Chemistry of Well Discharges in the Olkaria Geothermal Field, Kenya", United Nations University Geothermal Training Programme, Iceland. Report 1982-8, 38p.

Nehring, N.L. and D'Amore, F. (1981), "Gas Chemistry and Thermometry of the Cerro Prieto Geothermal Field," Proc. Third Symposium on the Cerro Prieto Geothermal Field, Baja California, Mexico, March 1981.

Stefánsson, V., Tómasson, J., Gunnlaugsson, E., Sigvaldason, H., Franzson, H. and Sigurdsson, Ó. (1983), "Nesjavellir, Well 6 - Drilling, Investigations and Production Characteristics," Report OS-83023/JHD-04 of the National Energy Authority, 100p. (In Icelandic).

Svanbjörnsson, A., Matthíasson, J., Frímannsson, H., Arnórsson, S., Björnsson, Sv. Stefánsson, V. and Saemundsson, K. (1983), "Overview of Geothermal Development at Olkaria in Kenya," This Workshop.

Xi-Xiang, Z. (1982), "Interpretation of Subsurface Temperature Measurements in the Mosfellssveit and Ölfusdalur Geothermal Areas, SW-Iceland," United Nations University Geothermal Training Programme, Iceland. Report 1980-7, 102p.

Proceedings Ninth Workshop Geothermal Reservoir Engineering
Stanford University, Stanford, California, December 1983
SGP-TR-74

PERMEABILITY REDUCTION DUE TO PRECIPITATION OF QUARTZ UNDER NONISOTHERMAL CONDITIONS

Laura A. Keith[1], Paul T. Delaney[1], and Diane E. Moore[2]

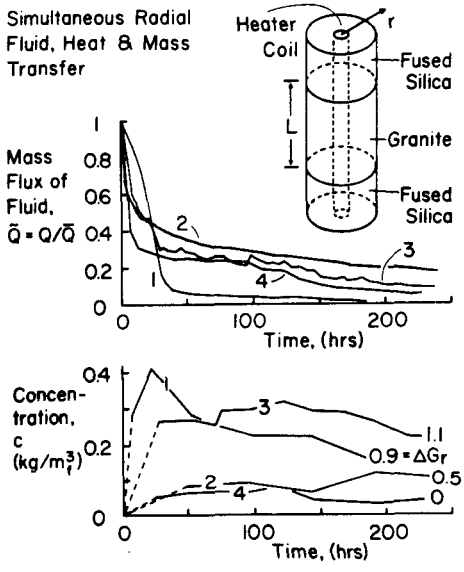
[1] U.S. Geological Survey
2255 North Gemini Dr.
Flagstaff, Ariz., 86001

[2] U.S. Geological Survey
345 Middlefield Rd.
Menlo Park, Calif., 94025

ABSTRACT. Many problems concerning the origin and exploitation of geothermal reservoirs demonstrate the need for models of reactive-solute transport. Of particular interest to us is the coupling between dissolution/precipitation reactions and transient-flow behavior. In an effort to account for observed flow-rate reductions during experiments on samples of granite held in a temperature gradient (summarized at this meeting in 1981 by Moore and others), we examine the effect of quartz precipitation on fluid flow. Our results confirm earlier inferences that reactions responsible for porosity reduction were affected by kinetic factors. Although our results show substantial flow-rate reductions, we are unable to reproduce measured silica concentrations of the outlet fluid by considering the behavior of silica phases without regard for that of the feldspars and micas.

INTRODUCTION. It is well established that quartz dissolves readily in geothermal and other hydrothermal settings. Silica precipitation, however, may be responsible for hydraulic seals in some reservoirs (Facca and Tonani, 1967). In a recent series of papers on simultaneous fluid, heat and mass transfer in granites (Summers and others, 1978; Lockner and others, 1978; Morrow and others, 1981; Moore and others, 1981, 1983), such processes were observed in a laboratory setting. These experiments were performed on cylindrical samples of the Westerly and Barre Granites, bounded by endpieces of fused silica (fig. 1). Distilled water was pumped into axial boreholes, which housed heater coils. Temperatures of 250° or 300°C were maintained at the inside of the sample; stable values of 84° to 103°C were recorded at the outside. Fluid-pressure differences of 0.5-1.0 MPa were maintained between the axial reservoir and the outside of the sample. Mass flux of water and various dissolved species were monitored over a period of a few weeks, and flow-rate reductions were observed (fig. 1). Concentrations of dissolved silica in the outlet fluid were typically, but not always, supersaturated with respect to amorphous silica in experiments with 250°C axial temperatures, whereas only quartz supersaturation was observed in experiments with 300°C temperatures. The pH of outlet fluids was neutral. Moore and coworkers concluded that quartz was the primary phase to precipitate, thus inducing flow-rate reductions.

Figure 1. Sketch of sample apparatus; graphs of mass fluid flux and aqueous silica concentration versus time for experiments 1, 2, 3 and 4, corresponding to B250-2, B300, W250 and W300, respectively, of Moore and others (1983). Conditions of experiments and dimensions of granite annulus are given in table 2. Flow rates are normalized by their initial values. Gibbs free energies of reaction ΔG_r, in kcal, are shown for the final fluid samples collected.



The purpose of this paper is to test the hypothesis that the reaction

$$SiO_2 + 2 \cdot H_2O \rightleftharpoons H_4SiO_4$$

where quartz and water combine to form aqueous silica is responsible for the hydraulic sealing of the samples. This hypothesis requires that the role of other silica phases, feldspars and micas in the overall mass transfer was unimportant. Li (1980) investigated a similar problem.

HEAT TRANSFER. Consider the energy equation:

$$(\rho C)\frac{\partial T}{\partial t} = \frac{1}{r}\frac{\partial}{\partial r} rk\frac{\partial T}{\partial r} + (\rho C)_f v \frac{\partial T}{\partial r} + (\Delta h)R \qquad (1)$$

which balances the accumulation of heat (LHS)

Table 1: Symbols and their Dimensionless Equivalents.

a Area of reaction surface;

c Concentration, $\zeta = c/\overline{s}_q$;

C Heat capacity, per unit mass;

G Reaction-rate group, $\overline{\phi}\overline{\mu}r_b^2\overline{a}_q\overline{k}_-/\overline{K}(P_a-P_b)\overline{m}_f$;

h Enthalpy of reaction;

k Thermal conductivity, $\tilde{k} = k/\overline{k}$, $\tilde{k}_0 = k_0/\overline{k}$, $\tilde{k}_1 = k_1/\overline{k}$;

k_- Precipitation rate constant, $\tilde{k}_- = k_-/\overline{k}_-$;

K Absolute permeability, $\tilde{K} = K/\overline{K} = \phi^3$;

m Mass of fluid available for reaction;

Q Fluid flux, $\tilde{Q} = Q/\overline{Q} = Q\cdot\overline{\mu}/2\pi L\overline{\rho}_f\overline{K}(P_a-P_b)$;

r Radial distance, $\eta = r/r_b$;

R Kinetic reaction rate;

P Pressure, $\psi = (P-P_b)/(P_a-P_b)$;

s Solubility, $\tilde{s} = s/\overline{s}_q$;

T Temperature, $\theta = (T-T_b)/(T_a-T_b)$, $\theta_1 = (273.15^oC+T_b)/(T_a-T_b)$;

t Time, $\tau = t/T$, $T = \overline{\phi}_f\overline{\mu}r_b^2\rho_q/\overline{K}(P_a-P_b)\upsilon_q\overline{s}_q$;

v Darcian velocity, $\tilde{v} = v/\overline{v} = v\cdot\overline{\mu}r_b/\overline{K}(P_a-P_b)$;

α Dispersivity, $A = \alpha/r_b$;

ϕ Volume fraction, $\Phi = \phi_f/\overline{\phi}_f$;

ρ Density, $\tilde{\rho} = \rho_f/\overline{\rho}_f$;

μ Dynamic viscosity, $\tilde{\mu} = \mu/\overline{\mu}$;

υ Atomic-weight ratio;

Superscripts and subscripts.

a Value at $r = r_a$, inside of annulus;

b Value at $r = r_b$, outside of annulus;

f Fluid;

q Quartz;

r Value in axial reservoir;

s Amorphous silica;

- denotes properties evaluated at the inside of the sample ($r=r_a$,t) for properties that do not vary with time, or initially (r,t=0) for those that do not initially vary spatially.

Table 2: Values of Properties.

$a^r_q = 8.8 \times 10^{-4}\ m^3{}_q$; $a^r_s = 3.9 \times 10^{-3}\ m^3{}_s$;
$k_0 = 0.586\ W/m\cdot s^oC$; $k_1 = 556\ W/m\cdot s$;
$L = 8.9$ cm; $r_a = 0.64$ cm; $r_b = 3.8$ cm;
$\rho_q = 2650\ kg/m^3$; $V^r_f = 4.9 \times 10^{-6}\ m^3{}_f$;
$\upsilon_f = 0.375$; $\upsilon_q = 0.675$

	1	2	3	4	= Experiment #
	(Barre)		(Westerly)		
$\overline{k}$ =	1.65	1.56	1.65	1.56	$W/m\cdot s^oC$;
$\overline{k}_-$ =	2.12	5.76	2.12	5.76	$\times10^{-6}\ kg_f/m^2{}_q\cdot s$;
$\overline{K}$ =	2000	74	740	240	$\times10^{-21}\ m^2$;
P_a =	10.5	21.0	10.5	20.5	MPa;
P_b =	10.0	20.0	10.0	20.0	MPa;
$\overline{s}_q$ =	0.61	0.86	0.61	0.86	$kg_{H_4SiO_4}/m^3{}_f$;
$\overline{s}_s$ =	1.66	1.90	1.65	1.90	$kg_{H_4SiO_4}/m^3{}_f$;
T_a =	250	300	250	300	^oC;
T_b =	103	94	84	92	^oC;
$\overline{\rho}$ =	806	736	806	736	kg/m^3;
$\overline{\mu}$ =	1.08	0.91	1.08	0.91	$\times10^{-4}$ Pa·s;

against its conduction, advection and rate of production through chemical reaction (RHS). (See table 1 for notation.) Although experiments ran for durations in excess of 100 hr, transient heating lasted less than 2 hr. Using the nondimensionalization shown in Table 1, the ratio of advective to conductive heat transfer scales as $(\rho C)_f\overline{K}(P_a-P_b)/\overline{\mu k}$ which is $<<1$; the influence of the heat of reaction is even less. Defining, nondimensional temperature θ, thermal conductivity $\tilde{k}$ and distance r/r_b, we can write the conduction equation

$$0 = \frac{1}{\eta}\frac{\partial}{\partial\eta}\eta\tilde{k}\frac{\partial\theta}{\partial\eta}\ , \text{ where } \tilde{k} = \tilde{k}_0 + \tilde{k}_1/(\theta+\theta_0) \qquad (2)$$

which reflects that thermal conductivity is inversely proportional to absolute temperature and has been fitted to data summarized by Touloukian and others (1981) for the Westerly and Barre Granites. (Values of parameters are given in table 2.) Boundary conditions are

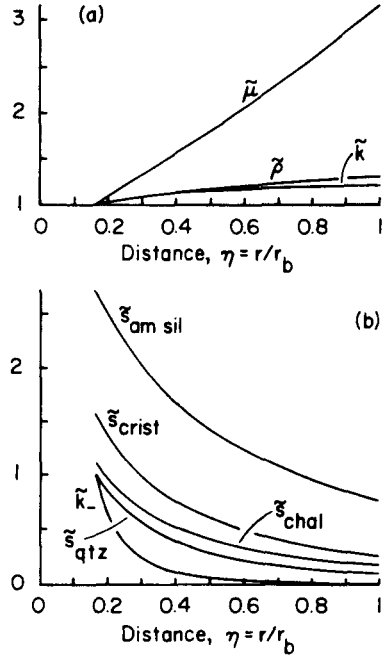
$$\theta(r_a/r_b) = 1,\quad \theta(1) = 0 \qquad (3)$$

The solution is transcendental:

$$\tilde{k}_0(1-\theta) + \tilde{k}_1\ln[(1+\theta_0)/(\theta+\theta_0)] = \qquad (4)$$
$$[1-\ln(\eta)/\ln(r_a/r_b)]\{\tilde{k}_0+\tilde{k}_1\ln[(1+\theta_0)/\theta_0]\}$$

Transport and thermodynamic properties are insensitive to variations in the pressure and concentration observed during the experiments. Therefore, profiles of nondimensional viscosity (Watson and others, 1980), thermal con-

Figure 2. Spatial distributions of (a) normalized fluid density $\tilde{\rho}$, thermal conductivity $\tilde{k}$ and viscosity $\tilde{\mu}$, and (b) solubility of quartz $\tilde{s}_q$, chalcedony $\tilde{s}_{chal}$, α-cristobalite $\tilde{s}_{crist}$ and amorphous silica $\tilde{s}_a$, and precipitation-rate constant $\tilde{k}_-$ for conditions of experiment 3.



ductivity, water density (Keenan and others, 1978), silica precipitation-rate constant (Rimstidt and Barnes, 1980) and solubility of quartz, chalcedony, α-cristobalite and amorphous silica (Fournier and Potter, 1982; Fournier, personal communication, 1983) can be determined from eq. 4 alone. Figure 2 shows profiles of these quantities for the conditions of experiment 3 and for silica dissolved in otherwise pure water. Note that the spatial gradients of the solubilites and precipitation-rate constant are steepest at the heated, inside of the sample. Overall, dissolution and precipitation should be greater at the interior of the sample. Although fluids may become supersaturated with respect to α-cristobalite or chalcedony, achievement of amorphous-silica saturation is unlikely. Only the quartz-water reaction is considered here.

FLUID FLOW. The equations for conservation of momentum (Darcy's law) and fluid mass are

$$v = -(K/\mu)\frac{\partial P}{\partial r}, \quad \frac{\partial}{\partial t}\phi_f\rho_f = \frac{-1}{r}\frac{\partial}{\partial r}r\rho_f v - \upsilon_f R \quad (5)$$

Order-of-magnitude calculations for a rock with flow porosity $\phi_f = 10^{-3}$ suggest that the residence time of water in the sample was less than 1 hr, so that the term on the LHS of the second equation above is small. The addition of water by quartz precipitation (the reaction term) is also small. Thus, conservation of fluid mass is assured if the mass flux of water is constant everywhere within the sample.

We postulate that flow porosity ϕ_f of granites can be idealized as microfractures of spacing d. Permeability and porosity are related by a model of flow along these orthogonal fractures (see Turcotte and Schubert, 1982), giving

$$K \propto \phi_f^3 d^2, \quad \text{or } \tilde{K} = \Phi^3 \quad (6)$$

where $\tilde{K}$ and Φ are nondimensional permeability and porosity, respectively. Initially, the permeability function $\Phi^3 = 1$; its subsequent behavior controls flow rate and pressure. Although the porosity function is not known independently of the mass transfer and dissolution/precipitation reactions, this cube--power relation assures that minor volumes of precipitated quartz will have a significant influence on fluid flux. Other more realistic relations than eq. 6 would not alter the conclusions reached by this study.

Introducing nondimensional mass flux $\tilde{Q}$, Darcian velocity $\tilde{v}$, fluid density $\tilde{\rho}$ and pressure ψ, we find

$$\tilde{Q}(\eta,\tau) = \tilde{Q}(\tau) = \eta\tilde{\rho}\tilde{v} = -\tilde{\eta\rho}(\Phi^3/\tilde{\mu})\frac{\partial\psi}{\partial\eta} \quad (7)$$

where τ is nondimensional time. Equation 7 is solved for $\tilde{Q}$ and ψ subject to the boundary conditions

$$\psi(r_a/r_b) = 1, \ \psi(1) = 0 \quad (8)$$

THE CASE OF QUARTZ SATURATION. Conservation of silica is assured by the equation

$$\frac{1}{\upsilon_q}\frac{\partial}{\partial t}\phi_q\rho_q + \frac{\partial}{\partial t}\phi_f c = \frac{-1}{r}\frac{\partial}{\partial r}rvc + \frac{\alpha}{r}\frac{\partial}{\partial r}rv\frac{\partial c}{\partial r} \quad (9)$$

where υ_q is the atomic weight ratio of quartz to aqueous silica, α is longitudinal dispersivity and c is concentration expressed as mass of aqueous silica per volume of water. Equation 9 is derived assuming that concentration gradients across pore channels are small. Mechanical dispersion, which refers to spreading caused by microscopic variations in velocity, is the major dispersive process. If quartz is the only reactive solid, the volume fractions of quartz and water are related by

$$\partial\phi_f/\partial\phi_q = -1 \quad (10)$$

The concentration of aqueous silica may be nearly at quartz saturation throughout most of the sample. If so, then after nondimensionalizing, we have $c/\bar{s}_q = s/\bar{s}_q = \tilde{s}$ and

$$\left(1-\upsilon_q\bar{s}_q/\rho_q\right)\frac{\partial\Phi}{\partial\tau} = \frac{1}{\eta}\frac{\partial}{\partial\eta}\eta\tilde{vs}_q - \frac{A}{\eta}\frac{\partial}{\partial\eta}\eta\tilde{v}\frac{\partial\tilde{s}}{\partial\eta}_q \quad (11)$$

The first term in parentheses on the LHS represents the accumulation of silica as quartz; the second term, the depletion of aqueous silica due to reduced pore space, which is of the order 10^{-4} and is henceforth neglected. Nondimensional time is

$$\tau = t/T, \text{ where } T = \bar{\phi}_f \bar{\mu} r_b^2 \rho_q / \bar{K}(P_a - P_b) \upsilon_q \bar{s}_q \quad (12)$$

and is composed of an advection rate and a ratio of densities of aqueous silica and quartz. We expect that sealing occurs over times $t \sim T$ for conditions dominated by quartz-saturated fluids. Equation 11 is subject to the initial condition:

$$\Phi(\eta, \tau=0) = 1 \quad (13)$$

Because the solubility gradient is nonzero (fig. 2), any other steady state is unlikely to exist for eq. 11 than $v = 0$ and, therefore, $\Phi = 0$.

Equations 7 and 11 are solved numerically for various values of nondimensional dispersivity A (fig. 3a). Although measurements have not been made, it is inferred that $0 < A < 1$ for intact specimens. The flux of aqueous silica increases with longitudinal dispersion, and so the rate of sealing increases with A. When cast in terms of nondimensional variables, these rates do not vary substantially among the experiments. The parameter A is the only parameter acting to increase the rate of flow-rate reductions in figure 3a. For $A = 0$, nondimensional pressure is calculated across the sample at various times (fig. 3b). Pressure, as well as porosity (not plotted, but similar to figure 4e), dramatically decreases at the inside of the sample, where solubility gradients are greatest. Therefore, if pore water is saturated with quartz, the sealing is complete and occurs dominantly near the inside wall of the sample.

To compare calculated flow rates with measured ones, we have to evaluate the time-scaling factor (eq. 12), where only the initial flow porosity $\bar{\phi}_f$ is unknown. We take $\bar{\phi}_f = 10^{-3}$ and $A = 0$ to superimpose calculated curves of fluid flux versus time for experiments 1 and 3 with the measured values (fig. 3c). This comparison shows good agreement for experiment 1, but poor agreement for experiment 3. An equivalent result has been obtained by Lichtner and coworkers (1983).

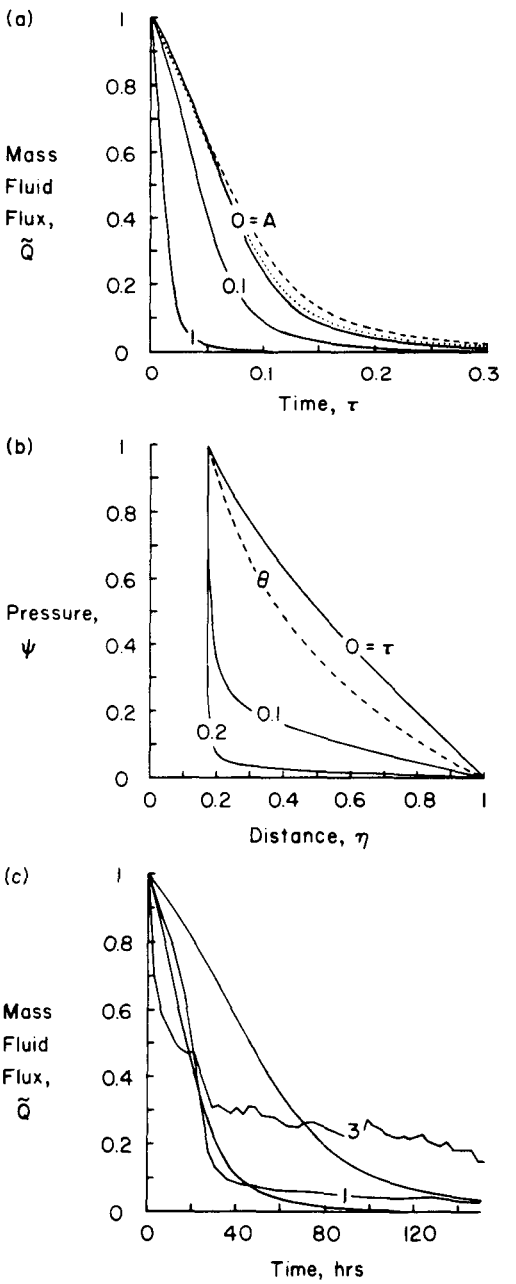
KINETICALLY CONTROLLED REACTION. The kinetics of the quartz-water reaction are now included in the transport model. Because we wish to isolate kinetic effects, we only consider the case of $A \ll 1$. Conservation of aqueous silica is

$$\frac{\partial}{\partial t}\phi_f c = \frac{-1}{r}\frac{\partial}{\partial r} rvc + R \quad (14)$$

where

$$R = (\phi_f a_q / m_f) k_- (\varepsilon_q - c) \quad (15)$$

Figure 3. (a) Normalized mass fluid flux versus nondimensional time τ where $A = \alpha/r_b = 0, 0.1, 1$ for conditions of experiment 3 (solid lines); dashed line, $A = 0$ for experiments 2 and 4; dotted line, $A = 0$ for experiment 1. (b) Normalized pressure versus distance for the case of $A = 0$ and conditions of experiment 3. (c) Normalized mass fluid flux versus time for $A = 0$, $\bar{\phi}_f = 10^{-3}$ and conditions of experiments 1 and 3 as calculated from eqs. 15 and 16, and as observed.



Equation 15 describes both dissolution and precipitation due to the reversible reaction between quartz and water, and aqueous silica (Rimstidt and Barnes, 1980). Although we are unaware of a rigorous development for the mass-conservation equations for nonisothermal-reacting porous media, eq. 14 is of the form discussed by Nguyen and others (1982) and Rubin (1983).

The value of the reaction parameter $\phi_f a_q / m_f$, which characterizes the extent of the reacting system, is unknown. Just as permeability can be related to flow porosity by a model of flow along orthogonal fractures, we find that

$$\phi_f a_q / m_f \propto 1/\rho_f d \qquad (16)$$

By introducing the nondimensional concentration $\zeta = c/\bar{s}_q$, eqs. 14-16 become

$$\frac{\upsilon_q \bar{s}_q}{\rho_q} \frac{\partial \phi \zeta}{\partial \tau} = \frac{-1}{\eta} \frac{\partial \eta \tilde{v} \zeta}{\partial \eta} + \frac{Gk_-}{\tilde{\rho}} (\tilde{s}_q - \zeta) \qquad (17)$$

where

$$G = \bar{\phi}_f \bar{\mu} r_b^2 \bar{a}_q \bar{k}_- / \bar{K} (P_a - P_b) \bar{m}_f \qquad (18)$$

is a ratio of kinetic-reaction rates to advection rates. For increasing values of G, the kinetics of the reaction are faster, concentrations approach saturation and the overall reaction rate becomes controlled by the advection rate. In the limit $G \to \infty$, eq. 11 is the special case $\zeta = \tilde{s}_q$ of eq. 17. Note that G is dependent upon the unknown quantities: initial flow porosity, area of quartz surface and mass of pore fluid. The LHS of eq. 17 is of the order 10^{-4} and is henceforth neglected. The boundary condition

$$\zeta(r_a/r_b) = 1 \qquad (19)$$

reflects that the inlet fluid is saturated with respect to quartz. An alternative boundary condition on concentration is incorporated below. Equation 11 (conservation of SiO_2) is

$$\frac{\partial \Phi}{\partial \tau} = \frac{1}{\eta} \frac{\partial}{\partial \eta} \eta \tilde{v} \zeta \qquad (20)$$

subject to the initial condition eq. 14.

Equations 7, 17 and 20 are solved numerically for the conditions of experiment 3 (table 2). Flow rate versus time curves (fig 4a) have

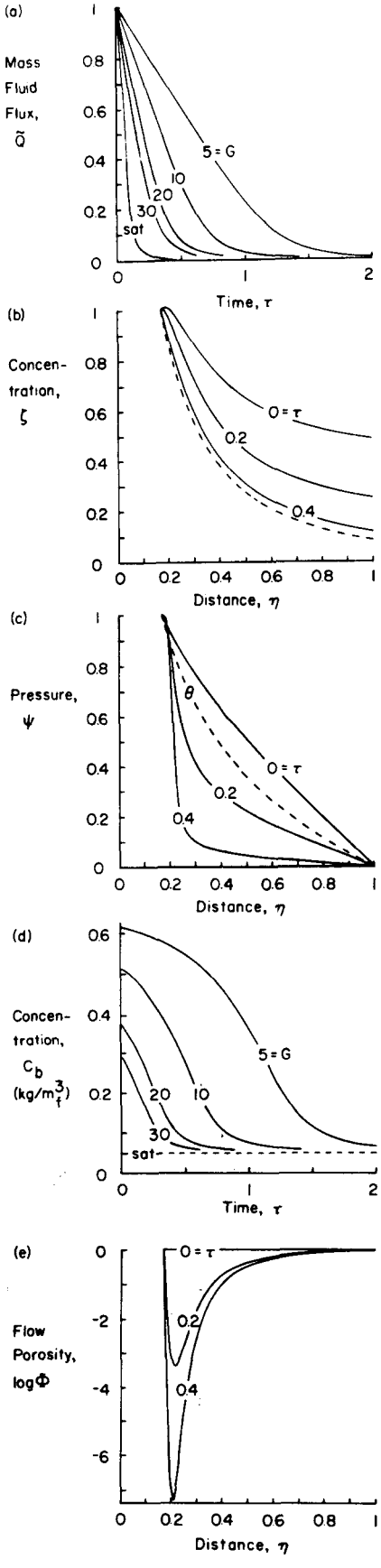


Figure 4. Inlet fluid is saturated. (a) Normalized mass fluid flux versus nondimensional time τ for G = 5, 10, 20, 30 and ∞ (saturation case, fig. 3). (b) Concentration ζ versus distance η for the case G = 30 at τ = 0, 0.2, 0.4; dashed line represents quartz solubility. (c) Pressure ψ versus η for G = 30. (d) Outlet concentration c_b versus τ for values of G. (e) Porosity Φ versus η for G = 30.

been calculated for various values of G. As G increases, the time for complete hydraulic sealing decreases. Figures 4b, 4c and 4e show how concentration, pressure and porosity, respectively, evolve in the sample over time for the case of G = 30. Concentrations approach quartz saturation only when pores are effectively sealed: that is, when pressure drops to an almost constant value throughout the sample. Porosity profiles reveal that quartz precipitates at the inside part of the sample, impeding flow from the heated reservoir. Because the inlet fluid is saturated, no dissolution of quartz occurs, and porosity only decreases from its initial value. Kinetic rates are most extreme near the high temperature end of the sample (fig. 2b) where porosity reductions are greatest. Outlet concentrations decrease steadily over time (fig. 4d) to quartz saturation, as compared to the relatively unchanging values measured (fig. 1b).

VARIABLE INLET CONCENTRATION. Although pure water was pumped into the axial reservoir, aqueous silica derived from quartz and fused silica on the reservoir wall accumulated during the course of the experiments. The presence of fused silica endpieces raises the possibility that the reservoir fluid became saturated with respect to quartz (the case above); results presented below indicate that this only occurred after complete sealing. To estimate the concentration of aqueous silica in the reservoir as a function of time, we employ the equation

$$\frac{d}{dt}c_a = \frac{-Qc_a}{\bar{\rho}_f V_f^r} + \frac{a_q^r \bar{k}}{m_f^r}(\bar{s}_q - c_a) + \frac{a_s^r \bar{k}}{m_f^r}(\bar{s}_s - c_a) \qquad (21)$$

which is a macroscopic mass balance (Bird and others, 1960, eq. 22.1-1) obtained by assuming that concentration gradients in the reservoir are small due to the presence of the heater coil. Although eq. 21 cannot be solved without knowledge of the mass flux of water into the pores (calculated from eq. 7), it nonetheless constitutes a boundary condition on the inlet concentration of aqueous silica. In nondimensional form, eq. 21 is

$$\frac{d}{d\tau}\zeta_a = \frac{-TQ\zeta_a}{\bar{\rho}_f V_f^r} + \frac{Ta_q^r \bar{k}}{m_f^r}(1-\zeta_a) + \frac{Ta_s^r \bar{k}\,\bar{s}}{m_f^r \bar{s}_q}(\zeta_a) \qquad (22)$$

Using eq. 22 and $\bar{\phi}_f = 10^{-3}$, the nondimensional time for sealing increases by more than a factor of 3 (compare figs. 4a and 5a). In the examples above, aqueous silica is introduced

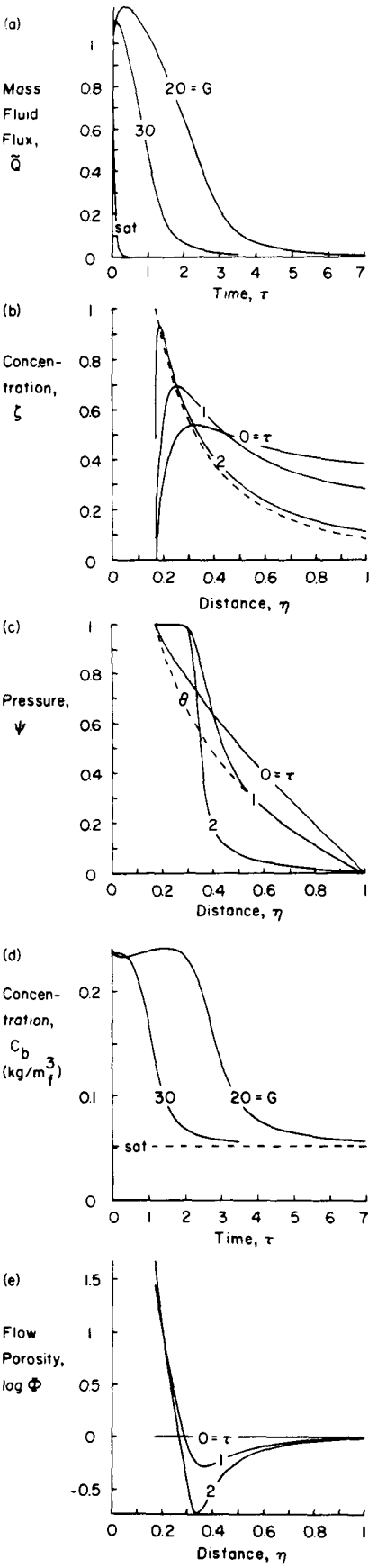


Figure 5. Concentration of inlet fluid varies with time. (a) Normalized mass fluid flux versus nondimensional τ for G = 20, 30 and ∞. (b) Concentration ζ versus distance η for the case G = 30 at τ = 0, 1 and 2. (c) Pressure ψ versus η for G = 30. (d) Outlet concentration c_b versus τ for values of G. (e) Porosity Φ versus η for G = 30.

into the samples from the reservoir; here much of the aqueous silica is derived from dissolution along pore walls, causing initial flow-rate increases. In fiqure 5b for G = 30, concentrations do not approach saturation until the sample is almost sealed ($\tau > 2$). Because dissolution occurs, pressures remain high (fig. 5c), and porosities increase at the inside of the sample (fig. 5e). As the concentration profiles intersect the quartz-solubility curve (near $\eta = 0.3$, fig. 5b), pressures and porosities correspondingly decrease due to precipitation. Outlet concentrations decrease with time (fig. 5d), although of lesser magnitude than in figure 4d, toward quartz saturation, whereas measured values do not.

CONCLUSIONS. Our results suggest that complete sealing would be achieved with model parameters appropriate for a low-permeability quartzite. However, we are unable to reproduce flow rates measured during experiments on granites, where sealing was incomplete. Furthermore, our results indicate that silica concentrations of the outlet fluid approach quartz saturation as the sample sealed; the measured concentrations did not change substantially and remained supersaturated through the length of the experiments. Effects of reactions with feldspar and mica are probably important. Because only small amounts of fluid were collected, aluminum concentrations could not be measured. Without this information and more complete kinetic data, the behavior of these minerals cannot be quantitatively examined. Order-of-magnitude calculations suggest that feldspar dissolution alone can account for observed silica concentrations and measured differences between the 250° and 300°C experiments, assuming that porosity reductions are governed entirely by the formation of clays--that is, no silica precipitates. In addition, at least three important parameters--dispersivity, flow porosity and mineral surface area--are either never or rarely measured. Further theoretical studies will require measurements of these properties.

REFERENCES.

Bird, R.B., W.E. Stewart and E.N. Lightfoot, 1960, Transport Phenomenon, John Wiley, New York, 780 p.

Facca, G., and F. Tonani, 1967, "The self-sealing geothermal field," Bull. Volcanology, 30, 271-273.

Fournier, R.O., and R.W. Potter, 1982, "An equation correlating the solubility of quartz in water from 25° to 900°C at pressures up to 10,000 bars," Geochim. Cosmochim. Acta, 46, 1969-1973.

Keenan, J.H., F. Keyes, P. Hill and J. Moore, 1978, Steam Tables, John Wiley, New York, 156 p.

Li, T. M. C., 1980, Axisymmetric Numerical Simulation of Hydrothermal Systems Including Changes in Porosity and Permeability due to the Quartz-Water Reaction, Ph.D. thesis, Penn. State Univ., 240 p.

Lichtner, P.C., H.C. Helgeson and K. Pruess, 1983, "Numerical modeling of fluid flow with simultaneous chemical reaction in hydrothermal systems," Geol. Soc. Am. Abstr.with Prog., 15, p. 627.

Lockner, D., D. Bartz and J. Byerlee, 1978, "Change in permeability during flow of water through granite subjected to a temperature gradient," Proc. Fourth Stanford Geothermal Workshop.

Moore, D.E., C.A. Morrow and J.D. Byerlee, 1981, "SiO_2 precipitation accompanying fluid flow through granite held in a temperature gradient," Proc. Seventh Stanford Geothermal Workshop.

_____, 1983, "Chemical reactions accompanying fluid flow through granite held in a temperature gradient," Geochim. Cosmochim. Acta, 47, 445-453.

Morrow, C.A., D. Lockner, D. Moore and J. Byerlee, 1981, "Permeability of granite in a temperature gradient," J. Geophys. Res., 86, 3002-3008.

Nguyen, V.V., W.G. Gray, G.F. Pinder, J.F. Botha and D.A. Crerar, 1982, "A theoretical investigation on the transport of chemicals in reactive porous media," Water Resources Res., 18, 1149-1156

Rimstidt, J.D., and H.L. Barnes, 1980, "The kinetics of silica-water reactions," Geochim. Cosmochim. Acta, 44, 1683-1699.

Rubin, Jacob, 1983, "Transport of reacting solutes in porous media: relation between mathematical nature of problem formulation and chemical nature of reactions," Water Resources Res., 19, 1231-1252

Summers, R., K. Winkler and J. Byerlee, 1978, "Permeability changes during the flow of water through Westerly granite at temperatures of 100°-400°C," J. Geophys. Res, 83, 339-344.

Touloukian, Y.S., W.R. Judd and R.F. Roy, 1981, Physical Properties of Rocks and Minerals, McGraw-Hill, New York, 548 p.

Turcotte, D.L., and G. Schubert, 1982, Geodynamics, John Wiley, New York, 450 p.

Watson, J.T.R., R.S. Basu and J.V. Sengers, 1980, "An Improved equation for the viscosity of water and steam," in Water and Steam: Their Properties and Current Industrial Applications, J. Straub and K. Scheffler, eds., Pergamon Press, New York, p. 336-343.

Proceedings Ninth Workshop Geothermal Reservoir Engineering
Stanford University, Stanford, California, December 1983
SGP-TR-74

HYPOTHESES ON POSSIBLE EQUILIBRIA BETWEEN N_2 AND OTHER GASES AT LARDERELLO AND CERRO PRIETO[+]

Franco D'Amore, Romano Celati, Claudio Calore

CNR, Istituto Internazionale per le Ricerche Geotermiche

Pisa, Italy

ABSTRACT

Considering various possible chemical reactions between N_2 and other gas species present in the geothermal fluid, the following reaction has been individuated:

$$C + 1/2\ N_2 + 7/2\ H_2 = NH_3 + CH_4$$

which is generally satisfied for plausible thermodynamic reservoir conditions (temperature and the relative contributions of steam and liquid to fluid production) at Larderello and Cerro Prieto.

INTRODUCTION

N_2, CH_4 and NH_3 are among the main components of uncondensable gas in the fluid of geothermal fields. A strong correlation was noted at Larderello between CH_4 and N_2 concentrations. Figure 1 shows the $\%CH_4$ in the uncondensable gas versus $\%N_2$ for three different zones of the field. The N_2/Ar ratio at Larderello is usually much higher than that of an air-saturated meteoric water (D'Amore and Nuti, 1977). Consequently N_2 may be assumed to be a reactive species connected in some way with methane.

An attempt was then made to individuate a chemical reaction capable of controlling the relative concentrations of N_2, CH_4 and NH_3 in the Larderello vapour-dominated system. Comparison was made with the water-dominated system of Cerro Prieto, which has much different reservoir thermodynamic conditions.

Chemical reactions considered

N_2 is generally considered at equilibrium with H_2 and NH_3 in the following reaction (D'Amore and Nuti, 1977; Ellis, 1979; Giggenbach, 1980; Nehring and D'Amore, 1984):

$$NH_3 = 1/2\ N_2 + 3/2\ H_2 \qquad (1)$$

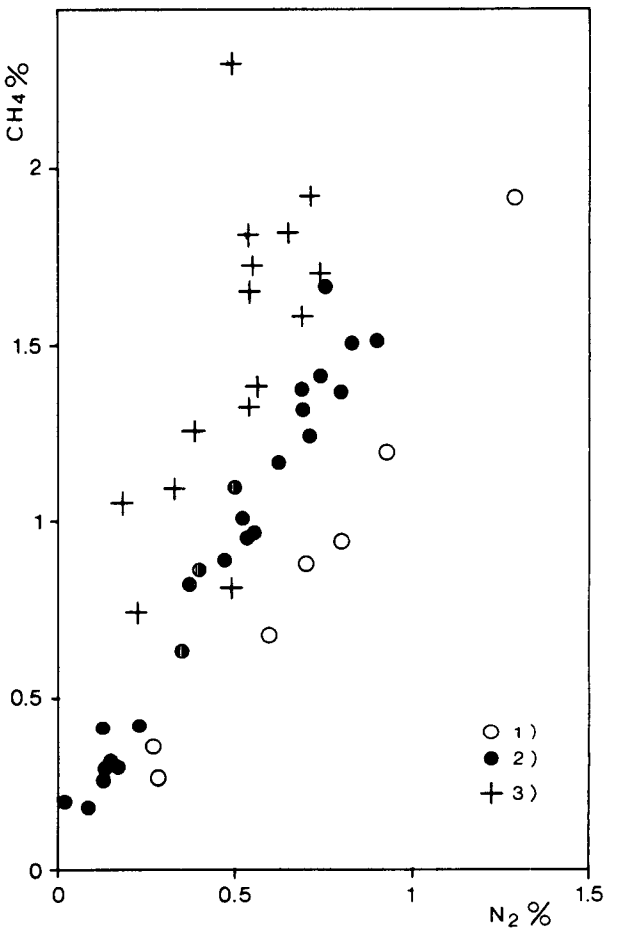


Figure 1. $\%CH_4$ in uncondensable gas versus $\%N_2$ for three different zones of the Larderello field. 1) Northeastern boundary zone; 2) central "classical" Larderello zone; 3) western and south-western zones of the field.

[+] Work conducted as part of the ENEL-CNR collaborative agreement.

However, this reaction is not in equilibrium at Larderello for plausible temperatures and reservoir steam fractions (D'Amore et al., 1982). Three different chemical reactions involving carbon were considered, since significant amounts of graphite have been detected in the Paleozoic basement in this area (Gianelli and Puxeddu,1979; Bagnoli et al., 1979). These reactions are:

$$3C + 4NH_3 = 3CH_4 + 2N_2 \quad (2)$$

$$C + NH_3 + 1/2\ H_2 = 1/2\ N_2 + CH_4 \quad (3)$$

$$C + 1/2\ N_2 + 7/2\ H_2 = NH_3 + CH_4 \quad (4)$$

These reactions were tested to discover whether any were consistent with the data from 22 wells at Larderello with different reservoir temperatures and fluid characteristics. The reservoir temperature assumed for each well was based on production data and in-hole measurements. Steam fractions in the reservoir fluid, y, which satisfy equilibrium conditions for reactions (1), (2), (3) and (4), were computed. In Table 1 the y_{NN} and y_{CN} values of y obtained from eqs. (1) and (4) respectively are compared with the y_{FT}, y_H and y_S values obtained from eqs.(5), (6) and (7) respectively:

$$H_2O = H_2 + 1/2\ O_2 \quad (5)$$

$$H_2S = H_2 + 1/2\ S_2 \quad (6)$$

$$CH_4 + 2H_2O = CO_2 + 4H_2 \quad (7)$$

Computations were based on the hypotheses described by D'Amore and Celati (1983), D'Amore et al.(1982, 1983). The equations used to calculate y are shown in Table 3. Two different equations were used for reaction (6), for Larderello and Cerro Prieto, to express sulphur fugacity as a function of temperature.

Table 1 does not include the y values obtained from reactions (2) and (3), since those obtained with reaction (2) are all near zero, and reaction (3) generally provides negative values.

Cerro Prieto field was considered since coaly material has been found to be ubiquitous in shaly layers of the reservoir (Barker and Elders, 1979). Furthermore, a good correlation was noted in the 1977 data (Nehring and D'Amore, 1984) between CH_4 and N_2. However, data scattering increases considerably in 1982. The data considered for Cerro Prieto (see Table 2) are from 1982 analyses of the fluid of 26 wells (Nehring and D'Amore, 1984). The reservoir temperatures used were those indicated by the Ca-Na-K geothermometer (Nehring and D'Amore, 1984). Reactions (2) and (3) once again are not in equilibrium for values of y exceeding 10^{-3}.

For both fields the y_{NN} values obtained with eq.(1) are generally one order of magnitude lower than those obtained with eqs.(4),(5),(6) and (7), while y_{CN} , with only a few exceptions, is satisfactorily consistent with y_H, y_S and y_{FT} . y_S at Cerro Prieto is at times much different from y calculated with the other methods. As mentioned by D'Amore et al.(1983), y_{FT} at Larderello is sometimes higher than y_H and y_S , usually where the $\%CH_4$ in the uncondensable gas is low. The investigation of the origin of these discrepancies is beyond the scope of the present study. Nevertheless, of all the chemical reactions considered relating N_2 to NH_3, eq.(4) provides the results closest to those obtained from eqs.(5), (6) and (7).

Acknowledgement

The authors wish to thank ENEL for providing data on gas compositions.

REFERENCES

Bagnoli, G., Gianelli, G., Puxeddu, M., Rau,A., Squarci, P., Tongiorgi, M. (1979), "A Tentative Stratigraphic Reconstruction of the Tuscan Paleozoic Basement", Mem.Soc.Geol.Ital., v.20, 99-116.

Barker, C.E., Elders, W.A. (1979), "Vitrinite Reflectance Geothermometry in the Cerro Prieto Geothermal Field, Baja California, Mexico", Geothermal Resources Council Trans., v.3, 27-30.

D'Amore, F., Celati, C. (1983), "Methodology for Calculating Steam Quality in Geothermal Reservoirs", Geothermics, v.12, no.2/3,129-140.

D'Amore, F., Celati, R., Calore, C. (1982), "Fluid Geochemistry Applications in Reservoir Engineering (Vapor-Dominated Systems)", Proc. 8th Workshop Geothermal Reservoir Engineering, Stanford, Dec.14-16,1982, 295-308.

D'Amore, F., Celati, R., Calore, C., Bertrami, R. (1983), "Effects of Natural Recharge on Gas Composition in the Larderello-Castelnuovo Area", this Workshop.

D'Amore, F., Gianelli, G. (1984), "Mineral Assemblages and Oxygen and Sulphur Fugacities in Natural Water-Rock Interaction Processes", Geochim. et Cosmochim.Acta, in press.

D'Amore, F., Nuti, S. (1977), "Notes on the Chemistry of Geothermal Gases", Geothermics,v. 6, 39-65.

Ellis, A.J. (1979), "Chemical Geothermometry in Geothermal Systems", Chem.Geom., v.25, 219-226.

Gianelli, G., Puxeddu, M. (1979),"An Attempt at Classifying the Tuscan Paleozoic: Geochemical Data", Mem.Soc.Geol.Ital.,v.20,435-446.

Giggenbach, W.F.(1980),"Geothermal Gas Equilibria", Geochim.Cosmochim.Acta,v.44,2021-2032.

Nehring, N.L., D'Amore,F. (1984),"Gas Chemistry and Thermometry of the Cerro Prieto, Mexico, Geothermal Field", Geothermics, v.13, no.1/2, 75-90.

Table 1. Molar gas concentrations and steam fractions (y),calculated from eqs.(7),(5),(6),(4) and (1), for Larderello field

Well	Year	T°C	$\frac{n_{gas}}{n_{H_2O}} .10^3$	$\log\frac{n_{H_2}}{n_{H_2O}}$	$\log\frac{n_{H_2S}}{n_{H_2O}}$	$\log\frac{n_{CH_4}}{n_{H_2O}}$	$\log\frac{n_{N_2}}{n_{H_2O}}$	$\log\frac{n_{NH_3}}{n_{H_2O}}$	$\log\frac{n_{CO_2}}{n_{H_2O}}$	y_{FT}	y_H	y_S	y_{CN}	y_{NN}
a	1978	240	97.2	-3.19	-3.43	-3.46	-3.58	-3.58	-1.02	> 1	0.71	0.93	0.63	0.04
b	1978	250	35.4	-3.19	-3.33	-3.58	-4.09	-3.79	-1.47	0.87	0.60	0.54	0.62	0.04
c	1978	240	108.7	-3.21	-3.42	-2.99	-3.04	-3.55	-0.98	0.87	0.68	0.53	0.47	0.05
d	1978	260	13.0	-3.55	-3.46	-3.85	-4.37	-3.65	-1.92	0.31	0.22	0.32	0.17	0.02
e	1978	270	22.4	-3.18	-3.25	-3.36	-3.80	-3.58	-1.69	0.56	0.45	0.43	0.41	0.04
f	1978	280	14.1	-3.33	-3.35	-3.73	-4.12	-3.75	-1.89	0.40	0.27	0.26	0.36	0.02
g	1976	270	5.9	-3.67	-3.68	-3.87	-4.54	-4.30	-2.28	0.17	0.14	0.14	0.19	0.02
h	1978	270	12.2	-3.35	-3.41	-3.70	-4.18	-4.05	-1.96	0.40	0.30	0.29	0.42	0.04
i	1978	270	12.6	-3.33	-3.39	-3.67	-4.03	-3.98	-1.95	0.41	0.32	0.30	0.43	0.04
j	1978	270	15.7	-3.25	-3.24	-3.54	-3.99	-3.98	-1.85	0.49	0.38	0.43	0.51	0.05
k	1978	260	5.6	-3.62	-3.64	-4.11	-4.49	-4.19	-2.30	0.24	0.19	0.20	0.26	0.02
l	1978	230	59.5	-3.47	-3.62	-3.92	-3.73	-3.69	-1.23	0.79	0.44	0.41	0.43	0.03
m	1978	240	13.2	-3.40	-3.50	-3.78	-4.30	-3.70	-1.92	0.51	0.44	0.44	0.34	0.02
n	1978	240	4.9	-3.79	-3.83	-4.40	-4.63	-4.40	-2.35	0.23	0.18	0.19	0.27	0.02
o	1977-78	220	48.4	-3.67	-3.71	-3.88	-3.87	-3.56	-1.32	0.52	0.32	0.40	0.21	0.015
p	1971-78	220	7.1	-3.80	-3.92	-4.20	-4.27	-4.23	-2.17	0.28	0.24	0.24	0.27	0.02
q	1971-78	220	20.6	-3.37	-3.56	-3.49	-3.85	-3.81	-1.71	0.66	0.65	0.57	0.48	0.04
r	1973-78	210	10.7	-3.62	-3.68	-3.73	-4.23	-3.96	-2.00	0.41	0.43	0.52	0.27	0.02
s	1971-78	220	12.1	-3.61	-3.65	-3.89	-4.47	-3.42	-1.94	0.41	0.37	0.46	0.17	0.01
t	1971-78	210	3.5	-3.96	-3.93	-4.20	-4.73	-4.26	-2.50	0.18	0.19	0.29	0.15	0.01
u	1976-78	220	16.7	-3.53	-3.79	-4.48	-5.48	-3.07	-1.79	0.76	0.45	0.33	0.17	0.00
v	1971-78	210	6.5	-3.62	-3.73	-3.55	-4.09	-4.32	-2.24	0.31	0.43	0.46	0.35	0.04

Table 2. Molar gas concentrations and steam fractions (y), calculated from eqs.(7),(5),(6),(4),(1), for Cerro Prieto field (1982 data)

Well	T°C	$\frac{n_{gas}}{n_{H_2O}} .10^3$	$\log\frac{n_{H_2}}{n_{H_2O}}$	$\log\frac{n_{H_2S}}{n_{H_2O}}$	$\log\frac{n_{CH_4}}{n_{H_2O}}$	$\log\frac{n_{N_2}}{n_{H_2O}}$	$\log\frac{n_{NH_3}}{n_{H_2O}}$	$\log\frac{n_{CO_2}}{n_{H_2O}}$	y_{FT}	y_H	y_S	y_{CN}	y_{NN}
M5	280	1.74	-4.26	-4.07	-4.13	-5.03	-4.56	-2.83	0.027	0.027	0.029	0.035	0.0045
M11	288	1.27	-4.58	-4.11	-4.32	-4.69	-4.64	-2.97	0.010	0.013	0.008	0.017	0.0010
M14	263	3.79	-3.61	-3.86	-3.82	-4.75	-4.63	-2.49	0.18	0.19	0.12	0.27	0.035
M19A	284	1.58	-4.30	-4.07	-4.19	-5.04	-4.60	-2.87	0.023	0.027	0.023	0.033	0.0037
M25	284	1.83	-4.24	-3.98	-4.12	-5.00	-4.55	-2.81	0.027	0.025	0.042	0.036	0.0042
M26	269	1.63	-4.36	-3.96	-4.19	-5.00	-4.60	-2.86	0.024	0.026	0.077	0.032	0.0047
M29	260	1.49	-4.37	-4.17	-4.25	-5.07	-4.63	-2.89	0.029	0.031	0.044	0.037	0.0053
M30	275	1.27	-4.31	-4.15	-4.33	-5.07	-4.61	-2.97	0.027	0.026	0.025	0.039	0.0047
M31	280	2.30	-3.98	-3.87	-3.93	-4.78	-4.46	-2.72	0.056	0.055	0.078	0.072	0.011
M35	275	1.04	-4.37	-4.26	-4.23	-5.00	-4.75	-3.07	0.020	0.022	0.009	0.033	0.0056
M43	281	1.13	-4.62	-4.18	-4.36	-5.12	-4.72	-3.02	0.009	0.008	0.011	0.015	0.0008
M48	308	1.09	-4.23	-4.22	-4.47	-5.07	-4.57	-3.04	0.020	0.009	< 0	0.039	< 0
M50	294	1.57	-4.22	-4.06	-4.17	-4.93	-4.57	-2.88	0.023	0.020	0.003	0.038	0.0032
M51	301	1.99	-4.06	-3.97	-4.13	-4.89	-4.53	-2.77	0.038	0.026	0.002	0.056	0.0046
M53	319	2.17	-3.99	-3.95	-4.12	-5.10	-4.51	-2.74	0.036	0.014	< 0	0.050	< 0
M84	317	4.51	-3.33	-3.60	-3.95	-4.77	-4.26	-2.44	0.25	0.13	0.059	0.36	0.024
M90	284	1.25	-4.37	-4.20	-4.18	-4.88	-4.69	-2.40	0.016	0.017	0.003	0.030	0.0043
M91	306	1.18	-4.34	-4.06	-4.38	-4.94	-4.56	-3.01	0.013	0.005	< 0	0.026	< 0
M101	301	1.46	-4.40	-3.92	-4.12	-4.95	-4.45	-2.93	0.010	0.006	0.013	0.014	< 0
M102	318	8.88	-3.34	-3.43	-3.54	-4.82	-3.76	-2.10	0.23	0.13	0.14	0.16	0.0045
M104	313	7.56	-3.27	-3.51	-3.50	-4.74	-4.10	-2.20	0.26	0.17	0.12	0.25	0.020
M105	304	2.04	-3.97	-3.92	-4.12	-4.79	-4.42	-2.77	0.046	0.031	0.005	0.056	0.0035
M114	271	0.94	-4.82	-4.23	-4.30	-5.11	-4.78	-3.10	0.005	0.006	0.020	0.009	0.0006
M130	290	2.00	-4.13	-3.97	-4.10	-4.04	-4.31	-2.77	0.035	0.030	0.031	0.056	0.0085
E2	318	1.61	-4.21	-3.95	-4.39	-5.09	-4.46	-2.87	0.002	0.002	< 0	0.028	< 0
E4	316	2.46	-3.65	-3.79	-4.19	-4.56	-4.55	-2.70	0.11	0.057	< 0	0.22	0.021

Table 3. Chemical reactions and related equations used in the text.

Reaction 1 $NH_3 = 1/2\ N_2 + 3/2\ H_2$ $(y = y_{NN})$

$$3/2 \log(n_{H_2}/n_{H_2O})_{WH} + 1/2 \log(n_{N_2}/n_{H_2O})_{WH} - \log(n_{NH_3}/n_{H_2O})_{WH}$$
$$= -4.63 - 255.2/T + 1.55 \log T + 3/2 \log A_{H_2} + 1/2 \log A_{N_2} - \log A_{NH_3}$$

Reaction 2 $3C + 4NH_3 = 3CH_4 + 2N_2$

$$3 \log(n_{CH_4}/n_{H_2O})_{WH} + 2 \log(n_{N_2}/n_{H_2O})_{WH} - 4 \log(n_{NH_3}/n_{H_2O})_{WH}$$
$$= -18.42 + 6038.6/T + 6.20 \log T + 3 \log A_{CH_4} + 2 \log A_{N_2} - 4 \log A_{NH_3}$$

Reaction 3 $C + NH_3 + 1/2\ H_2 = 1/2\ N_2 + CH_4$

$$\log(n_{CH_4}/n_{H_2O})_{WH} + 1/2 \log(n_{N_2}/n_{H_2O})_{WH} - 1/2 \log(n_{H_2}/n_{H_2O})_{WH} - \log(n_{NH_3}/n_{H_2O})_{WH}$$
$$= 0.569 + 1597.5/T + \log A_{CH_4} + 1/2 \log A_{N_2} - 1/2 \log A_{H_2} - \log A_{NH_3}$$

Reaction 4 $C + 1/2\ N_2 + 7/2\ H_2 = NH_3 + CH_4$ $(y = y_{CN})$

$$\log(n_{NH_3}/n_{H_2O})_{WH} + \log(n_{CH_4}/n_{H_2O})_{WH} - 7/2 \log(n_{H_2}/n_{H_2O})_{WH} - 1/2 \log(n_{N_2}/n_{H_2O})_{WH}$$
$$= 0.14 + 2737.5/T + \log A_{NH_3} + \log A_{CH_4} - 7/2 \log A_{H_2} - 1/2 \log A_{N_2}$$

Reaction 5 $H_2O = H_2 + 1/2\ O_2$ $(y = y_H)$

$$\log f_{O_2} = -3.808 - 13708.3/T - 2.075 \cdot 10^6/T^2 \quad \text{(D'Amore and Gianelli,1984)}$$

$$\log(n_{H_2}/n_{H_2O})_{WH} = 4.556 - 5922/T + 1.038 \cdot 10^6/T^2 + \log A_{H_2}$$

Reaction 6 $H_2S = H_2 + 1/2\ S_2$ $(y = y_S)$

Larderello : $\log f_{S_2} = 5.706 - 9767/T$ (temperature validity range = 210° - 280°C)

$$\log(n_{H_2S}/n_{H_2O})_{WH} = 7.539 - 6410.75/T - 0.79 \log T + 1.038 \cdot 10^6/T^2 + \log A_{H_2S}$$

Cerro Prieto : $\log f_{S_2} = 0.761 - 7186.4/T$ (temperature validity range = 260° - 320°C)

$$\log(n_{H_2S}/n_{H_2O})_{WH} = 5.067 - 5120.5/T + 1.038 \cdot 10^6/T^2 - 0.79 \log T + \log A_{H_2S}$$

Reaction 7 $CH_4 + 2H_2O = CO_2 + 4H_2$ $(y = y_{FT})$

$$4 \log(n_{H_2}/n_{H_2O})_{WH} + \log(n_{CO_2}/n_{CH_4})_{WH}$$
$$= -0.26 - 5227/T + 4 \log A_{H_2} + \log A_{CO_2} - \log A_{CH_4}$$

T = temperature, °K; $A_i = (y + \frac{1-y}{B_i})$; n = number of moles; WH = wellhead; f_{O_2} = oxygen fugacity; f_{S_2} = sulphur fugacity; y = molar steam fraction in the reservoir.

Proceedings Ninth Workshop Geothermal Reservoir Engineering
Stanford University, Stanford, California, December 1983
SGP-TR-74

HETEROGENEITY OF THE LIQUID PHASE, AND VAPOR SEPARATION IN LOS AZUFRES (MEXICO) GEOTHERMAL RESERVOIR

*Nieva D., +Quijano L., &Garfias A., *Barragán R.M. and &Laredo F.

*Instituto de Investigaciones Eléctricas, Apdo. Postal 475, Cuernavaca, Morelos 62000, México. +Subgerencia de Estudios and &Coordinadora Ejecutiva de Los Azufres, Gerencia de Proyectos Geotermoeléctricos, Comisión Federal de Electricidad

ABSTRACT

Data of chemical and isotopic composition of fluids from Los Azufres geothermal wells is interpreted in order to characterize the composition of the liquid phase, and to define the relation between this phase and fluids from steam-producing wells.

Chemical and specific enthalpy data show that most wells considered are fed a mixture of steam and liquid. Thus, flashing occurs in the formation. This poses a problem on the interpretation of isotopic data, because the composition of the feeding mixture need not be representative of the composition of the liquid phase in the reservoir. Two extreme alternatives for the interpretation of isotopic data are considered. In the first alternative the composition of the total discharge is considered to be the same as that of the liquid in the reservoir. In the second alternative the feeding fluid is considered to be a mixture of the liquid phase in the reservoir and the calculated fraction of steam. In addition, this steam is assumed to separate from a much larger mass of that liquid phase at the downhole temperature. The contribution of steam is then substracted from the total discharge to yield the composition of the liquid phase. Using data for silica concentration in total discharge and separated water, the chloride concentration in the reservoir liquid is calculated. This result is used to calculate the fraction of steam in the feeding mixture of each well. The isotopic data is then corrected as proposed for the second alternative, to yield the composition of the liquid phase.

Comparison of the corrected and uncorrected isotopic valuesshows that the correction has an important effect only when the steam mass fraction in the feeding mixture is large (> 20%). The correction tends to reduce the dispersion of data points in a δ D vs δ^{18}O diagram. Points representing composition of liquid phase show an approximately linear distribution, suggesting a process of mixing of two fluids. Available data appears to rule out the possibility of mixture with local meteoric or shallow ground waters. Some spatial correlations of composition are noted. The composition of fluids produced by two steam wells corresponds to steam separated from a much larger mass of liquid. Temporal variations in the composition of fluid produced by steam well A-6 suggests that this well might be fed with steam from more than one section in the reservoir.

INTRODUCTION

The chemical and isotopic composition of hydrothermal fluids constitute one of the early important sources of information, which could be used to begin the characterization of a geothermal reservoir. It is particularly important to assemble as complete a set of data as possible from the pre- and early exploitation stages, since this would provide valuable information on the natural state of the system. This in turn would make it possible to monitor the changes occurring in the reservoir as exploitation begins and proceeds.

Giggenbach and Quijano (1981) have assembled a set of data of isotopic and chemical composition of fluids from geothermal wells in Los Azufres field, as well as from hydrothermal springs and fumaroles of the area. They have interpreted the evidence in a study of the regional hydro - logy of the Cuitzeo - Los Azufres area. One of the major findings of this study is the clear difference between the isotopic composition of local meteoric and shallow underground waters, and the composition of the geothermal fluids. The authors have concluded that the reservoir fluid consists of paleowaters, and postulate a relation between the Los Azufres aquifer and thermal springs in the Cuitzeo - Araro area, some 30 kilometers north.

The explored area in Los Azufres field covers an extension of about 30 Km^2 (Fig. 1). The field is located in a mountain range, bounded on two sides by valleys. The average altitude of well heads is 2850-2900 meters above sea level; the valleys lie about 300 m to 500 m below. There are two main sections which have been selected for exploitation, based on favorable tempera - ture and permeability conditions. In the north ern section, known as the Maritaro area, one finds only wells that produce a mixture of water and steam. In the southern section, known as the Tejamaniles area, one finds steam-producing wells, interspersed with mixture - producing wells. The present contribution describes the results of a study of the hydrology of the Los Azufres reservoir. The main objective of this investigation has been to determine any possible differences among the liquid phases from the several sections of the field, and to determine the relation between the fluid emanating from steam-producing wells and the liquid phase. We have used a subset of the data included in the work of Giggenbach and Quijano (1981).

OBSERVATIONS

Table 1 shows a set of chemical and isotopic composition data for fluids produced by wells from Los Azufres. The specific enthalpy of

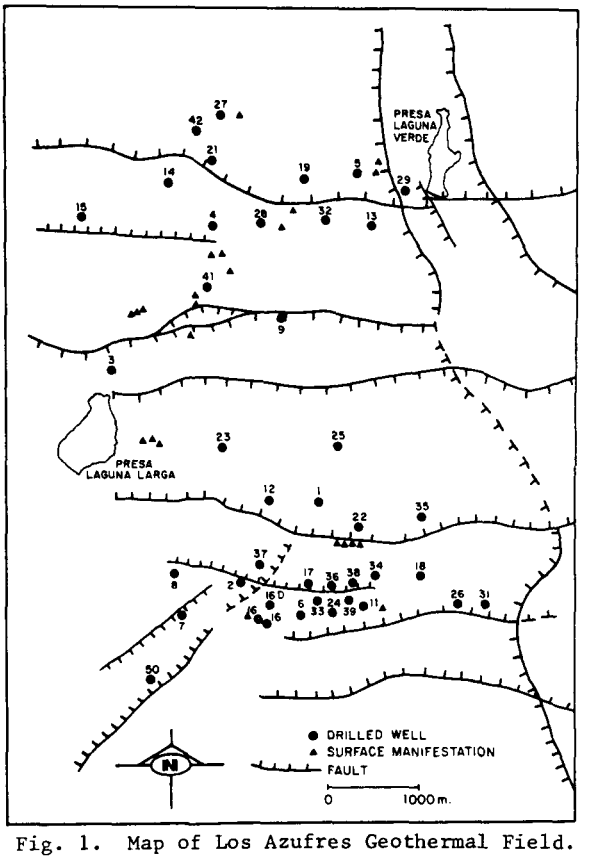


Fig. 1. Map of Los Azufres Geothermal Field.

the total discharge is also shown. Values for the ionic species and silica refer to their concentration in the liquid separated at atmospheric pressure. The boiling temperature in Los Azufres area is 92°C. The delta values for deuterium and ^{18}O refer to the composition of the total discharge. These values have been calculated from the composition of the liquid separated at atmospheric pressure, using data given by Truesdell et al (1977) for partition coefficients of deuterium and ^{18}O between the vapor and liquid phases.

The Table includes isotopic data for fluids from two steam-producing wells (A-6 and A-17). For some of the mixture-producing wells isotopic but not chemical data is available. Downhole temperatures obtained with Kuster type equipment are shown in Table 2. Also shown are temperatures calculated by means of a Cationic Composition Geothermometer (Nieva and Nieva, 1982), the Na-K-Ca geothermometer

TABLE 1.- Chemical and isotopic composition data of Los Azufres fluids.

WELL	H J/g	Na^+	K^+ ppm	Cl^-	SiO_2	^{18}O	D	DATE OF SAMPLING
A-1	1750	-	-	-	-	-3.94	-56.6	20/ 3/82
A-2	1400	-	-	-	-	-4.33	-62.6	20/ 3/82
A-4	1460	1804	499	3270		-4.44	-65.2	8/ 5/80
A-5	1885	1876	534	3320	1160	-4.03	-58.8	29/ 4/80
A-5	1671	1638	465	2870	1250	-4.06	-62.4	13/ 1/81
A-6	2660	-	-	-	-	-4.26	-53.4	8/ 5/80
A-6	2756	-	-	-	-	-4.83	-60.6	13/ 1/81
A-6	2673	-	-	-	-	-5.02	-55.7	20/ 3/82
A-7	1360	1496	250	2460	780	-4.23	-65.0	17/ 4/80
A-8	1570	1606	359	2760	1100	-4.67	-65.8	26/ 4/80
A-13	1234	1499	390	2580	1020	-2.76	-60.4	14/ 1/81
A-13	1490	-	-	-	-	-2.57	-57.2	20/ 3/82
A-16D	1230	-	-	-	-	-3.72	-58.9	20/ 3/82
A-17	2673	-	-	-	-	-5.06	-58.8	20/ 3/82
A-19	2452	1689	475	3060	1050	-5.21	-62.4	13/ 1/81

H = specific enthalpy

(Fournier and Truesdell, 1973) and the revised silica geothermometer (Fournier and Potter II, 1982). In all cases there is good agreement among the values calculated with the different geothermometers. The measured values, on the other hand, seem to be consistently below the calculated values. Furthermore, the measured values would appear to be low also from a consideration of the specific enthalpies of total discharge. Given these observations and the general agreement among the geothermometers, only the latter have been considered in selecting a value of downhole temperature for each well. The selected values are shown in Table 2.

TABLE 2.- Measured and calculated downhole temperatures for Los Azufres wells.

WELL	T MEAS. °C	*T CCG °C	°T Na-K-Ca °C	&T SiO_2 °C	DATE OF SAMPLING
A-1	292	304	-	-	
A-2	280	304	290	285	14/ 4/80
A-4	298	308	314	-	8/ 5/80
A-5	270	311	318	308	13/ 1/81
A-7	249	251	254	262	17/ 4/80
A-8	275	282	286	295	26/ 4/80
A-13	265	300	300	287	14/ 1/81
A-13	265	292	297	280	9/ 2/83
A-16D	260	261	265	255	9/ 2/83
A-18	250	284	290	266	2/ 3/82
A-19	271	310	312	290	13/ 1/81

*CCG = Cationic Composition Geothermometer (Nieva and Nieva, 1982).

°Na-K-Ca Geothermometer (Fournier and Truesdell, 1973).

&SiO_2 = Revised and expanded silica (quartz) Geothermometer (Fournier and Potter, 1982).

In most cases listed in Table 1, the specific enthalpy of the total discharge is considerably in excess of the specific enthalpy of liquid water at the downhole temperature. This implies that phase separation occurs in the formation, so that the wellbore is fed a mixture of steam and liquid. This poses a problem on the interpretation of the isotopic composition of total discharge. This problem arises from the fact that, if phase separation occurs in the formation, there is no certainty that the isotopic composition of the total mixture entering the well is representative of the undisturbed liquid phase in the reservoir. The problem is particularly complex because only part of the steam present in the feeding mixture might represent an excess, the rest of it originating from local boiling (see Truesdell et al, these Proceedings, and Nieva et al, 1982, for a discussion of this problem). In view of the unavailability of the necessary information for the estimation of excess steam, it is decided to consider two extreme alternatives and to compare the final conclusions. The first extreme position is to consider the

isotopic composition of the total discharge as identical to that of the liquid phase in the reservoir. The other alternative is to consider as excess all the steam present in the mixture. In this case, it is also to be assumed that the steam has separated from a much larger mass of the reservoir liquid at the downhole temperature. Using partition coefficients for deuterium and ^{18}O, calculated at that temperature, one can correct the isotopic composition of the total discharge in order to obtain the composition of the liquid phase, according to the following expressions:

$$\delta_x^{lp} = (\delta_x^{td} - \Theta) / \Phi \qquad (1)$$

$$\Theta = 1000\ f\ (1 - \alpha) / \alpha \qquad (2)$$

$$\Phi = 1 - f + (f/\alpha) \qquad (3)$$

where f is the fraction of excess steam in the mixture; α is the atomic ratio of ^{18}O over ^{16}O in the steam, divided by the corresponding ratio in the liquid phase, at the downhole temperature. The superscripts lp and td refer to liquid phase and total discharge, respectively. The symbol x stands for ^{18}O or D. In cases where a steam deficit is estimated, the composition of the liquid phase is calculated from:

$$\delta_x^{lp} = (\delta_x^{td} + \Theta) / \Phi \qquad (4)$$

The fraction of steam in the feeding mixture is calculated from the silica concentration in the total discharge and that in the liquid separated at atmospheric pressure. From the latter concentration, and the assumption that the flow inside the borehole occurs adiabatically, one can calculate the downhole temperature (Fournier and Potter II, 1982). In so doing one also obtains the equilibrium concentration of silica in the liquid phase at the calculated downhole temperature. Considering this value and the silica concentration in the total discharge, one obtains the fraction of steam in the feeding mixture by a simple mass balance calculation. Data and results for this calculation are presented in Table 3, for the cases where silica concentrations are available. In all cases except one, the results indicate the presence of a substantial fraction of steam in the feeding mixture; in the case of well A-19 the steam constituted the larger part (80% in weight). For well A-13 a small steam deficit is calculated; given the errors in enthalpy measurements and silica determination, this result probably means that the well was being fed only liquid.

TABLE 3.- Percent steam in feeding mixture calculated from silica concentration. Chloride concentration in the total discharge, and calculated concentration in liquid phase in the reservoir.

WELL	H J/g	T °C (SiO_2)	SiO_2 ppm			% VAPOR
			s.w.	t.d.	eq.	
A-5	1885	308	1250	427	703	39
A-5	1671	300	1160	505	673	25
A-7	1360	262	780	446	519	14
A-8	1570	295	1100	528	653	19
A-13	1234	287	1020	640	623	-3
A-19	2452	290	1050	97	635	85

H = specific enthalpy of total discharge.
s.w. = Water separated at atmospheric pressure.
t.d. = Total discharge.
e.q. = Equilibrium concentration of silica at estimated downhole temperature.

The values of steam fraction calculated above, and the chloride concentration in the separated water, could be used to estimate the chloride concentration in the liquid phase of the reservoir.

Results of these calculations are shown in Table 4. The general agreement between the several calculated values is clear. Two of the six values deviate noticeably from the rest. Since these values correspond to the cases where the steam fraction was largest, and thus are more likely to result from overcorrections, they were not taken into account for the estimation of an average value of chloride concentration in the reservoir. The value obtained is 1650 ppm.

TABLE 4.- Chloride concentration in total discharge and calculated concentration in the liquid phase of the reservoir.

WELL	CHLORIDE (ppm) total discharge	liquid phase in reservoir
A-5	1134	1868
A-5	1250	1667
A-7	1407	1638
A-8	1325	1638
A-13	1619	1575
A-19	284	1856

Inverting the mass balance calculation referred to in the last paragraph, it is possible to calculate the fraction of steam in the feeding mixture from the chloride concentration in the total discharge, and the average concentration in the liquid phase of the reservoir. Table 5 shows the results obtained for samples listed in Table 1. In a few cases of mixture-producing wells where chemical analysis data are not available, the fraction of steam was calculated by means of an enthalpy balance calculation.

TABLE 5.- Percent steam in feeding mixture calculated from chloride concentration in total discharge. Calculated isotopic composition of liquid phase.

WELL	% STEAM	^{18}O	D	DATE OF SAMPLING
A-1	°29	-3.67	-57.5	20/ 3/82
A-2	° 8	-4.25	-62.9	20/ 3/82
A-4	-4	-4.48	-65.1	8/ 5/80
A-5	31	-3.77	-59.6	29/ 4/80
A-5	24	-3.86	-63.7	13/ 1/81
A-7	15	-4.00	-65.5	17/ 4/80
A-8	20	-4.45	-66.5	26/ 4/80
A-13	2	-2.74	-60.4	20/ 3/82
A-13	°10	-2.47	-57.5	20/ 3/82
A-19	83	-4.53	-64.6	13/ 1/81
A-16D	4	-3.66	-59.1	20/ 3/82

°Chloride concentration not available; calculated from specific enthalpy of total discharge.

DISCUSSION

The uncorrected values of isotopic composition of total discharge are plotted in Fig. 2. It is evident that there is considerable dispersion of the compositions corresponding to mixture-producing wells (represented by circles). The values corresponding to fluids produced by steam wells (represented by triangles) tend to be in the upper left section of the distribution, as would be expected from the values of partition coefficients of the isotopic species

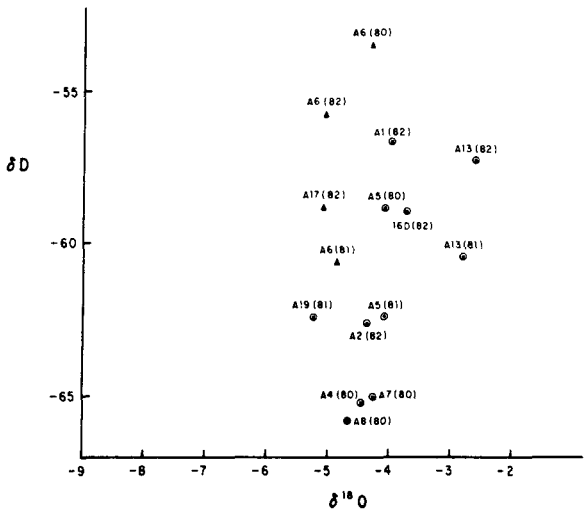


Fig. 2. Isotopic Composition of total discharge from Los Azufres wells. Circles and triangles represent fluids from mixture-producing and steam wells, respectively.

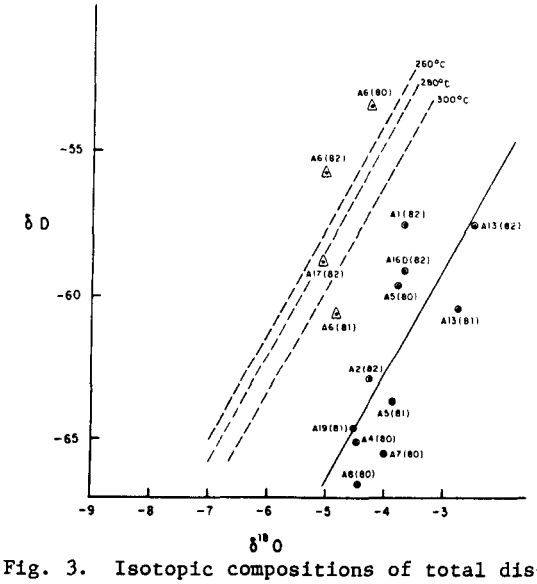


Fig. 3. Isotopic compositions of total discharge after correcting those corresponding to mixture-producing wells, in the manner described in the text. Symbols as for Fig. 2.

between steam and liquid at temperatures above 250 °C.

Fig. 3 presents a plot of the isotopic values, corrected as proposed under the second alternative. Superposition of Figs. 2 and 3 shows that the correction has a substantial effect only for those cases where 20% or more of the feeding mixture was constituted by steam, as is the case of wells A-19, A-5 (sample of 1980) and A-1. The correction tends to reduce the dispersion of the data points corresponding to liquid phase. I also increases the systematic difference between the compositions of liquid and steam phases. The data points for liquid phase show an aproximately linear distribution; the solid line corresponds to a least-squares fit with a correlation coefficient of 0.75.

The uncertainties in the measurement of δD and $\delta^{18}O$ are estimated as $\pm$ 0.5 and $\pm$ 0.05, respectively. The observed differences in isotopic composition of liquid phase are much larger than these error margins, and thus indicate a degree of heterogeneity in the aquifer. As reported by Giggenbach and Quijano (1981), the isotopic compositions of local shallow waters and the geothermal fluids are very different, ruling out the possibility of a direct origin of the latter from local meteoric precipitation. The approximately linear distribution in Fig. 3 suggests the possibility of mixture of two fluids in the aquifer. Extrapolation of the best-fit line gives an intercept with the meteoric line (Craig,1961) corresponding to an isotopic composition very different than that of any of the analysed local waters. Although there is a considerable scatter in the points along the adjusted line, it can be concluded that available evidence does not support the possibility of mixing of the geothermal fluid with local ground waters.

The wellheads of A-7 and A-8 are on different sides of a fault (see Fig. 1); however, well A-7 is very close to the fault and on the side of inclination of the fault plane, so that it probably intersects it. This is consistent with the two wells being fed by fluid of similar composition. The feeding zone of A-2 is on the other side of the fault, and this well receives fluid of a somewhat different composition. Well A-16D is relatively close to A-2, but separated by an inferred fault. The feeding fluid of A-16D is clearly different than that of the other three wells mentioned above.

The northern and southern sections of the field which have been chosen for exploitation are separated by a zone of high resistivity (Romero and Palma, 1983), and of relatively minor hydrothermal alteration at the surface and shallow levels. Thus, the two sections might appear to be unrelated. However, the available information from deep wells in the middle section show that there is a continuity of hydrothermal alteration at great depth (> 1800 m), which joins the northern and southern sections. This suggests that there is a deep aquifer which spans the entire area of the field (Cathelineau et al, this Proceedings). Well A-4, A-19, A-5 and A-13 are distributed along the Maritaro fault. The fluid feeding well A-4 is similar to that which feeds wells A-7 and A-8 in the southern part of the field. Well A-13, which is on the same side of the Maritaro fault than A-4, receives a fluid of very different composition. However, it should be noted that the feeding zones of these two wells are at very different depths. The slotted liner sections of A-4 and A-13 are at approximately 900-1300 meters and 1650-1850 meters above sea level, respectively. The slotted liner section of A-5, on the other side of the Maritaro fault, is at an intermediate depth (approximately 1400-1800 meters above sea level). The composition of the fluid feeding this well is also intermediate, but closer to that of A-13. Data for well A-19 can not be used to support or disprove this suspected correlation of composition

with depth, because its slotted liner section spans most of the depth range involved (1200-1850 meters above sea level). Clearly, information from more wells located in this area is needed, in order to investigate the possibility of the existence of two aquifers at different depths.

The compositions of steam phases separated at 300°C, 280°C and 260°C from liquid phases with compositions falling in the solid line of Fig. 3, have been calculated. The results fall in the broken lines shown in the same Figure. These calculations assume that the mass of the separated steam is negligible compared to that of the remaining liquid. If this is not so, than the composition of the separated steam will fall in the space bounded by the broken and solid lines, the closer to the latter the higher the fraction of separated steam. The points corresponding to the 1980 and 1982 samples from well A-6 seem to fall just out of the allowable range. However, taking into account the error margin in the determination of deuterium, and the scatter of the linear distribution of liquid phase compositions, these two points might fall in the extreme of the range. The other two points corresponding to samples from steam wells also fall near the extreme of the range, close to the broken lines. This implies that wells A-6 and A-17 are fed by steam separated from a much larger mass of liquid. The large variations with time shown by the composition of fluid produced by A-6, suggests that this well might receive steam from more than one section of the aquifer, at different times.

CONCLUSIONS

The chemical and specific enthalpy data show that there is phase separation in the feeding zones of most of the wells considered. The isotopic composition data shows no evidence of mixing of the geothermal fluid with local meteoric and shallow ground waters. These inferences are consistent with a situation in which the aquifer has no local recharge, although it may have lateral recharge from the low-lying surrounding valley. Under these circumstances, it would be expected that the system be underpressurized and flashing would occur in zones with a high degree of fracturing, as well as in zones of intake of producing wells.

The origin of the heterogeneity of the liquid phase in the reservoir remains obscure. The approximately linear distribution of isotopic compositions suggests a process of mixing of two fluids. Clearly, data from more of the wells in the field is needed in order to draw firmer conclusions in this regard. In particular, it is necessary to investigate the possible correlation of isotopic composition with depth in the northern section of the field.

ACKNOWLEDGMENTS

The work described in this report constitutes part of a project supported by Consejo Nacional de Ciencia y Tecnología de México, contract PIT/EN/NSF/1810. The authors want to express their indebtedness to much of the personnel of the Gerencia de Proyectos Geotermoeléctricos, Comisión Federal de Electricidad for their general support and assistance during the conduction of these studies. Thanks are also due to Bertha Solano, Ma. Eugenia Calderón and Ma. de Lourdes Calderón for expertly typing the manuscript, and to Adrián Patiño for drafting the figures.

REFERENCES

Cathelineau M., Oliver R., Izquierdo G., Garfias A., Nieva D. and Izaguirre O. (1983) "Mineralogy and Distribution of Hydrothermal Mineral Zones in Los Azufres (México) Geothermal Field. This Proceedings.

Craig H. (1961) "Isotopic Variations in Meteoric Waters". Science 133, 1702.

Fournier R.O., and Potter II, R.W. (1982) "A Revised and Expanded Silica (Quartz) Geothermometer". G.R.C. Bull. November, p 3.

Fournier R.O. and Truesdell A.H. (1973) "An Empirical Na-K-Ca Geothermometer for Natural Waters". Geochim. Cosmochim. Acta 37, 1255.

Giggenbach W. and Quijano L. (1981) "Estudio Isotópico de las Aguas del Campo Geotérmico de Los Azufres". Manuscript.

Nieva D., Fausto J.J., González J. and Garibaldi F. (1982) "Flow of Steam into the Feeding Zone of Wells of Cerro Prieto I". Proceedings, Fourth Symposium on the Cerro Prieto Geothermal Field".

Nieva D., and Nieva R. (1982) " A Cationic Composition Geothermometer for Prospection of Geothermal Resources". Manuscript.

Romero J.C., and Palma O. (1983) "Estudios Geoeléctricos en la Zona Geotérmica de Los Azufres, Michoacán". 1ª Reunión Informal Interdisciplinaria de Actividades sobre el Campo Geotérmico de Los Azufres. Resúmenes". Nov. 23-25, 1983. Los Azufres, Mich., México.

Truesdell A.H., D'Amore F., Nieva D., and Pruess K. (1983) "The Origin of Excess Steam in Discharges from Cerro Prieto Geothermal Wells". This Proceedings.

Truesdell A.H., Nathenson M., and Rye R.O. (1977) "The Effects of Subsurface Boiling and Dilution on the Isotopic Compositions of Yellowstone Thermal Waters". J. Geophys. Res. 82, 3694.

Proceedings Ninth Workshop Geothermal Reservoir Engineering
Stanford University, Stanford, California, December 1983
SGP-TR-74

SIMULATION OF RADON TRANSPORT IN GEOTHERMAL RESERVOIRS

Lewis Semprini and Paul Kruger

Civil Engineering Department
Stanford University
Stanford, CA 94305

Introduction

Numerical simulation of radon transport is a useful adjunct in the study of radon as an in situ tracer of hydrodynamic and thermodynamic processes in geothermal reservoirs. A numerical model has been developed to assist in the interpretation of field experiments. The model simulates transient response of radon concentration in wellhead geofluid as a function of prevailing reservoir conditions.

The radon simulation model has been used to simulate radon concentration response during production drawdown and two flowrate transient tests in vapor-dominated systems. Comparison of model simulation with experimental data from field tests provides insight in the analysis of reservoir phenomena such as propagation of boiling fronts, and estimates of reservoir properties of porosity and permeability thickness.

Radon as an In Situ Tracer

Radon-222 is a ubiquitous in situ tracer for studying dynamic processes in geothermal reservoirs. It is produced continuously from the decay of its parent radionuclide, 1600-yr Ra-226 which is distributed throughout the reservoir formation. The emanation of radon gas from the rock matrix to the reservoir pore volume constitutes a constant, steady flux of radon to the geothermal fluids.

As a radioactive, gaseous, chemically-inert element with a useful half life of 3.83 days, Rn-222 is an ideal short-term, in situ tracer in geothermal reservoirs. The first-order decay property is a precise sink term in the reservoir, which combined with its emanation, results in measurable changes in radon concentration due to changes in physical, thermodynamic, and transport conditions in the reservoir during fluid production. As a chemically-inert rare-gas element, conservation of the tracer is assured due to lack of chemical retardation during transport through the reservoir formation. As a component of the noncondensable gases, radon is expected to partition between vapor and liquid phases of the geofluds. Phase partitioning becomes an important process in a simulation model of noncondensable gas transport in geothermal reservoirs.

Radon Transport Models

Analytical models which describe convective transport of radon with hydrodynamic dispersion through porous media are limited to steady-state solutions. A review of such solutions was made by Serdyukova and Kapitanov (1978) and by the National Bureau of Standards (1981). Analyses of radon transport in incompressible fluids for various flow geometry were made by Stoker and Kruger (1975), D'Amore et al. (1978), and Warren and Kruger (1979). A steady-state solution for compressible gases in radial flow was given by Sakakura et al. (1959). These analytical models applied to geothermal reservoirs require several simplifying assumptions, such as steady-state, isothermal, and single-phase conditions. To carry analysis of such systems further, numerical models are generally required.

Numerical models for single-phase radon transport have been developed by Clements and Wilkening (1974) for incompressible gas and by Edwards and Bates (1980) for compressible gas. These models have been applied to studies of the effect of atmospheric pressure variation on radon exhalation from ground surfaces and in mine cavities. Our model attempts to generalize the transport of radon by convection and diffusion with the emanation and decay aspects of radon, and the effects of gas partitioning between phases.

The radon transport model was formulated on the basis of the following set of assumptions:

(1) Radon emanation into the pore volume is constant and independent of pore volume concentration.

(2) The partial pressure of radon gas (at a molar fraction of the geofluid of the order of 10^{-16}) is negligible.

(3) Partitioning of radon gas obeys Henry's law, with local phase equilibrium in the reservoir.

Constant radon emanation implies small effect of change of thermodyanmic conditions on the emanation (recoil/diffusion) processes in the rock. This assumption is supported by the observations of Satomi and Kruger (1982) that radon emanation was constant under experimental superheated conditions above a fractional saturation pressure of 0.5. The infinitesimal partial pressure of radon implies that radon transport can be resolved independent of the geothermal flow, and the assumption of local phase equilibrium implies that liquid and vapor terms can be combined.

The resulting equation for mass conservation includes terms for convective and dispersive transport, emanation source, and decay sink given by

$$\phi\frac{\partial}{\partial t}(\rho_l C_l S_l + \rho_v C_v S_v) = -\nabla(\rho_v C_v V_v) - \nabla(\rho_l C_l V_l) + \nabla D_v \nabla(\rho_v C_v) + \nabla D_l \nabla(\rho_l C_l) - \lambda(\rho_l C_l S_l + \rho_v C_v S_v) + E \quad (1)$$

where

ϕ = formation porosity (m^3/m^3)
ρ = fluid density (kg/m^3)
C = mass concentration (kg/kg)
V = fluid velocity (m/s)
S = volumetric saturation (m^3/m^3)
D = coefficient of hydrodynamic dispersion (m^2/s)
λ = decay constant for radon (s^{-1})
E = emanation rate ($kg/m^3 \cdot s$)

for the two phases: l = liquid; v = vapor

Solution of the equation is achieved by finite difference techniques, simplified by the decoupling of the radon transport equation and the geothermal flow simulation. In this solution, the reservoir hydrodynamic and thermodynamic conditions are determined from available reservoir simulators of the type described by Faust and Mercer (1979). For each time increment, the reservoir simulator calculates nodal values of fluid pressure, temperature, liquid and vapor saturation, density, and enthalpy. Values of temperature, saturation, and density, along with calculated liquid and vapor velocities, are used as input to the radon transport model.

The reservoir simulation model chosen for the radon transport model was developed by Zyvoloski et al. (1979). This model was tested by the Stanford and New Zealand groups in the SGP Model Intercomparison Study (1980) and found to be in good agreement with other models tested.

The radon transport model has constructed as a finite difference model with (1) upwind (upstream) differencing incorporating a correction for numerical dispersion as described by Chaudhari (1973) for convection, and central differencing for hydrodynamic dispersion. The coefficients of hydrodynamic dispersion were assumed to be linear functions of fluid velocity, given by

$$D = \alpha_L V + D^* \quad (2)$$

where

α_L = longitudinal dispersivity (m/s)

D^* = molecular diffusion coefficient (m^2/s)

The time derivative is solved by numerical integration using fourth-order Runge-Kutta techniques. The solution is therefore explicit in form, second-order in space, and fourth-order in time.

The output of the model is the concentration of radon in the pore volume expressed as $(\rho_l C_l S_l + \rho_v C_v S_v)$ kg/m^3. The liquid phase concentration required for the space derivative term is obtained from the total volumetric concentration by

$$\rho_l C_l = \frac{(\rho_l C_l S_l + \rho_v C_v S_v)}{(H - HS_l + S_l)} \quad (3)$$

where H = Henry coeff. $((kg/m^3)_v/(kg/m^3)_l)$

The vapor phase concentration is obtained from the Henry Law equation

$$\rho_v C_v = H\ \rho_l C_l \quad (4)$$

Initial and Boundary Conditions

Reservoir radon concentration in an unexploited geothermal system is assumed to be in equilibrium with emanation from the formation rock. The volumetric concentration (in units of nCi/m^3) is estimated by

$$C_e = \frac{E_m \rho_r (1-\phi)}{\phi} \quad (5)$$

where E_m = emanation from rock (nCi/kg)

ρ_r = rock density (kg/m^3)

Emanation can be expressed as a mass flux (kg/kg-sec) by the conversion 1 nCi (radon) = 1.36×10^{-20} kg/sec.

The initial volumetric concentration is used to calculate the phase concentrations with equations (2) and (3). For saturation of 1.0 for either phase, the volumetric concentra-

tion for that phase is the total volumetric concentration of the reservoir.

The boundary conditions are Dirichlet type (concentration specified) for the outer boundary, and transmissive type for the inner (discharge) boundary of the dispersion term.

Simulations

The radon transport model is being used to evaluate data from a number of field experiments, including transient drawdown at the vapor-dominated fields at The Geysers, the liquid-dominated reservoirs at Cerro Prieto, and the hot, dry rock experiment at Fenton Hill. This paper discusses the analysis of several drawdown transients at the vapor-dominated field at The Geysers observed by Stoker and Kruger (1975) and Warren and Kruger (1979). The model follows the transport characteristics of vapor-dominated reservoirs described by White et al. (1971) and Truesdell and White (1973). In vapor-dominated reservoirs, steam is produced from vaporization of water present in small pores in the formation. During exploitation, a boiling zone propagates out from the wellbore as pressure drops in the reservoir. Steam travels an increasing distance from its source to the wellbore with exploitation time. The radon transport model follows the response of emanated radon as a result of the vaporization process and its transport with the produced geofluid as the boiling zone propagates into the reservoir.

Vapor-Dominated Model

The radon transport model is based on radial flow in a homogeneous reservoir, in the same manner as well test simulation in vapor-dominated reservoirs as discussed by Moench and Atkinson (1978) and Moench (1980). Reservoir properties for the homogeneous reservoir used in the simulation are given in Table 1. The property values are in the range reported by Pruess and Narasimhan (1982) for The Geysers reservoirs. Our value for the emanation coefficient, E_m, is in the range of experimental values obtained from reservoir cores. The coefficient of hydrodynamic dispersivity was selected from Pickens and Grisak (1981).

The simulation of radon transients was run with radon concentration at the wellhead assumed equal to the concentration at the wellbore product node in the model mesh. Figure 1 shows the spatial response of pressure, saturation, mass flow, and radon concentration, with simulation outputs at 1.2, 12, and 36 days during a constant rate drawdown. For comparison, the concentration of a nonradioactive, conservative component of the noncondensable gases is shown for the same times. The conservative component has the same initial concentration as radon and the same Henry's law partition coefficient, but does not have a source or sink in the reservoir.

TABLE 1

PARAMETERS FOR NUMERICAL SIMULATION

Formation Properties	
Porosity	$\phi = 0.10$
Rock Density	$\rho_r = 2300$ kg/m^3
Rock Specific Heat	$C_r = 1000$ J/kg °C
Rock Thermal Conductivity	K = 0.0 w/m °C
Reservoir Thickness	h = 500 m
Matrix Porosity	$k = 1 \times 10^{-14}$ m^2 - 1×10^{-13} m^2
Rock Radon Emanation	$E_m = 0.005$ -0.015/kg
Dispersivity	$\alpha = 1$ m
Initial Conditions	
Liquid Saturation	Temperature T = 241°C
	S_l = .05, .20, .50
Production	
Wellbore radius	$r_w = 0.112$ m
Skin	S -4.50
Effective Wellbore Radius	$r_w' = r_w e^{-S} = 10$ m
Production Rate	10 kg/sec - 36 kg/sec

The pressure responses of this simulation show a drawdown extending into the formation. With time, the pressure drawdown results in vaporization, with a gradual decrease in liquid saturation. The mass flux responds to the outward propagation of the boiling zone during exploitation, with steam traveling to the wellbore from further in the formation.

The comparison of the response of radon concentration to the conservative noncondensable gas shows the influence of its source and sink properties on reequilibration to changing thermodynamic conditions. Radon concentration decreases near the wellbore at early drawdown time of 1.2 days by dilution of the original pore volume steam with newly produced steam from vaporization of liquid water of low radon content. The response of the conservative gas tracer is the same as radon, also due to the dilution process. After 12 days of drawdown, however, the distribution of radon concentration is different from that of the conservative gas. The radon concentration is observed to increase over the 12-day period while the conservative gas concentration remains constant. The increase in radon concentration is attributed to the emanation of radon into the steam over a larger reservoir volume as the travel distance increases, whereas the conservative gas component which does not have an emanation source remains diluted in

concentration. At 36 days, the boiling zone has progressed further into the formation, and the radon concentration continues to increase, but at a decreasing rate. Because of the 3.83-day half life of Rn-222, equilibrium is expected between its increased decay during the longer travel time to the wellhead and its increased concentration due to the expanding emanation volume. The conservative gas component concentration remains constant.

To estimate the usefulness of the model to the design of additional field experiments for evaluating reservoir properties such as permeability thickness, it is necessary to obtain experience on the sensitivity of model output to model input parameters. For this purpose, a second simulation was run with variations in permeability, initial liquid saturation, and production rate. The results of well node radon concentration as a function of log (time) are shown in Figure 2. The results show three generally distinct regions: (1) essentially linear decrease at early time (0 to 0.4 d); (2) a steady-state period (0.5 to 1 d); and (3) a period of almost linear increase (after 4 d). The two linear periods suggest a first-order dilution process for the early period and a first-order build-up during the latter period, consistent with the propagation of the boiling zone into the reservoir. These observations are in accord with the numerical results of Moench and Atkinson (1978) which show a linear relationship between dimensionless pressure drawdown (as p^2) and log (time). The form of pressure response governs the growth of the vaporization zone and changes in fluid density. Both of these parameters affect the radon concentration.

The effect of permeability is noted in Figure 2a. The data show a strong dependence of decrease in permeability on initial dilution at early time. The large dilution results from the steep pressure gradient near the wellbore with localized boiling. At higher permeability, where the pressure response is more rapid, boiling becomes more distributed. The increases of radon concentration at later time appear somewhat symmetric. The slopes of the two lower permeability values seem to increase with time. This may be due to the effects of fluid compressibility. With increased pressure drawdown, the resulting steam has a lower density and therefore greater specific volume exposing a greater rock volume for radon emanation to the steam.

The data in Figure 2b indicate that radon concentration does not appear to be highly sensitive to initial liquid saturation. This observation is surprising in that it was anticipated that the rate of boiling zone propagation from the well would be a function of the initial liquid saturation. Perhaps its influence is offset by radon enrichment by phase partitioning from liquid water to steam.

The results in Figure 2c show that radon concentration is influenced by production rate. The dilution rate at early time is more strongly dependent on production rate compared to the growth rate at later times. The factors influencing these observations are not clear at this time, and the results of the simulation support our prior conclusions that multiple flowrate drawdown tests with radon as a mass tracer may be a useful method for reservoir evaluation in conjunction with pressure drawdown tests.

Simulation of Field Experiments

Simulations of two types of radon drawdown experiments have been attempted. There are short-term (8-12 hours) tests reported by Stoker (1975) and the longer-term (75 day) drawdown reported by Warren (1980). Stoker ran several short tests during well production testing from bleed-rate shutin, whereas Warren ran a long-term production test that included two radon transients following rapid flowrate change.

A. Short-term Tests

Figure 3 shows the simulation results of the short-term drawdown test of Stoker for the repeated flows of 8 to 12 hours following shutin for periods of 12 to 16 hours over a three-day period. The simulations show good agreement with the observed data. The early decrease in radon concentration by dilution from near wellbore boiling is readily observed, especially in the second transient, when early wellhead sampling was achieved. The model shows enrichment of radon during shutin, indicative of the condensation of steam with pressure build-up near the well. The sensitivity of the model to these effects suggests that radon measurements of cyclic production testing of new wells can markedly assist in early reservoir evaluation.

The results of the simulations of three drawdown tests by Stoker in well IV-C and IV-D at The Geysers are given in Figure 4. For these simulations, a permeability thickness of 20 darcy-m was used, close to the value of 6.9 darcy-m reported by Ramey and Gringarten (1976) for a well in another part of The Geysers field. The effective wellbore radius of 5 m used in the simulation is equivalent to a skin factor of ~ 3.8, in the range reported by Economides and Fehlberg (1979) and Pruess and Narasimhan (1982). The three drawdowns show similar behavior, linear drawdown to pseudo steady state achieved at approximately 6 hours. The slopes are reasonably uniform. The difference between the two experiments in well IV-C may be attributed to time period of about one month between tests. One possibility is a change in near-wellbore permeability. Economides and Fehlberg (1979) suggested that an observed increase in negative skin with production may result from cleanup of well

damage and fractures. The results of the simulation (given by the dashed line) shows a good fit between the actual data for a similar production rate. The radon emanation coefficient of 0.008 nCi/kg is in the range of laboratory measurements from Geysers rock cores. The slope of the early period dilution is similar to the slope of the three tests, and the approach to steady state is also similar. The agreement for the two wells is rather good considering wells IV-C and D are 1.5 miles apart and the difference in steam entry levels was 560 ft. The agreement also suggests that the dilution process is the likely one to explain the observed data. Wellbore storage unloading is not considered important with the wellbore partially filled with steam during bleed-rate production. Approximately 40 wellbore volumes were produced before first samples were collected.

B. Long-term Drawdown Experiment

The long-term drawdown experiment conducted by Warren (1980) was a 75-day flow experiment with two changes in flowrate to observe the radon transients. The data reported by Warren show a growth in radon concentration during the first 38-day period of stabilizing flowrate, a transient decrease over the next 27 days at reduced flowrate, and a rise when the original flowrate was restored. Although the radon data showed a strong cyclic variation over a few-day period, Warren and Kruger (1979) indicated by cyclic averaging that the large fluctuations could be consistent with a boiling process with steam transport in cyclic bursts. Radon in higher concentration can be produced from small pores with larger fractional emanation and mixed with steam from larger pores of lower emanation.

Figure 5 shows the results of the simulation of the constant rate build-up period in relation to the observed data. The simulation was run with a permeability of 2×10^{-14} m^2, thickness of 500 m, effective wellbore radius of 10 m, representing an equivalent skin value of -4.5 and initial liquid saturation value of 50%, both within realistic values at The Geysers. The model reproduces the data fairly well.

A test of the simulation model occurred during the radon transient period after the wellhead flowrate was reduced instantaneously. Figure 6 shows that the simulation results, based on a homogeneous radial flow reservoir, produce the opposite results to those observed. The model predicts a sharp rise in response to the partial shutin with a gradual attenuation to a higher value than before shutin, whereas the observed transient is a continuous decrease in radon concentration. The increase in radon concentration predicted by the model for the flowrate change can be attributed to three effects: (1) a lower degree initial dilution in the zone of vaporization; (2) enrichment of radon in the steam phase as condensation occurs; and (3) increased residence time in the reservoir resulting in a greater approach to equilibrium radon concentration.

The change in flowrate could also have a large effect on radon concentration if the reservoir is inhomogeneous. Kruger et al. (1977) and D'Amore et al. (1978) suggested the decrease in wellhead radon concentration following rapid flowrate reduction to the longer decay period during transport through a reservoir with low radon emanation. Warren and Kruger (1979) also interpreted the observed increase in radon concentration in the long-term drawdown as production of steam from successively smaller and smaller pores, with larger fractional emanation values.

The two possibilities suggested that a dual-block model might be more representative of The Geysers' reservoir than a homogeneous radial model. The two-block model consists of an inner block of highly fractured, permeable, low liquid saturation, and low emanation, connected to an outer block of lower permeability, high liquid saturation and higher emanation. During expolitation, withdrawal occurs first from the high permeability fissure block with later production of steam originating from the outer block.

The data of Warren (1980) was evaluated with a two-block model in which three important parameters of the two blocks were varied: (1) emanation coefficient, (2) block volume, and (3) liquid saturation. Figure (6) shows the match between the simulation and the observed data. In this simulation an emanation coefficient in the fissure block which is a factor of 10 lower than in the outer reservoir is required for the match. This factor can be supported from the work of Sammis et al. (1981) who observed lower emanation with increased permeability in granite cores.

The match also required essentially no liquid saturation, $S_1 = 0.005$, in the fissure block. This requirement can be supported from the model of Truesdell and White (1973) and simulations of Pruess and Narasimhan (1982) for steam production from fractured systems based on low or zero liquid saturation. The reservoir volume of the fissure block is of the order of 3.4×10^7 m^3. In a reservoir of 20-acre well spacing, the corresponding reservoir thickness would be 425 m. This large fissure block pore volume of low emanation is needed for sufficient decay of radon during transport from the outer block to the wellbore. Thus as flowrate is reduced and residence time increases, the decay or radon also increases, resulting in the observed lower radon concentration. The dual block simulation shows radon concentration reaching a steady-state value after production from the outer block has been established. Radon concentration should remain

fairly constant with further constant rate drawdown.

Physical factors that are more difficult to simulate can also be important. For example, Holub and Brady (1981) show from experimental studies of radon emanation from stressed rock that temporary increases in emanation result from applied uniaxial stress. Emanation returns to original values when the stress is removed. In the reservoir, changes in pressure resulting from changes in flowrate could in turn produce temporary changes in emanating power from the reservoir rock. Another possibility is a multi-layered system of dual permeability where the flow from each layer responds to pressure changes in the formation. A further effect may be from water adsorption. Herkelrath et al. (1983) indicated that adsorption of water at superheat conditions could modify the pressure response of the formation.

Other suggestions for improvement of the current simulation model includes review of the assumption of thermodynamic equilibrium between rock and fluid phases. If thermodynamic equilibrium is not achieved, temperature changes in the fluid phase would be greater than predicted by the model. Since solubility of radon in the liquid phase is temperature dependent, partitioning of radon during evaporation/condensation processes would change, with corresponding changes in radon concentration.

Conclusions

The simulation model of radon concentration in fluids produced from vapor-dominated reservoirs appears to follow adequately the results observed from field experiments at The Geysers geothermal field for both short-term and one long-term drawdown. The simulations based on appropriate values of input parameters, such as reservoir permeability thickness, agrees well with the values determined by traditional reservoir engineering practices.

The results support the model of an expanding zone of vaporization during exploitation, resulting in corresponding increases in radon concentration. Simulation and field experimental results are in good agreement for constant flowrate drawdown tests. Simulation of two-flowrate tests resulted in the need to introduce a two-compartmental model with differing average properties in the two zones to reach agreement between simulated and observed results. The concept of a two-zone reservoir should be explored in greater detail.

References

Chaudhari, N. (1973), "A Numerical Solution with Second-Order Accuracy for Multicomponent Compressible State Miscible Flow," Society of Petroleum Engineering Journal, April, 84-92.

Clements, E. W. and M. H. Wilkening (1974), "Atmospheric Pressure Effects on Radon-222 Transport Across the Earth-air Interface," Journal of Geophysical Research, 79 (33), 5025-5029.

D'Amore, F., J. C. Sabroux, and P. Zettewoog, (1978-1979), "Determination of Characteristics of Steam Reservoirs by Radon-222 Measurements in Geothermal Fluids," Paleoph, 17, 253-261.

Economides, M. J. and E. L. Fehlberg (1979), "Two Short-Time Build-up Test Analysis for Shell's Geysers Well D-6, A Year Apart, Proceedings, Fifth Workshop Geothermal Reservoir Engineering, SGP-TR-40, Stanford University, Stanford, CA.

Edwards, J. C. and R. C. Bates (1980), "Theoretical Evaluation of Radon Emanation Under a Variety of Conditions, Health Physics, 39, 263-274.

Faust, C. R. and J. W. Mercer (1979), "Geothermal Reservoir Simulation, 1-Mathematical Models, 2-Numerical Solution Techniques for Liquid- and Vapor-Dominated Hydrothermal Systems, Water Resouces Research, 15, No. 1, 23-46.

Herkelrath, W. N., A. F. Moench, and C. F. O'Neal II (1983) "Laboratory Investigations of Steam Flow in a Porous Medium," Water Resources Research, 19, No. 4, 931-937.

Holub, R. F. and B. T. Brady, (1981), "The Effect of Stress on Radon Emanation From Rock," Journal of Geophysical Research, 86, B3, 1776-1784.

Kruger, P., A. Stoker, and A. Umaña (1977) "Radon in Geothermal Reservoir Engineering," Geothermics, 5, 13-19.

Moench, A. F. (1980) "Radial Steam Flow in Two Phase Geothermal Reservoir - Comparison of Analytical and Finite Difference Solutions," Society of Petroleum Engineers Journal," Oct., 359-362.

Moench, A. F. and P. G. Atkinson (1978), "Transient Pressure Analysis in Geothermal Reservoirs with an Immobile Vaporizing Liquid Phase," Geothermics, 7, 253-264.

National Bureau of Standards (1981), "Radon Transport and Exhalation From Building Materials, Technical Note 1139.

Pickens, J. F. and G. E. Grisak (1981), "Scale-Dependent Dispersion in a Stratified Granular Aquifer," Water Resources Research, 17, No. 4, 1191-1211.

Proceedings (1980), Special Panel on Geothermal Model Intercomparison Study (1980), Sixth Workshop on Geothermal Reservoir Engineering, SGP-TR-42, Stanford University, Stanford, CA.

Pruess, K. and T. N. Narasimhan (1982), "On Fluid Reserves and the Production of Superheated Steam from Fractured, Vapor Dominated Geothermal Reservoirs," Journal of Geophysical Research, 87, B11, 9329-9339

Ramey, H. J. and A. C. Gringarten (1975), "Effect of High-Volume Vertical Fractures on Geothermal Steam Well Behavior," Proceedings of Second United Nations Symposium on the Development and Use of Geothermal Resources, San Francisco, CA.

Sakakura, A. Y., C. Lindberg, and H. Faul (1959),"Equation of Continuity in Geology with Applications to the Transport of Radioactive Gas," U.S. Geological Survey Bulletin, 1052-1.

Sammis, C. Banerdt, and D. E. Hammond (1981) "Stress Release of Rn-222 and CH_4 to Percolating Water in Granitic Rock," Proceedings, Seventh Workshop Geothermal Reservoir Engineering, SGP-TR-55, Stanford University, Stanford, CA.

Satomi, K. and P. Kruger (1982), Radon Emanation Mechanism from Finely Ground Rocks, SGP-TR-63, Stanford University, Stanford, CA.

Serdyukova, A. S. and Yu. T. Kapitanov (1978), "Radon Isotopes and Short Lived Products of Their Disintegration in Nature (translated from Russian), U. S. Bureau of Mines, Washington, D.C., PB-295-940T.

Stoker, A. (1975), Radon Measurements in Geothermal Systems, Engineers Thesis, Stanford, University, Stanford, CA.

Stoker, A. and P. Kruger (1975), "Radon Measurements in Geothermal Reservoirs," Second United Nations Symposium on the Development and Use of Geothermal Resources, San Francisco, CA.

Truesdell, A. H. and D. E. White (1973), "Production of Superheated Steam from Vapor-Dominated Geothermal Reservoirs," Geothermics, 2, Nos. 3-4, 154-173.

Warren, G. (1980), Measurements in Geothermal Systems, Engineers Thesis, Stanford University, Stanford, CA.

Warren, G. and P. Kruger (1979), "Transients in Vapor-Dominated Geothermal Reservoirs," SPE-8000, Proceedings, SPE California Regional Meeting, Ventura, CA.

White, D. E., L. J. P. Muffler, and A. H. Truesdell (1971), "Vapor Dominated Hydrothermal Systems Compared with Hot-Water System, Econ., Geology, 66, 75-97.

Zyvoloski, G. A., M. J. O'Sullivan, and D. E. Krol (1979) "Finite Difference Techniques for Modelling Geothermal Reservoirs," International Journal For Numerical and Analytical Methods in Geomechanics, 3, 355-366.

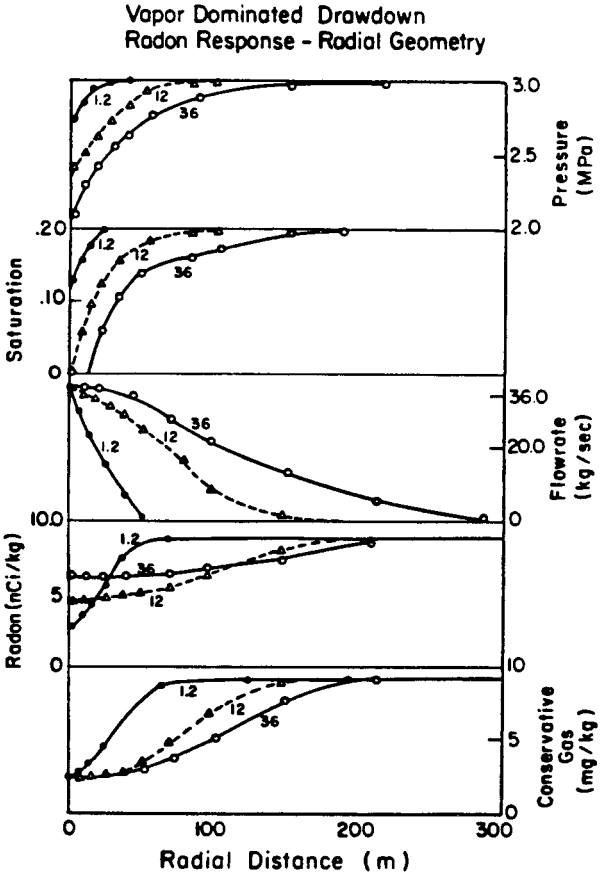


Figure. 1. Spatial and temporal response for a constant rate drawdown.

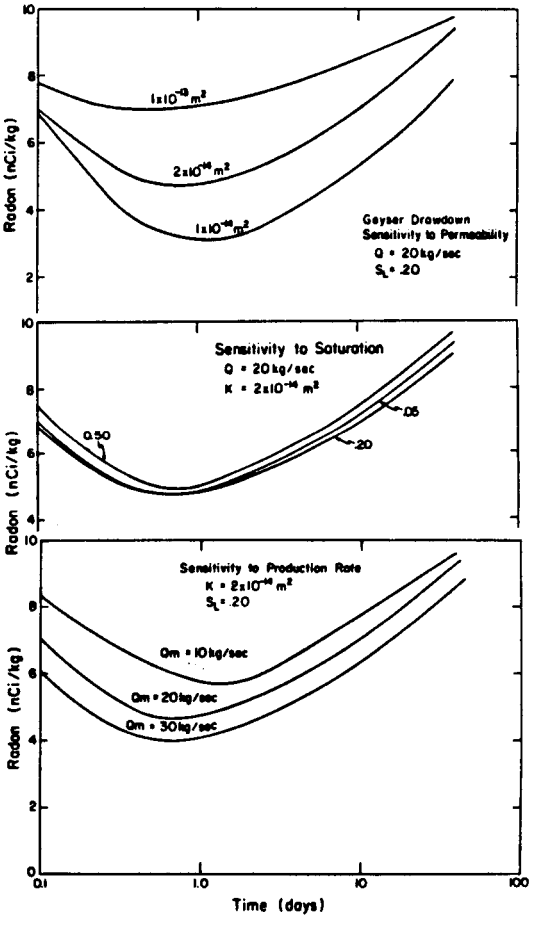


Figure 2a, b, c. Sensitivity to permeability, saturation, and flowrate.

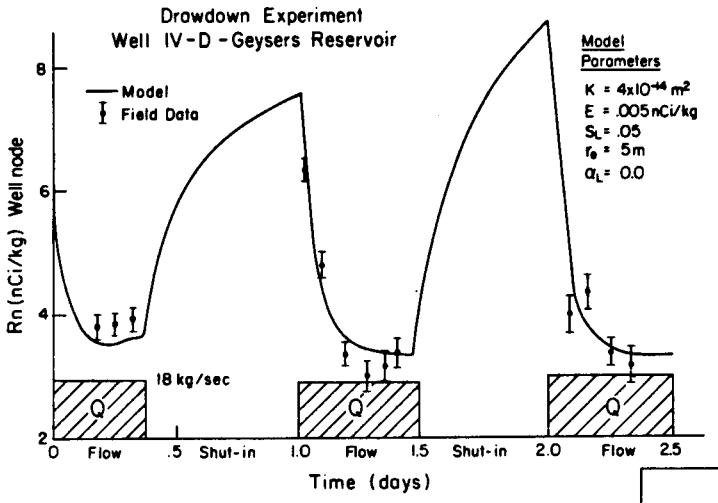


Figure 3. Comparison of model simulations to field transients during a cyclic drawdown experiment at The Geysers.

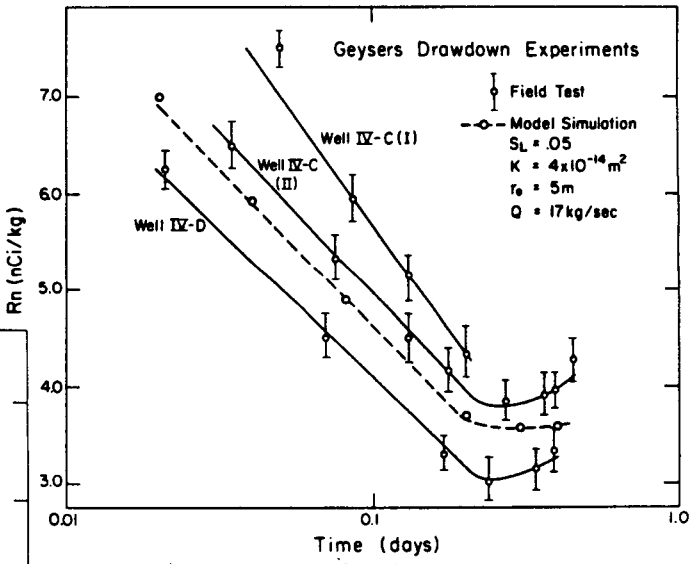


Figure 4. Response of radon concentration versus log (time) in short-term drawdown experiments at The Geysers.

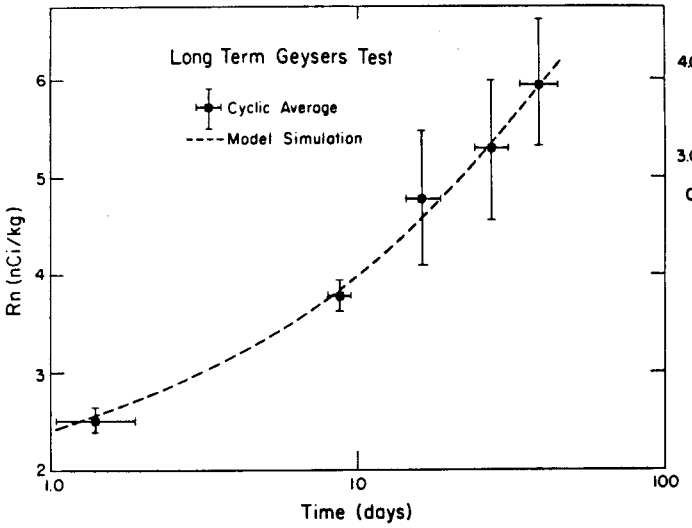


Figure 5. Comparison of a model simulation to radon build-up response in a 38-day constant rate drawdown experiment at The Geysers.

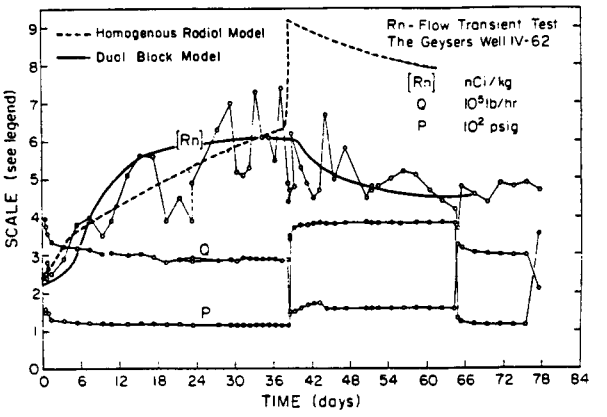


Figure 6. Dual-block model and homogeneous radial model responses to a two-rate drawdown test at The Geysers.

Proceedings Ninth Workshop Geothermal Reservoir Engineering
Stanford University, Stanford, California, December 1983
SGP-TR-74

MINERALOGY AND DISTRIBUTION OF HYDROTHERMAL MINERAL ZONES IN LOS AZUFRES (MEXICO) GEOTHERMAL FIELD.

+,*Cathelineau M., +Oliver R., +Izquierdo G., &Garfias A., +Nieva D., and &Izaguirre O.

(*) Centre de Recherches sur la Geologie de l'Uranium, Vandoeuvre, France (+) Instituto de Investigaciones Eléctricas, Depto. de Geotermia, Cuernavaca, México (&) Coordinadora de Los Azufres, Comisión Federal de Electricidad, México.

ABSTRACT

General features of the geometry of Los Azufres reservoir have been defined through the mapping of hydrothermal mineral alteration zones. Hydrothermal alteration has been studied in cuttings and drill cores from most of the active wells. X-ray diffraction microprobe analysis and classical optical methods have been employed for the identification of primary and authigenic minerals in fresh and altered samples. Observed patterns of alteration have been correlated with temperature and patterns of fluid circulation. The resulting model depicts a body of geothermal fluid at depth, which ascends and discharges through two main fracture systems. These two circulation zones are characterized by concentric aureoles of increasing hydrothermal alteration towards quasivertical axes. The overall pattern could be described as a dome structure produced by the abnormal thermal gradient, distorted by the effects of active upward circulation of the fluids.

INTRODUCTION

The Los Azufres (State of Michoacán) field is the second geothermal resource in México to undergo development, after the Cerro Prieto field in Baja California. Los Azufres field has an installed generating capacity of 25 MW, and the nearly forty wells that have been drilled offer ample opportunity for further development.

The primary geology of this field has been described by Camacho (1976), Gutiérrez-Negrin and Aumento (1981) and Oliver (1981). Briefly described, the geologic sequence consists of a series of volcanic layers, mostly andesites of a variety of textures, and rhyolites in the upper levels. Results of early studies of alteration mineralogy have been reported by Gutiérrez-Negrin and Aumento, (1981).

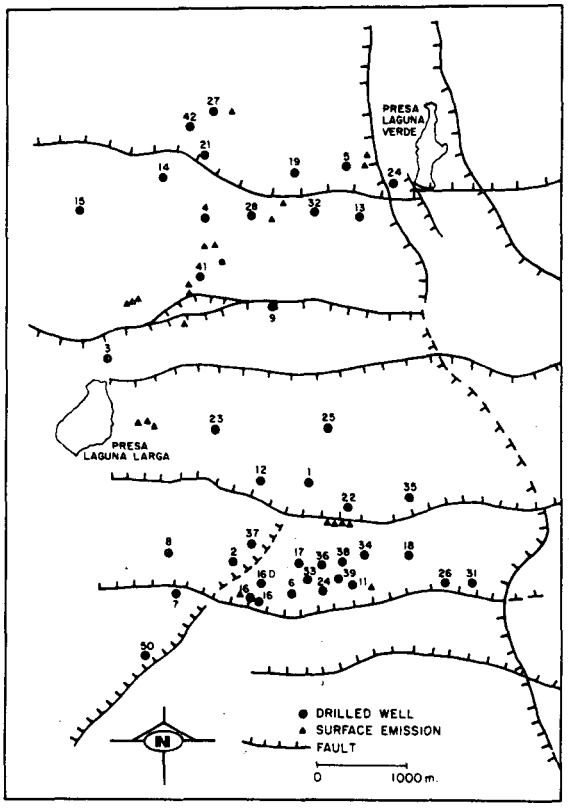


Fig. 1. Map of the Los Azufres Geothermal Field.

The extensive collection of drilling cores and cuttings available from new wells have provided the opportunity to study in more detail the effects of hydrothermal alteration. The present contribution describes the results of these studies, with evidence derived from X-ray diffractometry, microprobe analysis and optical micros copy applied to samples from most of the existing wells. The different associations of alteration minerals and their spatial distributions have been determined. The correlation of these distributions with measured temperature profiles has yielded a model which outlines the general geometry of the field and identifies the zones of circulation and discharge in the undisturbed system.

MATERIALS AND METHODS

Because of the lack of suitable outcrops, and the existence of pervasive weathering and hydrothermal alteration of shallow subsurface rocks, surface sampling was restricted to a few materials directly altered by surface manifestations. Most of the materials studied consisted of cores and cuttings obtained during drilling. Since cuttings from every 20 meters have been collected in the case of most wells, it has been possible to generate almost continuous profiles of nature and degree of alteration with depth.

Clays have been mechanically separated by crushing and centrifugation, and have been studied by classical methods of X-ray diffractometry. Mineralization in veins has been studied by optical methods, employing both reflected and transmitted light. More than 150 electron microprobe analyses have been performed, in order to define the exact composition of authigenic minerals.

Underground temperatures have been obtained from registers provided by field personnel. Only those registers obtained after proper thermal equilibration of the well have been considered. Downhole temperatures have been checked to be in good agreement with the estimates from chemical geothermometers.

MINERALOGY

Primary mineralogy: The authors distinguish two main groups of volcanic rocks in the area. One consists of spherulitic, glassy and pumicitic rhyolites, rhyolitic tuffs or ignimbrites, with essential constituents such as quartz, potassic feldspar, plagioclase, iron-rich biotite, zircon and glass. Other group is constituted by andesitic rocks, which show a variety of textures, grain size (aphanitic to porphyric) and mineral orientations. Essential constitutents of this second group include quartz, plagioclase, pyroxenes (augite, enstatite), magnetite, ilmenite, olivine and hornblende. Other volcanic units present are of minor interest and abundance, and occur as by lenses of basalt and dacite.

There are slight differences between previous reports (Camacho, 1976; Gutiérrez-Negrin and Aumento, 1982), and the primary mineralogy features described in this contribution. However these concern mainly nomenclature and terminology and the differences will not be discussed here.

Secondary mineralogy: The identification of alteration paragenesis has been facilitated by the lack of interference between primary and secondary mineralogy. Little evidence is found of the effect of external factors of alteration such as meteoric (except in shallow levels), sedimentary or diagenetic processes, which are normally important in geothermal fields located in sedimentary basins, e.g., Cerro Prieto (Elders et al , 1979), Salton Sea (McDowell and Elders, 1980).

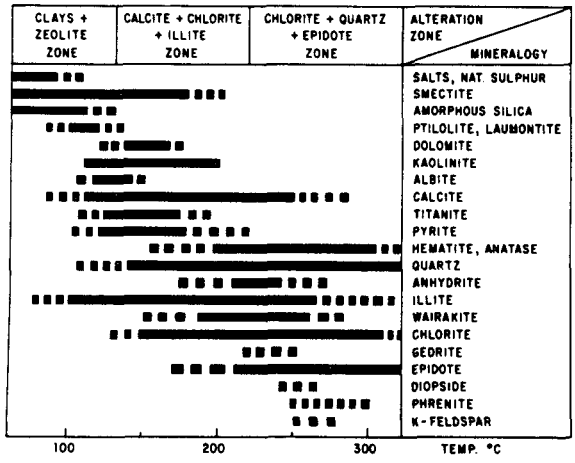


Fig. 2. Mineral Zonation in Andesites as a Function of Temperature.

Progressive changes in the mineralogy of the original andesites seem to be a function only of the temperature (Fig. 2), and of other chemical and physical conditions of the hydrothermal alteration process.

PARAGENESIS

Studies of veins and altered rocks show a regular sequence of mineral associations, which correlates with temperature and depth. Width of mineral zones varies as a function of local thermal gradients (Fig. 3). The observed mineralogy is compatible with metamorphism of Ca-Fe-Mg rich rocks. Signs of Na-K metamorphism apparently are absent in Los Azufres hydrothermal system, in contrast with findings in other current systems such as Salton Sea (Muffler and White, 1969) and Wairakei (Steiner, 1977), and fossil systems (Cathelineau, 1983; Cathelineau, 1984). Paragenesis corresponds to the zeolite, greenschist and amphibolite facies. The observed mineral associations, listed in order of increasing temperature of formation, are as follows:

- amorphous silica + native sulphur + smectites + gypsum + alunite.
- smectites + quartz + laumontite + ptilolite.
- calcite + chlorite + titanite + albite.
- calcite + wairakite + quartz + chlorite + anhydrite.
- chlorite + epidote + quartz + hematite + anatase.
- epidote + gedrite + chlorite.
- quartz + microcline + phrenite + epidote.
- epidote + diopside + quartz.

GEOMETRY OF DISTRIBUTIONS OF ALTERATION MINERALS

The information obtained from individual wells has been integrated in a three-dimensional map of distribution of alteration minerals. Horizontal cross-sections at 9 depth levels are shown in Fig. 3. Vertical cross-sections are shown in Fig. 4. Zero depth in these diagrams as well as in subsequent discussion corresponds to 2900 meters above sea level. The isobaths show the morfology of the surfaces of first appearance and the walls of dissapearance of selected minerals. Correlation of these mineral distributions with temperature profiles yield the following observations:

- Carbonates: Dolomite is scarce and replaced entirely by calcite at depths other than at the surface. Calcite disappears after a certain depth, yielding a flat, circumscribed zone of appearance.

- The level of appearance of epidote follows the isotherm 210-250°C. The epidote zone covers the entire horizontal spread of the field. Other calcsilicates such as amphibole and pyroxenes are found in localized sites, at depth greater than 2000 meters.

- Chlorite is distributed over the entire horizontal spread of the field at deep levels, but is restricted to two columns of alteration at levels shallower than 1500 meters. Detailed chemical composition data show a continuous evolution of chlorite solid solution parameters with temperature (Cathelineau and Nieva, 1983).

- Iron minerals: Magnetic and ilmenite are unstable and replaced by pyrite and titanite below the very shallow levels. The latter are replaced by hematite and anatase at deeper

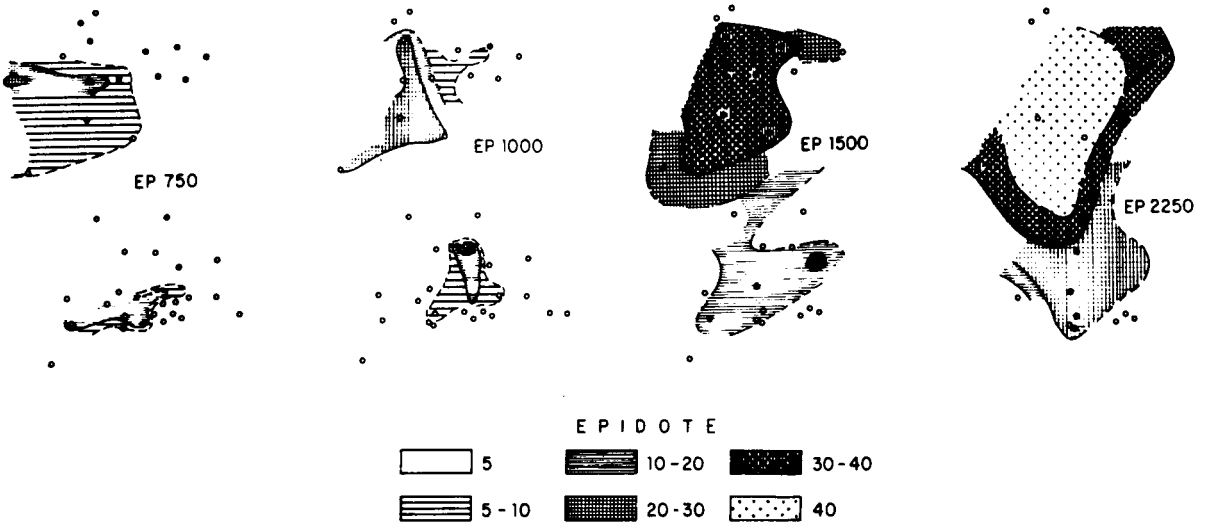
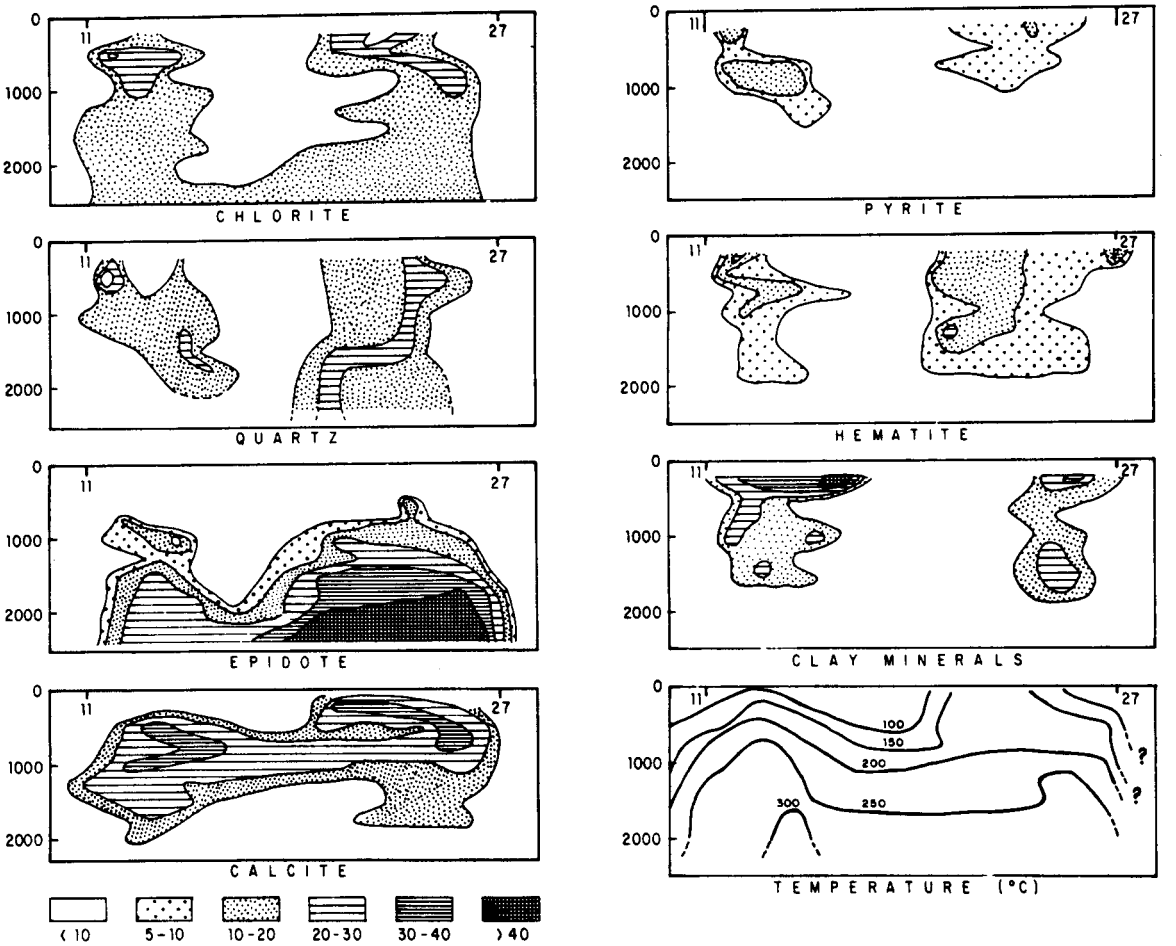


Fig. 3 = Maps of distribution of epidote at different levels _ arbitrary scale 0-40 indicates the relative abundance of the mineral.

Fig. 4 = Cross section along the line Well 11 - Well 27 of distribution of minerals and isotherms (depth is indicated in meters).



levels. The epidote-hematite association is noteworthy, since epidote-iron sulphide association are more common in most of the studied hydrothermal systems, such as Larderello (Cavaretta et al, 1980) and the Geysers (Steinfeld, 1981).

- Distribution zones of some of the alteration minerals follow quite closely the distribution of temperatures. The case of epidote is mentioned above. The distribution zone of calcite corresponds to temperatures of 100 - 250°C. Appearance of pyrite corresponds to temperatures of 100 - 150°C.

- Distribution zones of quartz, chlorite and clay minerals are contained within two columnar sections which appear to represent natural circulation and discharge zones.

DISCUSSION

The observed alteration patterns are indicative of prograde metamorphism. There is considerable coherence between temperature distribution and alteration patterns. No evidence was found of superposition of incompatible associations of alteration minerals, or of retrograde metamorphism.

The overall shape of hydrothermal alteration reflects the superposition of two main factors. One factor is the effect of the thermal gradient abnormality which produces a soft dome structure with sub-horizontal alteration zones. The second factor, which distorts this dome structure, is the hydrothermal alteration produced by ascending fluids in two main zones of circulation and discharge. These zones of circulation produce the two areas of alteration in the surface.

The southern zone consists of a well defined, narrow vertical zone of circulation. Short spacing of isotherms, and of lines of mineral stability, define aureoles of increasing alteration toward a center of activity. At the surface, this circulation zone produces hot springs, mud pots and mud lakes, which distribute roughly along the space between the Los Azufres and Agua Fría faults. This area of the field is known as Tejamaniles.

The northern circulation zone has a larger average diameter. It shows the same general pattern of aureoles of increasing alteration towards a center of activity. However, the lack of data points, particularly in the northern and southeastern sections of this zone, do not allow the definition of the horizontal spread of these aureoles. This circulation zone produces surface manifestations, which distribute roughly along the Maritaro fault. This area of the field is known as Maritaro.

SUMMARY

The mineralogy of hydrothermal alteration in Los Azufres field corresponds to that of a young system subjected to prograde metamorphism. A regular sequence of mineral associations is found as a function of depth and increasing temperature. The width of the different mineral zones varies horizontally with the thermal gradient. Some hydrothermal minerals such as epidote and pyrite could be used as indicators of certain ranges of subsurface temperature.

Mapping of the distribution of alteration minerals provides a picture of the general geometry of the field. There appears to be a main aquifer at depth, which discharges through two circulation zones, which probably originate from two main fracture systems. These circulation and discharge zones give rise to the Tejamaniles and Maritaro geothermal areas, which may appear to be unrelated at the surface.

ACKNOWLEDGMENTS

The work described in this report constitutes part of a project supported by Consejo Nacional de Ciencia y Tecnología of México under

contract PIT/EN/NSF/1810.

The authors want to express their indebtedness to the personnel of Los Azufres Field and Departamento de Exploración, Gerencia de Proyectos Geotermoeléctricos of Comisión Federal de Electricidad for their general support and assistance during the conduction of these studies.

Authors are indebted also to the Centre de Recherches sur la Geologie de L'Uranium for technical, analytical and scientific assistance.

REFERENCES

- Camacho, P. (1976) "Mapa Preliminar del Area Geotérmica de Los Azufres, Mich." Comisión Federal de Electricidad, México.

- Cathelineau M. (1983) "Potassic Alteration in French Uranium Vein Deposits". Mineral Deposita, 18, 89-97.

- Cathelineau M. (1984) "Quartz Leaching and Hydrothermal Alkali Metasomatism in Granites". (in press).

- Cathelineau M., and Nieva D., "Geothermometric Applications of Chlorite Solid Solutions". (submitted).

- Cavaretta G., Gianelli G., and Pudexxu M. (1980) "Hydrothermal Metamorphism in the Larderello Geothermal Field", Geothermics, 9, 297-314.

- Elders, W.A., Hoagland, J.R., Mc Dowell, S.O., and Cobo, J.M., (1979). "Hydrothermal Mineral Zones in the Geothermal Reservoir of Cerro Prieto", Geothermics, 8, 201-209.

- Gutiérrez, N.A.,and Aumento F., (1981), "The Los Azufres (Michoacán-México) Geothermal Field", Journ. of Hydrology, 56, 137-162.

- Mc Dowell S.D., and Elders W.A. (1980), "Authigenic Layer Silicate Minerals in Borehole Elmore 1, Salton Sea Geothermal Field, California, USA, Contr. Mineral. Petrol., 74, 293-310.

- Muffler L.J.P., and White, D.E., (1969), "Active Metamorphism of Upper Cenozoic Sediments in the Salton Sea Geothermal Field and the Salton through, Southeastern California, " Geol. Soc. of América Bull., 80, 157-182.

- Oliver R. (1981) "Geología de la Zona Geotérmica de Los Azufres, Michoacán". Tesis I.P.N., México.

- Steiner, A. (1977) "The Wairakei Geothermal Area, North Island, New Zealand. " Its Subsurface Geology and Hydrothermal Rock Alteration". N.Z. Geol. Surv. Bull., 90, 133p.

- Sternfeld J.N. (1981) "The Hydrothermal Petrology and Stable Isotope Geochemistry of Two Wells in the Geysers Geothermal Field (CA, USA)". Master's Thesis. Riverside, Univ.

Proceedings Ninth Workshop Geothermal Reservoir Engineering
Stanford University, Stanford, California, December 1983
SGP-TR-74

ONE YEAR EXPERIENCE WITH PORTABLE BACK-PRESSURE TURBINES IN LOS AZUFRES

Gerardo Hiriart L.

Comisión Federal de Electricidad
Dr. Salvador González Herrejón No. 52
Morelia, MEXICO 58020

ABSTRACT

This paper contains the experience gained after one year operating five 5 MW portable, back-pressure, geothermal power plants at Los Azufres. A brief description of the field and the equipment is given. Cost figures of the whole installation and a list of what we belive are the advantanges and disadvantages is also presented. The main conclusion is that the use of this type of turbogenerators is quite atractive in new undeveloped fields and also in countries with financial problems where initial capital cost investments must be kept as low as possible at the expenses of long term steam consumption.

INTRODUCTION

At the Los Azufres geothermal field, five wellhead turbogenerators were installed one year ago. The reasons in choosing back-pressure turbines were to have portable units in order to test this new field and to have the ability to move then to an other well in case of severe changes in the well conditions. The economical analysis showed that the investment (in turbogenerators only) could be completly recovered after three years of generation. That is, if one looks at the turbogenerators as tools for field testing, they pay off in three years. One should keep in mind that Los Azufres is 2,800 m over sea level, wich implies an atmospheric pressure of 0.7 atm.

In this paper the main characteristics of the field and of the equipment are presented; some idea about the cost and our opinion regarding the pros and counter of this type of installations is given. Finally a brief description of some of the problemas found at Los Azufres is presented.

THE FIELD

The Los Azufres geothermal field is located in central México over the Neovolcanic belt, one hour drive from the city of Morelia (Fig. 1) so far, 40 wells have been drilled. It is difficult to split them in exploratory and production wells. Enough is to say that ten have zero production or were abandoned during construction because of drilling problems. Six are very good inyection wells (more than 150 Ton/h acceptance) and the rest can be considered as " Producing wells " with an average of 50 (Ton/h) of steam at a separation pressure of 1 MPa. In the northern part of the field the mixture at separation conditions is half steam-half water, with 1 to 2 % of gas by weight and the wells are 1,500 m deep on the average. In the southern part, known as Tejamaniles, most of the wells produce dry (even superheated) steam with a gas content that goes fron 1 up to 25 % by weight; they are 800 m deep on the average.

Three of the 5 MW portable power plants are located (see Fig. 2) in the northern part, using saturated steam and two in the south-zone using superheated steam.

THE PLANTS

Each group is composed, as shown in Fig. 3, of a Weber-type steam water separator (soft in the superheated zone), one spherical valve, one spherical valve one chevron-type deshumidificator, a steam filter, two control valves, the Mitsubishi turbogenerator, a silencer on

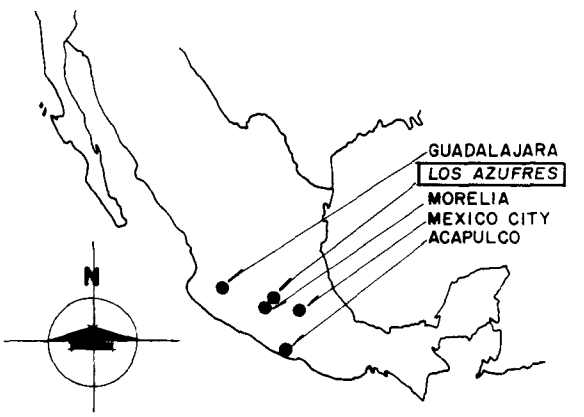


FIG. 1

top of the power house and a transformer.

The turbine is a five impulse stages, 3,600 -- rpm directly coupled to a 4,160 v syncronous - generator. The oil and the generator are air cooled. Inlet steam pressure 0.8 MPa, exhaust to the atmosphere at 70 KPa. Total saturated steam comsuption 60 Ton/h.

To start up the turbine no external source of electricity nor water is needed. For lubrica tion, an auxiliary Geothermal small turbine - is used. During operation no personnel is -- needed, in case of tripping a bell rings at a central station located at the headquarters - at Los Azufres.

Then main equipment is mounted over squids, - the time for setup in the field is about 10 - days. The teaviest piece is about 60 tons. - No alignement in the field is needed.

The five units are running since August 1982. In this particular case the time from the day the order was placed to the day of delivery - was 9 month. Parallel to that it took three month to prepare the platforms and to build - the foundations and the electrical ground --- grid. The time for instalation, tests and -- startup was 1 month per engine.

THE COST

In a country like México there is a great di- fference between import and domestic equip--- ment and labor wich makes the economical ana- lysis difficult to extrapolate to other coun-- tries. Any way, translating the figures to - 1983, those prices and its percentual weight become as shown in the following table:

COST OF THE 5 MW PLANT

Turbogenerator	61.0 %
Transformer	3.8 %
Mechanical Equipment ...	8.0 %
Electrical Equipment ...	6.3 %
Civil works	2.4 %
Egineering & design	2.5 %
Assembly	16.0 %
T O T A L	100. 00 %

Cost (1983 prices) 350 U$/KW

COST OF THE WELLS (1500 M AVE)

Drilling	44.3 %
Platform	1.3 %
Accesories	7.0 %
Cementation	6.3 %
Casing	41.1 %
T O T A L	100. %

Average production per well 70 (Ton/h) (*)

well cost (1983) U$ 1 850 000
Specific cost of the well 370 U$/KW

TOTAL COST AT LOS AZUFRES 720 U$/KW
* not including wells that didnot produce

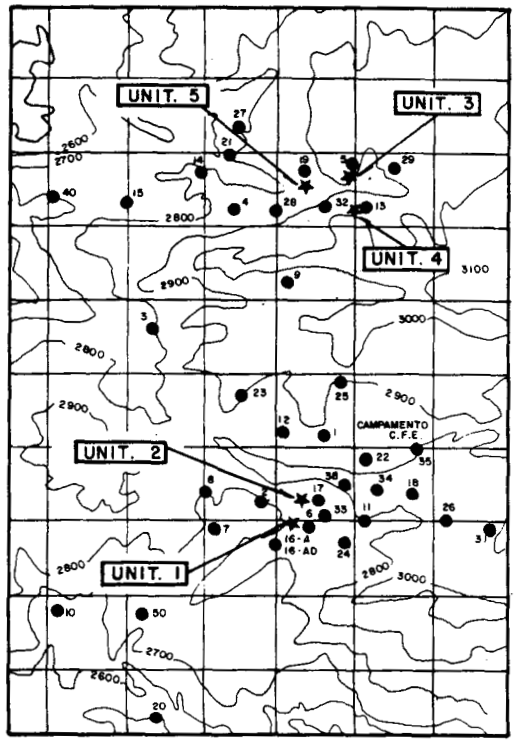


FIG. 2 WELLS AND PLANTS LOCATION AT LOS AZUFRES

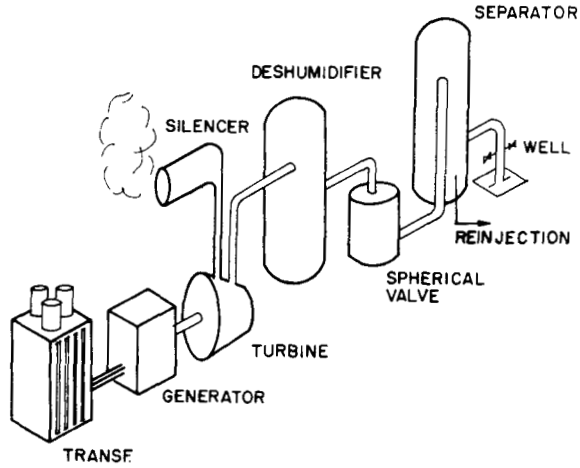


FIG. 3 GENERAL ARRANGEMENT OF THE 5 MW WELL - HEAD TURBINE.

PROS AND CONS

The use of back-pressure, well-head, 5 MW Geothermal power plants has some pros and some -- contras. According to our short experience -- they can be listed as follows.

DISADVANTAGES:- Steam consumption per kwh is - high. (12 kg/kwh in Los Azufres).

- The steam that enters the turbine is " Fresh flashed ", that is, it doesnt travel in long pipes where a small amount of condensation, drained later at the entrance of the turbine, helps to remove all the solids that were -- carried in the steam.

- It is practically impossible to use all the energy that the well produces or all the -- power that the turbine can deliver. In --- other words, if the turbine is for 5 MW, -- usually the well will deliver more steam -- than necessary (underuse of the well) or less than necessary (underuse of the turbine).

- Too many electrical transmission lines that increases the vulnerability to lightnigs -- and failiures.

- There is no control on the gases associated to the steam. They are discharged directly to the atmosphere, even though in this case the discharges are spreaded across the ---- field giving less concentration at each --- point.

ADVANTAGES:- Low capital investment in the -- equipment (specially atractive for the countries with financial problems due to high interest rates).

- Each well can begin production several --- years before than what would be,using a -- big central power plant.

- They can be installed in new wells, even - though the uncertainty about the evolution of their production characteristics.

- Specially atractive in fields with high gas content. If gas decreases with time, they leave a best well to be integrated latter - to a big central power plant.

- Because of the short distance from the --- well to the turbine, the heat losses are -- smaller (In a central power plant, heat -- and drainage losses in steam pipes repre--- sent 5 % of the total power produced).

- A new Geothermal field can be evaluated --- with enough confidence by extracting steam for months or years from several strategi-- cally located wells.

- Reliability of eleven 5 MW units is higher than one 55 MW power plant.

- Construction and engineering work is drastically simplified.

OUR EXPERIENCE

After more than one year experience opera--- ting those turbogenerators we have found that the equipment is highly reliable. The rea--- sons that have occasionaly caused tripping of the turbines can be grouped in

Mechanical trouble (mainly lubrication)	35 %
Precautorious inspection	7 %
Electrical transmission lines trouble	58 %

the power factor of the plants, having enough steam, is over 90 %. Unit 1 an 5 were generating less than 5 MW because the corresponding wells were not producing the 60 Ton/h of steam; recently, a second back up well was added to - each one to complete the 5 MW.

The main problems found have been, (appart --- from those in the electrical transmission li-- nes), of silica scaling in nozzles and blades. The origen can be explained as follows: In -- well 17, at the bottom of the well the steam - is not completly dry, it contains 1 % of water with all the impurities, such as silica and -- sodium. As it flows up, pressure decreases -- and the small amount of water evaporates lea-- ving the impurities suspended in the steam. - When this superheated steam passes through the deshumidifier, no silica is remove.

When the isoentropic expansion takes place in - the first row of nozzles, inside the turbine, - some water appears. Because of solubility differences, all the imipurities go to the water, -- oversaturating it and producind scaling at the leaving edge of the nozzles.

In well 5, where a half water half steam mixture is produced,scaling problems found have a - similar explanation. In this case the " Fresh-separated " steam that contains a certain ----- amount of water in suspension, because the -- friction losses (In the spherical valve for -- example) it decreases isoenthalpically its --- pressure allowing the droplets to flash, lea--- ving the salts in suspension, and repeating --- again the malfunctioning of the deshumidifier. In well 13 where we also have water and steam - mixture this problem does not appear because -- the distance from the separator to the deshumidifier is 300 m, inclined some 10° downward. - The pipe permits some cooling that produces a small amount of condensation. The condensated water flows in the stratified mode of the two-phase flow problem due to the 10° positive --- slope and this is easely removed by drainage - at the end of the pipe and also by the deshumidifier itself.



FIG. 4 Panoramic view of the Northern part of Los Azufres, Michoácan

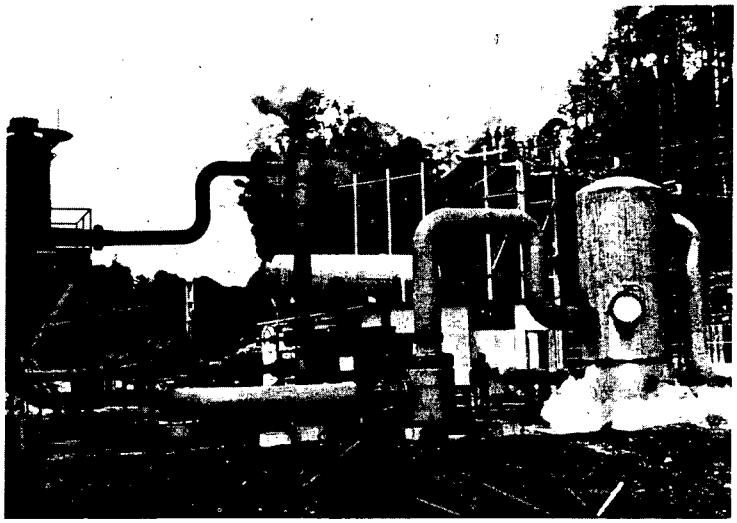


FIG. 5 Unit 2 at well 17, spherical valve and deshumidifier in -- first plane

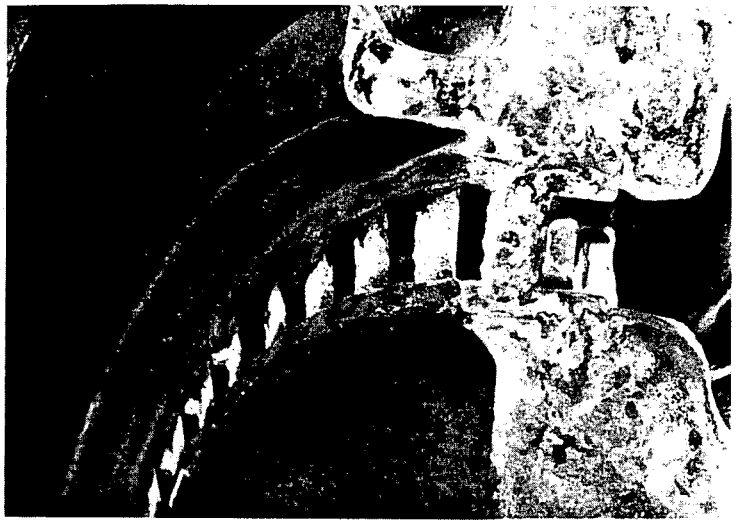


FIG. 6 Silica deposition in the second nozzle row of Unit 2 at well 17

Proceedings Ninth Workshop Geothermal Reservoir Engineering
Stanford University, Stanford, California, December 1983
SGP-TR-74

ONE COMPONENT TWO PHASE FLOW IN HORIZONTAL AND VERTICAL DUCTS: SOME BASIC CONSIDERATIONS

Paul F. Maeder, David A. Dickinson, Dimitris E. Nikitopoulos

Brown University
Providence, Rhode Island 02912

ABSTRACT

For a description and analysis of the flow we consider the conservation equations of the two phases separately, but in thermal and mechanical equilibrium, coupled by the interface shear forces (two fluid model, drift flux model). Coupling may be weak or strong, depending on Froude and Mach numbers of the flow. The fluid is highly compressible, not because the individual phases move at such speeds that their individual density changes are significant but because evaporation (phase change) results in large density changes of the system at moderate pressure or temperature changes once flashing occurs.

The slip between the phases is caused by unequal wall shear stress, acceleration of the fluid or gravitational forces and is hindered by the interface interaction. If we denote by γ the ratio of the liquid density to the vapor density and by σ the ratio of the vapor speed to the liquid speed we find that in horizontal flows $\sigma = \gamma^{1/2}$ yields the maximum slip (neglecting acceleration effects) that can be reached with no interface force acting (assuming equal friction coefficients for both phases at the wall).

If one investigates the conditions of thermodynamic flow similarity between different substances in two phase flow, one finds that the latent heat of vaporization is the principal controlling parameter. Thus, a 5 cm diameter test section in two phase R-114, at room temperature, corresponds to a 30 cm diameter duct in water-steam at boiling conditions at high temperatures such as encountered in geothermal and other power production systems.

1. INTRODUCTION

Two Phase Flow, as a branch of fluid mechanics, has commanded a great deal of attention for the last forty years. Most recently, research has been mainly concentrated on specific problems involved with the production of electricity from geothermal energy and the safety of nuclear power plants, in addition to the chemical engineering process problems which provided the original motivation. The number of approaches taken to the problem, however, is nearly as large as the number of investigators, and it seems as though a consensus has not been reached on some of the most basic questions.

Two basic approaches have been taken. The first encompassed nearly all of the earliest work and is characterized by phenomenological considerations or statistical methods. The development of flow-pattern diagrams [1] and the direct correlation of data [2] for pressure change and void fraction are examples. Notably, most work involved two-substance flow without phase change, such as air and water.

The second approach has been to seek deeper understanding of the physics of the flow in order to successfully and more accurately predict behavior over a fuller range of two phase conditions [7,8,9]. The importance of compressibility in determining the behavior of a single-substance flow is more readily recognized in the most recent work. An up-to-date collection and discussion is given in Ref. [10] and [11].

An investigation of the physical phenomena of two phase flow must center on the basic conservation equations of mass (continuity) momentum, and energy. These may be written in time-averaged form for each of the phases. The interface interaction must be properly accounted for, including the presence or absence of phase change. Hence, six basic equations can be written. Additional information is required for the nature of the interface coupling. If pressure and temperature equilibrium is assumed, combination of the conservation equations yields three independent equations, one each for momentum, energy and dissipation or mechanical energy (in addition to the two continuity equations).

The physical insight that can be gained from these basic considerations is the goal of the present paper.

2. THE BASIC PROBLEM

First, we will assume the case of a horizontal

pipe in which two separate fluids are flowing. We will assume that no phase change takes place. Each fluid has acting on it the pressure difference and the shear stresses as indicated in Fig. 1.

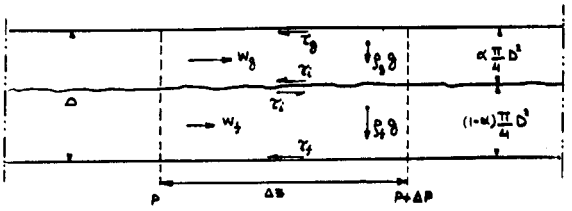


Figure 1.

The shear stress at the interface between the two fluids is shown schematically only. A simple calculation leads to the conclusion that, in this case, the pressure changes are so slight that both fluids can be considered as incompressible. We assume, as is conventional in fluid mechanics, that the pressure is constant throughout a cross-section. We further assume essentially one-dimensional flow and that the fraction of the wall circumference being wetted by one substance is proportional to the cross-section it occupies. Equilibrium between the forces acting on the two fluids then leads to

$$\alpha \frac{dP}{dz} = -\tau_{wg} \frac{\alpha}{R_h} - \tau_i \frac{N_i}{R_h C} \qquad (1a,b)$$

$$(1-\alpha) \frac{dP}{dz} = -\tau_{wf} \frac{(1-\alpha)}{R_h} + \tau_i \frac{N_i}{R_h C}.$$

We see that for the extreme case of negligible interface shear force, the wall shear stress for each component must be the same. Since this is given by the product of a friction factor and the dynamic pressures of the fluids, the latter must be in the inverse ratio of the friction factors. For flows of primary interest the Reynolds number will be large enough so the flow is turbulent and the friction factors as given by the Moody diagram will differ only slightly. In this case, i.e. steam-water flow with no phase change or air-water flow, the densities of the two fluids will be very different and therefore the velocities must differ greatly. Hence, slip between fluids ensues.

If we denote the density ratio of the two fluids by γ, we find that in the case of no interface stress, the slip ratio σ, i.e., the ratio of velocity in one fluid to that of the other, will be equal to the square root of the specific volume ratio. As the interface shear stress increases, this slip ratio will diminish and becomes essentially one if large interface stress is present. Thus, slip changes from $\sigma = \gamma^{1/2}$ for a strongly stratified flow, to $\sigma = 1$ for complete mixing. In the horizontal pipe, the amount of mixing that occurs will be related to the Froude number since the gravity is the agent which tends to stratify the flow.

Martinelli [2] has proposed to use as an independent variable, accounting for the friction effect, the ratio of the frictional pressure drop each fluid would experience if it were flowing separately in the absence of the other. If we do so (keeping in mind that the continuity equation establishes a relationship between the mass fraction ratio, the slip and the holdup) we obtain Fig. 2 which shows holdup (1 minus vapor void fraction) as a function of the Martinelli variable with slip ratio as a parameter. Some of the proposed correlations given in the literature have been shown [3,4,6] as well as some data from our facility [5].

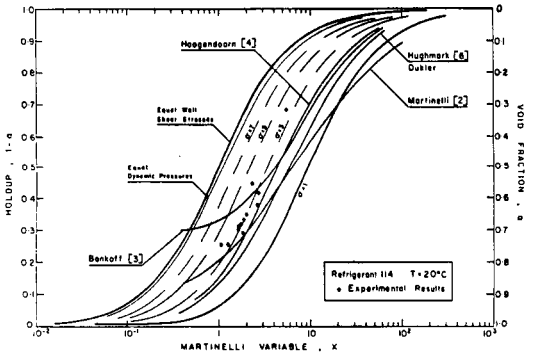


Figure 2.

A significantly different situation exists if the pipe or duct is oriented vertically. Figure 3 illustrates this case.

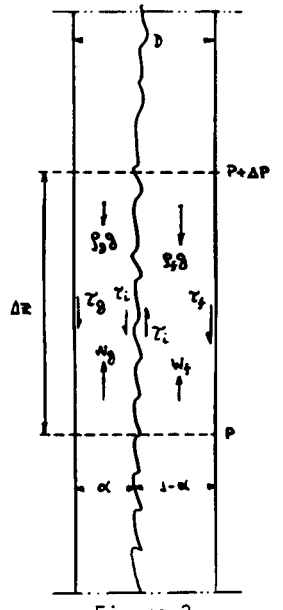


Figure 3.

The gravitational force acting on the two fluids will then be the primary cause of slip. Again, making the assumption that there is no interface shear stress the following relationship for slip ratio, friction factor and Froude number results:

$$\sigma = \gamma^{1/2}\left(1 + \frac{1}{fFr_f^2}\right)^{1/2} . \qquad (2)$$

Slip of the indicated magnitude is quite large. Violent mixing will occur leading to such flow patterns as slug flow, annular flow, etc. It should be noted and is significant that in the horizontal pipe, slip is caused by unequal wall shear stresses while in the vertical pipe slip is primarily caused by gravity acting on fluids of different densities. Since their densities will not change markedly neither fluid will be accelerated significantly. A fully developed flow whose character will not change along the pipe will result. Successive sections of pipe will be similar to each other.

3. COMPRESSIBILITY AND SIMILARITY

If the fluids are two phases of the same substance, the decrease in pressure due to gravitational forces and friction will cause liquid to evaporate. The accompanying large increase in specific volume (decrease in density) will cause acceleration of the flow in a constant area duct. The latter will be more pronounced if there is little or no slip between the phases. In order to accommodate the increased kinetic energy of the flow due to this acceleration, the pressure will decrease further. Finally, an increase in specific volume may produce such a large increase in kinetic energy that it can no longer be accommodated in an adiabatic system. The flow then chokes. We see that the flow is highly compressible even though the vapor phase is still moving at velocities far below its own velocity of sound.

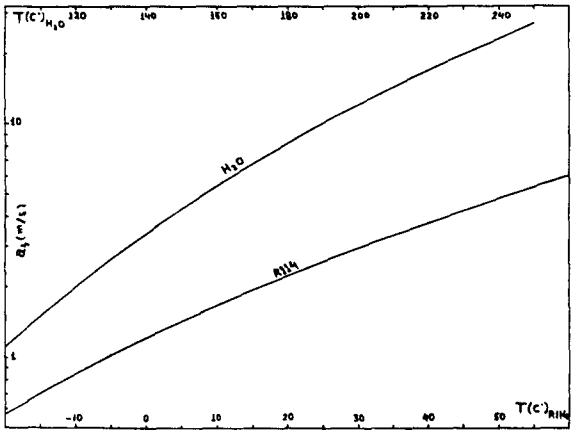


Figure 4.

The choking velocity with no slip is a property of the substance. Figure 4 shows the magnitude of this velocity of "sound" for saturated liquid as a function of temperature, for water and freon R-114 (the substance we are using in our laboratory).

Thus, we can define a Mach number at any point in our flow as the ratio of the flow velocity to the choking velocity at that point. This compressible fluid (two phases of a single substance) will progress from a point where flashing occurs at the flash Mach number, through a series of states until it finally chokes as shown in Fig. 5.

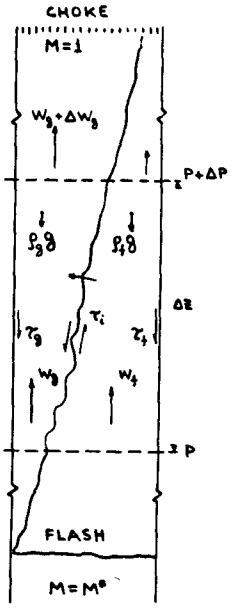


Figure 5.

This leads us to two basic questions: (1) Can we establish any similarity between such a flow of one substance and the flow of another substance? and (2) If we consider one substance only, what are the similarity parameters that are required to be met between the flow of this substance at one initial state and the flow of the same substance at another initial state?

Thermodynamic behavior of substances is complicated and we do not expect that exact similarity laws exist. However, we can create a simplified model of a fluid by assuming the latent heat to be constant, the specific heat and density of the liquid to be constant and the vapor to behave as a perfect gas with an apparent gas constant. For this we can establish a set of scaling parameters which will yield similarity of flows between substances or similarity within the flow regimes of one substance [12].

There is a single dimensionless similarity parameter between substances N_D, the "Dickinson number":

$$N_D = \frac{c_f h_{fg}}{RP_1 v_f} e^{\xi_1}, \tag{3}$$

where ξ_1 is the dimensionless temperature,

$$\xi_1 = -\frac{h_{fg}}{RT_1} \tag{4}$$

at a reference point.

The analysis also yields the proper scaling parameters for all variables, such as

$$\sqrt{\frac{c_f h_{fg}}{R}} \tag{5}$$

for velocity and

$$\frac{c_f h_{fg}}{gR} \tag{6}$$

for length. On the other hand for flow similarity the essential parameters are the Mach, Froude and Reynolds numbers, known from fluid mechanics.

Figure 6 shows the similarity parameter N_D for water substance and R-114 plotted against temperature.

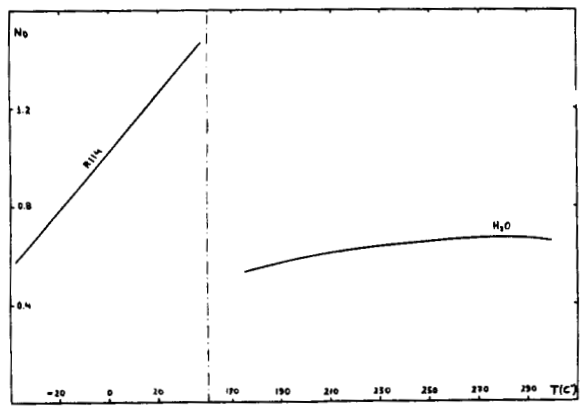


Figure 6.

We see that thermodynamic similarity exists between water substance at 200°C and R-114 at -20°C for instance.

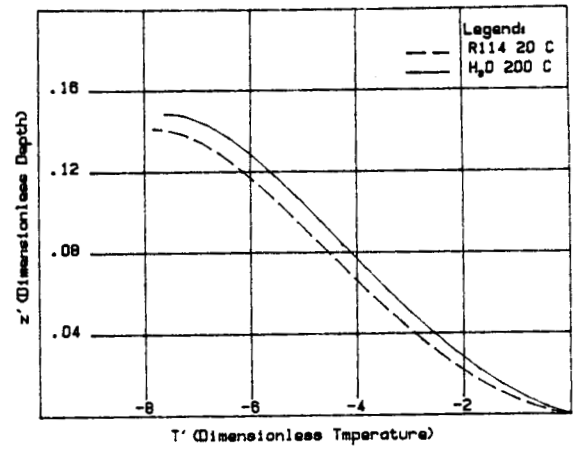


Figure 7.

Figure 7 shows the dimensionless length along a vertical pipe for water substance at 200°C and R-114 at 20°C plotted against the non-dimensional temperature.

The agreement between substances appears to be satisfactory. For purposes of illustration friction effects were neglected (i.e., isentropic flow was assumed). The physical depths are 319 m and 41.5 m for water and R-114, respectively.

4. EQUATIONS FOR THE TWO-FLUID SYSTEM

To complete the presentation in this paper we list the combined conservation equations for the two-fluid model with slip [5].

The conservation of mass equations:

$$\psi x_f = \rho_f \alpha_f w_f ; \ \psi x_g = \rho_g \alpha_g w_g \tag{7}$$

$$\text{or} \quad \frac{1-x}{x} = \frac{\gamma}{\sigma} \frac{1-\alpha}{\alpha} .$$

The conservation of momentum:

$$\frac{d}{d\tilde{z}} \{\psi w_{cm}\} = \tag{8}$$

$$-\frac{dP}{d\tilde{z}} + \bar{\tau}_{gw} + \bar{\tau}_{fw} - \rho_m g R_h$$

with $w_{cm} = \sum_p x_p w_p$, $\rho_m = \sum_p \rho_p \alpha_p$ and $\bar{\tau}_{pw} = \tau_{pw} \frac{N_p}{C}$.

The conservation of energy:

$$h + \frac{w_{rms}^2}{2} + g\tilde{z}R_h = h_0 \tag{9}$$

with $w^2_{rms} = \sum_p x_p w_p^2$, subscript p indicating the phase (f or g).

The dissipation equation:

$$\psi T \frac{ds}{d\tilde{z}} = \bar{\tau}_{wg} w_g + \bar{\tau}_i (w_g - w_f) + \bar{\tau}_{wf} w_f, \quad (10)$$

where $\bar{\tau}_i = \tau_i \frac{N_i}{C}$.

This last equation is independent of the rest, having been derived from individual phase conservation laws and the Gibbs relation.

Slip σ is contained in all these equations as a parameter while the interface shear stress appears in the dissipation equation. Slip and interface shear are related via the physical phenomena mentioned in the beginning of this paper. Such relationships are usually referred to as closures.

Very little is known about reasonable closures derived, as they should be, from the basic physical interactions between the fluids.

The work done by Taylor [13] and work related to the falling of droplets may serve as a guide to develop such relations. As a primitive approach to the problem one can introduce a pseudo friction factor f so that dissipation is proportional to the kinetic energy of the system $(w^2_{rms/2})$. This relation can be solved together with equations (7), (9) and (10) for fixed values of f and σ.

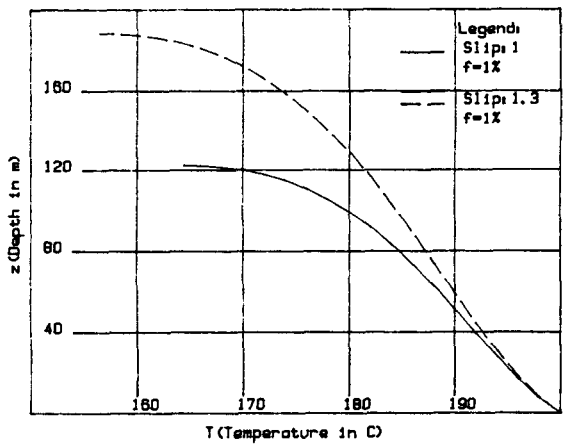


Figure 8.

Figure 8 shows the change in temperature versus length of the two phase flow (from flash to choke) upward in a vertical pipe, for f = 1% and two different values of σ.

We note the large effect on the length of the pipe from flash to choking produced by a relatively small increase of the slip ratio from 1 to 1.3. Void fraction measurements as reported in Fig. 2 indicate that slip ratios as high as 3 may be present even in horizontal ducts.

On the other hand, as the flow gets closer to choking the mixing of the phases becomes more violent, reducing slip, and the effect shown in Fig. 8 may be exaggerated.

5. CONCLUSIONS

It is clear from the foregoing that the qualitative behavior of the evaporating two phase system with its compressibility effects and choking is well understood. Also, well in hand is the formulation of the time-averaged two-fluid conservation equations. The present difficulties arise with the basic understanding and quantitative assessment of the interface interactions and forces inhibiting the slip between phases. The stronger these interactions are, the smaller will be the slip and the shorter will be the length of the duct from flashing to choking.

In the case of the geothermal reservoir or well in two phase flow, choking greatly reduces productivity. In the case of fluid transmission systems or other applications on the surface this is often recognized and efforts are made to separate vapor and liquid phases and transport them separately, greatly delaying or eliminating choking.

A better understanding, and a development of methods for calculation, of the interactions present if both phases flow together in one duct may lead to similarly effective methods in the Geothermal system.

ACKNOWLEDGEMENTS

The work described in this paper was performed under Grant No. 9X63-H4003-1 awarded to Brown University by Los Alamos National Laboratory on behalf of the Division of Geothermal Energy of the U.S. Department of Energy.

LIST OF SYMBOLS

Latin letters

w	velocity
P	pressure
z	length
D	diameter of pipe
g	acceleration of gravity
R	gas constant
T	temperature
x	flowing dryness fraction

Latin letters

h	enthalpy
h_o	stagnation enthalpy
f	friction factor
s	entropy
C	interior pipe circumference
N_i	length of interface
R_h	hydraulic radius of pipe
N_p	length of pipe circumference wetted by phase p
$Fr = \frac{w}{\sqrt{gD}}$	Froude number
$c_f = (\frac{\partial h}{\partial T})_{sat}$	specific heat of liquid on saturation line
h_{fg}	latent heat
N_D	Dickinson number
w_{cm}	velocity of the center of mass
w_{rms}	rms velocity
$\tilde{z} = z/R_h$	

Greek letters

$\sigma = \frac{w_g}{w_f}$	slip ratio
$\gamma = \frac{\rho_f}{\rho_g}$	density ratio
ρ	density
α	void fraction
τ_w	wall shear stress
ξ	dimensionless temperature
ψ	flowrate per unit area
τ_i	interface shear stress

Subscript g refers to vapor quantities

Subscript f refers to liquid quantities

Subscript p refers to f or g

Note: Change in subscript order on τ changes sign.

REFERENCES

[1] Baker, O. (1954), "Simultaneous Flow of Oil and Gas", Oil Gas J., 53, 185

[2] Lockhart, R.W. and Martinelli, R.C. (1949), "Proposed Correlation of Data for Isothermal Two Phase Two-Component Flow in Pipes", Chem. Eng. Prog., 45, 39.

[3] Bankoff, S.G. (1960), "A Variable Density Single-Fluid Model for Two Phase Flow with Particular Reference to Steam-Water Flow", Trans. ASME, J. Heat Trans., 82, 265.

[4] Hoogendoorn, C.J. (1959), "Gas-Liquid Flow in Horizontal Pipes", Chem. Eng. Sci., 9, 205.

[5] Dickinson, D.A. (1984), "An Investigation of Single-Substance, Horizontal Two Phase Flow", Ph.D. Thesis (in progress), Brown University, Providence, R.I..

[6] Hughmark, G.A. (1962), "Holdup in Gas-Liquid Flow", Chem. Eng. Prog., 58, 62.

[7] Dukler, A.E., Wicks, M., and Cleveland, R.G. (1964), "Frictional Pressure Drop in Two Phase Flow: B: An Approach Through Similarity Analysis", A.I.Ch.E. J., 10, 44.

[8] Zuber, N. and Findlay, J.A. (1965), "Average Volumetric Concentration in Two-Phase Systems", Trans. ASME, J. Heat Trans., 27, 453.

[9] Levy, S. (1963), "Prediction of Two-Phase Pressure Drop and Density Distribution from Mixing Length Theory", Trans. ASME, J. Heat Trans., 85, 137.

[10] Thermohydraulics of Two-Phase Systems for Industrial Design and Nuclear Engineering. J. M. Delhaye, M. Giot and M.L. Riethmueller, eds. Hemisphere, 1981.

[11] Advances in Two Phase Flow and Heat Transfer. S. Kakac and M. Ishii, eds. 2 vols., Martinus Nijhoff, 1983.

[12] Maeder, P.F.. Report in progress.

[13] Davies, R.M. and Taylor, G.I. (1950), "The Mechanics of Large Bubbles Rising Through Extended Liquids and Through Liquids in Tubes". Proc. Roy. Soc., A200, 375.

Proceedings Ninth Workshop Geothermal Reservoir Engineering
Stanford University, Stanford, California, December 1983
SGP-TR-74

A METHOD TO RECOVER USEFUL GEOTHERMAL-RESERVOIR PARAMETERS FROM PRODUCTION CHARACTERISTIC CURVES (1) STEAM RESERVOIRS.

E. Iglesias, V. Arellano *

A. Garfias, C. Miranda, J. Hernández and J. González +

* Instituto de Investigaciones Eléctricas
Cuernavaca, Mor., México.

+ Comisión Federal de Electricidad
Los Azufres, Mich., México.

ABSTRACT

In this paper we develop and demonstrate a method to estimate the reservoir pressure and a productivity index for vertical steam wells, from its production characteristic (also called output) curves. In addition, the method allows to estimate the radius of influence of the well, provided that a value of the reservoir transmisivity is available. The basic structure of the present method is: first, the measured well head mass flowrates and pressures are transformed to downhole conditions by means of a numerical simulator; then, the computed downhole variables are fitted to a simple radial model that predicts the sandface flowrate in terms of the flowing pressure. For demonstration, the method was applied to several steam wells from the Los Azufres geothermal field. We found excellent agreement of the model with this ample set of field data. As a bonus, the processed data allowed several inferences about the steam -producing zone of the reservoir: that the wells considered produce from relatively isolated pockets of steam, which are probably fed by nearby inmobile water; and that these feed zones are in poor hydraulic communication with the field surface waters. The main advantages of our method are that it provides a way to retrieve important reservoir information from usually available production characteristic curves, and that the method works from easily and accurately taken wellhead measurements.

INTRODUCTION

Production characteristic curves, also called output curves, are routinely determined for most geothermal wells. These curves relate mass flowrate at the wellhead with the corresponding wellhead pressure. Their normal uses include gathering cualitative information about reservoir properties(e.g. relative values of reservoir pressure, temperature or gas content, reservoir permeability) and about effects of scaling in the wellbore (eg. Grant et. al., 1982); estimating discharge enthalpy from the maximum discharging pressure (James, 1970, 1980 a,b); and, of course, predicting mass flow rates for given wellhead pressures and vice versa.

Output curves contain mixed information about both the reservoir and the intervening wellbore. As pointed out, only qualitative information about the reservoir is ussually recovered from these curves. The sole exception to this, James' maximum discharging pressure method to estimate discharge enthalpy, is based on the fact that at low flowrates resistive wellbore effects are unimportant; that is, in this case the wellbore and reservoir information are already separated.

In this paper we develop and demonstrate, via field examples, a method to recover important cuantitative information about the reservoir from output characteristic curves of steam wells. In a companion paper (Iglesias et. al., these Proceedings), we describe and demonstrate a similar method for water-fed wells. The method is based on unscrambling the wellbore and reservoir contributions to the output curves, by means of a wellbore flow numerical simulator. The reservoir information retrievable with our method can alternatively be obtained from transient pressure tests. These tests are difficult to run in high temperature wells which, more often than not, contain corrosive fluids. Moreover, the method presented in this paper uses as input data characteristic curves that have to be determined, anyway, for other uses. Our method is, therefore, an efficient way for retrieving important reservoir information from usually available wellhead data, without resorting to more difficult bottomhole measurements. No previous similar work is known to the authors.

METHOD

As outlined in the previous section, the first step of the method presented here consists of using a wellbore flow numerical simulator to unscramble the reservoir and the wellbore information contained in the production characteristic curves. This provides the values of the bottomhole variables corresponding to the data points on the wellhead output curves. The second step is to fit the computed bottomhole data to simple models that predict the behavior of the sandface flowrate as a function of the bottomhole flowing pressure. The fit provides estimates of the reservoir pressure p_e, and of

a productivity index J' of the well. If estimates of the reservoir transmissivity (kh/μ) are available, the radius of influence of the well can also be estimated.

Production characteristic curves are obtained measuring the stable or quasi-stable steam flowrates and acompanying wellhead pressures corresponding to different degrees of chocking of the well. Usually these measurements cover the range from fully open to nearly the maximum degree of chocking compatible with the existance of flow. The stable or quasi-stable state of the flow is important with regard to the types of wellbore and reservoir models appropriate for the present method.

The wellbore numerical model (WELFLO) used in this work is described by Goyal et. al. (1980) and references therein. WELFLO is a finite difference, one dimenssional, multiphase, steady-state geothermal wellbore flow simulator appropriate for vertical multidiameter wells. It has been extensively validated against field data (Goyal et. al., 1980,1981; Arellano, 1983). Two features of this code make it suitable for the problem at hand. First, the cappability to compute bottomhole conditions from wellhead input variables, as needed. Second, the assumtion of steady-state flow in the wellbore. This is required because, in order to obtain characteristic curves, wells are flown through the same orifice for several days, thus allowing transient wellbore effects to die out. The input variables of WELFLO are the geometry of the well (lengths, diameters, open or ranurated interval), mass flowrate, wellhead pressure, and wellhead flowing enthalpy. Conductive heat losses to the wellbore walls were neglected in our calculations. Our method requires to transform each and every measured data point of the characteristic curve to the corresponding bottomhole conditions. Of the complete set of bottomhole variables computed by means of WELFLO, we require only the flowing pressure and the mass flowrate (which equals the wellhead flowrate, due to the steady state conditions of the flow in the bore).

For the flow in the reservoir we chose a simple model suggested by experience: radial, horizontal, isothermal flow of steam through a porous, homogeneous, confined, cylindrical reservoir of constant thickness. If the outer boundary condition is constant pressure, then steady state can be achieved. In that case the mass flowrate is given by

$$W=\alpha \frac{kh}{\mu} \frac{(p_e^2 - p_{wf}^2)}{zT \ln (r_e/r_w)} , \qquad (1)$$

the well-known expression of Darcy's Law for steam flow in steady-state radial flow. Here α is a constant to accomodate different systems of units (nomenclature at the end of the paper). This steady-state model can approximately describe three situations of interest, with the restrictions commented below. (a) Infinite acting period, i.e. no boundary effects are felt during the time period Δt over which the output production data were collected; in this case Δt must be smaller than the time scale associated with the outward movement of the pressure perturbation in the reservoir, for (1) to be a valid approximation. (b) Constant pressure outer boundary condition, which may arise from the existence of a cylindrical boiling front some distance from the well; equation (1) is a valid approximation if Δt is smaller than the time scale associated with the outward movement of the boiling front. (c) Finite reservoir, no-flow condition at $r=r_e$; approximation (1) is valid when Δt is smaller than the time scale associated with the decrease of p_e.

If the reservoir flow model summarized by (1) is valid for a given set of output data (production characteristic curve), a plot of the computed sandface flowrate versus the corresponding squared flowing pressures should give a straight line. From (1) the intercept of this line is

$$a=\alpha \frac{kh}{\mu} \frac{p_e^2}{zT \ln (r_e/r_w)} , \qquad (2)$$

and its slope is

$$b= -\alpha \frac{kh}{\mu} \frac{1}{zT \ln (r_e/r_w)} . \qquad (3)$$

The reservoir pressure is then easily computed from

$$p_e = (-a/b)^{1/2} . \qquad (4)$$

A productivity index is naturally defined as

$$J' = W/(p_e^2 - p_{wf}^2) \qquad (5)$$

Then from (1), (3) and (5), the value of the productivity index is

$$J' = -b. \qquad (6)$$

Finally, if the transmisivity (kh/μ) of the reservoir is known, the radius of influence can be estimated from (6) as

$$r_e = r_w \exp (\alpha \frac{kh}{\mu} / z\, TJ') \qquad (7)$$

FIELD VALIDATION

To demonstrate our method we present a number of examples in this section. The data correspond to five steam wells from the Los Azufres (Michoacán, México) geothermal field. These and other steam wells are clustered on a relatively ample zone bounded on its North, West and East sides by wells that produce water and steam (Fig. 1).

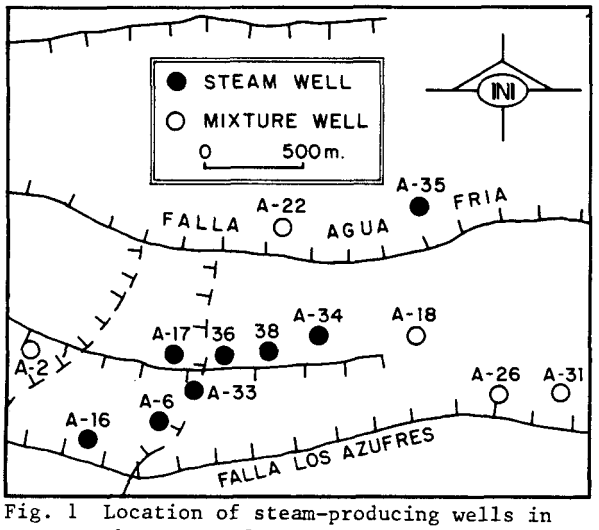


Fig. 1 Location of steam-producing wells in the Los Azufres geothermal field.

Figures 2 through 6 show the original production characteristic curves and their transformation to bottomhole conditions. Table 1 summarizes our results. The coefficients of correlation quoted in Table 1 correspond to the fit of the proposed reservoir flow model to the data -see also Figs. 2 through 6 (b)-. We conclude that the demonstrated excellent agreement with an ample set of field data constitutes strong evidence of the validity of our model.

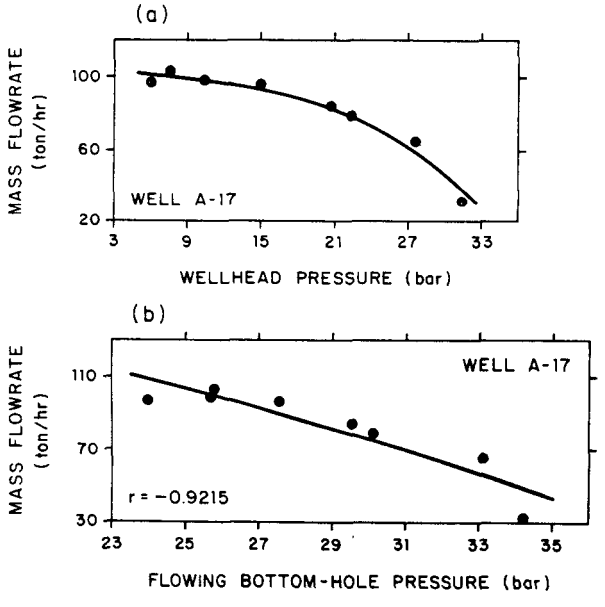


Fig. 2 (a) Characteristic curve of well A-17; (b) corresponding computed bottomhole variables, and fit of the steady-state radial steam flow model.

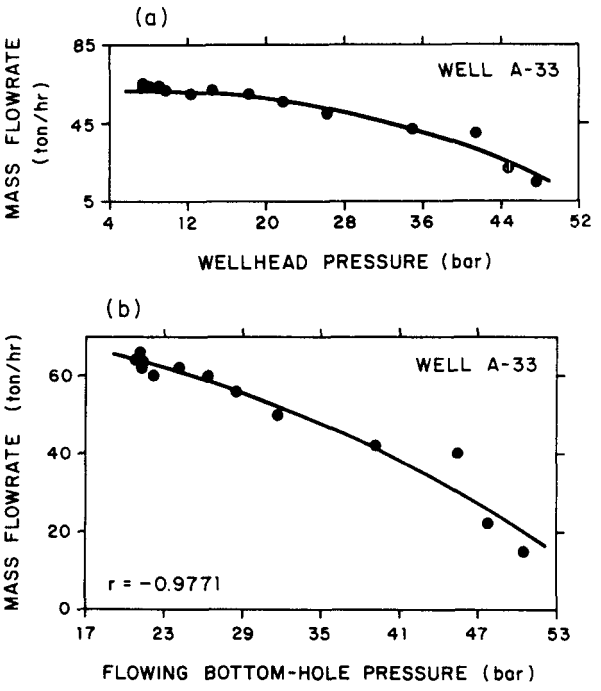


Fig. 3 (a) Characteristic curve of well A-33; (b) corresponding computed bottomhole variables, and fit of the steady-state radial steam flow model.

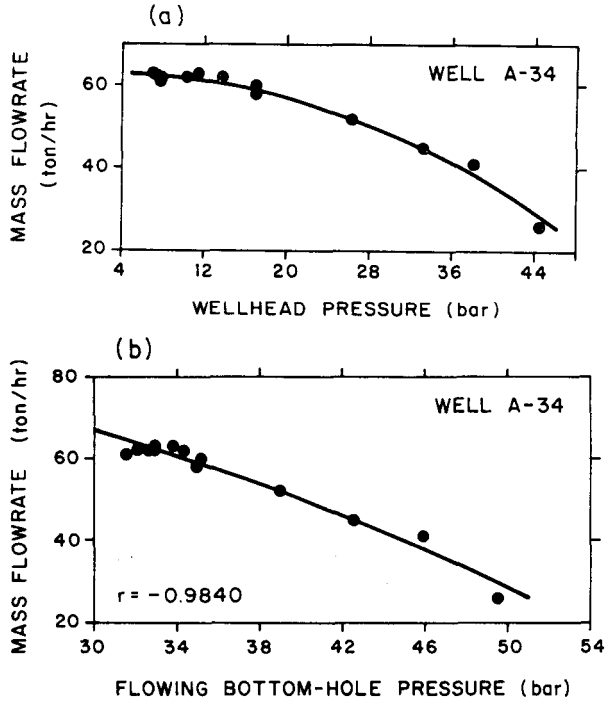


Fig. 4 (a) Characteristic curve of well A-34; (b) corresponding computed bottomhole variables, and fit of the steady-state radial steam flow model.

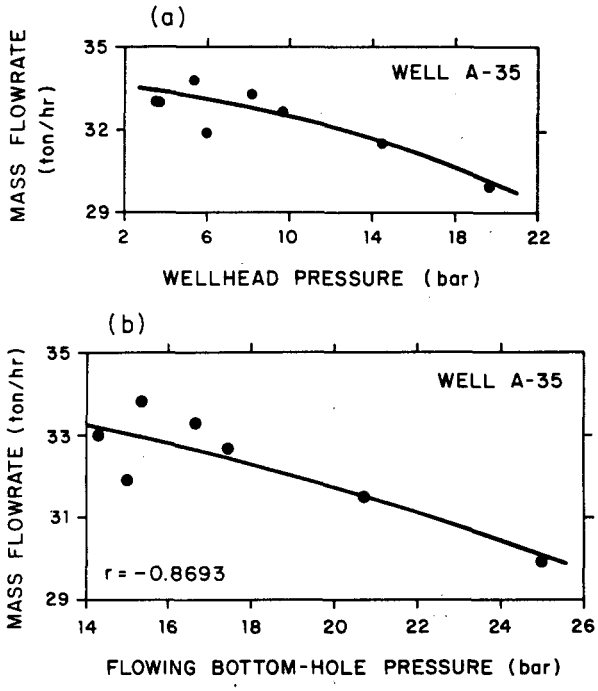


Fig. 5 (a) Characteristic curve of well A-35; (b) corresponding computed bottomhole variables, and fit of the steady-state radial steam flow model.

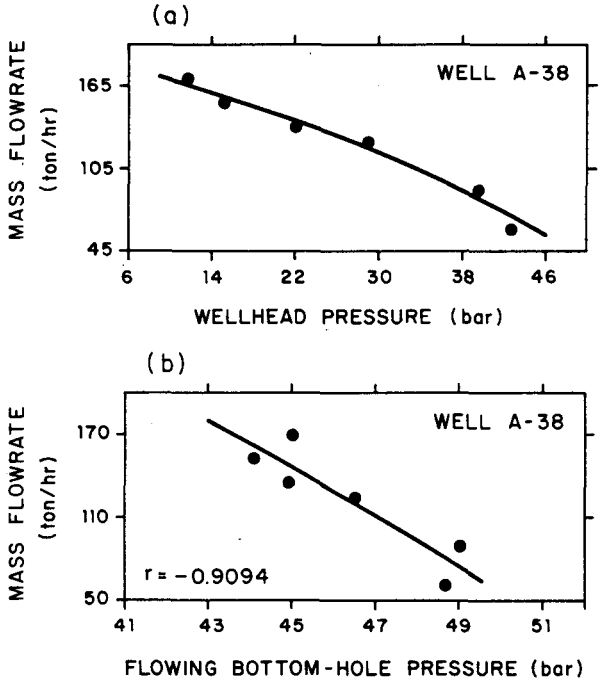


Fig. 6 (a) Characteristic curve of well A-38; (b) corresponding computed bottomhole variables, and fit of the steady-state radial steam flow model.

Table 1. Results of the method applied to wells from the Los Azufres geothermal field.

Well	Depth (m)	J' (ton h^{-1} bar^{-2})	Pe (bar)	Correlation Coefficient
A-38	752	0.1915	52.8	-0.9094
A-17	627	0.1015	40.5	-0.9215
A-34	856	0.0241	60.6	-0.9840
A-33	683	0.0210	59.1	-0.9771
A-35	1240	0.0074	68.5	-0.8693

Another check on our results, it would appear, should be to compare the computed reservoir pressures with measured shut-in bottomhole pressures. However, such comparison is not necessarily granted in geothermal wells (Grant, 1979; Grant et. al., 1981). The reason is that geothermal reservoirs are in a dynamic state of equilibrium which promotes the existence of non-hydrostatic internal pressure gradients. Since geothermal wells ussually have more than one feed zone, even shut - in wells may sustain internal flows. Thus, downhole profiles do not necessarily reflect reservoir pressure, except at the depths corresponding to feed points. Table 2 shows a comparison of measured bottomhole pressures with computed reservoir pressures. The former were measured in wells that had been shut-in for relatively long periods of time after their completion. In the cases presented in Table 2

Table 2. Computed reservoir pressures vs. measured bottomhole pressures.

Well	Well Depth. (m)	Pe (bar)	Depth of measurement (m)	Measured pressure (bar)
A-17	627	40.5	617	46.0
A-33	683	59.1	683	52.9
A-34	856	60.6	850	54.9
A-35	1240	68.5	1240	67.6
A-38	752	52.8	745	52.0

there is a remarkable good agreement between observed and predicted values. The average deviation is less than 6%. This constitutes further, though somewhat circumstantial, evidence supporting the applicability of the present model.

APPLICATIONS

As stated, if an estimate of the transmisivity is available, our method provides a way to estimate the radius of influence of the well. As an example, we present here such calculation for well A-35. A transient pressure test indicated a value $(kh/\mu) = 33{,}390$ md. m/cp for that well. The other relevant parameters are $J' = 0.0074$ ton. h^{-1}/bar^2 (from Table 1), $T = 473$ °K, $z = 0.87$, $\alpha = 2.3278 \times 10^{-4}$. Pluging these values into (7) we find $(r_e/r_w) = 12.84$, which implies a radius of influence of

the order of 1m. This result suggests the existence of a boiling front, and therefore of inmobile water, near the well.

As another application we plotted the computed reservoir pressures versus the corresponding depths (Fig. 7). The boiling point for depth curve is also indicated. The fact that well A-33 falls on the liquid region of the diagram was at first disturbing. However, this result was justified a-posteriori. Well A-33 was flown January 17 through March 24, 1983 to obtain the characteristic curve shown in Fig. 3 (a). During that period the well produced what appeared to be dry saturated steam. Consequently, a wellhead dryness fraction equal to unity was assumed in our calculations, with the result just noted. In early August the well was opened again, still apparently producing dry saturated steam. As time went by it was apparent that the steam produced became wetter. Finally, starting October 13, 1983, sizable amounts (few tons/hr) of separated water started to be recorded. In the authors' opinion, the accurate prediction that well A-33 should produce steam and water constitutes further evidence of the validity of the method presented in this work.

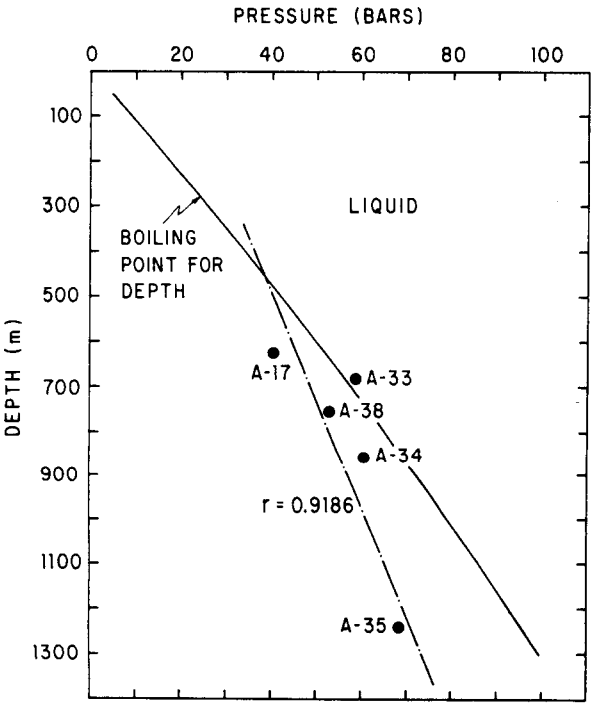


Fig. 7 Inferred reservoir pressures for steam wells vs. depth.

Other important inferences were drawn from Fig. 7. It has been assumed that a "steam dome" existed in the area defined by the steam wells of Fig. 1. The evidence summarized in Fig. 7 helps qualify that assumption. Excluding A-33 because of its status of a mixture producer, a straight line of slope 0.0414 bar/m and coefficient of correlation equal to 0.9186 can be fitted to the remaining steam wells. If a continuous steam phase existed interconecting these wells, the pressure profile should be nearly vertical. Therefore, we conclude that a steam dome constituted by a continuous steam phase does not exist in the area. Rather, the evidence points to the existence of relatively isolated pockets of steam, probably fed from nearby inmobile liquid water zones.

Another interesting inference from Fig. 7 is that the steam wells are underpressured with respect to the mean boiling for depth pressure profile, implying poor hydraulic communication of the feed zones with the field surface waters. Since the field is located in a highland, 300 to 500 meters above the neighboring valleys, this inference does not preclude recharge from the nearby lowlands.

SUMMARY AND CONCLUSIONS

We have developed and demonstrated a method to retrieve the reservoir pressure p_e and the productivity index J' corresponding to vertical steam wells from its production characteristic curves. If an estimate of the reservoir transmisivity (kh/μ) is available, our method provides a way to estimate the radius of influence of the well.
We found excellent agreement between predicted and observed values. This agreement provides strong evidence of the validity of our method.

The main advantages of the proposed method are as follows: It provides a way for retrieving important reservoir information from ussually available production characteristic curves; no extra measurements are needed. Unlike traditional methods that require significantly more difficult bottomhole measurements to evaluate the reservoir pressure and the productivity index, the present method works from easily taken wellhead measurements.

Concerning the steam producing zone of the Los Azufres geothermal field, we drawed the following inferences: The computed pressure profile of that zone indicates that a steam dome constituted by a continuous steam phase does not exist in the area. Rather, the evidence points to the existence of relatively isolated pockets of steam, probably fed by neighboring inmobile liquid water. Finally, the formations feeding the steam wells are underpressured with respect to the mean boiling for depth pressure profile, implying poor hydraulic communication with the field surface waters; however recharge from nearly lowlands is not precluded by our results.

AKNOWLEDGEMENTS

The authors wish to thank Ing. Ramón Reyes, Head of the Coordinadora Ejecutiva del Campo Geotérmico Los Azufres, for his encouragement. We are also indebted to the field personnel that laboriously and carefully gathered the data necessary for this paper. The manuscript was scrupulously and professionally typed by María Eugenia Calderón. The figures were drafted by Adrián Patiño.

NOMENCLATURE

a: Intercept of straight line (ton hr^{-1})

b: Slope of straight line (ton hr^{-1}/bar^2)

h: Reservoir thicknes (m)

J': Productivity index (ton hr^{-1}/bar^2)

k: Permeability (md)

p_e: Reservoir pressure (bar)

p_{wf}: Sandface flowing pressure (bar)

r_e: Radius of influence of the well (m)

r_w: Wellbore radius (m)

T: Absolute temperature (°K)

W: Mass flowrate (ton hr^{-1})

z: Gas deviation factor

α: Constant to accomodate different systems of units

μ: Viscosity (cp)

REFERENCES

Arellano, V. (1983) Project 1225 Estudios de Ingeniería de Yacimientos. Report IIE/11/1225/I 06/P.
Instituto de Investigaciones Eléctricas. Cuernavaca, Mor., México.

Goyal, K.P., C.W. Miller and M.J. Lippmann. (1980) Effect of Measured Wellhead Parameters and Well Scaling on the Computed Downhole Conditions in Cerro Prieto Wells. Sixth Workshop Geothermal Reservoir Engineering. Stanford University, SGP-TR-50, pp. 130-138.

Goyal, K.P., C.W. Miller, M.J. Lippmann and S. P. Vonder Haar. (1981). Analysis of Cerro Prieto Production Data. Third Symposium on the Cerro Prieto Geothermal Field, Baja California, México. pp. 496-500, San Fco. Ca., U.S.A.

Grant, M.A. (1979) Interpretation of Downhole Measurements in Geothermal Wells. Rep. No. 88. Appl. Math. Div. Dep. Sci. Ind. Res., New Zealand.

Grant, M.A., Bixley, P.F., and Donaldson, I.G. (1981) Internal Flows in Geothermal Wells: Their Identification and Effect on the Wellbore Pressure and Temperature Profiles. 56th. Annv. Fall Tech. Conf., SPE-AIME Paper SPE. 10317.

Grant, M.A., Donaldson, I.G., and Bixley, P.F. (1982) Geothermal Reservoir Engineering. Academic Press. New York., U.S.A.

James, R. (1970) Factors Controlling Borehole Performance. United Nations Symposium on the Development and Utilization of Geothermal Resources. Pisa, Italy. Vol. 2, pp. 1502-1515.

James, R. (1980a) Estimating Maximum Discharge of Geothermal Wells. Sixth Workshop Geothermal Reservoir Engineering. Stanford University. pp. 139-144.

James, R. (1980b) Significance of the Maximum Discharging Pressure of Geothermal Wells. Sixth Workshop Geothermal Reservoir Engineering. Stanford University. pp. 145-149.

Proceedings Ninth Workshop Geothermal Reservoir Engineering
Stanford University, Stanford, California, December 1983
SGP-TR-74

A METHOD TO RECOVER USEFUL GEOTHERMAL-RESERVOIR PARAMETERS FROM PRODUCTION CHARACTERISTIC CURVES. (2) HOT WATER RESERVOIRS.

E. Iglesias, V. Arellano *

R. Molinar +

* Instituto de Investigaciones Eléctricas
Cuernavaca, Mor., México

+ Comisión Federal de Electricidad
Los Azufres, Mich., México

ABSTRACT

In this paper we develop and demonstrate a method to estimate the reservoir pressure, a mass productivity index, and a thermal power productivity index for vertical water-fed geothermal wells, from its production characteristic (also called output) curves. In addition, the method allows to estimate the radius of influence of the well, provided that a value of the reservoir transmisivity is available. The basic structure of the present method is: first, the measured wellhead mass flowrates and pressures are transformed to downhole conditions by means of a numerical simulator; then, the computed downhole variables are fitted to a simple radial model that predicts the sandface flowrate in terms of the flowing pressure. For demonstration, the method was applied to several wells from the Cerro Prieto geothermal field. We found very good agreement of the model with this ample set of field data. The main advantages of our method are that it provides a way to retrieve important reservoir information from usually available production characteristic curves, that it works from easily and accurately taken wellhead measurements, and that its results address the two main aspects of geothermal resource utilization, namely, mass and heat production.

INTRODUCTION

Production characteristic curves, also called output curves, are routinely determinated for most geothermal wells. These curves relate mass flowrate at the wellhead with the corresponding wellhead pressure. Their normal uses include gathering qualitative information about reservoir properties (e.g. relative values of reservoir pressure, temperature or gas content, reservoir permeability) and about effects of scaling in the wellbore (eg. Grant et. al., 1982); estimating discharge enthalpy from the maximum discharging pressure (James, 1970, 1980 a,b); and, of course, predicting mass flow rates for given wellhead pressures and vice-versa.

Output curves contain mixed information about both the reservoir and the intervening wellbore. As pointed out, only qualitative information about the reservoir is ussually recovered from these curves. The sole exception to this, James' maximum discharging pressure method to estimate discharge enthalpy, is based on the fact that at low flowrates resistive wellbore effects are unimportant; that is, in this case the wellbore and reservoir information are already separated.

In this paper we develop and demonstrate, via field examples, a method to recover important quantitative information about the reservoir from output characteristic curves of water-fed wells. In a companion paper (Iglesias et. al., these Proceedings), we describe and demonstrate a similar method for steam wells. The method is based on unscrambling the wellbore and reservoir contributions to the output curves, by means of a wellbore flow numerical simulator, and then fitting these results to a simple radial model of the reservoir flow. The reservoir information retrievable with our method can alternatively be obtained by traditional methods, which require bottomhole measurements. These measurements are difficult to take in high temperature wells which, more often than not, contain corrosive fluids. Moreover, the method presented in this paper uses as input data characteristic curves that have to be determined, anyway, for other uses. Our method is, therefore, an efficient way for retrieving important reservoir information from usually available wellhead data, without resorting to more difficult bottomhole measurements. No previous similar work is known to the authors.

METHOD

The method presented here requires production characteristic curves as input data. These data are converted to the corresponding bottomhole quantities by means of a wellbore flow numerical simulator. Then, the computed bottomhole quantities are fitted with a simple model that predicts the sandface mass flowrate as a function of the bottomhole flowing pressure. The fit provides estimates of the reservoir pressure p_e, and the productivity index J_m of the well. If estimates of the reservoir transmissivity (kh/μ) are available, the radius of influence of the well can also be estimated.

Output characteristic curves are recorded during production tests. During these tests, the

wells are typically flown through several orifices of varying diameters. For each orifice the flow is mantained until stable or quasistable conditions are reached. At this point, the mass flowrate and the corresponding wellhead pressure are recorded. Liquid-fed wells in high enthalpy fields usually produce mixtures of water and steam at the surface. In this type of well the data recorded are the steam and water flowrates, and the wellhead pressure. After recording the data, the flow is diverted through another orifice of different diameter, and the process restarts. Thus, for high-enthalpy water-fed wells production tests provide two related curves: water and steam flowrates versus wellhead pressures. These constitute the raw data of the method presented here.

The wellbore numerical model (WELFLO) used in this work is described by Goyal et. al (1980) and references therein. WELFLO is a finite difference, one dimenssional, multiphase, steady-state geothermal wellbore flow simulator appropriate for vertical multidiameter wells. It has been extensively validated against field data (Goyal et. al., 1980; Arellano, 1983). Two features of this code make it adequate for the problem at hand. First, the cappability to compute bottomhole conditions from wellhead input variables, as needed. Second, the assumption of steady-state flow in the wellbore. This assumption is required because the stable or quasi-stable conditions attained during the production test allow wellbore transients to die out. The input variables of WELFLO are the geometry of the well (lenghts, diameters, extent of open or ranurated interval), total mass flow rate, wellhead pressure, and wellhead total specific flowing enthalpy. Conductive heat losses to the wellbore walls are unimportant in steady-state flow (Goyal et. al., 1980; Gould, 1974) and were neglected in our calculations.

Our method requires to transform each and every measured data point of the characteristic curve to the corresponding bottomhole conditions. Of the complete set of bottomhole variables computed by means of WELFLO, we require only the flowing pressure and the total mass flowrate (which equals the wellhead flowrate, due to the steady state conditions of the flow in the bore). Errors of the wellhead input quantities affect the bottomhole flowing pressures (BHP's) computed by means of WELFLO in different fashions, as follows (Goyal et. al., 1980). Computed BHP's are relatively insensitive to errors of the wellhead total mass flowrate. Errors of wellhead pressures have effects of the same order of magnitude on computed BHP's. Input enthalpies greater than the true value decrease calculated BHP's in approximate proportion to the error. Finally, computed BHP's are very sensitive to negative errors of the input enthalpy.

Once the output characteristic curves are recorded, little can be done with respect to the errors of the mass flowrates and of the corresponding wellhead pressures. Fortunately, this is not the case for the flowing total specific enthalpy, the most sensitive quantity with regard to BHP's errors. The individual specific enthalpies corresponding to each data point of the characteristic curve are computed from the related water and steam flowrates and known separation pressure. These individual enthalpies are affected by the random errors of the measured water and steam flowrates. Now, for liquid-fed geothermal wells the flowing total specific enthalpy is constant and independent of wellhead pressure or mass flowrate (e.g. Grant et. al., 1982). Therefore, we take the arithmetic mean h_T, which is the best statistical estimate of the true value in a set of random measures, as the value of the constant flowing specific enthalpy h_T. This approach minimizes the errors of the computed BHP's. As a further precaution, we check the set of individual enthalpies for possible correlations with wellhead pressures or mass flowrates. The existence of such correlations may indicate two-phase flow in the reservoir, which in turn would invalidate the present analysis.

For the flow in the reservoir we chose a simple model suggested by experience: radial, horizontal, isothermal flow of a liquid through a porous, homogeneous, confined, cylindrical reservoir of constant thickness. If the outer boundary condition is constant pressure, then steady state can be achieved. In that case the mass flowrate is given by

$$W = \alpha \frac{kh}{\nu} \frac{(p_e - p_{wf})}{\ln (r_e/r_w)} , \qquad (1)$$

the well-known expression of Darcy's Law for steady-state radial flow, in massic form. Here α is a constant to accomodate different systems of units (nomenclature at the end of the paper). This steady-state model can approximately describe three situations of interest, with the restrictions commented below. (a) Infinite acting period, i.e. no boundary effects are felt during the time period Δt over which the output production data were collected; in this case Δt must be smaller than the time scale associated with the outward movement of the pressure perturbation in the reservoir, for equation (1) to a valid approximation. (b) Constant pressure outer boundary condition, which may arise from the existence of a strong radial recharge some distance away from the well; equation (1) is valid with no restrictions on Δt. (c) Finite reservoir, no-flow condition at $r=r_e$; approximation (1) is valid when Δt is smaller than the time scale associated with the decrease of p_e.

If the reservoir flow model summarized by (1) is valid for a given set of output data (production characteristic curve), a plot of the computed sandface flowrates versus the corresponding flowing pressures should give a straight line. From (1) the intercept of this line is

$$a = \alpha \frac{kh}{\nu} \frac{p_e}{\ln (r_e/r_w)}, \quad (2)$$

and its slope is

$$b = -\alpha \frac{kh}{\nu} \frac{1}{\ln (r_e/r_w)}, \quad (3)$$

The reservoir pressure is then easily computed from

$$p_e = -(a/b) \quad (4)$$

A massic productivity index is naturally defined as

$$J_m = W/(p_e - p_{wf}) \quad (5)$$

Then, from (1), (3) and (5)

$$J_m = -b. \quad (6)$$

In geothermal applications a quantity of great interest is the thermal power of a given well. In analogy to (5), a useful power productivity index may be defined as

$$J_p = h_T J_m \quad (7)$$

for water-fed wells. In definition (6) we have used h_T, the total specific flowing enthalpy, which is constant and independent of wellhead pressure and total mass flowrate, as mentioned. In practice, we estimate h_T by $\bar{h}_T$, the total specific flowing enthalpy averaged over the characteristic curve, to minimize errors.

Finally, if the reservoir transmissivity (kh/μ) is known, the radius of influence of the well can be estimated from (6) as

$$r_e = r_w \exp\{(\alpha kh)/(\mu \nu J)\}, \quad (8)$$

where we have replaced $\nu = \mu v$, with v the specific volume of the liquid at reservoir conditions. In practice we estimate v by the specific volume of saturated water at the computed bottomhole temperature.

Estimates of r_e by this method are affected by the existence of a non-zero skin. This is because the permeability k in equation (8) represents the permeability "seen" by the well, which is not the reservoir permeability if there is a non-zero skin. In this case k should be replaced by the composite permeability

$$\bar{k} = \ln(r_e/r_w)/\{\frac{\ln(r_s/r_w)}{k_s} + \frac{\ln(r_e/r_s)}{k}\} \quad (9)$$

Taking $(r_s/r_w) \simeq 1 + \varepsilon$, with $\varepsilon \ll 1$ as usually assumed, it is easy to show from (9) that

$$\bar{k} < k \quad (10)$$

wether the skin is positive or negative. Expression (10) implies that (8) overestimates r_e if the reservoir permeability (e.g. as obtained from pressure tests) is used, when a non-zero skin exists. Given the exponential form of (8), these errors may be important.

FIELD VALIDATION

For validation purpouses we have applied our method to 5 wells from the Cerro Prieto geothermal field. Figure 1 shows their location.

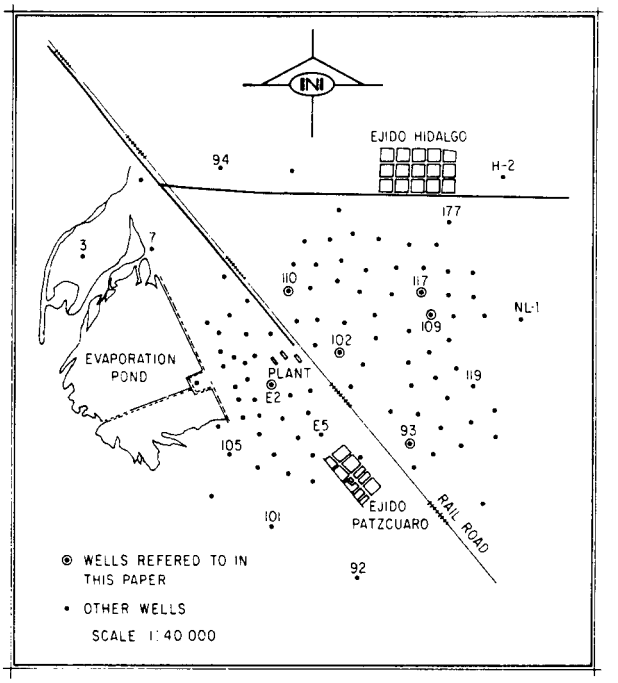


Fig. 1 Location of the processed wells from the Cerro Prieto geothermal field.

These wells were selected to satisfy the model assumption that the reservoir flow is exclusively single (liquid) phase. At the wellhead however, all these wells produce water and steam. This is because the liquid water entering the wellbore enventually flashes in its way up, due to the concomitant pressure decrease. During the production tests, from which the production characteristic curves were recorded, the wells were flown over wide ranges of wellhead pressures and flowrates. Our computations showed that, with one exception (M-93), two-phase flow developed in the reservoir around these wells at the higher flowrates. The points on the production characteristic curves corresponding to two-phase flow in the reservoir were discarded. All the results and figures in this section correspond to one-phase liquid flow in the reservoir.

The original production output curves and their transformation to bottomhole conditions are shown in Figs. 2 to 6. The corresponding re-

sults are summarized in Table 1. The excellent fits, evidenced by the high correlation coefficients, are strong evidence of the validity of the method presented here.

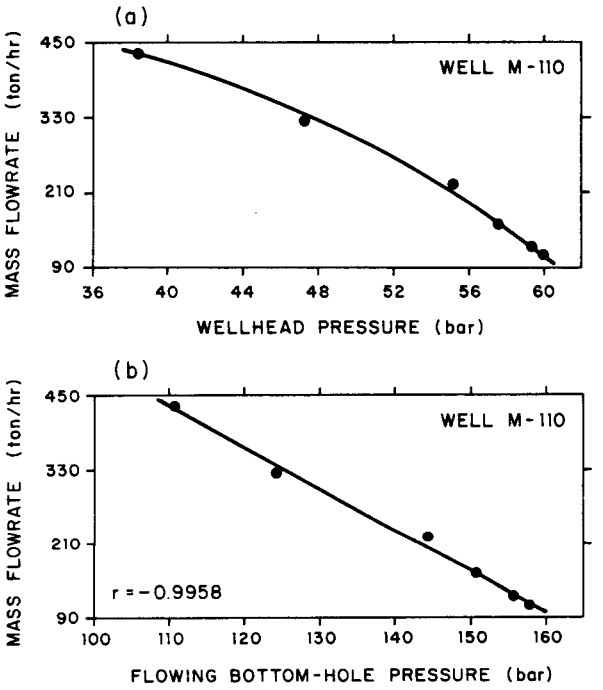


Fig. 2 (a) Characteristic curve of well M-110; (b) corresponding computed bottomhole variables, and fit to the steady-state radial liquid water flow model.

As another check on our method, we have compared the inferred reservoir pressures with measured shutin (or nearly shutin) downhole pressures. These results are shown in Table 2. The measured downhole pressures p_{meas} were corrected to the corresponding bottomhole depths by addition of the hydrostatic heads due to the differences of depth. Saturated liquid densities at the computed downhole temperatures were used in these calculations.

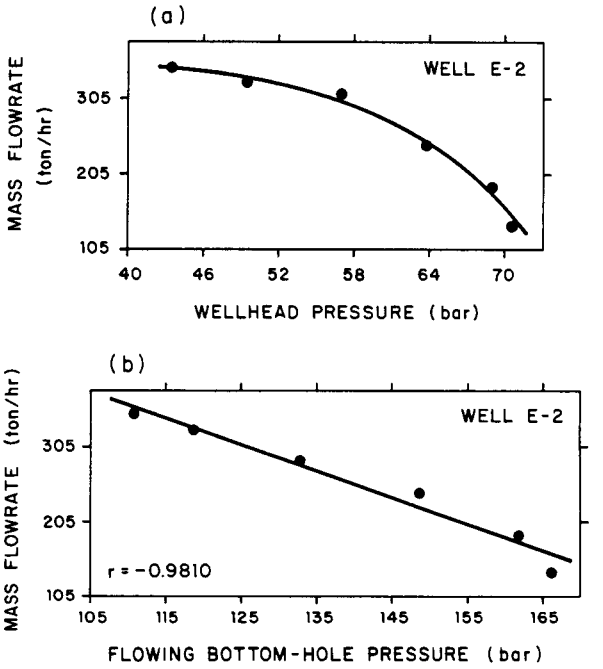


Fig. 3 (a) Characteristic curve of well E-2; (b) corresponding computed bottomhole variables, and fit to the steady-state radial liquid water flow model.

The inferred reservoir pressures agree with the measured shutin, or nearly shutin, downhole pressures to better than 17% in average. The agreement is good, considering the uncertainties involved, and the usual errors associated with alternative methods to estimate reservoir pressures. The uncertainties include errors in the measured or assumed input quantities of the

Table 1. Results of the method applied to hot water wells from the Cerro Prieto geothermal field.

Well	Correlation Coefficient	p_e (bar)	J_m (ton hr^{-1} bar^{-1})	$\bar{h}_T$ (MJ ton^{-1})	J_p^* (MW bar^{-1})
M-110	-0.9958	175.1	6.64	1411.1	2.60
E-2	-0.9810	212.1	3.53	1484.3	1.46
M-93	-0.9683	266.5	2.79	1332.5	1.03
M-109	-0.8737	316.0	2.53	1323.0	0.93
M-102	-0.9718	235.9	1.50	1488.1	0.62

*Expressed in thermal MW per bar.

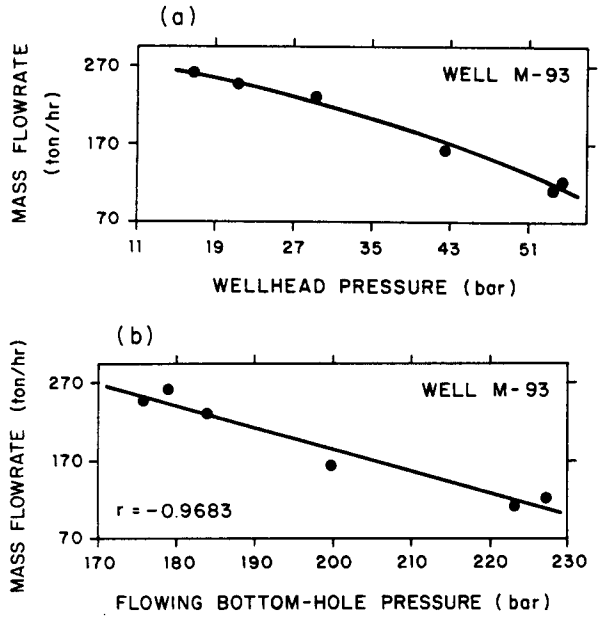


Fig. 4 (a) Characteristic curve of well M-93; (b) corresponding computed bottomhole variables, and fit to the steady-state radial liquid water flow model.

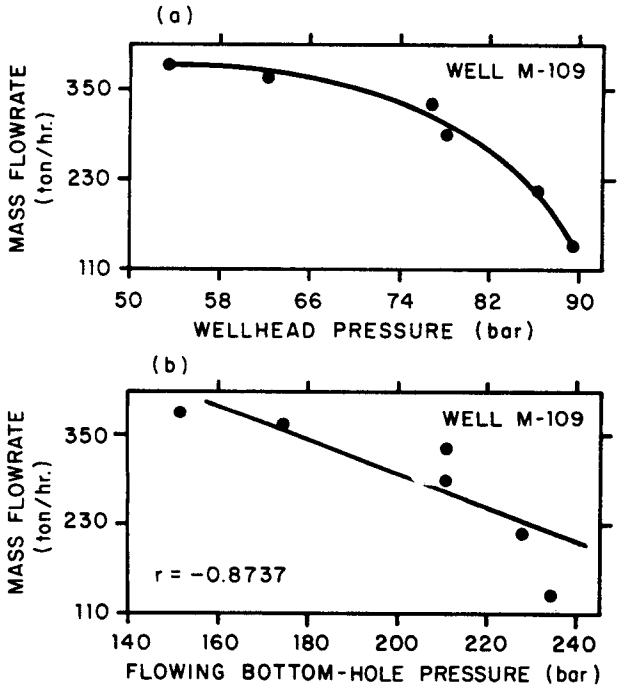


Fig. 5 (a) Characteristic curve of well M-109; (b) corresponding computed bottomhole variables, and fit to the steady-state radial liquid water flow model.

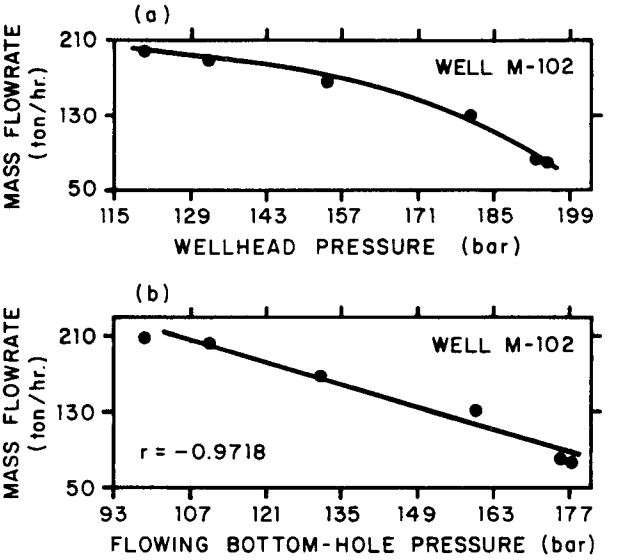


Fig. 6 (a) Characteristic curve of well M-102; (b) corresponding computed bottomhole variables, and fit to the steady-state radial liquid water flow model.

method, errors in the measured downhole pressures, and wether the measured downhole pressures represent reservoir pressures. As discussed in the previous section, errors in input variables of the method such as wellhead pressures, flowrates and enthalpies, or in the assumed inside diameters of the wells (possibly arising from scale deposits), might originate percentual errors of the order of magnitude shown in Table 2. On the other side, the measured shutin pressures, just like any other kind of measurement, are affected by instrumental and human errors. Finally, downhole pressure measurements may not represent true reservoir pressures, on two counts. First, it is often difficult to asses whether the shutin time has been long enough for equilibration. And second, geothermal shutin downhole profiles do not necessarily reflect reservoir pressure, except at the precise depth corresponding to feed points, even if shutin times are long enough (Grant, 1979; Grant et. al., 1981).

The inferred reservoir pressures shown in Table 2 appear to be systematically greater than the (corrected) measured pressures. This may be a random effect, masked by the relatively small size of the sample (5 cases), with the errors caused by the reasons discussed in the last paragraph. Alternatively, it may be a truly systematic effect introduced by the method presented here. More field data will be processed to solve this question.

Table 2. Inferred reservoir pressures vs. measured shutin (or nearly shutin) downhole pressures.

Well	MEASURED				INFERRED		DIFFERENCE
	p_{meas} (bar)	Depth (m)	Conditions	p_{corr}* (bar)	p_e (bar)	Depth (m)	$(p_e - p_{corr})/p_e$ (%)
M-110	163	1843	shutin	163.7	175.1	1854	+ 6.5
E-2	166.5	1762	flowing by ϕ=1" orifice	178.1	212.1	1946	+16.0
M-93	235	2553	flowing by ϕ=1" orifice	235.3	266.5	2558	+11.7
M-109	223	2385	flowing by ϕ=1/4" orifice	223.6	316.0	2395	+29.2
M-102	184	1900	shutin	189.6	235.9	1990	+19.6

*$p_{corr} = p_{meas}$ corrected to bottomhole depth (see text).

SUMMARY AND CONCLUSIONS

We have developed and demonstrated a method to retrieve the reservoir pressure p_e, a mass productivity index J_m, and a thermal power productivit index J_p corresponding to vertical water-fed wells from its production characteristic curves. If an estimate of the reservoir transmisivity (kh/μ) is available, our method provides a way to estimate the radius of influence of the well.

We have successfully validated the method against an ample set of field data. The quality of the agreement is very good.

The main advantages of the method are as follows: It provides a way for retrieving important reservoir information from ussually available production characteristic curves; no extra measurements are needed. Unlike traditional methods that require significantly more difficult bottomhole measurements to evaluate the reservoir pressure and the productivity index, the present method works from more easily taken wellhead measurements. Finally, the method provides important information concerning the two main aspects of geothermal resource utilization: mass and heat production.

A distinctive feature of the method described in this paper is that it combines two of the most important aspects of the geothermal resource, namely, mass and heat production. This useful feature is illustrated by the results presented in Table 1: reservoir pressures and mass productivity indexes on the one hand, and enthalpies on the other, are combined in a single parameter, the power productivity index.

The results of Table 1 show that the mass productivity indexes are mostly independent of both the reservoir pressure and the specific enthalpies. These results also show that the specific enthalpies of the wells are rather independent of the corresponding reservoir pressure. Finally, there is a strong correlation (linear correlation coefficient= +0.9969) between J_p and J_m. If representative of the whole field, these results indicate that in Cerro Prieto the controlling factor for mass and heat production is reservoir transmissivity.

AKNOWLEDGEMENTS

The authors wish to thank Ing. Arturo González S., Manager of the Subgerencia de Estudios Geotérmicos of Comisión Federal de Electricidad for his encouragement and cooperation. We are also thankfull to Ing. Alfredo Mañón M., Head of the Coordinadora Ejecutiva de Cerro Prieto for providing the field data necessary for this work. We are also indebted to the personnel of the Departamento de Evaluación de Yacimientos y Reinyección for skillfully handling data transfer and retrieval. The manuscript was accurately and professionally typed by María Eugenia Calderón. The figures drafted by Adrián Patiño.

NOMENCLATURE

a: Intercept of straight line (ton hr^{-1})

b: Slope of straight line (ton hr^{-1}/bar^2)

h: Reservoir thicknes (m)

h_T: Flowing total sprcific enthalpy (MJ ton^{-1})

$\bar{h}_T$: Flowing total specific enthalpy averaged over characteristic curve (MJ ton^{-1})

J_m: Mass productivity index (ton hr^{-1} bar^{-1})

J_p: Thermal power productivity index (MW bar^{-1})

k_s: Permeability of skin zone (md)

$\bar{k}$: Composite permeability seen by the well when there is a non-zero skin (md)

k: Permeability (md)

p_e: Reservoir pressure (bar)

p_{wf}: Sandface flowing pressure (bar)

p_{meas}: Measured shutin pressure (bar)

p_{corr}: p_{meas} corrected to bottomhole depth (bar)

r_e: Radius of influence of the well (m)

r_w: Wellbore radius (m)

r_s: Radius of the skin zone (m)

v: Specific volume of liquid water ($m^3\ kg^{-1}$)

W: Mass flowrate (ton hr^{-1})

α: Constant to accomodate different systems of units

μ: Viscosity (cp)

ν: Kinematic viscosity ($m^2\ s^{-1}$)

REFERENCES

Arellano, V. (1983) Project 1225 Estudios de Ingeniería de Yacimientos. Report IIE/11/1225/I 06/P. Instituto de Investigaciones Eléctricas. Cuernavaca, Mor., México.

Gould, T.L. (1974) Vertical Two Phase Steam-Water Flow in Geothermal Wells. J. Pet. Tech., August 1974, pp. 833-842.

Goyal, K.P., C.W. Miller and M.J. Lippmann. (1980) Effect of Measured Wellhead Parameters and Well Scaling on the Computed Downhole Conditions in Cerro Prieto Wells. Sixth Workshop Geothermal Reservoir Engineering. Stanford University, SGP-TR-50, pp. 130-138.

Goyal, K.P., C.W. Miller, M.J. Lippmann and S.P. Vonder Haar. (1981) Analysis of Cerro Prieto Production Data. Third Symposium on the Cerro Prieto Geothermal Field, Baja California, México. pp. 496-500, San Fco. Ca., U.S.A.

Grant, M.A. (1979) Interpretation of Downhole Measurements in Geothermal Wells. Ref. No. 88. Appl. Math. Div. Dep. Sci. Ind. Res., New Zealand.

Grant, M.A., Bixley, P.F., and Donaldson, I.G. (1981) Internal Flows in Geothermal Wells: Their Identification and Effect on the Wellbore Pressure and Temperature Profiles. 56th. Annu. Fall. Tech. Conf., SPE-AIME Paper SPE. 10317.

Grant, M.A., Donaldson, I.G., and Bixley, P.F. (1982) Geothermal Reservoir Engineering. Academic Press. New York, U.S.A.

James, R. (1970) Controlling Borehole Performance. United Nations Symposium on the Development and Utilization of Geothermal Resources. Pisa, Italy. Vol. 2, pp. 1502-1515.

James, R. (1980a) Estimating Maximum Discharge of Geothermal Wells. Sixth Workshop Geothermal Reservoir Engineering. Stanford University, pp. 139-144.

James, R. (1980b) Significance of the Maximum Discharging Pressure of Geothermal Wells. Sixth Workshop Geothermal Reservoir Engineering. Stanford University. pp. 145-149.

Proceedings Ninth Workshop Geothermal Reservoir Engineering
Stanford University, Stanford, California, December 1983
SGP-TR-74

TRACER RECOVERY AND MIXING FROM TWO GEOTHERMAL INJECTION-BACKFLOW STUDIES

R. M. Capuano, M. C. Adams and P. M. Wright

Earth Science Laboratory, University of Utah Research Institute
420 Chipeta Way, Suite 120
Salt Lake City, Utah 84108

ABSTRACT

Injection-backflow tracer testing on a single well is not a commonly used procedure for geothermal reservoir evaluation, and, consequently, there is little published information on the character or interpretation of tracer recovery curves. Two field experiments were conducted to develop chemical tracer procedures for use with injection-backflow testing, one on the fracture-permeability Raft River reservoir and the other on the matrix-permeability East Mesa reservoir. Results from tests conducted with incremental increases in the injection volume at both East Mesa and Raft River suggests that, for both reservoirs, permeability remained uniform with increasing distance from the well bore. Increased mixing during quiescent periods, between injection and backflow, at Raft River suggest an area near the well bore that has a hydrologic character different from the far well bore environment. Increased flow rates for East Mesa testing resulted in a general decrease in mixing. Comparison of recovery curves from the Raft River reservoir with those from the East Mesa reservoir suggests that mixing is greatest, and therefore permeability is greatest, in the fractured reservoir. These test results indicate that injection-backflow testing with tracers can be used successfully to characterize flow in the near-well bore environment.

INTRODUCTION

Injection of fluid into the ground has the potential to cause chemical effects, such as mineral precipitation or dissolution, and physical effects, such as seismic events and reservoir cooling. It is important to understand the nature of such phenomena and be able to predict the effects of injection beforehand. Increased use of injection appears to be the best solution to the problems of maintaining reservoir pressure, disposing of spent brine and preventing surface subsidence.

The U.S. Department of Energy, Division of Geothermal and Hydropower Technologies recognizes the need for research in injection. As part of their Injection Research Program, the Idaho Operations Office of DOE, the Earth Science Laboratory of the University of Utah Research Institute and EG&G, Idaho, Inc. have designed and carried out a series of field and laboratory experiments to develop new techniques useful to industry. Specifically, we have been developing methods for simultaneously determining the nature of fluid flow paths in the subsurface and the interaction of injected fluid with the reservoir rock and fluid through use of chemical tracers and geophysical surveys. The first set of field tests was carried out at Raft River, Idaho, in late 1982, and the second set, in which Republic Geothermal Inc. participated, was carried out at East Mesa, California, in the summer of 1983.

The first phase of our research, reported here, has been concerned with developing new methods that can be used with a single well. It is the usual case in a geothermal field that each well is hydrologically isolated from other wells in the same field to a greater or lesser extent. In considering a priori the several effects of interest that could be propagated between two wells, we realize that (a) a pressure transient created at one well may be observed at a second well after a certain length of time that in practice is highly variable both among fields and among wells in the same field, (b) an actual fluid packet would take a much greater time to propagate between wells, and (c) a thermal perturbation would take an even larger time to propagate between wells and, furthermore, would be unlikely to propagate at all if a fluid packet could not be propagated (neglecting the very slow thermal conduction effects). Reservoir engineering studies to date have been most concerned with treatment of the effects in (a) above, i.e. analysis of pressure transient data. Only the most advanced models today treat the chemical and physical changes that attend the movement of individual fluid packets and little application has been made of these models to geothermal fields. However, it is clear that if we are going to understand and predict thermal breakthrough (case (c)), we must understand movement of fluid packets in the reservoir.

Our field experiments have been designed to

help define movement of fluid packets around a single well. Fluid flow is set up by employing the so-called "huff-puff" technique of injecting fluid, into which suitable tracers have been introduced, and then withdrawing the fluid by backflowing. By monitoring the concentration of tracers recovered as a function of volume of fluid produced, information can be gained over and above that gained through the usual techniques of reservoir engineering measurement and analysis. These one-well tracer tests have an important advantage over two-well tracer tests in allowing us to quantify not only the dilution or mixing effects but also the chemical interaction of injected tracer and fluid with the reservoir rocks. In a two-well test if no tracer is detected at the second well from injection into the first well, one does not know whether fluid was not propagated between wells or whether the tracer was merely removed from solution by interaction in the reservoir.

This paper deals with the development of methods for the use of chemical tracers in injection-backflow testing at Raft River, Idaho, and East Mesa, California. Tracer recovery curves resulting from tests at these two sites are presented and compared. Other papers presented in these transactions deal with hydrologic evaluation of tracer recoveries from these tests (Downs and Russell), the effects of water-rock interactions on tracer behavior (Capuano), the results of laboratory experiments conducted on a physical model of a fractured reservoir (Hull and Koslow) work on development of reservoir analysis code to integrate dispersion and fracture flow (Miller), and the results of scale inhibitor experimentation conducted during injection testing (Michels).

GEOLOGIC SETTINGS

The Raft River thermal area is located in southeastern Idaho. There are two compositionally distinct thermal waters present in this system. The first is a slightly saline sodium chloride water, with dissolved solids up to 1400 ppm and measured temperatures up to 145°C. This water is found predominantly within a quartzite unit in the upper portion of the Precambrian basement. Unconformably overlying the Precambrian rocks are as much as 1600 m of Tertiary and Quaternary basin fill sediments (Blackett and Kolesar, 1983). These sediments host the second thermal water, which is also sodium chloride in character although it is more saline, with dissolved solids up to 6500 ppm, and is slightly hotter, with measured temperatures of up to 150°C.

Injection testing at Raft River was conducted on well RRGP-5, which is cased to the top of Precambrian quartzite at 1500 m. Thermal water produced from RRGP-5 is of the low-salinity type and flows predominantly from fractures in the quartzite. In the vicinity of RRGP-5 the overlying basin fill sediments are relatively impermeable and thermal water in the sediments around RRGP-5 is the low-salinity water believed to have traveled to the surface along faults in the sediments.

Well RRGE-3, which was used as the supply well for injection testing, is located approximately 2400 m from the injection well, RRGP-5. Thermal water produced from RRGE-3 is a mixture of the two thermal water types, and, therefore, is compositionally distinct from water encountered in the reservoir around injection well RRGP-5. This compositional difference can be used as a natural tracer for injection testing.

The East Mesa geothermal system is located in the Imperial Valley of southern California. The thermal reservoir occurs in a thick sequence of up to 4 km of clastic deltaic and lacustrine deposits of Tertiary and Quaternary age (Coplen, 1976). Hydrologic flow in the area is generally horizontal, with faults contributing to vertical permeability and recharge of thermal fluids (Bailey, 1977).

Two East Mesa wells were selected for injection-backflow testing, 56-19 and 56-30. These wells are located approximately 1600 m apart. Waters drawn from these wells have distinctly different compositions. Water flowing from 56-19 is 126°C, sodium chloride in character, with dissolved solids up to 5800 ppm. This solution is flowing from casing perforations extending between 800 m and 1400 m. Well 56-30 discharges a hotter, 174°C, less saline sodium chloride water, with 2700 ppm dissolved solids. This water is encountered at greater depth, 1600 to 2200 m, than 56-19 thermal water.

The supply well used for East Mesa testing, 38-30, is located only 600 m from well 56-30 and draws water of composition similar to well 56-30 from a similar depth.

TESTING

A total of eight injection-backflow tests were conducted on well RRGP-5 at the Raft River geothermal site. At East Mesa a total of four injection-backflow tests were conducted, one on well 56-30 and three on well 56-19. Several parameters can be altered during injection-backflow testing to aid in evaluation of the hydrodynamics of a geothermal reservoir. These parameters include: 1) chemical character of the tracer solution; 2) temperature of the tracer solution; 3) flow rate, during both injection and backflow; 4) quiescence time between injection and backflow; and 5) volume of tracer solution injected. During testing at Raft River and East Mesa, each of these parameters was varied. Table 1 lists a summary of the test conditions.

The chemical character of the injected solution was controlled by the composition of water from the supply well and the quantity of artificial tracers added to the water. In most cases, the supply well water was chemi-

TABLE 1. RAFT RIVER AND EAST MESA INJECTION-BACKFLOW TEST CONDITIONS

TEST	INJECTION				QUIESCENCE (hours)
	WELL	VOLUME (liters)[a]	RATE (liters/sec)	TEMP. (°C)	
RAFT RIVER					
2 Series					
2A-2	RRGP5	6.3×10^4	9.5	122	0
2C	RRGP5	1.5×10^6	9.5	122	0
2D	RRGP5	3.3×10^6	9.5	122	0
4 Series					
4A	RRGP5	1.1×10^4	9.5	122	28
4B	RRGP5	7.2×10^3	9.5	122	2
4C	RRGP5	6.1×10^3	9.5	122	12
4D	RRGP5	9.9×10^3	9.5	122	50
5 Series					
5	RRGP5	1.3×10^7	9.5	122	80
EAST MESA					
3(56-30)	56-30	7.1×10^5	19	93	12
3(56-19)	56-19	7.1×10^5	19	93	12
4(56-19)	56-19	7.5×10^5	32	93	13
6(56-19)	56-19	1.6×10^6	32	93	12

[a] Less volume remaining in the cased portion of the wellbore.

cally distinct from the reservoir water in the vicinity of the injection well. This compositional difference provided a suite of natural tracers such as Na, K, Ca, SiO_2, Cl, SO_4 and HCO_3. Artificial tracers added to the injected solution, both continuously and as slugs, were used to give the injected solution a distinct chemical composition for each test, thereby allowing prediction of contamination by solution unrecovered from previous tests. In addition, artificial tracer slugs were added at various times during injection to aid in understanding the effects of mixing on solution traveling different distances into the formation. Artificial tracers included Cl, Br, I, SCN (thiocyanate), B, Mg, K, Li and the organic dyes, disodium fluorescein and rhodamine-B. The composition of the injected solution and the use of artificial tracers are discussed in more detail by Capuano (1983).

TRACER RECOVERY

The variation in composition of the recovered solution reflects the amount of mixing that has taken place in the reservoir. To produce a mixing curve for each tracer, the fraction of tracer recovered in individual water samples was calculated using the mixing relationship, $X = (C_b - C_r)/(C_i - C_r)$, where "X" is the fraction of injectate in the backflow sample, and "C" is the concentration of tracer in the backflow sample, (b), reservoir water (r), and injection water (i).

The injection concentration, C_i, was taken as the average concentration in the injected solution. The concentration of the element in the reservoir water, C_r, was taken from analysis of water collected from the injection well prior to injection testing. Before testing began each of the injection wells was backflowed for up to 24 hours, while the water chemistry was monitored, to ensure that the reservoir would produce water with a relatively uniform composition. If less than 100% of the injected solution was recovered during backflow of any given test, natural and artificial tracers remained in the reservoir. These tracers were a source of contamination during subsequent injection tests. For all tests, with the exception of the Raft River 4 Series tests (see Table 1), the amount of solution injected was much greater than the amount of contamination from previous tests. Contamination, therefore, was assumed to have little effect on the character of tracer recovery from these tests. The Raft River 4 Series tests, however, had relatively small injection volumes ranging from 6000 to 11000 liters. Contamination of the reservoir by previous tests, therefore was relatively important. To account for this contamination, a corrected reservoir concentration equivalent to the concentration of that element in the last backflow sample, was used to calculate mixing.

Besides mixing, other processes can affect tracer concentrations in the recovered solution. These include tracer gains or losses as a result of adsorption or desorption, ion exchange, mineral dissolution or precipitation, and in the case of the organic dyes, disodium flourescein and rhodamine-B, thermal instability. Because these processes can have a substantial effect on tracer recovery, it is important to account for the resulting gains or losses in preparation of mixing curves. One means of doing this is to use a "conservative" tracer, one which is relatively unaffected by these processes. Ultimately the extent of these various effects on other tracers may then be estimated by comparing the recovery curves of conservative and nonconservative tracers.

An ideal conservative tracer is one which is unreactive with the geologic formations present in the study area, is not present in the rocks in a form that is readily released into the tracer solution, and whose concentration in the tracer solution can be well documented. For testing at Raft River the natural tracer Cl appears to best fit these criteria. Its solubility in natural waters is well above the maximum concentration of 3000 ppm injected during testing. Because Cl is not greatly affected by adsorption, desorption and ion exchange, minor gains and losses resulting from these processes would be relatively small compared to the high Cl concentrations in the injectate. In addition, Cl-bearing minerals were not identifed in the reservoir rocks in the vicinity of RRGP-5 (Blackett and Kolesar, 1983) and therefore Cl gains resulting from mineral dissolution were not of concern.

A generalized mixing curve for each Raft River test was, then, derived from a visual estimation of a best fit Cl curve. This is done under the assumption that the fraction

of conservative tracer in the recovered solution is proportional to the fraction of injectate in the recovered solution. Generalized mixing curves for the 2 Series tests and Test 5 are presented in Figure 1 and will be discussed below. The 4 Series curves are not presented because of space limitations. For further discussion of the 4 Series test results see Downs and Russell (1983).

Preliminary mixing curves for East Mesa injection-backflow tests are presented in Figure 2. Calculation of generalized mixing curves for East Mesa testing is not as straightforward because the presence of evaporite minerals in the reservoir rocks may not allow Cl to act conservatively. These and other problems will be evaluated further upon completion of additional analyses.

WELL-BORE RECOVERY

The effects of water-rock reactions and mixing are minimal in solution confined to the cased portion of the well bore. Therefore, the tracer content of the final solution injected into the well bore should equal the tracer content of the initial solution removed from the well bore. This comparison provides a unique opportunity to evaluate errors in data collection. For example, errors in chemical analyses or in measurement of flow rates, mixing in the well bore and accidental flow during quiescent periods are all potential problems that can be evaluated.

Comparison of the mass of the conservative tracer Cl, and for Raft River, Na and K, injected into and recovered from the cased portion of the well bore (hereafter called "well-bore recovery") shows less than 7% error for all Raft River and East Mesa injection-backflow tests, excepting Raft River Tests 4A, 4D and 5. Considering analytic precision, which ranges from 3 to 5%, and the probable 5% or greater error on flow rate determinations, these comparisons are surprisingly close.

Poor well-bore recoveries for Raft River Tests 4A, 4D and 5 are believed to be the result of backflow that occurred accidentally during the quiescent period. Solution lost from the well bore during quiescence is replaced with mixed water from the reservoir, thereby accounting for these poor comparisons. The exact volume of solution backflowed during the quiescent period for each of these tests is unknown.

RESULTS

Three test series were run on Raft River well RRGP-5. For the 2 Series tests all variables were held constant except injection volume, which was increased from 6.3×10^5 liters during Test 2A-2, to 1.5×10^6 liters during Test 2C, and to 3.3×10^6 liters during Test 2D. The shapes of the recovery curves from these three tests are very similar, indicating an almost exponential increase in mixing with increased backflow. These results suggest that the portion of the reservoir involved in testing is responding uniformly to the different injection volumes. Normalization of the recovery curves with respect to injection volume (Figure 3) shows that they not only have similar shapes but also overlap. The good agreement between the normalized recovery curves suggests that mixing varied in proportion to the volume of solution injected, and that the rate of mixing of the injected and reservoir waters was independent of the distance traveled by the solution. It is therefore concluded that the portion of the reservoir tested has uniform permeability. These generalizations, of course, only apply to the portion of the reservoir around RRGP-5 penetrated by the maximum volume of water involved in testing.

The addition of tracer slugs at various times during an injection test can also be useful in evaluating the character of a reservoir. Two five-minute tracer slugs were added to the injectate during Test 2D: an I slug was added at the start of injection and a B slug was added after one third of the injection was completed. Recovery curves for I and B, normalized with respect to the volume of solution injected after each respective slug, are shown in Figure 4. Despite the different injection schedules, there is excellent agreement between the normalized volumes of recovery needed for return of both tracer slugs. Furthermore, the slopes of these normalized recovery curves are very similar. The similarity of the response of these tracer slugs to mixing, independent of the distance traveled in the reservoir, further supports the conclusion that the portion of the reservoir tested has uniform permeability.

Raft River Test 5, which involved an injection volume of 1.3×10^7 liters (four times greater than that of Test 2D) can be compared with results of the 2 Series tests. In addition to injection volume, Test 5 also differed from the 2 Series tests by one other parameter, namely, the presence of a quiescent period between injection and backflow. Test 5 involved 80 hours of quiescence, whereas the 2 Series tests involved no quiescence. There are two distinct parts of the Test 5 recovery curve. The first is the curve for the initial 1.7×10^5 liters of backflow, which differs markedly from the 2 Series recovery curves. The second is the remaining backflow, beyond 1.7×10^5 liters, which in contrast, produces a recovery curve similar in trend to those of the 2 Series (Figure 1). These similarities are also apparent on Figure 4, which shows the normalized recovery curves. The Test 5 results, therefore, further support the conclusion of a uniform permeability reservoir. The Test 5 normalized recovery curve is however, slightly offset from the curves for Tests 2D

and 2C. This suggests a trend of slightly increased mixing rate with increased injection volumes used for Test 5.

The similarity of the latter portion of the Test 5 recovery curve with those of the 2 Series suggests that the initial portion of the Test 5 recovery curve should also be similar to the 2 Series curves if injection volume was the only parameter varied. The apparent truncation of the initial portion of the Test 5 recovery curve is therefore believed to be a product of increased mixing due to hydrologic effects during the 80 hour quiescent period.

At East Mesa, four injection-backflow tests were conducted. The first two, 3(56-30) and 3(56-19), were identical tests conducted on different wells in order to compare recovery curves from tests conducted on different portions of the reservoir. The recovery curves resulting from these two tests (Figure 2) show that less mixing has taken place in the reservoir surrounding 56-30 than in the reservoir surrounding 56-19. Preliminary calculation of the percentage of injectate recovered shows that, with a similar volume of backflow, 95% of the injectate was recovered from Test 3(56-30), whereas only 85% of the injectate was recovered from Test 3(56-19). This further supports the premise of less mixing during Test 3(56-30).

The remaining two East Mesa tests were both conducted on well 56-19. Test 4(56-19) was similar to Test 3(56-19) with the exception that the flow rate was nearly doubled for Test 4(56-19) (from 19 liters/sec (300 gal/min) to 32 liters/sec (500 gal/min)). Comparison of the recovery curves from these two tests shows that doubling the flow rate resulted in slightly less mixing.

Test 6(56-19) was run under the same test conditions as Test 4(56-19) (with the faster flow rate), with the exception of injection volume, which was doubled. Comparison of the recovery curves from Test 4(56-19) and Test 6(56-19) indicates that mixing varies in proportion to the volume of solution injected. This is further supported by the similarity in the recovery curves when normalized with respect to injection volumes for Tests 6(56-19) and 4(56-19) (Figure 5). The relationship between injection volume and mixing is similar to that noted for the Raft River tests, and suggested that the volume of reservoir tested has uniform permeability.

Comparison of the recovery curves from testing in the Raft River reservoir, in which fracture flow dominates, and the East Mesa reservoir, in which dispersive flow dominates, is difficult because of the preliminary nature of the East Mesa test results and the wide variation in parameters used. A general comparison of the normalized East Mesa recovery curves for Tests 3(56-19) and 3(56-30) with those of the Raft River 2 Series tests (Figures 3 and 5), suggests lesser mixing in the matrix-controlled East Mesa reservoir and therefore suggests lower permeability.

East Mesa Tests 3(56-19) and 3(56-30) were conducted with a flow rate of 19 liters/ sec, double that used for Raft River tests (9.5 liters/ sec.). As shown from East Mesa testing, an increase in flow rate resulted in a decrease in mixing in the porous reservoir. The effect of flow rate in the fractured reservoir was not tested. A portion of the decreased mixing noted in the East Mesa reservoir as compared to Raft River could be the result of the faster flow rate. On the other hand, East Mesa Tests 3(56-19) and 3(56-30) involved a 12-hour quiescent period, whereas the Raft River 2 Series tests involved no quiescence. In the Raft River reservoir it was found that increased quiescence could result in increased mixing. It is believed that a detailed evaluation of East Mesa tracer recoveries including that of tracer slugs, will allow a better comparison of these reservoirs.

CONCLUSIONS

Injection-backflow tracer tests have been used successfully in both fracture- and matrix-dominated geothermal reservoirs. Testing in the fractured reservoir at Raft River indicated that the portion of the reservoir tested has a relatively uniform permeability. This reservoir of uniform permeability, however, can be divided into a portion near the well bore in which hydrologic effects during quiescence resulted in increased mixing between the injectate and reservoir solution. At greater distances from the well bore increased quiescence had very little effect on mixing.

The maxtrix-controlled East Mesa reservoir also appears to have regions of near uniform permeability around the two wells tested. Results from tests on wells penetrating different portions of the reservoir, however, suggest that different areas of the reservoir have different permeabilities. In addition, it was found that, in the porous East Mesa reservoir, an increase in flow rate resulted in a decrease in mixing.

Comparison of the test results from the matrix-dominated reservoir at East Mesa with those of the fracture-dominated reservoir at Raft River suggests that at East Mesa the rate of mixing and therefore permeability is lower than at Raft River.

ACKNOWLEDGEMENTS

We wish to thank the employees of UURI, EG&G Idaho, Republic Geothermal and Westec Services who contributed to the success of this program. In particular, we would like to acknowledge the assistance of Frank Bakke, Gary Berglund, Richard McAtee, Joe Moore, Ruth Kroneman and Keith Yorgason, whose hard work, ideas and criticisms were invaluable contributions. This work was supported under

DOE Contract No. DE-AC07-80ID12079.

REFERENCES

Bailey, T. P. (1977), "A hydrogeological and subsurface study of Imperial Valley geothermal anomalies, Imperial Valley, California", University of Colorado, M.S. Thesis, 100 p.

Blackett, R. E., and Kolesar, P. T. (1983), "Mineral zonation within the Raft River geothermal system," Geothermal Resources Council Transactions, v. 7, p. 123-128.

Capuano, R. M. (1983), "Tracer behavior in geothermal systems", 9th Workshop on Geothermal Reservoir Engineering, Stanford, in press.

Coplen, T. B. (1976), "Cooperative geochemical resource assessment of the Mesa geothermal system", Inst. Geophysics and Planetary Physics, Univ. Calif. Riverside Report IGPP-UCR-76-1, 97 p.

Downs, W. F. and Russell (1983), "Response of the Raft River reservoir to injection-backflow studies", 9th Workshop on Geothermal Reservoir Engineering, Stanford, in press.

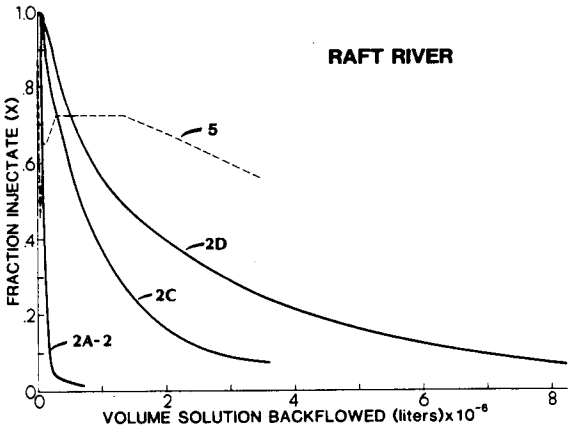


Figure 1. Recovery curves, Raft River tests.

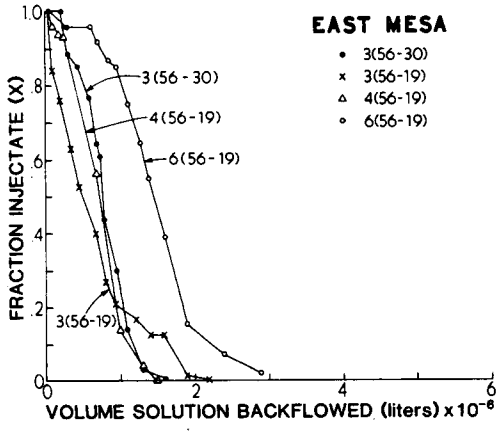


Figure 2. Preliminary recovery curves, East Mesa tests.

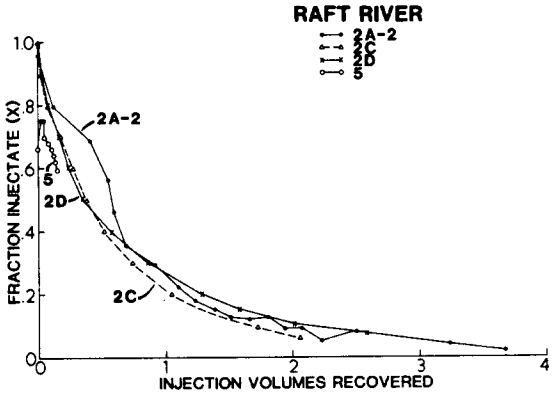


Figure 3. Recovery curves normalized with respect to injection volume, Raft River tests.

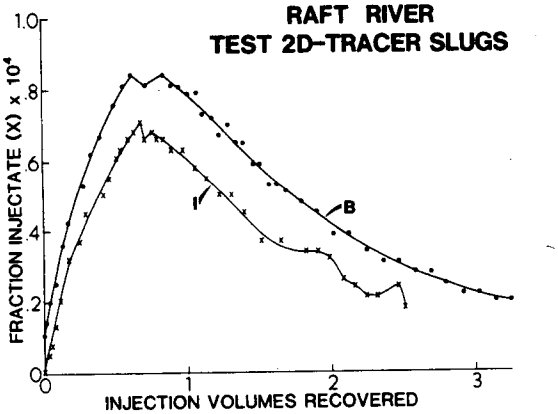


Figure 4. Tracer slug recovery curves normalized with respect to injection volumes, Raft River Test 2D.

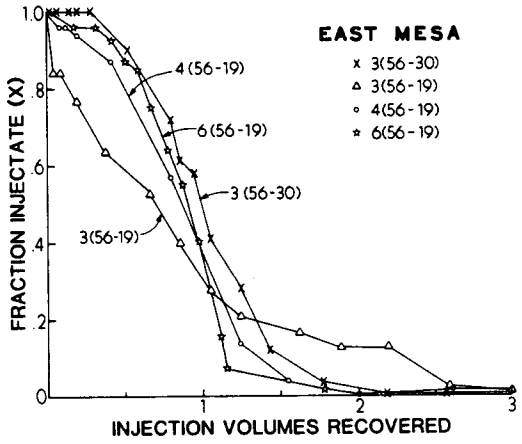


Figure 5. Recovery curves normalized with respect to injection volume, East Mesa tests.

Proceedings Ninth Workshop Geothermal Reservoir Engineering
Stanford University, Stanford, California, December 1983
SGP-TR-74

PHYSICAL MODEL OF A FRACTURED RESERVOIR

Laurence C. Hull and Karen N. Koslow

EG&G Idaho, Inc.
P.O. Box 1625
Idaho Falls, ID 83415

ABSTRACT

The objectives of the physical modeling effort are to: (1) evaluate injection-backflow testing for fractured reservoirs under conditions of known reservoir parameters (porosity, fracture width, etc.); (2) study the mechanisms controlling solute transport in fracture systems; and (3) provide data for validation of numerical models that explicitly simulate solute migration in fracture systems. The fracture network is 0.57-m wide, 1.7-m long, and consists of two sets of fractures at right angles to one another with a fracture spacing of 10.2 cm. A series of injection-backflow tests, similar to those performed at the Raft River Geothermal field, was conducted. These included variable volume injection and injection-backflow tests with varying quiescent periods between injection and backflow. This latter series of tests was conducted with a range of flow fields passing through the model. Tracer recovery is related to the flow field in the physical model and model parameters. Longer quiescent times and greater flow fields result in a lower tracer recovery. A plot of the fractional tracer recovery against quiescent time results in a straight line. This relationship, combined with classical reservoir engineering data, can be used to predict aquifer flow rate and porosity from known injection volumes and tracer recovery.

INTRODUCTION

Injection of spent geothermal fluids for environmental purposes or to maintain reservoir pressures can also have the detrimental effect of lowering the enthalpy of production fluids. In fields, such as Wairakei in New Zealand and Kakkonda and Hatchobaru in Japan, interconnection between injection and production wells appears to be along highly transmissive fractures (Fossum and Horne, 1982; Horne, 1982). Rapid breakthrough of injected fluids at production wells has resulted in significant enthalpy declines and required modifications in field operations. Such situations, where interwell travel times are on the order of days, can readily be studied using tracer tests between wells.

As travel times between wells become longer, the increased residence time permits greater thermal equilibration between injected fluids and reservoir rock. However, enthalpy loss can still occur after several years of plant operation, such as at Onikobe and Otake in Japan (Horne, 1982). It is important to be able to predict such effects in advance. Where residence times in the reservoir are on the order of several months or more, interwell tracer tests may not be feasible. Single-well tracer tests, combined with traditional reservoir assessment methods, can provide information on flow rates and reservoir porosity that can be used to predict future thermal breakthrough.

Methodology for interpretation of interwell tracer tests is well established (Lenda and Zuber, 1970; Grove and Beeten, 1971; Vetter and Zinnow, 1981). Single-well injection-backflow tests have been used to study the dispersion and adsorption characteristics of porous media reservoirs (Sternau et al., 1966; Drever and McKee, 1980; Pickens et al., 1981). Recently, methods have been developed to study interwell tracer tests in fractured reservoirs where well connections are along one or a few major fractures (Fossum and Horne, 1982; Horne and Rodriguez, 1983). Ground-water flow rates can be measured in a borehole using tracer injection techniques; however this flow rate could be very misleading in a fractured reservoir. This paper discusses a method for determining reservoir flow rate and porosity for a finite volume of reservoir and demonstrates its effectiveness using data collected from a laboratory-scale physical model of a fracture network.

METHOD DEVELOPMENT

For injection into a confined geothermal aquifer or into a planar fracture zone, the plume of injected fluid moves out radially from the injection well (Figure 1). If the well is shut in after the plume has been injected, the flow field will begin to carry the plume away from the well. When the well is pumped, after a quiescent time, not all of the initially-injected fluid is recovered after an equal volume has been pumped from

the well. The fraction of the fluid recovered is represented in Figure 1 by the shaded area where the two circles overlap. The fractional recovery is given by:

$$F = \frac{A_O}{A_T} \tag{1}$$

where

F = fractional tracer recovery

A_O = area of overlap

$$= 2[R^2 \cos^{-1}(d/R) - d(R^2 - d^2)^{1/2}] \tag{2}$$

A_T = area of injected plume

$$= \pi R^2 \tag{3}$$

Replacing A_O and A_T in Equation 1 by Equations 2 and 3 and simplifying gives:

$$F = \frac{2}{\pi}\left(\cos^{-1}\xi - \xi(1-\xi^2)^{1/2}\right) \tag{4}$$

where

$$\xi = d/R. \tag{5}$$

The relation between ξ and F is not linear over the entire range of ξ from 0 to 1. However, for the range $0 < \xi < 0.6$, the relation between ξ and F is well described by the equation:

$$\xi = 0.825(1-F). \tag{6}$$

Lateral displacement of the plume is 2d and equals:

$$2d = vt_q \tag{7}$$

where

v = flow-field velocity

t_q = quiescent time.

The radius of the injection plume is proportional to the volume of water injected,

$$R = \left(\frac{V}{\pi h \theta}\right)^{1/2} \tag{8}$$

where

V = volume of water injected

h = aquifer or fracture zone thickness

θ = porosity.

Fractional recovery can be related to reservoir parameters by combining Equations 5, 6, 7, and 8 to give:

$$(1-F) = 0.605\, v\left(\frac{V}{\pi h \theta}\right)^{-1/2} t_q . \tag{9}$$

By conducting a series of equal volume injection-backflow tracer tests with various quiescent times, a linear relation should be described between fractional tracer recovery and quiescent time. The slope of the relation is proportional to flow-field velocity and reservoir porosity.

Equation 9, unfortunately, still contains two unknowns, porosity and flow-field velocity. However, combining data collected from injection-backflow tests with traditional reservoir engineering data provides sufficient information for identification of both unknowns.

From geophysical logs, the thickness of the aquifer or fracture zone (h) can be estimated. Pump tests can then provide the hydraulic conductivity of the formation. If the hydraulic gradient of the reservoir in the vicinity of the well can be estimated, then the specific discharge can be calculated from Darcy's Law.

$$q = -KI \tag{10}$$

where

q = $v\theta$ = specific discharge

K = hydraulic conductivity

I = hydraulic gradient.

This gives two equations and two unknowns, and a unique solution for reservoir flow-field velocity and porosity can then be determined.

Two factors will complicate the use of the above outlined procedure and limit the conditions under which Equation 9 can be used. In the presence of a flow field, the injected plume will become distorted, with the distance to the upstream edge of the plume being shorter than the distance to the downstream edge. This will decrease the quantity of tracer recovery. This effect can be minimized by injecting and backflowing at a rate that dominates the flow field in the reservoir.

Another factor affecting tracer recovery is dispersion at the boundary between the plume and the native reservoir fluid. Intermixing between the two fluids produces a gradual interface rather than the abrupt interface shown in Figure 1.

Equation 9 may be easily used if its relative simplicity is retained. Including the effects of tracer dispersion and distortion of the plume by the flow field would add

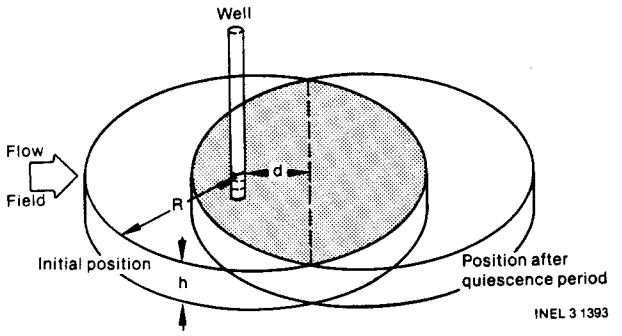


Figure 1. Schematic showing movement of an injected plume due to a flow field in the reservoir.

complexity and decrease reliability by adding additional unknown parameters. The effects of plume movement and tracer dispersion during injection and backflow can be quantified by conducting a test with no quiescent period. Effects of dispersion and movement of the plume during injection and backflow can be accounted for if tracer recovery during this no-quiescence test is used as the basis for calculating fractional recovery rather than the original quantity of tracer injected. All tests, therefore, must be of equal volume and equal injection-backflow rates. Not accounted for, is the dispersion of tracer as it moves under the influence of the flow field during quiescence. This latter factor is of secondary importance unless flow-field velocities are quite high.

PHYSICAL MODEL

To test this reservoir evaluation method, data were collected from a laboratory-scale fracture network. Injection-backflow tests were conducted at constant rate and volume in a simulated fracture network. The series of tests was carried out for a range of quiescent times for each of three different flow fields. This provided data to be compared to theory under circumstances where all reservoir parameters were known.

Description of Physical Model

The fracture network was built by cutting orthogonal fractures 0.32-cm wide and 1.91-cm deep into a 2.54-cm thick sheet of plexiglass (Figure 2). Fracture spacing is 10.16 cm, and fractures intersect the boundaries at 45 degrees. All fractures have uniform aperture and spacing. Plexiglass was selected as the material for model construction to allow for visual observation of tracer movement and because the matrix material is impermeable. Flow is evenly distributed to fractures at the inlet and collected from fractures at the outlet by manifolds. Piezometers and conductance probes are installed at various locations throughout the model to measure hydraulic gradients and tracer concentrations, respectively.

The flow field in the model is controlled by head loss between two constant head reservoirs and measured with a flow meter. Reservoir fluid is distilled water, dyed yellow, with a specific conductance of 10 μs. Injection is controlled by a syringe pump, and backflow by a third constant-head reservoir and a second flow meter. The injected fluid is a dilute sodium chloride solution, dyed blue, with a conductance of about 60 μs.

Conductance electrodes embedded in the fractures measure the breakthrough curves for the injected sodium chloride solution. A computerized data acquisition system allows point measurements of conductance to be made within a few seconds of each other. Data are recorded on a Hewlett-Packard 1000 computer and stored on magnetic tapes that can be transferred to the Cyber 176 computer for analysis.

Model Testing

Hydrologic testing was performed to determine the hydraulic conductivity of the model. Injection-backflow testing was performed to obtain time variations in tracer concentration data. A series of tests with variable quiescent periods was run to determine if reservoir flow velocity and porosity could be determined by the method outlined previously.

The hydraulic conductivity of the model was determined to be 25.65 ± 2.73 cm/sec. Hydraulic conductivity for a set of parallel fractures is given by (Freeze and Cherry, 1979):

$$K = \frac{\gamma}{\mu} \frac{N(2b)^3}{12} \qquad (11)$$

γ = specific weight

μ = dynamic viscosity

N = fracture density

$2b$ = fracture aperture.

Equation 11 is also valid for two sets of fractures having equal apertures that meet at 90 degrees. The calculated hydraulic conductivity for the physical model is 28.48 cm/sec at 25°C. There is an additional head loss of about 10% in the model over that predicted by theory.

Five tests, each with a different quiescent period, were run with three different flow-field velocities in the physical model (Table 1). Results from the test series conducted at a flow field of 1.57 cm/min are shown in Figure 3. For an injected volume of

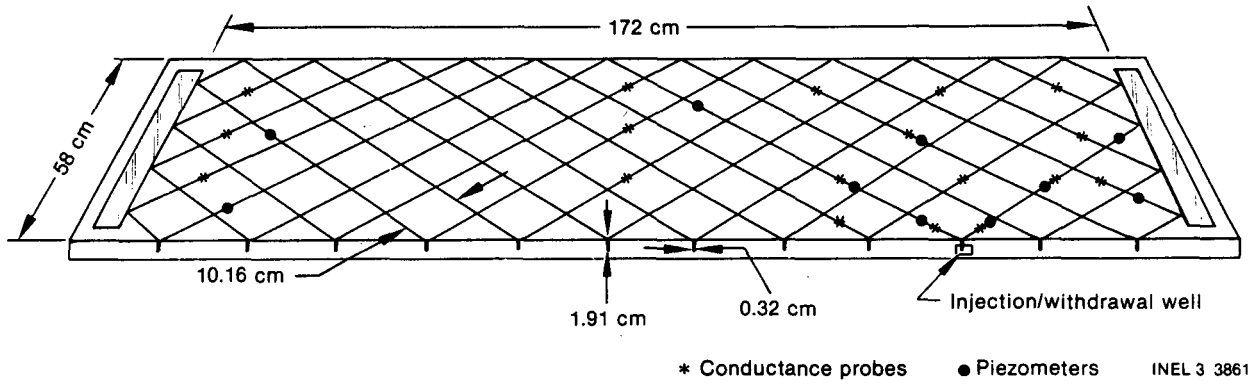


Figure 2. Fracture network used for variable quiescent time injection-backflow tests. Flow field is from right to left.

TABLE 1. QUIESCENCE TESTING SUMMARY

Injected Volume (cm^3)	Flow Field (cm/min)	Quiescent Times (min)	Injection-Backflow Rate (cm^3/min)
120	0.77	0, 1, 7, 15, 19	20
120	1.57	0, 3, 6, 10, 14	20
120	4.35	0, 1, 3, 3.33, 5	20

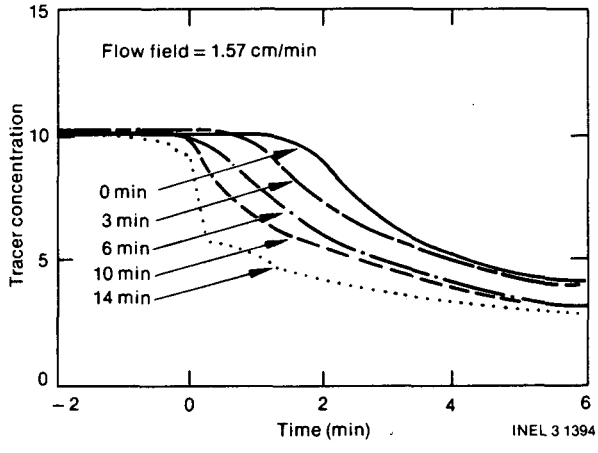


Figure 3. Tracer recovery curves at the injection-backflow port for different quiescent times. Reservoir flow field is 1.57 cm/min. Time = 0 refers to the beginning of backflow.

120 cm^3, the radius of the plume is 25 cm. With a flow field of 1.57 cm/min, it takes 16 min for the plume to move away from the injection well. From Figure 3, it can be seen that as quiescent time increases, the concentration curve drops off more rapidly. At a quiescent time of 14 min, the dropoff is immediate, indicating that the plume has already moved past the injection-withdrawal port. This difference is due to distortion of the injected plume by the flow field.

Because the curves drop off more rapidly with increasing quiescent times, fractional tracer recovery decreases. Tracer recovery was determined by integrating the area under the normalized tracer breakthrough curves. The zero quiescent-time curve was defined equal to 100%, and fractional recoveries calculated relative to that value.

Data collected from the physical model are plotted in Figure 4, along with predicted relations based on Equation 9 using known model parameters. To determine how well the data fit the model, linear regression was used to determine the best fit slope for the three sets of data points. A velocity was calculated from the best fit slopes and compared to the known flow-field velocities. The discrepancy between calculated velocities and known flow-field velocities is +30% for 4.35 cm/min and +20% for 1.57 cm/min. There is no significant difference between known and calculated velocities for 0.77 cm/min.

One of the assumptions upon which the derivation of Equation 9 is based is that the injection plume will be roughly circular. That is, the distortion caused by the presence of the flow field will be minor. This was not the case for the physical model tests with flow fields of 1.57 and 4.35 cm/min. The head change at the injection port is on the order of 2×10^{-2} cm. The head loss across the model for flow fields of 4.35, 1.56, and 0.77 cm/min is 3.1×10^{-2}, 2.0×10^{-2}, and 0.5×10^{-2} cm. Therefore, at the two higher flow rates, the injection plume is significantly distorted during injection. The successful application of the method, therefore, depends on dominating the reservoir hydraulic gradient with the cone of impression (depression) during injection (backflow).

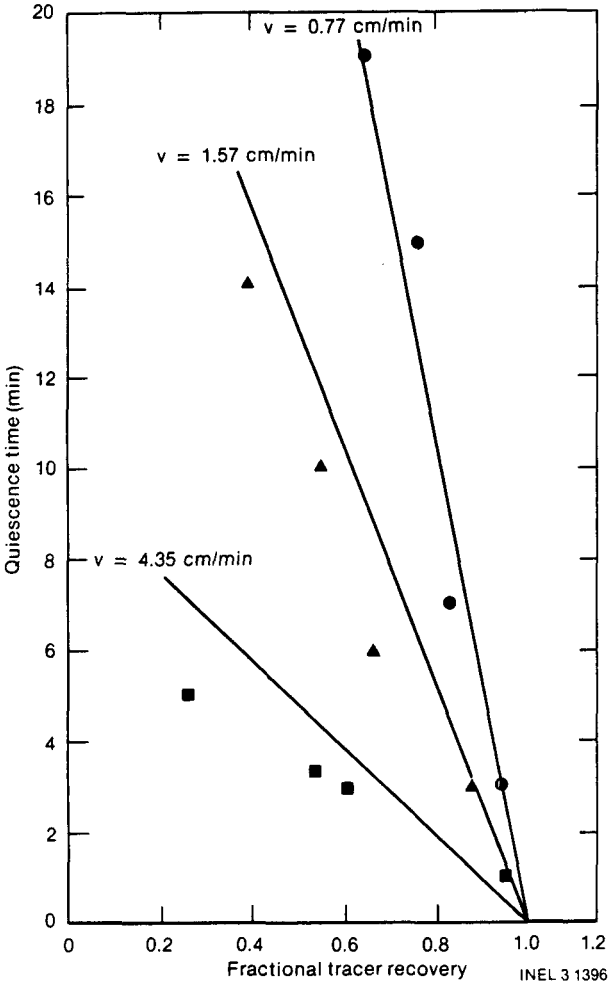


Figure 4. Predicted and measured relations between fractional tracer recovery and quiescent time for three flow-field velocities.

CONCLUSIONS

Single well injection-backflow tests using tracer solutions can provide valuable reservoir information when interwell tracer tests are not feasible. A method for determining reservoir flow-field velocity and porosity has been developed and tested against data collected from a laboratory-scale physical model. Agreement between measured and predicted values is excellent when the injection-backflow rate is much larger than the reservoir flow field. When reservoir flow rate equals or exceeds the injection-backflow rate, reservoir flow velocities are overestimated and porosities underestimated.

ACKNOWLEDGMENT

This work is supported by the U.S. Department of Energy under contract No. DE-AC07-76ID01570.

REFERENCES

Drever, J. I. and C. R. McKee (1980), "The Push-Pull Test, A Method of Evaluating Formation Adsorption Parameters for Predicting the Environmental Effects on In-Situ Coal Gasification and Uranium Recovery," In-Situ, 4, pp. 181-206.

Fossum, M. P. and R. N. Horne (1982), "Interpretation of Tracer Return Profiles at Wairakei Geothermal Field Using Fracture Analysis," Geothermal Resources Council, Transactions, 6, pp. 261-264.

Freeze, R. A. and J. A. Cherry (1979), Groundwater, Prentice-Hall, Inc., Englewood Cliffs, NJ.

Grove, D. B. and W. A. Beeten (1971), "Porosity and Dispersion Constant Calculations for a Fractured Carbonate Aquifer Using the Two Well Tracer Method," Water Resources Research, 7, pp. 128-134.

Horne, R. N. (1982), "Geothermal Reinjection Experience in Japan," Journal of Petroleum Technology, 34, pp. 495-503.

Horne, R. N and F. Rodriguez (1983), "Dispersion in Tracer Flow in Fractured Geothermal Systems," Geophysical Research Letters, 10, pp. 289-292.

Lenda, A. and A. Zuber (1970), "Tracer Dispersion in Groundwater Experiments," in Isotope Hydrology 1970, International Atomic Energy Agency, Vienna, pp. 619-637.

Pickens, J. F., R. E. Jackson, K. J. Inch, and W. F. Merritt (1981), "Measurement of Distribution Coefficients Using a Radial Injection Dual-Tracer Test," Water Resources Research, 17, pp. 529-544.

Sternau, R., J. Schwarz, A. Mercado, Y. Harpaz, A. Nir, and E. Halevy (1966), "Radioisotope Tracers in Large-Scale Recharge Studies of Groundwater," in Isotopes in Hydrology, International Atomic Energy Agency, Vienna, pp. 489-505.

Vetter, O. J. and K. P. Zinnow (1981), "Evaluation of Well-to-Well Tracers for Geothermal Reservoirs," LBL-11500, Lawrence Berkeley Laboratory.

Proceedings Ninth Workshop Geothermal Reservoir Engineering
Stanford University, Stanford, California, December 1983
SGP-TR-74

RESPONSE OF EAST MESA AND RAFT RIVER RESERVOIRS TO INJECTION-BACKFLOW TESTING

B. F. Russell, L. C. Hull and W. F. Downs

EG&G Idaho, Inc.
P.O. Box 1625
Idaho Falls, ID 83415

ABSTRACT

Analysis of tracer recovery curves from injection-backflow testing at two geothermal reservoirs reveals large differences in response between the two. The East Mesa reservoir is in a layered sandstone matrix, and tracer behavior can be adequately described by porous media theory. As the volume of water injected into the reservoir increases and, consequently, the depth of penetration into the formation, the ratio of dispersive flux to advective flux decreases, indicating the increasing importance of advective transport. This effect can be seen in normalized tracer recovery curves that become more symmetrical with greater injection volume. At the Raft River site, the reservoir is dominated by a single major fracture zone. Injecting larger volumes of water into the fracture does not change the shape of the normalized tracer recovery curves. This indicates that the dispersion coefficient increases proportionally to the distance traveled by the injection front. Differences in the shape of tracer recovery curves are related to fundamental differences in reservoir characteristics. Long tails on the tracer recovery curves at Raft River suggest a dual porosity reservoir with a secondary fracture network connected to the major fracture. Such findings may considerably affect calculations of secondary heat recovery using injection wells.

INTRODUCTION

Injection of spent geothermal fluids to maintain reservoir pressure may have the undesirable side effect of lowering the enthalpy of production fluids. Because of the fractured nature of many geothermal resources, they are frequently difficult to characterize. Without adequate characterization, it is difficult to predict the effects of injection. Tracer breakthrough tests (Horne, 1982; Fossum and Horne, 1982) have been used to study interconnections between wells where tracer travel times are on the order of days to a few weeks. Since breakthrough does not always occur within this time frame, alternative reservoir evaluation techniques have been proposed.

One such alternative under development is injection-backflow testing. This type of test consists of injecting water labeled with tracer(s) into a well for a predetermined period of time and then, immediately or after a quiescent period, withdrawing this labeled water through the same well. Tracer concentration is monitored to quantify the degree of mixing between injected and reservoir fluids. This type of testing provides enhanced ability to evaluate fracture-dominated geothermal systems and can assist in addressing concerns associated with long-term thermal breakthrough.

Methodology for interpretation of interwell tracer tests is well established (Lenda and Zuber, 1970; Grove and Beeten, 1971; Vetter and Zinnow, 1981). Single-well injection-backflow tests have been used to study the dispersion and adsorption characteristics of porous media reservoirs (Sternau et al., 1966; Drever and McKee, 1980; Pickens et al., 1981). Recently, methods have been developed to study interwell tracer tests in fractured reservoirs where well connections are along one or a few major fractures (Fossum and Horne, 1982; Horne and Rodriguez, 1983). Most of these techniques are based on an analytical solution to the advection-dispersion equation. The equation derived by Ogata and Banks (1961) for continuous injection and one-dimensional flow, in either porous media or in a single fracture, is:

$$C = \frac{Co}{2}\left\{\operatorname{erfc}\left(\frac{1-\tau}{2\sqrt{\xi\tau}}\right) + \exp(\xi^{-1})\ \operatorname{erfc}\left(\frac{1+\tau}{2\sqrt{\xi\tau}}\right)\right\} \quad (1)$$

where

C = measured tracer concentration

Co = injected tracer concentration

erfc = complementary error function

τ = reduced time = t/t_o

t_o = x/v

x = distance to measurement point

v = average linear velocity

ξ = D_L/vx = ratio of dispersive to advective flux

D_L = longitudinal dispersion coefficient.

When the ratio $D_L/vx < 0.005$, the product of the exponential and complementary error functions becomes negligible. Under such conditions, Equation 1 produces the symmetrical sigmoidal curve commonly associated with solute transport. When D_L/vx is large ($D_L/vx > 0.05$), the curve produced by Equation 1 is far from symmetrical.

Analytical solutions for radial-flow geometry have been presented by Hoopes and Harleman (1967) and Gelhar and Collins (1971). These solutions, however, are not applicable to situations where dispersive flux is significant relative to advective flux. Therefore, analytical solutions available for radial flow conditions cannot be used where injection is for a relatively short time period, and the injection plume remains near the well.

To aid in the refinement of the injection-backflow technique of well testing, two series of injection-backflow tests have been conducted. The first test sequence was carried out at the Raft River geothermal field in southern Idaho, and the second conducted during the summer of 1983 at the Republic geothermal field near East Mesa, California.

For preliminary analysis of test data collected from these two sites, simple one-dimensional analytical solutions are used to evaluate differences between tests, wells, and sites. Because many of the tests were conducted under circumstances where dispersive flux is important compared to advective flux, analytical solutions available for radial-flow geometry are not applicable. Further data analysis, using numerical simulations, will be conducted to refine the conceptual models of the two geothermal reservoirs and to estimate reservoir parameters.

EAST MESA

The East Mesa geothermal field is located in southern California, just northeast of El Centro. The reservoir is composed of interlayered sandstones and shales and is representative of a porous media reservoir. Wells 56-19 and 56-30 at the East Mesa facility were tested using the injection-backflow technique. Well 56-19 was completed as an injection well, although it has not been used extensively since the initial production tests. The well has 580 m of slotted liner and is highly productive with a productivity index of 1780 kg/hr/kPa. Spinner logs made during testing show 80 to 90 m of producing zones in the wellbore. Well 56-30 was completed as a production well and has been flowed for extended periods of time. The well has approximately 680 m of slotted liner, but only about 40 m of this length appears to produce geothermal fluids. The productivity index of Well 56-30 is 160 kg/hr/kPa, or about 10% that of Well 56-19.

These two wells were subjected to a parametric testing program designed to evaluate two injection variables, rate and volume. Tracer recovery data obtained from backflow portions of four of the East Mesa tests are shown in Figures 1 and 2. The data have been normalized, with reduced volume being the ratio of fluid recovered to fluid injected and reduced concentration being the ratio of tracer concentration measured to tracer concentration injected. In addition to measured tracer breakthrough, theoretical tracer breakthrough curves, calculated from Equation 1, are shown in the plots. These curves were fit to the early time recovery data (reduced volume <1) for each of the tests. These curves are described by the ratio of dispersive flux to advective flux (D_L/vx).

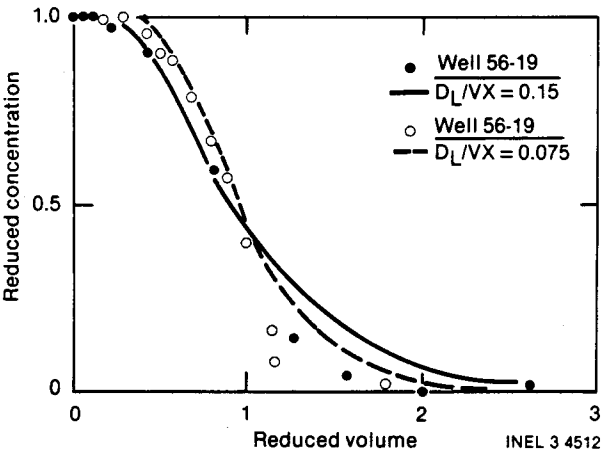


Figure 1. Tracer recovery from Test 4 (•) and Test 6 (o) on Well 56-19, East Mesa. During Test 4, 840 m^3 of tracer solution was injected and during Test 6, 1640 m^3 was injected into the well. The curves were calculated using Equation 1 and D_L/vx values indicated in the figure.

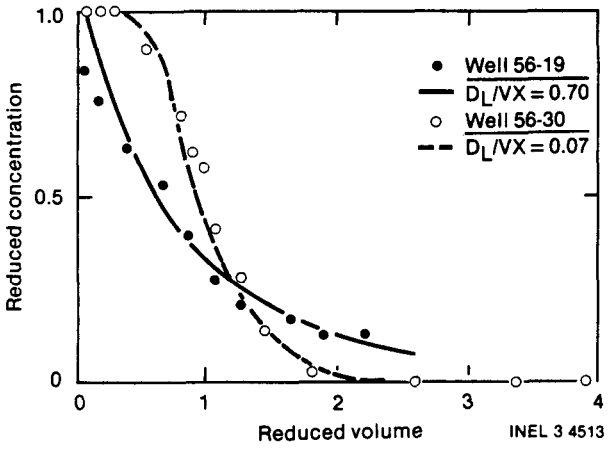


Figure 2. Tracer recovery after injecting 780 m^3 into Wells 56-19 and 56-30 at East Mesa. The curves were calculated using Equation 1 and D_L/vx values indicated in the figure.

Results from Tests 4 and 6 conducted on Well 56-19 are shown in Figure 1. Both tests were conducted at equal injection and backflow rates, but twice the volume of water was injected during Test 6. The calculated dispersion-advection ratio for the longer test is half the ratio for the shorter test. With a greater volume of fluid injected, the distance the front moved into the formation increased. This increased x in the D_L/vx ratio and, therefore, decreased the value of the overall ratio.

Results from Test 3 on Wells 56-19 and 56-30 are shown in Figure 2. Test 3 on both wells was at the same rate and of equal injected volume. The dispersive to advective flux ratio is very different for the two wells, with the ratio for Well 56-19 being about 10 times the ratio for Well 56-30. This suggests that the two wells have greatly different dispersive characteristics, or that the injected front travels significantly farther from the wellbore of Well 56-30. Because of the correlation between the productivity indices and the D_L/vx ratios, the change in ratios is probably related to a reservoir property. The most likely candidate is the length of the producing zone. Spinner surveys show twice the length of producing zones in Well 56-19 as in Well 56-30.

Tracer recovery curves from East Mesa wells follow behavior that corresponds to conventional theory for porous media. Analysis and interpretation of the data will be refined using radial-flow geometry and a numerical simulation code.

RAFT RIVER

The Raft River geothermal well field is located in southern Idaho and has been studied since the mid-1970s. Extensive data have been collected that show that the reservoir is fracture dominated and not amenable to conventional reservoir analysis (Dolenc et al., 1981; Russell, 1982).

The test well selected at Raft River was RRGP-5, a 1432-m deep production well. This well has been subjected to a series of tests including an experimental hydrofracture for well stimulation purposes. Logging operations conducted after the hydraulic fracturing indicated that a nearly vertical fracture had been generated, approximately 1.5 cm wide and 43 m long.

The results of the postfracturing pumping tests suggest the presence of a massive fracture with reservoir characteristics analogous to a constant-head recharge boundary. Although five producing zones have been identified in this well, spinner surveys indicate that there is one primary producing zone, associated with the major fracture. The tests conducted at Raft River were designed to evaluate the effects of variable volume and quiescence on tracer recovery curves (Downs et al., 1982). All tests were conducted at a constant rate of 34 m^3/hr.

Test 2A2 was a 4-hour injection test in which 137 m^3 of tracer solution was injected into the reservoir. Backflow immediately followed injection, with no quiescent period between. Test 2C was similar in format but required 48.5 hours to inject 1650 m^3 of tracer solution. Reduced tracer concentration curves versus time are shown in Figure 3. The recovery curve from Test 2C is much more spread out over time, indicating that greater mixing took place as the injection front moved farther from the wellbore. This follows classic dispersion theory with the length of the mixing zone increasing with distance traveled. Figure 4 shows tracer recovery curves during backflow in terms of reduced volume. This figure demonstrates that, in terms of injection volumes recovered, the tracer response was identical for the two tests.

Despite the 10-fold difference in injected volume, and presumably a significant difference in the distance traveled by the front, the recovery curves for the two tests are very similar. For the two curves to be the same, the ratio of dispersive to advective flux must be the same. Since the advective flux term increases as the distance traveled increases, the dispersive flux term must also increase. In the fracture-dominated

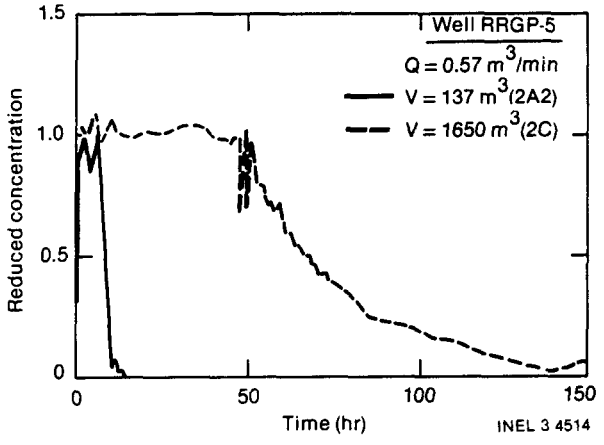


Figure 3. Tracer concentration during injection and backflow phases of Tests 2A2 and 2C at Raft River geothermal field. Test 2A2 was a 4-hour injection test and 2C a 48.5-hour injection test.

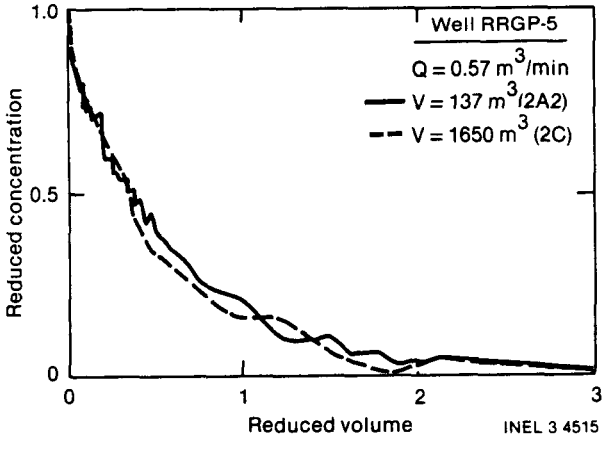


Figure 4. Normalized tracer recovery curves from backflow portions of Tests 2A2 and 2C.

system at Raft River, therefore, the dispersion coefficient must increase as the distance traveled increases. This increase in dispersion coefficient proportional to distance is consistent with theory for layered porous media or fracture networks where fracture apertures are log normally distributed (Neretnieks, 1983). The process causing this effect is the different velocities between layers or fractures. In the injection-backflow test mode, however, these velocity differences should cancel.

Taylor dispersion theory for parallel plates (Horne and Rodriguez, 1983) was applied to the test data in an effort to relate the tracer recovery curves to fracture aperture. Attempts to find a D_L/vx ratio for Equation 1 that fits the data from Tests 2A2 and 2C are shown in Figure 5. None of the curves has quite the right shape to fit the Raft River data, indicating that a single, relatively clean fracture is not a good model. Another model, which may fit the data better, is a dual porosity model. Tracer diffuses, or flows under a low gradient, into a fracture network off the major fracture. Tracer concentration drops off rapidly upon withdrawal because some of the tracer mass has been lost to this secondary fracture network. This "lost" tracer is then recovered slowly, producing a long, drawnout tail to the recovery curve. Attempts to fit the Raft River data to this latter conceptual model will be made in the near future using the FRACSL code (Miller, 1983).

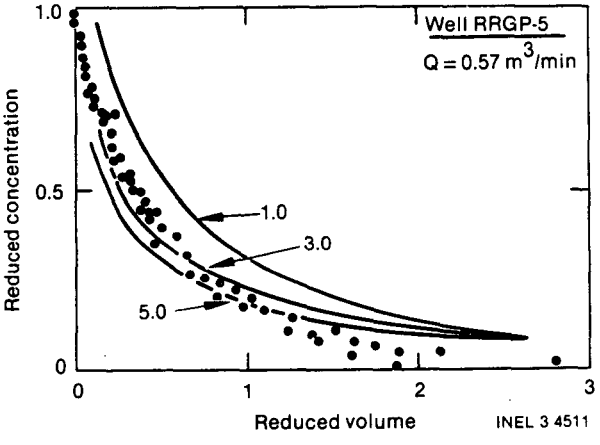


Figure 5. Comparison of normalized tracer recovery from Tests 2A2 and 2C with curves calculated using Equation 1 and D_L/vx ratios indicated for the three curves.

APPLICATIONS TO THERMAL BREAKTHROUGH

For tests conducted at Raft River and East Mesa, a cooler fluid was injected into a warmer reservoir. The temperature of the backflow was higher than injected due to mixing with reservoir fluid and exchange with reservoir rocks. Tracer recovery curves provide a measure of the ratio of the injected and native reservoir fluids from which an expected temperature response can be calculated. The difference between the expected and actual temperature response gives an estimate of the enthalpy added to the injected fluid. Downhole temperature measurements during backflow are necessary because thermal exchange in the wellbore will complicate data interpretation. Data collected at Raft River and East Mesa are being studied to evaluate this application of injection-backflow testing.

CONCLUSIONS

The East Mesa and Raft River reservoirs represent two very different configurations,

and tracer recovery curves from the two sites reflect these differences. The East Mesa data can be adequately addressed using existing porous media theory while the Raft River data appear significantly more complex. Data collected at Raft River imply that flow is dominated by a major fracture with some form of dual porosity comprised of secondary fractures or a porous matrix.

The injection-backflow tests have provided data that have assisted in refining the conceptual model for Raft River and have apparently confirmed the East Mesa reservoir configuration. The numerical simulations planned for this next year will aid in refining the interpretation of the test data and improve our understanding at the Raft River and East Mesa reservoirs.

ACKNOWLEDGMENT

This work is supported by the U.S. Department of Energy under contract No. DE-AC07-76ID01570.

REFERENCES

Dolenc, M. R. et al., "Raft River Geoscience Case Study," EG&G Formal Report No. 2125, 2 Volumes, November 1981.

Downs, W F., R. E. McAtee, R. M. Capuano, and C. W. Sill (1982), "Hydrothermal Injection Experiments at the Raft River KGRA, Idaho," SGP-TR-60, Proceedings Eighth Workshop Geothermal Reservoir Engineering, Stanford University, pp. 275-278.

Drever, J. I. and C. R. McKee (1980), "The Push-Pull Test, a Method of Evaluating Formation Adsorption Parameters for Predicting the Environmental Effects on In-Situ Coal Gasification and Uranium Recovery," In Situ, 4, pp. 181-206.

Fossum, M. P. and R. N. Horne (1982), "Interpretation of Tracer Return Profiles at Wairakei Geothermal Field Using Fracture Analysis," Geothermal Resources Council, Transactions, 6, pp. 261-264.

Gelhar, L. W. and M. A. Collins (1971), "General Analysis of Longitudinal Dispersion in Nonuniform Flow," Water Resources Research, 7, pp. 1511-1521.

Grove, D. B. and W. A. Beeten (1971), "Porosity and Dispersion Constant Calculations for a Fractured Carbonate Aquifer Using the Two Well Tracer Method," Water Resources Research, 7, pp. 128-134.

Hoopes, J. A. and D. R. F. Harleman (1967), "Dispersion in Radial Flow from a Recharge Well," Journal of Geophysical Research, 72, pp. 3595-3607.

Horne, R. N. (1982), "Geothermal Reinjection Experience in Japan," Journal of Petroleum Technology, 34, pp. 495-503.

Horne, R. N and F. Rodriguez (1983), "Dispersion in Tracer Flow in Fractured Geothermal Systems," Geophysical Research Letters, 10, pp. 289-292.

Lenda, A. and A. Zuber (1970), "Tracer Dispersion in Groundwater Experiments," in Isotope Hydrology 1970, International Atomic Energy Agency, Vienna, pp. 619-637.

Miller, J. D. (1983), "Fundamental Approach to the Simulation of Flow and Dispersion in Fractured Media," Ninth Workshop on Geothermal Reservoir Engineering, Stanford University.

Neretnieks, I. (1983), "A Note on Fracture Flow Dispersion Mechanisms in the Ground," Water Resources Research, 19, No. 2, pp. 364-370.

Ogata, A. and R. B. Banks (1961), "A Solution of the Differential Equation of Longitudinal Dispersion in Porous Media," U.S. Geological Survey Professional Paper 411-A, pp. A1-A7.

Pickens, J. F., R. E. Jackson, K. J. Inch, and W. F. Merritt (1981), "Measurement of Distribution Coefficients Using a Radial Injection Dual-Tracer Test," Water Resources Research, 17, pp. 529-544.

Russell, B. F. (1982), "Raft River Wellfield Testing and Analysis," Geothermal Resources Council Bulletin, April 1982, pp. 6-10.

Sternau, R., J. Schwarz, A. Mercado, Y. Harpaz, A. Nir, and E. Halevy (1966), "Radioisotope Tracers in Large-Scale Recharge Studies of Groundwater," in Isotopes in Hydrology, International Atomic Energy Agency, Vienna, pp. 489-505.

Vetter, O. J. and K. P. Zinnow (1981), "Evaluation of Well-to-Well Tracers for Geothermal Reservoirs," LBL-11500, Lawrence Berkeley Laboratory.

Proceedings Ninth Workshop Geothermal Reservoir Engineering
Stanford University, Stanford, California, December 1983
SGP-TR-74

DISPOSAL OF FLASHED BRINE DOSED WITH $CaCO_3$ SCALE INHIBITOR: WHAT HAPPENS WHEN THE INHIBITOR IS EXHAUSTED?

D. E. MICHELS
REPUBLIC GEOTHERMAL, INC.

in cooperation with

EG&G, IDAHO, INC.,
AND
UNIVERSITY OF UTAH RESEARCH INSTITUTE

ABSTRACT

A freshly flashed geothermal liquid, previously dosed with inhibitor and supersaturated with calcite was injected into another well where it displaced an unflashed counterpart of itself around the wellbore. Back-production of the injectate, and subsequently the native fluid, has yielded data for the rate that a scale inhibitor is degraded after injection. The circumstance also displays a novel mechanism whereby two fluids that do not physically mix nevertheless react with one another through the reservoir rock's serving a role of intermediary. The results have been further interpreted to conclude that in some circumstances a short lifetime for the scale inhibitor is not necessarily a problem for long-term injection.

INTRODUCTION

Commercialization of a geothermal resource requires that several different perspectives be pursued in regard to what happens when the reservoir fluids are moved around by production and disposal. Emphasis on reservoir management via hydraulic principles currently tends to dominate the issue despite examples where permeability changes are due to chemical reactions of injected fluids, mainly involving silica. Although $CaCO_3$ deposition has generally been regarded as a production problem, successful inhibitors displace that concern to the context of injection. It is that aspect of $CaCO_3$ deposition which is addressed in this report.

Flashed brine, dosed with inhibitor to retard deposition of $CaCO_3$ is, nevertheless, thermodynamically poised to deposit it. Eventually the scale inhibitor may be overcome. For example, an effective lifetime of less than 14 hours was indicated for one inhibitor. Consequences to the reservoir which receives the fluid apparently have not been previously explored. However, Huff-Puff tests (monitored backflow of injected tracers), carried out at East Mesa in the summer of 1983, have provided a starting point for addressing the questions.

Geothermal liquid for the 1983 Huff-Puff tests was produced by natural flow from a commercial-quality well (No. 38-30) at East Mesa. Although the liquid was available at the wellhead in an unflashed condition, the overall system required that steam flashing be allowed. Such flashing activates the $CaCO_3$ scale deposition reactions, hence scale inhibitor was added, before the flash.

Since the functional mechanism of the inhibitor does not affect the thermodynamic drive for scale deposition, one should anticipate deposition whenever the residual inhibitor in the brine diminishes to below a critical minimum concentration. Although the inhibitor has long-term stability at the temperature of flashed brine, its stability at rock temperatures in the injection zone is in question. Additionally, the large rock surface area of the injection zone may sorb some inhibitor from the injectate. Furthermore, a slow, but finite overgrowth of $CaCO_3$ on "inhibited" crystals also consumes some of the inhibitor. There may be other factors including some which intervene to limit deposition.

The engineering questions raised by this eventuality are: (1) How far is the fluid from the wellbore when the deposition occurs; (2) how much $CaCO_3$ will deposit compared to available space in the rock's porosity; and (3) what factors may limit deposition.

Huff-Puff experiments provide a means for direct measurement of the time involved with decay/degradation of the inhibitor's function in the real context of a receiver well. More significantly, these experiments have also provided insights about water-water reactions between the injectate and native fluid. We have obtained additional implications about chemical reactions between the reservoir rock and the injectate and also about what happens when native fluid returns to rocks that have previously reacted with injectate.

The present experimental results deserve to be viewed at two levels. Firstly, the data are site-specific and reflect an early attempt to discover what sorts of things can be learned. These are experiments in the truest sense, in that the eventual outcome was predicted only vaguely at the start.

Secondly, the experiments identify a new class of studies that yield important data not provided by any counterparts. These new data are complementary, without being redundant, to more traditional kinds of information in the issue of resource evaluation and reservoir management.

EXPERIMENTAL

Two test Wells, 56-30 and 56-19, and the supply well 38-30, were used in the overall program, but this report is limited to a test where fluid from 38-30 was dosed with scale inhibitor, allowed to flash, and separated liquid was then dosed with tracers and pumped into 56-30. The amount injected was not sufficient to enable a breakthrough into 38-30.

After injection, the fluid was allowed to rest there for 12 hours before back-production began. Back-production was made at the same rate as injection, but lasted longer, so that nearly five times the injected volume was removed. The injected volume (IV) constitutes a natural unit of volume when describing the results of these experiments.

During back-production, many liquid samples were collected to quantify the behavior of tracers, both added and natural. Several other physical measurements were made also, but this report is limited to selected chemical results and fluid volumes.

For the overall experimental program the calcium content in the supply liquid was about 7.0$\pm$ 0.1 ppm before flashing and about 6$\pm$ 1ppm after flashing when inhibitor was present. Table 1 shows compositions for the fluids involved. All inhibitors used were incompletely effective within the space of the surface equipment (this aspect will be covered in a separate report). Without inhibitor, the calcium content of flashed brine was about 2.0 $\pm$ 0.5 ppm.

The calcium serves as a tracer of the injectate's reactivity, hence also of the inhibitors effectiveness. Inhibited liquid shows a loss of calcium from its concentration at the time of injection to a lower concentration characteristic of uninhibited liquid.

Test 3 provides the subject for this report. It involved 11.5 hours of injection of inhibited, flashed liquid from 38-30 into 56-30 at a rate of 300 gpm (0.78 million liters total injected volume). The injectate was also dosed with a level increment of chloride intended to track the nature of the mixing front. After the 12-hour quiescence, 56-30 was back-produced at a rate of 300 gpm and samples were collected for chemical analysis.

Samples were taken from the wellhead through a probe that reached into the mainstream flow. Liquid entering the probe passed, without flashing, through a stainless steel tubing formed into a coil. The assembly was cooled by immersion in cool water. A valve downstream from the cooling coil controlled the flow. The liquid sample was then collected, briefly open to the atmosphere, into a glass vial with screw cap. The calcium contents of samples collected this way are stable. Samples were analyzed one to 20 hours later using atomic absorption calibrated with standards.

Results are shown in Figure 1 where the ordinate X/X_o represents a normalized calcium or chloride concentration. Specifically, the observed concentration X, in a sample is divided by the concentration in unaltered native fluid X_o.

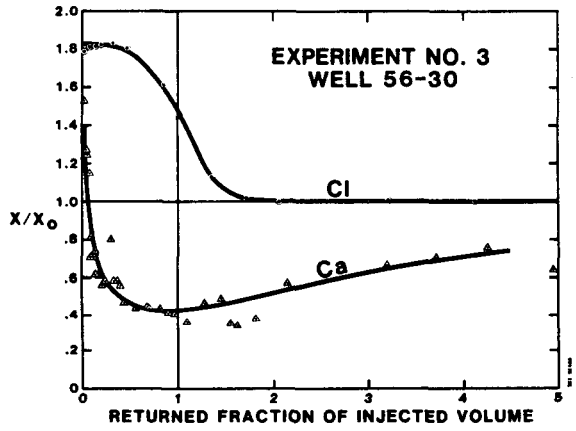


FIGURE 1. CALCIUM AND CHLORIDE IN BACKFLOW

The chloride concentrations initially exceeded the X_o values because KCl was added as a level tracer to the injected liquid. The native concentration of calcium in 56-30 is 6.55 $\pm$ .08 ppm, based on seven samples collected before Test 3 began. Several features of Figure 1 are worth noting.

1. The chloride returns indicate that unmixed native fluid was obtained by the time two injection volumes had been back-produced; the inflection point for chloride is distinct and near 1 IV.

2. The ordinate function for calcium decreases sharply and remains well below unity throughout all of the back-production. The inflection point is not distinct.

3. The calcium concentration is still small and near its minimum value after back-production of two injection volumes.

4. The overall deficit of calcium in the back-produced liquid is several times the amount that could have been stripped from the original injected liquid.

These results are startling because they show a substantial loss of calcium from native fluid that never mixed with the injectate that must have induced the loss.

DISCUSSION

1. Inhibitor Lifetime

Figure 1 shows that the calcium concentration in samples of returned fluid plunged sharply with the first increments of production. All the samples for which X/X_0 exceeds unity are from "injectate" that remained in the wellbore through the 12-hour hiatus between injection and back-production. These large values are taken to indicate dissolution of calcium-containing minerals from the wellbore. This is extraneous to the issue of water-rock reaction or stability of inhibitor in the reservoir and will not be discussed further.

Values of X/X_0 less the unity all pertain to the fluid which was exposed to reservoir rocks. The minimum values of about 0.4 correspond to actual calcium concentrations of about 2 ppm. This is the level expected for calcium in flashed brine which has not been dosed with inhibitor. Accordingly, such results indicate complete exhaustion of the inhibitor.

The time involved to reach exhaustion is indicated by the minimum in the trend line of Figure 1, namely, a return of about 0.8 IV. (Notwithstanding the scatter of data and a few lower values of X/X_0 between IV's of 1 and 2.) This is about 9.2 hours after start of backflow and about 21.2 hours after injection ceased. By symmetry the fluid involved with the minimum X/X_0 was dosed with inhibitor 9.2 hours before injection ceased, thus, the total time to complete exhaustion is about 30 hours.

On the other hand, even the first sample of fluid which contacted rock shows a loss of calcium. Since that sample was taken only about one hour into backflow, we can conclude that the inhibitor was detectably degraded in less than 14 hours.

A more sophisticated approach presumes that the inhibitor function degrades in the sense of a first order reaction. To measure this, one may plot X/X_0 vs IV on semi-log paper and examine it for linearity. Figure 2 shows that the 17 data points between 0.08 and 0.7 IV do indeed suggest linearity. Smaller IV values can be excluded because they involve fluid returning only from the wellbore; larger volumes can be excluded because a sensitivity limit has apparently been reached where the inhibitor's effect, if any, can no longer be resolved by the analytical results.

The slope of a least squares fitted line to those data yield a value of 0.65 IV for the half-volume, the amount of fluid production involved with a two-fold change in X/X_0.

Since the value of 0.0 IV belongs to fluid dosed 12 hours earlier and 1.0 IV is obtained 36 hours after dosing with inhibitor, a time half-life for the inhibitor of 15.7 hours can be deduced.

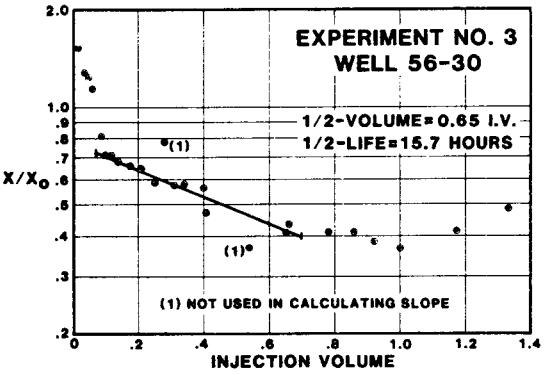


FIGURE 2. NORMALIZED CONCENTRATION OF CALCIUM vs. RETURNED FRACTION OF INJECTION VOLUME

This appears to be reasonable, considering that inhibitor dosage was nominally 3 ppm and that concentrations above about 1 ppm are without significant effect. In principle, a half-life of 15.7 hours would reduce 3 ppm of inhibitor to the 1 ppm threshold in about 25 hours. Thereafter, continued degradation of inhibitor would be discernible through the variable analytical results for residual calcium. That calculated 25-hour delay is larger than the apparent 14 hour delay described earlier, but not unreasonably so because neither the 3 ppm nor 1 ppm nominal values are precisely identified for this experiment. Also, the scatter of data in Figure 2 yields some uncertainty for the half-life calculated above.

The concept of half-life for the inhibitor, using units of time, might be appropriate for a degradation mechanism due to temperature instabilities. However, the maximum temperatures in 56-30 are approximately 175°C for which the inhibitors have elsewhere shown good stability in seawater-like salinities. Thus, unless there is a synergistic effect between temperature and some factor in the reservoir rocks, exposure temperature may be disregarded. Therefore, it would seem useful to interpret the half-life from Figure 2 in units of volume. Accordingly it would then be plausible to consider the degradation as being due to a water-rock reaction, perhaps akin to sorption, not readily reversible, but involving amounts of liquid on the order of the injection volume. This conclusion will be considered later in regard to where the calcium deposits.

2. Water-Rock Reaction

If the reactive potential of the injected liquid were truly transferred to the native fluid, beyond the extent to which they were physically mixed, then an intermediary must have been involved. The intermediary in this case would appear to be the rocks of the reservoir.

The nature of an intermediary is to respond in a chemically reversible way, in this case with a reaction that can also participate with the calcite deposition reaction. This statement is not intended to imply that the rocks react directly with calcium or calcium carbonate. Rather, it is proposed here that the acid-base exchange capacity of the rocks, which exists mainly in the clays, participates with the acid-base properties of the injectate and native fluid.

Specifically, the pH of native fluid, charged as it is with CO_2, and at an elevated temperature, is much lower than the pH of the flashed counterpart that has not only lost its free CO_2, but also carries significant $CO_3^=$ due to decomposition of HCO_3^- according to Equation 1.

$$2HCO_3^- \rightarrow H_2O + CO_2 + CO_3^= \qquad (1)$$

In the case at hand, pH in the native reservoir condition is calculated to be 6.7 whereas, pH of the flashed brine at the injection temperature is on the order of 9.0. The base capacity of the flashed brine is about 0.8 milliequivalents per kilogram (meq/kg) to pH's near 7. By contrast, the calcium content of native fluid is about 0.33 meq/kg.

The reservoir rocks, on the other hand, contain clays in variable amounts up to a few percent by weight. Of course, the active part of the injection zone must be a clay-poor region, but none of the East Mesa production zones are considered clay-free.

The acid-base exchange capacity of the clays there have not been measured, but published values for kaolinite between pH 6.7 and 9 suggest that 0.2 meq per gram of clay would be a reasonable presumption. If we further presume five weight percent clay in the reservoir sandstone and a 30 percent porosity, the rock's acid-base capacity would be 19 meq/liter of rock volume. This is about 80 times the acid-base capacity of flashed brine that could fill the porosity.

Two concepts derive from this approximation. The rock's over-capacity to react with injectate assures that the injection front which displaces native fluid will be largely equilibrated with the rock before much fluid-fluid mixing can occur. Since we would expect that two fluids in equilibrium with the same rock are also in equilibrium with each other, little water-water reaction can be expected as the injectate displaces native fluid. Furthermore, it appears that a unit of injectate will lose its thermodynamic drive to deposit calcite due to chemical equilibration with the rock and without deposition of calcite.

Secondly, the chemical base capacity carried by the injectate will be consumed near the wellbore. The estimated 80:1 capacity ratio suggests that the 0.78 million liters of injectate were titrated by only 9.8 cubic meters of rock. Since only about 120 meters of wellbore length are involved with significant production, the nominal depth of water-rock reaction, assuming radial symmetry, is about 0.090 meters. A somewhat larger estimate of chemical penetration depth can be derived for part of the well by noting that about 70 percent of the reservoir flow in 56-30 is associated with a 40-meter long interval of wellbore. For that zone, depth of water-rock reaction would be 0.154 meters.

By comparison, the total fluid injected into the rocks would involve 2,600 cubic meters of rock volume with radial penetrations corresponding to 2.6 and 3.8 meters, respectively.

Thus, although a zone of transition between unaffected rock and totally reacted rock may be expected for several reasons, its practical width would seem to be small relative to the gross depth of fluid penetration. Therefore, the calcium burden in the injectate would appear to soon become stable during injection, irrespective of whether inhibitor remained present.

For long-term injection, the vicinity of the wellbore expandingly acquires the chemical and thermal nature of the injectate. Of the several modes of inhibitor failure, all except overgrowth would become suppressed, trending toward a maximum lifetime for the inhibitor's function. That would be timely since for longer term injection, the distance from wellbore to rock that still could neutralize the calcite deposition potential will become greater. In this East Mesa example, the possibility of inhibitor exhaustion appears to have a negligible consequence for long-term injectability.

3. Calcium Loss to the Rocks

There is a great contrast between the acid-base reactivity, which was neutralized in a rock volume estimated to be only 1/80th of the injection volume, and the 0.65 IV half-volume for the inhibitor. This suggests that the inhibitor moves much further through the rock than do the chemical base properties of the injectate.

Returning to Figure 2, the space between the plot for calcium and the line $X/X_o = 1$ represents calcium lost from the liquids. The portion of that space to the right side of one IV, or more precisely, to the right of a vertical line through the inflection point in the chloride tracer curve, represents calcium lost from the native fluid.

The chemical equivalence of that calcium can be estimated by extrapolating the calcium recovery curve toward the right where it intersects $X/X_o = 1$. Unfortunately, the data are a bit scattered, so only the simplest extrapolation will be considered at this time.

A liner least squares fit to the last 11 data yields $X/X_0 = 1$ at 7.1 IV.

The average calcium deficit is thereby calculable as 2.3 ppm. The total amount of calcium lost by the 7.1 IV is 636 chemical equivalents of calcium:

$$(780000\ l/IV)\left(\frac{2.3 \times 2\ meq/l}{40.1}\right)(7.1\ IV) = 636\ eq$$

By comparison, the base capacity of the injected brine is 624 chemical equivalents.

$$(780000\ l/IV)(.80\ meq/l)(IV) = 624\ eq$$

This correspondence appears excellent, showing that the Huff-Puff techniques can yield quantitative results about water-rock interactions.

Significantly, the amount of calcite which deposits depends on the rock's base exchange capacity not on the volume of injectate or back-production.

The possibility of clogging the rock's porous space by this deposition mechanism appears slight. Using the approximation of rock reactivity applied earlier, namely 19 meq/l and 30 percent porosity, one can calculate that each liter of rock volume can become dosed with 0.95 gram of calcite. That amounts to about 0.35 ml of new calcite per 300 ml of porosity. Even accepting that deposition of calcite in the narrow throats which connect nodes of porosity has effects on permeability far beyond the volume proportions, it is difficult to expect a substantial effect. A laboratory verification of this matter would be simple to set up, however.

SUMMARY

The Huff-Puff experimental method has provided grist for several issues about how injected geothermal fluids behave in the reservoir rocks. Some data and estimates are provided for the survivability of an inhibitor, the fate of calcium that might be suspected to yield scale, the mixing of injectate with native fluid, and the nature of the water-rock reactions, including deposition of calcite in the porosity.

Significantly, some results are nonintuitive. It appears easy to design subsequent experiments for both field and laboratory, to yield still better tests of concepts.

The most significant result at this stage is that Huff-Puff experiments, as a class, are clearly powerful, experimental tools for applied geothermal engineering.

TABLE 1

NOMINAL LIQUID COMPOSITIONS*
ppm BY WEIGHT

COMPONENT	SUPPLY WELL 38-30 PRE-FLASH	SUPPLY WELL 38-30 POST-FLASH	TEST WELL 56-30 PRE-FLASH
Sodium	630	698	597
Potassium	25	27	25
Calcium	7	2.0,6.0**	6.1
Ammonium	4.0	0.9	6***
Strontium	2.7	3.0	0.8
Lithium	0.6	0.7	0.3
Magnesium	0.2	0.2	-
Chloride	533	586	505
HCO_3	600	585	596
CO_3	0.03***	45***	0.03***
Sulfate	172	190	177
Boron	1.4	1.5	0.8
Fluoride	3.0	3.3	2.4
Silica	193	210	180
CO_2	440	1	430
Temp. °C	170	94****	165

* Electrically balanced based on several analyses
** Without and with $CaCO_3$ scale inhibitor added pre-flash
*** Estimated
**** Upon injection into 56-30

Proceedings Ninth Workshop Geothermal Reservoir Engineering
Stanford University, Stanford, California, December 1983
SGP-TR-74

MATRIX DIFFUSION AND ITS EFFECT ON THE MODELING OF TRACER RETURNS FROM THE FRACTURED GEOTHERMAL RESERVOIR AT WAIRAKEI, NEW ZEALAND.

Clair L. Jensen and Roland N. Horne

Department of Petroleum Engineering
Stanford University, CA 94305

ABSTRACT

Tracer tests performed at the geothermal reservoir at Wairakei, New Zealand have been analyzed, using a mathematical and physical model in which tracer flows through individual fractures with diffusion into the surrounding porous matrix. Model calculations matched well with the observed tracer return profiles. From the model, first tracer arrival times and the number of individual fractures (the principal conduits of fluid flow in the reservoir) joining the injector-producer wells can be determined. If the porosity, adsorption distribution coefficient, bulk density and effective diffusion coefficent are known, fracture widths may be estimated. Hydrodynamic dispersion down the length of the fracture is a physical component not taken into account in this model. Future studies may be warranted in order to determine the necessity of including this factor. In addition to the tracer profile matching by the matrix diffusion model, comparisons with a simpler fracture flow model by Fossum and Horne (1982) were made. The inclusion of the matrix diffusion effects was seen to significantly improve the fit to the observed data.

INTRODUCTION

In many geothermal development schemes, produced geothermal waters are reinjected for the purpose of disposal and pressure maintenance. The known effects of reinjecting water are: improved or degraded thermal recovery (depending on underground flow paths and velocities); permeability changes in the reservoir; pressure maintenance of reservoir fluid; and possible re-routing of natural underground water pathways. Horne (1982) presents a summary of such experience on a worldwide basis.

Since both detrimental and beneficial effects have been observed, reservoir tests to determine the effects of a proposed reinjection system are desireable. Also, various reservoir parameters and the mechanics of fluid flow in the reservoir need be investigated. Interwell tracer tests have made significant contributions to the understanding of fluid flow in natural underground reservoirs. Radioactive and chemical tracers have been used for many years in groundwater hydrology to study the movement of water through porous media, but until recently little has been reported on their use in fractured geothermal systems.

In addition to the test itself, there needs to be some method to analyze the data obtained. To date, tracer returns from geothermal reservoirs have been analyzed in only a semi-quantitative sense to determine transit times, flow velocities and pathways.

In 1982, Fossum and Horne presented an analysis of tracer data from field results at Wairakei, New Zealand, including a model describing linear flow through a fracture with hydrodynamic dispersion. This physical and mathematical model unfortunately proved to be only partially adequate in modeling fluid flow, and does not fit well to many of the more recently obtained test results from the fractured Wairakei geothermal reservoir.

In searching for and testing of a physical model that would better mathematically fit the tracer return data, it has been found here that a 'double-porosity' model is more satisfactory. The 'double-porosity' model formulated in this work includes diffusion of tracer into the porous matrix in addition to flow through the fractures in the reservoir.

DISCUSSION

The tracer tests which produced the data used in this study were performed by the Institute of Nuclear Sciences, Department of Scientific and Industrial Research, New Zealand. Iodine-131 was used as the tracer. Its half-life is eight days. This eight-day half-life limited the field tests to four to five weeks, by which time a combination of decay corrections and

variation of background signals produced unacceptably large errors. This error becomes quite noticeable at late time for some of the tracer return data. For a detailed description of tracer injection methods, well monitoring and counting equipment used at Wairakei see McCabe, Barry and Manning (1983).

The data was corrected for decay and background responses. All negative values have been deleted. Missing data is due to instrument or field problems. Not all of the monitored wells gave sufficient tracer returns and therefore were not analyzed.

Until recently, most mathematical models were based upon a porous media physical model. These porous media type models are useful, but since most geothermal reservoirs are highly fractured they are not entirely applicable, for they assume some type of uniform sweep through the reservoir. Horne and Rodriguez (1983) presented a mathematical model based on the physics of dispersion during fluid flow through fractures, thus forming a basis for the derivation of a transfer function to be used in the interpretation of field observations. Fossum and Horne (1982) utilized this model to analyze some of the tracer return profiles from the Wairakei geothermal field. A double flowpath model was found to give a better data match than a single flowpath model, though interwell flow over long distances was interpreted to occur in only a very few open fissures. However, other tracer test data more recently obtained from Wairakei has proven to be poorly fitted by this simple model.

A possible explanation for this poor fit was indicated by laboratory studies performed by Breitenbach (1982). Significant retention of the tracer in reservoir rocks was observed. The processes producing tracer retention could include adsorption, diffusion, dissolution and ion exchange.

From experimentation, Neretnieks (1980) determined that diffusion into the rock matrix can enhance tracer retardation by many orders of magnitude compared to retardation by surface reaction in fissures only, and that the magnitude of the retardation depends very much on the fissure widths and spacings.

Grisak and Pickens (1980) presented a study concerning the effect of matrix diffusion on solute transport through fractured media. Transport is considered in a manner conceptually similar to 'double-porosity' or 'intra-aggregate' transport models. A finite element model was developed to simulate nonreactive and reactive solute transport by advection, mechanical dispersion, and diffusion in a unidirectional flow field. The numerical model and the laboratory tracer test data provided insight into the processes controlling solute transport in fractured media.

From studies of the migration of radionuclides in the bedrock surrounding nuclear waste repositories, Neretnieks, Eriksen, and Tahtinen (1982) developed a mathematical and physical model describing tracer movement in a single fissure of granitic rock. This model takes into account instantaneous sorption on the surface of the fissure, and loss of tracer from the fluid flowing in the fissure due to diffusion into the porous matrix. It is this model that is used to help gain insight and a physical understanding of the fluid flow implied by the tracer tests performed at the geothermal reservoir field at Wairakei, New Zealand.

Although fractures are the principal paths of groundwater flow and solute transport, the matrix adjacent to the fractures plays an important part in the overall solute transport process. The effect of matrix diffusion is to provide solute storage, with the rate of change of storage within the matrix related to Fick's second law of diffusion.

The net effect of matrix diffusion is to retard the arrival of the solute at any point along the fracture. If the source of the solute is discontinued, the effect will be to flush the fracture and reverse the concentration gradient, causing solute to move from the matrix into the fracture.

Two equations describing the physical situation of one-dimensional advective flow through a fracture with simultaneous tracer adsorption and diffusion into the surrounding porous matrix are as follows:

$$R\frac{\partial C_f}{\partial t} - \frac{2D_e}{\delta}\frac{\partial C_p}{\partial y}\bigg|_{y=0} + U_f\frac{\partial C_f}{\partial x} = 0 \qquad (1)$$

$$D_a\frac{\partial^2 C_p}{\partial y^2} = \frac{\partial C_p}{\partial t} \qquad (2)$$

A linear equilibrium relationship between the dissolved and sorbed phases of the solute has been assumed. Linear adsorption assumes that once the tracer and rock are brought sufficiently close together, adsorption will be an instantaneous process.

Two different diffusion coefficients, D_a and D_e, are presented in Equations 1 and 2. The apparent and effective diffusion coefficients are related as follows:

$$D_a = \frac{D_e}{K_d \rho_b} \tag{3}$$

The effective diffusion coefficient D_e is dependent on temperature, porosity, molecular diffusivity, and the geometry of the rock. $K_d\rho_b$ is a volumetric sorption equilibrium constant and is related to porosity ϕ, the solid rock density ρ_s and the adsorption distribution coefficient k by the equation,

$$K_d \rho_b = \phi + (1 - \phi)k\rho_s \tag{4}$$

Notice that if the solids are inert, i.e., k=0, the porous rock matrix still has a volumetric sorption equilibrium constant equal to its porosity ϕ. Rearrangement of Equation 4 gives,

$$R = \frac{K_d \rho_b}{\phi} = 1 + \frac{k\rho_b}{\phi} \tag{5}$$

where R is refered to as the retardation factor.

The retardation factor defines the mean velocity of the moving liquid relative to the mean velocity at which the tracer itself moves through the rock. This factor accounts for the slowing down of a tracer moving with the fluid due to the interaction with the solid. If there is no interaction between the tracer and the solid phase, k becomes zero and R reduces to one.

The initial and boundary conditions are a finite rectangular pulse of tracer with duration Δt introduced at the inlet of the fracture at time t=0, and the fracture and rock are originally free of tracer.

The solution to Equations 1 and 2 subject to the given initial and boundary conditions is,

$C_f = 0 \quad$ for $\quad t < t_w R$

and for $t > t_w R$,

$$C = \frac{E\alpha_1\alpha_2}{\sqrt{\pi}(\alpha_2 t-1)^{1.5}} \exp\left(-\frac{\alpha_1^2}{(\alpha_2 t-1)}\right) \tag{6}$$

where,

$$\alpha_1 = (D_e \phi t_w)^{0.5}/\delta \quad \text{and} \quad \alpha_2 = \frac{1}{t_w R}$$

The linear parameter E normalizes the flow fraction to one. This normalization is needed because precise information on the initial concentration injected into the fracture system connected with the producing well is not available. This does not affect the shape of the calculated tracer profile, but merely the size.

Tester, Bivens, and Potter (1982) proposed the use of an objective function F over N measured data points in order to analyze for optimum values α_1 and α_2 in the transfer function $C(t;\alpha_1,\alpha_2)$ for a given tracer return profile. When F, given by

$$F = \sum_{i=1}^{N} \left(C(t;\alpha_1,\alpha_2) - C_i\right)^2 \tag{7}$$

is minimized, optimum values of α_1 and α_2 result. A multifracture model assuming one-dimensional flow in separate fractures and which gives the predicted tracer concentration response is given by

$$C = \sum_{j=1}^{M} \varepsilon_j C_j(t;\alpha_{1j},\alpha_{2j}) \tag{8}$$

where ε_j is the fraction of flow in fracture path j. The relative flow fractions in the fracture system communicating with the production well and the injection well is given by

$$\sum_{j=1}^{M} \frac{\varepsilon_j}{E} = 1 \qquad (9)$$

This multifracture model is used to determine whether the tracer returns to a producing well is a result of flow through one or more fractures. Once the above objective function is minimized, the resulting optimized parameters are used to give information about the fracture system and flow mechanisms in the geothermal reservoir.

Optimization of the parameters in the transfer function $C(t;\alpha_1,\alpha_2)$ is accomplished using a nonlinear least-squares method of curve fitting based on a paper by Golub and Pereya (1973). A computer program calls for the input of the tracer return data, the number of parameters being used, and estimates of the nonlinear parameters. Subroutine VARPRO (written by Stanford University Department of Computer Science) and its accompaning subroutines are called to optimize the objective function. The main program then calls for the plotting of the tracer return data along with the computed best fit tracer return profile, and the optimal values of both the nonlinear and linear parameters of the given transfer function are printed.

RESULTS

The tracer return data for the various wells were fitted to the mathematical model using the computer program discussed previously. Figures 2, 4, and 6 show the fitted data profiles. The squares represent the data and the solid line is the calculated curve fit. For comparison purposes, Figures 1, 3, and 5 show corresponding curve fits using the model presented by Fossum and Horne (1982). Remember that their model includes only advection and dispersion along one or more non-connecting or channeled fractures. The model presented in this report includes adsorption, advection, and diffusion into the surrounding porous matrix. This inclusion of diffusion gives considerable improvement in the curve fit of the tracer return profiles. Furthermore, in many of the wells only a single fracture model is required to smoothly fit the data, whereas multi-fracture modeling was required in the cases presented by Fossum and Horne (1982). This is more pleasing since most curves can be fitted if several linear combinations of the single path equation are used, irrespective of the physical applicability.

Values for the flow fractions and nonlinear parameters α and β for the different calculated tracer return curve fits are given in Table 1.

For a few of the tracer return data, double fracture modeling was possible but did not substantially improve the single fracture curve fits. Where improvement was possible, however, these fits were used in place of the single curve fits.

Not all the tracer returns are well fitted. One such tracer return is from well WK121. The fit (Fig. 6) is better than that obtained with the non-diffusive model (Fig. 5), however it still does not reproduce the entire observed behavior. Reasons for poor fits may be that (1) hydrodynamic dispersion down the length of the fracture needs to be included to better model the fluid and tracer flow, (2) the instantaneous linear adsorption assumption is not valid, or (3) temperature effects on k, and D_e are of importance.

Well WK121 is an interesting case in that a good fit was obtained when modeled as a double fracture case. However, a negative flow fraction is calculated. This anomaly could have a physical or mathematical significance, but most likely is an artifact of the curve fitting technique itself, in that more than one approach to convergence may be possible.

The goal of tracer return analysis is to infer information concerning the flow velocities, fracture widths, flow pathways, and reservoir rock and fluid properties such as diffusion and adsorption coefficients. To do this with the Wairakei data at hand requires some knowledge of the parameters ρ_b, D_e, k, and ϕ.

If a nonsorbing tracer is used then k=0, R=1, and $K_d\rho_b=\phi$. In this nonsorbing case some knowledge of the porosity ϕ and effective diffusion coefficient D_e is required to calculate fracture width values for the corresponding curve fit. In Table 1, fracture width values are given based on the nonsorbed tracer assumption and the effective diffusion coefficient value of 4.32×10^{-6} m^2/day (5×10^{-11} m^2/s). The value for D_e is a medium value obtained from a range of values given by Neretnieks (1980) for nonsorbing tracers in granites. This value is not necessarily the proper value to be used in this case, but it does allow one to speculate on possible fracture widths. Also, since the matrix porosity of the Wairakei reservoir is not definitively known, porosity values of 1% and 5% were

used in the the calculations.

In Table 1, flow velocities have been calculated based on the injector-producer distances and calculated first tracer arrival times. An assumption of the tracer not being sorbed to the reservoir rock (R=1) is also made in these calculations. As the injector-producer distances are not necessarily representative of pathlengths in the reservoir, these calculated velocities are minimum values.

CONCLUSIONS

1. Tracer diffusion into the matrix of the Wairakei geothermal reservoir is an important factor in the mechanism of tracer flow. Estimated reservoir parameters such as fracture widths, fluid velocities and dispersion characteristics are difficult to accurately interpret in a fractured reservoir without accounting for matrix diffusion. The diffusion of tracers into the rock matrix and their sorption onto the surfaces of the rock are the main mechanisms retarding migration through fractures.

2. In using the fracture model presented by Fossum and Horne (1982) to analyze the Wairakei data, a double flowpath model gave a more accurate data match than a single component model. However, in using the matrix diffusion model presented in this report, single fracture flowpath modeling was sufficient in many of the cases.

3. Without further investigation of representative values for the effective diffusion coefficient D_e, bulk rock density ρ_b, porosity ϕ, and the adsorption distribution coefficient k, quantitative values for the various reservoir and fluid flow properties cannot be accurately calculated for the Wairakei reservoir.

4. Further study into the modeling of tracer flow through fractured media which takes into account hydrodynamic dispersion down the length of the fracture in addition to diffusion into the porous matrix may be warranted.

NOMENCLATURE

α	nonlinear parameters
C_f	concentration of tracer in fracture
C_p	concentration of tracer in porous matrix
D_a	apparent diffusion coefficient
D_e	effective diffusion coefficient
δ	fracture width
E	linear scaling factor
ϵ	fraction of flow
F	objective function
k	adsorption distribution coefficient
$K_d\rho_b$	volumetric sorption equilibrium constant
M	number of proposed fracture paths
N	number of data points
ρ_b	bulk density of the medium
ρ_s	solid rock density
R	retardation factor
t_w	water residence time
ϕ	porosity
U_f	fluid velocity in the fracture
x,y	Cartesian directions

ACKNOWLEDGEMENT

The data used in this work was collected at the Wairakei geothermal field by the Institute of Nuclear Sciences, Department of Industrial and Scientific Research, Gracefield, New Zealand, and was made available to the Stanford Geothermal Program by Dr. W.J. McCabe. Funding for Stanford University's participation in this work was provided by the U.S. Department of Energy under contract number DE-AT-03-80SF11459.

REFERENCES

Breitenbach, K.A., Chemical Tracer Retention in Porous Media, Stanford Geothermal Program, SGP-TR-53, Stanford CA, May 1982.

Fossum, M.P. and Horne, R.N., "Interpretation of Tracer Return Profiles at Wairakei Geothermal Field Using Fracture Analysis, "Geothermal Resources Council, Transactions, Vol. 6, October 1982.

Golub, G.H. and Pereya, V., "The Differentiation of Pseudo-Inverses and Nonlinear Least Squares Problems Whose Variables Separate," SIAM J. Numerical Analysis, Vol. 10, No. 2, 413-431, 1973.

Grisak, G.E. and Pickens, J.F., "Solute Transport Through Fractured Media," Water Resources Research, Vol. 16, No. 4, 719-739, 1980.

Horne, R.N., Effects of Water Injection Into Fractured Geothermal Reservoirs: A Summary of Experience Worldwide, Stanford Geothermal Program, SGP-TR-57, Stanford CA, June 1982.

Horne, R.N. and Rodriguez, F., "Dispersion in Tracer Flow in Fractured Geothermal Systems," Geophysical Research Letters, Vol. 10, No. 4, 289-292, 1983.

McCabe, W.J., Barry, B.J. and Manning, M.R., "Radioactive Tracers in Geothermal Underground Water Flow Studies," Geothermics, Vol. 12, 83-110, 1983.

Neretnieks, I., "Diffusion in the Rock Matrix: An Important Factor in Radionuclide Retardation?," J. of Geophysical Research, Vol. 85, No. B8, 4379-4397, 1980.

Neretnieks, I., Eriksen, T. and Tahtinen, P., "Tracer Movement in a Single Fissure in Granitic Rock: Some Experimental Results and Their Interpretation," Water Resources Research, Vol. 18, No. 4, 849-858, 1982.

Tester, J.N., Bivens, R.L. and Potter, R.M., "Interwell Tracer Analysis of a Hydraulically Fractured Granitic Geothermal Reservoir," Society of Petroleum Engineers Journal, Vol. 22, 537-545, 1982.

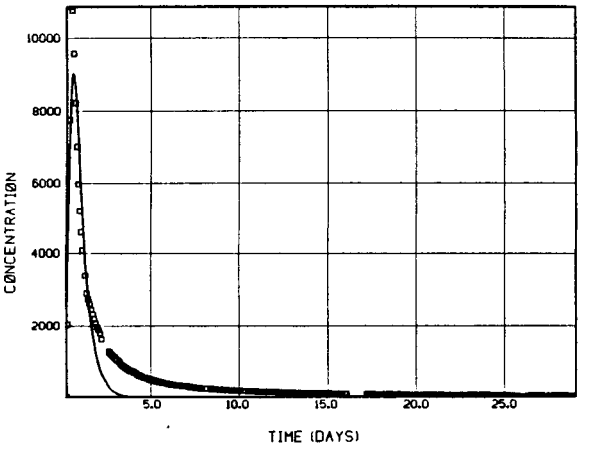


Figure 1: Wairakei (3/79) - CWK24 from WK107 Fossum model: single fracture fit

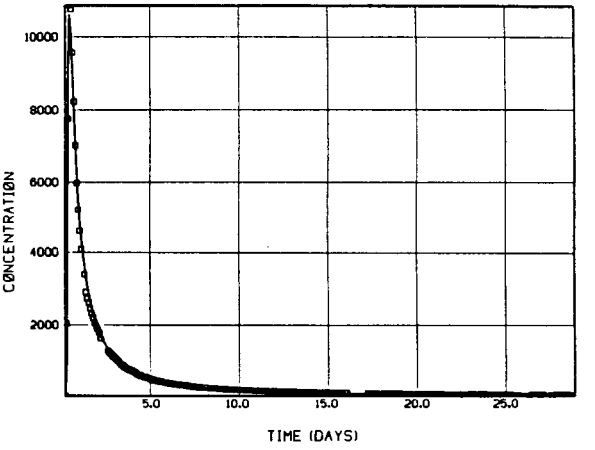


Figure 2: Wairakei (3/79) - CWK24 from WK107 Matrix diffusion model: single fracture fit

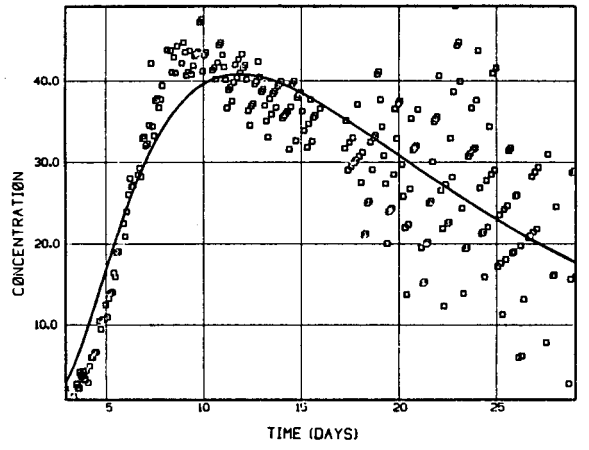


Figure 3: Wairakei (3/79) - CWK70 from WK107 Fossum model: single fracture fit

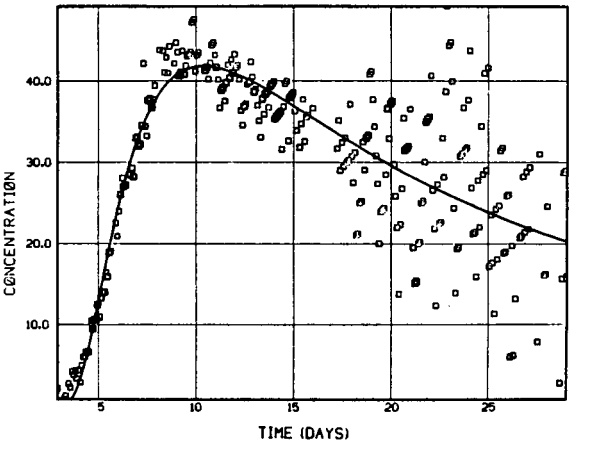


Figure 4: Wairakei (3/79) - CWK70 from WK107 Matrix diffusion model: single fracture fit

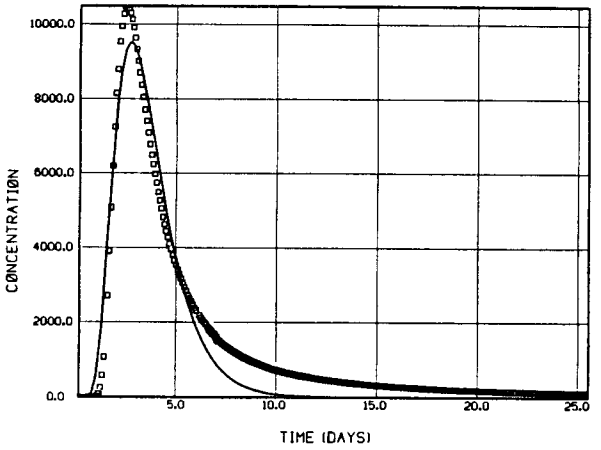


Figure 5: Wairakei (7/79) - CWK121 from WK101 Fossum model: single fracture fit

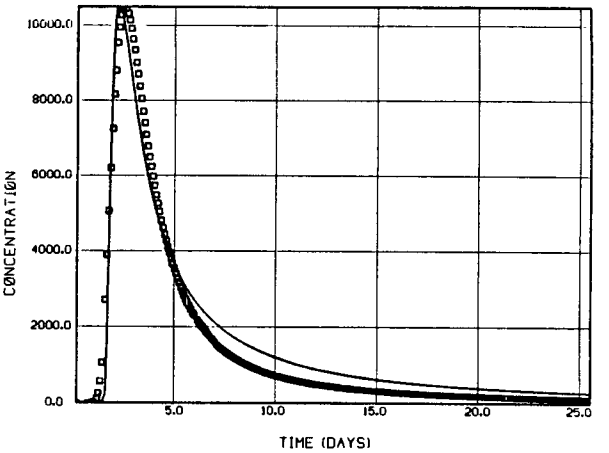


Figure 6: Wairakei (7/79) - CWK121 from WK101 Matrix diffusion model: single fracture fit

TABLE 1

Production well	Injector-Producer Distance (meters)	Flow Fraction ϵ_j/E	Nonlinear Parameters α_1	Nonlinear Parameters $1/\alpha_2$ (days)	Minimum Flow Velocity (m/hr)	Fracture Width (mm) ϕ=1%	Fracture Width (mm) ϕ=5%
WK24	210	1.000	1.250	0.231	37.9	0.08	0.18
WK30	240	0.811	1.370	4.367	2.3	0.32	0.71
		0.189	1.270	3.212	3.1	0.29	0.66
WK48	120	0.450	1.393	0.293	17.1	0.08	0.18
		0.550	1.669	1.040	4.8	0.13	0.28
WK55	220	1.000	2.578	2.671	3.4	0.13	0.29
WK67	120	1.000	2.736	1.651	3.0	0.10	0.22
WK68	120	1.000	2.049	2.919	1.7	0.17	0.39
WK70	170	1.000	2.483	2.033	3.5	0.12	0.27
WK81	175	1.000	1.535	3.659	_ 0	0.26	0.58
WK83	330	1.000	2.167	2.550	5.4	0.15	0.34
WK108	80	1.000	1.685	6.782	0.5	0.32	0.72
WK103	165	1.000	3.437	0.619	11.1	0.05	0.11
WK116	350	0.259	0.920	4.696	3.1	0.49	1.09
		0.741	3.844	0.626	23.4	0.04	0.10
WK121	490	1.000	0.916	1.451	14.1	0.27	0.61
		0.530	2.555	0.719	28.4	0.07	0.15
		-0.470	2.100	1.265	16.1	0.11	0.25

All production wells produce tracer injected at well WK107, except wells WK103, 116, and 121 which produce tracer injected at WK101.

Proceedings Ninth Workshop Geothermal Reservoir Engineering
Stanford University, Stanford, California, December 1983
SGP-TR-74

DOUBLET TRACER TESTING IN KLAMATH FALLS, OREGON

J. S. Gudmundsson, S. E. Johnson, R. N. Horne, P. B. Jackson
G. G. Culver*

Pet. Eng. Dept., Stanford University
* Geo-Heat Center, Oregon Institute of Technology

ABSTRACT

A tracer test was carried out in a geothermal doublet system to study the injection behavior of a developed reservoir known to be fractured. The doublet produces about 320 gpm of 160° F water that is used for space heating and then injected; the wells are spaced 250 ft apart. Tracer breakthrough was observed in 2 hours and 45 minutes in the production well, indicating fracture flow. However, the tracer concentrations were low and indicated porous media flow; the tracers mixed with a reservoir volume much larger than a fracture.

INTRODUCTION

The injection of spent geothermal fluids provides for an environmentally acceptable means of disposal and retards the impact of production on reservoir pressure. However, fluid injection also lowers the enthalpy of production wells so they become useless. What happens in a particular geothermal field is still a matter of speculation. Understanding of geothermal injection is made difficult because the reservoirs are highly fractured and isotropic. There is a need to extend our experience and know-how in geothermal injection technology.

The work reported in this paper was carried out in Klamath Falls, Oregon, in early-mid 1983. It is a progress report on a tracer test that was done as one part of a larger reservoir engineering research project. The main element of this project was an aquifer pump-injection-tracer test carried out in mid-late 1983. The Klamath Falls project had two main objectives: (1) to further our understanding of geothermal injection phenomena and (2) to provide reservoir engineering data to estimate the effect of pumping on wells with down-hole heat exchangers. The doublet tracer test addresses the first of these objectives.

The hydrogeology of the Klamath Falls area and the city's geothermal resources are discussed by Sammel (1980). The current status of hot water use in Klamath Falls is reported by Lund (1982); including institutional issues.

DOUBLET SYSTEMS

The Klamath Falls region is characterized by a network of northwest to southeast faults and fractures. The apparent geothermal resource is 3-4 miles long and about one mile wide, along the regional structure. It is a low to moderate temperature field and is located on the northeastern side of the city, where basin sediments meet uplifted rocks. The reservoir formation is almost nil to 1500 ft deep and consists of sedimentary deposits and volcanic rocks. The permeable zones of wells tend to be between basalt flows or granular sediments overlain by clay and silt deposits.

The main use of the geothermal resource in Klamath Falls is in space heating. More than 400 wells have been drilled since about 1930. The wells range in depth from 100-2000 ft (30-600 m) and reach temperatures of 70-230°F (20-110°C). The waters are of good quality with dissolved solids in the range 800-1200 mg/kg. Down-hole heat exchangers are used in most of the 400 wells.

Less well known, than the down-hole heat exchanger wells, are the doublet systems of Klamath Falls. These systems have one production well and one injection well. The hot water pumped from the production well is used for space heating via heat exchangers and then disposed of by injection. The two wells tend to be of similar depth and design; they are closely spaced. Several wells in the city are pumped but there is no injection of the spent fluids; the storm drain receives them. Also, some down-hole heat exchanger wells are pumped a little to maintain wellbore temperature.

Four doublet systems were identified as candidates for tracer testing: Klamath Union High School, Mazama High School, Mills School and the YMCA Center. The well data for these doublets are shown in Table 1. While these systems are the same in concept and similar in capacity, their operation is different. The main difference is the flowrate. The YMCA doublet is usually turned off during the night and has a low flowrate when in use. The wells in the Mills system are apparently

Table 1. Well data on doublet systems in Klamath Falls

Item \ Location	Union		Mazama		Mills		YMCA	
	P	I	P	I	P	I	P	I
Drilled (yr)	1964	?	?	1966	1961	1957	1979	1978
Depth (ft)	257	240	972	1210	800	809	1410	2016
Casing (ft)	257	120	934	1104	800	809	982	510
Perforated (ft)	176-180 236-257	-	60-400	-	680-800	769-809	-	-
Flow[a] (gpm)	?	?	360[b]	450[b]	250[c]	100[c]	310[b]	300[b]
Temp.[a] (^{o}F)	?	?	142	136	192	182	147	111
Spacing (ft)	~250		~300		~100		~400	
Pumping[d] (gpm)	~320		?		Low		20-40[e]	
Temp.[f] (^{o}F)	~160		~140		?		~140	

a: Completion flow test
b: Air lift pumping
c: Artesian flow
d: Current pumping
e: Intermittent flow
f: Production well

not always pumped because they also have down-hole heat exchangers; the wells are quite closely spaced. The Mazama doublet is operated all the time at a reasonable but unknown flowrate. It is located in the southeast of the city away from the area of greatest interest.

UNION DOUBLET

The Klamath Union High School doublet system is located where surface manifestations were found before, for example, Big Spring. The high school is close to the County Museum which is the area of main interest in the pumping-injection-tracer project. There are many other wells in the same area, some of which are pumped. The use of geothermal water at the high school dates back to 1946. The present doublet system started operating about twenty years ago.

The production well is 257 ft deep and perforated for 25 ft, most of which is near the bottom. A look at Table 1 shows that the injection well is 240 ft deep and cased to 120 ft; it was drilled at least ten years earlier than the production well. The wells are closely spaced, at a distance of about 250 ft. The Union doublet system was selected for this study because of the high flowrate and its location.

When school starts in the fall, the Union doublet system is turned on. It stays on until school is out in the spring. There is a down-hole pump in the production well which pumps a constant amount the whole school year. The flow is not measured. However, the pump installer estimates the flowrate to be about 320 gpm, based on the vertical turbine pump specifications, static water level and wellhead pressure. The doublet heating system is shown in Figure 1. At the wellsite, there are two buildings that are heated: a machine shed and a residence. They are heated by a slip stream from the wellhead. The shed system is turned on/off manually when needed and uses 4-5 gpm. The residence system is thermostatically controlled and uses 8-10 gpm when on. The return fluid from both of these systems is piped to the annulus of the production well, 5-6 ft below the wellhead. Therefore, the maximum slip stream flowrate is 15 gpm, or less than 5% of the total pumprate.

The high school is about 600 ft away from the doublet. The hot water goes to the school in a 6" pipeline and then passes through 13 shell-and-tube heat exchangers which are connected in a mixed series/parallel arrangement. The geothermal water is cooled in the heat exchangers and returned to the injection well. We need to know the travel time of the hot water from the production well to the injection well. This will depend

on the flowrate and the volume of the piping and heat exchangers. It takes about 3 minutes for water pumped at 305 gpm to travel 600 ft in a 6" pipe. If we assume that each of the 13 heat exchangers has the same volume as 600 ft of pipe, it will take 45 minutes for the geothermal water to go from one wellhead to the other. This is an order of magnitude estimate.

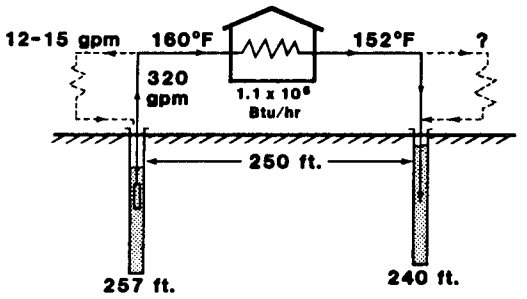


Figure 1: Klamath Union High School doublet and heating system

On pumping, the geothermal water cools a few degrees. At the start of the heating season the water temperature is 165°F (74°C) but it cools by 5°F in 3-10 days, depending on the heat load. Once this initial cooling has occurred, the water temperature remains constant until springtime. The following fall, the temperature is back to 165°F at startup. It seems likely that the injection of spent fluids causes this cooling of the production water. Long term cooling of the hot water has been observed by the operators of the Union doublet system. The records are not to be found, but it seems that the temperature dropped 6°F at about the same time as the Museum well (1235 ft deep) was drilled in 1975; there may or may not be a connection. The geothermal water enters the high school heat exchangers at 160°F (71°C) and leaves typically at 152°F (67°C). At 305 gpm this corresponds to 1.1 x 10^6 Btu/hr or 323 kW of thermal power.

At the site of the injection well, there is a swimming pool. It is heated by the cooled geothermal water returned from the high school building before it is injected. The arrangement is depicted in Figure 1. A slip stream is piped to two shell-and-tube heat exchangers in paralled. The amount of fluid used in the swimming pool exchangers is not known; neither are the discharge temperatures. A reasonable guess would be that the swimming pools system cooled the injection fluid by a degree or two and that it added a few minutes to the fluid residence time.

TEST PLANNING

The doublet tracer test was the first part of a larger reservoir engineering study of the Klamath Falls resource. This large study involved the wells of the recently constructed district heating system which has not yet been operated. The production well is located on the northeastern side of the resource about 3000 ft from the Museum well. This great distance and the many unknown factors in geothermal tracer testing called for a small-scale test beforehand: a doublet tracer test.

Iodide has been determined to be a useful chemical tracer for geothermal systems (Horne 1982). Its background concentration tends to be low and because it is a halide it is unlikely to interact much with the reservoir formation. Iodide salts are however expensive and difficult to analyze in most waters. Fluorescent dyes are commonly used in groundwater tracer studies (Smart and Leidlaw 1977). They are inexpensive and can easily be analyzed in low concentrations. The dyes used in water tracing are organic chemicals developed for low (ambient) temperature use. They are likely to break down and lose their fluorescent properties at geothermal temperatures. The nature and extent of this loss are however unknown; they are of no interest in common water tracing.

Rhodamine WT and fluorescein dyes were selected for use in the doublet tracer test. It was also decided to try potassium iodide because of its potential use in high temperature systems (at the time the authors were in the planning stage of a large high temperature reservoir tracer test elsewhere and wanted to try the chemical and the analytical method). The dyes are best measured in a fluorometer which is simple to use and inexpensive. To measure the iodide an ion specific electrode was used (Jackson 1983). The advantage of both methods (fluorometer and electrode) is that they are easily carried out in the field. The following detection limits were thought to apply for these techniques and materials:

Rhodamine WT	0.013	µg/kg
Fluorescein	0.29	µg/kg
Potassium iodide	1.0	mg/kg

The literature was searched for data on possible health risks associated with the tracer materials. It was found that no ill effects would be likely to occur upon drinking the geothermal water during the tracer test.

Two cases that represent the likely extremes were considered when estimating the mass of tracer materials to be injected: radial and doublet flow. When a fluid injected into one well moves radially, the breakthrough time t_r at distance r is given by the expression:

$$t_r = \frac{\pi r^2 \phi h}{Q}$$

where ϕ and h are the reservoir porosity and thickness, respectively, and Q the flowrate. The porosity-thickness product ϕh can be replaced by δ to represent the flow in a planar fracture of that thickness. A doublet configuration acts as a source-sink system. If x is the doublet spacing, the breakthrough time t_x will be 1/3 that of a radial system (Gove et al. 1970 and Klett et al. 1981), namely:

$$t_x = \frac{\pi x^2 \phi h}{3Q}$$

We assume that the tracer material mixes uniformly with all the fluid injected into the reservoir. Its concentration at the production well will then be the total mass of tracer divided by the fluid volume injected until breakthrough. The following data were used in the calculations:

Spacing	250 ft
Thickness	25 ft
Porosity	10 %
(Flowrate	305 gpm)

The corresponding radial and doublet volumes (V=Qt) were 13,800 m^3 and 4,600 m^3. If the desired tracer concentrations in the production well were empirically set 100x and 20x the detection limits of the dyes and potassium iodide, respectively, then the following shows the mass of tracers needed and the estimated breakthrough times:

	Radial	Doublet
Rhodamine WT	18 g	6 g
Fluorescein	400 g	133 g
Potassium iodide	276 kg	92 kg
Breakthrough time	200 hr	67 hr

Permits were obtained from the Department of Environmental Quality (State of Oregon) and the Department of Health Services (Klamath County) to inject 90 g and 900 g of rhodamine-WT and fluorescein, respectively, and 690 kg of potassium iodide (much less was injected). The price of the three tracers was similar on a pound-mass basis; 8-9 $/lb.

FIELD WORK

The rhodamine WT and fluorescein were mixed in 100 gallons of geothermal water. It took 15 minutes to pump this water into the injection well. One pound (450 g) of each material was injected. The rhodamine WT was in the form of a liquid 20% active; the one pound solution contained 90 g of this red-pink dye. Fluorescein comes in dry powder form and is greenish in water. All of this material was considered active. The potassium iodide was mixed in 150 gallons of geothermal water; it is readily soluable and colorless. The amount used was 500 lb (227 kg). It took 20 minutes to inject this solution. An ordinary agricultural sprayer was used for the injection. The tracers were injected at the wellhead of the injection well. The wellhead piping is such that the dyes are mixed immediately with the downflowing water. For the amounts of tracers injected (shown), the expected concentrations at the production well were:

	Radial	Doublet
Rhodamine WT (90 g)	0.0065 mg/kg	0.020 mg/kg
Fluorescein (450 g)	0.033 mg/kg	0.10 mg/kg
Potassium iodide (227 kg)	16.0 mg/kg	48.0 mg/kg

An automatic sampling apparatus was set up at the production well. It consisted of sixteen three-way solenoid valves that were operated by a programmable timer. The apparatus takes fifteen samples of any volume at any interval. The fluid to be sampled is directed through a filter and then cooled in a coil of tube. Flow is continuous through the apparatus until one of the three-way valves is activated by the timer. The flow is then directed into a sample bottle for a predetermined time. The apparatus was programmed to fill one bottle every 1/2 hour. Five other wells were sampled by hand during the tracer test. At first samples were collected every hour, then less frequently. The wells sampled are shown in Figure 2: Balsiger (260 ft deep), Creamery (765 ft), Eccles (787 ft), Friesen (563 ft) and Garrison (240 ft). The flowrate of the Creamery well was measured 75 gpm and the temperature 180°F. The flow in other wells had to be guessed; Balsiger 30 gpm, Eccles and Friesen 20 gpm and Garrison 10 gpm. Other wells in the area were not pumped at the time of the testing.

The dyes were measured in a Turner 112 fluorometer. One of the purposes of the tracer test was to evaluate which of the two dyes was better for geothermal tracer studies. We found out that injecting them at the same time was not desirable. A mixture of two dyes tends to have less color than just one dye. And although recommended lamps and filters were used in the fluorometer, there was measurable interference. A reading on the fluorometer could not be assigned to one dye only; the values obtained were therefore qualitative. During the tracer test, the water samples were analyzed the same or following day that they were collected, at least for the first week or so. The fluorometer was set (lamp and filters) to detect fluorescein. Not every sample collected was analyzed, but every second or third. We wanted to know where and when the tracers broke through. The idea was that we could later analyze the samples initially left out. However, a complicating factor is that the color of dye solutions decreases with time, more rapidly so for fluorescein than rhodamine WT. The samples from one well

were measured with the rhodamine WT setting of the fluorometer. The iodide was measured by ion-selective analysis; the Accument 750 meter from Fischer was used.

BREAKTHROUGH CURVES

A tracer breakthrough curve shows the concentration of a tracer with time; a sort of a travel log. It provides a record of what happens underground when a fluid flows between the wells of a doublet system, for example. The interpretation of a tracer breakthrough curve depends on knowing what physical and chemical principles apply. In geothermal reservoirs these principles are little known and field data are limited. The doublet tracer test was carried out to address this problem.

The flow pattern in the Klamath Union High School doublet is complicated by the fact that other pumped wells are in the area. The largest of these is the Creamery well about 450 ft away from the injection well and pumped 75 gpm. These and other wells are shown in Figure 2. The following breakthrough times were measured in the wells:

Production	2-3/4 hr
Creamery	20 hr
Balsiger	~100 hr

These times are only a fraction of what was expected. The tracer broke through in the production well 25-75 times faster than estimated (above) before the test. Tracer returns were not detected in the Friesen and Garrison wells.

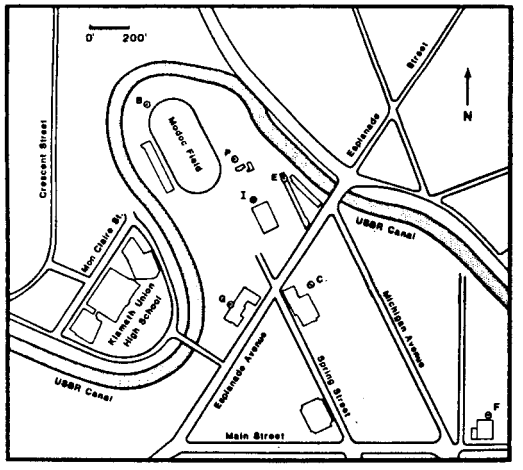


Figure 2: Location of wells in doublet tracer test: (I) Injection, (P) Production, (B) Balsiger, (C) Creamery, (E) Eccles, (F) Friesen and (G) Garrison

Breakthrough curves for the production and Creamery wells are shown in Figures 3, 4 and 5. Other data are not reported here for brevity. Figures 3 and 5 show the fluorometer reading (not calibrated) when set for fluorescein and rhodamine WT, respectively. The concentration readings are not comparable. In Figure 5 there are two data sets; the lower values were measured about two months later. Figure 4 shows the concentration of potassium iodide in the production well.

The potassium iodide concentration expected in the production well was 16-48 mg/kg; the maximum observed was about 60 mg/kg. An examination of Figure 4, and keeping in mind the circulation time, shows that the first breakthrough was similar to a doublet behavior. Also, the potassium iodide concentration falls to a level of about 20 mg/kg in a day or so. This would say that with time the system approaches radial behavior. These observations are based on radial and doublet fluid volumes of 13,600 m^3 and 4,600 m^3, respectively.

However, the fluid volume injected until breakthrough in the production well was small. In 2-3/4 hr at 305 gpm, only 191 m^3 of water was injected. The doublet and radial volumes that give appropriate tracer concentration (shown above) are 24 and 72 times larger! What is the cause of this order-of-magnitude discrepancy? In waterflooding (Craig 1971) the "area sweep efficiency at breakthrough" for common well patterns is usually 50-80%. This means that the area (volume) swept by injected water is typically of the same order-of-magnitude as the pattern drainage area. In geothermal we have more than simple displacement.

The doublet system at the high school has been in operation more than 20 years. For about nine months each year 305 gpm are pumped out at 160°F and injected at about 152°F. It is clear that the reservoir rock between the production and injection wells cannot sustain the thermal output of the system. There is likely to be intensive mixing of the injected and hotter fluids in the drainage volume of the production well; the cooled fluids tend to flow down and hotter fluids ascend. This mixing action must be rapid as evident from the experimental results. The following working hypothesis seems to fit the observations: the injected fluid moves rapidly along fractures to the production well, and on the way some of it mixes with fluids flowing up/down in crossflow fractures.

CONCLUDING REMARKS

The results presented in this paper are one part of a larger project. The data have not been fully analyzed, so the outcome of the

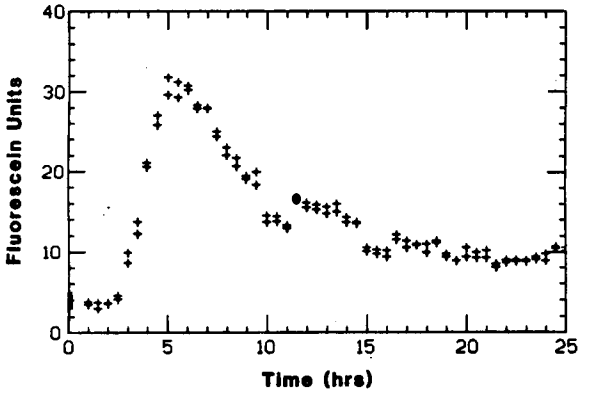


Figure 3: Fluorescein breakthrough curve in production well

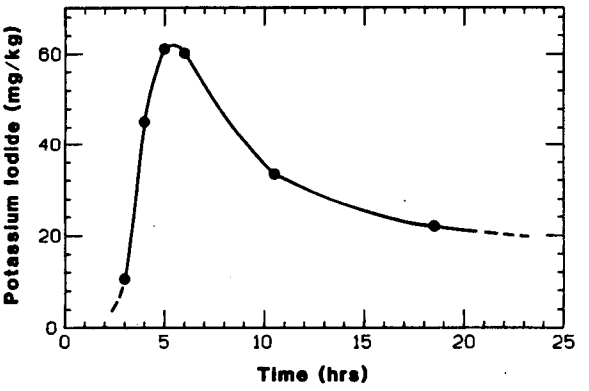


Figure 4: Potassium iodide breakthrough curve in production well

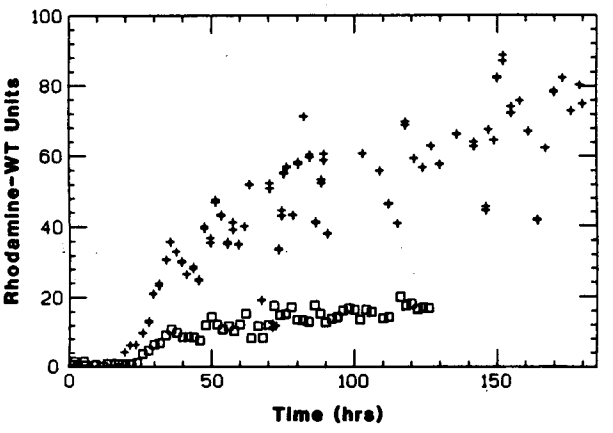


Figure 5: Rhodamine-WT breakthrough curve(s) in Creamery well. Samples measured during test (+) and two months later (□)

doublet tracer test reported here must be viewed as a progress report. Nevertheless, some conclusions are warranted from the observations made so far:

(1) The automatic sampling apparatus worked well and is a time saving device of great value. The two analytical methods, used to measure the halide ion and dyes concentrations, were found to be most applicable in the field. Better methods are available for measuring iodide in the laboratory, but fluorometry is best for dyes. More time and care was needed for the analytical techniques used than anticipated.

(2) Dyes are more cost effective than halides for tracer work in low to moderate temperature geothermal reservoirs.

(3) Rapid tracer breakthroughs were found in wells that were pumped at high rates. These also happen to lie parallel to the dominant fracture/fault direction northwest to southeast of the region.

(4) A great disparity was found between reservoir characterization based on tracer concentration and breakthrough times. The concentrations measured indicate doublet behavior initially, and radial behavior at later times. The tracer breakthrough times were rapid and indicated much lower porosity-thickness values than expected.

(5) The data point to an important consequence for geothermal injection. While tracer returns (breakthrough time) indicate small reservoir volumes, the mixing or contact volume of the fluid appears to be much larger. The consequences of injecting cold fluids would appear not to be as great as indicated by tracer tests.

ACKNOWLEDGEMENTS

We would like to thank our colleagues at the U.S. Geological Survey and Lawrence Berkeley Laboratory for their cooperation in this work. Our appreciation to the people of Klamath Falls, in particular, Earl Ferguson, superintendent, for his permission in carrying out the test. The following students at Stanford University also took part in this project: Gardner Walkup, Clair Jensen and John Gilardi. We want to thank the several students at Oregon Institute of Technology that helped in the sample taking and analysis. Thanks to Marty Molloy and Jane Hadley of U.S. Department of Energy for their contribution to this project. This work was carried out under the auspices of the Stanford Geothermal Program and the Geo-Heat Center with support from the U.S. Department of Energy.

REFERENCES

Craig, F.F., 1971: "The Reservoir Engineering Aspects of Waterflooding," SPE Monograph, 3.

Grove, D.B., Beetem, W.A. and Sower, F.B., 1970: "Fluid Travel Time between a Recharging and Discharging Well in an Aquifer having a Uniform Regional Flow Field," Water Resources Research, 6, 1404-1410.

Horne, R.N., 1982: "Geothermal Reinjection Experience in Japan," J. Pet. Tech., 34, 495-503.

Jackson, P.B., 1982: "Method for the Collection and Analysis of Sample Fluids during a Tracer Test," MS Report, Petroleum Engineering Department, Stanford University.

Klett, R.D., Tyner, C.E. and Hertel, E.S., 1981: "Geologic Flow Characterization using Tracer Techniques," Sandia National Laboratories, Report SAND80-0454.

Lund, J.W., 1982: "Current Status of Geothermal Utilization in Klamath Falls, Oregon, "Proc. Int. Conf. Geoth. Energy, Florence, Italy, 121-130

Sammel, E.A., 1980: "Hydrogeological Appraisal of the Klamath Falls Geothermal Area, Oregon," U.S.G.S. Professional Paper 1044-G.

Smart, P.L. and Laidlaw, I.M.S., 1977: "An Evaluation of Some Fluorescent Dyes for Water Tracing," Water Resources Research, 13, 15-33.

Proceedings Ninth Workshop Geothermal Reservoir Engineering
Stanford University, Stanford, California, December 1983
SGP-TR-74

LABORATORY PHYSICAL MODEL FOR PATTERN INJECTION IN GEOTHERMAL SYSTEMS

M. Parlaktuna and E. Okandan

Middle East Technical University
Ankara - Turkey

ABSTRACT

In the development of geothermal sources for power generation, production of geothermal fluids as well as reinjection becomes an important aspect for significant heat extraction from the reservoir rock.

The purpose of this work was to understand how cold water injection in five spot pattern affected the temperature distributions and production pressures in a physical model with a constant temperature heat source. The production and injection rates were varied as well as their respective depths.

The model is a hot water dominated system with crushed limestone of 0.6-0.9 cm particle size as the reservoir rock, which had 40% porosity, 58 darcy permeability. The analysis revealed that injection rate should be at least 2/3 of production rate (measured as condensed water) so that the pressure decline at the producing end was stopped. Heat extraction from the system was high when injection was done towards the top of the model while production horizon was deeper.

INTRODUCTION

Reinjection of waste waters in geothermal power generating plants had the prime reason of eleminating the danger of environmentally hazardous elements in geothermal fluids. However it was observed in certain field applications that reinjection if applied properly had the effect of pressure maintenance in the geothermal reservoir and power output was increased accordingly.(1)

The studies of reservoir performance becomes important in order to predict the behavior of geothermal fields under reinjection. There are several numerical modelling studies reported (2-3) but still there are several unknown physical phenomena which cause these models to be in limited use.

Physical laboratory model studies reported in literature are also limited. Stanford geothermal model(4) is a fracture stimulated model where cold water is injected from the bottom of the heated reservoir and temperature behavior is analyzed. Schrock and Laird(5) had studied the effects of cold water injection in a rectangular model which had a source and a sink located towards the center.

The study described in this paper deals with a three dimensional geothermal reservoir model, quadrant of a five spot pattern where the effects of cold water injection on temperature distribution and producing pressure was investigated.

EXPERIMENTAL SET UP AND PROCEDURE

The physical model is a metal box with 50 cm length and width and 20 cm depth. The porous medium is a crushed limestone pack with 0.6 cm-0.9 cm particle size. Porosity was 40% and permeability was measured as 58 darcies.

The heating elements were placed at the bottom of the model and their temperatures were controlled at 120°C thus a constant temperature heat source was created. The cold water injection was performed by a pump and outflow rates were measured as condensed water volume/unit time. The temperature at different locations in the model were measured using 54 thermocouples and a temperature scanner. Thermocouples were placed on 5 layers in the model and in the injection and production ports. The experimental set up and model configuration is given in Figure 1.

Each experiment was started by heating the model until constant temperatures were recorded in each thermocouple. In all experiments a temperature gradient along the depth of the model existed, which may be regarded as similar to a natural condition. After this heating period, production at constant rate was started from the producing end and initial producing pressures were recorded, which ranged from 99 kPa to 117 kPa. The production continued until pressure declined to 68 kPa and then water injection was initiated at a desired rate at a certain depth. The temperature, the producing pressure and production rates were recorded in 10 minute intervals during the experiments.

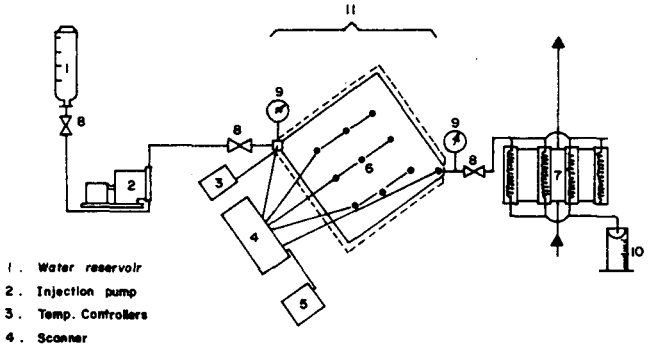


Figure 1. Experimental Set-up

RESULTS AND DISCUSSION

During the experiments the producing pressure was taken as the controlling parameter to initiate or to end the cold water injection. When the pressure at the producing end declined to 68 kPa (10 psig), injection was initiated. The pressure increased or decreased depending on the production and injection rates. When the pressure of the system increased, the experiments were terminated if the maximum pressure recorded did not change for the last 30 minutes. For the case where pressure decline was observed the tests were stopped when the difference between two successive pressure readings in the 10 minute interval was 0.1-0.2 psi.

The constant temperature heat source was set to 120°C. The injection and production rates and depths in experiments were varied as shown in Table 1. The results are discussed by grouping the conditions as the effect of production and injection rates and effect of injection and production depths on producing pressure behavior and temperature distribution in the model.

In the analysis two definitions were used. Production to injection ratio, P/I, is defined as

$$P/I = \frac{\text{Production rate before injection}}{\text{Injection rate}}$$

The range of P/I values obtained in the experiments is also given in Table 1.

Pressure recovery index is given as

$$PRI = \frac{\text{Prod.Press.after Inj. - Press.before Inj.}}{\text{Press.before Inj.}}$$

and it is an indication of how producing pressures had changed with the injection of cold water.

The Producing Pressure

The decline in producing pressures prior to injection had shown similar trend in all experiments depending on the production rates. The behavior after the start of injection changed depending on the P/I ratio of the experiment.

The first group of experiments showed a decline in pressure even after the injection. The second group had experienced almost constant production pressures while the third group had responded with increase in pressure. (Figure 2). As seen from the figure the experiment with P/I of 1.44 exhibits a very small increase in producing pressure after injection was started and stayed almost constant. For values of P/I less than 1.44 increase in pressure while for values greater than 1.44 decrease in pressure was observed.

The data is also analyzed by looking at the change in PRI as a function of P/I at 3 different injection periods namely 70, 90 and 110 minutes of injection. The results are shown in Figure 3. The zero PRI indicates that there will be no change in producing pressure after the start of injection while PRI less than zero means pressure will be decreasing while positive values indicate an increase in pressure. The relationship has two straight line portions. For P/I greater than 2 a steeper line is obtained than the straight line for P/I less than 2. So for P/I of 2 and greater, the system did not feel the injection and behaved as if only production was present. At zero PRI the P/I value is 1.5, which indicates that below this limit, pressure recovery from the model will be more efficient.

Table 1. Experimental Conditions

Injection Depth.	Exp. No.	Prod. Rate 10^{-3} m^3/D	Inj. Rate 10^{-3} m^3/D	P / I	Final Prod. Press (kPa)
17 cm from top of model	5	11.8	8.2	1.44	67.6
	6	11.3	8.4	1.35	80.0
	7	12.2	5.9	2.07	37.9
	8	14.4	4.7	3.06	29.6
	11	13.6	20.8	0.65	100.0
	12	8.1	8.0	1.01	89.6
4 cm from top of model	9	12.3	4.2	2.93	42.1
	10	14.5	18.9	0.77	99.3
	13	10.7	10.7	1.00	89.6
	14	8.5	15.8	0.54	110.3
	15	9.0	4.6	1.96	35.2

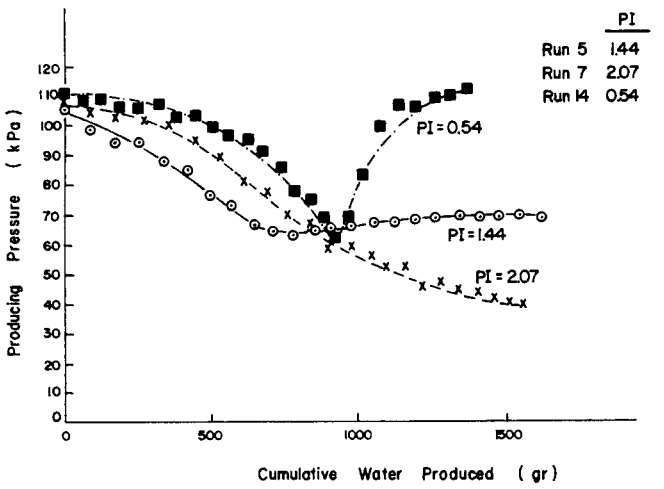


Figure 2. Effect of P/I on producing pressure

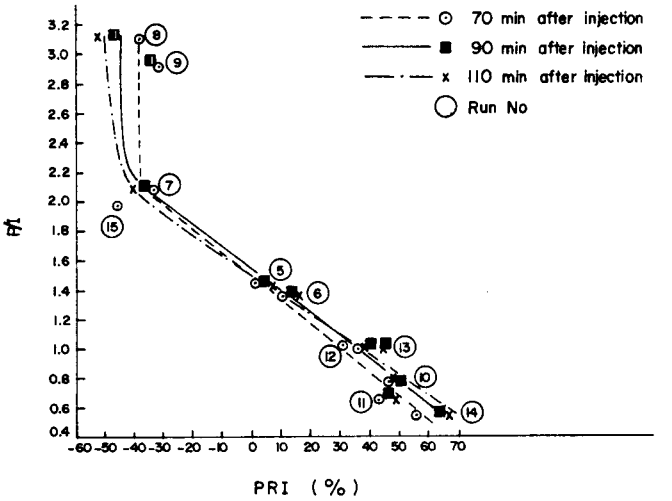


Figure 3. Effect of P/I on pressure recovery index

The producing pressures as a function of P/I at two different injection depths are shown in Figure 4. For low P/I values and shallow injection depths higher pressures were recorded.

Temperature Distribution

As may be expected from the producing pressure behavior, the temperature distributions were affected by the injection and production rates and their respective depths. The variations will be presented as areal temperature distributions and distributions along the vertical plane of the diagonal line.

The behavior before injection was dependent upon production rates where higher rates resulted in higher temperatures. Figure 5 illustrates areal and vertical diagonal temperatures when producing rates were $10x10^{-3}$ m^3/D and $14.4x10^{-3}$ m^3/D. Same distributions were observed in experiments where production rates were close to each other. This behavior is believed to be the result of efficient convective heat transfer from the heat source at higher rates.

The temperature behavior after injection, was analyzed as a function of P/I ratio and injection depth. The experiments were grouped as 1) injection port at a deeper level (17 cm from top) than production (11 cm from top) 2) injection port at a shallower depth (4 cm from top) than production, and for comparison temperature readings at 70 minutes of injection time were taken, to draw the following figures.

In each group increase in P/I resulted in a general decrease in temperature distribution in the model. In Figure 6a the effect of increasing P/I ratio is obvious. The higher rates of cold water injection caused a decrease in the temperature and towards the producing end gradual heating was observed. Figure 6b illustrates the same observation but at a shallower depth of injection. The comparison of Figures 6a and 6b which were drawn for similar P/I values but at two different injection depths shows that the temperature of the system was relatively higher when injection was performed at a shallower depth than production. This was observed in the areal temperature distributions also.

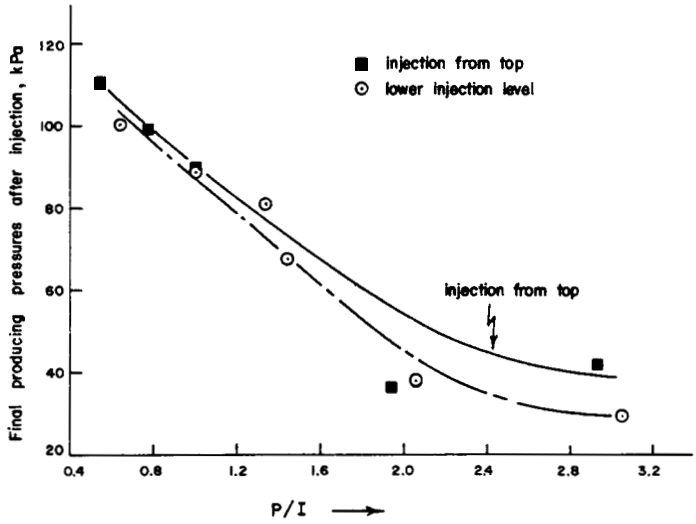
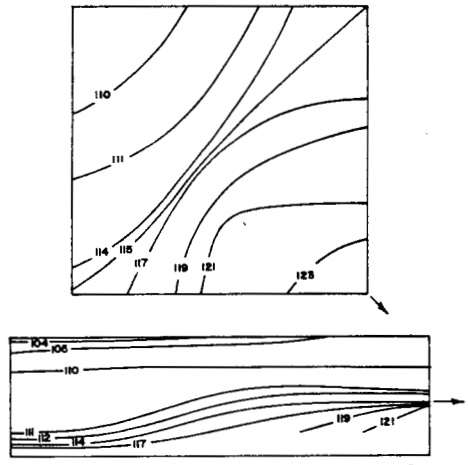
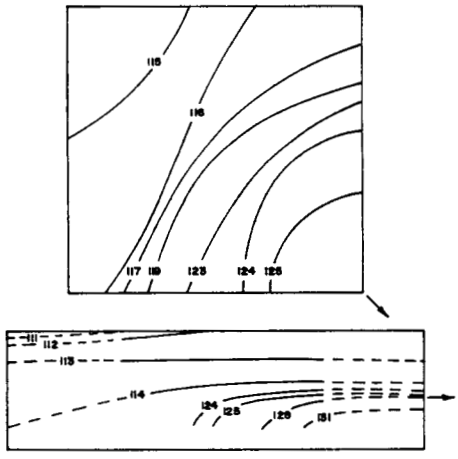


Figure 4. Variation of producing pressures with P/I and depth of injection

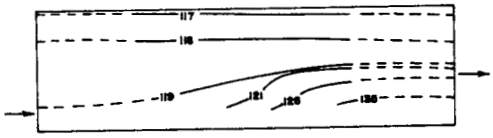


Run 13, Production rate : 10.7×10^{-3} m^3/D

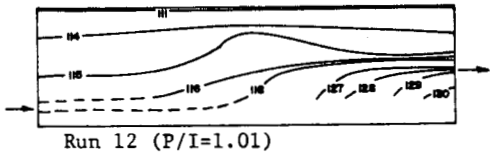


Run 8, Production rate : 14.4×10^{-3} m^3/D

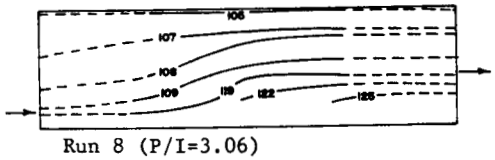
Figure 5. Effect of production rate on temperature distribution before injection



Run 11 (P/I=0.65)

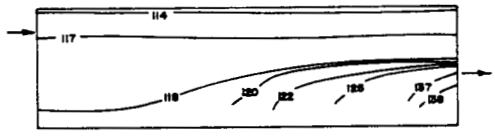


Run 12 (P/I=1.01)

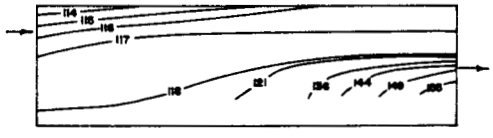


Run 8 (P/I=3.06)

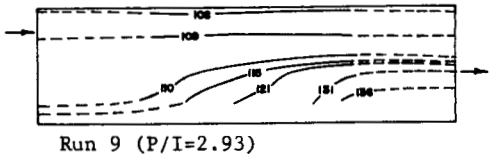
Figure 6a. Effect of P/I on vertical temperature distribution for injection at a deeper zone.



Run 14 (P/I=0.54)



Run 13 (P/I=1.00)



Run 9 (P/I=2.93)

Figure 6b. Effect of P/I on vertical temperature distribution for injection at a shallow depth.

Figure 7 was drawn for P/I of 0.65 and 0.54 and injection depths of 17 cm and 4 cm from the top of the model respectively. Figure 8 shows temperature at the producing end for Run 14 where P/I is 0.65. After the injection of cold water a slight decrease and then an increase in the produced fluid temperature even above that of the initial value was observed. This also indicates efficient heat recovery from the reservoir.

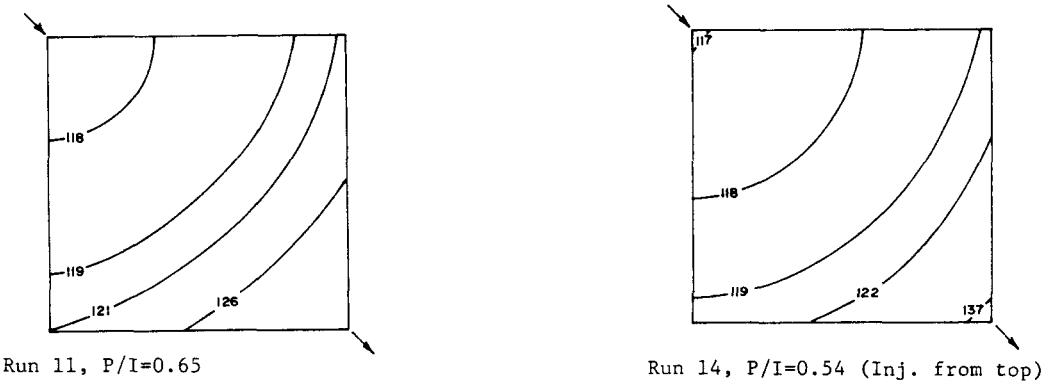
In all experiments, higher temperatures were recorded, in the lower section of the producing end. This may be due to stagnant fluid body in that section and/or extra heating from the heat source since thermocouple for temperature controller of the heating element was placed at the center of the model.

CONCLUSIONS

In the experiments conducted on a physical model of a water dominated geothermal system for cold water pattern injection, the following conclusions were reached:

1. The production rate to injection rate ratio was a critical parameter in the behavior of producing pressures as well as temperature distributions. The P/I ratio should be at least 1.5 in order that the pressure drop in the system was stopped, or in other words pressure recovery index to be zero. Lower P/I values resulted in pressure recovery while higher values caused continuous drop in producing pressure. Low P/I values also caused efficient heat extraction from the system.

2. The depth of injection relative to production also affected the behavior of the model. When injection was performed at favorable P/I values and at a shallower depth than production, extraction of heat by the injected water was more efficient.



Run 11, P/I=0.65

Run 14, P/I=0.54 (Inj. from top)

Figure 7. Effect of injection depth on areal temperature distribution

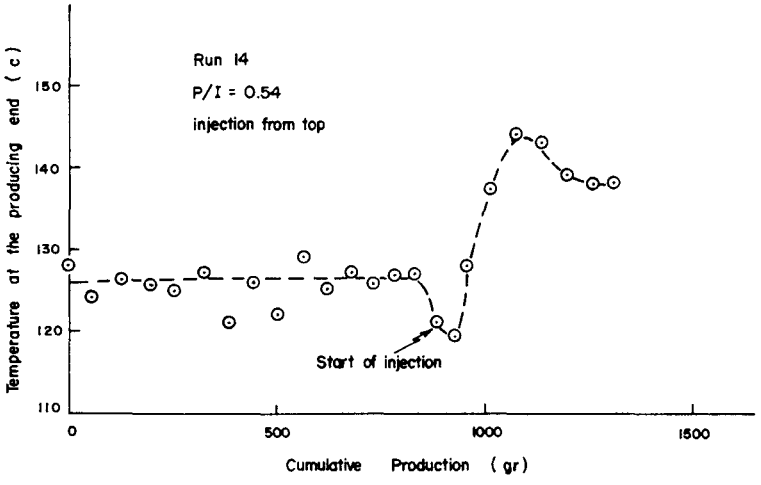


Figure 8. Temperature at the producing end for Run 14

REFERENCES

1. Horne, R.N. (1982) "Geothermal Reinjection Experience in Japan", Journal of Petroleum Technology, May 1982, 495.

2. Faust, C.R. and Mercer, J.W. (1979) Mathematical "Models for Liquid and Vapor Dominated Hydrothermal Systems" Water Resources Research, 15, 1, 23-46.

3. Thomas, L.K., Pierson, R.G. (1978) Three dimensional Geothermal Reservoir Simulation" SPEJ, 18, 2, 151-161.

4. Hunsbedt, A., P. Kruger, A.L. London (1978) "Laboratory Studies of Fluid Production from Artificially Fractured Geothermal Reservoirs", Journal of Petroleum Technology, May, 1978.

5. Schrock, V.E., Laird, A.D.K. (1976) "Physical Modeling of Combined Forced and Natural Convection in Wet Geothermal Formations", Journal of Heat Transfer, May 1976, 213.

Proceedings Ninth Workshop Geothermal Reservoir Engineering
Stanford University, Stanford, California, December 1983
SGP-TR-74

ANALYSIS OF PRODUCTION DATA FROM THE KRAFLA GEOTHERMAL FIELD, ICELAND

K. Pruess and G.S. Bodvarsson
Earth Sciences Division
Lawrence Berkeley Laboratory
University of California
Berkeley, California 94720

V. Stefansson
National Energy Authority of Iceland
Reykjavik, Iceland

Introduction

The Krafla geothermal field in northeastern Iceland consists of several zones, which contain fluids of different composition and thermodynamic state (Stefansson, 1981). In this paper we examine production data from wells which are completed in two-phase zones. Transient changes in flow rate and flowing enthalpy are analyzed to obtain insight into relative (liquid and gas phase) permeabilities, and other reservoir parameters.

Numerous studies have shown that predictions of geothermal reservoir behavior are strongly dependent upon the choice of relative permeability functions. There is an extensive literature on gas-oil and oil-water relative permeabilities, but steam-water relative permeabilities which are needed for geothermal reservoir analysis are poorly known. Laboratory experiments by Chen et al. (1978) and Counsil and Ramey (1979) have provided some data which, however, seem to be at variance with relative permeability characteristics deduced from field data by Grant (1977) and Horne and Ramey (1978). The differences may reflect uncertainties in the analysis methods used, or they may reflect "real" differences in relative permeability behavior of fractured reservoirs from that of porous medium-type laboratory cores. Recent theoretical work by Menzies (1982) and Gudmundsson et al. (1983) has substantiated the relative permeability characteristics obtained by Horne and Ramey (1978) for Wairakei wells.

Production Data

Krafla wells completed in two-phase zones show strong transients in flow rate and enthalpy when first put on production. As a typical example of this behavior, Figure 1 shows production data from well 12. Initially the well produced approximately 14 kg/s of water and 20 kg/s of steam from a reservoir at a temperature of approximately 320°C. Within a few days water production ceased, and steam production dropped to approximately 10 kg/s. After three months steam production had declined to 6 kg/s, while enthalpy continued to increase slowly.

The observed transients of flow rate and enthalpy are influenced by many reservoir properties in the vicinity of the well. In general, the main parameters governing well behavior are: permeability, porosity, effective wellbore radius (skin), in-place vapor saturation, and relative permeability characteristics of the medium. Many of these properties may be spatially variable, and a priori knowledge of the relevant parameters is limited.

In Figure 2 we have plotted flow rate on a logarithmic scale versus flowing enthalpy for several Krafla wells completed in two-phase zones. When plotted in this fashion, most data points fall on smooth curves, with some approximately linear sections (Stefansson et al., 1982). The sizeable scatter of the data present in some cases for wells 12 and 14 occurs because of variations in well head pressure. We have drawn smooth curves through the data points, which for wells 12, 13, and 15 are approximately parallel. This indicates similar relative permeability characteristics for these wells. Well 14, which is completed in a different reservoir zone (Bodvarsson et al., 1983a), is operated at a much higher well head pressure, and shows a different correlation between flow rate and enthalpy.

Relative Permeability Analysis

We have used the smoothed field data (see Figure 2) to study the relative permeability behavior of wells 12 through 15. Our method of analysis is similar to that of Grant (1977), and can be summarized with the following equations. The flow rate of a two-phase well is written

$$q = PI(p - p_{wb}) \left[\frac{k_{r\ell}\,\rho_\ell}{\mu_\ell} + \frac{k_{rv}\,\rho_v}{\mu_v} \right] \qquad (1)$$

Here PI is the productivity index of the well, p is an average reservoir pressure in the vicinity of the well, and p_{wb} is the flowing down-hole pressure. Parameters specific to the liquid phase are: relative permeability $k_{r\ell}$, density ρ_ℓ, and viscosity μ_ℓ, with analogous definitions applying to the vapor phase. The parameter group PI $(p-p_{wb})$ is identical to the parameter B used by Grant (1977).

Expressing flowing enthalpy as:

$$h = \frac{\frac{k_{r\ell}}{k_{rv}}\frac{\rho_\ell}{\mu_\ell}\,h_\ell + \frac{\rho_v}{\mu_v}\,h_v}{\frac{k_{r\ell}}{k_{rv}}\frac{\rho_\ell}{\mu_\ell} + \frac{\rho_v}{\mu_v}} \qquad (2)$$

we have two equations relating the measured quantities q and h to the three unknowns $k_{r\ell}$, k_{rv}, and B. Grant (1977) obtained the needed third equation by considering a well which at some time was flowing at single-phase liquid conditions, in which case

$$q_\ell = B \frac{\rho_\ell}{\mu_\ell} \qquad (3)$$

To obtain B-values for other wells, Grant shifted their log q vs. h-plots to obtain the best common plot. In our case this step is not necessary, because all wells considered here did actually reach single-phase (vapor) flow conditions, so that the vapor form of equation (3) can be used directly. The relative permeabilities obtained on this basis, assuming an average reservoir temperature of T = 300°C, are plotted versus flowing enthalpy in Figure 3. The curves for different wells are rather different, with well 12 relative permeabilities generally considerably larger than those for the other wells.

The above analysis was based on the assumption that B is a constant parameter for each well, independent of flowing enthalpy. We suggest that this is a rather poor approximation, because both flowing downhole pressure p_{wb} and average reservoir pressure p near the well may vary considerably with flowing enthalpy. Using the smoothed data as shown in Figure 2, we compute B both for single-phase liquid (h_ℓ = 1344 kJ/kg) and for single-phase vapor (h_v = 2749 kJ/kg). The results are given in Table 1. We then re-analyze the smoothed q vs. h data, using equations (1) and (2) with linear interpolation for the well indices between their liquid and vapor values:

$$B(h) = \left[PI\ (p-p_{wb})\right]_h$$

$$= B_\ell + \frac{h-h_\ell}{h_v-h_\ell}\left[B_v - B_\ell\right] \qquad (4)$$

Figure 4 shows that with this renormalization the relative permeabilities for wells 12, 13, and 15 practically collapse into single curves. This provides evidence that the relative permeabilities for these wells are in fact virtually identical, and that the approximation made in (4) is valid. Well 14 shows a somewhat different behavior, which may indicate a true difference in relative permeability characteristics between different reservoir zones.

Inspection of Figure 4 shows that $k_{r\ell} + k_{rv} \approx 1$ to a good approximation over the entire range $h_\ell < h < h_v$. A similar conclusion was reached by Bodvarsson et al. (1983b), based on observed transients in steam rate at the separators for well 13, in response to injection into nearby well 7. It is also interesting to note that the shape of the relative permeability curves is rather similar to the theoretical streamtube model predictions of Menzies (1982) and Gudmundsson et al. (1983).

It should be emphasized that the relative permeability information obtained from the above analysis remains incomplete. Figure 4 displays relative permeabilities as functions of flowing enthalpy. However, for applications in geothermal reservoir modeling it is necessary to express relative permeability as a function of thermodynamic state variables, such as in-place vapor saturation. The relationship between S and flowing enthalpy h is unknown, so that the relative permeabilities as given in Figure 4 cannot be used in a numerical model. In fact, any relative permeability functions $k_{r\ell}(S)$, $k_{rv}(S)$ with $k_{r\ell} + k_{rv} \approx 1$ and monotonic dependence upon S are consistent with the results of our analysis.

Modeling of flow rate and enthalpy transients

The foregoing relative permeability analysis employed only the observed correlation between flow rates and enthalpies. The actual temporal variation of q and h did not enter into the discussion. Here we shall examine the transients as observed for well 12 (see Figure 1) to deduce further information about reservoir parameters and conditions.

We have used our numerical simulators SHAFT79 (Pruess and Schroeder, 1980) and MULKOM (Pruess, 1983) to model the time dependence of flow rate and enthalpy. As a first approach we use the field-measured flow rates as input to the simulator, and attempt to match the observed enthalpy transients. Table 2 shows parameters which were kept fixed in the simulations. Assuming uniform initial vapor saturation, we made an extensive parameter search for porosity, permeability, effective formation thickness, and relative permeability, using both porous and fractured porous medium models. This particular effort failed to produce anything resembling the observed enthalpy transient. The main shortcoming of all models with uniform vapor saturation is that they predict a much more rapid rise in enthalpy than is observed in the actual test. This discrepancy suggests that vapor saturation at the time when well 12 was opened for discharge was in fact nonuniform, with smaller values near the well.

A possible explanation for a nonuniform saturation distribution may be found in the drilling and completion practice. During drilling the reservoir region around the bore is cooled by circulating drilling fluid, which may cause some steam condensation in the formation. Furthermore, at the end of the drilling process cold water is continuously injected for a few days during well logging, testing, and stimulation. The average total mass of injected water has been estimated as 3000-5000 tonnes (Benediktsson, personal communication, 1982). Subsequently the well heats up for several weeks before being placed on production. If steam condensate and injected water remain in the vicinity of the bore rather than being dispersed over a larger reservoir region, this would provide an explanation for a nonuniform initial vapor saturation. Changes in the N_2/H_2 ratio of produced waters show that indeed for several days after placing a well on production a mixture of injected and reservoir waters is produced (Gislason et al., 1978).

Based on these considerations a conceptual model was developed in which the bulk of the reservoir has a "background" vapor saturation S_b, while near the well the initial vapor saturation is $S_n<S_b$. The "excess mass" present near the well due to steam condensation and cold water injection is

$$M_{ex} = V_n \phi (S_b - S_n)(\rho_\ell - \rho_v) \qquad (5)$$

where V_n is the volume of the zone with $S=S_n$. Because of this excess mass enthalpy transients would be slower, as indicated by the field data. The radius of the "near-zone" V_n, which contains the excess mass and is in high-permeability contact with the well, was rather arbitrarily fixed at R_n = 10 m (corresponding to a negative skin value of s ◘ -4.5). By varying relative permeability functions and porosity in the near-zone, several excellent matches to the enthalpy transients were obtained. Examples are shown in Figure 5, while Table 3 gives the key parameters for different cases.

It is apparent that the data can be matched equally well with different values for irreducible water saturation and initial vapor saturation. The different cases all agree closely in the excess mass present near the well, which also agrees well with the total amount of water injected. This together with the good quality of the enthalpy match gives strong support for the conceptual model employed in the simulations.

Despite the success of the model in matching field data it provides only rather limited insight into reservoir parameters. It does show clearly that the injected water remains near the well for a period of weeks. Furthermore, the water is in high-permeability contact with the wellbore. However, none of the important reservoir parmeters, such as porosity, volume of the near-zone, initial vapor saturation in the near zone, functional form of relative permeabilities, and irreducible saturations, are uniquely defined.

Deliverability Model

The model discussed in the previous section employs part of the test data (time-dependent flow rates) to predict the enthalpy transients. While this has yielded a good match and a consistent description, it is desirable to develop a more comprehensive model in which all test data are matched with calculated values rather than prescribing some as input.

Here we present results from a "deliverability model", in which production rate depends upon reservoir pressure according to equation (1). Thus the time-dependence of both flow rate and enthalpy is predicted by the simulator. Evaluating equation (1) for single-phase vapor flow, using $q_v \simeq 10$ kg/s, $p_{wb} \simeq 2.0$ MPa, $p \simeq 10.7$ MPa, we obtain PI = 3.8×10^{-13} m^3. The permeability·thickness product was fixed at the value 1.20 dm obtained from injection tests (Bodvarsson et al., 1983a). Using different relative permeability functions, and different values for vapor saturation, reservoir porosity, and radius R_n of the near zone with excess liquid (see Table 4), we have been able to obtain a number of excellent matches to both flow rate and enthalpy (see Figures 6 and 7).

It turns out that the match is very sensitive to the choice of porosity and of S_n. Different choices of R_n can be compensated for by making appropriate adjustments in ϕ, such that ϕR_n^2 remains constant. The value of S_b must correspond to immobile or nearly immobile liquid, and is determined to within 5-10%. The excess mass present near the well due to condensation and injection is estimated as approximately 4.5×10^6 kg in most cases, which agrees very well with the injected mass. For Corey relative permeability functions a significantly larger M_{ex} is obtained than for linear functions. The quality of the fit for [q(t), h(t)] is good in all cases, indicating that the transients are very sensitive to the excess mass, but not sensitive to the functional form of $k_{r\ell}(S)$ and $k_{rv}(S)$.

Conclusions

Our analysis of flow rate and enthalpy data from several wells completed in the same two-phase zone of Krafla geothermal reservoir has yielded consistent relative permeability parameters. We find that $k_{r\ell} + k_{rv} \simeq 1$ over the entire range of two-phase flow conditions from immobile liquid to immobile vapor. The available data provide relative permeability parameters as a function of flowing enthalpy only. The relationship between flowing enthalpy and in-place vapor saturation remains unknown, so that the relative permeability information obtained is of limited value for quantitative modeling of geothermal reservoir performance.

Numerical simulation of flow rate and enthalpy transients has yielded excellent matches to production data from well 12. However, there is little information about the reservoir which can be deduced in an unambiguous way, because the field data could be matched with a variety of rather different parameter choices. The only unambiguous piece of information obtained is that the water injected into the well during drilling and completion remains in the vicinity of the wellbore during several weeks of warmup.

Acknowledgement

This work was supported by the State Electric Power Works of Iceland, and by the Assistant Secretary for Conservation and Renewable Energy, Division of Geothermal Energy and Hydropower Technologies of the U.S. Department of Energy under Contract No. DE-AC03-76SF00098.

References

Bodvarsson, G.S., Benson, S.M., Sigurdsson, O., Stefansson, V., and Eliasson, E.T., "The Krafla Geothermal Field, Iceland. 1. Analysis of Well Test Data", submitted to Water Resources Research, 1983a.

Bodvarsson, G.S., Pruess, K., and O'Sullivan, M. J. "Injection and Energy Recovery in Fractured Geothermal Reservoirs", paper SPE-11689, presented at the California Regional Meeting of the SPE, Ventura, Ca., March 1983b.

Chen, H.K., Counsil, J.R., and Ramey, H.J., Jr. "Experimental Steam-Water Relative Permeability Curves", GRC Transactions, Vol. 2, p. 103, July 1978.
Counsil, J.R., and Ramey, H.J., Jr. "Drainage Relative Permeabilities Obtained from Steam-Water Boiling Flow and External Gas Drive Experiments, GRC Transactions, Vol. 3, p. 141-143, September 1979.
Gislason, G., Armannsson, H., and Hauksson, T. "Krafla-Hitaastand og Gastegundir i Jardhitakerfinu, National Energy Authority, OSJHD-7846, 1978.
Grant, M.A. "Permeability Reduction Factors at Wairakei", paper 77-HT-52, presented at AICHE - ASME Heat Transfer Conference, Salt Lake City, Utah, August 1977.
Gudmundsson, J.S., Menzies, A.J., and Horne, R.N. "Streamtube Relative Permeability Functions for Flashing Steam-Water Flow in Fractures", paper SPE-11686, presented at the 1983 California Regional Meeting, Ventura, Ca., March 1983.
Horne, R.N., and Ramey, H.J., Jr. "Steam-Water Relative Permeabilities from Production Data", GRC Transactions, Vol. 2, p. 291-293, July 1978.
Menzies, A.J., "Flow Characteristics and Relative Permeability Functions For Two-Phase Geothermal Reservoirs From A One Dimensional Thermodynamic Model", Stanford Geothermal Program, Report SGP-TR-59, 1982.
Pruess, K., "Development of the General Purpose Simulator MULKOM", Annual Report 1982, Earth Sciences Division, Lawrence Berkeley Laboratory, 1983.
Pruess, K., and Schroeder, R.C. "SHAFT79 User's Manual", Lawrence Berkeley Laboratory Report LBL-10861, Berkeley, Ca.,
Stefansson, V., "The Krafla Geothermal Field, Northeast Iceland", in: Geothermal Systems, L. Rybach and L.J.P. Muffler (eds.), p. 273-294, 1981.
Stefansson, V., Gudmundsson, A., Steingrimsson, B., Armannsson, H., Franzson, H., Sigurdsson, O., and Hauksson, T., "Krafla Well KJ-13", Report by the Icelandic Energy Authority, OS82046/JHD07, 1982.

Table 1. Well indices.

Well	Well Index B (10^{-6} Pa·m^3)	
	Liquid	Vapor
12	8.3	4.1
13	3.1	2.5
14	4.4	5.7
15	1.7	1.6

Table 2. KG-12 Simulations - Fixed Parameters

Parameter	Value
produced flowrate	as observed in the field (time-dependent)
reservoir temperature	320°C
reservoir pressure	112.89 bars (=saturation pressure at T=320°C)
rock density	2650 kg/m^3
rock specific heat	1000 J/kg°C
rock heat conductivity	2.0 W/m°C
skin	-4.5
irreducible vapor saturation	0

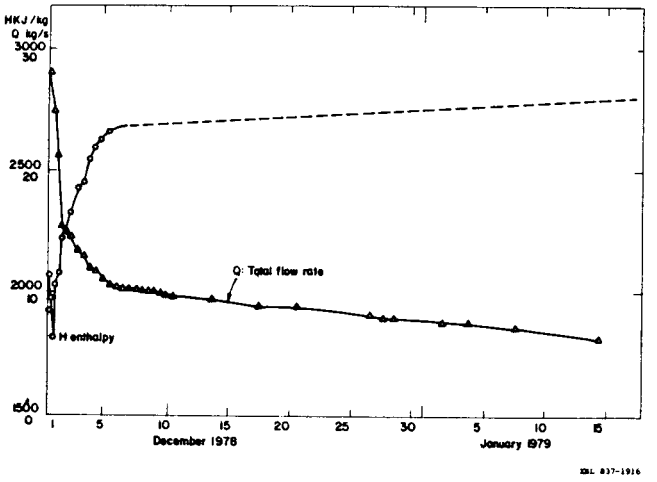
Table 3. Simulations with prescribed (observed) flow rate.

parameter	Case 1	Case 2	Case 3
kH (Dm)	2.0	1.2	1.2
relative permeability function	linear	Corey	smoothed linear
$S_{\ell r}^*$	.30	.30	.40
S_{sr}^+	.00	.00	.05
$S_{pv}^\#$	1.00	1.00	0.65
S_b	.70	.50	.65
S_n	.45	.30	.38
ϕ	.08	.11	.08
M_{ex}(10^6 kg)	3.78	4.16	4.09

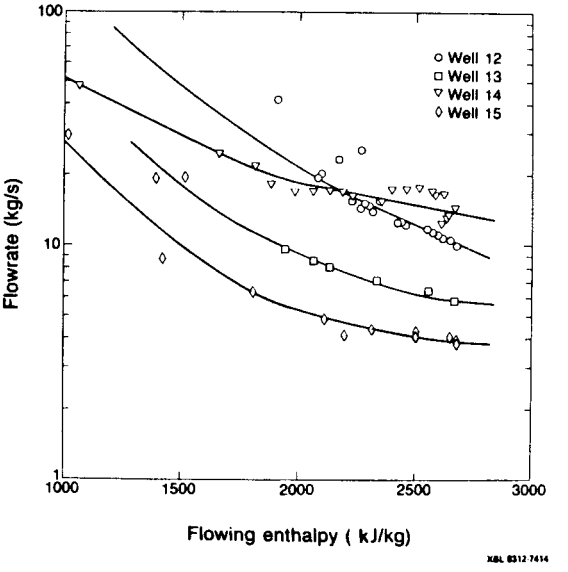
*irreducible liquid saturation
+irreducible vapor saturation
#perfectly mobile vapor saturation

Table 4. Simulations using a deliverability model.

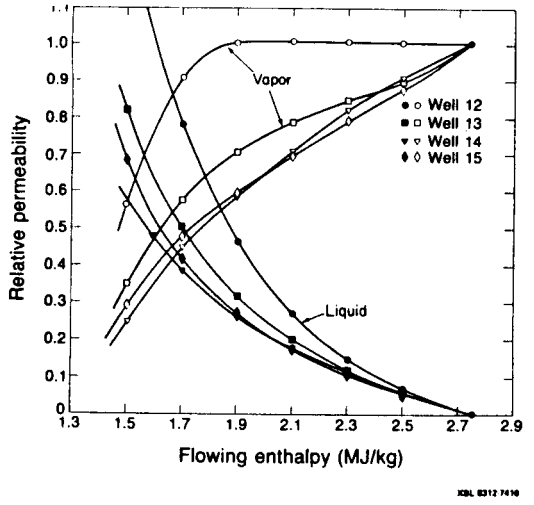
Parameter	Case 1	Case 2	Case 3	Case 4
relative permeability function	smoothed linear	smoothed linear	Corey	smoothed linear
$S_{\ell r}$	.40	.50	.30	.40
S_{sr}	.05	.05	.0	.05
S_b	.65	.55	.50	.65
S_n	.24	.16	.06	.24
ϕ	.015	.06	.06	.06
R_n(m)	20	10	10	10
$M_{ex}(10^6 kg)$	4.66	4.43	5.00	4.66



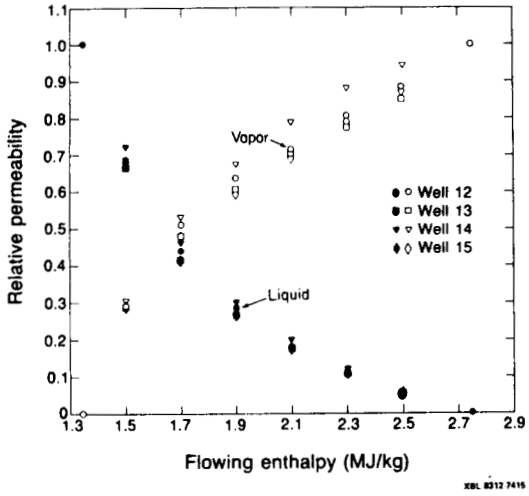
1. Production data for well 12.



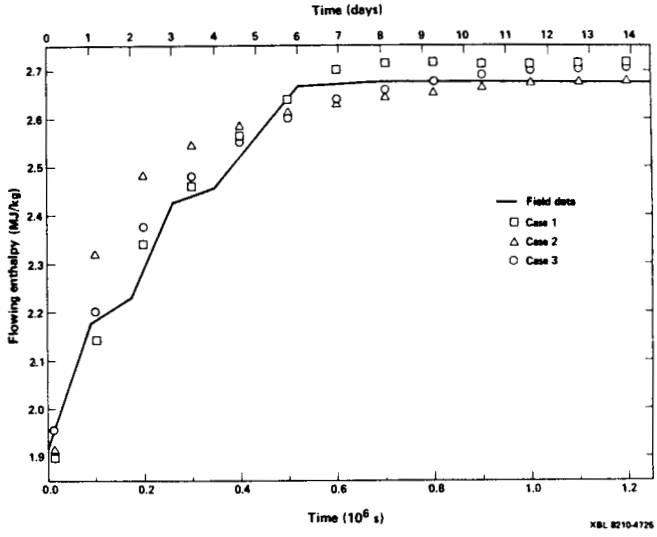
2. Observed correlation between flow rate and flowing enthalpy.



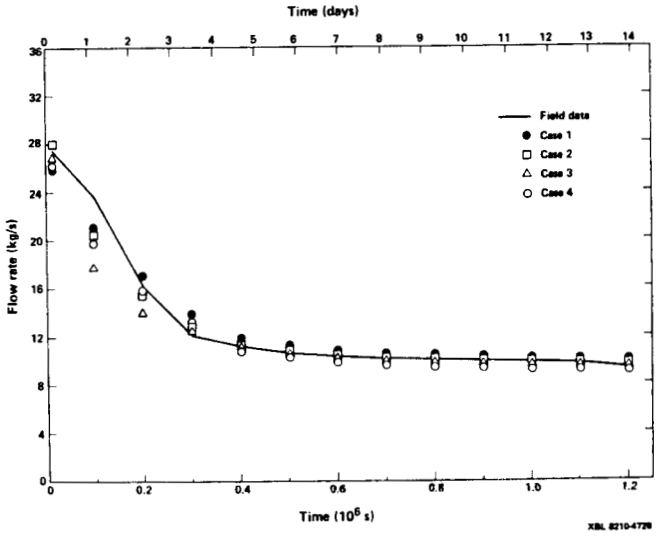
3. Relative permeabilities assuming constant well indices.



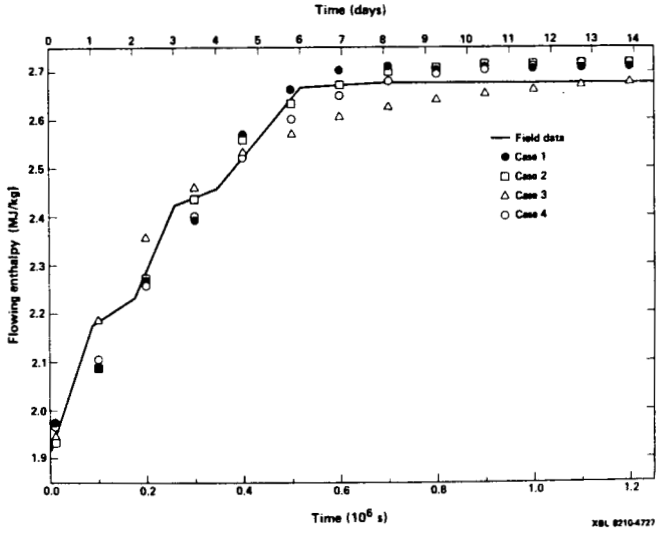
4. Renormalized relative permeabilities.



5. Comparison between calculated and observed enthalpies for well 12 (calculation uses observed flow rates).



6. Comparison between calculated and observed flow rates for well 12 (deliverability model).



7. Comparison between calculated and observed enthalpies for well 12 (deliverability model).

Proceedings Ninth Workshop Geothermal Reservoir Engineering
Stanford University, Stanford, California, December 1983
SGP-TR-74

MODELING STUDIES OF GEOTHERMAL SYSTEMS WITH A FREE WATER SURFACE

Gudmundur S. Bodvarsson and Karsti
Earth Sciences Division
Lawrence Berkeley Laborator
University of California
Berkeley, California 9472

Introduction

Numerical simulators developed for geothermal reservoir engineering applications generally only consider systems which are saturated with liquid water and/or steam. However, most geothermal fields are in hydraulic communication with shallow ground water aquifers having free surface (water level), so that production or injection operations will cause movement of the surface, and of the air in the pore spaces above the water level. In some geothermal fields the water level is located hundreds of meters below the surface (e.g. Olkaria, Kenya; Bjornsson, 1978), so that an extensive unsaturated zone is present. In others the caprock may be very leaky or nonexistent [e.g., Klamath Falls, Oregon (Sammel, 1976); Cerro Prieto, Mexico; (Grant et al., 1984] in which case there is good hydraulic communication between the geothermal reservoir and the shallow unconfined aquifers. Thus, there is a need to explore the effect of shallow free-surface aquifers on reservoir behavior during production or injection operations.

In a free-surface aquifer the water table moves depending upon the rate of recharge or discharge. This results in a high overall storativity; typically two orders of magnitude higher than that of compressed liquid systems, but one or two orders of magnitude lower than that for liquid-steam reservoirs. As a consequence, various data analysis methods developed for compressed liquid aquifers (such as conventional well test analysis methods) are not applicable to aquifer with a free surface (Bodvarsson and Zais, 1982).

We have developed a numerical simulator for the modeling of air-steam-water systems. In this paper we apply the simulator to various problems involving injection into or production from a geothermal reservoir in hydraulic communication with a shallow free-surface aquifer. First, we consider a one-dimensional column problem and study the water level movement during exploitation using different capillary pressure functions. Second, a two-dimensional radial model is used to study and compare reservoir depletion for cases with and without a free-surface aquifer. Finally, the contamination of a shallow free-surface aquifer due to cold water injection is investigated. The primary aim of these studies is to obtain an understanding of the response of a reservoir in hydraulic communication with a unconfined aquifer during exploitation or injection and to determine under which circumstances conventional modeling techniques (fully saturated systems) can be applied to such systems.

Methodology

In our modeling studies we employ a numerical simulator called "TOUGH" (= transport of unsaturated groundwater and heat; Pruess, 1983), which treats the two-phase flow of water and air in liquid and gaseous phases together with heat flow in a fully coupled way. The governing equations account for Darcy flow with relative permeability and capillary pressure effects. Gaseous diffusion can be handled also, but this has been omitted in the calculations presented here. The energy balance includes the latent heat effects of vaporization and condensation, along with conductive and convective heat flow. Water, air, and rock are assumed to be in local thermodynamic equilibrium at all times. The flow domain can include liquid, gaseous, and two-phase regions. The thermophysical properties of water substance are accurately represented by the steam table equations as given by the International Formulation Committee (1967). Air is approximated as an ideal gas, and additivity of partial pressures is assumed for air-vapor mixtures. The (small) solubility of air in liquid water is represented by Henry's law.

Production From A Vertical Column

The first problem considered is a vertical column with a main reservoir, caprock, shallow unconfined aquifer and an unsaturated zone. The grid used and the permeabilities assigned to different zones are shown in Figure 1. The water table is located at a depth of 200 m; below that there is a shallow aquifer. The aquifer is separated by a 200 m thick caprock from a 600 m thick geothermal reservoir. Atmospheric conditions are maintained at the ground surface (P = 1bar, T = 10°C). Other parameters that do not vary spatially are given in Table 1.

The capillary pressure function used and the relative permeabilities are shown in Figure 2. In general, capillary pressure functions depend greatly on the pore size distribution of the rocks, with larger capillary pressure for smaller pore size. As Figure 2 shows, we assume a maximum capillary pressure of 15 bars, which was chosen rather arbitrarily, but may be reasonable for the small pores typically found in volcanic rocks. The relative permeability functions used are linear with 30% irreducible liquid saturation and 5% irreducible gas saturation. We have found that these functions are compatible with field data from the Krafla geothermal field, Iceland (Pruess et al., 1983).

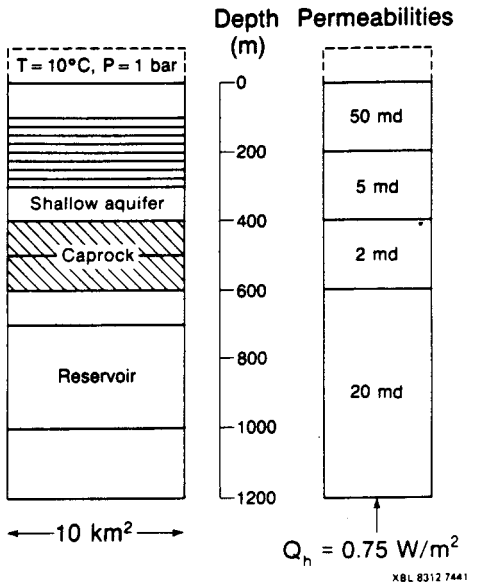


Figure 1. Schematic diagram of 1-D vertical column model.

Table 1. Specifications for column problems. Parameters that do not vary spatially.

Porosity	:	10%
Rock grain density	:	2650 kg/m^3
Rock specific heat	:	1000 J/kg
Heat conductivity	:	2.0 W/m·°C
Rock compressibility	:	0 pa^{-1}

Before exploitation, stable initial conditions were obtained for a constant heat flux of 0.75 W/m^2 (Fig. 3). Two cases were considered; one where the capillary effects were neglected (solid lines), and the second one where the capillary function shown in Figure 2 was used. Figure 3 shows that capillary effects tend to reduce sharp saturation gradients and expand the two-phase zone. On the other hand, when capillary effects are neglected, the gas saturation tends to stabilize at the irreducible liquid saturation (S_{ℓ} = 0.7 for our relative permeability curves). Because of the expanded unsaturated zone with pressure close to 1 bar, the case with capillary effects always has slightly lower pressure. The temperature profile (identical for both cases) shows the two possible heat transfer mechanism for this problem. In the upper part of the system the heat is transported mainly by conduction, resulting in a linear temperature profile with a large gradient. The main reservoir beneath the caprock is in two-phase conditions, and the heat is transported mainly by counter flow of steam and water with a smaller temperature gradient.

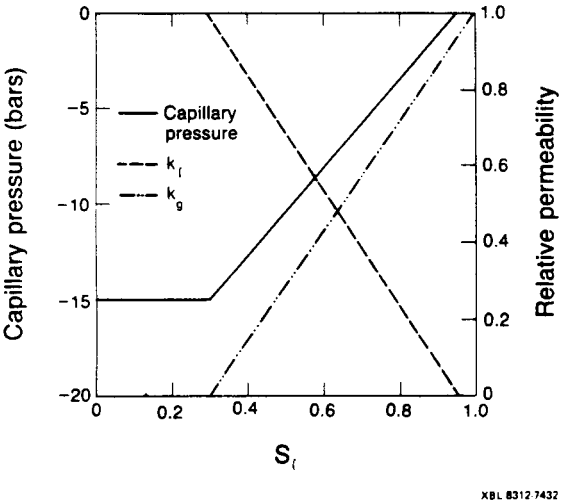


Figure 2. Capillary pressure and relative permeability functions used in the study.

During exploitation 500 kg/s of fluids were produced from the reservoir (approximately equivalent to 50 MW$_e$). The resulting pressure and gas saturation profiles at selected times are shown in Figures 4 and 5. The figures show that during exploitation the water level declines and steam saturation increases in the reservoir. In the case where capillary pressure is neglected this causes a distinct minimum in the gas saturation in the caprock. When capillary pressure effects are included the gas saturation in the caprock is much higher as they tend to diminish saturation differences. Near the bottom of the reservoir the capillary pressure effects tend to hold onto the liquid, resulting in lower gas saturations at late times (30 years). However, vapor static conditions develop in the reservoir at late times (Fig. 4).

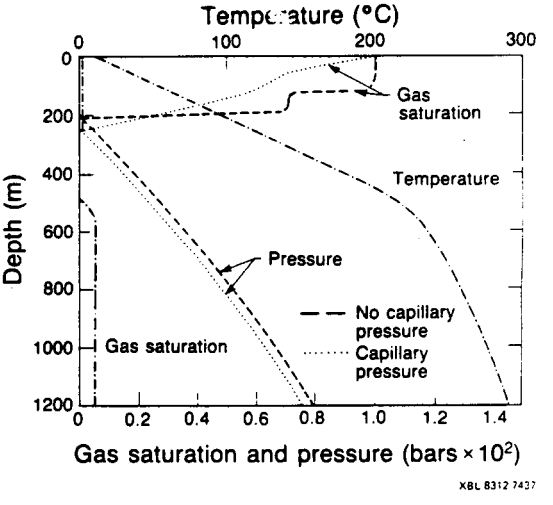


Figure 3. Initial thermodynamic conditions for the column problem.

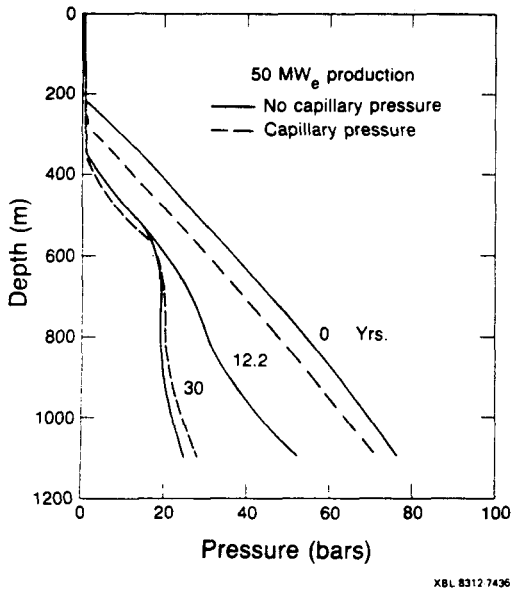


Figure 4. Pressure profiles at various times during expolitation.

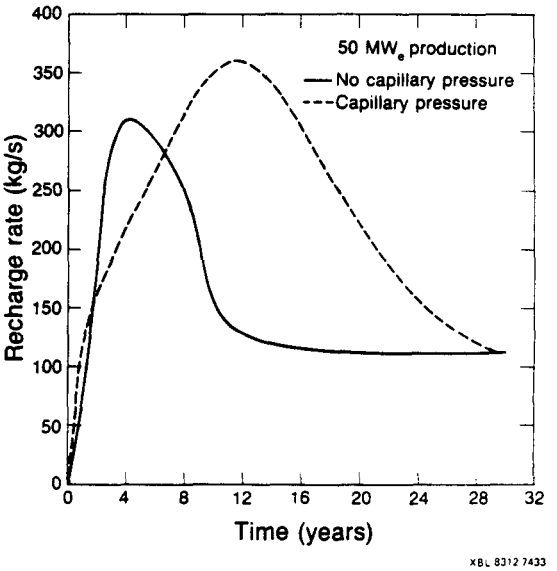


Figure 6. The recharge rate into the reservoir versus time.

Figure 6 shows the total fluid recharge from the shallow free surface aquifer to the reservoir for the two cases (with and without capillary pressure effects). Both cases show a rapid rise in the recharge rate reflecting pressure decline in the reservoir, but the maximum recharge rate occurs later when capillary effects are included. The reason for this is that capillary effects tend to slow the release of water in place in the caprock and the shallow aquifer. The decline of the recharge rate at later times occurs due to the lowering of the water table and increasing gas saturation in the shallow zones.

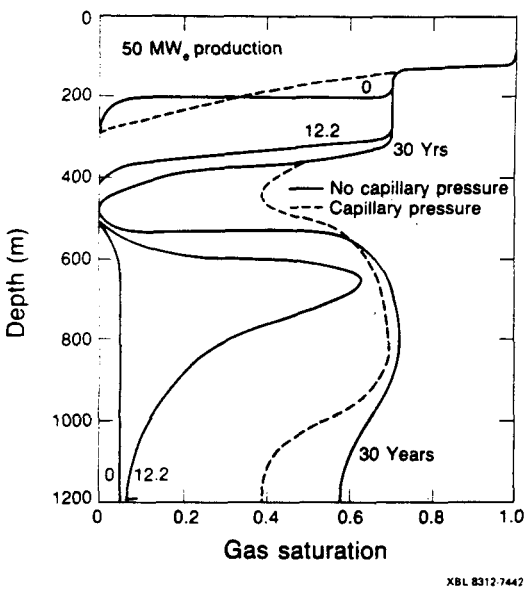


Figure 5. Gas saturation profiles at various times during exploitation.

Production From A Two-Dimensional Radial Model

The primary objective of this section and that immediately following is to examine to what extent conventional modeling techniques for single-component water systems can be applied to problems involving shallow unconfined aquifers. The approach employed is to simulate the same problem using the air-water formulation as well as using fully saturated (steam-water) approximations. Any differences that arise are then due to the approximations employed at the free-surface boundary.

The first problem selected is a two-dimensional radial problem using the same vertical space discretization employed in the column model (Fig. 7). In the radial direction we use a coarse grid consisting of 6 elements which extend to 10 km. The formation parameters and the initial conditions are also identical to those used in the column model. A fixed extraction rate of 1500 kg/s (~ 150 MW_e) is prescribed for the element labeled "P" in Figure 7. The enthalpy of the produced fluids from that node is determined from the mobilities of the individual phases. In this study we neglect capillary pressure effects.

In modeling the problem as a confined system, the unsaturated zone above the shallow aquifer (the top 200 m) is neglected. Thus, the top 5 layers in the grid (Fig. 7) as well as the boundary nodes at the top (for constant temperature and pressure) are deleted. However, in order to maintain stable initial conditions, heat sinks of appropriate strength corresponding to 0.75 W/m^2 are placed in the elements in the top row (top layer of the aquifer). In this manner, identical initial conditions can be used for both the unsaturated and the confined aquifer problem and the results should be directly comparable.

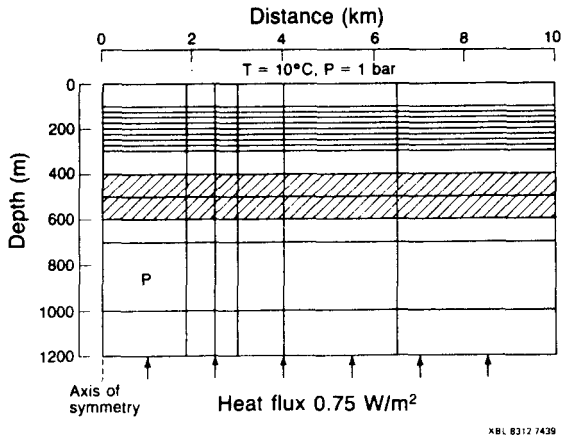


Figure 7. Mesh used in the 2-D radial production problems. "P" denotes the production node.

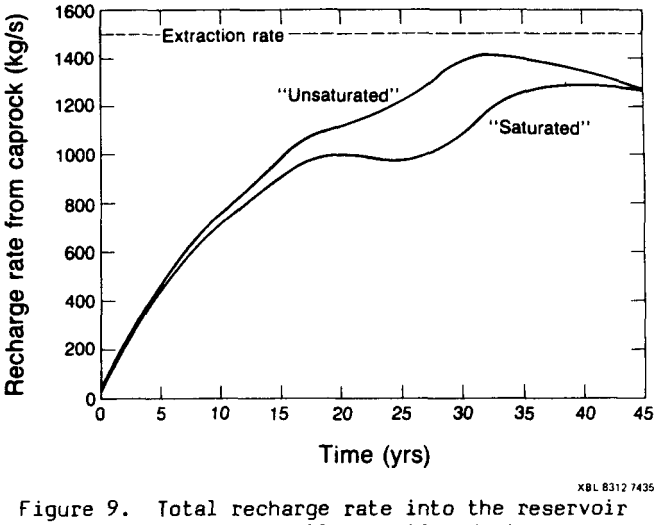


Figure 9. Total recharge rate into the reservoir from the shallow aquifer during exploitation.

The results for the pressure and vapor saturation in the production node versus time are shown in Figure 8; Figure 9 shows the total recharge rate from the caprock into the reservoir versus time. Figure 8 shows that at early times the effects of exploitation on the pressure decline and boiling at the production node are identical for the two cases. The recharge rates for both cases increase rapidly, partly because of the pressure decline in the reservoir and partly because of pressure rise in the shallow aquifer due to upflow of steam and condensation (Bodvarsson et al., 1982). Later on, the pressure decline in the "unsaturated" case is slower than in the "compressed liquid" case, because of greater recharge from the free-surface aquifer (Fig. 9). The high storage coefficient of the free-surface aquifer allows more rapid recharge to the reservoir without a large decline in the water table. The recharge rate for the "compressed liquid" reaches a stable level after about 20 years, due to the low compressibility, but then increases sharply after approximately 25 years when two phase conditions evolve at the top of the shallow aquifer. At intermediate times the recharge rate for the "unsaturated" case is 20-25% higher than that for the "compressed liquid" case, causing larger pressure declines and vapor saturation buildup in the production node for the latter case. At late times the recharge rates become very similar as rather uniform depletion of the entire system occurs.

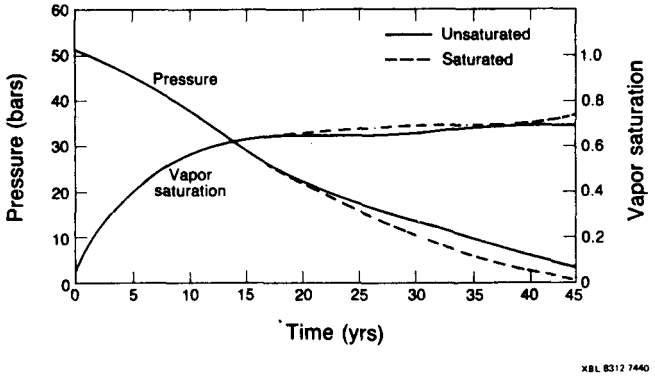


Figure 8. Pressure and gas saturation at the production mode.

In general the system behavior is very similar for both cases, mainly because a two-phase zone evolves at the top of the aquifer in the "compressed liquid" case. This two-phase zone has a high compressibility and thus behaves very similarly to a free surface boundary condition. However, in cases where the recharge from above is a serious problem, due to cooling of the reservoir, it may be necessary to accurately model the recharge by proper treatment of the free surface.

We have also considered cases where the caprock is non-existent and thus the entire resevoir is unconfined. In these cases we have considered low temperature reservoirs of rather high permeability so that boiling due to exploitation would not occur. One would expect a-priori that for such systems the upper boundary condition at the free surface would dominate the reservoir response, so that models that do not include the air component would give inaccurate results. However, the results from our preliminary studies indicate that this is not the case. For the "compressed liquid" models the initial pressure decline will be unrealistically large, but then a two-phase zone will develop at the top of the shallow aquifer with pressure corresponding to the saturation pressure at the prevailing temperature. Subsequently the two-phase zone will advance downward in the same manner as the unsaturated zone in the air-water model. In the air-water model the pressure in the unsaturated zone will be close to 1 bar whereas for the "compressed liquid" model the two-phase zone will typically have a pressure of 0.2 - 0.5 bars. However, this slight difference will not have a significant effect on the overall reservoir depletion, and thus for most practical purposes we feel that single-component water-steam models are adequate for the modeling of the exploitation of reservoirs with hydraulic connections to shallow free surface aquifers.

Injection into a Reservoir with a Fault Connection to a Shallow Aquifer

The example considered in this section illustrates effects of reinjection into a liquid-dominated geothermal reservoir which is hydraulically connected to a shallow unconfined aquifer by means of a vertical fault. Of particular interest in this type of problem is the migration of reservoir water into the shallow aquifer as a consequence of reinjection, which may create environmental hazards.

The injection configuration and the overall geometry of the flow system are shown in Figures 10 and 11. The injectors are placed in a "line drive" pattern at 100 m spacing. At a distance of 126 m from the injection line there is a vertical fault. The line connecting the injection wells is an approximate line of symmetry, because problem parameters were chosen in such a way (see Table 2) that the rate of flow up the fault is negligibly small compared to lateral flow in the reservoir (less than 5%). We model one symmetry element, which is a vertical slice with a thickness of 100 m. This is shown in the vertical cross section in Figure 2. The reservoir is represented by five grid layers of 100 m thickness each. The injection rate into each grid layer is constant at 10 kg/s. Constant pressure boundary conditions, corresponding to the initial gravity-equilibrated pressure distribution, are assumed at the left and right boundaries of reservoir and aquifer. The lower boundary of the reservoir, and the boundaries of the caprock, are assumed "no flow". Boundary conditions of p = 1 bar, T = 20°C are maintained at the ground surface. Detailed problem parameters are given in Table 2.

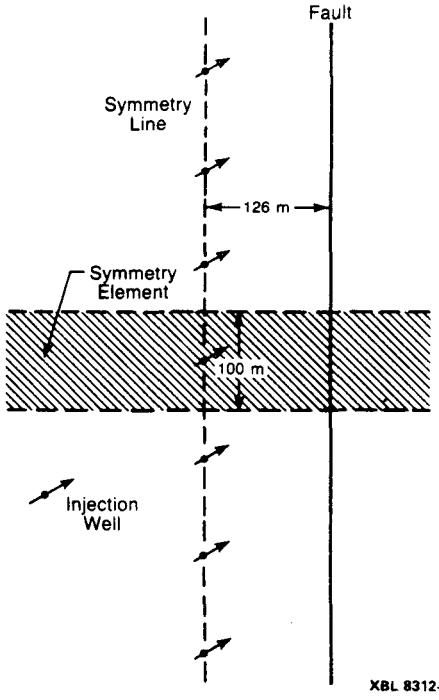


Figure 10. Schematic diagram of the injection well configuration and the leaky fault.

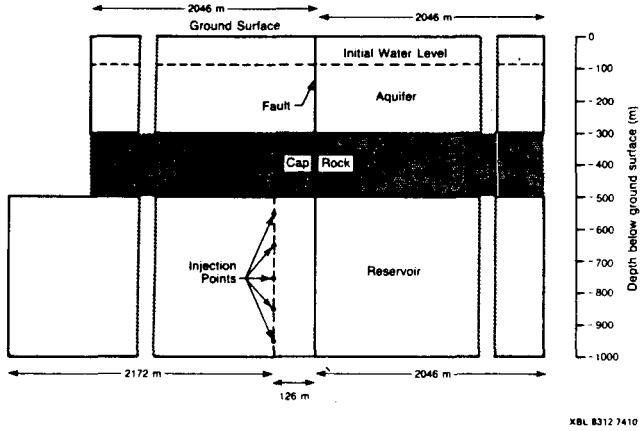


Figure 11. A vertical cross section of the interconnection between the shallow aquifer and the reservoir.

In response to injection, pressures in the reservoir increase, causing some upflow of water in the fault zone. The water levels in the fault zone and the shallow aquifer rise above their initial depth of -90 m. Figure 12 shows the water levels at various times as a function of the distance from the fault. For comparison we have also carried out a simulation using a fully saturated system, i.e., placing the upper boundary of the system at the initial water level of -90 m. (This corresponds to treating the aquifer as fully confined.) Figure 13 shows velocities of water migration up the fault for the two cases. The velocities differ by as much as 50%. Non-reactive solids dissolved in the reservoir water will begin to reach the shallow aquifer approximately 25 days after injection is started. In the confined case, pressures near the top of the aquifer rise to approximately 9.5 bars, whereas pressures remain near 1 bar at the free-water surface in the unconfined case. Pressures and temperatures in the reservoir differ by no more than 1-2% between the two cases. Thus an explicit treatment of the free surface is not necessary if only predictions of reservoir behavior are desired. However, reliable predictions of effects of injection on the shallow aquifer are only possible when a two-component water-air approach is used.

Table 2. Parameters for injection problem.

	Aquifer	Fault	Reservoir
Formation parameters			
Permeability $(m)^2$	100×10^{-15}	400×10^{-15}	50×10^{-15}
Porosity (%)	20	20	10
Initial conditions			
Initial Temperature (°C)	20	20/250	250
Initial Pressure (bars)	gravity equilibrium, with 1 bar at ground surface		
Initial Water Level (m)	-90	-90	
Injection			
Total Rate (kg/s)			50
Enthalpy (kJ/kg)			419
Width of fault (m)		1.0	

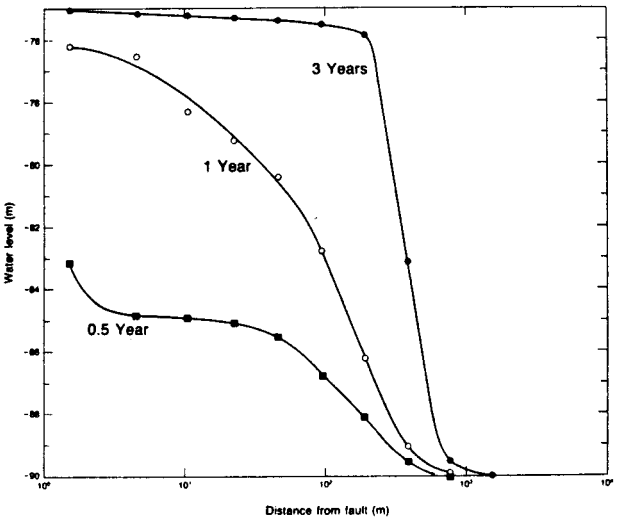


Figure 12. The rise of the water level in the shallow aquifer versus time during injection.

Summary and Conclusions

In this paper we solve some reservoir problems involving an unconfined shallow aquifer. The main purpose of these simulations is twofold:

(i) To obtain some understanding of the interaction between geothermal reservoirs and shallow unconfined aquifers and the effects of capillary pressure for such problems.

(ii) To study to what extent conventional geothermal simulators for fully saturated media can be applied to problems involving free-surface aquifers.

The results obtained indicate that capillary pressure effects tend to enlarge the two-phase zone and smooth out large gas saturation gradients within the zone. The free-surface aquifer provides recharge to the main geothermal reservoir, and if a rigorous air-water simulator is not used, the recharge rate may be underestimated. This can have serious implications especially in cases where the caprock is very leaky and problems with reservoir cooling due to recharge of cooler fluids from above are evident. However, for most reservoir problems our results show that the use of conventional single-component geothermal simulators for the modeling of the interaction of shallow unconfined aquifers with the reservoir during expolitation gives reasonable results. This is especially true in cases where boiling occurs in the reservoir or in the shallow aquifer as a result of exploition, because in these cases the reservoir response is dominated by the two-phase zone. On the other hand, our results indicate that for an assessment of possible contamination of shallow unconfined aquifers during injection, one must use a rigorous air-water model for a detailed analysis. In these cases, the discharge rate to the shallow aquifer and its pressure distribution during injection cannot be accurately calculated with a model for a saturated medium. As the discharge rate to the shallow aquifer is the most important parameter for contamination studies it appears that air-water models are necessary for such problems.

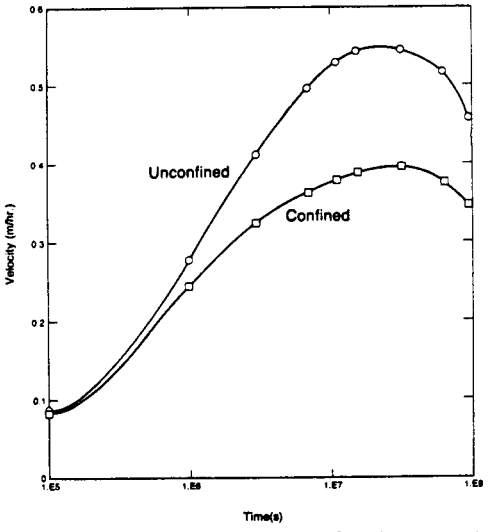


Figure 13. The velocity of the fluid migration up the fault as a function of time.

Acknowledgment

This work was supported by the Assistant Secretary for Conservation and Renewable Energy, Division of Geothermal Energy and Hydropower Technologies of the U.S. Department of Energy under Contract NO. DE-AC-3-76SF00098.

References

Bjornsson, S., 1978, "Estimation of the reservoir potential of the Olkaria geothermal field in Kenya", Nordic Symposium on Geothermal Energy, Goteborg, Sweden.

Bodvarsson, G., and Zais, E.J., 1982, Geothermal reservoir testing by piezometric surface drawdown/buildup", SPE-11142, paper presented at the 57th Annual meeting of the Society Of Petroleum Engineers, New Orleans. Sept. 26-29, 1982.

Bodvarsson, G.S., Pruess, K., Lippmann, M.J. and Bjornsson,S., 1982, "Improved Energy recovery from geothermal reservoirs". J Petro. Techn. Vol 34, No.9 p. 1920-1928.

Grant, M.A., Truesdell, A.H. and Manion, M.A., 1984, "Production induced boiling and cold water entry in the Cerro Prieto geothermal reservoir indicated by chemical and physical measurements", Geothermics, Vol.13, pp.117-140.

International Formulation Committee, 1967, "A formulation of the thermodynamic properties of ordinary water substance", IFC Secretariat, Dusseldorf, Germany.

Pruess, K., 1983 "Tough - a numerical model for strongly heat driven flow in partially saturated media". Annual report of the Earth Sciences Division, Lawrence Berkeley Laboratory, in preperation.

Pruess, K., Bodvarsson, G.S., Stefansson, V, and Eliasson, E.T., 1983, "The Krafla geothermal field. 4. Well performance and reservoir depletion", paper submitted to Water Resources Research.

Sammel, E.A, 1976 " Hydrologic reconnaissance of the geothermal area near Klamath Falls, Oregon", report WRI-76-127, U.S. Geological Survey Menlo Park, California, 129pp.

Proceedings Ninth Workshop Geothermal Reservoir Engineering
Stanford University, Stanford, California, December 1983
SGP-TR-74

RESERVOIR SIMULATION ON THE CERRO PRIETO GEOTHERMAL FIELD: A CONTINUING STUDY.

*M. Castañeda, **R. Márquez, *V. Arellano, **C.A. Esquer

*Instituto de Investigaciones Eléctricas
**Coordinadora Ejecutiva de Cerro Prieto
Mexicali, B.C., Mexico

INTRODUCTION

The Cerro Prieto geothermal field is a liquid-dominated geothermal reservoir of complex geological and hydrological structure. It is located at the southern end of the Salton-Mexicali trough which includes other geothermal annomalies as Heber and East Mesa. Although in 1973, the initial power plant installed capacity was 75 MW of electrical power, this amount increased to 180 MW in 1981 as field development continued. It is expected to have a generating capacity of 620 MW by the end of 1985, when two new plants will be completely in operation. Questions about field deliverability, reservoir life and ultimate recovery related to planned installations are being presently asked. Numerical modeling studies can give very valuable answers to these questions, even at the early stages in the development of a field.

An effort to simulate the Cerro Prieto geothermal reservoir has been undergoing for almost two years. A joint project among Comision Federal de Electricidad (CFE), Instituto de Investigaciones Electricas (IIE) and Intercomp of Houston, Texas, was created to perform reservoir engineering and simulation studies on this field. The final project objective is to simulate the behaviour of the old field region when production from additional wells located in the undeveloped field zones will be used for feeding the new power plants.

Early project results from a preliminary material balance applied to the old part of this field (Cerro Prieto I region) using a simplified geological model had indicated the existance of a strong cold water recharge into this region (Castañeda et. al., 1982). This conclusion agreed with the results presented by previous authors (Westwood, 1981; Grant, 1982; Bermejo, 1979).

Now, a tridimensional coarse grid reservoir model has been extended over the entire field as additional reservoir information has been generated and become available to this project. This study presents the simulation efforts to obtain a reservoir pressure and enthalpy history match of the Cerro Prieto I region, using this coarse grid model, when production from other field regions is taken into account. The influence of some reservoir features (i.e., geologic faults) on these match as well as predictive calculations are also presented.

RESERVOIR MODEL

The extended field area used in this simulation study is presented in figure 1. This area (19.5 Km^2) encloses the practical boundaries of the field, as they were defined by CFE[11].

The tridimensional coarse grid model imposed to this area was based on the geologic model presented by Cobo, 1981. Basing his model on well cuttings, he recognized five lithologic units within this area that showed differences in origin, mineralogy, grading, color, etc. From the oldest to most recent, these lithologic units are: biotite granite, gray shale, coffe-colored shale, mudstone and unconsolidated sediments. Most all Cerro Prieto wells are completed on the gray shale and/or coffe-colored shale units although there are some wells that have reached the granitic basement (Sánchez and De la Peña, 1981).

Although this geologic model replaced the one we had been using in the preliminary material balance calculation of this project (a model based on well logs interpretation, (Abril 1978), they showed some similarities on both proposed lithologic columns. Cobo's mineralogic model was then used mainly because there was not enough reservoir information in the other model to characterize the extended field area.

Figure 2 presents a tridimensional representation of Cobo's contour map of the top of the gray shale unit. This figure clearly suggests that the field area of study can be subdivided in 5 main blocks (blocks I through V) limited by the respective faults. This figure also suggests that hotter reservoir zones are expected to be found deeper in the southeast part of the field (Cerro Prieto II area) as it has been indicated by other authors and confirmed by drilling (Domínguez, 1982, Rivera et. al., 1982).

For simulation purposes, these five irregular blocks were replaced by rectangular blocks but the same respective block area was kept. Figure 3 shows this schematic representation.

Faults were included in this representation by assigning to them a defined dimension (thickness of 50 m). For this study, Hidalgo and Patzcuaro faults were considered only.

Figure 4 shows the model vertical representation. Mainly, each block consists of 4 units: 1) a cooler aquifer (unconsolidated sediments) overlying the main geothermal reservoir, 2) a shaly layer (Cobo's mudstone layer and sometimes referred as a "cap rock" by other authors), 3) a shaly sand layer (gray shale coffe-colored shale units), considered as the zone of geothermal interest (higher temperature and higher permeability zone, and 4) the granitic basement. The thickness of each unit represents an average value for each block. Cobo's contour maps of each unit were used for such purpose.

The geologic faults were only included in the gray shale_coffe-colored shale unit. Both faults were sealed at the mudstone layer and they did not continue through the unconsolidated sediments.

FORMATION PROPERTIES

For this study, the rock properties were determined by means of geophysical well log analysis and well test data (Castañeda et. al., 1982). This rather scarce data was not sufficient to define the entire area of study or to characterize all lithologic units. Some rock properties were inferred or assumed in zones where no information was available. Figure 5 presents the assigned reservoir parameters to all units.

INITIAL CONDITIONS

The initial field temperature distribution used in this work is presented in figure 6. These temperature profiles were obtained from isoterm maps elaborated from shut-in wells temperature data (Castañeda et. al., 1983). However, the temperature distribution of the eastern part of the field may have been affected by former explotation of the western area. Thus, the presented temperature profiles for the part of the field (blocks 3, 4, and 5) were only used as an approximation to the real initial temperature values.

The initial pressure distribution was computed by assuming an atmospheric pressure at the ground surface and then calculating a hydrostatic distribution of pressure with depth, subject to the initial temperature distribution. These initial conditions neglect any changes that might have occurred in the western field area before 1973. Although some wells were completed and tested in this area on the late 60's, full production started in 1973.

The initial conditions imply that the reservoir was at single phase (liquid) condition prior to production at Cerro Prieto. It has been indicated by some authors (Grant et. al. 1981) that although there was a region of boiling fluid initially in the reservoir, this region was local and very small and that most of reservoir rock contained fluid at single phase (liquid). If that condition of boiling existed in the reservoir, this was a local phenomeno and could not be represented in our coarse grid model.

BOUNDARY CONDITIONS

Presently, the fact that a strong recharge is taking place at the old part of the field (Cerro Prieto I region) is generally well accepted although there has been no agreement on the magnitude and direction of such recharge. Some authors (Bermejo, 1979; Sánchez and De la Peña, 1981) have suggested that there is a significant recharge into this region from the north and east. Others (Grant et. al., 1981; Lippman and Bodvarsson, 1982) have found that the most of the recharge comes from the west and shallower zones.

In this study, a steady-state recharge representation was selected. This required placing aquifer blocks (outer elements) to the rectangular grid model. Aquifer blocks are defined as those elements in the model that communicate directly with an aquifer that is not itself modeled as part of the calculation grid but whose effects are introduced through the specific aquifer terms. The influx into an aquifer block is calculated as:

$$\text{influx rate} = VAB \times (P_i - P_{n+1}) \text{ RB water/day}$$

where:

P_i = initial block pressure

P_{n+1} = block pressure at end of time step

VAB = aquifer influx coefficient RB/DAY/psi

The aquifer blocks in the model are: in the western side of the model, nodes I=1, J=1 to 7; in the northern side, J=1, I=1 to 4; in the eastern side, I=4, J=1 to 7 (in all three sides, layers K=1 to 18). In the southern side, no recharge was considered.

Initial temperature profiles of periphery wells were used to represent the recharge temperature. For the western side of the model, well M-6 (block I), well Q-743 (block II), well M-92 (block IV) and well M-189 (block V) were used for such purpose. Well M-94 (blocks I and III) was considered for the northern side. For the eastern side, well H-2 (block III) and well NL-1 (blocks IV and V). Figure 7 shows these profiles.

SIMULATION RUNS

Intercomp's geothermal reservoir simulator GEOTHERM) was used in this work. The finite difference formulation of this simulator is explained by Coats, 1974. This simulator does not account for the presence of inert gases or for varying concentration and precipitation of dissolved solids.

The grid model representation including main blocks, layers, faults as well as aquifer blocks gave a total of 504 elements.

Rather than simulating a single well, groups of wells were formed according to their location in the field (at a given main block) and their depths of open intervals. In the latter case, the open intervals of each well were projected onto the model vertical representation. This procedure determined the producing layers of the model. Figure 8 shows the 17 groups of wells formed in this manner and their location in the grid model. Some of these wells are not presently on production and they are not accounted for in the histoy match process. They are wells needed for the two new power plants and will become producers in the predictive calculations.

Production history was taken from the monthly production data reported by CFE. Figures 9, 10 and 11 show the production assigned to each well in the model for blocks I, II and some wells in block III, respectively, during the production period of March 1973-May 1983.

The prime objective was to match the observed Cerro Prieto I (block I in the model) reservoir pressure and enthalpy history under the steady-state recharge assumption. These histories are presented in figure 12 and 13, respectively. Both histories are representative of a 1200 m depth zone. The histories suggest that this region has remained single phase (liquid) during this production period (at least until 1979). Some authors (Grant et. al., 1981); Lippman and Bodvarsson, 1982) have shown that although local near-well boiling is a common phenomenon in Cerro Prieto, a more extensive steam zone has not been formed in this part of the field, under exploitation conditions.

HISTORY MATCH RUNS

To handle the recharge strength, aquifer influx coefficients (VAB) were assigned to the aquifer blocks. The same recharge strength (i.e., same VAB values) were given to each of the three recharge sides of the model. This combination may not be unique and it is possible that an acceptable history match could also be obtained with any other combination. However, at this point, there is not enough field information in this coarse grid model to determine such combination exactly.

Because of the single phase (liquid) characteristic of this part of the reservoir during the history match period, the relative permeability concept was not relevant in this set of runs. However, if a two-phase zone develops in other field regions within the model during these runs, the same Corey's curves presented in reference 3 are used, but with residual liquid saturation of 0.3 and residual vapor saturation of 0.05.

For simulation studies, the single most important reservoir parameter is its permeability. Although rock porosity, compressibility, heat conductivity and heat capacity data are also needed for simulation studies, the effects of these parameters are not as great as those of permeability (Lippman and Bodvarsson, 1982). Therefore, the matching procedure was to vary the reservoir permeabilities in the production zones (gray shale-coffe-colored shale units) in combination with the variation of the aquifer influx coefficients. For sake of space, only the most representative simulation runs are presented here.

Figure 12 shows the simulated pressure when the initial reservoir parameters presented in figure 5 were used, for aquifer influx coefficients of 25, 100 and 300. In this case, k_h = 50 md and k_v = 10 md, for the production zone. As it can be observed, simulated pressures were higher than the observed values. To obtain a more gradual pressure drop throughout time, this rather low k_h/k_v ratio of 5 was increased to 10 (an acceptable ratio value for sedimentary reservoirs). Keeping the same k_h value, the vertical permeability (k_v) was reduced to 5 md. Figure 12 also shows this case when a VAB value of 200 is used. The respective simulated enthalpy is presented in figure 13.

Although a perfect pressure match was obtained for three of the four observed values, it was decided that the same weight should be given to the four observed points. An additional pressure drop could be obtained if the aquifer influx coefficients were reduced (i.e., less recharge) but this procedure would tend to decrease the cooling of that region (i.e., give higher simulated enthalpies) and the enthalpy match could not be obtained. Another method to produce an additional pressure drop could be by reducing the reservoir horizontal permeability and retarding the effect of the recharge on the reservoir pressure. To avoid an excessive pressure drop, the aquifer influx coefficient values have to be increased. Figure 14 presents both pressure and enthalpy matches when k_h was reduced to 30 md and a VAB of 1500 was used (the k_h/k_v of 10 was held constant).

It is interesting to notice that the simulator predicts an increase on reservoir pressure in the Cerro Prieto I region, after the period of 84 months (i.e., after 1979). Although no Cerro Prieto I isobaric maps have been made

after that period to verify this result, the above could be explained if we observe the production history of the wells # 2 and 3 on the model. These wells are directly responsible for the pressure drop in that zone (see figure 9). Though the mass flowrate of well 3 remains almost constant during this period, the mass flowrate of well 2 increases to a maximum and then it is reduced to almost half of that value after the period of 84 months. If this part of the field was being over-exploited, this mass flowrate reduction of well 2 should result in a pressure increase on that zone due to the strong aquifer recharge that is taking place in that region.

The rise in the observed enthalpy during the first two years could not be reproduced by this model. It is believed that such rise was produced by taking into account wells that were producing from an initial small two-phase region (Grant et. al., 1981). in the calculation of the overall enthalpy of Cerro Prieto I for those years.

The cooling of the region is due to recharge fluid of lower temperature coming from the west and north sides of the model, as well as that coming from blocks II and III at the same depth. Additional cooler fluid may be coming from the upper unconsolidated layer. Although the vertical permeability of the mudstone layer was set to 5 md (a considerably lower value than the reservoir permeability), some authors have shown that this value could not be sufficiently small to exclude significant downward flow through this layer (Grant et. al., 1981). However, with this coarse grid model, it is only possible to observe an overall effect of this recharge phenomenon.

EFFECT OF FAULTS

The trend of the Cerro Prieto I observed enthalpy in Figure 13 suggests that such enthalpy could stabilize after the 84 months period. To explore such possibility, the vertical permeability of the faults was increased to allow for mixing of more hot fluid from the lower hayers with cooler recharge fluids. The desired overall effect was to decrease the decline rate of the Cerro Prieto I temperature (i.e., enthalpy) at that depth. Although the faults vertical permeability was increased to 500, 1000 and even 10,000 md, the effect was insignificant to be noticed on the corresponding enthalpy graph.

PREDICTION OF FUTURE PERFORMANCE

A single prediction of future performance of the Cerro Prieto I region (i.e., after 1983) was performed. The calculation was merely an extension of the matched performance up through May of 1983. The simulator was allowed to run for an additional 20 years. Figure 15 presents the required mass flow rate to integrate the two new power plants, the wells that will become producers and the approximated dates of the plants starting operation (POISE, 1983). The mass flow rate of the already producing wells was held constant at the value reported by CFE in May of 1983.

Figure 16 shows the predicted pressure and enthalpy performance of this region. At the end of this period, the pressure has slowly decreased to 96 bars. The reservoir enthalpy has decreased to 1030 KJ/Kg, corresponding to a liquid water temperature value of 237°C.

The enthalpy decline is not lineal during this period. The rate of enthalpy decline diminishes with time and could possibly reach a constant enthalpy value for a longer period of time. As mentioned before, this phenomenon could be already occurring with the observed Cerro Prieto I enthalpy. If this is the case, then the predicted enthalpy would be a pessimistic value. Therefore, it would be worthwhile to continue generating this kind of data to verify such field behaviour.

Figure 17 compares the predicted pressure and enthalpy values to that of the steam-water saturation curve. As it can be observed, the Cerro Prieto I region remained single phase (liquid) during the predicted period.

CONCLUSIONS

1.- An acceptable pressure and enthalpy history match of the Cerro Prieto I region was obtained considering a steady-state recharge assumption, for the production period of 1973-1979.

2.- A 30 years predictive calculations using this coarse grid model indicate that reservoir pressure in this part of the field will slowly decrease to 96 bars. However, the reservoir enthalpy will continue to decline but a lower decline rate than at the begining of the field explotation.

3.- Because of the strong recharge taking place in this part of the field, the model predicts that Cerro Prieto I will not come into two phase conditions during the predicted period, under the proposed explotation program.

4.- The Cerro Prieto I predicted enthalpy of 1030 KJ/Kg (a liquid water temperature of 237 C) could be a rather pessimistic value. Further enthalpy data is needed to validate this conclusion.

5.- This coarse grid model suggests that the eventual demise of the Cerro Prieto I region would be a thermal degradation (i.e., cooling effect) rather than a pressure decline in the classical sense.

ACKNOWLEDGEMENTS

The authors would like to thank Coordinadora Ejecutiva de Cerro Prieto and also Instituto de Investigaciones Electricas for the opportunity given to them in presenting this paper.

REFERENCES

The following abbreviations will avoid monotonous repetitions:

CPI : Proceedings of the First Symposium on the Cerro Prieto Geothermal Field, September 20-22, 1978, San Diego, Ca.

CPII : Proceedings of the Second Symposium on the Cerro Prieto Geothermal Field, October 17-19, 1979, Mexicali, B. C., Mexico.

CPIII: Proceedings of the Third Symposium on the Cerro Prieto Geothermal Field, March 24-26, 1981, San Francisco, Ca.

CPIV : Proceedings of the Fourth Symposium on the Cerro Prieto Geothermal Field, August 10-12, 1982, Guadalajara, Jal., Mexico.

1.- Abril, G.A., Noble, J.E., (1978): "Correlaciones de Secciones Transversales en Base a Registros Eléctricos de Pozos del Campo Geotérmico de Cerro Prieto", CPI, pp. 41-46.

2.- Bermejo et. al. (1979): "Variación de la Presión en el Yacimiento de Cerro Prieto durante su Explotación", CPII, pp. 473-493.

3.- Castañeda, M., Abril, A.G., Arellano, V., Márquez, R.M., Sánchez, J.R. (1982): "Entrenamiento para el Desarrollo Sistemático de la Ingeniería de Yacimientos en el Campo Geotérmico de Cerro Prieto", Instituto de Investigaciones Eléctricas, Internal Report IIE/11/FE-G30/1678/I 01/P, Sept 1982.

4.- Castañeda, M., Márquez, R., Esquer, C.A., Arellano, V. (1983): "Entrenamiento para el Desarrollo Sistemático de la Ingeniería de Yacimientos en el Campo Geotérmico de Cerro Prieto", Instituto de Investigaciones Eléctricas, Internal Report IIE/11/1678/I 03/F.

5.- Coats, K.H., George, W.D., Chu, C., and Marcum, B.E. (1974): "Three Dimensional Simulation of Steam Flooding", Society of Petroleum Engineering Journal, Vol. 14, Number 6.

6.- Cobo, J.M. (1981): "Configuración de los Cuerpos Litológicos de Lodolita, Lutita Café, Lutita Gris, Zonas de Sílice y Epidota y sus Relaciones con la Tectónica del Campo Geotérmico de Cerro Prieto", CPIII, pp. 29-42.

7.- Domínguez, B. (1982): Perforación Geotérmica en Cerro Prieto", CPIV, pp. 217-232.

8.- Grant, M.A., Truesdell, A.H., Mañón, M. A. (1981): "Production Induced Boiling and Cold Water Entry in the Cerro Prieto Geothermal Reservoir Indicated by Chemical and Physical Measurements", CPIII, pp. 221-237.

9.- Grant, M.A., Sullivan, M.J. (1982): "The Old Field at Cerro Prieto considered as a Leaky Aquifer", CPIV, pp. 123-132.

10.- Lippman, M.J., Bodvarsson, G.S. (1982): "Modeling Studies on Cerro Prieto", CPIV.

11.- Minutes of the Second Cerro Prieto Internal DOE/CFE Workshop, Hotel Fiesta, San Felipe, B.C., Mexico, January 19-21, 1982.

12.- Programa de Obras e Inversiones del Sector Eléctrico, (POISE), Comisión Federal de Electricidad, Enero 1983.

13.- Rivera, R., Bermejo, F.J., Castillo, F., Pérez, H., Abrajan, A. (1982): "Actualización en el Estudio del Comportamiento y Distribución de Temperaturas en Cerro Prieto II y III", CPIV, pp. 93-112.

14.- Sánchez, R.J., De la Peña, L.A. (1981): "Geohidrología del Aquífero Geotérmico de Cerro Prieto", CPIII, pp. 309-323.

15.- Westwood, J.D. (1981): "The Application of Lumped Parameter Modeling to the Cerro Prieto Geothermal Field", Geothermal Resources Council Trans,, Vol. 5, June 1981.

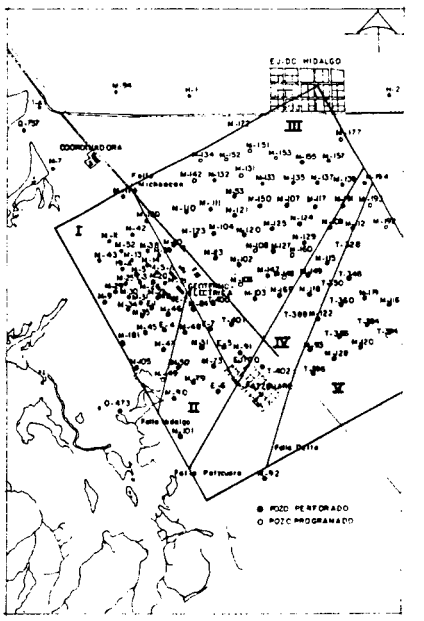


Fig. 1 Extended field area used in this work.

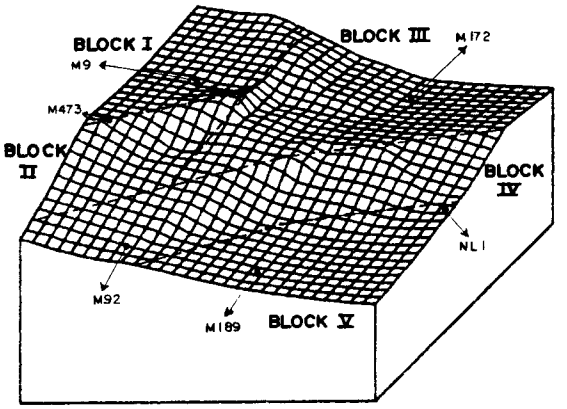


Fig. 2. Tridimensional representation of the top of the gray shale unit.

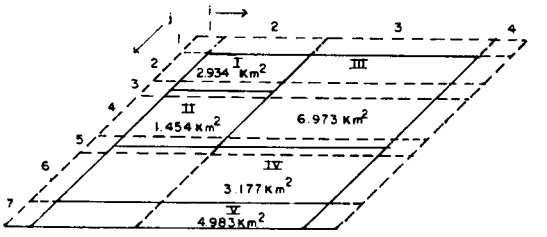


Fig. 3 . Schematic distribution of aereal grid elements.

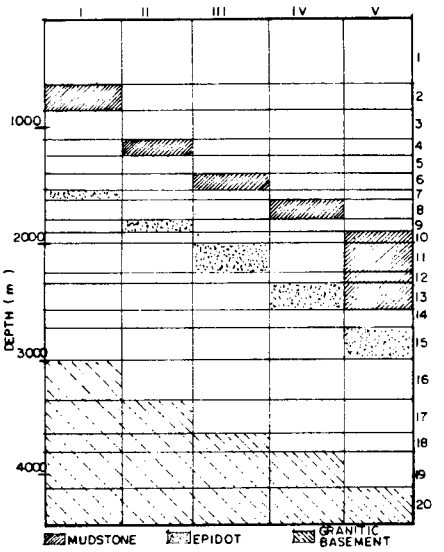


Fig. 4 . Vertical representation of the grid model.

PARAMETER \ UNIT	UNCONSOLIDATED SEDIMENTS	MUDSTONE	GRAY SHALE COFFEE-COLORED SHALE	BIOTITE GRANITE
POROSITY (fraction)	0.10	0.04	0.1	0.02
HORIZONTAL PERMEABILITY (md)	100	1	50	0.1
VERTICAL PERMEABILITY (md)	20	5	10	0.01
THERMAL CONDUCTIVITY BTU/ft.°F	35.0	35.0	35.0	35.0
ROCK HEAT CAPACITY BTU/ft³-°F	39.5	39.5	39.5	39.5
ROCK COMPRESSIBILITY (psi⁻¹)	4×10^{-6}	4×10^{-6}	4×10^{-6}	4×10^{-6}

Fig. 5 . Initial reservoir parameters for each model unit.

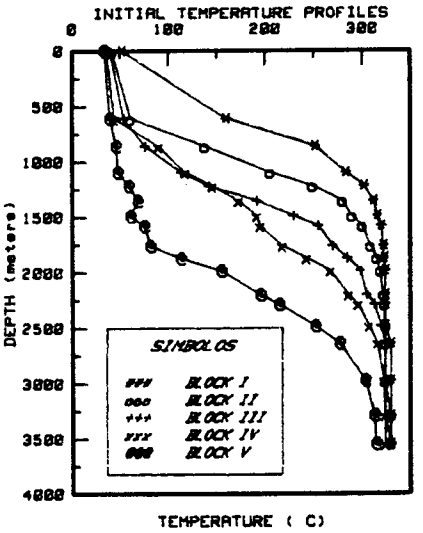


Fig. 6 . Initial temperature profile for each main block.

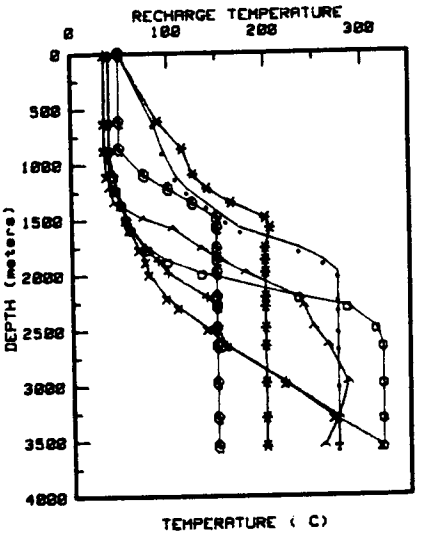


Fig. 7 . Recharge temperature profiles considered in this work.

MODEL WELL NUMBER	LOCATION I	J	K	WELL	BLOCK
1	2	2	2	M9, M291	I
2	2	2	4-5	M2911, M11, M31, M9A, M15A, M26, M27, M14, M5, M21A, M35, M8, M42.	I
3	2	2	5	M-20, M45, M25, M46, M39, M-30, M34, M43.	I
4	2	2	7		I
5	2	4	5	M48, M50, M90	II
6	2	4	5-7	M51,	II
7	2	4	10-11	M101	II
8	2	4	9	M84, M73, M79	II
9	3	2	11	M53, M91, M102, M103, M113, M117, M120, M121, M124, M125, M135, M137, M139, M150, M155, M157, M169, M177, M195, E5, E7.	III
10	3	2	9	M104, M110	III
11	2	4	13-14	E6	II
12	2	2	9	E2	I
13	3	2	12	M133, M127	III
14	3	2	13-14	M111	III
15	2	6	13	M109, M112, M115, M118, M122, M149, M191, M194, M328, M350 M388	IV
16	2	7	15	M93, M116, M119, M128, M348 M364, M366, M386, M395	V
17	3	4	11	M129, M147, T400	III

Fig. 8 . Location of the groups of wells in the coarse grid model.

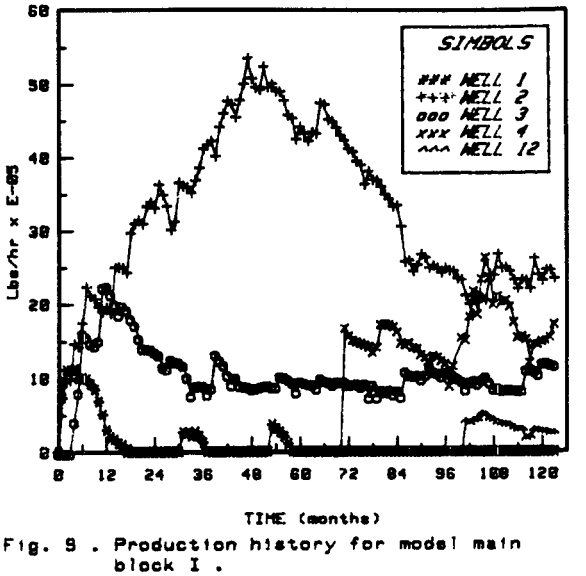


Fig. 9 . Production history for model main block I .

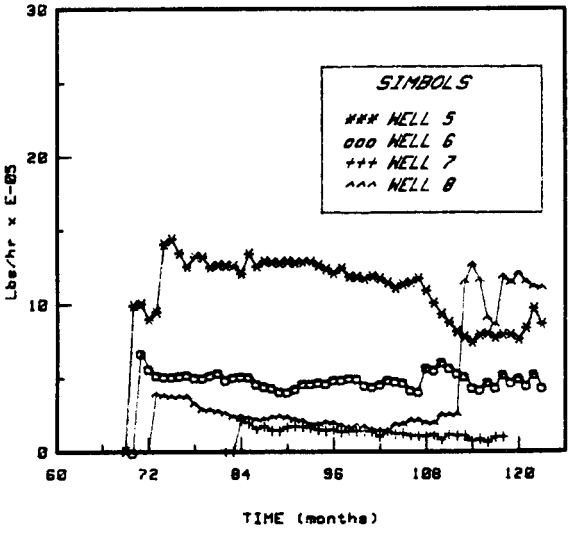


Fig. 10 . Production history for model main block II.

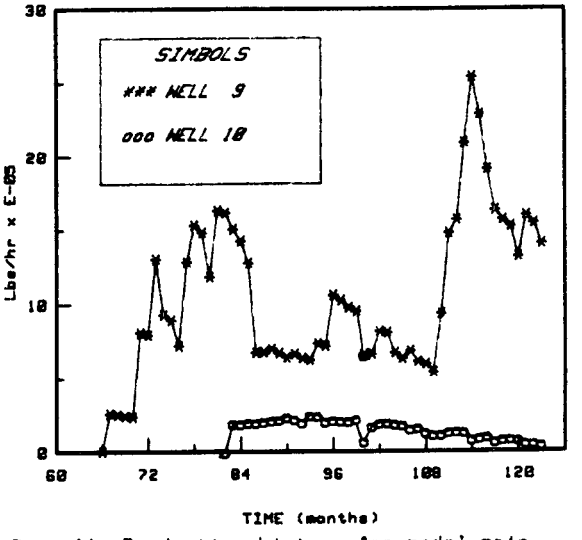


Fig. 11. Production history for model main block III.

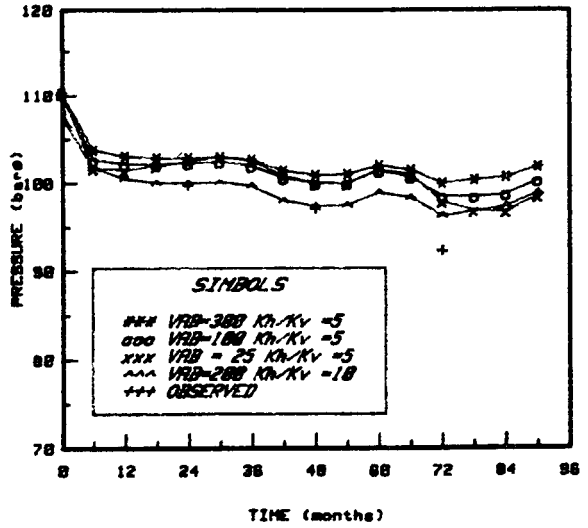


Fig. 12 . Simulated pressure for the initial reservoir parameters.

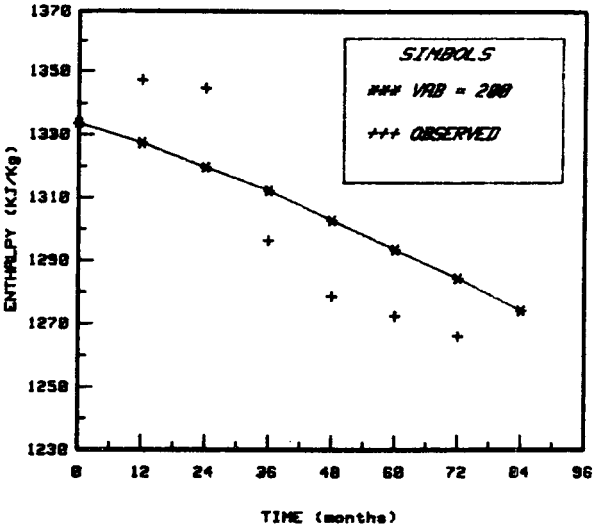


Fig. 13 . Simulated enthalpy for the case Kh/Kv = 10 , Kh = 50 md .

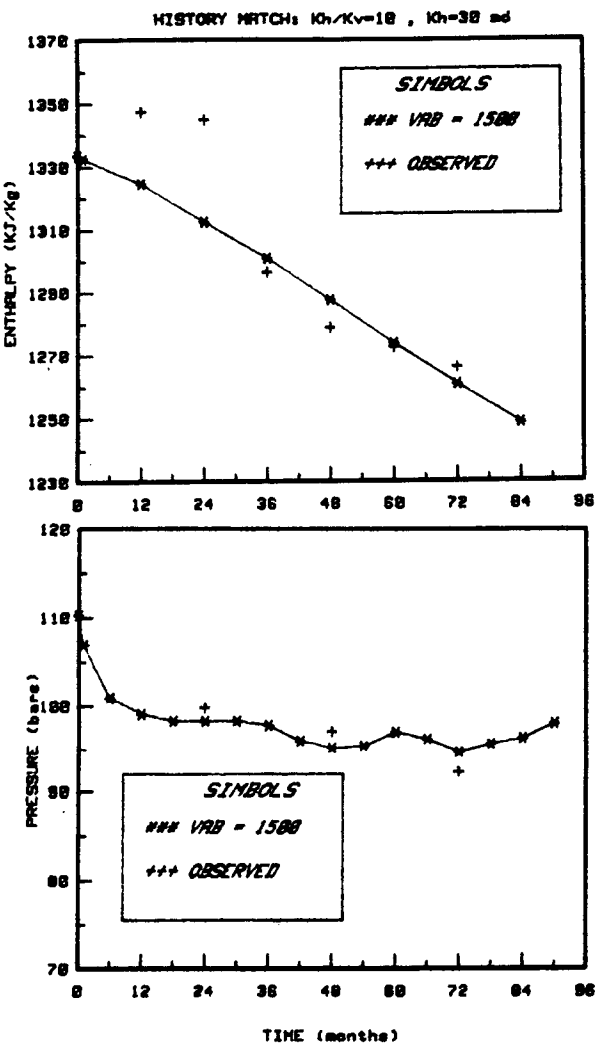


Fig. 14 . Pressure and enthalpy match for Cerro Prieto I (at depth of 1200 m)

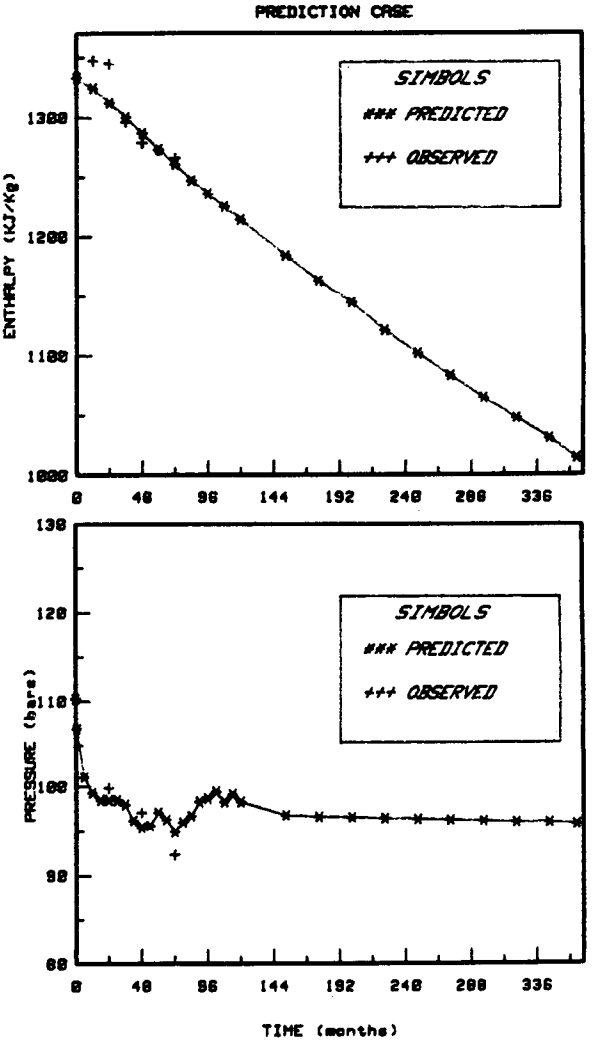


Fig. 16 . Predicted pressure and enthalpy for Cerro Prieto I region (period 1973-2003)

POWER PLANT	UNIT	DATE	WELLS	MASS RATE PER WELL (Ton/hr.)
CP II	1	DIC/1/83	M93, M116, M119, M128, M364, M366, M386, M395, M348, M122 T400.	233.1
	2	NOV/1/84	M129, M147, M27, M115, M118, M149, M328, M350, M388.	233.1
CP III	1	ENE/1/85	M150, M117, M121, M113, M124, M110, M109, M112, M125, M111.	233.1
	2	JUL/1/85	M135, M137, M139, M157, M155, M177, M195, M191, M194, M133.	233.1

Fig. 15. Required mass flow rate and approximated starting operation dates for the two new power plants.

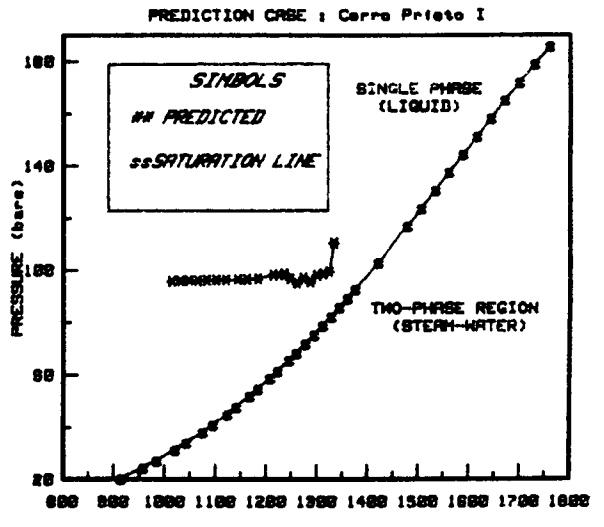


Fig. 17 . Comparison of predicted pressure and enthalpy with the steam-water saturation curve values

Proceedings Ninth Workshop Geothermal Reservoir Engineering
Stanford University, Stanford, California, December 1983
SGP-TR-74

NUMERICAL SIMULATIONS OF THE HYDROTHERMAL SYSTEM AT LASSEN VOLCANIC NATIONAL PARK

Michael L. Sorey and Steven E. Ingebritsen

U.S. Geological Survey, Menlo Park, California

ABSTRACT

The hydrothermal system in the vicinity of Lassen Volcanic National Park contains a central region of fluid upflow in which steam and liquid phases separate, with steam rising through a parasitic vapor-dominated zone and liquid flowing laterally toward areas of hot spring discharge south of the Park. A simplified numerical model was used to simulate the 10,000 - 20,000-year evolution of this system and to show that under certain circumstances fluid withdrawal from hot-water reservoirs south of the Park could significantly alter the discharge of steam from thermal areas within the Park.

INTRODUCTION

Thermal discharge from the Lassen hydrothermal system occurs in fumaroles and steam-heated springs within Lassen Volcanic National Park (LVNP) and in high-chloride neutral-pH hot springs within the Lassen Known Geothermal Resource Area (KGRA) south of the Park. Existing geochemical and geophysical data indicate that these features are connected to and fed by a single convection system at depth. Thus fluid production for geothermal energy development south of LVNP could potentially cause changes in flow rates and temperatures in discharge vents within the Park. The numerical simulations discussed in this paper were carried out in an effort to predict the magnitude of such changes.

Although the general nature of the Lassen system has been delineated, critical data regarding the location and properties of thermal-fluid reservoirs are lacking. Therefore, numerical simulations of the evolution of the present-day Lassen hydrothermal system were carried out to provide estimates of the rock properties and boundary conditions controlling heat and fluid flow.

Our simulation model is idealized and involves a relatively simple geometric configuration. Nevertheless, the results of this study indicate that under certain circumstances fluid production from reservoirs within Lassen KGRA could induce significant changes in steam discharge within LVNP. Such development is also likely to reduce or eliminate the discharge of hot springs within Lassen KGRA.

THE LASSEN HYDROTHERMAL SYSTEM

The Lassen area is in north-central California, approximately 50 km east of Redding and 20 to 30 km northwest of Lake Almanor (figure 1). It is at the southern end of the Cascade Range, which here is reduced to a broad ridge of Late Pliocene and Quaternary volcanic rocks, primarily pyroxene andesite flows and pyroclastics with minor basaltic and silicic flows and pyroclastics (Muffler and others, 1982).

Surficial hydrothermal features in the Lassen region are confined to the southern half of LVNP and to the Lassen

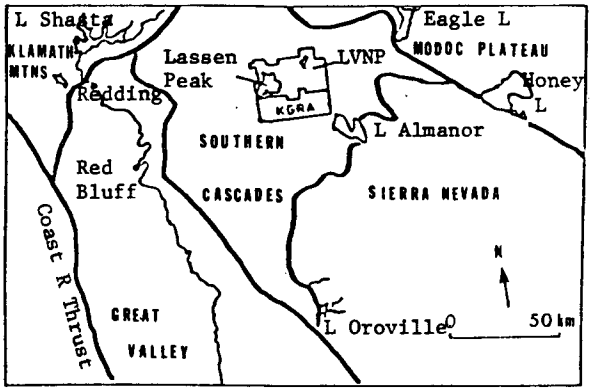


Figure 1. Physiographic provinces in Northern California and adjacent states and locations of Lassen Volcanic National Park (LVNP) and Lassen Known Geothermal Resource Area (KGRA).

KGRA (figure 2). They include fumaroles and acid-sulphate hot springs at relatively high elevations in LVNP and neutral-pH high-chloride hot springs at relatively low elevations in the KGRA. Although these features are widely separated, they are fed by a single convection system at depth. The Lassen system is similar in this respect to other high-temperature hydrothermal systems in regions of moderate to great relief, including the Valles Caldera in New Mexico and the Tongonan area in the Philippines. We refer to such systems as liquid hydrothermal systems with parasitic vapor-dominated zones (LHSPVZ). The essential characteristic of these systems is that steam and liquid phases separate within a zone of upflow, with steam rising through a parasitic vapor-dominated zone and liquid flowing laterally to discharge at lower elevations.

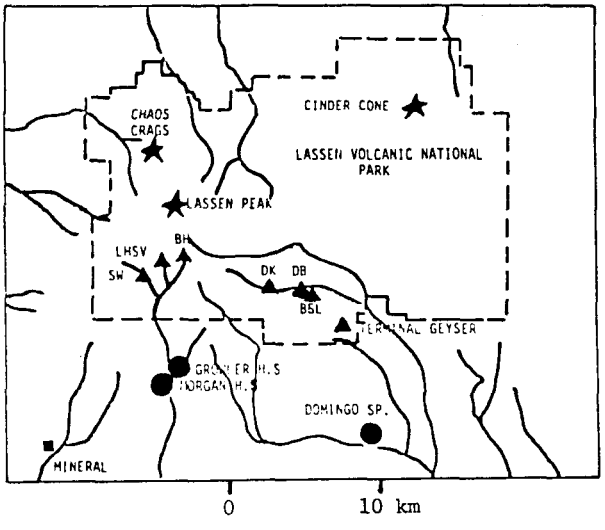


Figure 2. Map of areas of thermal fluid discharge and streams in the Lassen region. Areas of fumaroles, steam-heated springs, and low-chloride conductively heated springs shown as triangles (BH = Bumpass Hell, LHSV = Little Hot Springs Valley, SW == Sulphur Works, DK = Devils Kitchen, DB = Drakesbad, BSL = Boiling Springs Lake). Areas of high-chloride thermal water discharge shown as dots.

A generalized conceptual model for the Lassen system and other LHSPVZ is illustrated in figure 3. As seen in the accompanying diagram of pressure versus elevation, steam is the pressure-controlling phase within the vapor-dominated zone and the vertical pressure gradient in this zone is near vapor-static. Pressures in this zone are balanced by the weight of liquid in the overlying zone of steam condensate and shallow groundwater. The thickness of the vapor-dominated zone depends upon the difference in elevation between the steam-heated and high-chloride discharge areas, and on the pressure gradient required to drive the lateral outflow.

Studies of gas and stable isotope composition (Janik and others, 1983) and geothermometry (Thompson, 1983) indicate that thermal fluids in the Lassen region circulate outward from a common upflow zone beneath Bumpass Hell (figure 2). Recharge to the system occurs on the composite cone of the Lassen volcanic center that includes Lassen Peak. Fluid is heated at depth by conduction from the residual silicic magma chamber associated with this long-lived (0.6 m.y. to present) volcanic center, and possibly by small amounts of magmatic steam. The resulting high-enthalpy fluid circulates upward along the contact between the andesitic composite cone and the dacite dome field of the Lassen center (Muffler and others, 1982).

With the exception of Morgan and Growler Hot Springs, hot spring waters in the Lassen area are generally acidic and low in chloride (Thompson, 1983), indicating some degree of vapor-dominated conditions at depth. The widely separated areas of steam-heated discharge could be surface expressions of a single laterally extensive vapor-dominated zone or expressions of a number of "satellite" parasitic vapor zones. However, the composition of gas in steam discharging from the various thermal features suggests that vapor-dominated conditions do not extend continuously under the entire southwestern part of LVNP (Janik and others, 1983), and that the thermal features between Devil's Kitchen and Terminal Geyser and at Morgan and Growler Hot Springs are connected to the vapor-dominated zone beneath Bumpass Hell by liquid-dominated lateral flow zones. The 1200 m deep Walker "O" No. 1 well at Terminal Geyser - the only well drilled deeper than 250 m in the Lassen region - intercepts such a lateral flow zone at a depth of approximately 500 m (Beall, 1981).

Most of the lateral outflow eventually discharges in regions of high-chloride springs in the canyon of Mill Creek (at Morgan and Growler Hot Springs) and at Domingo Springs, where elevated chloride levels indicate a component of high-chloride thermal water. Available data supports a model of two areally restricted orientations of thermal fluid circulation in the Lassen system, between Bumpass Hell and Morgan and Growler Hot Springs and Bumpass Hell

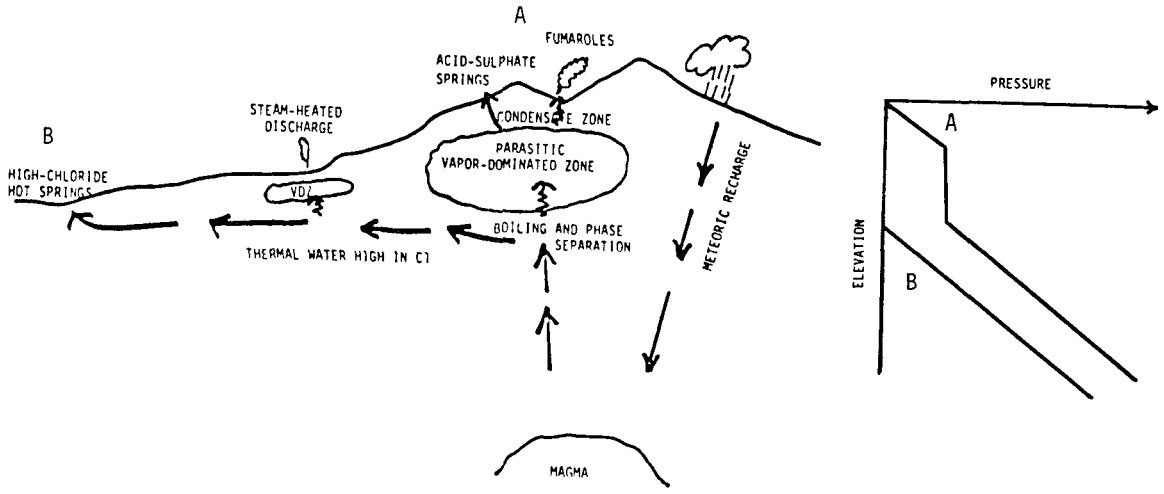


Figure 3. Generalized conceptual model of the Lassen hydrothermal system and other liquid-dominated systems with parasitic vapor-dominated zones, and corresponding pressure -elevation relations in the upflow region A and outflow region B.

and Terminal Geyser. Extension of the Bumpass Hell - Terminal Geyser orientation to Domingo Springs seems reasonable. All of the surface manifestations of the Lassen hydrothermal system lie along these orientations, and resistivity data (Christopherson and Pringle, 1981) show no evidence of high-temperature, high-chloride water underlying the central part of Lassen KGRA between the two flow zones. The areally restricted flow zones imply avenues of relatively high permeability leading away from the upflow zone beneath Bumpass Hell. Such avenues of permeability could be fault controlled.

Although the general nature of the Lassen system is well understood, quantitative constraints on this model are few. Temperatures and pressures in the vapor-dominated zone beneath Bumpass Hell are inferred to be near 235 °C and 31 bars, on the basis of superheated steam temperatures of up to 159 °C measured in the overlying fumarolic area during the California drought of 1976-1977 (Muffler and others, 1982). Temperatures in the lateral flow zone beneath Terminal Geyser intercepted by the Walker "O" well are approximately 176 °C (Beall, 1981), and high-chloride spring temperatures in the Morgan and Growler Hot Springs area are near-boiling.

Preliminary estimates of the rate of lateral outflow in the Lassen system were made based on data collected in the course of this study. Measurements of streamflow and chloride concentration at selected sites in the Morgan and Growler Hot Springs area indicate that the total flow of thermal water discharging at the surface is approximately 17 kg/s. This figure probably represents most of the lateral outflow along the Bumpass Hell - Morgan and Growler Hot Springs orientation; however, an anomolously high heat flow value (Mase and others, 1980) and low resistivity values (Christopherson and Pringle, 1981) in the Child's Meadow area south of Morgan and Growler suggest that an additional, unknown quantity of thermal fluid flows past the hot springs area in the subsurface. Some or all of the thermal fluid flowing under Terminal Geyser may eventually discharge at Domingo Springs. Measurements of chloride flux in Domingo Springs indicate a thermal component of approximately 2.7 kg/s. Additional thermal fluid from the Bumpass Hell - Terminal Geyser orientation may flow into the North Fork of the Feather River and Warner Creek, where relatively high flowrates could preclude detection of a thermal component.

NUMERICAL MODEL

The geometric configuration used in numerical simulations of the Lassen hydrothermal system is shown in figure 4. It consists of a vertical slab of uniform width with a sloping upper boundary representing land-surface elevations between Bumpass Hell and Morgan and Growler Hot Springs. Fluid circulation is confined to the vertical conduits along the sides of the model and to the 200 m-thick lateral conduit. Circulation is driven by a specified mass inflow of hot water at the lower right and discharge occurs at the upper right and left sides of the model. A conductive heat flow along the base of

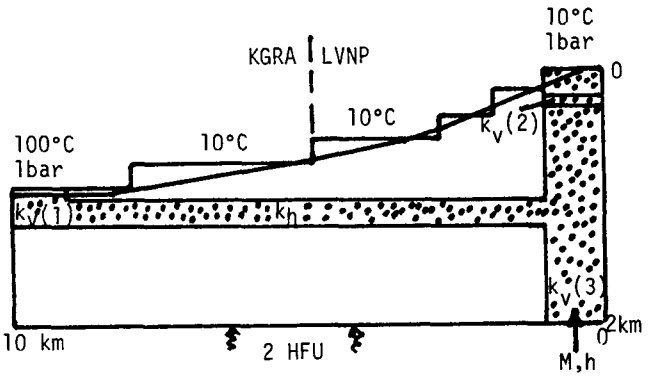


Figure 4. Geometric model used in simulations of the Lassen hydrothermal system. Arrow indicates inflow of hot water at mass flow rate M and enthalpy h. Fluid flow confined to regions with dotted pattern and across portions of the upper boundary held at 1 bar pressure. Upper boundary represents finite difference approximation to land surface between Bumpass Hell and Morgan and Growler Hot Springs. Horizontal and vertical permeabilities indicated by symbols k_h and k_v, respectively. The model width is 1 km.

85 mW m^{-2} represents the regional heat flow (Mase and others, 1980). With reference to the conceptual model shown in figure 3, the numerical model is restricted to the regions of upflow and lateral outflow and does not include the regions of downflow and magmatic heating.

A two-dimensional model was chosen in part because of computational difficulties and expense involved in three-dimensional simulations of multiphase flow over the time periods on the order of 10,000 years. In addition, the lack of quantitative information regarding rock and fluid properties within the Lassen system does not justify using a more detailed model. The available data do suggest that there are two areally restricted flow regimes originating from the central upflow zone beneath Bumpass Hell. Our model corresponds with the Bumpass Hell - Morgan and Growler Hot Springs orientation, which represents the most likely target for geothermal exploration and development in Lassen KGRA, and for which the discharge of high-chloride thermal fluid is reasonably well constrained. Inclusion in the model of the Bumpass Hell - Terminal Geyser orientation would have added useful constraints provided by the known temperature and elevation of the lateral conduit beneath Terminal Geyser. However, exclusion of this part of the flow system saves considerably on computational requirements and should not alter the basic conclusions derived from the numerical simulations.

For simplicity, the lateral conduit is assumed to be flat-lying at an average elevation of 1400 m and to be 200 m in thickness. These values match those for the hot-water aquifer penetrated in the Walker "O" No. 1 well. Modeling the lateral conduit at significantly greater depths would have resulted in the evolution of a vapor-dominated zone with pressures considerably in excess of the desired 31 bar-level. The model width of 1 km is the value suggested by the average width of the glacially eroded Mill Creek Canyon.

The computer code used in the numerical simulations is a modified version of a three-dimensional, two-phase fluid and heat transport program described by Faust and Mercer (1979) and used in a recent analysis of the effects of potential geothermal development in the Valles Caldera. Modifications were needed to improve the scheme for upstream weighting of fluid properties and relative permeabilities and to allow conductive heat flux to be specified as a boundary condition.

EVOLUTION SIMULATIONS

Simulations of the evolution of the Lassen hydrothermal system provided insight into the conditons required for the development of LHSPVZ in general, as well as estimates of the rock properties and boundary conditions controlling heat and fluid flow in the Lassen system. The simulations indicate that several conditions are necessary for the development of parasitic vapor-dominated zones: large-scale topographic relief that enables thermal fluids to discharge in regions of significantly different elevations; a change in hydrologic or geologic properties that initiates a period of drainage from a zone of high temperature; and low permeability barriers that inhibit drainage of cool water from surrounding regions into the evolving vapor-dominated zone. The evolution of LHSPVZ are discussed in greater detail by Sorey and Ingebritsen (1983).

Initial conditions for the evolution simulations were a temperature distribution corresponding to a uniform conductive heat input of 85 mWm^{-2} and a hydrostatic pressure distribution. Evolution simulations were carried out until the pressure distribution reached conditions similar to those in figure 3, with pressures near 31 bars in the vapor-dominated zone, and temperatures in the lateral conduit had become relatively stable (changing less than 1 °C per 1,000 years). The desired temperature and pressure distributions

in the lateral conduit at this quasi-steady-state condition were constrained only by the requirement that temperatures at the left side of the model be above the surface boiling point of 95 °C. Factors affecting the simulated end-point conditions include the mass inflow rate M, inflow enthalpy h, horizontal and vertical permeabilities k_h and k_v, and the relative permeability-liquid saturation functions. The lack of information on values of most of these parameters and the complex interactions between thermodynamic and hydraulic processes in the simulations made considerable experimentation necessary to find combinations of parameter values that would produce the desired results.

The evolution simulations suggest that times required for the evolution of the present-day Lassen hydrothermal system are of the same order of magnitude as the age of the volcanism which produced Lassen Peak (11,000 years). Quasi-steady-steady-state mass flux and temperature distributions for one of the evolution runs are shown in figure 5. Values of various parameters associated with this solution are listed below and defined in figure 4.

M = 20 kg/s
h = 1,125 J/gm (258 °C)
$k_h = 1.4 \times 10^{-9}$ cm^2
$k_v(1) = 1 \times 10^{-9}$ cm^2
$k_v(2) = 5 \times 10^{-13}$cm^2
$k_v(3) = 1 \times 10^{-9}$ cm^2

Corey relative permeability functions

Mass flow vectors at quasi-steady-state (figure 5) show a counterflow of liquid and steam within the vapor-dominated zone, with a net upflow of 0.54 kg/s. At the base of the lower permeability caprock layer [$k_v(2)$] overlying the vapor-dominated zone, some of the steam condenses and flows downward while the remainder flows into the caprock layer where it condenses before rising to the land surface. Although separate flows of steam and steam condensate at the land surface are not simulated, the net mass upflow of steam through the vapor-dominated zone is balanced by the mass upflow of liquid across the surface.

The parameter values listed above lead to a quasi-steady-state configuration involving a zone of two-phase flow conditions in the lateral conduit extending to the Park boundary. The presence of an extensive two-phase region in the lateral conduit would have a strong influence on the rate of propagation of pressure changes induced by fluid withdrawal, and whether such a region exists is as yet unknown.

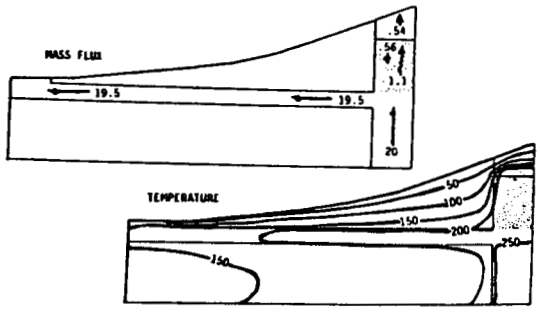


Figure 5. Quasi-steady state results from simulation of the evolution of the Lassen hydrothermal system, showing mass flow vectors (straight arrows for liquid, wavy arrows for steam) and the temperature distribution. Dotted pattern represents region of vapor-dominated conditions. Units of mass flow are kg/s.

Simulations with a much lower value of $k_v(1)$ (6×10^{-12}cm^2) and a slightly increased value of k (1.8×10^{-9} cm^2) resulted in higher conduit pressures and the absence of two-phase flow except immediately below the vapor-dominated zone. Quasi-steady-state results were also generated using the relative permeability functions suggested for fractured media by Sorey, Grant, and Bradford (1980) in place of the porous-media derived Corey functions.

Four quasi-steady-state results from the evolution simulations were used as initial conditions for simulations of fluid withdrawal for geothermal electric power generation. Two of these cases involved an extensive region of two-phase flow in the lateral conduit, one for each of the two sets of relative permeability functions referred to previously, and two involved single-phase flow in the conduit away from the region of phase separation, one for each of the relative permeability functions. One additional variable considered in the development simulations was the vertical permeability k (2) of the caprock layer above the vapor-dominated zone.

DEVELOPMENT SIMULATIONS

Development simulations were carried out for production rates of 50, 100, and 250 kg/s. For reservoir temperatures near 200 °C, these production rates correspond with electrical power generation of about 5, 10, and 25 MW_e, respectively. In the absence of reinjection, it was not possible to sustain production rates greater than 50 - 100 kg/s for periods of about 50 years without causing

pressures in the production block to fall below a realistic cutoff point of 3 bars. This reflects limitations imposed by the permeability and cross-sectional area of the conduit. Conduit permeability is constrained from the evolution simulations to the range 1.4 x 10^{-9} to about 2.0 x 10^{-9} cm^2, if the rate of mass outflow along the Bumpass Hell to Morgan-Growler Hot Springs axis is indeed near 20 kg/s, as suggested by the chloride flux measurements discussed above. The average value of permeability - thickness for the lateral conduit in our model would then be 34 darcy-meters, a value comparable to those found for exploited geothermal fields at Wairakei and Broadlands in New Zealand.

Production rates greater than 100 kg/s can be sustained with reinjection at 80 percent of the production rate. The maximum production rate sustainable for more than 30 years is near 250 kg/s; for greater rates either production-block pressures fall below 3 bars or production-block temperatures fall below a realistic cutoff point of 150 °C. Such declines in temperature in the production block are due to the injection of lower temperature water.

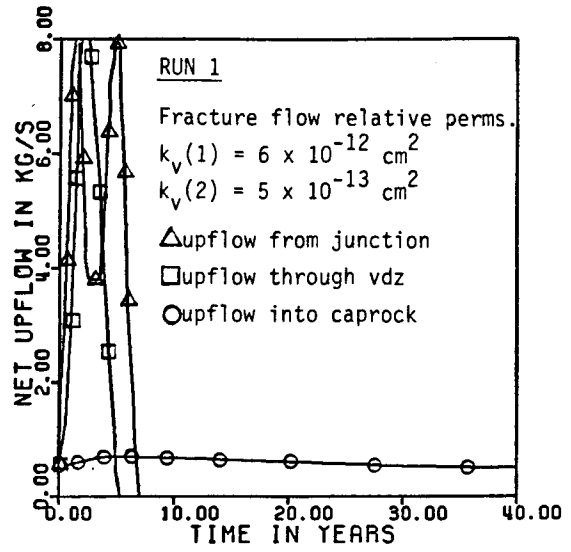
The development scheme involved a production block centered 4.5 km from the left side of the model and 1.5 km outside the Park boundary (see figure 4). Reinjection was specified either in the block centered 1 km upstream (towards the Park) from the production block or the block centered 1 km downstream from the production block.

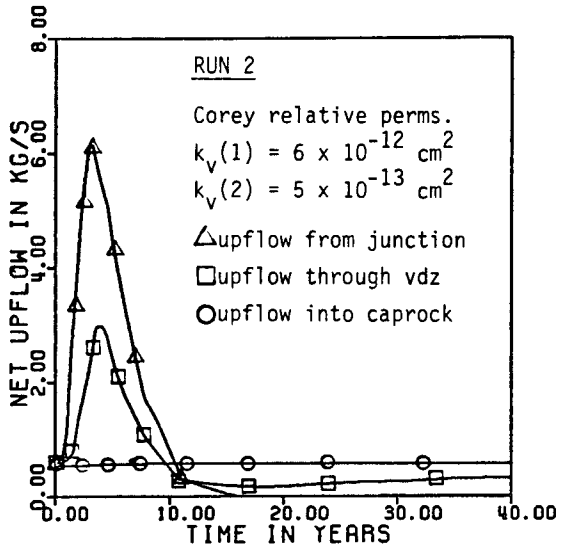
During the development simulations, the rate of fluid flow across the constant-pressure finite-difference block representing Morgan and Growler Hot Springs changes. Depending on the specified production-injection rates and the value of $k_v(1)$, the simulated flow across this boundary either decreases in magnitude or reverses in direction in response to production. A reversal in direction corresponds with the disappearance of hot-spring discharge and induced recharge of cold water from the land surface. For given production-injection rates, the simulated rate of induced recharge was greater and the pressure declines in the lateral conduit less for cases with a high value of $k_v(1)$ than for cases with a low value of $k_v(1)$.

Fluid production from the lateral conduit induces pressure drops that propogate upstream (toward the Park) as well as downstream from the production area. The rates and magnitudes of pressure changes induced within portions of the conduit beneath LVNP vary significantly depending on the difference between the specified production and injection rates, the relative permeability functions used, and, most significantly, on the extent of two-phase conditions in the conduit before development starts. For cases in which pressure declines can propogate into the region of phase separation beneath the central vapor-dominated zone, the net rate of steam upflow into the vapor-dominated zones is observed to increase significantly and then decrease within a time frame of less than 20 years. Such increases in upflow rate are damped within the vapor zone itself by condensation and accompanying pressure rises so that the observed changes in steam flow into the caprock layer are delayed and reduced in magnitude.

The plots in figure 6 show transient variations in net upflow of steam into and out of the vapor-dominated zone during selected development runs involving single-phase initial conditions in the lateral conduit away from the upflow zone. In each case, changes in steam upflow in the vapor-dominated zone are observed in response to fluid production. Although boiling and two-phase flow are induced in and near the production area in these runs, the drop in pressure to saturation values for the initial temperatures is transmitted relatively rapidly through the single-phase portions of the conduit and hence can reach the upflow zone during the development period. In runs in which the lateral conduit initially contained an extensive region of two-phase flow, the effects of fluid production did not propogate as far back as the upflow zone because of the low hydraulic diffusivity in the two-phase portion of the lateral conduit.

The development runs plotted in figure 6 involve production of 50 kg/s with no reinjection and show the effects of varying the relative permeability functions and the vertical permeability of the caprock layer on induced changes in steam upflow. With the higher value of $k_v(2)$ in Run 3, the initial rate of steam upflow from the quasi-steady-state simulation is about twice the value for the lower $k_v(2)$ cases, but changes in net upflow during development are more subdued and spread out over a longer period of time. This response may be due in part to differences in the initial pressure-temperature distributions in the lateral conduit, which for run 3 involved less overpressure with respect to the corresponding saturation





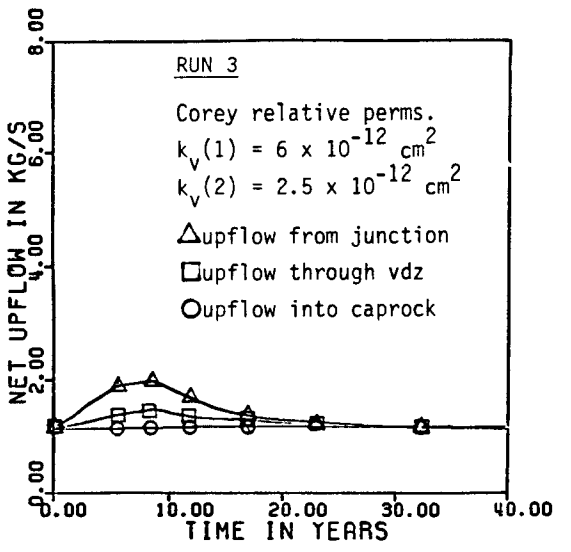


Figure 6. Development simulations involving production of 50 kg/s without reinjection. Production starts at 0 years.

pressures than for runs 1 and 2. The degree of overpressure affects the magnitude of pressure decline that can propogate from the production area before boiling occurs.

Changes in steam upflow are most pronounced for the case with fracture-flow relative permeability functions. Here, although the temporary increase in steam flow is greatly damped by condensation within the vapor-dominated zone, the increase in steam flow into the caprock amounts to about 32 percent of the initial flow rate. The oscillation seen within the first five years of production may represent a shift in the dynamic balance between steam upflow, liquid downflow, and pressures and saturations near the base of the vapor-dominated zone.

Results for development runs involving reinjection were qualitatively similar to the results in figure 6. Changes in net steam upflow increased with the production rate and, hence, the difference between production and injection.

Temporary increases in steam upflow seen in these simulations are followed by decreases to levels at or below initial flow rates. Pressures in the region of phase separation beneath the vapor-dominated zone continue to decline during the entire development period. At early times, corresponding decreases in liquid saturation and increases in steam relative permeability dominate and produce the observed rapid rise in steam upflow. After about 5 - 10 years, liquid saturation and steam relative permeability tend to stablize and the continued pressure decline beneath the vapor-dominated zone causes the rate of steam upflow to decrease. Within the vapor zone itself, steam relative permeability remains nearly constant so that changes in steam upflow can only occur if the vertical pressure gradient changes. Thus the observed increase in steam flow through the vapor zone at early times is accompanied by condensation of steam and resultant pressure increases, with more condensation and larger pressure increases at lower levels than at higher levels to increase the gradient. This condensation of excess steam results in the vapor zone acting as a buffer between relatively large changes in the region of phase separation and smaller changes at the base of the caprock.

Simulated changes in net steam upflow into the caprock layer ranged from 0 to

32 percent of the initial rate, and were in all cases very small compared with changes within and below the vapor-dominated zone. This primarily reflects the relatively low value of vertical permeability applied to the caprock layer. As the value of $k_v(2)$ is increased, the ratio of change in steam upflow into the caprock to the change in steam upflow at the base of the vapor zone increases. The value for caprock permeability of 2.5×10^{-12} cm^2 used in run 3 is near the upper limit for successful simulation of the evolution of the Lassen system. However, a more detailed model involving separate channels for steam and liquid flow through the condensate zone would be required to adequately describe the changes in steam flow at the land surface induced by geothermal development. Such changes are likely to be larger in magnitude than those found in our simulations.

Although no changes in pressure or upflow within the vapor-dominated zone were observed during development runs involving an extensive region of two-phase flow initially in the lateral conduit, such changes could occur if the permeability of the lateral conduit were at least an order of magnitude larger than the value used in these simulations. Higher permeability is possible if the conduit were thinner or less areally extensive than modeled. On the other hand, if outflow conduits at Lassen are more areally extensive than modeled in this study, conduit permeabilities may by lower and the speed of pressure propogation slower than our simulations indicate. In either event, the need for additional test drilling to delineate such conduits and to provide access for monitoring pressure and temperature changes near the Park boundary seems evident.

REFERENCES

Beall, J. J., 1981, A hydrologic model based on deep test data from the Walker "O" No. 1 well, Terminal Geyser, California: Transactions of the Geothermal Resources Council, v. 4, p. 153-156.

Christopherson, K. R., and Pringle, Laurel, 1981, Additional audio-magnetotelluric soundings in the Lassen Known Geothermal Resource Area, Plumas and Tehama Counties, California: U.S. Geological Survey Open-file Report 81-959, 18 p.

Faust, C. R., and Mercer, J. W., 1979, Geothermal resevoir simulation: 2. Numerical solution techniques for liquid and vapor-dominated hydrothermal systems: Water Resources Research v. 15, p. 31-46.

Janik, C. J., Nehring, N. L., and Truesdell, A. H., 1983, Isotope geochemistry of thermal fluids from Lassen Volcanic National Park: Geothermal Resources Council Transactions, v. 7, p. 295-300.

Mase, C. W., Sass, J. H., and Lachenbruch, A. H., 1980, Near-surface hydrothermal regime of the Lassen "Known Geothermal Resource Area", California: U.S. Geological Survey Open-file Report 80-1230, 18 p.

Muffler, L. J. P., Nehring, N. L., Truesdell, A. H., Janik, C. J., Clynne, M. A., and Thompson, J. M. 1982, The Lassen geothermal system: Proceedings of the Pacific Geothermal Conference, Auckland, New Zealand, p. 349-356.

Sorey, M. L., Grant, M. A., and Bradford, Elizabeth, 1980, Nonlinear effects in two-phase flow to wells in geothermal reservoirs: Water Resources Research, v. 16, p. 767-777.

Sorey, M. L., and Ingebritsen, S. E., 1983, Evolution of liquid-dominated hydrothermal systems with parasitic vapor-dominated zones: Proceedings of the Fifth New Zealand Workshop, University of Auckland, New Zealand, p. 17-22.

Thompson, J. M., 1983, Chemical analyses of thermal and nonthermal springs in Lassen Volcanic National Park and vicinity, California: U. S. Geological Survey Open-file Report 83-311, 23 p.

Proceedings Ninth Workshop Geothermal Reservoir Engineering
Stanford University, Stanford, California, December 1983
SGP-TR-74

A Fundamental Approach to the Simulation of Flow and Dispersion in Fractured Media

J. D. Miller

EG&G Idaho, Inc.
P. O. Box 1625
Idaho Falls, Idaho 83415

ABSTRACT

Fracture systems may be generalized in terms of number and orientation of sets of parallel fractures and the distribution of length, width, thickness and separation. Borehole measurements may be used to particularize these parameters for a specific site.

Global flow and dispersion in an aquifer occur in the interconnected fractures and may be related to specific fracture elements. A fluid dynamics code named SALE has been used to solve the Navier-Stokes equations for laminar flow in these elemental geometries. A marker particle calculation has been added to characterize longitudinal dispersion due to the velocity profile across the fracture and lateral dispersion due to flow disturbances at junctions.

Local flow and dispersion in the matrix occur in the finer fracture structure and are evaluated using porous media approaches.

These results or models are integrated in a 2D isothermal reservoir simulator named FRACSL. Discrete fractures are superimposed on the edges or diagonals of rectangular grid elements. Water may flow from node to node through the matrix or through the fracture. The heads are found by iterating for the distribution which conserves the appropriate local mass. Marker particles are used to monitor the tracer dispersion due to motion in the fractures, in the matrix and between the two.

Results are given showing flow and dispersion in an orthogonal junction and in a sample fractured reservoir.

INTRODUCTION

Geothermal, waste management and secondary and tertiary petroleum recovery activities have provided the stimulus for recent advances in the characterization of fractured reservoirs. Much of this work has been directed towards the evolution of specific fractured media approaches which depart significantly from those used for porous media. An essential characteristic of these approaches is the determination of fracture system geometric and flow characteristics.

A reservoir fracture system may be described in terms of two subsets: A number of interconnected fractures which constitute the global flow system and a system of progressively smaller fractures which begin at the global flow system and terminate in the matrix microcrack structure. The secondary system, while nominally quiescent, constitutes the bulk of the matrix porosity and surface area.

Fractured reservoir characterization for petroleum recovery is described by Nelson[1]. A basis for characterizing the geometry of fracture systems is presented by Nelson[2] and by Stearns and Friedman[3] and a significant body of data is available in the literature, particularly from the research at the Stripa mine in Sweden and from the Canadian waste management programs.

Numerical simulations of flow in fractured media depart from the use of heterogeneous and anisotropic porous media characteristics and model the flow in unique and discrete fractures or in repeated fracture patterns. Some flow simulations[4,5] superimpose discrete fractures onto the edges of porous media grid cells. This approach results in a single set of grid point pressures and distinct matrix and fracture flow paths between those grid points.

These flow simulations are essential to the study of solute transport, both as an end product and as another tool for characterizing fractured reservoirs. Typical solute transport models, however, revert to porous media theory. A common approach is to implement different dispersivities in the fracture and in the matrix.

While studies[6] have shown the significance of geometry and head gradient orientation on dispersion or mixing in individual fractures and fracture junctions, these characteristics have not been reflected in reservoir level numerical simulation.

This paper describes initial numerical studies aimed at characterizing the flow and dispersion characteristics of the global flow system in terms of those of its elements and

integrating those characteristics with those of the matrix in a complete reservoir simulation. One objective of this work is to develop a model whose parameters can be adjusted to describe a particular reservoir by matching measured hydrologic and tracer dispersion responses. This model will ultimately be used for assessing the thermal potential of a reservoir. Specific models will be developed to correlate data measured in 1982 and 1983 at Raft River, Idaho and East Mesa, California as part of the U.S. Department of Energy Hydrothermal Injection Research Program. Other phases of this program are reported elsewhere in these proceedings.

APPROACH

The complete numerical simulation effort, a portion of which is presented in this paper, includes the following tasks:

1) Integrate formation characterization data from the literature into a base which can be used together with site-specific data such as lithology, core samples and acoustic televiewer, spinner, temperature and conductivity logs to generate representative fracture patterns for the site being modeled.

2) Generate flow and dispersion characteristics for the elements of the global flow system as a function of geometry and flow conditions.

3) Integrate the element characteristics into a reservoir simulation.

4) Develop specific models of the Raft River and East Mesa reservoirs to correlate measured flow and tracer dispersion.

This work is an outgrowth of and is complemented by extensive laboratory scale physical modeling.[6,7]

The numerical simulation accomplished to date consists of initial development and demonstration of the fracture element and reservoir simulations. Completion of the current simulations and the addition of heat transfer and rock-water interactions is included in future planning.

ELEMENT SIMULATION

The specific motivation for this phase of the program is experimental work showing that complete mixing does not occur at fracture junctions.[6] This, together with consideration of the dispersion resulting from the velocity profile across a fracture, suggests that reservoir dispersion may be a strong function of identifiable fracture element characteristics.

The elements of interest, in the order traversed in injection, are the well-head piping, the wellbore, the junction of the wellbore and the initial fractures, single fractures, fracture junctions and the junctions of flowing and "dead-ended" fractures. Subsequent smaller fractures down to the micro-crack level are, for the present, treated using porous media models.

The essential capability required in the mathematical model is a flow simulation. Once the steady state velocity field has been established the dispersion characteristics are found by tracing imaginary marker particles through the flow element, thereby determining the lateral position at the exit as a function of that at the inlet. The resulting pressure drop and particle inlet-outlet displacement curve are then transferrable to the reservoir simulation. This process is a deterministic study of advective dispersion only. Diffusion, where significant, will be added in the reservoir simulation.

While the majority of the elements considered are essentially two dimensional, the wellbore -initial-fracture junction and the single fracture itself require three dimensional treatment.

The code selected for these simulations is SALE[8] (Simplified Arbitrary Lagrangian-Eulerian). This code is used extensively to solve a variety of fluid dynamics problems by numerical solution of the Navier-Stokes equations in two dimensions. This code is extremely well documented and was already installed (in two-dimensions) with plotting capability at the Idaho National Engineering Laboratory (INEL). A three dimensional version[9] is available but has not yet been installed.

SALE provides an implicit treatment of the pressure calculation for flow at the incompressible limit, thereby avoiding Courant-like time step restrictions While the grid may be moved with the fluid in the Lagrangian manner or arbitrarily rezoned, in the subject application it is held fixed in the Eulerian manner. A non-rectangular grid may be coded by the user. A problem may include the following boundary conditions: 1) a free Lagrangian surface, 2) a free-slip (symmetry or non-viscous) vertical or horizontal wall, 3) a curved or tilted free-slip wall, 4) a no-slip wall, 5) a continuative outflow boundary, 6) a specified inflow or outflow boundary and 7) a specified pressure boundary. Initial simulations of steady flow between parallel plates and accelerated flow in a pipe agreed well with theory.

A fracture junction model was built into the SALE code along with a marker particle calculation. Figure 1 shows the velocity vectors calculated for the orthogonal junction of two parallel sided fractures of

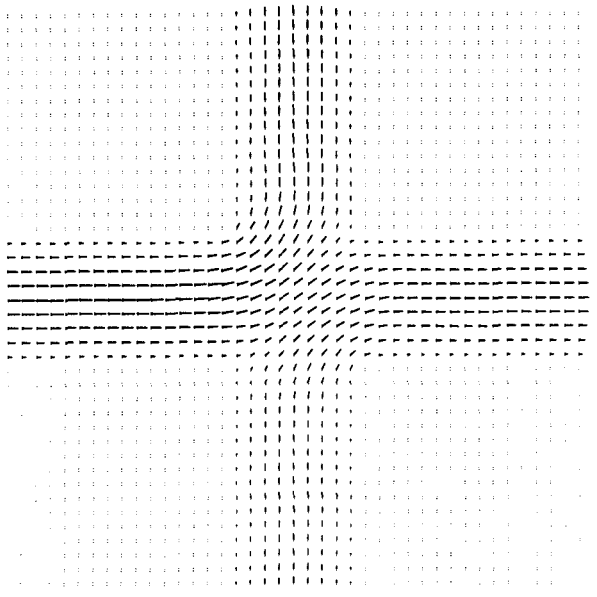


Figure 1. Velocity vectors for orthogonal junction of two fractures. Vertical inlet velocity at 50% of horizontal inlet velocity.

equal width. The case shown is a 40 cell by 40 cell grid with inlet (bottom and left) and exit (top and right) leg lengths double their widths. The left inlet flow is at a mean velocity of 312.4 ft/day, the bottom inlet flow is lower by a factor of two and the width of each fracture is .0625 inch. Poiseuille velocity profiles[10] are imposed at each of the inlets and both exits are at zero pressure. While the exit flow straightens within a length equal to one width, a length twice the width was found necessary to reestablish a symmetrical Poiseuille velocity profile.

The complete set of input parameters for the fracture junction include angle of intersection, relative width, and velocities in three of the legs. Three velocities are sufficient since the fourth is found from continuity. Since the pressure drops were found to be linear with velocity, the spectrum of velocities is defined by specifying two velocity ratios, e.g., leg B to leg A and leg C to leg A. Initial results are limited to orthogonal junctions and equal widths and were made for 3 different ratios of bottom and left inlet velocities with exit velocities corresponding to equal exit pressures.

Calculated dispersion characteristics are given as displacement functions. A displacement function relates the lateral position of a marker particle at the inlet to its position at the outlet and, in the case of an asymmetric junction, specifies which outlet. Lateral position in the fracture is an essential consideration since the advective movement varies so strongly from the wall to the centerline. The existence of multiple outlets leads to the plot format shown in Figure 2. The inlet lateral position is shown on a continuous abscissa for the two inlets and the exit lateral position is shown on a continuous ordinate for the two exits. The sketches at the top of the figure illustrate the graphical process of rotating the left inlet down to the x axis and rotating the top exit up to the y axis. The result is a continuous function, as shown for vertical inlet velocities of 10%, 50% and 100% of the horizontal inlet velocity. The three curves demonstrate the intrusion of the stronger horizontal stream into the horizontal exit for small vertical inlet velocities.

Steady state was achieved for each of these cases in .5 seconds of problem time. This calculation, at time steps of 5 ms, and the subsequent tracing of marker particles through the system was accomplished in 49 CP

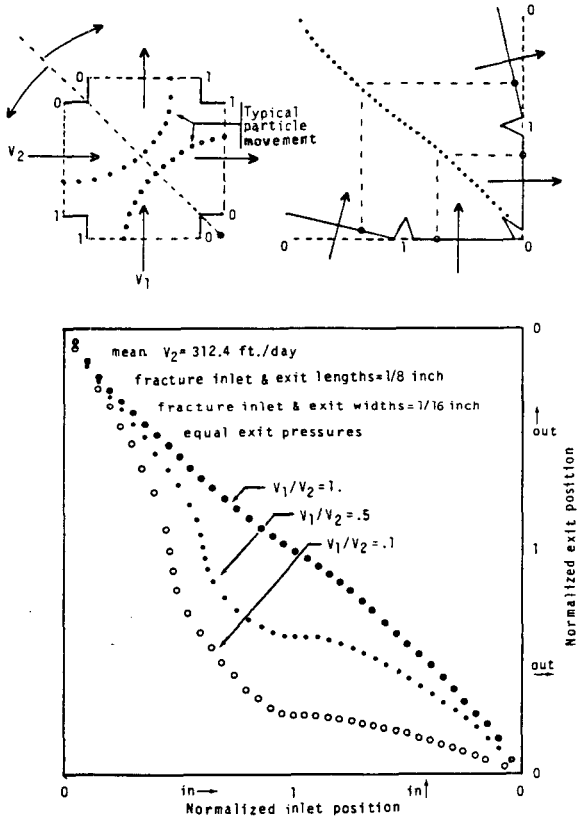


Figure 2. Displacement function for orthogonal junction of two fractures.

seconds on a CYBER 176 computer. While trivial levels of numerical (non-physical) stabilization were sufficient to maintain stability and avoid distortion due to alternate node coupling and donor cell differencing, a small spatial pressure oscillation was noted. Resolution of this problem and verification by comparison to physical model results are in progress.

RESERVOIR SIMULATION

Suitable codes described in the literature with the discrete fracture capability essential to this approach were unavailable for external use. A new code was therefore assembled from the basic flow relationships and simplified models of marker particle displacement processes. The model calculates flow between points on a rectangular grid through the matrix or through a fracture which may connect adjacent grid points horizontally, vertically or diagonally. The grid is two-dimensional, the boundaries are impermeable and specified external inflow or outflow may be applied at any grid point. The heads at the various grid points are found by dividing the grid into quarter-cells and assigning each quarter cell to the nearest grid point. Continuity is then applied to the matrix flow and fracture flow entering or leaving the volume assigned to each grid point.

The simulation was implemented within the ACSL[11] (Advanced Continuous Simulation Language) problem solver code. ACSL is a proprietary, author supported code which provides the input/output, function generation, integration, etc. software to solve a dynamic problem described by the user in terms of algebraic and first-order ordinary differential equations. It also provides a direct calculation of a steady state by a Newton-Raphson iteration which drives the derivatives towards zero. The resulting code is named FRACSL.

Sample flow calculations were performed on the fractured reservoir shown in Figure 3. The reservoir is 900 ft long by 360 ft high by 1 ft thick and incorporates a 9 cell by 9 cell grid, an open wellbore at the left edge and an extensive fracture system as shown by the heavy vertical or diagonal lines. Hydraulic parameters are given in Table 1. In this simplified model the junction resistance is not specifically selected as a function of junction characteristics. The ACSL direct steady state mode was used to calculate the head and flow distribution for a 25 gpm injection flow and a 25 gpm withdrawal flow. In each case, the head derivatives, after subtracting the steady state drawdown rate, were forced to zero. Table 1 and Figure 4 show the results for the injection case.

The following discussion summarizes the marker particle models incorporated in the code.

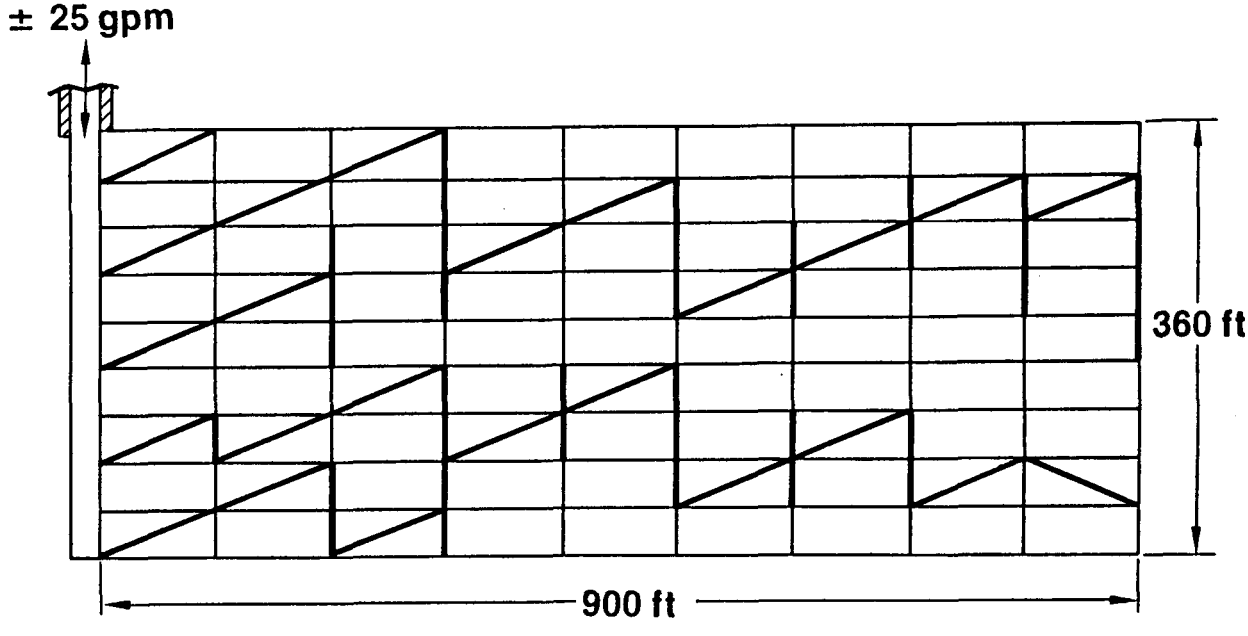


Figure 3. Sample Fractured Reservoir

Table 1. Sample Reservoir Flow Simulation

Water Temperature	70°F
Well Flow Rate	± 25 gpm
Fracture Aperture	±.01 ft
Fracture Conductivity	2.25E+6 ft/day
Matrix Conductivity	1.0 ft/day
Head at Well	100 ft
Minimum Head in Fracture (Injection)	35.2 ft
Minimum Head in Matrix (Injection)	11.3 ft
Fracture Velocity Range	1560-178500 ft/day
Matrix Velocity Range (x or y component)	.00069-.672 ft/day

A tracer slug injection is modeled by injecting ten groups of 25 particles into the fracture system at suitable time intervals. Each group of 25 is distributed across the width of the 5 fractures which intersect the well. Each particle is assigned a mass proportional to its velocity, thereby approximating a constant concentration input. Dispersion in the wellbore and the junctions of the wellbore and the initial fractures will be added later.

A particle in a fracture is moved with a velocity which corresponds to the local value on a Poiseuille velocity profile fitted to the mean fracture velocity. Diffusion is added by drawing a sample from an appropriately scaled normal distribution. Three dimensional dispersive effects will be determined using SALE-3D and incorporated in the reservoir model.

A particle traversing a junction completes the time increment in the exit fracture. The lateral position in the exit fracture is determined from the SALE generated displacement function for the appropriate inlet position, geometry and flow ratios.

Particles move from the fractures into the matrix based on the mass balances for the individual grid points and the matrix quarter cells and half fractures which terminate at that grid point. The volume of water moving from the fracture into the matrix in this regime is equal to the excess of fracture inflow over fracture outflow, multiplied by the time interval. This volume is distributed to the various half fractures at the grid point according to their length-times-volumetric-flow products. The assumption is made that the water enters the matrix in a "dead-ended" fracture which creates sufficient dispersion in the through-flow that the volume entering the matrix may come, with equal likelihood, from any depth in the flowing fracture. The validity of this simplification will be determined from fracture characterization and SALE dispersion studies.

The model is implemented numerically by dividing the volume to be transferred to the matrix into 10 equal cells and selecting those cells at random over the entire width and depth of

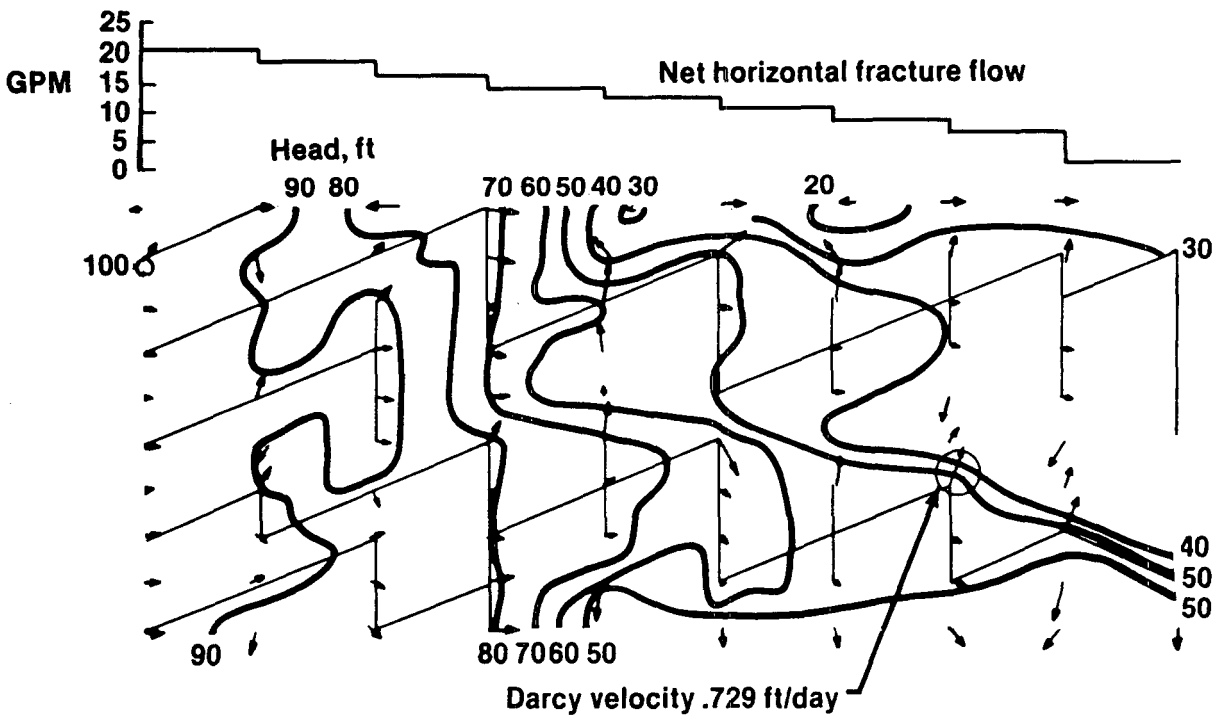


Figure 4. Fracture Flow, Head Contours and Matrix Velocities for 25 gpm Injection

the half-fracture. Any markers in these ten cells are removed from the fracture and assigned an equal position in the matrix.

Marker particle motion in the matrix is computed as the sum of advection, porous media based dispersion and molecular diffusion. The advective displacement is found by interpolating for the velocity vectors at the beginning of the time increment and multiplying by the time increment. Dispersive displacements in the direction of the advection and normal to it are found from separate normal distributions with standard deviations equal to the square root of twice the product of the appropriate dispersivity, in feet, times the advective displacement[12]. Molecular diffusion is computed in a similar manner.

The same models apply during the withdrawal phase except that the fracture-to-matrix transfers are reversed and the particles are counted as they leave the initial fractures to reenter the well. The matrix-to-fracture transfer is again based on the mass balance for the appropriate grid point and associated matrix and half fractures. The volume of water moving from matrix to fracture during a time increment is equal to the excess of fracture exit flow over fracture inlet flow, times the time increment. That volume is assigned to the individual half fractures on the basis of their flow-times-length products. The total volume of water associated with the grid point is equal to the area of matrix times the unit thickness times the matrix porosity. The transferred water is taken from a strip of appropriate width along the fracture. Any marker in that strip at the end of the time step or which crosses it during the time step is moved normally into the fracture and assigned a lateral position drawn from a random distribution.

Results have been generated for a simplified model without molecular diffusion and with particle lateral position at the exit of a junction equal to that at the inlet. The ten groups of 25 particles were released into the initial fractures at equal intervals during a

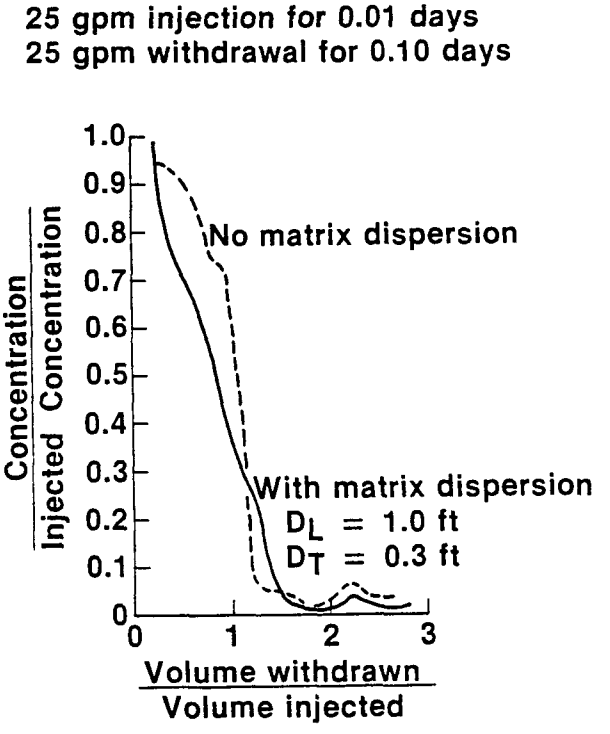


Figure 5. Recovery Curves

.01 day injection period with flow conditions as shown in Figure 4. Table 2 gives the initial and end-of-injection positions for the first 5 particles released into the lowest fracture in the reservoir for a case without matrix dispersion.

As shown in the table, three of the particles had transferred to the matrix by the end of injection.

Flow was then reversed for a period of 0.10 days and the particle mass returning to the well was monitored. The ratio of recovered-to-injected concentration was found by differentiating the total tracer return and divi-

Table 2. Marker Particle Positions (No Matrix Dispersion)

Particle	Initial Position in Fracture - Distance from Fracture Bottom	End-of-Injection Position in Reservoir: Longitudinal Distance from Left Edge	Vertical Distance fm. Bottom	Host - Fracture or Matrix	Distance from Fracture
1	10%	52.2%	41.1%	Fracture	---
2	30%	22.2%	6.7%	Matrix	.046' right
3	50%	3.4%	3.4%	Matrix	.015' below
4	70%	82.1%	15.5%	Fracture	---
5	90%	33.9%	22.8%	Matrix	.001' below

ding by the injection rate. Figure 5 shows the concentration ratio as a function of the withdrawn-to-injected volume ratio. A purely advective case would give a function which steps from 1.0 for volume ratios less than 1.0 to 0. for ratios greater than 1.0. Results for the injection-withdrawal sequence without matrix dispersion are shown by the dotted line. Substantial spreading of the sharp front has occurred and the tail of the curve extends to zero concentration at a volume ratio of 6.4. The solid curve shows the effect of the addition of matrix dispersion with longitudinal dispersivity of 1.0 ft and transverse dispersivity of 0.3 ft. The front is spread further and the tail is extended with 7.0% of the tracer still in the reservoir after 10 injection volumes have been withdrawn.

SUMMARY

An approach to numerical simulation of fractured reservoirs has been developed which includes characterization of fracture system geometry, numerical simulation of flow and dispersion in fracture elements, numerical simulation of flow and dispersion in fractured reservoirs and correlation with laboratory and field test data.

A general purpose fluid flow code has been modified to simulate flow and the dispersion of marker particles in orthogonal fracture junctions. Results are given for three different flow conditions.

A reservoir simulation code has been assembled. Flow is calculated in the matrix and in discrete fractures arranged along the edges or diagonals of the rectangular grid blocks. The dispersion of marker particles through the reservoir is simulated. Sample results are given.

This work was funded by the U.S. Department of Energy under Contract No. DE-AC07-76ID0 1570.

REFERENCES

1. R. A. Nelson, "An Approach to Evaluating Fractured Reservoirs", Journal of Petroleum Technology, Vol. 34, No. 9, Sept. 1982, pp. 2167-2170

2. R. A. Nelson, "Natural Fracture Systems: Description and Classification", AAPG Bulletin, Vol. 63, No. 12, Dec. 1979, pp. 2214 - 2232

3. D. W. Stearns and M. Friedman, "Reservoirs in Fractured Rock", AAPG Memoir, No. 16, 1972

4. R. G. Baca and R. C. Arnett, "Fluid Flow in Fractured-Porous Rock Masses by Finite-Element Techniques", Proceedings of the Fourth International Symposium on Finite Element Methods in Flow Problems, Tokyo, July 1982, University of Tokyo Press

5. J. Noorishad and M. Mehran, "An Upstream Finite Element Method for Solution of Transient Transport Equation in Fractured Porous Media", Water Resources Research, Vol. 18, No. 3, June 1982, pp. 588-596

6. L. C. Hull and K. N. Koslow, "Dispersion in Fracture Networks", Eighth Workshop on Geothermal Reservoir Engineering, Stanford University, Dec. 1982

7. L. C. Hull and K. N. Koslow, "Physical Model of a Fractured Reservoir", Ninth Workshop on Geothermal Reservoir Engineering, Stanford University, Dec. 1983

8. A. A. Amsden, H. M. Ruppel, C. W. Hirt, "SALE: A Simplified ALE Computer Program for Fluid Flow at All Speeds", Los Alamos Report LA-8095, UC-32, June 1980

9. A. A. Amsden and H. M. Ruppel, "SALE-3D: A Simplified ALE Computer Program for Calculating Three-Dimensional Fluid Flow", NUREG/CR-2185, LA-8905, Jan. 1982

10. D. T. Snow, "Anisotropic Permeability of Fractured Media", Water Resources Research, Vol. 5, No. 6, 1969, pp. 1273-1288

11. Mitchell and Gauthier, Assoc., Inc., Advanced Continuous Simulation Language (ACSL), User Guide/Reference Manual, 1981

12. T. A. Prickett, et. al., "A 'Random-Walk' Solute Transport Model for Selected Groundwater Quality Evaluation", Illinois State Water Supply, ISWS/BUL-65/81, 1981

Proceedings Ninth Workshop Geothermal Reservoir Engineering
Stanford University, Stanford, California, December 1983
SGP-TR-74

ROCK FAILURE IN COMPRESSION

S.Nemat-Nasser and H.Horii

Department of Civil Engineering
The Technological Institute
Northwestern University
Evanston, Illinois 60201

ABSTRACT

Mechanisms of rock failure in compression -- axial splitting and shear failure -- are studied, based on a microscopic consideration. Analytical models are constructed and model experiments on plates of a brittle polymer are performed. It is shown that unstable growth of tension cracks which propagate from the tips of pre-existing cracks and curve towards the maximum compressive direction, is the fundamental mechanism that produces axial splitting of a uniaxially compressed rock specimen, whereas shear failure of a triaxially compressed specimen is a result of sudden growth of tension cracks at tips of a suitably arranged interacting set of microcracks. The simultaneous out-of-plane unstable growth of a suitably oriented row of cracks is analyzed and, on the basis of this model, the variations of the "ultimate strength" and the orientation of the overall fault plane with the confining pressure are estimated. The brittle-ductile transition is discussed with the aid of a model which includes both tension crack extension and plastic zone development from the pre-existing cracks.

1 INTRODUCTION

Brittle solids such as rock and concrete by their nature contain numerous microcracks and inhomogeneities. Materials of this kind fail under uniaxial compression by axial splitting, where the fracture surface is parallel to the axial compression direction. Shear failure, on the other hand, is observed under triaxial compression; Peng and Johnson (1972). The ultimate strength and the orientation of the macroscopic failure plane depend on the confining pressure in a complex manner. Generally speaking, the strength versus confining pressure curve is non-linear under low confining pressures and is almost linear under moderate confining pressures; Mogi (1966). The inclination of the overall failure plane relative to the compression axis increases with increasing confining pressure, almost attaining the constant value of 30° under moderate confining pressures. In the brittle-ductile transition stage, plastic flow takes place along the failure plane; Griggs and Handin (1960).

Based on the idea that frictional sliding on pre-existing cracks results in the formation of tension cracks at their tips, models for microcracking under compression have been proposed; e.g., Brace and Bombolakis (1963) and McClintock and Walsh (1963). Nemat-Nasser and Horii (1982) present an analytical solution of compression-induced, out-of-plane crack extension, and study the mechanism of the axial splitting; see also Horii and Nemat-Nasser (1983a,b) and Nemat-Nasser (1983). Their results are summarized in Section 2.

Photographic studies of Hallbauer, Wagner and Cook (1973) show that under triaxial compression the microcrack distribution is almost uniform until the applied stress reaches the ultimate strength, and at the ultimate strength a region of high crack-density (tension cracks) emerges along a plane which eventually becomes a macroscopic shear failure plane. To reveal the mechanism of shear failure, Horii and Nemat-Nasser (1983b) consider a row of suitably oriented cracks, and examine their simultaneous out-of-plane unstable growth which may lead to possible macroscopic faulting. They estimate the variations of the "ultimate strength" and the orientation of the overall failure plane with confining pressure, using this model. These results are presented in Section 3.

As the confining pressure increases, the transition from brittle to ductile behavior is observed, where plastic flow occurs along the failure plane; Griggs and Handin (1960). Edmond and Paterson (1972) report that dilatancy persists well in this range. Following this observation and the results of our model experiments, a model for the mechanism dominant in the brittle-ductile transition range, which includes both the tension crack extension and the plastic zone development from the pre-existing cracks, is proposed in Section 4.

2 AXIAL SPLITTING

Under axial compression, a pre-existing crack undergoes frictional sliding which leads to the formation of tension cracks at its tips. The tension cracks grow at sharp angles relative to the orientation of the pre-existing crack and curve into a direction parallel to the maximum compressive direction. This is

illustrated in Fig. 1 which shows kinked-curved cracks at the tips of a pre-existing crack in an axially compressed plate of Columbia Resin CR36. This is considered to be the mechanism of microcracking under compression; Brace and Bombolakis (1963), Hoek and Bieniawski (1965), and Nemat-Nasser and Horii (1982).

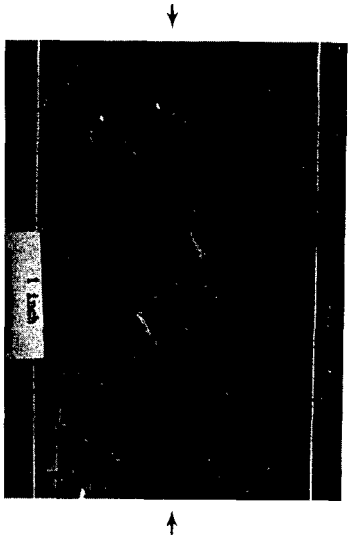


Fig.1 Kinked-curved crack extension from the tips of a pre-existing crack.

An analytic solution for the problem of out-of-plane curved crack growth, illustrated in Fig. 2, is obtained by Nemat-Nasser and Horii (1982); see also Nemat-Nasser (1983) and Horii and Nemat-Nasser (1983a,b).

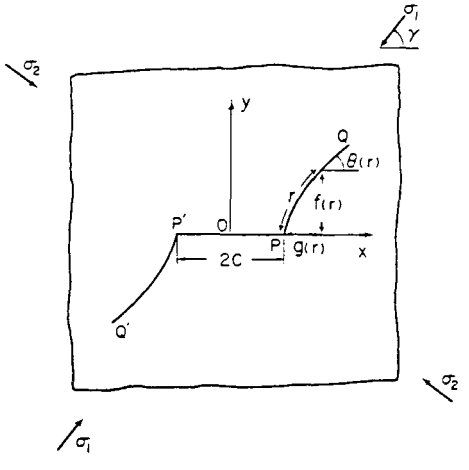


Fig.2 Pre-existing crack PP' and its extensions PQ and P'Q'.

The calculated crack profiles are compared with those observed on model experiments; Fig. 3. The most significant result is the variation of the axial load versus crack extension length curve with the lateral stress; see Fig. 4. Under axial compression with lateral compression, crack growth is stable and stops at a certain finite length. In the presence of small lateral tension, on the other hand, crack growth becomes unstable after a certain crack extension length is attained. This unstable crack growth is considered to be the fundamental mechanism which produces axial splitting of a uniaxially compressed rock specimen. Peng and Johnson (1972) report the presence of lateral tension in the uniaxially compressed specimen because of the end-boundary conditions. Different inserts affect the ultimate strength; the normalized strength becomes 9.5 for the steel insert, 7.3 for the teflon insert, and 5.9 for the neoprene insert. They also report a radial tensile stress of 6-8% of applied compression for the neoprene insert, and 4-6% for the teflon insert. These experimental data seem to support our analytical results.

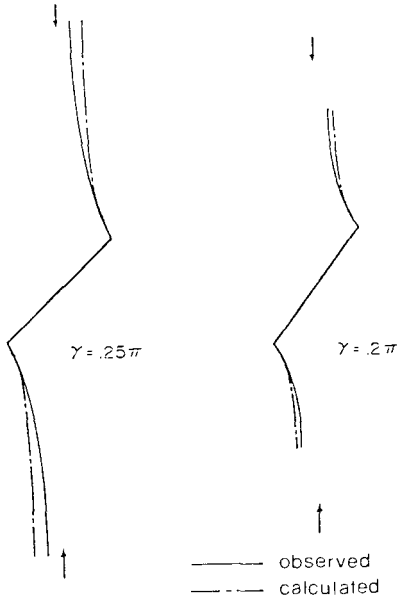


Fig.3 Calculated and observed crack profiles; Horii and Nemat-Nasser (1983b).

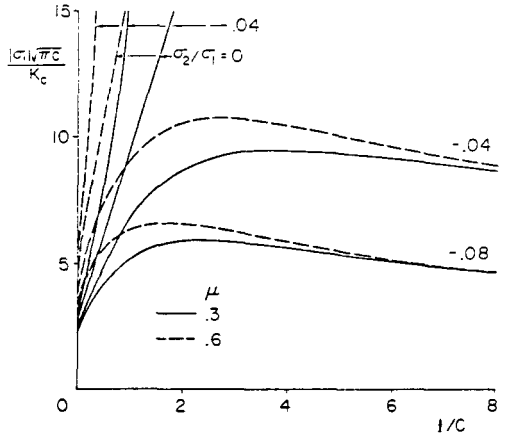


Fig.4 Normalized axial compression required to attain the associated crack extension length; Horii and Nemat-Nasser (1983b).

3 SHEAR FAILURE

A rock specimen contains microcracks of various sizes. Smaller cracks are greater in number and closer in spacing. Under axial compression, larger cracks become activated first. Without lateral confinement, they continue to grow, leading to axial splitting; Fig. 5. In the presence of lateral compression, on the other hand, their growth is soon arrested and, at a certain stress level, suitably oriented smaller cracks become activated because of their interaction. Then a narrow zone containing many microcracks is formed, which eventually becomes a macroscopic failure plane; Fig. 6.

Based on observations by Hallbauer *et al.* (1973) and our model experiments, it appears that shear failure may be considered to be the result of unstable growth of a suitably oriented set of interacting pre-existing cracks. To capture this feature, Horii and Nemat-Nasser (1983b) consider a row of equally spaced cracks of equal initial size and of common orientation; see Fig. 7. The required axial compression is calculated as a function of the crack extension length for constant confining pressure. Typical results are shown in Fig. 8.

For small values of ϕ of Fig. 7, the axial compression first increases with increasing crack extension length, attains a peak value,

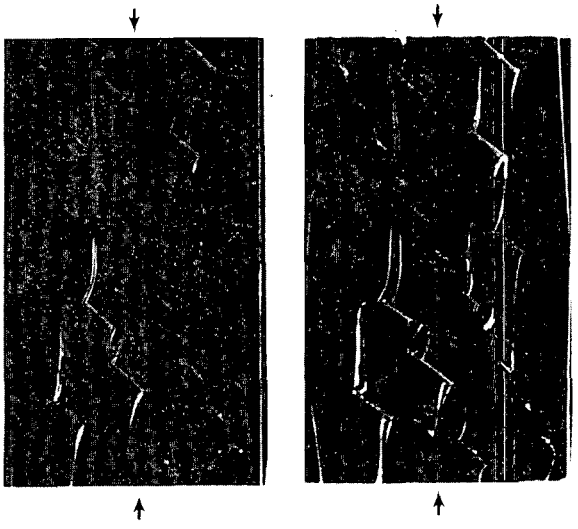


Fig.5 The axial splitting of the specimen under uniaxial compression; Horii and Nemat-Nasser (1983b).

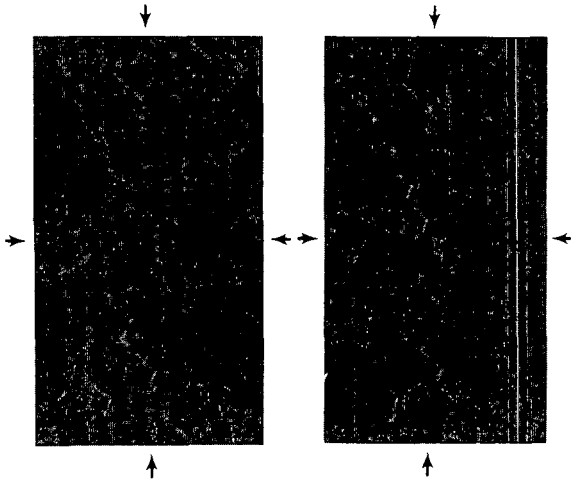


Fig.6 Unstable growth of tension cracks at tips of a row of interacting pre-existing cracks under triaxial compression; Horii and Nemat-Nasser (1983b).

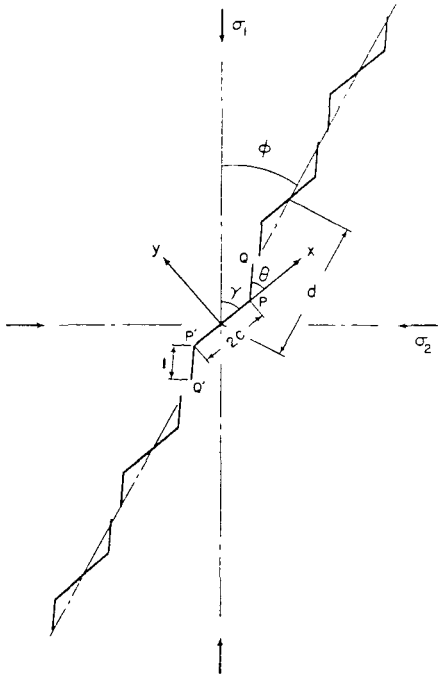


Fig.7 An infinite plate with a row of pre-existing cracks and their out-of-plane extensions.

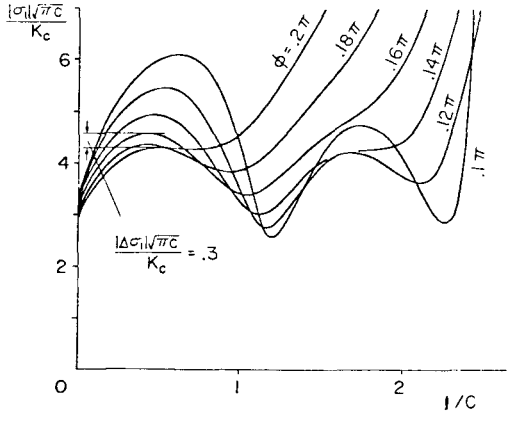


Fig.8 Axial stress versus crack extension length: $\gamma = .24\pi$ and the coefficient of friction $\mu = .4$; Horii and Nemat-Nasser (1983b).

decreases, and then begins to rise again. This suggests an unstable growth of optimally oriented cracks at a critical value of the axial stress, which is considered to correspond to the formation of a fault zone. It is seen from Fig. 8 that the peak values of the axial stress for the values of ϕ from 0.16π to 0.2π fall in a very narrow range, i.e. $|\Delta\sigma_1|\sqrt{\pi c}/K_c \sim 0.3$. This implies that the overall failure angle is sensitive to imperfection and other effects. Indeed, the orientation of the fracture plane observed in experiments often scatters over a wide range. The range of the overall failure angle, however, may be limited since the peak value of the axial stress increases sharply as ϕ decreases. We can specify the possible range of the overall orientation angle ϕ by prescribing the "stress barrier" $|\Delta\sigma_1|\sqrt{\pi c}/K_c$ which can be overcome. The value of γ of Fig. 7 is chosen such that the required axial compression for the instability is minimized.

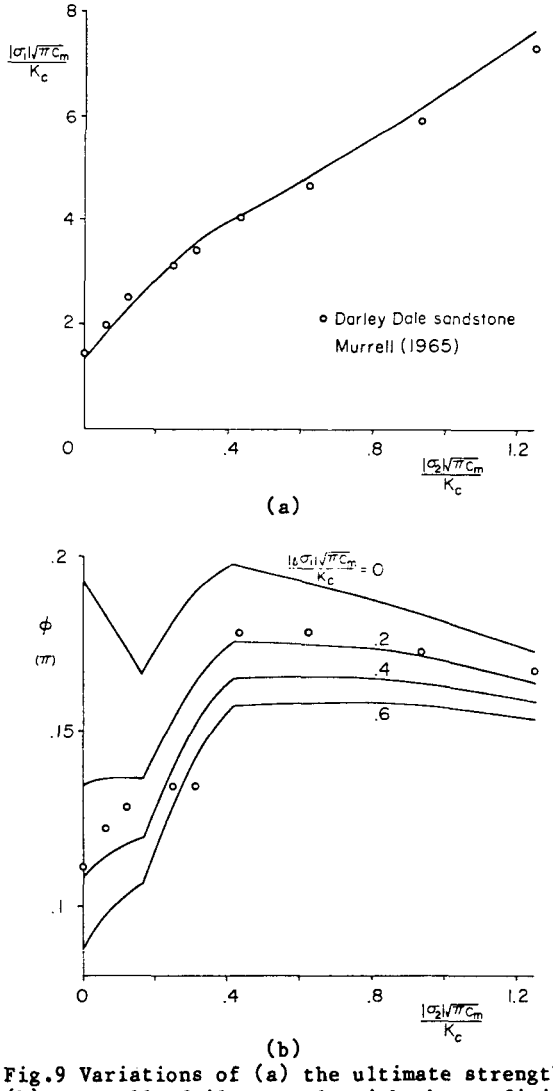


Fig.9 Variations of (a) the ultimate strength, (b) overall failure angle with the confining pressure; Horii and Nemat-Nasser (1983b).

Now we can calculate the critical axial load, $|\sigma_1|\sqrt{\pi c}/K_c$, and the possible range of the overall failure angle, ϕ, for a given confining pressure and crack spacing d/c. In the actual rock specimen, there are many cracks of various sizes. It is reasonable to expect that smaller cracks are greater in number and closer in spacing. Thus, one may assume that the spacing of the "optimally oriented" cracks is an increasing function of the crack size. We, therefore, introduce the simple relation,

$$d/c_m = b(c/c_m)^{1+a},\quad b = d_m/c_m,\quad a > 0,$$

where c_m and d_m denote the minimum crack size and the corresponding crack spacing, and a and b are constants. With this relation we can calculate the ultimate strength which is the minimum of the axial critical load and the possible range of the overall failure angle as functions of the confining pressure. Typical results are shown in Figs. 9a,b with $d_m/c_m = 3.0$, $a = 0.18$, and $K_c/\sqrt{\pi c_m} = 8\times10^3$ psi. The corresponding experimental data on Darley Dale sandstone reported by Murrell (1965) are also shown in these figures.

4 BRITTLE-DUCTILE TRANSITION

The model of brittle fracture discussed in Section 3 anticipates that the critical load for instability increases with increasing confining pressure. This is shown in Fig. 10, where the relation between the axial load and the crack extension length is plotted for different values of the confining pressure. Whereas at lower confining pressures the curves have distinct peaks, at higher pressures the peaks disappear. This suggests that the brittle fracture model discussed in Section 3 is no longer applicable at high confining pressures.

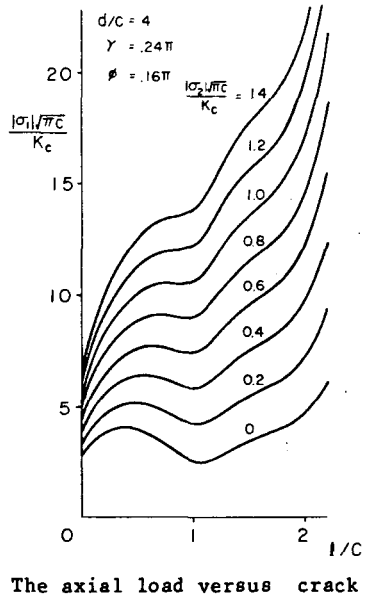


Fig.10 The axial load versus crack extension length curve for indicated values of the confining pressure.

In the brittle-ductile transition stage, plastic flow occurs along the failure plane; Griggs and Handin (1960). However, Edmond and Paterson (1972) report that dilatancy persists well in this range. Since dilatancy results from microcracking, it may be concluded that both microcracking and plastic flow occur in the brittle-ductile transition stage.

The photoelastic picture of Fig. 11 shows the residual strains in the unloaded specimen (shown in Fig.6). It illustrates the development of plastic zones after biaxial compression of the plate which contains pre-existing cracks.



Fig.11 The residual strains in the unloaded specimen of Fig.6.

In the brittle-ductile transition stage, the development of the plastic zones, and their interaction are considered to be the controlling mechanism of the overall deformation. A model which includes tension cracks and plastic zones at the tips of the pre-existing cracks is now being investigated by the present authors.

ACKNOWLEDGMENT

This work has been supported by the U.S. Air Force Office of Scientific Research grant AFOSR-84-0004 to Northwestern University.

REFERENCES

Brace, W.F., and E.G. Bombolakis (1963), "A note on brittle crack growth in compression", J. Geophys. Res., 68(12), 3709-3713.

Edmond, J.M., and M.S. Paterson (1972), "Volume changes during the deformation of rocks at high pressures", Int. J. Rock Mech. Min. Sci., 9, 161-182.

Griggs, D., and J. Handin (1960), "Observations on fracture and a hypothesis of earthquakes", Rock deformation (edited by D.Griggs and J.Handin), Mem. Geol. Soc. Am., 79, 347-364.

Hallbauer, D.K., H. Wagner, and G.W. Cook (1973), "Some observations concerning the microscopic and mechanical behaviour of quartzite specimens in stiff, triaxial compression tests", Int. J. Rock Mech. Min. Sci. & Geomech. Abstr., 10, 713-726.

Hoek, E., and Z.T. Bieniawski (1965), "Brittle fracture propagation in rock under compression", Int. J. Fract. Mech., 1, 137-155.

Horii, H., and S. Nemat-Nasser (1983a), "Estimate of stress intensity factors for interacting cracks", Advances in Aerospace Structures, Materials and Dynamics, AD-06, ASME, 111-117.

Horii, H., and S. Nemat-Nasser (1983b), "Compression-induced micro-crack growth in brittle solids: axial splitting and shear failure"; submitted to J. Geophys. Res..

McClintock, F.A., and J.B. Walsh (1963), "Friction on Griffith cracks in rocks under pressure", Proc. 4th U.S. Nat. Congr. Appl. Mech. 1962, ASME, New York, 2, 1015-1021.

Mogi, K. (1966), "Pressure dependence of rock strength and transition from brittle fracture to ductile flow", Bull. Earthquake Res. Inst., 44, 215-232.

Murrell, S.A.F. (1965), "The effect of triaxial stress systems on the strength of rocks at atmospheric temperatures", Geophys. J. Roy. Astr. Soc., 10, 231-281.

Nemat-Nasser, S. (1983), "Non-coplanar crack growth", Proc. ICE Int. Symp. on Fract. Mech., Beijing, China, Nov. 22-26, 185-197.

Nemat-Nasser, S., and H. Horii (1982), "Compression-induced nonplanar crack extension with application to splitting, exforliation, and rockburst", J. Geophys. Res., 87(B8), 6805-6821.

Peng, S.D., and A.M. Johnson (1972), "Crack growth and faulting in cylindrical specimens of Chelmsford granite", Int. J. Rock Mech. Min. Sci., 9, 37-86.

Proceedings Ninth Workshop Geothermal Reservoir Engineering
Stanford University, Stanford, California, December 1983
SGP-TR-74

PRESSURE TRANSIENT ANALYSIS FOR LARGE SCALE HYDRAULIC INJECTIONS IN THE CARNMENELLIS GRANITE, ENGLAND

R J PINE

GOLDER ASSOCIATES & CAMBORNE SCHOOL OF MINES GEOTHERMAL ENERGY PROJECT
PENRYN, CORNWALL, TR10 9DU, ENGLAND

ABSTRACT

Large volume hydraulic injections into the Carnmenellis granite have been completed at the CSM Hot Dry Rock Project during the period October 1982 to July 1983, with small volume injections before and after this period. The effects of the injections on the hydraulic properties of the rock mass have been estimated by pressure transient analysis. The growth of the reservoir zone was tracked with microseismic locations, and the growth mechanism modelled with the computer program FRIP.

The limited duration of the transients amenable to analysis and the tendency for growth below the injection zone meant that the interpretations could only describe hydraulic conditions within about 100 m of the wellbores. The effect of the large volume injections was to increase permeability values from less than 100 μd to greater than 5 md, and to decrease skin values from about -3 to about -6.

The FRIP modelling explained the observed reservoir growth in plan with reference to measured in-situ stresses, jointing and rock properties and showed some of the limitations of continuum modelling.

INTRODUCTION

The background to the Hot Dry Rock (HDR) research project operated by the Camborne School of Mines (CSM) in Cornwall, UK, was summarised by Batchelor (1982) at a previous Stanford workshop on geothermal energy. Details were included of the hydraulic tests conducted to late November 1982.

The purposes of this paper are to give a brief update on the tests and the results, and to examine in more detail the uses and limitations of pressure transient analysis as applied during the project.

The interpretation of pressure transients arising during tests on wells in fractured rock is widely recognised as a challenging problem and a number of approaches have developed; eg, Gringarten, Ramey and Raghavan (1975), Earlougher (1977), Gringarten (1982), and Agarwal et al (1979).

The approach at CSM has been to use such analyses based on radial and planar diffusion, which assume no pressure dependence of key parameters such as formation permeability and compressibility. These tests are used to provide index values for the hydraulic parameters as conditions change within the rock mass during successive injection, shut-in and venting cycles.

At the same time, interpretations have been attempted using the geometry of the apparent shape and size of the created reservoir defined by microseismic location. In addition, injections have been modelled using the two dimensional joint-block computer model, FRIP. This modelling gives an insight into the relatively complex behaviour of elastic rock blocks separated by joints whose apertures are controlled by fluid pressure, in situ stress, strength and stiffness conditions.

BACKGROUND INFORMATION

The CSM HDR site is located towards the centre of the Carnmenellis granite outcrop which probably extends to a depth of at least 10 km. It is regularly jointed with two main sets of orthogonal subvertical joints and a set of subhorizontal joints. Vertical joints are spaced at typically 1 to 3 m at the ground surface increasing to about 10 m at 0.8 to 2 km depth. The strikes of the subvertical joint sets are shown in Figure 1. The joint profiles visible at surface and underground exposures are typically smooth, nearly planar to smooth, undulating according to the classification of Barton (1976).

In situ stresses in the Carnmenellis granite are markedly anisotropic. Pine et al (1983 a and b) measured the stresses to a maximum depth of 2 km using a combination of overcoring and hydrofracturing methods. At a depth of 2 km, the maximum and minimum horizontal and vertical total stresses are approximately 60-70, 30 and 52 MPa respectively. The bearing of the maximum horizontal stress is about 130°-310° relative to true North.

Typical mechanical and hydraulic properties of the intact granite include a uniaxial compressive strength of 150 MPa, hydrofracture tensile strength of 15 MPa, deformation modulus

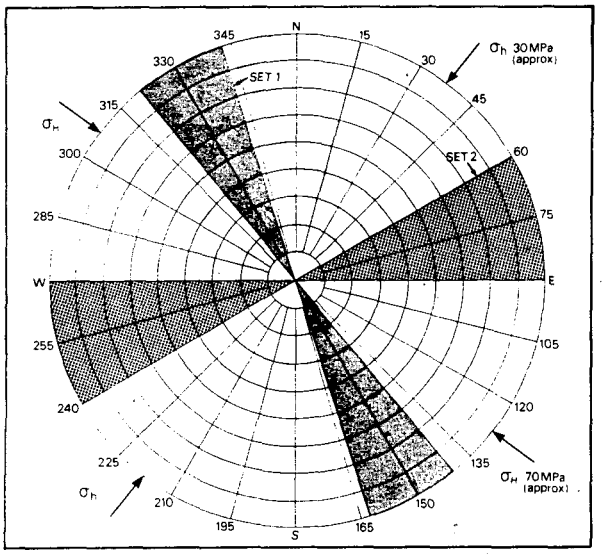


Figure 1: Directions of strikes of major joint sets and horizontal in situ stresses

of 60 GPa, Poisson's ratio of 0.2 and fluid permeability of 10 nanodarcy. The properties do not vary significantly from ground surface to a depth of 2 km.

Two deep wells have been drilled at the site to a vertical depth of about 2 km. The injection well, RH12, is cased to a vertical depth of about 1.75 km and the recovery well, RH11, to a depth of 1.45 km with open hole lengths of 357 m and 772 m respectively. The open hole diameters are approximately 0.22 m. Both wells are inclined at 30° from the vertical in the open hole sections, which lie in the same vertical plane on a bearing of about 125°-305°

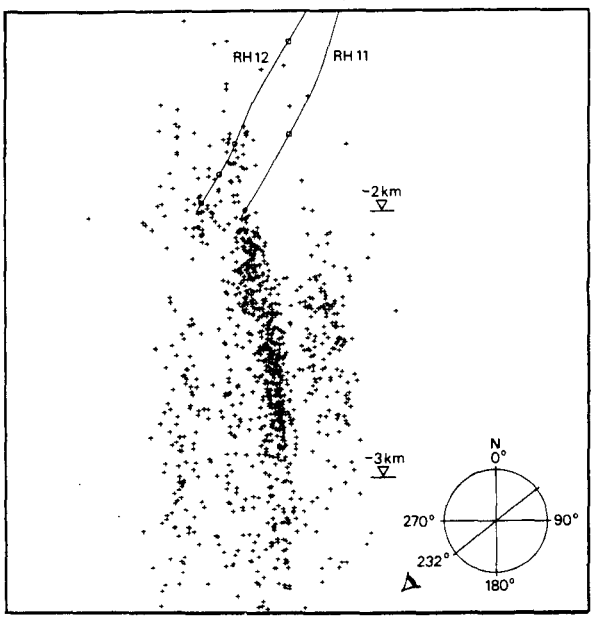


Figure 2: Vertical section showing micro-seismic locations viewed from the South West

with a vertical separation of 300 m. The relative positions of the wells in the injection zone are shown in Figures 2 and 3.

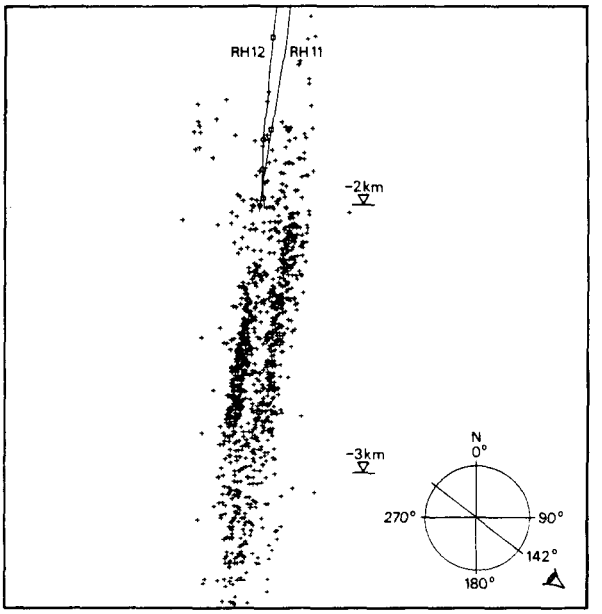


Figure 3: Vertical section showing micro-seismic locations viewed from the South East

SUMMARY OF HYDRAULIC TESTS UNDERTAKEN

The hydraulic tests which have been performed on the two deep wells can be divided into three groups:

i Low flowrate tests conducted before and after the major injections.
ii High flowrate major injections/stimulations.
iii Medium flowrate circulations.

The majority of the low flow rate tests were conducted from April to August 1982 and were described by Pine and Ledingham (1983). The purpose of these tests was to obtain datum values for the undisturbed hydraulic properties needed for quantifying the far field losses and the effect near the wells of the major injections. Constant pressure and flowrate injections and shut-in tests were conducted. Total water volumes of about 300 and 200 m^3 were injected into RH11 and RH12 respectively. The additional low flowrate check tests following the major injections were conducted in November 1983, when reservoir pressures had reduced to near hydrostatic.

The high flowrate tests were carried out mainly during the period October to November 1982, when a total net volume of about 100 000 m^3 of water was injected. The purpose of these tests was to stimulate the natural rock joints between the wells and create a relatively permeable flowing zone with sufficient surface area to keep thermal drawdown to an acceptable

minimum during subsequent circulations. Both the injection well, RH12, and the recovery well, RH11, were injected and vented. There were also several shut-in tests.

An additional experiment involving a 400 m^3 viscous injection was undertaken in RH11 in May 1983.

The medium flowrate circulation periods were from November 1982 to April 1983 and from late May to July 1983. The wells were then shut-in until the recent low flowrate tests. The main purpose of the circulation tests was to determine the steady state hydraulic behaviour of the stimulated reservoir, which is not covered in this paper. However, during the course of these tests there were several pressure transients due to changes in pumping and venting flowrates. Several of these transients were suitable for analysis. Further test details are included in Table 1.

THEORY

Basic analysis

Pressure transients were analysed in the conventional manner; eg, Earlougher (1977), using log-log, semi-log and root time plots of pressure change against time. The analysis due to Gringarten et al (1982), which is based on infinite fracture conductivity for fractured sytems, was found to be the most convenient log-log analysis. Interpretation in terms of double porosity per Gringarten (1982) and finite conductivity fractures per Agarwal et al (1979) were also attempted. The modified time scale due to Agarwal (1980) was found useful for shut-in test analyses with log-log drawdown type curves.

The majority of the transients analysed were for injections and shut-ins, with a few drawdown and two-rate injections. All tests were analysed for the individual wells without consideration of any (minor) interference effects from the adjacent well. The radius of investigation for radial flow tests was estimated per van Poollen (1964).

Reservoir growth mechanisms and directions

The water injected into a jointed crystalline rock mass with a low matrix permeability such as granite moves predominantly within the existing network of natural fractures. Where injection pressures are high enough the apertures of the joints are increased by either jacking (opening against normal closure stress) or shearing (as a result of anisotropic in situ stresses). Evidence for the shearing mechanism is provided by the nature of seismic and microseismic signals detected by monitoring networks; eg, Healy et al (1968), Pearson (1981), and Batchelor et al (1983).

It can be shown theoretically that shearing will precede jacking in most circumstances; eg, Pine and Batchelor (1982, 1983). For relatively high injection flow rates, fluid pressures can become high enough to cause jacking near the wells with shearing further out. Beyond the zone of shearing, fluid movement can be of a diffusive nature through unstimulated joints. Shear growth will be mostly within joints subject to the least normal closure stress with some additional growth in other joints, depending on the joint and in situ stress orientations and stress magnitudes.

When a joint has sheared, part of the dilation will be irreversible because of non matching joint surfaces. The irreversible shear dilation will cause a residual increased permeability even when fluid pressures subsequently decline. Where shearing occurs as a result of sustained hydraulic injections, there will be a tendency for an upward or downward component to the zone of stimulation (Pine and Batchelor, 1983). Downward growth will be associated with significant anisotropies in the in situ principal stress gradients. This is likely to be common in hard jointed rock to depths of at least 4 km; eg, McGarr (1980).

Test group	Test type	Peak pressure (MPa)	Flowrate (l/s)	Permeabilities (md)		Skin factors	
				Range	Mean	Range	Mean
LOW FLOW	Injection	5.5	0.1 to 3.0	0.001 to 0.06		-1 to -3	
HIGH FLOW	Injection Shut in	14.0	46 to 90	3.7 to 13.0 2.2 to 3.9	7.6 3.2	-2.4 to -4 -4.6 to -5.7	-3.4 -5.1
MEDIUM FLOW	Injection Shut in Drawdown	12.0 11.0 8.0	20 to 33 5 to 15	3.0 to 5.0 1.6 to 4.1 0.3 to 2.9	3.9 2.8 1.3	-3.7 to -5.3 -4.4 to -5.8 -4.2 to -6.6	-4.9 -5.4 -5.6
LOW FLOW CHECK TESTS	Injection Shut in		3.2	1.4 1.1		-4.9 -4.8	

TABLE 1 Summary of pressure transient test analyses for injection well, RH12

Joint-block modelling

In recognition of the probable physics of jacking and shearing processes in jointed rock, the Fluid Rock Interaction Program (FRIP) was developed for the CSM project. The model was originally specified by CSM and subsequently developed by an external consultant, Cundall (1982, 1983). The model has been used to interpret some of the low flow rate injections, summarised by Pine and Ledingham (1983).

The model permits dynamic simulation of fluid flow in joints of variable aperture between elastic blocks of a uniform size in a grid sufficiently large to eliminate important boundary effects. It is in a finite difference formulation and solves the equations of motion for the blocks and the flow conditions for the joints at each time step throughout the grid. Laminar flow is assumed.

RESULTS

Transient test analyses

The results of the pressure transient analyses for RH12 are summarised in Table 1. Results for RH11 were similar but less extensive. Permeability, k, skin, s, and fracture half length, x_f, values were determined on the assumption that conditions were uniform throughout the height of the open hole section, and that the formation compressibility, β, had a constant value of 10^{-10} Pa^{-1}. These assumptions are discussed later.

There was generally reasonable agreement between parameter values determined by log-log and semi-log or root-time analyses for the same tests. During injections there was a tendency for the flow to appear as a limited period of planar followed by a more prolonged period of radial diffusion with straight lines on root time then semi-log plots. During shut-in tests usually planar diffusion only was evident. There was no convincing evidence for double porosity type behaviour.

The undisturbed rock mass had very low values of permeability, a minimum of 1 μd in RH12 and 10 μd in RH11. These values were associated with s of about -1, and x_f of about 1 m. By completion of the low flow rate tests, the k had increased to about 60 μd and s had decreased to about -3, with x_f about 5 m.

The effect of the high flowrate injections was to cause very significant increases in k and decreases in s, as expected. The peak k value seen during a high flowrate injection was about 13 md. This was associated with a moderate s value of about -3. However, during subsequent shut-ins and medium flow rate injections these values fell to typically 3 md and -5 respectively.

Figure 4 shows a typical semi-log plot from part of an injection of 21 l/s which lasted for

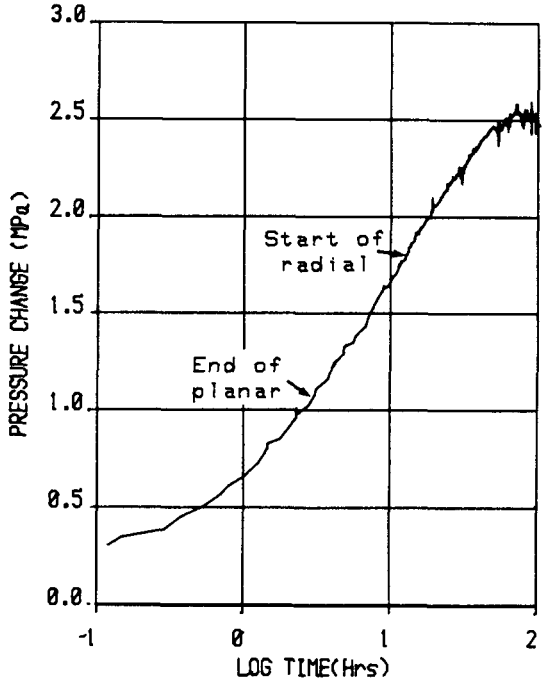


Figure 4: Pressure-log time trace for 21 l/sec injection into RH12, during main injection period

367 hrs. The end of the planar and beginning of the radial diffusion periods determined from log-log analysis were at about 3 and 12 hrs respectively. The values of k, s and x_f were about 4.5 md, -5.3 and 42 m respectively.

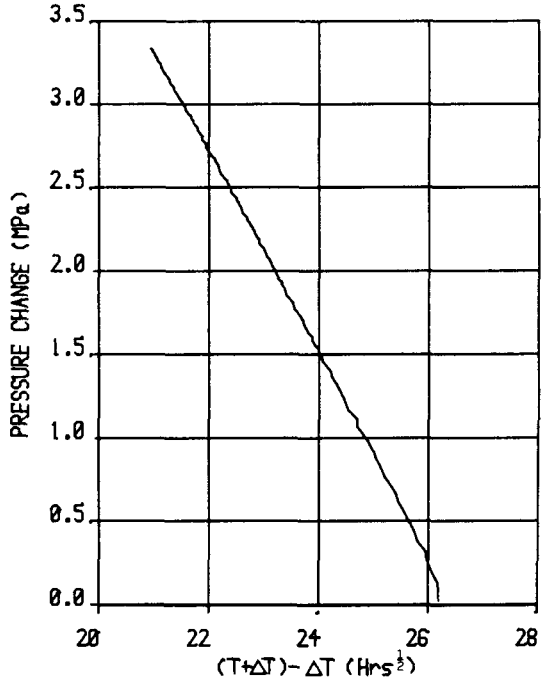


Figure 5: Pressure-root time function trace for shut-in of RH12, during main injection period

Figure 5 shows a plot of pressure vs the root time function $(t + \Delta t)^{\frac{1}{2}} - \Delta t^{\frac{1}{2}}$ for a shut-in period t of 35 hrs duration following an injection of 26 l/s for a period t of 700 hrs. There is a good straight line correlation, indicating planar diffusion. The theoretical end of the planar diffusion period from log-log analysis was at approximately 4 hrs although there is a similar slope for much longer. The product $A\sqrt{k\beta}$, where A is the total diffusive source area (one side), was about 3.3×10^{-8} m^3Pa^{-1}. Using a k value of 4 md from a previous injection and assuming a β value of 10^{-10} Pa^{-1} gives an A value of 52 000 m^2, equivalent to an x_f value of 73 m for a full height symmetrical fracture.

The low flowrate tests of November 1983 showed only planar diffusion behaviour during both injections and shut-ins. (The pressure-root time response of RH12 to a 3.2 l/sec injection is shown in Figure 6.) This made the deduction of k and s values difficult because radial diffusion had not developed by the end of the test and an independent value for k could not be derived. Note that k had itself been affected by the stimulations since early measurements.

The values shown in Table 1 are for the infinite conductivity fracture model per Gringarten (1982). The equivalent x_f values are about 30 m. Using the finite conductivity fracture model per Agarwal et al (1979), k is only 110 µd and x_f is 130 m. The product $A\sqrt{k\beta}$ is about 10^{-8} m^3Pa^{-1} in both cases. This can be compared with a value of only 3×10^{-10} m^3Pa^{-1} from similar tests before the main injections.

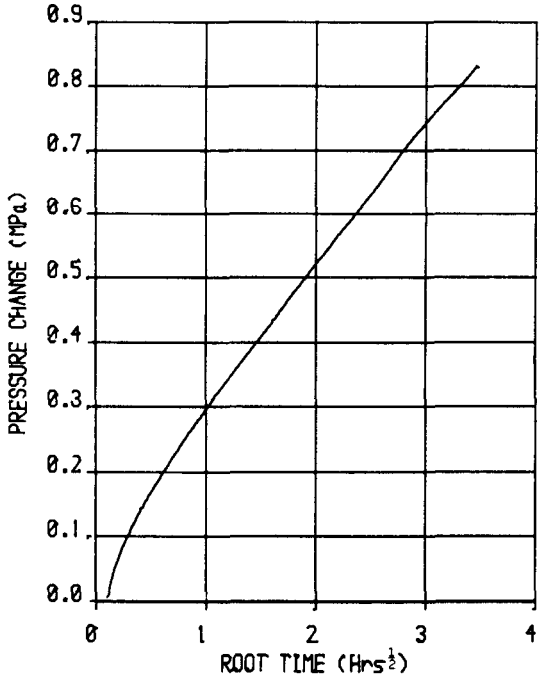


Figure 6: Pressure-root time trace for 3.2 l/sec injection into RH12, following main injection period

The viscous fracturing operation conducted on RH11 did not result in any significant increase in k or decrease in s. However, extensive new fracturing was observed in the wellbore with a TV survey, and subsequent circulation tests showed an improved connection between RH11 and the main reservoir.

Microseismic locations

The microseismic location system used at the CSM project and the progression of microseismic location with time during the high flow rate injections were described by Batcheor et al (1983). Figures 2 and 3 show the microseismic locations in vertical sections towards the end of these injections. Figure 7 shows a plan with the viewing direction approximately 10° off vertical to maximise the alignment of the locations. Preliminary versions of these plots were presented by Batchelor (1982).

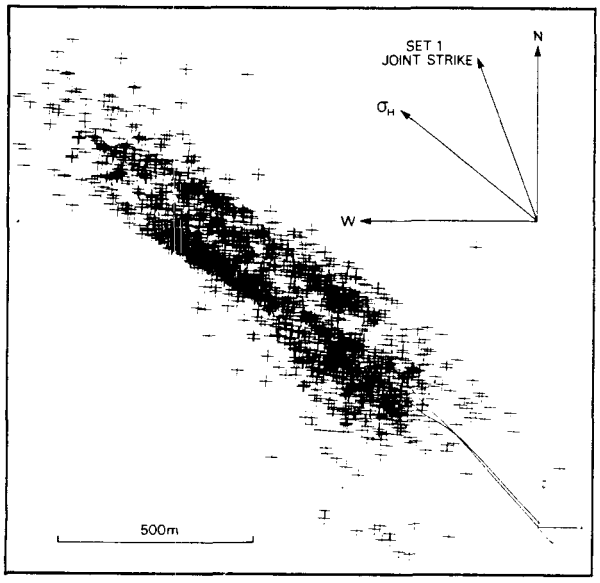


Figure 7: Plan view of microseimic locations viewed 10° from vertical

It is considered that the overall region defined by the microseismic locations contains zones of increased permeability, although it is not possible to conclude that individual locations are associated with the increased permeabilities.

Although the wells are enveloped by the microseismic locations, most of the reservoir growth has been downward. There is also a planarity to the stimulated zone aligned close to the maximum principal stress direction.

FRIP modelling

Some of the low flowrate injections have been successfully modelled using the FRIP program. Details are presented by Pine and Ledingham (1983). Modelling of the high flowrate injections using realistic rock and hydraulic parameters has been unsuccessful so far because

of the high computer CPU usage. This problem has been avoided to a certain extent by modelling injections with artificially high viscosities, within relatively compressible rock blocks (Murphy and Pine 1984). These adjustments have the effect of accelerating joint stimulation and damping out short pressure transients, thus increasing time steps and reducing CPU usage.

Some results are shown in Figures 8 and 9. Both figures show plan views of an orthogonal vertically jointed rock mass subjected to a maximum horizontal principal stress aligned 30° anticlockwise from the strike of joint set 1 as applicable at the CSM site. Fluid was injected into a joint intersection at the centre of the models. The figures show the joint stimulation pattern. The dilation of the joints due to both shearing and jacking is shown by line thickness. The ratios of the effective in situ horizontal stresses σ_H'/σ_h' were 2 and 5 in Figures 8 and 9 respectively. (The effective horizontal stresses are the total stresses minus the hydrostatic pressure presumed to exist in the joints before injection).

The growth of the reservoir shown in Figure 8 is similar to that shown by the microseismic locations in Figure 7. The shearing of joint set 1 induced by the injection reduced the normal stresses acting on set 2 sufficiently that fluid could penetrate and cause shearing in that set over a large area. This led to a step-like growth in an overall direction between those of joint set 1 and σ_H.

The growth shown in Figure 9 is quite different. Because of the still very high normal stresses acting on set 2 after shearing in set 1, shear growth in set 2 was inhibited. There was only a localised tendency for growth away from the direction of joint set 1, towards σ_H.

DISCUSSION

Pressure transient test results and analysis

The different responses to injections and shut-ins, as shown by the hydraulic parameters in Table 1, indicate the pressure dependent nature of the rock mass. The higher permeability and skin values seen during injections, with the apparent radial diffusion behaviour, suggests that the injections locally and temporarily overcome the influence of any planar structures, with joints opening up in all directions (sets 1 and 2). During the less energetic and prolonged shut-in and drawdown tests, joints not aligned near to the σ_H direction (set 2) close preferentially, resulting in a more planar type of diffusive behaviour.

The results of the November 1983 low flowrate tests show that the net effect of the main

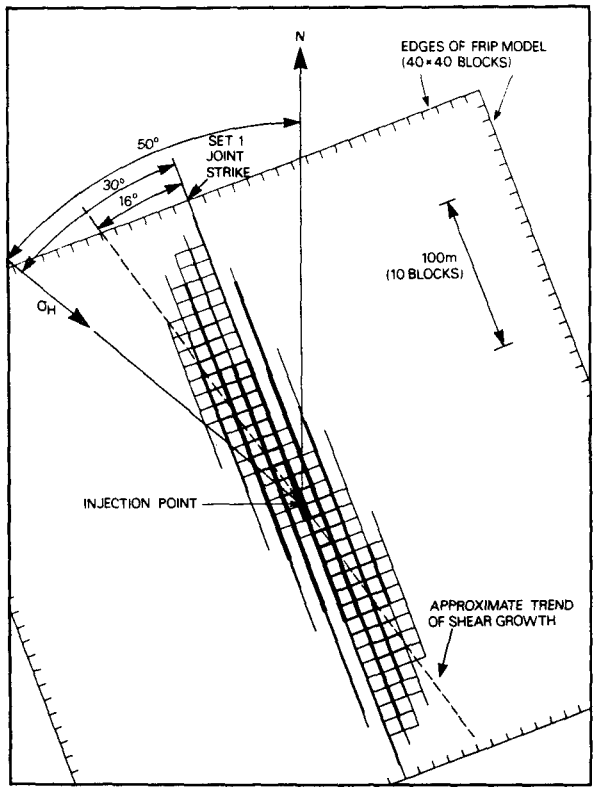


Figure 8: Plan view of hydraulically stimulated joint network from FRIP model; 2:1 horizontal stress ratio

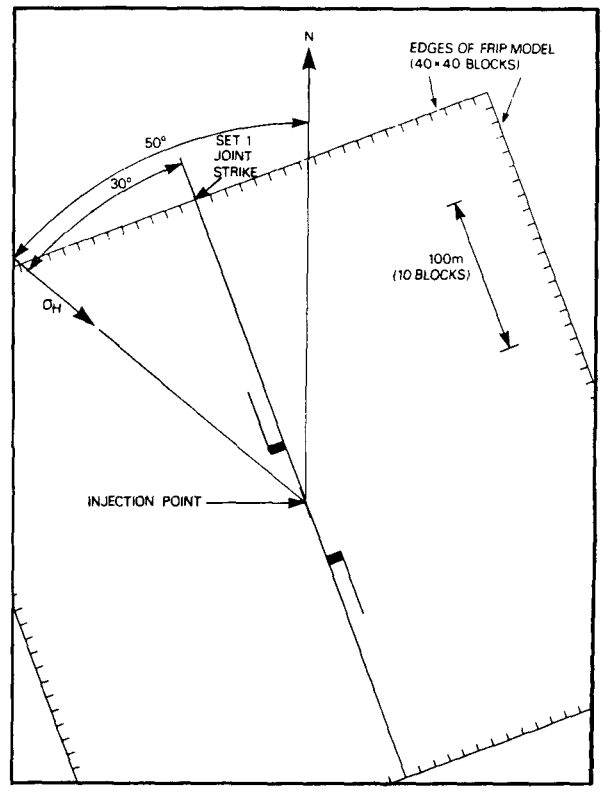


Figure 9: Plan view of hydraulically stimulated joint network from FRIP model; 5:1 horizontal stress ratio

injections was to create essentially planar permeable zones but with some uncertainty regarding dimensions and permeabilities. The higher permeability shorter fracture and lower permeability longer fracture options may be seen as compatible with the 2:1 and 5:1 stress FRIP models respectively. Further analysis of these recent results is in hand.

One difficulty with the pressure transient analysis was the selection of values for the formation compressibility β, needed for calculating s and x_f. When the joint system connected to the wellbore is actively dilating or compressing due to fluid pressure changes, the local formation compressibility, is lower than the overall value. The local compressibility depends on the joint porosity and the rate of joint dilation with fluid pressure changes.

Using dilation parameters for granite joints derived from Walsh (1981) and a local joint porosity of 0.1% to 1% results in compressibilities of about 5×10^{-11} to 2.5×10^{-10} Pa^{-1}. The overall compressibility for the Carnmenellis granite with a low joint porosity is about 2.5×10^{-11} Pa^{-1}. A constant value of 10^{-11} Pa^{-1} was selected for the pressure transient analyses.

Errors in the values of s due to errors in β will be small because of the logarithmic relationship. Errors in x_f are much greater, being approximately proportional to errors in β. The error magnitudes are probably less than 1 for s and less than 20 m for x_f for typical test results.

The shape and dimensions of the stimulated zone as defined by the microseismic locations show that only approximate values of near wellbore hydraulic conditions can be expected from pressure transient analysis. This is probably true for all HDR injection and recovery wells. It is evidently true for the CSM system where the major portion of the reservoir is below the open hole lengths of the boreholes.

Fracture half lengths of typically 50 to 100 m are inferred from the analyses conducted during the high and medium flowrate tests. Radius of investigation concepts for uniform radial flow conditions lead to similar dimensions for typical permeabilities and transient periods of up to about 100 hrs. These dimensions are much smaller than the overall reservoir dimensions.

The implicit assumption of uniform fracture conditions throughout the open hole length is also a simplification. Temperature and flowmeter logging have indicated discrete flowing zones, which have tended to polarise with increasing injection flowrates and pressures. Some of the fracture half lengths may be, therefore, significantly greater than calculated.

The results are, however, a useful measure of induced changes. They will be particularly relevant during the next phase of the project, when it is hoped to link a third, deeper well with RH12 via the existing stimulated zone. The planned separation of the wells is about 300-400 m.

Numerical modelling

The 5:1 effective stress ratio used in Figure 9 is closest to the measured stress conditions but the model with the 2:1 ratio shown in Figure 8 appears more compatible with the microseismic growth shown in Figure 7. Inspection of the joint directions shown in Figure 1 shows that set 2 is unlikely to be everywhere perpendicular to set 1. In this case joints in set 2 are likely to be oriented at considerably less than 60° to the σ_H direction (as in the model) and the types of shearing seen with the 2:1 stresses may well be possible with the 5:1 stresses.

The observed vertical growth of the reservoir by shearing during hydraulic injections cannot be demonstrated by the two dimensional FRIP formulation. A full three dimensional model would be necessary. However, this would raise further problems with computer CPU usage under current circumstances. Some efforts are being made to minimise the usage for the two dimensional model and there may then be some application to a three dimensional model.

The FRIP modelling has demonstrated some of the limitations of continuum modelling of pressure transients, whether of the conventional type with hydraulic parameters independent of fluid pressure or the more sophisticated finite element or finite difference formulations with pressure dependence. None of these approaches have to the author's knowledge satisfactorily addressed the interactions of rock joints and blocks, fluid pressure transients and in situ stresses.

Conceptual permeability model

The pressure transient analysis, microseismic location and FRIP modelling results indicate that a reasonable conceptual model for the permeability distribution associated with the injection well, RH12, would be as shown in Figure 10. There is an inner highly stimulated core, Zone A, with a permeability of up to 5 md and progressively lower permeabilities in the outer zones B (stimulated) and C (unstimulated). The figure shows a cross section. The lengths of zones A and B, approximately parallel to σ_H could be of the order of 100-200 m and 300-600 m respectively. It will be necessary to establish the main circulation of the system within zones A and B.

This model is applicable where the reservoir pressure is several MPa above hydrostatic. The sizes and permeabilities of these zones are probably smaller at reservoir pressures near hydrostatic.

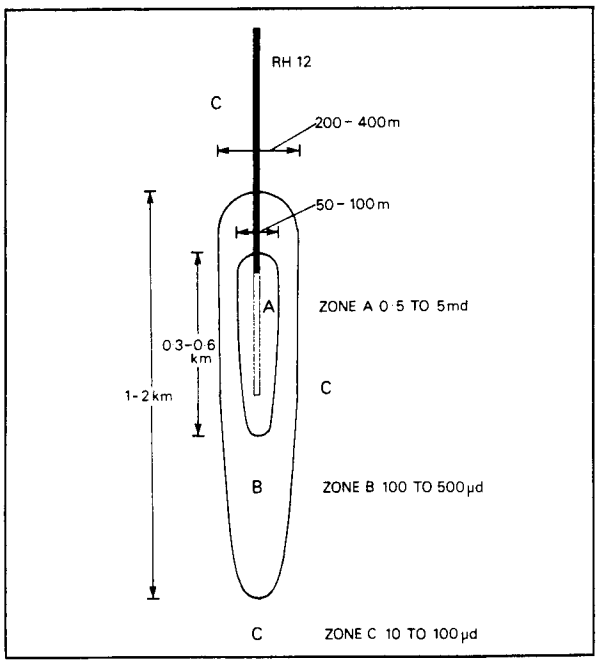


Figure 10: Conceptual model of permeability distribution in the hydraulically stimulated zone

CONCLUSIONS

The use of conventional diffusion theory for pressure transient analysis of the CSM HDR wells has provided a useful index of the changes caused to the rock mass near the wellbores by hydraulic injections. The penetration of the tests has been insufficient to determine hydraulic characteristics beyond about 100 m from the wells, and has more typically given information within about 50 m from the wells.

Reservoir growth as a result of the injections has been predominantly downwards and mostly beyond the range of influence of the pressure transient tests. The downward growth is believed to be due to a shearing mechanism in a significantly anisotropic in situ stress regime.

The effect of the high flow rate injections (up to 90 l/sec) was to increase the lumped permeability of the rock mass from less than 100 μd to greater than 5 md in the vicinity of the wells. Skin values were reduced to about -5 to -6.

The net effect after the reservoir pressure had returned to near hydrostatic was to increase the extent of more permeable fractures by a factor of about 30 compared with early values.

The use of the discrete joint-block model FRIP has given some useful insights into the interactions of rock mechanics and hydraulics in stressed jointed rock during hydraulic injections. Although the model is currently two dimensional and uses significant computer CPU time, it may be possible to develop a more efficient formulation with eventual three dimensional application.

It has been possible to use the results of the transient tests, microseismic locations and FRIP modelling to establish a conceptual permeability model for the reservoir zone adjacent to the injection well, RH12. The model will require further calibration from the results of circulation tests, tracers, well logging and thermal drawdown.

ACKNOWLEDGEMENTS

The work described in this paper was performed for the CSM HDR geothermal energy project, funded by the United Kingdom Department of Energy (Contract E/5A/CON/115/173/017) and the European Economic Community (Contract EG-D-2-003-UK(N)). The author wishes to acknowledge the considerable efforts made by the project staff which have made this paper possible, in particular the Project Director, Dr A S Batchelor, and Messrs P Ledingham and K Kwakwa.

All the views and conclusions expressed in this paper are the author's personal opinions and are not necessarily supported by either the United Kingdom Department of Energy or the European Economic Community Directorate General for Science and Research.

REFERENCES

Agarwal R G, Carter R D, Pollock C B. (1979), "Evaluation and performance of low-permeability gas wells stimulated by hydraulic fracturing". Transactions SPE, Volume 267, Part 1.

Agarwal R G. (1980), "A new method to account for producing time effects when drawdown type curves are used to analyze pressure buildup and other test data". In SPE-AIME 55th annual technical conference, Dallas, Sep 1980 (SPE 9289).

Barton N. (1976), "The shear strength of rock and rock joints". Int J Rock Mech Min Sci & Geomech Abstr, 13, 255-279.

Batchelor A S. (1982), "The stimulation of a hot dry rock geothermal reservoir in the Cornubian granite, England". Proc 8th Workshop Geothermal Reservoir Engineering, Stanford University, California. pp 237-248.

Batchelor A S, Baria R B, Hearn K. (1983), "Monitoring the effects of hydraulic stimulation by microseismic event location: a case study". SPE 12109. In SPE 58th annual technical conference and exhibition, San Francisco, Oct 1983.

Cundall P A. (1982), "Adaptive density-scaling for time-explicit calculations. In 4th International Conference on Numerical Methods in Geomechanics, Edmonton, May 1982.

Cundall P A. (1983), "Fluid-rock interaction program (FRIP): computer model of HDR reservoir". Phase 2 Group IV Part 2 report. Camborne School of Mines Geothermal Energy Project.

Earlougher R C. (1977), "Advances in well test analysis". Henry L Doherty Series monograph Vol V. SPE-AIME, Dallas, 264 pp.

Gringarten A C. (1982), "Interpretation of tests in fissured reservoirs and multilayered reservoirs with double porosity behaviour: theory and practice. SPE 10044. In SPE International Petroleum Exhibition and Technical Symposium, Bejing, China, Mar 1982.

Gringarten A C, Bourdet D P, Landel P A, Kniazeff V J. (1979), "A comparison between different skin and wellbore storage typecurves for early-time transient analysis. In SPE-AIME 54th annual technical conference, Las Vegas, Sep 1979. (SPE 8205), 16 pp.

Gringarten A C, Ramey H J, Raghavan R. (1975), "Applied pressure analysis for fractured wells". J Pet Tech. (July 1975). 887-892; Trans, AIME, 259.

Healy J H, Rubey W W, Griggs D T, Raleigh C B. (1968), "The Denver earthquakes". Science, 161, No 3848, 1301-1310.

McGarr A. (1980), "Some constraints on levels of shear stress in the crust from observations and theory". J Geophys Res, 85, No B11, 6231-6238.

Murphy H D, Pine R J. (1984), "Dendritic hydraulic fracturing in geothermal energy reservoirs". In ASME Petroleum Division Conference, New Orleans, Feb 1984. American Society of Mechanical Engineers.

Pearson C. (1981), "The relationship between microseismicity and high pore pressures during hydraulic stimulation experiments in low permeability granitic rocks". J Geophys Res, 86, No B9, 7855-7864.

Pine R J, Batchelor A S. (1982), "In situ stresses and jointing in the Carnmenellis granite and the implications for hydraulic behaviour". Camborne School of Mines Jnl, 82, 40-48.

Pine R J, Batchelor A S. (1983), "Downward growth of hydraulic stimulation by shearing in jointed rock". Submitted to Int J Rock Mech Min Sci & Geomech Abstr, Nov 1983.

Pine R J, Merrifield C M, Ledingham P. (1983), "In situ stress measurement in the Carnmenellis granite: 2 - Hydrofracturing tests at Rosemanowes Quarry to depths of 2000 m". Int J Rock Mech Min Sci & Geomech Abstr, 20, No 2, 63-72.

Pine R J, Tunbridge L W, Kwakwa K. (1983), In situ stress measurement in the Carnmenellis granite: 1 - Overcoring tests at South Crofty mine at a depth of 790 m". Int J Rock Mech Min Sci & Geomech Abstr, 20, No 2, 51-62.

Pine R J, Ledingham P. (1983), "In situ hydraulic parameters for the Carnmenellis granite hot dry rock geothermal energy research reservoir". SPE 12020. In SPE 58th Annual Technical Conference and Exhibition, San Francisco, Oct 1983.

Van Poollen H K. (1964), "Radius of drainage and stabilisation time equations". Oil and Gas J, (14 Sep 1964), 138-146.

Walsh J B. (1981), "Effect of pore pressure and confining pressure on fracture permeability". Int J Rock Mech Min Sci & Geomech. Abstr, V 18, pp 429-435.

Proceedings Ninth Workshop Geothermal Reservoir Engineering
Stanford University, Stanford, California, December 1983
SGP-TR-74

VARIATION OF FRACTURING PRESSURES WITH DEPTH NEAR THE VALLES CALDERA

Zora Dash and Hugh Murphy

Los Alamos National Laboratory, MS J981
Los Alamos, New Mexico 87545

ABSTRACT

Hydraulic Fracturing at the Fenton Hill Hot Dry Rock Geothermal site near the Valles Caldera has yielded fracturing pressures from 14 to 81 MPa (2030 to 11750 psi) at depths ranging from 0.7 to 4.4 km (2250 to 14400 ft). This data can be fit to a fracture gradient of 19 MPa/km (0.84 psi/ft), except for an anomalous region between 2.6 to 3.2 km where fracturing pressures are about 20 MPa lower than estimated using the above gradient. This anomaly coincides with a biotite granodiorite intrusive emplaced into a heterogeneous jointed metamorphic complex comprised of gneisses, schists and metavolcanic rocks. Microseismic events detected with sensitive downhole geophones suggest that shear failure is an important process during hydraulic fracturing of such jointed rock. Consequently the usual relation between minimum earth stress and fracture opening pressure, based upon classic tensile failure, cannot be used apriori; fracture opening pressure is instead a complex function of joint orientation and all three components of principal earth stress.

FRACTURING EXPERIMENTS

The Los Alamos National Laboratory, with financial support from the U.S. D.O.E., West Germany's Ministry for Science and Technology, and Japan's New Energy Development Organization, has drilled five wells into Precambrian crystalline basement rock as part of the Hot Dry Rock geothermal energy program. The experimental site, Fenton Hill, is located in the western flank of the Valles Caldera, a dormant volcano in the Jemez Mountains of northern New Mexico. The first well, GT-1, was drilled to 0.75 km for exploratory purposes. The second and third wells, GT-2 and EE-1, were drilled to approximately 3 km, and were used for numerous HDR heat extraction experiments.[1] These wells were connected by hydraulic fractures, one of which extended vertically 300 m from initiation point in EE-1 to intersection with GT-2. The fourth and fifth wells, EE-2 and EE-3, were drilled to 4.4 and 4.0 km respectively. The temperature at 4.4 km was 325°C. The bottom sections of these wells were directionally drilled, at an angle of 35° from vertical, with horizontal deviation in the ENE direction, parallel to the estimated direction of the minimum principal earth stress. These wells are to be connected by fractures which must be about 370 m high, because the wells are separated vertically by this distance.

In all fracturing experiments conducted to date, the fracturing fluid has been water, to which friction reducer and fine silica have been added occasionally to reduce wellbore friction and to increase fracturing efficiency by blocking permeability of the rock faces contiguous to the fracture. Other than the addition of friction reducer the water was not viscosified, and no proppants were injected. Injection rates have ranged from 1 to 76 ℓ/s, and injection volumes from 1 to 5000 m^3. The great depths and temperatures have so far precluded the successful use of impression packers or televiewers to determine fracture orientation, but monitoring of microseismic acoustic emissions during fracturing with 3 axis geophones installed to depths of 2.9 km in neighboring wells indicate that the fracture planes generally strike NS, nearly as expected. All fractures are vertical, or nearly so, except in the lower zone of EE-2, (below 4.3 km) where acoustic emission patterns suggest a fracture zone with a dip of 45°.

Table I summarizes total downhole fracture pressures, P_f, determined in all fracture experiments conducted in the Fenton Hill geothermal wells to date. Later we discuss the relationship of P_f and minimum horizontal earth stress. The designation ISIP indicates that a reasonably constant pressure was observed after shut-in, but extrapolated ISIP indicates that the "Muskat analysis" was required, in which a straight line fit of logarithm of pressure versus time is extrapolated back to actual time of shut-in.[2] "Fracture extension" indicates that re-injection provided such a clear arrest in the pressure-time curve, and at reasonably low flow rates, that this arrest could be taken as P_f. The designation "P from PTA" indicates the fracture extension pressure derived from noting the pressure required to change hydrological characteristics of the existing fracture, e.g. enlargement. The last two methods of P_f determination, termed P vs $Q^{0.25}$

Table I. Fenton Hill Fracture Pressures			
Well / Expt	Depth (km)	Fracture Opening Pressure (MPa)	Method Of Determination
GT-1			
	0.745	13.7-14.8	ISIP
GT-2			
	2.0	33.5-34.9	Extrapolated ISIP
	2.93	36.6-37.3	Fracture Extension
EE-1			
	1.96	30.6-31.5	Fracture Extension
	2.93	37.5	Fracture extension pressure from PTA
EE-2			
2018(82/07/19)	3.46-3.59	61.0(6)*	P vs Q^.25 Extrapolation
		67.5(6)	P vs Q^.5 Extrapolation
		62.7	ISIP
		75.0	Extrapolated ISIP
2020(82/10/06)	3.46-3.59	63.0(5)	P vs Q^.25 Extrapolation
		68.5(5)	P vs Q^.5 Extrapolation
		67.7-73.9	ISIP (4 measurements)
		70.0-74.2	Extrapolated ISIP (3)
2011(82/05/30)	4.25-4.36	59.2(2)	P vs Q^.25 Extrapolation
		69.9(2)	P vs Q^.5 Extrapolation
		80.2	ISIP
		80.3	Extrapolated ISIP
2012(82/06/04)	4.25-4.36	74.5(7)	P vs Q^.25 Extrapolation
		78.7(7)	P vs Q^.5 Extrapolation
		80.2	ISIP
		80.3	Extrapolated ISIP
2016(82/06/19)	4.25-4.36	71.7(9)	P vs Q^.25 Extrapolation
		77.0(9)	P vs Q^.5 Extrapolation
		81.2	ISIP
		81.3	Extrapolated ISIP
EE-3			
2006(82/01/19)	3.09-3.15	38.1	Extrapolated ISIP
2007(82/02/17)	3.09-3.15	33.6(3)	P vs Q^.25 Extrapolation
		35.9(3)	P vs Q^.5 Extrapolation
		38.4	Extrapolated ISIP
2023(82/11/08)	3.09-3.15	33.9(6)	P vs Q^.25 Extrapolation
		37.3(6)	P vs Q^.5 Extrapolation
		38.6	ISIP
		42.5	Extrapolated ISIP
2025(82/12/14)	3.35-3.44	45.4(14)	P vs Q^.25 Extrapolation
		56.6(14)	P vs Q^.5 Extrapolation

* Number in Parentheses is Number of P - Q Data Points in Curve Fit.

(laminar flow) and P vs $Q^{0.5}$ (turbulent flow) are scaling laws for refracturing pressure variation with flow rate, using a simple fracture aperture (opening) and pressure relation[3]. Figure 1 presents the variation of the fracture extension pressure with Q for Experiment 2012. As can be seen, reasonable fits to the data can be obtained with either $Q^{0.25}$ or $Q^{0.5}$ scaling, a typical value of the discrepancy between data and curve fit being only about 1%. The values of P_f obtained by extrapolation are 74.5 MPa for $Q^{0.25}$ scaling and 78.7 MPa for $Q^{0.5}$ scaling, but below we show that this difference, though small, is significant and we will argue that $Q^{0.5}$ scaling is more appropriate.

The single value of P_f derived from PTA was based upon 15 injection tests.[4] The range of ISIPs provided for Experiment 2020 represents four separate determinations[5] during the course of injecting 3300 m^3 (860,000 gallons) over 15 hours.

Table I demonstrates the excellent repeatability of all the methods of estimating P_f. For example, three separate fracturing experiments were conducted in EE-2 in the depth interval 4.25 to 4.36 km. The six separate P_f measurements by ISIP and extrapolated ISIP vary by a maximum of 1.4% from minimum to maximum.

For Experiment 2011, only two data points were available for P - Q curve fitting and, as can be seen, the value of P_f so derived is significantly different from the other estimates. For the other two experiments at 4.25 to 4.36 km, the number of data points was greater and the agreement is much better. In fact, if the P_f estimates based upon two point P vs Q extrapolation are excluded, the agreement of the remaining P_f estimates is excellent, ranging only from 71.7 to 81.3 MPa, or a variation of 6% about the mean. Similar observations pertain for the 8 measurements of P_f at 3.46 to 3.59 km in EE-2 and the 8 measurements at about 3.1 km in EE-3.

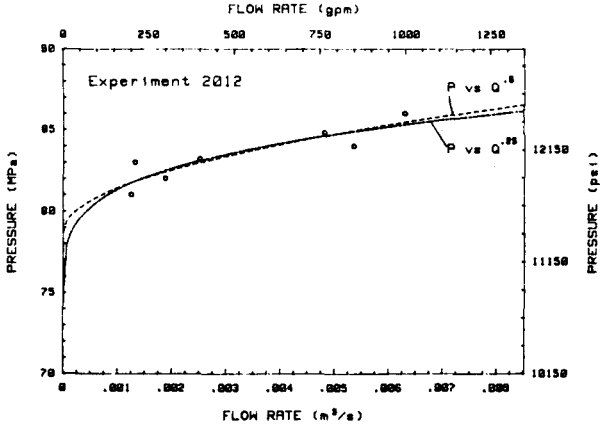


Figure 1. Variation of fracture extension pressure with injection rate.

With the possible exception of Experiment 2018, the P_f determined from $Q^{0.25}$ extrapolation is always significantly lower than the other determinations. This argues that a laminar flow rule is inappropriate, an entirely reasonable finding considering the high injection rates used in these experiments. If $Q^{0.25}$ extrapolation is excluded from consideration, the agreement of P_f determinations would be ±3% at 4.3 km, ± 8% at 3.5 km, and ± 8% at 3.1 km.

Figure 2 presents the variation of fracture pressure with depth. All measurements, with the exception of those from P - $Q^{0.25}$ extrapolation and the two-point $Q^{0.5}$ extrapolation are plotted. Also shown is the vertical overburden stress computed from the density of the overlying formations. Except for the biotite granodiorite intrusive located at 2.6 to 3.2 km, P_f can be represented as a linear function of depth, with a fracture pressure gradient of 19 MPa/km (0.84 psi/foot).

RELATIONSHIP OF FRACTURE PRESSURE AND EARTH STRESSES

According to conventional theory, the fracture pressure derived from shut-in or from fracture extension pressure is equivalent to the minimum principal earth stress, S_{min}. However, before this equivalence can be drawn for the present measurements it must be shown that the mode of fracturing is tensile in nature, not due to shear. In addition, because

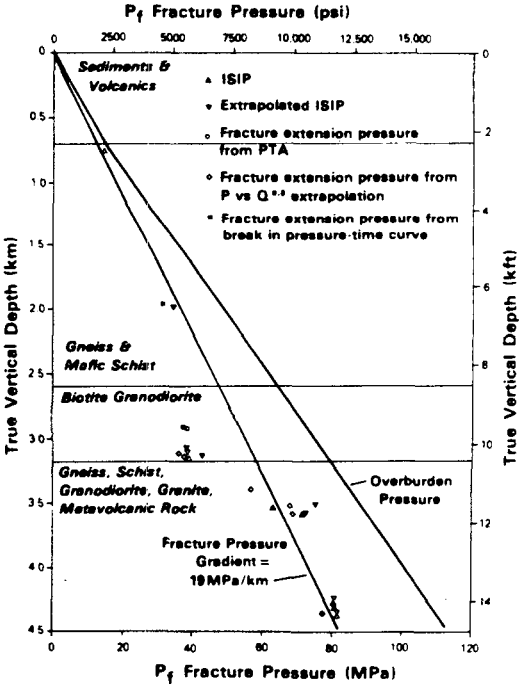


Figure 2. Variation of fracture pressure with depth.

fracturing in these crystalline rock formations undoubtedly opens up pre-existing fractures, or joints, rather than creating virgin rock failures, it must also be shown that the joints preferentially stimulated are perpendicular, or nearly so, to Smin, or else that the principal earth stresses are sufficiently close in magnitude that joint orientation makes little difference. Let us first consider the possibility of shear fracturing. For joints without strength or cohesion, it can be shown that as the fluid pressure is increased, eventually the effective normal stress on the joint will be reduced to the point where the joint can slip; theoretically shear slippage occurs before the effective stress is reduced to zero, and the joint completely opens ("jacking" is the descriptive term used in reference 6). Adopting Amonton's friction law, it can be shown that if β is the angle between a joint plane and the direction of the maximum principal stress, Smax, and ϕ is the friction angle, (the coefficient of friction is $\tan\phi$) then

$$\frac{S_{min}}{P_f} = \frac{2 + (\lambda - 1)\, S_{max}/P_f}{\lambda + 1} \qquad (1)$$

where $\lambda = \cos 2\beta + (\sin 2\beta)/\tan\phi$.

Thus S_{min} can be estimated from the measured P_f if independent estimates of Smax, β and ϕ are available. Usually Smax is the readily estimated overburden stress, but in tectonically active regions such as the Valles Caldera this must be established, and the means of doing so was derived from differential strain analysis (DSA) of core specimens[8] as well as fault plane solutions[9] of microseismic acoustic emissions. DSA earth stress measurements are based upon the stress required to close microcracks in the core, the assumption being that all such cracks are closed in situ. This method is consequently qualitative in nature, subject to considerable uncertainties, and with a tendency to overestimate actual earth stress. Figure 3 presents the results: the solid lines indicate the estimated minimum horizontal stresses, and the dashed lines represent the maximum horizontal stresses. The four core specimens were unoriented, so the direction of the DSA principal horizontal stresses are unknown. While considerable uncertainty is noted it appears that the maximum horizontal stress is less than, or approximately equal to, the vertical stress.

Microseismic accoustic emissions during hydraulic fracturing experiments were detected with a downhole, three-axis geophone (or occassionally an accelerometer) as well as a surface network of 13 stations located within 5 km of the geothermal wells. Full details are provided in reference 9, but can be summarized as follows: the fault plane solution for fracturing at the 4.3 km interval in EE-2 indicates strike slip faulting on a N-S vertical plane. The solution at 3.5 km indicates dip slip on a N-S vertical plane. These two solutions indicate that over a short depth interval, only 800 m, the maximum earth stress changes from nearly vertical to nearly horizontal, which strongly implies that the maximum horizontal stress is nearly equal to the overburden stress over this depth interval, being slightly greater at 3.5 km, and slightly less at 4.3 km. This result is entirely consistent with the DSA stress ranges shown in Figure 3. Consequently the magnitude of the maximum stress can be taken as that of the overburden stress. At 3.5 km the ratio S/P_f is then 1.30 while at 4.3 km the ratio is 1.37; both intervals can be characterized, on average, as $S_{max}/P_f = 1.34$. Substitution in equation (1) yields, in Table II, the ratios of S_{min}/P_f provided by the shearing criterion for various values of fracture orientation and friction angle. Friction angles of 30° to 60° encompass the range of reasonable values for crystalline granitic rock.

For the 3.5 km interval the fault plane was not well constrained, and the plane could dip from 50° to 90° (β = 0° to 40°). The fracture orientation provided by mapping the microseismic hypocenters is also poorly constrained, but the general pattern appears to be a vertical fracture striking roughly N-S. The fault plane solution for the 4.3 km interval is more tightly constrained, with dip of 85° and strike N10°E. Usual fault plane convention places the P axis direction at 45° to the fault, so β = 45°. However, hypocenter maps suggest a fracture dipping 45° and striking roughly N-S. This could be construed as a single fracture, with a dip at variance with that given by the fault plane solution (but still with $\beta \leq 45°$), or as a series of en echelon fractures, each with vertical fault plane, but joined to adjacent fractures by off-vertical natural joints.

In every case discussed, $\beta \leq 45°$, so that the minimum earth stresses in Table II are remarkably well constrained: $S_{min}/P_f = 1.08 \pm 8\%$, for $30° \leq \phi \leq 60°$. Thus the use of either the conventional interpretation or one

Table II

Ratios of Minimum Earth Stress To Fracture Pressure According to Shear Fracturing Criterion With $S_{max}/P_f = 1.34$.

β	ϕ = 30°	ϕ = 45°	ϕ = 60°
0°	1.00	1.00	1.00
15°	1.09	1.05	1.02
30°	1.17	1.05	1.00
45°	1.07	1.00	0.91
60°	1.00	0.84	0.64
75°	0.66	0.27	-0.26

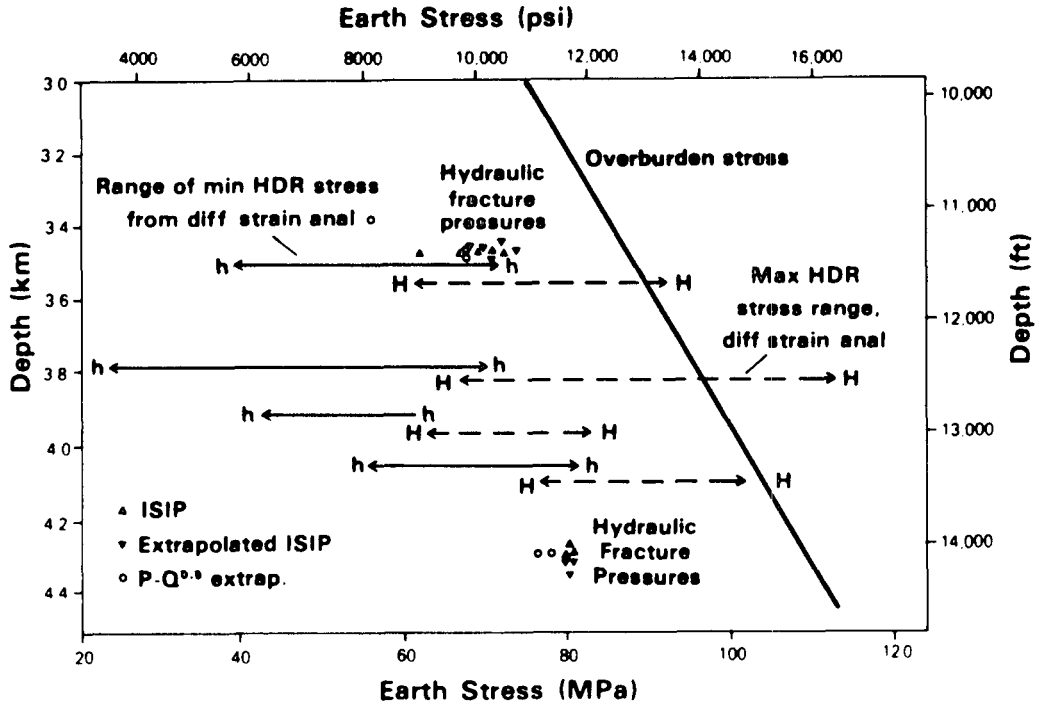


Figure 3. Comparison of DSA Earth Stresses and Fracture Pressures.

based upon shear fracturing results in essentially the same result, $S_{min} = P_f$, or $S_{min} = 1.08 (\pm 0.08) P_f$.

The final check is to consider the possibility of joint "jacking" on planes non-perpendicular to S_{max}. In this case the normal stress must be equal to P_f, and rotational stress transformation yields:

$$\frac{S_{min}}{P_f} = \frac{2 - (1 - \cos 2\beta) S_{max}/P_f}{1 + \cos 2\beta} \qquad (2)$$

Table III indicates that unlike shear fracturing, it requires a fracture pressure greater than S_{min} to jack open joints inclined significantly to the S_{max} direction. It may be concluded that static considerations alone preclude the opening of such off angle joints by jacking, because these would shear first.

Table III
Ratio of Minimum Earth Stress To Fracture Pressure For "Jacking"; $S_{max}/P_f = 1.34$

β	S_{min}/P_f
0°	1
15°	0.97
30°	0.89
45°	0.66

However dynamic factors must also be considered.[10] The injected fluid must be accommodated by fracture and formation porosity. Depending upon injection rate, fluid viscosity, fracture size, and formation permeability and compressibility some fluid permeates the rock adjacent to the fracture and is thus stored in existing porosity. The remaining fluid is stored in the dilated fracture. In principle, jacking requires higher pressures, which leads to greater dilation than shearing, but rough estimates[11] suggest that formation permeation accommodated 90% of the water injected in these fracturing experiments. Consequently little fracture dilation was required, and despite the vast differences in physical scale this fracturing was probably similar to the shear fracturing observed by Lockner and Byerlee[12] when core specimens were fractured at low injection rates. Thus, it is likely that jacking in the present experiments, if it occurred at all, was confined to low β joints, for which $S_{min}/P_f \approx 1$.

To briefly summarize estimated earth stresses at other depths, it is noted that the maximum ratio of S_{max}/P_f occurs for the biotite granodiorite intrusive, where the ratio is 2, resulting in $S_{min}/P_f = 1.25 \pm 0.25$ based upon the shear criterion for joints with $\beta < 45°$. However in this interval a completed reservoir was developed and simple geometrical relations between fracture initiation zones and intersection zones in the opposite well indicate

nearly vertical fractures, $\beta \leq 10°$, so S_{min}/P_f is constrained to less than 1.10. The jacking criterion for $\beta \leq 10°$ likewise results in $S_{min}/P_f = 0.95$. In summary $S_{min} \approx P_f$ closely for this interval. For depth intervals not yet discussed no similar geometrical constraints are available, but in these intervals $S_{max}/P_f \approx 1.5$; and the shear criterion results in $S_{min}/P_f = 1.12 \pm 0.12$.

CONCLUSIONS

Fracture pressures were estimated from direct ISIPs, extrapolated ISIPs, observed changes in hydrological characteristics, and extrapolations of fracture extension pressure versus injection rate. Excluding "laminar" flow scaling, and "turbulent" flow scaling where only a very few data sets (P vs Q) are available, excellent agreement is found for all five methods. Because of the nearly lithostatic state of stress at this site, in which the ratio of S_{max}/S_{min} was typically 1.5 (2.0 in the worst case), it was possible to show that $S_{min} \approx P_f$ even if the mode of fracturing is shear, or if off-vertical joints were "jacked" open. Except for the Biotite Granodiorite intrusive, where S_{min} appears to be 20 MPa lower than expected, the minimum principal earth stress is linear with depth, with a gradient of 19 MPa/km (0.84 psi/ft) and is horizontally oriented in approximately the EW direction. The maximum horizontal stress is nearly equal to the overburden stress.

REFERENCES

1. Dash, Z., et al, "Hot Dry Rock Geothermal Reservoir Testing: 1978 to 1980", J. Volcan. Geotherm. Res., 15, 59-99, 1983.

2. Aamodt, R. L., and Kuriyagawa, M., "Measurement of Instantaneous Shut-In Pressure in Crystalline Rock", appears in Hydraulic Fracturing Stress Measurements Nat'l Acad. Press Washington, DC. 1983.

3. Perkins, T. K. and Kern, L. R., "Widths of Hydraulic Fractures", J. Petr. Tech., 13, 937-946, September, 1966.

4. Murphy, H. D., Lawton, R. G., Tester, J. W., Potter, R. M., Brown, D. W., and Aamodt, R. L., "Preliminary Assessment of a Geothermal Energy Reservoir Formed by Hydraulic Fracturing", Soc. Petr. Engr. J., 317-326, August 1977.

5. Brown, D. W., "Recent Results - Los Alamos Hot Dry Rock Project", Proc. 8th Workshop Geothermal Reservoir Engineering, Stanford, Univ., December 1982.

6. Pine, R. J. and Batchelor, A. S., "Downward Growth of Hydraulic Stimulation by Shearing in Jointed Rock", submitted to Int. J. Rock Mech. Min. Sci. Geomech Abstr., 1983.

7. Bombolakis, E. G., "Some Constraints and Aids for Interpretation of Fracture and Fault Development", Proc. 2nd Int. Conf. Basement Tectonics, Denver, 1979.

8. Anon. "Differential Strain Curve Analysis and Differential Wave Velocity Analysis of Fenton Hill EE-2 Cores", Dowell Rock Mechanics Laboratory, Tulsa, Oklahoma, November 1983.

9. Cash, D., Homuth, E. F., Keppler, H., Pearson, C., and Sasaki, S., "Fault Plane Solutions for Micro Earthquakes Induced at Fenton Hill Hot Dry Rock Geothermal Site: Implications for the State of Stress Near a Quaternary Volcanic Center", to appear in Geophys. Rev. Lett., 1984.

10. Murphy, H. D., Pine, R. J., "Dendritic Hydraulic Fracturing in Geothermal Energy Reservoirs", Proc. Energy Tech. Conf. and Exhibit, New Orleans, Feb. 12-16, 1984.

11. Murphy, H. D. Keppler, H. and Dash, Z., "Does Hydraulic Fracturing Theory Work in Jointed Rock Masses?," Trans. Geotherm. Res. Council 7, 461-466, 1983.

12. Lockner, D. and Byerlee, J. D., "Hydrofracture in Weber Sandstone at High Confining Pressure and Differential Stress", J. Geophys, Res., 82, 2018-2026, 1977.

Proceedings Ninth Workshop Geothermal Reservoir Engineering
Stanford University, Stanford, California, December 1983
SGP-TR-74

BEHAVIORS OF CRACK-LIKE RESERVOIRS BY MEANS OF FRACTURING AT NIGORIKAWA AND KAKKONDA GEOTHERMAL FIELDS

Hiroyuki Abé, Hideaki Takahashi, Katsuto Nakatsuka,
Hiroaki Niitsuma and Morihiko Takanohashi*

Faculty of Engineering, Tohoku University, Sendai 980
*Japan Metals and Chemicals Co. Ltd., Takizawa 02001,
Japan

ABSTRACT

A basic concept of the geothermal reservoir as a set of cracks is first presented. Extensions of subsurface cracks during well stimulation treatments at Nigorikawa(Mori) and closure operations of production well-head valves at Kakkonda are analysed and their behaviors are demonstrated based on results of long-distance AE Measurements.

INTRODUCTION

It has become evident recently that the productivity of geothermal well is highly dependent on the existence of cracks in deep rock masses. In HDR projects subsurface cracks are known to serve for heat exchangers below the earth's surface. By applying the hydraulic fracturing technique as a well stimulation, subsurface cracks are created and used as channels of the geothermal fluid flow. The extension of subsurface cracks has been successfully measured at Nigorikawa(Mori) in 1980 by using a long-distance acoustic emission(AE) technique developed in Tohoku University(Niitsuma, H. et al., 1983). The movement of subsurface natural cracks during the closure operation of the well-head valves has also been measured at Kakkonda in 1982 and 1983 by using the same measurement technique.

In this paper a basic concept of the geothermal reservoir is first described, as it is suggested from experiments on geothermal energy extraction for both HDR and hydrothermal types that the geothermal reservoir is constituted by a set of cracks. The behaviors of subsurface cracks at both Nigorikawa(Mori) and Kakkonda geothermal fields are demonstrated by analysing the AE data.

BASIC CONCEPT OF GEOTHERMAL RESERVOIR

a. Geothermal reservoir

There are two kinds of geothermal reservoirs, i.e., natural and man-made reservoirs. Every geothermal reservoir is considered to be constituted by a set of cracks, most of which are connected each other and contain a geothermal fluid.

b. Cracks in geothermal reservoir

Faults, joints or thin layers subjected to alteration due to metamorphism have smaller values of the fracture toughness than that of the surrounding rock. Let these surfaces or thin layers be called "surfaces of weakness".

When the rock mass is fractured into two parts by a surface of weakness and the fluid is filled inside the newly created thin space, this space is said to be a crack in the sense of fracture mechanics applied to geothermal energy extraction. The fracture toughness of the (unfractured) surface of weakness is generally different from zero. A scheme of crack and surface of weakness is shown in Figure 1.

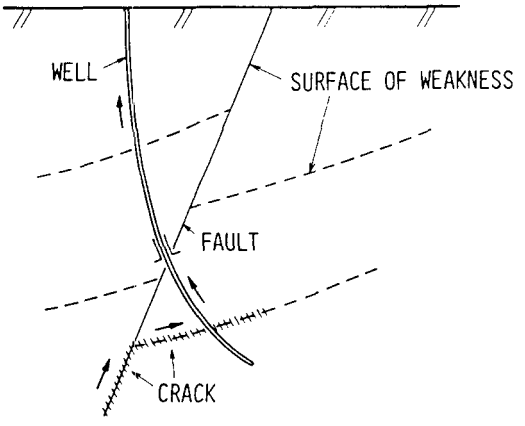


Figure 1. Cracks in geothermal reservoir and surfaces of weakness

c. Growth of geothermal reservoir cracks

c-1. Massive hydraulic fracturing using deep well pumps. The cracks created by massive hydraulic fracturing for both HDR and hydrothermal types are considered. In general the crack initiates on the line formed by intersecting the wellbore wall with the surface of weakness.

However if the fracturing operation is performed on the very small portion of the wellbore wall by using, for example, a pair of packers, the crack may be produced from a point of the matrix of the rock mass, which is different from a point on the surface of weakness.

When the crack grows by the injection of fluid, it has a tendency to extend along the surface of weakness which is probably vertical to the direction of the minimum principal tectonic stress. The crack ceases growing as the injection of water by pump is stopped, as shown in Figure 2. In a hydrothermal type, however, if the crack is connected with natural cracks with higher fluid pressure, some small branch cracks may grow even after the stop of the water injection by pump.

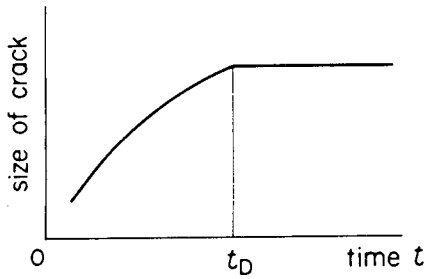


Figure 2. Size of crack as function of time t. (Injection of fluid is stopped at $t = t_D$)

c-2. Closure operation of well-head valves. It was found during the closure operation of production well-head valves that the cracks grow along surface of weakness as in the case of fracturing by using pumps. Two cases are considered; (i) hot water type, and (ii) vapor type. In Case (i) hot water is dominant in quantity compared with vapor, and Case (ii) is reversed. Figure 3 shows a schema for the variation of downhole pressure, where the closure operation of the well-head valve begins at $t = 0$ and it is completed at $t = t_D$ in both cases. The AE events are detected when the velocity of closure operation is larger than a certain value. The extension of cracks are known by

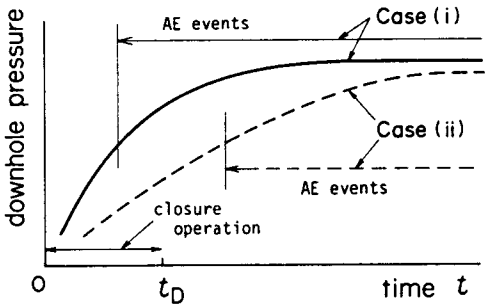


Figure 3. A schema for borehole pressure versus time

detecting these AE events. In Case (i) AE events are found even for $t < t_D$, while they could be detected for $t > t_D$ in Case (ii) because of the compressibility of the vapor. The fact that AE events are detected also during a dozen or so hours after the closure operation means that fluid pressures in small cracks continue to increase depending on the permeability and/or the fluid viscosity. Afterward the downhole pressure and also the number of AE events decrease slowly with time.

c-3. Supplements to growth of cracks. Hydraulically induced cracks both by the action of pumps and the closure operation of well-head valves extend with the increase of the fluid mass in each of the cracks and/or with the decrease of the fracture resistance which depends on the environmental effect near their tips. However, the cracks extend essentially in a stable manner different from those in the members in machines and structures (Abé, H. et al., 1976).

According to the AE measurements mentioned in this paper the cracks in hydrothermal systems are considered to extend mainly in downstream domains of the geothermal fluid flow.

CREATION OF RESERVOIR CRACKS BY FRACTURING AND ITS AE EVALUATION AT NIGORIKAWA(MORI) FIELD

A 50MWe geothermal electric power plant had been developed in the Nigorikawa(Mori) geothermal field in Hokkaido by Dohnan Geothermal Energy Co., Ltd., a subsidary of Japan Metals & Chemicals Co., Ltd., and was put into operation in November, 1982. A total of 17 geothermal wells at the depth ranging from 700m to 2400m had been drilled. In order to stimulate geothermal wells, massive hydraulic fracturing treatments were performed for 10 wells, in two separate projects in 1978 and 1980. The detailed information for this hydraulic fracturing was already described elsewhere (Katagiri, K. et al., 1980, Sato, K. et al., 1983).

On May 1, 1980, the massive hydraulic fracturing for D-1 well was carried out, where the long-distance AE measurement was also performed to monitor the crack extension during the fracturing. A large pre-existing crack was observed at the depth of about 1400m from the maximum lost circulation of mud water during well drilling. An AE instrumentation well of 30m depth was drilled. The AE hodogram technique and experimental details were reported already in the literature (Niitsuma, H. et al., 1983). The distance between the expected fractured location and the AE monitoring well was about 1600m.

AE monitoring had been continued for 3.5hr during the fracturing (about 1.5hr), and before and after the operation in order to check the background noise level. Twenty-one AE events could be detected during the hydraulic fracturing by the waveform monitoring. The maximum value of their amplitude is 0.86gal.

Normally a hydraulically induced fracture formation is estimated by an abrupt pressure drop, denoted as a breakdown, under a condition of increasing or constant flow rate. However, one could not determine the breakdown point clearly only from the pressure change. On the other hand, AE events would be generated potentially by tension elastic rebound at the fracture boundary and rock bursts near the fractured zone. Therefore, the AE technique is effectively used for the monitoring of the abrupt breakdown during hydraulic fracturing. All large AE signals detected are listed in Table 1.

Table 1. AE signals detected during hydraulic fracturing at D-1 well

TIME	No.	LOCATED AE SOURCE	
		DISTANCE(m)	DIRECTION(°)
1st STAGE			
10:41'12"	3	1603	W37.0S
10:51'22"	6	1613	W34.7S
10:59'55"	10	1325	W33.0S
11:07'45"	11	1238	W43.3S
11:10'42"	13	1100	W21.0S
2nd STAGE			
11:36'02"	17	1278	W43.5S
11:36'40"	19	1414	W25.1S
11:46'20"	24	1585	W15S-W22S
11:49'40"	25	1331	W34.5S
11:55'25"	26	1715	W26.0S
11:56'50"	29	1556	W15S-W18S
11:57'12"	30	1704	W23.1S
12:01'10"	31	1109	W30.0S

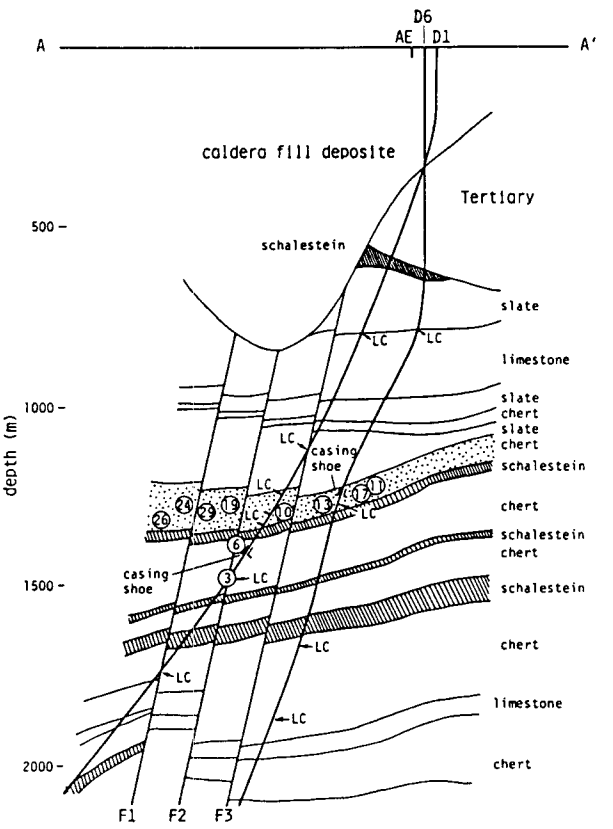


Figure 4. A-A'(E-W) section view of subsurface geological structure and AE source locations

Estimated distances between sonde and AE source by the hodogram method are presented in Table 1 where the wave velocities are assumed that v_p = 4330m/s, v_s = 2500m/s according to core sample data. Estimated relative directions in XY(horizontal) plane are also indicated in the table.

Figure 4 shows the subsurface geologic section view where the contour of D-1 well is in plane. The D-6 well had been treated before the treatment of D-1. Both D-1 and D-6 wells are almost in the same plane. A series of numbers and their locations indicate an order of AE occurrence and the source locations given in Table 1. F1, F2 and F3 represent three major faults and LC in the figure indicates the location of lost circulation of mud water during well drilling, and it shows the existence of a crack in the geothermal reservoir. The lost circulations mainly occurred along the fault, the upper part of limestone layer and the fractured chert layer(the dotted layer in Figure 4) at the depth ranging from 1200m to 1400m. It is confirmed from core samples that the fractured chert layer includes pre-existing cracks induced naturally having networks of pores caused by weathering. LC just below the casing bottom in D-1 well indicates the expected fractured point and D-1 well intersects with the fault F2 at this point.

After the hydraulic fracturing it is found from the tracer and well performance tests that the breakthrough between D-1 and D-6 wells occurred. When the production testing of D-1 well was carried out, both well-head pressures of D-1 and D-6 wells built-up simultaneously. Therefore, it can be considered that the crack extended along the fault F2 and the naturally fractured chert layer(dotted layer in Figure 4).

A horizontal distribution of AE source is plotted as shown in Figure 5, where F1, F2 and F3 show the location of the faults near the depth of the expected fractured zone (1300-1500m) and the crack extension is indicated over these faults. The crack extension process during the hydraulic fracturing of D-1 well may be explained by means of the AE data, as follows, referring Figs. 4 and 5: (1) The AE occurrences of #3 and 6, which are shear dominant type events, suggest that a shear crack extended from the point of the maximum lost circulation near the casing shoe along the fault plane F2. (2) The crack was kinked at the naturally fractured chert layer and extended in the layer toward the direction of the fault F3(#10), and

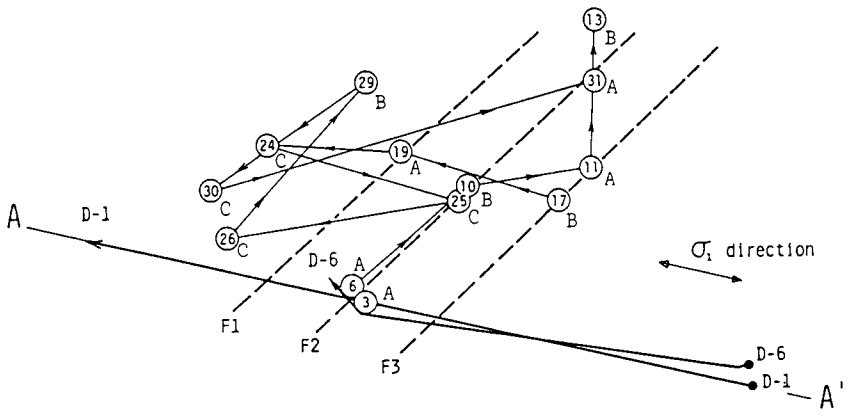


Figure 5. Horizontal distribution of AE sources

the data may suggest an occurrence of an opening mode cracking. (3) A shear mode cracking occurred again(#11) when the crack reached to the fault plane F3, where a hydraulically induced crack from D-6 well had already existed. (4) After that, the crack extended in the layer (#13-30), nearly parallel to the line A-A' which coincides with the maximum earth stress direction in the Nigorikawa(Mori) area (Nakamura, H., 1977).

EXTENSION OF RESERVOIR CRACKS DURING BUILT-UP TEST(VALVE CLOSURE OPERATION) AT KAKKONDA FIELD

Kakkonda geothermal field is located in Iwate prefecture. A 50MWe geothermal electric power plant had been developed in the field by Japan Metals and Chemicals Co., Ltd., and was put into operation in 1978 (Nakamura, H. and Sumi, K., 1981, Sato, K., 1982).

Eleven wells are being used for production and fourteen for reinjection of hot water.

The build-up tests of production wells have been carried out in 1982 and 1983 at Kakkonda field, after an interval of about one year. AE signals during the tests were measured. The well-head valves of the four wells (E-1, C-5, B-5 and B-3) were closed successively within six hours in 1982. After that, valves of remaining seven wells (A-1,-2,-3, B-1, C-2,-3, D-1) were closed within three hours. Both well-head pressure and flow rate were monitored during the test. AE were measured in an instrumentation well of 15m depth which had been drilled into the tuff(see Figure 9).

Figure 6 shows the ringdown count rate vs time along with flow rate. As shown in the figure, the acoustic emission activity increases with decreasing flow rate. It is also noted that the successive valve closures of multiple wells or the large change of flow rate within a short period induced a lot of acoustic emissions.

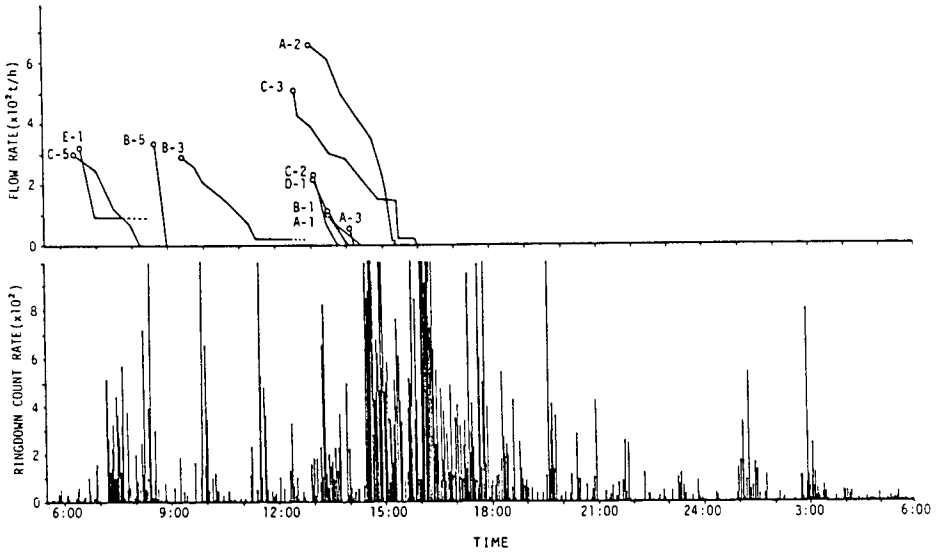


Figure 6. AE ringdown count rate and flow rate versus time during built-up test (July 15, 1982)

Figure 7 shows the change of each well-head pressure and the occurrences of individual AE as a function of time, where the height of open circle means AE event energy. Although a detailed analysis is needed to correlate the well-head pressure with the bottom pressure, the transient behavior of well-head pressure and the variation of AE activity is very similar to that suggested in Figure 3.

The AE signals detected were processed by the same procedure, and the AE source locations were determined by using the p- and s-wave velocities of 3560m/s and 2060m/s respectively. Figure 8 is a plane distribution of AE sources. The AE sources are localized in a southeast region of the field, surrounded by faults. It is also shown that the active area seems to extend gradually outward during the valve operation. Figure 9 shows the vertical projection of the AE sources detected near A-A' section of Fig.8.

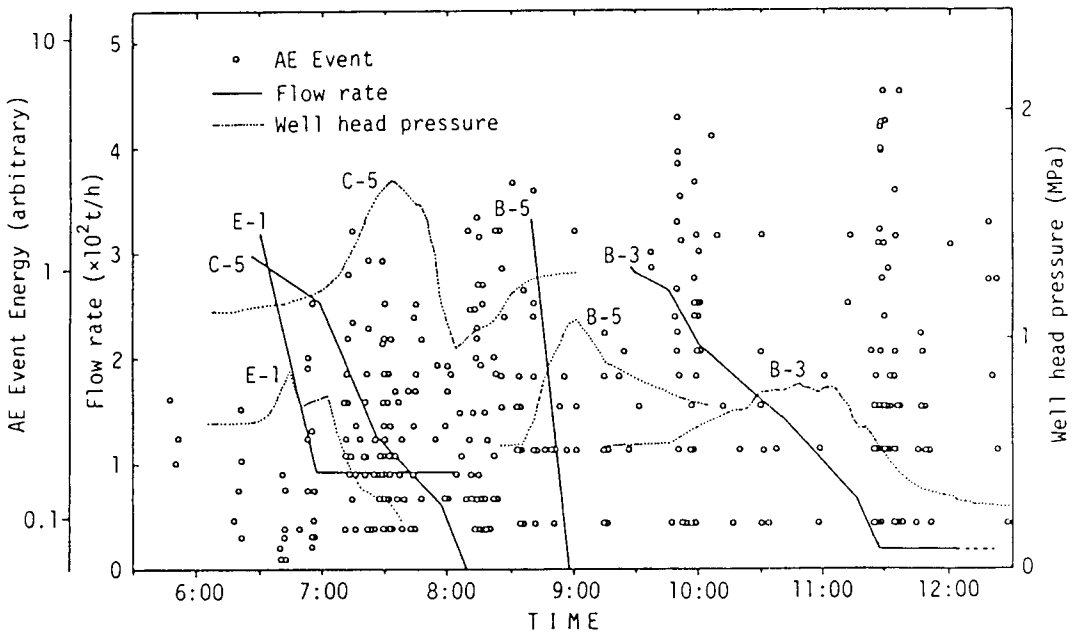


Figure 7. AE event energy, flow rate and well-head pressure versus time (July 15, 1982)

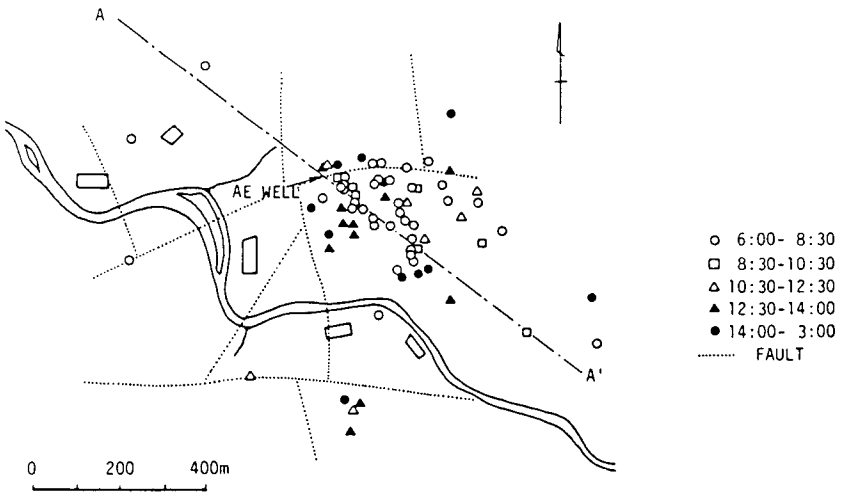


Figure 8. Plane distribution of AE sources detected during built-up test (July 15, 1982)

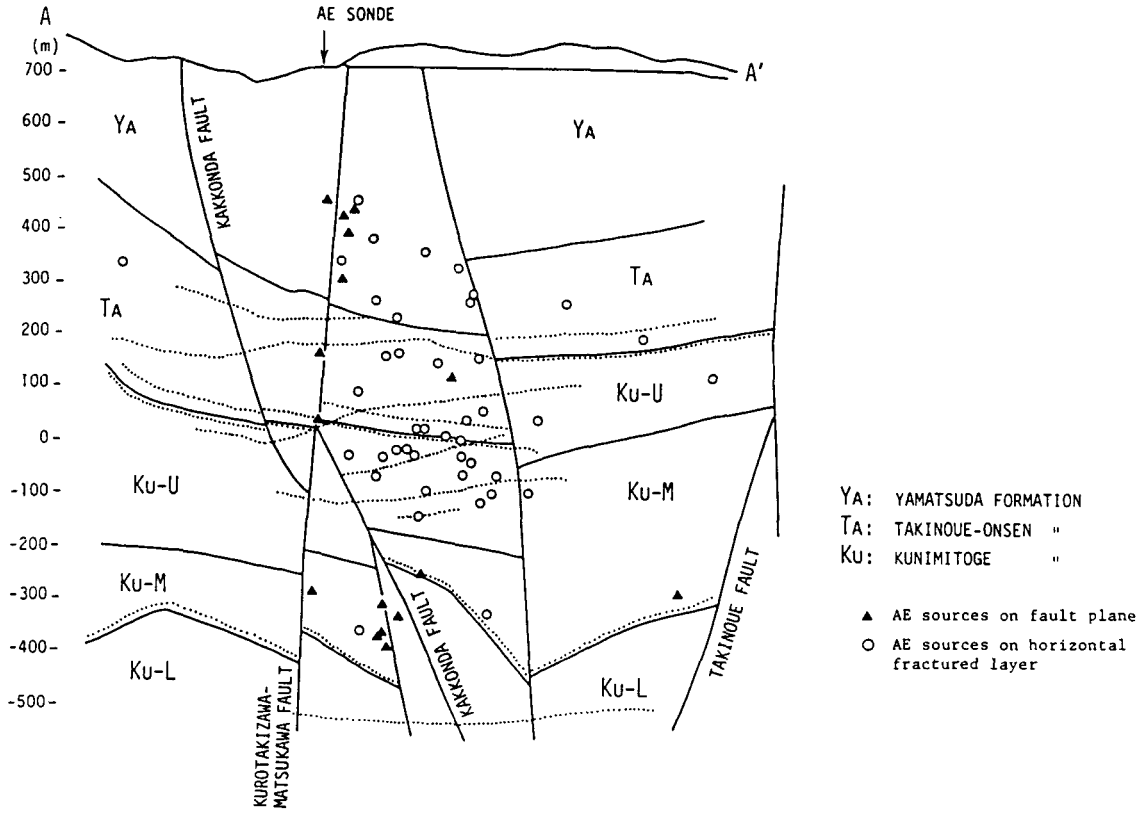


Figure 9. Vertical projection of AE sources detected near A-A' section of Fig. 8

It is found that AE sources and their time variation are closely related to the successive movements of reservoir cracks. Based on the built-up valve operation and AE data we can understand a detailed structure of the geothermal reservoir cracks at Kakkonda, with special reference to the geological fine discontinuities.

ACKNOWLEDGMENTS

The work was supported by Ministry of Education, Science and Culture under Grant-in-Aid for Energy Research Nos. 505514, 56045015, 57045014 and 58045010. The assistance of Mr. T. Shōji is gratefully acknowledged.

REFERENCES

Abé, H. et al., (1976), "Growth Rate of a Penny-Shaped Crack in Hydraulic Fracturing of Rocks," Journal of Geophysical Research, 81-29, pp. 5335-5340.

Katagiri, K. et al., (1980), "Hydraulic Fracturing Aids Geothermal Field Development," World Oil, 191-7, Dec., pp. 75-88.

Nakamura, H., (1977), "Volcanoes as Possible Indicators of Tectonic Stress Orientation-Principle and Proposal," J. Volcano, Geotherm. Res., 2-1, pp. 1-16.

Nakamura, H. and Sumi, K., (1981), "Exploration and Development at Takinoue, Japan," Geothermal Systems: Principle and Case Histories, Chapt. 9, John Wiley and Sons, pp. 241-271.

Niitsuma, H. et al., (1983), "In-Situ AE Measurement of Hydraulic Fracturing at Geothermal Fields," Hydraulic Fracturing and Geothermal Energy, Proc. 1st Japan-US Joint Seminar and Symposium, Nov. 1982, Martinus Nijhoff Publishers, Netherlands, pp. 357-371.

Sato, K., (1982), "Analysis of Geological Structure in the Takinoue Geothermal Area," J. Geothermal Res. Soc. Japan, 3-3, pp. 135-148.

Sato, K. et al., (1983), "Analysis of Hydraulic Fracturing Based on Fracture Mechanics in Japanese Geothermal Wells," Hydraulic Fracturing and Geothermal Energy, Proc. 1st Japan-US Joint Seminar and Symposium, Nov. 1982, Martinus Nijhoff Publishers, Netherlands, pp. 113-123.

Proceedings Ninth Workshop Geothermal Reservoir Engineering
Stanford University, Stanford, California, December 1983
SGP-TR-74

THE COST EFFECTIVENESS OF FRACTURE STIMULATION IN INCREASING THE FLOW FROM GEOTHERMAL WELLS*

Gerald L. Brown, The BDM Corporation

Albuquerque, New Mexico 87185

ABSTRACT

The cost effectiveness of fracture stimulation at The Geysers, the Imperial Valley, and other geothermal resource areas in the United States was studied using GEOCOM, a computer code for analyzing the impact of completion activities on the life-cycle costs of geothermal wells. Technologies for fracturing the reservoir near the wellbore involve the creation of a pressure pulse in the wellbore by means of either hydraulic or explosive force. The cost of a single fracture stimulation job can vary from $50,000 to over $500,000, with a typical cost of around $300,000. The code shows that additional flow achieved by fracture stimulation must exceed 10,000 pounds per hour for each $100,000 invested in stimulation in order for a fracture treatment to be cost effective. In some reservoirs, this additional flow must be as great as 30,000 pounds per hour. The cost effectiveness of fracturing has not yet been demonstrated in the field. The Geothermal Well Stimulation Program achieved an overall average of about 10,000 pounds per hour for each $100,000 invested.

INTRODUCTION

In many geothermal reservoirs the majority of the wells that are drilled produce sufficient flow of high temperature fluids to be economic, but this is not always the case. Even in the best fields, it is common to drill production wells in which there is inadequate flow of fluids even though the wellbore itself is free of problems that would impede flow. Techniques that are commonly used to increase or "stimulate" flow from such wells include:

(1) Redrilling the well (e.g., to deepen or underream it, or to drill a new leg)
(2) Pumping the well
(3) Treating the producing formation with chemicals (e.g., acid washing)
(4) Fracturing the producing formation.

A sometimes viable alternative is to abandon the existing well (perhaps using it as an injector) and to drill a new production well.

In determining which technique to use, it is important to estimate both the cost and the effectiveness of each option.

The stimulation procedure considered in this paper is fracturing the formation. This is achieved by increasing the pressure inside a wellbore to the point that the formation surrounding the wellbore fails in tension and parts (either at the site of a pre-existing crack or via a new fracture). Fracturing is intended to increase the flow into the well by increasing its surface area in the producing formation or by connecting it to existing fractures that will supply reservoir fluids.

Although stimulation, in general, and fracturing, in particular, are common completion practices in petroleum drilling, they have not been widely used in geothermal extraction. Accordingly, a U.S. DOE program was undertaken to investigate and develop stimulation techniques for geothermal wells.[2] Several different stimulation techniques were investigated in this program and tested at different geothermal fields. Most of the fracture stimulation tests that were run succeeded in producing new fractures, and some of the experiments resulted in additional flow into the wellbore. However, in spite of these technical successes, none of the experiments increased flow enough to be economically successful.

The results presented in this paper are part of those arising from a study investigating the additional flow is necessary for fracturing to be economically attractive.[1] The study was done using an existing economic model, GEOCOM[4,5], to analyze the cost-benefit ratio for stimulation operations. The analysis was performed to help establish priorities for tasks under consideration for Sandia National Laboratories' Geothermal Technology Development Program. Though derived for internal use, many of the conclusions are of general interest.

THE GEOCOM MODEL

The GEOCOM computer model was developed as an internal management tool to answer questions concerning the cost effectiveness of geothermal completion practices.[3] The model facil-

*Work performed under the auspices of the U.S. Department of Energy, Contract No. DE-AC0476-DP00789.

itates comparison of the potential cost effectiveness of various technology development options and aids in project selection. In particular, it considers the cost and revenue streams associated with a well and can be used to determine rates of return or life-cycle effectiveness. The GEOCOM model is implemented in ANSI FORTRAN.

The specific GEOCOM output utilized in this study is the ratio of life cycle cost to benefit (expressed in dollars per million Btus of energy produced) for a geothermal well. Life cycle costs include capital, operating, maintenance, workover and abandonment costs. The modeling of the energy produced includes the quality of the fluid (temperature, steam content, etc.) and the end use for it, and accounts for the time when the production takes place (considering reservoir decline rates, well shut-in periods, etc.). The model inflates and discounts both costs and benefits over the life of the well.

One aspect of the model that makes it particularly useful in evaluating and comparing completion alternatives is its default data base that summarizes well and reservoir performance, cost factors, and production histories for several U.S. geothermal areas. Due to the default data, analysis of the cost effectiveness of fracture stimulation required only the independent computation of representative stimulation costs in order to conduct parametric studies. Some of the default data for six U.S. geothermal areas are presented in Table 1. The bottom row of Table 1 presents the GEOCOM estimate of the cost benefit ratio for producing fluid from the "default well" at each area.

TECHNIQUES AND COSTS OF FRACTURE STIMULATION

Fracture stimulation requires the creation of a large pressure pulse within the wellbore that can be effectively coupled to the producing formation. The two most common methods of creating such a pulse are hydraulic pressure and chemical explosives. Both methods were developed for use in oil and gas wells and were tested in the Geothermal Stimulation Program.

Figure 1 schematically represents the physical setup for a hydraulic fracture stimulation. The zone to be fractured is sealed above and below by packers, hydraulic tubing is stabbed through the top packer, and proppants and gel (to suspend the proppants) are pumped through the tubing at high rates and pressures. The cost of hydraulic fracturing can be dominated by the costs of these materials (fluids and proppants). A typical stimulation would require 5000 barrels of fluid and 100,000 pounds of proppant for a total material cost of $100,000. Pumping and related services comprise the second largest component of cost in hydraulic fracturing. It might typically cost $70,000 to pump at the high rates (a barrel a second) and high pressures (3000 psi) necessary. Rig costs, for setting the packers and running tubing might add roughly $40,000; and other costs would bring the total to about $250,000 of direct costs for hydraulic fracturing.[4,7]

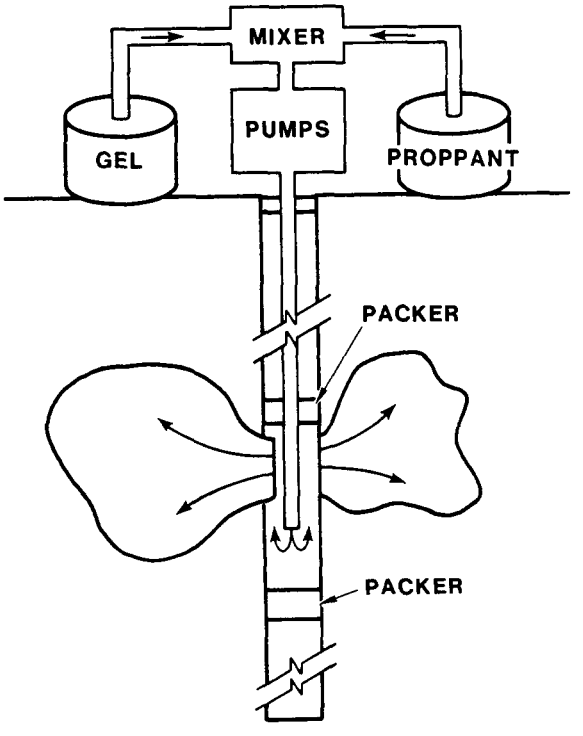


Figure 1. Schematic Representation of Hydraulic Fracturing

Explosive stimulation involves lowering explosives into the well and detonating them in the interval to be fractured. The direct costs for explosive fracturing are generally considerably less than for hydraulic fracturing. The major cost is the cost of expendable hardware which is likely to be in the neighborhood of $200 per linear foot of well to be stimulated[4]. An average stimulation (200-foot treatment interval) would require $40,000 in expendable hardware, including 1600 pounds of propellant, 30 sections of casing, and a detonator system. The costs of the services needed to support the stimulation would bring total direct costs to about $60,000. Though considerably less expensive than hydraulic fracturing, there are many situations in which explosive stimulation is impractical or ineffective.

The indirect costs of fracturing can sometimes exceed the direct costs. The major contributor to indirect cost is often the requirement for a compatible well completion. In general, neither hydraulic nor explosive stimulation can be accomplished from inside a production liner. Typically, an uncemented liner can be removed and replaced for approximately $100,000[4]. Similarly, stimulation may re-

quire a higher density of perforations in a cemented liner. A remedial perforation of a 200-foot interval would cost approximately $50,000[4]. In summary, the indirect costs of fracturing are scenario dependent and can add significantly to stimulation costs.

Table 2 presents the hydraulic fracturing costs that were experienced in the Geothermal Well Stimulation Program[7,8,9]. The table indicates a typical cost of about $300,000. The large indirect costs for the Raft River experiments reflect the fact that the wells had to be recompleted before they could be fractured.

Location	Cost $ (1000s) Direct	Indirect
Valles Caldera	360	40
Raft River	64	240
Raft River	129	281
East Mesa*	420	34
The Geysers	300	34

*Sum of costs for two experiments in the same well.

Table 2. Hydraulic Fracturing Costs from the Geothermal Well Stimulation Program

COST EFFECTIVENESS

The basic measure used to evaluate the effectiveness of fracture stimulation is its effect on the well's cost-benefit ratio in dollars per Btu of fluid produced over the life of the well. There are several ways that this ratio could be used to evaluate stimulation operations.

If the well being stimulated is subeconomic before stimulation, the true measure of effectiveness of the stimulation is whether it converted the well into an economic producer. This would require sufficient additional flow to significantly reduce the well's cost benefit ratio. Along this line, an indication is given in the "Results" section of the flow required for a relatively small reduction in the ratio. However, this standard is highly well-specific and cannot be applied in general analyses.

A second way to evaluate stimulation effectiveness is to compare the cost-benefit ratio for stimulation to the ratio for a good "default" producing well in the same field (as in Table 1). This would appear to indicate whether money is better spent in stimulating an existing well or in drilling a new one; although it ignores the probabilities of success for each.

A third, related way to evaluate effectiveness is to determine whether the stimulation improves the cost-benefit ratio of the well being stimulated. This is the standard used to evaluate effectiveness in this discussion and in the "Results" section below. This criterion can be expressed in a simplified form as

$$\frac{\text{well cost without stimulation}}{\text{energy produced without stimulation}} > \frac{\text{well cost with stimulation}}{\text{total energy produced}}$$

Since this criterion uses well cost and flow, it appears to be well specific. However, as shown below, in the cost and flow regions of interest, it is not. The major drawback to this criterion is that it ignores the well-specific questions of resulting total flow and overall well efficiency.

METHODOLOGY

The extensive GEOCOM data base allows the analysis of fracture stimulation to be done fairly easily. Building on the default values for each location, only the data on stimulation costs and additional flows are necessary as inputs. A parametric analysis of the cost effectiveness of fracture stimulation was carried out for the six geothermal sites included in Table 1.

Using its default data, GEOCOM was used to produce representative cost and revenue streams for different levels of initial flow for a well and to compute the appropriate cost-benefit ratios. Following this, numerous model runs were made in which stimulation cost and initial well flow were varied throughout their ranges of interest. These results were then used to develop iso-cost curves that connect values for which the cost-benefit ratio is constant. Since these curves (presented below) are roughly linear and parallel throughout the domain of interest, their common slope is important. Its value indicates the ratio between incremental additional stimulation cost and incremental additional flow for which the cost-benefit ratio for the well remains constant. That is, this slope represents the additional flow per stimulation dollar which must be exceeded by a fracture stimulation operation if it is to reduce the cost-benefit ratio of the well.

MODEL RESULTS

Wells were analyzed for several different geothermal fields. Typical results are shown for four areas in Figure 2.

For wells in the Imperial Valley, increases in initial flow of 25,000 to 30,000 pounds per hour are required per $100,000 invested in stimulation in order for the stimulation to maintain the same overall cost of energy from the well. On the other hand, at The Geysers only 6000 to 8000 pounds per hour of additional flow are needed for each $100,000. An intermediate value of 15,000 to 20,000 pounds per hour is required at Roosevelt Hot Springs. These differences arise from the varying qualities of the fluids produced and from the different well costs, well performances, and well lifetimes for the different areas.

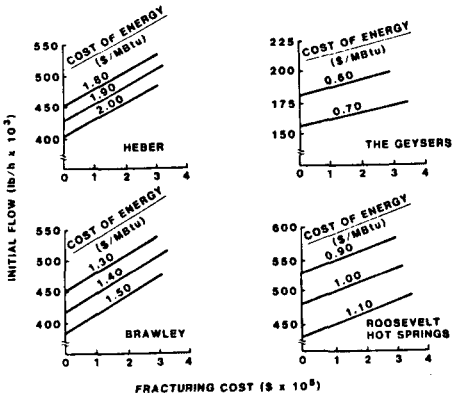


Figure 2. GEOCOM Results for Four Areas. The curves are iso-cost curves for different unit costs of energy.

The determination of the break-even values cited above for the various geothermal areas is illustrated in Figure 3. The common slope of the parametric iso-cost curves, denoted "a" in the figure, is the criterion value. The model was not used to determine energy costs outside the indicated ranges, and so there is no reason to assume that the linearity extends over greater ranges of either cost or flow. In addition, these results ignore reservoir-specific factors that drive cost and affect resulting flow. Nonetheless, the threshold values are important.

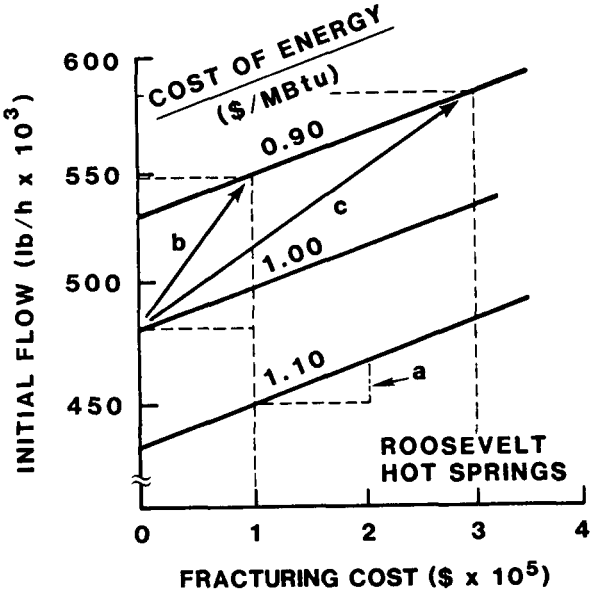


Figure 3. Sample Calculations

Even greater amounts of initial flow are required to significantly reduce the cost of producing energy. For example, lowering the cost of one MBtu from the Heber well by ten cents (5%) would require approximately 50,000 pounds per hour of additional flow for a $100,000 fracture stimulation. At Roosevelt Hot Springs approximately 70,000 pounds per hour of additional initial flow for a $100,000 expenditure would result in a 10% decrease in energy costs ("b" in Figure 3). However, these results are not proportional. Roughly 100,000 pounds per hour for a $300,000 expenditure at Roosevelt would have the same effect. These calculations are shown by "c" in Figure 3. Similar estimates can be made for other wells from the data shown in Figure 2.

Although these parametric results derived from the model are interesting, they represent only one way to evaluate cost effectiveness. They do not consider the reservoir parameters that affect whether or not stimulating the reservoir is possible or if it makes sense. The results also ignore the effect of the fluid temperature after stimulation. Higher temperature flow can be as valuable as greater quantities of flow. The GEOCOM model was used to study this and several other parameters, but the results are not discussed in this paper.[1]

EXPERIMENTAL RESULTS

The GEOCOM modeling results place in perspective the limited results of the geothermal fracture stimulation experiments. The field tests that have been conducted have averaged an increase of 8000 to 15,000 pounds of fluid in initial flow per $100,000 invested. This appears to be close to the breakeven point for some of the reservoirs; but for most reservoirs, it is considerably below the level necessary to significantly reduce the costs of producing fluid from a marginal well.

CONCLUSIONS

Fracture stimulation is an expensive operation with insufficient geothermal experience to allow high-confidence estimates of its cost effectiveness. Based on modeling and limited experimental results, it appears that for the most favorable geothermal fields, a successful fracture stimulation can be nearly a breakeven operation (in terms of its effect on total energy costs). However, analysis and experience indicate that the effectiveness of fracture stimulation must be greatly improved before it can be used with confidence to salvage nonproductive wells (by significantly reducing the total energy costs). Fracture stimulation has been used for years in oil and gas wells; and because of the maturity of this technology, the costs of fracture stimulation are not likely to fall. Instead, the most promising areas for work relative to geothermal wells would be in improving effectiveness (as measured by increased flow) and in increasing the probability of success. A key element in this work will be developing an understanding of the fractures that can be produced by different stimulation techniques and how they interact with geothermal reservoirs.

Table 1.

Default GEOCOM Data for Six U.S. Geothermal Areas

Parameter	1	2	3	4	5	6
Location	Brawley	Heber	E. Mesa	The Geysers	V. Caldera	Roosevelt H.S.
Temperature (°F)	344	360	340	365	358	344
Well Depth (ft.)	6000	8000	7600	8000	6000	7500
Well Life (mo.)	120	120	120	330	360	200
Flow (lbs./hr.)	500,000	500,000	500,000	200,000	200,000	580,000
Steam Fraction	.058	0	0	1.	.30	.20
Dissolved Solids (PPM)	80,000	14,000	2,200	0	6,100	6,500
Well Cost ($)	612,600	771,300	723,600	1,131,600	1,075,300	1,129,300
Workover Interval (yrs.)	1	2	5	5	5	5
Workover Delay (mo.)	.25	.25	.25	.25	.25	.25
Flow Decline-Reservoir (frac./mo.)	.004	.005	.005	.00195	.00308	.004
Flow Decline-Correctable (frac./mo.)	.03	.01	.005	0.0	.01	.01
Cost/Benefit of Fluid ($/MBTU)	1.17	1.60	1.71	0.54	1.58	0.87

Table 1. Default GEOCOM Data for Six U.S. Geothermal Areas

REFERENCES

1. Brown, G. L., "Geothermal Wells--The Cost Benefit of Fracture Stimulation Estimated by the GEOCOM Code," SAND83-7440, September 1983.

2. Cambell, D. A., et al., "A Review of the Geothermal Reservoir Well Stimulation Program," Proceedings of International Conference on Geothermal Drilling and Completion Technology, 1981.

3. Carson, C. C., "The Impact of Common Completion and Workover Activities on the Effective Costs of Geothermal Wells," SPE 11155, Society of Petroleum Engineers Conference, October 1982.

4. Mansure, A. J., et al., "Geothermal Completion Technology Life Cycle Cost Model (GEOCOM)," SAND82-7006, July 1982.

5. Mansure, A. J. and C. C. Carson, "Geothermal Completion Technology Life Cycle Cost Model (GEOCOM)," Geothermal Resources Council Transactions Vol. 6, October 1982, p. 203.

6. Morris, C. W., et al., "Fracture Stimulation Experiment in Baca 20," Geothermal Resources Council Transactions, Vol 6, October 1982, p. 211.

7. Republic Geothermal, et al., "Hydraulic Treatment of Well Baca 23," Geothermal Reservoir Well Stimulation Program DOE Contract DE-AC04-79- AL10563, June 1981.

8. -- "Raft River Well Stimulation Experiments," February 1981.

9. -- "Hydraulic Fracture Stimulation Experiments in East Mesa," February 1981.

Proceedings Ninth Workshop Geothermal Reservoir Engineering
Stanford University, Stanford, California, December 1983
SGP-TR-74

CRUSTAL ROCK FRACTURE MECHANICS FOR DESIGN AND CONTROL OF ARTIFICIAL SUBSURFACE CRACKS IN GEOTHERMAL ENERGY EXTRACTION ENGINEERING (Γ-PROJECT)

Hiroyuki Abé and Hideaki Takahashi

Faculty of Engineering, Tohoku University
Sendai 980, Japan

INTRODUCTION

Recently a significant role of artificial and/or natural cracks in the geothermal reservoir has been demonstrated in the literatures (Abé, H., et al., 1983, Nielson, D.L. and Hullen, J.B., 1983), where the cracks behave as fluid paths and/or heat exchanging surfaces. Until now, however, there are several problems such as a design procedure of hydraulic fracturing, and a quantitative estimate of fluid and heat transfer for reservoir design.

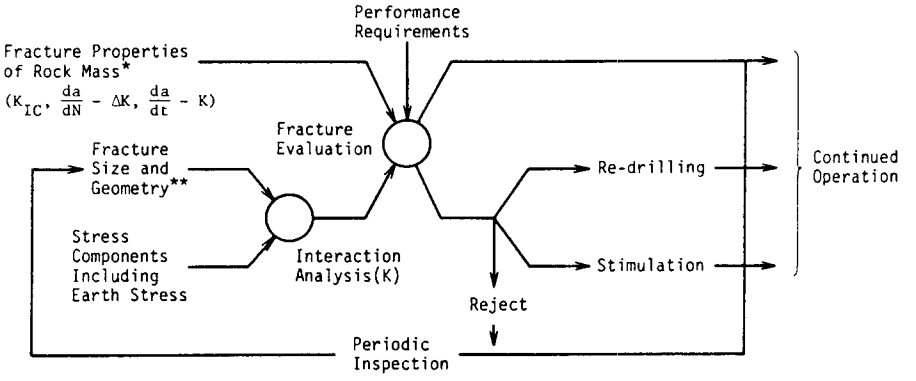
In order to develop a design methodology of geothermal reservoir cracks, a special distinguished research project, named as "Γ-Project", started at Tohoku University (5 years project, 1983-1988). In this project a basic fracture mechanics model of geothermal reservoir cracks is being demonstrated and its validation is being discussed both theoretically and experimentally. This paper descibes an outline of "Γ-Project".

FRACTURE MECHANICS CONCEPT OF GEOTHERMAL RESERVOIR: BACKGROUND OF "Γ-PROJECT"

Linear Elastic Fracture Mechanics has been shown to be a powerful tool for the study of cracking behavior in material engineers, who have analysed the brittle failure of structural engineering components. Now the fracture mechanics approach is being employed to provide new insight into the fracture of rocks, especially, in the design of crack-like geothermal reservoirs of both hot water/steam dominated and hot dry rock (HDR) types.

Figure 1(a) shows an evaluation procedure for crack-like geothermal reservoirs based on Fracture Mechanics, where a full understanding of three basic quantities, the fracture properties of rock mass under the crustal condition, the location and size(geometry) of cracks, and stress components including earth stress is prerequisite. Fracture extension can be analysed in terms of the stress intensity factor. If the stress intensity factor is raised above a critical value, K_c, which is a material constant, then the crack will propagate. recently it is found that the value K_c is influenced by the aggressive environment, when a crack tip strain rate is enough low for a chemical reaction. In addition, for many rocks, crack extension can occur at much lower values of K than K_c. Therefore, a variety of environmentally dependent mechanisms, notably stress corrosion cracking, can facilitate this stable, quasistatic subcritical crack propagation.

Figure 1(b) and (c) give an illustrative evaluation procedure of crack extension control both during hydraulic fracturing and heat extraction operation, respectively. Here the crack exten-



* Includes effect of operating environment, etc.
** Includes expected crack growth due to corrosion, fatigue, etc.

Figure 1(a) Schematic representation of an idealized fracture control for geothermal reservoir

sion behavior is evaluatied essentially by use of fracture mechanics parameter (K) analysed numerically and rock fracture data (K_{IC}, da/dN-ΔK, da/dt-K) determined experimentally. Considering a model construction of the geothermal reservoir, geological inhomogenuities such as faults, joints and layered structures should be taken into account. Figure 2 gives a new crack

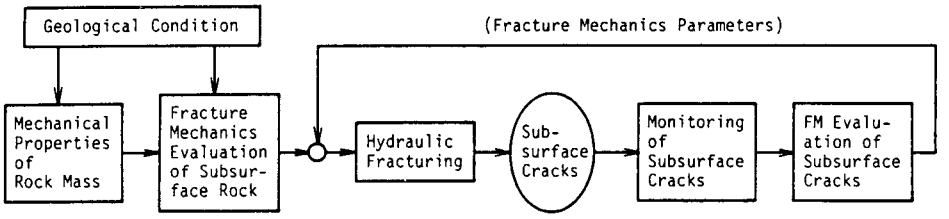


Figure 1(b) Illustrative procedure for creation of reservoir cracks by hydraulic fracturing

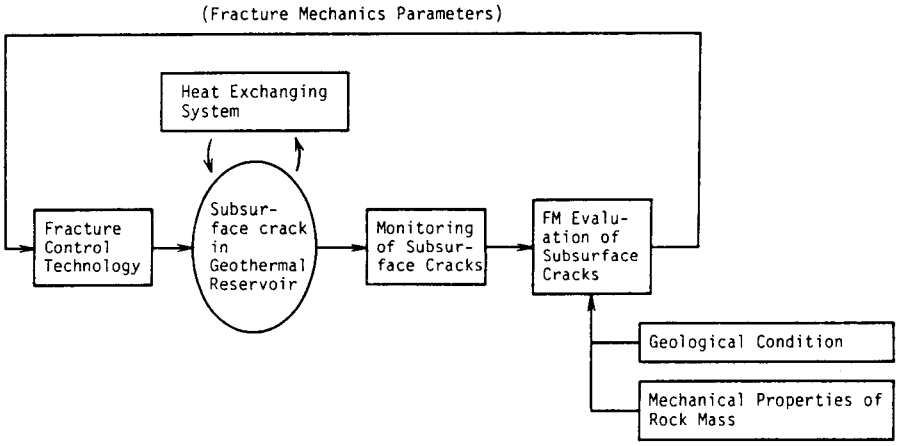


Figure 1(c) Illustrative procedure for control of reservoir cracks

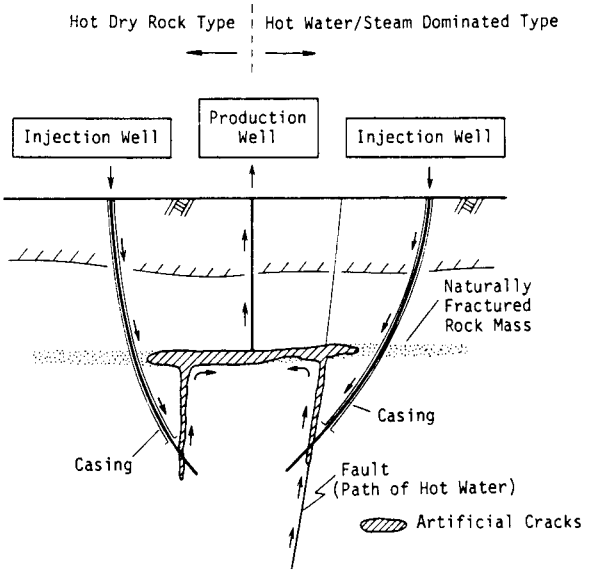


Figure 2 Role of cracks in geothermal energy extraction applicable to both HDR and hot water/steam dominated reservoir project by GEEE, Tohoku University

model proposed by GEEE, Tohoku University, where a role of a subsurface crack as a fluid path and/or a heat exchanging surface is demonstrated both for an HDR and a hot water/steam dominated reservoirs which consist of various geological inhomogeneity. Consequently, when the fracture mechanics description of geothermal crack is made accurately enough, we can design the location, size and geometry of cracks as well as the amount of heat extraction from the rock mass.

OUTLINES OF "Γ-PROJECT"

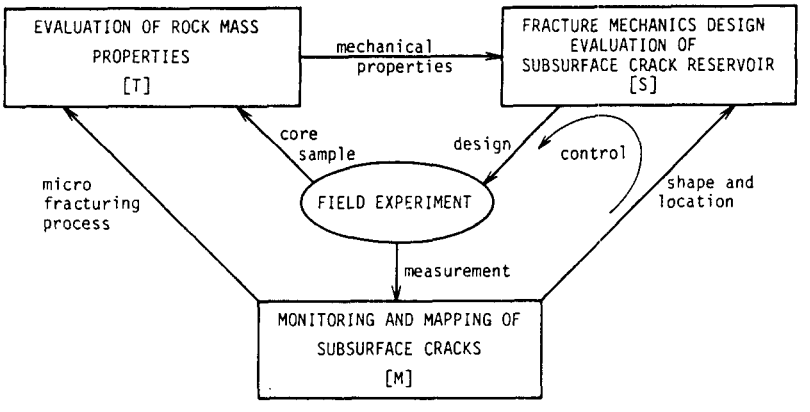
a. Research organization

"Γ-Project" is supported by the Government of Japan, Ministry of Education, Science and Culture (MESC), and is a grant-in-aid for special distinguished research. Table 1 shows a program organization, key personnels and their contributions in GEEE at Tohoku University. In this project field experiments such as hydraulic fracturing should be made to confirm a validation of the fracture mechanics approach, where an extensive cooperative investigation is planned in a variety of interdisciplinary fields as shown in Fig. 3.

Table 1 Research group of geothermal energy extraction engineering (GEEE), Tohoku University

Research Areas	Personnels and Organization	
[T] Evaluation of Rock Mass Mechanical Properties	Prof. H. Takahashi**	Research Institute for Strength and Fracture of Materials
	Ass. Prof. T. Shoji	
	Ass. Prof. H. Sekine	Dept. of Eng. Science
[S] Fracture Mechanics Design and Evaluation of Subsurface Reservoir Cracks	Prof. H. Abé*	Dept. of Mech. Eng.
	Ass. Prof. K. Hayashi	
	Ass. Prof. H. Sekine	Dept. of Eng. Science
[M] Monitoring and Mapping of Subsurface Cracks	Ass. Prof. K. Nakatsuka	Dept. of Mining and Minerals Eng.
	Ass. Prof. H. Niitsuma	Dept. of Elect. Eng.

* Chairman of GEEE ** Vice-chairman of GEEE



[T] EVALUATIONS OF ROCK MASS PROPERTIES

[S] FRACTURE MECHANICS DESIGN AND EVALUATIONS OF SUBSURFACE CRACK RESERVOIR

[M] MONITORING AND MAPPING OF SUBSURFACE CRACKS

Figure 3 GEEE organization showing the research areas and their cooperations

b. Main purposes of "Γ-Project"

Brief description of 5 years project research is given in Table 2. This project can be devided into three research phases, Phase I, II and III. The maximum crack sizes including specimen size or well depth are different in each phase as shown in Table 3.

Main topics and highlights in each project phase are as follows:

Phase I: Theoretical and experimental validation of rock fracture mechanics should be made during the hydraulic fracturing experiments of medium size specimen (1m × 1m × 1m sample size) and large size specimen (10m × 10m × 10m, "Field Laboratory") (see Fig. 4)

Phase II: Application phase of "Phase I Project"; Field experiment should be interpreted based on rock fracture mechanics. Several new exploration techniques and equipments will also be developed (see Fig. 5)

Phase III: (i) Data of rock fracture properties under the simulated geothermal reservoir condition will be collected by use of autoclave test facilities (see Fig. 6)
(ii) Theoretical modeling and computer simulation of fluid and heat transfer are made where the design procedure of an actual geothermal reservoir is discussed.

Table 2 Time schedule of "Γ-Project", (Total budget: ¥440 million)

	1983	1984	1985	1986	1987
Phase I	Labo hydraulic fracturing [1] (Specimen size: 0.5m×0.5m×0.5m)	Labo hydraulic fracturing [2] (Specimen size: 1m×1m×1m)	Hydraulic fracturing in "Field Laboratory" (1st and 2nd exp.) (Specimen size: 10m×10m×10m)		
Phase II	Selection of test site	Drilling of core sample and exploration (Well depth: ~500m)	Drilling of fracturing well (Well depth: ~500m)	Main hydraulic fracturing (1st and 2nd exp.) AE monitoring of subsurface cracks	Circulation and tracer tests
Phase III	Labo autoclave experiment: Rock fracture mechanics under the condition of actual geothermal reservoir (confining pressure: ~40MPa, temperature: ~350°C, in pressurized hot water) Transmission properties of elastic wave in rock mass				
	Computer simulation: Theoretical modeling of heat and fluid transfer, and heat extraction from subsurface rock mass				

Table 3 Crack size to be evaluated in Phase I, II and III projects

Project		Well depth (Crack Size) to be evaluated	Labo. Exp. Condition	Field Validation Exp.
Phase I	(1)	0.5 m (0.1 m)	room temperature no confining pressure	———
	(2)	5 m (1 m)	———	room temperature no confining pressure
Phase II		500 m (10~50 m)	———	test temp.: max. 100°C conf. press.: max. 10 MPa
Phase III		[1~5 km (~500 m)]*	test temp.: max. 350°C conf. press.: max. 40 MPa	———

* A deep well experiment is not carried out, but several case studies for reservoir crack design will be performed in Phase III project.

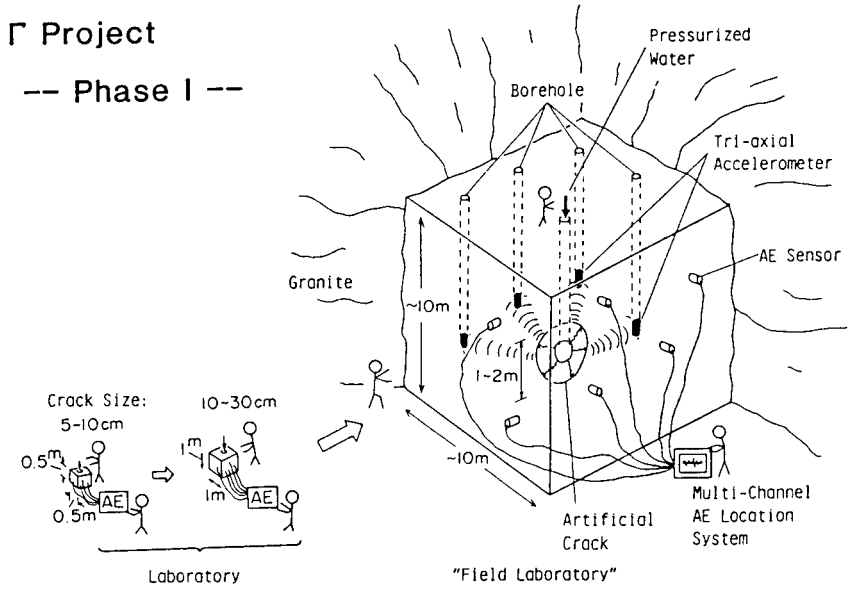
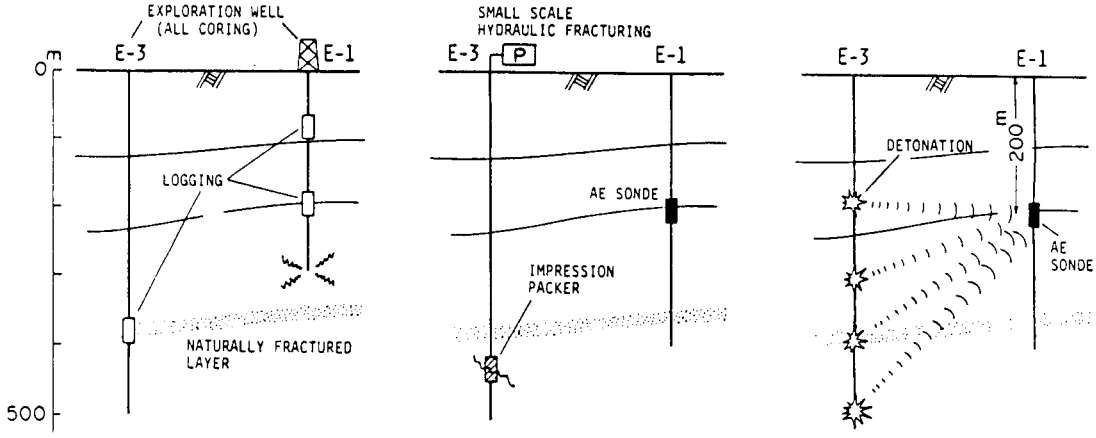


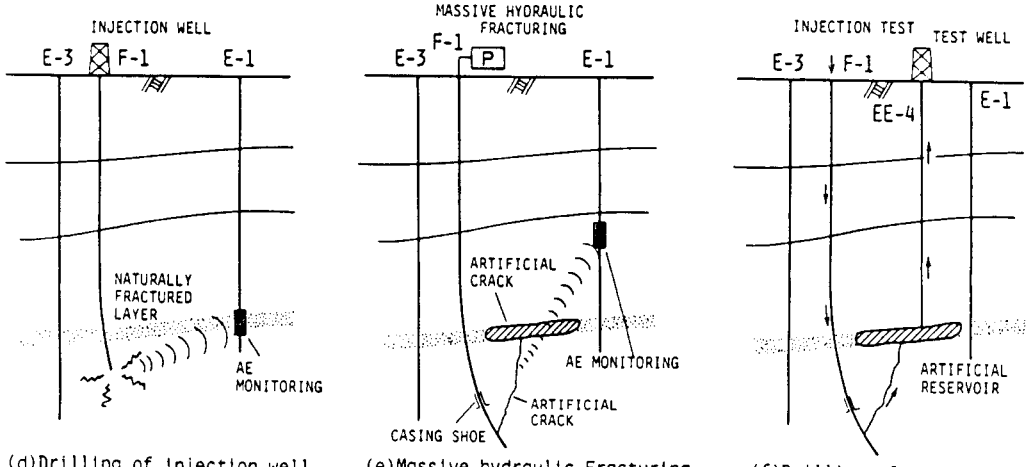
Figure 4 Hydraulic fracturing experiments in Phase I



(a)Survey of subsurface structure and evaluation of fracture toughness distribution by core sample data.

(b)Measurement of crustal stress distribution by means of small scale hydraulic fracturing.

(c)Calibration of velocity structure by detonation.



(d)Drilling of injection well with AE monitoring.

(e)Massive hydraulic Fracturing and formation of crack-like reservoir.

(f)Drilling of test well and injection test.

Γ Project

-- Phase II --

Figure 5 Field experiments and main hydraulic fracturing in Phase II project

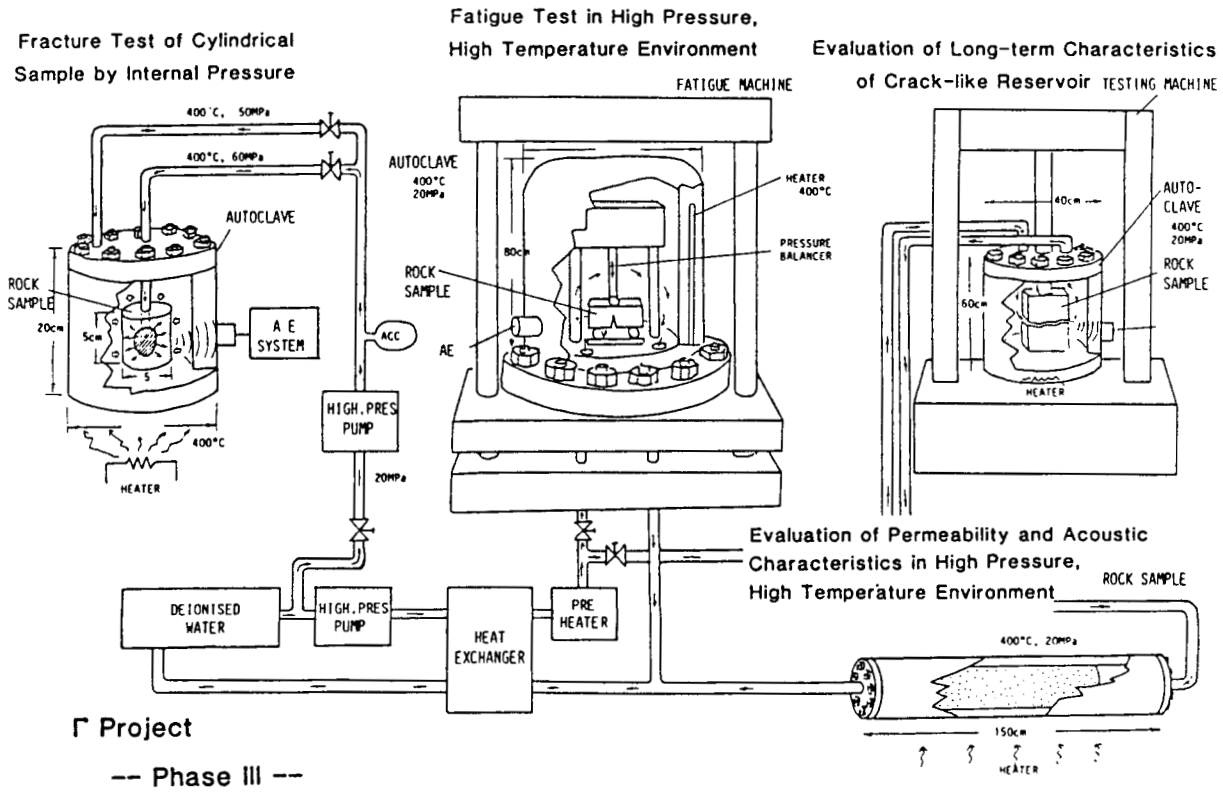


Figure 6 Autoclave test facilities in Phase III project

CONCLUDING REMARKS

With special reference to subsurface crack design methodologies applied to geothermal reservoir engineering, a validation of rock fracture mechanics concept will be demonstrated both theoretically and experimentally. Several case studies depicted in "Γ-Project" will provide an appropriate information of data interpretation in actual reservoir performances as well as well stimulations by hydraulic fracturing.

ACKNOWLEDGMENT

The authors wish express their hearty thanks to Mr. T. Shōji for his assistance in preparing the manuscript.

REFERENCES

Abé, H. et al., (1983), "Behavior of Crack-Like Reservoir by Means of Fracturing at Nigorikawa and Kakkonda Geothermal Field," in this Conference Volume.

Nielson, D.L. and Hullen, J.B., (1983), "Geologic Model of The Baca Geothermal Reservoir Valles Caldera, New Mexico," in this Conference Volume.

Proceedings Ninth Workshop Geothermal Reservoir Engineering
Stanford University, Stanford, California, December 1983
SGP-TR-74

MAPPING THE ACID STIMULATION IN THE BEOWAWE GEOTHERMAL FIELD USING SURFACE ELECTRICAL POTENTIALS

Carolyne M. Hart, Dennis Engi, and Harry E. Morris

Sandia National Laboratories
P. O. Box 5800
Albuquerque, NM 87185

ABSTRACT

A surface electrical potential system was fielded during the chemical stimulation of the Rossi 21-19 well in the Beowawe Geothermal Field. The technique, which measures variations in resistivity resulting from the flow of conductive fluid into the reservoir, was not only shown to be highly sensitive, not only to the chemical treatment, but also to the in situ conductive zones before any acid injection. A review of the experiment and a preliminary interpretation of the data are presented. The data provide convincing evidence that it should be possible to map the treated zone as well as the primary pretreatment in situ conductive zones.

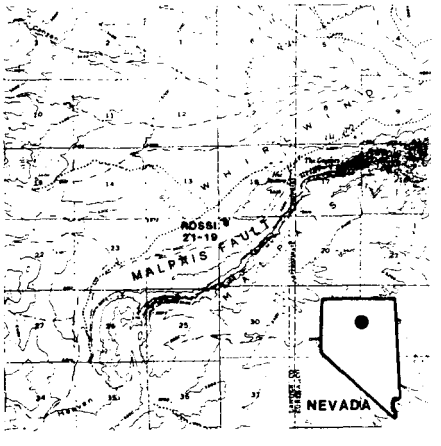
INTRODUCTION

Chevron has drilled a total of five deep wells in the Beowawe Geothermal Field in north-central Nevada. One of these wells, Rossi 21-19, has been subcommercial, even though it does intersect a high-temperature zone. Pressure interference tests have shown that all of the Chevron wells are hydraulically connected. Thus, it has been assumed that Rossi 21-19 was completed in a limited zone of restricted permeability and/or was damaged during drilling (Republic Geothermal, 1983 and Hanold, 1983).

As a part of DOE's comprehensive 8-well geothermal reservoir well stimulation program, Republic Geothermal, Inc. and its contractors performed a 60,000 gallon two-stage chemical stimulation treatment intended to remove the near-wellbore restriction suspected to exist in Rossi 21-19. Sandia National Laboratories participated in the acid stimulation experiment by fielding a surface electrical potential system that has been developed to map fracture treatments. This diagnostic technique has been used in the evaluation of hydraulic fracture treatments of oil and gas reservoirs, but had never been applied in a geothermal well or during an acid stimulation treatment. The objectives of its use at the Beowawe site were to determine whether or not the technique is sensitive to chemical treatments of geothermal wells and, if so, to map the directional nature of the treated zone.

SITE DESCRIPTION

The Beowawe Geothermal Field is located on an ENE striking Basin and Range normal fault which marks the southwest boundary of Whirlwind Valley, a few miles southwest of the town of Beowawe in north-central Nevada (see Figure 1). The complicated geology of this field has been the subject of many geologic studies, including Smith (1983), Struhsacker (1980), Zoback (1979), and Garside and Schilling (1979). The reservoir is thought to be in the lower Paleozoic carbonates at depths approaching 20,000 to 30,000 feet. The low salinity brine of the reservoir (1200 ppm TDS) flows upward from the carbonates by way of a complicated series of faults (Epperson, 1982). The east-northeast trending Malpais fault system is one of two major fault sets in the area. As shown in Figure 1, Rossi 21-19 lies along the Malpais fault zone at the base of the Malpais rim.



each square - 1 square mile

Figure 1. Map of the Beowawe Area Showing Rossi 21-19.

This work supported by the U.S.Department of Energy under Contract No. DE-AC06-76DO0789.

ROSSI 21-19

The stimulation well, Rossi 21-19, was drilled by Chevron Resources Company in 1979 to a depth of 7212 feet. A slotted liner is hung at the producing zone (4178 ft - 7213 ft). The actual production interval(s) in the well may lie anywhere in a range between 130 and 1000 ft. Interpretations of electric log data suggest possible productive intervals at 4400-4600 ft, 5000 ft and near 6100 ft. Downhole static temperature is near 386°F at 5100 ft (Republic Geothermal, 1983).

THE SURFACE ELECTRICAL POTENTIAL SYSTEM

The surface electrical potential system (SEPS) measures variations in resis- tivity contrasts resulting from the flow of a conductive fluid into the earth. This system, essentially a "misse a la masse" technique (Parasnis, 1973), utilizes the stimulation well as a current source electrode and an outlying well as the current sink. Hole-to-surface resistivity measurements are made by injecting bipolar pulses of current into the stimulation well and measuring the resultant distribution of electrical poten- tial on the earth's surface. A rigorous analysis of potential distributions resulting from a penetrating electrode has been pre- sented by Muskat (1932).

The surface distribution of equipotential lines surrounding the pole source buried in a laterally isotropic earth (a homogeneous halfspace) is in the form of concentric circles with the stimulation well as their center, as shown in Figure 2. During stimulation, the well casing, along with the associated reservoir matrix, when filled with a conducting fluid, acts as a changing current injection electrode. As the stimulation treatment progresses, the electrode geometry changes and the electrical potentials measured at the surface reflect this changing shape.

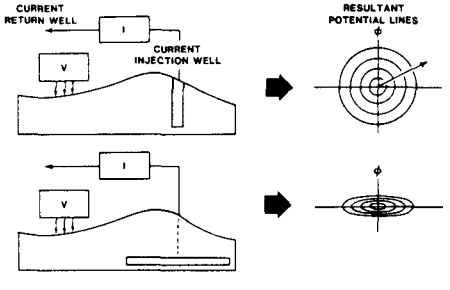


Figure 2. Surface Electrical Potential Distribution.

The SEPS da a are taken by periodically recording the induced potential differences at the earth's surface between an infinite reference probe and the data probes placed every 15° circumferentially around the stimulation well. Background data are taken to establish the induced potential levels around the well prior to the stimulation treatment. These data then become the reference data for detecting the changes produced when the conductive fluid alters the electrical geometry. If the electrical potentials before, during and after the stimulation are compared, diagnostic information about the directional nature of the treatment is obtained.

SEPS INSTRUMENTATION CONFIGURATION

The surface electrical potential data were taken by measuring potentials at 65 probe locations placed circumferentially around Rossi 21-19 at distances of 750 ft, 2000 ft and 4000 ft. A schematic of the probe array is presented in Figure 3. The probes were stainless steel rods measuring 18 inches in length and 1/2 inches in diameter and were driven approximately 6 inches into the ground. A wire from each probe was fed to an associated potential measurement box (PMB) located adjacent to the inner potential probe. The output from the PMB's was frequency multiplexed into cables which carried power from an instrumentation van (B-59) to the PMB's and transmitted data from each PMB to the instrumentation van.

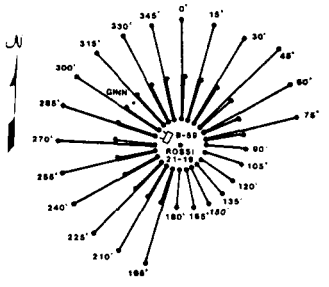


Figure 3. Surface Electrical Potential Array for Rossi 21-19 Acid Stimulation.

The potential field was created by injecting electrical current flow into Rossi 21-19. Bipolar current pulses from a series of solid gel batteries was injected at the Rossi 21-19 wellhead, and the current was returned via two current return (sink) wells. The first sink well, the Batz well, was approximately two miles NE of Rossi 21-19. Interference tests had previously suggested that Batz was hydrologically coupled to Rossi 21-19. Thus, this current return path was a part of the current injection electrode. The second current

return well was a windmill that was located approximately three miles SW of the injection well. This well was drilled in a shallow fresh water reservoir and had no hydraulic communication with Rossi 21-19.

The directional reversal of the injected current during each measurement was necessary to prevent polarization effects. The potential for each probe location was taken as the difference between the sampled positive and negative pulse referenced to infinity and normalized with respect to the current used to induce the field. The injected current and the data collection were controlled from the instrumentation van by a PDP 11/34 minicom- puter.

STIMULATION EXPERIMENT

The stimulation design for Rossi 21-19 was a two-stage chemical treatment confined to the slotted liner interval below 4369 ft. An abbreviated test schedule is given in Table 1. The first acid treatment included 500 bbl of 14.5 percent hydraulic acid (HCl)) displaced by 2400 bbl of water and the second treatment consisted of 982 bbl of 12 percent HCl and 3 percent hydro-floryl (HF) acid solution followed by 4000 bbl of water (Smith, M. C., 1983). Injectivity tests performed before and after stimulation indicated a 2.3 fold increase in injectivity by the end of the second treatment.

TABLE 1. TEST SCHEDULE

Date	Activity	Fluid Pumped
8/16-8/17	SEPS Background Data	None
8/20	Injectivity Test	Water
8/21	Acid Injection 1, Injectivity Test	Water & HCl Water
8/22	Acid Injection 2, Injectivity Test	Water,HCl,HF Water
8/23	SEPS Post-Test Data	None

Since the success of this diagnostic technique relies on changes in resistivity resulting from the flow of a conductive fluid into the formation, quantitative estimates of expected resistivity contrasts were made before SEP was fielded. Resistivity of the in situ brine was measured at 80 ohm-m. The effect of adding various concentrations of HCl to the sampled in situ water is shown in Figure 4. The reduction in resistivity by an order of magnitude is due almost entirely to the HCl. The addition of HF to the solutions has an insignificant effect due to the high acidity of HCl and the low ionization constant for HF. Thus, it was concluded that SEPS should easily detect the presence of HCl at the levels to be injected.

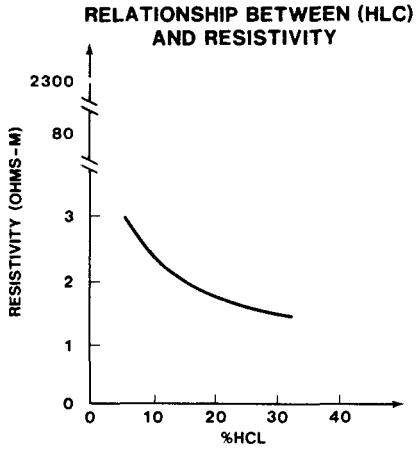


Figure 4. Resistivity vs (HCl).

PRELIMINARY DATA INTERPRETATION

SEPS data from both current return wells were collected during all of the experimental stages outlined in Table 1. A different set of data was acquired approximately every five minutes. The data was displayed in the field during real-time, so some indication of the directional nature of the treatment zone was available on site. Since that time, data from discrete times that are representative of the various experimental stages (background, injectivity tests, acid injections and post-test) have been more thoroughly examined. Analysis of these "snapshots" along with the real-time observations provide a preliminary interpretation of the subsurface activity during the chemical stimulation.

Polar plots of the background data collected around Rossi 21-19, using the Batz well for current return, are shown in Figure 5. The

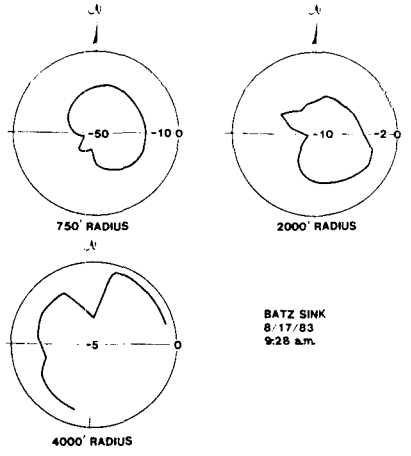


Figure 5. Polar Plot of Pre-Stimulation Potentials (mV/A) around Rossi 21-19.

windmill current return data provided similar plots. These data remained stable over a two day period. Because of the resistivity contrast between the in situ brine and the surrounding earth, the Malpais fault (60°/255°) is seen in the background data from all three radii. Also apparent in the data are a near surface conductive body at the 195°, 750 ft probe and a near surface anomaly at the 4000 ft radius in the vicinity of the 0° and 345° probes. A neighboring well, Ginn 1-13, is depicted by the protrusion in the 2000' radius, 315° probe. This probe location was within 100 ft of the 9000+ ft well. Notice that the magnitude of the potential measurement decreased because the current was sinking in this deep well.

No observations were made during the injectivity tests. This is not surprising because the water was being pumped from and reinjected to the same reservoir, thereby creating no resistivity contrast.

Some activity was observed along the known predominant fracture direction and toward the Ginn well during the hydrochloric acid stage, but the data did not indicate any significant movement during this stage. The HCl was not expected to produce any measurable stimulation effect, but was necessary to prevent formation of insoluble calcium fluoride precipitate in the formation during the second stage (Hanold, 1983).

Data from the second acid injection portray definite acid flow patterns as exemplified in Figure 6. Major acid flow paths were along the Malpais fault line (60°/255°) and along a 15°/195° path. Although not obvious from the "snapshot" displayed in Figure 6, some movement of the treatment fluids was seen along an east-west path approximately 2000 ft north of Rossi 21-19 with activity centered at Ginn 1-13. The conductive paths observed during the HCl/HF treatment are illustrated in Figure 7.

Post-stimulation data (Figure 8), when compared to the background data of Figure 5, indicate that the chemical treatments altered the in situ flow patterns. The predominant 60°/255° fracture is still present but the flow appears to be enhanced along the 60° azimuth. This is most obvious in Figure 8 from the 4000 ft radius data. The stimulation also appears to have increased permeability between Rossi 21-19 and Ginn 1-13.

Although data from the windmill sink was not presented in this paper, the response was consistent with that of the Batz well.

SUMMARY

The surface electrical potential system was fielded during the chemical treatment of

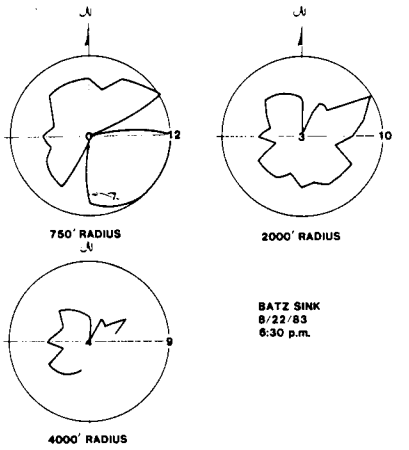


Figure 6. Polar Plot of Acid Injection 2 Potentials (mV/A) around Rossi 21-19.

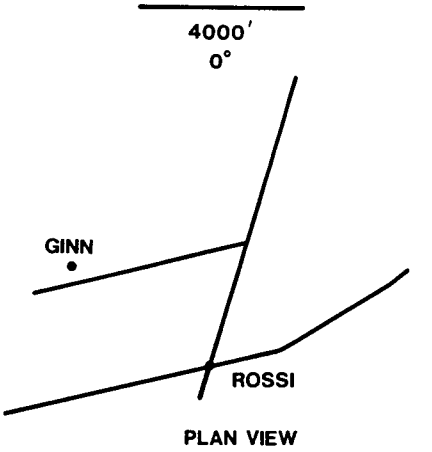


Figure 7. Plan View of Conductive Paths During Acid Injection 2.

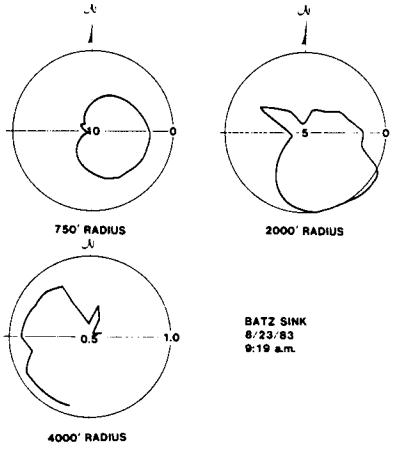


Figure 8. Polar Plot of Post-Stimulation Potentials (mV/A) around Rossi 21-19.

Rossi 21-19 in the Beowawe Geothermal Field in north-central Nevada. The objectives of its use at the Beowawe site were to determine the sensitivity of the technique to chemical treatments of geothermal wells and to map the directional nature of the treated zone.

Post-test data indicate that the stimulation indeed altered flow patterns. Moreover, the SEPS was, in fact, sensitive to the chemical treatment and there appears to be substantive data relative to the directionality of the treatment.

Because of the high conductivity of the in situ fluid, the system was able to detect a major conductive path extending along azimuths ENE and WSW from Rossi 21-19 before any acid injection. This path of flow was enhanced during the stimulation treatment and a second major flow path appeared to the NNE. Some activity was also evident in the vicinity of an adjacent well (Ginn 1-13).

REFERENCES

Epperson, I. J., "Beowawe, Nevada, Well Testing: History and Results," GRC Transactions, Vol. 6, 1982, pp 257-260.

Garside, L. J. and Schilling, J. H., Thermal Waters of Nevada, Nevada Bureau of Mines, Geological Bulletin 91, 1979.

Hanold, R. J., "Geothermal Well Stimulation Program Quarterly Progress Report," prepared for the U. S. Dept. of Energy Geothermal and Hydropower Technologies Division, October 28, 1983.

Muskat, M., "Potential Distributions in Large Cylindrical Disks with Partially Penetrating Electrodes," Physics, Vol. 2, 1932, pp 329-364.

Parasnis, D. S., Mining Geophysics, New York, Elsevier, 1973.

Republic Geothermal, Inc., "Proposal for Producing Well Chemical Stimulation Treatment, Beowawe Geothermal Field, Experiment No. 8," prepared for the U. S. Dept. of Energy Geothermal and Hydropower Technologies Division, May 1983.

Smith, C., "Thermal Hydrology and Heat Flow of Beowawe Geothermal Area, Nevada," Geophysics, Vol. 48, No. 5, May 1983, pp 618-626.

Smith, M. C., ed., Geothermal Report, Vol. xii, No. 21, November 1, 1983, pp 1-2.

Struhsacker, E. M., The Geology of the Beowawe Geothermal System, Eureka and Lander Counties, Nevada, University of Utah Research Institute, Earth Science Lab, Rep. No. 37, 1980.

Zoback, M.L.C., A Geologic and Geophysical Investigation of the Beowawe Geothermal Area, North-Central Nevada, Stanford University Publications, Geological Sciences, Vol. 16, 1979.

Proceedings Ninth Workshop Geothermal Reservoir Engineering
Stanford University, Stanford, California, December 1983
SGP-TR-74

THERMAL EXPANSION BEHAVIOR OF CERRO PRIETO SANDSTONES AND OTHER SEDIMENTARY ROCKS UNDER STRESS.

E. CONTRERAS

INSTITUTO DE INVESTIGACIONES ELECTRICAS. CUERNAVACA, MOR., MEXICO.

F. BERMEJO

COMISION FEDERAL DE ELECTRICIDAD. CERRO PRIETO, B.C., MEXICO.

ABSTRACT

This paper describes the experimental work and presents the results of a research program - carried out to investigate the thermal expansion behavior of sedimentary rocks under high stress conditions. The aspects that were investigated include the effects of temperature, temperature cycling, and confining pressure . Furthermore, the validity of the usual assumption on thermal expansion isotropy was investigated. On the other hand, the matrix thermal expansion concept is analyzed and its physical meaning and aplications are discussed. The effect of temperature on porosity is also a subject investigated regarding experimental methods for its estimation and comparison of earlier results.

The experiments carried out consisted basically of thermal strain versus temperature measurements on jacketed and unjacketed samples subjected to different confining pressures and covering the temperature range from 25°C to 280°C and the pressure range from 3.0 MPa to 34.4 MPa. A review of earlier work is included as a reference frame to discuss and compare the results of this work, as well as to emphasize the limited extent of the research on thermal expansion behavior of sedimentary rocks that had been accomplished.

Results are presented by means of thermal strain versus temperature curves and tabular data of thermal expansion coefficients. Several important conclusions for laboratory and field applications are reached from each of the aspects investigated.

The wide research scope of this work and the considerable amount of data reported may represent an important contribution to the knowledge of thermal expansion behavior of sedimentary rocks.

INTRODUCTION

The thermal expansion behavior of rocks is a subject of great interest in many reservoir engineering, geophysical, mining and similar underground applications where rocks are heated. The limited data available on thermal expansion of rocks are mostly bulk expansion data for low porosity rocks, the majority of which are igneous, generally corresponding to either atmospheric pressure and wide temperature ranges, or high pressure and narrow temperature range conditions. That is, very few results have been reported in which samples were subjected simultaneously to high stress and a wide range of temperature variations

It is well known that sandstones constitute the main producing-horizons in various geothermal fields; therefore, the importance of the thermal expansion behavior of sedimentary rocks in geothermal applications is self-evident. However, this subject has not yet been covered extensively.

In order to obtain a good knowledge about the thermal expansion behavior of rocks, it is mandatory to understand the effects of parameters such as temperature, temperature cycling, heating rate, stress, saturation, expansion anisotropy, and effect of temperature on porosity. Such an understanding is also necessary to plan the experimental measurements more adequately, thus reducing considerably the amount of experimental work required. Concerning sedimentary rocks, the effects of only some of the above mentioned parameters have so far been partially investigated. A brief review of the existing studies on this subject is included in the following.

Ashqar (1979), Somerton (1980) and Somerton et. al. (1981) reported the results of bulk thermal expansion of liquid-saturated specimens of Boise, Berea and Bandera sandstones that were subjected to 20.7 MPa confining pressure and 6.9 MPa pore pressure, while increasing the temperature from 30°C to 175°C at a rate of about 1°C/min. The samples were not subjected to temperature cycling, hence only heating strain-temperature curves were reported. These curves were compared with the strain-temperature curves for the same outcrop sandstones reported by Somerton and Selim (1961) run under dry and no confining or pore pressure conditions, and a fair agreement was found, indicating that thermal expansivities of Boise, Berea and Bandera sandstones were not strongly dependent of stress and fluid saturation.

Janah (1980), Somerton (1980) and Somerton et. al. (1981) reported results of a series of tests focused to investigate the influence of temperature on pore volume contraction for the same outcrop sandstones under stress. The specimens studied were subjected to 20.7 MPa confining pressure and 6.9 MPa pore pressure. Changes in pore volume were measured as temperature was increased from 30°C to 170°C. From their results, the authors concluded that the pore volume of liquid saturated sandstones under stress decreases with increasing temperature, and that the pore volume thermal contraction is a function of porosity, values decreasing with increased porosities. The fractional pore volume contractions reported by the authors for the Boise, Berea and Bandera sandstones for the 30°C to 170°C temperature range are 0.55%, 1.04% and 1.53%, respectively.

Janah (1980) also studied the effects of stress level on pore volume thermal contraction and noted that differences in confining stress level had little effect on it; on the other hand, increase in pore fluid pressure level had a marked effect, the pore volume contraction decreasing substantially with increased pore fluid pressure.

Greenwald et. al. (1982) presented a new set of results for exactly the same kind of experiments as carried out by Ashqar (1979) and Janah (1980) on bulk thermal expansion and thermal pore volume contraction of Boise, Berea and Bandera sandstones.

The strain-temperature curves reported by Greenwald et. al. (1982) differ to some extent from the ones obtained by Ashqar (1979), especially regarding Berea sandstone strain curves; the agreement for Boise and Bandera is fairly good. On the other hand, the fractional pore volume contractions reported by Greenwald et. al. for the Boise, Berea and Bandera sandstones for the 30°C to 170°C temperature increment are 3.0%, 3.7% and 4%, respectively, which compare badly to the 0.55%, 1.04% and 1.53% values reported by Janah (1980) and Somerton (1981). However no comments or explanations of these big dissimilarities were provided by the authors.

Assuming that all three sandstones are isotropic and thus, that the bulk volumetric strain is three times the axial strain, Greenwald et. al. (1982) combined their results of both pore volume contraction and axial thermal expansion measurements to calculate decrease in the original porosity. The results they reported are 3.0%, 3.8% and 4.4% porosity reduction for the 30°C -170°C temperature range for the Boise, Berea and Bandera sandstones, respectively. Greenwald et. al. (1982) concluded that the inclusion of bulk volume thermal expansion values in porosity determinations is a second-order correction, which led to the observation that the calculated fractional changes in porosity resulted very similar to their results for fractional pore volume changes. The authors of the present work would like to point out that such a conclusion is not always correct and would lead to significant errors in the cases where the fractional pore volume changes are of the same order of magnitude as the bulk volume thermal strain; such is the case if the pore volume contractions after Janah are considered instead of Greenwald's results.

Contreras et. al. (1982) measured the thermal strain of Berea sandstone and of a sandstone from Cerro Prieto Well M-94. The samples were tested at two different constant confining pressures of 3 MPa and 20.7 MPa, with the temperature being increased at a uniform rate of about 1.5°C/min. in the range from 20°C to 280°C. Thermal expansion measurements were made both on jacketed samples with no pore pressure, hence obtaining information about the usual bulk thermal strain, and on unjacketed samples with the confining fluid filling the rock pore volume, thus obtaining data about the so called "matrix thermal strain", a new concept that had not been introduced before in the scientific investigation on behavior of rocks. The results by Contreras et. al. (1982) showed that both, bulk and matrix thermal expansivities are dependent of the confining pressure applied to the rock. Further evidence was found that the bulk and the matrix thermal expansion coefficients depend of the temperature range itself. Furthermore, combining bulk and matrix thermal strain data and using a novel approach, Contreras et. al. (1982) presented estimates of the effect of temperature on porosity.

This short review of the existing literature clearly shows that there are several parameters whose influence on thermal expansion behavior of sedimentary rocks has not been investigated at all and that the effect of others has been investigated only in a very limited extension and mostly on outcrop sandstones.

The objectives of the present study were established to contribute to fill the main gaps of knowledge described above; consequently, in this work the following aspects are investigated in relation with thermal expansion behavior of sedimentary rocks: (1) effect of temperature cycling, (2) effect of heating rate, (3) effect of confining pressure, (4) effect of orientation with respect to the bedding plane, (5) comparison between bulk and matrix thermal strain and analysis of its significance, (6) effect of temperature on porosity. Furthermore, a big deal of data about thermal expansion coefficients of several sedimentary rocks is provided as another main result of the investigations accomplished. Unlike previous studies involving outcrop sandstones, the results presented in this paper correspond mostly to rocks from wells drilled in a very important geothermal region (the Cerro Prieto Geothermal Field area), thus increasing their importance for practical applications.

EXPERIMENTAL ASPECTS

The identification, origin and porosity at room conditions of the samples used in this work are given in Table 1. The porosities reported were measured using the liquid saturation under vacuum method. The three kinds of outcrop sandstones were chosen so as to cover a wide range of porosities. The geothermal samples were obtained from wells M-94, M-127 and M-149 drilled in the Cerro Prieto Geothermal Field, located in Baja California, México. These geothermal samples were cut perpendicular to their bedding planes from field cores using a 2.5 cm. diameter diamond drill bit, except the sample M-127-HA that was drilled out parallel to its bedding plane. After cutting the samples to a lenght of approximately 5 cm., their ends were ground flat and parallel to within 2.5×10^{-3} cm.

TABLE 1. Origin and Porosity of the Sandstones Studied.

SAMPLE IDENTIFICATION	WELL	DEPTH (METERS)	POROSITY (%)
M94-A	M94	2417	15.8
M94-B	M94	2417	15.8
M127-A	M127	2195	20.2
M127-HA	M127	2195	20.2
M149-A	M149	2160	15
KAYENTA K1	OUTCROP	----	18.6
KAYENTA K2	OUTCROP	----	18.6
KAYENTA K3	OUTCROP	----	18.6
BEREA 1	OUTCROP	----	18.8
BEREA 2	OUTCROP	----	18.8
COLTON 1	OUTCROP	----	10.9
COLTON 2	OUTCROP	----	10.9

In order to fulfill the objectives established for this work, four basic types of tests were planned and run. Their description is presented below.

Type A Tests. Intended to investigate the effect of temperature cycling on the bulk thermal strain. For these tests, a constant confining pressure of 8 MPa was applied on dry jacketed samples that were then subjected to two heating-cooling cycles in the range from 25°C to 280°C, with the temperature being changed both for the heating and cooling parts at a uniform rate of about 2°C/min. Strain and temperature were recorded during the temperature cycles once every minute. Type A tests were run on samples M127-A and M127-HA.

Type B Tests. Intended to investigate the combined effect of heating rate and temperature cycling on the bulk thermal strain. These tests were run on dry jacketed samples subjected to a constant confining pressure of 8 MPa. Each sample tested was subjected to three consecutive temperature cycles at 1, 2 and 3°C/min in the range from 25°C to 280°C. Strain and temperature were recorded during the three cycles once every minute. Type B tests were run on samples M149-A and KAYENTA K1.

Type C Tests. Intended to investigate the effect of confining pressure and temperature cycling on the bulk thermal strain. These tests were run on dry jacketed samples subjected at two or three temperature cycles in the range 25°C to 280°C; for each consecutive cycle a different confining pressure was applied to the rock, keeping the heating and cooling rates constant at 2°C/min. The values of confining pressures chosen for these tests were 3, 17.2, 20.7 and 34.4 MPa. Samples M94-A and KAYENTA K2 were subjected to temperature cycles at 3, 17.2 and 34.4 MPa. Samples BEREA 1 and COLTON 1 were subjected only to heating from 25°C to 280°C at 3 and 20.7 MPa. Strain and temperature were recorded during the tests once a minute.

Type D Test. Intended to investigate the concept of matrix thermal expansion and determine the influence of confining pressure and temperature cycling on it. These tests were run on unjacketed samples, thus enabling the confining fluid to fill the rock pore volume. The samples tested were subjected to temperature variation in the range from 25°C to 280°C at two different confining pressures. Samples M94-B and KAYENTA K3 were subjected to temperature cycles at 3 and 34.4 MPa. Samples BEREA 2 and COLTON 2 were subjected only to heating from 25°C to 280°C at 3 and 20.7 MPa. Strain and temperature were recorded during the tests once a minute.

A summary of the tests description and the experimental work accomplished is shown in Table 2.

The experimental equipment used is shown schematicaly in Fig. 1. It consists primarily of the pressure vessel, a servocontrolled pressurizing system, an automatized heating system, strain and temperature sensors and transducers and a computer based data acquisition system.

Linear thermal expansion for both jacketed and unjacketed samples was measured along their axis by means of high resolution LVDT's (linearly variable differential transducers) attached to the top of the test specimen by quartz rods. Deformation of up to 2.5×10^{-2} cm. can be measured with an accuracy of $\pm 6.2 \times 10^{-5}$ cm. Averaging the outputs of the two LVDT's removes any false strain due to tilting. More details

TABLE 2. Summary of Testing Conditions and Experimental Work Carried Out.

TEST TYPE (SAMPLES TESTED)	SAMPLE CONDITION	CONFINING PRESS MPa	TEMPERATURE VARIATION (°C)	HEATING RATE °C/MIN.
A	JACKETED	8	25-280-25	2
(M127-A,M127-HA)			25-280-25	2
B	JACKETED	8	25-280-25	1
(M149-A,KAYENTA K1)		8	25-280-25	2
		8	25-280-25	3
C	JACKETED	3	25-280-25	2
(M94-A,KAYENTA K2)		17.2	25-280-25	2
		34.4	25-280-25	2
C	JACKETED	3	25-280	2
(BEREA 1,COLTON 1)		20.7	25-280	2
D	UNJACKETED	3	25-280-25	2
(M94-B,KAYENTA K3)		34.4	25-280-25	2
D	UNJACKETED	3	25-280	2
(BEREA 2,COLTON 2)		20.7	25-280	2

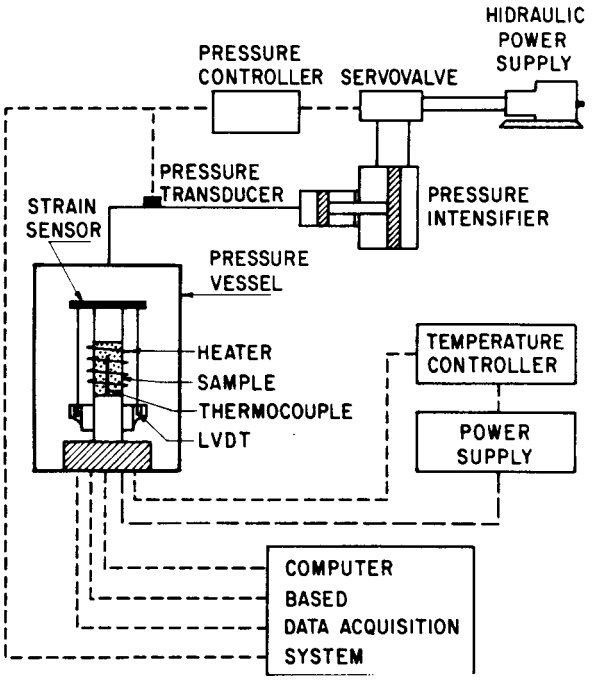


Figure 1. Schematic of experimental equipment.

on the experimental configuration used are given by Ennis et. al. (1979).

The temperature cycles and heating rates were tailored by means of a Honeywell programmable controller that regulated the power to an electric heater located inside the pressure vessel around the sample. By using the servocontrolled pressurizing system, confining pressure was kept constant at the chosen values within ± .01 MPa.

Data collected during the tests consisted of deformation output from the two LVDT's, sample temperature and confining pressure. Data was collected once every minute and stored by means of a computer based acquisition system.

In order to take into account the thermal expansion of the measuring system, calibration tests were run using fused quartz as the standard.

RESULTS AND DISCUSSION

Effect of Repeated Temperature Cycles on Bulk Thermal Expansion:

The results of type A tests carried out to investigate the effect of two consecutive temperature cycles on the bulk thermal expansion of sandstones are shown graphically in figures 2 and 3 by means of strain versus temperature curves. Description of the test conditions were given before and are also included as inset in the figures. The general strain-temperature behavior exhibited by the samples M127 - Ā and M127-HA is very similar, as it can be inferred from figures 2 and 3. Several interesting features of the strain-temperature curves can be appreciated and will be analyzed and discussed in the following.

For both samples, the heating and cooling strain-temperature curves of the first cycle show significant differences, with the cooling curve lying below the heating curve almost for the whole temperature range, resulting in a negative strain or compaction at the end of the first cycle. On the other hand, the strain-temperature behavior for the second cycle is highly reversible, since the discrepancies between its heating and cooling curves are almost inexistente; further, the compactions observed after completion of the second cycle are smaller than the ones for the first cycle. Using the strain marks drawn on figures 2 and 3, it is also noted that for both temperature cycles, the sum of the heating thermal strain, ε_T, and the corresponding compaction, ε_C, is almost a constant value, ε, for each sample. The parameter ε physically represents the cooling thermal strain experimented by the rock.

From these observations, we can draw an important conclusion, although still somewhat preliminary, concerning the strain-temperature behavior of sandstones. It appears that after a few temperature cycles, the rock will become thermomecanically stabilized, and that further recycling will not cause additional compaction in it. Under these circumstances, bulk thermal strain of sedimentary rocks would be reversible provided the rock has been previously subjected to a few temperature cycles. More experimental evidence supporting the conclusion of reversibility will be presented in the forthcoming subsection.

Further, since the parameter ε is the cooling thermal strain experimented by the rock, and such a parameter has the same value for both cycles as was noted before, it would be reasonable to propose that the thermal strain versus temperature curve of the cooling part of the temperature cycle does not depend on the thermal history of the rock, (as oppossed to the heating strain-temperature curve that does depend on the thermal history). The validity of the above proposed concept is strong-

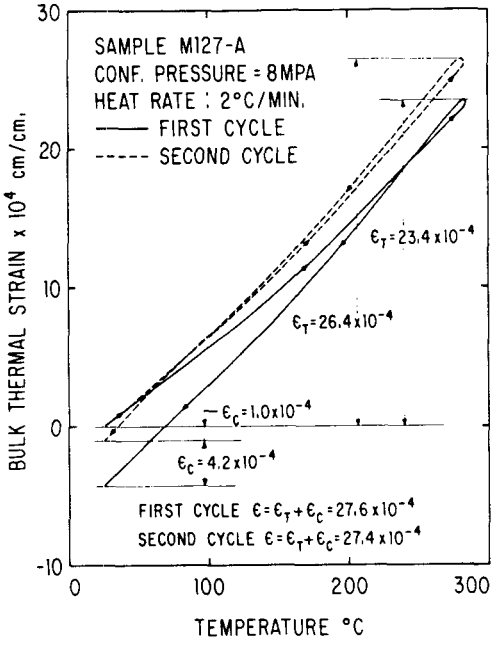


Figure 2. Effect of repeated temperature cycles on bulk thermal expansion of sample M127-A.

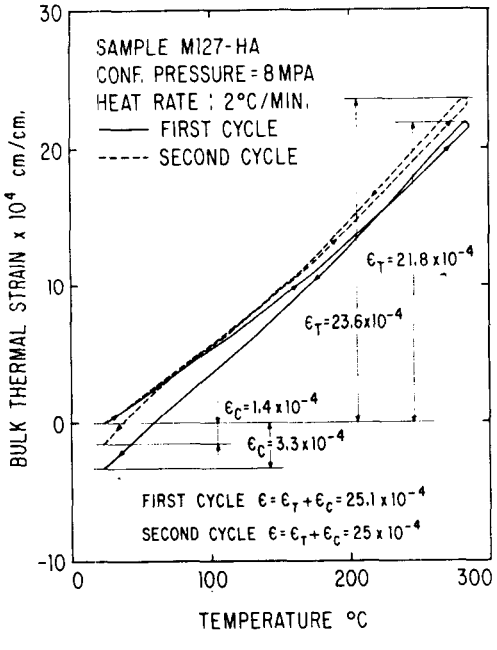


Figure 3. Effect of repeated temperature cycles on bulk thermal expansion of sample M127-HA.

ly supported by the experimental evidence that will be presented later in this work.

Combining the concept about the invariability of the cooling strain-temperature curve with the conclusion on the reversibility of the bulk thermal strain after a few temperature cycles, it is possible to determine the bulk thermal strain versus temperature behavior of a thermomecanically stabilized rock from the knowledge of any cooling strain curve, even the one corresponding to the first cycle. The importance of this conclusion is evident for the planning of experimental measurements as well as for analysis and application of results.

Effect of Heating Rate and Temperature Cycling on Bulk Thermal Expansion.

The results of type B tests carried out to investigate the effect of different heating rate values are shown in figures 4 and 5 for the samples M149-A and KAYENTA K1, respectively. Again, it is observed that for both samples the heating strain and the cooling strain versus temperature curves of the first cycle differ to a large extent, and a considerable compaction results at the end of this cycle. However, this compaction is more noticeable for sample KAYENTA K1 than for sample M149-A.

Both the latter strain-temperature cycles (two and three) differ markedly from cycle one. However, discrepancies between the cycles two and three are nearly indistinguishable from each other, thus providing evidence that the change in heating rate from 2°C/min to 3°C/min does not affect the strain-temperature pattern.

Furthermore, thermal expansion for cycles two and three is highly reversible upon cooling; the heating and cooling curves show only a small hysteresis loop, which can be related to the existence during the heating period of a lag of the inside-the-sample temperature with respect to the temperature sensed by the thermocouple attached to the external surface of the sample. The opposite phenomenon occurs during the cooling period. This observation is supported by the fact that the hysteresis loop is wider for the 3°C/min heating rate than for the 2°C/min heating rate.

The notorious similarity between cycles two and three provides enough evidence so as to reasonably conclude that their discrepancy from cycle one is not due to the different heating rates, but to the compaction mechanism, which was discussed before. Therefore, it can be concluded that differences in heating rates in the range from 1°C/min to 3°C/min do not affect the thermal strain-temperature behavior of sedimentary rocks nor do they produce irreversible structural damage. As it is noted, the actual value of the heating rate influences only the extension of the hysteresis loop. A 2°C/min heating rate is recom-

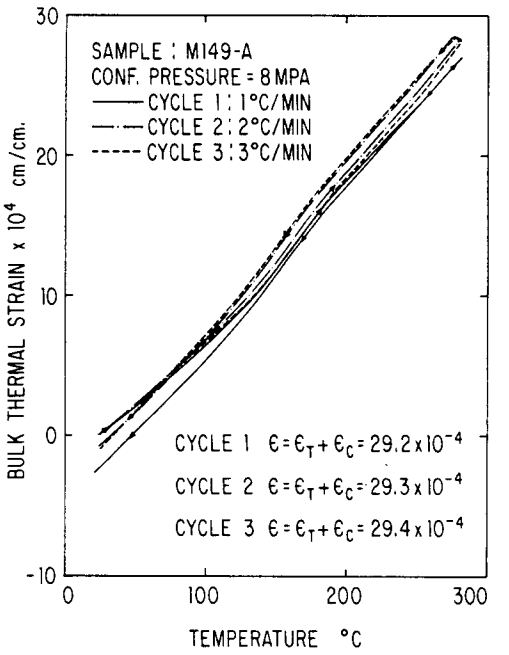


Figure 4. Effect of heating rate and temperature cycling on bulk thermal expansion of sample M149-A.

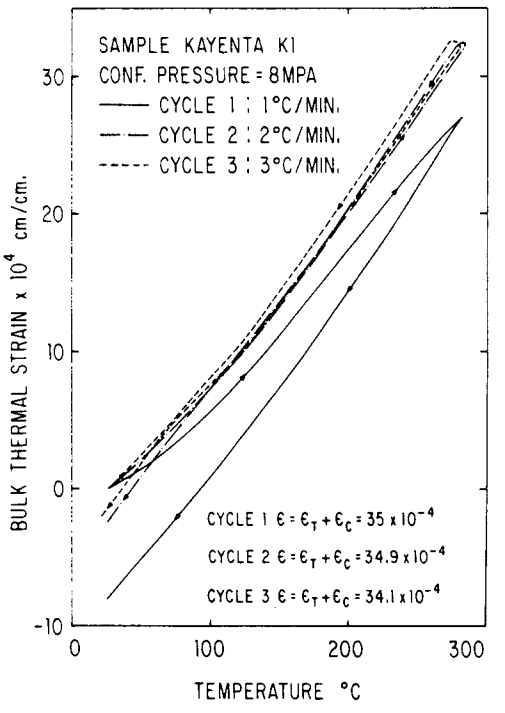


Figure 5. Effect of heating rate and temperature cycling on bulk thermal expansion of sample KAYENTA K1.

mended by the authors of this work, since the hysteresis loop associated to it is small enough so as to avoid significant experimental errors.

Concerning the heating and cooling thermal strains for the three cycles, it is interesting to note that for each sample the cooling thermal strain associated to the total temperature range covered is practically constant, regardless of the cycle considered. The same conclusion was drawn in the earlier subsection as well. The numerical values of the cooling thermal strain for the three cycles of both samples studied, M149-A and KAYENTA K1, are shown on figures 4 and 5, respectively.

Invariability of the Cooling Thermal Strain-Temperature Curve.

The observations that have been made regarding the constant value exhibited by the cooling thermal strain in the total temperature range for a given sample, regardless of its thermal history, strongly suggest the possibility that, provided the stress conditions on the rock are kept constant, the cooling thermal strain versus temperature curves exhibit the same pattern independently of the thermal history of the rock. In order to confirm such an assumption, the cooling strain-temperature curves of the cycles shown in figures 2 - 5 were redrawn using a common origin at 280°C, and the results are shown in figures 6 - 9, which provide enough experimental evidence in favor of the proposed concept about the invariability of the cooling thermal strain.

A practical application of this concept, as it was mentioned before, is the inferrence of the thermal expansion behavior corresponding to a stabilized rock from the cooling thermal strain-temperature curve of any cycle. This means that all the information regarding the thermal expansion behavior of a rock subjected to a given confining pressure, can be obtained from a single first cycle, but not from the heating thermal strain versus temperature curve only, since this curve is dependent on the thermal history of the rock. Another application of the invariability of the cooling thermal strain-temperature curve will be shown in the next subsection.

Effect of Confining Pressure on Bulk Thermal Expansion.

Type C tests were carried out to investigate the effect of confining pressure on bulk thermal expansion behavior. Information on the experimental conditions and the samples tested was given before and is summarized in table 2. The results for samples M94-A and KAYENTA K2 are shown in figures 10 and 11, respectively. The bulk thermal strain versus temperature cycles for the confining pressures of 3 MPa, 17.2 MPa and 34.4 MPa are plotted using a common origin at 25°C.

The problem involved in analizing the effect of confining pressure on bulk thermal expansion from figures 10 and 11, is that the heating strain-temperature curves are influenced by the previous thermal tratment underwent by the rock sample. Thus, the differences that may exist between any two heating curves are the sum of the influence of confining pressure itself plus the effect associated to the thermal history of the rock. Therefore, an analysis of the effect of confining pressure from heating strain-temperature curves requires that these effects be separated. On the other hand, the invariability of the cooling strain-temperature curves with respect to the thermal history was demonstrated before; thus, any observable discrepancies between cooling strain curves can be attributed to the effect of the confining pressure only. Using this approach and taking into account that for a thermomecanically stabilized rock at a given pressure, the heating strain curve is very similar to its corresponding cooling strain curve (see figures 2 - 5), the isolated effect of confining pressure on bulk thermal expansion can be estimated by plotting the cooling strain-temperature curves from a common origin at 25°C. Applying this method to the cases under study, samples M94-A and KAYENTA K2, the results shown in figures 12 and 13 were obtained. For sample M94-A, the effect of confining pressure on bulk thermal expansion in the range from 3 MPa to 34.4 MPa is rather small and erratic. On the other hand, for sample KAYENTA K2 the effect of increasing confining pressure is to reduce the thermal strain at a given temperature. At high temperatures (> 150°C), this effect is more significant for the 3 MPa to 17.2 MPa interval than for the 17.2 MPa to 34.4 MPa interval.

Bulk thermal expansion measurements at 3 MPa and 20.7 MPa were also carried out on samples BEREA 1 and COLTON 1 in the range from 25°C to 280°C with no temperature cycling. The results of these measurements are presented in table 3 by means of average thermal expansion coeffi - cients for the 25°C to 280°C range, from which the effect of confining pressure on bulk thermal expansion can be inferred.

The Matrix Thermal Expansion Concept:

In the following, the concept of matrix thermal expansion introduced by Contreras et. al. (1982) is analyzed with relation to its physical significance and applications. It has been pointed out by some authors, Somerton et. al. (1981) among others, that it is the expansion of mineral grains into the pore space that causes the decrease in pore volume with increased temperature, since there is less resistance to grain expansion into the pore space than to displac - ing adjacent grains. From this observation it can be inferred that for a confined sample, that is a jacketed sample subjected to a confining pressure higher than a pore pressure, the observable bulk thermal expansion should be

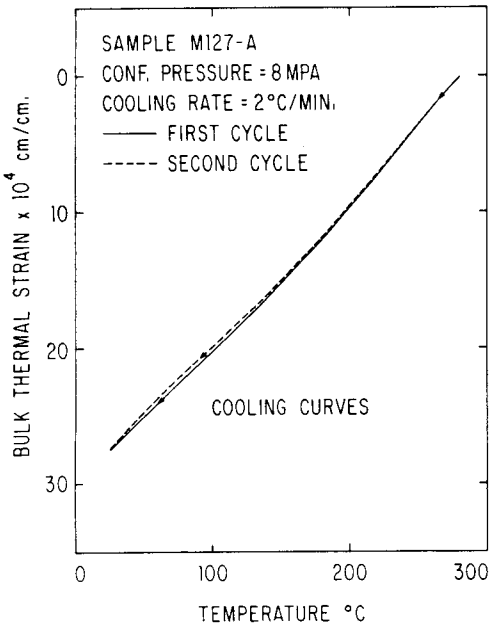


Figure 6. Strain-temperature cooling curves of sample M127-A. (Redrawn from Fig.2 using a common origin at 280°C).

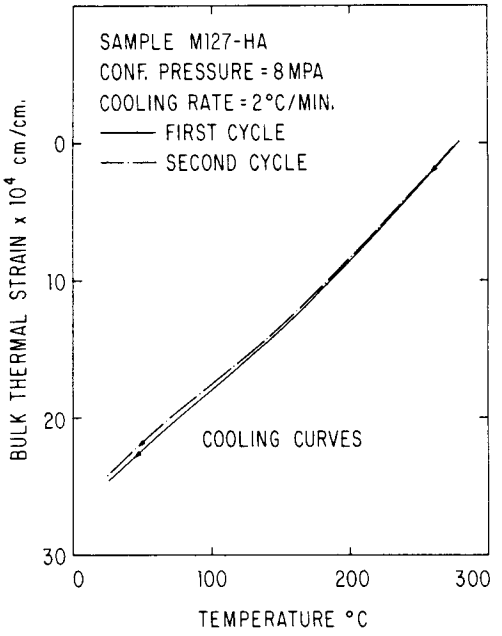


Figure 7. Strain-temperature cooling curves of sample M127-HA, (Redrawn -- from Fig.3 using a common origin at 280°C).

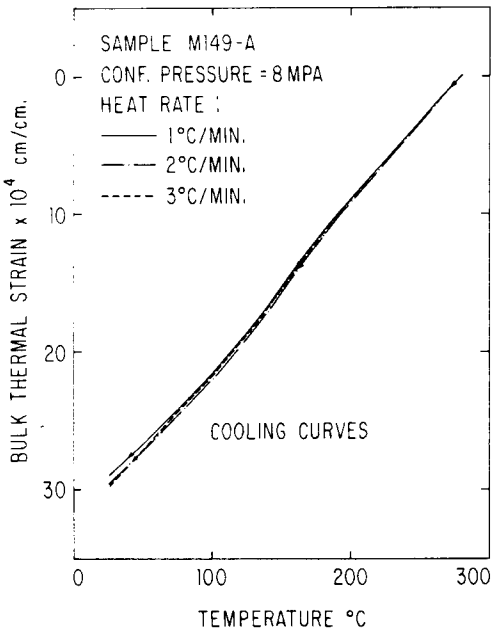


Figure 8. Strain-temperature cooling curves of sample M149-A. (Redrawn from Fig.4 using a common origin at 280°C).

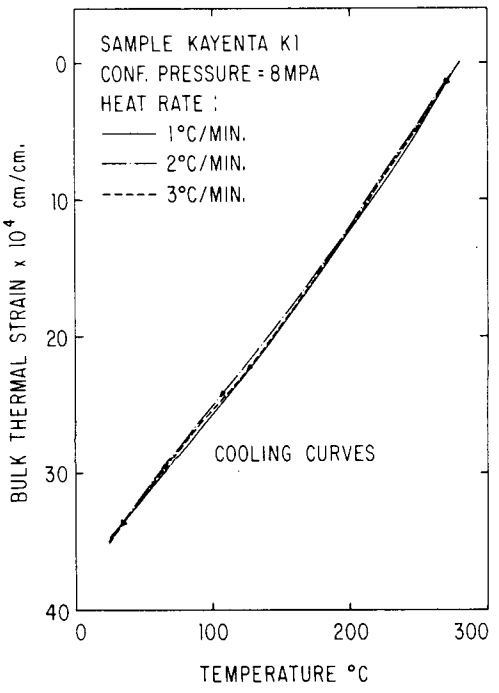


Figure 9. Strain-temperature cooling curves of sample KAYENTA K1, (Redrawn from Fig.5 using a common origin at 280°C).

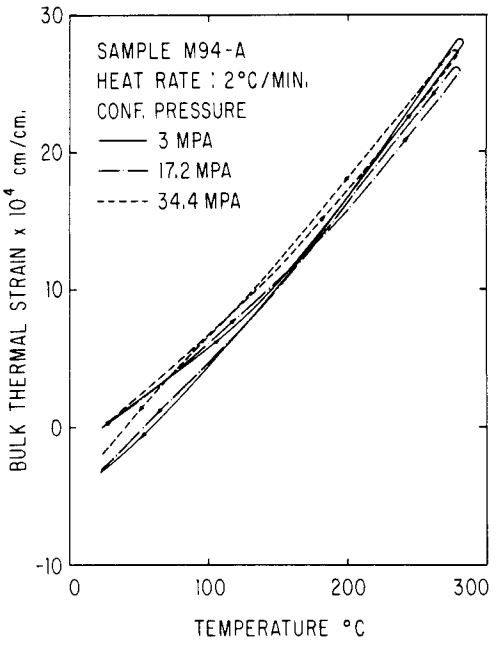


Figure 10. Combined effect of confining pressure and temperature cycling on bulk thermal expansion of sample M94-A.

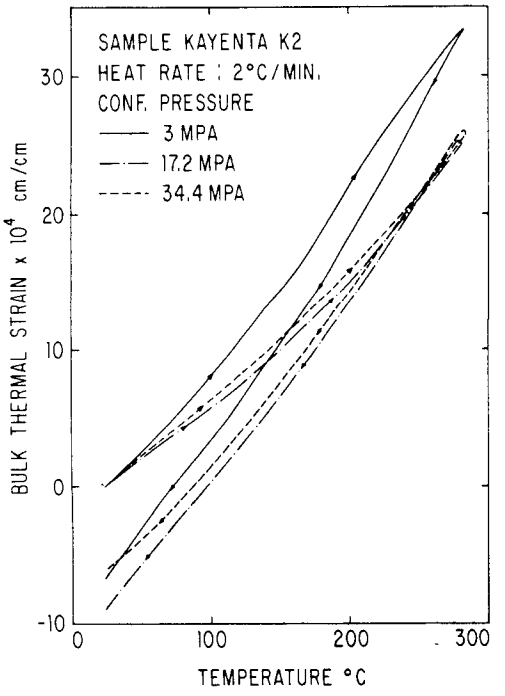


Figure 11. Combined effect of confining pressure and temperature cycling on bulk thermal expansion of sample KAYENTA K2.

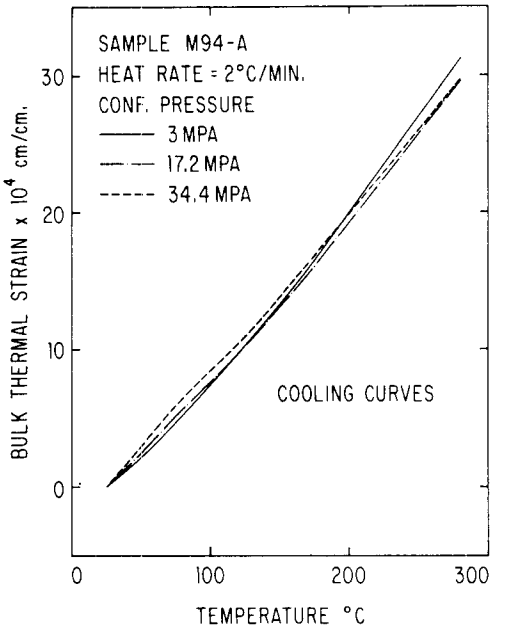


Figure 12. Isolated effect of confining pressure on bulk thermal expansion of sample M94-A.(As inferred - from strain-temperature cooling curves).

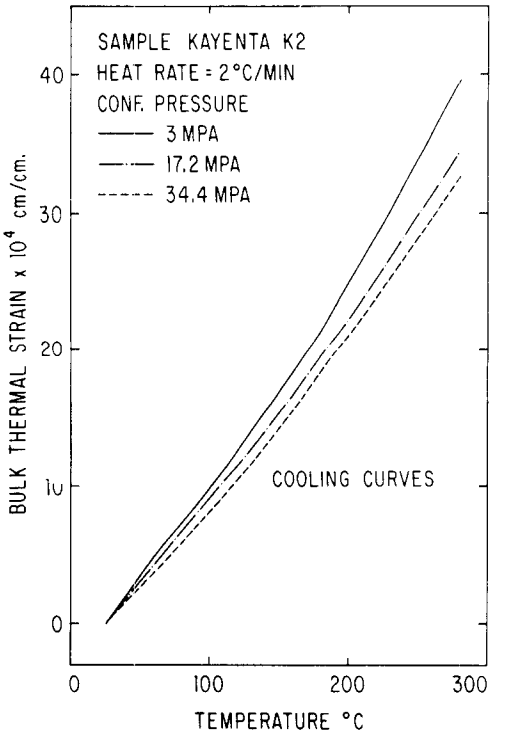


Figure 13. Isolated effect of confining pressure on bulk thermal expansion of sample KAYENTA K2.(As inferred from strain-temperature cooling curves).

smaller than the thermal expansion experimented by the solid material or rock matrix.

In order to evaluate the matrix thermal expansion of a confined rock subjected to given confining pressure P_c and pore pressure P_p, it is required to supress the preferential expansion of the mineral grains into the pore space by making the resistance opposed to the expansion of grains equal towards any direction. This can be accomplished if a pressure equal to the mean isotropic stress in the rock is applied in the pore space in such a way that the isotropic stress is kept constant to avoid any stress difference which could affect the matrix thermal expansion to be determined. It can be shown that these conditions are achieved by increasing both the confining pressure and the pore pressure up to a common value P_o given by

$$(1) \quad P_o = \frac{P_c - \phi P_p}{1 - \phi}$$

where ϕ is the porosity of the rock. Therefore the matrix thermal expansion behavior of a rock subjected to P_c and P_p can be inferred from thermal expansion measurements carried out either on the jacketed rock subjected to $P_c' = P_p' = P_o$ or on the unjacketed rock subjected to a hydrostatic pressureequal to P_o.

The matrix thermal expansion behavior of some sandstones was determined by running tests type D. In order to provide a comparison frame to analyze differences between matrix and bulk thermal expansions, matrix tests were run on samples obtained from the same piece of rock as the samples used for type C bulk tests. The effect of temperature cycling and confining pressure on matrix thermal expansion behavior of samples M94-B and KAYENTA K2 is shown in figures 14 and 15 respectively. It is interesting to note that at the end of the first temperature cycle (confining pressure = 3 MPa) a permanent positive strain results, which is probably indicative that some kind of irreversible microestructural alteration occurs in the rock. On the other hand, the thermal strain versus temperature behavior for the second cycle (confining pressure = 34.4 MPa) is highly reversible. This suggests that the assumed microestructural damage is temperature-dependent only.

Matrix and bulk thermal strain-temperature curves for the heating part of temperature cycles are shown in Fig. 16 for samples M94-A (matrix data) and M94-B (bulk data). The differences that exist between matrix strain and bulk strain for the same confining pressure at given temperature, provide evidence in favor of the concept that preferential expansion of the mineral grains occurs towards the pore space. To this point, it has to be pointed out in accordance with the discussion of the latter subsection, that to accomplish a better comparison with bulk thermal expansion data for 3MPa and 34.4 confining pressure matrix thermal expansion measurements should have been carried out at 3.6 MPa and 40.9 MPa respectively.

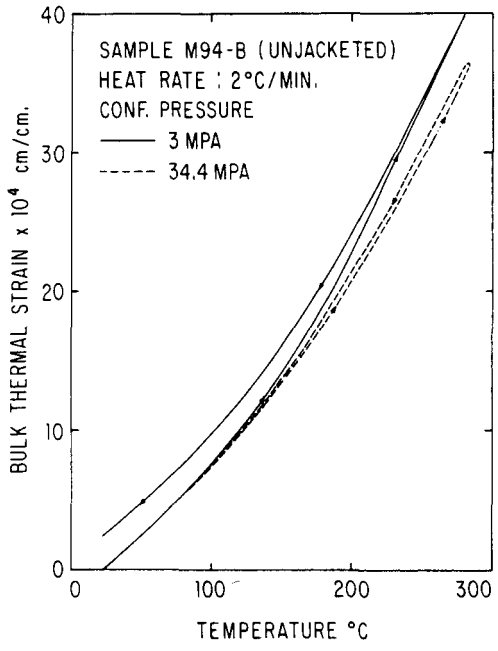


Figure 14. Effect of confining pressure and temperature cycling on matrix thermal expansion of sample -- M94-B.

Estimation of the Effect of Temperature on Porosity from Bulk and Matrix Thermal Expansion Measurements.

Determination of the effect of temperature on porosity is a subject of interest because of its practical implications in reservoir engineering. The traditional approach proposed to investigate this effect consists of calculating the fractional change in porosity $\Delta\phi/\phi_o$ from experimental data on fractionalchange in bulk volume $\Delta V_B/V_B$ (normally considered to be three times the linear bulk strain) and fractional change in pore volume $\Delta V_P/V_P$. The basic equation used is

$$(2) \quad \frac{\Delta\phi}{\phi_o} = 1 - \frac{1 - \frac{\Delta V_P}{V_P}}{1 - \frac{\Delta V_B}{V_B}}$$

Greenwald et. al. (1982) used this method to calculate the effect of temperature in the range from 40° to 170°C on fractional porosity change for Boise, Berea and Bandera sandstones under 20.7 MPa confining pressure and 6.9 MPa pore pressure. The result reported by Greenwald for the Berea sandstone is shown in Fig. 17. Further, from data on linear thermal expansion and pore volume contraction for the same outcrop rock by Somerton (1980) and Somerton et. al.

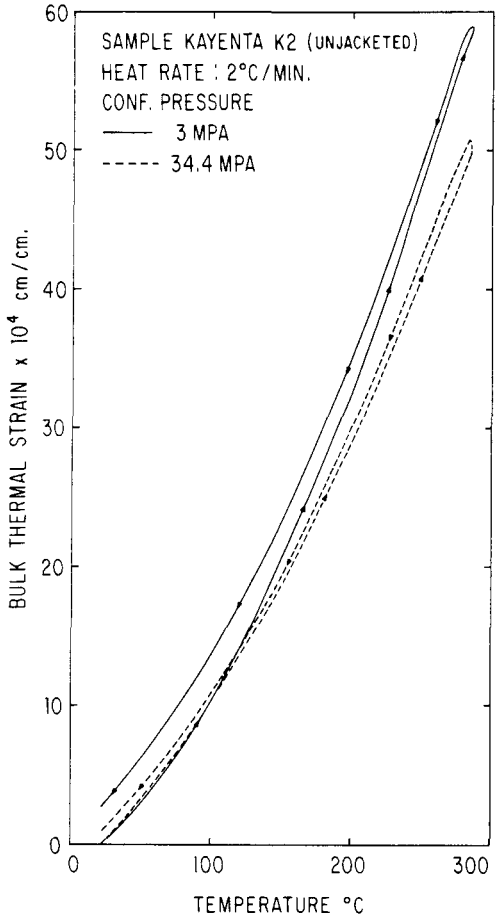


Figure 15. Effect of confining pressure and temperature cycling on matrix thermal expansion of sample -- KAYENTA K2.

(1981), we calculate the effect of temperature on porosity and the result is also shown in Fig. 17. The discrepancy exhibited by the results shown arises from the differences between the pore volume contraction data used by Greenwald and the data presented by Somerton. This matter was referred to in the literature review of the present work.

On the other hand, provided the rock is isotropic, the effect of temperature on porosity may also be expressed mathematically as

$$(3)\quad \left(\frac{\phi_T}{\phi_{T_o}}\right) = \frac{1}{\phi_o}\left\{1+(\phi_o - 1)\, e^{3(E_s - E_B)}\right\}$$

where:

ϕ_T = Porosity at temperature T

ϕ_{T_o} = Porosity at temperature T_o

E_s = Linear matrix thermal strain at temperature T

E_B = Linear bulk thermal strain at temperature T.

Using matrix and bulk linear thermal expansion data obtained from type C and D tests, we calculated through equation (3) the effect of temperature on porosities for sandstones BEREA and KAYENTA and the results are presented in Figs. 17 and 18 respectively. Our results for BEREA sandstone show a fair agreement with the values we calculated from Somerton's data, but they differ considerably from the results reported by Greenwald.

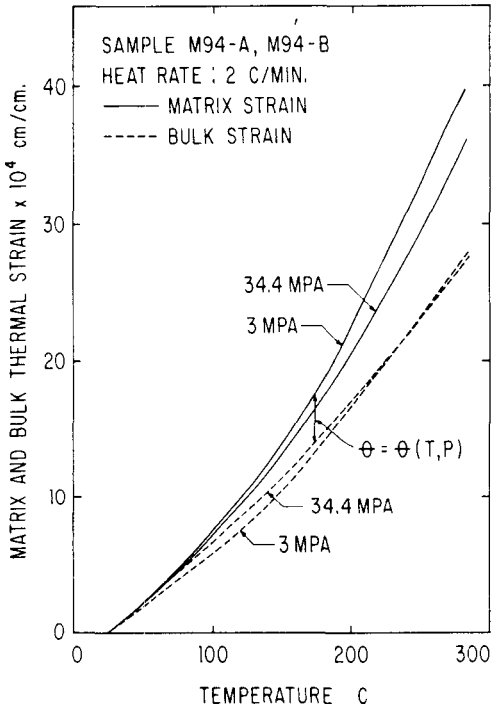


Figure 16. Comparison between matrix and bulk thermal strain of samples M94-A and M94-B.

Results of Research on Thermal Expansion Isotropy:

The assumption that sedimentary rocks are isotropic concerning thermal expansion behavior is very frequently adopted; for example when it is considered that the volumetric strain equals three times the linear strain. The validity of

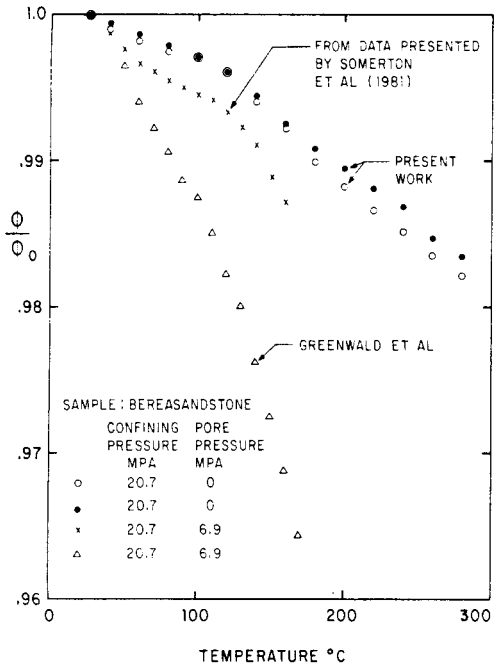


Figure 17. Effect of temperature on - porosity of Berea sandstone as reported by different authors.

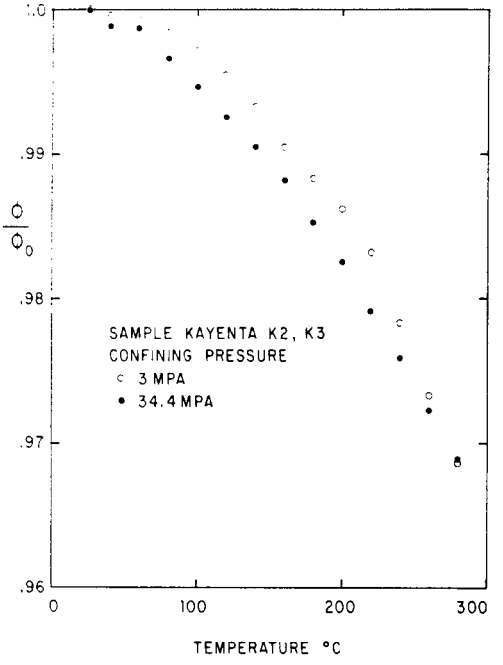


Figure 18. Effect of temperature on - porosity of sample KAYENTA K2,K3.

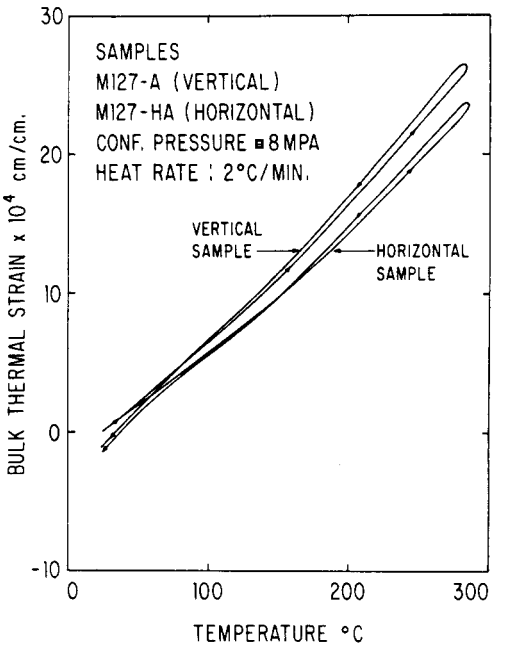


Figure 19. Effect of orientation with respect to the bedding plane on bulk thermal expansion. (From data presented in Figs. 2 and 3).

this assumption was investigated in the present work by measuring the bulk thermal expansion of two twin samples obtained from the same piece of rock; one of them was cut parallel to the bedding plane (sample M127-HA) and the other one was cut perpendicular to the bedding plane (sample M127-A). These samples were also used to investigate temperature cycling effects and the results obtained were presented before (see Figs. 2 and 3). Overlapping the thermal strain versus temperature curves for the second cycles of samples M127-A and M127-HA, as taken from Figs. 2 and 3, the result shown in Fig. 19 is obtained. The thermal strain exhibited by the vertical sample is higher than the thermal strain exhibited by the horizontal sample at a given temperature, thus suggesting that the thermal expansion isotropy assumption for sedimentary rocks may not be a good approach to simplify analysis. Of course, more investigation has to be conducted to determine the extent of thermal expansion anisotropy in sedimentary rocks.

Thermal Expansion Coefficients:

The results of some of the tests carried out are not presented explicitly by means of thermal strain-temperature curves. However, thermal expansion coefficients were calculated from al strain versus temperature data for all of -- the tests carried out. The results are presented in Table 3.

TABLE 3. Thermal Expansion Coefficients of the Samples Tested.

SAMPLE	CONFINING PRESSURE MPa		LINEAR THERMAL EXPANSION COEFFICIENTS $°C^{-1} \times 10^6$							
			BULK				MATRIX			
			TEMPERATURE INTERVAL °C				TEMPERATURE INTERVAL °C			
			40-70	140-170	240-270	AVG(25-280)	40-70	140-170	240-270	AVG(25-280)
M94-A	3	H-2	7.2	12.3	13.5	10.8				
(1)		C-2	9.9	12.8	14.3	12.3				
	17.2	H-2	8.2	10.5	12.7	10.0				
		C-2	10.7	11.7	13.0	11.5				
	34.4	H-2	9.0	10.7	12.7	10.7				
		C-2	11.9	11.7	12.2	11.7				
M94-B	3	H-2					10.1	15.9	20.6	
(2)	34.4	H-2					9.4	13.6	19.7	
M127-A	8	H-2	7.8	9.4	10.3	10.0				
(3)		C-2	9.7	10.9	12.9	10.7				
		H-2	8.9	10.2	11.3	8.1				
		C-2	10.7	10.6	12.3	9.7				
M127-HA	8	H-2	7.5	8.2	9.4	8.1				
(4)		C-2	9.5	9.7	11.3	9.7				
		H-2	7.9	8.3	9.8	8.9				
		C-2	9.4	9.4	11.1	9.7				
M149-A	8	H-2	8.3	13.5	10.9	10.5				
(5)		C-2	9.9	13.8	10.9	11.5				
		H-2	8.7	14.0	12.0	11.0				
		C-2	11.3	13.8	11.9	11.6				
		H-3	8.7	13.3	12.6	11.0				
		C-3	11.6	14.7	11.0	11.7				
KAYENTA K1	8	H-1	7.7	12.1	11.3	10.6				
(6)		C-1	12.0	14.3	16.1	13.8				
		H-2	9.0	14.3	12.1	12.4				
		C-2	13.1	14.0	15.9	13.7				
		H-3	9.9	14.2	15.3	12.6				
		C-3	13.0	14.1	16.1	13.8				
KAYENTA K2	3	H-2	10.9	14.6	11.7	12.9				
(7)		C-2	14.2	15.1	20.1	15.5				
	17.2	H-2	7.9	10.3	13.0	9.9				
		C-2	12.8	13.8	15.2	13.5				
	34.4	H-2	8.8	10.4	12.2	10.1				
		C-2	10.7	13.5	14.9	13.0				
KAYENTA K3	3	H-2					13.5	24.3	33.4	22.1
(8)	34.4	H-2					12.6	20.2	25.1	18.9
BEREA 1	3	H-2	10.2	14.5	15.4	12.8				
(9)	20.7	H-2	10.6	13.0	15.8	12.5				
BEREA 2	3	H-2					12.1	21.9	20.5	18.0
(10)	20.7	H-2					13.1	19.6	18.4	17.3
COLTON 1	3	H-2	10.9	17.1	16.3	14.8				
(11)	20.7	H-2	9.8	12.5	13.6	11.7				
COLTON 2	3	H-2					12.7	18.5	14.8	15.9
(12)	20.7	H-2					12.7	14.8	17.2	14.3

Note: H and C in the confining pressure column indicate whether the reported data in the row correspond to the heating or to the cooling part of the temperature cycling respectively.

Thermal expansion coefficients were calculated both for heating and cooling curves in the intervals of 40°C to 70°C, 140°C to 170°C and 240°C to 270°C, using a linear regression scheme with at least ten experimental data points for each interval. The correlation coefficient was higher than 0.99 in all the cases. Furthermore, average thermal expansion coefficients for the total temperature range covered (25°C to 280°C) were also calculated and the results are also reported in Table 3.

SUMMARY AND CONCLUSIONS

An extensive experimental program focused to investigate the thermal expansion behavior of sedimentary rocks has been carried out. The significant findings and conclusions from this work can be summarized as follows:

1. At a given confining pressure, after a first irreversible thermal strain-temperature cycle samples become thermomecanically stabilized and further cycles are almost reversible, repeteable and with no considerable hysteresis. However, a rock sample stabilized at a given pressure will again exhibit an irreversible thermal strain-temperature behavior if the confining pressure is increased up to a new value. This suggests that the compaction experimented by the rock arises from a combined effect of temperature and pressure.

2. Differences in heating rates in the range from 1°C/min to 3°C/min do not affect the thermal expansion behavior of the sedimentary rocks studied.

3. At a given confining pressure, the cooling thermal strain versus temperature curves show the same pattern independently of the thermal history of the rock (as opposed to the heating curves that exhibit thermal hystory dependence).

4. The bulk thermal expansion behavior that a stabilized rock at a given pressure would exhibit, can be inferred from the cooling thermal strain-temperature curve of any cycle, even the first one, but not from the first heating strain temperature curve.

5. The effect of confining pressure on bulk thermal expansion is significant and well behaved for one of the two samples studied, but is rather small and erratic for the other sample. More investigation on this aspect has to be carried out to obtain further evidence to support some sort of conclusion.

6. The matrix thermal expansion behavior corresponding to a rock subjected to given confining pressure P_c and pore pressure P_p, can be inferred by measuring the thermal expansion of the rock subjected to confining pressure P_c^* and to a pore pressure P_p^* given by

$$P_p^* = P_c^* = \frac{P_c - \phi P_p}{1-\phi}$$

where ϕ is the porosity of the rock.

7. For a rock subjected to given pressure conditions, the matrix thermal strain is higher than the bulk thermal strain at a given temperature; this is in agreement with the concept of preferential thermal expansion of mineral grains into the pore space.

8. The matrix thermal expansion behavior exhibited by the samples studied shows that strain remains in the rock after completion of the first temperature cycle. On the other hand, for the second cycle the thermal strain versus temperature behavior is highly reversible and with no hysteresis, even though a different confining pressure was applied on the samples during the second cycle. This suggests that the remaining strain of the first cycle arises because of structural damage caused by differential thermal expansion of the mineral grains when are heated during the first cycle. This structural damage is temperature dependent and occurs during the first temperature cycle only. Furthermore, it can be noted that the effect of increased confining pressure is to reduce the matrix thermal expansion at a given temperature.

9. The effect of temperature on porosity was estimated from matrix and bulk thermal expansion data for two sandstones and results were compared with earlier available data calculated from pore volume contraction and bulk thermal expansion data. Although the observed effect is rather small, more investigation on this particular subject should be conducted to establish ranges of porosity change as well as to determine a pattern of influence upon variable confining pressure.

10. Thermal expansion isotropy for sedimentary rocks is an assumption that should be adopted cautiosly

11. A big deal of data about thermal expansion coefficients of the samples tested is reported. Information concerning magnitudes and variation ranges of this parameter may be useful for reservoir engineering calculations that involve the thermal expansion behavior of sedimentary rocks.

ACKNOWLEDGEMENTS

We wish to thank Ing. Alfredo Mañón M. at Comisión Federal de Electricidad, Coordinadora Ejecutiva de Cerro Prieto, for his interest in this work. We also thank Ing. Sergio Mercado G., at Instituto de Investigaciones Eléctricas,

for his permission to accomplish the experimental program leading to this paper as part of project IIE-1663. Martín Uribe collaborated in the experimental work, Adrián Patiño drafted the figures and Mrs. María Eugenia Calderón and Mrs. Ma. de Lourdes Calderón made the typing; their participation is duly acknowledged.

REFERENCES

Ashqar, P. I., (1979), "Thermal Expansion of Poous Rocks Under Stress". Master of Science Project Report, University of California, Berkeley, December 1979.

Contreras, E., Iglesias, E., Bermejo, F. (1982), "Effects of Temperature and Stress on the Compressibilities, Thermal Expansivities, and Porosities of Cerro Prieto and Berea Sandstones to 9000 psi and 280°C". Proceedings 8th Workshop on Geothermal Reservoir Engineering. Stanford, California, December 14-16, 1982.

Ennis, D. O., Butters, S. W., Lingle, R., Van Buskirk, R. G., Prater, F. R. (1979). "Capabilities to Measure Geothermal Material Properties at Simulated In-Situ Conditions". Terratek Report TR79-49.

Greenwald, R. F., Ashqar, P. I., Somerton, W.H., (1982). "Thermal Expansion Behavior of Porous Rocks Under Stress". Proceedings of the Thermal Expansion Conference N° 7. Plenum Press, 1982. David C. Larsen, Editor.

Janah, A., (1980). "Pore Volume Variation with Temperature for Porous Rocks Under Stress". M. S. Report, University of California, Berkeley. Department of Mechanical Engineering.

Somerton, W. H., Selim, M. A., (1961). "Additional Thermal Data for Porous Rocks-Thermal Expansion and Heat of Reaction". 31st Annual California Regional Meeting of SPE, Octobre 21-22, 1961.

Somerton, W. H., (1980). "The Behavior of Rock-Fluid Systems at Elevated Temperatures and Pressures". Annual Report 1981, Earth Sciences Division, Lawrence Berkeley Laboratory, University of California.

Somerton, W. H., Janah, A. H., Ashqar, P. I., (1981). "Thermal Expansion of Fluid Saturated Rocks Under Stress". SPWLA Twenty-Second Annual Logging Symposium. June 23-26, 1981.

Proceedings Ninth Workshop Geothermal Reservoir Engineering
Stanford University, Stanford, California, December 1983
SGP-TR-74

Design and Development of a Test Facility to Study Two-Phase Steam/Water Flow in Porous Media

Ashok K. Verma, Karsten Pruess, G. S. Bodvarsson,
C. F. Tsang and Paul A. Witherspoon

Lawrence Berkeley Laboratory
University of California
1 Cyclotron Road
Berkeley,CA, 94720

INTRODUCTION

The concept of relative permeability is the key concept in extending Darcy's law for single phase flow through porous media to the two-phase flow regime. Relative permeability functions are needed for simulation studies of two-phase geothermal reservoirs. These are poorly known inspite of considerable theoretical and experimental investigations during the last decade. Since no conclusive results exist, many investigators use ad hoc parametrization, or adopt results obtained from flow of oil and gas (Corey,1954). It has been shown by Reda and Eaton (1980) that this can lead to serious deficiencies. Sensitivity of the relative permeability curves for prediction of mass flow rate and flowing enthalpy into geothermal wells has been studied by many investigators (eg. Eaton and Reda (1980), Bodvarsson et al (1980), Sun and Ershagi (1979) etc.) It can be concluded from these studies that the behavior of a two-phase steam/water reservoir depends greatly on the relative permeability curves used. Hence, there exists a need for obtaining reliable relative permeability functions.

The approach taken at Lawrence Berkeley Laboratory to obtain relative permeability curves and their dependence on fluid and matrix properties is summarized in Fig. 1. Thermodynamic studies are carried out to develop the equations governing two-phase steam/water flow in porous media and to analyze the relationship between mass flow rate and flowing enthalpy. These relationships will be verified against experimental results and subsequently will be used to develop a field analysis technique to obtain in-situ relative permeability parameters. Currently our effort is concentrated on thermodynamic analysis and development of an experimental facility. This paper presents some of the findings of our theoretical work and also describes the design and development effort for the experimental facility.

In the first part of this paper we present some basic theoretical studies of the mechanism of phase trapping and the effect of pore geometry on the relative permeability functions. The flow conditions which may support phase trapping are identified and it is recommended that these operating conditions be avoided during the experiment. The effect of pore geometry on the relative permeability functions is studied by considering two different flow configurations, a circular tube and a plane fracture.

In the second part of this paper a description of the experimental setup is given. The proposed experimental setup is similar to that of Reda and Eaton (1981). However, a significant improvement in the analysis of the operating conditions is achieved by considering the effects of capillary pressure and the end effects resulting from it. We also propose to use a capillary pressure probe to obtain the dependence of capillary pressure on saturation under dynamic conditions.

PREVIOUS WORK

Various investigators have attempted to determine the relative permeability curves for steam/water flow in porous media. Experimental works to determine the relative permeability curves have been reported, among others, by Corey (1954), Chen et. al (1978), and Counsil and Ramey (1979). Grant (1977), Horne and Ramey (1978) and Shinohara (1978) used flow rate and enthalpy data from the Wairaki geothermal field in New Zealand to obtain information about in-situ relative permeability functions. A completely theoretical model was proposed by Menzies (1982), and Gudmundsson et al (1983), who used a streamtube model to obtain relative permeability functions.

BASIC STUDIES

In this section we study the mechanism of phase trapping and the effect of pore geometry on the relative permeability functions.

Phase Trapping

Phase trapping can occur when one of the phases becomes immobile under the action of capillary pressure in a channel full of the other phase which flows around it. Both water and steam can be trapped in flow channels when the thermodynamic conditions are such that the net rate of phase transformation, at the interface of the trapped phase and the flowing phase, equals zero. This phenomenon is important in this study because of two reasons:

(i) phase trapping is an important mechanism of permeability reduction

(ii) phase trapping can lead to local changes that are hysteretic in nature. (Observed by Udell (1983) in his "Hot Wire" experiment).

To study the phase trapping mechanism in a two-phase steam/water flow in porous media, the following assumptions are made:

a) flow is one dimensional and horizontal

b) water is the wetting fluid. Steam resides on the concave side of the steam/water interface and both the liquid and the steam phases are superheated (Udell,1983)

c) pores are large enough so that the effect of adsorption on phase equlibrium can be neglected

d) water, vapor and the matrix are locally in thermodynamic equlibrium and any phase transformation is quasistatic.

With these assumptions we can show that, (see appendix-I)

i) the vapor phase can be trapped when liquid is flowing in the direction of increasing temperature

ii) the liquid phase can be trapped if vapor is flowing in the direction of decreasing temperature and also

$$\frac{\partial}{\partial x}\left(\frac{T}{P_c}\right) < 0$$

This indicates that relative permeability of a phase may depend not just on saturation but also on the local temperature gradient.

Effect of pore geometry

To study the effect of pore geometry on relative permeability functions we use an approach similar to that of Yuster (1951). The two different flow channel geometrics considered are (i) a circular tube, and (ii) a plane fracture.

In both these cases the flow is assumed to be separated with water being the wetting fluid. We also assume that the surface temperature distribution is such that no flashing or condensation can occur. Under these conditions, the relative permeability functions for the circular tubes are (Yuster, 1951)

$$k_{rw} = (1 - S_v)^2 \qquad (1)$$

$$k_{rv} = 2\, S_v \frac{\mu_v}{\mu_w} + S_v^2 \left(1 - 2\frac{\mu_v}{\mu_w}\right) \qquad (2)$$

Following the same line of reasoning we can show that for plane fractures

$$k_{rw} = 1 - 1.5\, S_v + 0.5\, S_v^3 \qquad (3)$$

and

$$k_{rv} = 1.5 \frac{\mu_v}{\mu_w} S_v - S_v^3 \left(1.5 \frac{\mu_v}{\mu_w} - 1\right) \qquad (4)$$

A plot of these relative permeability curves, for

$$\frac{\mu_v}{\mu_w} = 0.4 \text{ and } 0.1,$$

is shown in Fig. 2. From these curves we can see that for a given saturation the parallel plate configuration has a higher relative permeability for the water phase than the circular tube model. However, the vapor phase relative permeability has the opposite trend. This phenomenon occurs because for a given saturation the parallel plate configuration will have a thicker water layer than the circular tube model.

It is easy to show from equations 1-4 that in the two-phase zone (i.e. $0 < S_v < 1$) the sum of relative permeabilities is less than one (i.e. $k_{rw} + k_{rv} < 1$) as long as the viscosity ratio (μ_v/μ_w) remains less than unity.

However, this model is rather simplistic and further studies are needed in which effects of phase transformation should be included.

PROPOSED EXPERIMENTAL SETUP AND OPERATING CONDITIONS

The proposed experimental setup (Fig.3) is similar to that of Reda and Eaton (1981). The test sample is a sand pack in a glass cylinder (3" I.D. x 36" length), mounted vertically to avoid the problem of flow stratification. The outer surfaces of this cylinder are made adiabatic with the aid of computer controlled guard heaters. Liquid water at constant temperature is pumped into the inlet end of the test sample at a constant flow rate with the aid of a dual-cylinder, constant-flow rate, metering pump.

Electric heaters are installed inside the porous matrix at the inlet end. A controlled amount of power is supplied to these heaters through a stabilized power supply to cause boiling and the power input is adjusted to achieve the required flow quality. The mixture of steam and water leaves the test sample through an exit chamber designed to reduce the end effects. The exit end is maintained at constant pressure with the aid of a back pressure regulator.

Pressure, temperature, capillary pressure and saturation readings will be taken at regular intervals in the central portion of the test column. Saturation readings will be taken with the aid of a γ-ray densitometer, which avoids disturbing the flow while taking readings.

Desirable operating conditions have been studied with the aid of numerical modeling. It was speculated that the effect of capillary pressure, and the end effects resulting from it, would be very significant. To study these effects, various capillary pressure curves were incorporated in a numerical code MULKOM (Pruess, 1983), and test runs were simulated. A typical result of a simulation with the end effects is shown in Fig. 4 and for the purpose of comparison, a typical result without the end effect is shown in Fig. 5. From these figures we can see that, while the four parameters of interest, P_v, P_c, T and S_v, vary monotonically with more or less constant gradient in Fig. 5, the end effects cause a very sharp gradient of P_v, P_c and S_v (Fig. 4) over the last 20 cm of the test column near the exit end. This phenomenon occurs because of the physical nature of the problem which requires that the capillary pressure must equal zero at the exit.

We have also considered the effects of matrix properties, boundary conditions and the relative permeability functions on the proposed experiment. Results of simulations using many parameter combinations show that it is possible to obtain a region of almost constant saturation over an extended length of the test column. Readings taken in this region can be analyzed to yield relative permeabilities without much difficulty.

The analysis technique follows that of Reda and Eaton (1981). By considering the conservation of mass and energy in a two-phase concurrent flow in a vertical test section, we derive the following relationships.

$$f = \frac{m_o (h_o - h_w) - m_o g z + q_o - q}{m_o (h_v - h_w)} \qquad (5)$$

$$k_{rw} = \frac{(f - 1)\, m_o\, \mu_w\, v_w}{kA \frac{d}{dz} (P_w + \rho_w g z)} \qquad (6)$$

$$k_{rv} = - \frac{f\, m_o\, \mu_v\, P_v}{kA \frac{dPv}{dz}} \qquad (7)$$

The right hand side of equations 5-7 consists of quantities which are either known or can be measured from the experiment and hence equations 6 and 7 can be used to calculate the relative permeabilities.

SUMMARY

Criteria for phase trapping in flow channels have been developed based on the thermodynamics of curved interfaces. It is shown that the vapor phase can be trapped if liquid is flowing in the direction of higher temperature. On the other hand, liquid can be trapped if vapor is flowing in the direction of lower temperature. Based on an ideal capillary analysis we conclude that the shape of the relative permeability functions depend on the pore geometry and the viscosity ratio of steam and water. We also show that the sum of the relative permeabilities in the two-phase zone is generally less than unity. Our analysis neglects phase change, and a more realistic treatment of steam-water flow is needed before conclusive results can be obtained. From the basic studies we conclude that the relative permeability functions may depend, among other parameters, on the fluid properties, pore geometry and flow conditions.

Results of the numerical studies show that the end effects can be very significant. However, it is possible to design and experiment such that a nearly constant vapor saturation region exists over an extended portion of the test sample. In this region, the capillary pressure gradient is small and thus the experimental data can be easily interpreted.

NOMENCLATURE

A core cross-sectional area

f dynamic quality $(m_v/(m_v + m_w))$

g acceleration of gravity

h specific enthalpy

k intrinsic permeability of the sample

k_r relative permeability

m mass flow rate

P Pressure

q heat flux due to conduction

R gas constant for vapor

r_{eq} equivalent radius of curvature

$r_{eq} = 2\gamma/p_c$

S inplace saturation

T temperature

v specific volume

x linear distance

z vertical distance along the core holder

μ absolute viscosity

γ Gibb's free energy per unit area of interface

SUBSCRIPTS

c capillary

o condition at the inlet of the test sample

v vapor phase

w water phase

∞ infinite radius of curvature

ACKNOWLEDGEMENT

This work was supported by the Assistant Secretary for Conservation and Renewable Energy, Office of Renewal Technology, Division of Geothermal and Hydropower Technologies of the U.S. Department of Energy under Contract No. DE-AC03-76SF00098.

REFERENCES

Bodvarsson, G.S., O'Sullivan, M.J. and Tsang, C.F., 1980, "The Sensitivity of Geothermal Reservoir Behavior to Relative Permeability Parameters", Proc. 6th Workshop Geothermal Res. Eng., Stanford.

Chen, H.K., Counsil, J.R., and Ramey, H.J., 1978, "Experimental Steam-water Relative Permeability Curves," Trans. Geothermal Resources Council, Vol. 2, 102-104.

Corey, A.T., 1954, "The Interrelation Between Gas and Oil Relative Permeabilities", Prod. Mon., 19, 38-41.

Counsil, J.R., and Ramey, H.J., 1979, "Drainage Relative Permeabilities Obtained from Steam-Water Boiling - Flow and External Gas Drive Experiments", Transactions, Geothermal Resources Council, Vol. 3, 141-143.

Grant, M.A., 1977, "Permeability Reduction Factors at Wairaki," Paper presented at AIChE-ASME Heat Transfer Conference, AIChE, Salt Lake City, Utah, Aug. 15-17.

Gundmundsson, J.S., Menzies, A. J., and Horne, R. N., 1983, "Streamtube Relative Permeability Functions for Flashing Steam-Water Flow in Fractures", SPE Paper No. 11686 presented at the California Regional Meeting of the SPE, Ventura.

Horne, R.N. and Ramey, H.J., 1978, "Steam/water Relative Permeability From Production Data", Transactions, Geothermal Research Council, Vol. 2, 291-293.

Menzies, A.J., 1982, "Flow Characteristics and Relative Permeability Functions for Two-Phase Geothermal Reservoirs from a One-Dimensional Thermodynamic Model", M.S. Report, Stanford University.

Pruess, K., 1983, "Development of the General Purpose Simulator MULKOM," Annual Report 1982, Earth Sciences Division, Lawrence Berkeley Laboratory, Berkeley, CA.

Reda, D.C. and Eaton, R.R., 1980, "Influence of Steam/Water Relative Permeability Models on Predicted Geothermal Reservoir Performance: A Sensitivity Study", 6th Annual Workshop on Geothermal Reservoir Engineering, Stanford, Dec. 15-18.

Reda, D.C. and Eaton, R.R., 1981, "Definition of a Facility for Experimental Studies of Two-Phase Flows and Heat Transfer in Porous Materials", AIAA 16th Thermophysics Conference, Paper No. AIAA-81-1190.

Shinohara, K., 1978, "Calculations and Use of Steam/Water Relative Permeabilities in Geothermal Reservoirs," M.S. Report, Stanford University.

Sun, H. and Ershaghi, I., 1979, "The Influence of Steam-Water Relative Permeability Curves on the Numerical Results of Liquid Dominated Geothermal Reservoirs", Transaction, Geothermal Resources Council, Vol. 3, 697-700.

Udell, K., 1983, "Heat Transfer in Porous Media Heated from Above with Evaporation, Condensation and Capillary Effects", Journal of Heat Transfer, Aug. 1983, 485-492.

Yuster, S.T., 1951, "Theoretical Considerations of Multiphase Flow in Idealized Capillary Systems", Proc. 3rd World Petroleum Congress.

APPENDIX

Mechanism of phase trapping in flow channels.

The required thermodynamic relations are:
Laplace's equation

$$P_c = P_v - P_w = 2\gamma/r_{eq}, \text{ and} \qquad A.1$$

Kelvin's equation

$$RT \ln (P_v/P_\infty) = \frac{v_w \gamma}{r_{eq}} \qquad A.2$$

First we apply these to a trapped vapor bubble in a channel full of flowing water (Fig. 6). Considering a horizontal flow,

$$\frac{\partial P_w}{\partial x} < 0 \qquad A.3$$

Since the vapor bubble does not flow it must have constant pressure throughout (i.e. P_v = const. inside the bubble). Therefore

$$\frac{\partial P_c}{\partial x} = -\frac{\partial P_w}{\partial x} = -\frac{2\gamma}{r_{eq}^2}\frac{\partial r_{eq}}{\partial x} \qquad A.4$$

Assuming that the vapor phase and the liquid phase are in thermodynamic equlibrium along their interface, the temperature gradient is obtained by differentiating eqn. A.2

$$\frac{\partial T}{\partial x} = -\left[\frac{v_w \gamma}{R \ln (P_\infty/P_v)\, r_{eq}^2}\right]\frac{\partial r_{eq}}{\partial x} \qquad A.5$$

In the assumed configuration the vapor is superheated and hence $P_\infty > P_v$. Therefore the quantity in the square bracket in eqn. A.5 is positive.

Considering eqns. A.3, A.4 and A.5 it can be concluded that for the mechanical and thermodynamic equilibrium of the trapped vapor bubble

$$\frac{\partial r_{eq}}{\partial x} < 0 \qquad \text{A.6}$$

$$\frac{\partial T}{\partial x} > 0 \qquad \text{A.7}$$

Now we consider trapping of liquid phase in a flow channel (Fig. 7). In the trapped section liquid has constant pressure (i.e. P_w = constant). For mechanical equilibrium, eqn. A.1 yields

$$\frac{\partial P_c}{\partial x} = \frac{P_v}{\partial x} = -\frac{2\gamma}{r_{eq}^2}\frac{\partial r_{eq}}{\partial x} \qquad \text{A.8}$$

Since

$$\frac{\partial P_c}{\partial x} < 0$$

we must have $\frac{\partial r_{eq}}{\partial x} > 0$

Considering the thermodynamic equilibrium of the phases along the interface, eqn. A.2 yields

$$\frac{1}{P_v}\frac{\partial P_v}{\partial x} = \frac{\gamma\ v_w}{RT^2\ r_{eq}^2}\frac{\partial(T\ r_{eq})}{\partial x} \qquad \text{A.9}$$

Since

$$\frac{\partial P_v}{\partial x} < 0$$

equations A.8 and A.9 yield that for mechanical and thermodynamic equilibrium of the trapped liquid phase T and r_{eq} must satisfy

$$\frac{\partial\ (T\ r_{eq})}{\partial x} < 0 \qquad \text{A.10}$$

or

$$r_{eq}\frac{\partial T}{\partial x} < -\ T\frac{\partial r_{eq}}{\partial x}$$

Incorporating the eqn. A.8

$$\frac{\partial T}{\partial x} < 0 \qquad \text{A.11}$$

From eqn. A.1, A.10 and A.11

$$\frac{\partial}{\partial x}\left(\frac{T}{P_c}\right) < 0 \qquad \text{A.12}$$

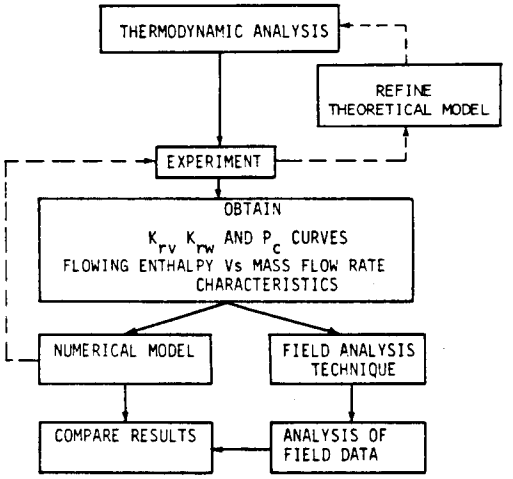


Fig. 1. Overall approach to determination of relative permeability functions for steam/water flow.

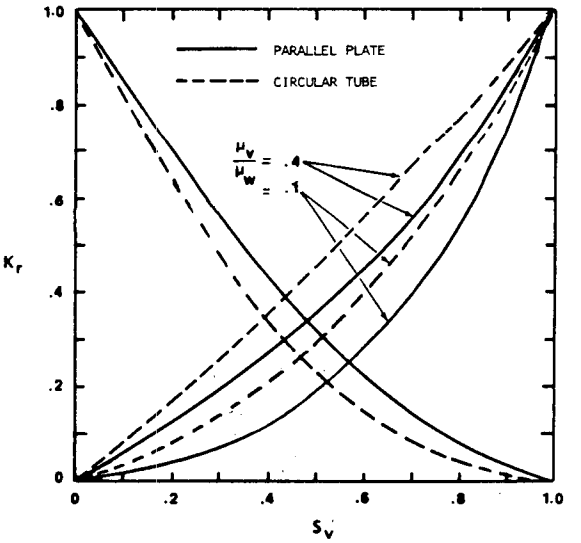


Fig. 2. Relative permeability curves for idealized capillary tubes.

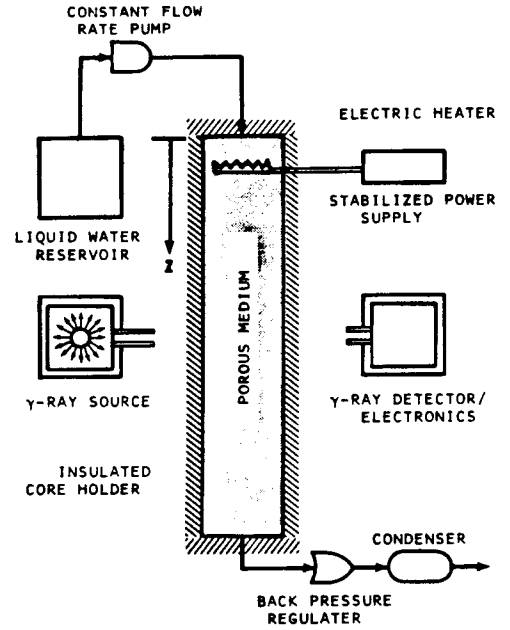


Fig. 3. Schematic of the experimental setup.

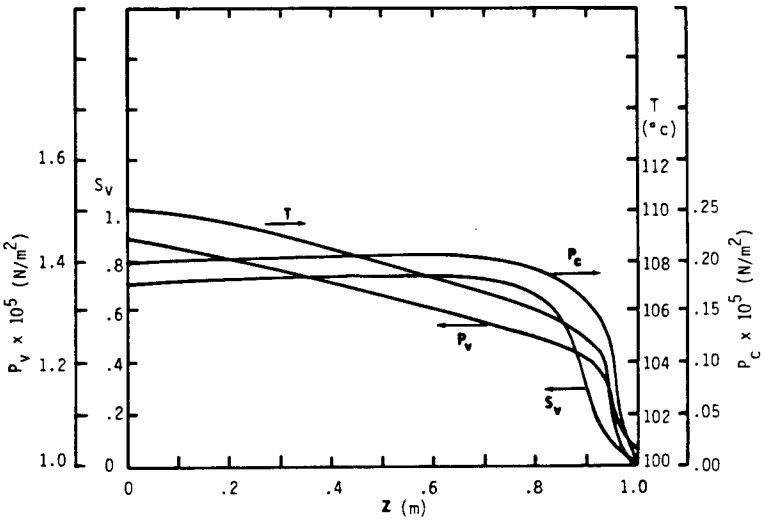


Fig. 4. Simulated test results with the end effects.

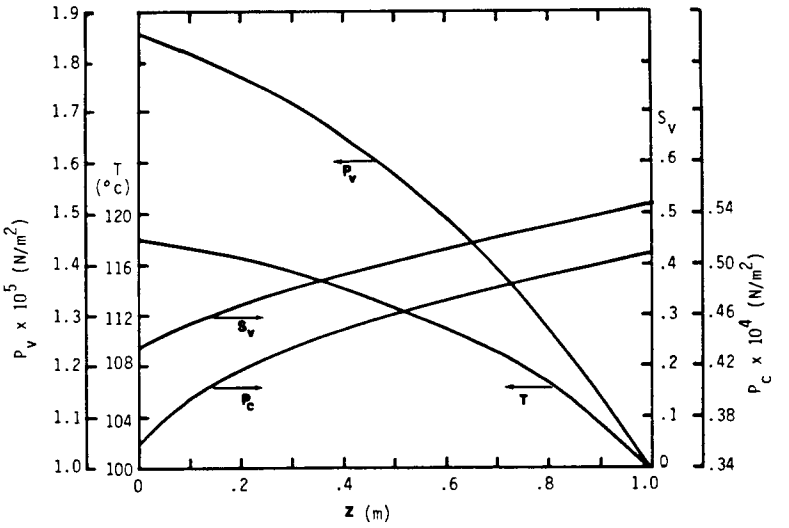


Fig. 5. Simulated test results without the end effects.

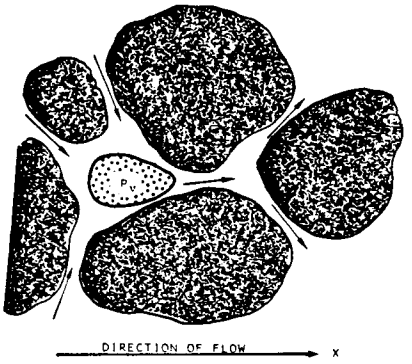


Fig. 6. Vapor trapping in a flow channel.

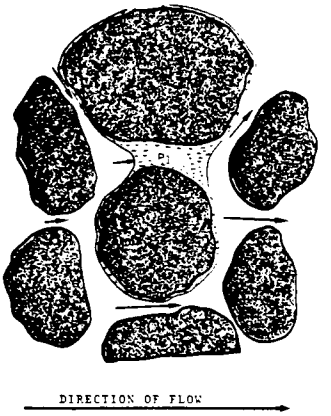


Fig. 7. Liquid trapping in a flow channel.

Proceedings Ninth Workshop Geothermal Reservoir Engineering
Stanford University, Stanford, California, December 1983
SGP-TR-74

RADIAL FLOW OF PRESSURED HOT WATER THROUGH NARROW CRACKS

Russell James

D.S.I.R., Wairakei
Private Bag, Taupo
New Zealand

ABSTRACT

Geothermal wells discharging hundreds of tonnes/hour of steam-water mixtures may be supplied at depth from one very narrow crack of width 1 to 2 mm, or alternatively, from some hundreds of hairline cracks. In the former case, turbulent flow takes place out to tens of metres from the well while the sum of frictional and kinetic pressure-drop indicates the flashing distance to be of the order of 10 cm from the well wall for pressure-temperature equilibrium. However it is unlikely that equilibrium obtains because of the high water velocity (order of 100 m/s) near the well giving no time for bubble nucleation. Flashing and hence mineral deposition are therefore not at all likely in the crack but can occur within the well from the crack horizon upwards. In the case of a multitude of fine cracks giving the same total flow, streamline conditions prevail over the flow path with the flash front a metre or so from the well, hence deposition is a possibility.

INTRODUCTION

The flow of hot water to the feed level of geothermal wells may be considered as either through one crack or for the same flow through a large number of much finer cracks. The latter condition is analogous to flow through granulated beds but has the advantage of avoiding concepts of permeability expressed by units such as the darcy.

The radial flow of pressurised hot water has been studied, James, (1975a) using test results from a well with a maximum discharge of 77 kg s^{-1} (277 t h^{-1}) with a crack width calculated at about 1.5 mm. Pressure fell rapidly within the crack when close to the well to below the value at which it would boil under stable equilibrium conditions. However, it was determined that the time interval for bubble nucleation was too short and hence that the fluid remained as a single-phase until it burst into the well, at which point exposive generation of steam takes place followed by a continuous generation as the mixture ascends to the wellhead. This result is of some importance as if flashing commonly occurs within cracks, there would be a strong likelihood of deposition of minerals taking place which would be impossible - or extremely difficult - to remove, whereas deposition within the well casing is a tractable condition even if not an attractive one.

However, if the flow was distributed over a number of fine cracks, streamline (viscous) conditions would prevail over the flow-path requiring a different calculation and in this case, the fluid velocity would be severely restricted and the radius at which pressure falls to the boiling point would be increased. Both these effects lead to steam generation within the crack and hence a potential for mineral deposition would now exist. Because geothermal wells commonly have sharply defined horizons of good inflow within the depth of interest with the remainder giving little, if any, feed over hundreds of metres of uncased hole, it appears that flow from a large number of minute cracks is rare compared with the case of one (or a few) large cracks.

It would be useful to study a well with a comparatively poor output (as a commercial proposition) and see which of these two conditions best apply. Fortunately such a well has been described recently by Menzies and others (1982) with a few values of flow and feed-horizon pressures reproduced below as Table 1.

TABLE 1: Flow Characteristics of Well 403, Tongonan, Philippines.

w Flow, kg s^{-1}	P_b Feed horizon pressure, bar
0	120
9	113.3
22.8	72
28.8	37.3
30.2	not available

RADIAL FLOW CALCULATIONS

Taking the largest flow with its associated pressure from the table; 28.8 kg s^{-1} and 37.3 bar, we can calculate the crack width, t, from the equation of James (ibid) making the assumption that turbulent flow conditions operate from the well outwards to a distance of

at least a hundred well radii. This will be checked after provisionally determining the crack width. The fluid is considered as hot water using the published enthalpy of 1270 J g^{-1} for this well giving an associated water temperature of 286.5°C, specific volume 1.3535 l g^{-1} and viscosity of 0.088 centipoise. Notation is given later. Using the metric form, the pressure-drop along the radial flow-path is:

$$P_o - P_b = 515.32 \left(\frac{w}{t\ d}\right)^2 V_f + \frac{w^{1.85} V_f\ \mu_f^{0.15}}{t^3\ d^{0.85}} \qquad (1)$$

For a well bore diameter of 220 mm and feed horizon pressure in the reservoir of 120 bar, we have:

$$120 - 37.3 = 515.32 \left(\frac{28.8}{t\ 220}\right)^2 1.3535 + 3.034 \frac{(28.8)^{1.85}\ 1.3535\ (0.088)^{0.15}}{t^3 \qquad 220^{0.85}}$$

Solving, $t = 0.64615$ mm

The changeover from viscous to turbulent flow is generally regarded as taking place at a Reynolds Number, $N_r = 2000$, Perry (1963).

where $$N_r = \frac{G\ t}{\mu_f}$$

and $$G = \frac{w}{2\ \pi\ R \left(\frac{t}{1000}\right)} \text{ kg m}^{-2} \text{ s}^{-1}$$

Hence,

$$2000 = \frac{w}{2\ \pi\ R \left(\frac{t}{1000}\right)} \quad \frac{t}{\mu_f}$$

and

$$R = \frac{w}{4\ \pi\ \mu_f} \text{ metres} \qquad (2)$$

For a flow of 28.8 kg s^{-1} and viscosity of 0.088 c'poise, the radius at the viscous-turbulent interface is 26.04 mtres. Equation (2) is surprisingly independent of crack width and gives a radius to the viscous condition which is roughly equivalent numerically to the flow-rate, and at a distance of 237 well bore radii.

We may take it therefore that Equation (1) is applicable and hence we can estimate the feed horizon pressure P_b for various flows through the crack width above, as follows:

$$120 - P_b = 515.32 \left(\frac{w}{0.646\ (220)}\right)^2 1.3535 + 3.034 \frac{w^{1.85}\ 1.3535\ (0.6945)}{(0.646)^3 \quad 220^{0.85}}$$

Hence

$$P_b = 120 - \left(\frac{w^2}{28.972} + \frac{w^{1.85}}{9.2664}\right) \qquad (3)$$

Equation (3) is used to evaluate values of P_b for various values of w and these are plotted on Fig. 1 together with test results from Table 1 and it is seen that good agreement is obtained. No sign of choking is indicated, as suggested by Menzies, et al. (ibid) and it appears that flow progressively increases with lowering of feed horizon pressure.

PRESSURE PROFILE TOWARDS WELL

To determine the fluid pressure as it flows radially towards the well, we employ Equation (1) with d replaced by radius R in metres where

$$R = \frac{d}{2\ (1000)}$$

Flow is taken as w = 28.8 kg s^{-1} and t = 0.646 mm with other factors as before.

$$120 - P_b = 515.32 \left(\frac{28.8}{t\ 2000\ R}\right) 1.3535 + 3.034 \frac{(28.8)^{1.85}\ 1.3535\ (0.6945)}{t^3\ (2000\ R)^{0.85}}$$

$$P_b = 120 - \left(\frac{0.3464}{R^2} + \frac{8.2822}{R^{0.85}}\right) \qquad (4)$$

Equation (4) enables the pressure profile to be determined from values of radius R and results are plotted on Fig. 2, where it is seen that pressure only starts to fall significantly when within a radius of about 1 m from the well centre-line. As the boiling pressure for water at 286.5°C is 70.14 bar, the associated radius is 0.1684 - 0.11 = 0.058 m. To evaluate the time taken in passing from this radius to the well, we require the water velocity

$$u_f = \frac{\left(\frac{w}{1000}\right) V_f}{2 \pi R \left(\frac{t}{1000}\right)} = \frac{w V_f}{2 \pi R t}$$

For $w = 28.8$, $V_f = 1.3535$, $t = 0.646$ and assuming provisionally that there is no flashing (steam generation),

$$u_f = \frac{28.8 (1.3535)}{2 \pi R 0.646} = \frac{9.601}{R} \quad m\ s^{-1}$$

Time in seconds =

$$\begin{cases} R = 0.1684 \\ \qquad \dfrac{\delta R}{u_f} \\ r_w = 0.11 \end{cases} = \begin{cases} R = 0.1684 \\ \qquad \dfrac{R.\ \delta R}{9.601} \\ r_w = 0.11 \end{cases}$$

$= 0.000847$ seconds

It is submitted that this is much too short a time to permit bubble nucleation, hence the water remains steam-free before it enters the well even though the pressure declines significantly below the boiling (saturated) value.

WHAT CRACK SIZE FOR COMPLETE VISCOUS FLOW?

From Equation (2) and taking R as equivalent to the well radius of 0.11 m we obtain;

$$0.11 = \frac{w}{4 \pi (0.088)}$$

hence $w = 0.1216$ kg s^{-1} and for this flow, viscous conditions apply over the whole flow-path. To determine the crack width, we employ the basic equation of James (1975b) in the metric form and for Reynolds Numbers less than 2000.

$$P_o - P_b = \frac{\mu_f w V_f \ln \left(\frac{50}{r_w}\right)}{39.37 t^3} \qquad (5)$$

To obtain the identical flow as before, we require

$$\frac{28.8}{0.1216} = 237 \text{ cracks each with}$$

the same pressure drop from 120 to 37.3 bar. We take a value of the peripheral radius of 50 m approximating to half the distance between wells.

$$120 - 37.3 = \frac{0.088 (0.1216) 1.3535 \ln \frac{50}{0.11}}{39.37 t^3}$$

$$t = 0.030 \text{ mm}$$

To obtain the pressure profile with radial flow towards the well, we have:

$$120 - P_b = \frac{0.088 (0.1216) 1.3535 \ln \left(\frac{50}{R}\right)}{39.37 (0.030)^3}$$

$$P_b = 120 - 13.51 \ln \left(\frac{50}{R}\right) \qquad (6)$$

Equation (6) is used to plot the pressure profile for viscous flow on Fig. 2 and can be compared with the case of turbulent flow. Identical flows are assumed with one crack of width 0.646 mm passing a turbulent flow of 28.8 kg s^{-1} while for viscous flow 237 cracks are required each of 0.03 mm width and passing 0.1216 kg s^{-1}. For cracks narrower than 0.03 mm a larger number is required to sustain the same flow, but the pressure profile remains the same. For all such viscous curves of Fig. 2, the pressure falls to the boiling value of 70.14 bar at a radius of 1.25 m from the well centre-line and from there to the well wall takes about 0.9 seconds for the 0.03 mm crack and much longer for narrow cracks. Hence flashing of steam is certain and the potential for mineral deposition exists, creating a 'skin' effect close to the well with increasing resistance and hence diminishing flow with time.

For viscous conditions and sufficient cracks to give equivalent flows, a straight line relationship is obtained on Fig. 1 which can be compared with the curve derived for the same flows through one crack. Downhole measurements of flowing wells should permit differentiation between these flow types as suggested in James (1975a).

CONCLUSIONS

Probably the feed to geothermal wells is from solo fissures of a size greater than 1 mm for reasonable commercial discharges. For minute cracks of total equivalent flow, a very large number is required approaching thousands, and is analogous to flow through granulated beds, which appears to be relatively rare, otherwise mineral scaling in the neighbourhood of wells, would be common in regions where the deep water has a high chemical content. Even wells which scale right down to the feed zone are rejuvenated after reaming, indicating that solids are not deposited within the rock fractures. If the opposite were true, geothermal science would be faced with potentially serious problems of descaling the matrix.

REFERENCES

Menzies, A.J., Gudmundsson, J.S. and Horne, R.N. 1982: Flashing Flow in Fractured Geothermal Reservoirs. Proc. 8th Workshop, Geothermal Reservoir Engineering, Stanford University, California, U.S.A.

James, R. 1975a: Drawdown Test Results Differentiate between Crack Flow and Porous Bed Permeability. 2nd U.N. Symp. Development and Use of Geothermal Resources. San Francisco California, U.S.A.

James, R. 1975b: Optimum Well Spacing for Geothermal Power. 2nd U.N. Symp. Development and Use of Geothermal Resources. San Francisco, California, U.S.A.

Perry, J.H. 1963: Chemical Engineers' Handbook. McGraw-Hill, U.S.A.

NOTATION

d	Diameter, mm.
G	Mass-velocity, kg m^{-2} s^{-1}.
N_r	Reynold's Number (non-dimensional).
P_o	Reservoir pressure (no-flow) at feed horizon, bar.
P_b	Pressure at feed horizon, bar.
r_w	Radius of well, mm.
R	Radius, m.
t	Crack width, mm.
u_f	Velocity of hot water, m s^{-1}.
V_f	Specific volume of hot water, kg m^{-3}.
w	Flow-rate, kg s^{-1}.
μ_f	Viscosity of hot water, centipoise.

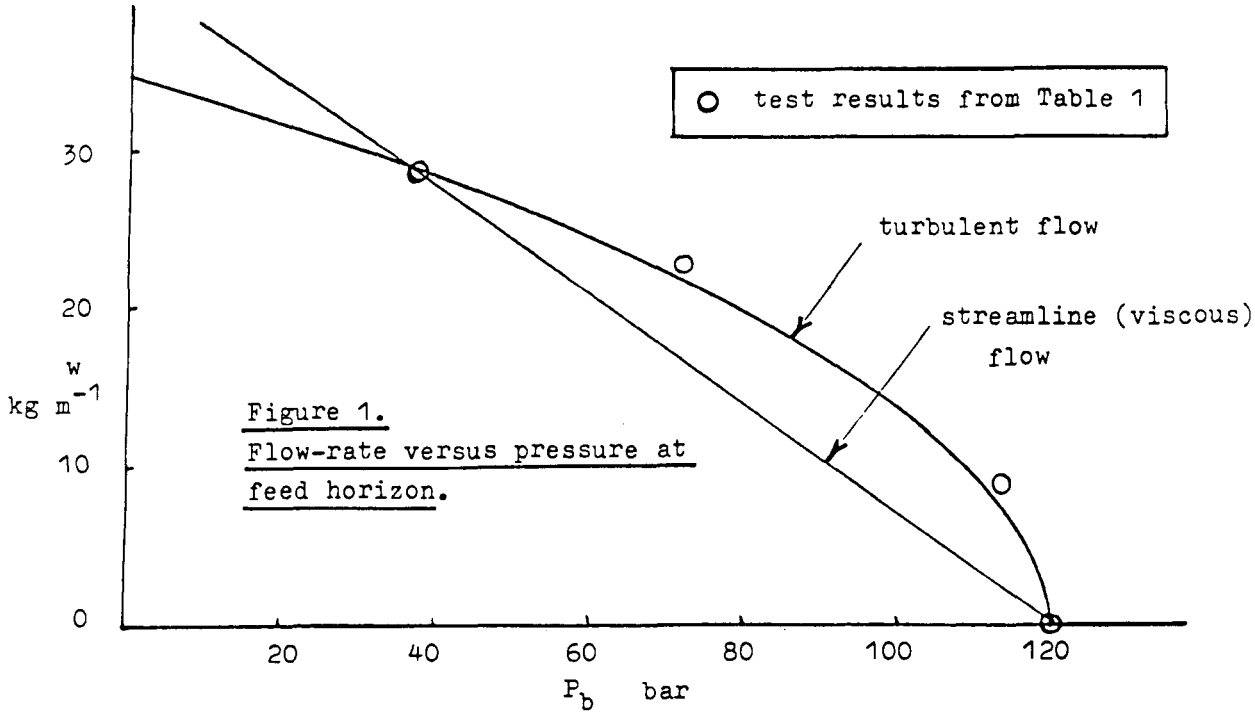


Figure 1.
Flow-rate versus pressure at feed horizon.

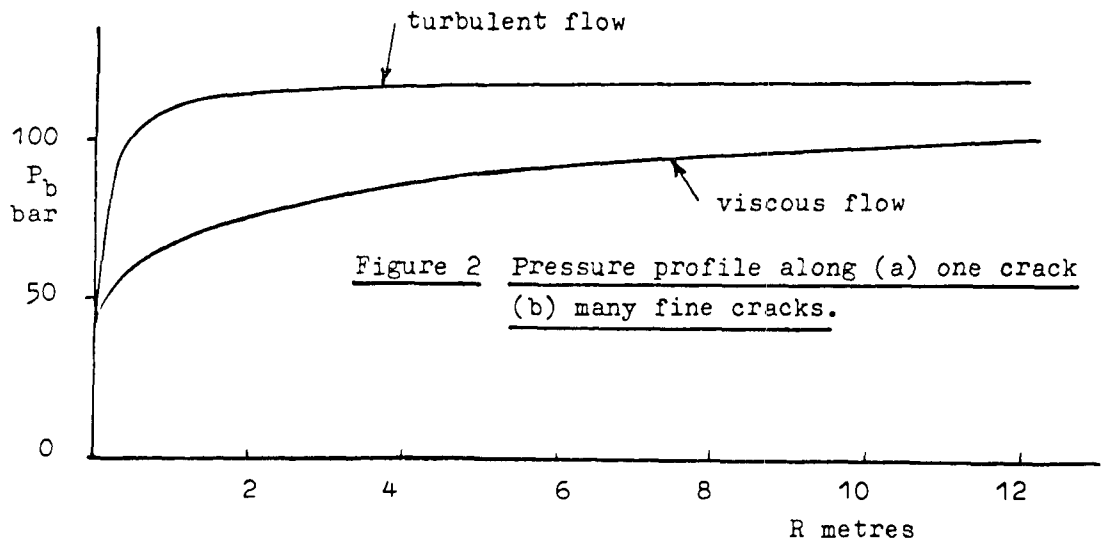


Figure 2 Pressure profile along (a) one crack (b) many fine cracks.

NINTH WORKSHOP ON GEOTHERMAL RESERVOIR ENGINEERING

Participants List

Hiroyuki Abe
Department of Mechanical Engineering
Faculty of Engineering, Tohoku University
Sendai, Japan

Hemendra Acharya
Stone & Webster Eng. Corp.
245 Summer Street
Boston, MA 02110

Richard Adams
California Energy Co.
3333 Mendocino Avenue
Santa Rosa, CA

Stefan Arnorsson
University of Iceland
Science Institute,
Dunhagi 3
107 Reykjavik, Iceland

Paul Atkinson
Union Oil Company of California
P.O. Box 6854
Santa Rosa, CA 95406

Miguel Angel Ayuso
Comision Federal de Electricidad
Ave. de las Camelinas 3527, 10° Piso
Morelia-Mich. Mexico 25231

Sally Benson
Lawrence Berkeley Laboratory
One Cyclotron Rd., Bldg. 90, M/S 1106
Berkeley, CA 94720

Alain Boisdet
BRGM-AFME
BP6009 45060
Orleans, France

William E. Brigham
Petroleum Engineering Department
Stanford University

Myron Burr
Union Oil Company
2099 Range Avenue
Santa Rosa, CA 95406

Gudmundur S. Bodvarsson
Lawrence Berkeley Laboratory
One Cyclotron Road
Berkeley, CA 94720

Claudio Calore
CNR, Instituto Internazionale per le Ricerche
Geotermiche, Via del Buongusto, 1
56100 Pisa, Italy

Regina M. Capuano
Earth Science Laboratory
420 Chipeta Way, Suite 120
Salt Lake City, UT 84108

Charles Carson
Sandia National Laboratories
Division 6241, P. O. Box 5800
Albuquerque, NM 87185

Louis Castanier
Petroleum Engineering Department
Stanford University

Michel Cathelineau
Instituto de Investigaciones Electricas
Interior Internado Palmira,
Apartado Postal 475
Cuernavaca, Morelos, Mexico

Raffaele Cataldi
ENEL/National Geothermal Unit
14, Piazza B. da Sassoferrato
56100 Pisa, Italy

Jim Combs
Geothermal Resources International, Inc.
545 Middlefield Rd., #200
Menlo Park, CA 94025

John R. Counsil
Aminoil USA
2300 County Center Drive, Suite 260
Santa Rosa, CA 95406

Gene Culver
Geo-Heat Center
Oregon Institute of Technology
Klamath Falls, OR 97601

Franco D'Amore
CNR, Instituto Internazionale per le Ricerche
Geotermiche, Via del Buongusto, 1 - 56100
Pisa, Italy

Charles Darby
KRTA
Box 4498
Auckland, New Zealand

William DaSie
Chevron Resources
595 Market St.
San Francisco, CA 94120

Paul Delaney
U.S. Geological Survey
2255 N. Gemini Dr.
Flagstaff, AZ 86001

Richard DiTommaso
Union Oil Company of California
2099 Range Avenue
Santa Rosa, CA 95401

William D'Olier
Thermal Power Company
601 California Street
San Francisco, CA 94108

Bernardo A. Dominguez
Comision Federal de Electricidad
Av. de las Camelinas No. 3527 - 7° Piso
Edific io Financiero
Fraccionamiento las Americas
Morelia, Michoacan, C.P. 58270

Richard F. Dondanville
Union Oil Company of California
Geothermal Division
P.O. Box 6854
Santa Rosa, CA 95406

Andy Drenick
Geothermal Resources International
2300 County Center Dr., Suite 264
Santa Rosa, CA 95401

Herman Dykstra
Petroleum Engineering Consultant
4180 Treat Blvd., Suite I
Concord, CA 94518

Michael J. Economides
Petroleum Engineering Department
University of Alaska
Fairbanks, AK 99701

Kathleen L. Enedy
Aminoil USA
P.O. Box 11279
Santa Rosa, CA 95406

Steven Enedy
Union Oil Company
P.O. Box 6854
Santa Rosa, CA 95406

J. C. Fernandez
Union Oil Company
P.O. Box 6854
Santa Rosa, CA 95406

Robert O. Fournier
U.S. Geological Survey
345 Middlefield Road
Menlo Park, CA 94025

Keshav Goyal
Phillips Petroleum Company
655 East 4500 South
Salt Lake City, UT 84107

Jon S. Gudmundsson
Petroleum Engineering Department
Stanford University

Massimiliano Guglielminetti
Agip
20097 S. Donato Milanese (Milano)
Posta: C.P. 12069
20120 Milano, Italy

Mohinder Gulati
Union Oil Company
P.O. Box 6854
Santa Rosa, CA 95404

Carolyne Hart
Sandia National Laboratories
Division 6256, P.O. Box 5800
Albuquerque, NM 87185

Jeffrey Hebein
MCR Geothermal Corp.
10880 Wilshire Blvd.
Los Angeles, CA 90025

Seiichi Hirakawa
Faculty of Engineering
University of Tokyo, Bunkyo-ku
Tokyo 113, Japan

Viet T. Hoang
Chevron Resources Co.
P.O. Box 7147
San Francisco, CA 94120-7147

Susan F. Hodgson
Div. of Oil and Gas
1416 Ninth Street, Room 1310
Sacramento, CA 95814

Bill Holman
Department of Energy
1333 Broadway
Oakland, CA 94612

Roland N. Horne
Petroleum Engineering Department
Stanford University

Larry Hull
EG&G Idaho
P.O. Box 1625
Idaho Falls, ID 83415

Eduardo Iglesias
Instituto de Investigaciones Electricas
Interior Internado Palmira
Apartado Postal 475
Departamento de Geotermia
Cuernavaca, Morelos, Mexico

Joe Iovenitti
Thermal Power Company
601 California Street
San Francisco, CA 94108

Mr. Ishido
NEDO (New Energy Development Organization)
Sunshine 60, 29 F, 1-1, 3-Chome
Higashi-Ikebukuro, Toshima-ku
Tokyo, 170 Japan

Jim Jackson
EPRI
Palo Alto, CA 94303

Cathy Janik
U.S. Geological Survey
345 Middlefield Road, M/S 910
Menlo Park, CA 94025

Laura A. Keith
U.S. Geological Survey
2255 N. Gemini Drive
Flagstaff, AZ 86001

Paul Kruger
Civil Engineering Department
Stanford University

Stephen T. Lam
Mechanical Engineering Department
Stanford University

Erik Layman
Chevron Resources Company
Geothermal Division
P.O. Box 7147
San Francisco, CA 94120

Stephen C. Lipman
Union Oil Company
Geothermal Division
2099 Range Avenue
Santa Rosa, CA 95401

Marcelo J. Lippmann
Lawrence Berkeley Laboratory
Earth Sciences Division
Berkeley, CA 94720

Tom Lyons
Pacific Gas and Electric Company
77 Beale Street
San Francisco, CA 94106

Luis Macias-Chapa
Petroleum Engineering Department
Stanford University

Paul F. Maeder
Division of Engineering
Brown University
182 Hope Street
Providence, Rhode Island 02912

Mark Magers
Union Oil Co. of California
Geothermal Division
2099 Range Avenue
Santa Rosa, CA 95406

Dennis S. McMurdie
Grace Geothermal Corporation
970 East 4800 South, Suite 2
Salt Lake City, UT 84117

Tsvi Meidav
Trans-Pacific Geothermal, Inc.
Suite 415
1419 Broadway
Oakland, CA 94612

Philip H. Messer
Union Oil Company of California
81-711 Highway 111
Indio, CA 92201

Donald Michels
Republic Geothermal
11823 E. Slauson Avenue
Santa Fe Springs, CA 90601

Frank G. Miller
Petroleum Engineering Department
Stanford University

John D. Miller
EG&G Idaho
Box 1625
Idaho Falls, ID 83401

Allen Moench
U.S. Geological Survey, M/S 96
345 Middlefield Road
Menlo Park, CA 94025

Phil Mogen
Union Oil Company
P.O. Box 6854
Santa Rosa, CA 95406

Rafael Molinar Cesena
Comision Federal de Electricidad
Gerencia de Proyectos Geothermoelectricos
Centro Financiero de Michoacan
Av. de las Camelinas #3527-7 Piso
Morelia, Mich., Mexico 58270

Martin M. Molloy
U.S. Department of Energy
1333 Broadway
Oakland, CA 94612

Malcolm H. Mossman
Occidental Geothermal, Inc.
5000 Stockdale Highway
Bakersfield, CA 93309

Hugh Murphy
Los Alamos National Lab.
Los Alamos, NM 87544

Manuel Nathenson
U.S. Geological Survey, M/S 910
345 Middlefield Road
Menlo Park, CA 94025

S. Nemat-Nasser
Northwestern University
Evanston, Illinois 60201

Dennis L. Nielson
Earth Science Lab/UURI
420 Chipeta Way
Salt Lake City, UT 84108

David Nieva Gomez
Instituto de Investigaciones Electricas
Interior Internado Palmira
Apartado Postal 475
Departmento de Geotermia
Cuernavaca, Morelos, Mexico

Gerald Niimi
ThermaSource Inc.
725 Farmers Lane
Santa Rosa, CA 95402

Gudmundur Palmason
Orkustofnun
(Iceland National Energy Authority)
Grensasvegur 9
108 Reykjavik, Iceland

Susan Petty
Well Production Testing, Inc.
P.O. Box 69
Carlsbad, CA 92008

R. J. Pine
Camborne School of Mines
Geothermal Energy Project
Rosemanowes Quarry, Herniss, Penryn
Cornwall TR10 9DU, England

Alfonso S. Pingol
Union Oil of California
Geothermal Division
P.O. Box 6854
Santa Rosa, CA 95406

Lyndon Pittinger
Union Oil of California
P.O. Box 6854
Santa Rosa, CA 95406

Robert W. Potter
Occidental Geothermal, Inc.
5000 Stockdale Highway
Bakersfield, CA 93309

Thomas Powell
Union Oil Geothermal Division
P.O. Box 6854
Santa Rosa, CA 95406

Susan M. Prestwich
U.S. Department of Energy
550 Second Street
Idaho Falls, ID 83401

Karsten Pruess
Lawrence Berkeley Lab.
One Cyclotron Road
Berkeley, CA 94720

Gregory Raasch
Union Oil Company
P.O. Box 6854
Santa Rosa, CA 95406

Henry J. Ramey, Jr.
Petroleum Engineering Department
Stanford University

Jack Ramsthaler
EG&G Idaho
Idaho Falls, ID 83401

Marshall Reed
Berkeley Group, Inc.
2000 Center Street, Suite 108
Berkeley, CA 94704

T. David Riney
S-Cubed
3398 Carmel Mountain Road
San Diego, CA 92121

Jesus Rivera
Seccion de Ingenieria Petrolera
Division de Estudios de Posgrado
Facultad de Ingenieria
Ciudad Universitaria
04510 Mexico, D.F.

Jill Robinson
GRI Operator Corporation
2300 County Center Dr., Suite 250
Santa Rosa, CA 95401

Mark M. Robinson
Southern California Edison Company
P.O. Box 800
Rosemead, CA 91770

Abraham Sageev
Petroleum Engineering Department
Stanford University

Edward A. Sammel
U.S. Geological Survey
345 Middlefield Road, M/S 39
Menlo Park, CA 94025

Alex Schriener
Union Oil - Geothermal
P.O. Box 6854
Santa Rosa, CA 95406

Ron Schroeder
Berkeley Group, Inc.
2000 Center St., Suite 108
Berkeley, CA 94704

Lewis Semprini
Civil Engineering Department
Stanford University

Omar Sigurdsson
Orkustofnun
Grensasvegur 9
108 Reykjavik, Iceland

Ray Solbau
Lawrence Berkeley Lab.
University of California
Berkeley, CA 94720

Michael L. Sorey
U.S. Geological Survey
345 Middlefield Road, M/S 39
Menlo Park, CA 94025

Kenneth F. Stelling
State of California
Division of Oil & Gas
50 "D" Street, Room 300
Santa Rosa, CA 95404

Cal Strobel
Union Oil Company
P.O. Box 6854
Santa Rosa, CA 95404

Mary K. Stroh-Twichell
Aminoil USA - Geothermal Area
P.O. Box 11279
Santa Rosa, CA 95406

Mr. Suzuki
New Energy Development Organization
Sunshine 60, 29 F, 1-1, 3-Chome
Higashi-Ikebukuro, Toshima-Ku
Tokyo, 170 Japan

Hideaki Takahashi
Research Institute for Strength and
Fracture of Materials
Faculty of Engineering
Tohoku University
Sendai, Japan

Richard P. Thomas
Department of Conservation
State of California - Div. of Oil & Gas
1416 Ninth Street, Room 1316-35
Sacramento, CA 95814

Randolph C. Thompson
Union Oil Co. of California
P.O. Box 6854
Santa Rosa, CA 95406

Ronald S.H. Toms
Department of Energy
1000 Independence Ave., SW
Washington, D.C. 20585

Alfred H. Truesdell
U.S. Geological Survey
345 Middlefield Road, M/S 911
Menlo Park, CA 94025

Ashok K. Verma
Lawrence Berkeley Lab.
One Cyclotron Road, M/S 1106
Berkeley, CA 94720

Pierre Ungemach
Commission of the European Communities
Rue de la Loi 200
1049 Brussels, Belgium

Raymond H. Wallace, Jr.
U.S. Geological Survey, WRD
Gulf Coast Hydroscience Center
NSTL, MS 39529

A. Watson
KRTA, Ltd.
CPO Box 4498
Auckland, New Zealand

E. R. Western
Sunedco
12700 Park Central, Suite 1500
Dallas, TX 75251

Donald E. White
U.S. Geological Survey
345 Middlefield Road, M/S 110
Menlo Park, CA 94025

Andrew J. Whittome
Chevron Resources Company
595 Market Street
San Francisco, CA 94108

Ken Williamson
Union Oil Company
P.O. Box 6854
Santa Rosa, CA 95406

Phillip Wright
Earth Science Laboratory
420 Chipeta Way, Suite 120
Salt Lake City, UT 84108

Dick Yarter
Republic Geothermal
11823 E. Slauson Ave.
Santa Fe Springs, CA 90670

SUBJECT INDEX VOLUMES 1-10

Acid stimulation: IX 421

Acoustic emission: IX 403

Adsorption: X 247

Ahuachapan field: IX 97

Air-steam-water systems: IX 351

Alaska: VI 66, VIII 25, VIII 31, X 227

Albano field: IX 17

Alfina field: I 93

Amiata field: IX 17

Aquifer:
- contamination: IX 351
- Free surface: IX 351
- geopressured-geothermal: VIII 261
- linear: X 97

Aquitaine basin: IX 5

Autoclave test facilities: IX 415

Axial splitting: IX 381

Azores: VIII 73

Baca field: VI 28, VII 47, VII 53, VIII 91, VIII 97, IX 145

Back-pressure turbines: IX 275

Basalt: VIII 189

Bejing field: IX 127

Beowaw field: IX 421

Berea sandstone: VIII 197, VIII 205

Boise KGRA: III 130

Boiling processes: IX 231

Borehole televiewer: X 13

Bottle Rock (The Geysers): IX 135

Bottom-hole pressure: IX 289, IX 291

Brady hot springs: IV 218

Brines: II 176, VII 61, VIII 309, VIII 329, X 265
- reinjection: IV 42
- scaling: IV 42
- thermodynamic properties: II 247

Brittle-ductile transition: IX 381

Broadlands field: IV 139, IV 332, V 37, V 313, VI 28, VI 238, VIII 127, VIII 183, IX 107, X 189

Build-up tests: IX 403

Bulalo field: IV 228, V 255

Calcite: IX 317, X 247

Calcium: IX 317, X 37

California: I 52, I 74, I 84, I 89, I 135, I 143, I 146, I 153, II 9, II 16, II 30, II 39, II 61, II 75, II 116, II 126, II 143, II 159, II 324, III 18, III 61, III 107, III 116, III 145, III 178, III 209, IV 96, IV 106, IV 118, IV 300, V 83, V 131, V 139, V 189, V 211, VI 13, VI 279, VI 303, VI 344, VI 351, VI 361, VII 161, VIII 31, VIII 39, VIII 45, VIII 177, VIII 295, IX 5, IX 157, IX 205, IX 299, IX 311, IX 365, IX 409, X 89, X 123, X 129, X 133, X 141, X 195, X 247, X 297

Campi Flegrei Caldera: IX 17, IX 53

Canada: X 253

Capillary pressure effects: IX 351, IX 443

Carbon dioxide: X 233, X 273

Casa Diablo: X 297

Cascade volcanic belt: X 253

Castelnuovo: VIII 323, IX 17, IX 221

Casing corrosion: X 189

Cell boundaries: X 89

Cements:
- testing: VI 126

Cerro Prieto: IV 5, V 44, V 55, V 228, VI 121, VI 130, VI 258, VI 344, VII 23, VII 29, VII 35, VIII 49, VIII 161, VIII 171, VIII 197, VIII 205, VIII 231, IX 81, IX 247, IX 291, IX 357, IX 427, X 73, X 301

Chemical analysis:
- standardization: V 139

Chemical tracers: VIII 289

China: IX 127

Chingshin field: V 64, V 96, V 277, IX 193

Chingshui field: IX 193

Choking: IX 279

Chloride concentration studies: IV 239

Chloride tracer: X 265

Circulation: X 195

Cold water injection: VII 175, VIII 279, IX 339

Comision Federal de Electricidad (CFE) research: VIII 49, IX 81

Composite reservoir: VIII 103

Compressibility: VIII 197, IX 279, IX 381

Computer codes: V 147, V 169, V 222, V 195
FRACSL: X 287, X 293
FRIP: IX 387
GEOCOM: IX 409
NSCGREATS: VIII 149
liquid-dominated systems: V 199

Computerized well test analysis: IX 199

Conceptual model: X 29, X 279

Confining pressure: IX 427

Contamination of aquifers: IX 351

Continuum model: VII 157

Convection: VIII 5

Cooling effects: IX 351, X 73, X 195

Corrosion: X 189

Coso field: VIII 45

Coso Hot Springs: IV 118

Costa Rica: VII 13, X 37

Costs: IX 409, X 31

Crack-like reservoirs: IX 403

Cracks: IX 415, IX 449

Critical flow slip model: VIII 143

Decline curve: X 105, X 163

Deliverability: X 31, X 97, X 105

Denmark: IX 5

Desert Peak: IX 151

Dilatancy: IX 381

Discrete fracture model: VII 157

Dispersion: VII 103, VIII 283, IX 253, IX 311, IX 373, X 259, X 287

Double porosity: VIII 115, VIII 219, IX 175, IX 181, X 163, X 293

Doublet systems: IX 331

Downhole pressure transient data: IX 217

Drawdown: IX 261, X 45

Drift velocity: X 287

Drill cores:
data acquisition systems: II 46

Drilling mud: VIII 205

Dry steam: X 23, X 65

Dual permeability: X 293

Ducts: IX 279

East Africa: I 113

East Brawley: VIII 39

East Mesa: IX 299, IX 311, X 247, X 287

East Mesa field: I 23, I 52, I 146, II 9, II 39, II 75

Electrical potential: IX 421

Electric Power Research Institute (EPRI) VII 21

Ellidaar field: IX 37, X 279

El Salvador: VII 13, IX 97

England: VIII 237, IX 387

Enthalpy data: VII 143, VII 151, VIII 127, IX 253, IX 345, IX 357, X 133, X 241, X 273

Environmental effects: VIII 329

Epidote: IX 269

Europe: IX 5

Expansion: IX 427

Exploration: IX 167

Explosive fracturing: IX 409

Explosive stimulation: VIII 237

Falloff data: X 151

Fault-charged systems: VII 161

Fenton Hill: II 188, IV 244, IV 249, IV 256, VI 272, VI 367, VII 97, VIII 249, VIII 269, IX 397

Ferrara: IX 17

Fissured reservoirs: IX 175

Flashing: VIII 143, IX 253, IX 279, IX 449, X 37

Flow and gas extraction model: VII 133

Flow data analysis: VII 47, VII 131, VIII 119, VIII 133, VIII 175, IX 199, IX 205, IX 345, IX 443, X 227

Flow, interporosity: X 163

Flowmeter: IX 205

Flowrate analysis: IX 345, IX 443

Flowrate prediction: IX 305, IX 365, IX 373

Fluid and heat model: VII 151, VIII 219

Fluid behavior: VIII 225

Fluid depletion: VIII 177

Fluid flow: VII 151, VIII 211, VIII 219, X 37

Fluid flow:
- measuring methods: III 198, VI 126

Fluid migration: VIII 161

Fluid reserves: X 113

FRACSL code: X 287, X 293

Fracture:
- detection: X 13
- explosive: IX 409
- ladders: VIII 139
- mechanics: IX 415
- networks: VIII 285, X 287, X 293
- skin: IX 175
- stimulation: VII 53, IX 409
- widths: IX 323

Fractured reservoirs: II 16, II 21, II 34, II 168, V 293, VII 151, VII 169, VIII 97, VIII 111, VIII 115, VIII 119, VIII 143, VIII 219, VIII 275, IX 135, IX 151, IX 299, IX 305, IX 311, IX 323, IX 331, IX 373, X 145, X 259
- flow models: I 45, VI 178
- heat transfer: V 175
- permeability: V 103

Fractures:
- deformation: I 37

Fracturing pressure: IX 397, IX 409

France: IX 5

Fujian: IX 127

Fumarole steam: IX 231

Gabbro zone: X 97

Galzignano: IX 17

Garibaldi volcanic belt: X 253

Gas:
- composition: IX 221
- concentration: IX 247
- correction: VIII 133
- geothermometers: IX 231
- noncondensable: X 37

Gas-steam ratio: VIII 323

Gas-water ratio: VIII 261

Generating capacity: IX 157

GEOCOM model: IX 409

Geological model: VIII 231

Geologic structures: I 37, III 209,
- geothermal exploration: I 113
- mathematical models: III 214

Geologic surveys:
- Alaskan sites: VIII 31
- Cerro Prieto: VIII 49
- Imperial Valley: VIII 39
- Los Humeros: VIII 19
- Pilgrim Springs: VIII 25
- Sarukawa: X 207

Geophysical surveys: I 52, III 18, III 36, III 61, III 70, VI 328, VI 338
- evaluation: V 115

Geopressured-geothermal aquifer: VIII 261

Geopressured systems: I 130, I 146, VI 76, VI 84, VI 98, VI 105
- geologic faults: III 209
- geothermal wells: IV 280
- ground subsidence: IV 280
- mathematical models: II 299
- sandstones: IV 280
- simulation: II 299, V 159

Geothermal energy:
- research programs: I 23, I 198, I 199, I 219, III 192, IV 15, V 5, VI 150
- resource assessment: VI 3
- resource development: IV 5

Geothermal exploration: III 130, VI 338, VI 361

Geothermal fields:
geologic faults: II 46
geologic structure: II 46, VI 21
heat flow: II 30
mathematical models: IV 36
recharge: II 40, II 150, II 159, II 339, V 55, VI 21
reinjection: II 8, II 46, II 98, II 116, II 181, IV 322, V 26, V 37
rock-fluid interactions: II 34
tracer techniques: IV 249, VI 344
well temperature: II 290, VI 272, VI 279, VI 297, VI 316, VI 328

Geothermal fluids: V 278
chemical analysis: II 30, II 116, VI 21,
chemical composition: IV 96, V 262 VI 279
geochemistry: VI 84, VI 367
plugging: III 163, IV 275
reinjection: IV 294, V 355
scaling: I 185, IV 42
thermodynamic properties: I 247, II 247, IV 294
transport: V 329
water chemistry: VI 98

Geothermal power plants: I 117, I 153, II 9, II 116
economics: I 153
performance: I 135
steam separators: I 135

Geothermal reserves: IX 193

Geothermal resources:
brines: I 135
economic analysis: II 150, III 158, VI 3, VI 238
economics: I 161, I 167
geothermal fluids: I 113
management: II 181, V 5
remote sensing: II 30
reservoir engineering: IV 234
resource assessment: II 12, III 145, VI 238
resource development: VI 13, VI 34, VI 41, VI 374, VI 380
resource potential: III 3, III 9, III 70, III 96, III 107
risk assessment: VI 374, VI 380
temperature surveys: II 30, II 40, VI 28

Geothermal space heating: II 181

Geothermal systems:
convection: I 206, I 213, II 236, II 251, II 339, IV 300
flow models: I 26, I 42, I 45, I 52, I 62, I 201, I 213, I 267, II 193, II 200, II 229, III 188, III 209, IV 286, IV 300, IV 308, V 11, VI 194, VI 218, VI 322
fluid injection: VI 98, VI 204
heat extraction: II 46, II 181, II 188, II 200, VI 264, VI 272
heat transfer: I 50, I 52, I 249, II 46, II 222, II 236, II 251, II 263, II 268, IV 112, IV 286, IV 300, IV 308, VI 243
hydrodynamics: IV 146, IV 160
mass transfer: II 268, IV 286, IV 300, IV 308
mathematical models: I 26, I 65, I 146, I 242, I 247, I 267, II 46, II 126, II 193, II 263, II 268, II 308, II 324, III 203, III 214, IV 36, IV 286, IV 300, IV 308, VI 194, VI 213, VI 264
natural convection: VI 194
reinjection: I 62
reservoir engineering: I 146, II 3, II 6, II 9, IV 36, V 5, VI 66, VI 253
rock-fluid interactions: I 240, IV 275, VI 322
simulation: I 130, I 198, I 201, I 225, I 232, I 247, II 116, II 159, II 222, II 308, II 310, III 178, III 185, III 188, IV 308, IV 332, VI 188, VI 204, VI 213, VI 253
thermodynamic properties: VI 213
two-phase flow: I 42, III 185, III 192, IV 308, VI 28, VI 49, VI 170, VI 288
vapor pressure: IV 60
water chemistry: IV 42, IV 275, IV 294

Geothermal wells:
enthalpy: VI 224
explosive stimulation: I 192, II 213, II 219
field tests: II 109, II 176, IV 96
flow models: V 322, VI 130, VI 159, VI 188
flow rate: VI 139
fluid withdrawal: VI 139
hydraulic fracturing: I 174, I 178, I 180, II 188, II 198, II 200, III 36, VI 272, VI 303
mathematical models: VI 130, VI 159
measuring instruments: II 101, II 109, II 176, VI 126
performance: VI 218
plugging: III 163, IV 106
pressure measurement: IV 96
sampling: VI 84
scale control: I 185
sonic logging: IV 256
temperature measurement: II 136, IV 96
testing: I 69, I 74, I 77, I 93, I 101, I 117, I 124, II 21, II 75, II 85, II 98, II 116, II 143, II 168, III 64, III 96, III 116, III 125, III 130, III 138, III 145, III 172, IV 106, IV 112, IV 118, IV 133, IV 139, IV 146, IV 153, IV 160, IV 165, IV 176, IV 188, IV 201, IV 207, IV 213, IV 218, IV 322, V 11, V 44, V 55, V 64, V 77, V 83, V 90, V 115, VI 322, VI 76, VI 105, VI 145, VI 150, VI 159, VI 170, VI 288
transients: I 93, I 124, III 172, VI 159, VI 170

two-phase flow: I 77, II 21, III 198
well logging: I 74, II 21, II 66, III 36, III 70, III 81, V 282, V 316, VI 258, VI 279, VI 303, VI 310
well pressure: I 157, VI 28, VI 145, VI 150

Geothermometry: II 34, VI 367, VI 351, IX 231

Germany: IX 5

Geysers: I 84, I 89, I 153, II 16, II 30, II 61, II 143, III 18, III 61, IV 96, IV 106, IV 201, V 83, V 127, V 175, V 302, VI 13, VI 279, VI 344, VI 351, VI 361, VIII 177, VIII 295, IX 135, IX 409, X 89, X 105, X 123, X 129, X 133, X 141

Goddard Springs: VIII 31

Granite: VII 127, VII 133, IX 387

Gravity change/subsidence ratio: VIII 177

Greece: IX 73

Ground subsidence: I 65

Guangdong: IX 127

Gulf coast, U.S.: VI 84

Hatchobaru, IX 115, X 79

Hawaii: I 219, II 109, III 138, IV 133, IV 201, VIII 155, VIII 309, X 65, X 201

Heat:
conduction: X 195
extraction: VII 169, VIII 255, X 73
flow: VII 151, VIII 211, VIII 219, VIII 225
sweep model: X 73
transfer: VII 151, X 151
transmission model: VIII 269

Heat transfer: III 49

Heber field: I 74, I 135, II 9, II 126 IX 157

Hengill geothermal area: X 23

High-temperature logging: VII 115

History matching: X 97

Hoki: X 79

Hot-dry-rock reservoirs: VII 97, VIII 237, VIII 249, VIII 269, IX 5, IX 387, IX 397, IX 403

Hot-dry-rock systems: I 174, I 258, II 188, II 193, II 198, II 200, II 213, III 49, V 103, VI 272, VI 303, VI 367
fluid flow: IV 244, IV 249, IV 256, IV 264

Hot-dry-rock systems:
fracture properties: IV 244, IV 249, IV 256, IV 264, IV 270
growth: IV 270
heat extraction: IV 244
resource assessment: III 3

Hot springs: IX 365, X 123

Hot-water reservoirs: IX 291

Hot-water systems: VI 351
economics: III 158
reservoir engineering: VI 3

Hydraulic conductivity: X 287

Hydraulic fracturing: IX 397, IX 409, IX 415

Hydraulic injections: IX 387

Hydrogeologic model: VIII 171

Hydrogen sulfides:
renewal: I 153

Hydrology: VIII 67, VIII 275, VIII 285

Hydrothermal alteration: II 34, III 361, IX 145, IX 269, X 253

Hydrothermal convection systems: VIII 5

Hydrothermal systems: VIII 5, VIII 19, VIII 25, VIII 31, VIII 39, VIII 45, IX 135, IX 145, IX 151, IX 157, X 89

Hydrothermal systems:
ground subsidence: II 310
mathematical models: I 126, I 161, VI 21, VI 69
simulation: V 147, V 159, V 212

Iceland: IV 153, V 169, V 329, VI 49, VII 13, VII 61, VII 71, VII 139, VIII 111, VIII 189, VIII 211, IX 37, IX 345, X 23, X 45, X 177, X 279

Ihaho: I 117, I 124, II 75, II 168, III 125, III 130, V 26, V 120, V 183, VI 115, VIII 275, VIII 279, IX 299, IX 311, X 287

Imperial Valley: III 107, VIII 39, VIII 197, IX 5, IX 205, IX 409

Industry advisory panel: X 5

Inhibitor degradation rate: IX 317

Injected fluid monitoring: X 297

Injection-backflow tracer tests:
IX 299, IX 305, IX 311, X 247

Injection depth: IX 339

Injection tests: VII 71, VII 77, VII 175, VIII 73, VIII 97, VIII 103, VIII 111, VIII 249, VIII 275, VIII 279, VIII 283, IX 299, IX 305, X 195

Injection wells:
performance: V 255
plugging: III 163
testing: V 26, V 37, VI 115

Interference testing: IX 151, IX 187, IX 193

Isotopic studies: VIII 45, VIII 309, VIII 323, IX 253, X 253

Italy: I 37, I 93, I 101, II 21, II 40, II 150, IV 201, IV 165, III 214, V 90, V 197, V 212, V 262, VI 21, VI 351, VII 13, VII 77, VII 85, VII 91, VIII 295, VIII 315, VIII 323, IX 5, IX 17, IX 53, IX 221, IX 247

Ixtlan de los Hervores: IX 81

Japan: III 70, VII 13, VII 103, VII 115, VIII 149, VIII 155, IX 115, IX 403, X 79, X 207

Kakkonda: IX 115, IX 403

Kawerau field: VI 170, VIII 183

Kenya: IX 65

Kilauea volcano: VIII 309, X 65, X 201

Kirishima field: VIII 149

Kizildere field: X 53

Klamath Falls: IX 187, IX 331

Krafla field: V 169, VI 49, VII 71, VIII 211, IX 37, IX 211, IX 345, X 177

Land leasing
legal aspects: I 153

La Primavera: IX 81, IX 87

Lardarello field: I 37, II 21, II 40, II 150, III 214, V 90, V 212, V 262, VI 21, VI 351, VII 77, VII 85, VII 91, VIII 295, VIII 315, VIII 323, IX 5, IX 17, IX 221, IX 247, X 113, X 273

Lassen hydrothermal system: IX 365

Latera field: IX 5, IX 17

Laugarnes field: IX 37

Lawrence Berkeley Laboratory: IX 205, IX 443

Lawrence Berkeley Laboratory numerical simulator: VIII 255, IX 157

Leyte: IX 121

Linear acquifer: X 97

Linear elastic fracture mechanics: IX 415

Lip-pressure method: VIII 133

Liquid-dominated system: X 189

Liquid-phase heterogeneity: IX 253

Log-log type curve: X 163

Longevity: IX 157

Long Valley: II 324

Los Alamos: VIII 249, VIII 269

Los Azufres field: IV 176, VII 41, VII 143, IX 81, IX 253, IX 269, IX 275, IX 285, X 213, X 219, X 233, X 241, X 265

Los Humeros field: VIII 19, IX 81

Los Negritos: IX 81

Louisiana: VI 76, VIII 261

Low-temperature reservoirs: VII 109

Lumped double porosity: VIII 189

Lumped parameter model: VII 23, X 45, X 97

Mak-Ban field: VI 34

Makushin volcano: VIII 31, IX 167, X 227

Mammoth-Pacific power plant: X 297

Maritaro: IX 269

Mathematical models
comparative evaluations: VI 121
wellbore: VI 130

Matrix diffusion: IX 323

Matrix-dominated reservoirs: IX 299

Matrix thermal expansion: IX 427

Matsukawa: IX 115

Meager Creek: X 253

Methane: VII 133

Mexico: IV 5, IV 239, IV 176, V 44, V 55, V 228, VI 60, VI 130, VI 258, VI 328, VI 344, VII 13, VII 23, VII 29, VII 35, VII 41, VII 53, VIII 19, VIII 49, VIII 161, VIII 171, VIII 197, VIII 231, IX 81, IX 87, IX 253, IX 269, IX 275, IX 285, IX 357, IX 427, X 73, X 213, X 219, X 233, X 241, X 265, X 273, X 301

Microcracking: IX 381

Milos Island: IX 73

Mineral alteration zones: IX 269

Mineralogy: IX 269, X 89, X 253

Mineral precipitation: X 247

Miravalles field: X 37

Mofete: IX 5, IX 17, IX 53

Mokai field: IX 107, X 29

Momotombo: III 96

Monroe field: V 115

Monte Amiata: IX 5, IX 17

Mori: IX 115

Mountain Home field: V 183

Moving front: VIII 103

Mud contamination: VIII 205

Multi-component modeling: X 279

Multiple interacting continua (MINC): VIII 219

Namafjall field: VI 49, IX 37

Natural gas wells: III 29

Nesjavellir field: IX 37, X 23

Nevada: IV 218, V 329, IX 151, IX 421

New Mexico: II 88, V 103, V 238, VI 28, VI 272, VI 367, VII 97, VIII 91, VIII 97, VIII 249, IX 145, IX 397

New Zealand: I 126, II 40, II 308, II 310, III 185, IV 36, IV 139, IV 217, IV 332, V 37, V 199, V 205, V 302, V 309, VI 28, VI 41, VI 126, VI 139, VI 145, VI 170, VI 238, VII 13, VIII 67, VIII 111, VIII 127, VIII 133, VIII 183, IX 107, IX 323, X 31, X 189

Nicaragua: III 96

Niland field: I 135, I 143, II 9

Ngawha field: V 309, VIII 133, IX 107

Nicaragua: VII 13

Nigorikawa: IX 403

Noncondensible gases: X 113, X 233

Nonisothermal injection: VIII 103, IX 211, X 151

NSCGREATS model: VIII 149

Ohtake: X 79

Okoy field: VI 69

Olkaria: IX 65

One-dimensional sweep model: VIII 255

Onikobe: IX 115

Onuma: IX 115

Optimization: X 31

Oregon: IX 187, IX 331

Orthogonal fracture junctions: IX 373

Otake: IX 115

Output curve: X 37

Overexploitation: IX 97

Paragenesis: IX 269

Paris basin: IX 5

Pauzhetka field: X 57

Permeability: VII 121, VII 127, VIII 111, VIII 127, VIII 205, VIII 211, VIII 261, IX 145, IX 239, IX 299, IX 345, IX 387, IX 443, X 301

Permeability-thickness ratio: VIII 261

Petrochemistry: VIII 39

Petrothermal energy: IX 381, IX 387, IX 397, IX 403, IX 409, IX 415

Phase separation: IX 253

Phase studies:
aqueous solutions: IV 66

Phase trapping: IX 443

Philippines: IV 228, V 255, VI 34, VI 69, IX 121

Phlaegrean fields (Mofete): IX 5, IX 17

Pilgrim Springs field: VIII 25
flow models: II 229, VI 218
two-phase flow: IV 66

Plastic flow: IX 381

Porosity logging: VIII 189

Porosity prediction: IX 305

Porosity-thickness product: IX 193

Porous media: IX 443, X 287, X 293

Potassium concentration studies: IV 239

Power generation: VII 35, VII 21, IX 81, IX 275, X 53, X 219, X 227

Pressure build-up tests: IX 193, X 177

Pressure drawdown: X 97, X 233

Pressure measurements: V 96, V 103, VIII 67, VIII 91,VIII 103, VIII 119, VIII 279, IX 199, X 241

Pressure prediction: IX 351

Pressurized tests: X 169

Pressure transient analysis: VII 161, IX 387, X 133, X 151, X 163

La Primavera field: VI 328

Production data: IX 345, X 57

Production engineering: X 183, X 189, X 195

Production/injection ratio: IX 339

Productivity index: IX 289, IX 291

Productivity (inferred): IX 211

Proximity functions: VIII 219

Pseudo-steady state flow: IX 175, IX 181

Puhagan field: IX 121

Puna: X 65, X 201

Pyrite: IX 269

p/Z analysis: X 97

Quartz precipitation: IX 239

Quasi-three-dimensional model: VIII 225

Radial flow: IX 449

Radicondoli: IX 17

Radon: VII 133, VIII 315, IX 261
simulation model: IX 261
transport: IX 261

Radon 222:
diffusion: V 302
monitoring: II 61, V 309, VI 344
tracer studies: IV 201

Raft River: VIII 275, VIII 279, IX 299, IX 311

Raft River field: I 117, I 124, II 75, II 168, III 125, V 26, V 120, VI 115, VI 159

Rate testing: VIII 73, VIII 119, X 163

Reactive-solute transport: IX 239

Recharge (natural): IX 221, IX 351, IX 357, X 73

Redondo Creek: VIII 91, VIII 97, IX 145

Reinjection: VII 41, VII 77, VII 85, VIII 49, VIII 275, VIII 279, VIII 289, IX 17, IX 97, IX 121, IX 339, X 259, X 265

Relative permeability: IX 443

Remote sensing: X 13

Research programs: DOE: VIII 1, VIII 49, IX 1; EPRI: VII 21
International cooperation: VII 13, VII 29, VIII 49, IX 1
University: VII 5, VIII 255
U.S.: VII 7, VII 11

Reservoir:
behavior: VII 143
boundaries: X 89
decay: X 213
evaluation: X 201, X 207, X 213, X 219, X 227
longevity: VII 161
performance study: X 207
scale: IX 217
simulation: VIII 137

Reservoir chemistry: VII 91, VII 127, VII 133, VII 143, VIII 45, VIII 295, VIII 309, VIII 315, VIII 323, VIII 329, IX 65, IX 221, IX 231, IX 239, IX 247, IX 253, IX 261, IX 269, X 113, X 133, X 233, X 241, X 247, X 253, X 259, X 265

Reservoir engineering: III 87, IV 36, VII 1, VII 5, VII 7, VII 11, VII 13, VII 21, VII 161, VIII 25, VIII 49, VIII 171, VIII 231, VIII 275, IX 17, IX 107, IX 121, IX 415, X 1, X 5, X 13, X 97, X 207, X 273

Reservoir physics: VII 115, VII 121, VII 139, VII 143, VIII 19, VIII 49, VIII 161, VIII 171, VIII 177, VIII 183, VIII 189, VIII 197, VIII 205, IX 421, IX 427, IX 443, IX 449, X 293, X 297, X 301, X 307

Reservoir rock:
- permeability: I 26, I 192, II 16, II 34, II 188, II 198, III 24, III 172, III 192, IV 50, VI 218, VI 224, VI 288, VI 297, VI 316, VI 361
- plugging: II 34
- rock mechanics: II 263

Resistivity monitoring: VIII 161, VIII 189, IX 421, X 45

Resistivity-porosity relationship: VIII 189

Resource assessment: VII 109, VIII 1, VIII 31

Resource development: VII 23, VII 29, VII 35, VII 41, VII 47, VII 53, VII 61, VII 71, VII 77, VII 85, VII 91, VIII 1, VIII 49, VIII 67, VIII 73, IX 5, IX 17, IX 37, IX 53, IX 65, IX 73, IX 81, IX 87, IX 97, IX 107, IX 115, IX 121, IX 127, X 23, X 31, X 37, X 45, X 53, X 57, X 65, X 73, X 79

Reykjanes field: VII 61, IX 37, X 45

Ribiera Grande field: VIII 73

Rift zone: X 65

Rock failure: IX 381

Roosevelt KGRA: I 77, III 89

Rotorua field: IX 107

Rotarua-Whakarewarewa Field: VI 41

Rotary drilling: II 3

Salton Sea area: X 195

Salton Sea field: III 145, III 178, V 120

San Donato: IX 17

Sandstone: VIII 197, VIII 205, IX 427, X 287

San Miguel Island: VIII 73

San Vito: IX 5

Sarukawa waterflood project: X 207

Scale inhibitor: IX 317

Scaling: VI 130

Scaling effects: IX 217, IX 277, IX 449, X 37

Sedimentary rocks: IX 427

Seismicity: II 101

Seismic study: X 297

Seltjarnarnes field: IX 37

Serrazzano Field: IV 201, V 169

Shear failure: IX 383, IX 397

Silica: X 247, X 279

Simulation: VIII 115, VIII 149, VIII 211, VIII 219, VIII 225, VIII 231, VIII 255, VIII 261, IX 261, IX 351, IX 357, IX 365, IX 373, X 105, X 151, X 195, X 273, X 279, X 287

Sitka: VIII 31

Skin: X 169

Slug test: IX 181, X 169

Sodium concentration studies: IV 239

Solute breakthrough: VIII 285

Solute transport: IX 305, X 287

Southern Negros: IX 121

Spinner measurements: IX 199, IX 205

Stanford Geothermal Program: VIII 255, IX 199

Stanford hydrothermal model: VII 169

Steam:
- condensation: IX 231
- excess: X 233
- flow model: VII 179
- quality: IX 231
- reservoirs: IX 285

Step-rate injection tests: VIII 103

Stimulation: VIII 237

Stochastic fracture distributions: VIII 219

Storage capacity: X 169

Stratigraphy: IX 145

Stress: IX 387, IX 397, IX 415, IX 427

Streamtube model: VIII 143

Subsidence: VIII 177, VIII 183

Suginoi: IX 115

Summer Bay: VIII 31

Surface electrical potential: IX 421

Surprise Valley: VI 303

Svartsengi field: IX 37

Sweet Lake aquifer: VIII 261

Tainjin field: IX 127

Taiwan: V 64, V 96, V 249, VII 13, IX 193

Tauhara field: VIII 67

Tectonics: VIII 39

Tejamaniles: IX 269

Temperature:
cycling: IX 427
distribution: IX 339
drop model: X 183
monitoring: X 265
reversals: X 31

Temperature gradients:
mathematical models: V 337, V 343

Temperature measurement: III 55, III 89, III 107

Tenakee Springs: VIII 31

Test well: IX 167

Texas: II 299, IV 280, VI 76, VI 105

Thermal conductivity: VIII 214

Thermal degradation: IX 351

Thermal expansion: VIII 197, IX 427

Thermal landslide: X 123

Thermal Shallow Reservoir: X 129, X 133, X 141

Thermodynamic behavior: X 213, X 241

Thermohydrodynamic model: X 57

Tibet: IX 127

Tiwi field: VI 34

Tongonan field: IX 121

Torre Alfina: IX 5, IX 17

Torvaliga: IX 17

Tracer:
dispersivity: X 259
recovery: IX 299, IX 305, IX 311
retention: VIII 289

Tracer tests: VII 41, VII 85, VII 103, VII 135, VIII 289, IX 261, IX 323, IX 331, X 133, X 247, X 265

Transient flow: IX 175, IX 181

Transmissivity: VIII 279, IX 211, X 23

Travale: IX 5, IX 17

Travale KGRA: I 101, IV 165

Triangular probability: X 31

Tritium: VIII 323

Turbogenerators: IX 275

Two-phase flow: VII 175, VIII 91, VIII 127, VIII 133, VIII 137, VIII 143, VIII 149, VIII 155, IX 283, IX 443, X 23, X 65, X 183, X 227, X 241

Two-phase flow:
monitoring: III 43

Unalaska Island: VIII 31, IX 167, X 227

United Kingdom: VIII 237, IX 5, IX 387

U.S. Department of Energy (DOE)
research: VIII 1, VIII 9, IX 1, X 1

U.S. Geological Survey: VII 11

USSR: VIII 329, X 57

Utah: I 77, III 89, V 115

Valles Caldera: V 238, VI 272, IX 145, IX 397

Valve closure: IX 403

Vapor-dominated system: VIII 295, VIII 315, IX 247, IX 261, X 89, X 97, X 105, X 113, X 65, X 227, X 273

Vapor-dominated systems: VI 194
bottom hole pressure: V 127
two-dimensional calculations: VI 194

Vapor separation: IX 253

Vertical flow model: VIII 155

Vertical steam wells: IX 285

Vicenza: IX 17

Viscosity: IX 211, IX 443

Volcanic regions:
heat transfer: VI 243

Volcanoes:
Garibaldi belt: X 253
Kilauea: VIII 309, X 65, X 201
Makushin: VIII 31, IX 167, X 227

Vulcano: IX 17

Wairakei: II 40, II 308, II 310, III 185, IV 36, IV 217, V 199, V 205, V 302, V 309, VI 121, VI 126, VI 139, VI 145, VI 28, VI 41, VI 238, VI 253

Wairakei field: VIII 67, VIII 183, IX 107, IX 323

Water influx: X 45, X 97

Water-rock reaction: IX 317

Water reservoirs:
hydrodynamics: IV 146

Well:
completion: X 37
discharge: VII 61
drilling: VII 35, VIII 25, X 31
stimulation: VII 53, VIII 237, IX 17, IX 121

Wellbore:
heat transmission code: VIII 269
scale: IX 217, X 37
simulation: VIII 137

Wellhead power plant start-up: X 219

Wellhead pressure: IX 285, IX 291

Well logging: VII 29, VII 115, VIII 161, VIII 171, VIII 177, VIII 183, VIII 189, VIII 197, VIII 205, VIII 237, IX 205, X 13, X 189

Well siting: VII 161

Well testing: VIII 73, VIII 91, VIII 97, VIII 103, VIII 111, VIII 115, VIII 119, VIII 137, VIII 261, IX 17, IX 53, IX 73, IX 167, IX 175, IX 181, IX 187, IX 193, IX 199, IX 205, IX 211, IX 217, X 145, X 151, X 163, X 169, X 177

Wyoming: VI 28

X-ray diffraction: IX 269

Yangbajain field: IX 127

Yunnan: IX 127

Yellowstone: VI 28

AUTHOR INDEX VOLUMES 1-10

Aamont, R.L.: II 188

Abe, H.: I 180, II 200, IX 403, IX 415

Abou-Sayed, A.S.: V 26

Abriola, L.: V 175

Abril, A.: VII 29, VIII 231

Adams, M.C.: IX 299, X 247, X 253

Adams, R.H.: III 96

Aguilar, R.G.,: VI 367

Ahmed, U.: V 26

Albright, J.N.: IV 256

Allegrini, G.: VII 77, VIII 231

Allen, C.A.: III 125

Allis, R.G.: VIII 67, VIII 177, VIII 183

Alonso-E., H.A.: IV 5, V 228, IX 81

Andrade, M.: VIII 261

Ansari, J.: VIII 31

Antonelli, G.: V 147

Aragon, A.: X 219, X 241

Archambeau, C.: II 263

Arce, G.N.: VIII 31

Arellano, V.: VII 29, IX 291, IX 357, X 241, X 301

Arenas, A.: VIII 205

Arnorsson, S.: IX 65, IX 321

Asseus, G.E.: II 268

Atherton, R.W.: I 267

Atkinson, P.G.: II 46, III 29, III 64, V 257

Axelsson, G.: VIII 189

Ayatollahi, M.S.: IV 264

Banerdt, M.: VII 133

Barelli, A.: I 93, I 101, IV 165, V 11

Barkman, J.H.: II 116, III 116

Barnes, H.L.: I 185, II 176

Barr, H.: X 31

Barragan, R.M.: IX 253, X 219, X 265

Bartz, D.: IV 50

Batchelor, A.S.: VIII 237

Bazant, Z.P.: I 232, IV 270

Bjornsson, S.: IX 65

Benoit, W.R.: IX 151

Benson, S.: VII 71, VII 161, VIII 103, IX 187, IX 205

Bermejo M., F.: VII 25, VIII 197, IX 427

Bertrami, R.: IX 221

Bickham, R.E.: V 316

Bixley, P.F.: V 37, VI 126, VI 238, VIII 133, IX 107, X 189

Blair, C.K.: V 115, VI 98

Bloomster, C.H.: I 167

Bodvarsson, G.: I 45, II 52, III 203, IV 146, IV 153, IV 160, V 64, V 329, VI 338, VII 139

Bodvarsson, G.S.: VII 71, VII 161, VIII 161, VIII 211, IX 157, IX 211, IX 345, IX 351, IX 443, X 105, X 151, X 279

Bories, S.: I 247, IV 66

Breitenbach, K.A.: VIII 289

Brigham, W.E.: I 26, IV 165, V 212, VI 297, VI 150, X 97

Brown, D.W.: II 188, VIII 249

Brown, G.L.: IX 409

Brown, L.S.: VI 279

Brown, S.: V 183, V 343

Brownell, D.H.: II 310, IV 280

Bunyak, M.J.: VII 53

Byerlee, J.D.: II 198, IV 50, VII 127

Cabrera, J.: X 265

Calamai, A.: IX 17

Calore, C.: VI 21, VII 85, VII 91, VIII 295, IX 221, IX 247, X 273

Campbell, D.A.: II 116, III 116, IX 167, X 227

Cappetti, G.: VII 77

Capuano, R.M.: VIII 275, IX 299

Carella, R.: IX 53

Castaneda, M.: VII 29, VIII 231, IX 357

Castanier, L.M.: IV 66, VII 23

Cataldi, R.: IX 17

Cathelineau, M.: IX 269

Cederberg, G.: IV 201

Celati, R.: I 37, I 101, I 242, II 21, II 150, VI 21, VII 77, VII 91, VIII 295, IX 221, IX 247, X 273

Chang, C.R.Y.: V 64, V 96, V 249, V 337

Chang, S.P.: II 193

Champman, D.S.: V 115

Chen, B: II 109, III 138, IV 133, X 201

Cheng, P.: I 219, II 236, V 192, V 322, VI 243

Chiang, C.Y.: V 337, IX 193

Chiang, S.C.: V 249

Chiu, T.L.: IX 193

Cillerai, V: II 21

Cinco, H.: IV 165

Clemo, T.M.: X 287

Cofo, J.: X 73

Contreras, E.: VIII 197, IX 427, X 307

Corona, A.: X 265

Counce, D.A.: VI 367

Counsil, J.: III 192, IV 60

Cox, B.L.: X 151

Crosby, G.: III 89

Cuella, G.: IX 97

Culver, G.C.: IX 331

D'Amore, F.: V 262, VI 21, VI 351, VII 91, VIII 295, VIII 315, IX 221, IX 247, X 113, X 273

Danesh, A.: IV 60

DaPrat, G.: VIII 119, X 163

Dash, Z.V.: VII 97, VIII 269, IX 397

Dee, J.F.: X 97

Delaney, P.T.: IX 239

de las Alas, V.F.: IV 228

Denlinger, R.: VI 178

DeVilgiss, J.: IV 84

Dibble, W.E.: VI 316

Dickinson, D.A.: IX 279

Dominguez A.,B.: IV 5, V 228, VII 35, IX 87

Donaldson, I.G.: IV 36, V 222, VI 41, VII 1

Dorfman, M.H.: I 130, II 299, VI 105, VIII 261

Dougherty, D.E.: VIII 115

Downs, W.F.: II 34, II 176, VIII 275, IX 311

Duda, L.E.: X 195

Duffield, W.A.: VII 11

Dundurs, J.: I 178

Dvorov, I.M.: VIII 329

Dvorov, V.I.: VIII 329

Dykstra, H.: III 96, VI 13

Eaton, R.R.: VI 218

Economides, M.: IV 165, V 83, V 127, VI 66, VIII 25, VIII 31, IX 73, IX 167, X 227

Ehlig-Economides, C.: IV 60, IV 188, VI 66, VIII 25, IX 73

Eliasson, E.T.: VIII 211

Eliasson, J.: VI 288

Engi, D.: IX 421

Ershaghi, I.: V 282, VI 258

Esquer, C.A.: IX 357, X 73

Fallon, J.B.: VIII 91

Fandriana, L.: V 183

Farrell, W.E.: X 79

Faust, C.R.: I 198, II 308, III 185, IV 275

Fehlberg, E.L.: I 84, II 16, V 83

Ferriz, H.: VIII 19

Fisher, H.N.: V 103

Fossum, M.P.: VIII 289

Fournier, R.O.: VIII 45

Fradkin, L.J.: V 199

Frimannsson, H.: IX 65

Frye, G.: I 89, II 30, IV 96

Fujinaga, Y.: VI 188, X 207

Gale, R.O.: IV 139

Garfias, A.: IX 253, IX 269, X 233, X 241, X 265

Garg, S.K.: I 65, II 310, III 178, IV 217, IV 280, V 195, VI 76, VII 47, VII 175, VIII 97, X 79

Ghaemian, S.: VI 258

Gilardi, J.: X 259

Giovannoni, A.: VII 77

Glover, R.B.: VIII 127

Gobran, B.D.: VI 279, VI 297, VII 121

Golabi, K.: II 181, III 158, VI 374, VI 380

Goldman, D.: II 168, III 130

Goldstein, N.E.: VIII 161, X 13

Gonzalez, A.: VI 60

Gonzalez, J.: X 233

Goranson, C.: III 116, IV 118, IX 205

Gould, T.L.: I 146

Goyal, K.P.: III 209, IV 300, V 205, VI 130, IX 151

Graj, A.N.: IV 15

Granados, E.E.: X 37

Grant, M.A.: IV 78, IV 139, V 37, V 242, VI 170, VI 28, VIII 111, VIII 127, VIII 133, IX 107, X 31

Gray, W.G.: II 222

Greenfield, R.J.: IV 275

Grisgsby, O.C.: IV 249, VI 367

Gringarten, A.C.: I 113

Gudmundsson, J.S.: VII 61, VIII 143, IX 331, X 45

Guevara, M.: VIII 205

Guglielminetti, M.: IX 53

Guillot, A.: IX 199

Gulati, M.S.: I 69, V 238

Gunnarsson, G.: VI 288

Gunnlaugsson, E.: IX 231

Haas, J.L.: II 247

Halfman, S.E.: VIII 171

Halldorsson, G.K.: VII 71

Hammond, D.E.: VII 133

Handy, L.L.: V 282

Haney, J.: IV 118

Hanson, J.M.: II 46, IV 160, V 120

Hanson, M.E.: I 192

Harban, D.C.: I 77

Harrar, J.E. VI 98

Harrison, R.F.: IV 272, V 115

Hart, C.M.: IX 421

Hauksson, T.: VII 61

Hebein, J.J.: IX 135, X 89

Herkelrath, W.N.: III 43, IV 54, VI 322, VII 179

Hernandez, L.: X 73

Hinrichs, T.C.: I 143

Hirakawa, S.: III 70, IV 234, VI 188, VII 115, VIII 225, IX 115, X 207

Hiriart, G.: VII 41, IX 275, X 213

Hite, J.R.: II 16

Hoang, V.T.: VIII 137

Holcomb, D.: II 263

Horii, H.: IX 381

Horne, R.N.: III 192, IV 138, VI 150, VII 5, VII 103, VIII 143, VIII 289, IX 199, IX 323, IX 331, X 259

Howard, J.H.: III 9, IV 15, V 5, VI 3

Hsieh, C.H.: III 192, IV 60

Hsieh, P.A.: X 169

Hulen, J.B.: IX 145

Hull, L.C.: VIII 285, IX 305, IX 311, X 293

Hunsbedt, A.: II 213, III 49, V 293, VI 264 VII 169, VIII 255, X 73

Ichikawa, M.: VIII 225

Ingebritsen, S.E.: IX 365

Inglesias, E.R.: VI 84, VII 41, VIII 197, VIII 205, IX 291, X 241, X 265, X 301

Iregui, R.: II 213, III 49

Isherwood, W.: III 18

Ishido, T.: X 79

Isokrari, O.F.: I 130, II 299

Izaguirre, O.: IX 269

Izquierdo, G.: VIII 205

Jackson, P.B.: IX 331

James, R.: I 52, III 198, V 355, VI 139, VI 145, VIII 133, IX 449

Jamieson, I.: III 61

Jensen, C.L.: IX 323

Jig, H.: IV 84

Johnson, S.E.: IX 331

Jones, A.H.: V 26

Jones, T.: VI 328

Juprasest, S.: V 183

Karasaki, K.: VIII 219, X 145

Karmarkar, M.: IV 207, V 322

Kasameyer, P.W.: I 249, II 290, III 163, X 297

Kassoy, D.R.: I 23, II 263, III 209, IV 300

Keer, L.M.: I 180, II 200

Keith, L.A.: IX 239

Kelsey, F.J.: II 251

Keskinen, M.: VIII 39

Keys, W.S.: II 66

Kihara, D.: II 109, III 138, IV 133

Killup, M.W.: VIII 127

King, M.S.: X 307

Kingston, R.: IX 121

Kiryukhin, A.V.: X 57

Kjaran, S.P.: VI 288

Klein, C.W.: X 37

Knapp, R.M.: I 130, II 299

Koslow, K.N.: VIII 285, IX 305

Kruger, P.: I 169, II 61, II 213, III 49, III 192, IV 201, V 327, VI 264, VI 344, VII 1, VIII 255, VIII 315, IX 261, X 73, X 219

Kuide, X.: IX 127

Kunze, J.F.: I 117, II 168, III 125, III 130 VIII 25

Kuo, T.M.C.: V 139

Kuwada, J.T.: I 157

Lai, C.H.: X 279

Lam, S.T.: VIII 255, X 73

Laredo, F.: IX 253, IX 253

Lawton, R.G.: II 188

Leaver, J.D.: IX 107

Li, T.M.C.: II 34

Lin, J.J.: V 249

Lipman, S.C.: II 6

Lippmann, M.J.: IV 5, V 228, VI 130, VII 35, VIII 49, VIII 171, IX 87, IX 157

Liguori, P.E.: V 147

Lockner, D.: II 198, IV 50

Lofgren, B.: VIII 25

Lombard, G.L.: I 135

London, A.L.: II 213, III 49

Long, J.C.S.: X 145

Lowell, M.G.: I 117

Maas, J.P.: IX 151

MacDonald, R.C.: VI 105

Macias-Chapa, L.: V 302, IV 201

Maeder, P.F.: IX 279

Maes, M.E.: II 219

Maini, T.: I 258

Manetti, G.: I 93, I 101, I 242, II 150, IX 17

Maney, J.: X 141

Mangold, D.C.: VII 161

Mann, L.: I 74

Mannon, L.S.: III 29

Manon, A.: IV 5

Marconcini, R.: II 21, II 150

Marquez, R.: VIII 231, IX 357, X 73

Martin, J.C.: I 42, II 251, IV 42

Martinez, A.: X 265

Mateen, K.: IX 181

Mathews, M.: VI 303

Mathias, K.E.: II 39

Matthiasson, J.: IX 65

Mazor, E.: III 55

McAtee, R.E.: VIII 275

McCoy, R.L.: VII 29

McEdwards, D.G.: II 75, III 116

McKee, C.R.: I 192

McNitt, J.R.: X 37

Meidav, T.: I 52, II 126

Menzies, A.J.: VIII 143

Mercado, S.: VI 60

Mercer, J.W.: I 198, II 308, III 185, IV 275

Messer, P.H.: II 136, IV 228, V 255

Mete, L.: VIII 73

Michels, D.E.: IX 317, X 183

Miller, C.W.: VI 130, VI 159

Miller, F.G.: II 3, IV 165, VI 150, VII 13

Miller, J.D.: IX 373

Miller, L.G.: II 168

Miranda, C.: X 219, X 241, X 265

Miyoshi, M.: VI 188

Mlodinow, L.D.: III 172

Mock, J.E.: X 1

Moench, A.F.: II 229, III 64, IV 54, IV 112, V 90, VI 178, VI 322, VII 179, IX 175, X 169

Mogen, P.: X 141

Molinar, R.: V 228, IX 291, X 219, X 301

Moore, D.: VI 361

Moore, D.E.: VII 127, IX 239

Moore, J.N.: X 253

Morris, C.W.: VII 53, X 227

Morris, H.E.: IX 421

Morrow, C.A.: VII 127

Morse, J.G.: III 145

Muffler, L.J.P.: III 3

Mura, T.: I 180, II 200

Murakami, K.: X 79

Murphy, H.D.: I 174, II 188, IV 244, VI 272, VII 97, IX 397

Murphy, W.: VI 328

Nair, K.: VI 380

Nakanishi, S.: X 79

Nakatsuka, K.: IX 403

Narasimhan, T.N.: I 124, II 75, III 116, V 205

Nathenson, M.: I 50, II 40, IV 96

Nelson, D.V.: V 293, VI 264

Nelson, L.B.: III 130

Nemet-Nasser, S.: I 232, IX 381

Neri, G.: I 37, I 101, I 242, II 21, II 150, V 90, V 229, IX 17, IX 97

Netherton, R.: III 163, VI 98

Nguyen, V.V.: VI 213

Nielson, D.: IX 145

Nieva, D.: IX 253, IX 269, X 233, X 265

Niitsuma, H.: IX 403

Nikitopoulos, D.E.: IX 279

Noble, J.E.: IV 15

Noto, P.: VII 85

Nugent, J.M.: I 135

Nur, A.: IV 84, VI 316, VI 328

Nuti, S.: VII 85

Ohkuma, H.: VIII 261

Ohtsubo, H.: I 232

Okandan, E.: IX 339, X 53

Okazaki, J.: V 139

Oliver, R.: VIII 205, IX 269

Olhoeft, G.R.: V 282

Olsen, G.: X 45

O'Neill, K.: II 222

Ortiz, J.: X 219

O'Sullivan, M.J.: IV 332, VI 204, VI 224 IX 107

Owen, L.B.: III 163, VI 98

Palmason, G.: IX 37

Parlaktuna, M.: IX 339

Perusini, P.: I 37

Peters, E.: VIII 261

Petty, S.: VI 115, IX 217

Pinder, G.F.: I 199, II 222, III 188, IV 286, V 175, VI 213, VII 157, VIII 115

Pine, R.J.: IX 387

Piwinskii, A.J. & Netherton, R.: III 21

Pohoiki, H.I.: IV 201

Polat, T.: X 53

Potter, J.M.: VI 316

Potter, R.M.: II 188, III 36, VI 272

Potter, R.W.: II 247, III 55

Pritchett, J.W.: I 201, II 310, III 178, V 159, V 195, IV 217, VII 175, X 79

Pruess, K.: IV 308, V 169, VI 194, VI 204, VII 151, VIII 161, VIII 211, VIII 219, VIII 255, IX 345, IX 443, X 113, X 273

Qilong, Y.: IX 127

Quijano, L.: IX 253

Raasch, G.D.: VI 34, X 129

Rago, F.: VIII 261

Ramey, H.J., Jr.: II 3, III 49, III 192, IV 1, IV 60, IV 165, V 64, V 175, VI 150, VI 297, VII 13, IX 181, X 163

Randall, G.S.: IV 272

Reda, D.C.: VI 218

Reed, M.: IV 3, VII 109, X 1

Reeder, J.W.: VIII 31

Rex, R.W.: II 116

Rice, L.F.: II 159, IV 217, V 195

Rigby, F.A.: VI 310

Rimstidt, J.D.: I 185, II 176

Rinehart, J.S.: II 263

Riney, T.D.: III 178, IV 280, V 195, VII 47, VIII 97

Ritz, C.L.: VII 19

Rivera-Rodriguez, J.: VIII 73, IX 97

Roberts, V.W.: II 9, VII 21

Rodriguez, F.: VII 103

Rodriguez, J.: IV 176

Rosa, A.: IX 199

Rosser, J.R.: IX 151

Rothstein, S.: VI 380

Roux, B.: V 343

Rudisill, J.M.: IV 218

Russell, B.F.: IX 311

Safai, N.M.: III 188

Sageev, A.: VI 297, X 163

Saltuklaroglu, M.: IV 176, V 44, V 55, VII 143

Samaniego-V, F.: IX 97

Sammis, C.G.: I 240, II 34, VII 133

Samundsson, K.: IX 65

Sanchez, E.: X 213

Santoyo, S.: VIII 205

Sanyal, S.K.: I 52, II 126, III 81, V 183, V 316, V 343, VI 279, X 37

Scherer, C.R.: I 161, II 181, III 158

Schroeder, R.C.: I 249, II 85, II 290, III 116, IV 118, IV 308, V 169, IV 5, V 228

Schultz, A.: IV 165

Schwarz, W.J.: III 9, IV 15, V 5

Seki, A.: IV 133, X 201

Semprini, L.: IV 201, V 302, VI 344, VIII 315, IX 261, X 219

Sengul, M.: II 126

Sepehrnoori, K.: VIII 261

Shapiro, A.: V 175, VII 157

Sharme, D.: I 258

Shen, H.W.: I 213

Shen, K.Y.: V 96

Sigurdsson, O.: VII 71, VIII 189, IX 211, X 177

Sill, W.: VIII 275

Sioshansi, F.: VI 380

Skiba, P.A.: VIII 279

Smith, A.T.: X 297

Smith, E.W.: VI 69

Smith, J.L.: II 116

Solbau, R.D.: IX 205

Sorey, M.L.: I 225, II 324, V 199, V 222, VI 253, VII 109, VIII 5, IX 365

Speliotis, G.: IX 73

Spivak, A.: II 159

Squarci, P.: VI 21

Squerci, P.: I 37

Stauder, J.J. X 253

Stefansson, V.: VI 49, VII 71, VIII 189, VIII 211, IX 37, IX 65, IX 211, IX 345, X 23, X 177

Steingrimsson, B.: VI 49, X 177

Sternfeld, J.: VIII 39

Stieltjes, L.: I 113

Stoker, R.C.: I 117, II 168, III 125, III 130

Strobel, C.J.: II 143, IV 106

Sugrobov, V.M.: X 57

Summers, R.: II 198

Svanbjornsson, A.: IX 65

Swenson, L.W., Jr.: VII 169

Syms, M. C.: VI 126

Syms, P. H.: VI 126

Tachimori, M.: VIII 149, VIII 155

Takahashi, H.: IX 403, IX 415

Takahashi, P.: II 109, III 138, X 201

Takanohashi, M.: IX 403

Tansev, E.: III 107, IV 213

Tester, J.W.: II 188, IV 249, V 103, VI 272

Thomas, D.M.: VIII 309

Thompson, J.M.: VIII 45

Thorhallsson, S.: IX 37, X 45

Thorson, L.: III 163

Thorsteinsson, T.: IX 37

Todd, M.C.: IV 275

Tomasson, J.: VII 61

Toms, R.S.H.: VIII 1, IX 1

Truesdell, A.H.: III 55, IV 96, IV 239, V 262, VI 21, V 277, VI 194, VI 351

Trujillo, P.E.: VI 367

Tsang, C.F.: I 62, II 75, II 85, III 172, IV 322, VI 224, VII 7, IX 443

Tsang, Y.W.: IV 322

Tsao, L.: IV 294

Ucok, H.: V 282

Ungemach, P.: IX 5

Verma, A.K.: VI 243, IX 443

Verma, S.: X 219, X 265

Vides-R., A.: IX 97

Voss, C.I.: IV 286

Vrouzi, F.: IX 73

Warren, G.: II 61

Wasserman, M.L.: III 107

Watson, A.: IX 121

Weertman, J.: II 193

Wegner, R.E.: II 251

Wells, L.E.: V 373

Weres, O.: III 214, IV 294

Wescott, E.: VI 60

Westwood, J.D.: VII 23

Whitehead, N.E.: V 309

Wilson, D.M.: X 189

Wilt, M.J.: VIII 161

Witherspoon, P.A.: I 62, I 124, IV 5, V 228, VII 7, IX 443, X 105, X 145, X 279

Woitke, L.J.: I 153

Wolgemuth, K.M.: V 26

Wooding, R.A.: I 126, I 206, II 339

Wright, P.M.: IX 299

Wu, T.M.: V 249

Wu, T.S.: IX 193

Yamaguchi, S.: VII 115, X 207

Yee, A.: IV 294

Yoshimura, T.: X 79

Yuen, P.: III 138, IV 133

Zais, E.: III 85, IV 153, V 190, VI 121

Zebib, A.: II 263

Zelwer, R.: VIII 171

Zerzan, J.: IV 308

Zyvoloski, G.A.: IV 332, VIII 269